National Library
of Canada

Canadian Theses Service

Ottawa, Canada
K1A 0N4

Bibliothèque nationale
du Canada

Service des thèses canadiennes

NOTICE

The quality of this microform is heavily dependent upon the quality of the original thesis submitted for microfilming. Every effort has been made to ensure the highest quality of reproduction possible.

If pages are missing, contact the university which granted the degree.

Some pages may have indistinct print especially if the original pages were typed with a poor typewriter ribbon or if the university sent us an inferior photocopy.

Previously copyrighted materials (journal articles, published tests, etc.) are not filmed.

Reproduction in full or in part of this microform is governed by the Canadian Copyright Act, R.S.C. 1970, c. C-30.

AVIS

La qualité de cette microforme dépend grandement de la qualité de la thèse soumise au microfilmage. Nous avons tout fait pour assurer une qualité supérieure de reproduction.

S'il manque des pages, veuillez communiquer avec l'université qui a conféré le grade.

La qualité d'impression de certaines pages peut laisser à désirer, surtout si les pages originales ont été dactylographiées à l'aide d'un ruban usé ou si l'université nous a fait parvenir une photocopie de qualité inférieure.

Les documents qui font déjà l'objet d'un droit d'auteur (articles de revue, tests publiés, etc.) ne sont pas microfilmés.

La reproduction, même partielle, de cette microforme est soumise à la Loi canadienne sur le droit d'auteur, SRC 1970, c. C-30.

NL-339 (r. 88/04)

Canada

THE UNIVERSITY OF ALBERTA

SCALED MODEL STUDIES OF SOLVENT–STEAM INJECTION UNDER BOTTOM WATER CONDITIONS

BY

DANIEL JOHN ORACHESKI

©

A THESIS
SUBMITTED TO THE FACULTY OF GRADUATE STUDIES AND RESEARCH
IN PARTIAL FULFILLMENT OF THE REQUIREMENTS FOR THE DEGREE
OF MASTER OF SCIENCE
IN
PETROLEUM ENGINEERING

DEPARTMENT OF MINING, METALLURGICAL AND PETROLEUM
ENGINEERING

EDMONTON, ALBERTA
FALL, 1988

Permission has been granted to the National Library of Canada to microfilm this thesis and to lend or sell copies of the film.

The author (copyright owner) has reserved other publication rights, and neither the thesis nor extensive extracts from it may be printed or otherwise reproduced without his/her written permission.

L'autorisation a été accordée à la Bibliothèque nationale du Canada de microfilmer cette thèse et de prêter ou de vendre des exemplaires du film.

L'auteur (titulaire du droit d'auteur) se réserve les autres droits de publication; ni la thèse ni de longs extraits de celle-ci ne doivent être imprimés ou autrement reproduits sans son autorisation écrite.

ISBN 0-315-45648-5

THE UNIVERSITY OF ALBERTA

RELEASE FORM

NAME OF AUTHOR Daniel John Oracheski

TITLE OF THESIS Scaled Model Studies of Solvent-Steam Injection, Under Bottom Water Conditions

DEGREE FOR WHICH THESIS WAS PRESENTED : MASTER OF SCIENCE

YEAR THE DEGREE WAS GRANTED : FALL, 1988

Permission is hereby granted to the UNIVERSITY OF ALBERTA LIBRARY to reproduce single copies of this thesis and to lend or sell such copies for private, scholarly or scientific research purposes only.

The author reserves other publication rights, and neither the thesis nor extensive extracts from it may be printed or otherwise reproduced without the author's written permission.

(SIGNED) Danny Oracheski

PERMANENT ADDRESS:

1402 - Galbraith House, Michener Park,

Edmonton, Alberta, Canada

T6H 5B5

DATED: May 10, 1988

THE UNIVERSITY OF ALBERTA

FACULTY OF GRADUATE STUDIES AND RESEARCH

The undersigned certify that they have read and recommend to the Faculty of Graduate Studies and Research, for acceptance, a thesis entitled SCALED MODEL STUDIES OF SOLVENT–STEAM INJECTION, UNDER BOTTOM WATER CONDITIONS submitted by DANIEL JOHN ORACHESKI in partial fulfillment of the requirements for the degree of MASTER OF SCIENCE in PETROLEUM ENGINEERING.

....

Dr. S.M. Farouq Ali (Supervisor)

D L Flock
....

Dr. D.L. Flock

JM Whiting
....

Dr. J.M. Whiting

J. D. Scott
....

Dr. J.D. Scott (External Examiner)

DATED : May 10, 1988

To My Wife, Colleen,

and to My Parents, Louis and Carol,

For Their Boundless Dedication, Encouragement and Love

Abstract

The research project was based upon examining the use of a solvent in combination with a steamflood as a thermal recovery technique in thin heavy oil formations with underlying water. The research consisted of conducting steam injection experiments in a low pressure, scaled physical model of the Aberfeldy heavy oil reservoir which is located in Lloydminster, Saskatchewan.

The low pressure apparatus used for this study was designed to represent one quarter of an eight hectare (twenty acre) five-spot pattern. The scaling of the vacuum model was based upon low pressure scaling criteria.

The main emphasis of the research was directed towards studying the effectiveness of a solvent-steamflood process conducted in a bottom water model and comparing this technique to a conventional steamflood performed in a similar model. As expected, the bottom water had a very adverse effect on the thermal efficiency of the recovery processes due to the underlying water acting as a heat sink and high conductivity channel for the injected steam. It was determined that a solvent-steamflood process conducted in a bottom water model displayed improved oil recovery compared to a conventional steamflood method. The use of a solvent slug prior to steam injection improved the thermal efficiency of the steamflood by partially guiding the steam away from the heat scavenging bottom water and into the desired oil zone.

Recovery schemes other than the solvent-steamflood method in a bottom water formation were also investigated. The alternate methods consisted of gas injection prior to steamflooding, gas injection prior to a solvent-steamflood and implementing a limited barrier at the oil/water contact in the vicinity of the injection well prior to steamflooding. Experimental results indicated that these three methods improved recovery compared to the conventional steamflood, however, the solvent-steamflood process still exhibited the highest recovery. A solvent-steamflood experiment conducted in a previously

waterflooded model yielded the best recovery of all the experiments, suggesting that this process may also be a viable tertiary recovery method.

A heat flow analysis of a conventional steamflood in a homogeneous model was conducted. It was concluded that the Mandl-Volek steam injection model best represented the steam zone development in the model and that heat loss from the model was substantial throughout the experiment.

Results of the research indicated that the implementation of a solvent-steamflood technique to optimize oil recovery in thin heavy oil reservoirs containing bottom water, warrants further investigation. The alternate methods studied also merit further examination since these schemes appeared to improve oil recovery from these types of formations as well.

Acknowledgements

Extreme gratitude is expressed to Dr. S.M. Farouq Ali for his expert guidance and support, as well as his geniune and overwhelming generosity. The affiliation with Dr. Farouq Ali has provided the author with valuable experience and knowledge, and most importantly helped develop the author into a better person. The author is very proud to have had the opportunity to be associated with such a distinguished individual as Dr. Farouq Ali.

The author wishes to acknowledge Mr. Marty Proctor for his patience and commitment in helping to familarize the author with the experimental equipment and procedure related with the research project. The friendship developed with Mr. Proctor, alone has made the author's experience as a graduate student more than worthwhile.

The author is grateful to Mr. Lyle Oracheski for his capable and irreplaceable assistance in conducting the experiments and processing the experimental data.

The expertise and advice of Mr. Bob Smith used to modify the experimental apparatus used in this project was appreciated.

Special thanks are given to Dr. K.W.A. Miller, of Husky Oil Operations Ltd., for providing data on the Aberfeldy formation, which was used in designing the prototype reservoir.

The financial assistance and technical assistance provided by the Department of Energy, Mines and Resources, CANMET, and the members of this organization, particularly Dr. Albert George and Mr. Roger Lafleur, are gratefully acknowledged.

Table of Contents

Chapter Page

I Introduction 1

II Statement of the Problem 3

III Literature Review 6

  Scaled Model Studies of Steam Injection Processes 6

    Experimental Approaches to Steam Injection 7

      High Pressure and Low Pressure Scaled Models 8

    Studies of Thin, Bottom Water Reservoirs 12

  Incorporation of Solvent with Steam Injection Processes 14

    Dispersion and Diffusion of Solvents in a Porous Medium 14

    Non-Thermal Miscible Displacement Processes 15

    Solvent Scaling Criteria 17

    Incorporation of Solvent Injection into Thermal Recovery Methods 18

    Asphaltene Flocculation 22

IV Scaling of the Solvent-Steamflood Process in the Low Pressure Model 24

  Derivation of the Model Scaling Parameters 24

  Designing the Low Pressure Model of the Aberfeldy Reservoir 29

    Field Representation 29

    Length Scale Selection 31

    Scaling of Model Pressure 31

    Scaling of Model Temperature 33

    Determination of the Required Steam Quality 35

    Scaling of Model Oil Viscosity 36

    Time Scale Determination 36

    Scaling of Model Permeability 37

Scaling of Injection and Production Rates 38
Determination of Water Proportion for Steam Quality 39
Scaling of Wells in the Model 40
Scaling of Solvent in the Model 41
V Experimental Apparatus and Procedure 43
Physical Model 43
Data Acquisition System 47
Solvent and Steam Injection System 50
Produced Fluid Collection System 51
Model Cart, Rail System and Cold Storage Compartment 53
Model Fluids 53
Selection of the Aberfeldy Model Oil 53
Selection of the Solvent 54
Preparation of the Model for an Experiment 56
Packing of the Model 56
Saturation of the Model 60
Preparation of Bottom Water Model 61
Creation of a Gas Cap in the Model 64
Conducting the Experiments 65
Clean Up of the Apparatus 68
Analysis of Experimental Data 68
VI Discussion of the Results 74
Presentation of of the Results 74
Steamflood versus Solvent-Steamflood Process 79
Typical Steamflood History in a Bottom Water Reservoir 81
Base Experiments for Comparison Purposes 89
Continuous Solvent Flood 89

Solvent-Steamflood 95
Steamflood of a Bottom Water Model With Prior Gas Injection 114
Effect of Solvent Slug Size on Oil Recovery by a Steamflood 128
Effect of Bottom Water Thickness on Steamflood Response 149
Effect of Bottom Water Thickness on Solvent-Steamflood Response 151
Role of Gas Injection in Steamflooding 186
Gas Injection in a Steamflood 187
Gas Injection Prior to Steam Injection with Bottom Water 187
Gas Injection with Solvent and Steam Injection 188
Gas Injection Prior to Solvent & Steam Injection with Bottom Water 202
Effect of Injection-Production Interval Locations 223
Use of a Physical Barrier in a Bottom Water Steamflood 226
Effectiveness of Waterflooding Prior to Solvent and Steam Injection 242
Heat Flow Analysis 259
Lauwerier Equation 259
Comparison of Marx-Langenheim and Mandl-Volek Models 264
A. Marx-Langenheim Theory 264
B. Mandl-Volek Theory 266
Heat Loss Analysis 269
Experimental Limitations and Sources of Error 273
VII Conclusions 275
References 278
Appendix A 283
Appendix B 576

List of Tables

Table		Page
4.1	Scaling Parameters for Steam Injection Process	25
4.2	Prototype and Model Values for the Aberfeldy Reservoir	30
4.3	Prototype and Model Scaling Values	34
4.4	Steam Enthalpy at Various Model Pressures	40
5.1	Temperature Vs. Oil Viscosity for Prototype and Ideal Model Oils	54
6.1	List and Description of Solvent and Steam Injection Experiments	75
6.2	Experimental Data for Run 39: Steamflood in Bottom Water Model	83
6.3	Experimental Data for Run 40: Solvent Flood in Homogeneous Model	90
6.4	Experimental Data for Run 44: Solvent-Steamflood in Homogeneous Model	97
6.5	Experimental Data for Run 45: Solvent-Steamflood in Homogeneous Model	102
6.6	Experimental Data for Run 46: Solvent-Steamflood in Homogeneous Model	107
6.7	Experimental Data for Run 60: Gas Injection Prior to a Steamflood in Homogeneous Model	116
6.8	Experimental Data for Run 61: Gas Injection Prior to a Steamflood in Homogeneous Model	121
6.9	Experimental Data for Run 65: Solvent-Steamflood in Bottom Water Model	130
6.10	Experimental Data for Run 66: Solvent-Steamflood in Homogeneous Model	137
6.11	Experimental Data for Run 67: Solvent-Steamflood in Homogeneous Model	142
6.12	Experimental Data for Run 49: Solvent-Steamflood in Bottom Water Model	155
6.13	Experimental Data for Run 50: Solvent-Steamflood in Bottom Water Model	160

6.14 Experimental Data for Run 51:
Solvent-Steamflood in Bottom Water Model ____ 165

6.15 Experimental Data for Run 53:
Solvent-Steamflood in Bottom Water Model ____ 170

6.16 Experimental Data for Run 54:
Solvent-Steamflood in Bottom Water Model ____ 175

6.17 Experimental Data for Run 55:
Gas Injection Prior to a Solvent-Steamflood in Homogeneous Model ____ 190

6.18 Experimental Data for Run 56:
Gas Injection Prior to a Solvent-Steamflood in Homogeneous Model ____ 195

6.19 Experimental Data for Run 58:
Gas Injection Prior to a Solvent-Steamflood in Bottom Water Model ____ 204

6.20 Experimental Data for Run 59:
Gas Injection Prior to a Solvent-Steamflood in Bottom Water Model ____ 209

6.21 Experimental Data for Run 62:
Gas Injection Prior to a Solvent-Steamflood in Bottom Water Model ____ 214

6.22 Experimental Data for Run 63:
Steamflood in Bottom Water Model With a Partial Barrier ____ 229

6.23 Experimental Data for Run 64:
Steamflood in Bottom Water Model With a Partial Barrier ____ 234

6.24 Experimental Data for Run 47A:
Waterflood Prior to a Solvent-Steamflood in Homogeneous Model ____ 244

6.25 Experimental Data for Run 47B:
Solvent-Steamflood Following a Waterflood in Homogeneous Model ____ 245

6.26 Experimental Data for Run 48A:
Waterflood Prior to a Solvent-Steamflood in Homogeneous Model ____ 250

6.27 Experimental Data for Run 48B:
Solvent-Steamflood Following a Waterflood in Homogeneous Model ____ 251

6.28 Heat Flow Analysis of Model Using Lauwerier Equation (Run 26):
1/2 of Injection in Top Portion and 1/2 of Injection in Bottom Portion ____ 261

6.29 Heat Flow Analysis of Model Using Lauwerier Equation (Run 26):
3/4 of Injection in Top Portion and 1/4 of Injection in Bottom Portion ____ 262

6.30 Comparison of Marx-Langenheim and Mandl-Volek Models of Formation
Heating by Steam Injection for the Low Pressure Model in Run 26 ____ 268

6.31 Analysis of Heat Loss Occurring During a Base Steamflood (Run 26) ____ 271

List of Figures

Figure Page

5.1 Schematic Diagram of Low Pressure Apparatus 44

5.2 Schematic Diagram of Model Illustrating Thermocouple Positions 49

5.3 Diagram of Collection System for Produced Fluids 52

5.4 Temperature-Viscosity Profiles for Ideal and Actual Model Oils 55

5.5 Mixture Viscosity Vs. Heavy Virgin Naphtha Concentration 57

5.6 Diagram of Particle Distributor Used as a Packing Device for Model 59

5.7 Refractive Index Vs. Percentage of NaCl in a Salt Water Solution 63

5.8 Refractive Index Vs. Volumetric Fraction of Heavy Virgin Naphtha 67

5.9 Sample of a Top View Temperature Profile 71

5.10 Sample of a Cross-Sectional Temperature Profile 72

6.1 Map of Experimental Runs Conducted During the Research Project 78

6.2 Schematic Diagram of a Steamflood Process 80

6.3 Schematic Diagram of a Solvent-Steamflood Process 81

6.4 Run 39: Cumulative Oil Recovery Vs. Pore Volumes Injected 84

6.5 Run 39: Oleic Phase in Each Sample Vs.Cumulative Volume Injected 85

6.6 Run 39: Instantaneous Produced WOR Vs. Cumulative Volume Injected 86

6.7 Run 39: Instantaneous Oil/Steam Ratio Vs. Cumulative Oil Produced 87

6.8 Run 40: Cumulative Oil Recovery Vs. Pore Volumes Injected 92

6.9 Run 40: Oleic Phase in Each Sample Vs. Cumulative Volume Injected 93

6.10 Run 44: Cumulative Oil Recovery Vs. Pore Volumes Injected 98

6.11 Run 44: Oleic Phase in Each Sample Vs. Cumulative Volume Injected 99

6.12 Run 44: Instantaneous Produced WOR Vs. Cumulative Volume Injected ____ 100

6.13 Run 44: Instantaneous Oil/Steam Ratio Vs. Cumulative Oil Produced ____ 101

6.14 Run 45: Cumulative Oil Recovery Vs. Pore Volumes Injected ____ 103

6.15 Run 45: Oleic Phase in Each Sample Vs. Cumulative Volume Injected ____ 104

6.16 Run 45: Instantaneous Produced WOR Vs. Cumulative Volume Injected ____ 105

6.17 Run 45: Instantaneous Oil/Steam Ratio Vs. Cumulative Oil Produced ____ 106

6.18 Run 46: Cumulative Oil Recovery Vs. Pore Volumes Injected ____ 108

6.19 Run 46: Oleic Phase in Each Sample Vs. Cumulative Volume Injected ____ 109

6.20 Run 46: Instantaneous Produced WOR Vs. Cumulative Volume Injected ____ 110

6.21 Run 46: Instantaneous Oil/Steam Ratio Vs. Cumulative Oil Produced ____ 111

6.22 Run 60: Cumulative Oil Recovery Vs. Pore Volumes Injected ____ 117

6.23 Run 60: Oleic Phase in Each Sample Vs. Cumulative Volume Injected ____ 118

6.24 Run 60: Instantaneous Produced WOR Vs. Cumulative Volume Injected ____ 119

6.25 Run 60: Instantaneous Oil/Steam Ratio Vs. Cumulative Oil Produced ____ 120

6.26 Run 61: Cumulative Oil Recovery Vs. Pore Volumes Injected ____ 122

6.27 Run 61: Oleic Phase in Each Sample Vs. Cumulative Volume Injected ____ 123

6.28 Run 61: Instantaneous Produced WOR Vs. Cumulative Volume Injected ____ 124

6.29 Run 61: Instantaneous Oil/Steam Ratio Vs. Cumulative Oil Produced ____ 125

6.30 Comparison of Steamflood Run 39 & Gas Injection Prior to a Steamflood Run 61 Recoveries Performed in a Bottom Water Model 127

6.31 Run 65: Cumulative Oil Recovery Vs. Pore Volumes Injected 131

6.32 Run 65: Oleic Phase in Each Sample Vs. Cumulative Volume Injected 132

6.33 Run 65: Instantaneous Produced WOR Vs. Cumulative Volume Injected 133

6.34 Run 65: Instantaneous Oil/Steam Ratio Vs. Cumulative Oil Produced 134

6.35 Run 66: Cumulative Oil Recovery Vs. Pore Volumes Injected 138

6.36 Run 66: Oleic Phase in Each Sample Vs. Cumulative Volume Injected 139

6.37 Run 66: Instantaneous Produced WOR Vs. Cumulative Volume Injected 140

6.38 Run 66: Instantaneous Oil/Steam Ratio Vs. Cumulative Oil Produced 141

6.39 Run 67: Cumulative Oil Recovery Vs. Pore Volumes Injected 143

6.40 Run 67: Oleic Phase in Each Sample Vs. Cumulative Volume Injected 144

6.41 Run 67: Instantaneous Produced WOR Vs. Cumulative Volume Injected 145

6.42 Run 67: Instantaneous Oil/Steam Ratio Vs. Cumulative Oil Produced 146

6.43 Comparison of the Effect of Solvent Slug Size on Solvent-Steamflood Recoveries for Runs 45, 66 & 67 148

6.44 Run 49: Cumulative Oil Recovery Vs. Pore Volumes Injected 156

6.45 Run 49: Oleic Phase in Each Sample Vs. Cumulative Volume Injected 157

6.46 Run 49: Instantaneous Produced WOR Vs. Cumulative Volume Injected 158

6.47 Run 49: Instantaneous Oil/Steam Ratio Vs. Cumulative Oil Produced 159

6.48 Run 50: Cumulative Oil Recovery Vs. Pore Volumes Injected 161

6.49 Run 50: Oleic Phase in Each Sample Vs. Cumulative Volume Injected 162

6.50 Run 50: Instantaneous Produced WOR Vs. Cumulative Volume Injected 163

6.51 Run 50: Instantaneous Oil/Steam Ratio Vs. Cumulative Oil Produced 164

6.52 Run 51: Cumulative Oil Recovery Vs. Pore Volumes Injected 166

6.53 Run 51: Oleic Phase in Each Sample Vs. Cumulative Volume Injected 167

6.54 Run 51: Instantaneous Produced WOR Vs. Cumulative Volume Injected 168

6.55 Run 51: Instantaneous Oil/Steam Ratio Vs. Cumulative Oil Produced 169

6.56 Run 53: Cumulative Oil Recovery Vs. Pore Volumes Injected 171

6.57 Run 53: Oleic Phase in Each Sample Vs. Cumulative Volume Injected 172

6.58 Run 53: Instantaneous Produced WOR Vs. Cumulative Volume Injected 173

6.59 Run 53: Instantaneous Oil/Steam Ratio Vs. Cumulative Oil Produced 174

6.60 Run 54: Cumulative Oil Recovery Vs. Pore Volumes Injected 176

6.61 Run 54: Oleic Phase in Each Sample Vs. Cumulative Volume Injected 177

6.62 Run 54: Instantaneous Produced WOR Vs. Cumulative Volume Injected 178

6.63 Run 54: Instantaneous Oil/Steam Ratio Vs. Cumulative Oil Produced 179

6.64 Total Oil Recovery Vs. Bottom Water Thickness for Solvent-Steamfloods 182

6.65 Comparison of Steamflood Run 39 & Solvent-Steamflood Run 54 Recoveries Performed in a Bottom Water Model 185

6.66. Run 55: Cumulative Oil Recovery Vs. Pore Volumes Injected 191

6.67 Run 55: Oleic Phase in Each Sample Vs. Cumulative Volume Injected 192

6.68 Run 55: Instantaneous Produced WOR Vs. Cumulative Volume Injected 193

6.69 Run 55: Instantaneous Oil/Steam Ratio Vs. Cumulative Oil Produced 194

6.70 Run 56: Cumulative Oil Recovery Vs. Pore Volumes Injected 196

6.71 Run 56: Oleic Phase in Each Sample Vs. Cumulative Volume Injected 197

6.72 Run 56: Instantaneous Produced WOR Vs. Cumulative Volume Injected 198

6.73 Run 56: Instantaneous Oil/Steam Ratio Vs. Cumulative Oil Produced 199

6.74 Comparison of Solvent-Steamflood Run 45 & Gas Injection Prior to Solvent-Steamflood Run 56 Recoveries Performed in a Homogeneous Model 201

6.75 Run 58: Cumulative Oil Recovery Vs. Pore Volumes Injected 205

6.76 Run 58: Oleic Phase in Each Sample Vs. Cumulative Volume Injected 206

6.77 Run 58: Instantaneous Produced WOR Vs. Cumulative Volume Injected 207

6.78 Run 58: Instantaneous Oil/Steam Ratio Vs. Cumulative Oil Produced 208

6.79 Run 59: Cumulative Oil Recovery Vs. Pore Volumes Injected 210

6.80 Run 59: Oleic Phase in Each Sample Vs. Cumulative Volume Injected 211

6.81 Run 59: Instantaneous Produced WOR Vs. Cumulative Volume Injected 212

6.82 Run 59: Instantaneous Oil/Steam Ratio Vs. Cumulative Oil Produced 213

6.83 Run 62: Cumulative Oil Recovery Vs. Pore Volumes Injected 215

6.84 Run 62: Oleic Phase in Each Sample Vs. Cumulative Volume Injected ____ 216

6.85 Run 62: Instantaneous Produced WOR Vs. Cumulative Volume Injected ____ 217

6.86 Run 62: Instantaneous Oil/Steam Ratio Vs. Cumulative Oil Produced ____ 218

6.87 Comparison of Solvent-Steamflood Run 50 & Gas Injection Prior to Solvent-Steamflood Run 58 Recoveries Performed in a Bottom Water Model ____ 221

6.88 Comparison of Effect of Injection-Production Interval Locations Runs 49 & 50 ____ 224

6.89 Schematic of Partial Barrier Installed in a Bottom Water Model ____ 227

6.90 Run 63: Cumulative Oil Recovery Vs. Pore Volumes Injected ____ 230

6.91 Run 63: Oleic Phase in Each Sample Vs. Cumulative Volume Injected ____ 231

6.92 Run 63: Instantaneous Produced WOR Vs. Cumulative Volume Injected ____ 232

6.93 Run 63: Instantaneous Oil/Steam Ratio Vs. Cumulative Oil Produced ____ 233

6.94 Run 64: Cumulative Oil Recovery Vs. Pore Volumes Injected ____ 235

6.95 Run 64: Oleic Phase in Each Sample Vs. Cumulative Volume Injected ____ 236

6.96 Run 64: Instantaneous Produced WOR Vs. Cumulative Volume Injected ____ 237

6.97 Run 64: Instantaneous Oil/Steam Ratio Vs. Cumulative Oil Produced ____ 238

6.98 Comparison of Recoveries of a Solvent-Steamflood With Bottom Water Run 50 & a Steamflood With a Partial Bottom Water Barrier Run 64 ____ 240

6.99 Run 47: Cumulative Oil Recovery Vs. Pore Volumes Injected ____ 246

6.100 Run 47: Oleic Phase in Each Sample Vs. Cumulative Volume Injected ____ 247

6.101 Run 47: Instantaneous Produced WOR Vs. Cumulative Volume Injected ____ 248

6.102 Run 47: Instantaneous Oil/Steam Ratio Vs. Cumulative Oil Produced ____ 249

6.103 Run 48: Cumulative Oil Recovery Vs. Pore Volumes Injected ____ 252

6.104 Run 48: Oleic Phase in Each Sample Vs. Cumulative Volume Injected ____ 253

6.105 Run 48: Instantaneous Produced WOR Vs. Volume Injected ____ 254

6.106 Run 48: Instantaneous Oil/Steam Ratio Vs. Cumulative Oil Produced ____ 255

6.107 Schematic Diagram of the Marx-Langenheim Model for Reservoir Heating by Steam Injection ____ 265

A.1 Run 39: Top View Temperature Profile at 0.25 Pore Volumes Injected ____ 284

A.2 Run 39: Top View Temperature Profile at 0.50 Pore Volumes Injected ____ 285

A.3 Run 39: Top View Temperature Profile at 0.75 Pore Volumes Injected ____ 286

A.4 Run 39: Top View Temperature Profile at 1.00 Pore Volumes Injected ____ 287

A.5 Run 39: Top View Temperature Profile at 1.25 Pore Volumes Injected ____ 288

A.6 Run 39: Top View Temperature Profile at 1.50 Pore Volumes Injected ____ 289

A.7 Run 39: Cross-Sectional Temperature Profile at 0.25 Pore Volumes Injected ____ 290

A.8 Run 39: Cross-Sectional Temperature Profile at 0.50 Pore Volumes Injected ____ 291

A.9 Run 39: Cross-Sectional Temperature Profile at 0.75 Pore Volumes Injected ____ 292

A.10 Run 39: Cross-Sectional Temperature Profile at 1.00 Pore Volumes Injected ____ 293

A.11 Run 40: Top View Temperature Profile at 0.25 Pore Volumes Injected ____ 294

A.12 Run 40: Top View Temperature Profile at 0.50 Pore Volumes Injected ____ 295

A.13 Run 40: Top View Temperature Profile at 0.75 Pore Volumes Injected 296

A.14 Run 40: Top View Temperature Profile at 1.00 Pore Volumes Injected 297

A.15 Run 40: Top View Temperature Profile at 1.25 Pore Volumes Injected 298

A.16 Run 40: Top View Temperature Profile at 1.50 Pore Volumes Injected 299

A.17 Run 40: Top View Temperature Profile at 1.75 Pore Volumes Injected 300

A.18 Run 40: Top View Temperature Profile at 2.00 Pore Volumes Injected 301

A.19 Run 40: Cross-Sectional Temperature Profile at 0.25 Pore Volumes Injected 302

A.20 Run 40: Cross-Sectional Temperature Profile at 0.50 Pore Volumes Injected 303

A.21 Run 40: Cross-Sectional Temperature Profile at 0.75 Pore Volumes Injected 304

A.22 Run 40: Cross-Sectional Temperature Profile at 1.00 Pore Volumes Injected 305

A.23 Run 44: Top View Temperature Profile at 0.25 Pore Volumes Injected 306

A.24 Run 44: Top View Temperature Profile at 0.50 Pore Volumes Injected 307

A.25 Run 44: Top View Temperature Profile at 0.75 Pore Volumes Injected 308

A.26 Run 44: Top View Temperature Profile at 1.00 Pore Volumes Injected 309

A.27 Run 44: Top View Temperature Profile at 1.25 Pore Volumes Injected 310

A.28 Run 44: Top View Temperature Profile at 1.50 Pore Volumes Injected 311

A.29 Run 44: Top View Temperature Profile at 1.75 Pore Volumes Injected 312

A.30 Run 44: Top View Temperature Profile at 2.00 Pore Volumes Injected 313

A.31 Run 44: Cross-Sectional Temperature Profile at 0.25 Pore Volumes Injected 314

A.32 Run 44: Cross-Sectional Temperature Profile at 0.50 Pore Volumes Injected 315

A.33 Run 44: Cross-Sectional Temperature Profile at 0.75 Pore Volumes Injected 316

A.34 Run 44: Cross-Sectional Temperature Profile at 1.00 Pore Volumes Injected 317

A.35 Run 45: Top View Temperature Profile at 0.25 Pore Volumes Injected 318

A.36 Run 45: Top View Temperature Profile at 0.50 Pore Volumes Injected 319

A.37 Run 45: Top View Temperature Profile at 0.75 Pore Volumes Injected 320

A.38 Run 45: Top View Temperature Profile at 1.00 Pore Volumes Injected 321

A.39 Run 45: Top View Temperature Profile at 1.25 Pore Volumes Injected 322

A.40 Run 45: Top View Temperature Profile at 1.50 Pore Volumes Injected 323

A.41 Run 45: Top View Temperature Profile at 1.75 Pore Volumes Injected 324

A.42 Run 45: Top View Temperature Profile at 2.00 Pore Volumes Injected 325

A.43 Run 45: Cross-Sectional Temperature Profile at 0.25 Pore Volumes Injected 326

A.44 Run 45: Cross-Sectional Temperature Profile at 0.50 Pore Volumes Injected 327

A.45 Run 45: Cross-Sectional Temperature Profile at 0.75 Pore Volumes Injected 328

A.46 Run 45: Cross-Sectional Temperature Profile at 1.00 Pore Volumes Injected 329

A.47 Run 46: Top View Temperature Profile at 0.25 Pore Volumes Injected 330

A.48 Run 46: Top View Temperature Profile at 0.50 Pore Volumes Injected 331

A.49 Run 46: Top View Temperature Profile at 0.75 Pore Volumes Injected 332

A.50 Run 46: Top View Temperature Profile at 1.00 Pore Volumes Injected 333

A.51 Run 46: Top View Temperature Profile at 1.25 Pore Volumes Injected 334

A.52 Run 46: Top View Temperature Profile at 1.50 Pore Volumes Injected 335

A.53 Run 46: Top View Temperature Profile at 1.75 Pore Volumes Injected 336

A.54 Run 46: Top View Temperature Profile at 2.00 Pore Volumes Injected 337

A.55 Run 46: Cross-Sectional Temperature Profile at 0.25 Pore Volumes Injected 338

A.56 Run 46: Cross-Sectional Temperature Profile at 0.50 Pore Volumes Injected 339

A.57 Run 46: Cross-Sectional Temperature Profile at 0.75 Pore Volumes Injected 340

A.58 Run 46 : Cross-Sectional Temperature Profile at 1.00 Pore Volumes Injected 341

A.59 Run 60: Top View Temperature Profile at 0.25 Pore Volumes Injected 342

A.60 Run 60: Top View Temperature Profile at 0.50 Pore Volumes Injected 343

A.61 Run 60: Top View Temperature Profile at 0.75 Pore Volumes Injected 344

A.62 Run 60: Top View Temperature Profile at 1.00 Pore Volumes Injected 345

A.63 Run 60: Top View Temperature Profile at 1.25 Pore Volumes Injected 346

A.64 Run 60: Top View Temperature Profile at 1.50 Pore Volumes Injected 347

A.65 Run 60: Top View Temperature Profile at 1.75 Pore Volumes Injected 348

A.66 Run 60: Top View Temperature Profile at 2.00 Pore Volumes Injected 349

A.67 Run 60: Cross-Sectional Temperature Profile at 0.25 Pore Volumes Injected 350

A.68 Run 60: Cross-Sectional Temperature Profile at 0.50 Pore Volumes Injected 351

A.69 Run 60: Cross-Sectional Temperature Profile at 0.75 Pore Volumes Injected 352

A.70 Run 60: Cross-Sectional Temperature Profile at 1.00 Pore Volumes Injected 353

A.71 Run 61: Top View Temperature Profile at 0.25 Pore Volumes Injected 354

A.72 Run 61: Top View Temperature Profile at 0.50 Pore Volumes Injected 355

A.73 Run 61: Top View Temperature Profile at 0.75 Pore Volumes Injected 356

A.74 Run 61: Top View Temperature Profile at 1.00 Pore Volumes Injected 357

A.75 Run 61: Top View Temperature Profile at 1.25 Pore Volumes Injected 358

A.76 Run 61: Top View Temperature Profile at 1.50 Pore Volumes Injected 359

A.77 Run 61: Top View Temperature Profile at 1.75 Pore Volumes Injected 360

A.78 Run 61: Top View Temperature Profile at 2.00 Pore Volumes Injected 361

A.79 Run 61: Cross-Sectional Temperature Profile at 0.25 Pore Volumes Injected 362

A.80 Run 61: Cross-Sectional Temperature Profile at 0.50 Pore Volumes Injected 363

A.81 Run 61: Cross-Sectional Temperature Profile at 0.75 Pore Volumes Injected 364

A.82 Run 61: Cross-Sectional Temperature Profile at 1.00 Pore Volumes Injected 365

A.83 Run 65: Top View Temperature Profile at 0.25 Pore Volumes Injected 366

A.84 Run 65: Top View Temperature Profile at 0.50 Pore Volumes Injected 367

A.85 Run 65: Top View Temperature Profile at 0.75 Pore Volumes Injected ____ 368

A.86 Run 65: Top View Temperature Profile at 1.00 Pore Volumes Injected ____ 369

A.87 Run 65: Top View Temperature Profile at 1.25 Pore Volumes Injected ____ 370

A.88 Run 65: Top View Temperature Profile at 1.50 Pore Volumes Injected ____ 371

A.89 Run 65: Top View Temperature Profile at 1.75 Pore Volumes Injected ____ 372

A.90 Run 65: Top View Temperature Profile at 2.00 Pore Volumes Injected ____ 373

A.91 Run 65: Cross-Sectional Temperature Profile at 0.25 Pore Volumes Injected ____ 374

A.92 Run 65: Cross-Sectional Temperature Profile at 0.50 Pore Volumes Injected ____ 375

A.93 Run 65: Cross-Sectional Temperature Profile at 0.75 Pore Volumes Injected ____ 376

A.94 Run 65: Cross-Sectional Temperature Profile at 1.00 Pore Volumes Injected ____ 377

A.95 Run 66: Top View Temperature Profile at 0.25 Pore Volumes Injected ____ 378

A.96 Run 66: Top View Temperature Profile at 0.50 Pore Volumes Injected ____ 379

A.97 Run 66: Top View Temperature Profile at 0.75 Pore Volumes Injected ____ 380

A.98 Run 66: Top View Temperature Profile at 1.00 Pore Volumes Injected ____ 381

A.99 Run 66: Top View Temperature Profile at 1.25 Pore Volumes Injected ____ 382

A.100 Run 66: Top View Temperature Profile at 1.50 Pore Volumes Injected ____ 383

A.101 Run 66: Top View Temperature Profile at 1.75 Pore Volumes Injected ____ 384

A.102 Run 66: Top View Temperature Profile at 2.00 Pore Volumes Injected ____ 385

A.103 Run 66: Cross-Sectional Temperature Profile at 0.25 Pore Volumes Injected 386

A.104 Run 66: Cross-Sectional Temperature Profile at 0.50 Pore Volumes Injected 387

A.105 Run 66: Cross-Sectional Temperature Profile at 0.75 Pore Volumes Injected 388

A.106 Run 66: Cross-Sectional Temperature Profile at 1.00 Pore Volumes Injected 389

A.107 Run 67: Top View Temperature Profile at 0.25 Pore Volumes Injected 390

A.108 Run 67: Top View Temperature Profile at 0.50 Pore Volumes Injected 391

A.109 Run 67: Top View Temperature Profile at 0.75 Pore Volumes Injected 392

A.110 Run 67: Top View Temperature Profile at 1.00 Pore Volumes Injected 393

A.111 Run 67: Top View Temperature Profile at 1.25 Pore Volumes Injected 394

A.112 Run 67: Top View Temperature Profile at 1.50 Pore Volumes Injected 395

A.113 Run 67: Top View Temperature Profile at 1.75 Pore Volumes Injected 396

A.114 Run 67: Top View Temperature Profile at 2.00 Pore Volumes Injected 397

A.115 Run 67: Cross-Sectional Temperature Profile at 0.25 Pore Volumes Injected 398

A.116 Run 67: Cross-Sectional Temperature Profile at 0.50 Pore Volumes Injected 399

A.117 Run 67: Cross-Sectional Temperature Profile at 0.75 Pore Volumes Injected 400

A.118 Run 67: Cross-Sectional Temperature Profile at 1.00 Pore Volumes Injected 401

A.119 Run 49: Top View Temperature Profile at 0.25 Pore Volumes Injected 402

A.120 Run 49: Top View Temperature Profile at 0.50 Pore Volumes Injected 403

A.121 Run 49: Top View Temperature Profile at 0.75 Pore Volumes Injected 404

A.122 Run 49: Top View Temperature Profile at 1.00 Pore Volumes Injected 405

A.123 Run 49: Top View Temperature Profile at 1.25 Pore Volumes Injected 406

A.124 Run 49: Top View Temperature Profile at 1.50 Pore Volumes Injected 407

A.125 Run 49: Top View Temperature Profile at 1.75 Pore Volumes Injected 408

A.126 Run 49: Top View Temperature Profile at 2.00 Pore Volumes Injected 409

A.127 Run 49: Cross-Sectional Temperature Profile at 0.25 Pore Volumes Injected 410

A.128 Run 49: Cross-Sectional Temperature Profile at 0.50 Pore Volumes Injected 411

A.129 Run 49: Cross-Sectional Temperature Profile at 0.75 Pore Volumes Injected 412

A.130 Run 49: Cross-Sectional Temperature Profile at 1.00 Pore Volumes Injected 413

A.131 Run 50: Top View Temperature Profile at 0.25 Pore Volumes Injected 414

A.132 Run 50: Top View Temperature Profile at 0.50 Pore Volumes Injected 415

A.133 Run 50: Top View Temperature Profile at 0.75 Pore Volumes Injected 416

A.134 Run 50: Top View Temperature Profile at 1.00 Pore Volumes Injected 417

A.135 Run 50: Top View Temperature Profile at 1.25 Pore Volumes Injected 418

A.136 Run 50: Top View Temperature Profile at 1.50 Pore Volumes Injected 419

A.137 Run 50: Top View Temperature Profile at 1.75 Pore Volumes Injected 420

A.138 Run 50: Top View Temperature Profile at 2.00 Pore Volumes Injected 421

A.139 Run 50: Cross-Sectional Temperature Profile at 0.25 Pore Volumes Injected ____ 422

A.140 Run 50: Cross-Sectional Temperature Profile at 0.50 Pore Volumes Injected ____ 423

A.141 Run 50: Cross-Sectional Temperature Profile at 0.75 Pore Volumes Injected ____ 424

A.142 Run 50: Cross-Sectional Temperature Profile at 1.00 Pore Volumes Injected ____ 425

A.143 Run 51: Top View Temperature Profile at 0.25 Pore Volumes Injected ____ 426

A.144 Run 51: Top View Temperature Profile at 0.50 Pore Volumes Injected ____ 427

A.145 Run 51: Top View Temperature Profile at 0.75 Pore Volumes Injected ____ 428

A.146 Run 51: Top View Temperature Profile at 1.00 Pore Volumes Injected ____ 429

A.147 Run 51: Top View Temperature Profile at 1.25 Pore Volumes Injected ____ 430

A.148 Run 51: Top View Temperature Profile at 1.50 Pore Volumes Injected ____ 431

A.149 Run 51: Top View Temperature Profile at 1.75 Pore Volumes Injected ____ 432

A.150 Run 51: Top View Temperature Profile at 2.00 Pore Volumes Injected ____ 433

A.151 Run 51: Cross-Sectional Temperature Profile at 0.25 Pore Volumes Injected ____ 434

A.152 Run 51: Cross-Sectional Temperature Profile at 0.50 Pore Volumes Injected ____ 435

A.153 Run 51: Cross-Sectional Temperature Profile at 0.75 Pore Volumes Injected ____ 436

A.154 Run 51: Cross-Sectional Temperature Profile at 1.00 Pore Volumes Injected ____ 437

A.155 Run 53: Top View Temperature Profile at 0.25 Pore Volumes Injected ____ 438

A.156 Run 53: Top View Temperature Profile at 0.50 Pore Volumes Injected ____ 439

A.157 Run 53: Top View Temperature Profile at 0.75 Pore Volumes Injected 440

A.158 Run 53: Top View Temperature Profile at 1.00 Pore Volumes Injected 441

A.159 Run 53: Top View Temperature Profile at 1.25 Pore Volumes Injected 442

A.160 Run 53: Top View Temperature Profile at 1.50 Pore Volumes Injected 443

A.161 Run 53: Top View Temperature Profile at 1.75 Pore Volumes Injected 444

A.162 Run 53: Top View Temperature Profile at 2.00 Pore Volumes Injected 445

A.163 Run 53: Cross-Sectional Temperature Profile at 0.25 Pore Volumes Injected 446

A.164 Run 53: Cross-Sectional Temperature Profile at 0.50 Pore Volumes Injected 447

A.165 Run 53: Cross-Sectional Temperature Profile at 0.75 Pore Volumes Injected 448

A.166 Run 53: Cross-Sectional Temperature Profile at 1.00 Pore Volumes Injected 449

A.167 Run 54: Top View Temperature Profile at 0.25 Pore Volumes Injected 450

A.168 Run 54: Top View Temperature Profile at 0.50 Pore Volumes Injected 451

A.169 Run 54: Top View Temperature Profile at 0.75 Pore Volumes Injected 452

A.170 Run 54: Top View Temperature Profile at 1.00 Pore Volumes Injected 453

A.171 Run 54: Top View Temperature Profile at 1.25 Pore Volumes Injected 454

A.172 Run 54: Top View Temperature Profile at 1.50 Pore Volumes Injected 455

A.173 Run 54: Top View Temperature Profile at 1.75 Pore Volumes Injected 456

A.174 Run 54: Top View Temperature Profile at 2.00 Pore Volumes Injected 457

A.175 Run 54: Cross-Sectional Temperature Profile at 0.25 Pore Volumes Injected 458

A.176 Run 54: Cross-Sectional Temperature Profile at 0.50 Pore Volumes Injected 459

A.177 Run 54: Cross-Sectional Temperature Profile at 0.75 Pore Volumes Injected 460

A.178 Run 54: Cross-Sectional Temperature Profile at 1.00 Pore Volumes Injected 461

A.179 Run 55: Top View Temperature Profile at 0.25 Pore Volumes Injected 462

A.180 Run 55: Top View Temperature Profile at 0.50 Pore Volumes Injected 463

A.181 Run 55: Top View Temperature Profile at 0.75 Pore Volumes Injected 464

A.182 Run 55: Top View Temperature Profile at 1.00 Pore Volumes Injected 465

A.183 Run 55: Top View Temperature Profile at 1.25 Pore Volumes Injected 466

A.184 Run 55: Top View Temperature Profile at 1.50 Pore Volumes Injected 467

A.185 Run 55: Top View Temperature Profile at 1.75 Pore Volumes Injected 468

A.186 Run 55: Top View Temperature Profile at 2.00 Pore Volumes Injected 469

A.187 Run 55: Cross-Sectional Temperature Profile at 0.25 Pore Volumes Injected 470

A.188 Run 55: Cross-Sectional Temperature Profile at 0.50 Pore Volumes Injected 471

A.189 Run 55: Cross-Sectional Temperature Profile at 0.75 Pore Volumes Injected 472

A.190 Run 55: Cross-Sectional Temperature Profile at 1.00 Pore Volumes Injected 473

A.191 Run 56: Top View Temperature Profile at 0.25 Pore Volumes Injected 474

A.192 Run 56: Top View Temperature Profile at 0.50 Pore Volumes Injected 475

A.193 Run 56: Top View Temperature Profile at 0.75 Pore Volumes Injected 476

A.194 Run 56: Top View Temperature Profile at 1.00 Pore Volumes Injected 477

A.195 Run 56: Top View Temperature Profile at 1.25 Pore Volumes Injected 478

A.196 Run 56: Top View Temperature Profile at 1.50 Pore Volumes Injected 479

A.197 Run 56: Top View Temperature Profile at 1.75 Pore Volumes Injected 480

A.198 Run 56: Top View Temperature Profile at 2.00 Pore Volumes Injected 481

A.199 Run 56: Cross-Sectional Temperature Profile at 0.25 Pore Volumes Injected 482

A.200 Run 56: Cross-Sectional Temperature Profile at 0.50 Pore Volumes Injected 483

A.201 Run 56: Cross-Sectional Temperature Profile at 0.75 Pore Volumes Injected 484

A.202 Run 56: Cross-Sectional Temperature Profile at 1.00 Pore Volumes Injected 485

A.203 Run 58: Top View Temperature Profile at 0.25 Pore Volumes Injected 486

A.204 Run 58: Top View Temperature Profile at 0.50 Pore Volumes Injected 487

A.205 Run 58: Top View Temperature Profile at 0.75 Pore Volumes Injected 488

A.206 Run 58: Top View Temperature Profile at 1.00 Pore Volumes Injected 489

A.207 Run 58: Top View Temperature Profile at 1.25 Pore Volumes Injected 490

A.208 Run 58: Top View Temperature Profile at 1.50 Pore Volumes Injected 491

A.209 Run 58: Top View Temperature Profile at 1.75 Pore Volumes Injected 492

A.210 Run 58: Top View Temperature Profile at 2.00 Pore Volumes Injected 493

A.211 Run 58: Cross-Sectional Temperature Profile at 0.25 Pore Volumes Injected 494

A.212 Run 58: Cross-Sectional Temperature Profile at 0.50 Pore Volumes Injected 495

A.213 Run 58: Cross-Sectional Temperature Profile at 0.75 Pore Volumes Injected 496

A.214 Run 58: Cross-Sectional Temperature Profile at 1.00 Pore Volumes Injected 497

A.215 Run 59: Top View Temperature Profile at 0.25 Pore Volumes Injected 498

A.216 Run 59: Top View Temperature Profile at 0.50 Pore Volumes Injected 499

A.217 Run 59: Top View Temperature Profile at 0.75 Pore Volumes Injected 500

A.218 Run 59: Top View Temperature Profile at 1.00 Pore Volumes Injected 501

A.219 Run 59: Top View Temperature Profile at 1.25 Pore Volumes Injected 502

A.220 Run 59: Top View Temperature Profile at 1.50 Pore Volumes Injected 503

A.221 Run 59: Top View Temperature Profile at 1.75 Pore Volumes Injected 504

A.222 Run 59: Top View Temperature Profile at 2.00 Pore Volumes Injected 505

A.223 Run 59: Cross-Sectional Temperature Profile at 0.25 Pore Volumes Injected 506

A.224 Run 59: Cross-Sectional Temperature Profile at 0.50 Pore Volumes Injected 507

A.225 Run 59: Cross-Sectional Temperature Profile at 0.75 Pore Volumes Injected 508

A.226 Run 59: Cross-Sectional Temperature Profile at 1.00 Pore Volumes Injected 509

A.227 Run 62: Top View Temperature Profile at 0.25 Pore Volumes Injected 510

A.228 Run 62: Top View Temperature Profile at 0.50 Pore Volumes Injected 511

A.229 Run 62: Top View Temperature Profile at 0.75 Pore Volumes Injected 512

A.230 Run 62: Top View Temperature Profile at 1.00 Pore Volumes Injected 513

A.231 Run 62: Top View Temperature Profile at 1.25 Pore Volumes Injected 514

A.232 Run 62: Top View Temperature Profile at 1.50 Pore Volumes Injected 515

A.233 Run 62: Top View Temperature Profile at 1.75 Pore Volumes Injected 516

A.234 Run 62: Top View Temperature Profile at 2.00 Pore Volumes Injected 517

A.235 Run 62: Cross-Sectional Temperature Profile at 0.25 Pore Volumes Injected 518

A.236 Run 62: Cross-Sectional Temperature Profile at 0.50 Pore Volumes Injected 519

A.237 Run 62: Cross-Sectional Temperature Profile at 0.75 Pore Volumes Injected 520

A.238 Run 62: Cross-Sectional Temperature Profile at 1.00 Pore Volumes Injected 521

A.239 Run 63: Top View Temperature Profile at 0.25 Pore Volumes Injected 522

A.240 Run 63: Top View Temperature Profile at 0.50 Pore Volumes Injected 523

A.241 Run 63: Top View Temperature Profile at 0.75 Pore Volumes Injected 524

A.242 Run 63: Top View Temperature Profile at 1.00 Pore Volumes Injected 525

A.243 Run 63: Top View Temperature Profile at 1.25 Pore Volumes Injected 526

A.244 Run 63: Top View Temperature Profile at 1.50 Pore Volumes Injected 527

A.245 Run 63: Top View Temperature Profile at 1.75 Pore Volumes Injected 528

A.246 Run 63: Top View Temperature Profile at 2.00 Pore Volumes Injected 529

A.247 Run 63: Cross-Sectional Temperature Profile at 0.25 Pore Volumes Injected 530

A.248 Run 63: Cross-Sectional Temperature Profile at 0.50 Pore Volumes Injected 531

A.249 Run 63: Cross-Sectional Temperature Profile at 0.75 Pore Volumes Injected 532

A.250 Run 63: Cross-Sectional Temperature Profile at 1.00 Pore Volumes Injected 533

A.251 Run 64: Top View Temperature Profile at 0.25 Pore Volumes Injected 534

A.252 Run 64: Top View Temperature Profile at 0.50 Pore Volumes Injected 535

A.253 Run 64: Top View Temperature Profile at 0.75 Pore Volumes Injected 536

A.254 Run 64: Top View Temperature Profile at 1.00 Pore Volumes Injected 537

A.255 Run 64: Top View Temperature Profile at 1.25 Pore Volumes Injected 538

A.256 Run 64: Top View Temperature Profile at 1.50 Pore Volumes Injected 539

A.257 Run 64: Top View Temperature Profile at 1.75 Pore Volumes Injected 540

A.258 Run 64: Top View Temperature Profile at 2.00 Pore Volumes Injected 541

A.259 Run 64: Cross-Sectional Temperature Profile at 0.25 Pore Volumes Injected 542

A.260 Run 64: Cross-Sectional Temperature Profile at 0.50 Pore Volumes Injected 543

A.261 Run 64: Cross-Sectional Temperature Profile at 0.75 Pore Volumes Injected 544

A.262 Run 64: Cross-Sectional Temperature Profile at 1.00 Pore Volumes Injected 545

A.263 Run 47: Top View Temperature Profile at 0.25 Pore Volumes Injected 546

A.264 Run 47: Top View Temperature Profile at 0.50 Pore Volumes Injected 547

A.265 Run 47: Top View Temperature Profile at 0.75 Pore Volumes Injected 548

A.266 Run 47: Top View Temperature Profile at 1.00 Pore Volumes Injected 549

A.267 Run 47: Top View Temperature Profile at 1.50 Pore Volumes Injected 550

A.268 Run 47: Top View Temperature Profile at 2.00 Pore Volumes Injected 551

A.269 Run 47: Top View Temperature Profile at 2.50 Pore Volumes Injected 552

A.270 Run 47: Top View Temperature Profile at 3.00 Pore Volumes Injected 553

A.271 Run 47: Cross-Sectional Temperature Profile at 2.00 Pore Volumes Injected 554

A.272 Run 47: Cross-Sectional Temperature Profile at 2.50 Pore Volumes Injected 555

A.273 Run 47: Cross-Sectional Temperature Profile at 3.00 Pore Volumes Injected 556

A.274 Run 48: Top View Temperature Profile at 0.25 Pore Volumes Injected 557

A.275 Run 48: Top View Temperature Profile at 0.50 Pore Volumes Injected 558

A.276 Run 48: Top View Temperature Profile at 1.00 Pore Volumes Injected 559

A.277 Run 48: Top View Temperature Profile at 1.50 Pore Volumes Injected 560

A.278 Run 48: Top View Temperature Profile at 2.00 Pore Volumes Injected 561

A.279 Run 48: Top View Temperature Profile at 2.50 Pore Volumes Injected 562

A.280 Run 48: Top View Temperature Profile at 3.00 Pore Volumes Injected 563

A.281 Run 48: Top View Temperature Profile at 3.50 Pore Volumes Injected 564

A.282 Run 48: Top View Temperature Profile at 2.00 Pore Volumes Injected 565

A.283 Run 48: Cross-Sectional Temperature Profile at 2.50 Pore Volumes Injected 566

A.284 Run 40: Cross-Sectional Temperature Profile at 3.00 Pore Volumes Injected 567

A.285 Run 40: Cross-Sectional Temperature Profile at 3.50 Pore Volumes Injected 568

A.286 Run 26: Top View Temperature Profile at 0.25 Pore Volumes Injected 569

A.287 Run 26: Top View Temperature Profile at 0.50 Pore Volumes Injected 570

A.288 Run 26: Top View Temperature Profile at 0.75 Pore Volumes Injected 571

A.289 Run 26: Top View Temperature Profile at 1.00 Pore Volumes Injected 572

A.290 Run 26: Top View Temperature Profile at 1.25 Pore Volumes Injected 573

A.291 Run 26: Top View Temperature Profile at 1.50 Pore Volumes Injected 574

A.292 Run 26: Top View Temperature Profile at 1.75 Pore Volumes Injected 575

List of Plates

Plates Page

5.1 Overall View of Low Pressure Apparatus ____ 45

5.2 Close-up of Model Situated on Cart Between the Granite Blocks ____ 48

Nomenclature

C - Specific heat. (kJ/kg· ^{0}C)

f_s - Steam quality. (Dimensionless)

g - Acceleration due to gravity. (m/s^2)

k - Enthalpy per unit mass. (kJ/kg)

k - Permeability. (darcies)

k_h - Thermal conductivity. (kW/m· ^{0}C)

k_r - Relative permeability. (Dimensionless)

L - Length or Distance.

L_v - Latent heat of vaporization. (kJ/kg)

p - Pressure. (MPa or kPa)

$\dot{Q}_{loss}$ - Heat loss rate. (kJ/kg)

$\vec{q}$ - Conductive heat flux. (kW/m)

S - Saturation. (Dimensionless)

T - Temperature. (^{0}C)

t - Time. (Prototype (days) & Model (minutes))

$\vec{u}$ - Volumetric flux (Darcy velocity). (m/s)

w - Mass rate of flow. (cm^3 /min.)

$\gamma(m)$ - Function equal to ratio of values of its argument (m) in the prototype to that in the model. (Dimensionless)

μ - Viscosity. (mPa· s)

ϕ - Porosity. (Dimensionless)

ρ - Density. (kg/m^3)

Subscripts

a - aqueous phase for quality control

c - Cap or base rock

HVN -Heavy Virgin Naphtha

i - Initial condition

M - Model

o - oil

ors - Residual oil saturation to steam

P - Prototype

p - Production

R - Reference quantity used to obtain dimensionless number.

s - steam

sat - Saturation pressure or temperature

sc - Calculated steam temperature

ss - superheated steam

t - Total interval

w - water

wc -Connate Water

Chapter I

Introduction

At the present time steam injection processes account for the recovery of over one million barrels of heavy oil each day. The two major types of steam injection techniques are cyclic steam stimulation and steamflooding. To-date, cyclic steaming is the only proven commercial heavy oil recovery scheme to be successful in recovering heavy oil from the Cold Lake oil sands formations. Steamflooding has been quite suitable for some California heavy oil reservoirs such as San Ardo, Kern River and Midway Sunset fields. Recently the steamflood process has been implemented in some Saskatchewan fields such as the Aberfeldy.

Many heavy oil reservoirs in Alberta and Saskatchewan contain a characteristic bottom water layer which creates a serious field problem when a steamflood process is implemented. The presence of the underlying water zone causes a large amount of the injected steam to be diverted away from the target oil zone and into the bottom water layer. This results in the steamflood process having a low thermal efficiency and therefore the steamflood is uneconomical in these types of reservoirs.

The main focus of this research was to incorporate solvent injection with a steamflood process in an attempt to improve oil recovery from thin heavy oil formations with underlying water zones. The purpose of the solvent slug injection prior to steamflooding was to create highly conductive flow channels into the oil zone for the steam to penetrate. It was thought that the solvent channels formed in the oil region would aid in partially diverting the steam away from the detrimental bottom water zone, resulting in a greater volume of oil being heated, mobilized and consequently produced. The objective of the solvent-steamflood method was to guide the steam into the upper portion (oil layer) of the bottom water formation and keep the steam there as long as possible.

Other recovery schemes were investigated which also attempted to divert the steam away from the underlying water and into the oil region. The alternate methods considered were gas injection prior to a steamflood or solvent-steamflood and prior to steamflooding a limited barrier was formed at the oil/water contact of the formation which extended radially outward from the injection well.

Statement of the Problem

Prior to conducting any of the experiments, various modifications were carried out on the low pressure, scaled steamflood model which represents one-quarter of an eight hectare five spot pattern in the Aberfeldy reservoir, located in Saskatchewan. The modifications performed were as follows:

i. Incorporate a solvent injection system into the low pressure apparatus which consists of a controlled volume, Milroyal pump, a solvent storage bottle, and injection tubing from the Milroyal pump to the model.

ii. Set up a gas injection system which consists of a low pressure regulator, a nitrogen gas cylinder and an injection line to the model. The gas injection system was used to create a gas cap in the model in order to study its effect on different oil recovery strategies.

iii. Design a procedure which will allow the formation of various thicknesses of bottom water in the model.

iv. Modify various parts of the apparatus such as the walk-in, cold storage compartment and the rack and pinion system situated on the model cart to allow for easier operation of the apparatus during the experiments.

The major objectives of the research investigation were as follows:

1. To conduct a series of base experiments, which could be used to compare with the various types of solvent-steamflood experiments in order to determine the effectiveness of the solvent-steamflood recovery process.
    i. Continuous solvent flood to observe the injection behaviour of the solvent (Heavy Virgin Naphtha) in a homogeneous model.

  - ii. Solvent-steamflood in a homogeneous model in order to compare to a solvent-steamflood carried out in a bottom water model.
  - iii. Gas injection prior to a steamflood in a bottom water model in order to compare to experiments involving gas injection before the implementation of a solvent-steamflood of a bottom water model.

2. To perform a series of different solvent-steamfloods and compare the results with the corresponding base experiments, as follows:
  - i. Solvent-steamflood in a bottom water model in order to study the effects of solvent injection and bottom water thicknesses on the overall oil recovery.
  - ii. Compare a solvent-steamflood of a bottom water model to a base run using gas injection prior to the steamflood of a bottom water model.
  - iii. Gas injection prior to a solvent-steamflood of a bottom water model and compare to a solvent-steamflood of a bottom water model.

3. To perform experiments for analyzing the effect of various parameters on the overall oil recovery, as well as runs to study an alternative recovery technique, viz.:
  - i. Examine the effect of bottom water thickness on oil recovery and effectiveness of a recovery process.
  - ii. Analyze the effect of the solvent slug size on oil recovery.
  - iii. Study the effect of the injection and production interval locations on the efficiency of oil recovery.
  - iv. Compare an alternative recovery method to the solvent-steamflood technique such as forming a partial barrier between the bottom water and the oil zone in order to prevent the steam from channelling into the bottom water region of the reservoir.
  - v. Waterflood prior to a solvent-steamflood in a homogeneous model

4. Investigate the various heat flow and heat transfer mechanisms existing in the homogeneous, low pressure model during a straight steamflood experiment, as follows:

   i. Use Lauwerier, Marx-Langenheim and Mandl-Volek methods to determine heat flow characteristics of the model and provide steam zone volume estimates throughout the steamflood and compare the results.

   ii. Perform a heat balance on the model during the steamflood in order to predict heat losses from the model during the experiment.

Chapter III

Literature Review

This chapter provides a review of literature describing past scaled model studies which were used for investigating steam injection techniques, miscible (solvent) displacements and recovery processes combining solvent with steam into one process in an attempt to improve the overall oil recovery.

The first half of the review is a discussion of some of the important high and low pressure model investigations as well as studies which involved deriving the scaling criteria used to design the models. The section also reviews studies which investigated oil recovery by steam injection into oil reservoirs containing bottom water.

The last half of the literature survey deals with miscible displacement research and studies involving the incorporation of miscible (solvent) displacement with a steam injection process. Important mechanisms of miscible displacement (dispersion and diffusion) and some non-thermal miscible displacement studies are described. Also included are research studies which attempted to develop scaling criteria which would adequately represent a process combining solvent and steam injection. Experiments which examined the implementation of solvent injection with thermal recovery techniques such as hot waterflooding and steam injection are discussed, and research investigations involving asphaltene flocculation, often caused by solvents, are reported.

Scaled Model Studies of Steam Injection Processes

Several in-depth reviews detailing the current state of steamflood (or steam drive) technology have been presented in the literature [1,2]. Farouq Ali [3] gives a comprehensive description of the theories that have been proposed to explain the mechanics of steam advance in oil bearing strata.

Models for obtaining a good understanding of the physical processes involved in a steamflood operation have also been extensively employed as predictive tools designing the best recovery program for a particular reservoir. Most of these models were unscaled. Only in a few instances scaled models were used.

Experimental Approaches to Steam Injection

Various types of physical models have been used to examine many types of thermal recovery processes. Some models have been used to study various relevant operating parameters such as steam injection rate and pressure, steam quality, pattern size and type, and reservoir thickness. Other laboratory models have been used examine steam injection strategies in which recovery was from reservoirs with specific characteristics such as gas caps, high oil viscosity, bottom water, shale stringers, or a high waterflood residual oil saturation.

There are three basic types of physical models which can represent various types of prototype reservoirs; these are: unscaled, partially scaled and scaled.

Unscaled models, sometimes called "elemental models", involve neglecting scaling criteria completely and focussing on a certain aspect of the process in order to try to obtain the qualitative nature of a particular recovery mechanism such as steam distillation. The experimental conditions and materials for a unscaled model are chosen to represent an element of the prototype reservoir under investigation. Even though the unscaled model does not provide a quantitative analysis, unscaled experiments can yield critical information about the specific processes being investigated. Unscaled models are used to obtain a better understanding of the fluid-rock interactions occurring in the reservoir at various conditions .

Willman, Valleroy, Runberg, Cornelius and Powers [4] were the first investigators to carry out unscaled laboratory studies on steam injection. Their research produced valuable data on the various mechanisms that exist during a steamflooding operation. Linear cores saturated with refined oils and crudes, which had different viscosities and steam distillation properties, were used in the experiments. Results of the study produced steam injection oil recoveries one hundred percent better than previously recorded waterflood oil recoveries. Thermal expansion of the oil, viscosity reduction, and steam distillation were the specific mechanisms responsible for the improved recovery by steam injection. Marx and Langenheim [5] presented the first equations to predict the performance of a steamflood.

Baker [6] investigated heat flow during steam injection and found that heat losses from the reservoir were a function of time, reservoir thickness and thermal diffusivity. He also concluded that gravity override during steam injection was a common phenomenon. Oil was not used in these experiments.

Flock and Lee [7] examined the use of steam injection to displace a medium gravity crude from an unconsolidated sand pack. Results of this investigation were similar to those obtained by Baker [6]. Flock and Lee [7] concluded that steam injection into a medium gravity crude oil formation, that had previously been waterflooded, could be a viable tertiary recovery technique.

Scaled and partially scaled model studies have been performed to determine the effect of changes in various operational parameters such as completion intervals, flood pattern and size, steam quality, steam additives, slug size, injection rate, production pressure and reservoir heterogeneities.

An extensive review of the methods used in scaling steam injection processes was given by Farouq Ali and Redford [8] in which they used the Principle of Similarity as the basis of design for a scaled physical model. The Principle of Similarity is based on equivalence of ratios of forces, velocities, dimensions, temperature differences, and concentration differences which exist in the model and the prototype reservoir.

High Pressure and Low Pressure Scaled Models

When performing scaled model studies of thermal recovery processes, two types of scaling methods can be utilized. One can design either a high pressure model or a low pressure model, where each type has its advantages and disadvantages.

Often high pressure models use the same fluids as the prototype and therefore are thought to provide an improved scaling of the rock-fluid interactions such as permeability, relative permeability, and capillary pressure alterations. The low pressure model according to Stegemeier, Laumbach and Volek [9] better conforms to the Clausius-Clapeyron relation due to the subatmospheric pressures and low temperatures that can be achieved with a vacuum model. The improved matching of the Clausius-Clapeyron relationship results in improved modeling of the temperature distribution in the prototype. The temperature distribution can be related to the viscosity distribution, internal energy distribution, and the steam zone pressure gradient, which are all significant features of a thermal recovery process. In practical terms, the vacuum model is more economical, safer and can turn out results much faster than a high pressure model.

Compressibility cannot be accounted for by either one of the models. Kimber, Puttagunta and Farouq Ali [10] noted that reservoir fluids and porous media could only be used in a high pressure model if the geometric similarity could be distorted in the vertical dimension, which would affect other scaling parameters.

Prats [11] stated that relative permeability could not be incorporated into the scaling of a vacuum model. This was also found to be true for a high pressure model, but to a lesser degree, especially if the model scaling parameters permit the use of the reservoir rock and fluids.

The use of both high and low pressure scaled models provides a valuable insight into the various mechanisms that exist during the steamflood process.

Geertsma, Croes and Schwarz [12] were the first to develop a set of dimensionless groups for scaling a displacement process in which hot water was injected in order to increase the recovery in viscous crude reservoirs. They also derived scaling groups for a solvent injection process and a conventional water drive. Loomis and Crowell [13], Leverett, Lewis and True [14], Rapoport [15] and Perkins and Collins [16] have performed other scaled model studies using different scaling criteria related to waterfloods.

A set of high pressure scaling criteria involving multidimensional steam injection was developed by Pujol and Boberg [17]. These steam injection scaling criteria have served as a basis for other scaled model studies such as those performed by Pursley [18] and Ehrlich[19].

Pursley [18] incorporated the Pujol-Boberg scaling criteria to model reservoir conditions of a Cold Lake, Alberta, reservoir using a number of three-dimensional models. Among the purposes of the scaled model study it was intended to determine whether a gas cap or bottom water zone could be utilized during a steam injection process. Pursley [18] concluded that during a steam injection process the presence of bottom water aided oil recovery due to steam override, which caused a large region of the oil to be contacted. It was also proposed that a steam drive through a bottom water zone was possible if heating close to the base of the oil could be achieved and good vertical permeability existed. However, for thicker bottom water layers bottom water had a detrimental effect, and significantly reduced oil recovery. In other experiments, Pursley [18] found that the existence of a gas cap could help oil recovery if a thin bottom water layer was separated from the oil by an impermeable layer. Pursley [18] also performed experiments studying pattern size, steam bank size and additives to steam.

Experiments performed by Ehrlich [19] implemented a three-dimensional model which scaled a steam displacement in the Wabasca Grand Rapids 'A' sand. This model was developed according to the Pujol-Boberg scaling criteria. Ehrlich [19] found that areal sweep efficiency was high due to low effective steam mobilities and vertical sweep efficiency was low as a result of steam override.

Huygen and Lowry [20] carried out unscaled, high pressure model experiments studying steam injection in the presence of bottom water. The unscaled model used was a three-dimensional, high pressure model which considered only heat flow in the scaling calculations. Results showed that the bottom water counteracted the overriding tendency of steam. It was also concluded that bottom water can provide the much needed steam injectivity in immobile tar sands but it could also scavenge the steams heat from the oil, creating an inefficient recovery process in the case of a thicker bottom water region.

The first low pressure scaled model studies were performed by Stegemeier, Laumbach and Volek [9]. They noted that the low pressure model porous media had to be different from those in the prototype reservoir. The scaling criteria derived were used to develop the low pressure model used in this study.

The scaled experiments performed by Stegemeier et al. [9] were designed to provide operational assistance for numerous steamflood field operations implemented by the Shell Oil Company. Some of these operations included Tatums, Slocum, Peace River, Coalinga, Mt. Poso, Midway Sunset and Yorba Linda, fields.

Stegemeier et al. [9] reported vacuum model study results for both the Midway Sunset and Mt. Poso fields. Results of the Mt. Poso suggested that steam override would be a governing feature in the field. The Mt. Poso experiments enabled recommendations to be made which made Mt. Poso a successful steamflood. The Midway Sunset experiments were directed towards comparing steamflood and steam soak results. Harmsen[21] discussed the distinct advantages steamflooding had over cyclic steaming in specific situations.

Utilizing the scaling criteria developed by Stegemeier et al. [9], Prats [11] performed numerous vacuum model experiments studying the Peace River, Alberta, oil sand formation in which a bottom water layer is present. Various operational parameters such as injection rates, completion interval, steam quality, pressure levels and heat scavenging by water injection after steam injection were investigated.

Based on the scaling criteria developed by Stegemeier et al. [9], Doscher [22] designed a low pressure model. The scaling parameters were developed from similarities in an integral form, derived from a study by Yortsos [23] as opposed to the differential form used by Stegemeier et al. [9]. The model was utilized by Doscher and Huang [24] to examine the steam drive performance in a heavy oil field similar to Kern River. The effect of bottom water, injection rate, steam quality, reservoir permeability and oil viscosity were studied in this investigation. It was concluded from the study that an optimum steam injection rate existed, with the performance (cumulative oil recovered) falling off above and below this injection rate. Experiments carried out by Doscher and Ghassemi [25] used this vacuum model to study the effect crude oil viscosity has on the efficiency of a steam injection operation.

Proctor [26] constructed a three-dimensional, low pressure model of the Aberfeldy formation which is a thin, heavy oil reservoir. The design of the model was based on the scaling criteria derived by Stegemeier, Laumbach and Volek [9]. From the results of steam injection experiments performed in the model Proctor [26] concluded that the presence of bottom water in the reservoir had an extremely detrimental effect on the thermal efficiency of a steam injection process.

Studies of Thin, Bottom Water Reservoirs

Several studies have investigated oil recovery by steam injection into oil reservoirs containing bottom water. However, none of these studies dealt with thin reservoirs containing relatively thick bottom water regions and/or a gas cap zone. For this study a "thin heavy oil reservoir" was considered to be a heavy oil formation with a thickness of less than about 20 meters (65 feet). The prototype reservoir studied in this research is the thin, Aberfeldy reservoir which does not have a gas cap and a bottom water layer only exists in parts of the field. However the versatility of the equipment used in this research allows one to create a bottom water layer and/or a gas cap in the model of the Aberfeldy reservoir.

Prats [11] modelled the Peace River reservoir which is characterized by a large oil saturation (45%) in the bottom water layer. In his experiments he injected steam into the bottom water and increased pressure in the reservoir in an attempt to heat up the bottom water zone. This procedure enabled the overlying, highly viscous oil zone (65% oil saturation) to be mobilized by the heating effects of the bottom water zone. Due to the relatively high oil saturation in the bottom water zone the initial injection of steam into this zone resulted in a significant amount of oil being produced which increased the economic attractiveness of the recovery process. To further improve oil recovery, steam was injected directly into the oil zone once the oil saturation in this region was reduced to a predetermined value. The Wabasca reservoir examined by Huygen and Lowry [20] and the Cold Lake reservoir studied by Pursley [18] were both characterized by a relatively thin bottom water layers. These investigations therefore do not provide a reasonable representation of Aberfeldy type thin reservoirs. Other than the study performed by Doscher and Ghassemi [25] there has been little work done on steamflooding thin oil reservoirs such as the Aberfeldy.

A variety of production mechanisms are called into play during thermal stimulation of bottom water reservoirs as pointed out by Kasraie and Farouq Ali [27]. A study of present field and laboratory information by the authors concluded that cyclic steaming becomes uneconomical when a water zone exists that is thicker than one-fifth of the oil zone thickness. As well the presence of a gas saturation may be effective in a steamflood of a thin reservoir with bottom water if vertical permeability is high, which will promote gravity flow of the steam. In such an instance, it may be possible to spread the injected steam over the entire formation and develop a downward steam drive. This would improve the thermal efficiency of the steamflood due to less of the injected heat being scavenged by the underlying bottom water layer. It was also pointed out that many heavy oil formations in Alberta and Saskatchewan have underlying water sands. A well-known steamflood, where both bottom water and a gas cap exist is the Smackover flood [27] in Arkansas, which is operated at below atmospheric pressure. It is possible that the presence of the gas cap counteracts the channelling of steam into the bottom water.

A subsequent study by Kasraie and Farouq Ali [28] further discussed the application of thermal recovery techniques to "marginal" heavy oil reservoirs. Such reservoirs are defined to have one or more of the following characteristics: thin formation (less than 6 metres), bottom water, gas cap or very high oil viscosity (over 10 Pa.s). Thermal recovery applications under such conditions depend strongly on the extent of bottom water, oil viscosity, vertical permeability, oil saturation and fluid injection rate. Vertical permeability was found to be an important factor in marginal reservoirs, which are characterized by bottom water, a gas cap, thin pay and extra-heavy oil. The vertical permeability is of considerable importance in these types of formations since even a limited barrier between the oil and water zones would drastically reduce the tendency of the steam to channel down into the water layer. Therefore any shale breaks, silt zones or other heterogeneities at the base of the oil sand would serve to improve the oil recovery performance. Also the implementation of high temperature polymers, foams or additives, such as solvents, may also help to divert the steam away from the bottom water.

Incorporation of Solvent with Steam Injection Processes

Dispersion and Diffusion of Solvents in a Porous Medium

A thorough review of diffusion and dispersion in porous media was presented by Perkins and Johnston [29]. Dispersion was defined as the mixing of solvent and oil in a porous medium caused by uneven fluid flow or concentration gradients resulting from fluid flow. It was also noted that dispersion could occur in the longitudinal direction (direction of gross fluid flow) or transversely (perpendicular to gross fluid flow direction). Diffusion was described as the mixing of two miscible fluids arising from the random motion of the molecules in each fluid.

Along with dispersion and diffusion, imbibition plays an important role in oil recovery during a solvent and/or steam injection process. Graham and Richardson [30] performed theoretical and experimental studies of water imbibition in which they stated that an understanding of the role of imbibition in implementing the recovery of oil is deemed essential to proper control of reservoirs to achieve maximum oil recovery. In the study, imbibition was defined as the spontaneous taking up of a liquid by a porous solid. The spontaneous process of imbibition occurs when the fluid-filled solid is immersed or brought in contact with another fluid which preferentially wets the solid. In the process of wetting and flowing into the solid, the imbibing fluid displaces the non-wetting resident fluid.

Non-Thermal Miscible Displacement Processes

A vast amount of literature exists on miscible displacement. In the following, only the papers relevant to the present research will be reviewed. As reported by Holm [31] miscible displacement of oil is defined as the displacement of crude oil from pore space in a rock using a solvent action that prevents the formation of interfaces between the driven and the driving fluids.

Stalkup [32] performed work studying oil displacement by solvent at high water saturations. He concluded that in a miscible displacement in the presence of a high water saturation, some of the oil is blocked by water so that it is bypassed by the solvent front and is therefore not recovered. For the case of a miscible displacement in the presence of a high water saturation the dominant mechanisms responsible for oil recovery are miscible flushing by solvent of the portion of the hydrocarbon pore volume that contains mobile oil and molecular diffusion of the region of the hydrocarbon pore volume that is stagnant. In general, the higher the water saturation, the greater the longitudinal dispersion and the more oil is bypassed by the injected solvent.

In miscible slug flooding, the formation of mixing zones occurs between the reservoir oil and the solvent bank as well as the solvent bank and the scavenging fluid. The dimensionally scaled model test results of Craig [33] have shown that there is a tendency for channelling to occur due to gravity segregation of the oil, solvent, and scavenging fluid, resulting in more bypassing of in-place oil. He showed that these effects are reduced when the process is carried out in a permeable, steeply dipping reservoir. It was also noted that in order to maintain miscibility in field miscible floods the solvent slug volume should range from two to ten percent of the total in-place hydrocarbon pore volume of the reservoir.

Due to the high costs of solvents, the amount of solvent to be injected is a critical factor in the success of a miscible displacement process. If the solvent slug used is larger than required, then the solvent cost will be increased without a compensating rise in the oil recovery, and if too small a slug is employed then a large portion of recoverable oil is left behind in the reservoir. This was the basis for a study conducted by Baker [34], which predicted solvent slug requirements in an idealized linear system where gravity, mobility ratio and areal sweep effects were unimportant, but longitudinal dispersion (mixing at the leading and trailing edges of the bank) and capacitance effects were significant. Capacitance is defined as the growth of a mixing zone caused by the trapping of oil and solvent in heterogeneities in the reservoir. The fluids were trapped by the shielding effects of the water films in the rock heterogeneities. From the study Baker [34] found that slug size was affected by several variables, including reservoir geometry, interwell spacing, gravity effects and mobility ratio. He also determined that slug degradation was caused by mixing (by dispersion) of the solvent with oil at the leading edge of the solvent bank and with the drive fluid at the trailing edge.

Similarly to numerous other investigators, Rodriguez [35] also found that at an unfavourable mobility ratio, viscous fingering is the controlling factor in a miscible displacement. Totonji [36], conducting miscible displacements in consolidated and unconsolidated sandpacks, found that the absolute viscosities of the liquids involved had little effect on the process if conducted at a constant unfavourable viscosity ratio.

Experimental results of a number of investigators [37,38,39] have shown that a gradual change from a more to a less viscous injected fluid can mitigate the detrimental effects of viscous fingering on areal sweep efficiency in reservoir displacement processes. Research performed by Claridge [40] indicated that it is unlikely that viscous fingering can be completely prevented during unstable miscible displacement in oil reservoirs but the use of a graded bank often may result in improvements in both overall oil recovery and/or economic viability.

The relative economic attractiveness of miscible slug floods depends upon both the cost of solvent and oil recovery performance expected of competing oil recovery techniques. To-date about forty percent of all miscible slug field projects operated under favourable conditions have yielded either good or encouraging oil recovery efficiencies. In recent years, considerable interest has been shown in the use of solvents as a means of recovering oil left in a reservoir at the end of secondary recovery operations.

Solvent Scaling Criteria

A non-rigorous set of criteria, which treated a steam plus additive process as a steam recovery process plus a miscible drive, was derived by Kennedy and Crawford [41]. The study concluded that scaling of the combined steam and solvent processes could not be achieved as the scaling requirements for the flow rate in the steam recovery process contradicted the scaling requirements for the flow rate in the miscible drive process. As well Pursley [18] attempted a partially scaled model investigation of the process in which solvent was simply added to his steamflood model.

Pozzi and Blackwell [42] studied the scaling of isothermal miscible displacements. They determined that under specific conditions, the requirements of geometric similarity and gravitational scaling can be relaxed to allow scaling of miscible displacement, whether transverse mixing is by molecular diffusion or by convective dispersion.

Kimber, Puttagunta and Farouq Ali [10] presented new scaling criteria for steam and steam additive recovery experiments. From this study, the authors derived a complete set of similarity groups required to scale the steam or steam plus an additive (eg. solvent) process as defined by governing differential equations, constraints, constitutive relationships and initial and boundary conditions which had been developed. Five sets of scaling criteria, each representing a subset of the more complete set of scaling requirements, were developed by relaxing the scaling of various phenomena. The best approach to use would depend on the particular process to be scaled. The approach chosen should correctly scale the major mechanisms of the process and not cause minor mechanisms in the process to have significant effects on the response of the experimental model.

Incorporation of Solvent Injection into Thermal Recovery Methods

Alikhan and Farouq Ali [43] investigated a recovery process, which incorporated miscible displacement with hot waterflooding. The study considered oil recovery from a formation containing either a residual oil saturation or a connate water saturation, sealed above and below by heat-conducting strata. The recovery process involved introducing a small slug of a light hydrocarbon prior to the injection of one-half pore volume of hot water followed by a conventional cold waterflood. Results indicated that pre-injection of the light hydrocarbon slug preceding the waterflood led to a greater oil recovery than that obtained for a conventional waterflood. Alikhan and Farouq Ali [43] also found that the overall oil recovery by this technique was dependent on oil viscosity, light hydrocarbon slug viscosity and the injection rate. The process was also found to be more effective when the reservoir had been previously waterflooded as opposed to a connate water saturation initially existing in the formation. Solvent recovery was found to be better if a higher initial oil saturation existed.

In studying the application of solvent slugs in thermal operations Farouq Ali [44] investigated the change in phase behaviour characteristics due to an increase in temperature of the fluids involved in a solvent/steam recovery process. He concluded that at elevated temperatures the overall phase behaviour of a typical alcohol-brine system would shift in such a direction as to make displacement of oil by alcohol more efficient. This could be achieved by injecting a small alcohol or solvent slug ahead of a steamflood.

A study by Pirela and Farouq Ali [45] investigated the ternary phase behaviour of solvent-oil-water systems at high temperatures. An increase in the temperature of the system resulted in an increase in the miscibility of the system, which was found to be advantageous from the standpoint of oil recovery.

The chief objective of a study performed by Totonji and Farouq Ali [46] was to exercise control on the system phase behaviour through the use of mixtures of two alcohols exhibiting opposite phase behaviour characteristics in the alcohol-hydrocarbon-water system involved. Such systems were employed in displacements in porous media to ascertain the effectiveness of the systems and it was found that the oil recovery could be improved using these systems.

Experiments conducted by Ozen and Farouq Ali [47] using linear, consolidated cores under isothermal conditions revealed that a steam drive could be an effective technique for recovering the residual oil from a waterflood. They also found that the introduction of a small slug of light hydrocarbon (naphtha) preceding steam injection improved the overall oil recovery.

Hernandez and Farouq Ali [48] used a one-dimensional model (linear) to examine the use of solvent injection to form a channel through the tar sand, connecting the injection and production wells prior to the injection of steam into the tar sand. Results of the study indicated that the injection of a solvent slug preceding steam injection created improved steam injectivity into the oil zone and a higher overall recovery. It was also noted that the smaller solvent slugs aided forming a channel into the tar sand for the steam, whereas the larger solvent slugs created a permeability block which inhibited steam flow.

Snyder and Farouq Ali [49] proposed the use of solvents as a means of developing flow channels in the tight tar sand to provide the initial flow paths for the injected steam. In this study the authors investigated the recovery efficiency of naphtha injection into a two-dimensional homogeneous tar sand pack at various injection rates, the effectiveness of gravity segregation and conductive heating in tar packs with a highly permeable channel joining the inlet to the outlet. A permeable layer existed near the base of the pack. Information obtained from the study indicated that during steam injection the steam action is concentrated around the inlet and did not directly contact the majority of the pack and therefore naphtha injection prior to steam injection in a homogeneous pack was highly effective in opening a steam flow path. Once created, it allowed the steam to become more concentrated towards the production outlet resulting in improved overall oil recovery. It was also noted that total oil recovery improved as solvent residence time increased and as displacement rate in the recovery process decreased.

Farouq Ali and Abad [50] studied the use of solvents in combination with steam using a three-dimensional elemental model. These authors found that the type of solvent, the volume of solvent slug, and the placement of the solvent in the reservoir determined the extent of the bitumen recovery. They found that smaller solvent slugs were more effective than larger slugs and that there existed an optimum combination of solvent and steam slug sizes which optimized the overall bitumen recovery.

A study performed by Farouq Ali, Look Yee, Cordero and Figueroa [51] reported that implementing a thermal recovery method requires the creation of flow paths for the initial injection of a hot fluid. Comparisons of the base steamfloods and the solvent-steamfloods performed during the investigation show that the solvent-steamfloods did improve oil recovery. It was also determined in the study that the injected solvent spread over a large area by viscous fingering if the injection rate was very high, while if the rate was low the solvent essentially diffused into the bitumen and was largely confined to the immediate vicinity of the injection well.

In an economic evaluation of solvent/steam stimulation Doscher, Ershaghi, Herzberg and Gourene [52] suggested that by reducing the viscosity of crude oil before contact with steam by use of a solvent, the overall steam requirement to achieve the same recovery without solvent might be reduced. The success of this type of proposal was found to depend on whether it was possible to obtain a marginally greater reduction in viscosity by the mixing of solvent and crude oil as compared to using an economically equivalent amount of steam. Doscher et al. [52] also stated that for reservoirs where steam soaking operations were not attractive due to extreme heat losses, the utilization of a solvent/steam process needed to be investigated more carefully. The authors also suggested that solvent should be used in combination with steam to achieve specific advantages in a steam drive operation such as establishing or increasing conductivity between injection and production wells or increasing sweep efficiency.

Redford and McKay [53] found that the use of a solvent in a steam process may reduce the residual saturation in the water-swept areas of the reservoir and thus improve the overall oil recovery. For solvents which are mixed hydrocarbons the more volatile additive (light ends) may act as a drive agent while the less volatile (heavier ends) one may act as a viscosity-reducing agent during the pressure depletion portion of the cycle which further improved recovery.

Redford [54] reported that the use of naphtha in combination with steam improved oil recovery by reducing bitumen viscosity and thereby improving recovery in the water-swept portions of the reservoir, thus making more efficient use of the drive energy provided by the steam.

A comprehensive study carried out by Alikhan and Farouq Ali [43] investigated a combination of three different processes for the recovery of light and relatively viscous oils, using two approaches: injection of a slug of a light hydrocarbon miscible with the viscous oil, followed by the injection of hot water in one series of experiments, and a steam slug in another series, each of which was then driven by water. Essentially the mechanism of the process was a combination of miscible displacement, hot waterflooding and steamflooding. The process was designed for a high thermal efficiency utilizing the maximum amount of heat injected. Conclusions drawn from the investigation suggested that the solvent slug injected prior to the hot water or steam slug in a sandpack improved oil recovery as compared to a straight hot water or steam slug run. The solvent, in view of the prevailing adverse mobility ratio, mixed with the original in-place oil, and helped to lower the oil viscosity. The viscosity was further reduced by the heat from the injected hot water or steam slug, which led to an improvement in the mobility ratio and hence an improvement in the displacement efficiency. A large proportion of the light hydrocarbon slug was recovered by the steam distillation effect. It was also determined that the recovery ratio was higher and the steam residual oil saturation was lower when a steam slug was employed rather than a hot water slug. Recovery ratio was defined as the total hydrocarbon produced divided by the amount of hydrocarbon slug injected. The recovery ratio gave a basic indication of the rise in oil recovery due to the injection of the additional hydrocarbon in conjunction with the hot water.

In a recent study, Yamazaki, Matsuzawa, Abdeldarim and Ono [55] reported that when solvent was injected with steam, bitumen recovery increased and this increase was directly proportional to the rate at which solvent was injected. Yamazaki et al. [55] examined the use of benzene, cyclohexane and halide with steam injection and found that benzene and cyclohexane had nearly the same effect on the bitumen recovery enhancement, whereas halide appeared to be the least effective solvent.

Asphaltene Flocculation

In some instances, when bitumen is mixed with certain light, saturated hydrocarbons such as paraffinic solvents, hard friable materials called asphaltenes, may be precipitated. Asphaltene precipitation can create serious problems in the reservoir, such as constriction of fluid flow passages which results in a reduction in the formation permeability. An investigation by Knobloch, Farouq Ali and Treviño Diaz [56] found that the asphaltenes that precipitate out are not single molecules, but clusters of molecules often coated with paraffin and resin molecules strongly bonded to the exterior of the clusters. A conclusion of the study was that asphaltene precipitation increased with an increase in solvent concentration.

A study by Snyder and Farouq Ali [49] stated that naphtha injection may cause formation plugging by asphaltene flocculation but plugging was found to occur only when large volumes of naphtha were injected. The injection of a small amount of naphtha during a slug process would not initiate asphaltene flocculation. In the present research asphaltene precipitation was not considered to be a significant factor.

Chapter IV

Scaling of the Solvent-Steamflood Process in the Low Pressure Model

The following chapter describes the scaling method used in developing the low pressure model of the Aberfeldy reservoir which is utilized in the study. The governing equations used to create the scaling criteria and a list of the assumptions incorporated in the scaling procedure are provided. Two of the major assumptions are discussed in further detail. An extensive description of the scaling procedure designed by Stegemeier, Laumbach and Volek [9] is presented along with detailed calculations which were used in modelling the Aberfeldy heavy oil reservoir and determining the related operating parameters for the experiments. Also the new scaling criteria derived by Kimber, Puttagunta and Farouq Ali [10] for steam and steam additive recovery experiments is discussed.

Derivation of the Model Scaling Parameters

The scaling rules used in designing the low pressure model of the Aberfeldy were developed by Stegemeier, Laumbach and Volek [9]. The first step in modelling a steam injection process required deriving the proper scaling parameters.

In order to obtain the scaling parameters, a very involved procedure was performed. The first step involved formulating the governing differential equations into dimensionless form and then indentifying the similarity parameters by inspectional analysis. Next characteristic quantities were selected based upon the most important property values and constraints. The similarity parameters were then modified using engineering judgement resulting in a set of scaling parameters that could basically be matched between the prototype and the model. These scaling parameters are illustrated in Table 4.1.

Table 4.1. : Scaling Parameters for Steam Injection Processes.

Number	Scaling Parameter	Name of Scaling Parameter
1.	$\dfrac{p_r}{\rho_r g_r L_r}$	Poiseuille number divided by Stokes number.
2.	$\left\{\dfrac{f_{sr} L_{vr}}{C_r T_r} + 1\right\} \cdot A^*$	Modified Jacob number + 1.
3.	$\dfrac{f_{sr} \mu_{sr} \rho_r}{\mu_r \rho_{sr}}$	Ratio of steam pressure gradient to oil pressure gradient.
4.	$\dfrac{k_{hr} t_r}{\phi_r S_r \rho_r C_r L_r^2} \cdot A^*$	Fourier number or Peclet number.
5.	$\dfrac{\phi_r S_r \mu_r L_r}{k_r \rho_r g_r t_r}$	Stokes number.
6.	$\dfrac{w_r t_r}{\rho_r \phi_r S_r L_r^3}$	Poiseuille number divided by modified Poiseuille number.

Subscript ' r ' indicates that the variable is a reference quantity used to obtain a dimensionless term.

* When $\phi \, \Delta S$ is not matched, A takes on a value between unity and $\phi_r S_r \, (\rho_r C_r / \rho_{cr} C_{cr})$. If reservoir heating or heat production predominates, use unity; if cap and base rock heating predominates, use $\phi_r S_r \, (\rho_r C_r / \rho_{cr} C_{cr})$.

After Stegemeier, Laumbach and Volek [9]

Formulation of the governing equations into dimensionless form was carried out using various equations. The first equation involved the conservation of mass as applied to the oil phase which yielded

$$\phi \frac{\partial (\rho_o S_o)}{\partial t} + \nabla \cdot (\rho_o \vec{u_o}) = 0\,, \tag{1}$$

where the subscript o symbolizes oil.

The second equation was the continuity equation for the water given in both the liquid and vapor phases by

$$\phi \frac{\partial (\rho_w S_w)}{\partial t} + \nabla \cdot (\rho_w \vec{u_w}) + \phi \frac{\partial (\rho_s S_s)}{\partial t} + \nabla \cdot (\rho_s \vec{u_s}) = 0\,, \tag{2}$$

where the subscript w signifies water in the liquid phase and s represents water in the vapor phase (steam).

Darcy's flow equation was also applied which can be written for any species j, where $j = o, w$ or s as

$$\vec{u_j} = - \frac{k\, k_{rj}}{\mu_j} (\nabla p - \rho_j \vec{g})\,. \tag{3}$$

The conservation of energy for the reservoir was expressed by

$$\left[(1 - \phi)\rho_r C_r + \phi \left(\rho_o C_o S_o + \rho_w C_w S_w\right)\right] \frac{\partial T}{\partial t} + L_v \left[\phi \frac{\partial \left(\rho_s S_s\right)}{\partial t} + \nabla \cdot \rho_s \vec{u_s}\right]$$

$$+ \left(\rho_o C_o \vec{u_o} + \rho_w C_w \vec{u_w}\right) \cdot \nabla T + \rho_s \vec{u_s} \cdot \nabla h_s + \nabla \cdot \vec{q} = 0. \tag{4}$$

The conductive heat flux was represented by the Fourier equation,

$$\vec{q} = - k_h \nabla T\ . \tag{5}$$

The saturation relationship became

$$S_o + S_w + S_s = 1, \tag{6}$$

when three phases were present.

The pressure and temperature of the steam are interdependent at saturated conditions and are related by the Clausius-Clapeyron equation, which in its functional form was represented by

$$p_{sat} = p_{sat}(T_{sat}). \tag{7}$$

The dependence of the material properties in the reservoir on the thermodynamic-state variables were represented by constitutive equations and were expressed in functional form.

$$\phi = \phi(x, y, z) \tag{8}$$

$$\rho_j = \rho_j(p, T) \tag{9}$$

$$k = k(x, y, z) \tag{10}$$

$$k_{rj} = k_{rj}(S) \tag{11}$$

$$\mu_j = \mu_j(T) \tag{12}$$

$$h_s = h_s(T) \tag{13}$$

$$L_v = L_v(T) \tag{14}$$

$$k_h = k_h(x, y, z) \tag{15}$$

$$\rho_r = \rho_r(x, y, z) \tag{16}$$

S denotes the dependence of the property on the phase saturations.

Stegemeier et al. [9] made various assumptions when deriving the scaling criteria for a vacuum model. These assumptions are listed below.

1. Three phases may exist which consist of an oleic phase, an aqueous phase and a steam-vapor phase with no volatile hydrocarbons.
2. No partitioning into or out of the oil phase (dead-oil assumption).
3. Rock compressibility and thermal expansion are negligible.
4. Darcy's and Fourier's equations are valid.
5. Capillary-pressure effects are negligible.
6. The system is in local thermodynamic equilibrium.

7. Kinetic energy, potential energy, and viscous dissipation energy are negligible compared to the thermal energy.
8. The enthalpy and internal energy are essentially equal for the oleic phase and for the aqueous phase and are linear functions of the temperature.
9. The difference between the steam enthalpy and internal energy can be neglected.
10. The time rate of change of the specific steam enthalpy in the steam zone is negligible.
11. The internal energy of the rock is a linear function of the temperature.
12. The saturated steam temperature is the maximum temperature at any location.
13. Relative permeabilities depend exclusively on the saturations.
14. S_{ors} and S_{iw} are constant and uniform throughout the model.
15. Critical saturation for steam flow is assumed to be zero.
16. The changes in the density of the immovable water and residual oil are negligible.

Due to the assumptions listed above it is unavoidable that strict scaling of the relationships of relative permeability and capillary pressure could not be achieved. The relative permeability and capillary pressure relationships would have to be equal functions of saturation in both the model and prototype for strict scaling to be achieved. Additional error in scaling occurs due to the problem associated with obtaining model fluids and materials with properties needed for totally satisfying the scaling groups in Table 4.1.

Bentsen [57] found that the mobility ratio was the most prevalent in a displacement process of a linear system which made it possible to neglect the requirement that relative permeabilities be equal in both the prototype and model for certain conditions. As mentioned previously Bentsen [57] dealt with a linear system but Proctor [26] suggested that more complex problems such as the low pressure model used in this research could be handled in a similar manner. The inability to scale capillary pressure was believed to be valid due to the high crude oil viscosity in the prototype reservoir. Demetre, Bentsen and Flock [58] stated that for a large value of mobility ratio, the breakthrough recovery was a weak function of the capillary number during a stable displacement. Therefore the assumption of Stegemeier et al. [9] that capillary pressure effects be neglected was valid for this situation.

It was determined by Prats [11] that the three-phase relative permeability curves used for a prototype at anticipated operating conditions could not be determined. Similarly, it wasn't known how to set up the relative permeability properties for the laboratory model. This also made it difficult to determine if the relative permeability relationships between the model and the prototype were scaled or unscaled. He found from his Peace River model study that despite the limitation, good agreement was obtained between the field and model relative permeability relationships.

Confirmation of the validity of the assumptions made in deriving the scaling rules was further demonstrated by the agreement of laboratory model results and results of actual field operations as reported in the study by Stegemeier, Laumbach and Volek [9].

Designing the Low Pressure Model of the Aberfeldy Reservoir

Once the set of scaling parameters were developed various engineering decisions had to be made in order to apply the derived scaling parameters.

Field Representation

The first step of the model design involved selecting prototype values that would be representative of typical field values of the Aberfeldy reservoir. Field characteristics that were to be specified were well spacing, net and gross pay thickness, porosity, permeability, thermal conductivity, heat capacity, movable saturation, oil density and density as a function of temperature, initial reservoir temperature, and range of injection pressure. A list of the selected prototype values along with the corresponding model values are given in Table 4.2. Calculations of the model values are provided further on in this section.

Table 4.2 : Prototype and Model Values for The Aberfeldy Reservoir

Feature	Prototype	Model
Well Spacing	20 Acre (8 hectare) 5-spot	Quarter of a 5-spot
Length of Pattern (Quarter of a 5-spot)	140.8 metres (461.9 feet)	81.3 centimetres (32.0 inches)
Time Scale	1 year	12.1836 minutes
Net Pay Thickness	11 metres	6.35 centimetres
Gross Pay Thickness	10 to 13 metres	6.35 centimetres
Porosity	0.31	0.32
Permeability	2000 millidarcies	4216.5 darcies
Thermal Conductivity	0.002077 KW/m.K (1.2 Btu/hr-ft.F)	0.003266 KW/m.K
Heat Capacity	2.1803 KJ/kg.K	2.3824 KJ/kg.K
Initial Oil, Gas & Water Saturations	So=0.75 Sg=0.02 Sw=0.23	So=0.75 Sg=0.05 Sw=0.20
Steamflood Residual Oil Saturation	Sor = 0.15	Sor = 0.145
Oil Viscosity	1275 mPa.s @ 23.9 C 560 mPa.s @ 32.2 C 90 mPa.s @ 65.6 C 12.5 mPa.s @ 135.0 C 1.29 mPa.s @ 301.7 C	9256.5 mPa.s @ 3.2 C 4065.6 mPa.s @ 5.6 C 653.4 mPa.s @ 15.1 C 90.75 mPa.s @ 35.0 C 9.37 mPa.s @ 82.6 C
Water Viscosity	0.894 mPa.s @ 25.8 C	------------
Gas Viscosity	0.013 mPa.s @ 23.3 C 0.016 mPa.s @ 134.4 C	------------ ------------
Specific Gravity of Gas	0.55	------------
Initial Reservoir Temperature	23.3 C	3 C
Initial Reservoir Pressure	3.45 MPa	26.82 kPa
Steam Injection Pressure	1.90 MPa	16.87 kPa
Inj. & Prod. Rates	1 m3/day	9.0728 cm3/min
Injection Rate of Steam	100 m3/day	226.8 cm3/min.
Injection of Solvent	88.4 m3/day	200 cm3/min.
Steam Quality	0.7	0.08324
Reservoir Depth	522.4 metres	------------
Bottom Water Thickness	Varies from 0 to 6.9 metres	Varies from 8 - 20 % of Gross Model Thickness
Upper Pressure Boundary	Fracture Gradient of Reservoir	------------
Lower Pressure Boundary	0.345 MPa (50 psia) Back Pressure	7 kPa (1 psia)

The model designed for this study represented one-quarter of an eight hectare (20 acre), five spot pattern. Since the Aberfeldy reservoir is characterized by a thin pay zone overlying a bottom water layer, the model was scaled in all three dimensions. To achieve the best scaling in the model and obtain the best predictions from the experimental results the model was designed as large as was practical.

Length Scale Selection

Although somewhat arbitrary, the determination of the length scale was based on the temperature/pressure relations as well as the constraints of practical model size. Stegemeier et al. [9] stated that to achieve the best temperature/pressure match for saturated steam the length scale factor, γ (*L*), should be as small as possible, thus the model should be as large as possible. The size of the model depends on the practical limitations of time and the time required to saturate, cool and clean. The higher probability of leaks and the greater structural requirements of a larger model must also be considered.

The model used for this study represented one-quarter of an eight hectare (20 acre), five spot pattern of the Aberfeldy heavy oil reservoir. Prototype dimensions of the one-quarter of a five spot pattern were 140.8 m (461.9 ft.) x 140.8 m (461.9 ft.) square x 11 m (36.1 ft.) thick. The dimensions of the model were 81.3 cm (32 in.) x 81.3 cm (32 in.) square with a thickness of 6.4 cm (2.5 in.) which resulted in a length scale factor in all three dimensions of about 173.2.

$$\gamma (L) = \frac{L_P}{L_M} = 173.2 \qquad (4.1)$$

Scaling of Model Pressure

Deciding on what model production pressure to choose was considerably straightforward. For typical length scales of 100 to 200 and prototype production pressures as low as 0.345 MPa (50 psia), the Clausius-Clapeyron temperature/pressure relation at saturation could be best matched if the lowest possible model production pressure can achieved.

$$\therefore\ (p_p)_P \ = \ 0.345 \text{ MPa}$$

The lowest model production pressure that could be maintained was limited, from a practical standpoint by vapor pressure constraints and vacuum pump limitations. The initial value recommended by Stegemeier et al.[9] to be used in scaling calculations was 6.895 kPa (1 psia).

$$\therefore\ (p_p)_M \ = \ 6.895 \text{ kPa}$$

The upper limit of the prototype production pressure range was bounded by the fracture gradient of the reservoir.

Once the initial value for model production pressure , $(p_p)_M$, was selected, an expression for scaling the model pressure could be created using scaling parameter 1 from Table 4.1.

$$\gamma\ (\Delta p\ ) = \frac{(p\ - p_p)_P}{(p\ - p_p)_M} = \frac{\rho_P\, g_P\, L_P}{\rho_M\, g_M\, L_M} \tag{4.2}$$

Since the ratio of gravitational accelerations was unity and the length scale had already been calculated from Equation 4.1, the only unknown term in Equation 4.2 was the ratio of densities. A value was assumed for the density ratio that would be corrected later and was found to be approximately equal to 0.9. By substituting the known values into Equation 4.2, a relationship involving model pressure, p_M , as a function of prototype pressure, p_P , could be developed.

$$\gamma\ (\Delta p\ ) = \frac{(p\ - p_p)_P}{(p\ - p_p)_M} \ = \ (0.9)\ (1.0)\ (173.2)$$

$$p_M \ = (p_p\ )_M + 0.0064152\, p_P \ - 0.0064152\ (p_p\ )_P$$

$$p_M = 0.006895 - (0.0064152)\ (0.34475) + 0.0064152\, p_P$$

$$\therefore p_M \ = 0.004683 + 0.006415\, p_P \tag{4.3}$$

Where p_M was the model pressure and p_P was the corresponding prototype pressure, with p_M and p_P calculated in MPa. Table 4.3 lists some tabulated values for p_P along with corresponding p_M values.

Scaling of Model Temperature

To achieve the best match between model and prototype oil-viscosity curves, Stegemeier et al. [9] suggested that model temperature range be made as large as possible. This also allows for a better match of the Clausius-Clapeyron temperature/pressure relation for saturated steam. From a practical standpoint, the lowest initial model temperature that could be obtained in the laboratory was approximately 3^0C. Therefore the initial model temperature was set at $(T_i)_M = 3^0$C. In order to scale the temperature, corresponding prototype and model temperatures at only one other point was needed.

Stegemeier et al. [9] reported that it is usually best to choose a pressure value from the middle of the pressure range when determining the temperature difference ratio. A majority of the oil production will occur when these middle range temperatures exist. As well the lower region of the Clausius-Clapeyron relation for saturated steam is more difficult to match, therefore it is better to fit the middle and upper portions of the temperature/pressure relation.

A prototype pressure of 2.00 MPa was chosen from Table 4.3 as the middle range pressure. The corresponding model and prototype temperatures for 2.00 MPa were determined from the temperature/pressure relation and from these values the temperature ratio was calculated.

$$\frac{(\Delta T)_P}{(\Delta T)_M} = \frac{(T - T_i)_P}{(T - T_i)_M} = \frac{(212.42 - 23.30)}{(57.03 - 3.0)} \tag{4.4}$$

$$\therefore \frac{(\Delta T)_P}{(\Delta T)_M} = 3.5 \tag{4.5}$$

Table 4.3 : Prototype and Model Scaling Values

Prototype Values							Model Values										
P (MPa)	Ts (C)	hw (kJ/kg)	CwΔT (kJ/kg)	Lv (kJ/kg)	ps (kg/m3)	μs (cp)	P (MPa)	Ts (C)	Tsc (C)	hw (kJ/kg)	CwΔT (kJ/kg)	Lv (kJ/kg)	ps (kg/m3)	μs (cp)	fs	μom/μop (cp/cp)	wa/wi
3.45	241.73	1045.9	947.84	1757.9	17.2322	0.0173	0.02682	66.47	65.48	274.07	261.50	2342.59	0.17100	0.01090	0.06965	7.1095	0.8854
3.00	233.90	1008.4	910.64	1795.7	14.9970	0.0170	0.02393	63.92	63.24	264.69	252.12	2349.28	0.15110	0.01080	0.07319	7.3253	0.8827
2.50	223.99	962.11	864.33	1841.0	12.5031	0.0166	0.02072	60.77	60.40	252.80	240.23	2356.40	0.13520	0.01060	0.07750	7.2644	0.8793
2.00	212.42	908.79	811.01	1890.7	10.0371	0.0162	0.01751	57.03	57.10	238.99	226.42	2365.72	0.11290	0.01040	0.08230	7.4558	0.8776
1.50	198.32	844.89	747.11	1947.3	7.5890	0.0156	0.01431	52.84	53.06	222.12	209.55	2373.60	0.08820	0.01020	0.08792	7.8512	0.8765
1.00	179.91	762.61	665.03	2015.3	5.1430	0.0149	0.01110	47.61	47.80	200.15	187.58	2386.99	0.07816	0.01000	0.09474	6.6411	0.8758
0.50	151.86	640.23	542.45	2108.5	2.6674	0.0140	0.00789	41.15	39.77	166.61	154.04	2403.94	0.06170	0.00970	0.10440	4.9637	0.8754
0.34475	138.34	582.00	484.22	2149.7	0.5322	0.1330	0.00690	38.50	35.91	150.48	137.91	2409.19	0.04556	0.00950	0.10790	1.4290	0.8751

After Proctor (26)

The temperature ratio must be constant for the entire temperature range in order to have a proper proportion of energy stored as internal energy. If the temperature ratio is constant the model temperature relation between the model and the prototype can be developed.

$$T_M - (T_i)_M = \frac{T_P - (T_i)_P}{3.5}$$

$$\therefore\ T_M = 0.286\, T_P - 3.657 \qquad (4.6)$$

The model temperatures determined using Equation 4.6 are listed in Table 4.3 and are represented by T_{sc} to denote that these are calculated values.

As illustrated in Table 4.3 the calculated values, T_{sc}, do not correspond exactly with the saturation values, T_s. It can be seen from Table 4.3 that the values of T_s and T_{sc} match quite well for all of the bottom lines of the table which corresponds to the lowest prototype pressure, $(p_p)_P$, of 0.345 MPa. If one attempts to sacrifice the upper temperatures due to constraints on minimum model temperatures greater errors will be introduced. Therefore it was concluded by Stegemeier et al. [9] that better scaling was obtained by allowing the error to exist at the low temperature.

It was also noted by Stegemeier et al. [9] that the portion of the temperature/pressure saturation relation that was the most difficult to match was the region corresponding to a prototype pressure of about 0.690 MPa (100 psia). However these low prototype pressures are not usually encountered during ordinary field operations.

Determination of the Required Steam Quality

By incorporating scaling parameter 2 from Table 4.1 the model steam quality could be calculated. If the relationship of $\phi\, \Delta S$ does not match and cap and base rock heating is predominant, which usually occurs during steam injection processes of thin formations, the term A in scaling parameter 2 can be replaced by $\phi\, S_R\, (\rho_R\, c_R / \rho_{cR}\, c_{cR})$. Therefore the model steam quality could be calculated using the following equation.

$$f_{sM} = \left(\frac{C_w \, \Delta T}{L_v}\right)_M \left\{ \left(\frac{f_s L_v}{C_w \, \Delta T} + 1\right)_P \left[\left(\frac{\phi_P \, \Delta S_P}{\phi_M \, \Delta S_M}\right) \cdot \left(\frac{\rho_P C_P}{\rho_M C_M}\right) \left(\frac{\rho_{cM} C_{cM}}{\rho_{cP} C_{cP}}\right) \right] - 1 \right\} \tag{4.7}$$

It was assumed that a porosity, ϕ_M , of 0.32 existed in the model and a change in the oil saturation within the model, ΔS_M ,would be 0.85. The change in the oil saturation in the prototype, $\Delta S_P = 1 - S_{or} - S_{wc}$, was assumed to be 0.62, where $S_{or} = 0.15$ and $S_{wc} = 0.23$. Various values of model steam quality at various pressures were calculated using Equation 4.7 and are listed in Table 4.3.

Scaling of Model Oil Viscosity

According to Stegemeier et al. [9] it was essential to scale the oil production subsequent to steam breakthrough as closely as possible. In order to match the pressure gradient in the oil zone and the steam region, the oil viscosity in the model should be scaled using scaling parameter 3 from Table 4.1. The following expression was utilized to scale the model oil viscosity.

$$\frac{\mu_{oM}}{\mu_{oP}} = \left(\frac{f_{sM}}{f_{sP}}\right)\left(\frac{\mu_{sM}}{\mu_{sP}}\right)\left(\frac{\rho_{sP}}{\rho_{sM}}\right)\left(\frac{\rho_{oM}}{\rho_{oP}}\right) \tag{4.8}$$

Values for the known quantities were inserted into Equation 4.8 to yield the corresponding model oil viscosities which are listed in Table 4.3.

Time Scale Determination

Since the study involves thermal recovery from a thin reservoir it was assumed that cap and base rock heating was predominant, as was assumed previously when calculating the model steam quality. Therefore the time-scale ratio was determined using scaling parameter 4 where A was equal to $\phi \, S_R \, (\rho_R \, c_R \, / \, \rho_{cR} \, c_{cR})$. By implementing scaling parameter 4, the following time-scale ratio equation was derived.

$$\frac{t_M}{t_P} = \left(\frac{k_{hP}}{k_{hM}}\right)\left(\frac{\rho_{cM}\, C_{cM}}{\rho_{cP}\, C_{cP}}\right)\left(\frac{L_M}{L_P}\right)^2 \tag{4.9}$$

Where the thermal conductivity of the model (granite), k_{hM}, was found to be 2.81 kcal/(m· hr.· ^{0}C)[59].

$$\therefore\ k_{hM} = 0.003266 \text{ kW/m} \cdot {}^0\text{K}$$

From Table 4.2 the thermal conductivity of the prototype (sandstone), k_{hP}, was 0.002077 kW/m· ^{0}K[26].

$$\therefore\ k_{hP} = 0.002077 \text{ kW/m} \cdot {}^0\text{K}$$

According to Proctor[26] the values for $(\rho_{cM}\, C_{cM})$ and $(\rho_{cP}\, C_{cP})$ are as follows.

$$(\rho_{cM}\, C_{cM}) = 2.3824 \text{ kJ/kg} \cdot \text{K}$$

& $$(\rho_{cP}\, C_{cP}) = 2.1803 \text{ kJ/kg} \cdot \text{K}$$

Where c represented values for the cap and base rock.

Substituting the above values into Equation 4.9 the time scale can determined as follows.

$$\frac{t_M}{t_P} = \left(\frac{0.002077}{0.003266}\right)\left(\frac{2.3824}{2.1803}\right)\left(\frac{1}{173.2}\right)^2 \cdot \left(525{,}960 \text{ min./yr.}\right)$$

$$\frac{t_M}{t_P} = 12.1836 \text{ min./yr.} \tag{4.10}$$

Where the conversion to min./yr. is based on a four year average (ie. one year = 365.25 days = 525,960 min.)

Scaling of Model Permeability

Scaling parameter 5 from Table 4.1 was used to scale the model permeability. The following equation was developed using this scaling parameter.

$$\frac{k_M}{k_P} = \left(\frac{\phi_M\, \Delta S_M}{\phi_P\, \Delta S_P}\right)\left(\frac{L_M}{L_P}\right)\left(\frac{\mu_M}{\mu_P}\right)\left(\frac{\rho_P}{\rho_M}\right)\left(\frac{t_P}{t_M}\right) \tag{4.11}$$

The ratio of μ_M / μ_P was temperature dependent which meant that Equation 4.11 was also a function of temperature. However Equation 4.11 couldn't be temperature dependent therefore according to Stegemeier et al.[9] a single value must be selected.

In choosing a representative value for the viscosity ratio, it was noted that the actual value of the ratio was important only after steam breakthrough occurred, at which time the steam pressures were low. Also the viscosity ratio was more significant in the area of the production well. Therefore Stegemeier et al.[9] concluded that viscosity ratio values should be chosen from the lower section of Table 4.3. The viscosity ratio value chosen corresponded to a prototype pressure of 1 MPa. Substitution of known values and prototype data into Equation 4.11 yielded the following model permeability.

$$\therefore \; k_M = 4216.5 \text{ darcies}$$

Scaling of Injection and Production Rates

Scaling of both the injection rates and production rates involved using scaling parameter 6 from Table 4.1 which was used to derive the proceeding equation.

$$\frac{w_M}{w_P} = \left(\frac{\rho_{oM}}{\rho_{oP}}\right)\left(\frac{L_M^3}{L_P^3}\right)\left(\frac{\phi_M \, \Delta S_M}{\phi_P \, \Delta S_P}\right)\left(\frac{t_M}{t_P}\right) \tag{4.12}$$

Inserting the appropriate values into Equation 4.12 gave

$$\frac{w_M}{w_P} = 9.0728 \, \frac{\text{cm}^3/\text{min.}}{\text{m}^3/\text{day}},$$

where the volumetric rates are at standard conditions.

To represent an injection rate of 100 m^3/day in the prototype, the corresponding injection rate in the model was one-quarter of 907.3 cm^3/min or 226.8 cm^3/min.

Determination of Water Proportion for Steam Quality

In order for complete scaling, the fractions of injected steam and water must be calculated to determine the appropriate model steam quality. The value depends on the heat loss from the lines, the desired steam quality, the enthalpy of steam produced by the steam generator and quality-control water temperature which is usually at room temperature.

The amounts of water and steam injected were based upon the enthalpy rate of the two inlet streams that were combined. The total enthalpy rate of the two streams had to be equal to the required enthalpy rate of the wet steam introduced into the model, as well as any existing heat losses.

$$\therefore w_{ss}h_{ss} + w_a h_a = \left(w_{ss} + w_a\right)\left(f_{sM}L_v + C_w\Delta T\right) + \dot{Q}_{loss} \qquad (4.13)$$

Where w_{ss} and w_a represented mass flow rates of the superheated steam and the feed water for quality control, h_{ss} and h_a were the entering enthalpies for the superheated steam and the quality control water and $\dot{Q}_{loss}$ was the heat loss rate. Rearranging Equation 4.13 and noting that $w_{wt} = w_{ss} + w_a$, where w_{wt} is the total mass rate of injected water, gave Equation 4.14.

$$\frac{w_a}{w_{wt}} = \frac{h_{ss} - f_s L_v - C_w\,\Delta T - \left(\dot{Q}_{loss}/w_{wt}\right)}{h_{ss} - h_{wa}} \qquad (4.14)$$

Enthalpy of quality control feed water was 96.52 kJ/kg (from basic steam tables) at a temperature of 23 ^{0}C. The temperature of the superheated steam was assumed to be 120 ^{0}C and the corresponding steam enthalpy was 2706.07 kJ/kg (also from basic steam tables). Therefore at various pressures, h_{ss} could be determined and substituted into Equation 4.14 to yield values for w_a/w_t at different pressures. The calculated values are listed in Table 4.4.

Table 4.4 : Steam Enthalpy at Corresponding Model Pressures

Model Pressure (MPa)	Steam Enthalpy (kJ/kg)
0.006895	2726.00
0.007891	2725.92
0.01110	2725.59
0.01431	2725.25
0.01751	2724.92
0.02072	2724.59
0.02393	2724.25
0.02682	2723.95

After Proctor [26]

Scaling of Wells in the Model

Direct geometrical scaling of wells could not be achieved for the small size needed in the low pressure model. Stegemeier et al. [9] implemented a well scaling method that utilized a slit well at the wall of the model. The slit wells effective radius was dependent on the slit width and the bead pack arrangement directly in front of the slit. The slit width was determined from the following equation.

$$w = 2\pi r_w = \pi d_w \qquad (4.15)$$

Where w = slit width

r_w = scaled radius of well

d_w = scaled diameter of well

Since the length scale for the model was 173.2 and the prototype well diameter was assumed to be 6 inches, the model wells required a scaled diameter of 6"/173.2 which equalled 0.03464 inches. The models well slit width was determined using Equation 4.15.

$$w = \pi\,(0.03464") = 0.1088" \quad (0.2764\text{ cm})$$

Design of the slit wells in the model allowed for relatively easy alteration of injection and production intervals. The nature of the reservoir (bottom water) studied and the recovery process (solvent-steamflood) required the injection interval to be in the upper region of the model and therefore the production interval was situated over the entire model thickness. The injection well contained four slots opposite the upper region of the model and the production well consisted of eight slots over length of the well.

Scaling of Solvent in the Model

Since the project dealt with the use of solvent in combination with a steam injection process it was thought that the new scaling criteria derived by Kimber, Puttagunta and Farouq Ali [10] could be incorporated into the low pressure model which was based on the scaling criteria of Stegemeier, Laumbach and Volek [9]. The scaling criteria developed by Kimber et al.[10] consisted of a complete set of similarity groups derived to scale the solvent plus steam process as defined by the governing differential equations, constraints, constitutive relationships and initial and boundary conditions set out by Kimber et al.[10]. By relaxing the scaling of various phenomena, five sets of scaling criteria were developed, each representing a subset of the more complete set of scaling requirements. The most appropriate approach to use would depend on the particular process to be scaled. The approach chosen should correctly scale the major mechanisms of the process and not cause minor mechanisms in the process to have significant effects on the response of the experimental model. The scaling criteria presented by Kimber et al. [10] for solvent-steam injection processes required the use of the same fluids under similar conditions of pressure and temperature as in the prototype reservoir which involved the implementation of a high pressure model. However as discussed previously the research project was based on experiments performed in the low pressure or vacuum model. Therefore the scaling criteria derived by Kimber et al. [10] could not be integrated into the low pressure model experiments studying the recoveries of solvent-steam injection techniques. Since the scaling criteria of Kimber et al.[10] could not be properly employed it was decided to carry out the solvent-steam injection experiments for the Aberfeldy research project in a similar manner to the scaled experiments of Pursley [18]. Pursley [18] used the Pujol-Boberg scaling criteria to create a three-dimensional, high pressure, physical model representing steam injection into a Cold Lake reservoir. He performed partially scaled model experiments of the solvent-steam injection process in which solvent was simply added to his steamflood model. In the same manner as Pursley [18], solvent was simply incorporated into the steamflood experiments of the Aberfeldy low pressure model used in the present research.

Chapter V

Experimental Apparatus and Procedure

The following chapter provides a description of the apparatus and materials used for the present research. The section describes the procedure for packing and saturating the model prior to each experiment. Details are also provided describing how the different types of runs such as homogeneous, bottom water and gas cap experiments were prepared and performed. A discussion of how an experiment was conducted once the model packing and saturation were complete is also provided. Figure 5.1 gives a schematic illustration of the apparatus used for these scaled model studies.

The apparatus used in this study comprised of the following major components: physical model, data acquisition system, solvent and steam injection equipment, produced fluids collection system and model cart, rail system and cold storage compartment. These are described in detail in the following sections. Plate 5.1 provides an overall view of the apparatus with the cold storage room located to the left of the model.

Physical Model

The model used for this study consisted of a fiberglass tray which was filled with glass beads (porous medium). Granite blocks were situated above and below the tray to simulate overburden and underburden, as well two slit wells were positioned in opposite corners of the fiberglass tray to represent the injection and production wells. The model of the Aberfeldy reservoir was constructed to simulate one-quarter of an eight hectare (20 acre), five-spot pattern having the dimensions 281.55 m x 281.55 m x 11 m thick.

The models length scale was 173.2. Therefore the dimensions to which the model was constructed were 81.28 cm (32 in) x 81.28 cm (32 in) x 6.35 cm (2.5 in) thick. In all of the experiments it was attempted to satisfy the scaling groups in order to better represent the steam properties and conditions that existing in the Aberfeldy reservoir. To improve scaling of steam behaviour the runs were conducted under vacuum conditions. At these

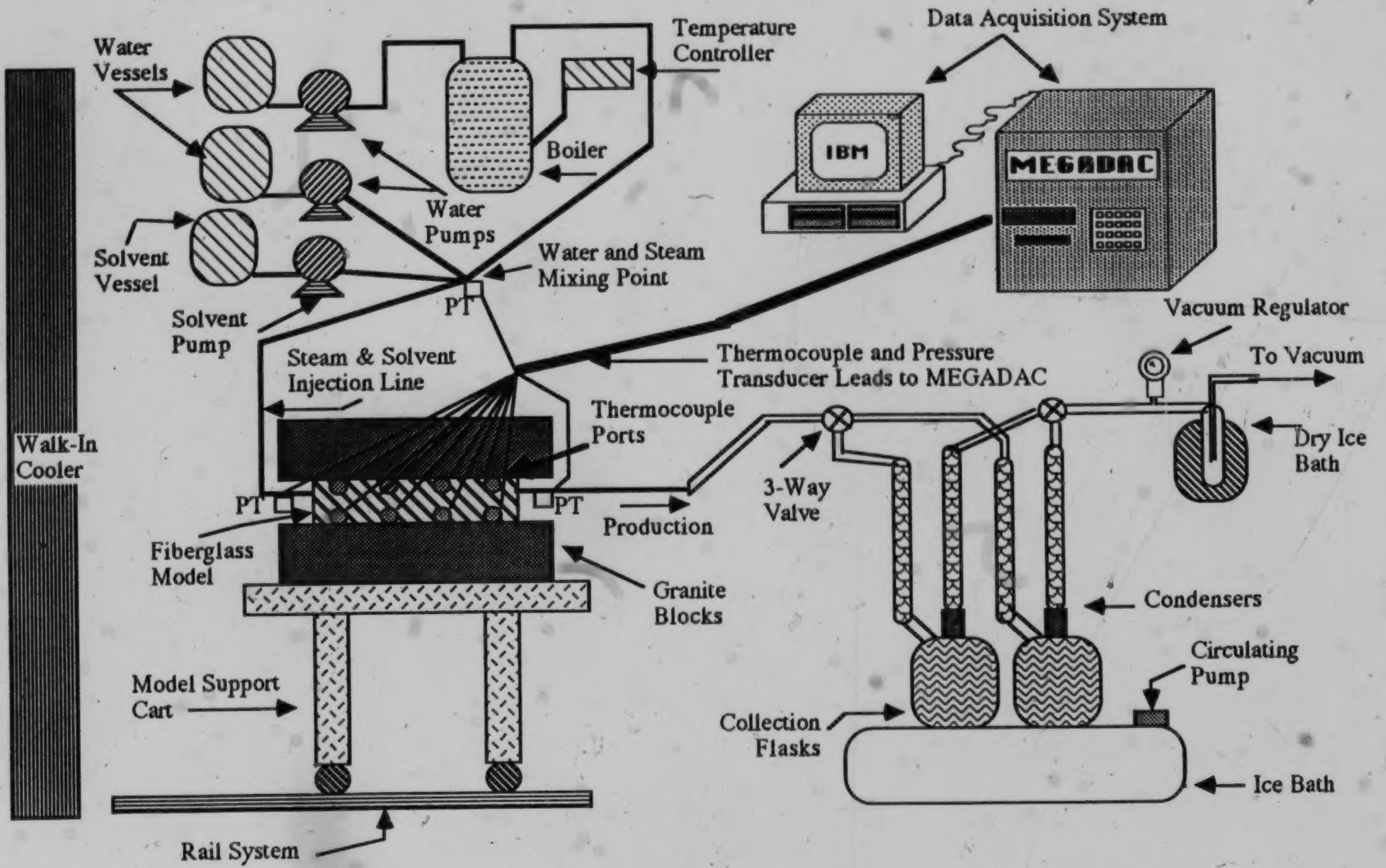
Walk-In Cooler
Water Vessels
Solvent Vessel
Solvent Pump
Water Pumps
Boiler
Temperature Controller
Water and Steam Mixing Point
PT
Data Acquisition System
IBM
MEGADAC
Steam & Solvent Injection Line
Thermocouple and Pressure Transducer Leads to MEGADAC
Thermocouple Ports
PT
PT
Fiberglass Model
Production
Granite Blocks
Model Support Cart
Rail System
3-Way Valve
Vacuum Regulator
To Vacuum
Dry Ice Bath
Condensers
Circulating Pump
Collection Flasks
Ice Bath

Figure 5.1 : Schematic Diagram of Low Pressure Apparatus

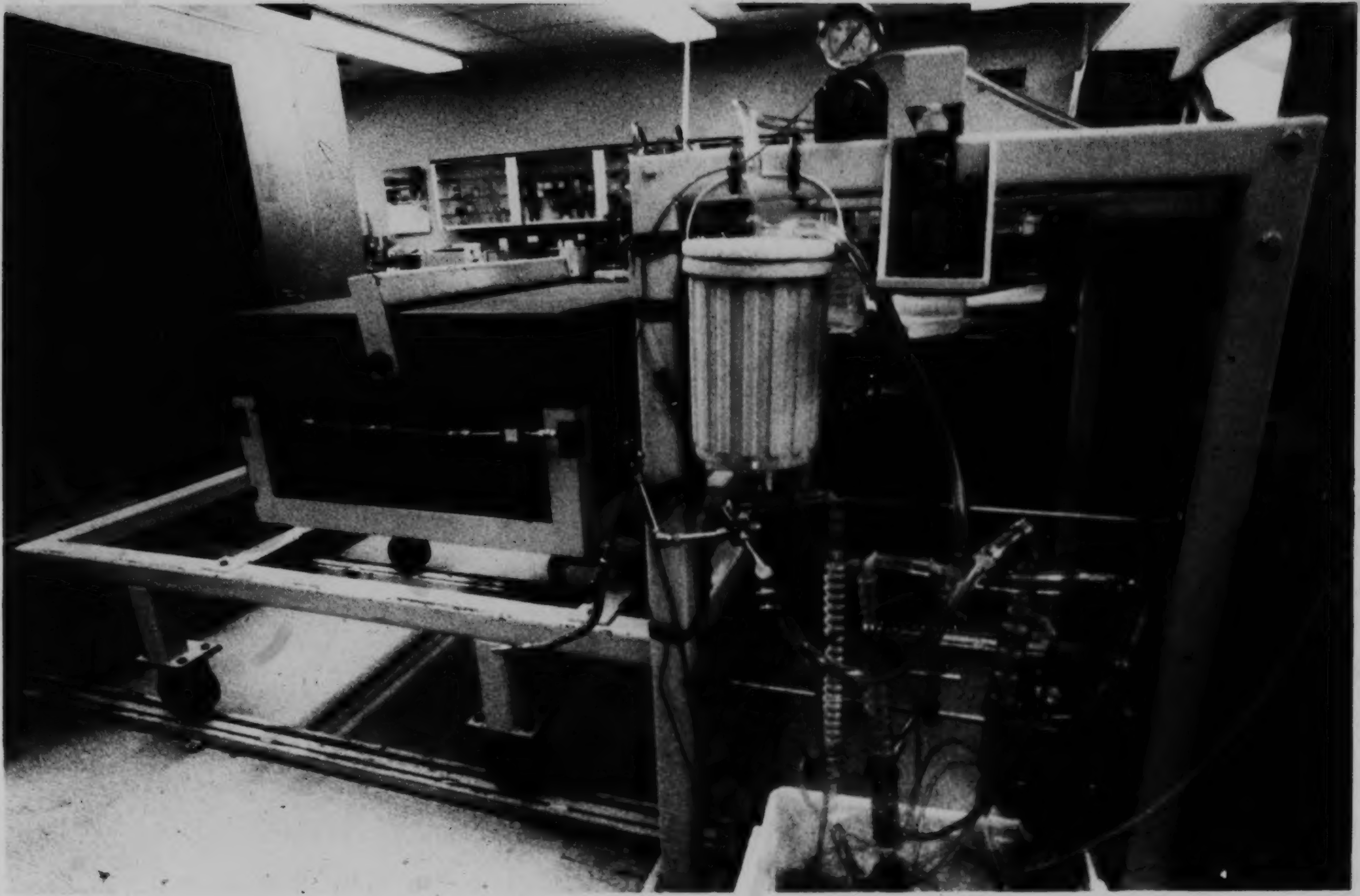

Plate 5.1: Overall View of Low Pressure Apparatus

low pressure conditions the model had to be able to withstand severe loading over a large surface area. Therefore the model was constructed of fiberglass, which could stand up to the high degree of loading. Also considered when selecting fiberglass as the model material is the fact that fiberglass is strong, inexpensive and reasonably easy to machine, which allowed for easy installation of the wells. The fiberglass tray was manufactured to desired specifications by a local manufacturer*.

The injection and production wells installed in the fiberglass tray were essential to the operation of the model. The wells were installed in diagonally opposite corners of the fiberglass tray and were constructed from aluminum rod. The desired production and injection intervals could be achieved in the model quite simply, since the wells were designed with a gate mechanism that could be inserted into the well at various postitions.

As was discussed in the chapter on scaling, a high model permeability of approximately 4200 darcies was required in the model. It was therefore decided that glass beads** approximately 3 mm (6 - 8 mesh) in diameter would have to be used as porous media to achieve the high permeability. Since the glass beads were quite expensive, a procedure was devised to clean and dry the beads after each run so they could be reused.

The purpose of the granite blocks situated above and below the model was to simulate the heat transfer characteristics of the cap and base rock of the Aberfeldy reservoir. The dimensions of each granite block were 91.4 cm (36 in) x 91.4 cm (36 in) square x 21.6 cm (8.5 in) thick†. Each block of granite weighed approximately 2000 pounds. Two metal clamps were attached around the blocks and the fiberglass tray to aid in preventing the top granite block from lifting off the model due to a pressure buildup in the model during an experiment. Cellular neoprene was applied to the open surfaces of the fiberglass tray to minimize heat losses adjacent to the model. Plate 5.2 shows the model situated on the cart with the granite blocks situated above and below the fiberglass tray.

---

* Triple M Fiberglass, 8135 Wagner Road, Edmonton, Alberta.
Cost = $ 400

** Canasphere Industries Ltd., 3344-58th Ave. S.E., Calgary, Alberta.
Cost = $ 9.25 / lb.

† DoAll Edmonton Ltd., 9743-45th Ave., Edmonton, Alberta, 436-0373.

Data Acquisition System

An extensive network of thermocouples[*] and pressure transducers[**] was installed throughout the model in order to collect as much data from each experiment as possible. Thirty-one thermocouples were installed in two layers at strategic locations within the model for recording the heat advance through the model. The approximate positions of thermocouples are illustrated in Figure 5.2. Other thermocouples and pressure transducers were situated at the mixing point, injection well, and the production well. The thermocouples and pressure transducers were connected to a MEGADAC[†] data acquisition device in order to record and store the temperature and pressure readings in the model throughout each run. The MEGADAC data acquisition unit had the capability of monitoring 128 input channels and scanning each of these channels as quickly as 20000 samples per second or as slowly as one sample every 30 minutes. The MEGADAC was programmed to scan each thermocouple and pressure transducer once every thirty seconds. One of the major reasons the MEGADAC was chosen as the data acquisition system was due to its compatibility with the IBM PC. By utilizing an IBM PC along with the computer software provided with the MEGADAC, the IBM PC could be employed to control the data acquisition system and record and store the results of each experiment.

By using the IBM PC along with the MEGADAC, the IBM PC served as a common link between the data acquisition system and the experimenter. The IBM PC allowed one to introduce instructions into the MEGADAC, which then carried out the respective operation and then returned the results of the operation back to the IBM PC. As

---

[*] Thermo Electric (Canada) Ltd., 8425 Argyll Road, Edmonton, Alberta.
Cost = $ 72.99 (thermocouple and wire)

[**] Validyne Engineering Corporation, 8626 Wilbur Avenue, Northridge, California.

[†] Optim Electronics Corporation, Middlebrook Tech Park, 12401 Middlebrook Road, Germantown, Maryland. Cost = $ 26,000

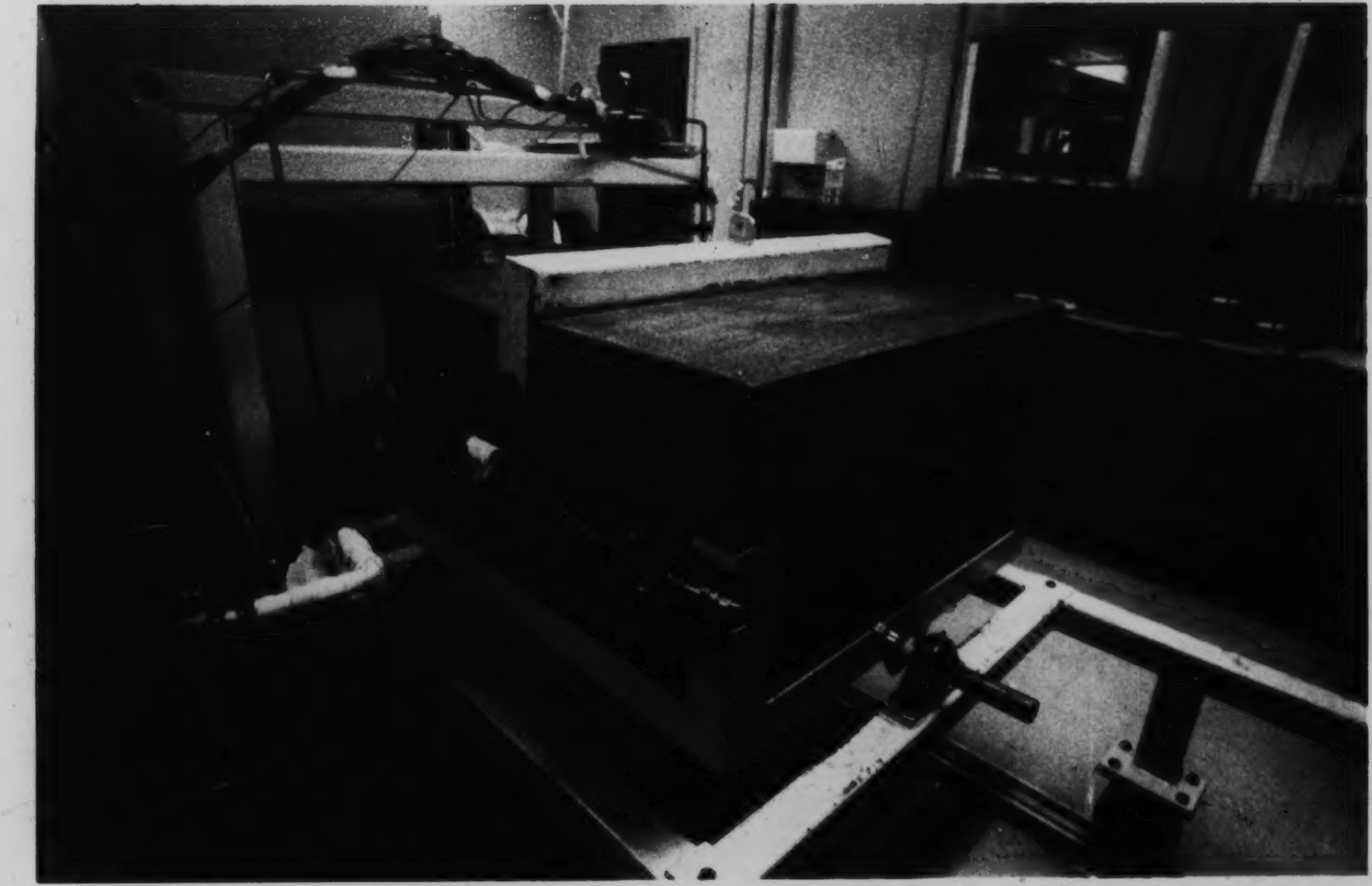

Plate 5.2: Close-up of Model Situated on Cart Between the Granite Blocks

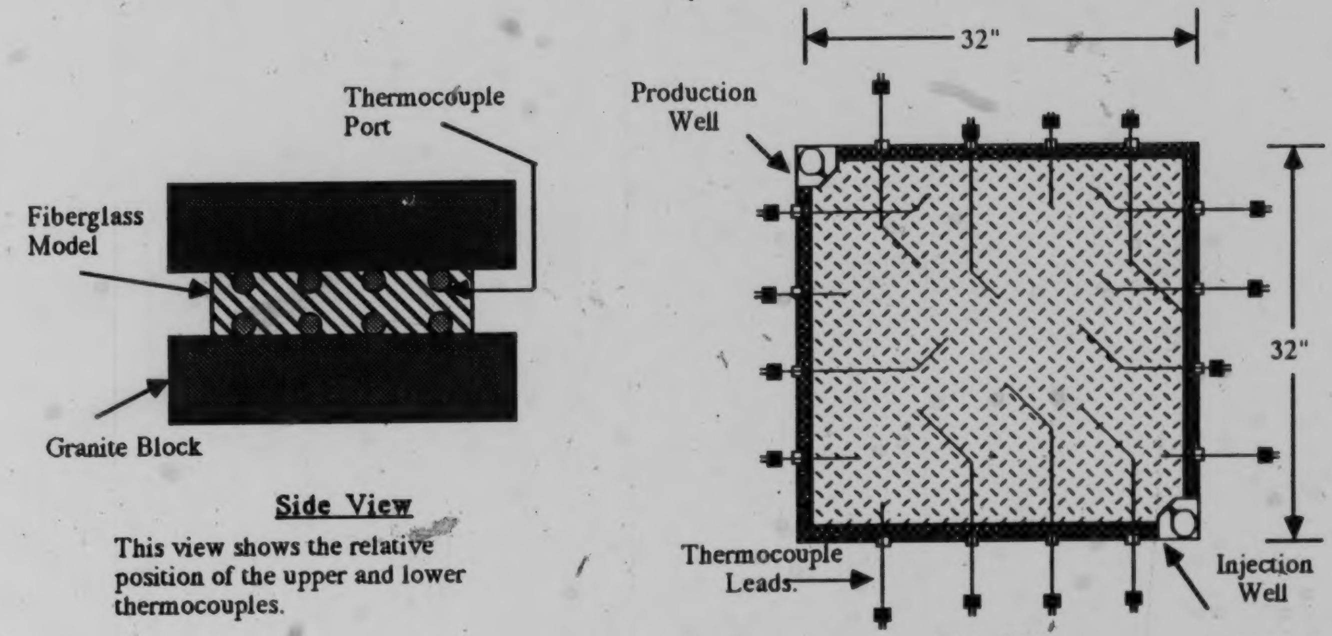
Thermocouple Port
Fiberglass Model
Granite Block
32"
Production Well
32"
Thermocouple Leads
Injection Well

Side View

This view shows the relative position of the upper and lower thermocouples.

Top View

This view illustrates the approximate position of the top layer of thermocouples.

Figure 5.2 : Schematic Diagram of Model Illustrating Thermocouple Positions.

well as these controlling features, the software contained other important capabilities such as being able to graph results of the experiment. Since relatively short experiment times were involved in this research, the MEGADAC data acquisition system was an integral component of the apparatus due to its scanning, recording and storing capabilities.

Solvent and Steam Injection System

The solvent was injected into the model during each experiment using a controlled volume, Milroyal pump. Injection of the solvent into the model was at a relatively large rate (200 cc/min.) so that solvent channelling into the oil zone would be more distinct and extensive. The channelling of the solvent into the oil region was aimed to provide a more conductive path for the steam in the oil zone.

The steam injection system comprised of two Milroyal controlled volume pumps and a low pressure steam generator. One of the pumps pumped water into the steam generator which produced superheated steam while the other pumped quality control water to the mixing point of the steam and water. The water pumped by both Milroyal pumps was distilled and deaerated. Steam at a constant temperature of 120 ^{0}C was generated in the steam generator by electrical heating. The purpose of the two injection lines was to achieve steam quality control. The desired steam quality was controlled by injecting the quality control water at appropriate rates and temperatures into the steam line at the mixing point. The appropriate pumping rates and temperatures were obtained using the heat transfer and mass balance principles discussed in the chapter on scaling.

The stainless steel tubing and fittings needed for the steam injection system were partially insulated between the model and the steam generator in an attempt to minimize heat loss from the lines as much as possible.

Produced Fluid Collection System

The collection system consisted of two series of condensers, two 2000 ml collection vessels, a circulating pump for the condensers, an ice bath, a dry ice cold trap and a vacuum regulator. Figure 5.3 provides a schematic diagram of the collection system.

Due to the vacuum conditions existing during the experiments, the collection system was designed with special features to facilitate the low pressure conditions. The large pore volume of the model (approximately 14000 cm^3) would not permit the use of a single container to collect the produced fluids and with this large a sample little instantaneous results could have been gathered during an experiment. Therefore, two 2000 ml flasks were used to collect the produced fluids. The collection system was designed so that each flask could be individually isolated from the vacuum so that each flask could be emptied separately.

Under vacuum conditions a portion of the produced fluids may vaporize, therefore the collection system was equipped with a dry ice cold trap and a series of condensers to prevent produced fluid loss from the system. During early production, the fluids were at a relatively low temperature (about 3^{0}C) resulting in a partial blockage of the production lines due to the high viscosity of the cold oil being produced. Therefore during the initial stages of an experiment, hot water was circulated through the first series of condensers in order to reduce the produced oil viscosity. As the experiment progressed the temperature of the produced fluids increased, therefore ice water was circulated through the condensers to inhibit vaporization of produced fluids in the collection system. A dry ice (carbon dioxide) trap was installed downstream of the condensers in order to condense any produced vapours that had passed through the condensers.

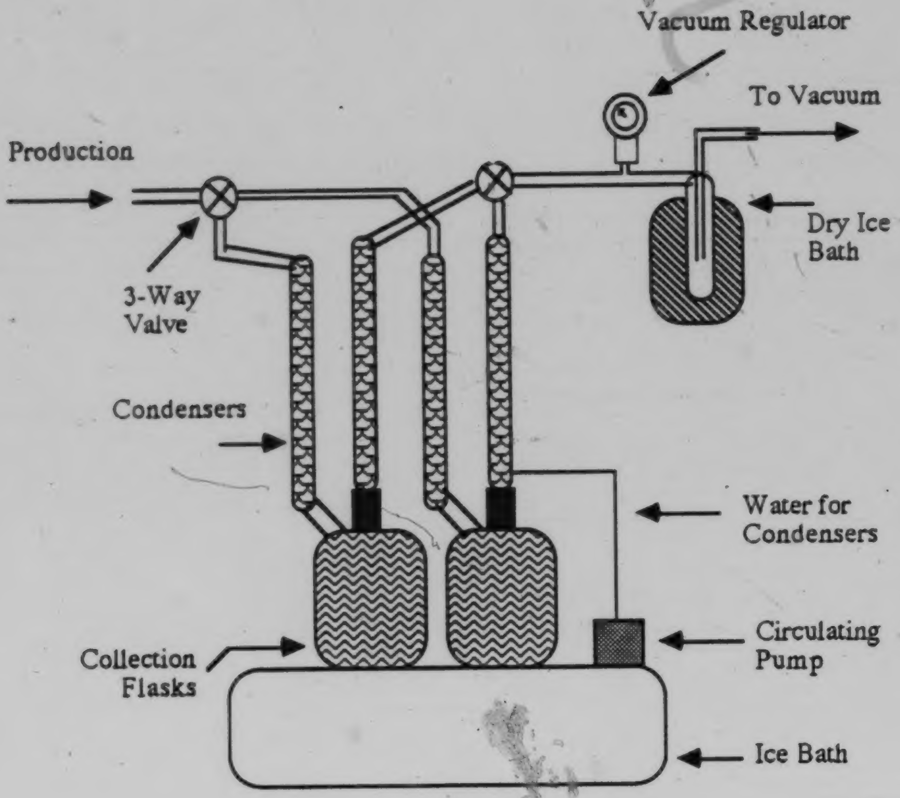
Vacuum Regulator
To Vacuum
Production
Dry Ice Bath
3-Way Valve
Condensers
Water for Condensers
Circulating Pump
Collection Flasks
Ice Bath

Figure 5.3 : Diagram of Collection System for Produced Fluids

Model Cart, Rail System and Cold Storage Compartment

According to the scaling criteria the initial temperature of the model was required to be approximately 3^{0}C. To achieve this low initial model temperature, a castor-equipped support cart and a rail system were included in the design of the model. The support cart and rail system allowed transporting of the model and the two granite blocks into the large cold storage compartment to be cooled prior to each experiment. The 8 ft x 10 ft x 7 ft high, cold storage room was custom built and installed by a local manufacturer*.

The support cart was equipped with a gear box and a rack and pinion system which allowed the model (fiberglass tray and granite blocks) to be easily inclined up to an angle of 45^0 from the horizontal. This capability allowed for a more efficient gravity stabilized front to be achieved during the saturation of the model. Due to the tilting ability of the model, experiments simulating dipping reservoirs could be performed, although there were not part of this research.

Placement and removal of the upper granite block on top of the model (fiberglass tray) was achieved by a hydraulic hoist system. The granite block was placed on the model prior to saturation and removed immediately after each experiment.

Model Fluids

Selection of the Aberfeldy Model Oil

Table 4.3 presented in the previous chapter provides a column detailing the relationship between the required model oil viscosity and the Aberfeldy prototype oil viscosity. Stegemeier et al. [9] stated that the values of μ_{oM} / μ_{oP} in the upper portion of Table 4.3 provide more accurate values, therefore choosing the average of these upper values yielded an average ratio of μ_{oM} / μ_{oP} of 7.26. Applying the prototype versus model temperature relationship (Equation 4.6) along with the calculated viscosity ratio yielded the ideal model oil viscosity at different model temperatures as shown in Table 5.1.

---

* Alberta Zero-Temp Industries Ltd., 11440-81 St., Edmonton, Alberta.
Cost = $ 5387

The actual model oil chosen for the Aberfeldy model that most closely resembled the viscosity-temperature profile of the model oil is the Faxam-100 oil. Figure 5.4 provides a comparison of the viscosity-temperature profiles for the ideal model oil and the Faxam-100 oil, which indicates that the viscosity relationships for both oils match reasonably well. The Faxam-100 was supplied by Imperial Oil Limited*.

Table 5.1 : Temperature Vs. Oil Viscosity for Prototype and Ideal Model Oil

Prototype Temperature (C)	Prototype Oil Viscosity (mPa· s)	Model Temperature (C)	Ideal Model Oil Viscosity (mPa· s)
23.9	1275	3.2	9256.5
32.2	560	5.6	4065.6
65.6	90	15.1	653.4
135.0	12.5	35.0	90.75
301.7	1.29	82.6	9.37

Selection of the Solvent

An extensive viscosity analysis was performed in order to decide upon an appropriate solvent that could be employed in the steamflood experiments of the vacuum model.

The viscosity study involved analyzing Heavy Virgin Naphtha, Light Virgin Naphtha and Synthethic Crude. Each solvent was combined with the model oil (Faxam-100) and the viscosity behaviour of these solvent mixtures was measured at different temperatures and mixture concentrations.

The upper temperature range of the model during a steamflood run was approximately 60^0 to 80^0C, which meant that the Heavy Virgin Naphtha was partially

---

* McEwen's Fuels and Fertilizers Ltd., ESSO Bulk Plant Agent, 3704-92nd Ave., Edmonton, Alberta.

Figure 5.4 : Temperature—Viscosity Profiles for Ideal and Actual Model Oil

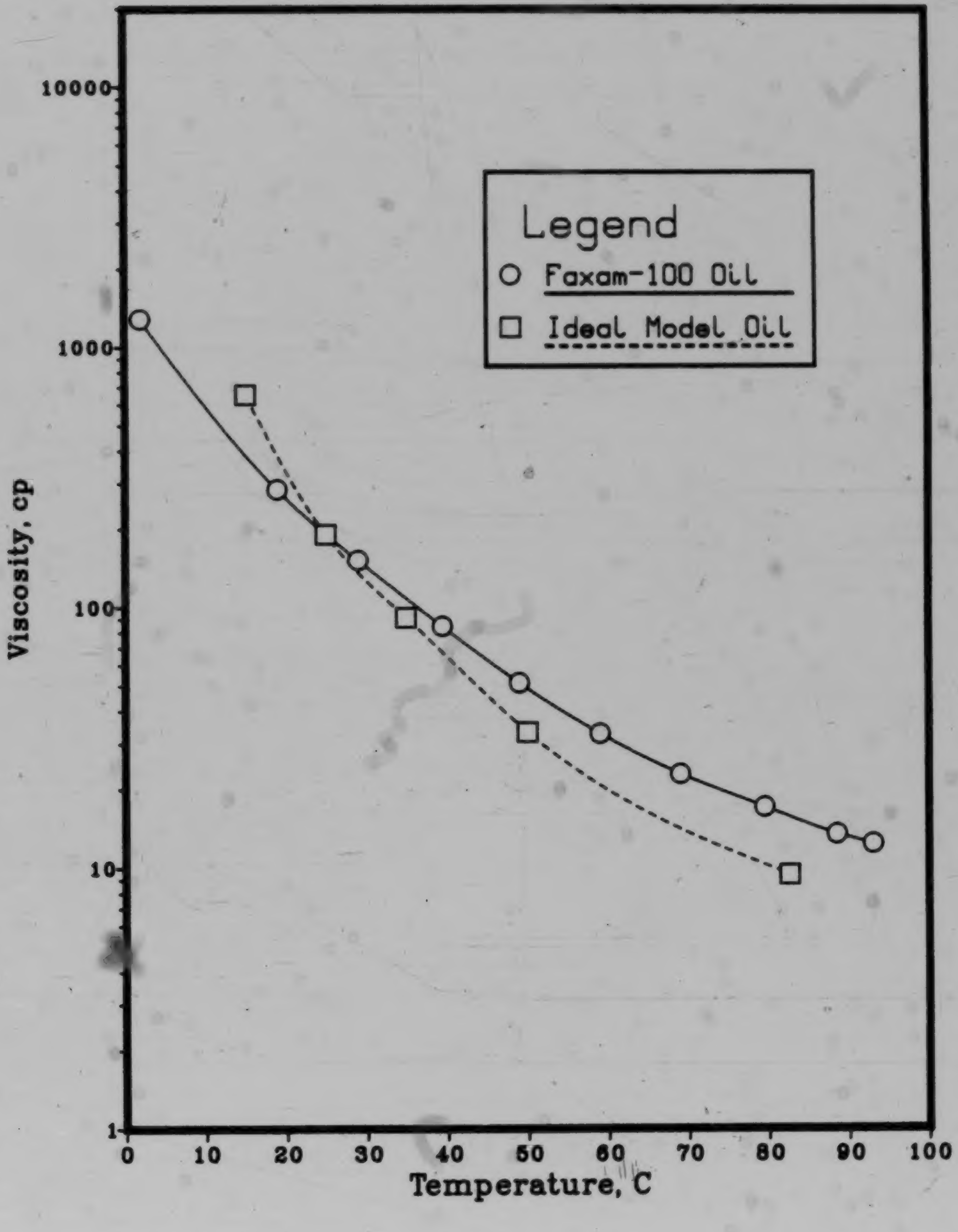

vaporized in this range. Partial vaporization of the solvent was favourable since this further enhanced the mobilization of oil by the diffusion of solvent vapour into the oil ahead of the solvent bank. The Heavy Virgin Naphtha and the Light Virgin Naphtha had very similar viscosities but the Light Virgin Naphtha was not chosen because it had a relatively low initial boiling point (30.5^{0}C) compared to the other two solvents and would almost entirely be vaporized at the model steamflood temperatures. The Heavy Virgin Naphtha was chosen as the solvent since it had a higher initial boiling point (61.0^{0}C) than the Light Virgin Naphtha and lower viscosity values than the Synthetic Crude. By overlaying the viscosity profiles for the Heavy Virgin Naphtha and the Synthetic Crude it was concluded that the Heavy Virgin Naphtha had a greater viscosity reduction capability, which was desirable for the solvent-steamflood recovery process. The viscosity profile for the Heavy Virgin Naphtha is provided in Figure 5.5.

Some pertinent properties of the Heavy Virgin Naphtha are listed below.

$\rho_{HVN} = 0.7320$ g/cm^3
API Gravity = 61.7418^0 API
Initial Boiling Point = 61.0^{0}C
Final Boiling Point = 131.5^{0}C

The Heavy Virgin Naphtha was supplied by ESSO Petroleum Canada, Strathcona Refinery.

Preparation of the Model for an Experiment

Packing of the Model

The first step in performing an experiment involved packing the fiberglass tray with clean, dry glass beads which represented the porous medium. Packing procedures such as vibrating or tamping were not feasible due to the size and shape of the fiberglass tray. Packing of the glass beads in the model was performed using a "particle distributor". Currie and Gregory [60] first devised the particle distributor and Wygal [61] made further modifications to the design of the distributor. Wygal [61] stated that the device could be used

Figure 5.5 : Mixture Viscosity Vs. Heavy Virgin Naphtha Concentration

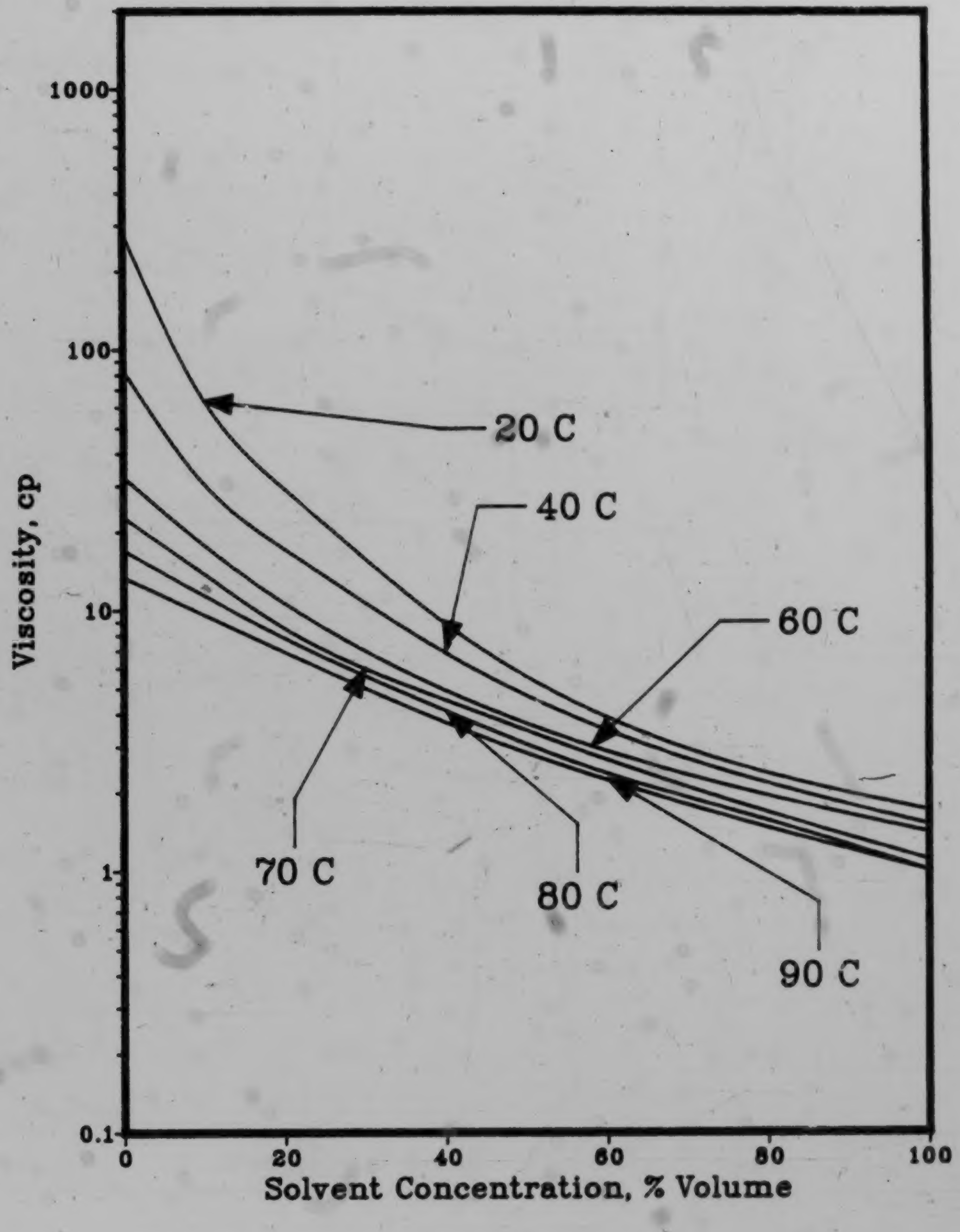

to consistently create many isotropic, homogeneous and stable unconsolidated packs with good results.

As stated by Wygal [61], the use of a particle distributor resulted in more mechanically stable packs with uniform properties throughout, that could be more accurately reproduced. The particle distributor has advantages over other packing methods such as vibrating and tamping, which often give less uniform packs.

The excellent results of the particle distributor were due to the beads striking the pack individually after being thoroughly spread out by a series of five offset wire mesh screens. The openings in the wire mesh screens were offset from one another. This offset in the wire matrix resulted in numerous deflecting surfaces which ensured thorough particle distribution. The offsetting nature of the wire mesh system prevented any dead areas from existing immediately below the screens. A diagram of the side view of the particle distributor is provided in Figure 5.6. A portion of the energy of the falling glass bead was transferred to the surface beads in the pack which were thereby displaced into more stable positions. Wygal [61] reported that the surface of the pack appeared fluid and alive for a depth of two or three particle diameters, as the pack grew.

. Construction of the particle distributor was quite simple. The particle distributor consisted of a plywood box frame with a series of five wire mesh screens having 5/8 inch openings. A gap of two inches existed between each screen and the screens were situated in the upper region of the plywood box frame to allow for adequate separation between the screens and the model tray. The plywood box frame was designed to be placed overtop of the model. The dimensions of the box were 32" x 32" x 26" high. A metering board was placed overtop of the screens to enable the beads to pass through the screens at a constant rate. This provided a continuous supply of beads to all the orifices of the particle distributor until the model was completely filled. Once an adequate amount of beads had passed through the particle distributor and into the model, the distributor was removed and the excess beads were scraped from the top of the bead pack surface. Bead pack porosities

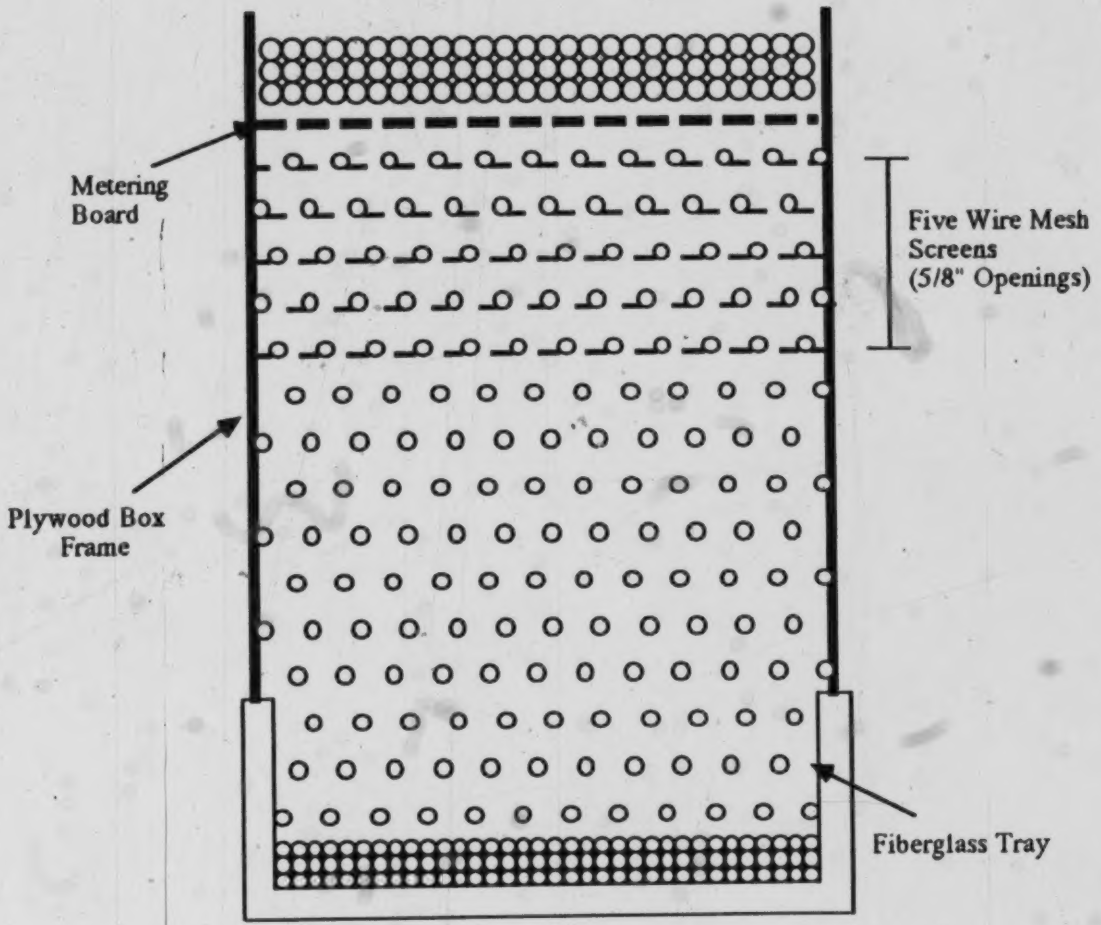
Metering Board
Plywood Box Frame
Five Wire Mesh Screens (5/8" Openings)
Fiberglass Tray

Figure 5.6 : Particle Distributor Used as a Packing Device for Model

obtained using the particle distributor were reasonably consistent at about 33% for homogeneous packs. For the bottom water models the porosity of the bead packs were slightly higher due to the packing procedure required to form the bottom water layer. The porosities obtained in the bottom water models were around 36%. The slight increase in porosity was due to a less uniform bead pack in the bottom water zone as a result of the packing procedure for the bottom water model.

Saturation of the Model

Once the bead pack was complete, a Teflon sheet was placed over the fiberglass tray and was affixed to the tray by a silicone sealant which was evenly applied to the rim of the tray. A vacuum was then applied to the model to ensure an adequate vacuum seal. When a proper vacuum seal was achieved the model was evacuated and the bead pack became a very solid and stable structure. After the model was totally evacuated, a rubber sheet was placed on top of the Teflon sheet to ensure complete contact between the porous medium and the upper granite block which was placed on the model using the hydraulic hoist system.

The apparatus was then tilted using the gear box and rack and pinion system. In the tilted position the fluids enter the model from downdip and are drawn upward through the model due to the vacuum applied at the updip end. Flow of fluids from downdip to the updip end created a more efficient gravity stabilized front which allowed a more thorough and uniform saturation of the model. Six large saturation ports were installed in the model. Three ports were situated at the downdip end and the other three were located at the updip end. The ports also improved the efficiency of the saturation process since the fluids were introduced into the model over the entire width.

The initial stage of the saturation involved drawing distilled, deaerated water up into the model through the three saturation ports at the downdip end. The porosity of the bead pack was calculated by measuring the volume of water pulled into the model and dividing this volume by the bulk volume of the model which was measured prior to packing. Once the model was saturated with water it was then saturated with the Faxam-100 oil in the same manner as the water. The amount of water displaced by the oil was measured in order to determine the irreducible water saturation and the initial oil saturation existing in the model.

With oil and water saturation complete, two metal clamps were attached to the model to help maintain the models vacuum in the event of an internal pressure surge during a run, which could exceed atmospheric pressure. This would have resulted in the vacuum seal being broken.

When the saturation procedure was complete, the valves at the production and injection ends of the model were closed to isolate the evacuated model from atmospheric conditions. The model was then moved into the cold storage room in order to lower the model temperature to 3^0C as required by the scaling criteria. Cooling of the model in the cold storage room required 24 to 36 hours.

Preparation of Bottom Water Model

Since the investigation dealt with marginal reservoirs containing bottom water and/or a gas cap, a procedure was designed that allowed a bottom water region to be created in the model.

The procedure involved filling the lower portion of the model with glass beads and a 5% salt (NaCl) water solution. After the bottom water layer was frozen, the remaining upper portion of the model was packed with glass beads and saturated with oil and water according to the procedure discussed previously. As mentioned earlier, the porosities of the bottom water models (36%) were higher than the porosities achieved for the homogeneous models (33%). Since the glass beads in the bottom water layer were not packed using the particle distributor, the resulting porosities were higher due to a less uniform bead pack in the bottom water layer.

The bottom water thicknesses achieved in the various experiments of this study ranged from about 8% to 26% of the gross model thickness. The thickness of the bottom water was somewhat controlled by the volume of the 5% salt water solution frozen in the model. The larger the volume of salt water solution frozen in the model, the thicker the bottom water layer created. The usual volume of 5% NaCl solution frozen in the model was 8000 ml, whereas the thicker bottom water cases used a volume of 10000 ml. Exact control of the bottom water thickness could not be achieved, because during the saturation of the upper portion of the model some of the frozen bottom water was contacted by the overlying water and oil which saturated the upper model region. This resulted in some of the bottom water melting and consequently being produced.

The actual thickness of the bottom layer created in the model was determined by measuring the amount of the 5% NaCl solution that was produced from the model with the saturation water. The amount of 5% salt water solution contained in each produced saturation sample was determined by measuring the refractive index of each sample and comparing the measured refractive index-concentration relationship given in Figure 5.7. The points of the graph were determined by measuring the refractive indices of various NaCl solutions with concentrations between 0% and 5% NaCl. Plotting these measured refractive indices yielded a relatively linear relationship of refractive index to NaCl concentration. The fraction of 5% NaCl solution in the sample was calculated by applying the lever rule to Figure 5.7. The total amount of 5% NaCl solution produced from the model during saturation could be used to determine the amount of 5% NaCl solution remaining in the model which represents the bottom water zone pore volume. In other words, the approximate amount of bottom water in the model is known and the amount of bottom water lost in the saturation process is corrected for. The thickness of the bottom water zone was calculated as a fraction of the total model thickness by dividing the bottom water zone pore volume by the total model pore volume.

Figure 5.7 : Refractive Index Vs. Percentage of NaCl in a Salt Water Solution

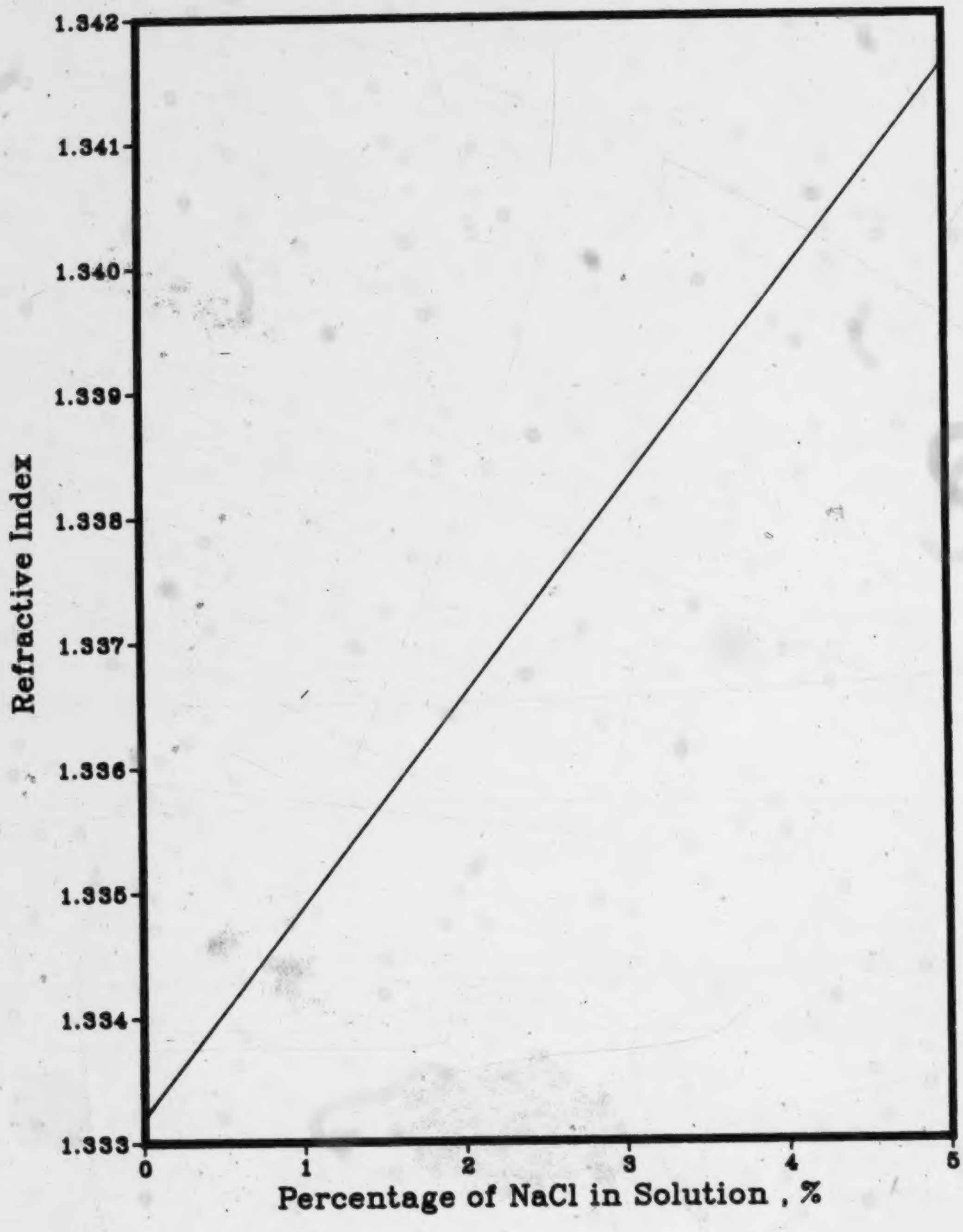

The packing and saturation procedure for the upper region of a bottom water model was identical to a homogeneous model except that due to the presence of the frozen bottom water layer in the model, less beads, water and oil were required to pack and saturate the top portion of the model.

Creation of a Gas Cap in the Model

As was mentioned previously, this investigation was devoted to oil recovery from marginal reservoirs containing bottom water and/or a gas saturation "gas cap". By injecting a small portion of an inert gas prior to an experiment, it was believed that a gas cap could be created which would divert the injected fluid away from the bottom water region and into the oil zone. The heat scavenging effects of the bottom water zone was believed to be somewhat mitigated by the presence of the gas cap.

The gas cap was created by injecting nitrogen gas into the upper region of the model which displaced a small portion of oil in the model. Prior to a run, a gas cap was formed by applying a vacuum to the production well end and then injecting nitrogen into the model through the injection well at an injection pressure of 1 psig. The low injection pressure was chosen to prevent the top granite block from lifting off of the model and breaking the vacuum seal. To provide a consistent gas injection procedure for each experiment the nitrogen gas was injected until no more oil was produced, or one prototype year (12.18 minutes) of gas injection was reached. The volume of the gas cap formed was assumed to be the amount of oil displaced by the injected gas. Nitrogen gas was selected as the gas since it is inert and therefore would not initiate a chemical reaction in the model during the recovery experiments.

The gas saturations created in the gas cap experiments were relatively small and ranged from 0.3% to 0.6% of the total model pore volume. Since the gas saturations were small it was concluded that the injected gas created a narrow gas channel in the top region of the bead pack between the injection and production wells. This procedure was adequate for the study since it was desired to observe what effect a gas saturation in the upper region of the model had on the injectivity of the solvent and steam in the oil zone of the model.

Conducting the Experiments

While the model was cooling in the cold storage compartment other tasks were carried out in preparation for the experiment. Preparation involved filling the water and solvent injection bottles and applying a vacuum to the water bottles to deaerate the water. All lines to and from the model were checked for any leaks and the oil was changed in the vacuum pumps.

Once the model had cooled to the desired temperature of 3^{0}C it was moved out of the cold storage compartment. The thermocouples and pressure transducers installed in the model were connected to the MEGADAC data acquisition unit. Test scans were performed by the MEGADAC on the thermocouples and pressure transducers to determine if they were operating properly. When all of the thermocouples and pressure transducers were found to be working properly the MEGADAC was programmed for the experiment during which the MEGADAC would scan each thermocouple and pressure transducer every thirty seconds. During the run the recorded data would be printed and stored on the IBM hard disk drive. Once the MEGADAC had been initiated for the experiment the injection and production lines were connected to the model and a vacuum was applied to the production system. The steam generator and both of the Milroyal pumps delivering the water and steam to the model were activated in order to achieve the desired steam temperature (between 60^{0}C and 70^{0}C) and quality. The steam was passed through the bypass line to the production system until the required steam temperature was reached. With this temperature reached the bypass was closed and the Milroyal pumps for the steam were shut down.

With preparation complete the experiment was ready to begin. To initiate the run, the production well was opened with the vacuum still applied to the production end. The injection well was then opened and the appropriate pumps were activated to inject the desired fluid into the model. During the solvent-steamflood experiments the desired slug of solvent (Heavy Virgin Naphtha) was injected into the model followed by the continuous injection of steam. For the continuous steamflood experiments, the steam was the only fluid injected into the model. During the experiments, produced liquids from the model were gathered in the two, 2000 ml production vessels. As the produced fluid filled each collection flask it was transferred to a numbered 2000 ml graduated cylinder, in which the amount of oil, solvent and water were later measured.

The amount of solvent present in the oil-solvent sample of each cylinder was determined by measuring the refractive index of each sample. The measured refractive indices were compared to the plot of refractive index versus solvent concentration of the sample (Figure 5.8). The points for the curve in Figure 5.8 were determined by measuring the refractive index of various Faxam-100 and solvent (Heavy Virgin Naphtha) mixtures at solvent concentrations ranging from 0 to 100%. These measured values were then plotted to yield Figure 5.8. The amount of solvent in each oil-solvent sample was calculated by applying the lever rule to Figure 5.8 which provided the amount of solvent in each oil-solvent sample.

Since the experiments carried out were time-dependent, the samples contained in the graduated cylinders were kept in chronological order so to measure the changing amount of solvent, oil and water in each cylinder as the experiment progressed.

The experiment was continued until approximately two pore volumes of steam had been injected into the model. Upon completion of the run both the vacuum pump and the Milroyal pump were shut down, the model was disconnected from the injection and production systems and the MEGADAC was turned off. The granite block and Teflon sheet were removed from the top of the model in order to visually analyze what portions of the model were affected most by the recovery process during the experiment. The amounts of oil, water and solvent in each cylinder were measured and recorded for future analysis.

Figure 5.8 : Refractive Index Vs. Volumetric Fraction of Heavy Virgin Naphtha

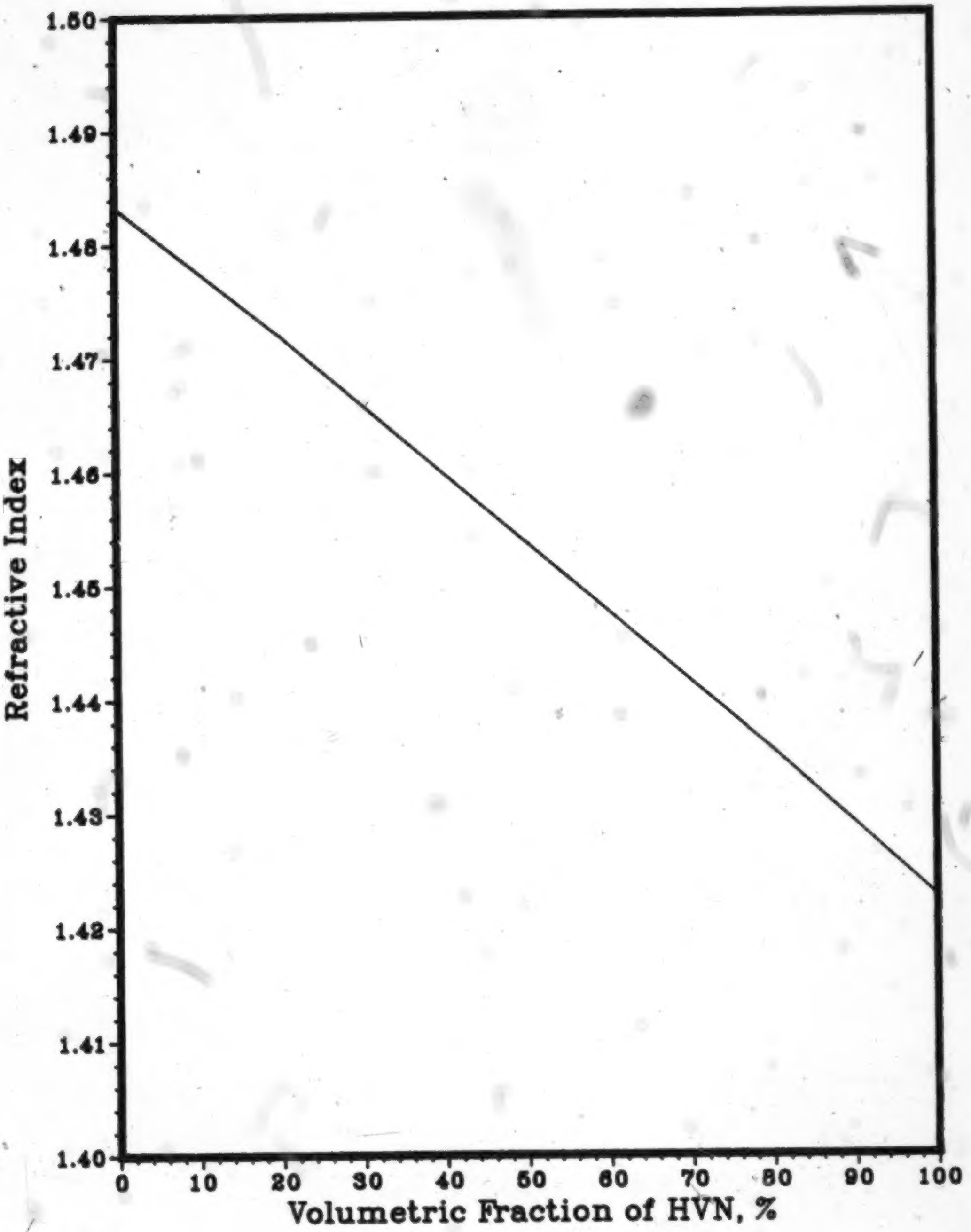

Clean Up of the Apparatus

With the experiment complete and all of the run data collected, the model and other experimental apparatus were cleaned in preparation for the next experiment.

The glass beads were first removed from the model and washed with a degreasing agent* which removed a majority of the oil from the beads. A laboratory detergent was then used to remove any remaining oil from the beads. The beads were then placed in a five foot tall, stainless steel cylinder where they were dried by forcing air to flow through the beads.

The excess oil, water and beads were cleaned from the model and silicone remaining on the edges of the fiberglass tray and Teflon sheet were scraped off. Once the model had been cleaned, the bent thermocouples were straightened to their original positions and any that were broken were replaced. Finally, the cylinders and production system were thoroughly emptied and washed. The model was then ready for the next experiment.

Analysis of Experimental Data

Following each experiment, the data accumulated and stored by the MEGADAC data acquisition unit was arranged in tabular form. The table generated for each experiment lists the pertinent data recorded from each run and from this information, oil and solvent recoveries were determined. Also presented in the table are the percentage of oleic phase in each sample, bead pack characteristics, initial and final oil and water saturations, solvent and steam injection rates and volume of injected solvent and steam. The data from the table was then used to generate a series of descriptive plots, which were analyzed to determine what occurred in the model during the experiment and the effectiveness of the recovery process that was implemented.

---

* Slik No. 5 degreaser, supplied by Baroid of Canada, Ltd., Calgary, Alberta, 263-8740.
Cost = $ 2.40 / litre.

The first graph involved plotting the cumulative oil (Faxam-100) recovered versus the pore volumes of fluids injected into the model. The shape of the curve provided generalized information on the mechanics of the run, such as at what stage of the experiment was the bulk of the recovered oil produced, approximately how long it took breakthrough to occur and how evident the banking of oil in the model was. The recovery plots of different experiments were compared to determine which recovery process yielded the highest and the quickest recovery of oil from the model.

The next two plots created were bar graphs. One plot illustrates the relationship of the volume as a percentage of oleic phase for each sample taken versus the cumulative volume of fluid injected. The other bar graph gives the instantaneous produced water-oil ratio versus the cumulative volume fluid injected. As with the recovery curves, analysis of the bar plots provided an indication of when breakthrough took place during a run as well as a limited indication of the stability of the displacement existing in the model.

Another plot generated from the experimental data was instantaneous oil/steam ratio versus cumulative oil produced. The plot indicated when breakthrough occurred as well as when other events took place during a run such as the production of the oil bank at the production well.

Implementation of a commercially available contouring package* made it possible to generate temperature profiles of the model at various times throughout the experiments.

Two sets of temperature profiles were constructed for each experiment. The first group consisted of isotherms from a top view perspective at different times during a run (0.25 to 2.00 pore volumes, every 0.25 pore volumes injected). Since two layers of thermocouples were installed in the model the profile contained two sets of isotherms, one set representing the temperature profile in the upper half of the model and the other set describing the temperature distribution in the lower portion of the model. To distinguish between the upper model profile and the lower model profile, a different line type was used for each set of isotherms so not to confuse the upper and lower sets of contour lines. Figure 5.9 represents a sample of a top view temperature profile.

---

* DISSPLA, a proprietary software product of Integrated Software Systems Corporation, 10505 Sorrento Valley Road, San Diego, Ca.

Observation of these profiles may show that in some cases the heat front advanced faster through the upper part of the model, which was indicated by the upper isotherms extending further out into the model than the lower isotherms. Similarly, if the heat front was travelling faster through the lower section of the model the temperature profile would indicate the lower isotherms moving faster than the upper contour lines.

The second group of plots gave cross-sectional temperature profiles of the model at various instances throughout an experiment (0.25 to 1.00 pore volumes, every 0.25 pore volumes injected). Similarly to the top view temperature profiles, the cross-sectional temperature profiles could also be used to determine how the heat advanced through the model during an experiment. Figure 5.10 represents a sample of a cross-sectional temperature profile.

Asymmetrical movement of the contour lines in the profiles may have been due to non-uniform movement of the heat front, caused by such factors as an irregularity in the bead pack or a variation in the saturation. However, some deviations in the contour lines resulted from shortcomings of the contouring package used. For example, cases existed where an isotherm overlapped itself or where two different isotherms crossed over one another. In other instances, the contouring package improperly interpreted the existence of zero degree isotherms which were not present. It was concluded that these defects were due to imperfections in the software of the contouring package. Despite the defects in the contouring package, the temperature profiles created gave a fair representation of the heat front movement through the model. Keeping in mind the defects of the contouring package, the temperature profiles were utilized to investigate the heat advance in the model for each experiment.

Figure 5.9 : Run 39

Steamflood of Bottom Water Model

Temperature Profile for
0.25 Pore Volumes Injected

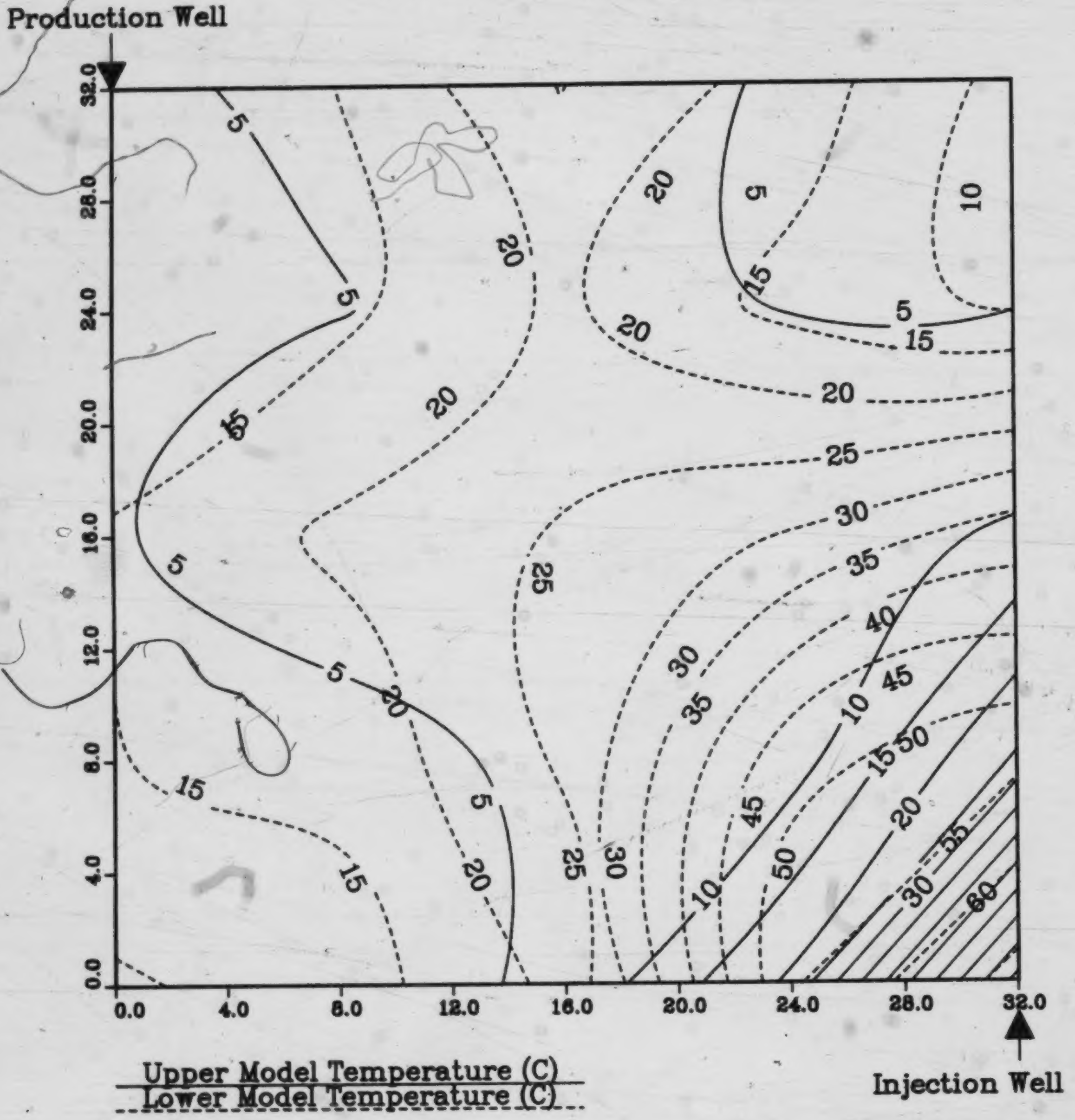

Figure 5.10 :Run 39 Temp Profile
Injector to Producer Cross–Section

0.25 Pore Volumes Injected.

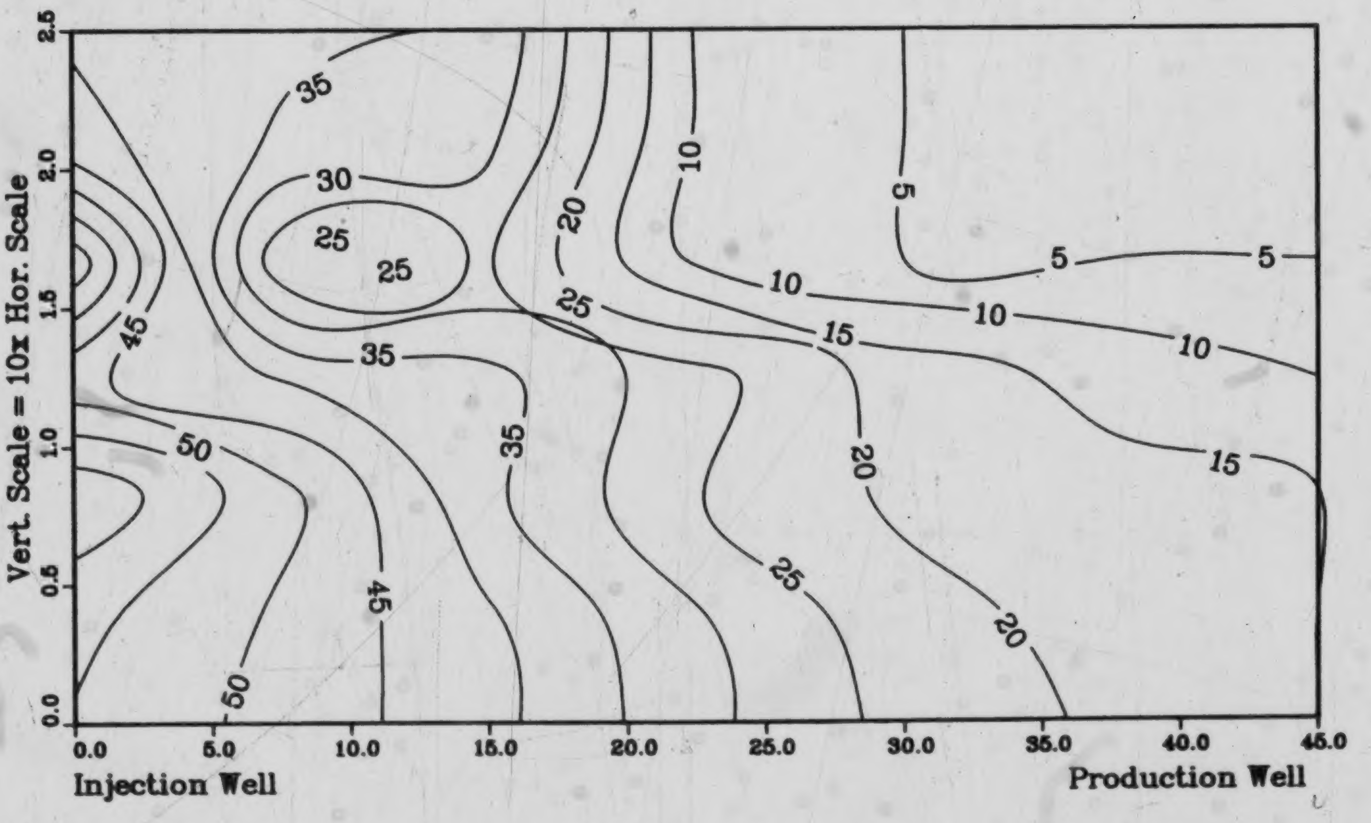

The plots and temperature profiles generated for each experiment were compared with those for other runs in order to examine the variation in production response and overall oil recovery caused by altering the recovery techniques, experimental parameters or run conditions. Some of the run parameters varied were the thickness of the bottom water layer, the presence of bottom water and/or a gas cap, the injection of a solvent slug prior to steamflooding, the solvent slug size, and the injection and production intervals.

Chapter VI

Discussion of the Results

Presentation of the Results

The following chapter is a discussion of the results of the present experimental study, using the low pressure, scaled model for investigating the steamflood process under bottom water conditions. The main emphasis of the study was on the use of a small amount of solvent with steam in an attempt to improve the steamflood efficiency. The purpose of using solvents in combination with steam was to increase steam injectivity in the oil zone, and create an initial flow path in the oil layer to divert the steam partially from the underlying water. The results of experiments using other strategies to better the steamflood efficiencies are included. Also provided in the section is a theoretical heat flow analysis performed on a selected steamflood experiment.

Various types of experiments were performed during the research investigation. Table 6.1 lists the pertinent values and results for all the experiments conducted during this investigation. The first group of runs consisted of base experiments which were compared with later experiments in order to observe the effects of different parameters such as solvent injection, solvent slug size, bottom water thickness, gas injection, injection-production interval locations and the use of alternative recovery schemes. These base experiments involved a continuous solvent flood in a homogeneous model, a solvent-steamflood in a homogeneous model and a steamflood with prior gas injection in a bottom model.

There were numerous, different runs carried out after the preliminary base experiments. A series of these proceeding experiments examined the effect of solvent slug size on oil recovery by a steamflood for cases of bottom water and no bottom water. Also studied was the effect of bottom water thickness on steamflood and solvent-steamflood responses. From these experiments one was able to determine if and why a solvent-steamflood was more effective than straight steam injection when bottom water was

Table 6.1 : List of Experiments

Run No.	Model Type	Type of Process	Inj. & Prod. Intervals	Porosity (%)	Soi (%)	Swi (%)	Sgi (%)	Bottom Water (%)	Slug Size (% P.V.)	Cum. Rec. (%OOIP) *	Solv. Rec. (%) *	Cum. P.V. Injected
39	BWM	SF	IE -PU	37.1	86.0	14.0	---	12.5	---	16.8	---	1.78
40	HM	CSI	IE - PU	33.7	92.5	7.5	---	---	---	26.8	89.5	2.25
41	HM	USR	IE - PU	---	---	---	---	---	---	---	---	---
42	HM	USR	IE - PU	---	---	---	---	---	---	---	---	---
43	HM	USR	IE - PU	---	---	---	---	---	---	---	---	---
44	HM	SSF	IE - PU	33.7	92.9	7.1	---	---	10.0	27.1	70.4	2.33
45	HM	SSF	IE - PU	34.1	92.0	8.0	---	---	10.0	30.0	71.2	2.59
46	HM	SSF	IE - PU	38.7	80.9	19.1	---	---	10.0	27.7	33.1	2.07
47A	HM	WF	IE - PU	33.6	93.0	7.0	---	---	---	19.1	---	1.54
47B	HM	SSF	IE - PU	33.6	75.3	24.7	---	---	10.0	33.5	44.9	2.03
48A	HM	WF	IE - PU	33.4	92.7	7.3	---	---	---	19.8	---	1.69
48B	HM	SSF	IE - PU	33.4	74.3	25.7	---	---	10.0	33.5	58.9	2.25
49	BWM	SSF	IE - PU	37.0	86.7	13.3	---	8.8	10.0	23.3	84.6	2.13
50	BWM	SSF	IU - PE	35.8	91.2	8.8	---	10.2	10.0	25.4	88.5	2.26
51	BWM	SSF	IU - PE	37.7	66.9	33.1	---	26.2	10.0	14.3	40.8	2.05
52	BWM	USR	IU - PE	---	---	---	---	---	---	---	---	---
53	BWM	SSF	IU - PE	36.5	76.2	23.8	---	15.2	10.0	19.0	54.4	2.16
54	BWM	SSF	IU - PE	36.1	91.0	9.0	---	12.2	10.0	22.6	89.8	2.39
55	HM	GISSF	IU - PE	34.3	90.3	9.1	0.6	---	10.0	26.8	87.7	2.37
56	HM	GISSF	IU - PE	33.6	93.0	6.3	0.6	---	10.0	27.0	90.9	2.43
57	BWM	USR	IU - PE	---	---	---	---	---	---	---	---	---
58	BWM	GISSF	IU - PE	35.6	86.4	13.0	0.6	9.8	10.0	18.2	88.6	2.27

Table 6.1 : Continued

Run No.	Model Type	Type of Process	Inj. & Prod. Intervals	Porosity (%)	Soi (%)	Swi (%)	Sgi (%)	Bottom Water (%)	Slug Size (% P.V.)	Cum. Rec. (%OOIP) *	Solv. Rec. (%) *	Cum. P.V. Injected
59	BWM	GISSF	IU - PE	35.7	85.3	14.1	0.6	13.6	10.0	24.7	96.7	2.30
60	BWM	GISF	IU - PE	35.9	76.3	23.4	0.3	17.6	---	13.6	---	2.31
61	BWM	GISF	IU - PE	36.0	83.5	16.2	0.4	12.1	---	19.5	---	2.30
62	BWM	GISSF	IU - PE	36.3	83.4	16.3	0.3	12.0	10.0	20.0	94.7	2.29
63	BWM	SFPBW	IU - PE	36.3	77.5	22.5	---	15.4	---	17.0	---	2.26
64	BWM	SFPBW	IU - PE	36.7	87.5	12.5	---	9.9	---	22.0	---	2.27
65	BWM	SSF	IU - PE	36.1	73.4	26.6	---	19.6	20.0	19.8	73.0	2.29
66	HM	SSF	IU - PE	33.5	93.3	6.7	---	---	5.0	24.2	91.4	2.59
67	HM	SSF	IU - PE	33.5	92.5	7.5	---	---	15.0	25.9	97.0	2.43

HM - Homogeneous Model
BWM - Bottom Water Model
SF - Continuous Steamflood
CSI - Continuous Solvent Injection
SF - Steamflood
SSF - Solvent-Steamflood
WF - Waterflood
GISF - Gas Injection Prior to Steamflood

GISSF - Gas Injection Prior to Solvent-Steamflood
SFPBW - Steamflood with Partial Bottom Water Barrier
USR - Unsuccessful Run
IU - Injection Into Upper Portion of Model
IE - Injection Over Entire Model Interval
PU - Production From Upper Portion of Model
PE - Production From Entire Model Interval

* - The Cumulative Oil and Solvent Recoveries listed in the table correspond to the Cumulative Pore Volume Injected which is provided in the last column of this table.

present. The effect of gas injection prior to steamflooding on oil recovery from homogeneous and bottom water formations was studied in another set of runs. A similar group of experiments examined the change in oil recovery due to gas injection prior to the solvent-steamflood of reservoirs with or without a bottom water zone. Other experiments investigated the effect of injection-production interval locations. Another set of runs considered the implementation of a physical barrier between the oil and water zones during a steamflood to divert the steam away from the bottom water. In other experiments the model was waterflooded prior to solvent and steam injection. A map of the various experiments conducted is provided in Figure 6.1, where the abbreviations in the figure are the same as used in Table 6.1.

The corresponding tables and figures (recovery curves, bar plots and oil/steam ratio plots) for each experiment are included throughout the chapter as each experiment is discussed. The two sets of temperature profiles (top view and cross-sectional view) are referred to throughout the discussion and are grouped in Appendix A, in view of the massive volume of data processed.

The final stage of the research study involved a theoretical heat flow analysis of a steamflood. The analysis consisted of estimating the growth and volumes of the steam zone and hot water region during the steamflood using three classical steam injection theories developed by Lauwerier [68], Marx and Langenheim [5] and Mandl and Volek [69]. A heat balance of the model was performed throughout the steamflood in order to estimate the amount of heat lost from the model during the experiment. The results of the analysis are provided in tabular form and are included throughout the discussion of the heat flow analysis. The four computer programs developed and implemented in this analysis are provided in Appendix B. These programs utilized the theories of Lauwerier, Marx and Langenheim and Mandl and Volek, as well as performing a heat balance in order to yield estimates of the generalized heat transfer behaviour that occurred in the model during an experiment.

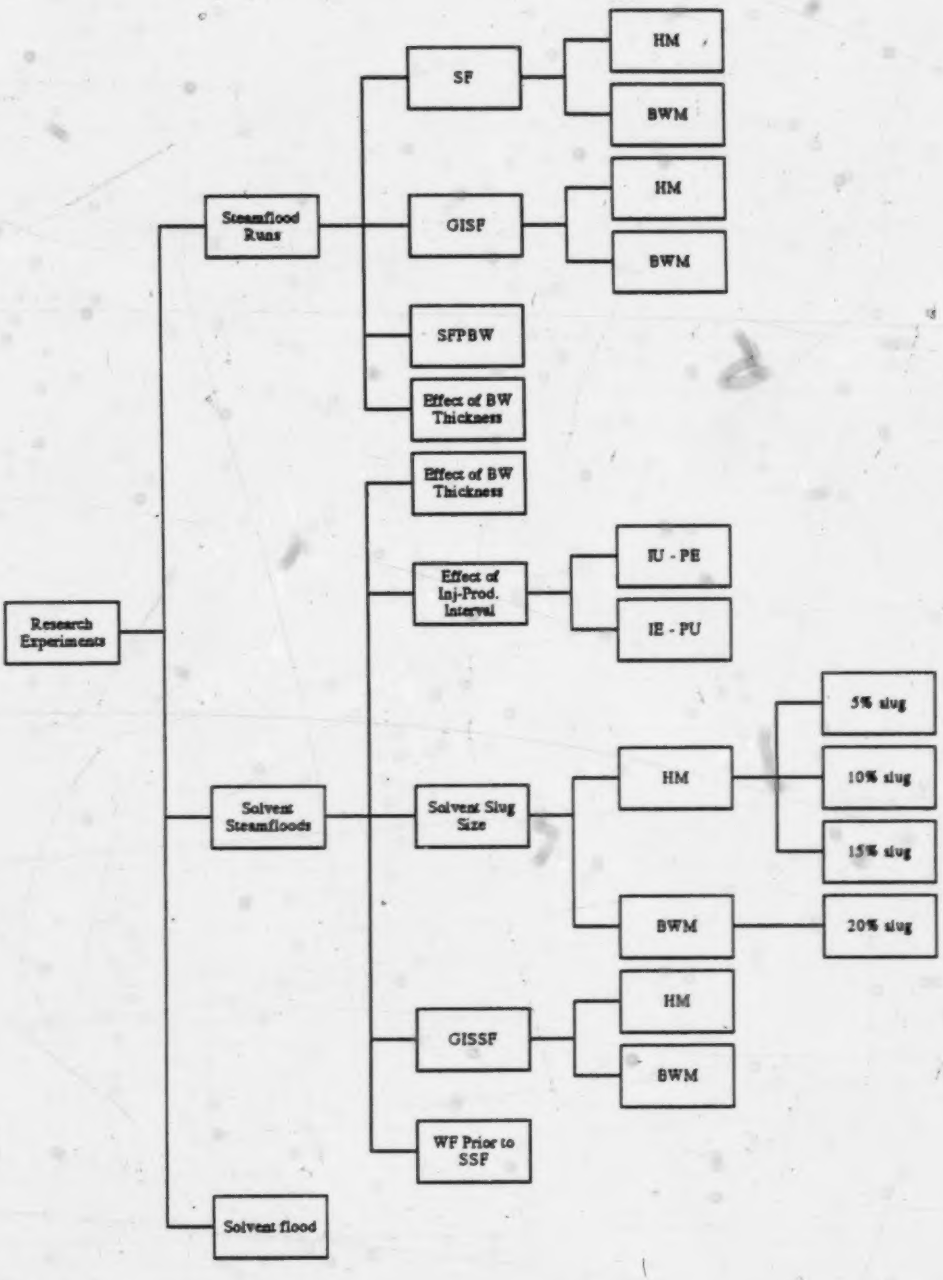
HM
SF
BWM
HM
Steamflood Runs
GISF
BWM
SFPBW
Effect of BW Thickness
Effect of BW Thickness
IU - PE
Effect of Inj-Prod. Interval
IE - PU
Research Experiments
5% slug
HM
10% slug
Solvent Steamfloods
Solvent Slug Size
15% slug
BWM
20% slug
HM
GISSF
BWM
WF Prior to SSF
Solvent flood

Figure 6.1 : Map of Experimental Runs Conducted During the Research Project

Steamflood versus Solvent-Steamflood Process

The steamflood process which is also known as a steam drive or steam displacement is a very important heavy oil recovery technique. Steamflooding is analagous to a waterflood in that steam is injected into the reservoir on a pattern basis, as in a waterflood. It has been reported [62] that a steamflood can be used quite effectively in light and moderately viscous oil reservoirs, also.

During a steamflood, steam is injected into the injection well resulting in the creation of a steam zone which expands radially outward from the injector into the reservoir as more steam is injected. The hot condensate leaving the steam zone creates a hot waterflood in front of the steam zone. As the hot condensate cools down to the formation temperature, it creates a cold waterflood effect ahead of the hot water and the steam zones. Therefore a steamflood process consists of a steam zone, a hot waterflood zone, and a cold waterflood zone. The oil recovery is due to the recovery mechanisms operating in each of the zones.

The steam zone which is at an approximately constant temperature T_s is the most essential component of a steamflood. Oil in this region is highly mobilized by the heating effect of the steam and is displaced by the gas drive effect of steam. Also the thermal expansion of oil further mobilizes the oil, and steam distillation of lighter fractions of the oil helps to lower the oil saturation as well.

The mobilized oil is displaced and banked up ahead of the steam zone in the condensate region. Before the steam invades the oil region ahead of the steam zone, the undisturbed oil zone has already been swept by the cold condensate and then the hot condensate. In essence, the advancing steam zone contacts the same oil saturation, whether the formation is previously waterflooded or not. An illustration of the different regions that exist in the reservoir during a steamflood is provided in Figure 6.2.

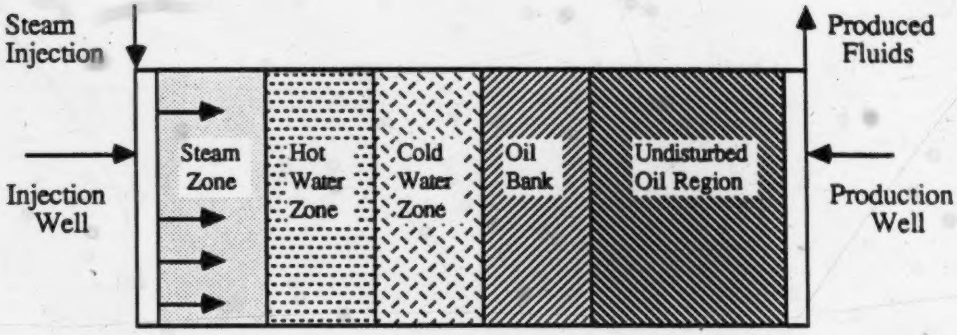

Figure 6.2 : Schematic Diagram of a Steamflood Process

Excellent areal coverage is usually obtained during a steamflood due to the gravity segregation of the steam which causes the steam to rise up through the formation until it condenses. Gravity segregation of the steam is always present and can limit vertical sweep in thick reservoirs.

The efficiency of a steamflood process is strongly dependent on formation thickness, steam quality, steam temperature and the presence of bottom water, since these factors determine the rate of growth of the steam zone.

The presence of a bottom water layer in a thin heavy oil formation is undesirable since it provides a highly conductive flow path for the injected steam to underride the oil layer. This lowers the thermal efficiency of a steamflood because a majority of the steams heat is scavenged by the underlying water.

The solvent-steamflood process is quite similar in nature to a steamflood except that a small slug of solvent is injected into the formation prior to steamflooding. The injected solvent channels directly into the oil region which forms an initial flow path for the steam. Therefore the heating effect of the steam can be more effectively utilized to mobilize and displace the oil in the reservoir. A schematic diagram of the solvent-steamflood process is given in Figure 6.3.

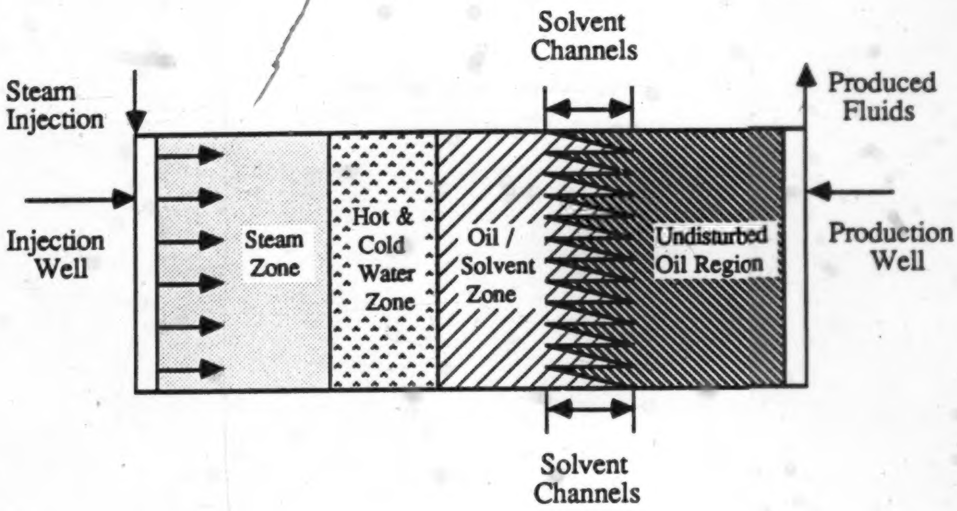
Solvent Channels
Steam Injection
Produced Fluids
Injection Well
Steam Zone
Hot & Cold Water Zone
Oil / Solvent Zone
Undisturbed Oil Region
Production Well
Solvent Channels

Figure 6.3 : Schematic Diagram of Solvent - Steamflood Process

Thin heavy oil formations, with underlying water are considered to be uneconomic for a conventional steamflood for reasons discussed previously. Therefore the purpose of using solvents in combination with a steamflood is to improve steam injectivity in the oil zone, and create an initial flow path in the oil layer in order to divert the steam partially from the underlying water. It is believed that the solvent-steamflood process can be a economically viable heavy oil recovery method.

Typical Steamflood History in a Bottom Water Reservoir

To obtain a better understanding of the production history of a typical steamflood in a bottom water formation, consider Run 39, which consisted of a steamflood in a bottom water model. The purpose of the experiment was to provide one with reasonable insight into what results were to be expected in a continuous steamflood of a thin heavy oil formation, with underlying water. The model used in Run 39 had a bottom water layer thickness which was 12.5% of the gross model thickness, i.e. one-eighth of the model thickness. The experimental results of Run 39 are listed in Table 6.2.

The net oil recovery of Run 39 was 16.8% which was substantially less than the recovery yielded by Run 26 which was a conventional steamflood of a homogeneous model. The oil recovery in Run 26 was 31.8%, as reported by Proctor, George and Farouq Ali [63], which indicates that the bottom water layer in Run 39 had an adverse effect on the effectiveness of the steamflood process.

The recovery curve created for Run 39, given in Figure 6.4, appeared to be a fairly linear relationship with no drastic increase or drop in the oil recovery at any time during the experiment. This suggested that the steam preferentially flowed underneath the oil layer into the less flow resistant bottom water region due to lower steam injectivity of the above oil layer. Therefore a majority of the steam heat was scavenged by the underlying water zone. Due to the bottom water layer, the formation of a well-pronounced steam zone and oil bank in the model was inhibited which resulted in an unstable steam displacement of the oil and thus a poor oil recovery.

Two bar plots of volume as a percentage of oleic phase in each sample taken versus cumulative volume injected and instantaneous produced water-oil ratio (WOR) versus cumulative volume injected were generated from the results of Run 39 and are provided in Figures 6.5 and 6.6, respectively. As well as indicating little oil production, both plots gave no indication that a well-defined steam breakthrough occurred during the experiment. It was therefore concluded that a very unstable steam displacement existed in the model due to a poorly developed steam zone. The absence of a pronounced steam breakthrough and the lack of an established steam zone both pertained to the presence of bottom water in the model.

Figure 6.7 provides a graph of instantaneous oil/steam ratio versus cumulative oil produced for Run 39. The plot does not have a very drastic rise in the oil/steam ratio values during the first part of the experiment which again suggested that the steam displacement of the oil was not as efficient during the steamflood process due to the bottom water zone.

The top view temperature profiles given in Figures A.1 through A.6 and the cross-sectional temperature profiles provided in Figures A.7 through A.10 for Run 39 illustrate

Table 6.2 : Run 39 Conventional Steamflood of Bottom Water Model

HC Pore Volume : 13400.0 cc
Pore Volume : 15580.0 cc
Bulk Volume : 42005.0 cc
Porosity : 37.1%
Initial Oil Satn. : 86.0%
Initial H2O Satn. : 14.0%

Type of Oil Used : Faxam-100
Initial Model Temperature : 3.00 C
Water Feed Flow Rate : 200.00 cc/min
Boiler Feed Flow Rate : 29.20 cc/min
Total Flow Rate of Steam : 229.20 cc/min
Steam Vol. Inj. : 27775.0 cc (1.78 PV)
Bottom Water Layer Thickness : 12.5% (% Gross Thickness)

Net Oil Recovery : 16.8%

Final Oil Saturation : 71.6%

Cyl. No.	Tot. Vol. Inj. (cc)	Cum. Vol. Inj.		Oil Prod. (cc)	Cum. Oil Rec.		Oil-Steam Ratio	Inst Prod. WOR	Inst. Oil Prod. % of Sample
		(cc)	(P.V.)		(cc)	(%OOIP)			
1	1895	1895	0.12	125	125	0.9%	0.0706	14.16	6.6%
2	2130	4025	0.26	250	375	2.8%	0.1330	7.52	11.7%
3	1910	5935	0.38	290	665	5.0%	0.1790	5.59	15.2%
4	2050	7985	0.51	205	870	6.5%	0.1111	9.00	10.0%
5	1990	9975	0.64	240	1110	8.3%	0.1371	7.29	12.1%
6	2005	11980	0.77	170	1280	9.6%	0.0926	10.79	8.5%
7	1930	13910	0.89	205	1485	11.1%	0.1188	8.41	10.6%
8	1965	15875	1.02	140	1625	12.1%	0.0767	13.04	7.1%
9	1910	17785	1.14	130	1755	13.1%	0.0730	13.69	6.8%
10	2020	19805	1.27	35	1790	13.4%	0.0176	56.71	1.7%
11	1920	21725	1.39	110	1900	14.2%	0.0608	16.45	5.7%
12	2020	23745	1.52	115	2015	15.0%	0.0604	16.57	5.7%
13	2030	25775	1.65	115	2130	15.9%	0.0601	16.65	5.7%
14	2000	27775	1.78	120	2250	16.8%	0.0638	15.67	6.0%

Figure 6.4 :Run 39 Continuous Steamflood
Cumulative Oil Recovery Vs. Pore Volumes Injected

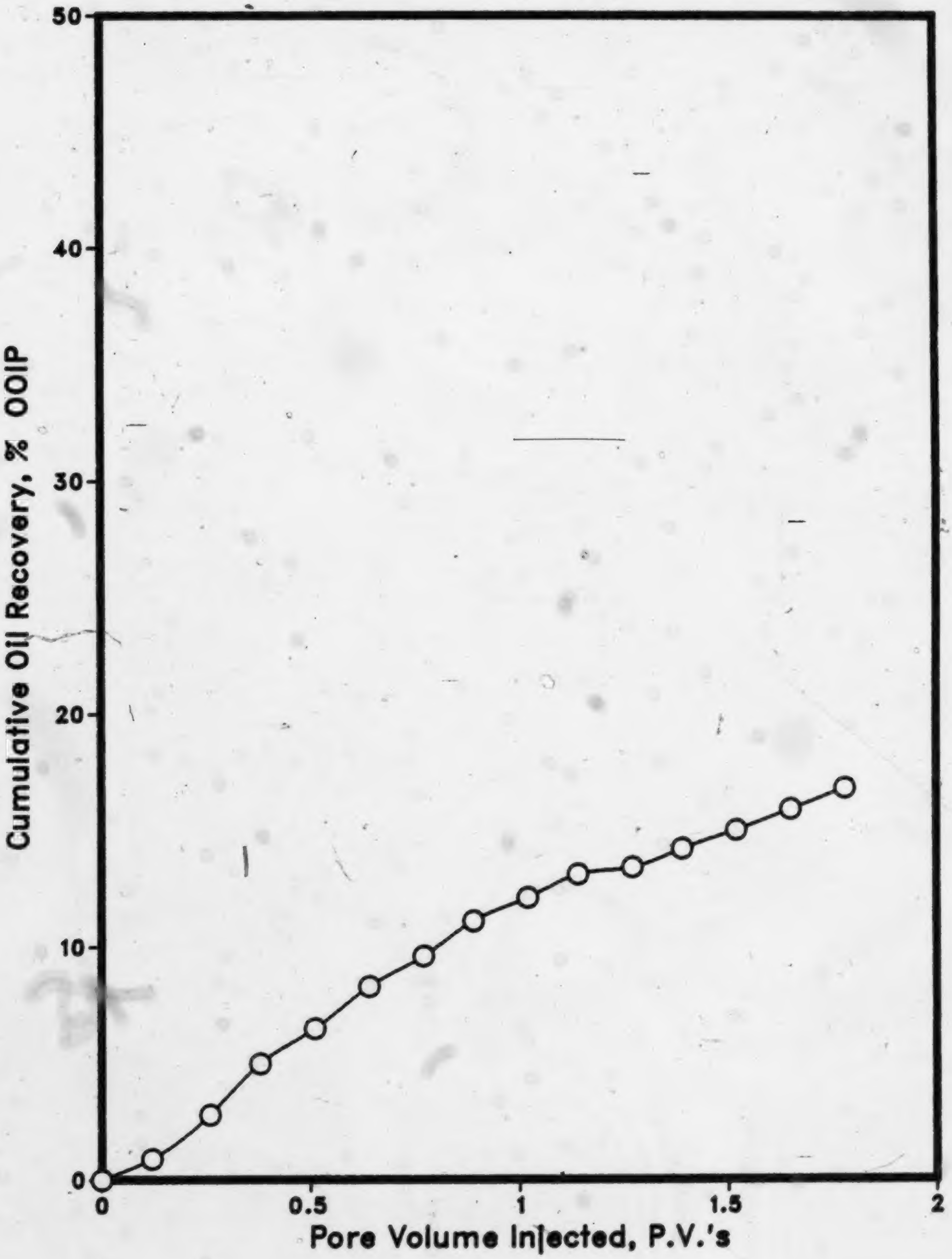

Figure 6.5 :Run 39 Continuous Steamflood
Oleic Phase in Each Sample Vs. Cumulative Volume Injected

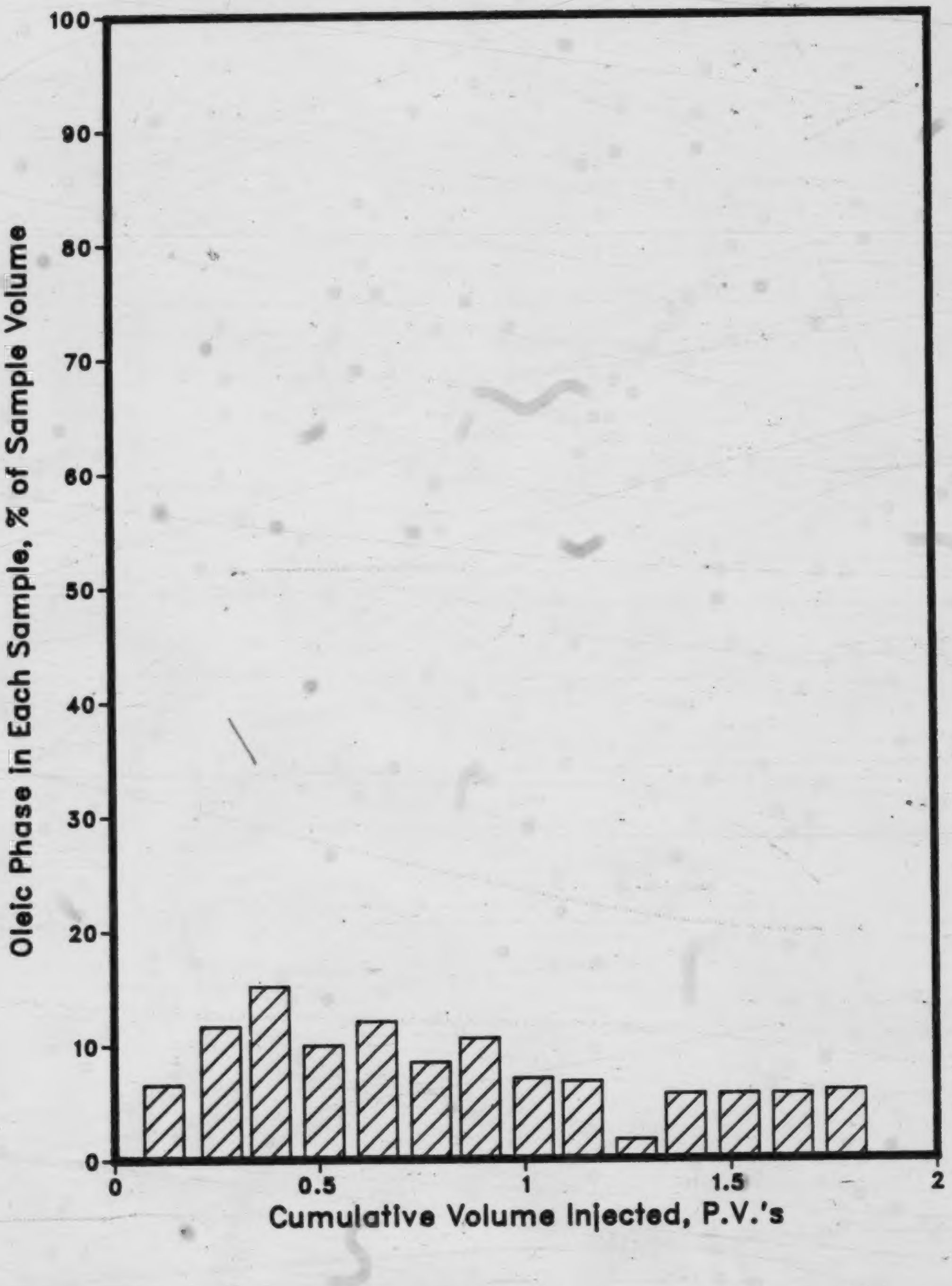

Figure 6.6 :Run 39 Continuous Steamflood
Instantaneous Produced WOR Vs. Cumulative Volume Injected

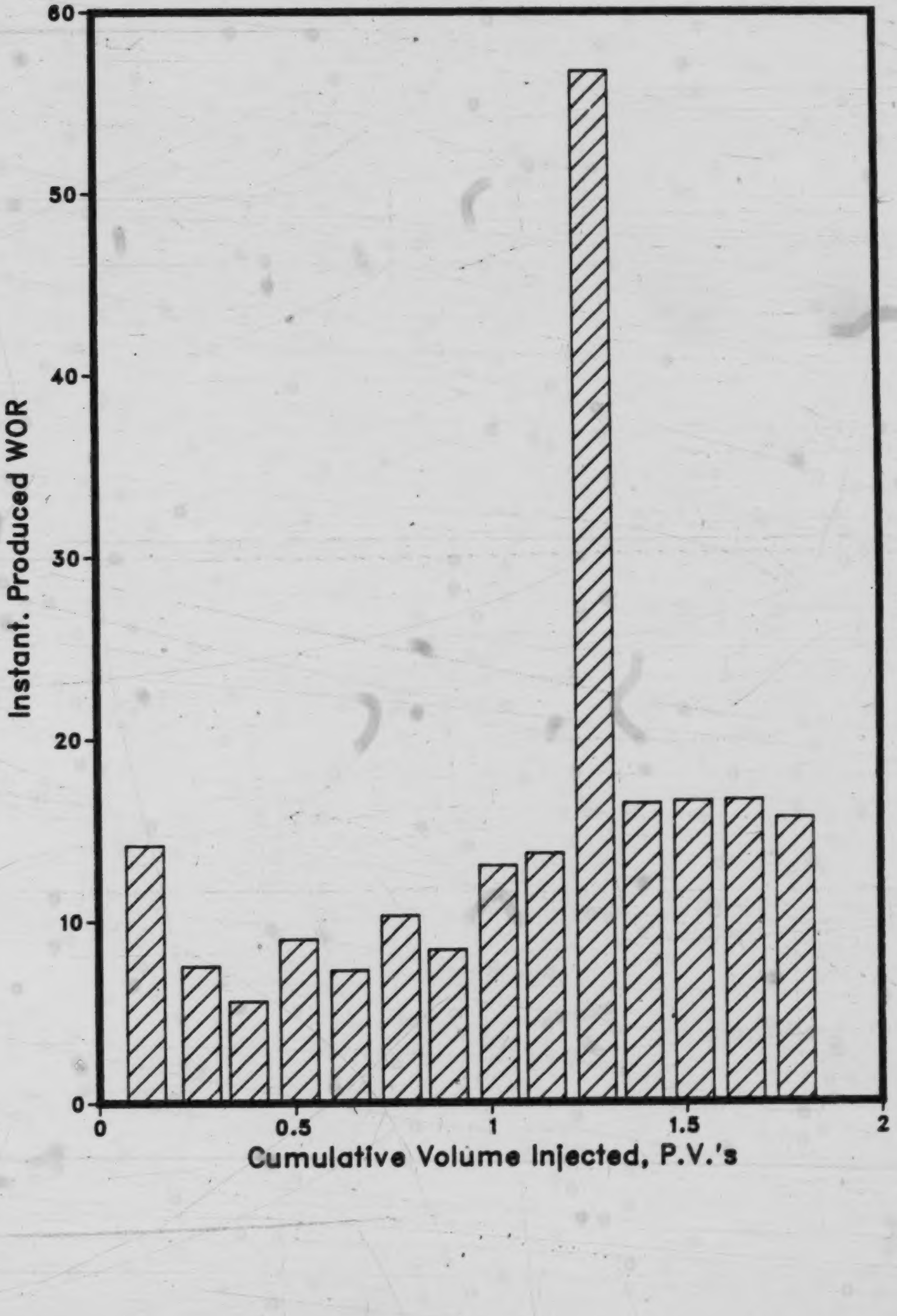

Figure 6.7 :Run 39 Continuous Steamflood
Instantaneous Oil/Steam Ratio Vs. Cumulative Oil Produced

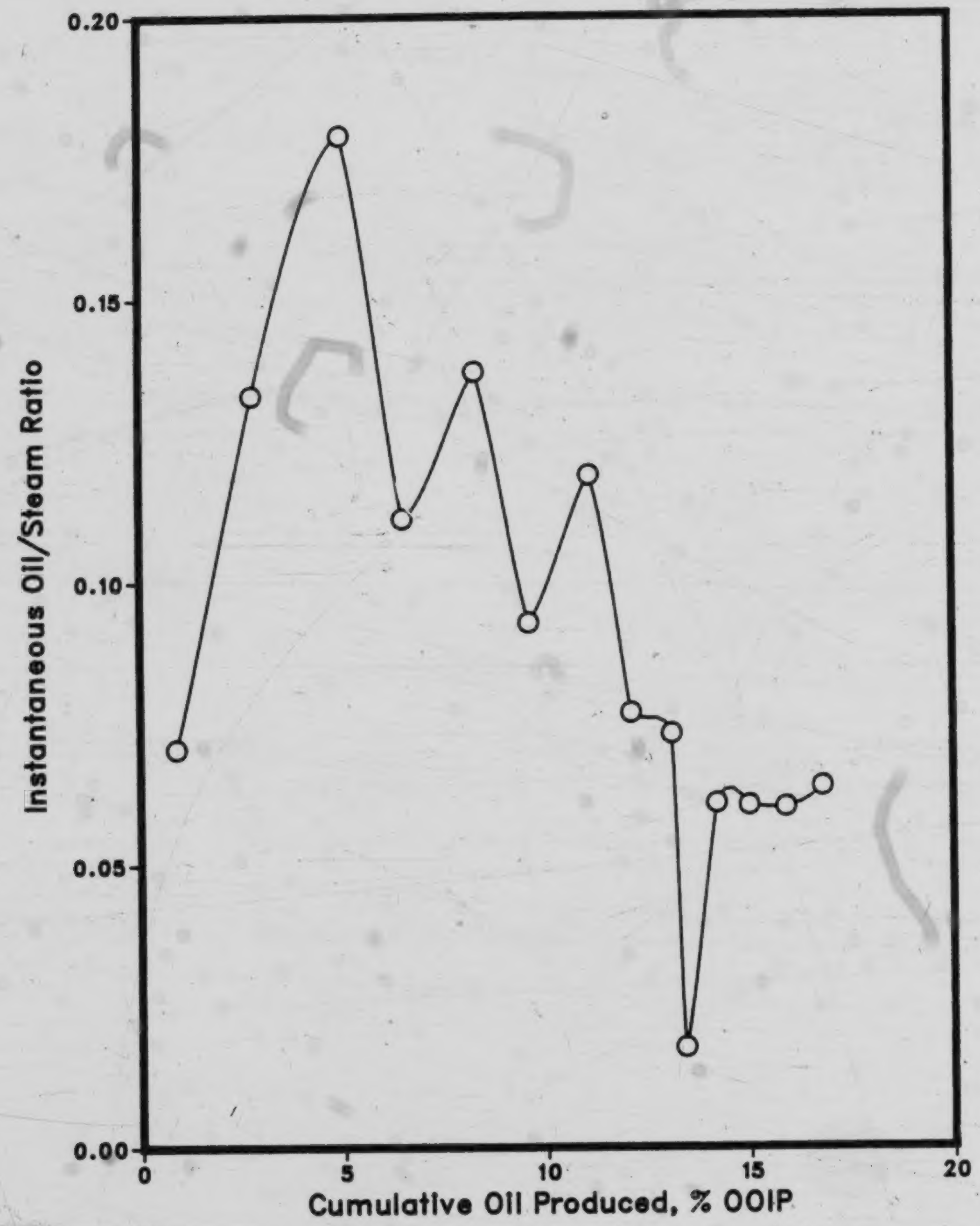

that the injected heat of the steam advanced faster through the lower half of the model than the upper section. The heat travelled faster through the lower section of the model since the steam had a higher injectivity in the underlying water zone than in the highly viscous oil layer. Therefore less of the injected steam was utilized to mobilize and displace the oil in the upper portion of the model due to the heat scavenging properties of the bottom water zone. Only at advanced times heating of the upper oil layer was significant enough to give additional oil recovery, and arrest the drop in oil/steam ratio.

All of the plots and temperature profiles for Run 39 indicated that the presence of bottom water during a steamflood process had a very unfavourable effect on the total amount of oil recovered from the model. The lower steam injectivity of the viscous oil zone forced the steam to flow into the underlying water which hindered the growth of the steam zone in the model. The lack of a steam zone allowed for a poor steam displacement of the inplace oil and therefore less oil was mobilized and displaced by the injected steam. The consequence of this inefficient displacement was a reduced oil recovery. The results of Run 39 enabled one to achieve a better idea of what to expect during a continuous steamflood of a bottom water formation.

Base Experiments for Comparison Purposes

A wide range of base experiments were carried out during the research. The data collected from these base runs were used to determine the injection properties of the solvent in the oil-saturated model. The results of the base experiments were also compared with later experiments to decide what effect such parameters as solvent slug injection, solvent slug size, bottom water thickness, gas injection, injection-production interval location and a physical barrier had on the oil recovery and thermal efficiency of a steamflood process implemented in a thin heavy oil formation, with underlying water.

The first base run was a continuous solvent flood in the homogeneous (i.e. no bottom water) model. The intention of the solvent flood was to enable one to estimate the injection behaviour of the solvent in the homogeneous model during the experiment. Another series of base experiments involved implementing a solvent-steamflood process in a homogeneous model. The results of these runs were then be compared to later solvent-steamflood experiments carried out in a bottom water model. The process of gas injection prior to a steamflood of a bottom water model was conducted in order to represent a base run which could be compared to the results of solvent-steamflood runs carried out in a bottom water model to determine how effective the use of a solvent slug prior to steamflooding would be.

Continuous Solvent Flood

Run 40 involved flooding a oil-saturated, homogeneous model with the chosen solvent (Heavy Virgin Naphtha). Table 6.3 lists pertinent data recorded from Run 40 such as the oil and solvent recoveries obtained during the experiment. Production began shortly after solvent injection was initiated and the majority of this production was solvent, suggesting that solvent breakthrough occurred almost immediately. This indicated that solvent channelling occurred almost immediately and thus the solventflood was an unstable

Table 6.3 : Run 40 Solventflood Performed With Homogeneous Model

Porosity = 33.7 %
Bulk Volume = 42005 cc
Pore Volume = 14140 cc

Initial HC Pore Volume = 13075 cc
Initial Oil Saturation = 92.47 %
Initial Water Saturation = 7.53 %

Total Solvent Injected = 2.25 P.V. (31700 cc)
Solvent Injection Rate = 200 cc/min.

Net Oil Recovery : 26.8 %

Solvent Recovery : 89.5 %

Cylinder No.	Solvent Conc. (%)	Total Volume Prod. (cc)	Cum. HC Vol. Prod		Oil Prod. (cc)	Cum. Oil Prod. (cc)	Cum. Oil Rec. (%)	Cum. Solvent Rec.		Inst. HC Prod. % of Sample
			(cc)	(P.V.)				(cc)	(%)	
1	59	1700	1700	0.12	697.00	697.00	5.33	1003.0	3.16	41.0%
2	79	1515	3215	0.23	318.15	1015.15	7.76	2199.9	6.94	21.0%
3	80	1510	4725	0.33	302.00	1317.15	10.07	3407.9	10.75	20.0%
4	84	1120	5845	0.41	179.20	1496.35	11.44	4348.7	13.72	16.0%
5	85	1730	7575	0.54	259.50	1755.85	13.43	5819.2	18.36	15.0%
6	88	1480	9055	0.64	177.60	1933.45	14.79	7121.6	22.47	12.0%
7	87	1705	10760	0.76	221.65	2155.10	16.48	8605.0	27.15	13.0%
8	89	1345	12105	0.86	147.95	2303.05	17.61	9802.1	30.92	11.0%
9	90	1570	13675	0.97	157.00	2460.05	18.81	11215.1	35.38	10.0%
10	91	1455	15130	1.07	130.95	2591.00	19.82	12539.2	39.56	9.0%
11	91	1675	16805	1.19	150.75	2741.75	20.97	14063.5	44.36	9.0%
12	94	1595	18400	1.30	95.70	2837.45	21.70	15562.8	49.09	6.0%
13	94	1895	20295	1.44	113.70	2951.15	22.57	17344.1	54.71	6.0%
14	94	1550	21845	1.54	93.00	3044.15	23.28	18801.1	59.31	6.0%
15	95	1740	23585	1.67	87.00	3131.15	23.95	20454.1	64.52	5.0%
16	95	1680	25265	1.79	84.00	3215.15	24.59	22050.1	69.56	5.0%
17	96	1750	27015	1.91	70.00	3285.15	25.13	23730.1	74.86	4.0%
18	96	1690	28705	2.03	67.60	3352.75	25.64	25352.5	79.98	4.0%
19	95	1790	30495	2.16	89.50	3442.25	26.33	27053.0	85.34	5.0%
20	96	1380	31875	2.25	55.20	3497.45	26.75	28377.8	89.52	4.0%

displacement. The cumulative oil recovery curve (Figure 6.8) is smooth and gradually increases, also suggesting that an oil bank did not form in the model during the experiment.

All samples taken during Run 40 were mostly solvent with the remainder of the sample being oil as is evident in Figure 6.9. The gradual drop in oil content of each sample and lack of pressure fluctuations at the production well during the solventflood again suggested that a poorly defined oil bank formed due to immediate solvent channelling which is characteristic of an unstable displacement.

Figures A.11 through A.18 display the top view temperature profiles of the model at upper and lower levels for every 0.25 pore volumes for the first two pore volumes of solvent injected during the experiment. The injected solvent was at room temperature (21^0C) which was different than the initial model temperature of 3^0C. The solvent was not at the same temperature as the model so that the temperature profiles could provide a better indication of where the solvent was going in the model during the run. These temperature contours indicate that the solvent advanced faster through the lower portion than the upper region of the model. The first few profiles also suggest that solvent channelling was quite prevalent in the model. The cross-sectional temperature profiles for the first pore volume of solvent injected are given in Figures A.19 through A.22 and also illustrate that the solvent tended to channel in the lower half of the model throughout the experiment.

During the initial stages of the run, channelling started soon after solvent injection. As the run progressed the solvent was dispersed transversely outwards from the swept zone causing an increased oil mobility in parts of the unswept region. The newly mobilized oil of the unswept area entered the main solvent flow path resulting in the growth of the swept zone. A gradual rise in the cumulative oil recovery then occurred due to the subsequent production of this newly mobilized oil. The rise in cumulative oil recovery could also be partially attributed to the flowing solvent further reducing the oil saturation in the swept zone. The overall low oil recovery was due to solvent channelling creating a

Figure 6.8 :Run 40 Solventflood of Aberfeldy Model
Cumulative Oil Recovery Vs. Cumulative Volume Injected

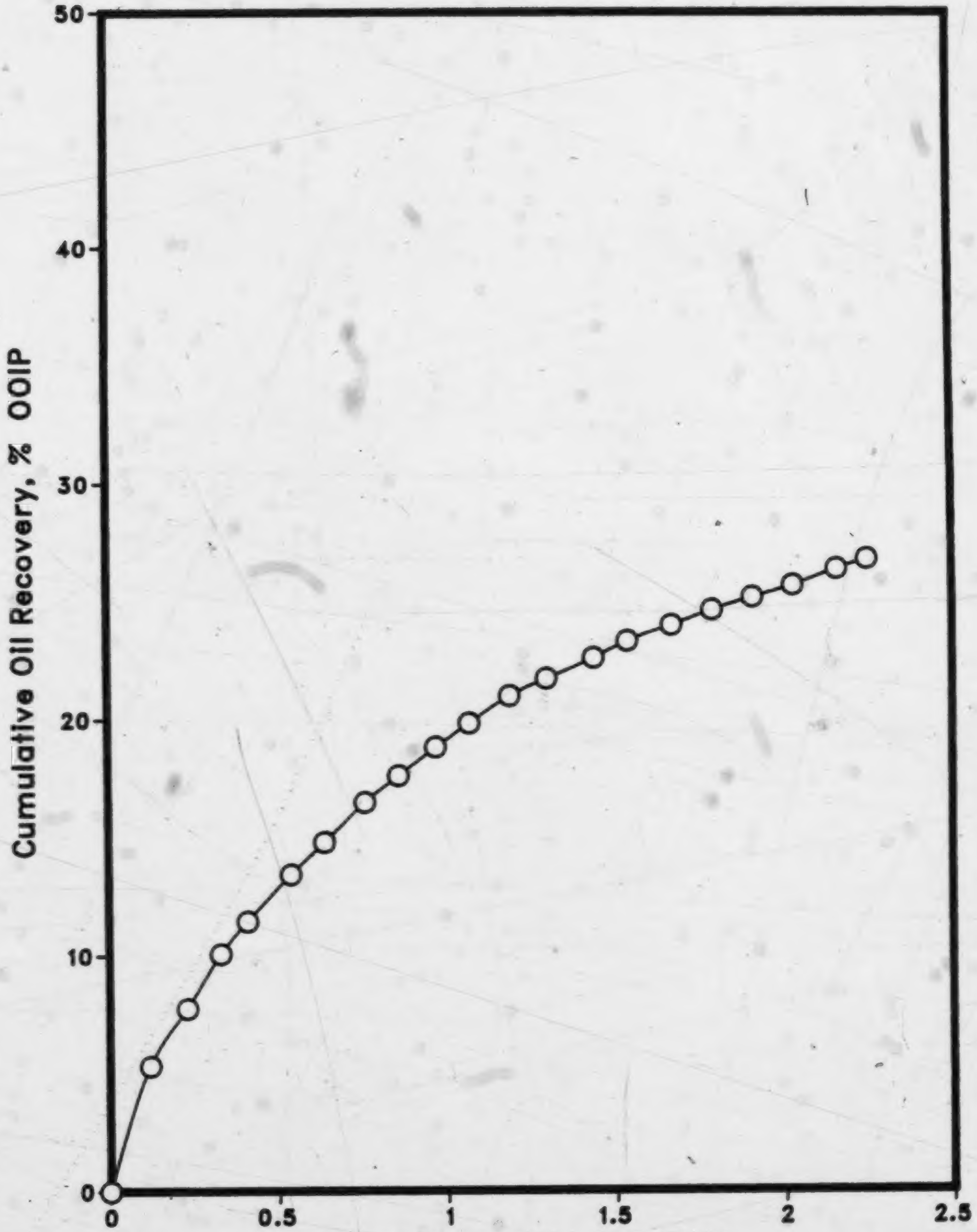

Figure 6.9 :Run 40 Solventflood of Aberfeldy Model
Instantaneous Oil Produced Vs. Cumulative Volume Injected

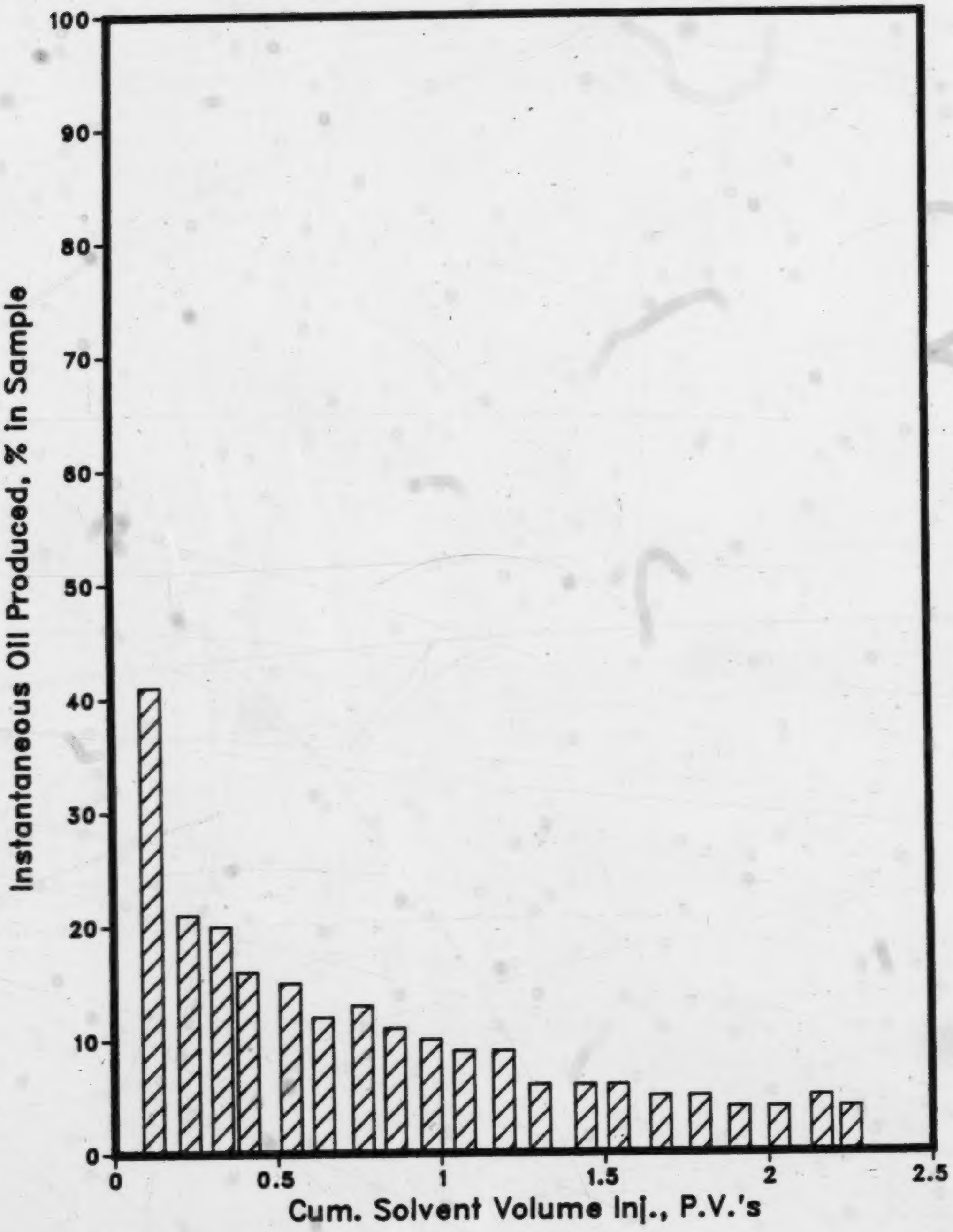

small swept zone that prevented an oil bank from developing and a stable displacement from being realized.

The oil recovery for Run 40 was relatively poor at 26.75 % which is comparable to previous waterfloods such as Run 7 (26.47 %) and Run 22 (25.91 %). Cumulative solvent recovery was at 89.52 %. The high solvent recovery was due to the immediate and continuous solvent channelling towards the production well during the run which resulted in less solvent being left in the model as a residual hydrocarbon saturation.

From the experimental results of Run 40 it appeared that the solvent channelled through the oil immediately upon injection and continued to do so throughout the experiment. This type of injection behaviour of the solvent was desirable in the context of a steamflood, because the solvent channels formed would aid in increasing the injectivity of steam into the oil during a steam injection process. The higher steam injectivity could allow a steam injection process to be more thermally efficient since less of the steams heat would be lost to such heat sinks as overburden, underburden, adjacent formations and bottom water zones. Therefore the injected steam could be utilized more effectively in mobilizing and displacing the in-place oil.

Solvent-Steamflood

Runs 44, 45 and 46 involved injecting a small solvent slug into an oil-saturated, homogeneous model prior to a continuous steamflood. Tables 6.4, 6.5 and 6.6 present the pertinent data and results for Runs 44, 45 and 46, respectively. These runs were designed to evaluate the reproducibility of the experimental results and gain experience with this type of experiment.

The purpose of the solvent slug prior to steam injection was to create solvent channels into the oil region through which the injected steam could more easily penetrate and thus, more efficiently mobilize the oil. Since more oil could be mobilized and displaced, a larger oil bank (actually solvent and oil) would form and a more stable steam displacement would result. The greater stability of the steam injection process resulted in a prolonged time until steam breakthrough and an improved overall oil recovery.

The solvent slug size used in these experiments was 10 % of the pore volume. This value was chosen because Alikhan [64] stated that beyond a particular slug size, which he found to be about 10% of the pore volume depending upon the viscosity contrast between the oil and the solvent, the solvent slug would not be efficiently produced and the net result would be a decrease in total oil and solvent recovery.

Comparing the oil recovery curves for Runs 44, 45 and 46 (Figures 6.10, 6.14 and 6.18, respectively) to that of Run 40 (Figure 6.8) it is evident that the shapes of the solvent-steamflood curves are not as smooth as Figure 6.8 where only the solvent was injected continuously. In the very early stages of the solvent-steamfloods the oil recovery rose quite sharply. The steep increase in the recovery curves (Figures 6.10, 6.14 and 6.18) represented the oil and solvent, positioned ahead of the steam zone, forming a bank in the vicinity of the production well which was subsequently produced during the initial stages of the run. The curve then gradually started to level off due to the breakthrough of the steam and water at the production well. The steam breakthrough resulted in a less stable, less efficient displacement and led to a drop in oil production as illustrated in

Figures 6.11, 6.12, 6.15, 6.16, 6.19 and 6.20. After the solvent-steamflood recovery curves began to level off these curves once again started to increase and were shaped similar to the latter part of the solvent flood recovery curve. The gradual rise in oil production was caused by additional oil being mobilized in the unswept and swept zones. Oil recovered from the unswept region was mobilized (viscosity reduction) by the heating characteristics of the steam. The oil produced from the swept zone was also recovered due to the heating properties of the steam which lowered the viscosity of the remaining oil and further reduced the oil saturation in the swept region. The final stages of the solvent-steamflood curves were not as smooth as the solvent flood curve due to small humps existing near the end of the solvent-steamflood curves. These small humps were probably linked to small pockets of oil in the swept region that were finally mobilized and produced.

The bar plots of volume as a percentage of oleic phase in each sample collected versus the cumulative volume injected for Runs 44 (Figure 6.11), 45 (Figure 6.15) and 46 (Figure 6.19) were similar to one another. The peaks represent increased oil content in production and the lows reflect a decrease in the oil content of the production. The highs and lows of these plots correspond quite closely to slope variations in the recovery curves. An increase in the recovery curve slope indicates a rise in oil production and a decrease reflected a drop in oil production. Figures 6.12 (Run 44), 6.16 (Run 45) and 6.20 (Run 46) are bar graphs representing instantaneous water/oil ratio versus cumulative volume injected. For Figures 6.12, 6.16 and 6.20 the peaks are increases in the water/oil ratio of the instantaneous production and the valleys indicate drops in the instantaneous water/oil ratio. The highs and lows for Figures 6.12, 6.16 and 6.20 also correspond reasonably well with the slope variations of the recovery curves.

Figures 6.13, 6.17 and 6.21 are plots of instantaneous oil/steam ratio versus cumulative oil produced. A distinct peak in the oil/steam ratio occurred for all three runs between 10 and 20% production of the original oil in place. After the peak the curve drops and then gradually levels off. The peak represents the oil produced due to the steam

Table 6.4 : Run 44 Solvent-Steamflood With Homogeneous Model

HC Pore Volume : 13140.0 cc
Pore Volume : 14140.0 cc
Bulk Volume : 42005.0 cc
Porosity : 33.7%
Initial Oil Satn. : 92.9%
Initial H2O Satn. : 7.1%
Solvent Vol. Inj.: 1400.0 cc (10.0% PV)

Type of Oil Used : Faxam-100
Initial Model Temperature : 3.00 C
Water Feed Flow Rate : 213.60 cc/min
Boiler Feed Flow Rate : 29.20 cc/min
Total Flow Rate of Steam : 242.80 cc/min
Solvent Flow Rate : 200.00 cc/min
Steam Vol. Injected : 31575 cc (2.23 PV)

Net Oil Recovery : 27.1% **Solvent Recovery : 70.4%** **Final Oil Saturation : 67.8%**

Cyl. No.	Solvent Conc. (%)	Tot. Vol. Inj. (cc)	Cum. Vol. Inj.		HC Prod. (cc)	Oil Prod. (cc)	Cum. Oil Rec.		Cum. Sol. Rec.		Oil-Steam Ratio	Inst Prod WOR	Inst. HC Prod. % of Sample
			(cc)	(P.V.)			(cc)	(%OOIP)	(cc)	(%)			
1	52%	965	965	0.07	965	463	463	3.5%	502	35.9%	0.0000	0.00	100.0%
2	52%	1620	2585	0.18	785	377	840	6.4%	910	65.0%	0.0000	1.06	48.5%
3	8%	1990	4575	0.32	270	248	1088	8.3%	932	66.6%	0.1570	6.37	13.6%
4	6%	2100	6675	0.47	435	409	1497	11.4%	958	68.4%	0.2613	3.83	20.7%
5	4%	2090	8765	0.62	510	490	1987	15.1%	978	69.9%	0.3228	3.10	24.4%
6	2%	2115	10880	0.77	370	363	2350	17.9%	985	70.4%	0.2120	4.72	17.5%
7	0%	1985	12865	0.91	230	230	2580	19.6%	985	70.4%	0.1311	7.63	11.6%
8	0%	2020	14885	1.05	160	160	2740	20.9%	985	70.4%	0.0860	11.63	7.9%
9	0%	1985	16870	1.19	130	130	2870	21.8%	985	70.4%	0.0701	14.27	6.5%
10	0%	2040	18910	1.34	100	100	2970	22.6%	985	70.4%	0.0515	19.40	4.9%
11	0%	2015	20925	1.48	105	105	3075	23.4%	985	70.4%	0.0550	18.19	5.2%
12	0%	2000	22925	1.62	85	85	3160	24.0%	985	70.4%	0.0444	22.53	4.3%
13	0%	1955	24880	1.76	85	85	3245	24.7%	985	70.4%	0.0455	22.00	4.3%
14	0%	2015	26895	1.90	75	75	3320	25.3%	985	70.4%	0.0387	25.87	3.7%
15	0%	2010	28905	2.04	85	85	3405	25.9%	985	70.4%	0.0442	22.65	4.2%
16	0%	2075	30980	2.19	70	70	3475	26.4%	985	70.4%	0.0349	28.64	3.4%
17	0%	1995	32975	2.33	80	80	3555	27.1%	985	70.4%	0.0418	23.94	4.0%

Figure 6.10 :Run 44 Solvent–Steamflood
Cumulative Oil Recovery Vs. Cumulative Volume Injected

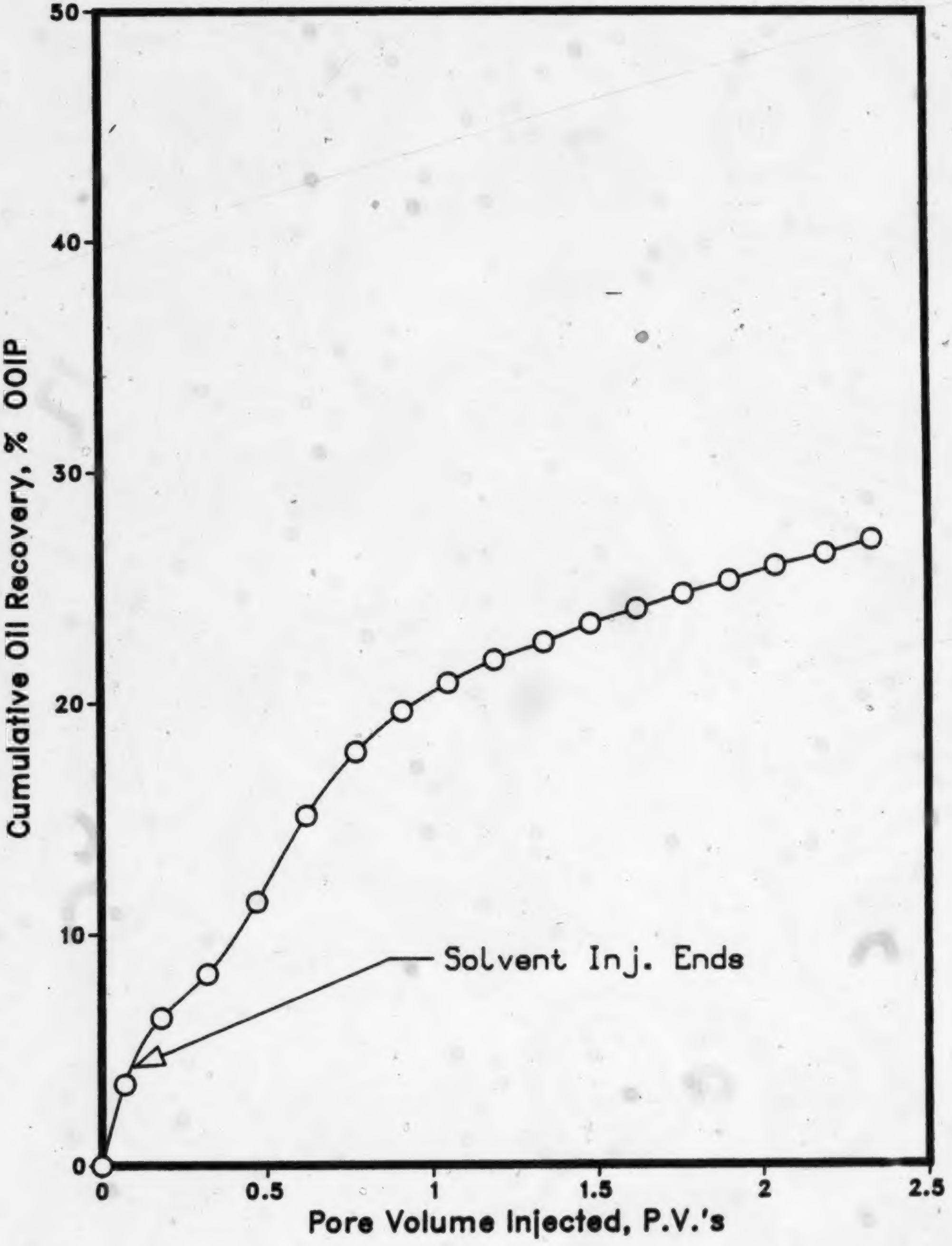

Figure 6.11 :Run 44 Solvent–Steamflood
Oleic Phase In Each Sample Vs. Cumulative Volume Injected

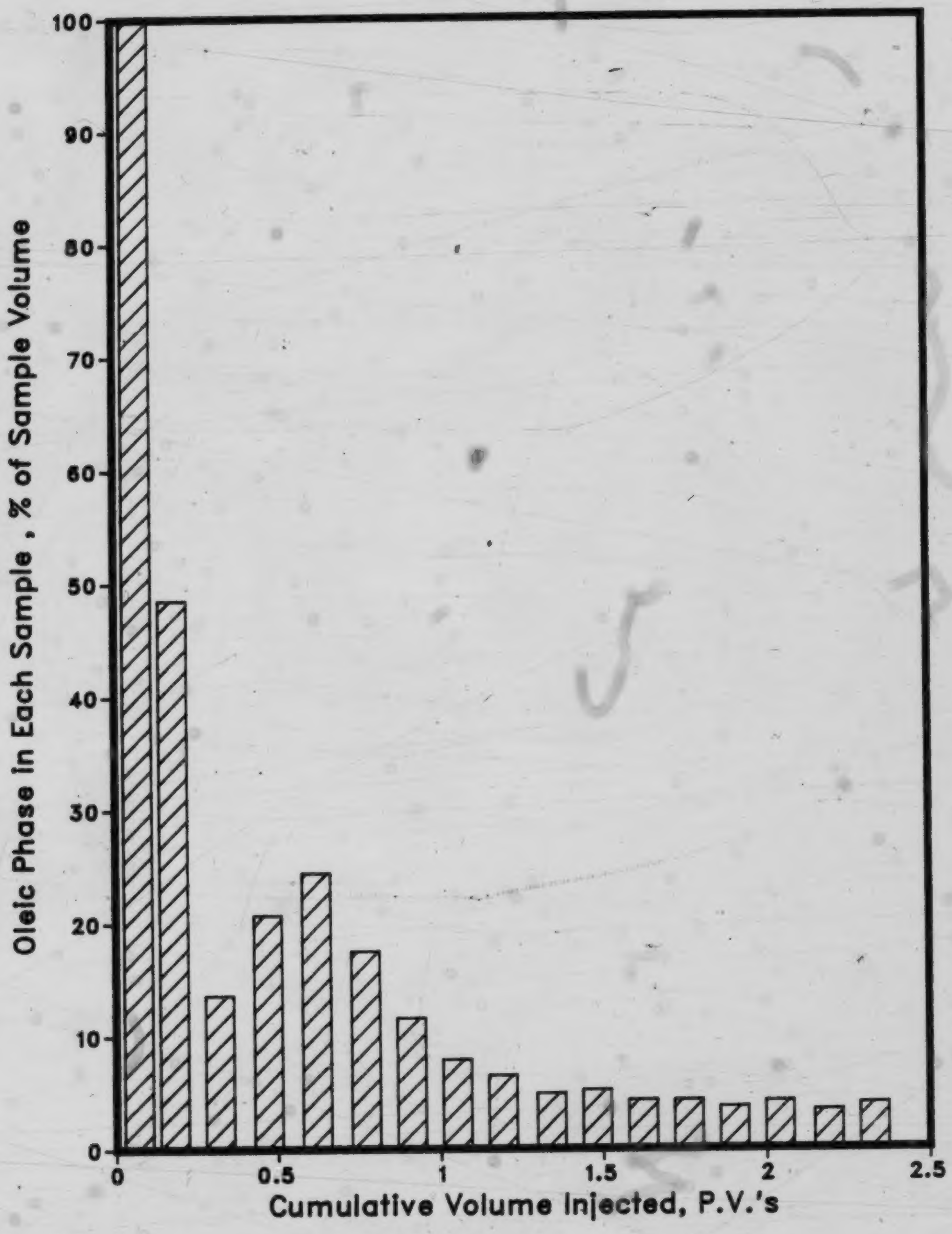

<

Figure 6.12 :Run 44 Solvent–Steamflood
Instantaneous Produced WOR Vs. Cumulative Volume Injected

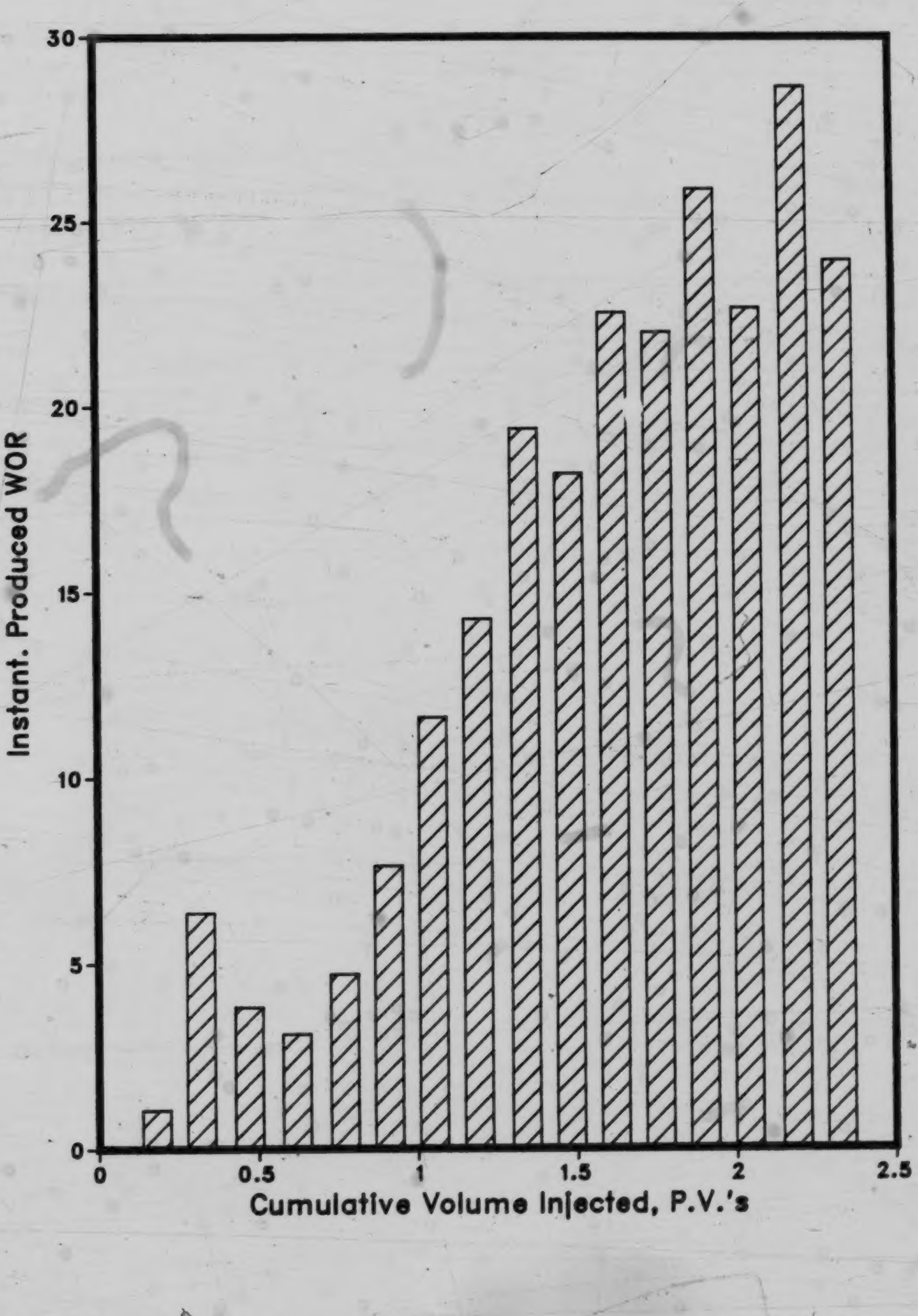

Figure 6.13 :Run 44 Solvent–Steamflood Instantaneous Oil/Steam Ratio Vs. Cumulative Oil Produced

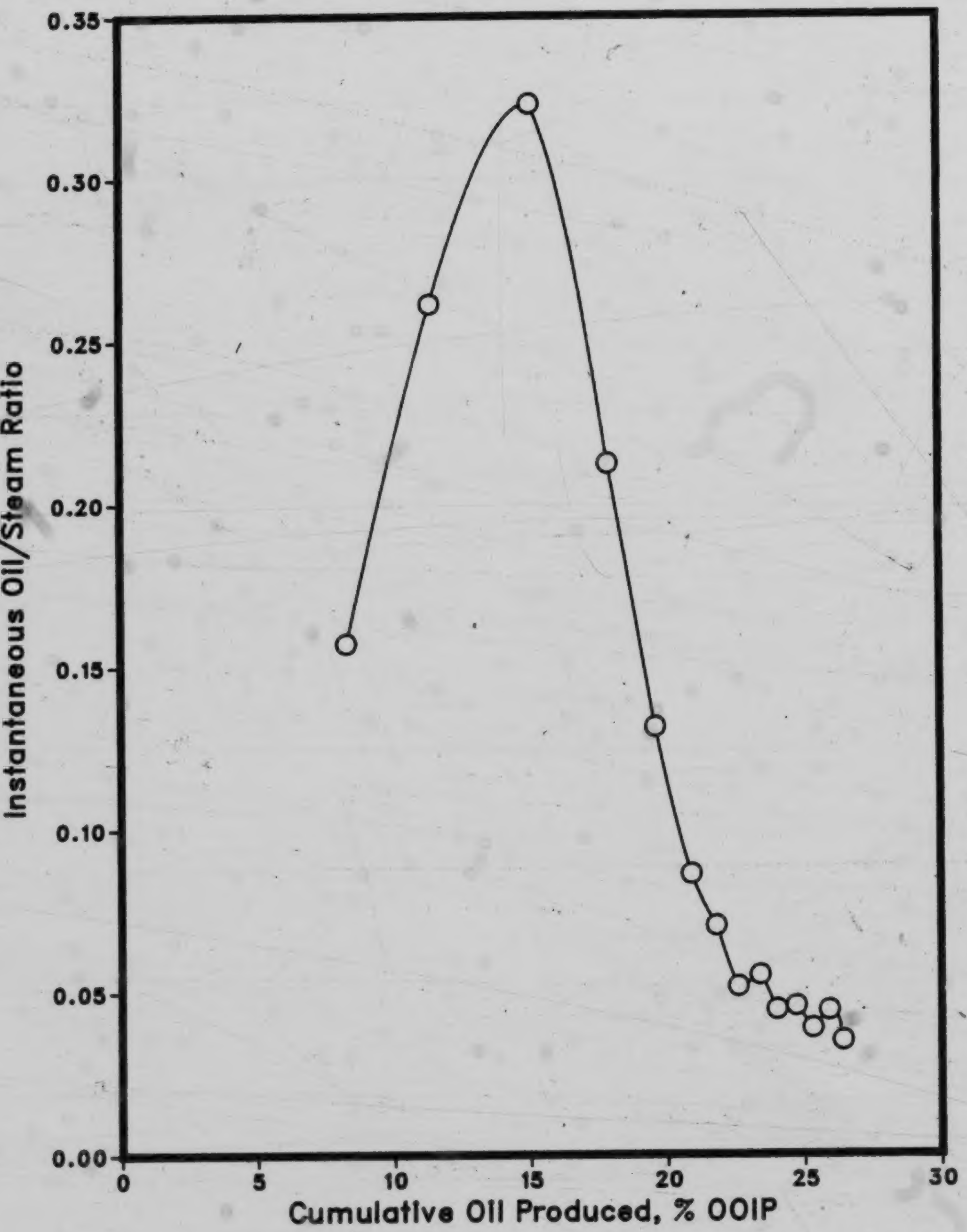

Table 6.5 : Run 45 Solvent-Steamflood With Homogeneous Model

HC Pore Volume : 13180.0 cc
Pore Volume : 14320.0 cc
Bulk Volume : 42005.0 cc
Porosity : 34.1%
Initial Oil Satn. : 92.0%
Initial H2O Satn. : 8.0%
Solvent Vol. Inj.: 1400.0 cc (10.0% PV)

Type of Oil Used : Faxam-100
Initial Model Temperature : 3.00 C
Water Feed Flow Rate : 213.60 cc/min
Boiler Feed Flow Rate : 29.20 cc/min
Total Flow Rate of Steam : 242.80 cc/min
Solvent Flow Rate : 200.00 cc/min
Steam Vol. Injected : 35655 cc (2.49 PV)

Net Oil Recovery : 30.0% **Solvent Recovery : 71.2%** **Final Oil Saturation : 64.5%**

Cyl. No.	Solvent Conc. (%)	Tot. Vol Inj. (cc)	Cum. Vol. Inj. (cc)	Cum. Vol. Inj. (P.V.)	HC Prod. (cc)	Oil Prod. (cc)	Cum. Oil Rec. (cc)	Cum. Oil Rec. (%OOIP)	Cum. Sol. Rec. (cc)	Cum. Sol. Rec. (%)	Oil-Steam Ratio	Inst Prod. WOR	Inst. HC Prod. % of Sample
1	47%	575	575	0.04	575	305	305	2.3%	270	19.3%	0.0000	0.00	100.0%
2	62%	640	1215	0.08	620	236	541	4.1%	654	46.7%	0.0000	0.03	96.9%
3	59%	395	1610	0.11	345	141	682	5.2%	858	61.3%	0.0000	0.14	87.3%
4	24%	1965	3575	0.25	320	243	925	7.0%	935	66.8%	0.1945	5.14	16.3%
5	8%	2030	5605	0.39	375	345	1270	9.6%	965	68.9%	0.2266	4.41	18.5%
6	4%	1800	7405	0.52	465	446	1716	13.0%	984	70.3%	0.3483	2.87	25.8%
7	3%	2000	9405	0.66	330	320	2036	15.4%	994	71.0%	0.1976	5.06	16.5%
8	1%	1960	11365	0.79	290	287	2323	17.6%	997	71.2%	0.1737	5.76	14.8%
9	0%	2020	13385	0.93	245	245	2568	19.5%	997	71.2%	0.1380	7.24	12.1%
10	0%	1950	15335	1.07	185	185	2753	20.9%	997	71.2%	0.1048	9.54	9.5%
11	0%	1965	17300	1.21	145	145	2898	22.0%	997	71.2%	0.0797	12.55	7.4%
12	0%	1920	19220	1.34	130	130	3028	23.0%	997	71.2%	0.0726	13.77	6.8%
13	0%	2025	21245	1.48	100	100	3128	23.7%	997	71.2%	0.0519	19.25	4.9%
14	0%	1970	23215	1.62	105	105	3233	24.5%	997	71.2%	0.0563	17.76	5.3%
15	0%	1990	25205	1.76	90	90	3323	25.2%	997	71.2%	0.0474	21.11	4.5%
16	0%	2000	27205	1.90	85	85	3408	25.9%	997	71.2%	0.0444	22.53	4.3%
17	0%	2030	29235	2.04	75	75	3483	26.4%	997	71.2%	0.0384	26.07	3.7%
18	0%	1900	31135	2.17	175	175	3658	27.8%	997	71.2%	0.1014	9.86	9.2%
19	0%	1980	33115	2.31	105	105	3763	28.6%	997	71.2%	0.0560	17.86	5.3%
20	0%	1940	35055	2.45	105	105	3868	29.3%	997	71.2%	0.0572	17.48	5.4%
21	0%	2000	37055	2.59	80	80	3948	30.0%	997	71.2%	0.0417	24.00	4.0%

Figure 6.14 :Run 45 Solvent–Steamflood
Cumulative Oil Recovery Vs. Pore Volumes Injected

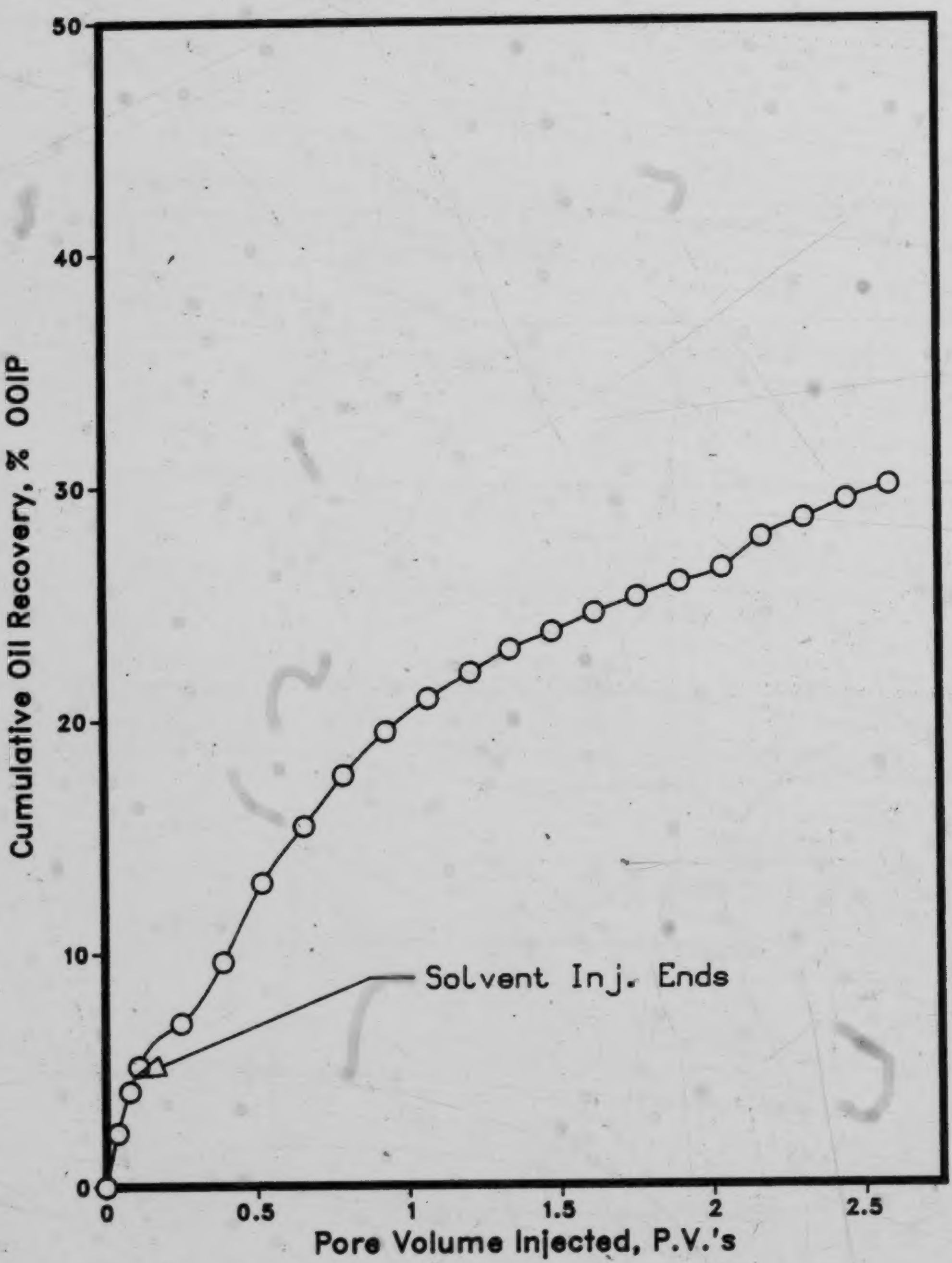

Figure 6.15 :Run 45 Solvent–Steamflood
Oleic Phase in Each Sample Vs. Cumulative Volume Injected

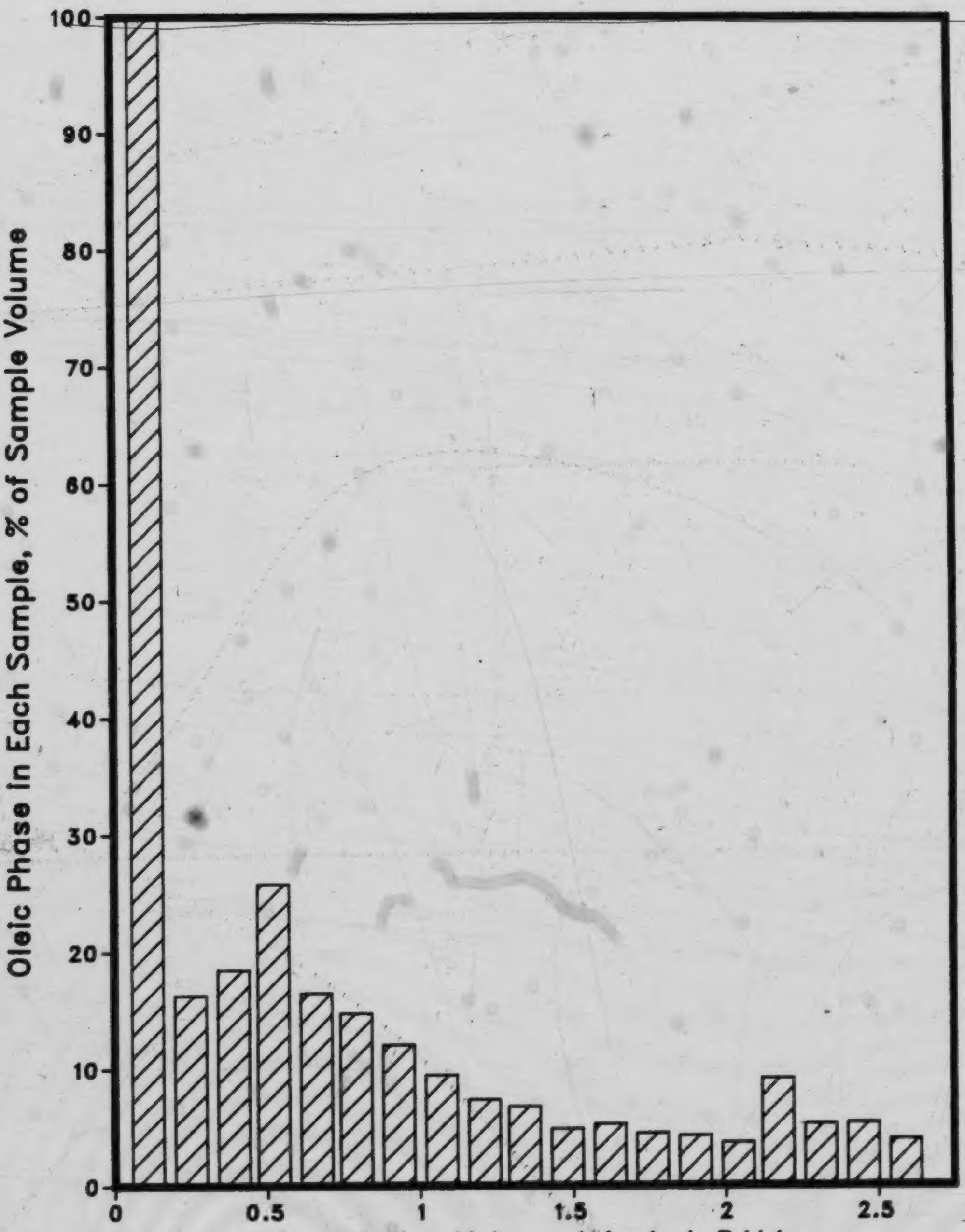

Figure 6.16 :Run 45 Solvent–Steamflood
Instantaneous Produced WOR Vs. Cumulative Volume Injected .

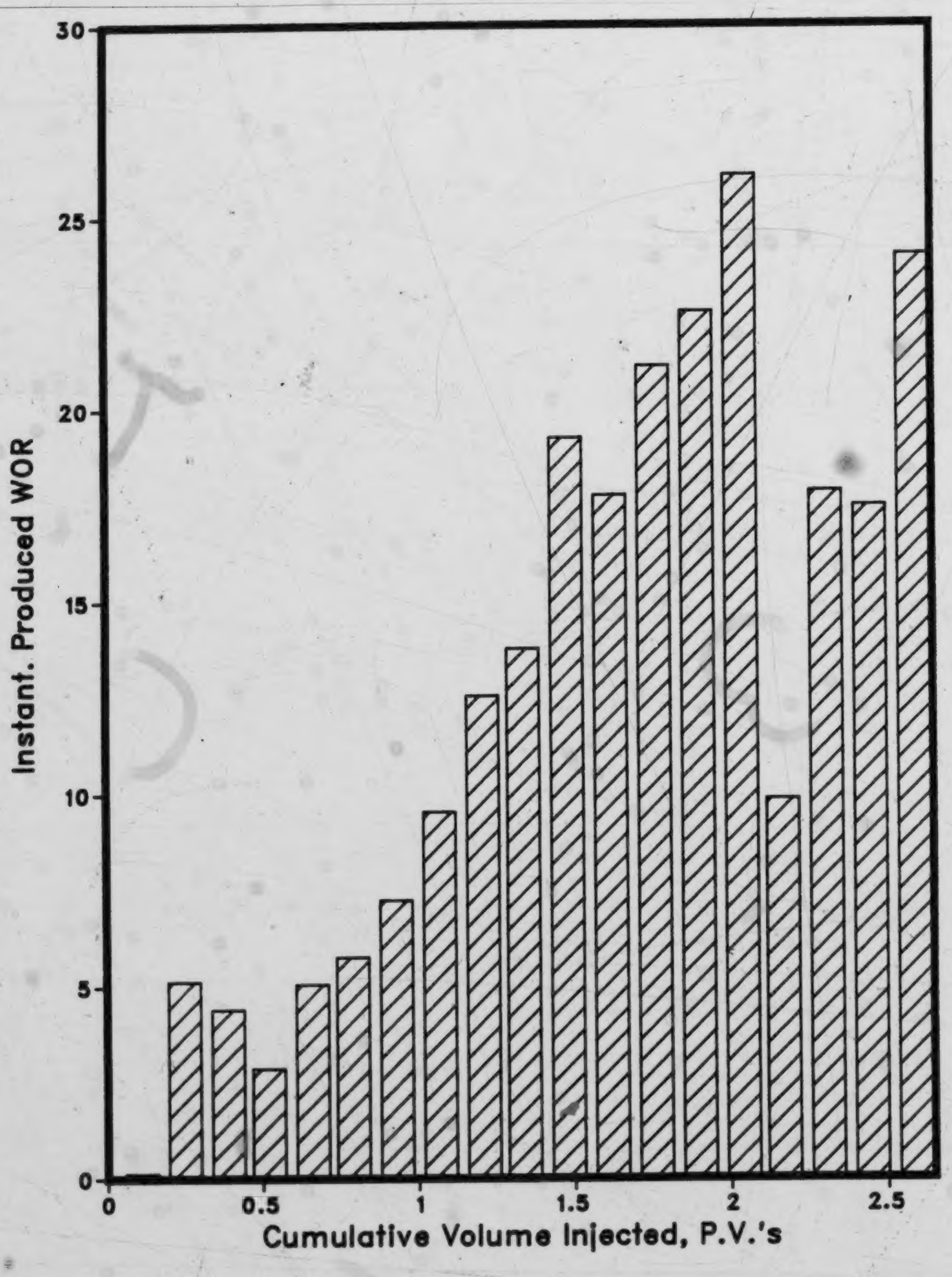

Figure 6.17 :Run 45 Solvent–Steamflood
Instantaneous Oil/Steam Ratio Vs. Cumulative Oil Produced

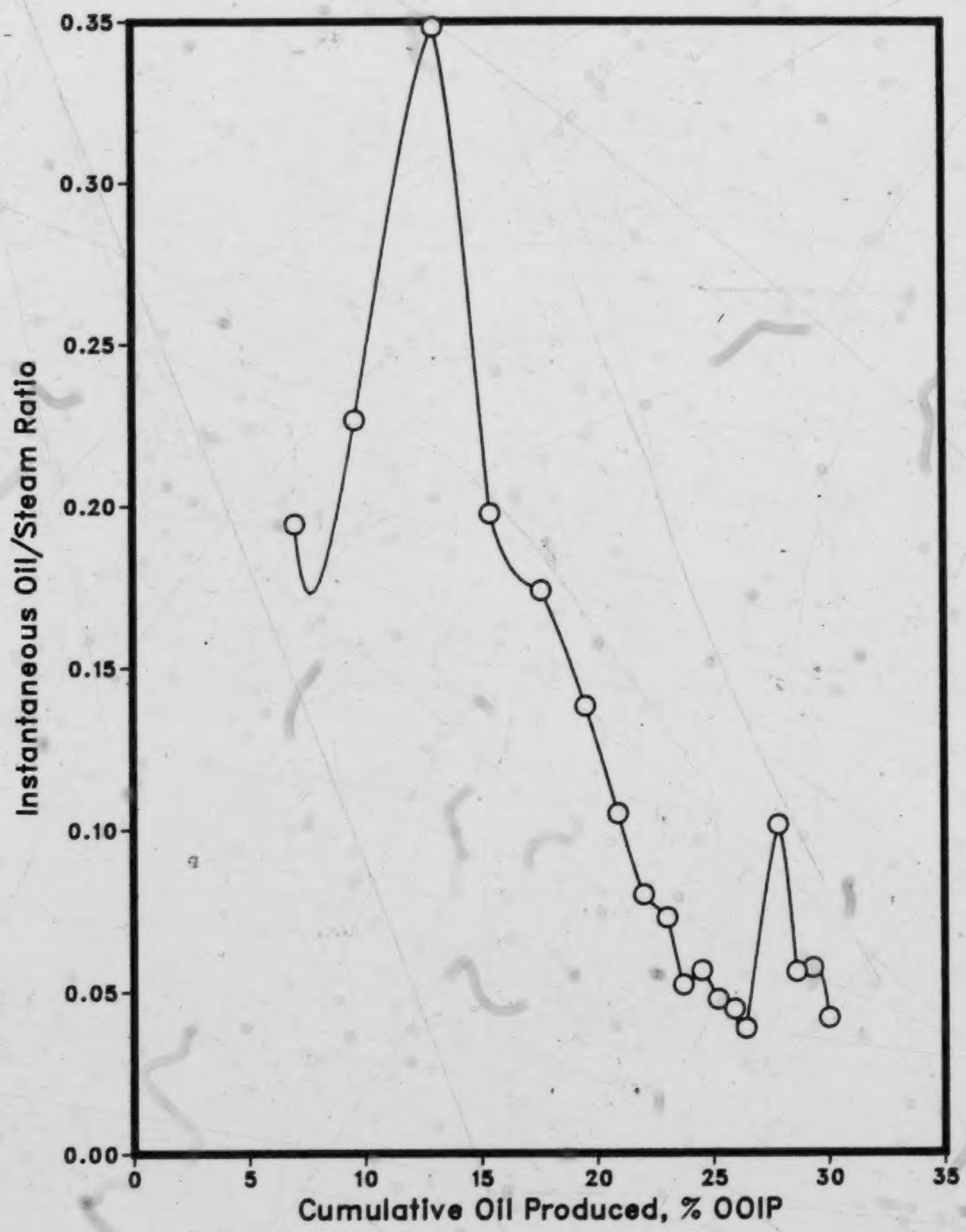

Table 6.6 : Run 46 Solvent-Steamflood With Homogeneous Model

HC Pore Volume : 13140.0 cc
Pore Volume : 16250.0 cc
Bulk Volume : 42005.0 cc
Porosity : 38.7%
Initial Oil Satn. : 80.9%
Initial H2O Satn. : 19.1%
Solvent Vol. Inj.: 1500.0 cc (10.0% PV)

Type of Oil Used : Faxam-100
Initial Model Temperature : 3.00 C
Water Feed Flow Rate : 213.60 cc/min
Boiler Feed Flow Rate : 29.20 cc/min
Total Flow Rate of Steam : 242.80 cc/min
Solvent Flow Rate : 200.00 cc/min
Steam Vol. Injected : 32170 cc (1.98 PV)

Net Oil Recovery : 27.7% **Solvent Recovery : 33.1%** **Final Oil Saturation : 58.5%**

Cyl. No.	Solvent Conc. (%)	Tot. Vol. Inj. (cc)	Cum. Vol. Inj.		HC Prod (cc)	Oil Prod. (cc)	Cum. Oil Rec.		Cum. Sol. Rec.		Oil-Steam Ratio	Inst Prod. WOR	Inst. HC Prod. % of Sample
			(cc)	(P.V.)			(cc)	(%OOIP)	(cc)	(%)			
1	26%	350	350	0.02	350	259	259	2.0%	91	6.1%	0.0000	0.00	100.0%
2	39%	380	730	0.04	380	232	491	3.7%	239	15.9%	0.0000	0.00	100.0%
3	42%	680	1410	0.09	370	215	706	5.4%	394	26.3%	0.0000	0.84	54.4%
4	16%	385	1795	0.11	95	80	786	6.0%	409	27.3%	0.3276	3.05	24.7%
5	15%	1820	3615	0.22	260	221	1007	7.7%	448	29.9%	0.1667	6.00	14.3%
6	5%	1920	5535	0.34	245	233	1240	9.4%	460	30.7%	0.1463	6.84	12.8%
7	4%	2075	7610	0.47	410	394	1634	12.4%	476	31.7%	0.2462	4.06	19.8%
8	3%	2000	9610	0.59	375	364	1998	15.2%	487	32.5%	0.2308	4.33	18.8%
9	2%	1880	11490	0.71	330	323	2321	17.7%	494	32.9%	0.2129	4.70	17.6%
10	1%	1950	13440	0.83	250	248	2569	19.6%	496	33.1%	0.1471	6.80	12.8%
11	0%	2100	15540	0.96	220	220	2789	21.2%	496	33.1%	0.1170	8.55	10.5%
12	0%	2080	17620	1.08	165	165	2954	22.5%	496	33.1%	0.0862	11.61	7.9%
13	0%	1990	19610	1.21	150	150	3104	23.6%	496	33.1%	0.0815	12.27	7.5%
14	0%	2035	21645	1.33	95	95	3199	24.3%	496	33.1%	0.0490	20.42	4.7%
15	0%	1950	23595	1.45	90	90	3289	25.0%	496	33.1%	0.0484	20.67	4.6%
16	0%	2045	25640	1.58	70	70	3359	25.6%	496	33.1%	0.0354	28.21	3.4%
17	0%	1975	27615	1.70	85	85	3444	26.2%	496	33.1%	0.0450	22.24	4.3%
18	0%	2020	29635	1.82	80	80	3524	26.8%	496	33.1%	0.0412	24.25	4.0%
19	0%	1900	31535	1.94	70	70	3594	27.4%	496	33.1%	0.0383	26.14	3.7%
20	0%	2135	33670	2.07	45	45	3639	27.7%	496	33.1%	0.0215	46.44	2.1%

Figure 6.18 :Run 46 Solvent–Steamflood
Cumulative Oil Recovery Vs. Pore Volumes Injected

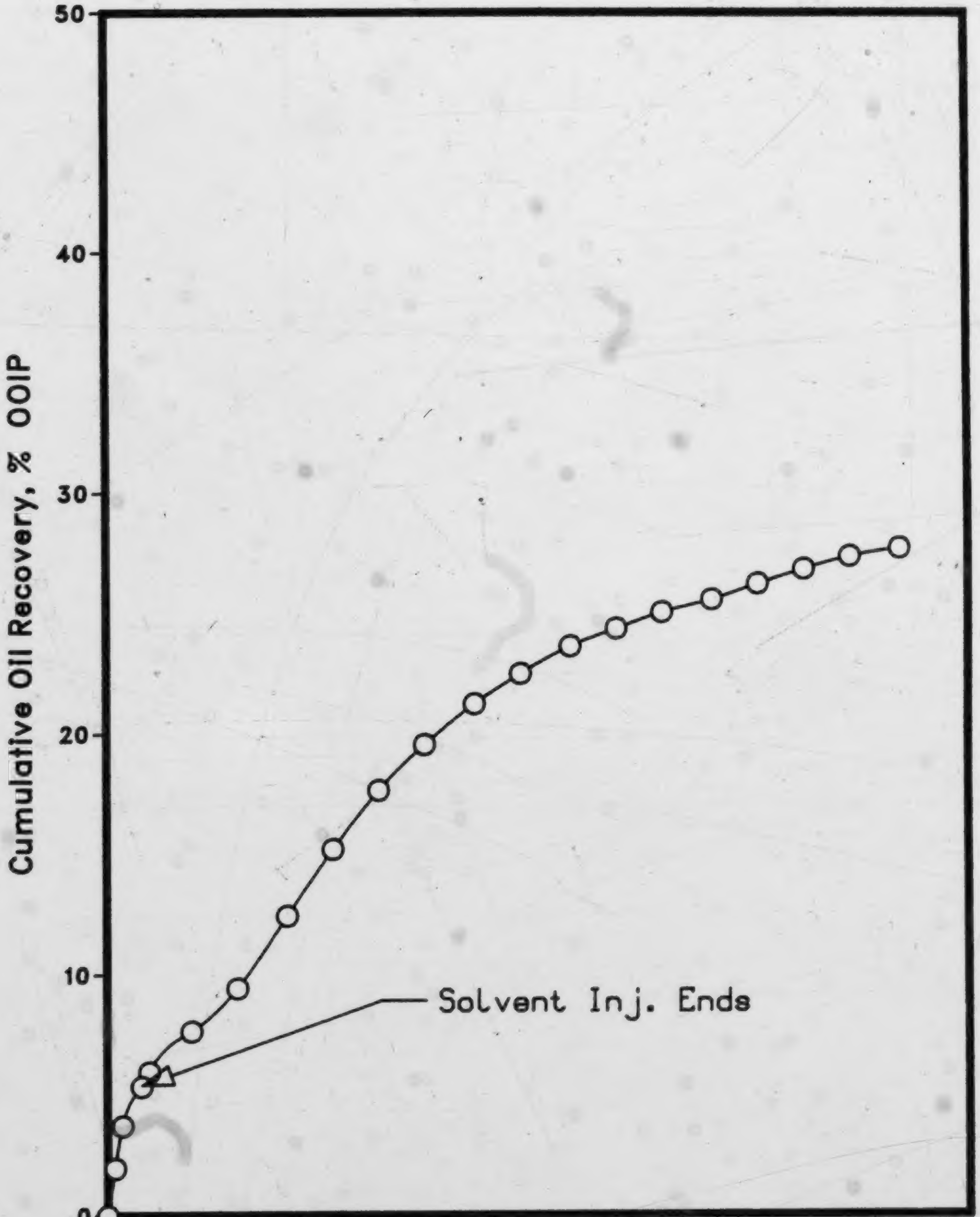

Figure 6.19 :Run 46 Solvent–Steamflood
OleicPhase in Each Sample Vs. Cumulative Volume Injected

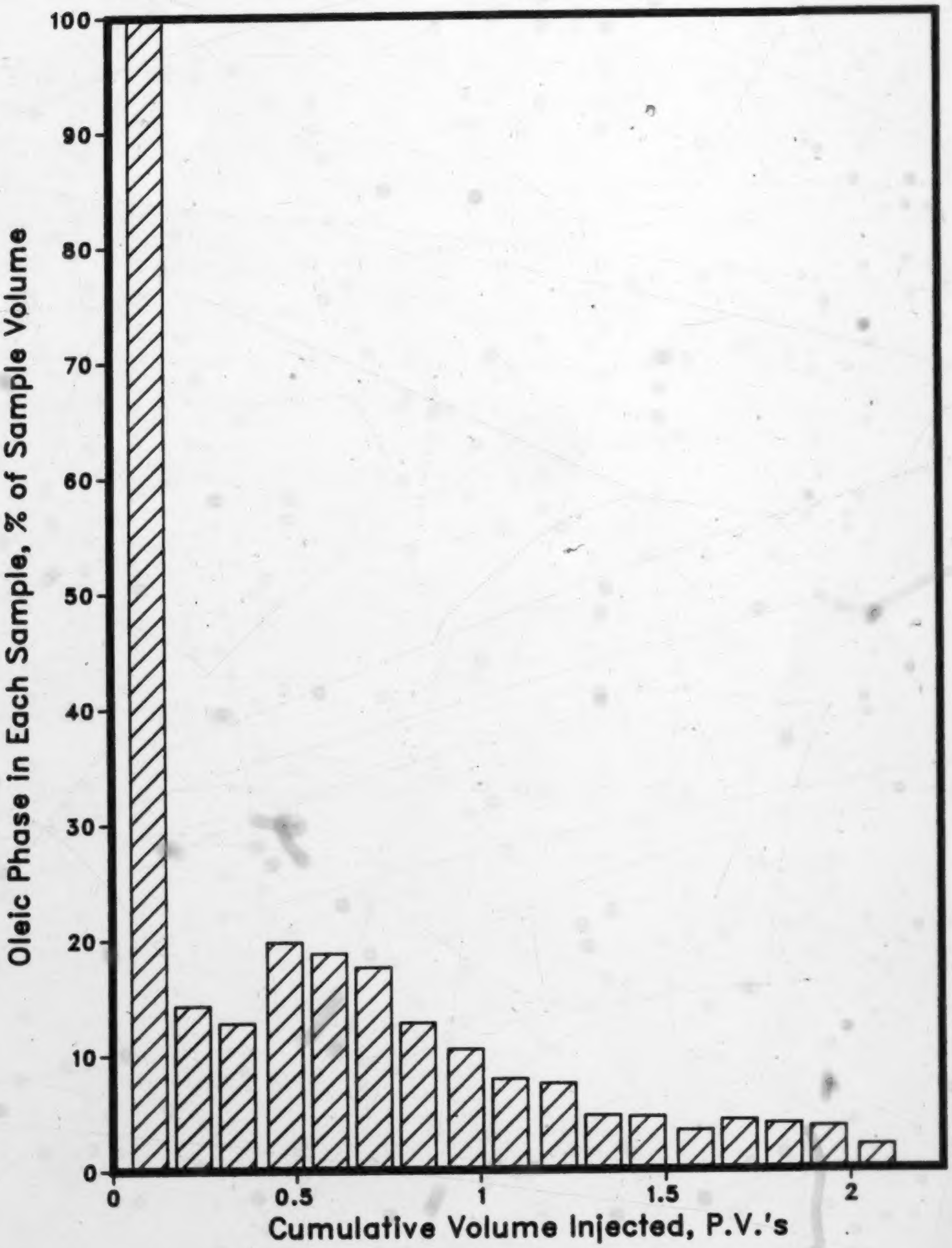

Figure 6.20 :Run 46 Solvent–Steamflood
Instantaneous Produced WOR Vs. Cumulative Volume Injected

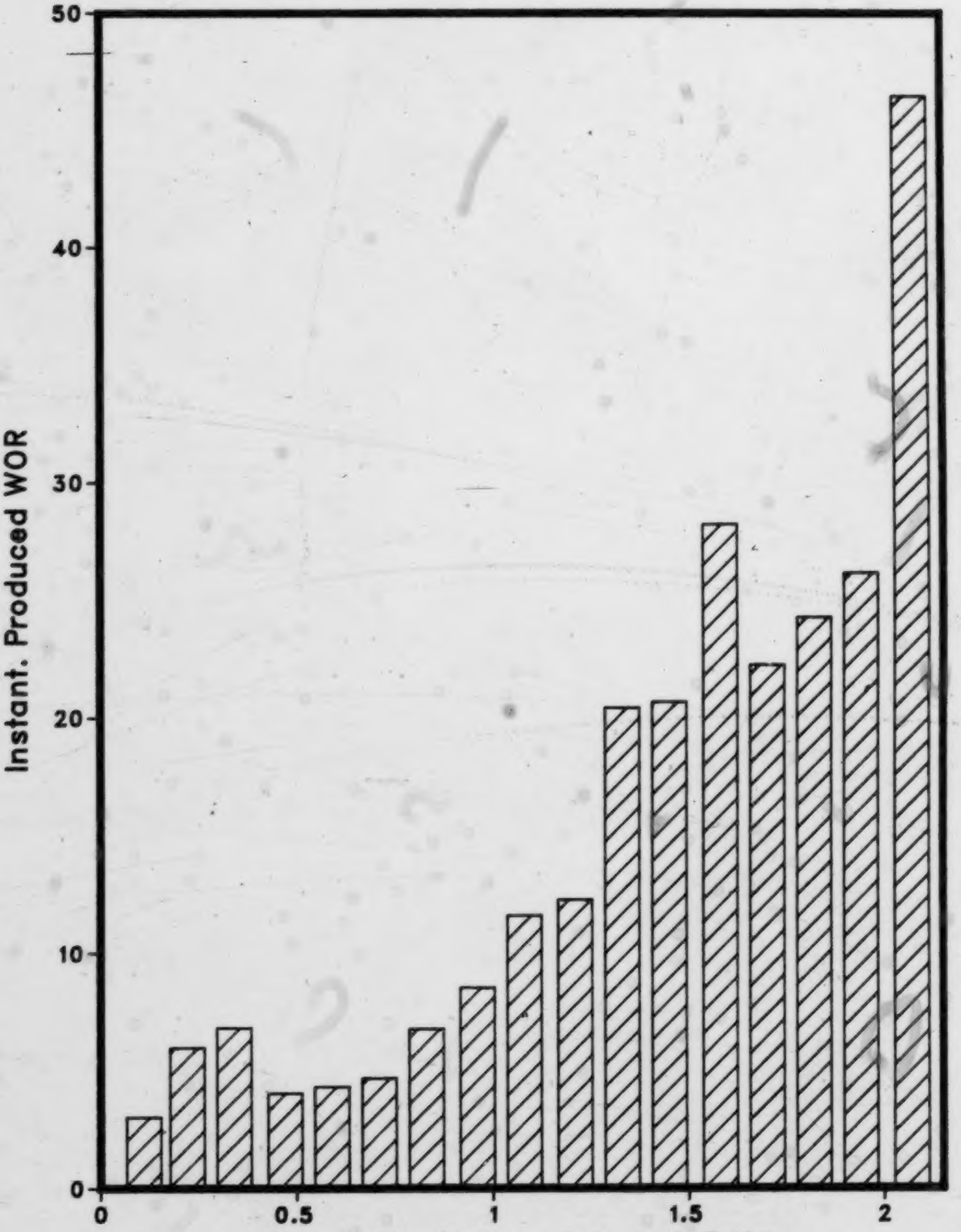

Figure 6.21 :Run 46 Solvent–Steamflood
Instantaneous Oil/Steam Ratio Vs. Cumulative Oil Produced

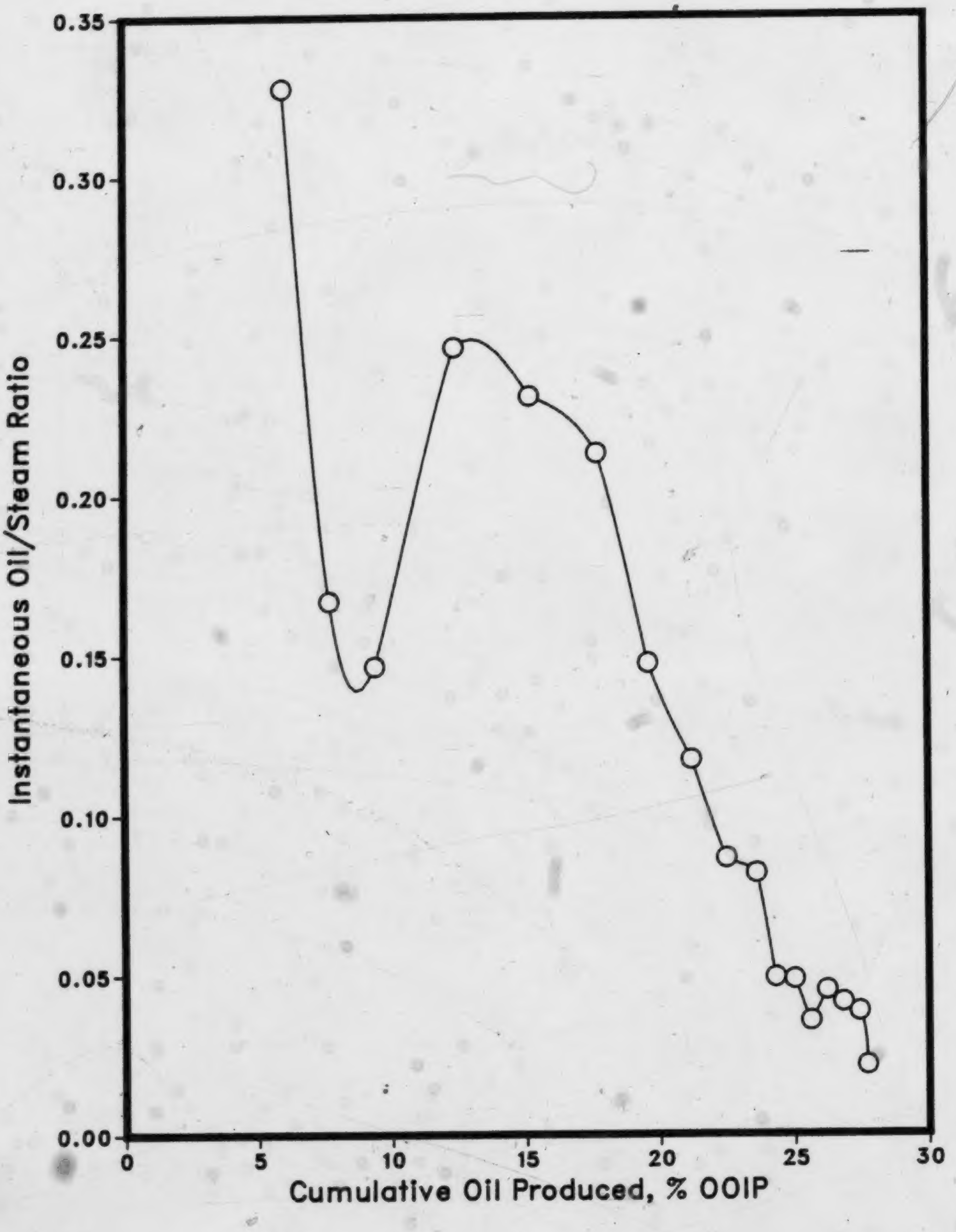

sweeping the model and creating an oil bank. Production of additional oil from the unswept and swept areas was indicated by the gradual decline of the curve after the peak.

Opposite to what occurred in the solvent flood, the top view temperature profiles for Runs 44 (Figures A.23-A.30), 45 (Figures A.35-A.42) and 46 (Figures A.47-A.54) indicate that the steam advanced faster through the upper level of the model than the lower section. The heat also appears to be moving slightly faster in the upper half of the model according to the cross-sectional temperature profiles provided in Figures A.31-A.34 (Run 44), Figures A.43-A.46 (Run 45) and Figures A.55-A.58 (Run 46). The faster heat advance in the upper section of the model was probably due to the gravity segregation behaviour of the steam in which the less dense steam tended to rise in the formation.

During the initial stages of the solvent-steamflood the solvent slug channelled into the oil zone and created a less resistant path for the steam to travel into oil, than would exist by simply injecting steam into an undisturbed oil region. This allowed the steam heat to be used more effectively to mobilize and displace the oil. The mobilized oil and solvent banked up at the production well creating a pressure buildup at the well. Once the banked up oil was produced and steam breakthrough occurred the high temperature steam continued to sweep through the model producing additional oil from both swept and unswept regions. The low solvent recovery of 33.1% in Run 46 is attributed to the higher water saturation in this run, which caused greater trapping of the injected solvent. The solvent recoveries for these runs were much lower than the solvent recovery of the solvent flood because less extensive channelling took place during the solvent-steamfloods and therefore more solvent mixed with the oil. This resulted in more solvent being trapped in the model as a residual hydrocarbon saturation. The three solvent-steamfloods required less solvent than Run 40 which also contributed to the lower solvent recovery. The use of the solvent slug before steam injection in the three solvent-steamflood experiments allowed the steam to contact a large area of oil which resulted in a more stable displacement of oil than in the case of a solvent flood (Run 40).

Oil recoveries for Runs 44 (27.1% OOIP), 45 (30.0% OOIP) and 46 (27.7% OOIP) were higher than that obtained for Run 40 (26.8% OOIP). However, the oil recovery for the solvent-steamfloods was about the same as previous continuous steamfloods such as Runs 26 (31.8% OOIP) and 27 (32.2 % OOIP), reported by Proctor, George and Farouq Ali [63]. Therefore using a solvent-steamflood process does not appear to be as economically attractive as a conventional steamflood performed in a homogeneous model. However, in the case of a heavy oil formation without bottom water and displaying a very low steam injectivity the implementation of solvent injection would help to raise steam injectivity. This would make steam penetration more extensive in the oil and therefore increase recovery compared to a conventional steamflood. The use of a solvent-steamflood process in a bottom water formation may also be better suited than a conventional steamflood process, which will be discussed later in this chapter.

Steamflood of a Bottom Water Model With Prior Gas Injection

It is believed that injecting a small portion of inert gas before performing a steamflood, a flow channel would form, which would divert the injected steam away from the bottom water region and into the oil zone. This would aid in minimizing the heat scavenging effects of the bottom water zone. The process of gas injection in combination with a conventional steamflood was first performed in a bottom water model which represents a base experiment.

Runs 60 and 61 investigated oil recoveries of a steamflood performed on a bottom model which contained a gas cap. The recoveries were carefully studied in order to determine the effectiveness of a steamflood in a reservoir containing a gas cap and bottom water layer. Tables 6.7 and 6.8 provide a list of the results for Runs 60 and 61, respectively. Bottom water thicknesses were 17.6% and 12.1% of the gross model thickness for Runs 60 and 61, respectively, and the initial gas saturations were 0.3% and 0.4% for Runs 60 and 61, respectively.

Runs 60 and 61 consisted of creating a gas cap in a bottom water model prior to a conventional steamflood. The gas cap was created by injecting nitrogen gas which displaced a small portion of oil in the model. The volume of the gas cap was considered to be the amount of oil displaced by the gas. Nitrogen gas was chosen since it was an inert gas and therefore would not initiate a chemical reaction in the model during the gas injection experiments. Since the initial gas saturation was relatively small the gas cap developed in the upper portion of the model and probably consisted of a small narrow channel extending from the injection well to the production well.

The recovery curves of Runs 60 (Figure 6.22) and 61 (Figure 6.26) gave an early indication that the presence of a gas cap and bottom water hindered the overall oil recovery. The oil recovery for Run 61 (19.5% OOIP) showed a higher recovery than Run 60 (13.6% OOIP) due to the thinner bottom water zone present in Run 61. The thinner bottom water layer resulted in less of the steams heat being scavenged and thus, more oil was mobilized and recovered during Run 61.

The bar plots of volume as a percentage of oleic phase in each sample taken versus cumulative volume injected and instantaneous produced WOR versus cumulative volume injected are provided for Runs 60 (Fig. 6.23 & 6.24) and 61 (Fig. 6.27 & 6.28). The values of instantaneous hydrocarbon produced were relatively low and there was no evidence of a prevalent peak in either of Figures 6.23 or 6.27 indicating that a well defined steam breakthrough did not occur during either experiment. Therefore a very unstable displacement appeared to exist during Runs 60 and 61, as also indicated by Figures 6.24 and 6.28. It was concluded that a majority of the injected steam flowed into the underlying bottom water or passed over the oil region into the gas cap.

The plots of instantaneous oil/steam ratio versus cumulative oil produced are displayed in Figures 6.25 (Run 60) and 6.29 (Run 61). Due to the thicker bottom water zone, Run 60 shows smaller oil/steam ratio values than Run 61. The oil/steam ratio curves in Runs 60 and 61 are quite different. In Run 60, steam clearly displaced the oil efficiently at first, but later breakthrough occurred, and the oil/steam ratio dropped. To a first approximation it can be said that the oil/steam ratio was relatively constant at 0.075. In Run 61, on the other hand, although the oil/steam ratios are generally higher than those in Run 60, the oil/steam ratio steadily drops. Overall the oil/steam ratio values for both experiments were low, which suggested that the underriding of the oil by the injected steam into the bottom water zone was quite prevalent in Runs 60 and 61 due to the lack of steam penetration into the oil layer.

Study of the temperature profiles for Runs 60 (Fig. A.59-A.66) and 61 (Fig. A.71-A.78) revealed that the injected heat advanced much more quickly through the lower region of the model due to the steam underriding the oil layer into the bottom water. The cross-sectional temperature profiles given in Figures A.67-A.70 (Run 60) and Figures A.79-

Table 6.7 : Run 60 Gas Injection Prior to Steamflood of Bottom Water Model

HC Pore Volume : 11500.0 cc
Pore Volume : 15080.0 cc
Bulk Volume : 42005.0 cc
Porosity : 35.9%
Initial Oil Satn. : 76.3%
Initial H2O Satn. : 23.4%
Initial Gas Satn. : 0.3%

Type of Oil Used : Faxam-100
Initial Model Temperature : 3.00 C
Water Feed Flow Rate : 200.00 cc/min
Boiler Feed Flow Rate : 29.20 cc/min
Total Flow Rate of Steam : 229.20 cc/min
Gas Cap Volume : 50.0 cc
Steam Vol. Inj. : 34850.0 cc (2.31 PV)
Bottom Water Layer Thickness : 17.6% (% Gross Thickness)

Net Oil Recovery : 13.6%

Final Oil Saturation : 65.9%

Cyl. No.	Tot. Vol. Inj. (cc)	Cum. Vol. Inj.		Oil Prod. (cc)	Cum. Oil Rec.		Oil-Steam Ratio	Inst Prod. WOR	Inst. Oil Prod. % of Sample
		(cc)	(P.V.)		(cc)	(%OOIP)			
1	1980	1980	0.13	65	65	0.6%	0.0339	29.46	3.3%
2	2195	4175	0.28	15	80	0.7%	0.0069	45.00	0.7%
3	1960	6135	0.41	45	125	1.1%	0.0235	42.56	2.3%
4	2210	8345	0.55	60	185	1.6%	0.0279	35.83	2.7%
5	2030	10375	0.69	145	330	2.9%	0.0769	13.00	7.1%
6	2030	12405	0.82	140	470	4.1%	0.0741	13.50	6.9%
7	1990	14395	0.95	130	600	5.2%	0.0699	14.31	6.5%
8	2025	16420	1.09	120	720	6.3%	0.0630	15.88	5.9%
9	2000	18420	1.22	120	840	7.3%	0.0638	15.67	6.0%
10	2135	20555	1.36	105	945	8.2%	0.0517	19.33	4.9%
11	2065	22620	1.50	60	1005	8.7%	0.0299	33.42	2.9%
12	2095	24715	1.64	135	1140	9.9%	0.0689	14.52	6.4%
13	1985	26700	1.77	105	1245	10.8%	0.0559	17.90	5.3%
14	2070	28770	1.91	85	1330	11.6%	0.0428	23.35	4.1%
15	2005	30775	2.04	80	1410	12.3%	0.0416	24.06	4.0%
16	2095	32870	2.18	75	1485	12.9%	0.0371	26.93	3.6%
17	1980	34850	2.31	80	1565	13.6%	0.0421	23.75	4.0%

Figure 6.22 :Run 60 Gas Injection Prior to Steamflood Cumulative Oil Recovery Vs. Pore Volumes Injected

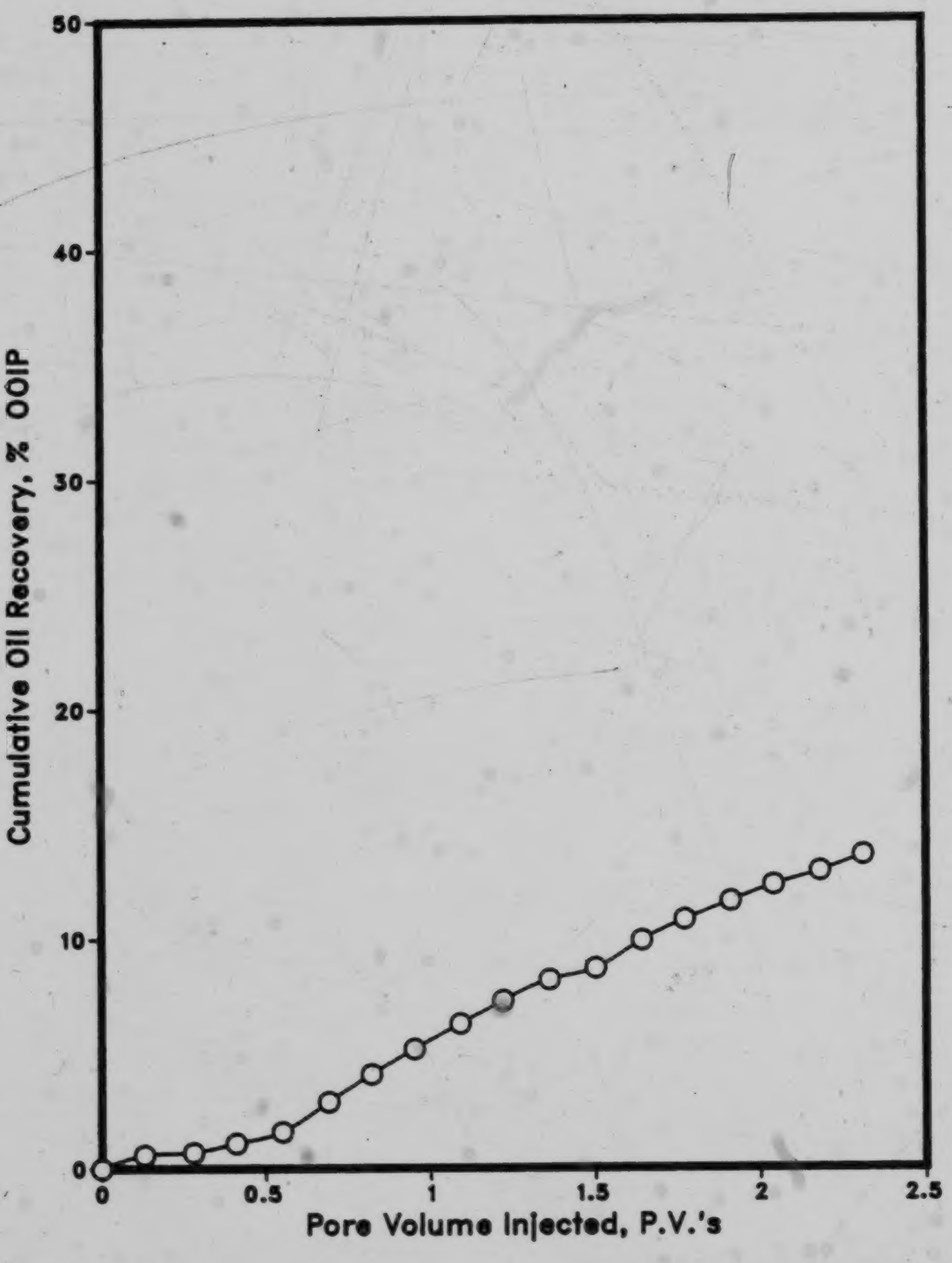

Figure 6.23 :Run 60 Gas Injection Prior to Steamflood
Oleic Phase in Each Sample Vs. Cumulative Volume Injected

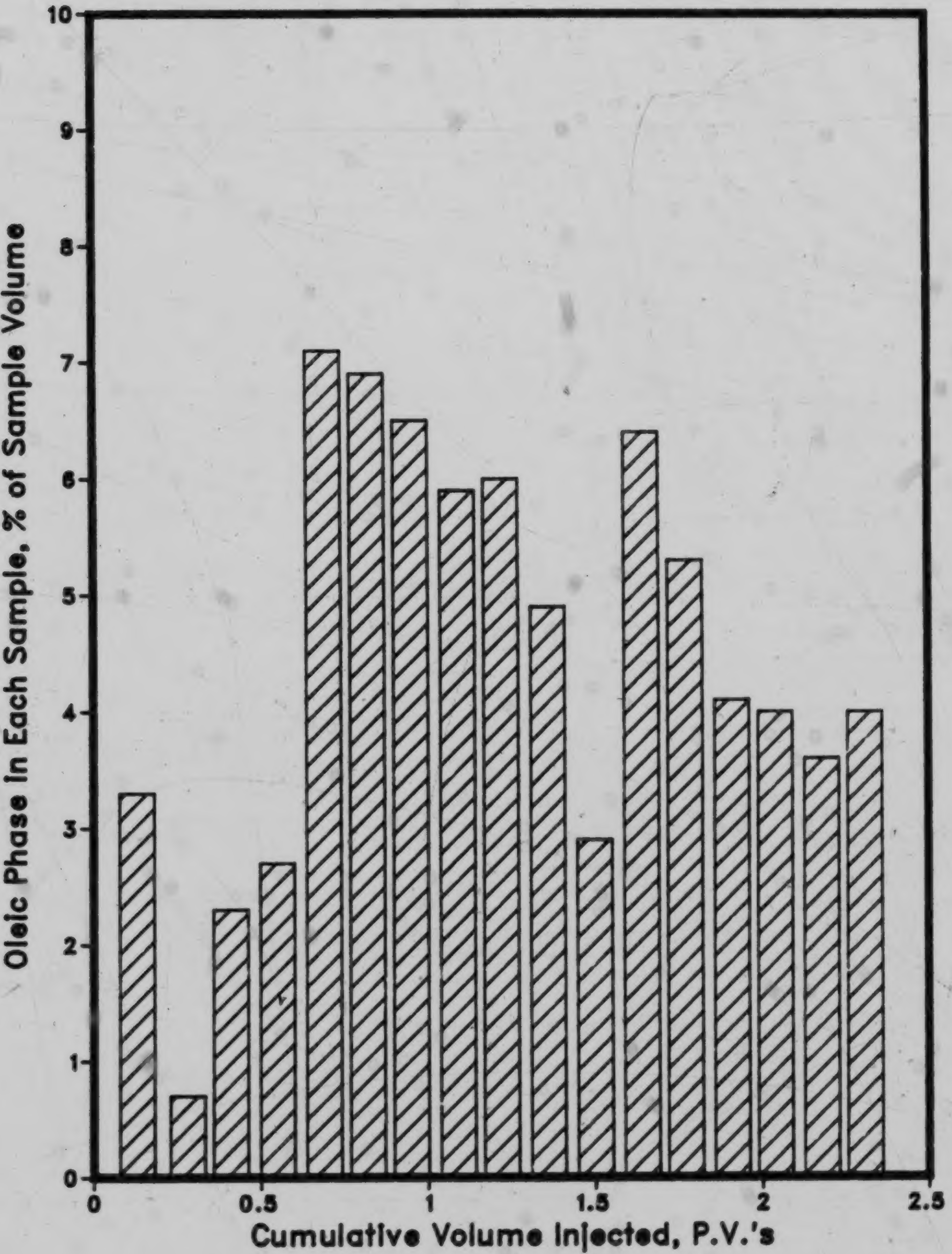

Figure 6.24 :Run 60 Gas Injection Prior to Steamflood Instantaneous Produced WOR Vs. Cumulative Volume Injected

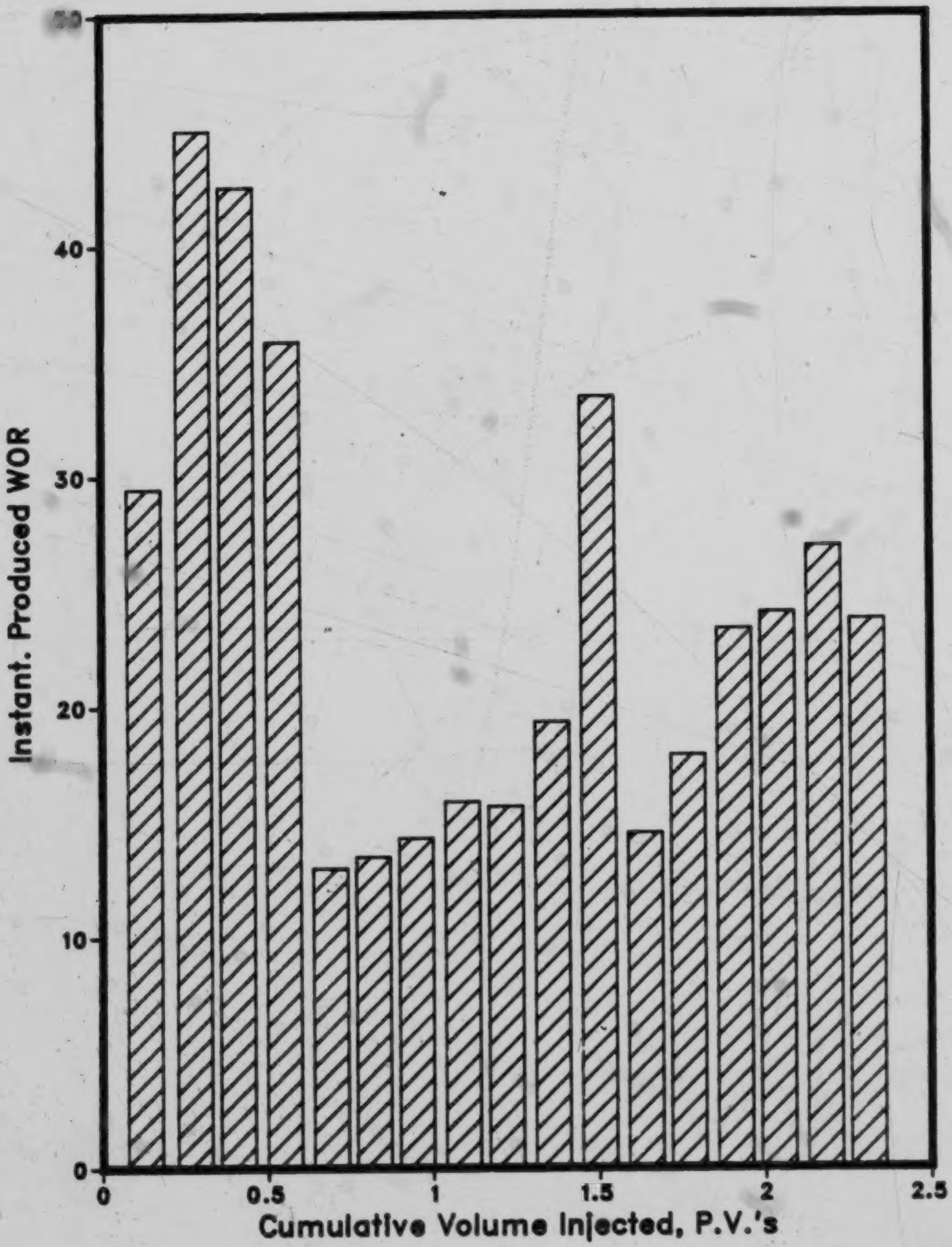

Figure 6.25 :Run 60 Gas Injection Prior to Steamflood Instanteous Oil/Steam Ratio vs. Cumulative Oil Produced

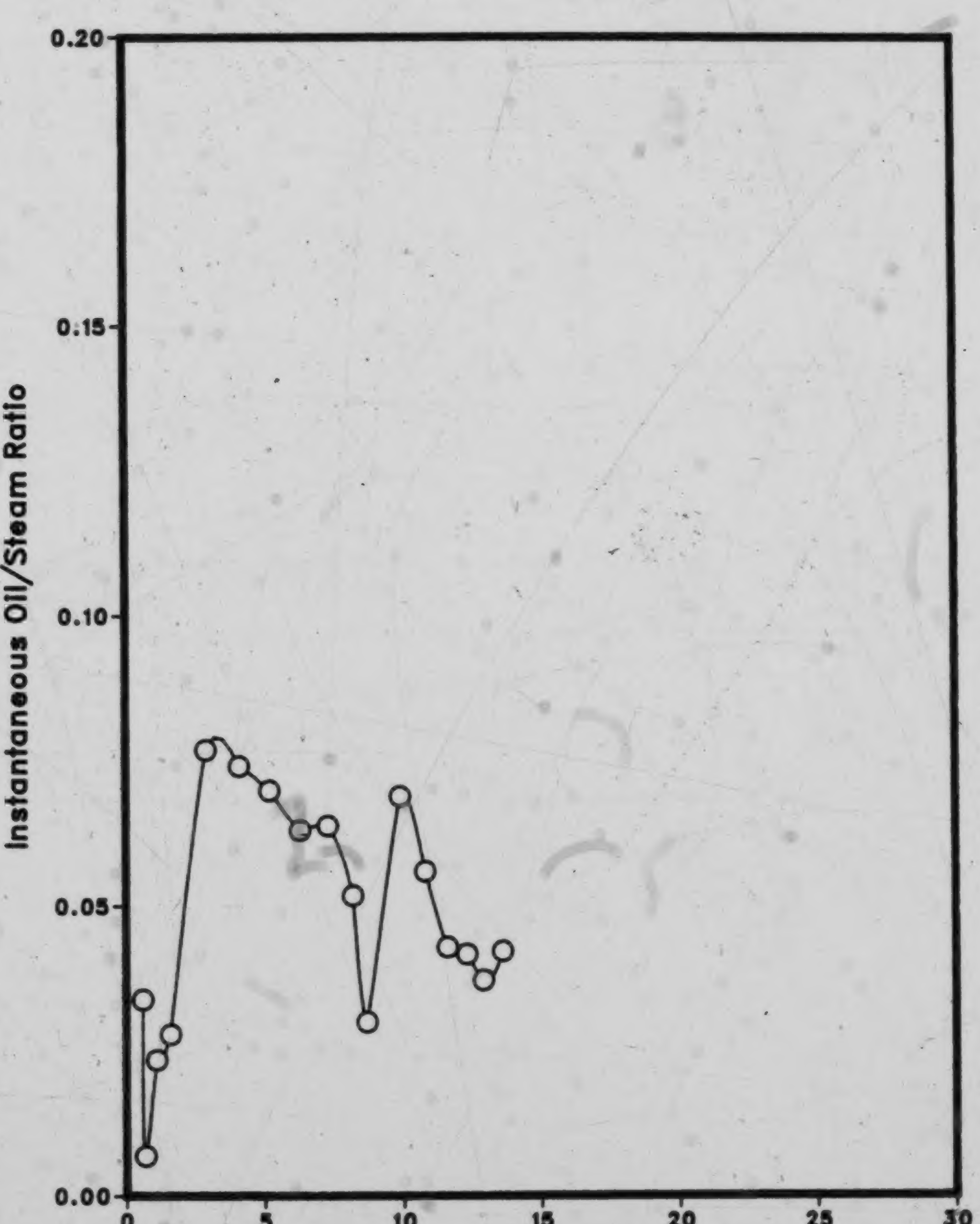

Table 6.8 : Run 61 Gas Injection Prior to Steamflood of Bottom Water Model

HC Pore Volume : 12615.0 cc
Pore Volume : 15115.0 cc
Bulk Volume : 42005.0 cc
Porosity : 36.0%
Initial Oil Satn. : 83.5%
Initial H2O Satn. : 16.2%
Initial Gas Satn. : 0.4%

Type of Oil Used : Faxam-100
Initial Model Temperature : 3.00 C
Water Feed Flow Rate : 200.00 cc/min
Boiler Feed Flow Rate : 29.20 cc/min
Total Flow Rate of Steam : 229.20 cc/min
Gas Cap Volume : 55.0 cc
Steam Vol. Inj. : 34800.0 cc (2.30 PV)
Bottom Water Layer Thickness : 12.1% (% Gross Thickness)

Net Oil Recovery : 19.5%

Final Oil Saturation : 67.2%

Cyl. No.	Tot. Vol. Inj. (cc)	Cum. Vol. Inj.		Oil Prod. (cc)	Cum. Oil Rec.		Oil-Steam Ratio	Inst Prod. WOR	Inst. Oil Prod. % of Sample
		(cc)	(P.V.)		(cc)	(%OOIP)			
1	1850	1850	0.12	260	260	2.1%	0.1635	6.12	14.1%
2	2180	4030	0.27	145	405	3.2%	0.0713	14.03	6.7%
3	2055	6085	0.40	225	630	5.0%	0.1230	8.13	10.9%
4	2020	8105	0.54	195	825	6.5%	0.1068	9.36	9.7%
5	2025	10130	0.67	185	1010	8.0%	0.1005	9.95	9.1%
6	2060	12190	0.81	160	1170	9.3%	0.0842	11.88	7.8%
7	1985	14175	0.94	160	1330	10.5%	0.0877	11.41	8.1%
8	2065	16240	1.07	145	1475	11.7%	0.0755	13.24	7.0%
9	1995	18235	1.21	135	1610	12.8%	0.0726	13.78	6.8%
10	2360	20595	1.36	120	1730	13.7%	0.0536	18.67	5.1%
11	1940	22535	1.49	125	1855	14.7%	0.0689	14.52	6.4%
12	2085	24620	1.63	105	1960	15.5%	0.0530	18.86	5.0%
13	1985	26605	1.76	85	2045	16.2%	0.0447	22.35	4.3%
14	2175	28780	1.90	160	2205	17.5%	0.0794	12.59	7.4%
15	1980	30760	2.04	80	2285	18.1%	0.0421	23.75	4.0%
16	2070	32830	2.17	90	2375	18.8%	0.0455	22.00	4.3%
17	1970	34800	2.30	85	2460	19.5%	0.0451	22.18	4.3%

Figure 6.26 :Run 61 Gas Injection Prior to Steamflood
Cumulative Oil Recovery Vs. Pore Volumes Injected

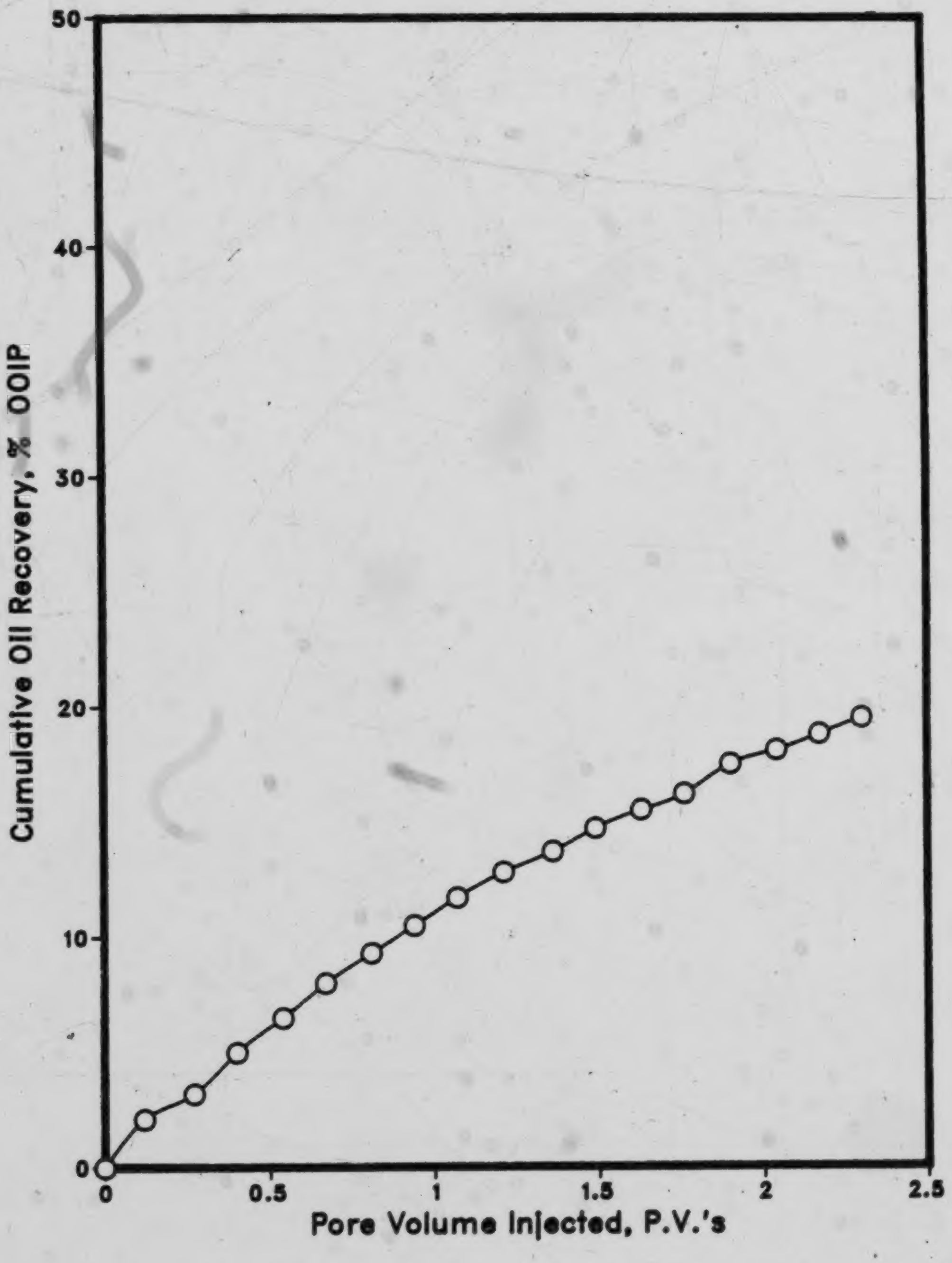

Figure 6.27 :Run 61 Gas Injection Prior to Steamflood
Oleic Phase In Each Sample Vs. Cumulative Volume Injected

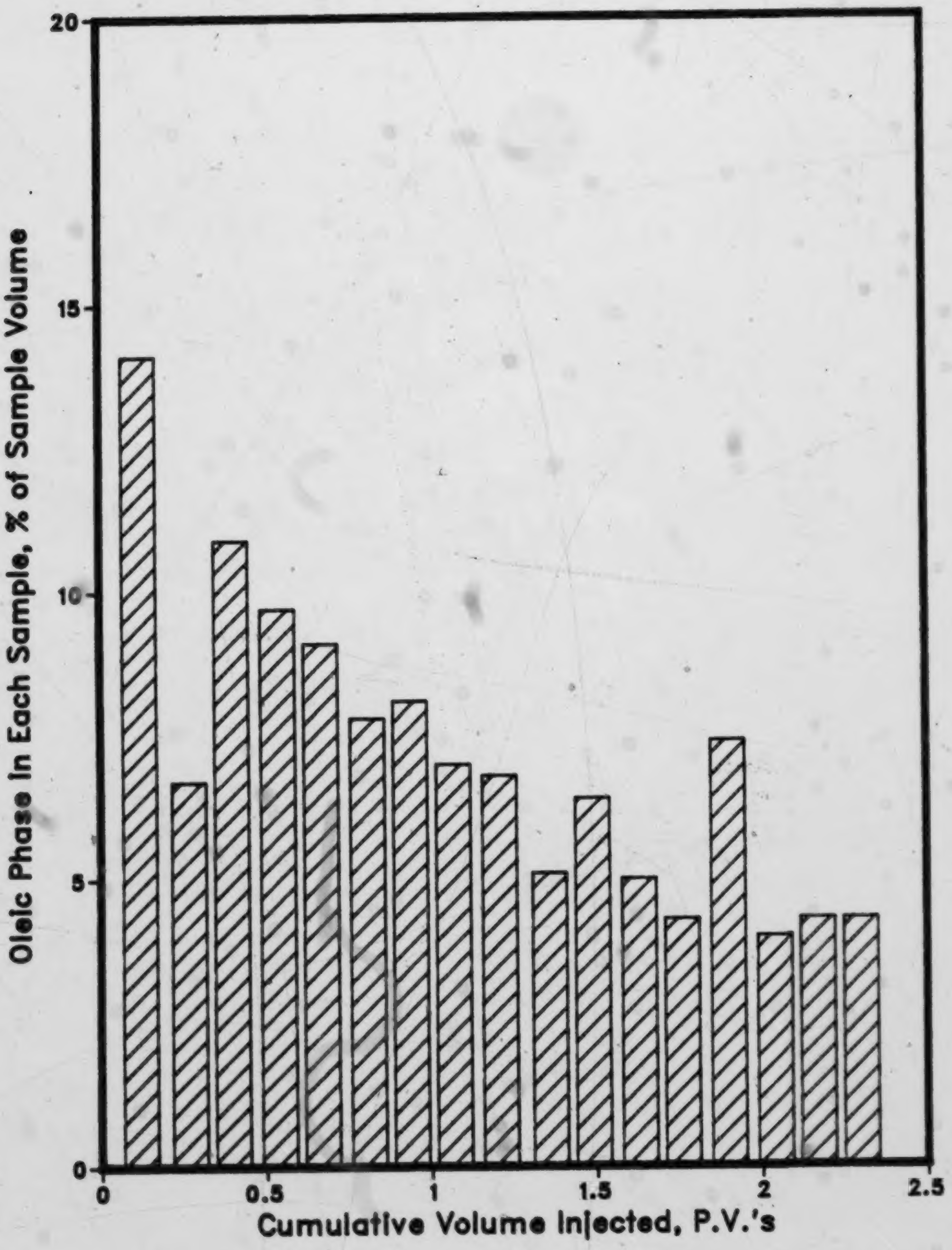

Figure 6.28 :Run 61 Gas Injection Prior to Steamflood Instantaneous Produced WOR Vs. Cumulative Volume Injected

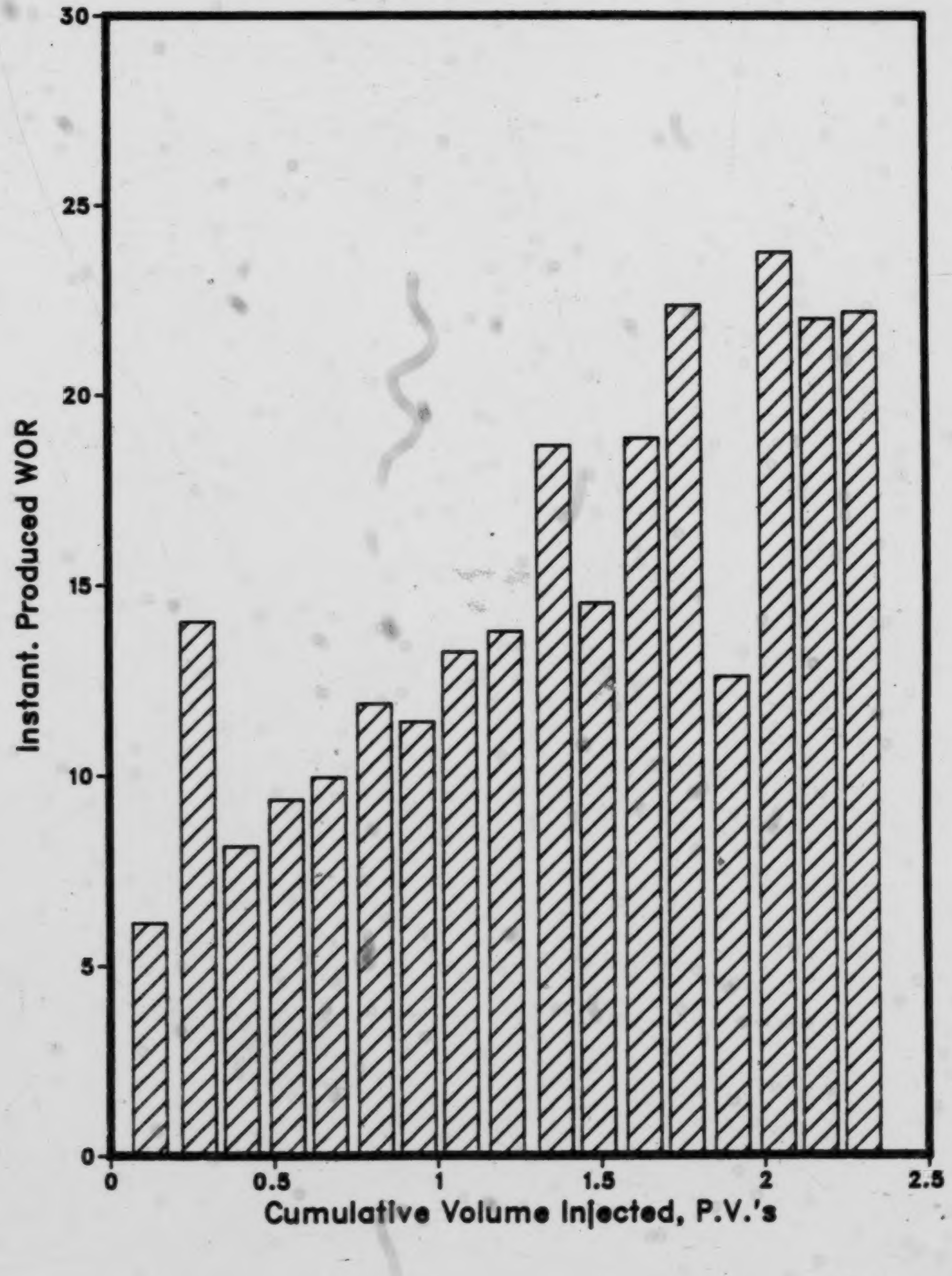

Figure 6.29 :Run 61 Gas Injection Prior to Steamflood Instanteous Oil/Steam Ratio vs. Cumulative Oil Produced

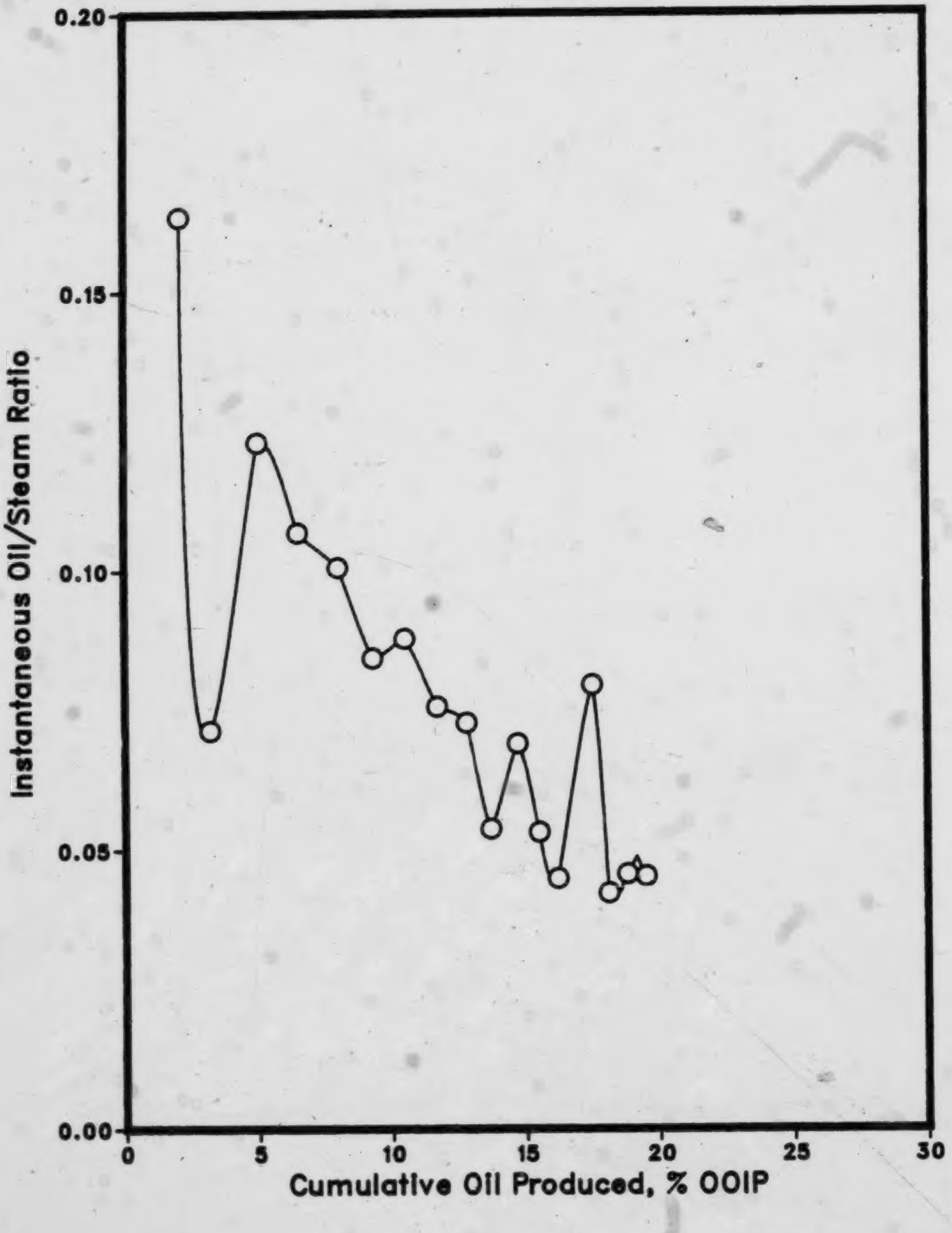

A.82 (Run 61) illustrate the prevalent heat scavenging nature of the bottom water since the heat appeared to travel faster in the lower section of the model.

It was concluded from the results of Runs 60 and 61 that the presence of a gas cap during a steamflood of a bottom water model tended to partially divert the steam away form the bottom water so that it could be used more effectively to heat up and mobilize the oil region. Comparison of the recoveries (Figure 6.30) of Run 39, a conventional steamflood, and Run 61, a steamflood preceded by gas injection, which had similar bottom water thicknesses, indicated that the presence of a gas cap somewhat improved the initial recovery response of a steamflood performed in a bottom water model. Also a comparison of the other plots generated for Runs 39 and 61 indicated steam breakthrough occurred sooner and was less distinct in the case of Run 39, which again confirmed that the implementation of a gas cap has the potential to improve the oil recovery during the steamflood of a bottom water formation.

From the results of Runs 60 and 61 the implementation of a solvent-steamflood process in a model with a gas cap and bottom water may further improve oil recovery by partially diverting more injected steam away from the detrimental bottom water zone.

Figure 6.30 :Comparison of Steamflood Run 39 & Gas Injection Prior to a Steamflood Run 61 Recoveries Performed in a Bottom Water Model

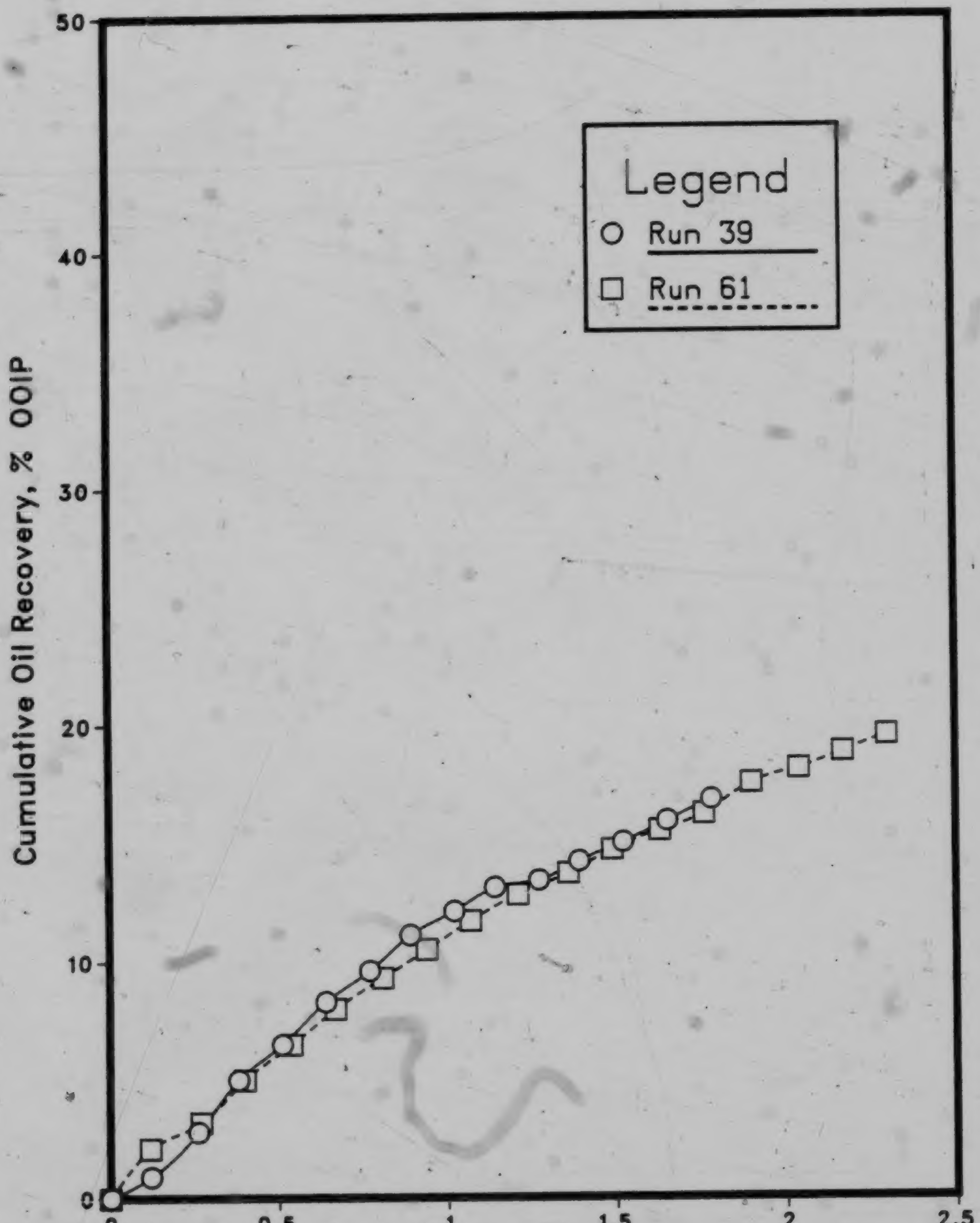

Effect of Solvent Slug Size on Oil Recovery by a Steamflood

It was important in this study to determine the effect of different solvent slug sizes on the overall oil recovery of a solvent-steamflood process. By determing the effect of solvent slug size, an optimal slug size might be established in order to increase oil recovery of a solvent-steamflood process.

Run 65 was conducted to investigate the effect of varying the amount of solvent injected into a bottom water model prior to steamflooding. The experiment involved doubling the solvent slug size from 10% of the model pore volume to 20%. The bottom water layer in the model was thick (19.6% of the gross model thickness). The results of Run 65 are provided in Table 6.9.

The oil recovery yielded in Run 65 was 19.8% of the original oil in place. The recovery curve of Run 65 is given in Figure 6.31. Runs 53 and 54 involved solvent-steamfloods of bottom water models with reasonably thick bottom water thicknesses of 15.2% and 12.2% of the gross model thickness, respectively and a solvent slug size of 10% of the model pore volume. These two similar experiments were compared with Run 65 in order to determine the effect of a larger solvent slug. The shape of the curve in Figure 6.31 was similar to that of the recovery curves obtained in Runs 53 and 54 even though Run 65 had a greater bottom water thickness. This suggested that the increase in the solvent slug size to 20% of the model pore volume somewhat improved the overall oil recovery. Due to the thick bottom water layer, the loss of injected solvent to the bottom water was prevalent, explaining the solvent recovery of 73.0%. However, solvent recovery was still comparable to the solvent recoveries of Runs 53 and 54 which were 54.4% and 89.8%, respectively.

The bar plots of volume as a percentage of oleic phase in each sample collected versus cumulative volume injected and instantaneous produced WOR versus cumulative volume injected are provided for Run 65 (Fig. 6.32 & 6.33). It was observed from

Figures 6.32 and 6.33 that Run 65 required longer for steam breakthrough to occur, compared to the steam breakthrough times for Runs 53 and 54. The longer steam breakthrough time was probably due to the larger solvent slug used which mobilized and displaced more of the in-place oil than the 10% solvent slug run. Therefore a larger volume of solvent and oil banked up at the production well. Steam breakthrough was prolonged because of the larger oil/solvent bank at the production well which required longer to be produced.

The plot of instantaneous oil/steam ratio versus cumulative oil produced for Run 65 is provided in Figure 6.34. Comparing the similar plots of Runs 53 and 54 it was noted that the initial values of oil/steam ratio in Figure 6.34 were much larger than the initial oil/steam ratio values for Runs 53 and 54. This suggested, as did the previously discussed bar plots (Figures 6.32 & 6.33), that a larger oil/solvent bank formed at the production well during Run 65. It seems that one-half of the oil is displaced very efficiently with large oil/steam ratios. Following that steam seems to channel into the water and recovery slows down. As more oil was produced the oil/steam ratios of Figure 6.34 dropped until they were less than the later oil/steam ratio values for Runs 53 and 54. The thicker bottom water layer present in Run 65 appeared to be more prevalent during the final stages of the experiment.

The temperature profiles for Run 65 are given in Figures A.83-A.90. Careful examination of the temperature profiles revealed that the injected heat travelled at about the same rate in both the upper and lower sections of the model during Run 65 as compared to Runs 53 and 54, despite the thicker bottom water layer of Run 65. This would indicate that the larger solvent slug created more extensive channels in the oil zone allowing the injected steam to be more efficiently used throughout the oil region instead of being lost to the bottom water. The cross-sectional temperature profiles in Figures A.91 through A.94 also indicate this.

Table 6.9 : Run 65 Solvent-Steamflood With Bottom Water

HC Pore Volume : 11140.0 cc
Pore Volume : 15180.0 cc
Bulk Volume : 42005.0 cc
Porosity : 36.1%
Initial Oil Satn. : 73.4%
Initial H2O Satn. : 26.6%
Solvent Vol. Inj.: 2800.0 cc (20.0% PV)
Steam Vol. Inj. : 32005.0 cc (2.09 PV)

Type of Oil Used : Faxam-100
Initial Model Temperature : 3.00 C
Water Feed Flow Rate : 200.00 cc/min
Boiler Feed Flow Rate : 29.20 cc/min
Total Flow Rate of Steam : 229.20 cc/min
Solvent Flow Rate : 200.00 cc/min
Bottom Water Layer Thickness : 19.6 % (% Gross Thickness)

Net Oil Recovery : 19.8% **Solvent Recovery : 73.0%** **Final Oil Saturation : 58.9%**

Cyl. No.	Solvent Conc. (%)	Tot. Vol. Inj. (cc)	Cum. Vol. Inj.		HC Prod. (cc)	Oil Prod. (cc)	Cum. Oil Rec.		Cum. Sol. Rec.		Oil-Steam Ratio	Inst Prod. WOR	Inst. HC Prod. % of Sample
			(cc)	(P.V.)			(cc)	(%OOIP)	(cc)	(%)			
1	0%	1400	1400	0.09	25	25	25	0.2%	0	0.0%	0.0182	55.00	1.8%
2	69%	1205	2605	0.17	845	262	287	2.6%	583	20.8%	2.3472	0.43	70.1%
3	82%	1500	4105	0.27	1095	197	484	4.3%	1481	52.9%	2.7037	0.37	73.0%
4	53%	1705	5810	0.38	795	374	858	7.7%	1902	67.9%	0.8736	1.14	46.6%
5	30%	2050	7860	0.52	235	165	1023	9.2%	1972	70.4%	0.1295	7.72	11.5%
6	21%	2025	9885	0.65	130	103	1126	10.1%	1999	71.4%	0.0686	14.58	6.4%
7	16%	2135	12020	0.79	45	38	1164	10.4%	2006	71.6%	0.0215	46.44	2.1%
8	12%	2205	14225	0.94	55	48	1212	10.9%	2013	71.9%	0.0256	39.09	2.5%
9	11%	2120	16345	1.08	70	62	1274	11.4%	2021	72.2%	0.0341	29.29	3.3%
10	9%	2000	18345	1.21	105	96	1370	12.3%	2030	72.5%	0.0554	18.05	5.3%
11	6%	1940	20285	1.34	105	99	1469	13.2%	2036	72.7%	0.0572	17.48	5.4%
12	3%	2075	22360	1.47	100	97	1566	14.1%	2039	72.8%	0.0506	19.75	4.8%
13	2%	1955	24315	1.60	105	103	1669	15.0%	2041	72.9%	0.0568	17.62	5.4%
14	1%	2055	26370	1.74	135	134	1803	16.2%	2042	72.9%	0.0703	14.22	6.6%
15	1%	2080	28450	1.87	115	114	1917	17.2%	2043	73.0%	0.0585	17.09	5.5%
16	0%	2190	30640	2.02	95	95	2012	18.1%	2043	73.0%	0.0453	22.05	4.3%
17	0%	1985	32625	2.15	95	95	2107	18.9%	2043	73.0%	0.0503	19.89	4.8%
18	0%	2180	34805	2.29	95	95	2202	19.8%	2043	73.0%	0.0456	21.95	4.4%

Figure 6.31 :Run 65 Solvent–Steamflood With Bottom Water
Cumulative Oil Recovery Vs. Pore Volumes Injected

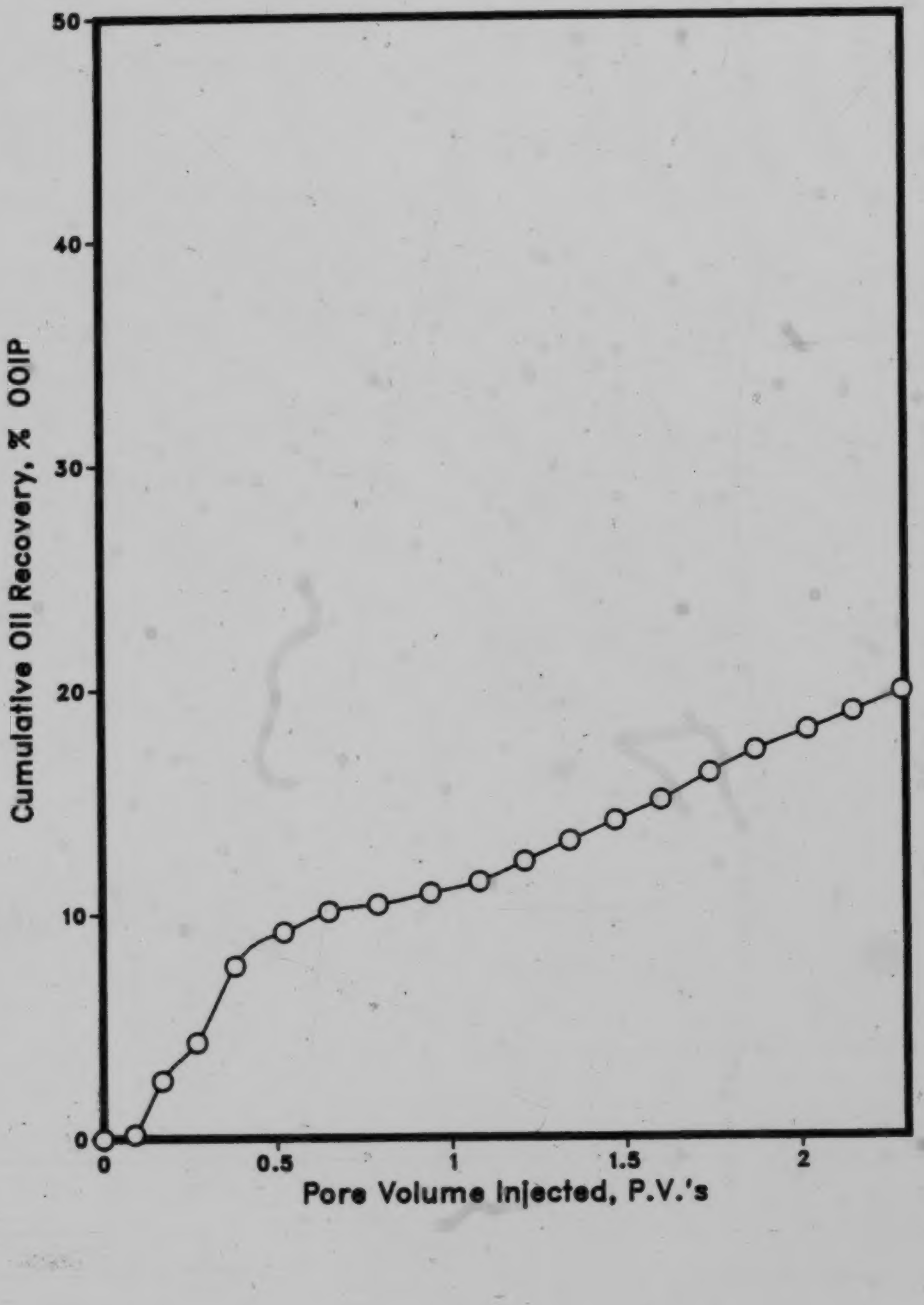

Figure 6.32 :Run 65 Solventflood–Steamflood With Bottom Water Oleic Phase In Each Sample Vs. Cumulative Volume Injected

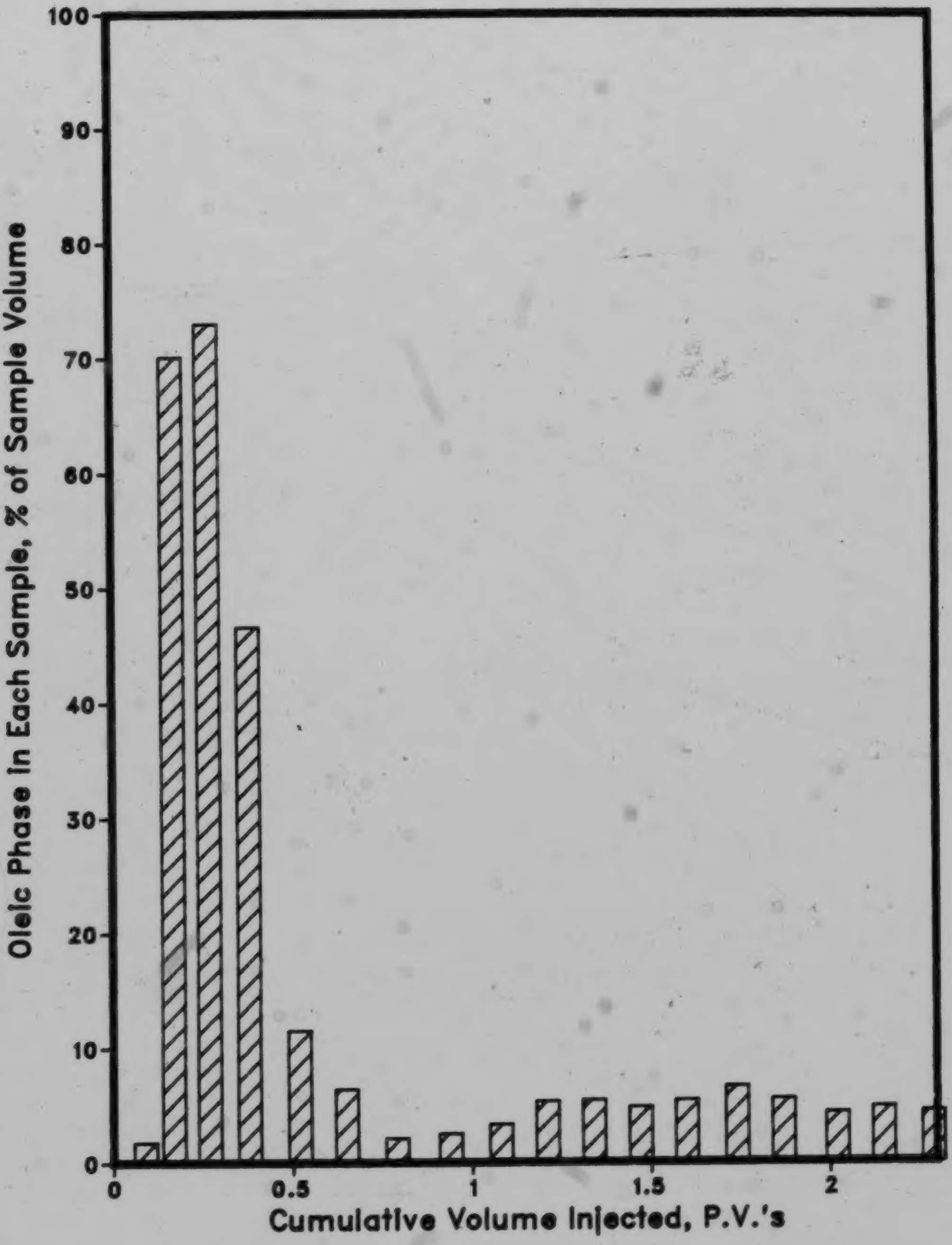

Figure 6.33 :Run 65 Solvent–Steamflood With Bottom Water Instantaneous Produced WOR Vs. Cumulative Volume Injected

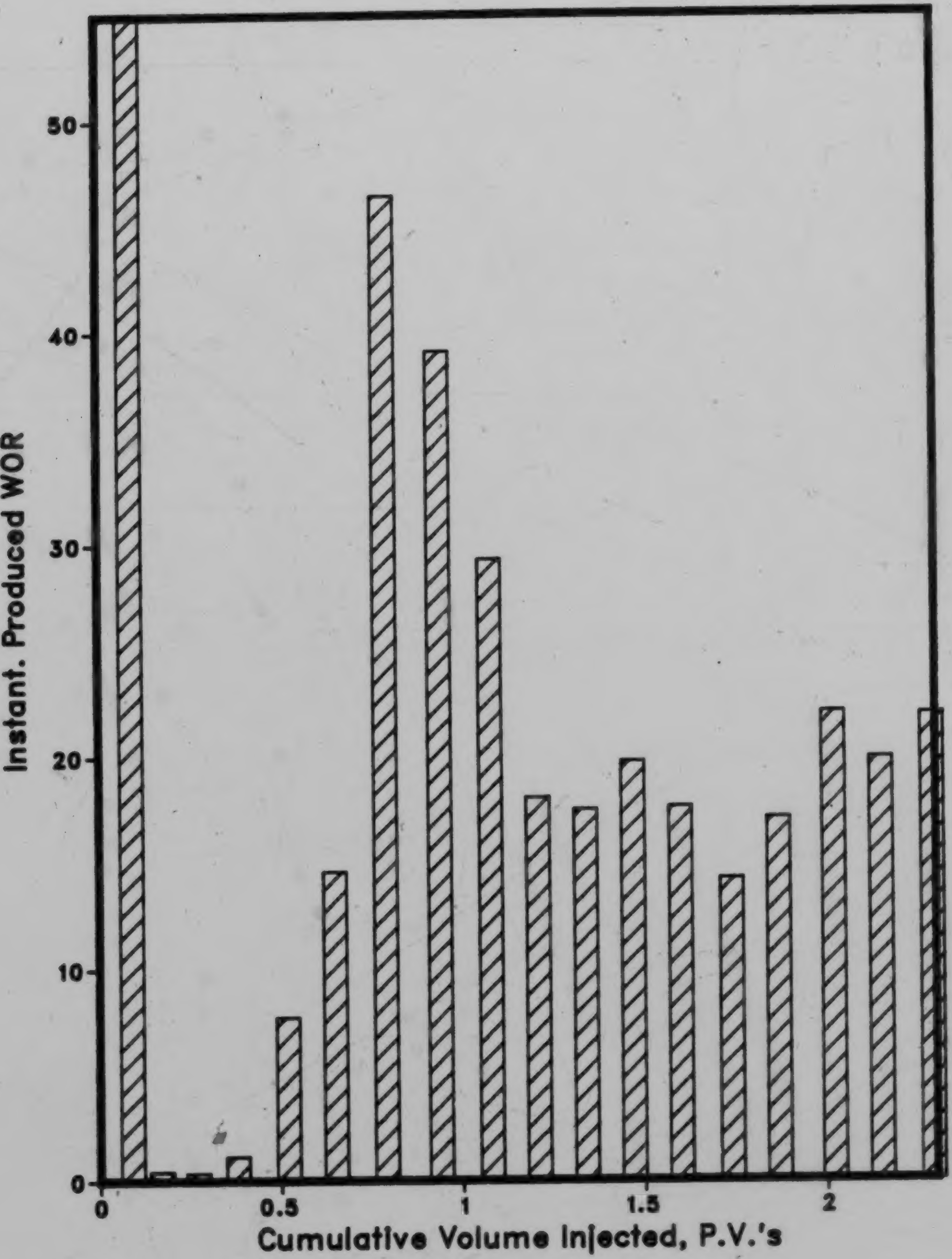

Figure 6.34 :Run 65 Solvent–Steamflood With Bottom Water Instanteous Oil/Steam Ratio vs. Cumulative Oil Produced

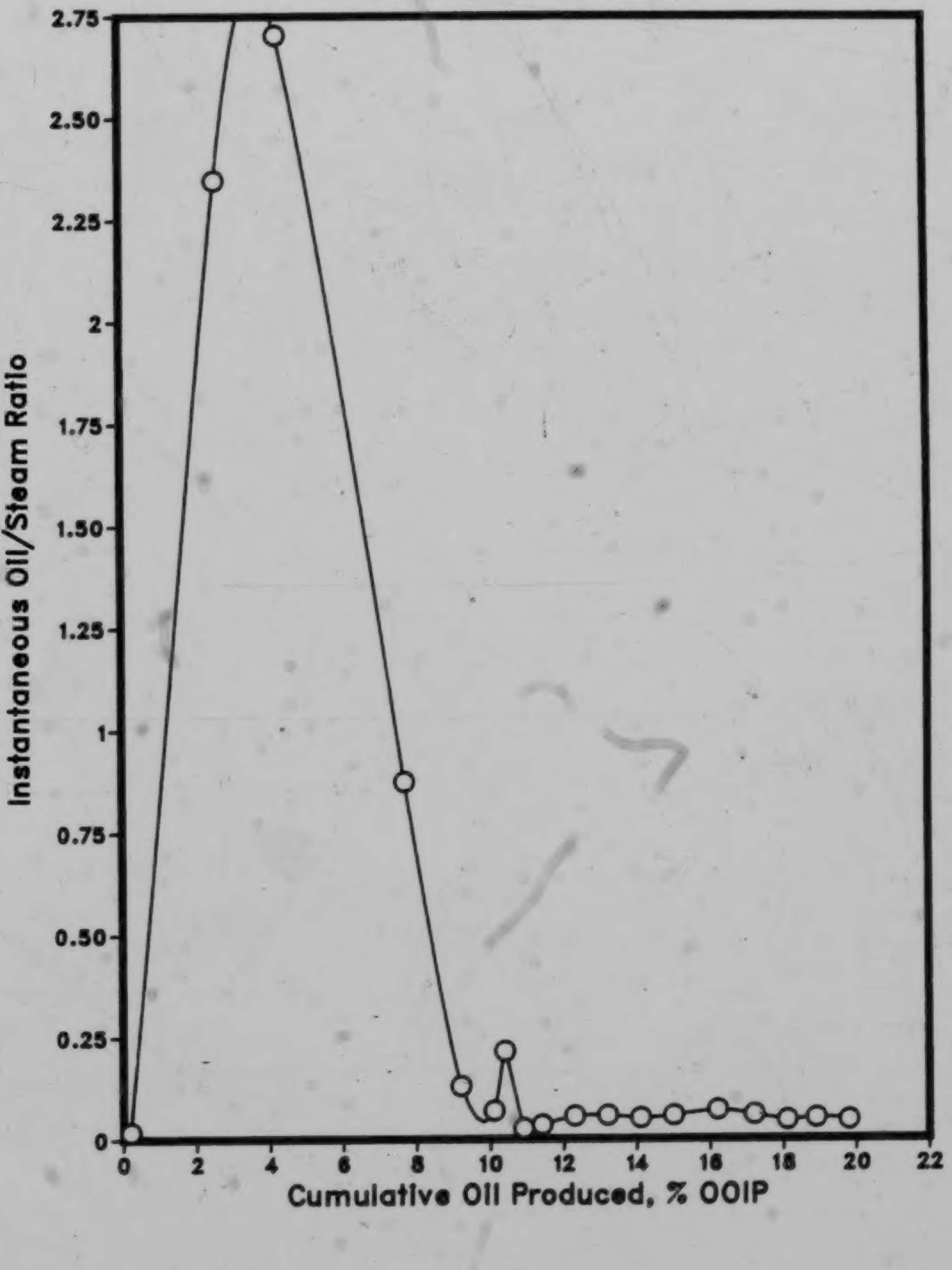

A comparison of the results of Run 65 with those of Runs 53 and 54 indicates that increasing solvent slug size may be beneficial to the overall oil recovery. However, one must also consider the extra cost of using additional solvent. This points to an optimal solvent slug size that would produce enough additional oil from the reservoir to warrant the additional expense of using more solvent in the recovery process.

It was decided to use homogeneous models instead of bottom water models, in the further examination of the effect of solvent slug size on recovery, so as to provide more consistent initial model conditions. In the case of the bottom water models the bottom water thicknesses could vary appreciably from one experiment to another, and thus the homogeneous models offered better reproducibility of initial model conditions than the bottom water models. The experimental results of the homogeneous model runs would therefore be more representative of the effect of solvent slug size.

Runs 66, 45 and 67 used solvent slug sizes of 5, 10 and 15% of the total pore volume, respectively. The three experiments involved solvent-steamfloods of a homogeneous model with varying solvent slug sizes. The results of Runs 66, 67 and 45 are provided in Tables 6.10, 6.11 and 6.5, respectively.

Analysis of the recovery curves for Runs 66 (Figure 6.35), 67 (Figure 6.39) and 45 (Figure 6.14) indicate that the experiment implementing the 10% solvent slug (Run 45) provided the best recovery. The recoveries for the 5% (Run 66) and 15% (Run 67) solvent slug experiments were 24.2% OOIP and 25.9% OOIP, which were somewhat less than that obtained in Run 45 (30.0% OOIP).

The bar plots of the amount of oleic phase in each sample as a percentage of each sample volume versus cumulative volume injected and instantaneous produced WOR versus cumulative volume injected are provided for Runs 66 (Fig. 6.36-6.37), 67 (Fig. 6.40-6.41) and 45 (Fig. 6.15-6.16). Figures 6.40 (Run 67) and 6.15 (Run 45) exhibited similar behaviours. The same plot for Run 66 (Figure 6.36) displayed less favorable behaviour than Figures 6.40 and 6.15 due to the smaller solvent (5%) used. The steam breakthrough for Run 66 occurred sooner and was not clear since a smaller oil/solvent bank formed due to less solvent injected. This caused the hydrocarbon bank to be produced more quickly and resulted in early steam breakthrough. Run 45 displayed a slightly more stable steam displacement of oil than Run 67 (ie. longer time until steam breakthrough and a more distinct breakthrough), which explains the higher recovery yielded by Run 45. The WOR bar plots also indicate a more stable displacement for Run 45 (Figure 6.16) compared to Runs 66 (Figure 6.37) and 67 (Figure 6.41). The displacement in Run 67 (15% solvent slug) appears to be only slightly less stable than for Run 45 from observation of Figures 6.41 and 6.16.

The plots of instantaneous oil/steam ratio versus cumulative oil produced for Runs 66 (Figure 6.38), 67 (Figure 6.42) and 45 (Figure 6.17) suggest that Run 45 was the most effective displacement, followed by Run 67, and finally Run 66 was the least stable displacement of the three experiments.

The top view temperatures profiles for Runs 66 (Fig. A.95-A.102), 67 (Fig. A.107-A.114) and 45 (Fig. A.35-A.42) all indicated that the heat advanced through both the upper and lower sections of the model at about the same rate for all three experiments. Observation of Figures A.35-A.42 for Run 45 indicated that the heat was retained in the upper region of the model for a longer period than it was during Runs 66 and 67. This suggested that the 10% solvent slug used in Run 45 formed more effective channels in the oil zone for the steam to penetrate and mobilize the inplace oil. Comparison of the cross-sectional profiles for Runs 66 (Fig. A.103-A.106), 67 (Fig. A.115-A.118) and 45 (Fig. A.43-A.46) also pointed out that the heat remained in the upper portion of the model longest during Run 45.

The solvent recoveries yielded for Runs 66 , 45 and 67 were 91.4%, 71.2% and 97.0%, respectively, which are quite reasonable recovery values.

As reported by Alikhan [64] the use of a 10% solvent slug prior to steam injection provided the best oil recovery compared to the 5% and 15% solvent slug runs. A

Table 6.10 : Run 66 Solvent-Steamflood With Homogeneous Model

HC Pore Volume : 13120.0 cc
Pore Volume : 14060.0 cc
Bulk Volume : 42005.0 cc
Porosity : 33.5%
Initial Oil Satn. : 93.3%
Initial H2O Satn. : 6.7%
Solvent Vol. Inj.: 700.0 cc (5.0% PV)

Type of Oil Used : Faxam-100
Initial Model Temperature : 3.00 C
Water Feed Flow Rate : 213.60 cc/min
Boiler Feed Flow Rate : 29.20 cc/min
Total Flow Rate of Steam : 242.80 cc/min
Solvent Flow Rate : 200.00 cc/min
Steam Vol. Injected : 35780 cc (2.55 PV)

Net Oil Recovery : 24.2% **Solvent Recovery : 91.4%** **Final Oil Saturation : 70.8%**

Cyl. No.	Solvent Conc. (%)	Tot. Vol Inj. (cc)	Cum. Vol. Inj.		HC Prod. (cc)	Oil Prod. (cc)	Cum. Oil Rec.		Cum. Sol. Rec.		Oil-Steam Ratio	Inst Prod. WOR	Inst. HC Prod. % of Sample
			(cc)	(P.V.)			(cc)	(%OOIP)	(cc)	(%)			
1	54%	1780	1780	0.13	855	393	393	3.0%	462	66.0%	0.0000	1.08	48.0%
2	20%	2020	3800	0.27	325	260	653	5.0%	527	75.3%	0.1917	5.22	16.1%
3	8%	1980	5780	0.41	320	294	947	7.2%	553	79.0%	0.1928	5.19	16.2%
4	7%	2110	7890	0.56	355	330	1277	9.7%	578	82.6%	0.2023	4.94	16.8%
5	6%	1945	9835	0.70	300	282	1559	11.9%	596	85.1%	0.1824	5.48	15.4%
6	5%	2035	11870	0.84	230	219	1778	13.6%	607	86.7%	0.1274	7.85	11.3%
7	5%	2035	13905	0.99	215	204	1982	15.1%	618	88.3%	0.1181	8.47	10.6%
8	5%	2040	15945	1.13	155	147	2129	16.2%	626	89.4%	0.0822	12.16	7.6%
9	4%	1930	17875	1.27	140	134	2263	17.2%	632	90.3%	0.0782	12.79	7.3%
10	3%	2135	20010	1.42	130	126	2389	18.2%	636	90.9%	0.0648	15.42	6.1%
11	2%	2015	22025	1.57	115	113	2502	19.1%	638	91.1%	0.0605	16.52	5.7%
12	1%	2030	24055	1.71	145	144	2646	20.2%	639	91.3%	0.0769	13.00	7.1%
13	1%	2000	26055	1.85	120	119	2765	21.1%	640	91.4%	0.0638	15.67	6.0%
14	0%	2070	28125	2.00	110	110	2875	21.9%	640	91.4%	0.0561	17.82	5.3%
15	0%	1890	30015	2.13	95	95	2970	22.6%	640	91.4%	0.0529	18.89	5.0%
16	0%	2225	32240	2.29	50	50	3020	23.0%	640	91.4%	0.0230	43.50	2.2%
17	0%	2055	34295	2.44	70	70	3090	23.6%	640	91.4%	0.0353	28.36	3.4%
18	0%	2185	36480	2.59	80	80	3170	24.2%	640	91.4%	0.0380	26.31	3.7%

Figure 6.35 :Run 66 Solvent–Steamflood Cumulative Oil Recovery Vs. Pore Volumes Injected

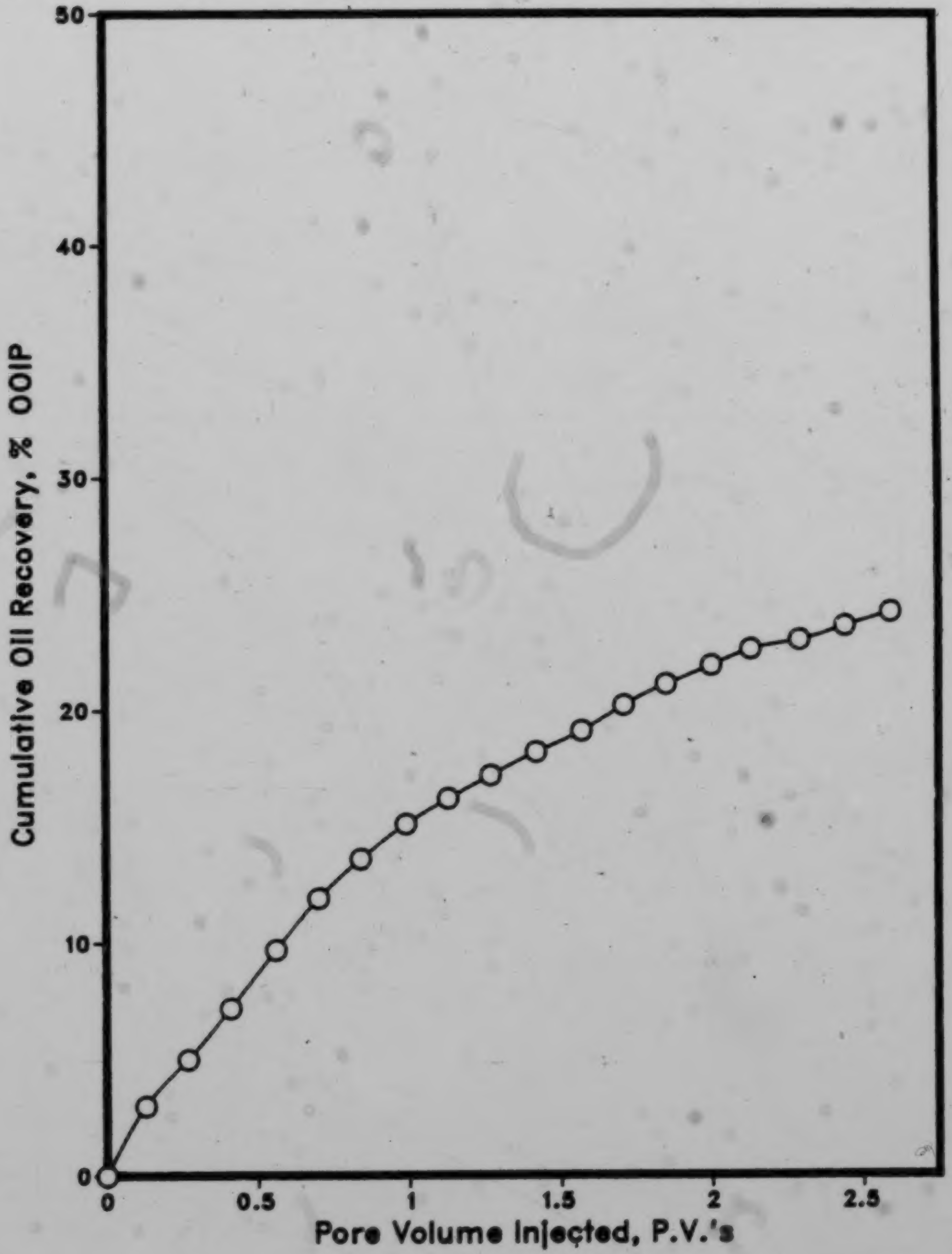

Figure 6.36 :Run 66 Solvent–Steamflood
Oleic Phase In Each Sample Vs. Cumulative Volume Injected

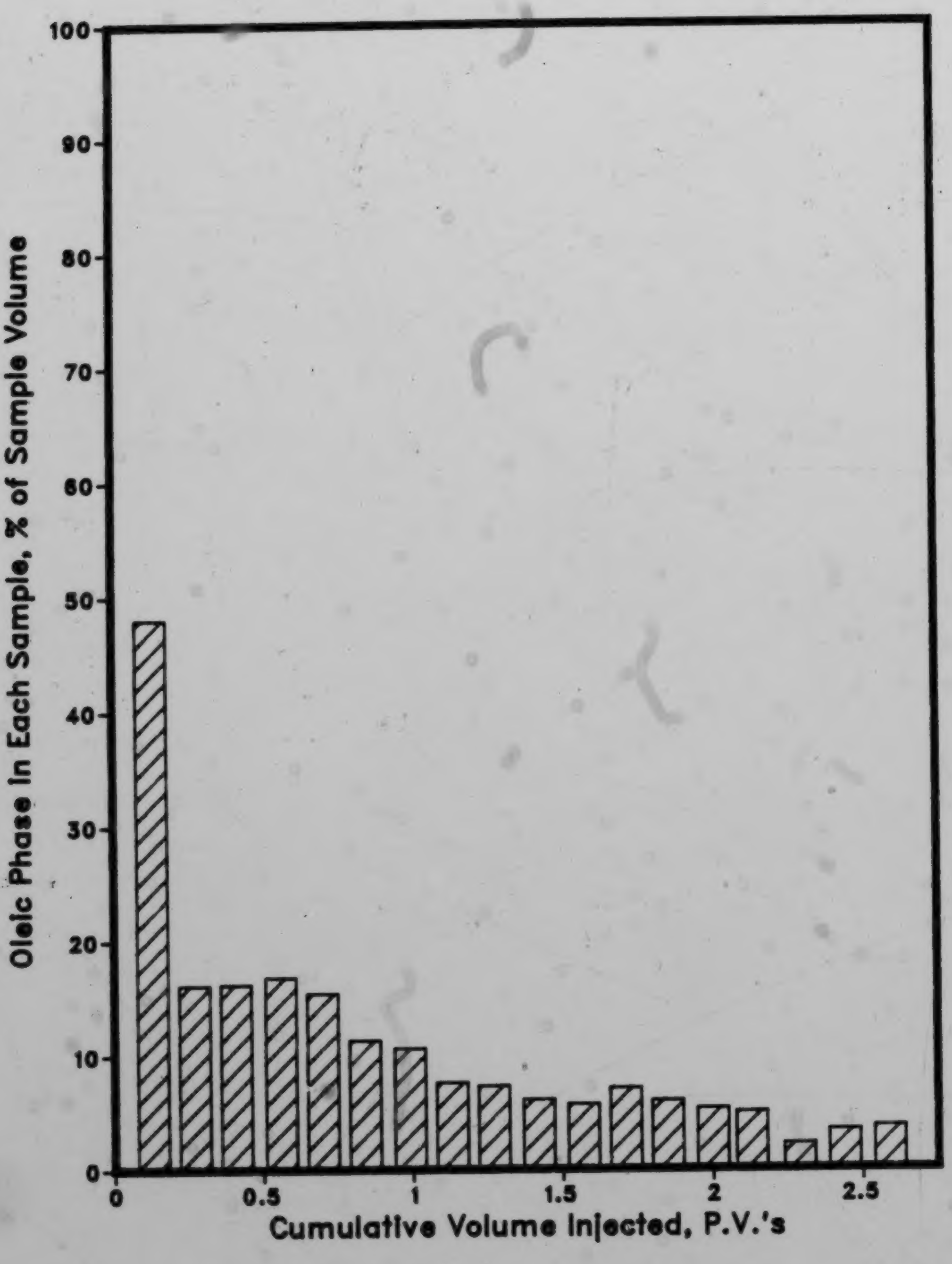

Figure 6.37 :Run 66 Solvent–Steamflood
Instantaneous Produced WOR Vs. Cumulative Volume Injected

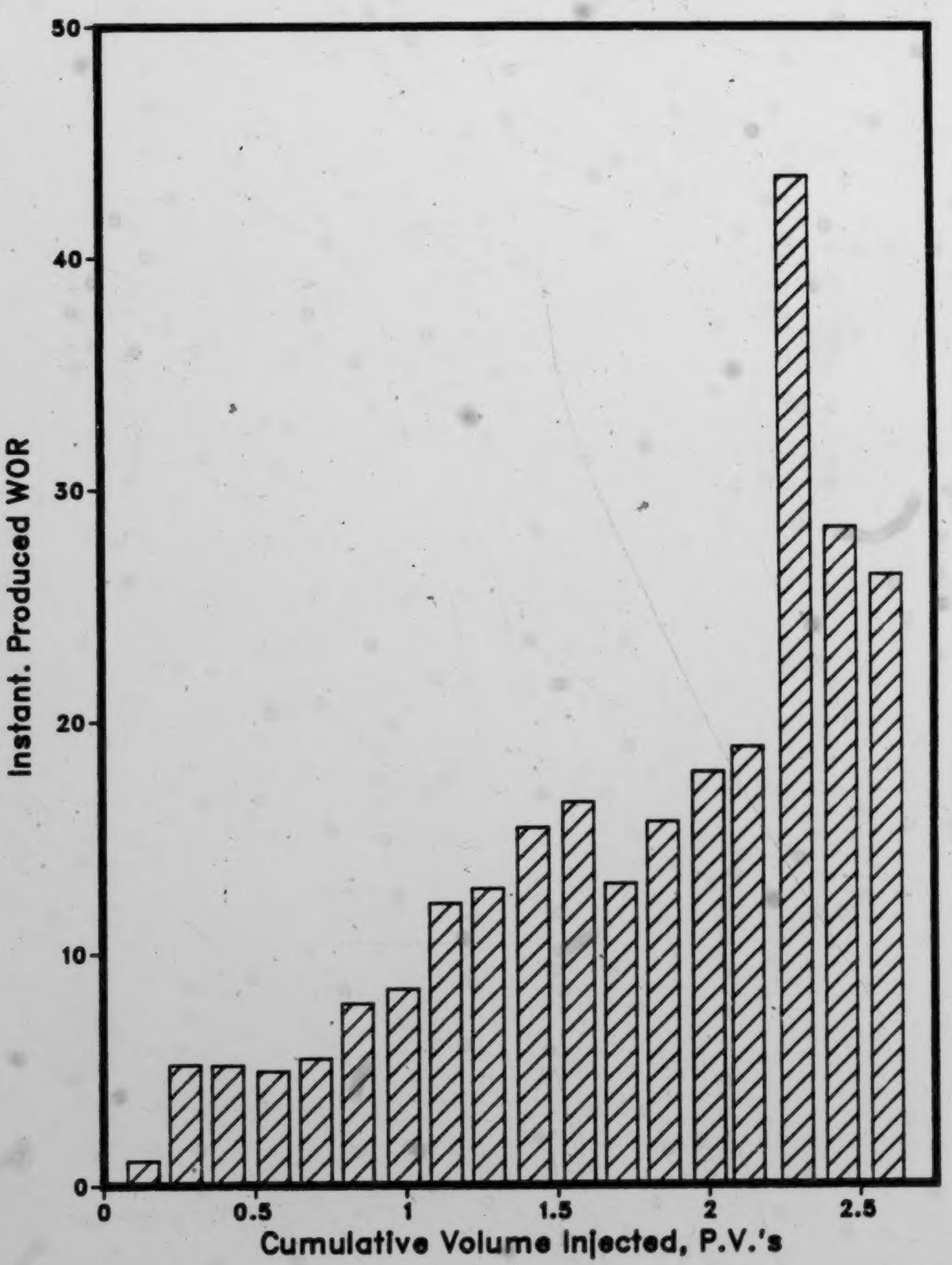

Figure 6.38 :Run 66 Solvent–Steamflood
Instantaneous Oil/Steam Ratio Vs. Cumulative Oil Produced

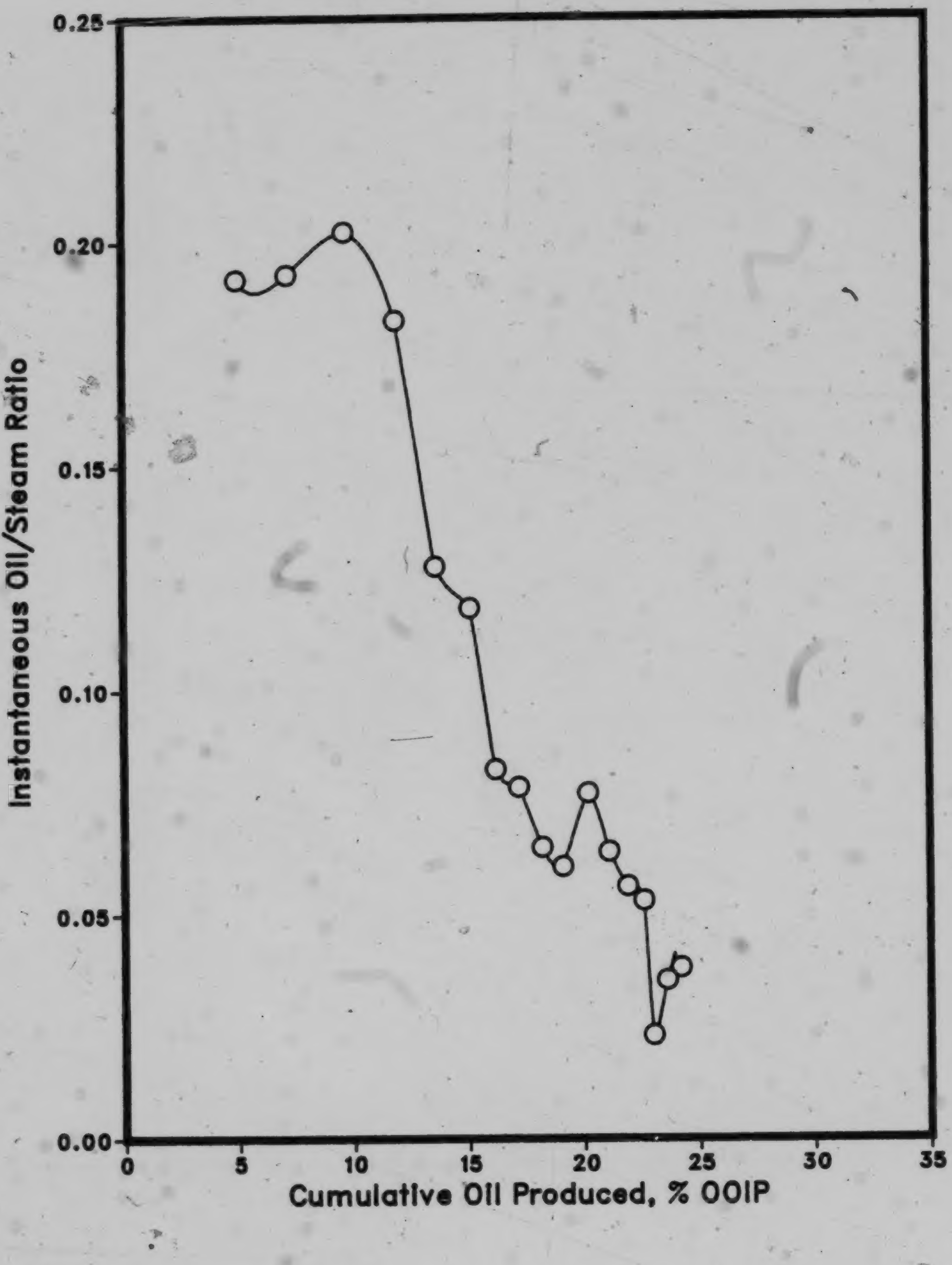

Table 6.11 : Run 67 Solvent-Steamflood With Homogeneous Model

HC Pore Volume : 13030.0 cc
Pore Volume : 14080.0 cc
Bulk Volume : 42005.0 cc
Porosity : 33.5%
Initial Oil Satn. : 92.5%
Initial H2O Satn. : 7.5%
Solvent Vol. Inj.: 2100.0 cc (15.0% PV)

Type of Oil Used : Faxam-100
Initial Model Temperature : 3.00 C
Water Feed Flow Rate : 213.60 cc/min
Boiler Feed Flow Rate : 29.20 cc/min
Total Flow Rate of Steam : 242.80 cc/min
Solvent Flow Rate : 200.00 cc/min
Steam Vol. Injected : 32160 cc (2.28 PV)

Net Oil Recovery : 25.9% **Solvent Recovery : 97.0%** **Final Oil Saturation : 68.6%**

Cyl. No.	Solvent Conc. (%)	Tot. Vol. Inj. (cc)	Cum. Vol. Inj.		HC Prod. (cc)	Oil Prod. (cc)	Cum. Oil Rec.		Cum. Sol. Rec.		Oil-Steam Ratio	Inst Prod. WOR	Inst. HC Prod. % of Sample
			(cc)	(P.V.)			(cc)	(%OOIP)	(cc)	(%)			
1	71%	980	980	0.07	980	284	284	2.2%	696	33.1%	0.0000	0.00	100.0%
2	88%	1225	2205	0.16	1115	134	418	3.2%	1677	79.9%	0.0000	0.10	91.0%
3	56%	1590	3795	0.27	410	180	598	4.6%	1907	90.8%	0.3475	2.88	25.8%
4	16%	1920	5715	0.41	265	223	821	6.3%	1949	92.8%	0.1601	6.25	13.8%
5	7%	2030	7745	0.55	375	349	1170	9.0%	1975	94.0%	0.2266	4.41	18.5%
6	6%	1935	9680	0.69	405	381	1551	11.9%	1999	95.2%	0.2647	3.78	20.9%
7	5%	2040	11720	0.83	385	366	1917	14.7%	2018	96.1%	0.2326	4.30	18.9%
8	3%	1980	13700	0.97	330	320	2237	17.2%	2028	96.6%	0.2000	5.00	16.7%
9	2%	2030	15730	1.12	230	225	2462	18.9%	2033	96.8%	0.1278	7.83	11.3%
10	1%	2030	17760	1.26	195	193	2655	20.4%	2035	96.9%	0.1063	9.41	9.6%
11	1%	2025	19785	1.41	135	134	2789	21.4%	2036	97.0%	0.0714	14.00	6.7%
12	0%	1985	21770	1.55	130	130	2919	22.4%	2036	97.0%	0.0701	14.27	6.5%
13	0%	2165	23935	1.70	80	80	2999	23.0%	2036	97.0%	0.0384	26.06	3.7%
14	0%	2055	25990	1.85	75	75	3074	23.6%	2036	97.0%	0.0379	26.40	3.6%
15	0%	2115	28105	2.00	85	85	3159	24.2%	2036	97.0%	0.0419	23.88	4.0%
16	0%	2000	30105	2.14	90	90	3249	24.9%	2036	97.0%	0.0471	21.22	4.5%
17	0%	2135	32240	2.29	50	50	3299	25.3%	2036	97.0%	0.0240	41.70	2.3%
18	0%	2020	34260	2.43	70	70	3369	25.9%	2036	97.0%	0.0359	27.86	3.5%

Figure 39 :Run 67 Solvent–Steamflood
Cumulative Oil Recovery Vs. Pore Volumes Injected

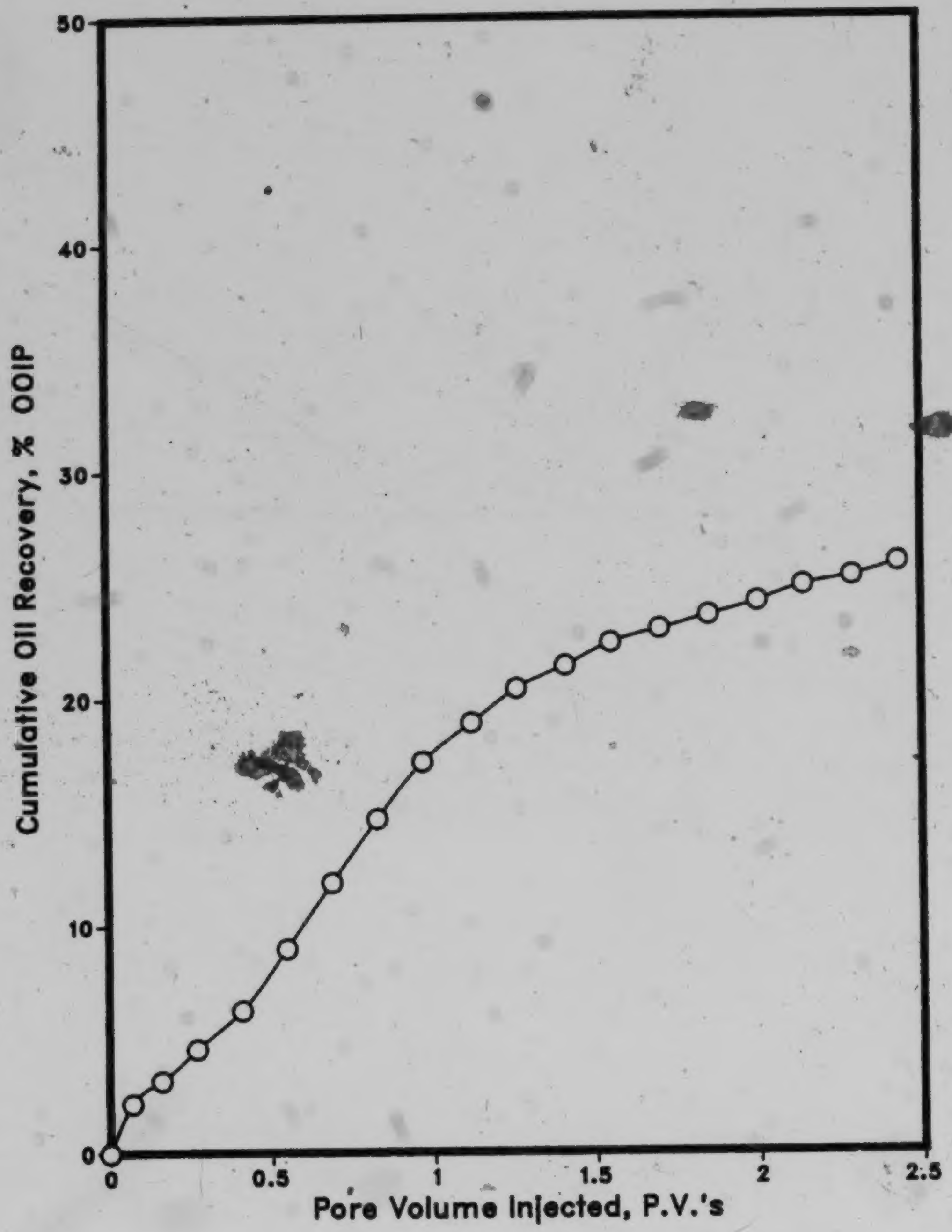

Figure 6.40 :Run 67 Solvent–Steamflood
Oleic Phase In Each Sample Vs. Cumulative Volume Injected

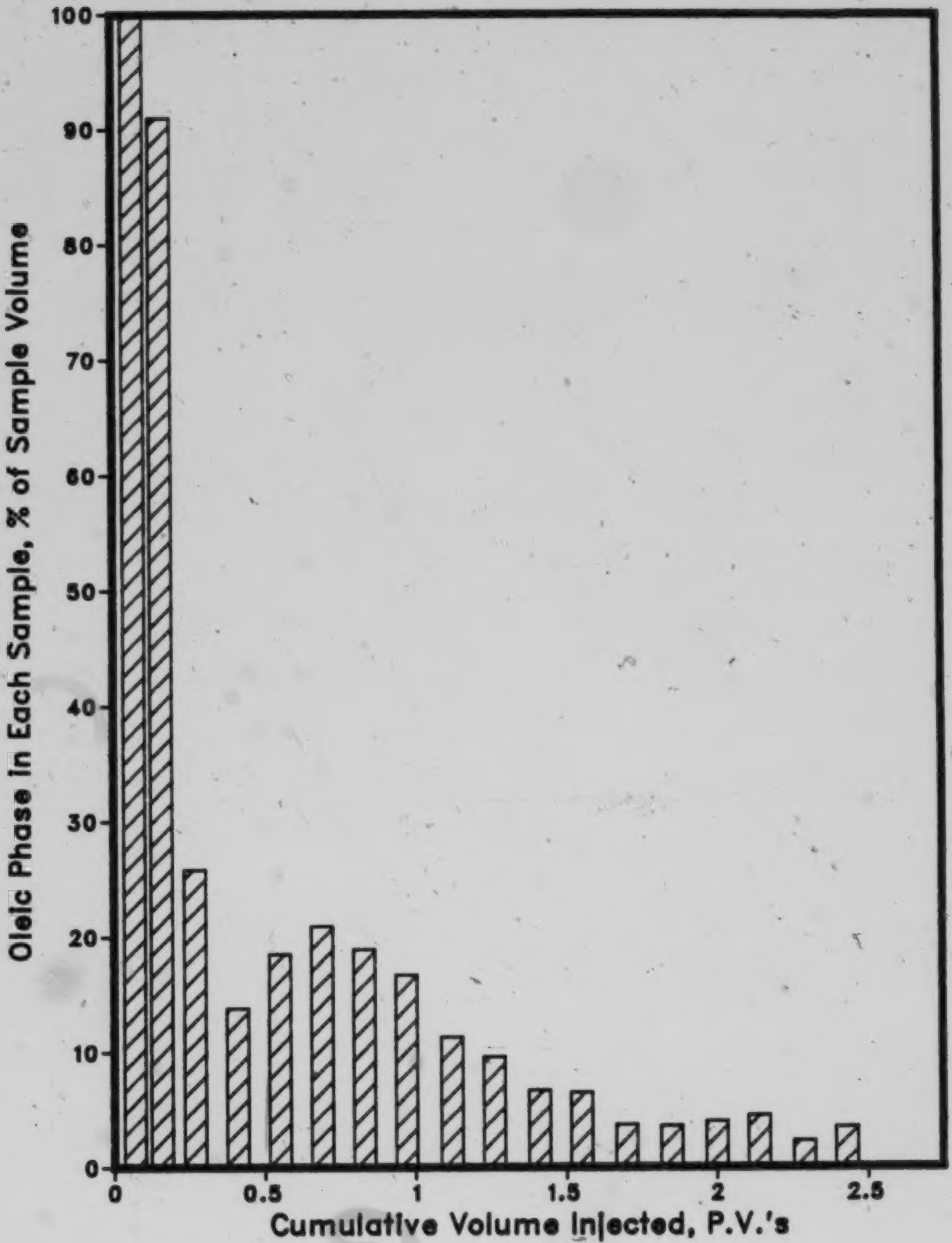

Figure 6.41 :Run 67 Solvent–Steamflood
Instantaneous Produced WOR Vs. Cumulative Volume Injected

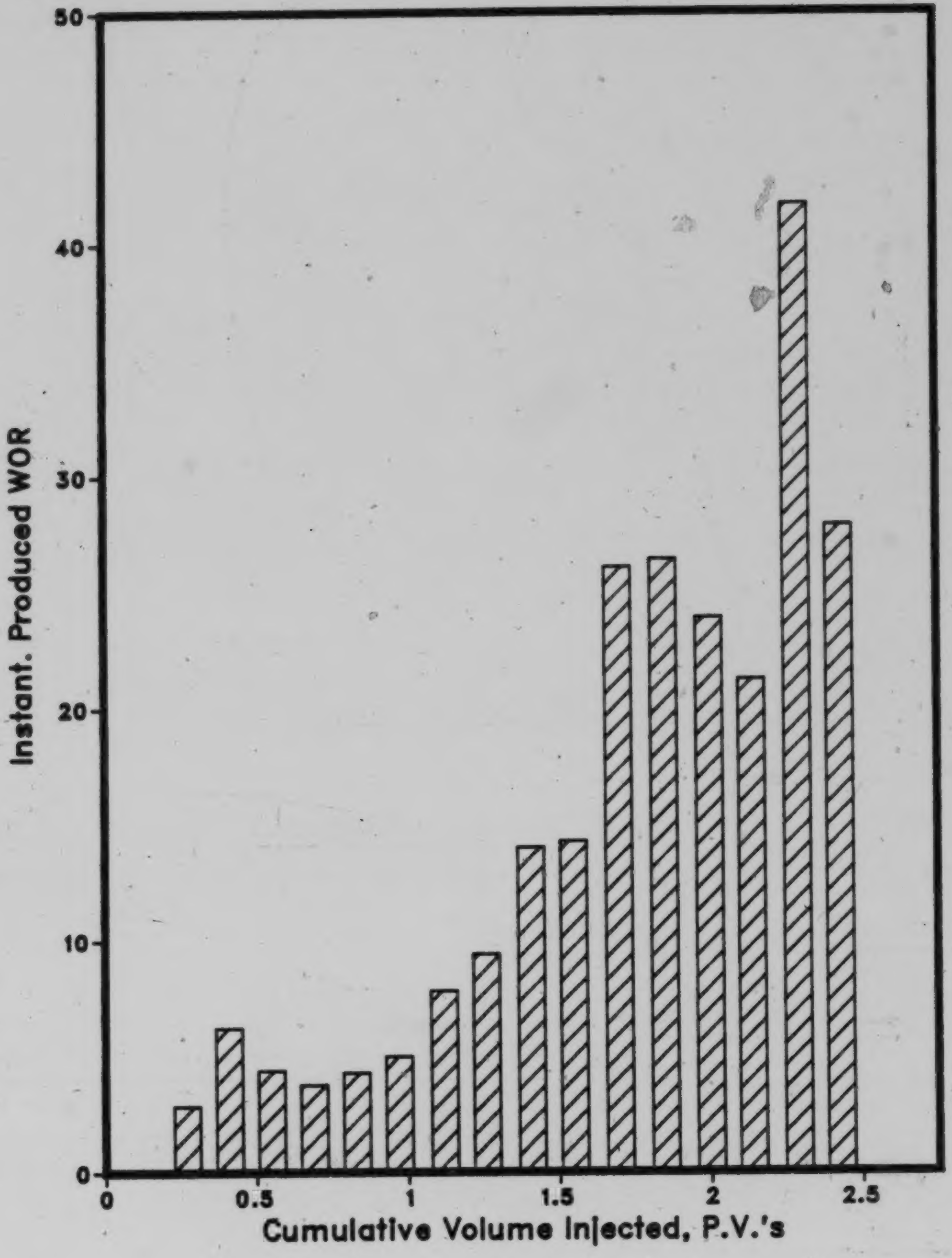

Figure 6.42 :Run 67 Solvent–Steamflood
Instantaneous Oil/Steam Ratio Vs. Cumulative Oil Produced

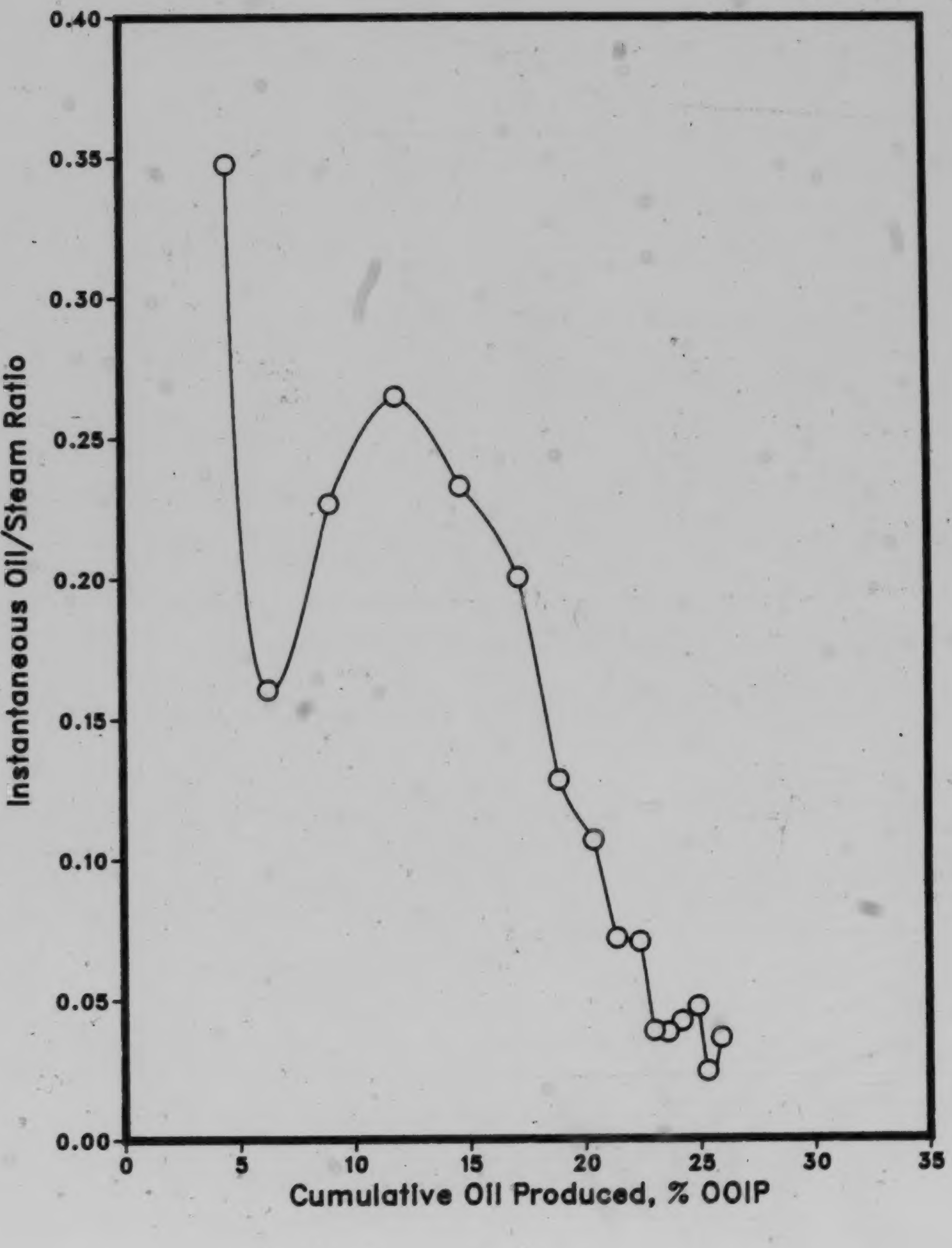

comparison plot (Figure 6.43) of the recovery curves for the three experiments indicates that Run 45 had the best recovery with Run 67 second and Run 66 having the least attractive recovery. From the results of the three experiments it appeared that the 10% solvent slug run allowed a more stable displacement to occur in the model and thus a greater recovery. Run 45 (10% slug) achieved the optimal balance between oil viscosity reduction and channelling which means that some of the oil does not contact the solvent. In the case of the 5% solvent slug experiment, less solvent channelling existed in the oil, thus less extensive steam penetration of the oil occurred and consequently less oil was mobilized. Steam advance in Run 66 (5% slug) is quite unusual, and departs strongly from a radial type advance. It seems that the solvent was displaced along the right edge of the model and from there on, steam advanced as a front from right to left (see Figure A.102 for the terminal time). For the 15% solvent slug run the larger solvent slug used created larger solvent channels in the model which allowed the steam to flow more directly from the injection to production wells and therefore more of the steam was partially diverted away from heating the oil than during Run 45. It was concluded from the results of Runs 66, 67 and 45 that there exists an optimal slug size of approximately 10% of the model pore volume which maximizes the oil recovered by a solvent-steamflood process.

Figure 6.43 :Comparison of the Effect of Solvent Slug Size on Solvent–Steamflood Recoveries for Runs 45, 66 & 67

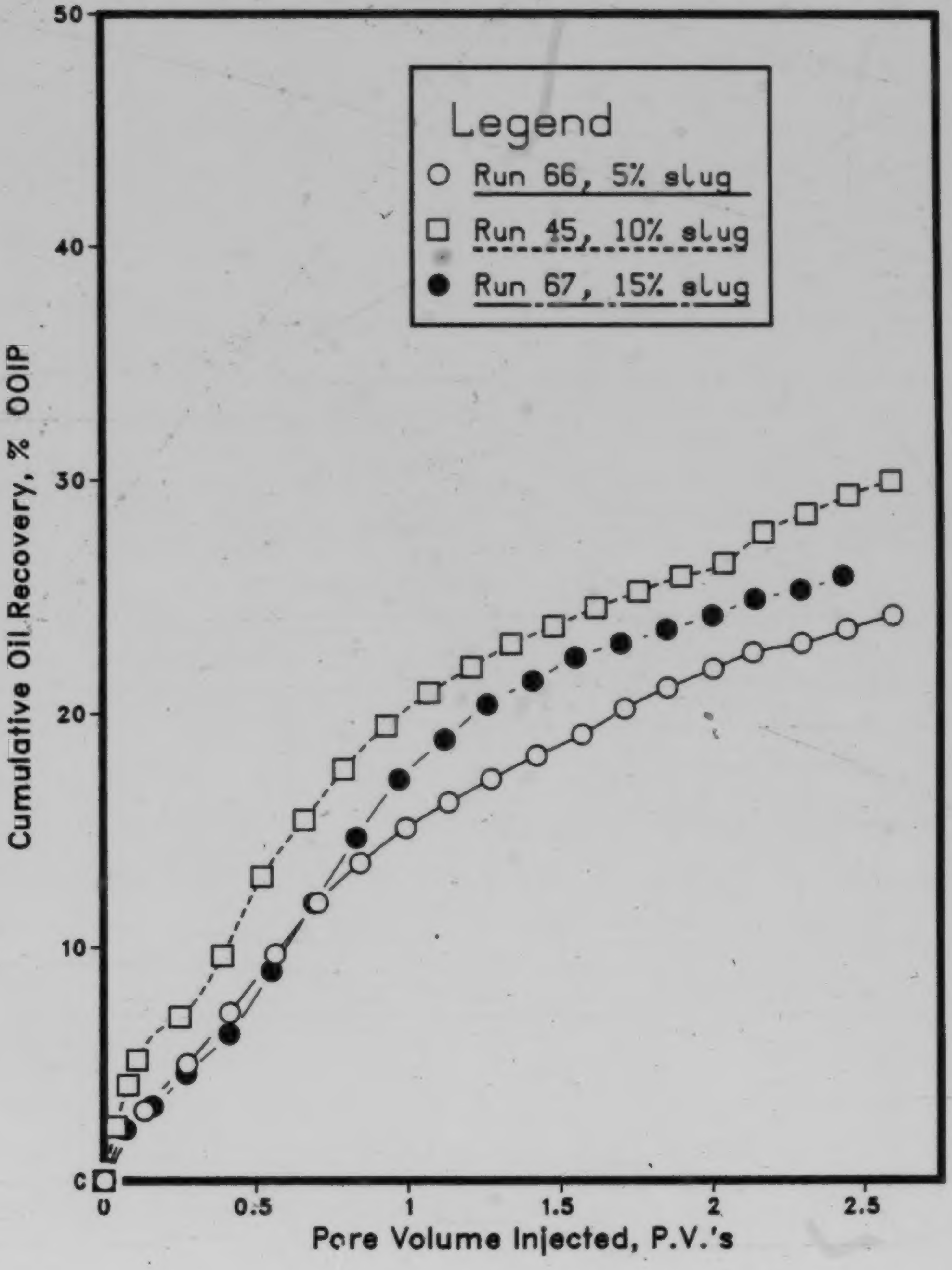

Effect of Bottom Water Thickness on Steamflood Response

Studies [63,65] similar to the present research investigated the effect of bottom water thickness on the steamflood response in the Aberfeldy heavy oil reservoir. In each of the studies carried out by Kasraie and Farouq Ali (numerical) [65] and Proctor, George and Farouq Ali (experimental)[63], it was observed that when bottom water was present during a steamflood, much less steam flowed in the oil region than that in the absence of water.

Kasraie and Farouq Ali [65] performed mathematical simulations of steamfloods in the Aberfeldy formation to investigate the effect of bottom water thickness on the overall oil recovery yielded by a steamflood. In these simulations, steam was injected into the oil zone only, and the producers were completed in the oil zone. The results quite clearly indicated that oil recovery declined steeply as the bottom water thickness increased. It was also reported that the oil-steam ratio reached a low earlier for the thicker bottom water zones than it did for the thinner water regions. This implied that in thicker water zones, the steam penetrated the bottom water earlier, and from then on, there was little improvement in the oil displacement efficiency. It was therefore concluded that when bottom water exists, much less steam travels in the oil zone than when bottom water is absent and thus even though oil is mobilized, considerable amounts of water continue to advance from the water zone into the producers.

The scaled model study carried out by Proctor, George and Farouq Ali [63] involved experiments in which the bottom water model of the Aberfeldy was steamflooded. Runs 32, 33 and 39 involved steamflooding a model of the Aberfeldy formation with varying bottom water thicknesses of 2.3%, 4.0% and 12.5% of the total model thickness, respectively. The oil recoveries obtained from Runs 32, 33 and 39 were 22.8%, 22.9% and 16.8% OOIP, respectively. Recoveries for the three runs indicate that as the bottom water layer thickness increased, oil recovery correspondingly decreased. The substantially greater oil recovery of 31.8% OOIP for Run 26, which was a conventional steamflood of the homogeneous model of the Aberfeldy, pointed out the deleterious effects that the bottom water had on the displacement efficiencies and recoveries of Runs 32, 33 and 39. Temperature profiles of the experiments suggested that the injected heat moved rapidly in the bottom water layer and heat advance in the upper part of the model was virtually stationary. This indicated that a hot waterflood existed once the steam condensed and the condensate quickly migrated into the less flow resistant bottom water. It was concluded from this study that the bottom water had very detrimental effects on the thermal efficiency of the steamflood and as the bottom water thickness increased the heat loss of the steam to the bottom water was intensified.

The results of these two studies [63,65] agreed in that as the bottom water thickness increased, the thermal efficiency, sweep efficiency and net oil recovery of the steamflood dropped. These findings support the possibility of employing a small solvent slug prior to a steamflood process in order to partially divert the steam away from the underlying water and into the above oil zone, so to delay the movement of steam downward into the bottom water. The use of solvent in combination with a steamflood process will be discussed in the following section.

Effect of Bottom Water Thickness on Solvent-Steamflood Response

The purpose of the initial solvent injection into the oil layer prior to steamflooding was to create a pathway in the oil layer for the steam to follow in an attempt to improve the oil recovery compared to conventionally steamflooding a bottom water formation.

An assumption of this study was that during initial solvent injection into the oil zone of the model, channelling or viscous fingering of the injected solvent into the oil region was predominant. This assumption was confirmed by the results of the solvent flood (Run 40) which was previously discussed. The extensive viscous fingering of the solvent into the oil was caused by the large contrast in mobilities between the solvent (k_{rd}/μ_d) and the oil (k_{ro}/μ_o) as well as a high solvent injection rate. The huge contrast in mobilities was mainly due to the large difference in viscosities of the solvent (μ_d) and the model oil (μ_o) at the initial model temperature of approximately 3.0^{0}C. The solvent had a much smaller viscosity (about 10 cp) than the heavy oil (approximately 1300 cp) at the initial temperature conditions. As well, the solvent permeability (k_{rd}) is higher than the heavy oil permeability (k_{ro}) initially during the solvent injection, the corresponding value for mobility ratio in this case, as defined by the equation below and discussed by Collins [66], would be even larger.

$$\text{Mobility Ratio} = M = \frac{\text{mobility of displacing fluid}}{\text{mobility of displaced fluid}} = \frac{k_{rd}/\mu_d}{k_{ro}/\mu_o}$$

The higher the value of mobility ratio and the solvent injection rate, the less stable the displacement would be, therefore for this situation the large mobility ratio would be unfavourable due to the large discrepancy between the solvent and oil viscosities. The displacement of the heavy oil by the solvent would be considered highly unstable due to the unfavourable mobility ratio governing the displacement and the relatively high solvent injection rate. Therefore the desired mixing of the solvent with the oil region of the model would be highly probable and thus solvent channelling was assumed to occur during the initial stages of the solvent-steamflood experiments.

Runs 49, 50, 51, 53 and 54 all involved injecting 0.10 pore volume of solvent (Heavy Virgin Naphtha) followed by a continuous steamflood of a model containing a bottom water layer. The only difference between the five bottom water experiments was that the bottom water thickness varied for each run. Bottom water thickness was altered in each run so to investigate its effect on the oil recovery.

The tabulated results for Runs 49, 50, 51, 53 and 54 are presented in Tables 6.12, 6.13, 6.14, 6.15 and 6.16, respectively. The bottom water thicknesses for Runs 49 (8.8% of gross model thickness), 50 (10.2% of gross model thickness) and 54 (12.2% of gross model thickness) were about the same, whereas Runs 51 (26.2% of gross model thickness) and 53 (15.2% of gross model thickness) had much thicker bottom water layers. The injection well for the model was situated so to inject fluids into the upper portion of the model. This was to ensure that the solvent and steam would not flow directly into the bottom water layer and underride the oil immediately upon injection.

Comparison of the recovery curves for Runs 49 (Figure 6.44), 50 (Figure 6.48), 51 (Figure 6.52), 53 (Figure 6.56) and 54 (Figure 6.60) demonstrate the deleterious effect bottom water thickness had on oil recovery. The recovery curves for Runs 49, 51 and 54 were much the same due to similarities in bottom water thicknesses, whereas the curves for Run 51 and 53 differed from Figures 6.44, 6.48 and 6.60 due to thicker bottom water layers. During the initial stages of the Runs 49, 50 and 54 the recovery curves moderately increased up to about 0.50 pore volumes at which point the slope of the curves became constant forming a relatively straight line for the remainder of the experiment. Due to the presence of bottom water the initial increase in the recovery curves for these three experiments was not as marked as in the previous solvent-steamflood base runs (Runs 44, 45 & 46). The moderate rise of oil recovery in Figures 6.44, 6.48 and 6.60 during the primary run stages represents the injected solvent forming flow paths into the oil layer.

This helped prevent the steam from being entirely lost to the bottom water layer and thus assisted in mobilizing more of the in-place oil. However the existence of bottom water eventually hindered the stability of the steam displacement in the model and reduced the heating efficiency of the steam in the oil region. This yielded a smaller oil recovery compared to previous homogeneous solvent-steamfloods (Runs 44, 45 & 46). The straight line segment of the three curves (Figures 6.44, 6.48 & 6.60) symbolizes the steam continuing to sweep through the oil section recovering additional oil while being partially lost to the bottom water. Runs 51 and 53 had much thicker bottom water layers than Runs 49, 50 and 54 which hampered solvent and steam injection into the oil zone. The consequence was a substantial reduction in the overall oil recovery. Figures 6.52 (Run 51) and 6.56 (Run 53) are in contrast with the recovery curves for Runs 49, 50 and 54 in that the plots are basically straight lines with much lower recoveries than Figures 6.44, 6.48 and 6.60. The straight line in Figures 6.52 and 6.56 represented the continuous injection of steam which mobilized oil in the upper portion of the model while throughout the run a majority of the steam's heat was scavenged by the underlying bottom water. Therefore the steam displacements in Runs 51 and 53 were considerably less stable then the displacements in Run 49, 50 and 54 due to the thicker bottom water zones of Runs 51 and 53.

The bar graphs of volume as a percentage of oleic phase in each sample taken versus cumulative volume injected and instantaneous produced WOR versus cumulative volume injected for Runs 49 (Fig. 6.45 & 6.46), 50 (Fig. 6.49 & 6.50), 51 (Fig. 6.53 & 6.54), 53 (Fig. 6.57 & 6.58) and 54 (Fig. 6.61 & 6.62) indicate that the bottom water was a dominating factor in the experiments. Figures 6.45, 6.49, 6.53, 6.57 and 6.61 suggested that during the initial stages of the five runs the injected steam penetrated into the oil layer and formed an oil bank ahead of the steam zone. Soon after the formation of the oil bank, steam breakthrough occurred. For Runs 49, 50, and 54 steam breakthrough existed at about 0.50 pore volumes injected and at about 0.25 pore volumes injected for

Runs 51 and 53. The values of instantaneous hydrocarbon produced in the sample for Run 51 and 53 were considerably lower than those for Runs 49, 50 and 54, due to the thicker bottom water zones of Runs 51 and 53. Figures 6.46, 6.50, 6.54, 6.58 and 6.62 also indicated that a distinct steam breakthrough occurred during all of the five bottom water runs. Again steam breakthrough appearred to occur sooner and was less distinct for Runs 51 and 53 due to the thicker bottom water zones.

The plots of instantaneous oil/steam ratio versus cumulative oil produced are displayed in Figures 6.47 (Run 49), 6.51 (Run 50), 6.55 (Run 51), 6.59 (Run 53) and 6.63 (Run 54). A distinct breakthrough was again observed in these figures which was distinguished by the steep decline in the instantaneous oil/steam ratio values between the first few points of each plot. In the case of Runs 51 and 53 the reduced oil/steam ratio settles down to a value of approximately 0.5, showing that the oil layer above continues to be heated by steam.

Top view temperature contour plots for Run 49 (Fig. A.119-A.126), 50 (Fig. A.131-A.138), 51 (Fig. A.143-A.150), 53 (Fig. A.155-A.162) and 54 (Fig. A.167-A.174) exhibits the temperature profiles for each of the experiments at every 0.25 pore volumes injected into the model. For Runs 49, 50 and 54, the temperature profiles revealed that early in the experiments the solvent created a flow path into the oil zone enabling the steam to flow more readily through the oil layer and as the steamflood progressed the steam eventually began to underride the oil by travelling through the bottom water. At this point the steam displacement became less stable. The underriding of the oil zone by the steam is demonstrated in the temperature contours. Comparison of the all the temperatures profiles for the five runs revealed that the steam began to underride the oil layer sooner during Runs 51 and 53, due to the thicker bottom water layer of the two runs. The cross-sectional temperature profiles for Runs 49 (Fig. A.127-130), 50 (Fig. A.139-142) and 54 (Fig. A.175-A.178) also indicated that the heat advanced through the entire

Table 6.12 : Run 49 Solvent-Steamflood With Bottom Water

HC Pore Volume : 13460.0 cc
Pore Volume : 15530.0 cc
Bulk Volume : 42005.0 cc
Porosity : 37.0%
Initial Oil Satn. : 86.7%
Initial H2O Satn. : 13.3%
Solvent Vol. Inj.: 1400.0 cc (10.0% PV)
Steam Vol. Inj. : 31630.0 cc (2.04 PV)

Type of Oil Used : Faxam-100
Initial Model Temperature : 3.00 C
Water Feed Flow Rate : 200.00 cc/min
Boiler Feed Flow Rate : 29.20 cc/min
Total Flow Rate of Steam : 229.20 cc/min
Solvent Flow Rate : 200.00 cc/min
Bottom Water Layer Thickness : 8.8 % (% Gross Thickness)

Net Oil Recovery : 23.3% **Solvent Recovery : 84.6%** **Final Oil Saturation : 66.5%**

Cyl. No.	Solvent Conc. (%)	Tot. Vol. Inj. (cc)	Cum. Vol. Inj.		HC Prod (cc)	Oil Prod. (cc)	Cum. Oil Rec.		Cum. Sol. Rec.		Oil-Steam Ratio	Inst Prod. WOR	Inst. HC Prod. % of Sample
			(cc)	(P.V.)			(cc)	(%OOIP)	(cc)	(%)			
1	7%	405	1340	0.09	185	172	172	1.3%	13	0.9%	0.0000	1.19	45.7%
2	60%	905	2245	0.14	740	296	468	3.5%	457	32.6%	0.0000	0.22	81.8%
3	72%	840	3085	0.20	740	207	675	5.0%	990	70.7%	0.0000	0.14	88.1%
4	32%	1980	5065	0.33	490	333	1008	7.5%	1147	81.9%	0.3289	3.04	24.7%
5	8%	2085	7150	0.46	205	189	1197	8.9%	1163	83.1%	0.1090	9.17	9.8%
6	5%	1980	9130	0.59	190	181	1378	10.2%	1172	83.7%	0.1061	9.42	9.6%
7	3%	2065	11195	0.72	195	189	1567	11.6%	1178	84.1%	0.1043	9.59	9.4%
8	2%	2005	13200	0.85	170	167	1734	12.9%	1181	84.4%	0.0926	10.79	8.5%
9	2%	2065	15265	0.98	150	147	1881	14.0%	1184	84.6%	0.0783	12.77	7.3%
10	0%	2000	17265	1.11	140	140	2021	15.0%	1184	84.6%	0.0753	13.29	7.0%
11	0%	2000	19265	1.24	125	125	2146	15.9%	1184	84.6%	0.0667	15.00	6.3%
12	0%	1935	21200	1.37	120	120	2266	16.8%	1184	84.6%	0.0661	15.13	6.2%
13	0%	2035	23235	1.50	120	120	2386	17.7%	1184	84.6%	0.0627	15.96	5.9%
14	0%	1970	25205	1.62	110	110	2496	18.5%	1184	84.6%	0.0591	16.91	5.6%
15	0%	1945	27150	1.75	230	230	2726	20.3%	1184	84.6%	0.1341	7.46	11.8%
16	0%	1915	29065	1.87	165	165	2891	21.5%	1184	84.6%	0.0943	10.61	8.6%
17	0%	2040	31105	2.00	75	75	2966	22.0%	1184	84.6%	0.0382	26.20	3.7%
18	0%	1925	33030	2.13	165	165	3131	23.3%	1184	84.6%	0.0938	10.67	8.6%

Figure 6.44 :Run 49 Solvent-Steamflood With Bottom Water
Cumulative Oil Recovery Vs. Pore Volumes Injected

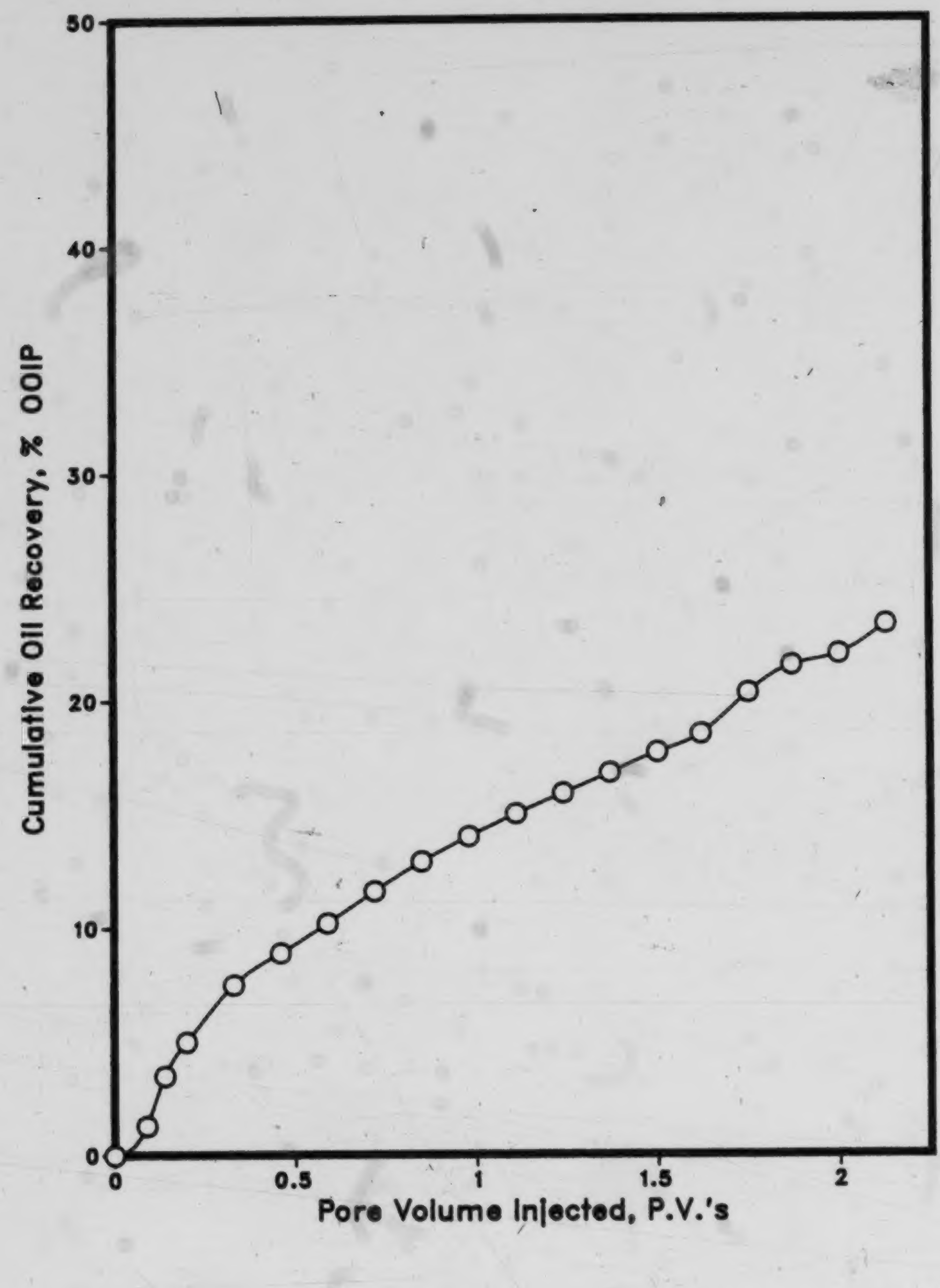

Figure 6.45 :Run 49 Solvent–Steamflood With Bottom Water
Oleic Phase in Each Sample Vs. Cumulative Volume Injected

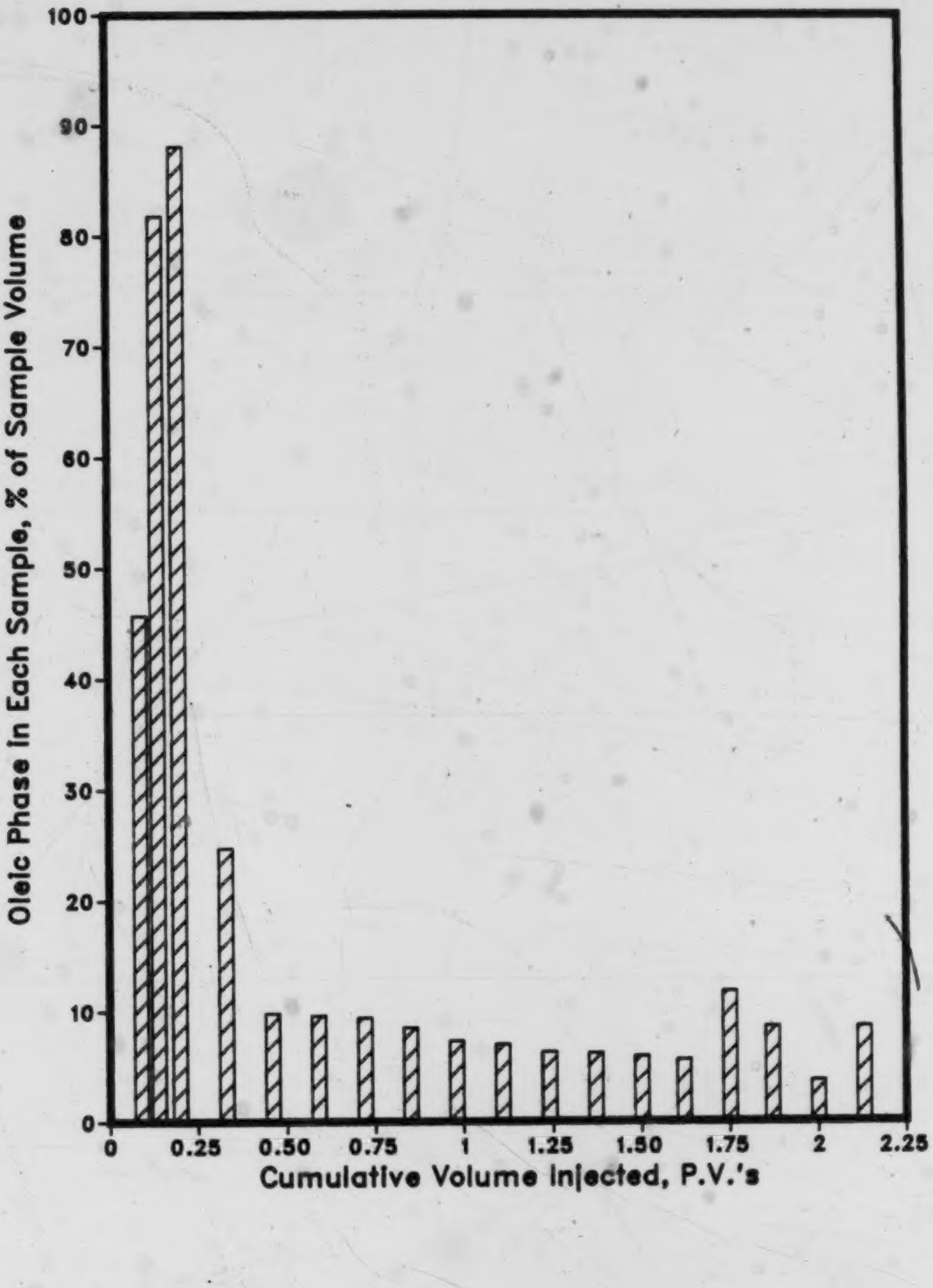

Figure 6.46 :Run 49 Solvent-Steamflood With Bottom Water Instantaneous Produced WOR Vs. Cumulative Volume Injected

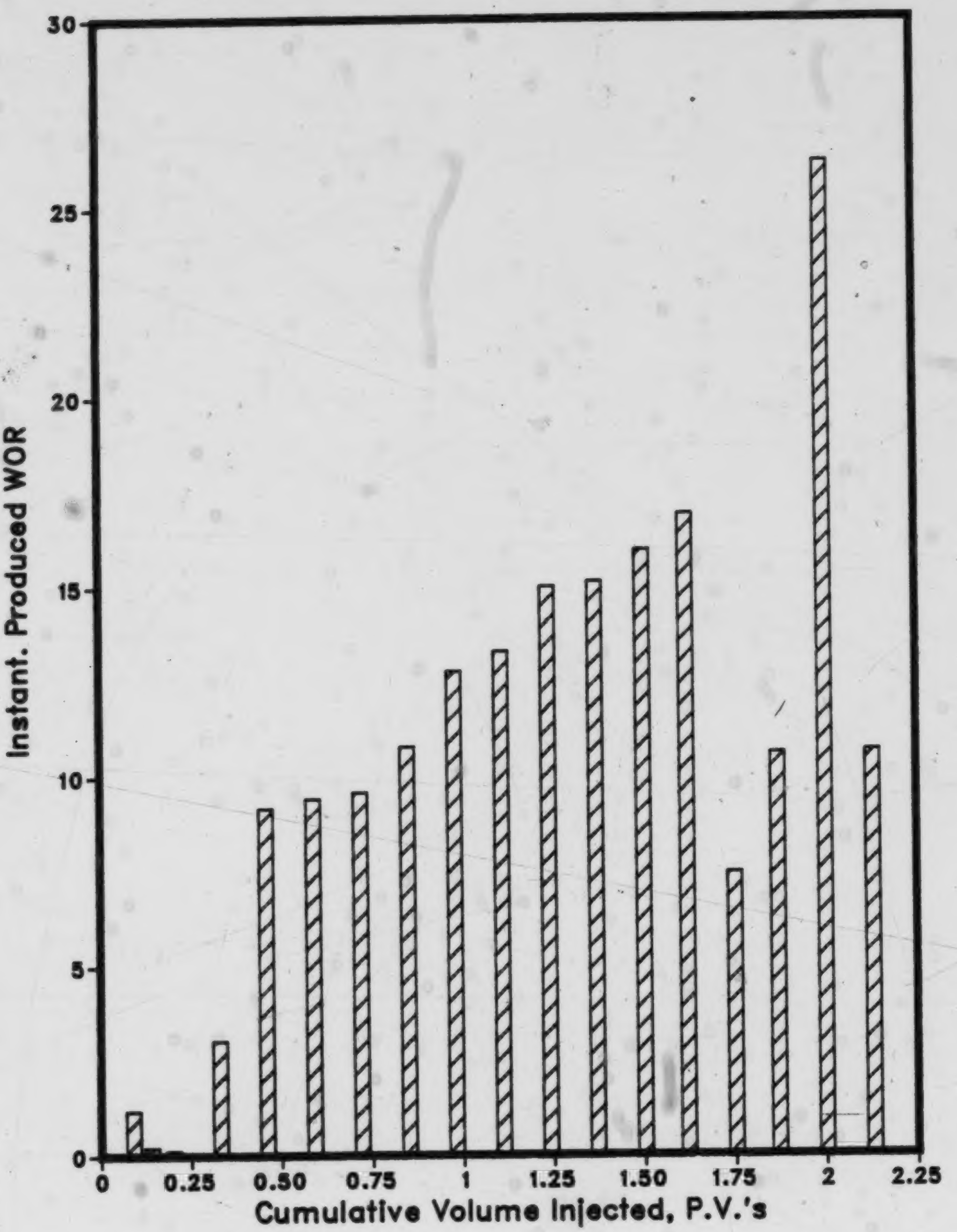

Figure 6.47 :Run 49 Solvent–Steamflood With Bottom Water Instanteous Oil/Steam Ratio vs. Cumulative Oil Produced

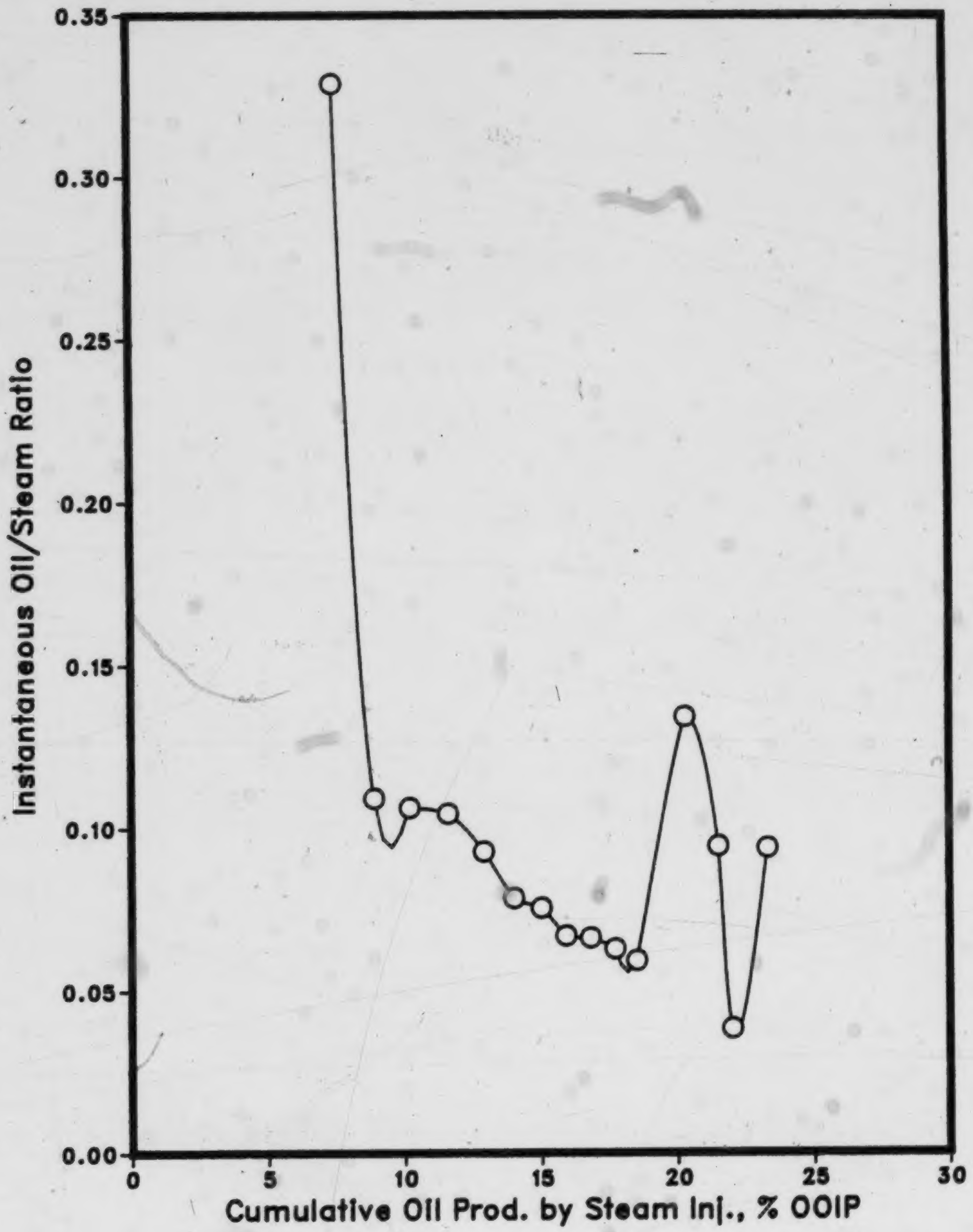

Table 6.13 : Run 50 Solvent-Steamflood With Bottom Water

HC Pore Volume : 13720.0 cc
Pore Volume : 15037.0 cc
Bulk Volume : 42005.0 cc
Porosity : 35.8%
Initial Oil Satn. : 91.2%
Initial H2O Satn. : 8.8%
Solvent Vol. Inj.: 1400.0 cc (10.0% PV)
Steam Vol. Inj.: 32635.0 cc (2.16 PV)

Type of Oil Used : Faxam-100
Initial Model Temperature : 3.00 C
Water Feed Flow Rate : 200.00 cc/min
Boiler Feed Flow Rate : 29.20 cc/min
Total Flow Rate of Steam : 229.20 cc/min
Solvent Flow Rate : 200.00 cc/min
Bottom Water Thickness : 10.2 % (% Gross Thickness)

Net Oil Recovery : 25.4% **Solvent Recovery : 88.5%** **Final Oil Saturation : 68.0%**

Cyl. No.	Solvent Conc. (%)	Tot. Vol. Inj. (cc)	Cum. Vol. Inj.		HC Prod (cc)	Oil Prod. (cc)	Cum. Oil Rec.		Cum. Sol. Rec.		Oil-Steam Ratio	Inst Prod. WOR	Inst. HC Prod. % of Sample
			(cc)	(P.V.)			(cc)	(%OOIP)	(cc)	(%)			
1	60%	1120	1120	0.07	1120	448	448	3.3%	672	48.0%	0.0000	0.00	100.0%
2	65%	1005	2125	0.14	665	233	681	5.0%	1104	78.9%	0.0000	0.51	66.2%
3	28%	1435	3560	0.24	235	169	850	6.2%	1170	83.6%	0.1958	5.11	16.4%
4	9%	2080	5640	0.38	410	373	1223	8.9%	1207	86.2%	0.2455	4.07	19.7%
5	5%	1940	7580	0.50	440	418	1641	12.0%	1229	87.8%	0.2933	3.41	22.7%
6	2%	2060	9640	0.64	225	221	1862	13.6%	1233	88.1%	0.1226	8.16	10.9%
7	1%	2040	11680	0.78	225	223	2085	15.2%	1235	88.2%	0.1240	8.07	11.0%
8	1%	2095	13775	0.92	190	188	2273	16.6%	1237	88.4%	0.0997	10.03	9.1%
9	1%	1980	15755	1.05	155	153	2426	17.7%	1239	88.5%	0.0849	11.77	7.8%
10	0%	2035	17790	1.18	125	125	2551	18.6%	1239	88.5%	0.0654	15.28	6.1%
11	0%	1975	19765	1.31	115	115	2666	19.4%	1239	88.5%	0.0618	16.17	5.8%
12	0%	2140	21905	1.46	110	110	2776	20.2%	1239	88.5%	0.0542	18.45	5.1%
13	0%	2020	23925	1.59	140	140	2916	21.3%	1239	88.5%	0.0745	13.43	6.9%
14	0%	2035	25960	1.73	105	105	3021	22.0%	1239	88.5%	0.0544	18.38	5.2%
15	0%	1960	27920	1.86	115	115	3136	22.9%	1239	88.5%	0.0623	16.04	5.9%
16	0%	2065	29985	1.99	105	105	3241	23.6%	1239	88.5%	0.0536	18.67	5.1%
17	0%	1940	31925	2.12	100	100	3341	24.4%	1239	88.5%	0.0543	18.40	5.2%
18	0%	2110	34035	2.26	150	150	3491	25.4%	1239	88.5%	0.0765	13.07	7.1%

Figure 6.48 :Run 50 Solvent–Steamflood With Bottom Water
Cumulative Oil Recovery Vs. Pore Volumes Injected

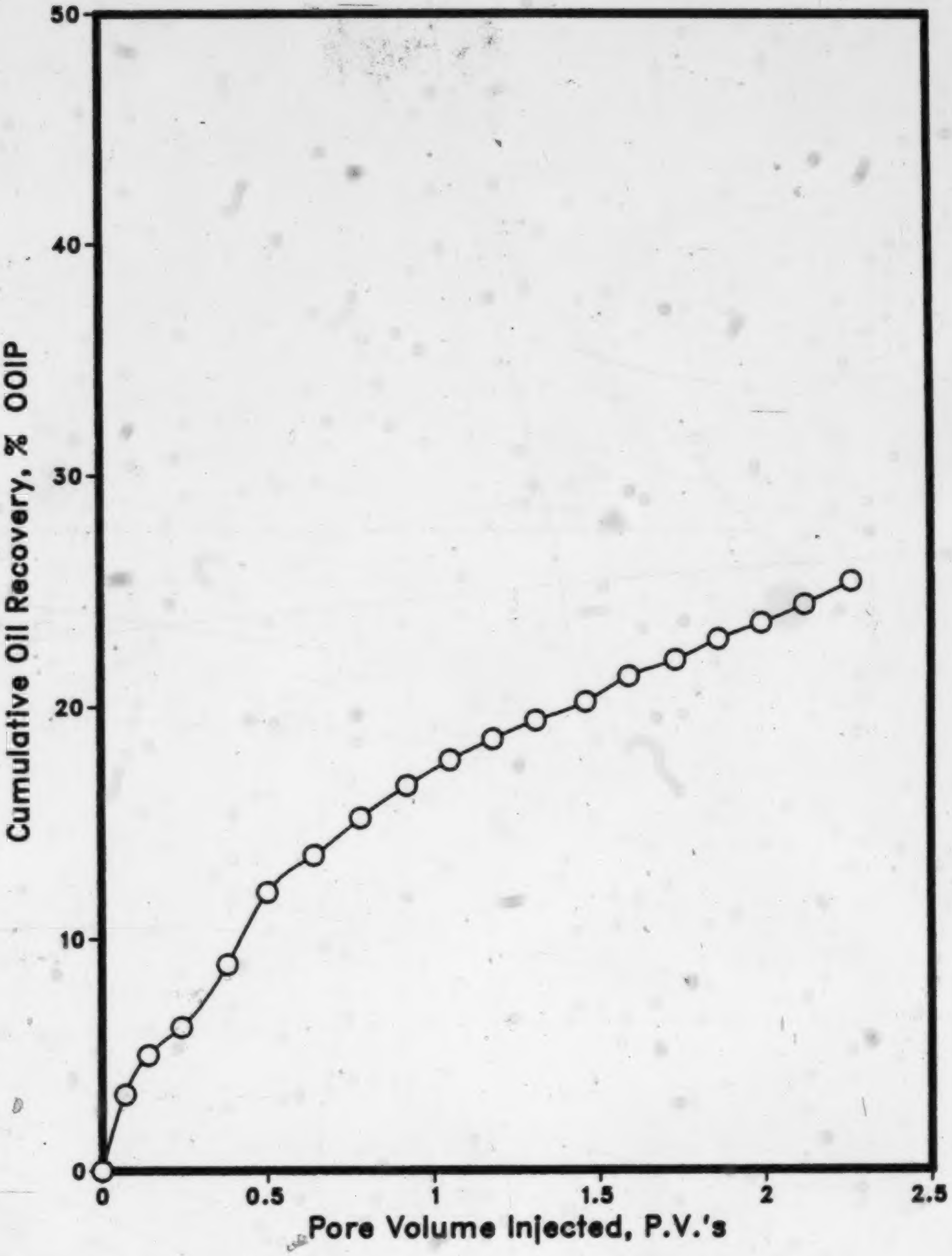

Figure 6.49 :Run 50 Solventflood–Steamflood With Bottom Water Oleic Phase In Each Sample Vs. Cumulative Volume Injected

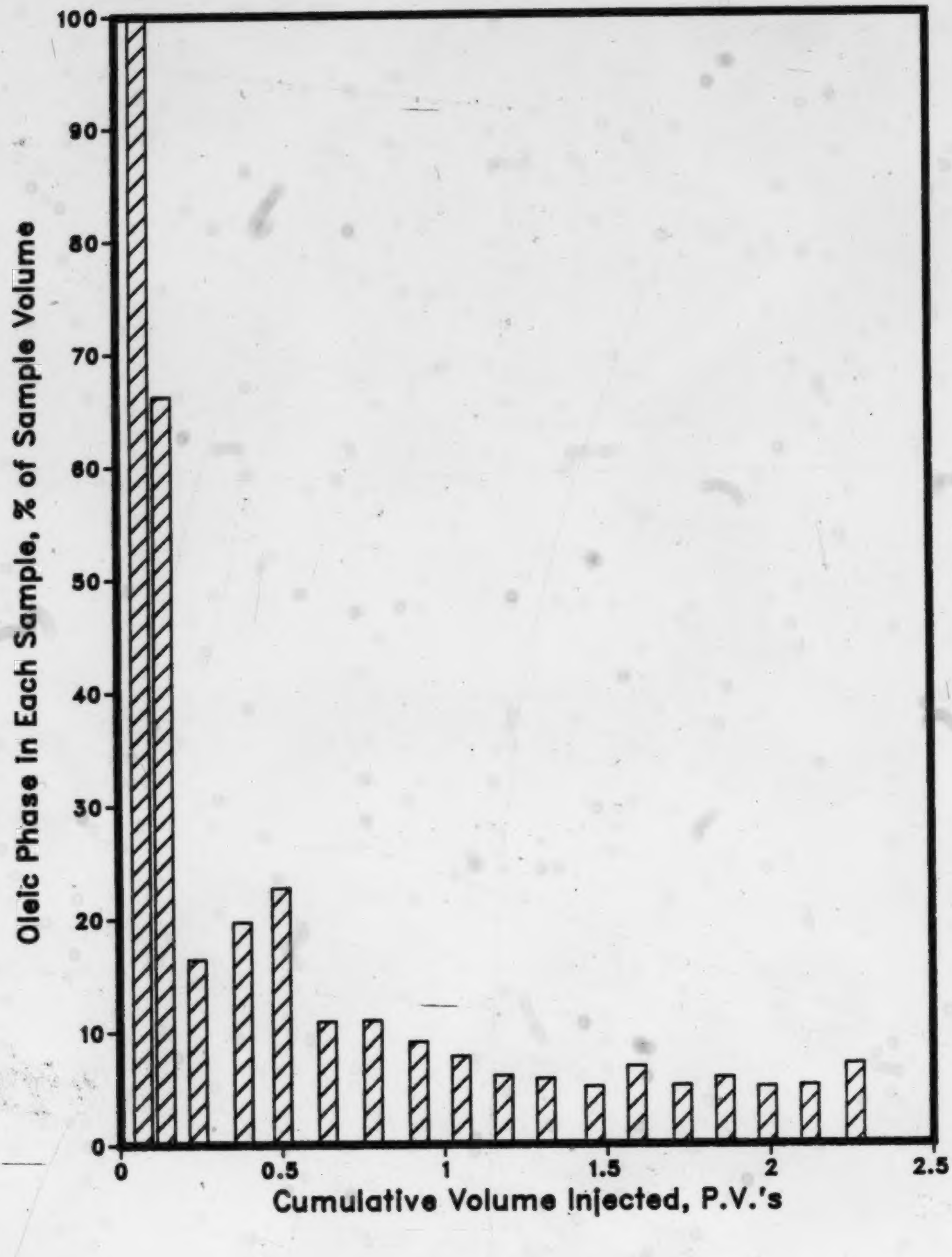

Figure 6.50 :Run 50 Solvent–Steamflood With Bottom Water Instantaneous Produced WOR Vs. Cumulative Volume Injected

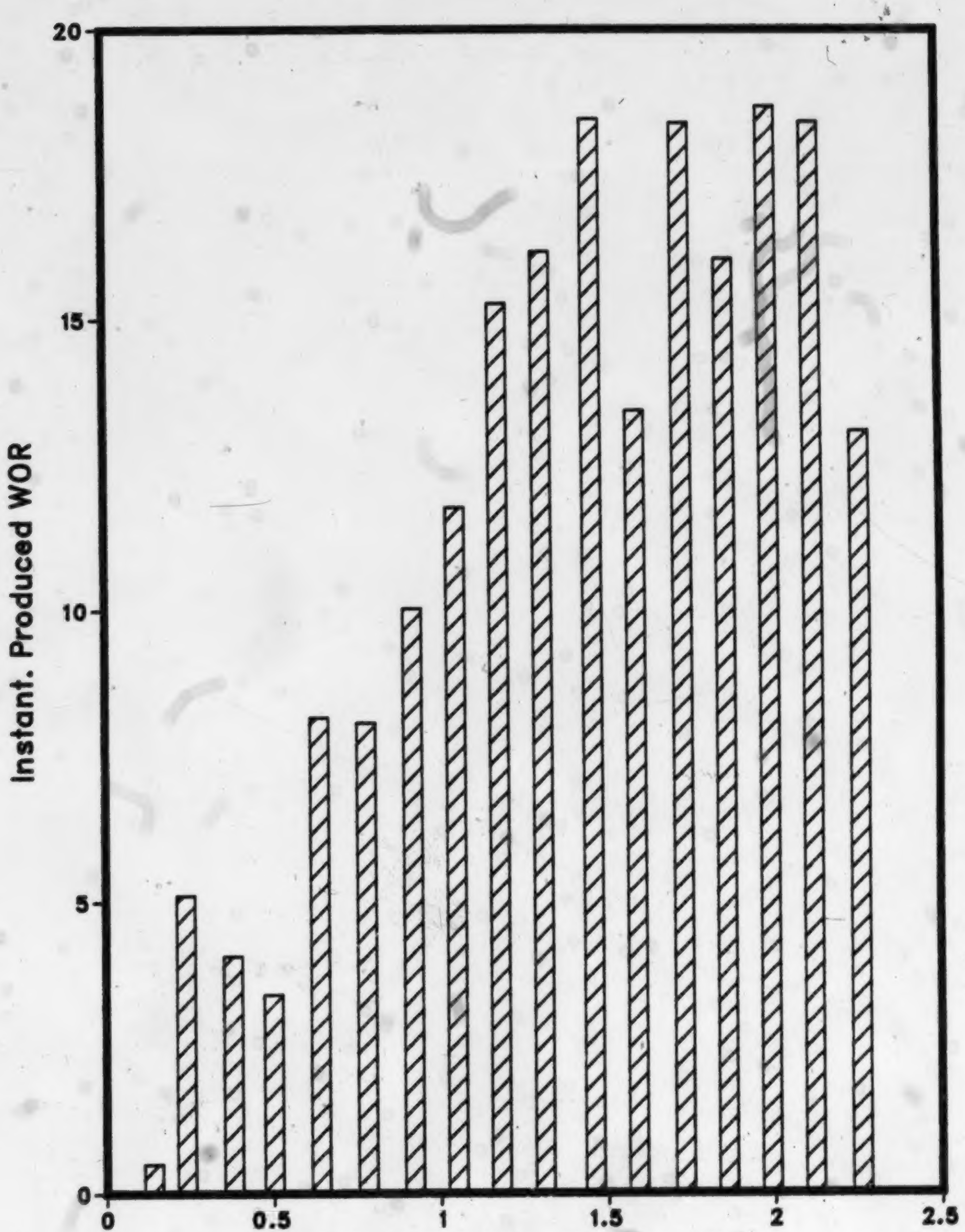

Figure 6.51 :Run 50 Solvent–Steamflood With Bottom Water Instantaneous Oil/Steam Ratio Vs. Cumulative Oil Produced

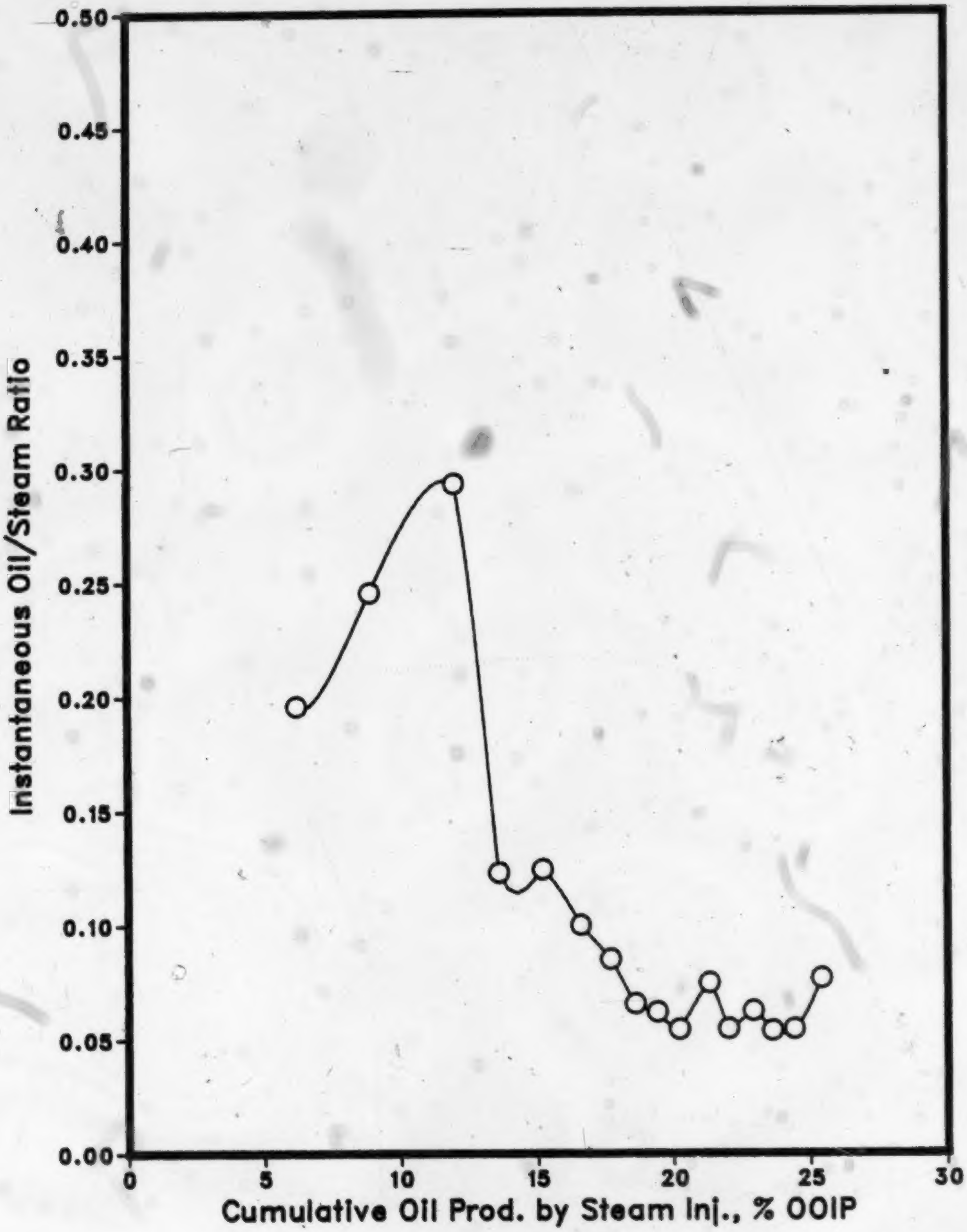

Table 6.14 : Run 51 Solvent-Steamflood With Bottom Water

HC Pore Volume : 10590.0 cc
Pore Volume : 15820.0 cc
Bulk Volume : 42005.0 cc
Porosity : 37.7%
Initial Oil Satn. : 66.9%
Initial H2O Satn. : 33.1%
Solvent Vol. Inj.: 1400.0 cc (10.0% PV)
Steam Vol. Inj. : 30980.0 cc (1.96 PV)

Type of Oil Used : Faxam-100
Initial Model Temperature : 3.00 C
Water Feed Flow Rate : 200.00 cc/min
Boiler Feed Flow Rate : 29.20 cc/min
Total Flow Rate of Steam : 229.20 cc/min
Solvent Flow Rate : 200.00 cc/min
Bottom Water Thickness : 26.2 % (% Gross Model Thickness)

Net Oil Recovery : 14.3% **Solvent Recovery : 40.8%** **Final Oil Saturation : 57.3%**

Cyl. No.	Solvent Conc. (%)	Tot. Vol. Inj. (cc)	Cum. Vol. Inj. (cc)	Cum. Vol. Inj. (P.V.)	HC Prod (cc)	Oil Prod. (cc)	Cum. Oil Rec. (cc)	Cum. Oil Rec. (%OOIP)	Cum. Sol. Rec. (cc)	Cum. Sol. Rec. (%)	Oil-Steam Ratio	Inst Prod. WOR	Inst. HC Prod. % of Sample
1	0%	1360	1360	0.09	35	35	35	0.3%	0	0.0%	0.0000	37.86	2.6%
2	68%	1020	2380	0.15	270	86	121	1.1%	184	13.1%	0.0000	2.78	26.5%
3	65%	760	3140	0.20	215	75	196	1.9%	324	23.1%	0.3945	2.53	28.3%
4	50%	1900	5040	0.32	265	133	329	3.1%	456	32.6%	0.1621	6.17	13.9%
5	31%	1900	6940	0.44	135	93	422	4.0%	498	35.6%	0.0765	13.07	7.1%
6	15%	1895	8835	0.56	65	55	477	4.5%	508	36.3%	0.0355	28.15	3.4%
7	10%	2000	10835	0.68	65	59	536	5.1%	514	36.7%	0.0336	29.77	3.3%
8	6%	1915	12750	0.81	60	56	592	5.6%	518	37.0%	0.0323	30.92	3.1%
9	7%	2105	14855	0.94	75	70	662	6.3%	523	37.4%	0.0369	27.07	3.6%
10	11%	1940	16795	1.06	120	107	769	7.3%	536	38.3%	0.0659	15.17	6.2%
11	6%	2020	18815	1.19	125	118	887	8.4%	543	38.8%	0.0660	15.16	6.2%
12	7%	1910	20725	1.31	115	107	994	9.4%	551	39.4%	0.0641	15.61	6.0%
13	4%	2110	22835	1.44	110	106	1100	10.4%	555	39.6%	0.0550	18.18	5.2%
14	4%	1930	24765	1.57	90	86	1186	11.2%	559	39.9%	0.0489	20.44	4.7%
15	4%	1945	26710	1.69	100	96	1282	12.1%	563	40.2%	0.0542	18.45	5.1%
16	4%	1860	28570	1.81	85	82	1364	12.9%	566	40.4%	0.0479	20.88	4.6%
17	4%	1880	30450	1.92	85	82	1446	13.7%	569	40.6%	0.0474	21.12	4.5%
18	3%	1930	32380	2.05	75	73	1519	14.3%	571	40.8%	0.0404	24.73	3.9%

Figure 6.52 :Run 51 Solvent–Steamflood With Bottom Water Cumulative Oil Recovery Vs. Pore Volumes Injected

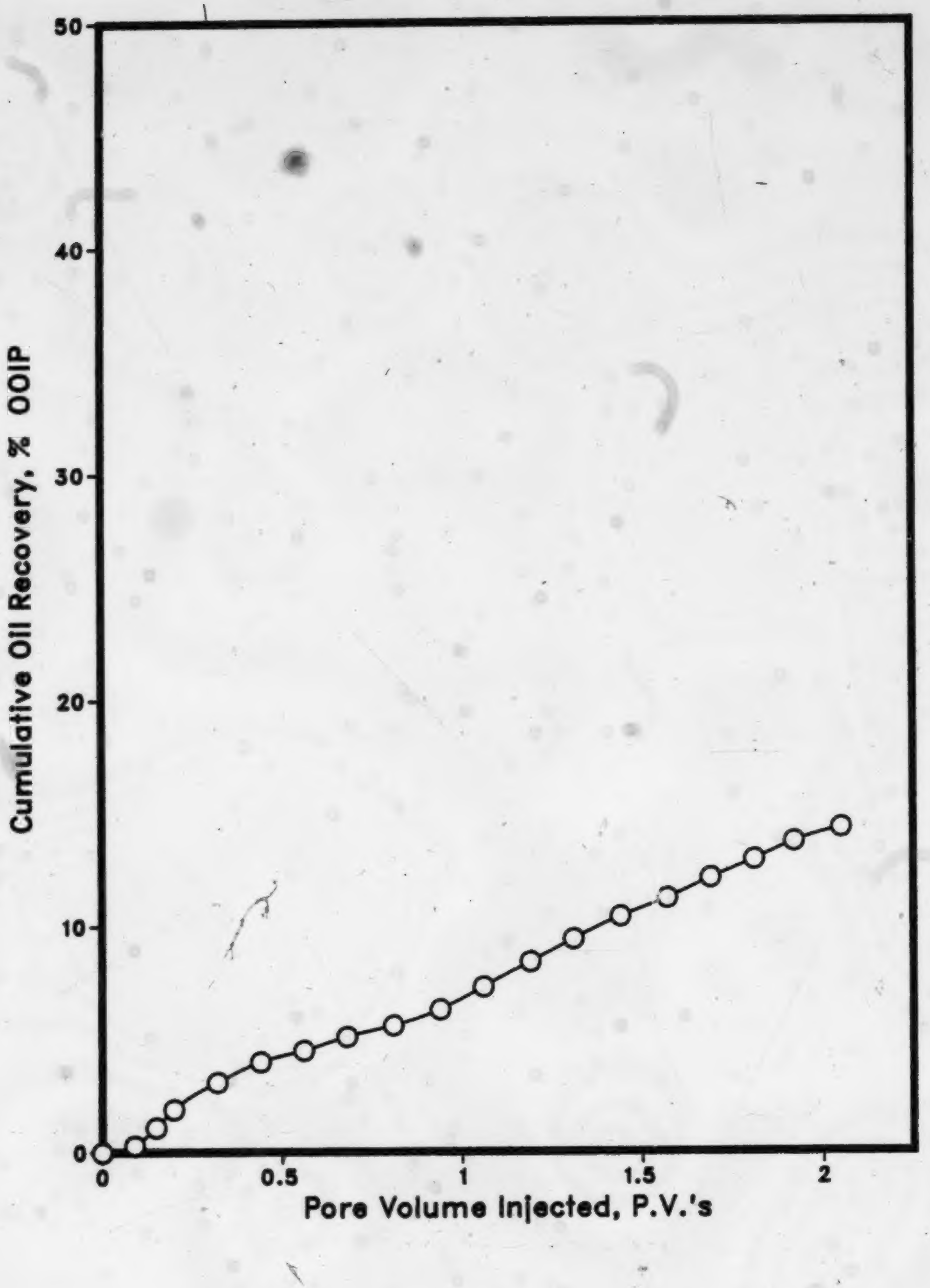

Figure 6.53 :Run 51 Solventflood–Steamflood With Bottom Water
Oleic Phase In Each Sample Vs. Cumulative Volume Injected

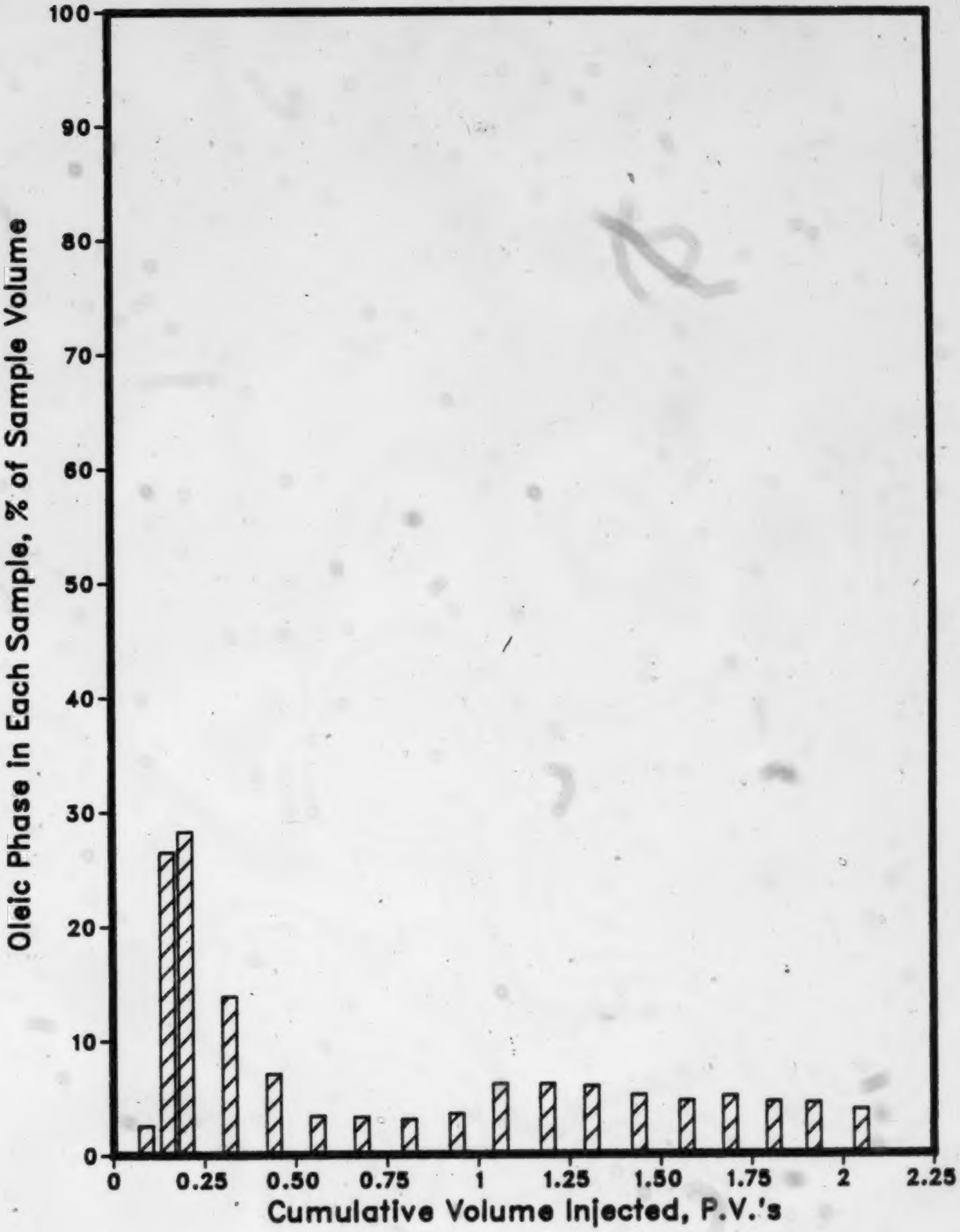

Figure 6.54 :Run 51 Solvent–Steamflood With Bottom Water Instantaneous Produced WOR Vs. Cumulative Volume Injected

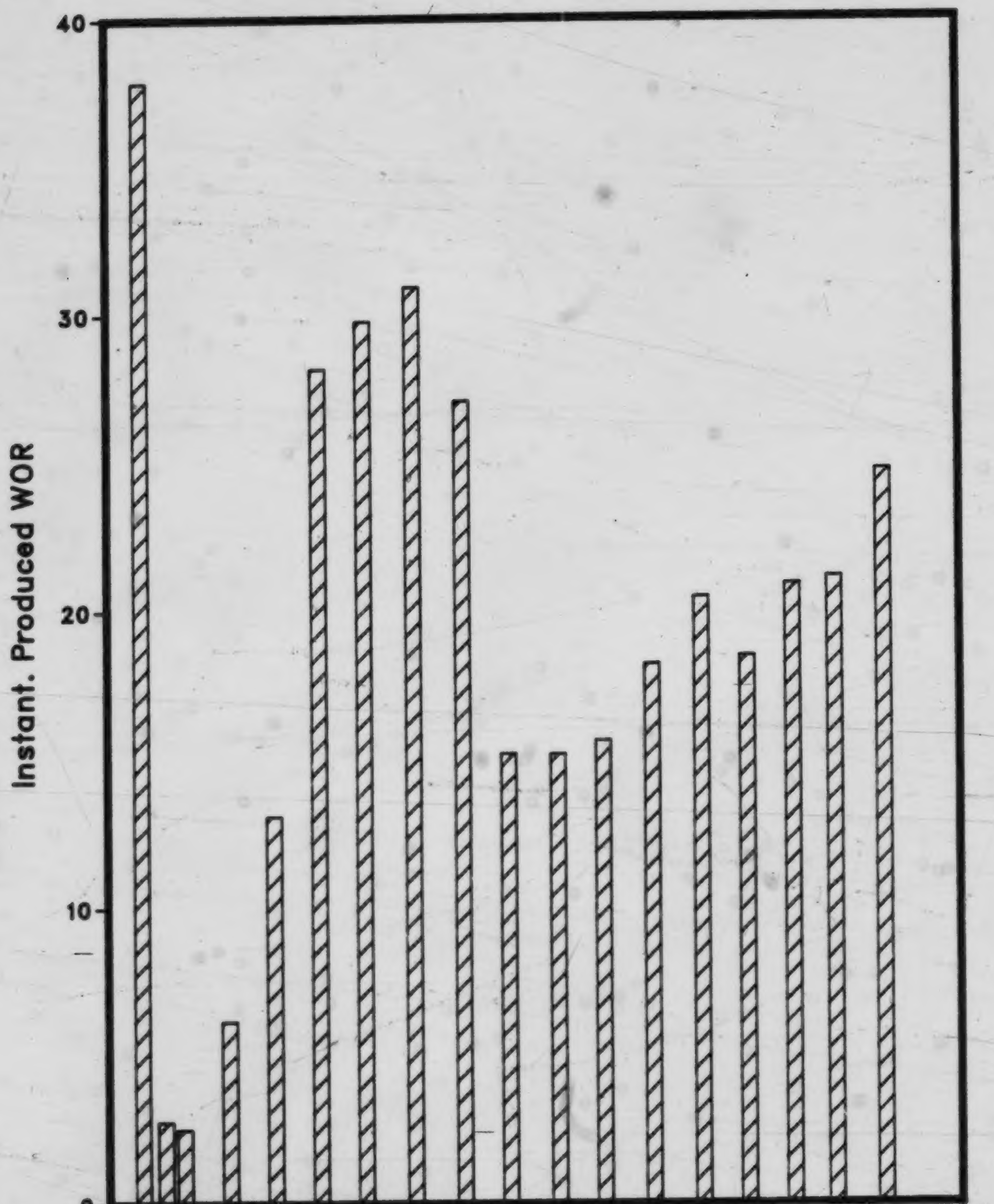

Figure 6.55 :Run 51 Solvent–Steamflood With Bottom Water Instantaneous Oil/Steam Ratio Vs. Cumulative Oil Produced

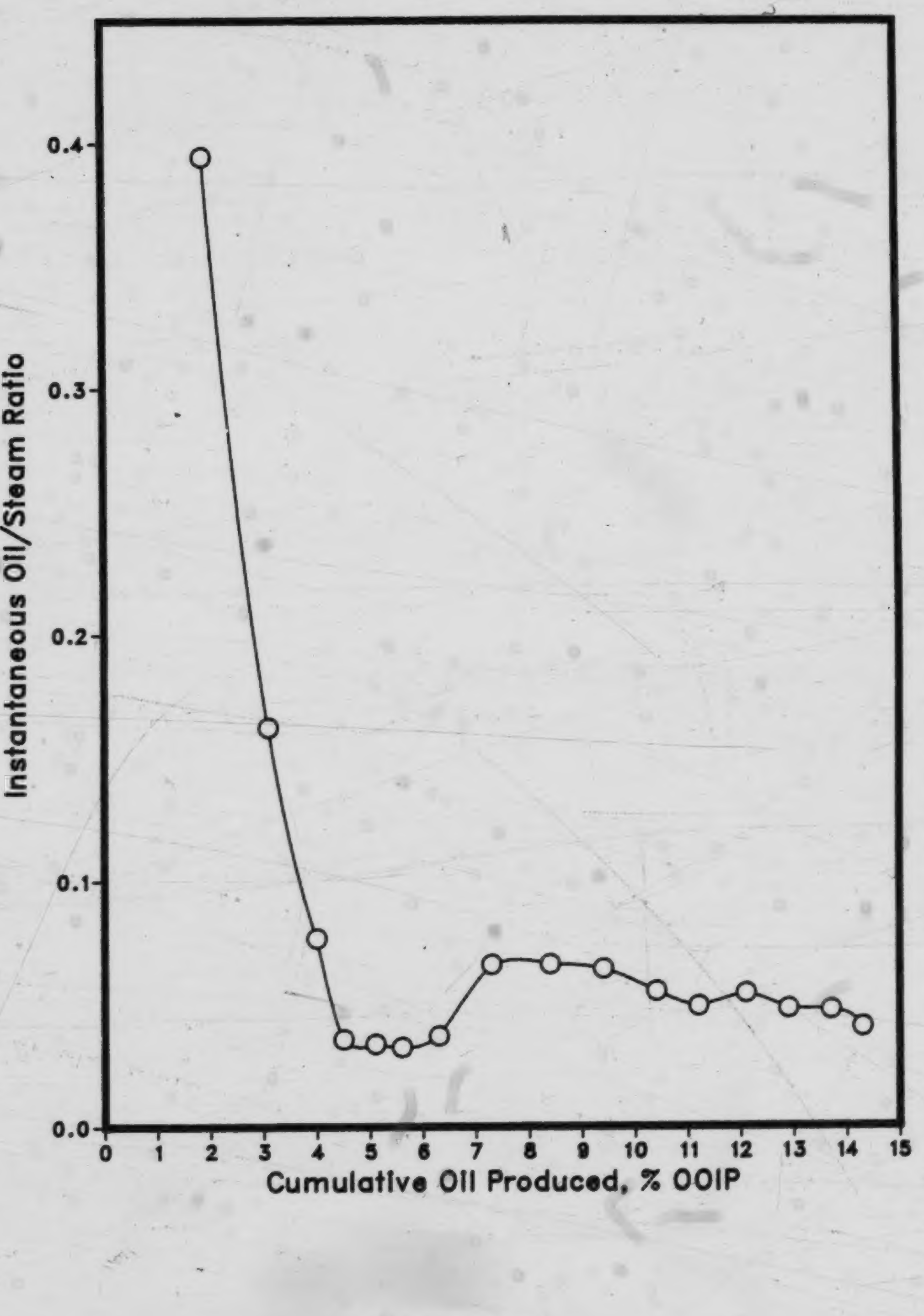

Table 6.15 : Run 53 Solvent-Steamflood With Bottom Water

HC Pore Volume : 11685.0 cc
Pore Volume : 15340.0 cc
Bulk Volume : 42005.0 cc
Porosity : 36.5%
Initial Oil Satn. : 76.2%
Initial H2O Satn. : 23.8%
Solvent Vol. Inj.: 1400.0 cc (10.0% PV)
Steam Vol. Inj. : 31670.0 cc (2.06 PV)

Type of Oil Used : Faxam-100
Initial Model Temperature : 3.00 C
Water Feed Flow Rate : 200.00 cc/min
Boiler Feed Flow Rate : 29.20 cc/min
Total Flow Rate of Steam : 229.20 cc/min
Solvent Flow Rate : 200.00 cc/min
Bottom Water Thickness : 15.6 % (% Gross Model Thickness)

Net Oil Recovery : 19.0%

Solvent Recovery : 54.4%

Final Oil Saturation: 61.7%

Cyl. No.	Solvent Conc. (%)	Tot. Vol. Inj. (cc)	Cum. Vol. Inj. (cc)	Cum. Vol. Inj. (P.V.)	HC Prod (cc)	Oil Prod. (cc)	Cum. Oil Rec. (cc)	Cum. Oil Rec. (%OOIP)	Cum. Sol. Rec. (cc)	Cum. Sol. Rec. (%)	Oil-Steam Ratio	Inst Prod. WOR	Inst. HC Prod. % of Sample
1	4%	1380	1380	0.09	80	77	77	0.7%	3	0.2%	0.0000	16.25	5.8%
2	67%	920	2300	0.15	740	244	321	2.7%	499	35.6%	0.0000	0.24	80.4%
3	50%	1100	3400	0.22	370	185	506	4.3%	684	48.9%	0.5068	1.97	33.6%
4	20%	1940	5340	0.35	210	168	674	5.8%	726	51.9%	0.1214	8.24	10.8%
5	7%	1810	7150	0.47	100	93	767	6.6%	733	52.4%	0.0585	17.10	5.5%
6	5%	2055	9205	0.60	100	95	862	7.4%	738	52.7%	0.0512	19.55	4.9%
7	4%	1980	11185	0.73	105	101	963	8.2%	742	53.0%	0.0560	17.86	5.3%
8	3%	1985	13170	0.86	110	107	1070	9.2%	745	53.2%	0.0587	17.05	5.5%
9	3%	2020	15190	0.99	125	121	1191	10.2%	749	53.5%	0.0660	15.16	6.2%
10	3%	2165	17355	1.13	135	131	1322	11.3%	753	53.8%	0.0665	15.04	6.2%
11	3%	1905	19260	1.26	155	150	1472	12.6%	758	54.1%	0.0886	11.29	8.1%
12	1%	2010	21270	1.39	125	124	1596	13.7%	759	54.2%	0.0663	15.08	6.2%
13	1%	1940	23210	1.51	110	109	1705	14.6%	760	54.3%	0.0601	16.64	5.7%
14	1%	2080	25290	1.65	105	104	1809	15.5%	761	54.4%	0.0532	18.81	5.0%
15	0%	2030	27320	1.78	125	125	1934	16.6%	761	54.4%	0.0656	15.24	6.2%
16	0%	1910	29230	1.91	105	105	2039	17.4%	761	54.4%	0.0582	17.19	5.5%
17	0%	1990	31220	2.04	100	100	2139	18.3%	761	54.4%	0.0529	18.90	5.0%
18	0%	1850	33070	2.16	80	80	2219	19.0%	761	54.4%	0.0452	22.13	4.3%

Figure 6.56 :Run 53 Solvent–Steamflood With Bottom Water Cumulative Oil Recovery Vs. Pore Volumes Injected

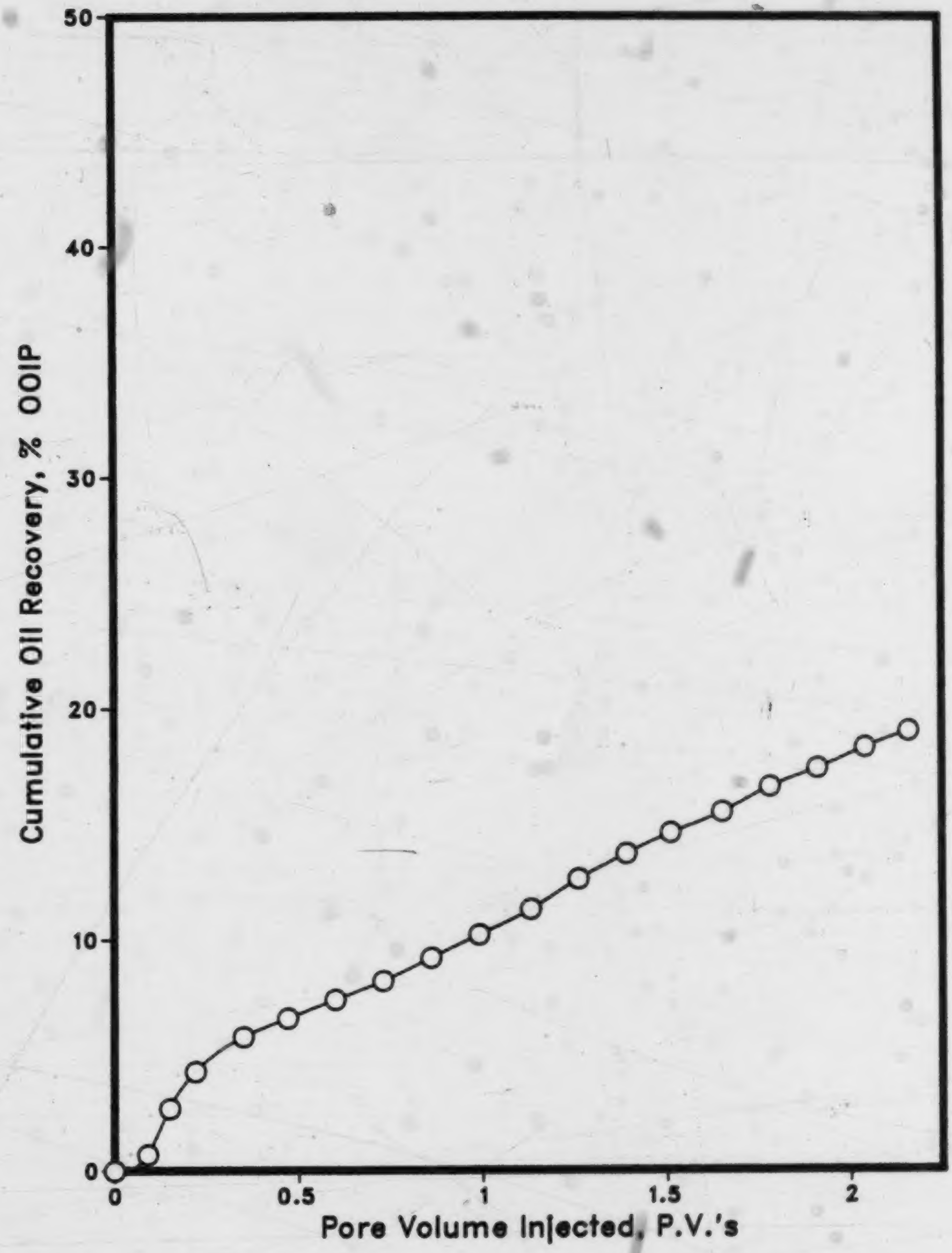

Figure 6.57 :Run 53 Solventflood—Steamflood With Bottom Water Oleic Phase In Each Sample Vs. Cumulative Volume Injected

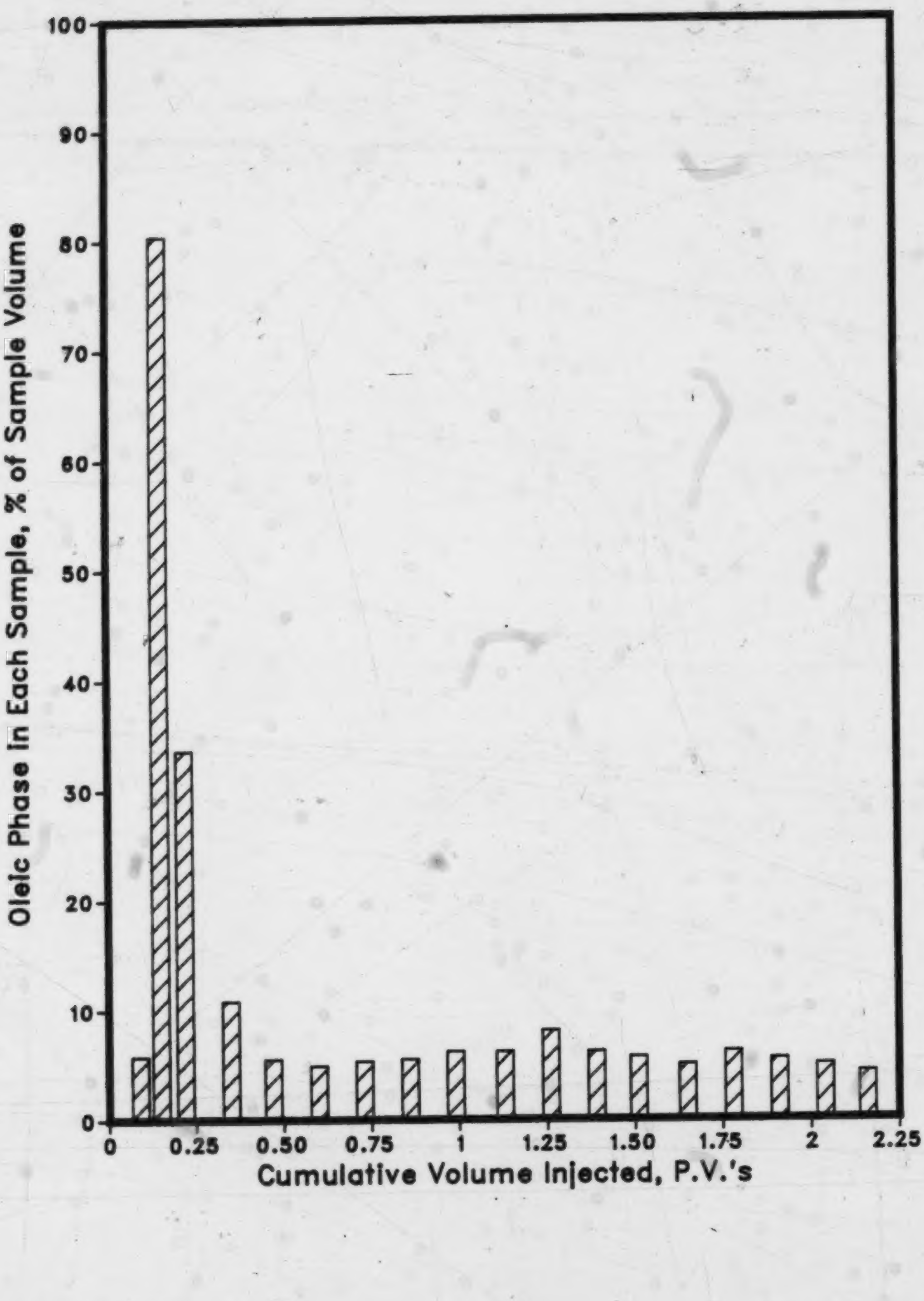

Figure 6.58 :Run 53 Solvent–Steamflood With Bottom Water
Instantaneous Produced WOR Vs. Cumulative Volume Injected

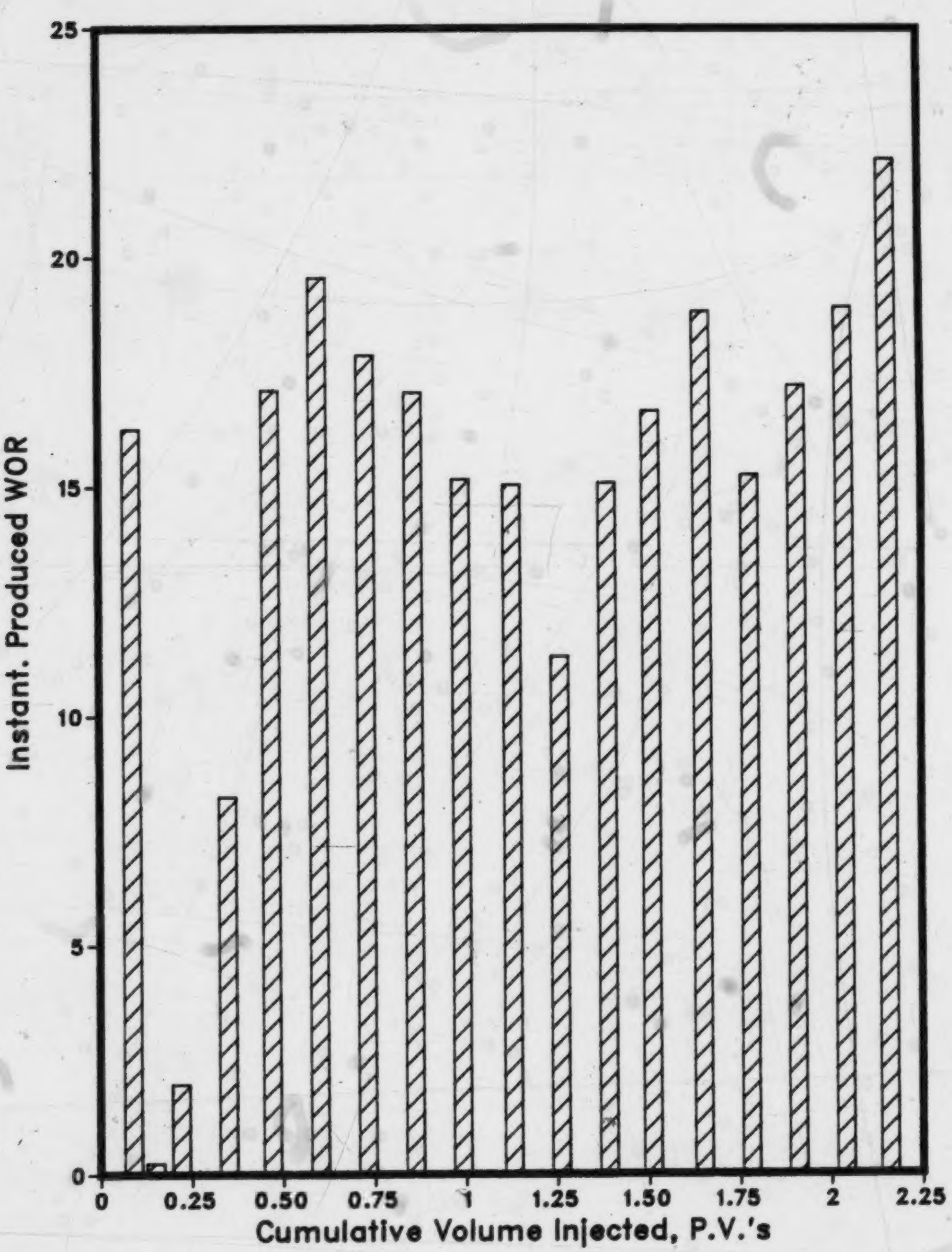

Figure 6.59 :Run 53 Solvent–Steamflood With Bottom Water Instanteous Oil/Steam Ratio vs. Cumulative Oil Produced

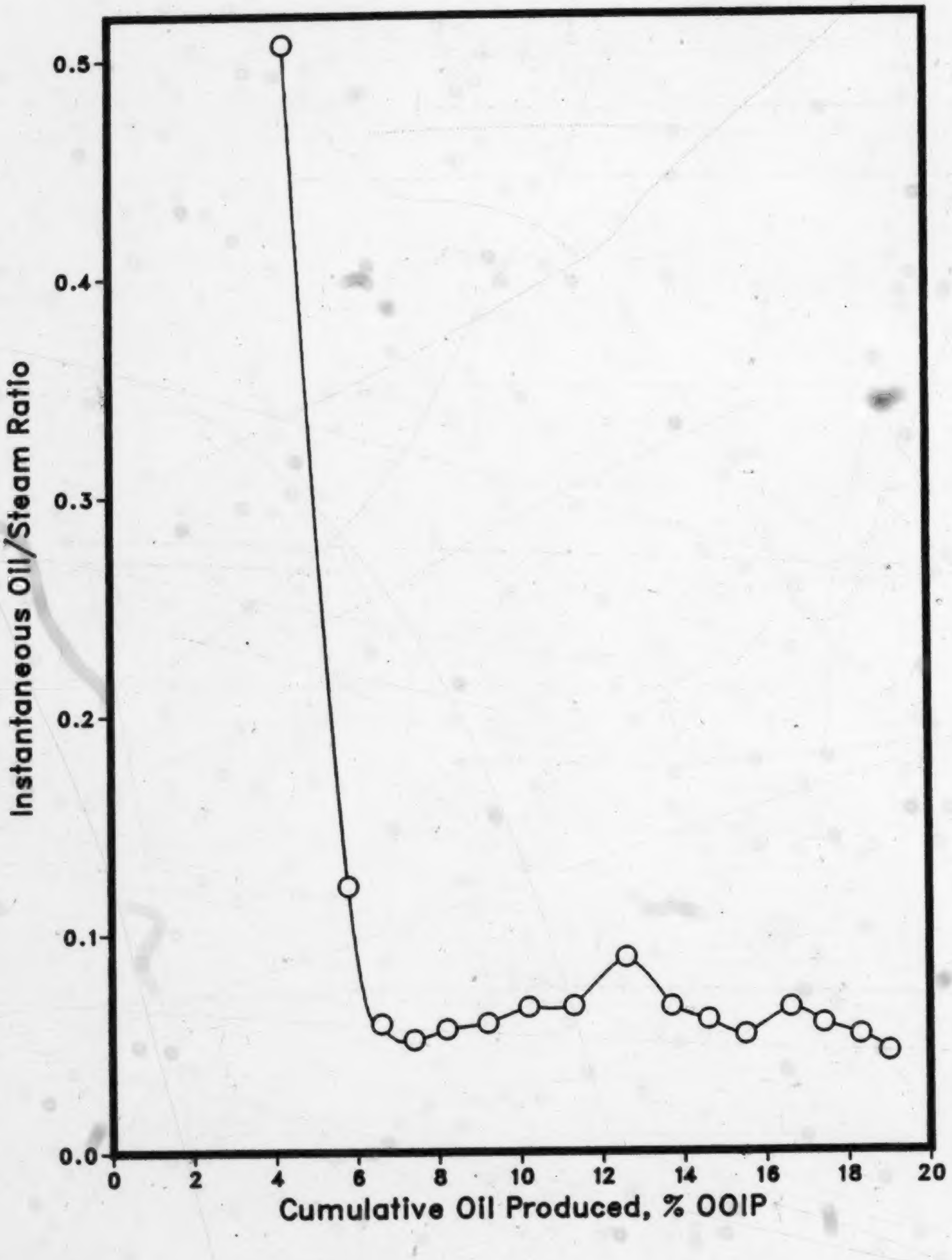

Table 6.16 : Run 54 Solvent-Steamflood With Bottom Water

HC Pore Volume : 13805.0 cc
Pore Volume : 15165.0 cc
Bulk Volume : 42005.0 cc
Porosity : 36.1%
Initial Oil Satn. : 91.0%
Initial H2O Satn. : 9.0%
Solvent Vol. Inj.: 1400.0 cc (10.0% PV)
Steam Vol. Inj. : 31885.0 cc (2.10 PV)

Type of Oil Used : Faxam-100
Initial Model Temperature : 3.00 C
Water Feed Flow Rate : 200.00 cc/min
Boiler Feed Flow Rate : 29.20 cc/min
Total Flow Rate of Steam : 229.20 cc/min
Solvent Flow Rate : 200.00 cc/min
Bottom Water Layer Thickness : 12.2 % (% Gross Thickness)

Net Oil Recovery : 22.6% **Solvent Recovery : 89.8%** **Final Oil Saturation : 70.4%**

Cyl. No.	Solvent Conc. (%)	Tot. Vol. Inj. (cc)	Cum. Vol. Inj.		HC Prod. (cc)	Oil Prod. (cc)	Cum. Oil Rec.		Cum. Sol. Rec.		Oil-Steam Ratio	Inst Prod. WOR	Inst. HC Prod. % of Sample
			(cc)	(P.V.)			(cc)	(%OOIP)	(cc)	(%)			
1	60%	1185	1185	0.08	1170	468	468	3.4%	702	50.1%	0.0000	0.01	98.7%
2	59%	985	2170	0.14	750	308	776	5.6%	1144	81.7%	0.0000	0.31	76.1%
3	27%	1175	3345	0.22	175	128	904	6.5%	1191	85.1%	0.1750	5.71	14.9%
4	9%	1895	5240	0.35	630	573	1477	10.7%	1248	89.1%	0.4980	2.01	33.2%
5	4%	2020	7260	0.48	165	158	1635	11.8%	1255	89.6%	0.0889	11.24	8.2%
6	1%	1940	9200	0.61	175	173	1808	13.1%	1257	89.8%	0.0992	10.09	9.0%
7	0%	2070	11270	0.74	150	150	1958	14.2%	1257	89.8%	0.0781	12.80	7.2%
8	0%	1940	13210	0.87	130	130	2088	15.1%	1257	89.8%	0.0718	13.92	6.7%
9	0%	2040	15250	1.01	120	120	2208	16.0%	1257	89.8%	0.0625	16.00	5.9%
10	0%	1935	17185	1.13	110	110	2318	16.8%	1257	89.8%	0.0603	16.59	5.7%
11	0%	1995	19180	1.26	110	110	2428	17.6%	1257	89.8%	0.0584	17.14	5.5%
12	0%	1965	21145	1.39	95	95	2523	18.3%	1257	89.8%	0.0508	19.68	4.8%
13	0%	2035	23180	1.53	85	85	2608	18.9%	1257	89.8%	0.0436	22.94	4.2%
14	0%	1970	25150	1.66	145	145	2753	19.9%	1257	89.8%	0.0795	12.59	7.4%
15	0%	2065	27215	1.79	105	105	2858	20.7%	1257	89.8%	0.0536	18.67	5.1%
16	0%	1980	29195	1.93	85	85	2943	21.3%	1257	89.8%	0.0449	22.29	4.3%
17	0%	1980	31175	2.06	75	75	3018	21.9%	1257	89.8%	0.0394	25.40	3.8%
18	0%	2110	33285	2.19	105	105	3123	22.6%	1257	89.8%	0.0524	19.10	5.0%

Figure 6.60 :Run 54 Solvent-Steamflood With Bottom Water Cumulative Oil Recovery Vs. Pore Volumes Injected

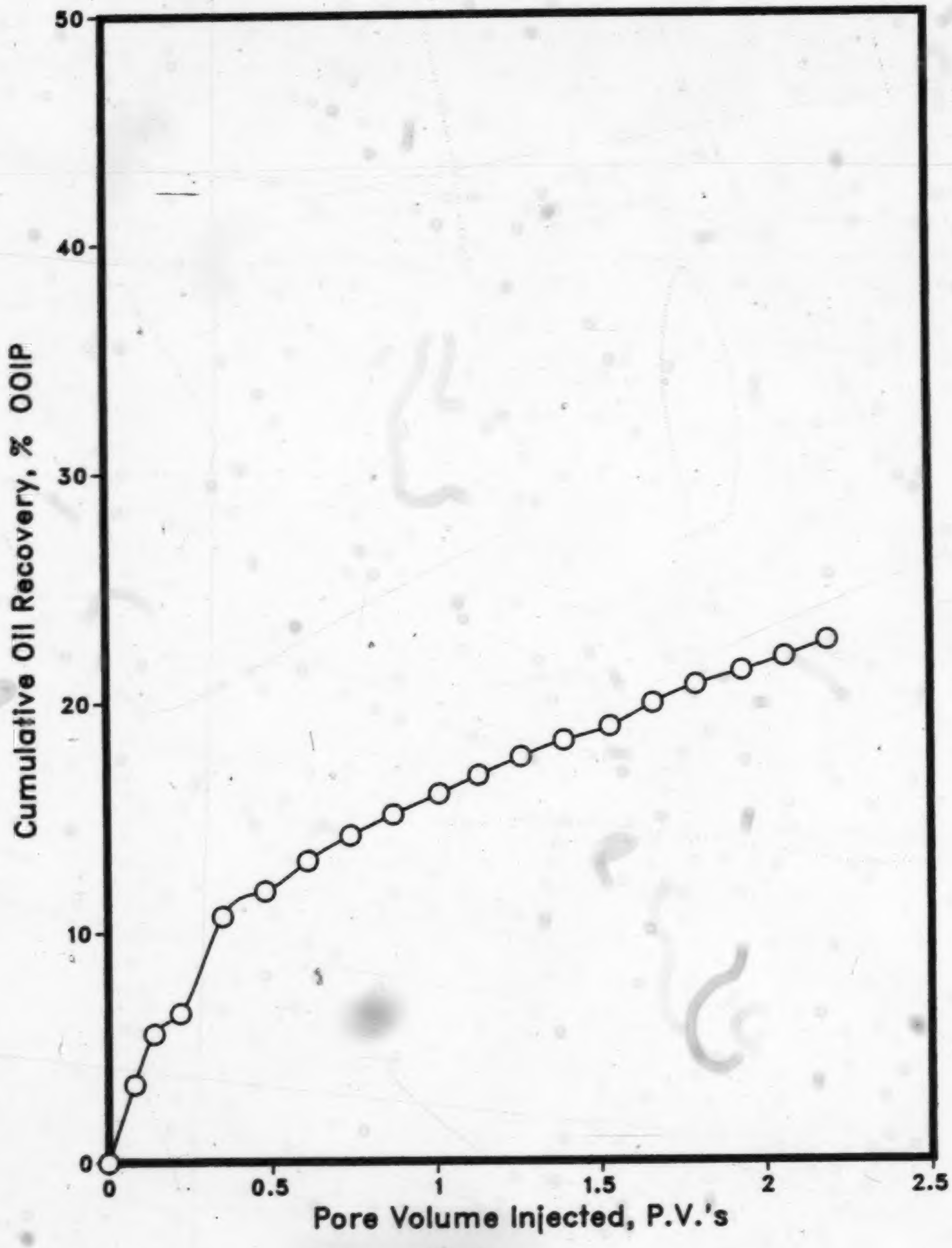

Figure 6.61 :Run 54 Solventflood—Steamflood With Bottom Water
Oleic Phase in Each Sample Vs. Cumulative Volume Injected

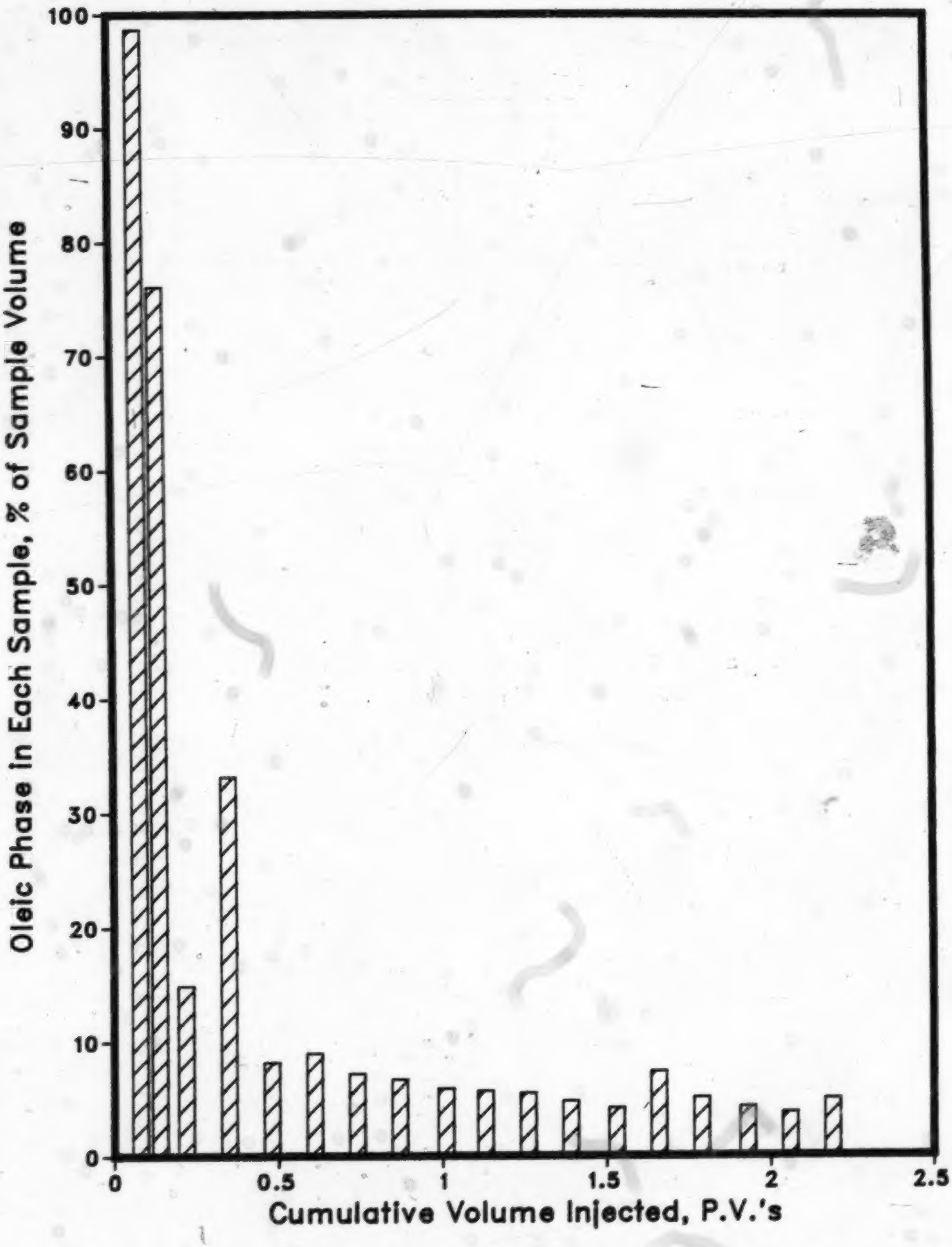

Figure 6.62 :Run 54 Solvent–Steamflood With Bottom Water Instantaneous Produced WOR Vs. Cumulative Volume Injected

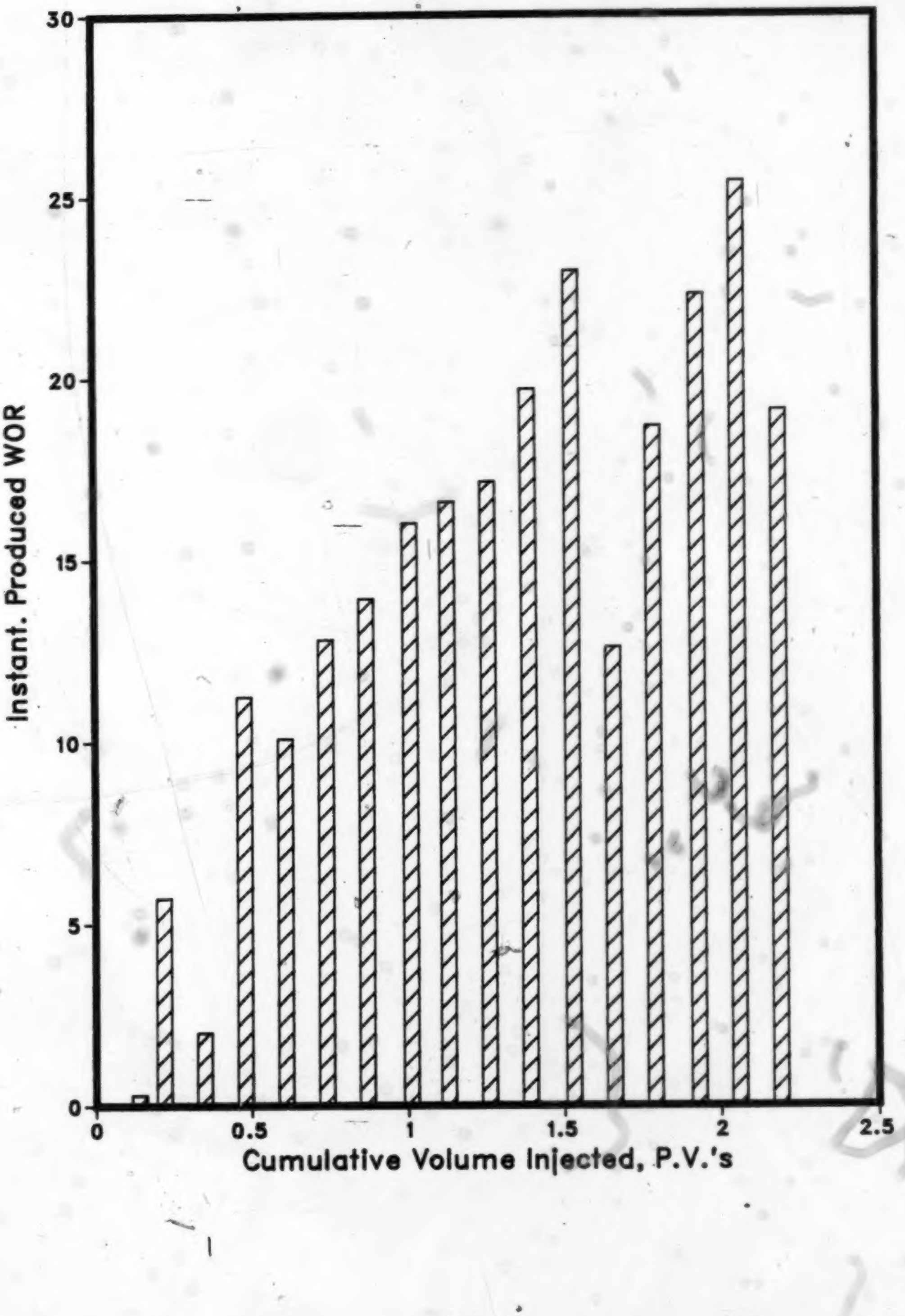

Figure 6.63 :Run 54 Solvent–Steamflood With Bottom Water Instanteous Oil/Steam Ratio vs. Cumulative Oil Produced

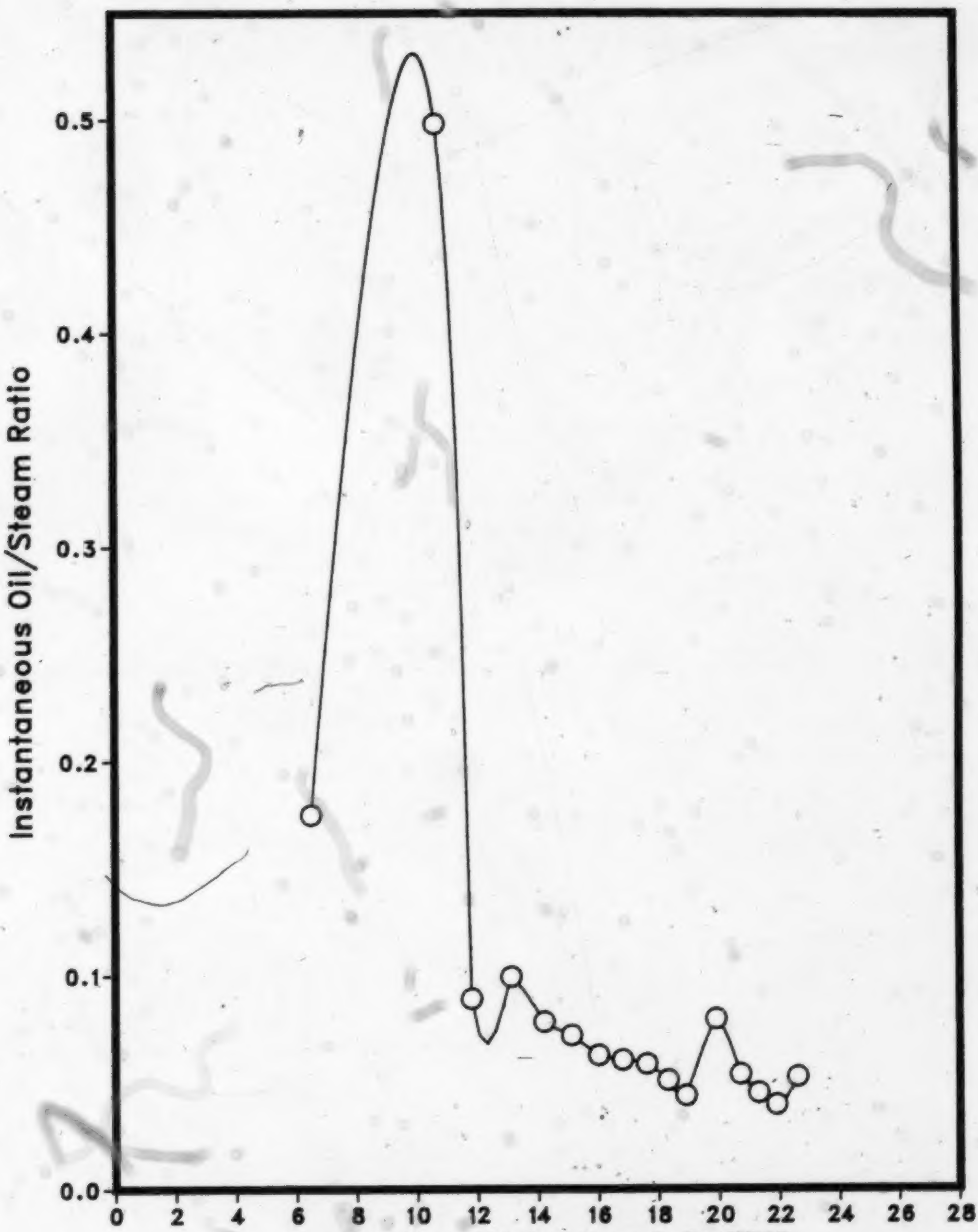

thickness of the model at about the same rate, whereas for Runs 51 (Fig. A.151-A.154) and 53 (Fig. A.163-A.166) heat advance was noticeably faster in the bottom water zone.

The solvent recoveries for Runs 49 (84.6%), 50 (88.5%) and 54 (89.8%) were considerably higher than those obtained in Runs 51 (40.8%) and 53 (54.4%). The solvent recoveries indicated that the higher the initial oil saturation in the core the better the solvent recovery. Since Runs 49, 50 and 54 had less bottom water and higher initial oil saturations than Runs 51 and 53, the solvent recoveries for these three runs were far better than those obtained for Runs 51 and 53.

The solvent recovery results were consistent with what Alikhan [64] has reported. He stated that a solvent-steamflood process implemented in an oil saturated model yielded a greater solvent recovery than when performed in a waterflooded model. The nature of the solvent recovery in these two instances could be related to increased mixing of solvent with oil in the waterflooded situation which caused more solvent to remain in the model as a residual hydrocarbon saturation. The two instances of an initially oil saturated model and an initially waterflooded model could be considered analagous to a thin bottom water situation and a thicker bottom water case, respectively. The varying degree of oil-solvent mixing in the two different types of runs may have been a result of the solvent having a higher relative permeability in the thinner bottom water layer experiments than the thicker bottom water cases. The higher relative permeability would create more distinct solvent channelling and less mixing with the inplace oil thus a larger solvent recovery. For the thicker bottom water situation the difference in relative permeability between the water and the solvent would be less than that for the thicker underlying water case due to the higher initial water saturation. The solvent would not flow through the model as easily thus blending more thoroughly with the in-place oil. Mixing of solvent and oil would be more pronounced in the thinner bottom water case. This would decrease the amount solvent recovered due to the remainder of a higher residual solvent slug material saturation.

The overall oil recoveries for Runs 49 (23.3% OOIP), 50 (25.4% OOIP), 51 (14.3% OOIP), 53 (19.0% OOIP) and 54 (22.6% OOIP) illustrate that bottom water can significantly reduce the amount of oil recovered by a solvent-steamflood. The effect of the bottom water on solvent and steam injection resulted in a considerably lower oil recovery than that obtained with a solvent-steamflood implemented on a homogeneous reservoir. Results of Runs 49, 50, 51, 53 and 54 confirm that the use of a solvent slug assisted in improving the overall oil recovery by partially diverting the steam away from the bottom water and into the oil layer during the initial stages of the steamflood. It was also noted that the bottom water had a more detrimental effect on the overall oil recovery as it increased in thickness. Figure 6.64, a plot of oil recovery after two pore volumes injected versus bottom water thickness for the five experiments as well as Run 46 (solvent-steamflood without bottom water), demonstrates the effect varying bottom water thickness has on overall oil recovery. Figure 6.64 is similar to the plot created in the study by Proctor, George and Farouq Ali [63] which investigated conventional steamflooding of thin bottom water formations without the use of a solvent. Similarly to what was reported by Proctor, George and Farouq Ali [63], Figure 6.64 indicates that for bottom thicknesses less than approximately 10% of the gross model thickness, the oil recovery due to the solvent-steamflood process is close to that obtained by solvent-steamfloods implemented in homogeneous models. For bottom water thicknesses greater than about 10% of the total model thickness the overall oil recovery of the solvent-steamflood process is greatly reduced. The experimental results suggest that the injection of a solvent slug prior to steamflooding a bottom water reservoir could improve the overall oil recovery up until a limiting bottom water thickness is reached. Based upon Figure 6.64 the limiting bottom water thickness is estimated to be somewhere between 25 and 30% of the total model thickness. It is concluded that as the bottom water thickness increases in the model the oil recovery is decreased until a limiting bottom water thickness value is reached, above which the use of a solvent slug does not significantly improve the oil recovery.

Figure 6.64 :Total Oil Recovery versus Bottom Water Thickness For Solvent–Steamfloods

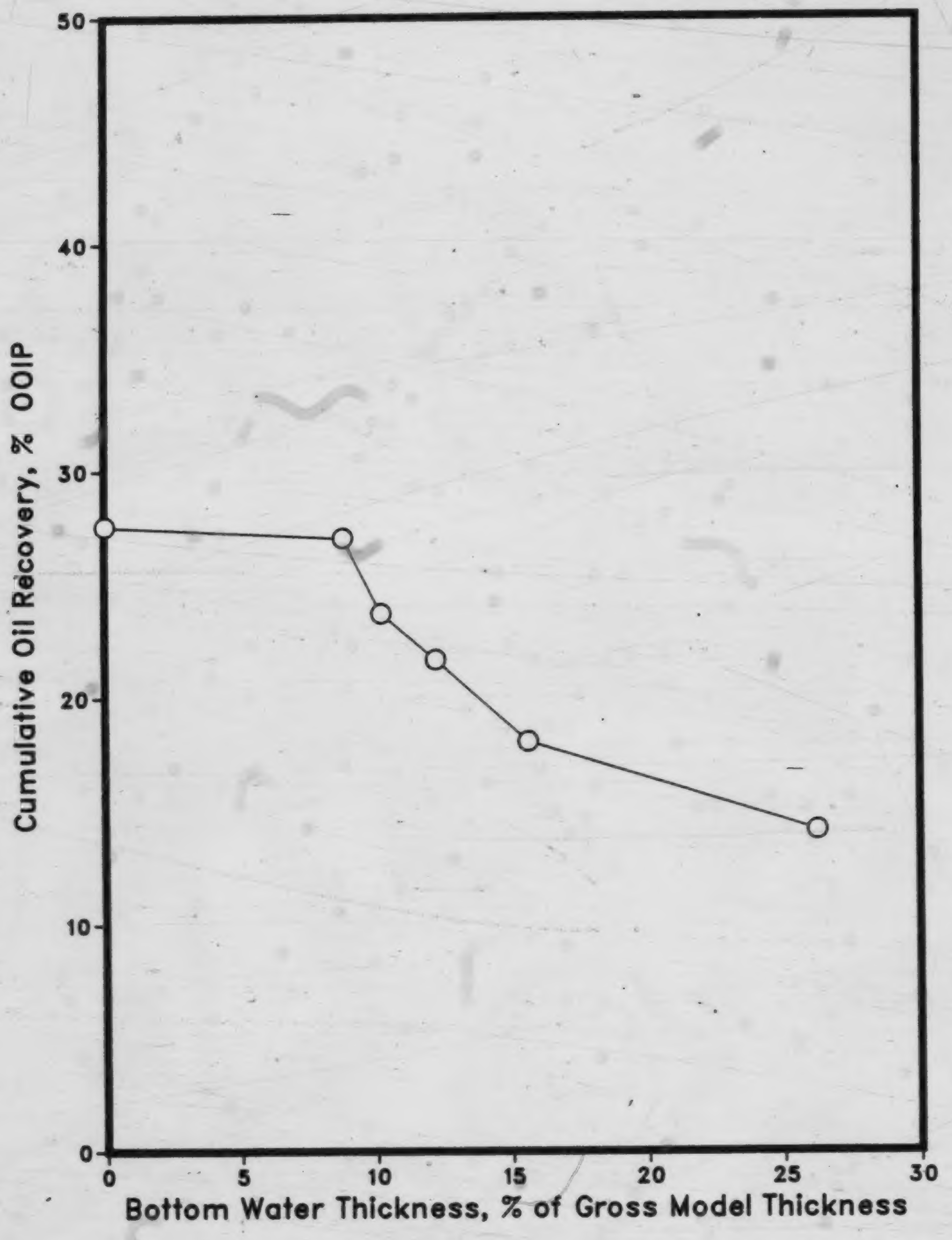

One of the major objectives of this study was to investigate the use of solvents in combination with steam as a recovery method for marginal heavy oil reservoirs containing bottom water and/or a gas cap. Solvent injection into the oil layer during the initial period of the runs created a temporary preferential path for the steam to follow, preventing the steam from immediately channelling into the bottom water. The steam progressed through the oil layer for a short period of time until it finally moved downward and advanced through the bottom water section. Once the steam moved into the bottom water layer the heating efficiency dropped in the oil zone and a severe drop in the overall oil recovery resulted.

Comparison of the results of Runs 49, 50 and 54 with previous continuous steamfloods (Runs 32, 33 & 39) carried out with similar bottom water thicknesses, revealed that the solvent slug injection prior to steamflooding partially alleviated the effect of bottom water and resulted in improved oil recovery. Due to partial diversion of the steam into the solvent channels in the oil region the steam displacement achieved was more stable, causing a delayed and more pronounced steam breakthrough to occur at the production well. In the case of a conventional steamflood, the bottom water had a greater and more immediate effect on steam displacement resulting in a much less stable displacement. This led to earlier and less distinct steam breakthrough at the producer. Oil recovery results for Runs 32 (BW=2.3%), 33 (BW=4.0%) and 39 (BW=12.5%) were 22.8%, 22.9% and 16.8% of the original oil in place, respectively. These recoveries were appreciably less than the recoveries yielded by Runs 49 (23.3% OOIP), 50 (25.4% OOIP), 53 (19.0% OOIP) and 54 (22.6% OOIP). In the case of Run 51 there did not seem to be an improvement in the oil recovery compared to the Runs 32, 33 and 39. Because of the extensive bottom water layer in Run 51 the steam was not able to flow through the oil layer for as long as in Runs 49, 50, 53 and 54 resulting in a considerable decline in the oil recovery of Run 51. Comparing the results of the two different types of experiments (ie. steamflood versus solvent-steamflood) revealed that the solvent-steamflood does exhibit an improved oil recovery capability from bottom water formations in relation to a conventional steamflood. A crossplot of the recovery curves for Runs 39 and 54 is provided in Figure 6.65 which compares the effectiveness of a solvent-steamflood process as opposed to a steamflood in similar bottom water formations. The difference in the initial behaviour of these two curves demonstrates the effectiveness of the solvent slug. The recovery curve for Run 54 in the primary stages of the run rises sharply compared to the recovery curve of Run 39. This was due to solvent channelling in Run 54 allowing the steam to penetrate the oil zone more easily which increased the stability of the steam displacement of oil in the model and resulted in more oil being mobilized and subsequently recovered. Figure 6.65 illustrates the increased oil recovery potential of the solvent-steamflood process over a conventional steamflood in bottom water formations.

It is concluded from the results of Runs 32, 33, 39, 49, 50, 51, 53 and 54 that the solvent slug assisted in improving the overall oil recovery in bottom water formations by partially diverting the steam away from the bottom water zone during the initial stages of the steamflood.

Figure 6.65 :Comparison of Steamflood Run 39 & Solvent–Steamflood Run 54 Recoveries Performed in a Bottom Water Model

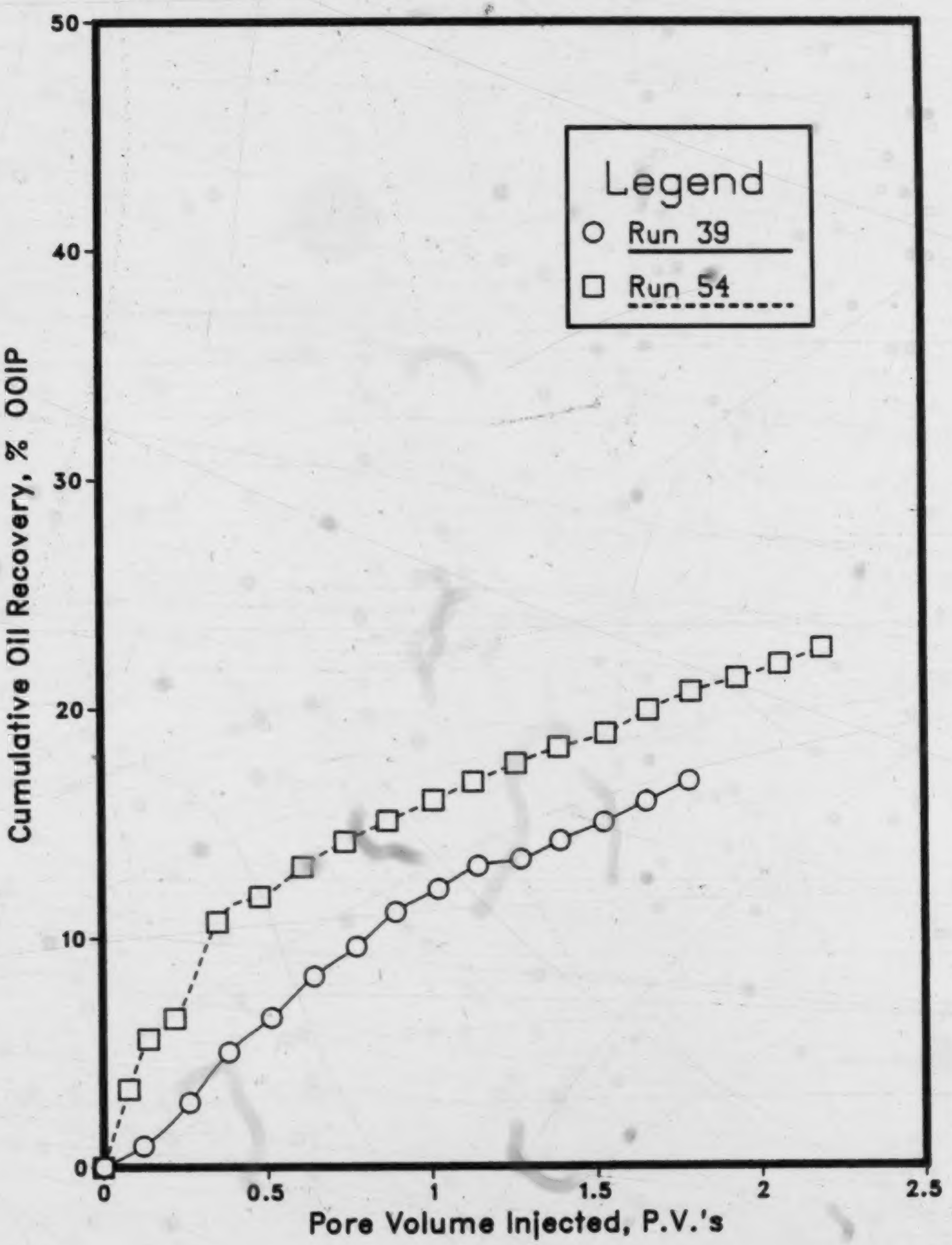

Role of Gas Injection in Steamflooding

In this research study, three different types of runs were conducted using gas injection prior to the specific recovery method being investigated. The first type of run involved gas injection prior to steam injection in a bottom water model and was discussed in the previous section dealing with base experiments. The second type of experiment conducted gas injection prior to a solvent-steamflood of a homogeneous model and the final type of run performed a solvent-steamflood in a bottom water model. The purpose for carrying out these gas injection runs was based on the principle reasoning that the injected gas would create a gas cap or channel in the upper portion of the model which would form a more conductive path for the injected fluid (ie. solvent and/or steam) to enter the oil zone. The less resistant gas path would aid in partially diverting the injected fluid away from the bottom water so that the oil mobilizing properties of the injected fluids could be used more effectively to recovery the overlying oil.

Proctor, George and Farouq Ali [63] performed a set of experiments (Runs 24 & 25) in the same low pressure model of the Aberfeldy formation as was used in the present research investigation. These two runs involved gas injection proceeded by a steamflood of a homogeneous model. The results reported by Proctor et al. [63] are briefly described in the proceeding section.

The first set of gas runs (Runs 60 & 61) carried out in the present research study were base experiments which involved creating a gas zone in a bottom water model before performing a steamflood. The results of these two experiments have already been discussed in the previous base experiment section "Steamflood of a Bottom Water Model With Prior Gas Injection". However, a brief summary of the results of the two experiments will be included in the following section.

The next group of experiments (Runs 55 & 56) utilized gas injection prior to conducting a solvent-steamflood of a homogeneous model, with the results provided and interpreted in the preceding section.

During the final set of runs (Runs 58, 59 & 62) gas injection was performed prior to the solvent-steamflood of a bottom water model. The results and discussion of the these three gas injection experiments are also included in this section.

Gas Injection in a Steamflood

Proctor, George and Farouq Ali [63] suggested that the injection of a small amount of inert gas prior to steamflooding may result in a flow channel away from the bottom water zone, thus minimizing the heat scavenging effect of the bottom water zone. They first tested this idea in a homogeneous pack and found that the implementation of gas injection may also be suitable in formations without the presence of bottom water. The gas injection strategy had the advantage of drastically increasing the steam injectivity in the oil region and therefore, could be quite useful in formations where steam injectivity is very low in the oil zone. It was also reported that the production response for the gas injection process was slightly less than that obtained for a continuous steam injection scheme. However, for a formation where steam injectivity is low, the increase in injectivity due to gas injection may justify the slight drop in the initial oil production response.

Gas Injection Prior to Steam Injection with Bottom Water

Results of Runs 60 and 61 indicated that the existence of a gas region in a bottom water model during a steamflood helped to partially divert the injected steam into the oil zone away from the bottom water so that the steam could be used more efficiently to heat and displace the oil in the model. When comparing the results of Run 39 (steamflood of a bottom water model) and Run 61 (gas injection prior to a steamflood of a bottom water model), which had similar bottom water thicknesses, it was evident during Run 61 that the presence of a gas zone in the model resulted in an improvement in the initial recovery response of a steamflood process in a bottom water formation. Also in Run 61, time until steam breakthrough was prolonged and steam breakthrough was more distinct than in Run 39, as indicated by the differences between the comparative plots generated from the results of each experiment. This was due to the gas zone partially preventing the steam from being lost to bottom water zone and therefore the steam could more effectively mobilize and recover the inplace oil.

Gas Injection with Solvent and Steam Injection

By injecting a small value of inert gas before performing a solvent-steamflood it is believed that a flow channel can be created which would divert the injected solvent and steam away from the bottom water region and into the oil zone. This would further minimize the heat scavenging effects of the bottom water zone. The process of gas injection in combination with a solvent-steamflood was first performed in a homogeneous model. Runs 55 and 56 consisted of creating a gas cap in a homogeneous model prior to a solvent-steamflood which used a 10% pore volume slug of solvent. The initial gas saturation in the model for the two runs was 0.6%. Tables 6.17 and 6.18 contain the tabulated results for Runs 55 and 56, respectively.

The oil recovery curves of Runs 55 and 56 are shown in Figures 6.66 and 6.70, respectively. Both curves rise sharply during the initial stages of the experiments which represent the production of oil mobilized by the solvent slug and steam. Following the sharp increase the curves begin to level off slightly and soon after started to rise again. However, the rise was less drastic than the initial increase. These regions of the recovery curves represent steam breakthrough at the production well which was preceded by the continued mobilization of oil due to steam injection. Figures 6.66 and 6.70 were similar to the recovery curves obtained for the straight solvent-steamfloods performed in a homogeneous model (Runs 44, 45 & 46).

The bar graphs of volume as a percentage of oleic phase in each sample taken versus cumulative volume injected and instantaneous produced WOR versus cumulative volume injected for Runs 55 (Fig. 6.67-6.68)and 56 (Fig. 6.71-6.72) indicate that steam breakthrough occurred in the primary stages of both experiments. The peaks and valleys of these bar plots corresponded very closely with the respective recovery curves. Again the plots were quite similar in nature to those of Runs 44, 45 and46.

Figures 6.69 and 6.73 are plots of instantaneous oil/steam ratio versus cumulative oil produced for Runs 55 and 56, respectively. Initially the oil/steam ratio drops steeply and then a distinct peak in the oil/steam ratio occurs in both figures between approximately 10 to 20% production of the original oil in place. Oil produced due to the steam sweeping the model prior to initial steam breakthrough was represented by this peak in the oil/steam ratio plots. The gradual levelling of the curves after the peak was created by further mobilizing of oil by the steam after breakthrough.

As in the case of Runs 44, 45 and 46, the temperature profiles for Runs 55 (Fig. A.179-A.186) and 56 (Fig. A.191-A.198) indicated that the solvent and steam advanced faster through the upper level of the model than the lower section. By comparing the profiles of Runs 44, 45 and 46 to those of Runs 55 and 56 it appeared that the injected solvent and steam moved slightly faster through the upper portion of the model when a gas saturation existed. The injectivity of the solvent and steam in the model was improved due to the existence of the gas saturation which resulted in the solvent and steam progressing more rapidly through the upper portion of the reservoir than the lower region. The cross-sectional temperature profiles for Runs 55 (Fig. A.187-A.190) and 56 (Fig. A.199-A.202) agreed with the top view profiles in that the solvent and steam advanced faster through the upper portion of the model than the lower part.

The oil recoveries for Runs 55 (26.8%) and 56 (27.0%) were fairly close to one another. These results were much the same due to the similarities in porosities and initial saturations for both experiments. The overall oil recovery for continuous steamfloods

Table 6.17 : Run 55 Gas Injection Prior to Solvent-Steamflood of Homogeneous Model

HC Pore Volume : 13015.0 cc
Pore Volume : 14410.0 cc
Bulk Volume : 42005.0 cc
Porosity : 34.3%
Initial Oil Satn. : 90.3%
Initial H2O Satn. : 9.1%
Initial Gas Satn. : 0.6%
Solvent Vol. Inj. ; 1400.0 cc

Type of Oil Used : Faxam-100
Initial Model Temperature 3.00 C
Water Feed Flow Rate : 200.00 cc/min
Boiler Feed Flow Rate : 29.20 cc/min
Total Flow Rate of Steam : 229.20 cc/min
Solvent Flow Rate : 200.00 cc/min
Gas Cap Volume : 85.0 cc
Steam Vol. Inj. : 32690.0 cc (2.27 PV)

Net Oil Recovery : 26.8% **Solvent Recovery : 87.7%** **Final Oil Saturation : 66.1%**

Cyl. No.	Solvent Conc. (%)	Tot. Vol. Inj. (cc)	Cum. Vol. Inj.		HC Prod (cc)	Oil Prod. (cc)	Cum. Oil Rec.		Cum. Sol. Rec.		Oil-Steam Ratio	Inst Prod. WOR	Inst. HC Prod. % of Sample
			(cc)	(P.V.)			(cc)	(%OOIP)	(cc)	(%)			
1	64%	1000	1000	0.07	1000	360	360	2.8%	640	45.7%	0.0000	0.00	100.0%
2	63%	1005	2005	0.14	700	259	619	4.8%	1081	77.2%	0.0000	0.44	69.7%
3	25%	1500	3505	0.24	220	165	784	6.0%	1136	81.1%	0.1719	5.82	14.7%
4	12%	2140	5645	0.39	180	158	942	7.2%	1158	82.7%	0.0918	10.89	8.4%
5	8%	2085	7730	0.54	205	189	1131	8.7%	1174	83.9%	0.1090	9.17	9.8%
6	7%	1865	9595	0.67	180	167	1298	10.0%	1187	84.8%	0.1068	9.36	9.7%
7	5%	2090	11685	0.81	195	185	1483	11.4%	1197	85.5%	0.1029	9.72	9.3%
8	4%	1965	13650	0.95	205	197	1680	12.9%	1205	86.1%	0.1165	8.59	10.4%
9	3%	2055	15705	1.09	265	257	1937	14.9%	1213	86.6%	0.1480	6.75	12.9%
10	2%	1955	17660	1.23	295	289	2226	17.1%	1219	87.1%	0.1777	5.63	15.1%
11	2%	2035	19695	1.37	330	323	2549	19.6%	1226	87.6%	0.1935	5.17	16.2%
12	1%	2015	21710	1.51	225	223	2772	21.3%	1228	87.7%	0.1257	7.96	11.2%
13	0%	2105	23815	1.65	170	170	2942	22.6%	1228	87.7%	0.0879	11.38	8.1%
14	0%	2010	25825	1.79	135	135	3077	23.6%	1228	87.7%	0.0720	13.89	6.7%
15	0%	2095	27920	1.94	145	145	3222	24.8%	1228	87.7%	0.0744	13.45	6.9%
16	0%	2070	29990	2.08	90	90	3312	25.4%	1228	87.7%	0.0455	22.00	4.3%
17	0%	2060	32050	2.22	100	100	3412	26.2%	1228	87.7%	0.0510	19.60	4.9%
18	0%	2040	34090	2.37	80	80	3492	26.8%	1228	87.7%	0.0408	24.50	3.9%

Figure 6.66 :Run 55 Gas Injection Prior to Solvent–Steamflood
Cumulative Oil Recovery Vs. Pore Volumes Injected

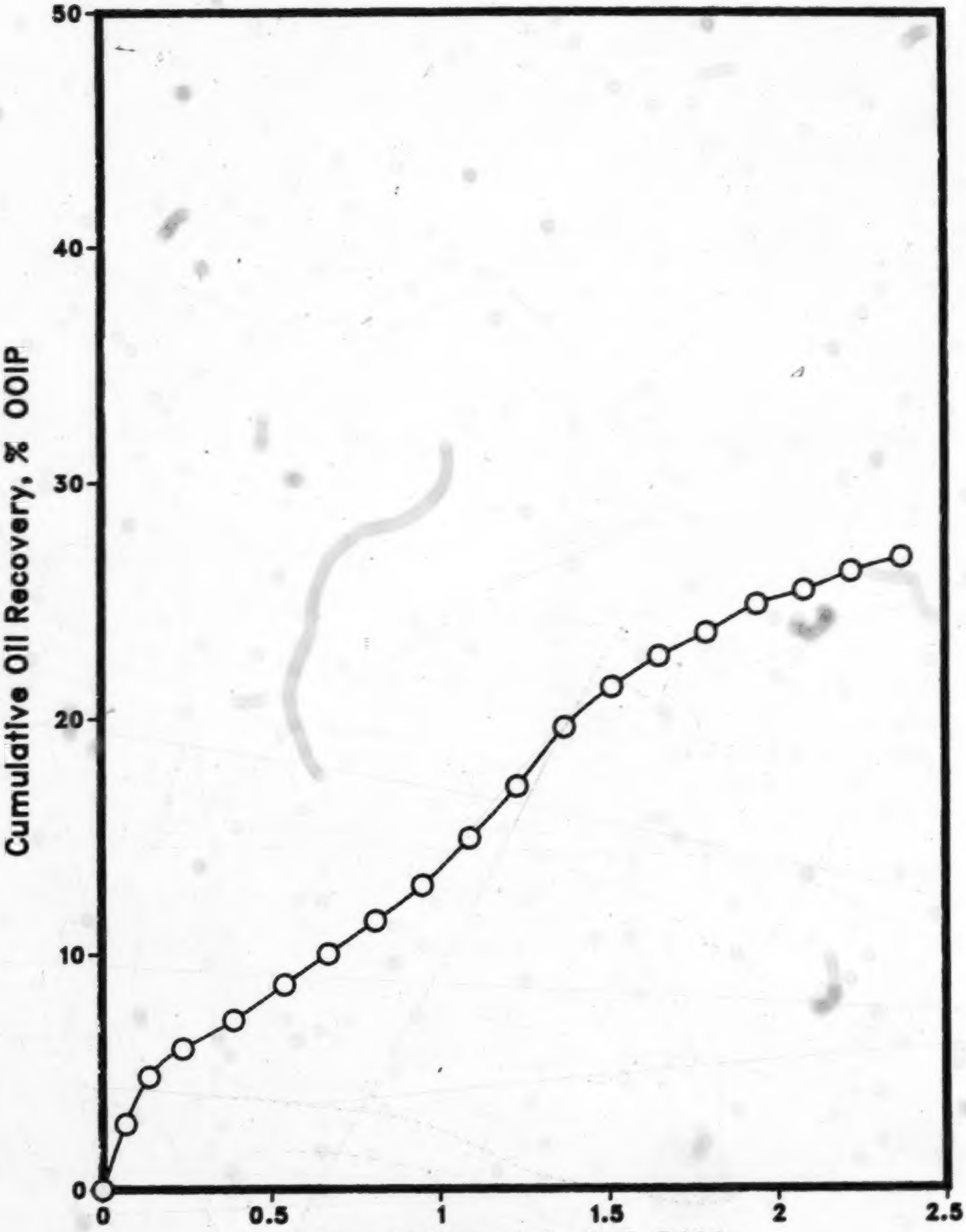

Figure 6.67 :Run 55 Gas Injection Prior to Solvent–Steamflood
Oleic Phase In Each Sample Vs. Cumulative Volume Injected

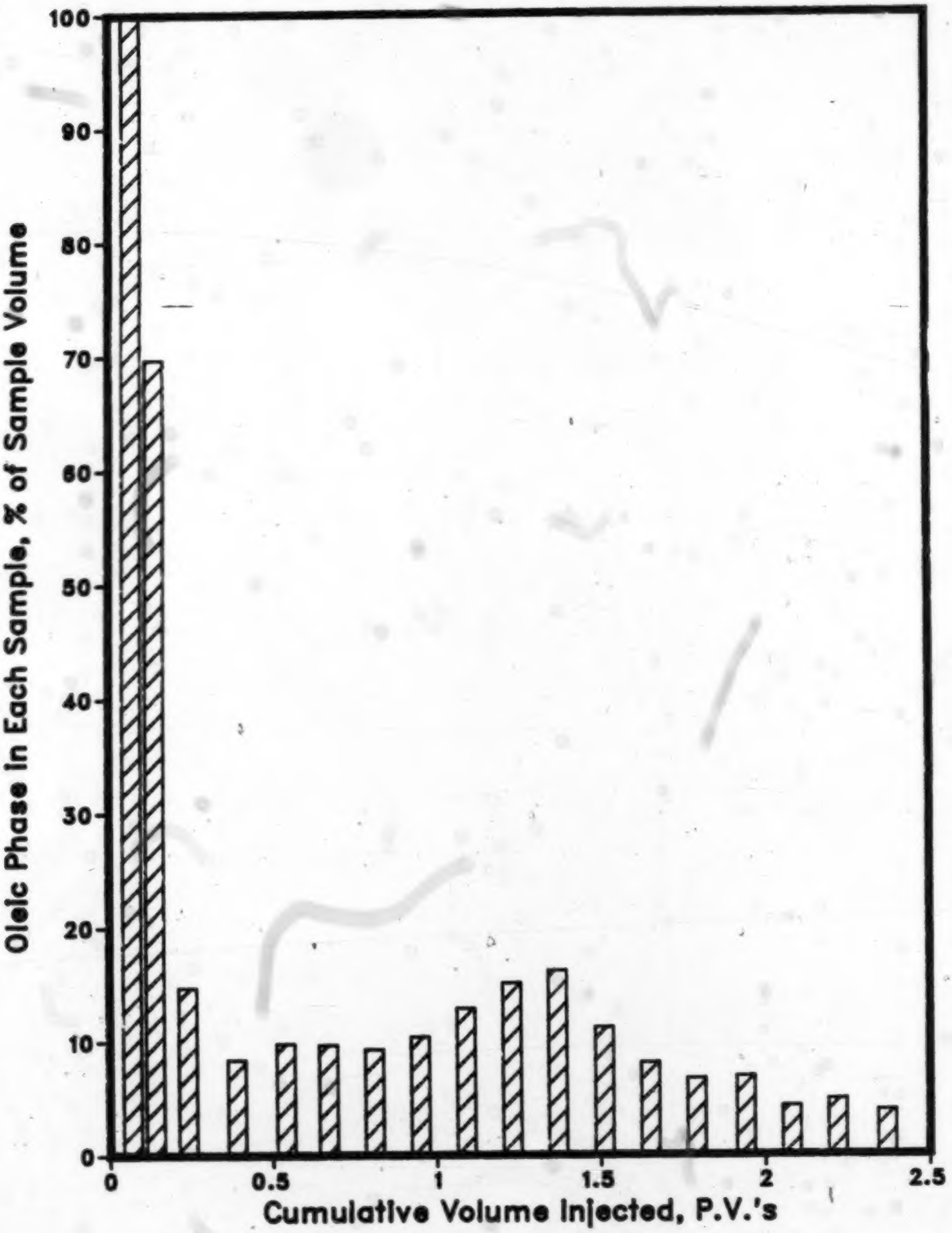

Figure 6.68 :Run 55 Gas Injection Prior to Solvent–Steamflood
Instantaneous Produced WOR Vs. Cumulative Volume Injected

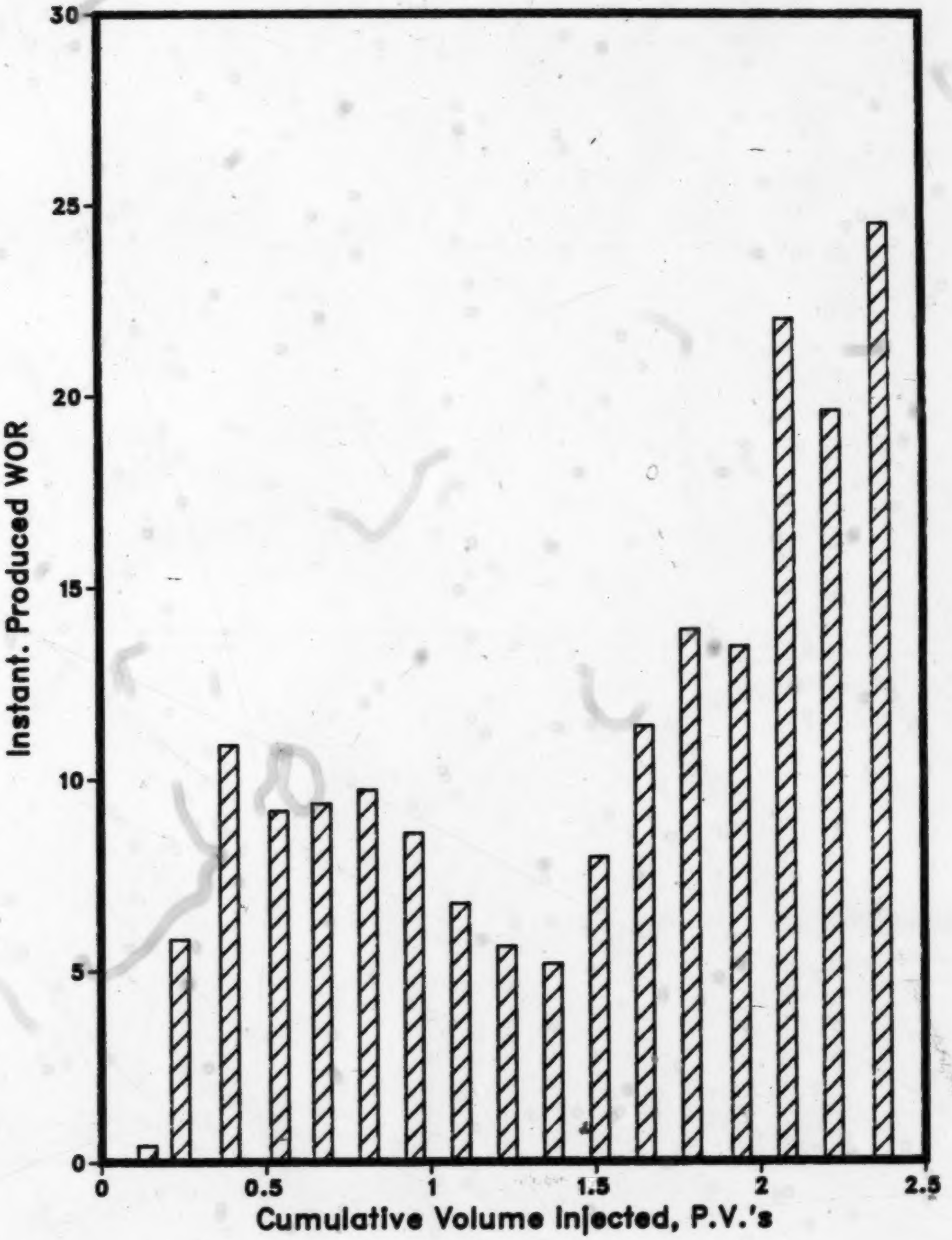

Figure 6.69 :Run 55 Gas Injection Prior to Solvent–Steamflood Instanteous Oil/Steam Ratio vs. Cumulative Oil Produced

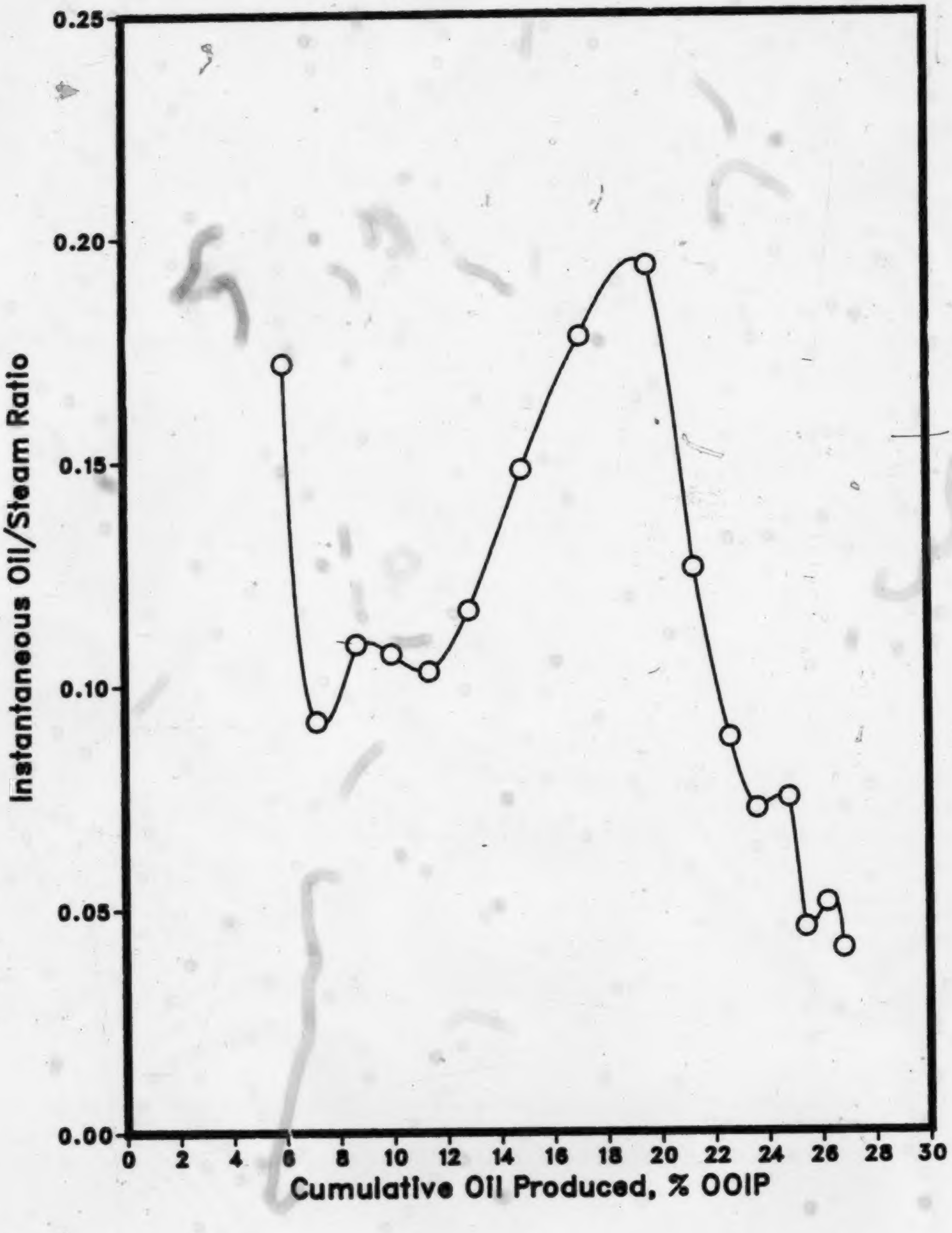

Table 6.18 : Run 56 Gas Injection Prior to Solvent-Steamflood of Homogeneous Model

HC Pore Volume : 13120.0 cc
Pore Volume : 14105.0 cc
Bulk Volume : 42005.0 cc
Porosity : 33.6%
Initial Oil Satn. : 93.0%
Initial H2O Satn. : 6.3%
Initial Gas Satn. : 0.6%
Solvent Vol. Inj. : 1400.0 cc

Type of Oil Used : Faxam-100
Initial Model Temperature : 3.00 C
Water Feed Flow Rate : 200.00 cc/min
Boiler Feed Flow Rate : 29.20 cc/min
Total Flow Rate of Steam : 229.20 cc/min
Solvent Flow Rate : 200.00 cc/min
Gas Cap Volume : 90.0 cc
Steam Vol. Inj. : 32845.0 cc (2.33 PV)

Net Oil Recovery : 27.0% **Solvent Recovery : 90.9%** **Final Oil Saturation : 67.9%**

Cyl. No.	Solvent Conc. (%)	Tot. Vol. Inj. (cc)	Cum. Vol. Inj.		HC Prod (cc)	Oil Prod. (cc)	Cum. Oil Rec.		Cum. Sol. Rec.		Oil-Steam Ratio	Inst Prod. WOR	Inst. HC Prod. % of Sample
			(cc)	(P.V.)			(cc)	(%OOIP)	(cc)	(%)			
1	66%	875	875	0.06	875	298	298	2.3%	577	41.2%	0.0000	0.00	100.0%
2	60%	1425	2300	0.16	700	280	578	4.4%	997	71.2%	0.0000	1.04	49.1%
3	53%	1475	3775	0.27	400	188	766	5.8%	1209	86.4%	0.3721	2.69	27.1%
4	10%	1920	5695	0.40	275	248	1014	7.7%	1236	88.3%	0.1672	5.98	14.3%
5	4%	2085	7780	0.55	580	557	1571	12.0%	1259	89.9%	0.3854	2.59	27.8%
6	2%	1885	9665	0.69	350	343	1914	14.6%	1266	90.4%	0.2280	4.39	18.6%
7	1%	2075	11740	0.83	295	292	2206	16.8%	1269	90.6%	0.1657	6.03	14.2%
8	1%	2105	13845	0.98	180	178	2384	18.2%	1271	90.8%	0.0935	10.69	8.6%
9	1%	2165	16010	1.14	150	149	2533	19.3%	1272	90.9%	0.0744	13.43	6.9%
10	0%	2000	18010	1.28	160	160	2693	20.5%	1272	90.9%	0.0870	11.50	8.0%
11	0%	2065	20075	1.42	145	145	2838	21.6%	1272	90.9%	0.0755	13.24	7.0%
12	0%	1860	21935	1.56	110	110	2948	22.5%	1272	90.9%	0.0629	15.91	5.9%
13	0%	2020	23955	1.70	140	140	3088	23.5%	1272	90.9%	0.0745	13.43	6.9%
14	0%	1920	25875	1.83	120	120	3208	24.5%	1272	90.9%	0.0667	15.00	6.3%
15	0%	2110	27985	1.98	95	95	3303	25.2%	1272	90.9%	0.0471	21.21	4.5%
16	0%	2065	30050	2.13	80	80	3383	25.8%	1272	90.9%	0.0403	24.81	3.9%
17	0%	2160	32210	2.28	90	90	3473	26.5%	1272	90.9%	0.0435	23.00	4.2%
18	0%	2035	34245	2.43	75	75	3548	27.0%	1272	90.9%	0.0383	26.13	3.7%

Figure 6.70 :Run 56 Gas Injection Prior to Solvent–Steamflood Cumulative Oil Recovery Vs. Pore Volumes Injected

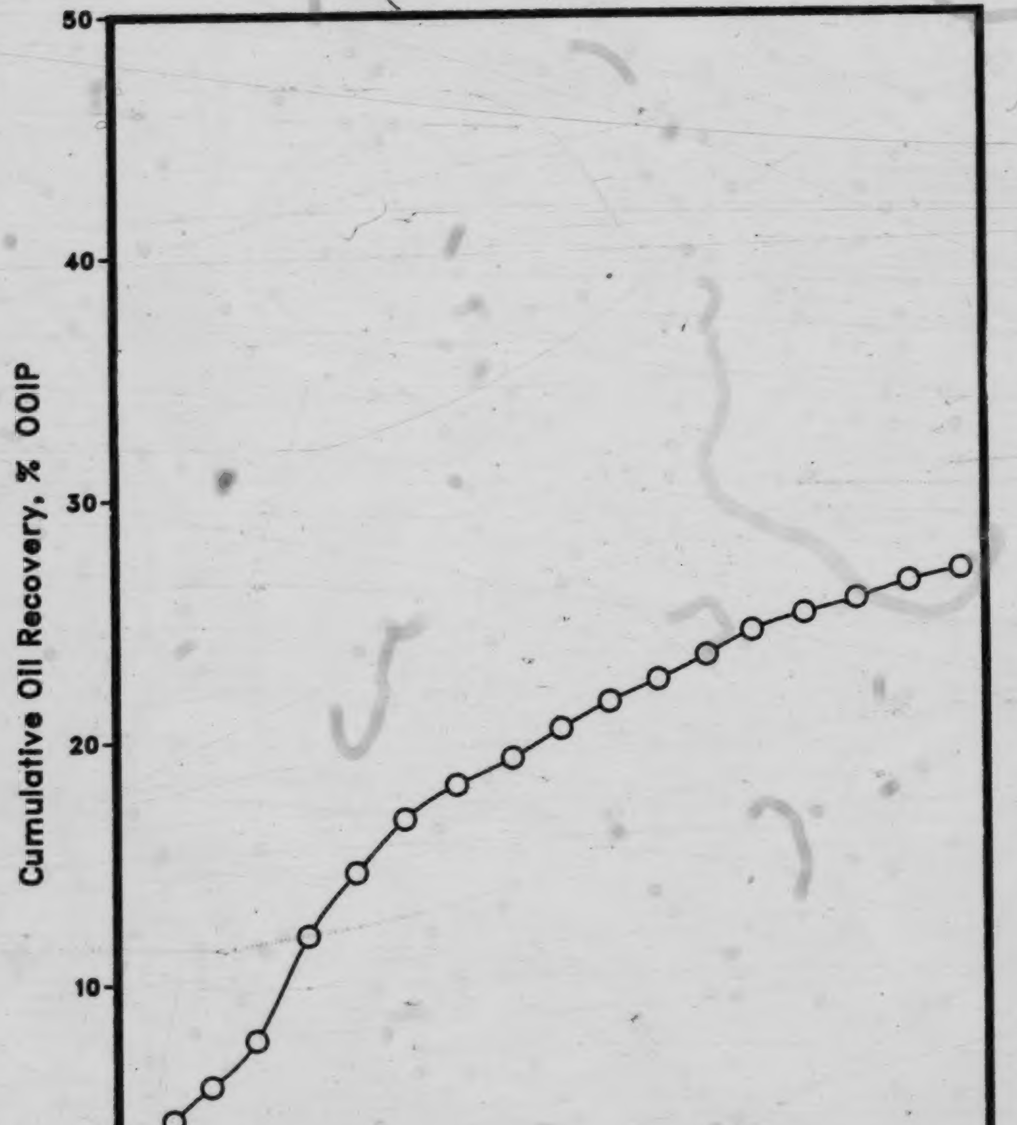

Figure 6.71 :Run 56 Gas Injection Prior to Solvent-Steamflood Oleic Phase in Each Sample Vs. Cumulative Volume Injected

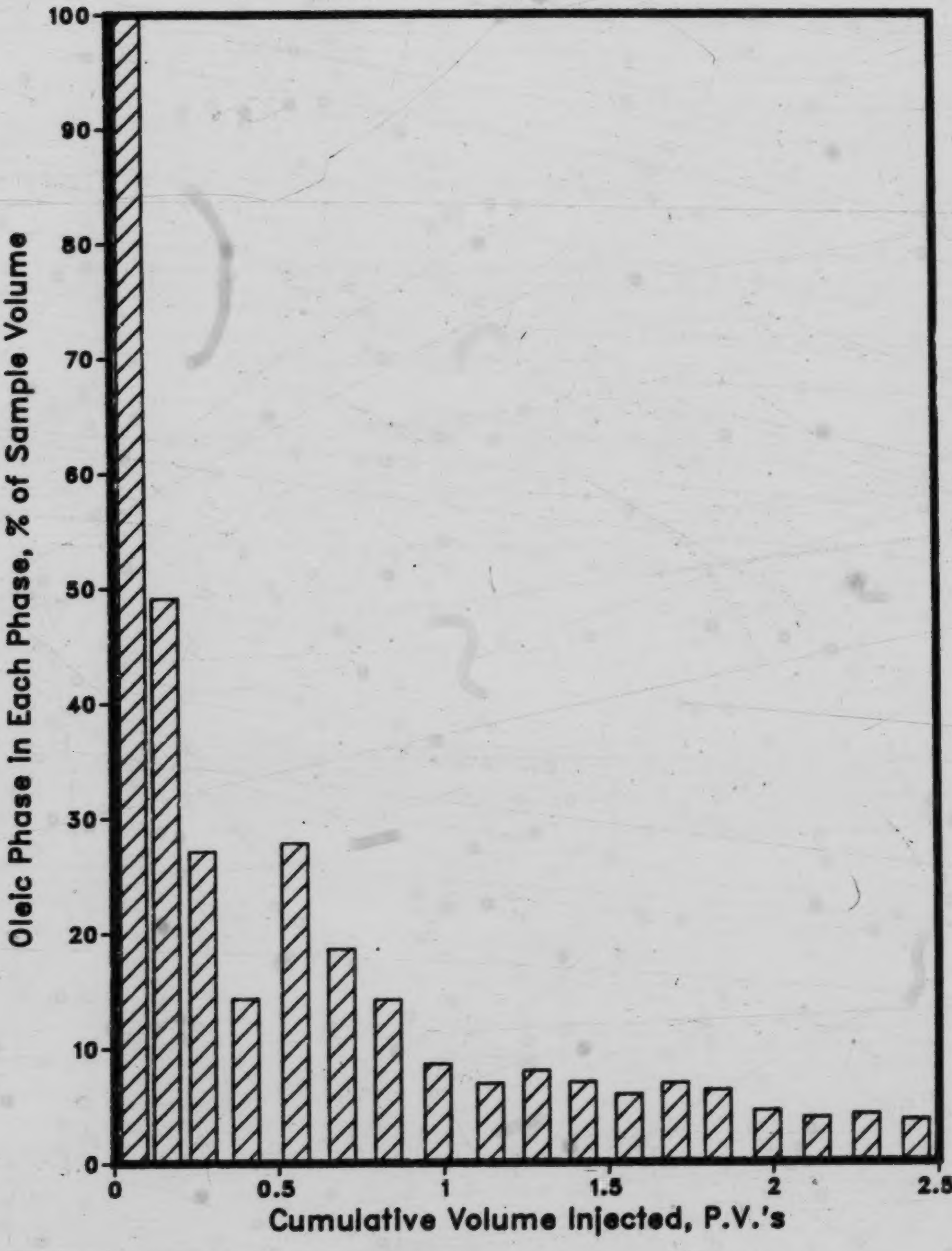

Figure 6.72 :Run 56 Gas Injection Prior to Solvent–Steamflood Instantaneous Produced WOR Vs. Cumulative Volume Injected

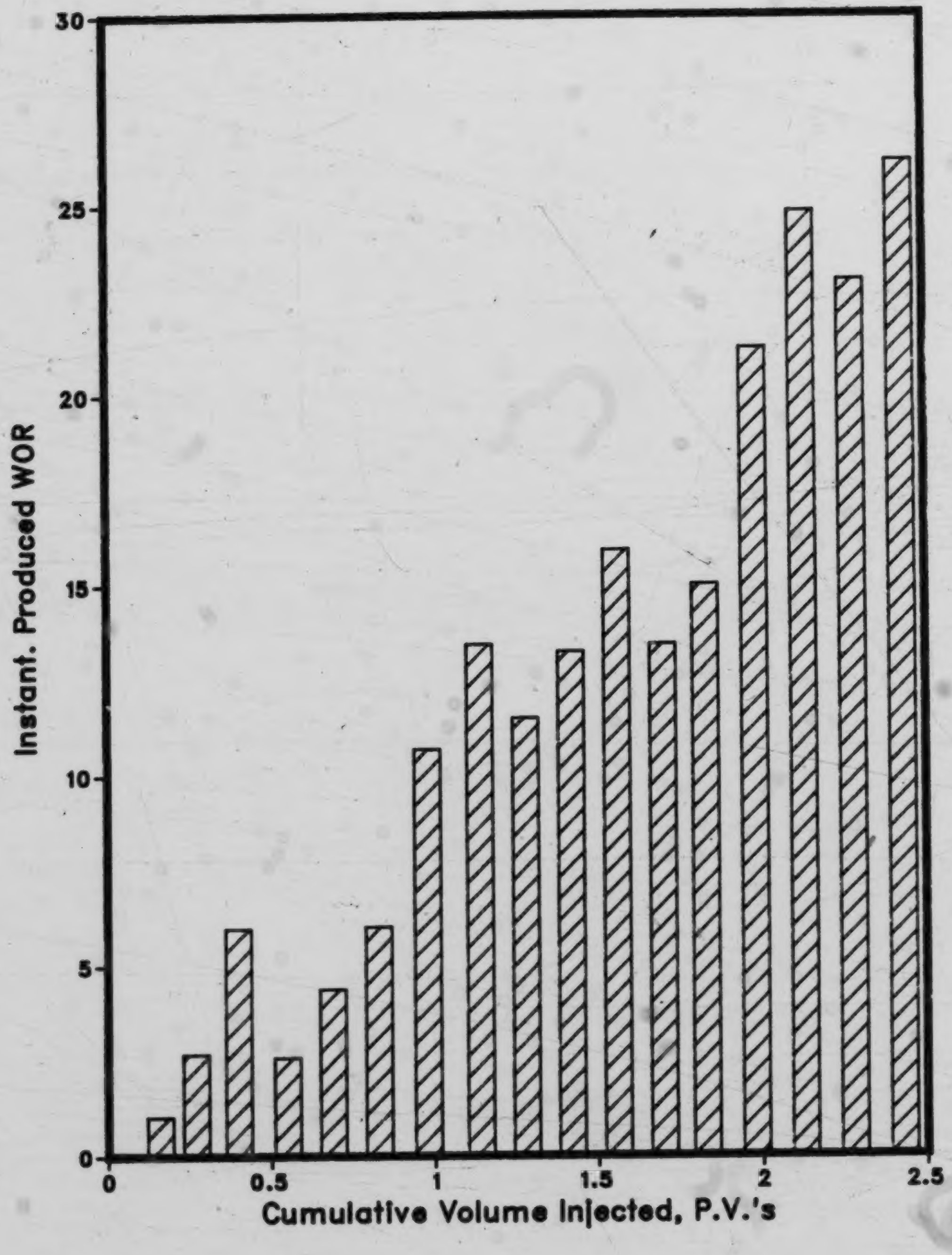

Figure 6.73 :Run 56 Gas Injection Prior to Solvent-Steamflood Instanteous Oil/Steam Ratio vs. Cumulative Oil Produced

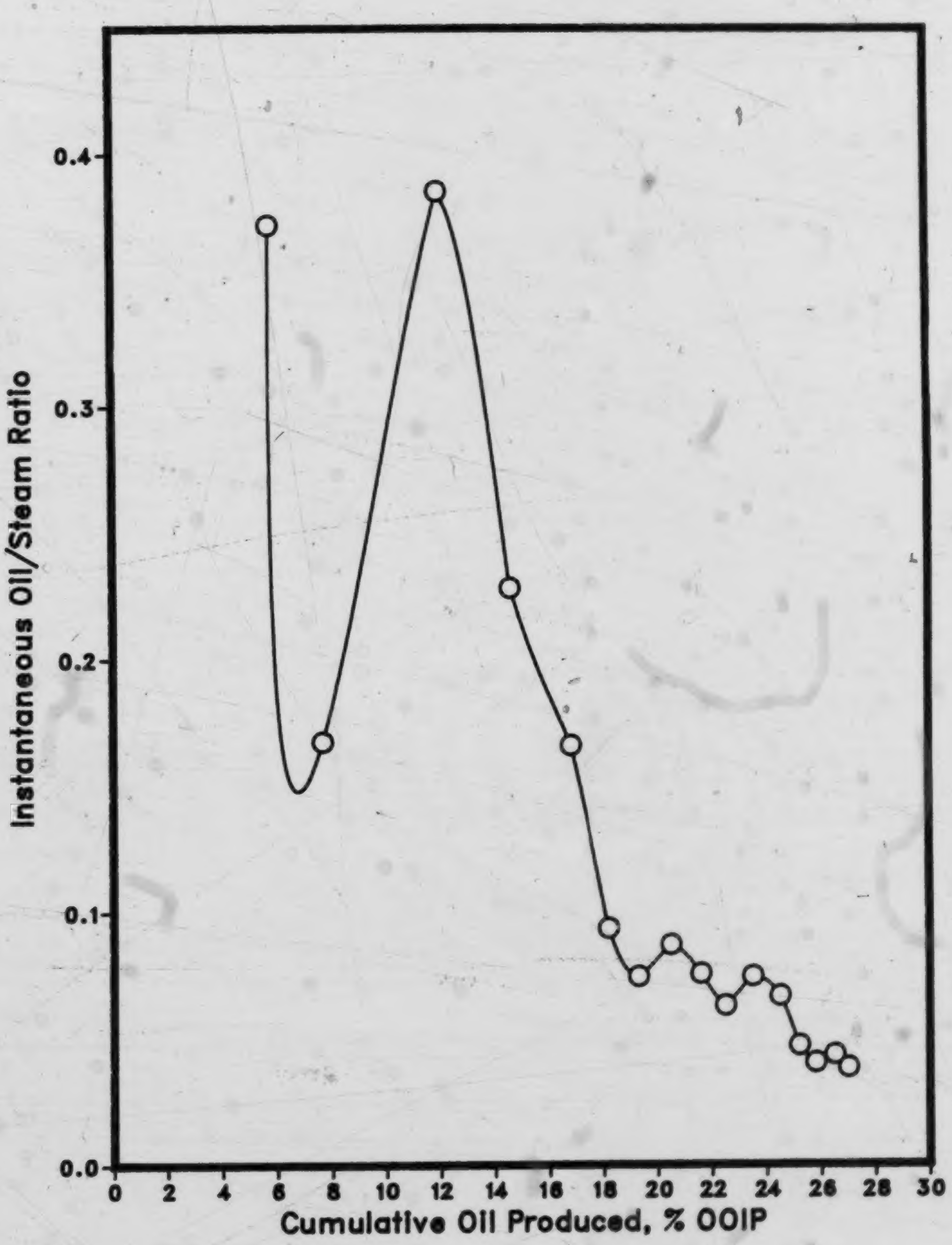

performed in a homogeneous model were slightly better than the oil recoveries achieved by Runs 55 and 56. The slight drop in oil recovery was probably due the gas cap partially diverting the steam over top of the oil and resulting in less oil being contacted by the solvent and steam. Solvent recoveries for Runs 55 (87.7%) and 56 (90.9%) were quite favourable due to the solvent flowing to the production well over top of the oil in the gas channel. The larger solvent recoveries were also due to the high initial oil saturations in both experiments. The reason for this solvent recovery behaviour was discussed earlier in the chapter.

During Runs 55 and 56 the solvent and steam tended to partially override the oil zone through the lower resistance "gas cap". Therefore the solvent and steam could not penetrate the oil zone as effectively as when a gas cap was not present (Runs 44, 45 & 46). This resulted in a slighty lower oil recovery for the two experiments as compared to Runs 44, 45 and 46. It was noted from the experimental results of Runs 55 and 56 that the presence of a gas cap slightly decreased the overall oil recovery. Figure 6.74 provides a comparison of the recovery curves for a solvent-steamflood of a homogeneous model (Run 45) and a solvent-steamflood preceding gas injection in a homogeneous model (Run 56). An examination of Figure 6.74 shows little difference between the two experiments except that the oil recovery for Run 45 (30.0% OOIP) was slightly higher due to a more stable displacement by the steam more thoroughly penetrating the oil zone through the channels formed by the viscous fingering of the injected solvent. The recovery for Run 56 (27.0% OOIP) was a bit less since the solvent and steam had a tendency to override the oil zone into the gas channel resulting in less solvent and oil penetrating, mobilizing and displacing the in-place oil. Run 45 was able to more effectively use the heating characteristics of the steam to recover the oil in the model.

This study deals with bottom water reservoirs, and therefore the presence of a gas cap would aid in diverting the injected solvent and steam away from the underlying bottom water layer. From the results of the two experiments it is concluded that the injection of a

Figure 6.74 :Comparison of Solvent-Steamflood Run 45 & Gas Injection Prior to Solvent-Steamflood Run 56 Recoveries Performed in a Homogeneous Model

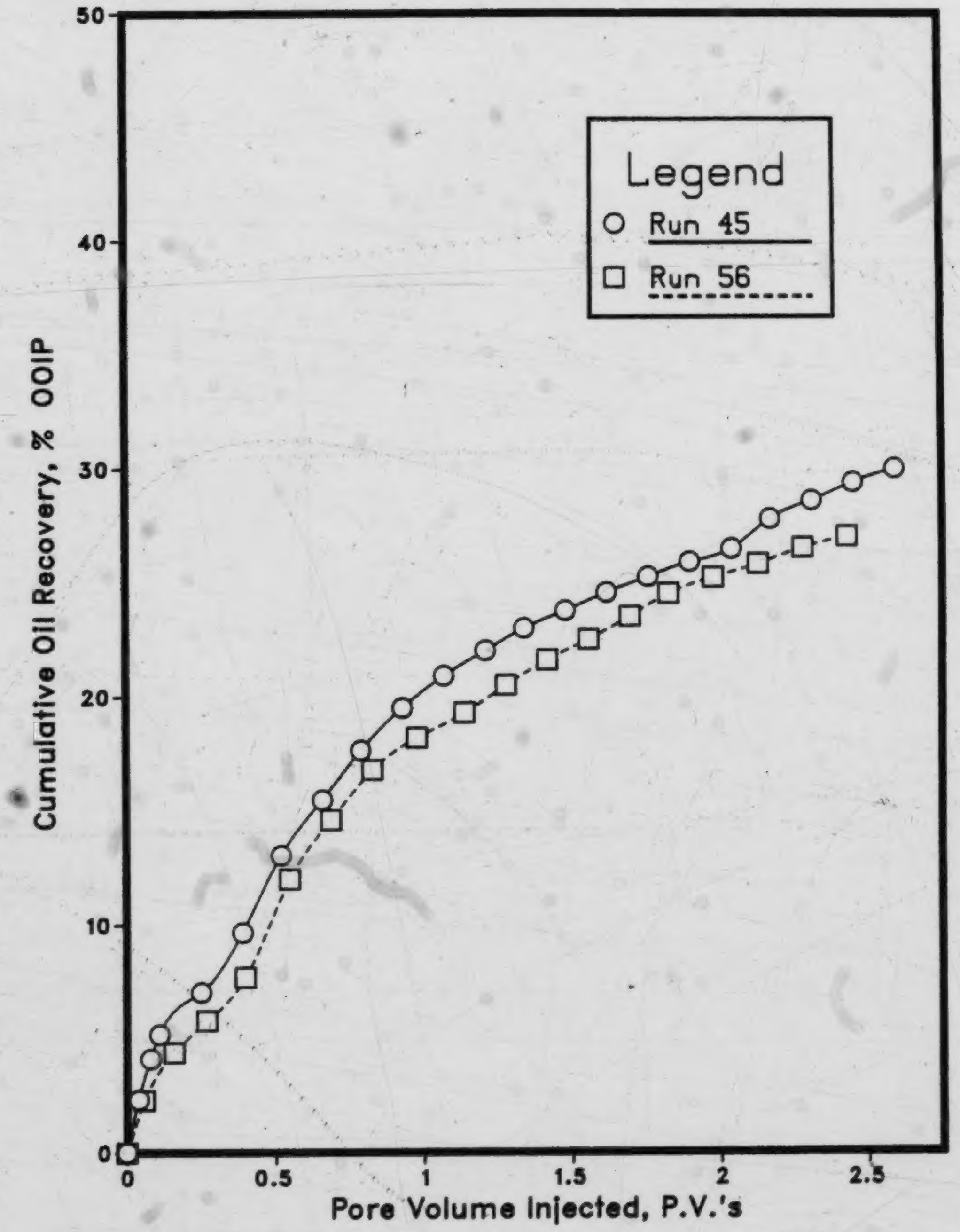

small amount of an inert gas prior to a solvent-steamflood would create a flow channel away from the bottom water zone and thus minimize the heat scavenging nature of the underlying bottom water layer. Also a comparison of Runs 55 and 56 to Runs 44, 45 and 46 revealed that the production response of the gas injection process was slightly lower than that for the straight solvent-steamflood process. However, in a reservoir where injectivity is a problem, the injectivity improvement obtained by gas injection may justify the small decrease in oil recovery response.

Gas Injection Prior to Solvent and Steam Injection with Bottom Water

Runs 58, 59 and 62 involved performing a solvent-steamflood on a bottom water/gas cap reservoir. Results of each experiment are given in Tables 6.19, 6.20 and 6.21, respectively. These experiments were similar to Runs 49, 50, 51, 53 and 54 except that Runs 58, 59 and 62 incorporated a gas cap in the low pressure model. The bottom water thicknesses for Runs 58, 59 and 62 were 9.8%, 13.6% and 12.0% of the gross model thickness, respectively, and the initial gas saturations were 0.6% (Run 58), 0.6% (Run 59) and 0.3% (Run 62).

The recovery curves for Runs 58 (Figure 6.75), 59 (Figure 6.79) and 62 (Figure 6.83) all indicated that the presence of bottom water and a gas cap affected the total oil recovery yielded by the solvent-steamflood process. The recovery curve for Run 58 (Figure 6.75) showed a relatively lower oil recovery (18.2%) than was obtained in Runs 59 (24.7%)and 62 (20.0%). The lower recovery may have been due to the slightly larger gas cap of Run 58 which caused the solvent and steam to be further diverted away from both the bottom water and oil zone. This resulted in less solvent and steam penetrating the oil region and therefore less oil was mobilized and subsequently recovered. Therefore the gas saturation should be optimized to increase oil recovery. Figure 6.79 illustrates that Run 59 had the highest overall oil recovery (24.7%) of the three experiments. Run 59 had a slightly smaller gas cap than Run 58 which may have caused more steam to penetrate the oil zone resulting in a better oil recovery. The recovery curve for Run 62 (Figure 6.83) indicates that Run 62 also had a higher recovery (20.0%) than Run 58. As mentioned before this higher recovery was probably caused by the slightly smaller gas cap contained in Run 62, and therefore a greater invasion of the oil zone by the injected solvent and steam resulted.

The bar plots of volume as a percentage of oleic phase in each sample collected injected and instantaneous produced WOR versus cumulative volume injected for Runs 58 (Fig. 6.76 & 6.77), 59 (Fig. 6.80 & 6.81) and 62 (Fig. 6.84 & 6.85) suggest that the introduction of a "gas cap" in the model was a dominating factor in the overall recovery for all the experiments. Observation of all of these plots indicates that breakthrough during the experiments occurred very early. Early breakthrough was caused by the very unstable displacement of oil by the solvent and steam. The lack of stability was a result of the presence of bottom water and gas cap which enabled the injected solvent and steam to flow above and below the oil layer. Once breakthrough had occurred, the instantaneous hydrocarbon produced for Figures 6.76, 6.80 and 6.84 dropped to relatively small values. Comparison of Figures 6.76, 6.80 and 6.84 with the corresponding plots of Runs 49, 50, 51, 53 and 54 (solvent-steamflood in a bottom water model) indicates that breakthrough occurred sooner in experiments 58, 59 and 62 which suggests that the gas cap was detrimental to the stability of the displacement. In these three runs, the solvent and steam were diverted away from the oil to a greater extent by the bottom water and gas cap than in the case of only bottom water.

The plots of instantaneous oil/steam ratio versus cumulative oil produced are displayed in Figures 6.78 (Run 58), 6.82 (Run 59) and 6.86 (Run 62). Overall the oil/steam ratios were slightly higher for Runs 58, 59 and 62 as compared to Runs 49, 50, 51, 53 and 54 which were experiments involving the solvent-steamflood of a bottom water model.

Table 6.19 : Run 58 Gas Injection Prior to Solvent-Steamflood of Bottom Water Model

HC Pore Volume : 12920.0 cc
Pore Volume : 14955.0 cc
Bulk Volume : 42005.0 cc
Porosity : 35.6%
Initial Oil Satn. : 86.4%
Initial H2O Satn. : 13.0%
Initial Gas Satn. : 0.6%
Solvent Vol. Inj. : 1400.0 cc

Type of Oil Used : Faxam-100
Initial Model Temperature 3.00 C
Water Feed Flow Rate : 200.00 cc/min
Boiler Feed Flow Rate : 29.20 cc/min
Total Flow Rate of Steam 229.20 cc/min
Solvent Flow Rate : 200.00 cc/min
Gas Cap Volume : 90.0 cc
Steam Vol. Inj. : 32515.0 cc (2.17 PV)
Bottom Water Layer Thickness : 9.8% (% Gross Thickness)

Net Oil Recovery : 18.2% **Solvent Recovery : 88.7%** **Final Oil Saturation : 70.7%**

Cyl. No.	Solvent Conc. (%)	Tot. Vol. Inj. (cc)	Cum. Vol. Inj. (cc)	Cum. Vol. Inj. (P.V.)	HC Prod. (cc)	Oil Prod. (cc)	Cum. Oil Rec. (cc)	Cum. Oil Rec. (%OOIP)	Cum. Sol. Rec. (cc)	Cum. Sol. Rec. (%)	Oil-Steam Ratio	Inst Prod. WOR	Inst. HC Prod. % of Sample
1	61%	875	875	0.06	465	181	181	1.4%	284	20.3%	0.0000	0.88	53.1%
2	74%	1195	2070	0.14	985	256	437	3.4%	1013	72.4%	0.0000	0.21	82.4%
3	54%	1340	3410	0.23	230	106	543	4.2%	1137	81.2%	0.2072	4.83	17.2%
4	28%	1855	5265	0.35	195	140	683	5.3%	1192	85.1%	0.1175	8.51	10.5%
5	17%	2015	7280	0.49	100	83	766	5.9%	1209	86.4%	0.0522	19.15	5.0%
6	13%	1940	9220	0.62	70	61	827	6.4%	1218	87.0%	0.0374	26.71	3.6%
7	5%	2065	11285	0.75	180	171	998	7.7%	1227	87.6%	0.0955	10.47	8.7%
8	4%	1975	13260	0.89	145	139	1137	8.8%	1233	88.1%	0.0792	12.62	7.3%
9	3%	2185	15445	1.03	135	131	1268	9.8%	1237	88.4%	0.0659	15.19	6.2%
10	2%	1915	17360	1.16	135	132	1400	10.8%	1240	88.6%	0.0758	13.19	7.0%
11	1%	2055	19415	1.30	190	188	1588	12.3%	1242	88.7%	0.1019	9.82	9.2%
12	0%	2035	21450	1.43	160	160	1748	13.5%	1242	88.7%	0.0853	11.72	7.9%
13	0%	2125	23575	1.58	140	140	1888	14.6%	1242	88.7%	0.0705	14.18	6.6%
14	0%	2075	25650	1.72	105	105	1993	15.4%	1242	88.7%	0.0533	18.76	5.1%
15	0%	2200	27850	1.86	75	75	2068	16.0%	1242	88.7%	0.0353	28.33	3.4%
16	0%	1945	29795	1.99	90	90	2158	16.7%	1242	88.7%	0.0485	20.61	4.6%
17	0%	2140	31935	2.14	115	115	2273	17.6%	1242	88.7%	0.0568	17.61	5.4%
18	0%	1980	33915	2.27	80	80	2353	18.2%	1242	88.7%	0.0421	23.75	4.0%

Figure 6.75 :Run 58 Gas Injection Prior to Solvent–Steamflood Cumulative Oil Recovery Vs. Pore Volumes Injected

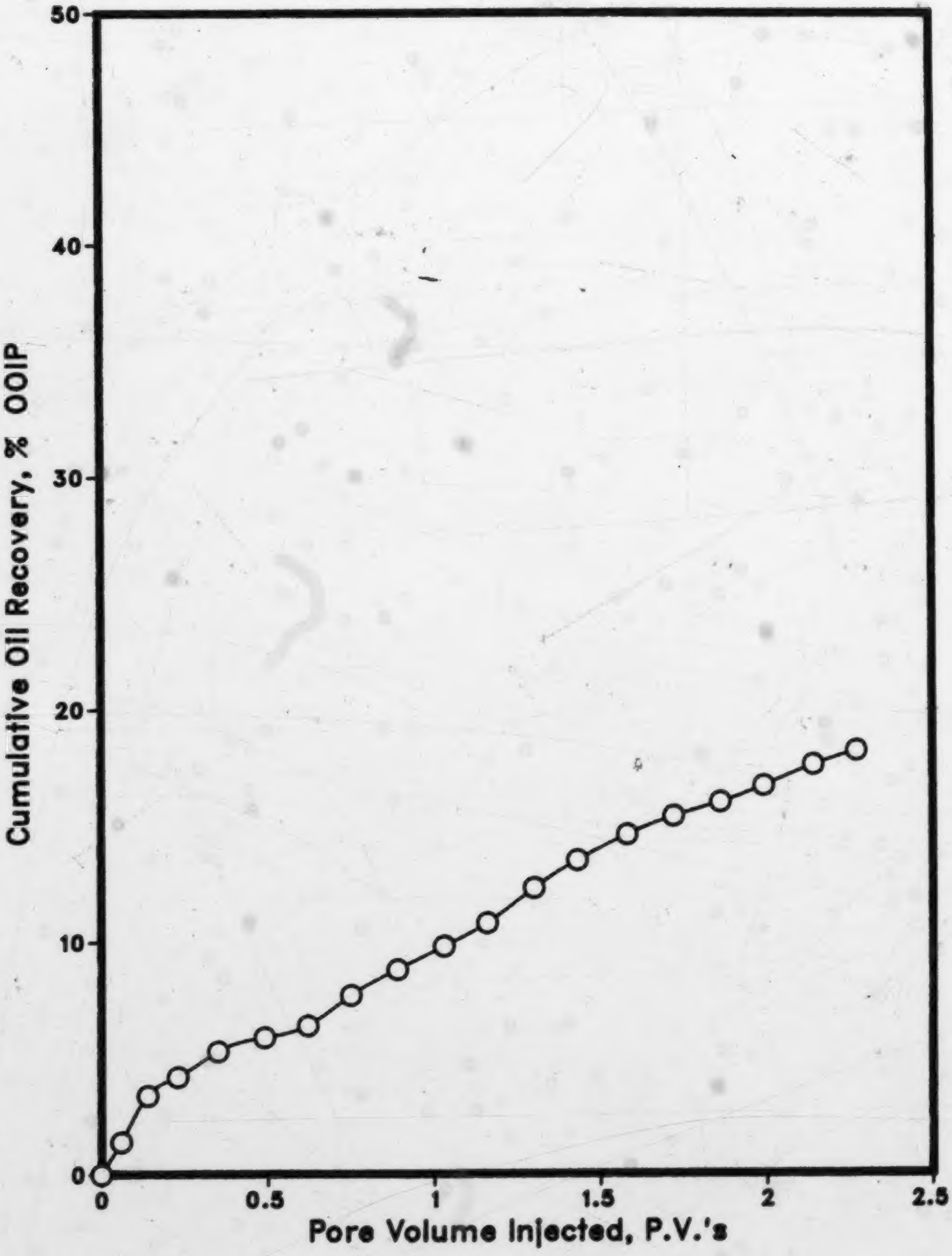

Figure 6.76 \:Run 58 Gas Injection Prior to Solvent–Steamflood
Oleic Phase in Each Sample Vs. Cumulative Volume Injected

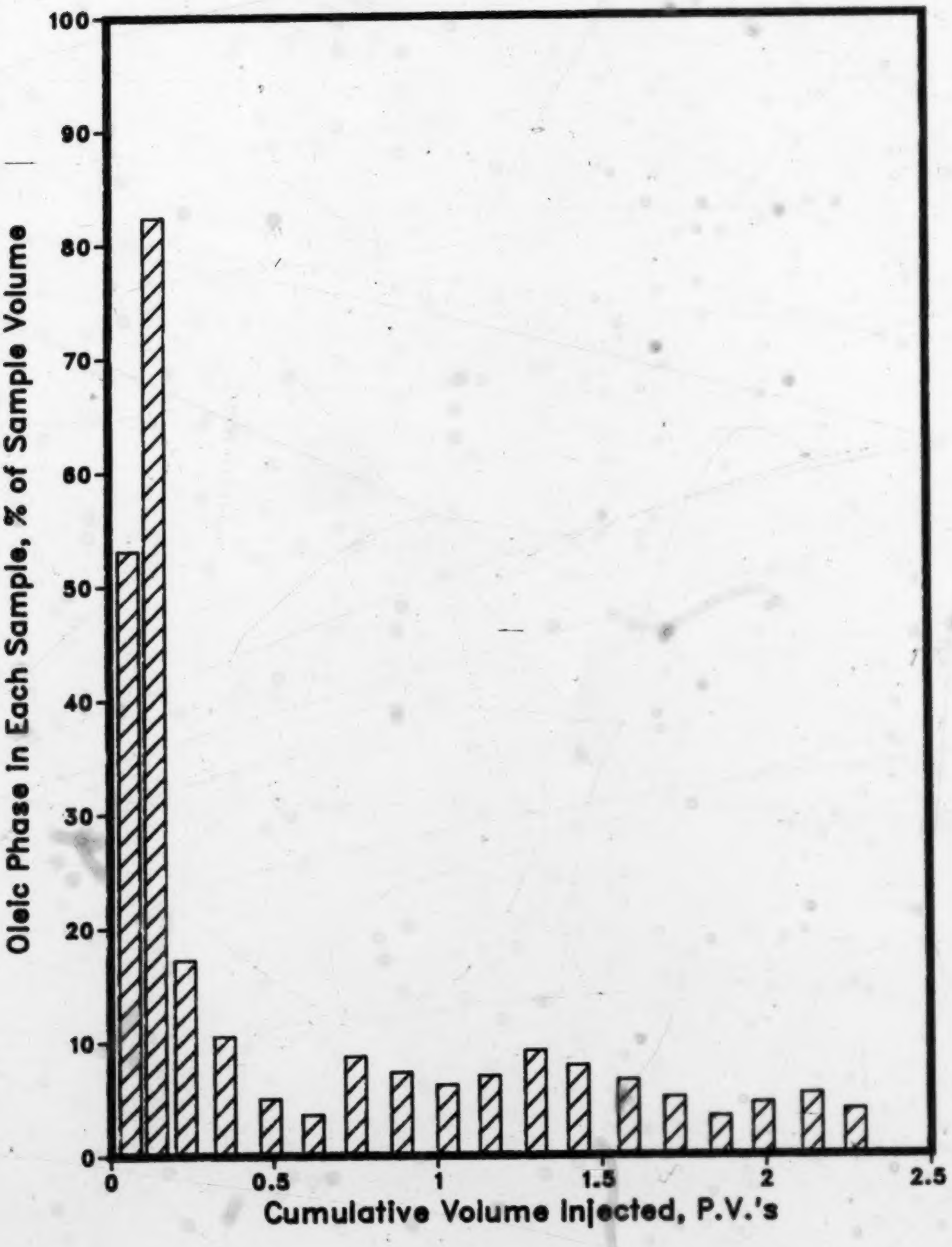

Figure 6.77 :Run 58 Gas Injection Prior to Solvent–Steamflood Instantaneous Produced WOR Vs. Cumulative Volume Injected

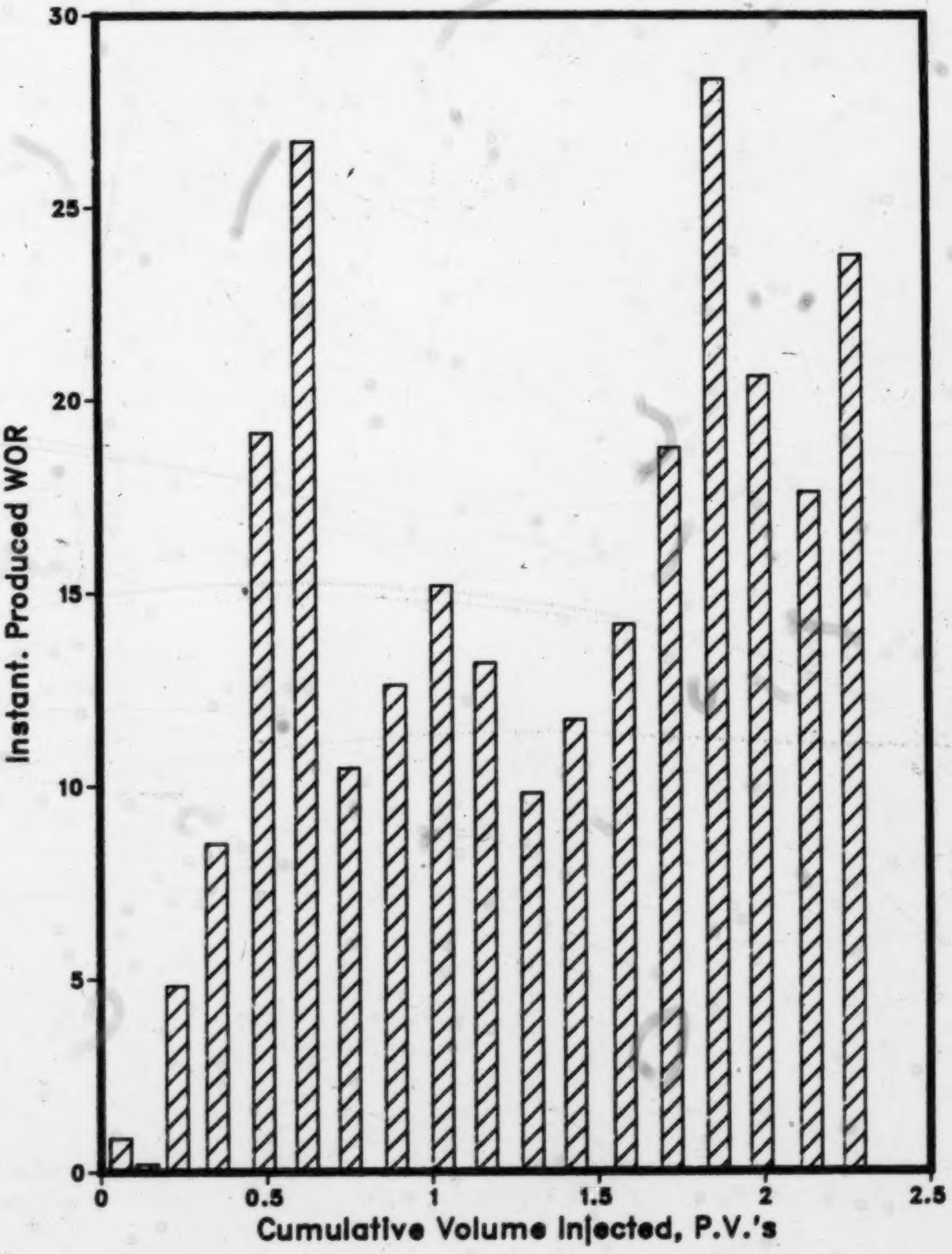

Figure 6.78 :Run 58 Gas Injection Prior to Solvent–Steamflood Instanteous Oil/Steam Ratio vs. Cumulative Oil Produced

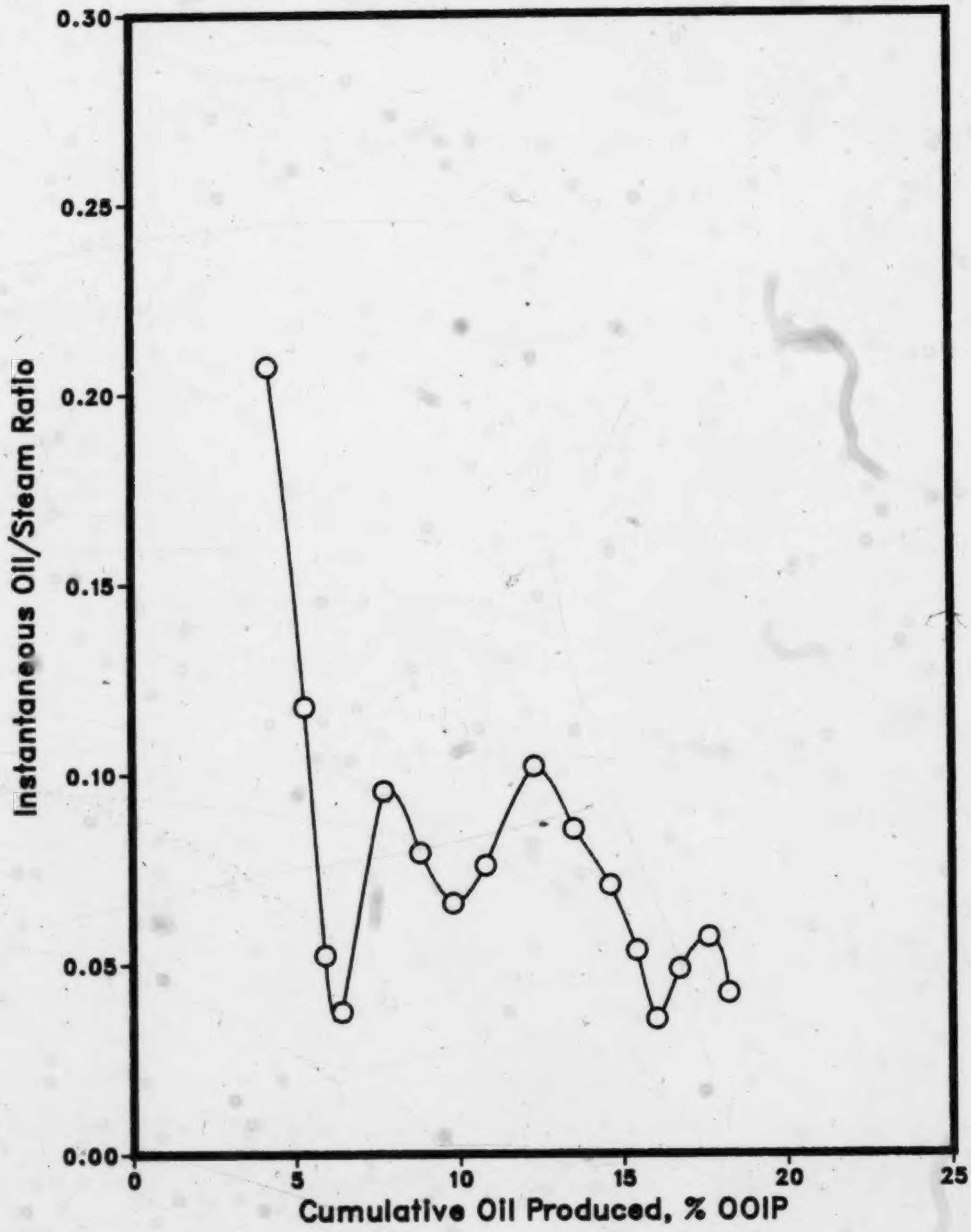

Table 6.20 : Run 59 Gas Injection Prior to Solvent-Steamflood of Bottom Water Model

HC Pore Volume : 12805.0 cc
Pore Volume : 15005.0 cc
Bulk Volume : 42005.0 cc
Porosity : 35.7%
Initial Oil Satn. : 85.3%
Initial H2O Satn. : 14.1%
Initial Gas Satn. : 0.6%
Solvent Vol. Inj. : 1400.0 cc

Type of Oil Used : Faxam-100
Initial Model Temperature : 3.00 C
Water Feed Flow Rate : 200.00 cc/min
Boiler Feed Flow Rate : 29.20 cc/min
Total Flow Rate of Steam : 229.20 cc/min
Solvent Flow Rate : 200.00 cc/min
Gas Cap Volume : 85.0 cc
Steam Vol. Inj. : 33070.0 cc (2.20 PV)
Bottom Water Layer Thickness : 13.6% (% Gross Thickness)

Net Oil Recovery : 24.7% **Solvent Recovery : 96.5%** **Final Oil Saturation : 64.2%**

Cyl. No.	Solvent Conc. (%)	Tot. Vol. Inj. (cc)	Cum. Vol. Inj.		HC Prod. (cc)	Oil Prod. (cc)	Cum. Oil Rec.		Cum. Sol. Rec.		Oil-Steam Ratio	Inst Prod. WOR	Inst. HC Prod. % of Sample
			(cc)	(P.V.)			(cc)	(%OOIP)	(cc)	(%)			
1	68%	1375	1375	0.09	1305	418	418	3.3%	887	63.4%	0.0000	0.05	94.9%
2	62%	1425	2800	0.19	575	219	637	5.0%	1243	88.8%	0.0000	1.48	40.4%
3	16%	1580	4380	0.29	390	328	965	7.5%	1305	93.2%	0.3277	3.05	24.7%
4	7%	2040	6420	0.43	205	191	1156	9.0%	1319	94.2%	0.1117	8.95	10.0%
5	5%	1860	8280	0.55	180	171	1327	10.4%	1328	94.9%	0.1071	9.33	9.7%
6	3%	2015	10295	0.69	190	184	1511	11.8%	1334	95.3%	0.1041	9.61	9.4%
7	3%	1930	12225	0.81	175	170	1681	13.1%	1339	95.6%	0.0997	10.03	9.1%
8	2%	2020	14245	0.95	180	176	1857	14.5%	1343	95.9%	0.0978	10.22	8.9%
9	2%	1950	16195	1.08	170	167	2024	15.8%	1346	96.1%	0.0955	10.47	8.7%
10	2%	2055	18250	1.22	155	152	2176	17.0%	1349	96.4%	0.0816	12.26	7.5%
11	1%	2010	20260	1.35	135	134	2310	18.0%	1350	96.4%	0.0720	13.89	6.7%
12	1%	2020	22280	1.48	135	134	2444	19.1%	1351	96.5%	0.0716	13.96	6.7%
13	0%	1970	24250	1.62	130	130	2574	20.1%	1351	96.5%	0.0707	14.15	6.6%
14	0%	2145	26395	1.76	130	130	2704	21.1%	1351	96.5%	0.0645	15.50	6.1%
15	0%	1970	28365	1.89	110	110	2814	22.0%	1351	96.5%	0.0591	16.91	5.6%
16	0%	2035	30400	2.03	130	130	2944	23.0%	1351	96.5%	0.0682	14.65	6.4%
17	0%	1950	32350	2.16	120	120	3064	23.9%	1351	96.5%	0.0656	15.25	6.2%
18	0%	2120	34470	2.30	105	105	3169	24.7%	1351	96.5%	0.0521	19.19	5.0%

Figure 6.79 :Run 59 Gas Injection Prior to Solvent-Steamflood Cumulative Oil Recovery Vs. Pore Volumes Injected

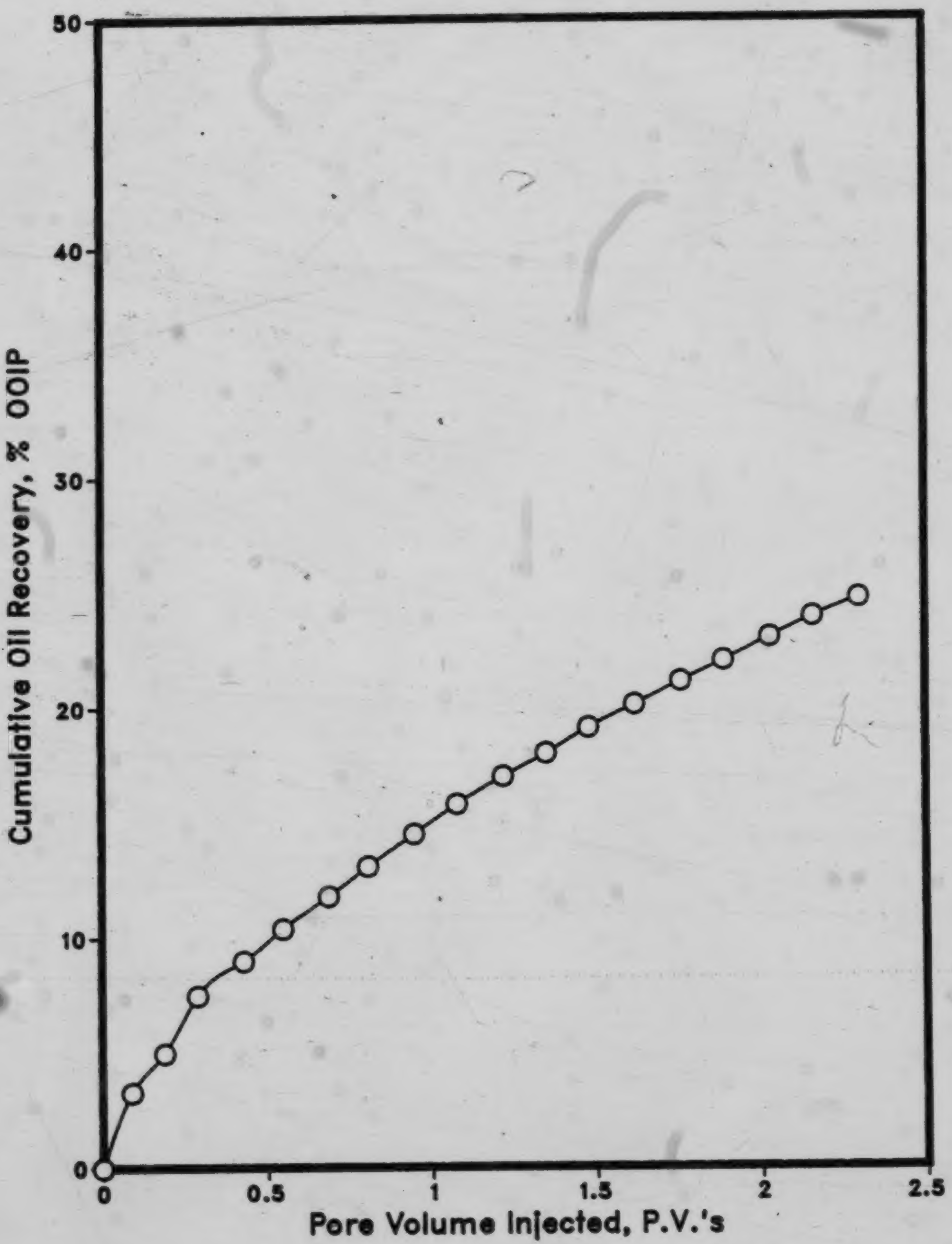

Figure 6.80 :Run 59 Gas Injection Prior to Solvent–Steamflood Oleic Phase in Each Sample Vs. Cumulative Volume Injected

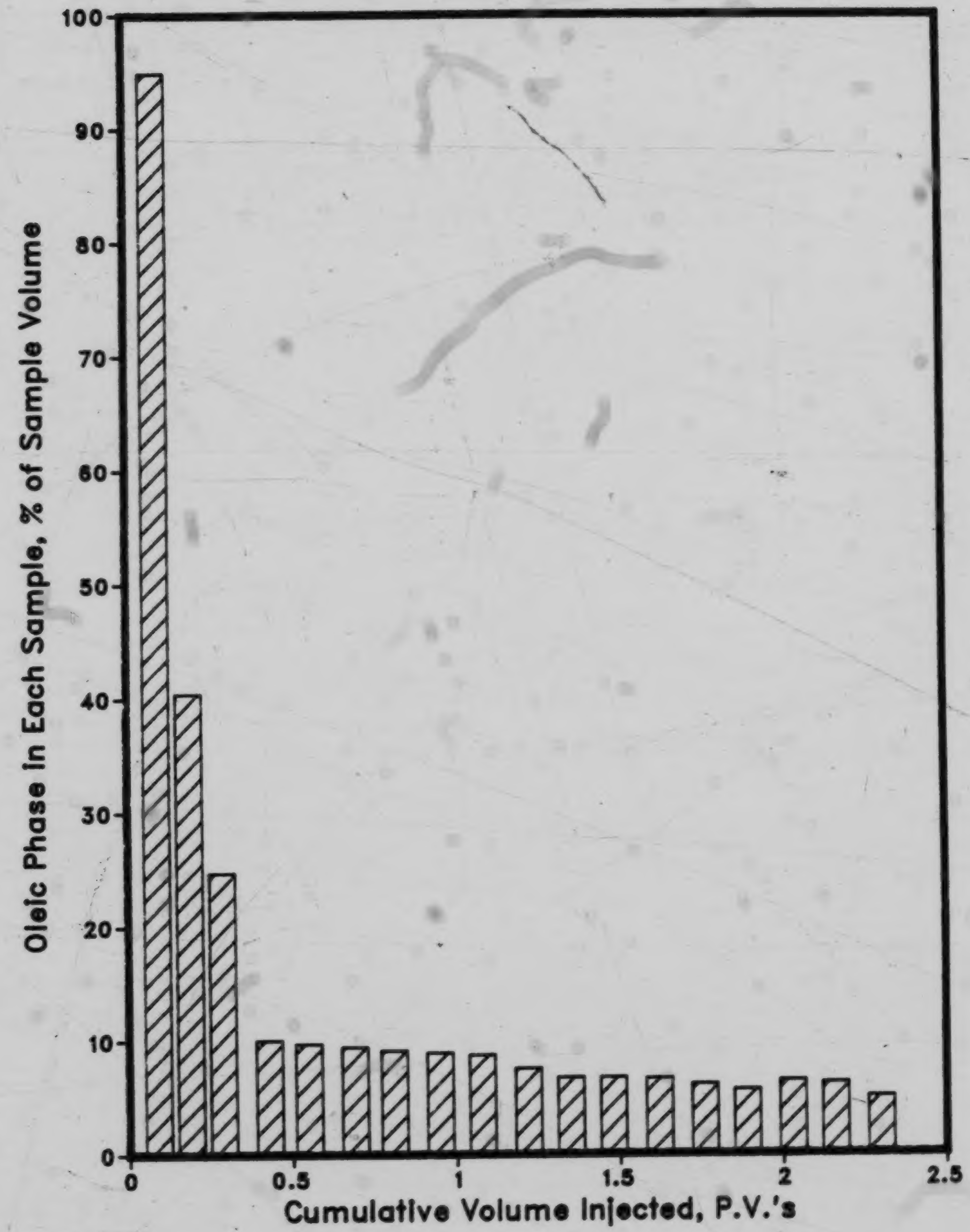

Figure 6.81 :Run 59 Gas Injection Prior to Solvent–Steamflood Instantaneous Produced WOR Vs. Cumulative Volume Injected

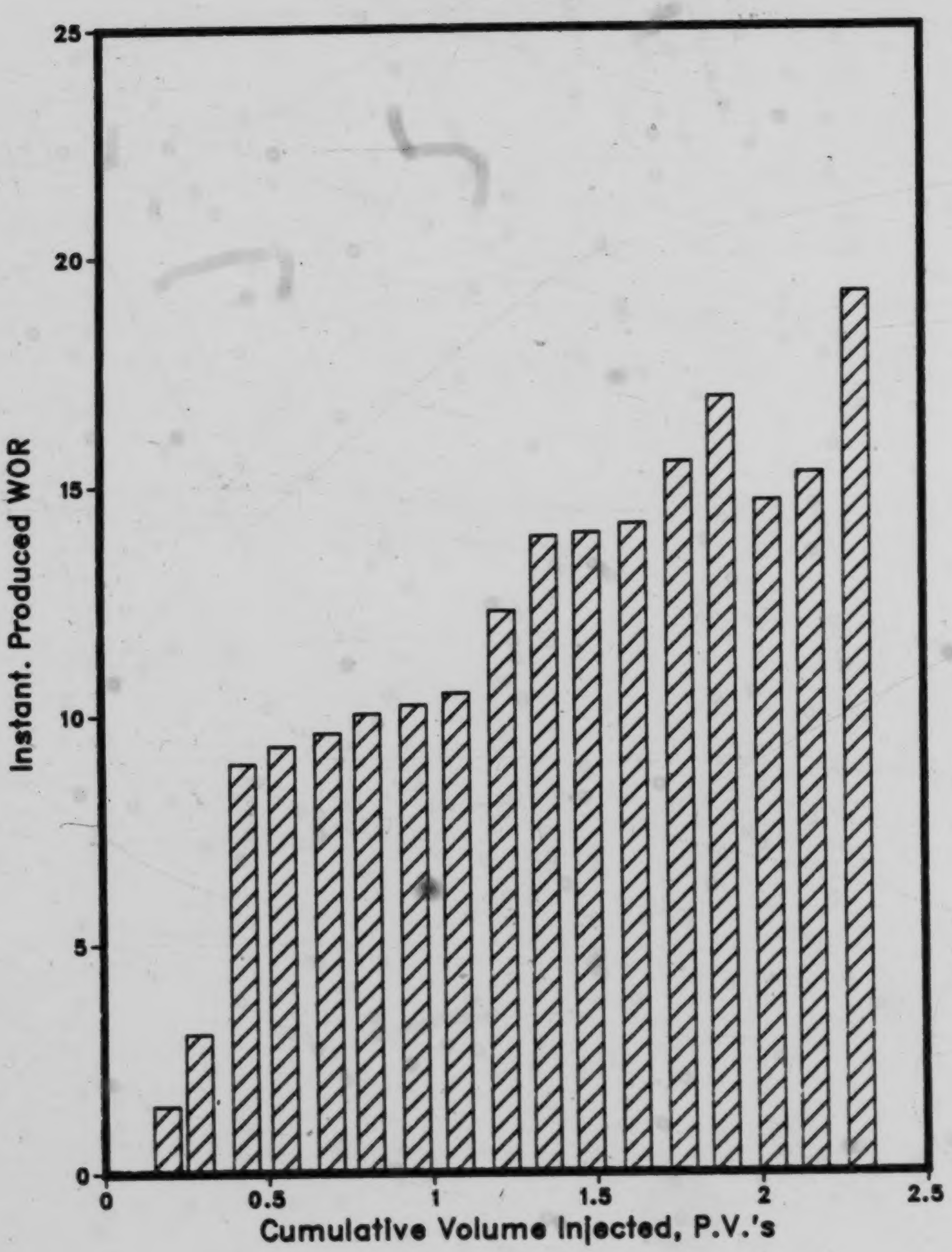

Figure 6.82 :Run 59 Gas Injection Prior to Solvent–Steamflood
Instanteous Oil/Steam Ratio vs. Cumulative Oil Produced

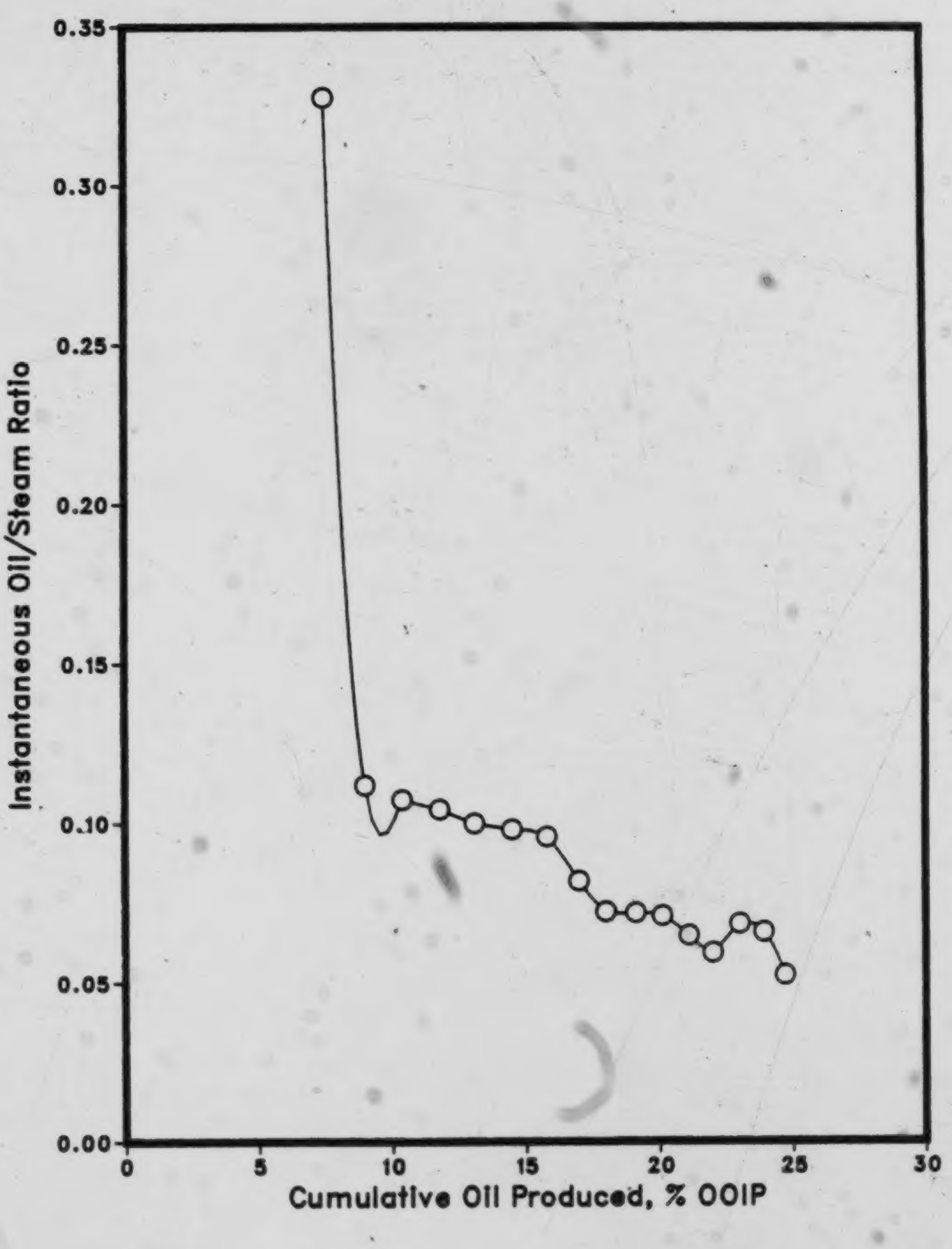

Table 6.21 : Run 62 Gas Injection Prior to Solvent-Steamflood of Bottom Water Model

HC Pore Volume 12730.0 cc
Pore Volume : 15260.0 cc
Bulk Volume : 42005.0 cc
Porosity : 36.3%
Initial Oil Satn. : 83.4%
Initial H2O Satn. 16.3%
Initial Gas Satn. : 0.3%
Solvent Vol. Inj. : 1400.0 cc

Type of Oil Used : Faxam-100
Initial Model Temperature 3.00 C
Water Feed Flow Rate : 200.00 cc/min
Boiler Feed Flow Rate : 29.20 cc/min
Total Flow Rate of Steam 229.20 cc/min
Solvent Flow Rate : 200.00 cc/min
Gas Cap Volume : 45.0 cc
Steam Vol. Inj. : 33595.0 cc (2.19 PV)
Bottom Water Layer Thickness : 12.0% (% Gross Thickness)

Net Oil Recovery : 20.0% **Solvent Recovery : 94.7%** **Final Oil Saturation : 66.7%**

Cyl. No.	Solvent Conc. (%)	Tot. Vol. Inj. (cc)	Cum. Vol. Inj. (cc)	Cum. Vol. Inj. (P.V.)	HC Prod. (cc)	Oil Prod. (cc)	Cum. Oil Rec. (cc)	Cum. Oil Rec. (%OOIP)	Cum. Sol. Rec. (cc)	Cum. Sol. Rec. (%)	Oil-Steam Ratio	Inst Prod. WOR	Inst. HC Prod. % of Sample
1	66%	1025	1025	0.07	760	258	258	2.0%	502	35.9%	0.0000	0.35	74.1%
2	64%	1800	2825	0.19	940	338	596	4.7%	1104	78.9%	0.0000	0.91	52.2%
3	24%	1905	4730	0.31	435	331	927	7.3%	1208	86.3%	0.2959	3.38	22.8%
4	12%	2000	6730	0.44	140	123	1050	8.2%	1225	87.5%	0.0753	13.29	7.0%
5	22%	2130	8860	0.58	195	152	1202	9.4%	1268	90.6%	0.1008	9.92	9.2%
6	21%	1900	10760	0.71	140	111	1313	10.3%	1297	92.6%	0.0795	12.57	7.4%
7	6%	2015	12775	0.84	250	235	1548	12.2%	1312	93.7%	0.1416	7.06	12.4%
8	4%	1990	14765	0.97	155	149	1697	13.3%	1318	94.1%	0.0845	11.84	7.8%
9	2%	2040	16805	1.10	145	142	1839	14.4%	1321	94.4%	0.0765	13.07	7.1%
10	2%	1900	18705	1.23	120	118	1957	15.4%	1323	94.5%	0.0674	14.83	6.3%
11	1%	2085	20790	1.36	125	124	2081	16.3%	1324	94.6%	0.0638	15.68	6.0%
12	1%	2040	22830	1.50	155	153	2234	17.5%	1326	94.7%	0.0822	12.16	7.6%
13	0%	2290	25120	1.65	50	50	2284	17.9%	1326	94.7%	0.0223	44.80	2.2%
14	0%	1920	27040	1.77	60	60	2344	18.4%	1326	94.7%	0.0323	31.00	3.1%
15	0%	2035	29075	1.91	55	55	2399	18.8%	1326	94.7%	0.0278	36.00	2.7%
16	0%	1865	30940	2.03	60	60	2459	19.3%	1326	94.7%	0.0332	30.08	3.2%
17	0%	2040	32980	2.16	35	35	2494	19.6%	1326	94.7%	0.0175	57.29	1.7%
18	0%	2015	34995	2.29	55	55	2549	20.0%	1326	94.7%	0.0281	35.64	2.7%

Figure 6.83 :Run 62 Gas Injection Prior to Solvent–Steamflood Cumulative Oil Recovery Vs. Pore Volumes Injected

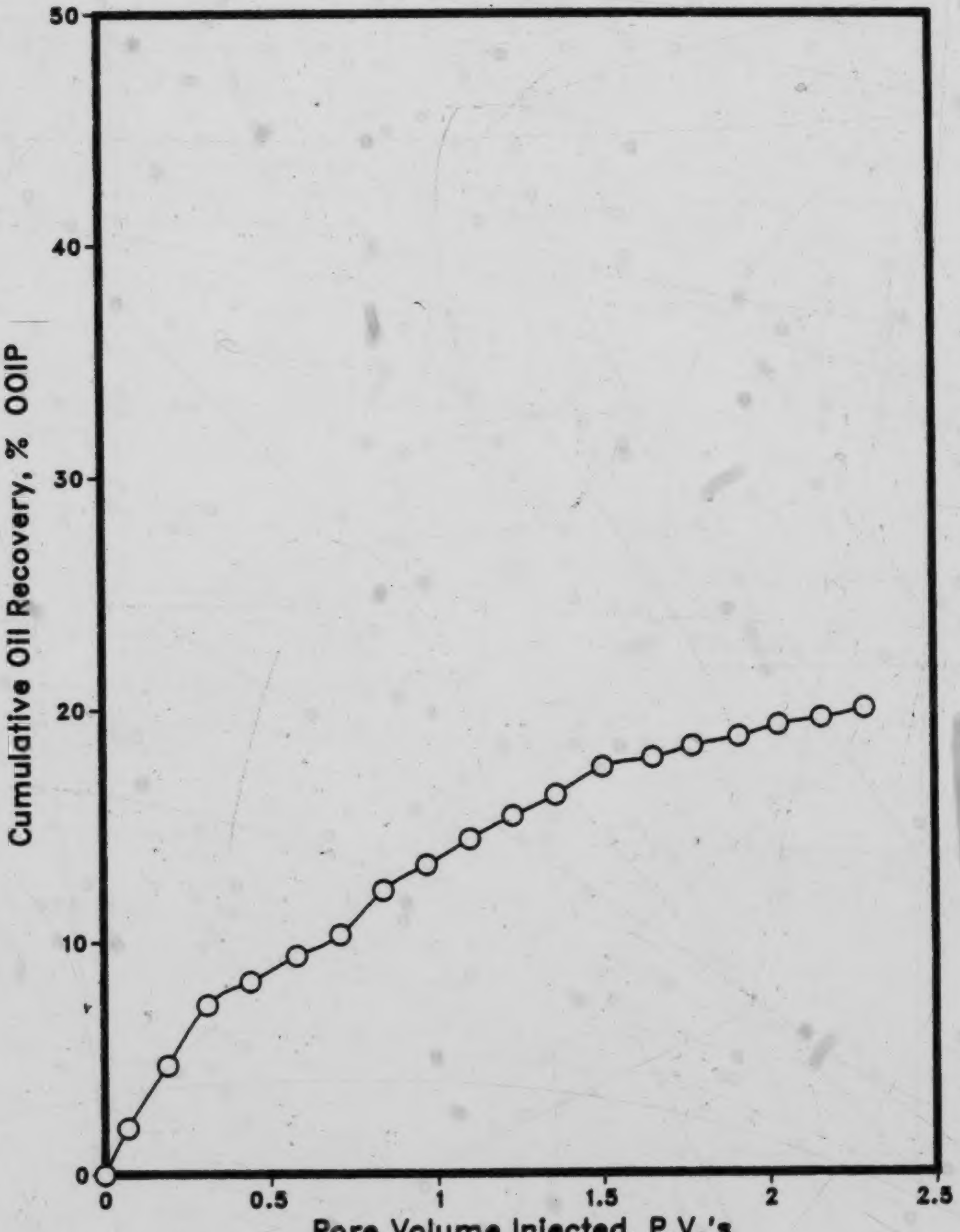

Figure 6.84 :Run 62 Gas Injection Prior to Solvent–Steamflood Oleic Phase in Each Sample Vs. Cumulative Volume Injected

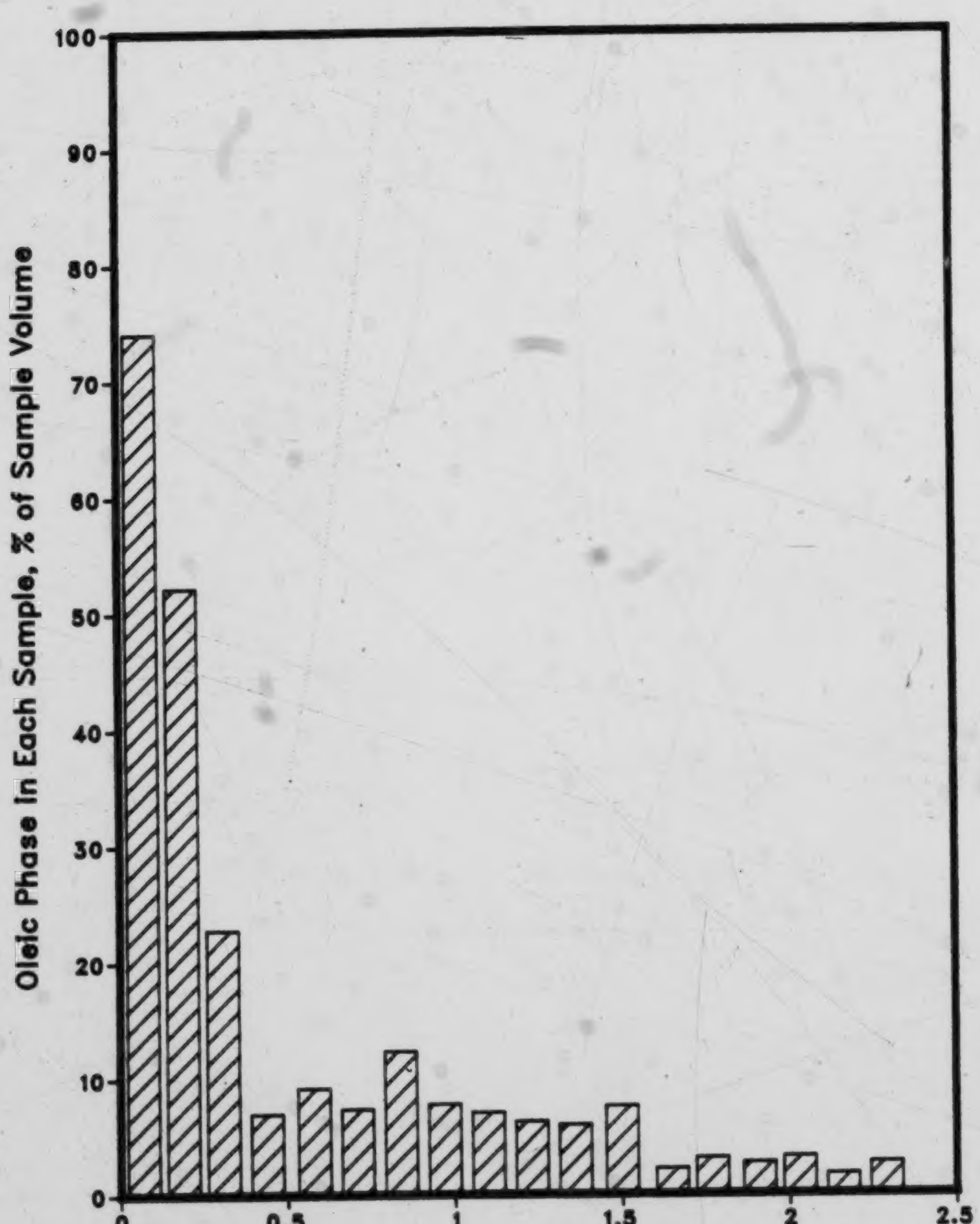

Figure 6.85 :Run 62 Gas Injection Prior to Solvent–Steamflood Instantaneous Produced WOR Vs. Cumulative Volume Injected

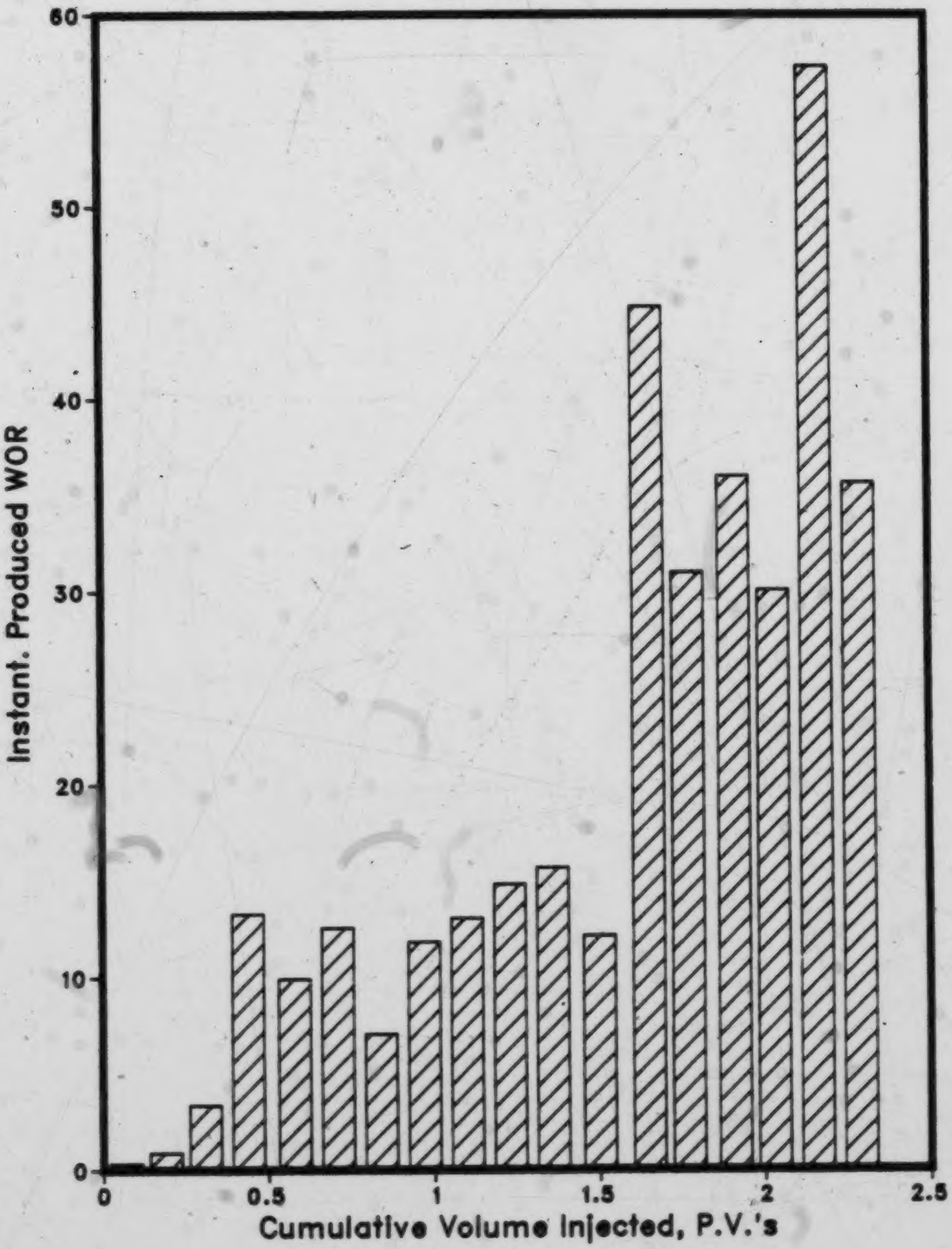

Figure 6.86 :Run 62 Gas Injection Prior to Solvent–Steamflood Instanteous Oil/Steam Ratio vs. Cumulative Oil Produced

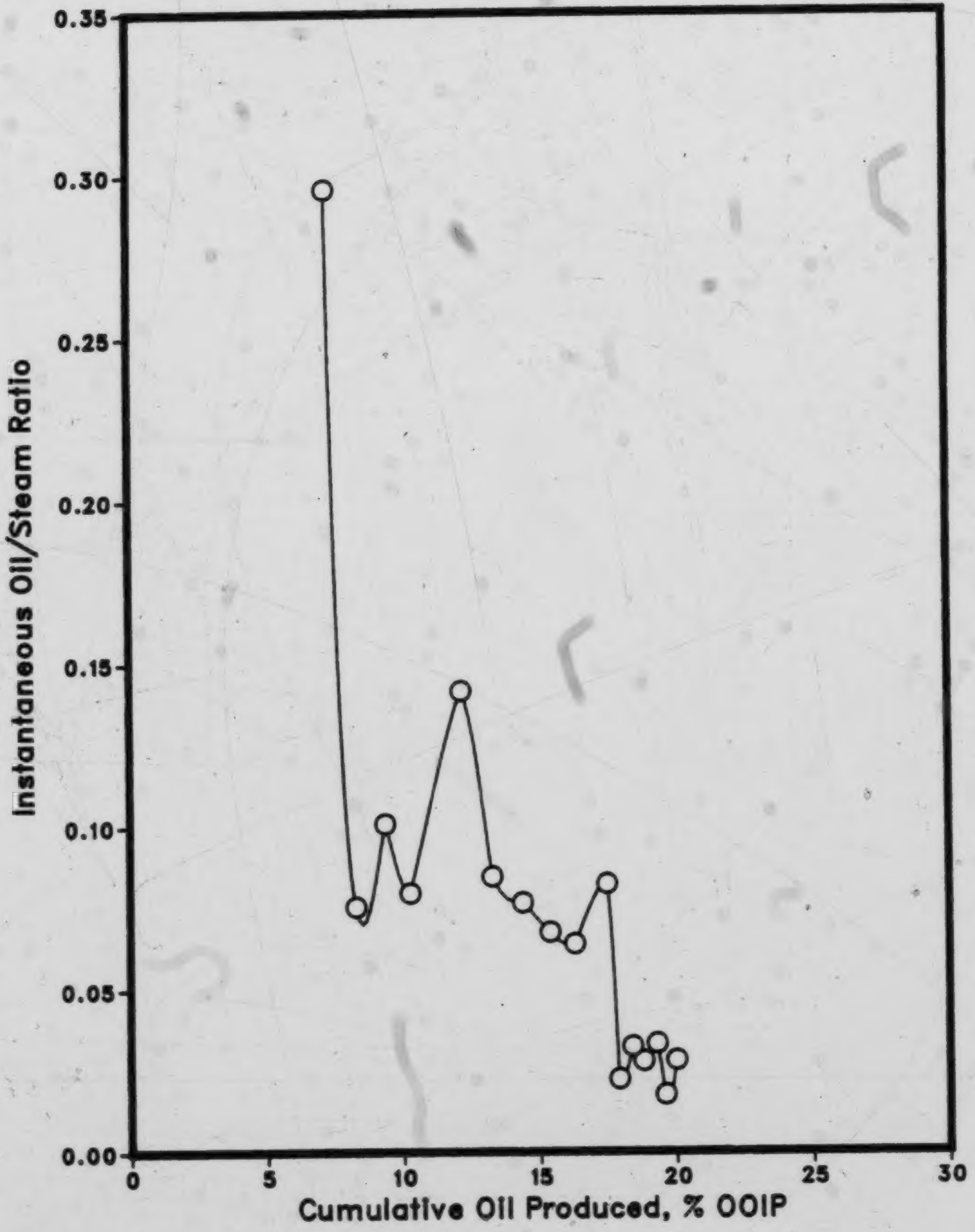

Examination of the temperature profiles for Runs 58 (Fig. A.203-A.210), 59 (Fig. A.215-A.222) and 62 (Fig. A.227-A.234) reveals that the presence of a gas cap allowed the heat to advance through the upper and lower portions of the model at about the same rate. The advancement of the heat through the lower region was only slightly faster due to some of the steam underriding the oil and gas cap into the bottom water. Of the three experiments the heat advanced fastest through the bottom portion of the model in Run 59 since a thicker bottom water region existed (13.6%). The cross-sectional temperature profiles of the three experiments are provided in Figures A.211-A.214 (Run 58), Figures A.223-A.226 (Run 59) and Figures A.235-A.238 (Run 62). These profiles also indicate that the existence of a gas cap permitted heat flow through the upper and lower sections at about the same rate. The cross-sectional profiles (Figures A.223-A.226) for the thicker bottom water case (Run 59) also demonstrated that heat advance was quicker in the bottom water zone during this experiment. These results imply that the gas cap aided partially in diverting the solvent and steam into the upper part of the model which reduced the heat lost to the bottom water. As well the gas cap partially diverted the solvent and steam away from the oil which resulted in less solvent and steam penetrating the oil layer and thus less oil was mobilized.

The solvent recoveries for Runs 58 (88.6%), 59 (96.7%) and 62 (94.7%) were all rather high. This indicates that solvent flowed to the production well mainly through the gas channel, resulting in less solvent mixing with the oil zone and less channelling of solvent in the bottom water zone. The lower solvent and oil recoveries for Run 58 was probably caused by less solvent channelling into the oil and more solvent flowing through the gas channel over top of the oil, therefore more heat from the injected steam was diverted to the top part of the oil zone or was lost to the bottom water and subsequently less oil was mobilized.

From the three experiments, the presence of a gas cap and bottom water had an obvious effect on the overall solvent and oil recoveries as was also described by Kasraie and Farouq Ali [27,28]. Results of Runs 58, 59 and 62 gave an indication that if a gas cap was present in the bottom water model more steam would be diverted away from the bottom water into the upper portion of the model.

Figure 6.87 provides a comparison of the recovery curves for a solvent-steamflood in a bottom water model (Run 50) and a solvent-steamflood with previous gas injection in a bottom water model (Run 58). Runs 50 and 58 had similar bottom water thicknesses of 10.2% and 9.8%, respectively. It is quite evident from Figure 6.87 that Run 50 (solvent-steamflood) achieved a considerably greater oil recovery than Run 58 (gas injection prior to solvent-steamflood). The main difference between the curves occurred during the initial stages of the two recovery relationships. Run 50 had a more drastic initial increase in recovery (25.4% OOIP) compared to Run 58 (18.2% OOIP) due to the solvent and oil more effectively penetrating the oil zone and creating a more stable steam displacement of oil during Run 50. Run 58 had a less pronounced solvent and oil invasion in the oil region since more solvent and oil flowed over top of the oil zone through the channel formed by the previous gas injection. Steam breakthrough was earlier and less distinct for Run 58 due to the existence of a less stable displacement of oil caused by the gas channel.

A gas cap in a reservoir can be helpful or detrimental to the effectiveness of a steam injection process depending on certain characteristics of the reservoir such as heat loss, reservoir thickness, bottom water thickness and the gas cap size. During the steamflood of a bottom water reservoir the gas cap allowed the steam to remain in the upper portion of the formation away from the bottom water, thus heating and mobilizing the inplace oil from above. How effectively the oil was mobilized from above depends on the magnitude of the heat lost to the overburden, adjacent formations and the bottom water zone. However, in the case of the solvent-steamflood process the gas cap enabled the solvent to flow over top of the oil zone. Overriding of the oil by the solvent caused fewer flow channels to form in the oil layer. Lack of solvent channelling into the oil zone hindered the penetration of the oil layer by the steam. Consequently, less oil was mobilized by the steam resulting in a

Figure 6.87 :Comparison of Solvent–Steamflood Run 50 & Gas Injection Prior to Solvent–Steamflood Run 58 Recoveries Performed in a Bottom Water Model

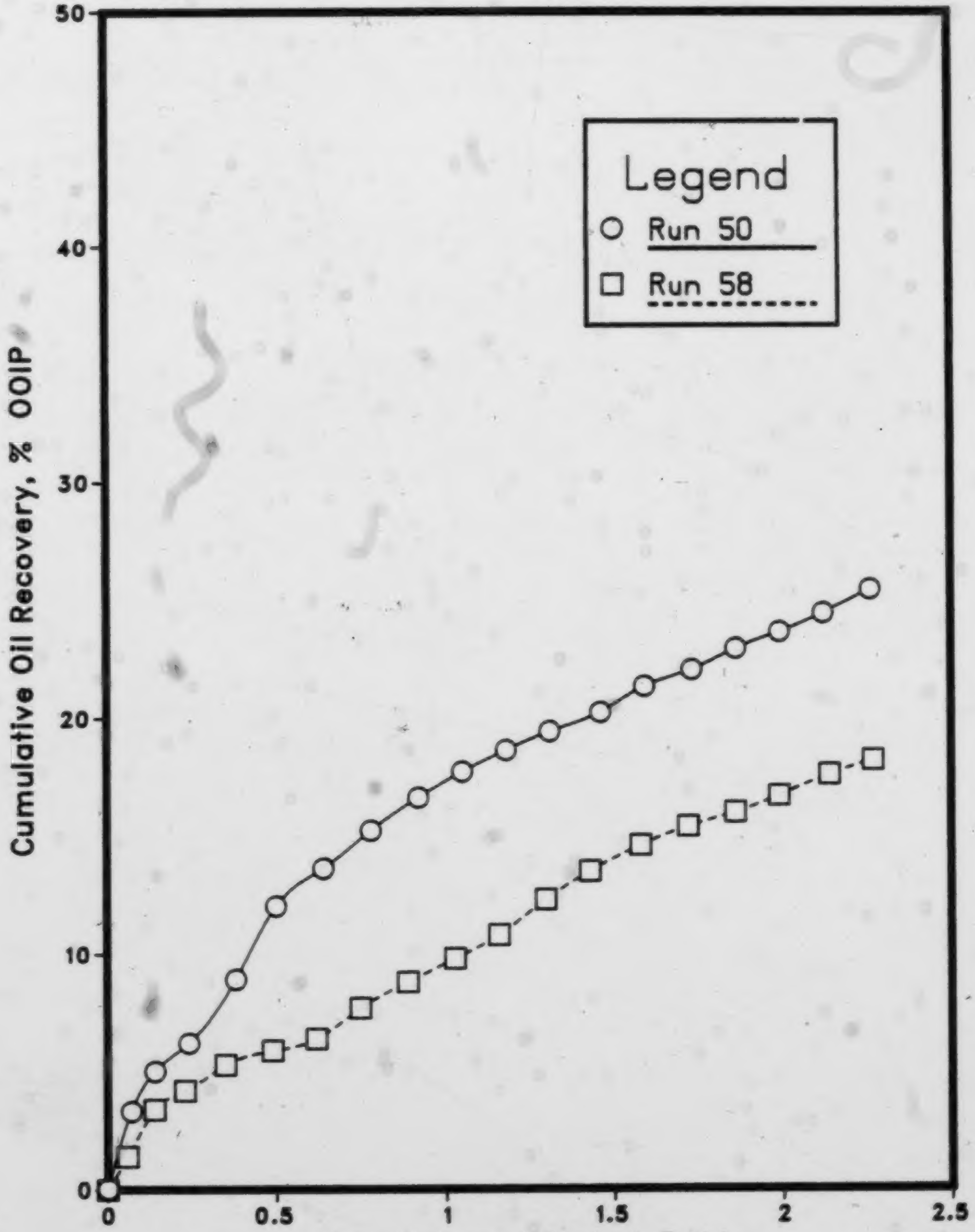

decline in the overall recovery of a solvent-steamflood process as compared to its implementation in a heavy oil reservoir with bottom water but no gas cap or gas channel.

Effect of Injection-Production Interval Locations

The effect of injection-production interval locations on the success of the solvent-steamflood process in bottom water reservoirs was found to be very important. By optimizing the injection-production interval positions the injected solvent and steam could be utilized most effectively to recover the inplace oil.

Two experiments were performed (Runs 49 & 50) in order to determine the effect of injection-production interval locations on the solvent-steamflood recovery from a bottom water model. Runs 49 and 50 had similar bottom water water thicknesses of 8.8% and 10.2% of the total model thickness, respectively. The injection interval was situated over the entire model thickness, while the production interval was in the top half of the model for Run 49. Whereas in Run 50 the injection was completed in the upper half of the model and production was from the entire model thickness.

A comparison of the recovery curves from the two experiments (Runs 49 & 50), provided in Figure 6.88, indicates that the most effective injection-production intervals appeared to be those used in Run 50 where injection was into the upper half and production was from the entire model thickness. As illustrated by Figure 6.88, Run 50 had a higher oil recovery than Run 49 throughout the entire run. In the case of Run 50, solvent and steam were injected into the upper half of the model and therefore less of the solvent and steam was affected by the underlying water, compared to Run 49. During Run 49, the solvent and steam were injected over the entire model thickness which resulted a larger percentage of the injected fluids being channelled by the bottom water, even though Run 49 had a slightly thinner bottom water layer. Solvent channelling in the oil zone was more extensive for Run 50 than Run 49 due to the more preferential solvent injection into the oil layer. Injection into the upper portion of the model increased solvent channelling in the oil and allowed more steam to penetrate the oil zone, causing more oil to be mobilized. However, for Run 49, less extensive solvent channelling occurred in the oil zone since

Figure 6.88 :Comparison of the Effect of Inj.-Prod. Interval Locations For Runs 49, Inj-Entire & Prod-Upper, & Run 50, Inj-Upper & Prod-Entire

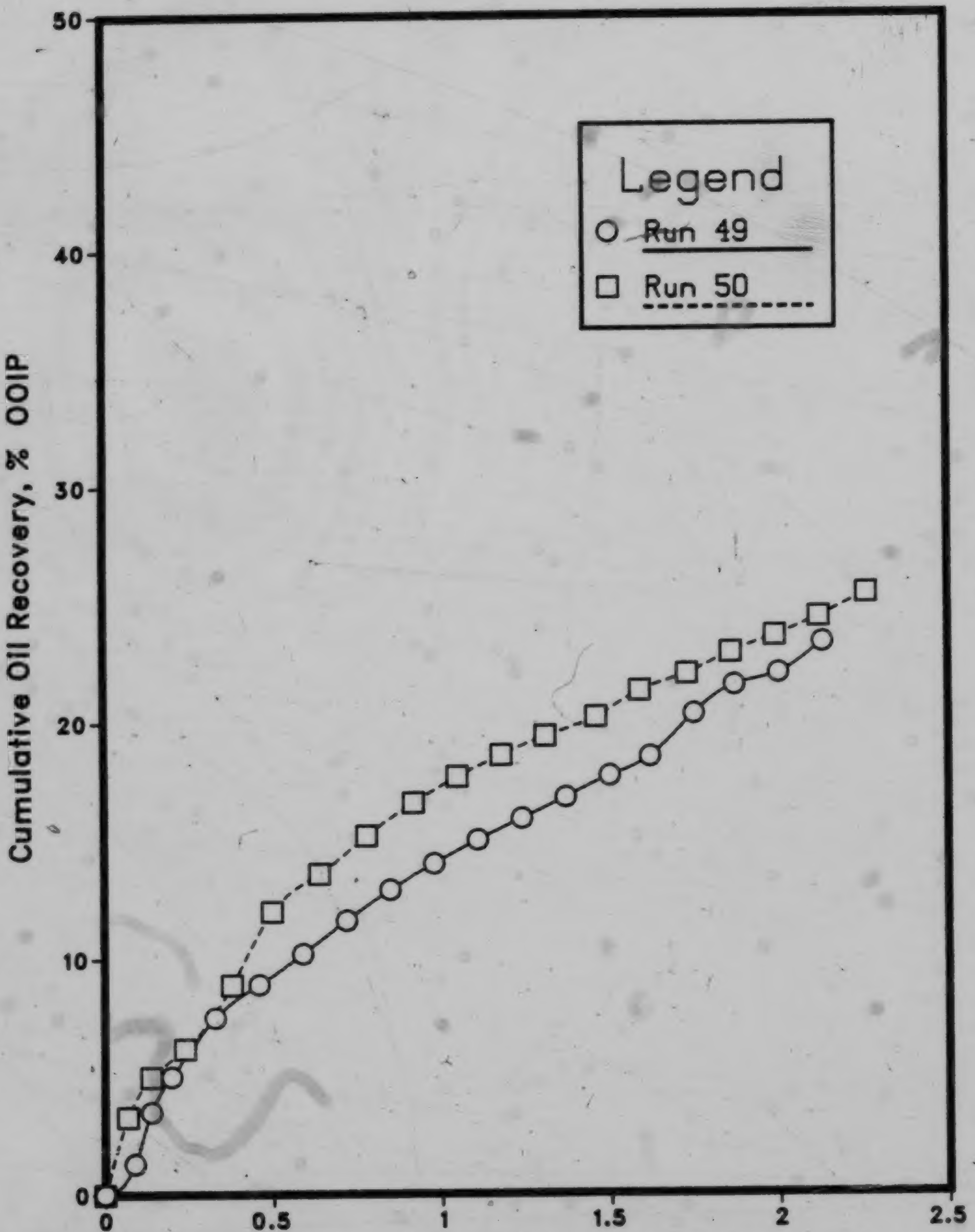

injection was spread over the entire model thickness as opposed to only half the model thickness as in Run 50. Less steam penetrated the oil zone in Run 49 and a greater amount of steam was lost to the bottom water as a result of reduced solvent channelling in the oil layer and a larger injection interval, which included the bottom water zone.

An examination of the top view temperature profiles for Runs 49 (Fig. A.119-A.126) and 50 (Fig. A.131-A.138) also indicates that the steam was being used more efficiently in the upper oil zone of the model during Run 50. Figures A.119-A.126 for Run 49 show that the injected heat from the steam was travelling faster through the bottom half than the upper region of the model. Compared to the temperature contours for Run 49, the temperature profiles for Run 50 (Fig. A.131-A.138) indicate the injected heat was retained longer in the upper region of the model, where the oil was located. The cross-sectional temperature profiles provided in Figures A.127-A.130 (Run 49) and Figures A.139-A.142 (Run 50) verify these observations.

The injection interval location for Run 50 permitted more efficient use of the injected solvent and steam, by directing these fluids into the oil zone and away from the bottom water, thus yielding a higher overall oil recovery. However, for Run 49, more solvent and steam were lost to the underlying water zone, making this solvent-steamflood process less efficient than the solvent-steamflood conducted during Run 50.

Use of a Physical Barrier in a Bottom Water Steamflood

One of the objectives of this study was to investigate an alternate recovery strategy to the solvent-steamflood process, which also attempted to divert the injected steam away from the bottom water layer. The experimental results of this type of run could then be compared to the findings of the solvent-steamflood experiments in order to determine the relative effectiveness of this recovery technique. This recovery method involved the placement of a partial barrier between the bottom water and oil zone to prevent the injected steam from flowing directly into the less flow resistant bottom water. A notable advantage of using a partial bottom water barrier as discussed by Alikhan and Farouq Ali [67] was that a barrier at the water-oil contact of a reservoir aided in reducing water coning. Runs 63 and 64 attempted to represent a bottom water reservoir containing a partial barrier which could be created in the field by selectively injecting a suitable blocking agent, such as a foam or gel, at the oil-water contact. The purpose of the partial barrier was to help prevent the steam from travelling directly into the bottom water so that it could flow through the overlying oil zone and more efficiently heat and mobilize the inplace oil. A thin plastic sheet was placed between the bottom water layer and the oil layer to represent a partial bottom water barrier. The barrier installed in the model extended radially outward from the injection well in the shape of a quarter circle with a radius of 16 inches. The area covered by the partial barrier was approximately 20% of the total model area as illustrated in the following schematic diagram (Figure 6.89).

Runs 63 and 64 were continuous steamfloods in a bottom water model containing a partial bottom water barrier between the oil zone and the underlying bottom water interval. The results of Runs 63 and 64 are given in tabular form and are displayed in Tables 6.22 and 6.23, respectively.

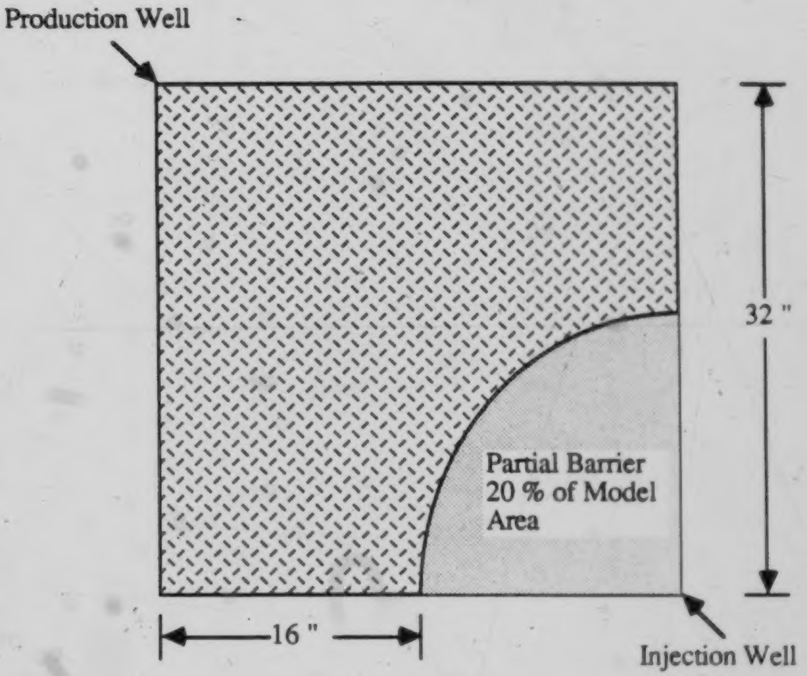

Figure 6.89 :Schematic of Partial Barrier Installed in a Bottom Water Model

The recovery curves plotted for Runs 63 and 64 are presented in Figures 6.90 and 6.94, respectively. The overall oil recovery for Run 63 (17.0% OOIP) was less favourable than that obtained in Run 64 (22.0% OOIP). The reason for the lower recovery in Run 63 is the thicker bottom water layer (15.4% of gross model thickness). Run 64 had a bottom water region that was 9.9% of the gross model thickness. Since less bottom water existed in Run 64 a larger percentage of the injected heat was utilized in mobilizing the oil instead of being scavenged by the bottom water. The recovery curves for Runs 63 (Figure 6.90) and 64 (Figure 6.94) appeared to have much slower initial recovery responses compared to the recovery curves of most of the previous solvent-steamflood experiments (Runs 49, 50, 51, 53 & 54). This suggests that the partial barrier experiments were not as effective as the solvent-steamflood runs since the steam appeared to have a tendency to travel between the partial barrier and the oil zone out to the point in the model where the barrier no longer existed. During the partial barrier experiments a larger amount of injected heat moved downward into the detrimental bottom water region with a smaller portion filtering upward into the oil zone. However, during the initial stages of the solvent-steamflood the steam flowed directly into the oil zone through the solvent channels, which more effectively utilized the oil mobilizing capability of the injected steam. This would explain the slower initial recovery responses of the partial barrier experiments. In the later stages of Run 63 (Figures 6.90) and Run 64 (Figure 6.94) the recovery responses become similar (ie. increased) to the responses observed in the recovery curves of the solvent-steamflood experiments. This indicates that some of the heat in the steam moved upward into the oil region resulting in a larger amount of oil being mobilized and subsequently produced.

The bar plots of the volume percentage of oleic phase in each sample versus cumulative volume injected and instantaneous produced WOR versus cumulative volume injected are provided for Runs 63 (Fig. 6.91 & 6.92) and 64 (Fig. 6.95 & 6.96). Study of the bar plots for both experiments shows that the thicker bottom water layer of Run 63 resulted in earlier solvent and steam breakthrough and a less stable displacement of the oil within the model as compared to Run 64.

The plots of instantaneous oil/steam ratio versus cumulative oil produced for Runs 63 (Figure 6.93) and 64 (Figure 6.97) also indicate the adverse effects of the thicker bottom water zone in Run 63. The average instantaneous oil/steam ratio in Run 63 (Figure 6.93) was somewhat lower than the average instantaneous oil/steam ratio in Run 64 (Figure 6.97) which was due to the larger bottom water zone in Run 63. The thicker bottom water layer in Run 63 caused a greater portion of water to be produced in each recovery sample of the experiment.

The temperature profiles for Runs 63 (Figures A.239-A.246) and 64 (Figures A.251-A.258) illustrate that during both experiments the heat advanced quicker through the lower portion of the model due to the presence of the bottom water. Due to the thicker bottom water in Run 63 the heat advanced faster through the lower half of the model and more slowly through the upper half as compared to Run 64. Since the injected heat

Table 6.22 : Run 63 Steamflood of Bottom Water Model With a Partial Barrier

HC Pore Volume :	11820.0 cc	Type of Oil Used :	Faxam-100
Pore Volume :	15245.0 cc	Initial Model Temperature :	3.00 C
Bulk Volume :	42005.0 cc	Water Feed Flow Rate :	200.00 cc/min
Porosity :	36.3%	Boiler Feed Flow Rate :	29.20 cc/min
Initial Oil Satn. :	77.5%	Total Flow Rate of Steam :	229.20 cc/min
Initial H2O Satn. :	22.5%	Bottom Water Layer Thickness :	15.4% (% Gross Model Thickness)
Steam Vol. Inj. :	34460.0 cc (2.26 PV)		

Net Oil Recovery : 17.0% **Final Oil Saturation : 64.3%**

Cyl. No.	Tot. Vol. Inj. (cc)	Cum. Vol. Inj.		Oil Prod.	Cum. Oil Rec.		Oil-Steam Ratio	Inst Prod. WOR	Inst. Oil Prod. % of Sample
		(cc)	(P.V.)	(cc)	(cc)	(%OOIP)			
1	2090	2090	0.14	45	45	0.4%	0.0220	45.44	2.2%
2	1940	4030	0.26	10	55	0.5%	0.0052	193.00	0.5%
3	2125	6155	0.40	45	100	0.8%	0.0216	46.22	2.1%
4	2020	8175	0.54	50	150	1.3%	0.0254	39.40	2.5%
5	2055	10230	0.67	85	235	2.0%	0.0431	23.18	4.1%
6	1940	12170	0.80	135	370	3.1%	0.0748	13.37	7.0%
7	2060	14230	0.93	195	565	4.8%	0.1046	9.56	9.5%
8	1900	16130	1.06	215	780	6.6%	0.1276	7.84	11.3%
9	2125	18255	1.20	165	945	8.0%	0.0842	11.88	7.8%
10	1985	20240	1.33	125	1070	9.1%	0.0672	14.88	6.3%
11	2045	22285	1.46	130	1200	10.2%	0.0679	14.73	6.4%
12	1970	24255	1.59	120	1320	11.2%	0.0649	15.42	6.1%
13	2040	26295	1.72	200	1520	12.9%	0.1087	9.20	9.8%
14	1950	28245	1.85	170	1690	14.3%	0.0955	10.47	8.7%
15	2050	30295	1.99	130	1820	15.4%	0.0677	14.77	6.3%
16	1985	32280	2.12	115	1935	16.4%	0.0615	16.26	5.8%
17	2180	34460	2.26	75	2010	17.0%	0.0356	28.07	3.4%

Figure 6.90 :Run 63 Steamflood of Bottom Water Model With a Partial Barrier Cumulative Oil Recovery Vs. Pore Volumes Injected

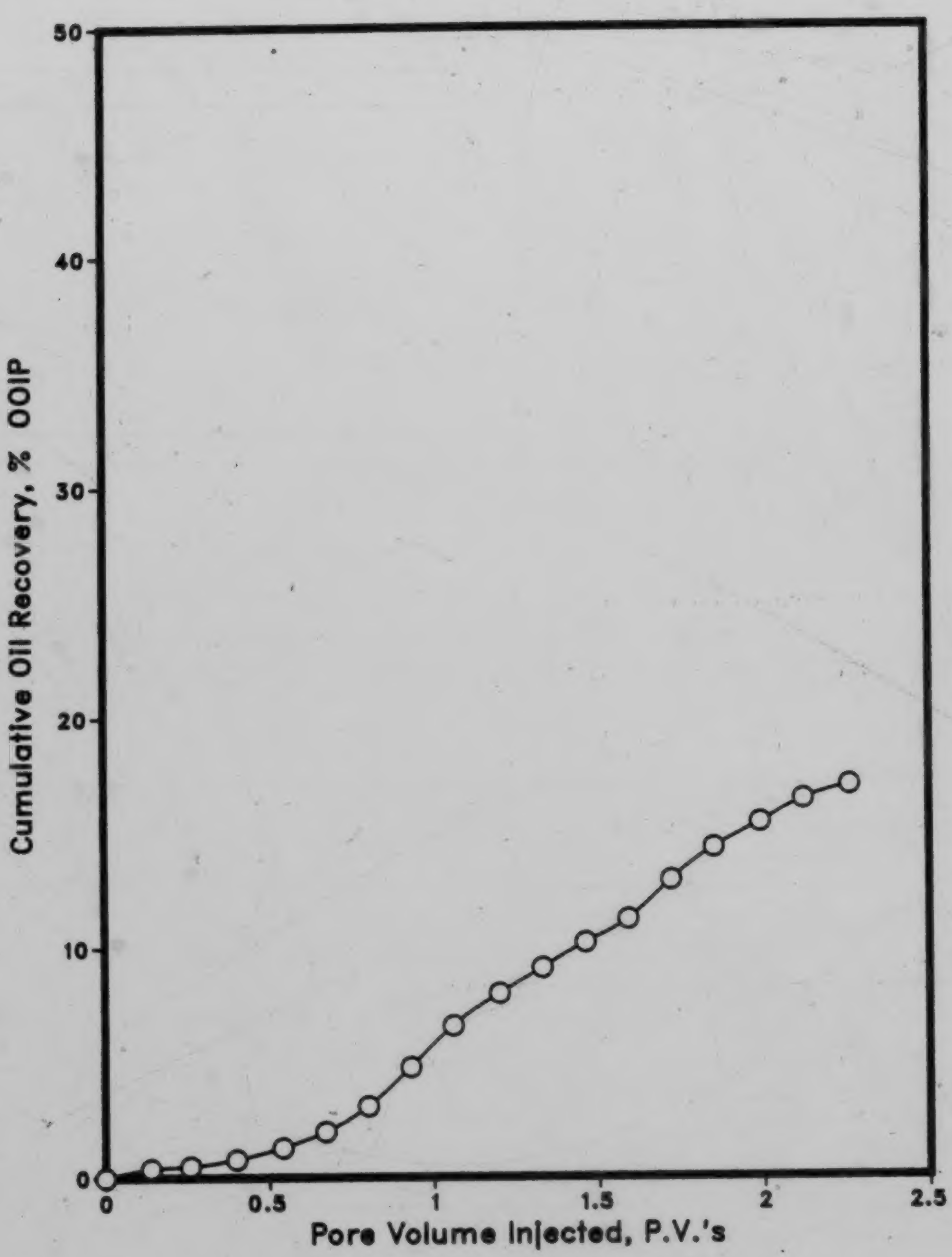

Figure 6.91 :Run 63 Steamflood of Bottom Water Model With a Partial Barrier Oleic Phase In Each Sample Vs. Cumulative Volume Injected

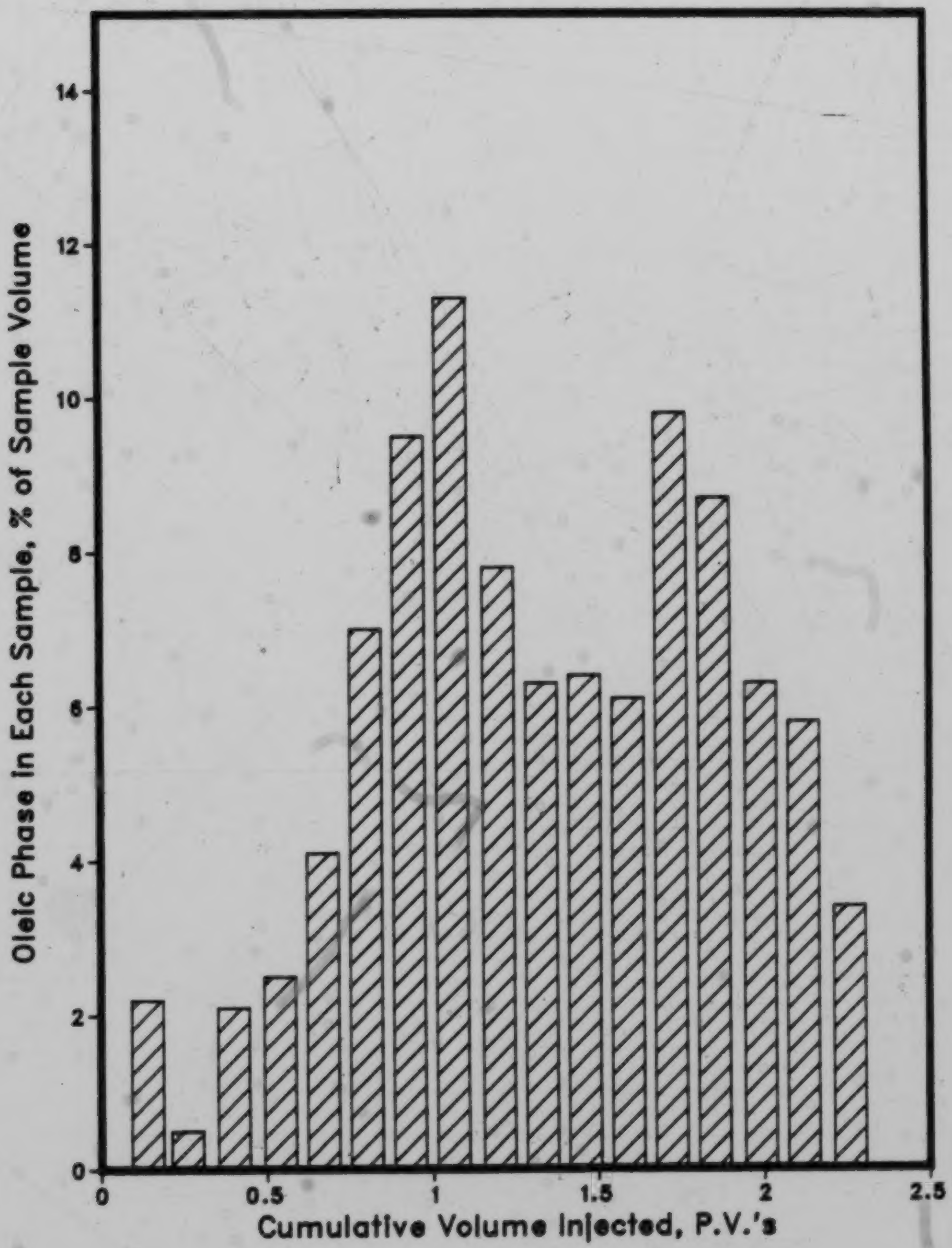

Figure 6.92 :Run 63 Steamflood of Bottom Water Model With a Partial Barrier Instantaneous Produced WOR Vs. Cumulative Volume Injected

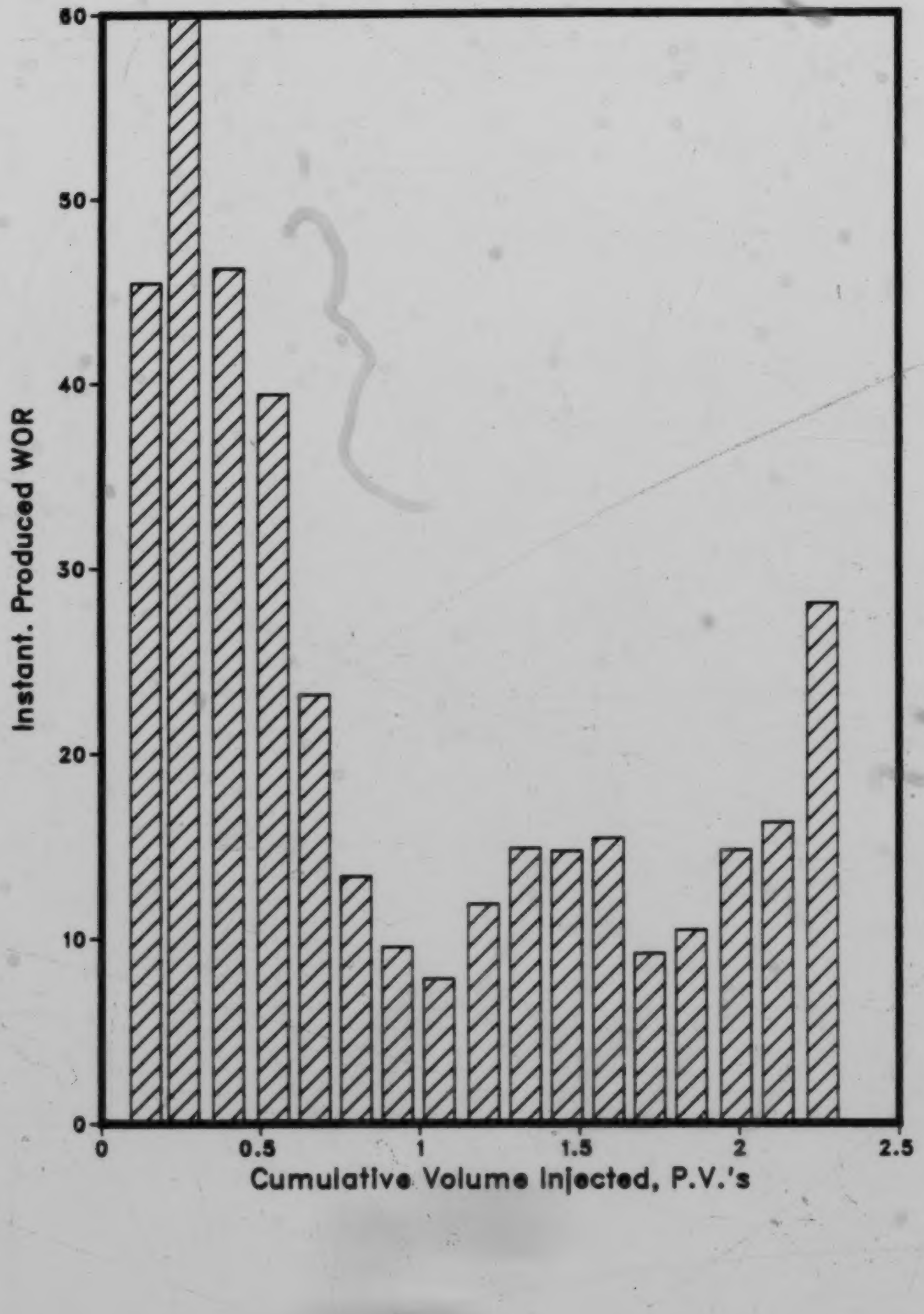

Figure 6.93 :Run 63 Steamflood of Bottom Water Model With a Partial Barrier Instanteous Oil/Steam Ratio vs. Cumulative Oil Produced

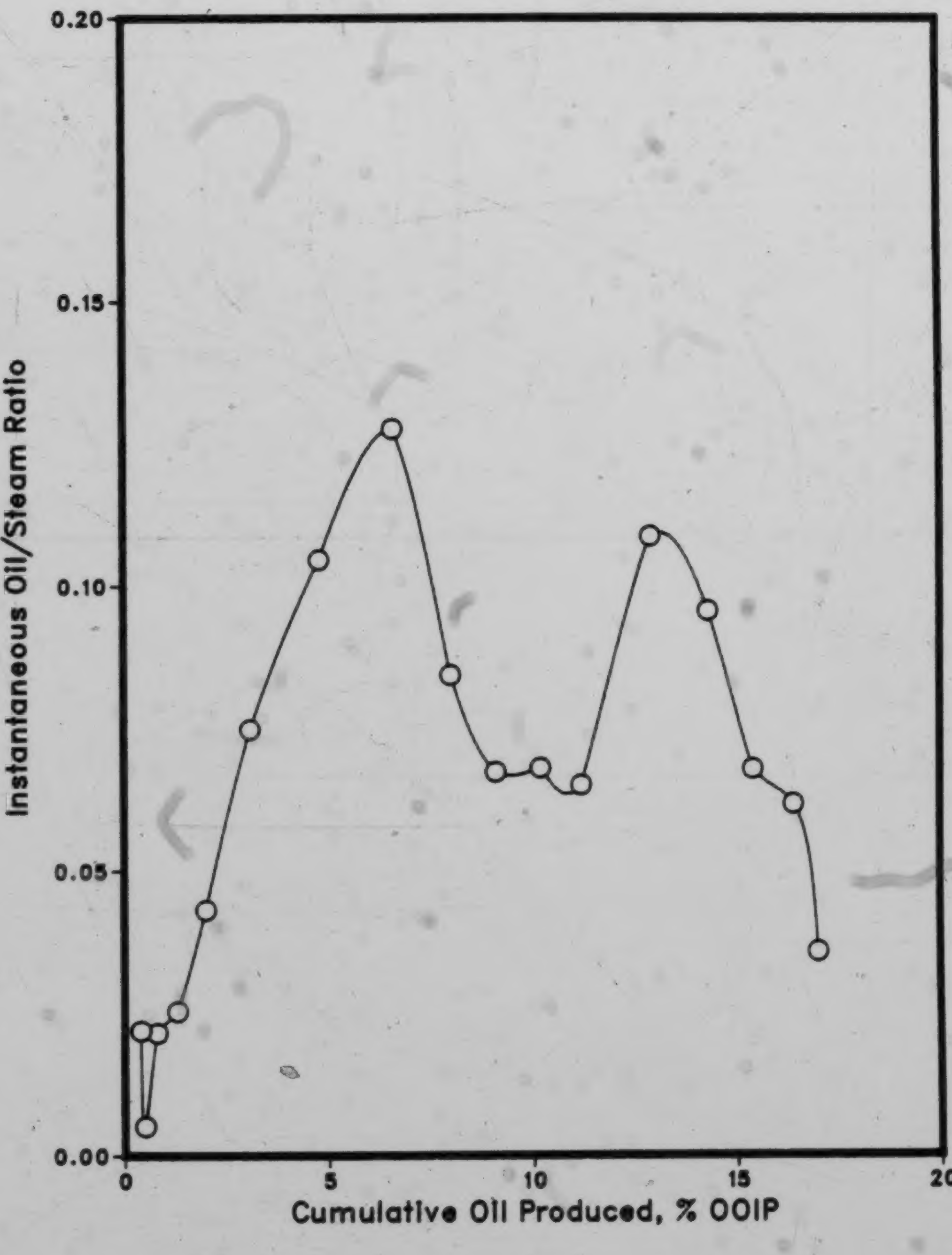

Table 6.23 : Run 64 Steamflood of Bottom Water Model With a Partial Barrier

HC Pore Volume : 13500.0 cc
Pore Volume : 15425.0 cc
Bulk Volume : 42005.0 cc
Porosity : 36.7%
Initial Oil Satn. : 87.5%
Initial H2O Satn. : 12.5%
Steam Vol. Inj. : 34950.0 cc (2.27 PV)

Type of Oil Used : Faxam-100
Initial Model Temperature : 3.00 C
Water Feed Flow Rate : 200.00 cc/min
Boiler Feed Flow Rate : 29.20 cc/min
Total Flow Rate of Steam : 229.20 cc/min
Bottom Water Layer Thickness : 9.9% (% Gross Model Thickness)

Net Oil Recovery : 22.0%

Final Oil Saturation : 68.2%

Cyl. No.	Tot. Vol. Inj. (cc)	Cum. Vol. Inj.		Oil Prod.	Cum. Oil Rec.		Oil-Steam Ratio	Inst Prod. WOR	Inst. Oil Prod. % of Sample
		(cc)	(P.V.)	(cc)	(cc)	(%OOIP)			
1	1975	1975	0.13	510	510	3.8%	0.3481	2.87	25.8%
2	2235	4210	0.27	155	665	4.9%	0.0745	13.42	6.9%
3	1980	6190	0.40	200	865	6.4%	0.1124	8.90	10.1%
4	2105	8295	0.54	230	1095	8.1%	0.1227	8.15	10.9%
5	2045	10340	0.67	275	1370	10.1%	0.1554	6.44	13.4%
6	2110	12450	0.81	145	1515	11.2%	0.0738	13.55	6.9%
7	1925	14375	0.93	180	1695	12.6%	0.1032	9.69	9.4%
8	2095	16470	1.07	145	1840	13.6%	0.0744	13.45	6.9%
9	2015	18485	1.20	110	1950	14.4%	0.0577	17.32	5.5%
10	2085	20570	1.33	140	2090	15.5%	0.0720	13.89	6.7%
11	1940	22510	1.46	125	2215	16.4%	0.0689	14.52	6.4%
12	2060	24570	1.59	125	2340	17.3%	0.0646	15.48	6.1%
13	1955	26525	1.72	135	2475	18.3%	0.0742	13.48	6.9%
14	2200	28725	1.86	120	2595	19.2%	0.0577	17.33	5.5%
15	1960	30685	1.99	140	2735	20.3%	0.0769	13.00	7.1%
16	2200	32885	2.13	140	2875	21.3%	0.0680	14.71	6.4%
17	2065	34950	2.27	100	2975	22.0%	0.0509	19.65	4.8%

Figure 6.94 :Run 64 Steamflood of Bottom Water Model With a Partial Barrier
Cumulative Oil Recovery Vs. Pore Volumes Injected

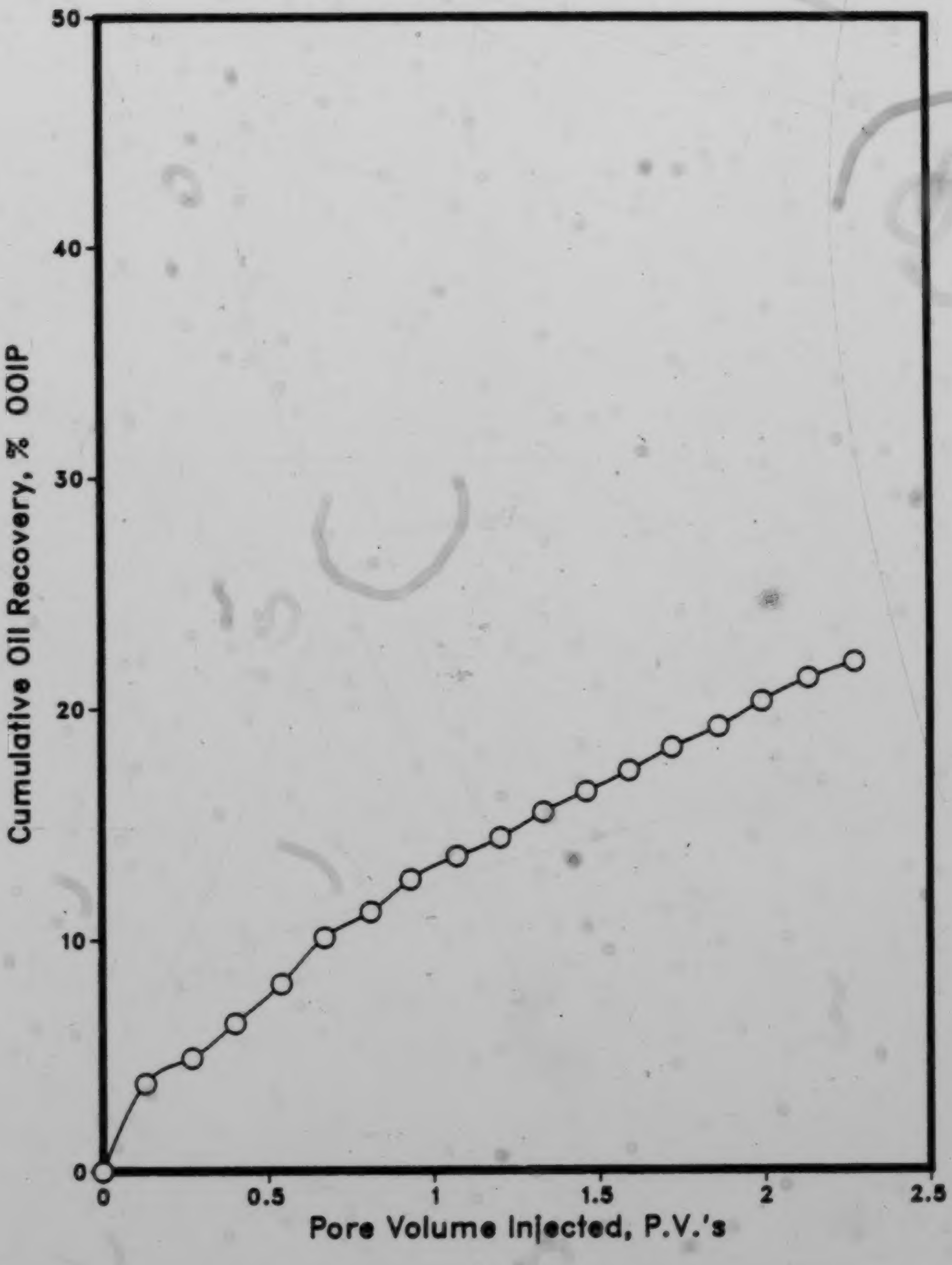

Figure 6.95 :Run 64 Steamflood of Bottom Water Model With a Partial Barrier
Oleic Phase in Each Sample Vs. Cumulative Volume Injected

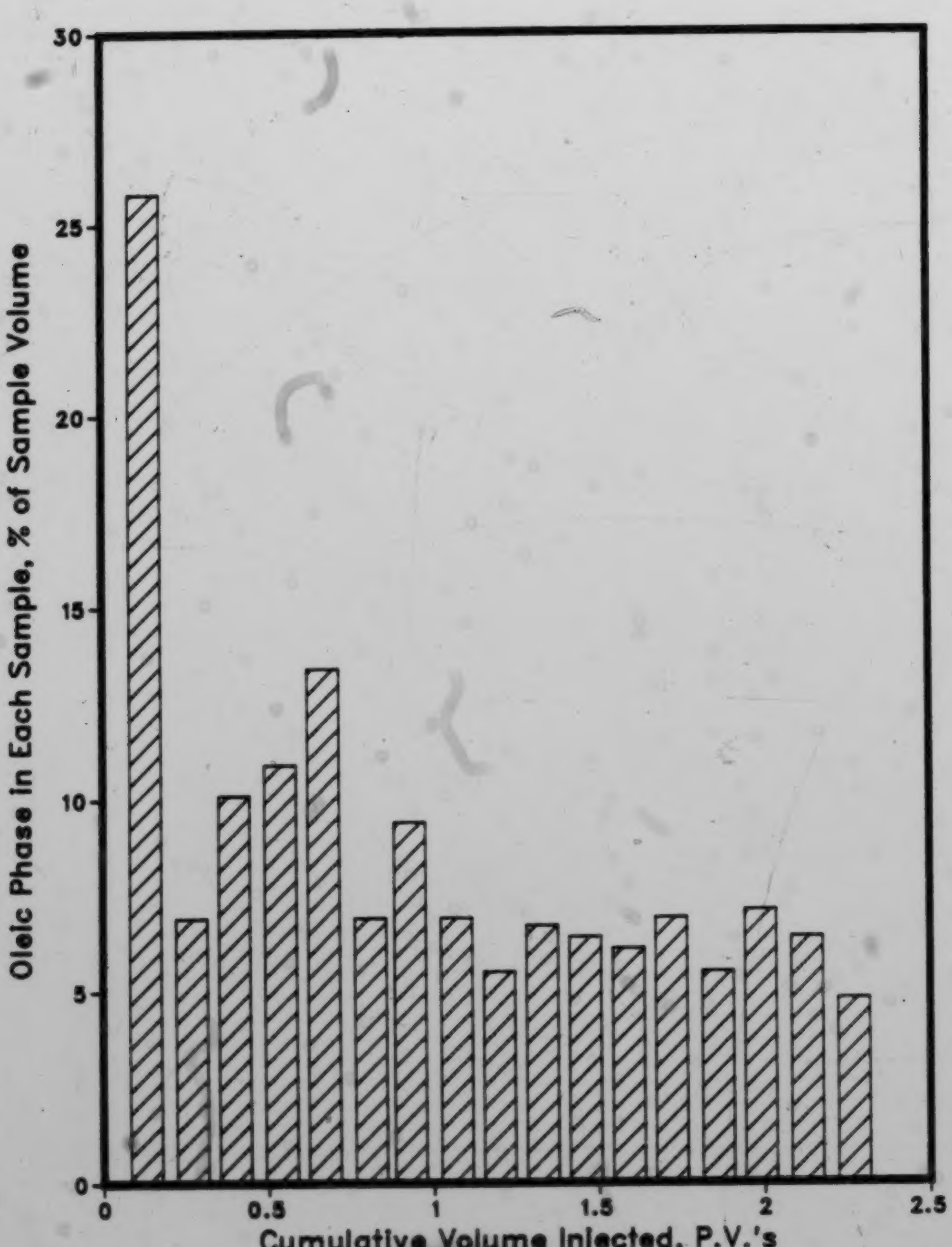

Figure 6.96 :Run 64 Steamflood of Bottom Water Model With a Partial Barrier Instantaneous Produced WOR Vs. Cumulative Volume Injected

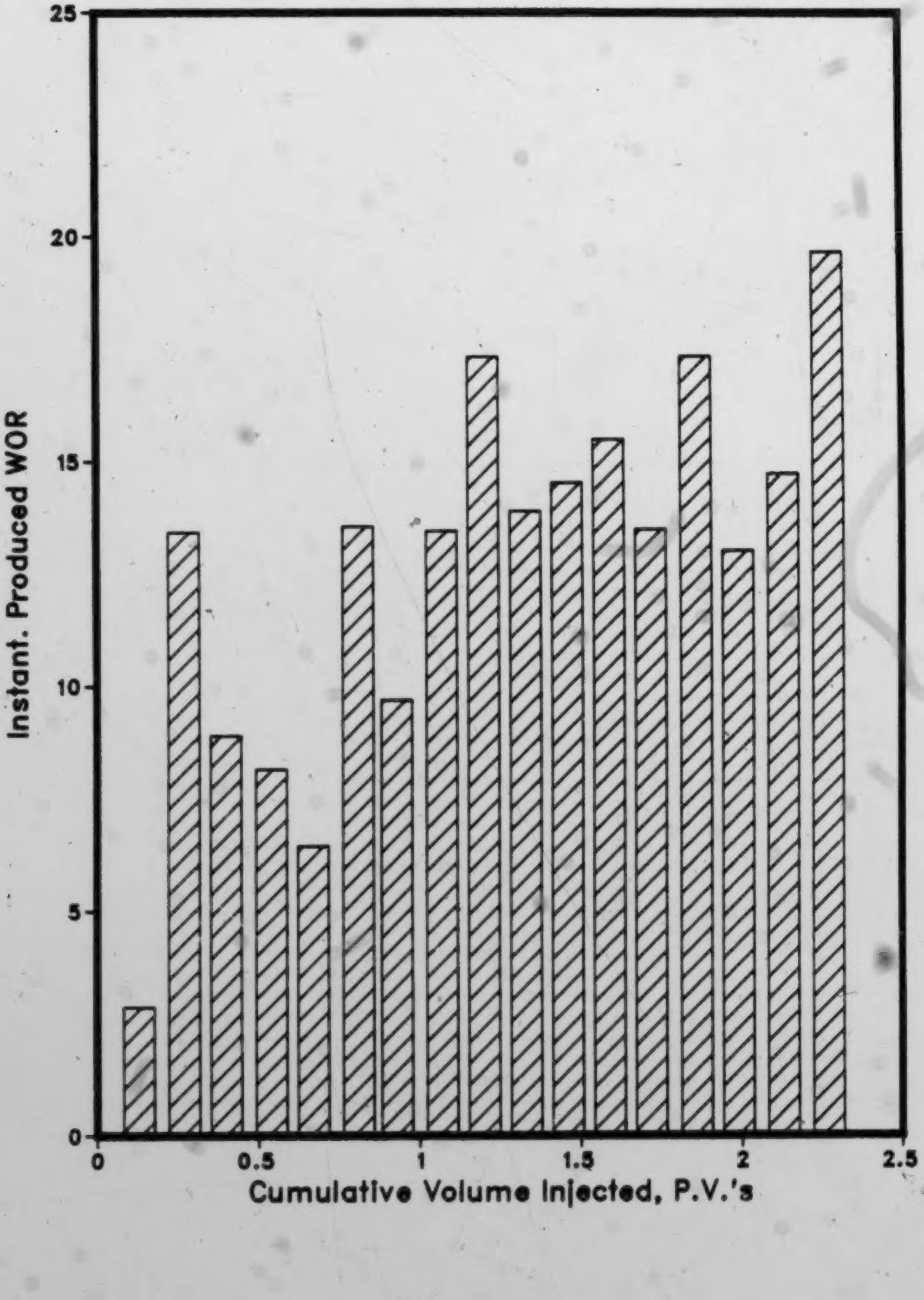

Figure 6.97 :Run 64 Steamflood of Bottom Water Model With a Partial Barrier Instanteous Oil/Steam Ratio vs. Cumulative Oil Produced

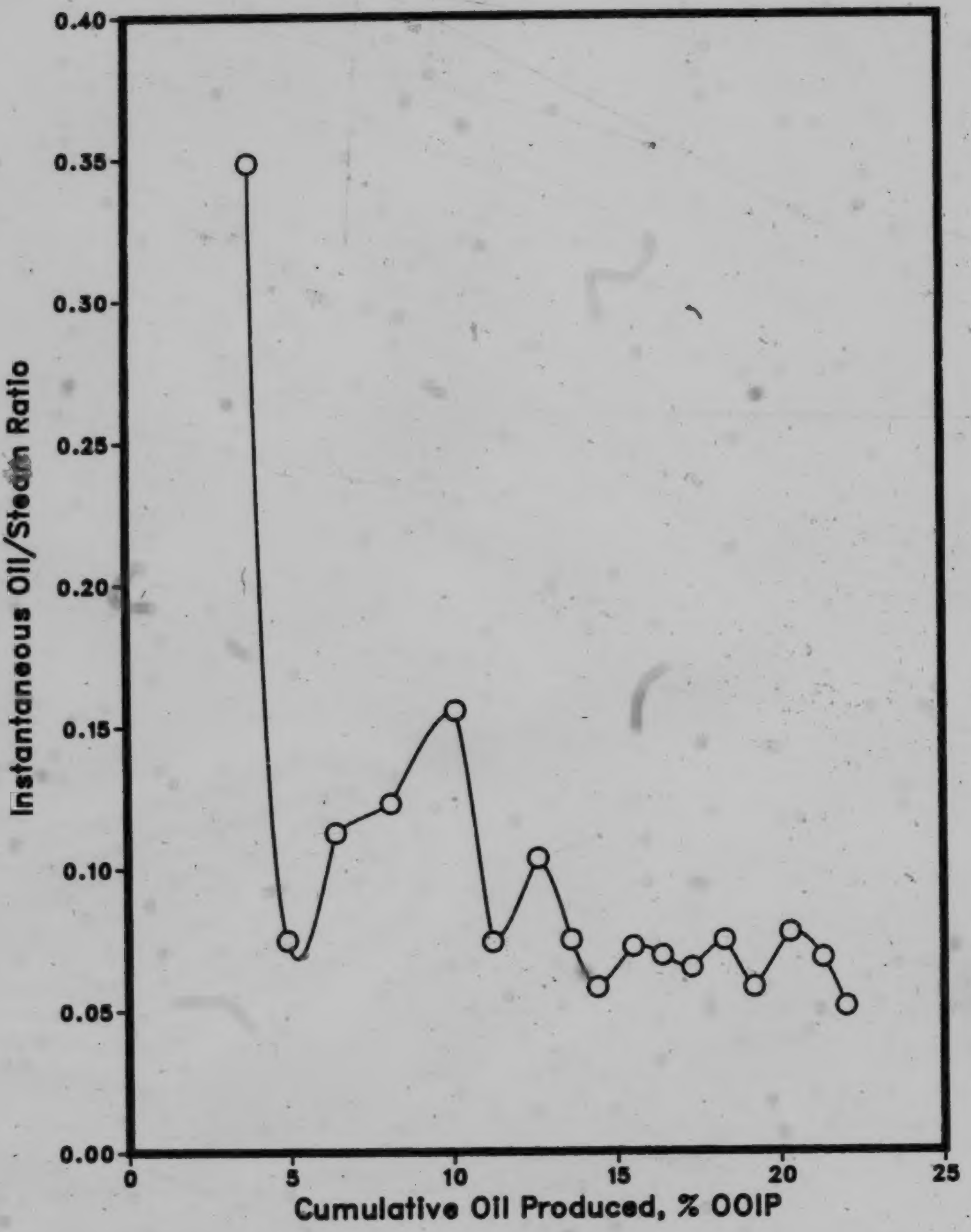

appeared to move faster through the upper half (oil zone) of the model during Run 64 it was concluded that less heat was lost to the underlying bottom water. Therefore Run 64 made better use of the injected steam than Run 63. A comparison of the temperature profiles of Runs 63 and 64 with Runs 49, 50, 51, 53 and 54 shows that the heat travelled faster in the lower region and slower in the upper region of the model during Runs 63 and 64. This indicates that the solvent-steamflood technique had a greater thermal efficiency than the partial barrier recovery strategy, due to reduced heat loss to the bottom water during the solvent-steamflood experiments. The cross-sectional temperature profiles for Runs 63 (Fig. A.247-A.250) and 64 (Fig. A.259-A.262) confirm the previous observations.

A comparison of the results of Runs 63 and 64 with the results of the previous solvent-steamflood experiments (Runs 49, 50, 51, 53 & 54) also indicates that the solvent-steamflood strategy was a more effective recovery technique. Figure 6.98 provides a comparison of a typical solvent-steamflood process conducted in a bottom water model (Run 50) and a conventional steamflood performed in the presence of a partial bottom water barrier (Run 64), both of which had similar bottom water thicknesses of 10.2% and 9.9% of the total model thickness, respectively. The comparison indicates that the recovery obtained in Run 50 (25.4% OOIP) was somewhat higher than that yielded by Run 64 (22.0% OOIP) even though Run 50 had a slightly thicker bottom water layer. The more favorable outcome of the solvent-steamflood process was due to steam being more directly injected into the oil region through the solvent channels. The injected heat had to travel upwards in the oil zone during the partial barrier experiments, which was not as thermally efficient as a solvent-steamflood. It was also reported by Alikhan and Farouq Ali [67] that the creation of a barrier in the field is generally difficult which makes this recovery method even less attractive.

Even though the solvent-steamfloods appeared to utilize the injected heat more efficiently, the partial barrier recovery technique did show promise. As well as a solvent-

Figure 6.98 :Comparison of Recoveries of a Solvent–Steamflood With Bottom Water Run 50 & a Steamflood with a Partial Bottom Water Barrier Run 64

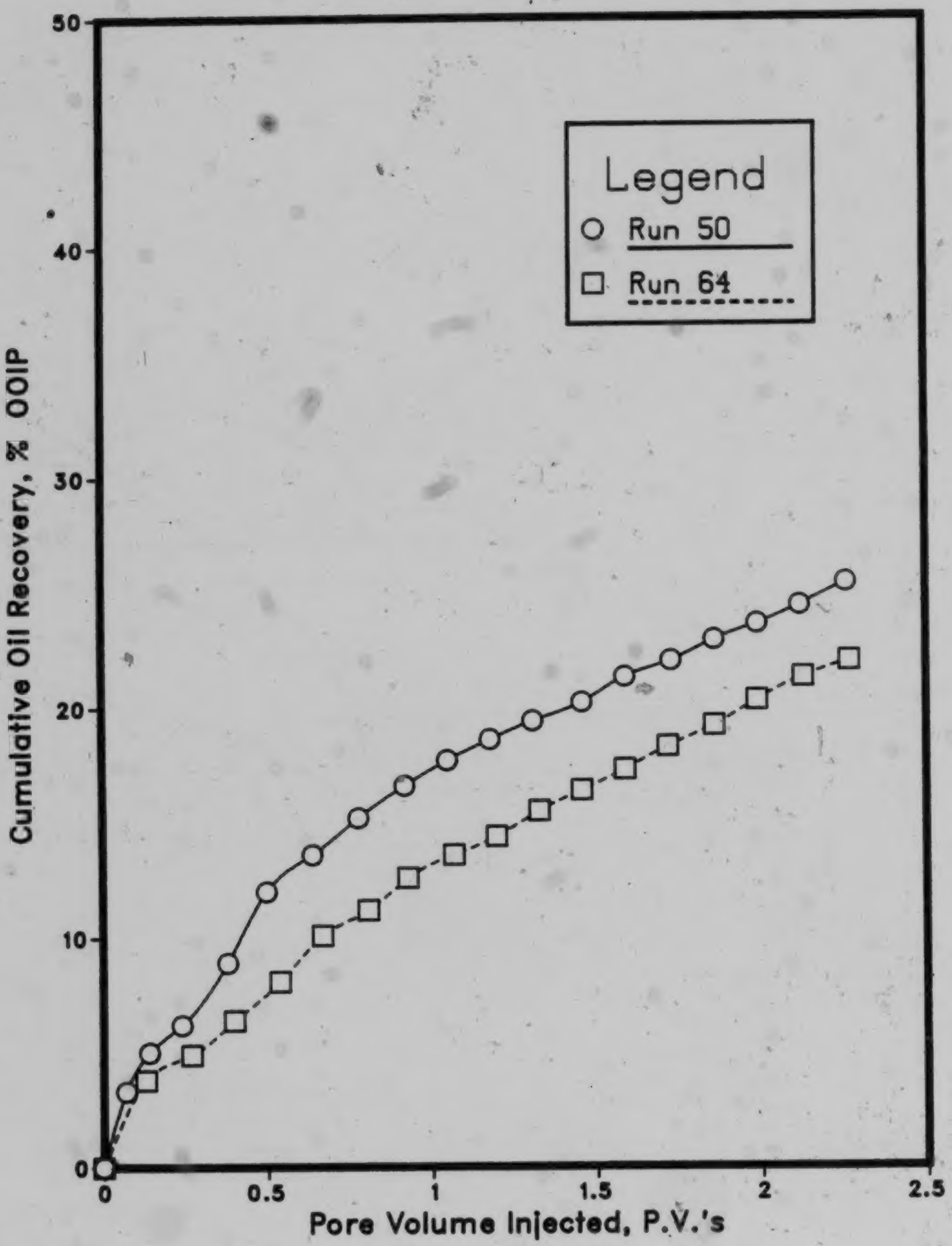

steamflood, the partial barrier method could also be used as a more thermally efficient alternative to a straight steamflood in a bottom water formation. Depending on the difference in costs and difficulties between injecting solvent (ie. solvent-steamflood) or creating a partial bottom water barrier as well as the comparative overall oil and solvent recoveries yielded for each recovery technique, the partial barrier method may in fact be more economical to implement in the field than a solvent-steamflood process. But from the experimental results of this study the solvent-steamflood appeared to be a better recovery process.

Effectiveness of Waterflooding Prior to Solvent and Steam Injection

Another objective of the research conducted was to determine the effectiveness of the solvent-steamflood process as an enhanced recovery technique. In Runs 47 and 48 a solvent-steamflood was conducted following a waterflood of a homogeneous model.

Both Runs 47 and 48 involved waterflooding the oil saturated model prior to injecting 0.10 pore volume of solvent and continuously steamflooding. The results for Runs 47 and 48 are provided in Tables 6.24 & 6.25 and 6.26 & 6.27, respectively. Initial model characteristics and the experimental results from the two runs were quite similar in many aspects such as porosities, initial and final oil and water saturations, and oil and solvent recoveries. The curves and bar plots provided for Runs 47 and 48 were also quite similar.

The similar recovery curves for the experiments are shown in Figures 6.99 (Run 47) and 6.103 (Run 48). A sharp rise is seen in the initial part of Figures 6.99 and 6.103 followed by a gradual decrease in the slope up until solvent injection and steamflooding. The initial rise in the curves represented the banking of oil at the production well due to waterflooding. The following decrease in the slope of the curves represents the breakthrough of the injected water. Further oil production occurred after water breakthrough due to the injected water displacing oil still existing in the model. The waterflood was continued until a water-oil ratio of approximately 20:1 was achieved. This value was chosen since many field waterflood operations are based on a WOR cutoff between 15 to 20. During solvent injection, the curves levelled off due to solvent mobilizing a small portion of oil in the model by viscosity reduction. Initiation of the steamflood resulted in another rise in the recovery curves because the oil mobilized by the solvent injection tended to form a bank in front of the steam zone. The mobilized oil was subsequently produced leading to a substantial increase in oil recovery at this stage of the experiment. After the steep increase, the slope of the recovery curves gradually declined due to the breakthrough of the injected steam at the production well. The gradual increase in the curves after steam breakthrough represents the additional oil recovered from both swept and unswept regions as a result of the steam mobilizing additional oil.

The bar plots of volume as a percentage of oleic phase in each sample collected versus the cumulative volume injected and instantaneous water/oil ratio versus cumulative volume injected for Runs 47 (Figures 6.100 & 6.101) and 48 (Figures 6.104 & 6.105) provide a good indication of when waterflooding and steamflooding were implemented and when water and steam breakthrough occurred during the experiments. Overlaying the bar plots on the respective recovery curves demonstrates how well the bar graphs correspond to the different stages of the runs such as water and steam breakthrough. Study of the water/oil ratio plots also revealed small peaks in the later stages of the steamflood which represent the eventual production of small pockets of oil in the model.

The plots of instantaneous oil/steam ratio versus cumulative oil produced shown in Figures 6.102 (Run 47) and 6.106 (Run 48) also confirm that steam breakthrough took place early in the continuous steamflood due to the high initial water saturation.

The top view temperature contours provided for Runs 47 (Fig. A.263-A.270) and 48 (Fig. A.274-A.281) demonstrate that during the waterflood and the solvent-steamflood the injected water, solvent and steam advanced slightly faster through the lower portion of the model. The cross-sectional temperature profiles for Runs 47 (Fig. A.271-A.273) and 48 (Fig. A.282-A.285) provided the profiles for both experiments after every 0.50 pore volumes injected once the solvent-steamflood had been initiated (ie. after waterflooding). The cross-sectional profiles for both runs indicated, as did the top view temperature profiles, the injected heat of the steam advanced faster through the lower portion of the model.

During the initial stages of the run an oil bank formed ahead of the water front resulting in an increased amount of oil being produced. Water breakthrough occurred at the production well once the oil bank had been produced and a subsequent drop in oil

Table 6.24 : Run 47A Waterflood Prior to Solvent-Steamflood of Homogeneous Model

HC Pore Volume : 13125.0 cc
Pore Volume : 14110.0 cc
Bulk Volume : 42005.0 cc
Porosity : 33.6%

Type of Oil Used : Faxam-100
Initial Model Temperature : 3.00 C
Water Feed Flow Rate : 200.00 cc/min
Initial Oil Saturation : 93.0%
Initial Water Saturation : 7.0%

Net Oil Recovery : 19.1%

Final Oil Saturation : 75.3%

Cylinder No.	Tot. Vol. Inj. (cc)	Cum. Vol. Inj (cc)	Cum. Vol. Inj (P.V.)	Oil Prod. (cc)	Cum. Oil Rec. (cc)	Cum. Oil Rec. (%OOIP)	Inst. Prod. WOR	Inst. Oil Prod. % of Sample
1	1830.0	1830.0	0.13	1055.0	1055.0	8.0%	0.73	57.7%
2	2010.0	3840.0	0.27	290.0	1345.0	10.2%	5.93	14.4%
3	1955.0	5795.0	0.41	260.0	1605.0	12.2%	6.52	13.3%
4	2005.0	7800.0	0.55	165.0	1770.0	13.5%	11.15	8.2%
5	1960.0	9760.0	0.69	150.0	1920.0	14.6%	12.07	7.7%
6	2060.0	11820.0	0.84	125.0	2045.0	15.6%	15.48	6.1%
7	1940.0	13760.0	0.98	110.0	2155.0	16.4%	16.64	5.7%
8	2030.0	15790.0	1.12	95.0	2250.0	17.1%	20.37	4.7%
9	1925.0	17715.0	1.26	85.0	2335.0	17.8%	21.65	4.4%
10	2005.0	19720.0	1.40	85.0	2420.0	18.4%	22.59	4.2%
11	1960.0	21680.0	1.54	85.0	2505.0	19.1%	22.06	4.3%

Table 6.25 : Run 47B Solventflood Following a Waterflood of Homogeneous Model

HC Pore Volume :	10620.0 cc	Type of Oil Used :	Faxam-100
Pore Volume :	14110.0 cc	Initial Model Temperature :	3.00 C
Bulk Volume :	42005.0 cc	Water Feed Flow Rate :	200.00 cc/min
Porosity :	33.6%	Boiler Feed Flow Rate :	29.20 cc/min
Initial Oil Satn. :	75.3%	Total Flow Rate of Steam :	229.20 cc/min
Initial H2O Satn. :	24.7%	Solvent Flow Rate :	200.00 cc/min
Solvent Vol. Inj.:	1400.0 cc (10.0% PV)	Steam Vol. Injected :	27235 cc (1.93 PV)

Net Oil Recovery : 33.5% **Solvent Recovery : 44.9%** **Final Oil Saturation : 61.9%**

Cyl. No.	Solvent Conc. (%)	Tot. Vol. Inj. (cc)	Cum. Vol. Inj.		HC Prod. (cc)	Oil Prod. (cc)	Cum. Oil Rec.		Cum. Sol. Rec.		Oil-Steam Ratio	Inst Prod. WOR	Inst. HC Prod. % of Sample
			(cc)	(P.V.)			(cc)	(%OOIP)	(cc)	(%)			
1	6%	1340	1340	0.09	45	42	42	0.3%	3	0.2%	0.0000	28.78	3.4%
2	60%	1440	2780	0.20	960	384	426	3.2%	579	41.4%	0.0000	0.50	66.7%
3	12%	1820	4600	0.33	260	229	655	5.0%	610	43.6%	0.1667	6.00	14.3%
4	6%	2070	6670	0.47	190	179	834	6.4%	621	44.4%	0.1011	9.89	9.2%
5	4%	1980	8650	0.61	120	115	949	7.2%	626	44.7%	0.0645	15.50	6.1%
6	2%	2100	10750	0.76	100	98	1047	8.0%	628	44.9%	0.0500	20.00	4.8%
7	1%	1920	12670	0.90	80	79	1126	8.6%	629	44.9%	0.0435	23.00	4.2%
8	0%	1895	14565	1.03	75	75	1201	9.2%	629	44.9%	0.0412	24.27	4.0%
9	0%	1975	16540	1.17	85	85	1286	9.8%	629	44.9%	0.0450	22.24	4.3%
10	0%	2000	18540	1.31	90	90	1376	10.5%	629	44.9%	0.0471	21.22	4.5%
11	0%	2060	20600	1.46	150	150	1526	11.6%	629	44.9%	0.0785	12.73	7.3%
12	0%	2030	22630	1.60	115	115	1641	12.5%	629	44.9%	0.0601	16.65	5.7%
13	0%	2005	24635	1.75	85	85	1726	13.2%	629	44.9%	0.0443	22.59	4.2%
14	0%	2000	26635	1.89	80	80	1806	13.8%	629	44.9%	0.0417	24.00	4.0%
15	0%	2000	28635	2.03	85	85	1891	14.4%	629	44.9%	0.0444	22.53	4.3%

Figure 6.99 :Run 47 Waterflood Followed by Solvent–Steamflood
Cumulative Oil Recovery Vs. Pore Volumes Injected

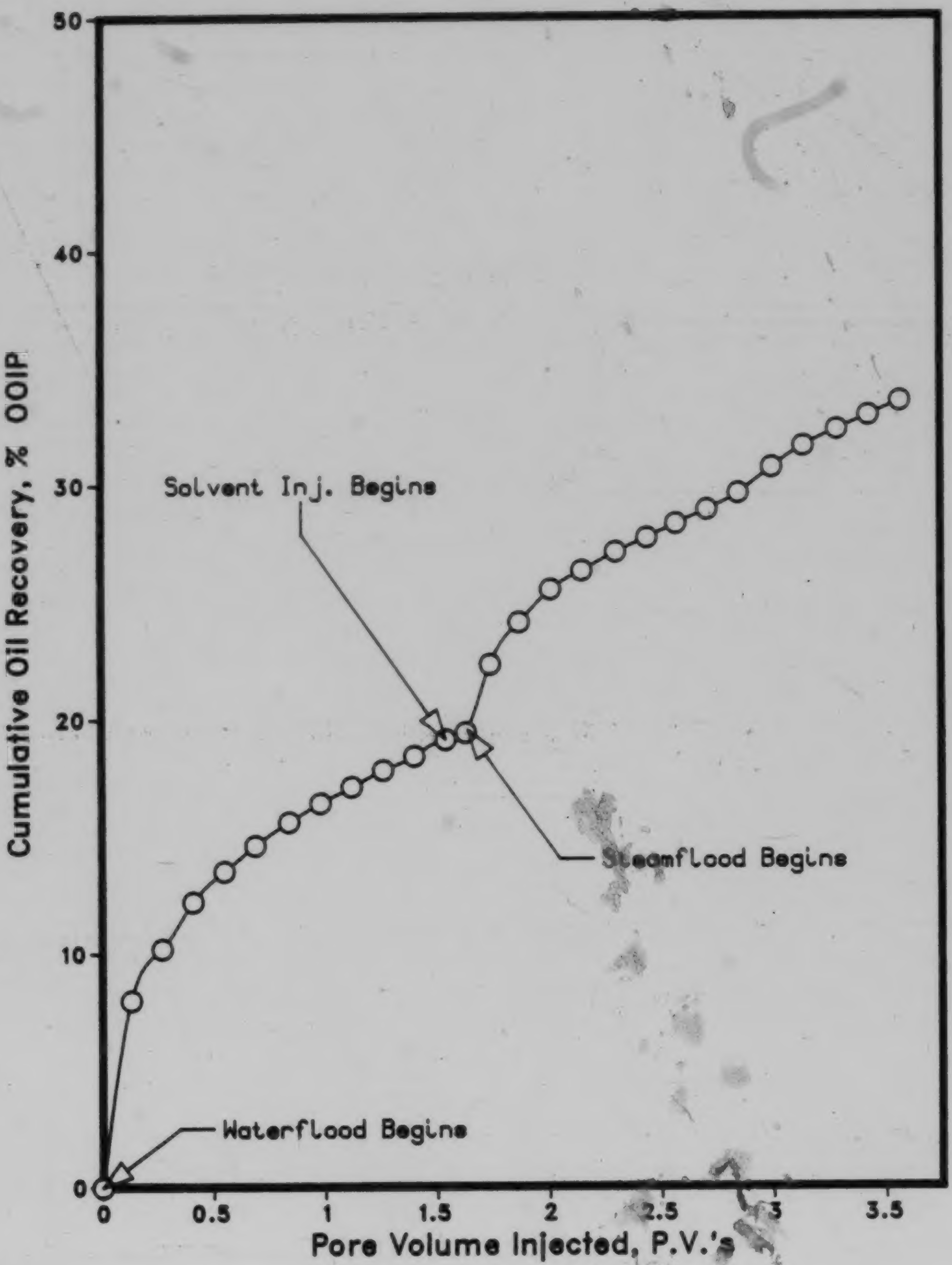

Figure 6.100 :Run 47 Waterflood Followed By Solvent–Steamflood
Oleic Phase in Each Sample Vs. Cumulative Volume Injected

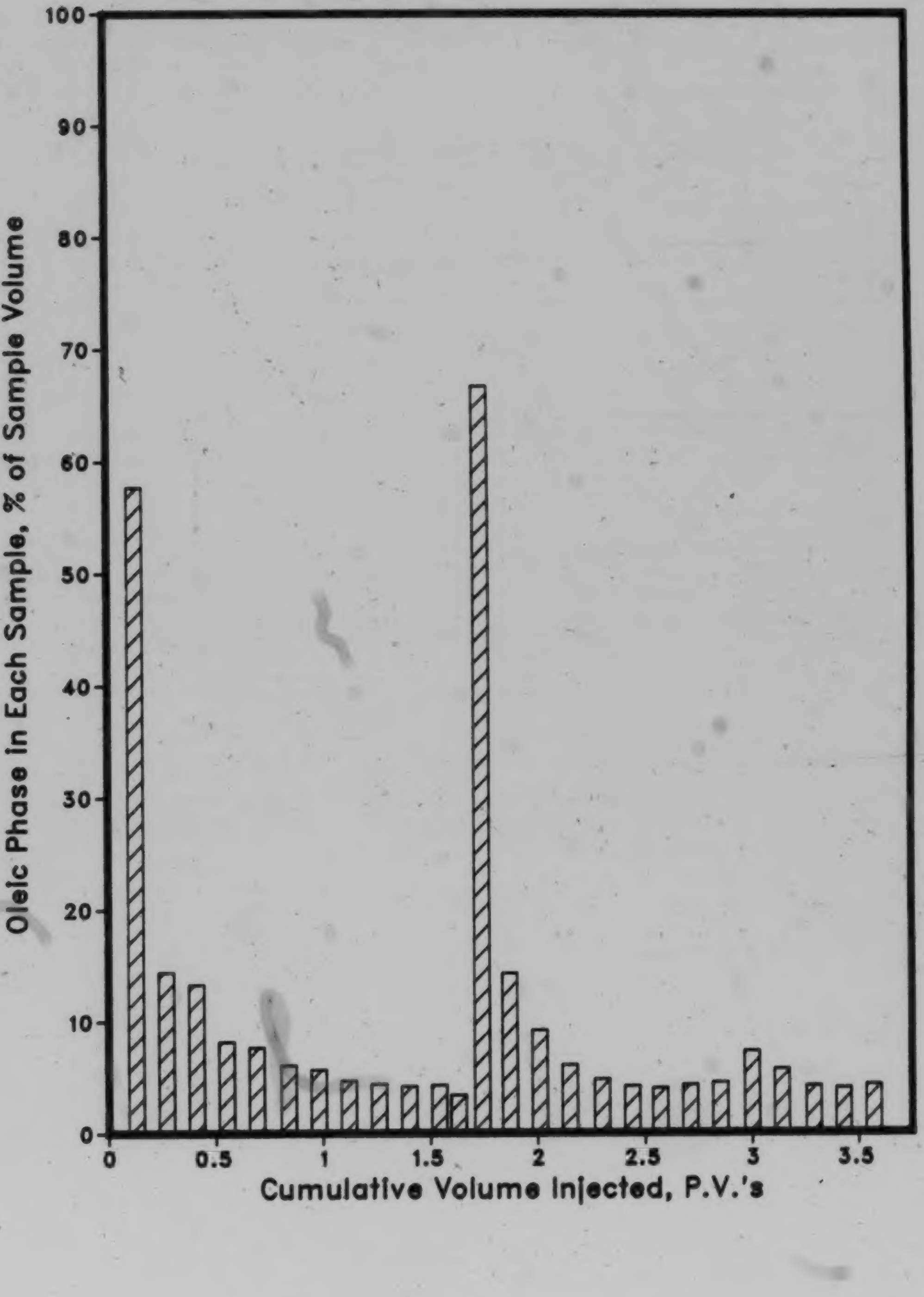

Figure 6.101 :Run 47 Waterflood Followed By Solvent--Steamflood Instantaneous Produced WOR Vs. Cumulative Volume Injected

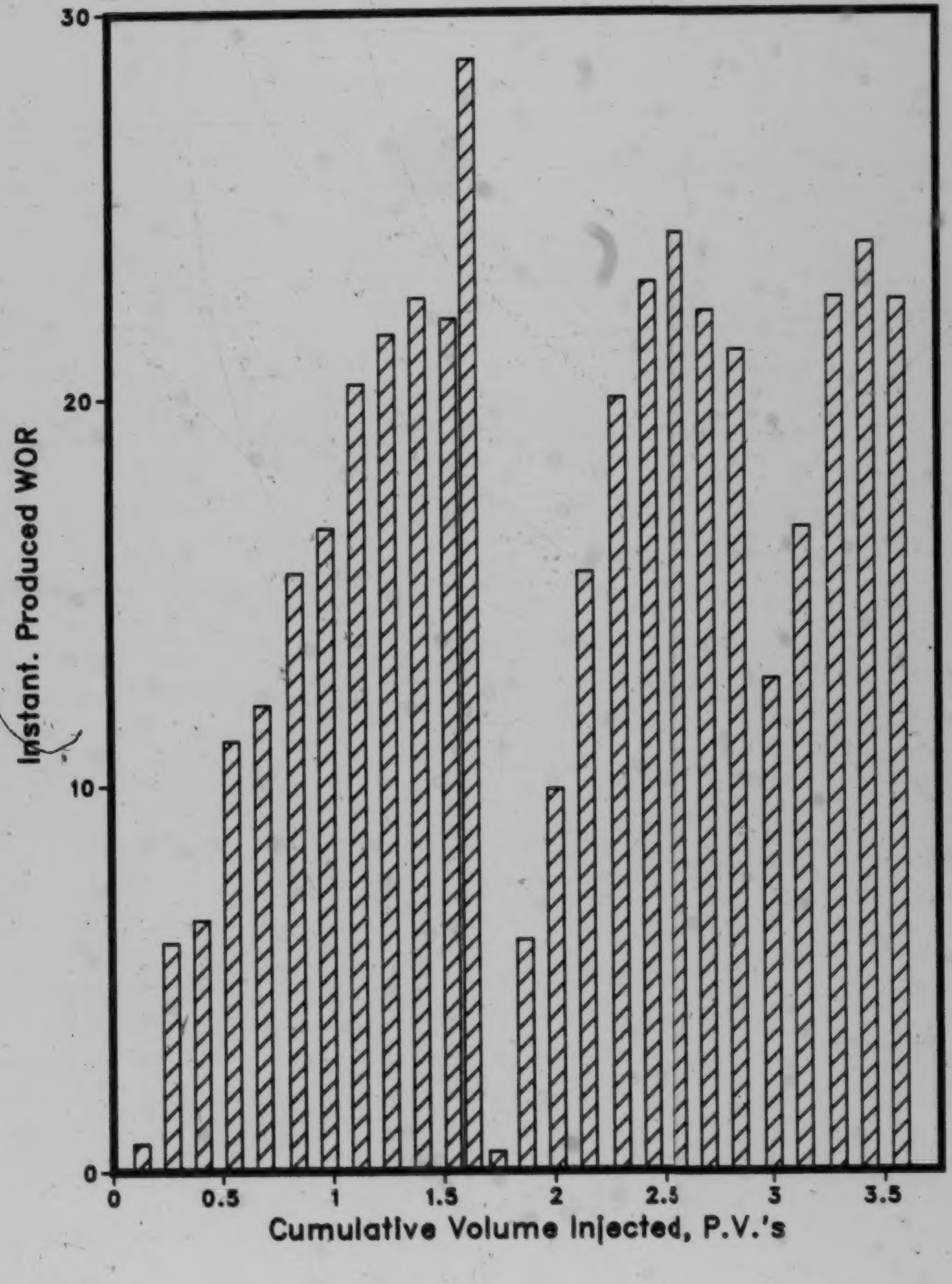

Figure 6.102 :Run 47 Waterflood Followed by Solvent–Steamflood Instantaneous Oil/Steam Ratio Vs. Cumulative Oil Produced

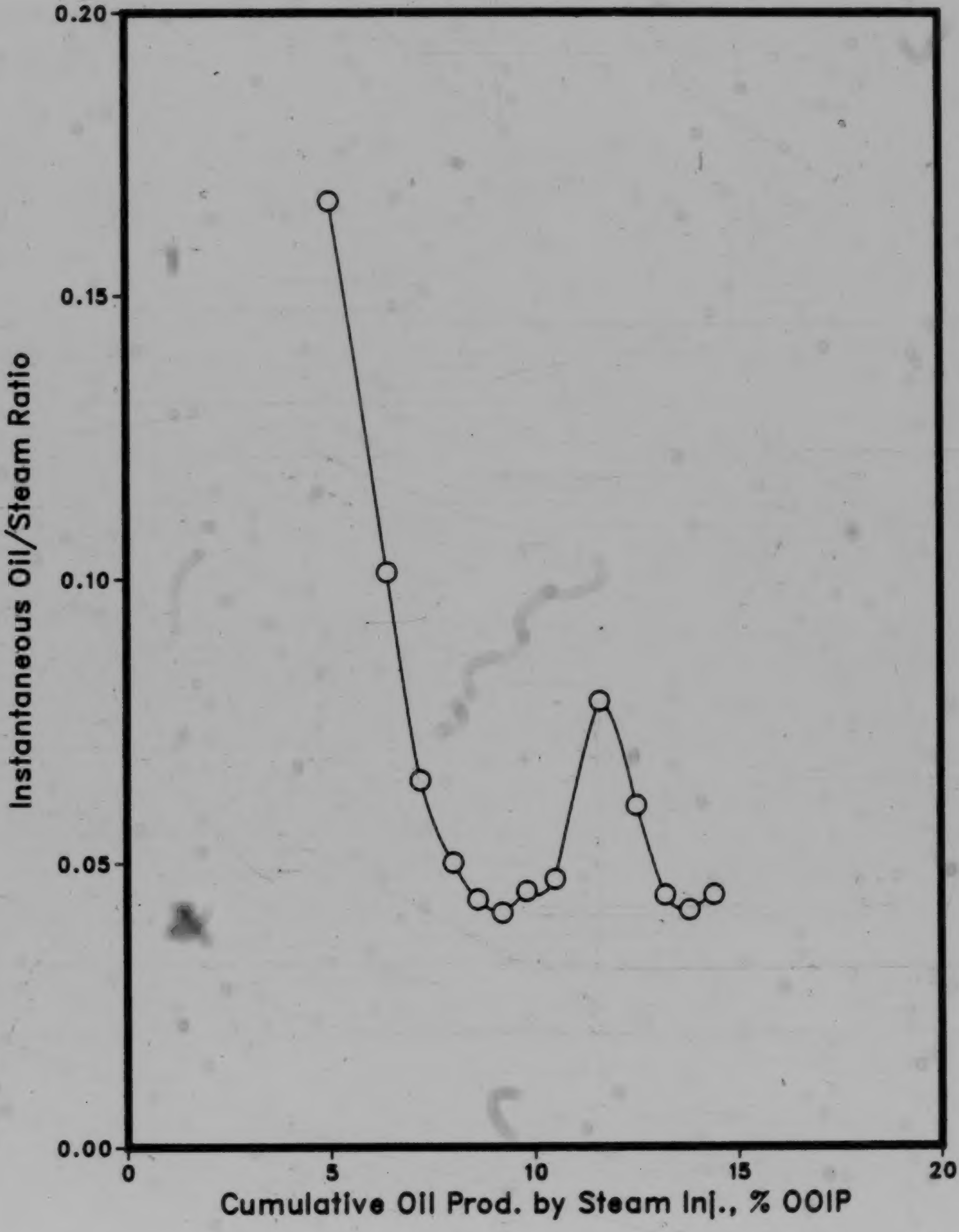

Table 6.26 : Run 48A Waterflood Prior to Solvent-Steamflood of Homogeneous Model

HC Pore Volume : 13000.0 cc
Pore Volume : 14030.0 cc
Bulk Volume : 42005.0 cc
Porosity : 33.4%

Type of Oil Used : Faxam-100
Initial Model Temperature : 3.00 C
Water Feed Flow Rate : 200.00 cc/min
Initial Oil Saturation : 92.7%
Initial Water Saturation : 7.3%

Net Oil Recovery : 19.8%

Final Oil Saturation : 74.3%

Cylinder No.	Tot. Vol. Inj. (cc)	Cum. Vol. Inj (cc)	Cum. Vol. Inj (P.V.)	Oil Prod. (cc)	Cum. Oil Rec (cc)	Cum. Oil Rec (%OOIP)	Inst. Prod. WOR	Inst. Oil Prod. % of Sample
1	2030.0	2030.0	0.14	1035.0	1035.0	8.0%	0.96	51.0%
2	2020.0	4050.0	0.29	320.0	1355.0	10.4%	5.31	15.8%
3	1865.0	5915.0	0.42	240.0	1595.0	12.3%	6.77	12.9%
4	2000.0	7915.0	0.56	165.0	1760.0	13.5%	11.12	8.3%
5	1870.0	9785.0	0.70	135.0	1895.0	14.6%	12.85	7.2%
6	1985.0	11770.0	0.84	110.0	2005.0	15.4%	17.05	5.5%
7	1885.0	13655.0	0.97	105.0	2110.0	16.2%	16.95	5.6%
8	2040.0	15695.0	1.12	100.0	2210.0	17.0%	19.40	4.9%
9	2045.0	17740.0	1.26	95.0	2305.0	17.7%	20.53	4.6%
10	1980.0	19720.0	1.41	90.0	2395.0	18.4%	21.00	4.5%
11	1935.0	21655.0	1.54	90.0	2485.0	19.1%	20.50	4.7%
12	2085.0	23740.0	1.69	85.0	2570.0	19.8%	23.53	4.1%

Table 6.27 : Run 48B Solvent-Steamflood Following a Waterflood of Homogeneous Model

HC Pore Volume :	10430.0 cc	Type of Oil Used :	Faxam-100
Pore Volume :	14030.0 cc	Initial Model Temperature :	3.00 C
Bulk Volume :	42005.0 cc	Water Feed Flow Rate :	200.00 cc/min
Porosity :	33.4%	Boiler Feed Flow Rate :	29.20 cc/min
Initial Oil Satn. :	74.3%	Total Flow Rate of Steam :	229.20 cc/min
Initial H2O Satn. :	25.7%	Solvent Flow Rate :	200.00 cc/min
Solvent Vol. Inj.:	1400.0 cc (10.0% PV)	Steam Vol. Injected :	30235 cc (2.16 PV)

Net Oil Recovery : 35.5% **Solvent Recovery : 58.9%** **Final Oil Saturation : 59.8%**

Cyl. No.	Solvent Conc. (%)	Tot. Vol. Inj. (cc)	Cum. Vol. Inj.		HC Prod (cc)	Oil Prod. (cc)	Cum. Oil Rec.		Cum. Sol. Rec.		Oil-Steam Ratio	Inst Prod. WOR	Inst. HC Prod. % of Sample
			(cc)	(P.V.)			(cc)	(%OOIP)	(cc)	(%)			
1	6%	1120	1340	0.10	30	28	28	0.2%	2	0.1%	0.0000	36.33	2.7%
2	58%	1940	3280	0.23	1195	502	530	4.1%	695	49.6%	0.0000	0.62	61.6%
3	25%	1900	5180	0.37	315	236	766	5.9%	774	55.3%	0.1987	5.03	16.6%
4	13%	2090	7270	0.52	180	157	923	7.1%	797	56.9%	0.0942	10.61	8.6%
5	8%	1960	9230	0.66	80	74	997	7.7%	803	57.4%	0.0426	23.50	4.1%
6	6%	2105	11335	0.81	100	94	1091	8.4%	809	57.8%	0.0499	20.05	4.8%
7	4%	1940	13275	0.95	80	77	1168	9.0%	812	58.0%	0.0430	23.25	4.1%
8	5%	2015	15290	1.09	150	143	1311	10.1%	819	58.5%	0.0804	12.43	7.4%
9	3%	1975	17265	1.23	95	92	1403	10.8%	822	58.7%	0.0505	19.79	4.8%
10	2%	2095	19360	1.38	95	93	1496	11.5%	824	58.9%	0.0475	21.05	4.5%
11	0%	2045	21405	1.53	50	50	1546	11.9%	824	58.9%	0.0251	39.90	2.4%
12	0%	2180	23585	1.68	100	100	1646	12.7%	824	58.9%	0.0481	20.80	4.6%
13	0%	1960	25545	1.82	110	110	1756	13.5%	824	58.9%	0.0595	16.82	5.6%
14	0%	2030	27575	1.97	100	100	1856	14.3%	824	58.9%	0.0518	19.30	4.9%
15	0%	1975	29550	2.11	95	95	1951	15.0%	824	58.9%	0.0505	19.79	4.8%
16	0%	2085	31635	2.25	95	95	2046	15.7%	824	58.9%	0.0477	20.95	4.6%

Figure 6.103 :Run 48 Waterflood Followed By Solvent–Steamflood Cumulative Oil Recovery Vs. Pore Volumes Injected

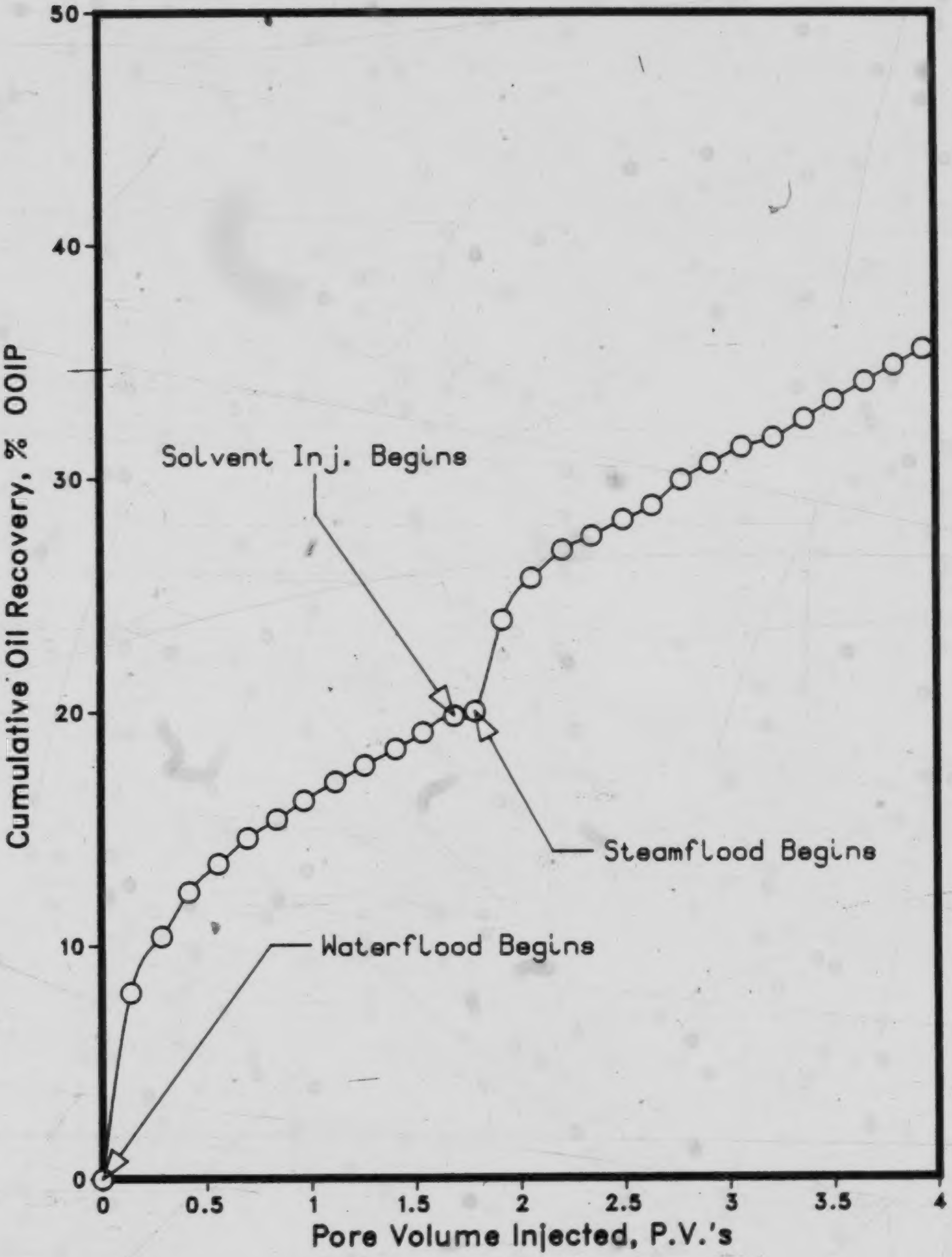

Figure 6.104 :Run 48 Waterflood Followed By Solvent–Steamflood Oleic Phase in Each Sample Vs. Cumulative Volume Injected

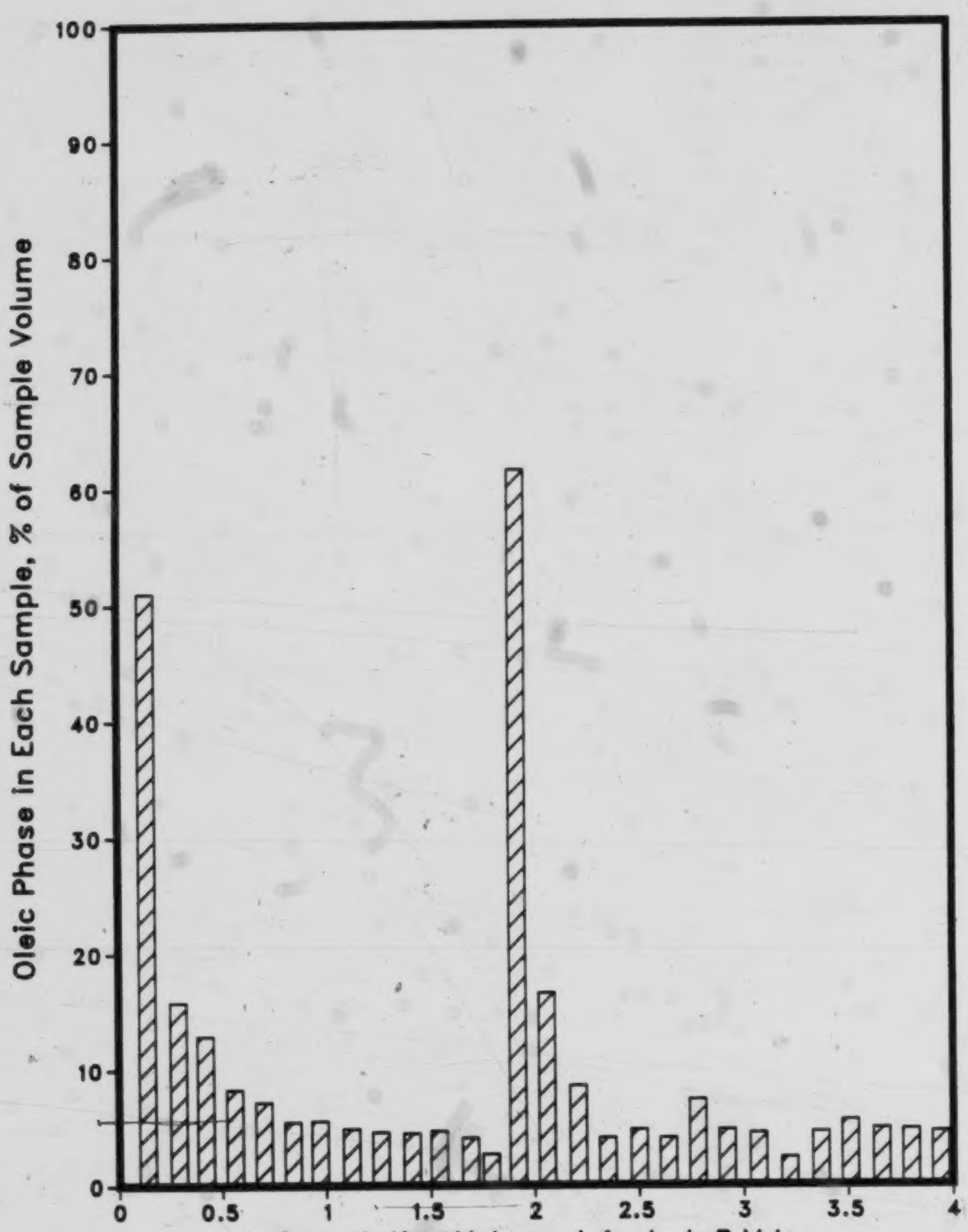

Figure 6.105 :Run 48 Waterflood Followed By Solvent-Steamflood Instantaneous Produced WOR Vs. Cumulative Volume Injected

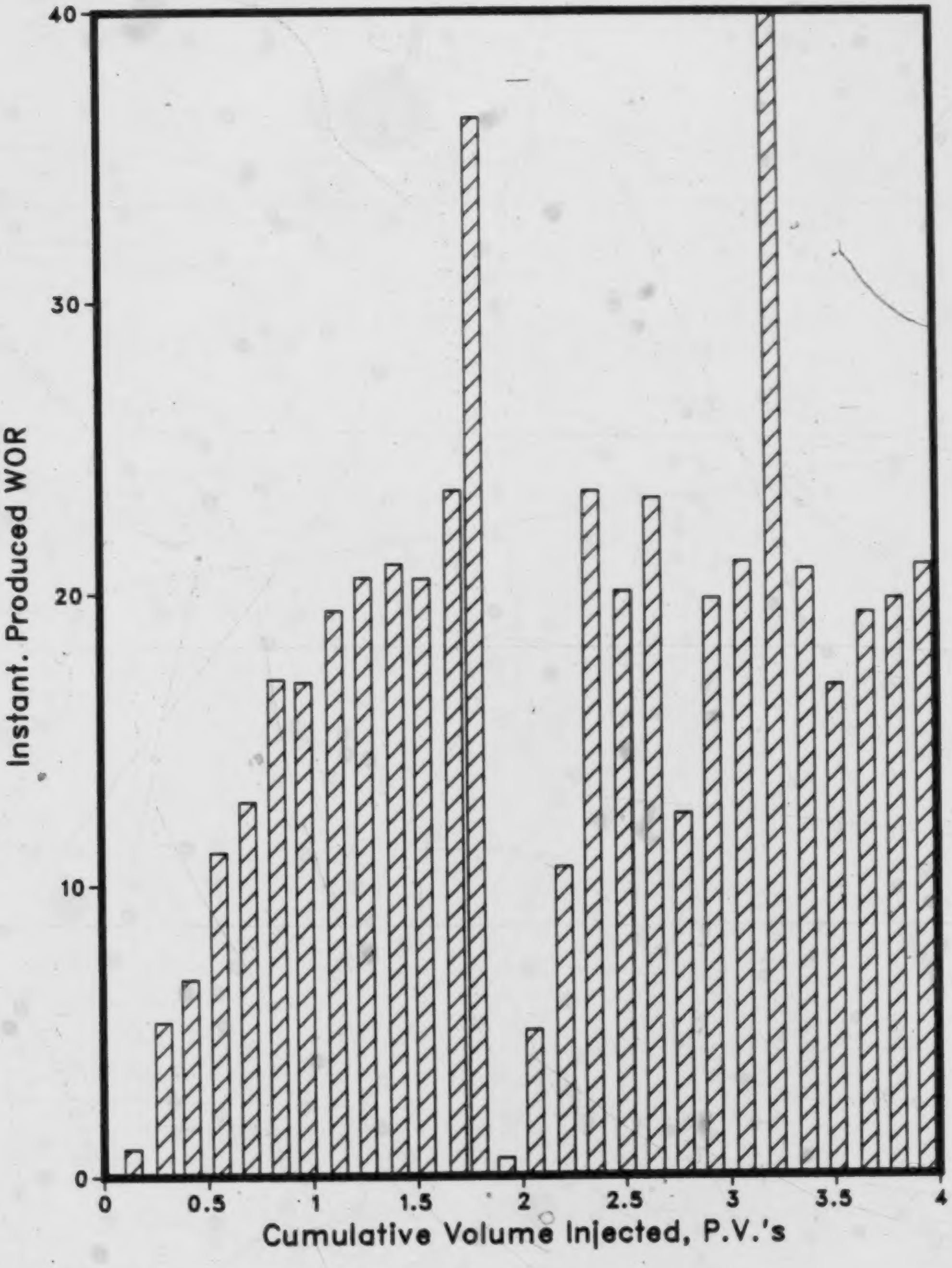

Figure 6.106 :Run 48 Waterflood Followed by Solvent-Steamflood
Instanteous Oil/Steam Ratio vs.Cumulative Oil Produced

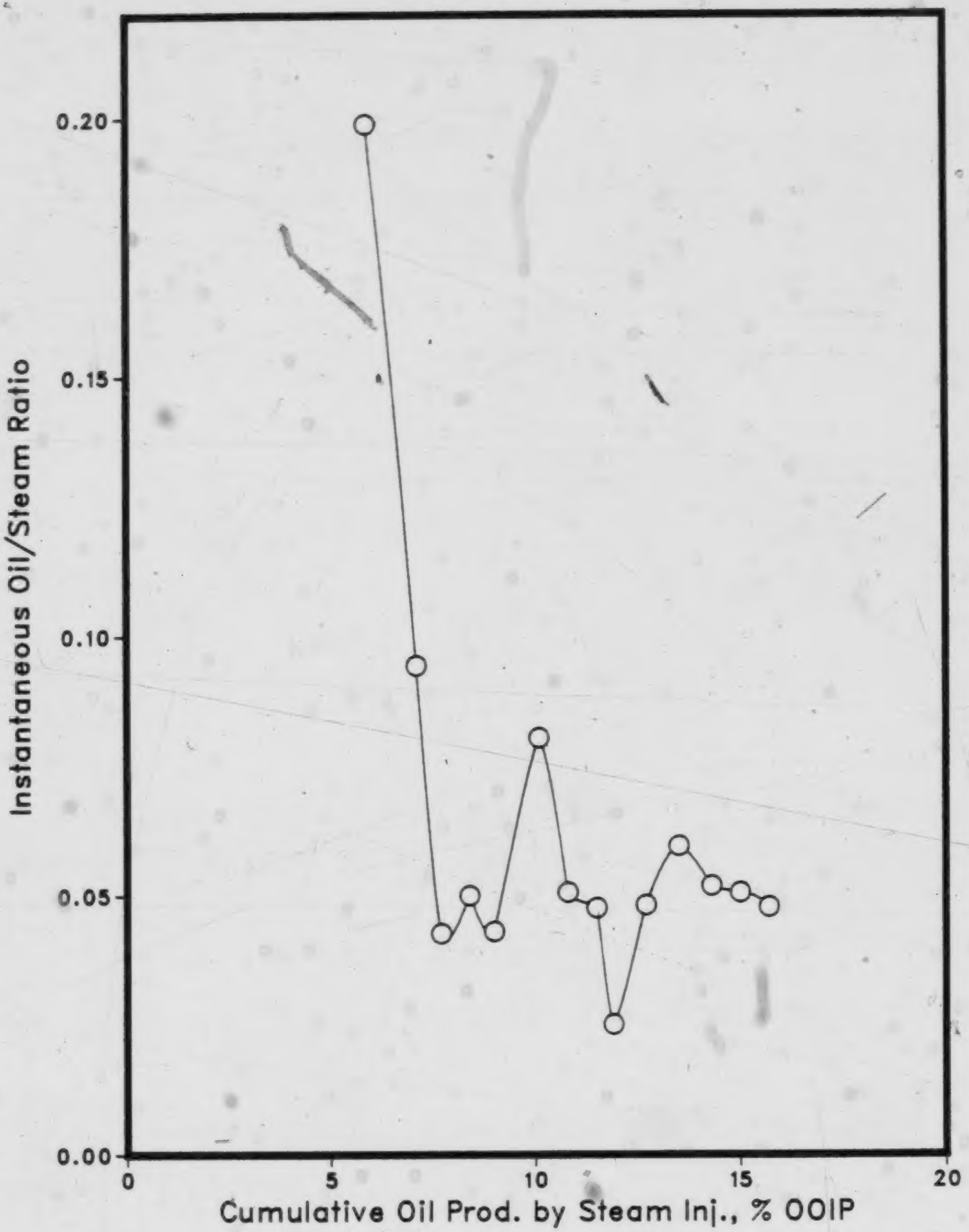

production resulted. When the desired WOR was attained, a 0.10 pore volume solvent slug was injected into the model which immediately began mixing with the immobile oil, reducing the oil viscosity. Initiation of continuous steam injection caused the oil/solvent mixture in the model to bank up ahead of the steam front. This resulted in additional oil production due to the recovery of the oil/solvent bank at the production well. Steam breakthrough and a preceding slump in oil output took place after the larger portion of the oil/solvent bank had been produced. Following steam breakthrough, the high temperature steam continued to sweep through the model mobilizing more oil from both the swept and unswept zones.

Solvent recoveries for Runs 47 (44.9%) and 48 (58.9%) varied slightly but were still relatively similar. Comparing the solvent recoveries for these two runs to Runs 44 (70.4%) and 45 (71.2%), it is apparent that Runs 47 and 48 have much lower solvent recoveries. In Runs 44 and 45 the solvent was injected into a model that was oil saturated with a connate water saturation. However, in Runs 47 and 48 the solvent was injected into the model after it had been waterflooded, and therefore the initial water saturation was much higher and a residual oil saturation existed.

As was discussed in the previous section dealing with the solvent recovery, results for Runs 47 and 48 were consistent with Alikhan [64]'s findings. He stated that a solvent-steamflood process implemented in an oil saturated model yielded a greater solvent recovery than when performed in a waterflooded model. The nature of the solvent recovery in these two instances could be related to increased mixing of solvent with oil in the waterflooded situation which caused more solvent to remain in the model as a residual hydrocarbon saturation. The varying degree of oil-solvent mixing in the two different types of runs may be a result of the solvent having a higher relative permeability in the oil saturated experiments than the waterflooded cases. The higher relative permeability would create more distinct solvent channelling and less mixing with the in-place oil, and hence a larger solvent recovery. For the waterflooded situation, the difference in relative permeability between the water and the solvent would be less than for the oil saturated case due to the higher initial water saturation. The solvent would not flow through the model as easily thus blending more thoroughly with the inplace oil. Mixing of solvent and oil would be more pronounced in the waterflooded case. This would decrease the amount solvent recovered due to the remainder of a higher residual solvent slug material saturation. The difference in the solvent recoveries in the two runs may also be due to changes in interfacial tension when solvent mixes with the in-place oil.

The overall oil recoveries for Runs 47 (33.5% OOIP) and 48 (35.5% OOIP) were higher than the recoveries obtained from the conventional steamfloods of the homogeneous model performed in Runs 26 (31.8% OOIP) and 27 (32.2% OOIP) as reported by Proctor, George and Farouq Ali [63]. The recoveries for the solvent-steamfloods of a homogeneous model (Runs 44 (27.1% OOIP), 45 (30.0% OOIP) & 46 (27.7% OOIP)) reported in this study also indicate that Runs 47 and 48 yielded a greater overall oil recovery. The oil recoveries for the waterflood cases (Runs 47 & 48) were higher because the solvent was able to blend with inplace oil more thoroughly than during the oil saturated experiments (Runs 26, 27, 44, 45 & 46). Alikhan also stated that for a high initial oil saturation the solvent slug is displaced as efficiently as the in-place oil, thus the advantage of using the solvent is partially lost and the oil recovery is diminished. However, for a waterflooded porous media the solvent is able to mix more extensively with the oil allowing the injected steam to contact a higher saturation of the solvent slug material leading to improved oil recovery.

Comparing the oil recovery for Runs 47 and 48 with those for the previous experiments using a homogeneous model and Faxam-100, it was noted that Runs 47 and 48 supplied the highest oil recovery of all the experiments performed using a homogeneous model saturated with Faxam-100 oil which includes the steamfloods reported by Proctor, George and Farouq Ali [63] (Runs 26 & 27) and the solvent-steamfloods conducted in this research (Runs 44, 45 & 46). The information obtained from Runs 47 and 48 agrees closely with the results recorded by Alikhan [64]. Performing solvent-steamfloods on waterflooded reservoirs to improve oil recovery shows promise as an enhanced heavy oil recovery technique.

Heat Flow Analysis

The objective of this analysis was to obtain an understanding of the heat transfer occurring in the low pressure model during an experiment. In order to simplify the analysis a base steamflood (Run 26) experiment was used in the study.

Lauwerier Equation

The first stage of the analysis involved comparing the temperature contours constructed for Run 26 (Fig. A.286-A.292) with results obtained by applying the Lauwerier equation to the temperature profiles. The purpose of this comparison was to observe if the injection process in the model more closely represented a hot waterflood as opposed to the desired steamflood.

The Lauwerier equation represents formation heating by hot fluid injection which does not possess latent heat of vaporization. If hot water is injected into a formation, a well-defined temperature distribution is established in the porous medium. Since hot water is the injected fluid the heating in the formation is due to sensible heat content and not the latent heat as is the case in steam injection. According to Lauwerier, the temperature at any particular time at the injection point is the same as the temperature of the injected fluid. The temperature in the reservoir decreases steadily with distance, eventually approaching the initial reservoir temperature (T_R) as one moves away from the injection point. As greater amounts of the hot fluid are introduced the temperature at each point in the formation increases until the injected fluid temperature is reached at the infinite time.

As derived by Lauwerier[68], the temperature (T) at any linear distance (x) or radial distance (r) from the injection point is given by the proceeding equation.

$$T = T_R + (T_F - T_R)\,\mathrm{erfc}\left[\frac{x_D}{2\sqrt{t_D - x_D}}\right] \qquad \text{for} \quad t_D > x_D$$

$$T = T_R \qquad \text{for} \quad t_D \leq x_D$$

Dimensionless distance $x_D = \dfrac{4\,(24)\,k_{hob} M_{ob} A}{5.615\, M_s \rho_w i_w h_t}$

Dimensionless time $t_D = \dfrac{4\, k_{hob} M_{ob} A}{M_s^2} \cdot \dfrac{t}{h_t^2}$

Where k_{hob} - thermal conductivity of overburden (BTU/hr-ft-^{0}F)
M_{ob} - heat capacity of overburden (BTU/ft^3-^{0}F)
M_s - heat capacity of heated sand (BTU/ft^3-^{0}F)
t - time (hr)
h_t - gross thickness (ft)
ρ_w - density of injected fluid (lb/ft^3)
c_w - specific heat of injected fluid (BTU/lb-^{0}F)
A - area (ft^2)

Where A = bx or $A = \pi r^2$
b - width (ft)
r - radial distance (ft)
x - linear distance (ft)

All of the temperarture profiles for Run 26 consist of two sets of contours. One set represents the upper half of the model while the other contour describes the lower portion. A computer program was created which utilized the Lauwerier equation and the temperature contours for Run 26 (0.25 to 1.00 P.V.). The computer program is given on page 577 of Appendix B. The area (A) used in this study was defined as the area existing between a particular temperature contour and the injection point. The area covered by each corresponding temperature on each profile was measured by a planimeter and then substituted into the Lauwerier equation in order to obtain a estimated temperature related to the measured area.

From the analysis, Tables 6.28 and 6.29 were prepared, which list the portion of model being represented, the amount of fluid injected in pore volumes prior the specific contour, the actual contour line temperature used to measure the previously discussed area and the temperature yielded by the Lauwerier equation corresponding to the area.

Table 6.28 : Heat Flow Analysis of Model Using The Lauwerier Equation (Experiment 26)

Portion of Model	Pore Volume Injected	Actual Contour Temp. (C)	Lauwerier Equation Temp. (C)	Portion of Model	Pore Volume Injected	Actual Contour Temp. (C)	Lauwerier Equation Temp. (C)
Upper	0.25	10	15.17	Upper	0.75	10	3.00
		20	41.08			20	36.41
Inj. Rate		30	55.49	Inj. Rate		30	54.53
1.0270 B/D		40	59.74	1.0270 B/D		40	61.94
		50	63.45			50	64.51
		60	65.84			60	66.39
		70	67.15			70	67.62
Lower	0.25	10	3.00	Lower	0.75	10	3.00
		20	11.15			20	3.00
Inj. Rate		30	49.61	Inj. Rate		30	4.91
1.0270 B/D		40	57.85	1.0270 B/D		40	15.78
		50	62.37			50	33.72
		60	65.58			60	57.11
		70	66.82			70	65.83
Upper	0.50	10	16.33	Upper	1.00	10	3.00
		20	39.50			20	25.29
Inj. Rate		30	52.99	Inj. Rate		30	49.45
1.0270 B/D		40	59.12	1.0270 B/D		40	61.08
		50	61.08			50	63.48
		60	63.53			60	65.34
		70	65.07			70	67.02
Lower	0.50	10	3.00	Lower	1.00	10	3.00
		20	3.00			20	3.00
Inj. Rate		30	4.58	Inj. Rate		30	3.00
1.0270 B/D		40	16.88	1.0270 B/D		40	6.50
		50	34.71			50	18.49
		60	58.54			60	36.31
		70	67.52			70	55.79

Table 6.29 : Heat Flow Analysis of Model Using The Lauwerier Equation (Experiment 26)

Portion of Model	Pore Volume Injected	Actual Contour Temp. (C)	Lauwerier Equation Temp. (C)	Portion of Model	Pore Volume Injected	Actual Contour Temp. (C)	Lauwerier Equation Temp. (C)
Upper Inj. Rate 1.5405 B/D	0.25	10	32.61	Upper Inj. Rate 1.5405 B/D	0.75	10	4.32
		20	50.65			20	47.02
		30	59.88			30	59.16
		40	62.63			40	64.04
		50	65.05			50	65.74
		60	66.63			60	66.99
		70	67.49			70	67.80
Lower Inj. Rate 0.5135 B/D	0.25	10	3.00	Lower Inj. Rate 0.5135 B/D	0.75	10	3.00
		20	3.00			20	3.00
		30	29.19			30	3.00
		40	46.59			40	3.00
		50	56.24			50	8.68
		60	62.92			60	45.69
		70	65.45			70	63.46
Upper Inj. Rate 1.5405 B/D	0.50	10	32.15	Upper Inj. Rate 1.5405 B/D	1.00	10	3.00
		20	49.30			20	38.74
		30	58.19			30	55.78
		40	62.20			40	63.47
		50	63.48			50	65.06
		60	65.09			60	66.29
		70	66.11			70	67.40
Lower Inj. Rate 0.5135 B/D	0.50	10	3.00	Lower Inj. Rate 0.5135 B/D	1.00	10	3.00
		20	3.00			20	3.00
		30	3.00			30	3.00
		40	3.00			40	3.00
		50	8.53			50	3.10
		60	48.44			60	11.81
		70	66.86			70	43.18

In this analysis the model was divided to the upper and lower portion. The fluid injection rate used for each interval is an estimate only: in Table 6.28 it is assumed that each portion of the model received one half of the total injected fluid. However, the greater part of the injection interval for Run 26 was situated in the upper portion of the model. Therefore, in Table 6.29 it was assumed that three-quarters of the total fluid injected entered the upper zone of the model while the remaining one-quarter went into the bottom portion.

For Table 6.28, a comparison of the temperatures calculated for the upper and lower portions, using Lauwerier's equation, suggests that the upper part of the model was being heated faster than the lower portion. This indicates gravity override of the steam rather than the usual underriding of the formation by injected water. This is also evident in Table 6.29 but to a larger extent due to a higher injection rate in the upper region of the model. A steamflood occurs in the model since the upper portion heats up faster than the lower zone, which leads one to believe that steam override was present in the model.

Comparing the actual contour temperature to that obtained from the Lauwerier equation can also be useful in determining if steam existed in the model. The actual contour temperatures, which are at the approximate steam temperature of 70^{0}C, are greater than the Lauwerier equation temperatures in the upper and lower portions of the model in both Tables 6.28 and 6.29. Since the actual temperature is greater than the assumed Lauwerier hot waterflood temperature, the existence of the steam in the model is evident. As well, the actual contour temperatures at 60^{0}C are only slightly less than the Lauwerier equation temperatures which indicates that a hot water or condensate bank existed ahead of the steam zone. The lower actual contour temperatures, compared to the Lauwerier equation, are for the most part considerably less which indicates the heating and subsequent displacement of in-place oil ahead of the steam and hot water regions. At the lowest actual contour temperatures the Lauwerier equation temperatures are equal to or approach the initial reservoir temperature meaning that the oil in this region of the model has not been affected by the advancing hot water and steam zones at this point in time.

From the comparison of the actual and calculated temperatures as well as the indication of gravity overriding by the injected fluid, it is concluded that steam was present in the model throughout Run 26. Also a hot water or condensate region is believed to form ahead of the steam front.

Comparison of Marx-Langenheim and Mandl-Volek Models

A. Marx-Langenheim Theory

The second portion of the heat flow analysis consisted of a comparison of the Marx-Langenheim [5] and Mandl-Volek [69] models of formation heating by steam injection for the low pressure model in Run 26. Both steam injection theories give the steam zone volume at any point in time during a steam injection process.

According to Marx-Langenheim theory, when steam is introduced into an oil bearing formation at an initial reservoir temperature (T_R), a certain amount of oil is displaced by the steam. At the same, time the injected steam condenses and heats the reservoir rock and fluids. The hot water region formed ahead of the steam, which is assumed to be at the steam temperature (T_S), preheats the reservoir ahead of the steam. The Marx-Langenheim theory assumes idealized conditions, and therefore the heated zone is at a constant temperature (T_S) which extends from the injection end to a point where the temperature sharply drops from T_S to T_R. For this to occur Marx-Langenheim theory assumes no gravity segregation of steam, uniform thickness, injection over entire thickness at a constant rate and no temperature drop in the steam zone.

Figure 6.107 shows a schematic representation of the idealized temperature and steam quality distributions for the Marx-Langenheim model of reservoir heating by steam injection. The steam zone or heated region represents the volume of fluids and rocks heated to steam temperature (T_S), regardless of the steam quality. Marx-Langenheim

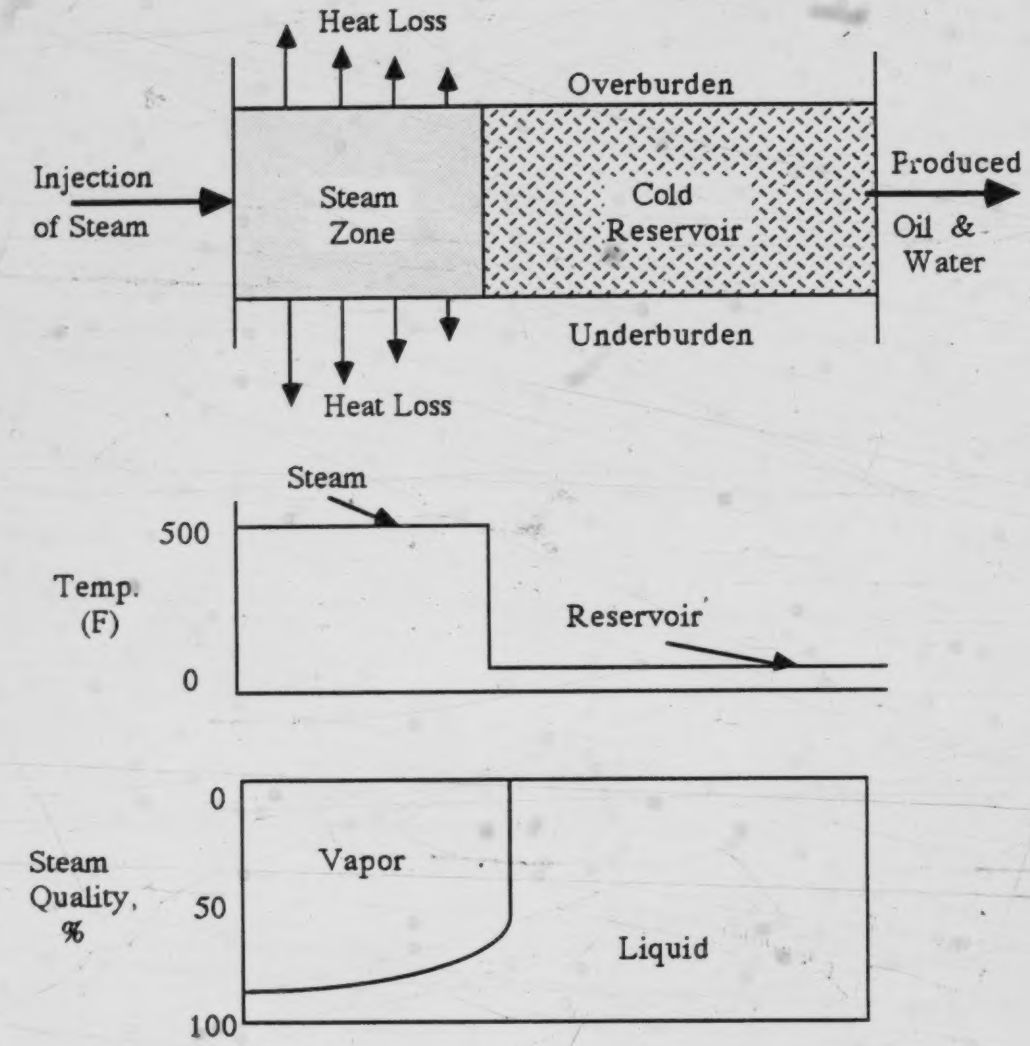
Heat Loss
Overburden
Injection of Steam
Steam Zone
Cold Reservoir
Produced Oil & Water
Underburden
Heat Loss
Steam
500
Temp. (F)
Reservoir
0
0
Steam Quality, %
Vapor
50
Liquid
100

Key Assumptions

- * No Gravity Effects
  - Entire Thickness Heated to Steam Temperature
  - No Hot Water Flow Ahead of Condensation Front
- *Homogeneous Sands and Shale
- *No Pressure Drop
- *Constant Injection Rate

Figure 6.107 : Schematic Diagram of the Marx-Langenheim model for reservoir heating by steam injection.

theory assumes that the condensate transfers the sensible heat over an infinitesimal distance which constitutes the condensate front.

Marx and Langenheim developed an equation to calculate the steam zone volume (V_S), which is as follows:.

$$V_s = \frac{Q_i M_s h_t^2 F_1}{4 k_{hob} M_{ob} (T_s - T_R)}$$

Where $Q_i = \left(\frac{350}{24}\right) i_s \left\{ h_w - h_R + f_{st} L_v \right\}$

Q_i - heat injection rate (BTU/hr)
i_s - steam injection rate (B/D - water equivalent)
h_w - saturated water enthalpy (BTU/lb)
h_R - enthalpy of water at reservoir temperature, T_R (BTU/lb)
f_{st} - steam quality
L_v - latent heat of vaporization for the steam (BTU/lb)

F_1 is a function of the dimensionless time, t_D.

$$F_1 = e^{t_D} \operatorname{erfc} \sqrt{t_D} + 2\sqrt{t_D/\pi} - 1 \qquad \text{or} \qquad F_1 \cong \frac{t_D}{1 + 0.85\sqrt{t_D}}$$

B. Mandl-Volek Theory

The major weakness of the Marx-Langenheim model, apart from neglecting gravity effects is that the injected steam continues to furnish the latent heat contained in the newly invaded strata as well as supplying heat for heat loss to adjacent formations. As long as the latent heat injection rate is greater than its consumption rate the Marx-Langenheim model is valid. However, at a particular time, called "critical time" by Mandl and Volek, this ceases to occur, and therefore an allowance must be made for convective heat transport by hot water ahead of the condensation front.

In the Mandl-Volek model, as long as the time is less than critical time, Marx-Langenheim theory can be implemented. If the time is greater than the critical time then the Mandl-Volek theory applies.

Estimation of the steam zone volume by the Mandl-Volek model is the average for two boundary conditions which are analytically solved. The first condition assumes no hot water movement infront of the condensation zone and therefore is the same as the Marx-Langenheim solution. The second condition assumes hot water movement and heat loss ahead of the front with no preheating of the overburden at the front.

Therefore the steam zone volume is calculated as shown below.

$$V_s = \frac{Q_i h_t^2}{(T_s - T_R)} \cdot \frac{M_s F_1}{4 k_{hob} M_{ob}} \qquad \text{for} \quad t \leq t_c \quad \text{(Marx-Langenheim)}$$

$$V_s = \frac{Q_i h_t^2}{(T_s - T_R)} \cdot \frac{M_s F_3}{4 k_{hob} M_{ob}} \qquad \text{for} \quad t > t_c \quad \text{(Mandl-Volek)}$$

Where $F_3 = e^{t_D} \operatorname{erfc} \sqrt{t_D} + 2\sqrt{t_D/\pi} - 1 - \sqrt{\frac{t_D - t_{DC}}{\pi}} \cdot$

$$\left\{ \left[1 + \frac{f_{st} L_v}{c_w (T_S - T_R)} \right]^{-1} + \left(\frac{t_D - t_{DC} - 3}{3} \right) e^{t_D} \operatorname{erfc} \sqrt{t_D} - \frac{t_D - t_{DC}}{3\sqrt{\pi t_D}} \right\}$$

Two computer programs were developed, which calculate the steam zone volume after every quarter of a pore volume of steam injected for experiment 26. The first program (page 579, Appendix B) incorporate the Marx-Langenheim solution to determine the steam zone volume. The second program (page 581, Appendix B) utilizes the Mandl-Volek theory for steam zone volume calculation.

Results of the comparison of the Marx-Langenheim and Mandl-Volek models are shown in Table 6.30. The table lists estimated steam zone volumes for both the Marx-Langenheim and Mandl-Volek situations at every quarter of a pore volume of steam injected for Run 26.

The results listed in Table 6.30 indicate that the steam zone volume calculated using the Marx-Langenheim theory was approximately 20% greater than the volume estimated using the Mandl-Volek theory. After two pore volumes of steam had been injected the predicted steam zone volume according to Marx-Langenheim theory was 65.55 % of the

Table 6.30 : Comparision of Marx-Langenheim & Mandl-Volek Models of Formation Heating by Steam Injection For the Low Pressure Model in Run 26

Pore Volumes of Steam Injected into the Model (P.V.)	Steam Zone Volume Using Marx-Langenheim Theory (% of Model's Bulk Volume)	Steam Zone Volume Using Mandl-Volek Theory (% of Model's Bulk Volume)
0.25	16.21	14.43
0.50	26.62	22.25
0.75	35.05	28.44
1.00	42.35	33.76
1.25	48.89	38.51
1.50	54.85	42.83
1.75	60.38	46.84
2.00	65.55	50.58

model's bulk volume, while the Mandl-Volek model estimated the steam zone volume to be 50.58 % of the model bulk volume. A comparison of the results of the two models indicates the critical time was reached soon after steam injection was initiated, therefore the Mandl-Volek model provided a better representation of the steam injection process which occurred in the low pressure model. It is also implied that the latent heat injection rate was less than the consumption rate of the injected heat.

From the results it was concluded that the Mandl-Volek model provides the more accurate representation of the steam zone developement in the model, which suggests that the latent heat injection rate was less than its consumption rate.

Heat Loss Analysis

A heat balance was performed on Run 26 to determine the total heat injected total heat remaining in the model and the total heat lost from within the model. The equations used for the heat balance were obtained from Farouq Ali's [70] text on heavy oil recovery.

Therefore the heat balance for Run 26 according to Farouq Ali [70] is as follows.

	Total Amount of Heat Injected in the Model	=	Total Heat Lost to the Surroundings and the Produced Fluids	+	Total Heat Existing in the Low Pressure Model
or	$Q_i(t)$	=	Q_{ob}	+	Q_s

Where $Q_i(t) = \left(\frac{350}{24}\right) i_s \left\{ h_w - h_R + f_{st} L_v \right\} t$

$Q_i(t)$ - total amount of heat injected (BTU)

i_s - steam injection rate (B/D - water equivalent)

h_w - saturated water enthalpy (BTU/lb)

h_R - enthalpy of water at reservoir temperature, T_R (BTU/lb)

f_{st} - steam quality

L_v - latent heat of vaporization for the steam (BTU/lb)

t - time (hr)

Determination of the total heat lost from the model (Q_{ob}) involved calculating the volume that each contour temperature occupied in the upper and lower temperature profiles for Run 26 (Fig. A.286-A.292). The volumes were calculated by measuring the area encompassed by each contour line for the upper and lower sections of the model. The area measured using a planimeter was then multiplied by one half the thickness of the model since the model was divided into upper and lower portions, each being half the thickness of the entire model. This calculation yielded the volume which each specific temperature contour occupied in the model.

The heat content of each elemental volume was determined using the following equation.

$$H_i = M_s V_i (T_i - T_R)$$

Where H_i - heat content of volume i (BTU)
M_s - heat capacity of heated model
V_i - volume of element i (ft^3)
T_i - temperature of element i (^0F)
T_R - initial model temperature (^0F)

The total heat existing in the model (Q_s) was then determined by summing the heat contained in each elemental volume, i.

$$Q_s = \sum_{i=1}^{n} H_i$$

Since values for $Q_i\ (t)$ and Q_s were obtained, a value for the total heat lost from the model (Q_{ob}) during experiment 26 could be predicted using the previously described heat balance equation.

Values of $Q_i(t)$, Q_s and Q_{ob} are listed respectively in Table 6.31 for every one quarter of a pore volume of steam injected into the model during Run 26. Total heat injected was given in BTU's while the heat lost and the heat remaining were listed as a percentage of the total heat injected into the model. A computer program (page 583, Appendix B) was developed which calculates the total heat injected into the model, the amount of heat contained in the model and the amount of heat lost from the model in Run 26, which was a base steamflood.

Table 6.31 : *Analysis of Heat Loss Occurring During a Base Steamflood (Experiment 26)*

Pore Volumes of Steam Injected into the Model (P.V.)	Total Amount of Heat Injected into the Model (Btu's)	Heat Remaining in the Model (% of Total Heat Injected)	Heat Lost to Surroundings & Produced Fluids (% of Total Heat Injected)
0.25	1438.74	24.45%	75.55%
0.50	2877.47	29.17%	70.83%
0.75	4316.21	20.61%	79.39%
1.00	5754.94	36.60%	63.40%
1.25	7193.68	29.60%	70.40%
1.50	8632.41	26.02%	73.98%
1.75	10071.15	27.14%	72.86%

Results of the heat balance analysis in Table 6.31 reveal that heat loss from the model was considerable, and that approximately one-quarter of the total heat injected into the model remained in the model. Therefore about 75 % of the total heat injected was lost to the surruoundings and the produced fluids. The magnitude of this heat loss is typical of steam injection processes in thin reservoirs. It was also noted from the results that the heat loss rate from the model was reasonably constant throughout the experiment.

Experimental Limitations and Sources of Error

As mentioned previously in the section dealing with scaling (Chapter IV), the assumptions made by Stegemeier, Laumbach and Volek lead to a certain degree of error in scaling the experiments. To adhere to strict scaling the capillary pressure and the relative permeability relationships would be required to be same functions of saturation in both model and the prototype. As well, there are practical considerations regarding the selection of model materials and fluids with properties that would exactly satisfy the scaling groups.

The inability to scale capillary pressure is believed to cause only a small error since a highly viscous crude oil occurs in the prototype reservoir. Demetre, Bentsen and Flock [58] reported that breakthrough recovery is only a weak function of the capillary number for large values of mobility ratio and provided a stable displacement exists. Bentsen [57] found that a displacement process in a linear system was dominated by mobility ratio. This made it possible to eliminate the requirement that relative permeabilities or their ratio be equal in the model and prototype for certain circumstances. It was suggested by Proctor [26] that two- and three-dimensional systems could also be dealt with in a similar manner.

Prats [11] reported that three-phase relative permeability curves used for a prototype at proper operating conditions could not be determined. Correspondingly it was not known how to establish the relative permeability properties for the laboratory model. Therefore it was difficult to determine if relative permeability relationships between the model and prototype were scaled or unscaled. Despite the limitation, Prats [11] found from his Peace River model study that good agreement was achieved between field and model performances.

Since different fluids and porous media are used in the model and prototype the relative permeability curves for the model and prototype will also be expected to be different. This is true even for the end points.

A feature of the Aberfeldy is that it is very stratified, however a limitation of the low pressure model was that representation of the stratification that exists in the reservoir could not be achieved (i.e. the model permeability in the vertical and horizontal directions was the same). Despite this limitation, the effect of stratification decreases vertical permeability which would probably help to hinder the movement of solvent and steam downward into the bottom water zone and therefore improve oil recovery.

Chapter VII

Conclusions

Based upon the results the research the following conclusions were reached:

1. The solvent-steamflood process exhibits an improved oil recovery capability from a bottom water formation as compared a conventional steamflood in the same type of reservoir. The higher recovery of the solvent-steamflood was due to the solvent slug channelling into the oil region and away from the bottom water, allowing the steam to penetrate the oil zone more easily. This increased the stability of the steam displacement of oil and resulted in more oil being mobilized and subsequently recovered.

2. (i) The implementation of gas injection prior to a steamflood of a thin formation with underlying water appears to improve oil recovery, compared to a conventional steamflood, by partially diverting the injected steam away from the bottom water zone and increasing the steam injectivity in the oil zone. The solvent-steamflood method yields the highest oil recovery compared to injecting gas prior to the steamflood of a bottom water model.

   (ii) Gas injection prior to a solvent-steamflood of a bottom water formation tends to diminish solvent channelling in the oil, due to the solvent travelling over top of the oil zone. This results in less steam penetrating the oil layer. Consequently, less oil is mobilized by the steam causing a drop in oil recovery of a solvent-steamflood as compared to its implementation in a heavy oil formation with underlying water but without a gas cap or gas channel.

3. Bottom water has very detrimental effects on the thermal and sweep efficiencies of a steamflood, and as the bottom water thickness increases the loss of the steam to the underlying water correspondingly increases.

4. In the case of a solvent-steamflood process on a bottom water formation, as the bottom water thickness increased in the model, the oil recovery decreased until a limiting bottom water thickness was reached. Above this value the use of a solvent would not significantly improve the oil recovery. The bottom water thickness above which improved oil recovery by a solvent-steamflood is negligible was estimated to be somewhere between 25% and 30% of the total formation thickness.

5. There exists an optimal solvent slug size of approximately 10% of the model pore volume which maximizes the amount of oil recovered by a solvent-steamflood process.

6. Location of the injection interval in the upper portion of the formation (ie. oil zone) enables more efficient use of the injected solvent and steam and increases oil recovery by directing the fluids into the oil zone and away from the harmful bottom water layer, as compared to injection over the entire interval or into the bottom portion of the formation.

7. The use of a partial bottom water barrier in combination with a steamflood of a bottom water formation helped to prevent steam from travelling directly into the water zone so it could more efficiently heat and mobilize the overling oil zone.

8. Conducting solvent-steamfloods of previous waterflooded reservoirs to improve oil recovery shows promise as an enhanced heavy oil recovery scheme.

9. A comparison of the experimental results for a solvent-steamflood, conventional steamflood, gas injection prior to a steamflood or solvent-steamflood and a partial bottom water barrier method all conducted in a bottom water model, shows that the solvent-steamflood technique yielded the highest oil recovery.

10. An analysis of formation heating for a conventional steamflood of a homogeneous, oil-saturated model (Run 26) was carried out using classical methods. It is concluded that:

    (i) The Mandl-Volek steam injection model provides the best representation of steam zone development in the model compared to the Marx-Langenheim and Lauwerier theories. This indicates that the latent heat injection rate fell below the consumption rate needed for continued steam zone advance.

    (ii) The heat loss from the model was considerable which is typical of steam injection processes in thin reservoirs. Results indicate that approximately one quarter of the total heat injected remained in the model to be used to mobilize the in-place oil.

References

1. Farouq Ali, S.M. and Meldau, R.F.: "Current Steamflood Technology," *JPT* (Oct. 1979) 1332.

2. Blevins, T.R., Duerksen, J.H., Ault, J.W.: "Light Oil Steamflooding -- An Emerging Technology," paper presented at the 1982 SPE/DOE Third Joint Symposium on Enhanced Oil Recovery of the Society of Petroleum Engineers, Tulsa, Oklahoma, April 4-7.

3. Farouq Ali, S.M.: "Steam Injection Theories -- A Unified Approach," paper presented at the 1982 California Regional Meeting of the SPE, San Francisco, California, March 24-26.

4. Willman, B.T., Valleroy, V.V., Runberg, G.W., Cornelius, A.J., and Powers, L.W.: "Laboratory Studies of Oil Recovery by Steam Injection," JPT (July 1961) 681-690.

5. Marx, J.W. and Langenheim, R.H.: "Reservoir Heating by Hot Fluid Injection," *Trans.*, AIME, **216** (1959).

6. Baker, P.E.: "An Experimental Study of Heat Flow in Steamflooding," *SPEJ* (March 1969) 89-99.

7. Flock, D.L. and Lee, J.: "An Experimental Investigation of Steam Displacement of a Medium Gravity Crude Oil," 28th Annual Technical Meeting of the Petroleum Society of the CIM, Canada-Venezuala Oil Sands Symposium, Edmonton (1977) 386-394.

8. Farouq Ali, S.M. and Redford, D.A.: "Physical Modeling of In Situ Recovery Methods For Oil Sands," 28th Annual Technical Meeting of the Petroleum Society of the CIM, Canada-Venezuala Oil Sands Symposium, Edmonton (1977).319-326.

9. Stegemeier, G.L., Laumbach, D.D. and Volek, C.W.: "Representing Steam Processes With Vacuum Models," paper SPE 6787 presented at the 52nd Annual Fall Technical Conference of SPE of AIME in Denver, Colorado, Oct. 9-12, 1977.

10. Kimber, K.D., Puttagunta, V.R., and Farouq Ali, S.M.: "New Scaling Criteria and Their Relative Merits for Steam Recovery Experiments," paper 86-37-22 presented at 37th Annual Technical Meeting of the Petroleum Society of CIM, Calgary, Alberta, June 8-11, 1986.

11. Prats, M.: "Peace River Steam Drive Scaled Model Experiments," 28th Annual Technical Meeting of the Petroleum Society of the CIM, Canada-Venezuala Oil Sands Symposium, Edmonton (1977).

12. Geertsma, J., Croes, G.A. and Schwarz, N.: "Theory of Dimensionally Scaled Models of Petroleum Reservoirs," *Trans.*, AIME, **207** (1956).

13. Loomis, A.G. and Crowell, D.C.: "Theory and Application of Dimensional and Inspectional Analysis to Model Study of Fluid Displacements in Petroleum Reservoirs," Bureau of Mines Report RI6546 (1964)..

14. Leverett, M.C., Lewis, W.B. and True, M.E.: "Dimensional-Model Studies of Oil-Field Behaviour," *Trans.*, AIME, **146** (1942).

15. Rapoport, L.A.: "Scaling Laws for Use in Design and Operation of Water-Oil Flow Models," *Trans.*, AIME, **204** (1955).

16. Perkins, F.M. and Collins, R.E.: "Scaling Laws for Laboratory Flow Models of Oil Reservoirs," *Trans.*, AIME, **219** (1960).

17. Pujol, L. and Boberg, T.C.: "Scaling Accuracy of Laboratory Steam Flooding Models", paper SPE 4191 presented at the California Regional Meeting of the Society of Petroleum Engineers, Bakersfield, Nov. 8-10, 1972.

18. Pursley, S.A.: "Experimental Studies of Thermal Recovery Processes," Paper presented at the Heavy Oil Symposium, Maracaibo (1974).

19. Ehrlich, R.: "Laboratory Investigation of Steam Displacement in Wabasca Grand Rapids A Sand," paper presented at the Canada-Venezuala Oil Sands Symposium, Edmonton, May 1977, 364-379.

20. Huygen, H.H.A. and Lowry, W.E.: "Steamflooding Wabasca Tar Sand Through the Bottom Water Zone -- Scaled Lab Experiments," paper presented at the 54th Annual Fall Meeting of the Society of Petroleum Engineers, Las Vegas, Sept. 23-26, 1979.

21. Harmsen, G.J.: "Oil Recovery by Hot-Water and Steam Injection," Eighth World Petroleum Congress, Moscow, 243-251.

22. Doscher, T.M.: "Scaled Physical Model Studies of the Steam Drive Process," First Annual Report (Sept., 1977 to Sept. 1978), U.S. Department of Energy, Contract DOE/ET/12075-1.

23. Yortsos, Y.C.: "Analytical Modelling of Oil Recovery by Steam Injection", Ph. D. Dissertation, California Institute of Technology (1979).

24. Doscher, T.M. and Huang, W.: "Steam-drive Performance Judged Quickly From Use of Physical Models," *Oil and Gas Journal* (Oct. 22, 1979) 52-57.

25. Doscher, T.M. and Ghassemi, F.: "The Influence of Oil Viscosity and Thickness on the Steam Drive," *JPT* (February 1983) 291-298.

26. Proctor, M.L.: "Steam Injection in a Scaled Physical Model," M.Sc. Thesis, The University of Alberta, 1985.

27. Kasraie, M. and Farouq Ali, S.M.: "Heavy Oil Recovery in the Presence of Bottom Water," paper 84-35-122 presented at the 35th Annual Technical Meeting of the Petroleum Society of CIM, Calgary, June 10-13, 1984.

28. Kasraie, M. and Farouq Ali, S.M.: "Application of Thermal Recovery Techniques to Marginal Reservoirs," paper presented at the Third European Meeting on Improved Oil Recovery, Rome, April 16-18, 1985.

29. Perkins, T.K. and Johnston, O.C.: "A Review of Diffusion and Dispersion in Porous Media," *SPEJ* (March 1963) 70.

30. Graham, J.W. and Richardson, J.G.: "Theory and Application of Imbibition Phenomena in Recovery of Oil," *Trans.*, AIME, **216**.

31. Holm, L.W.: "Status of CO_2 and Hydrocarbon Miscible Oil Recovery Methods," *JPT* (Jan. 1976) 76.

32. Stalkup, F.I.: "Displacement of Oil by Solvent at High Water Saturation," *SPEJ* (Dec. 1970) 337.

33. Craig, F.F.: "A Current Appraisal of Field Miscible Slug Projects," *JPT* (May 1970) 529.

34. Baker, L.E.: "Effects of Dispersion and Dead End Pore-Volume in Miscible Flooding," *SPEJ* (June 1977) 219.

35. Rodriguez, H.: "An Investigation of the Mechanics of Miscible Fluid Displacement in Natural Porous Pack," M.S. Thesis, The Pennsylvania State University, 1957.

36. Totonji, A.H.M.: "A Unified Study of Viscous Fingering and Other Viscosity Phenomena in Miscible Displacement," M.S. Thesis, The Pennsylvania State University, 1964.

37. Kyle, C.R. and Perrine, R.L.: "Experimental Studies of Miscible Displacement Instability," *SPEJ* (Sept. 1965) 189-195.

38. Mungan, N.: "Improved Waterflooding Through Mobility Control," *Cdn. J. Chem. Eng.* (Feb. 1971), vol. 49, 32.

39. Slobod, R.L. and Lestz, S.I.: "Use of a Graded Viscosity Zone to Reduce Fingering in Miscible Displacements," *Prod. Monthly* (Aug. 1960) 12.

40. Claridge, E.L.: "A Method for Designing Graded Viscosity Banks," *SPEJ* (Oct. 1978) 315.

41. Kennedy, W.A. and Crawford, G.W.: "Derivation of the Dimensionless Scaling Groups Governing Miscible and Steam Drive Processes," Report No. UT 59-8, Texas Petroleum Research Commitee, Austin, Texas, August 13, 1959.

42. Pozzi, A.L. and Blackwell, R.J.: "Design of Laboratory Models for Study of Miscible Displacement," *SPEJ* (March 1963) 28-40.

43. Alikhan, A.A. and Farouq Ali, S.M.: "Oil Recovery by Hydrocarbon Slugs Driven by a Hot Water Bank," *SPEJ* (Dec, 1971) 342.

44. Farouq Ali, S.M.: "Application of Solvent Slugs In Thermal Recovery Operations," *Producers Monthly* (July,1965) 6.

45. Pirela, L.V. and Farouq Ali, S.M.: "Ternary Phase Behaviour at High Temperatures," *SPEJ* (Dec. 1968) 381.

46. Toronji, A.H.M. and Farouq Ali, S.M. : "Solvent Flooding Displacement Efficiency in Relation to Ternary Phase Behaviour," *SPEJ* (April 1972) 89.

47. Ozen, A.S. and Farouq Ali, S.M.: "An Investigation of the Recovery of the Bradford Crude by Steam Injection," *JPT* (June 1969) 692-698.

48. Hernandez, O.E. and Farouq Ali, S.M.: "Oil Recovery From Athabasca Tar Sand by Miscible-Thermal Methods," paper No. 7249 presented at the 23rd Annual Technical Meeting of the Petroleum Society of CIM in Calgary, May 16-19, 1972.

49. Farouq Ali, S.M. and Snyder, S.G.: "Miscible Thermal Methods Applied to a Two-Dimensional, Vertical Tar Sand Pack, With Restricted Fluid Entry," *JCPT* (Oct.-Dec. 1973) 20.

50. Farouq Ali, S.M. and Abad, B.: " Bitumen Recovery from Oil Sands, Using Solvents in Conjunction with Steam," *JPT* (July-Sept. 1976) 80.

51. Farouq Ali, S.M., Look Yee, K,C., Cordero, F.J. and Figueroa, J.M.: "Role of Injection-Production Strategy in the Solvent-Steamflooding of the Athabasca Oil Sands," paper No. 78-29-36 presented at the 29th Annual Technical Meeting of the Petroleum Society of CIM, Calgary, June 13-16, 1978.

52. Doscher, T.M., Ershaghi, I., Herzberg, D.E. and Gourene, Z.S.: "An Economic Evaluation of Solvent/Steam Stimulation," *JPT* (Aug. 1979) 951.

53. Redford, D.A. and McKay, A.S.: "Hydrocarbon-Steam Processes for Recovery of Bitumen From Oil Sands," paper SPE 8823 presented at the First Joint SPE/DOE Syposium on Enhanced Oil Recovery, Tulsa, April 20-23, 1980.

54. Redford, D.A.: "The Use of Solvents and Gases With Steam in the Recovery of Bitumen From Oil Sands," paper No. 81-32-29 presented at the 32nd Annual Technical Meeting of the Petroleum Society of CIM, Calgary, May 3-6, 1981.

55. Yamazaki, T., Matsuzawa, N., Abdelkarim, O.A. and Ono, Y.: "Recovery of Bitumen From Oil Sand by Steam With Chemicals"," paper presented at AIChE National Meeting, New Orleans, March 8-10, 1988.

56. Knobloch, T.S., Farouq Ali, S.M. and Trevino Diaz, M.J.: "The Role of Acid-Additive Mixtures on Asphaltene Precipitation," paper SPE 7627 presented at the SPE of AIME Eastern Regional Meeting, Washington, D.C., Nov. 1-3, 1978.

57. Bentsen, R.G.: "Scaled Fluid-Flow Models With Permeabilities Differing From That of the Prototype," *JCPT* (July - September, 1976), 47-52.

58. Demetre, G.P., Bentsen, R.G. and Flock, D.L.: "A Multi-Dimensional Approach to Scaled Immiscible Fluid Displacement," *JCPT* (July - Augusı 1982) 49 -61.

59. CRC Handbook of Chemistry and Physics, 53 rd Edition, 1972 - 1973, page E-5.

60. Currie, J.B. & Gregory, A.R : "Homogeneously Distributed Particles," U.S. Patent 2,808,242 (Oct. 1, 1957).

61. Wygal, R.J.: "Construction of Models that Simulate Oil Reservoirs," *SPEJ* (Dec. 1963) 281.

62. Proctor, M.L. and Farouq Ali, S.M.: "Steamflooding Light and Moderately Viscous Oil Reservoirs in Alberta," paper 86-37-52 presented at 37th Annual Technical Meeting of the Petroleum Society of CIM, Calgary, June 8-11, 1986.

63. Proctor, M.L., George, A.E. and Farouq Ali, S.M.: "Steam Injection Strategies for Thin, Bottomwater Reservoirs," paper SPE 16338 presented at the 1987 California Regional Meeting of the SPE, Ventura, April 8-10.

64. Alikhan, A.A.: Oil Recovery by Hot Water and Steam-Driven Hydrocarbon Slugs in a Linear Porous Medium, Kuwait University, 1986.

65. Kasraie, M. and Farouq Ali, S.M.: "Steamflooding Bottom Water Reservoirs," paper No. 5 presented at 1st Annual Technical Meeting of the South Saskatchewan Section of the Petroleum Society of CIM, Regina, October 6 - 8, 1987.

66. Collins, R.E.: Flow of Fluids Through Porous Materials, Reinhold Publishing Corporation, 1961.

67. Alikhan, A.A. and Farouq Ali, S.M.: "State-of-the-Art of Water Coning Modelling and Operation," paper SPE 13744 presented at the 4th Middle East Oil Show,Society of Petroleum Engineers of AIME, Bahrain, March 11-14, 1985.

68. Lauwerier, H.A.: "The Transport of Heat in an Oil Layer Caused by the Injection of Hot Fluid," *Appl. Sc. Res.*, Sec. A, No. 5 (1955), 145.

69. Mandl, G. and Volek, C.W.: "Heat and Mass Transport in Steam-Drive Processes," *SPEJ* (March 1969) 59-79.

70. Farouq Ali, S.M.: Elements of Heavy Oil Recovery, (1982).

Appendix A

Temperature Profiles

Figure A.1 : Run 39

Steamflood in Bottom Water Model

Temperature Profile for 0.25 Pore Volumes Injected

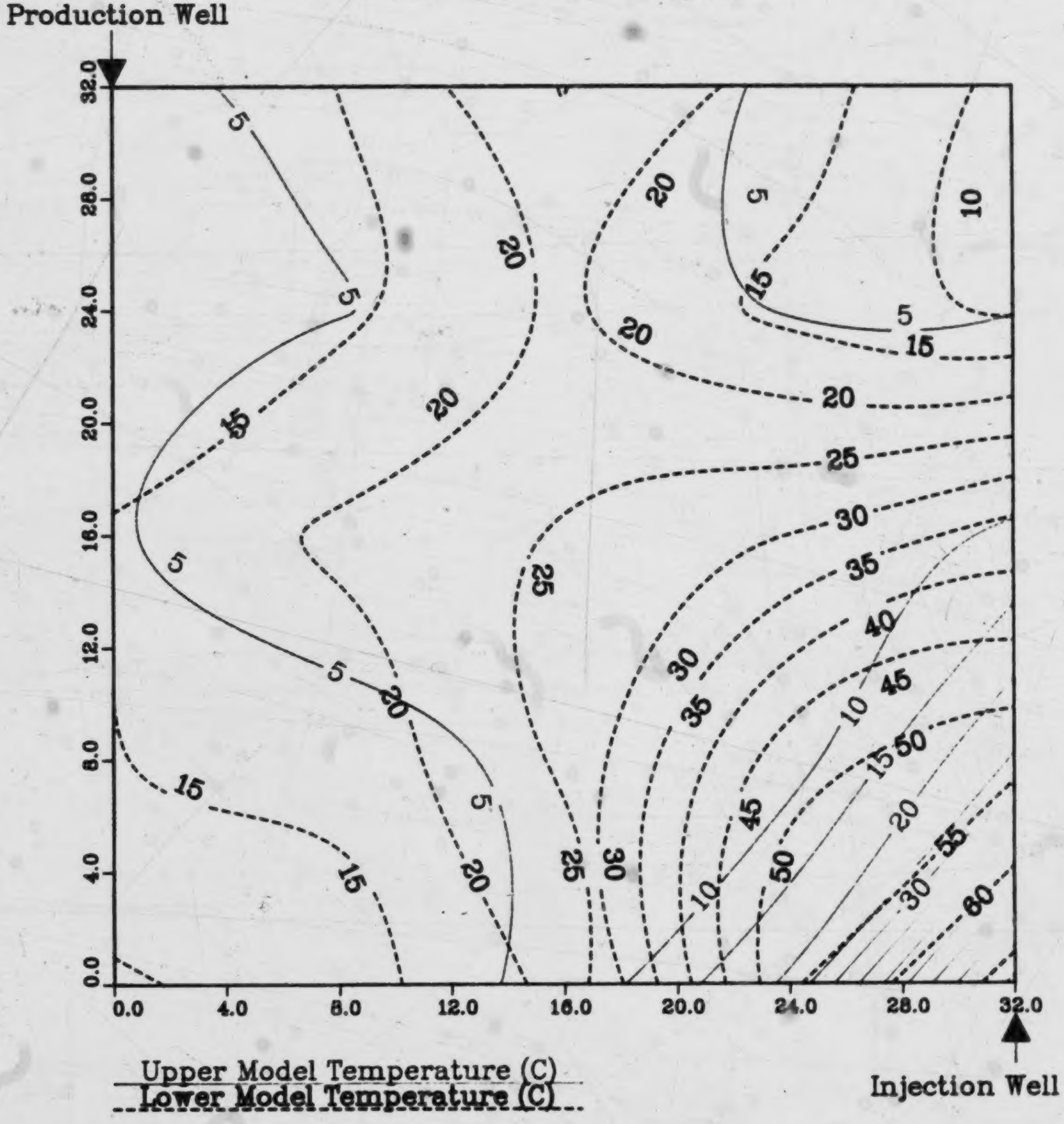

Figure A.2 : Run 39

Steamflood in Bottom Water Model

Temperature Profile for
0.50 Pore Volumes Injected

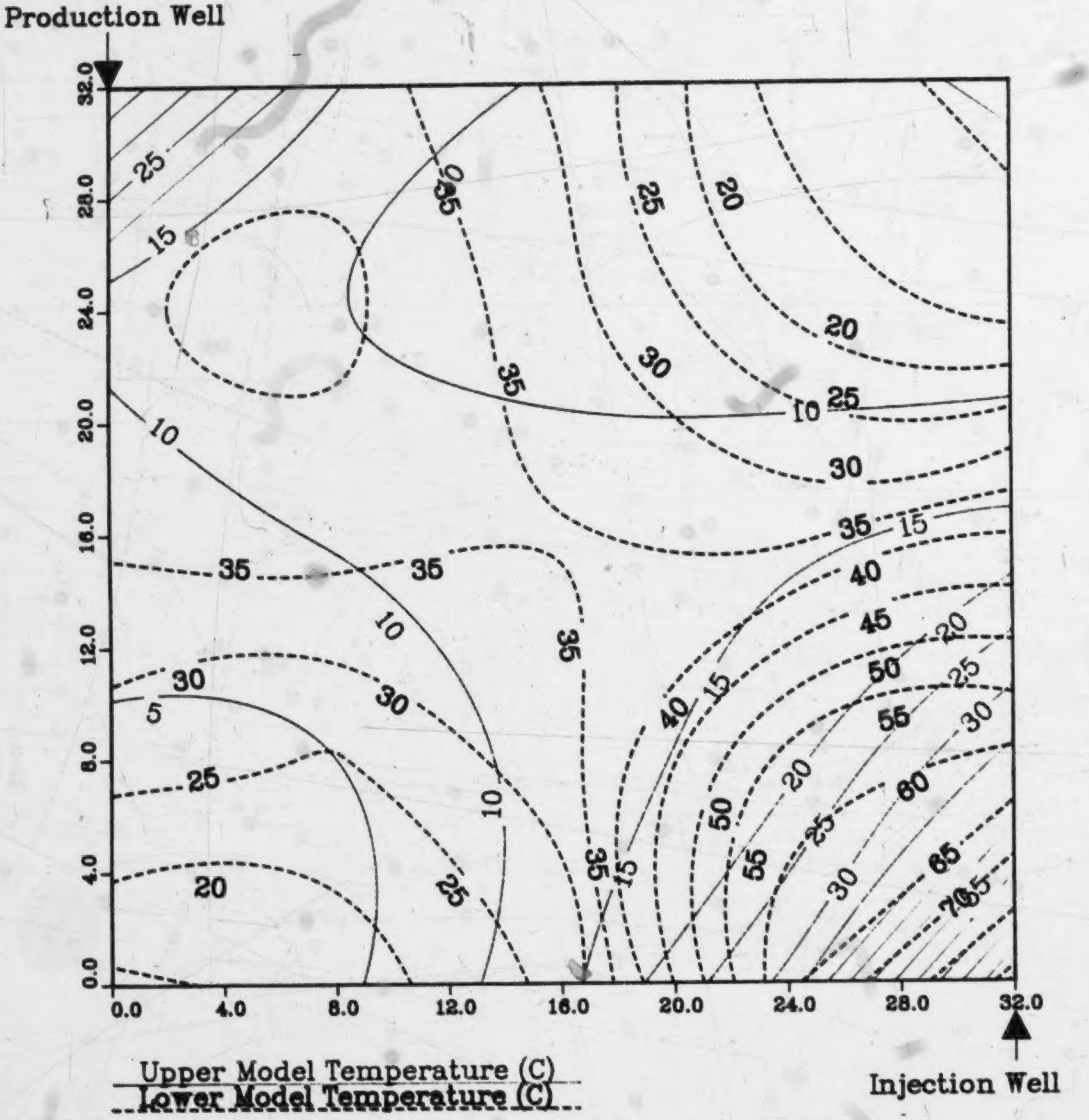

Figure A.3 : Run 39

Steamflood in Bottom Water Model

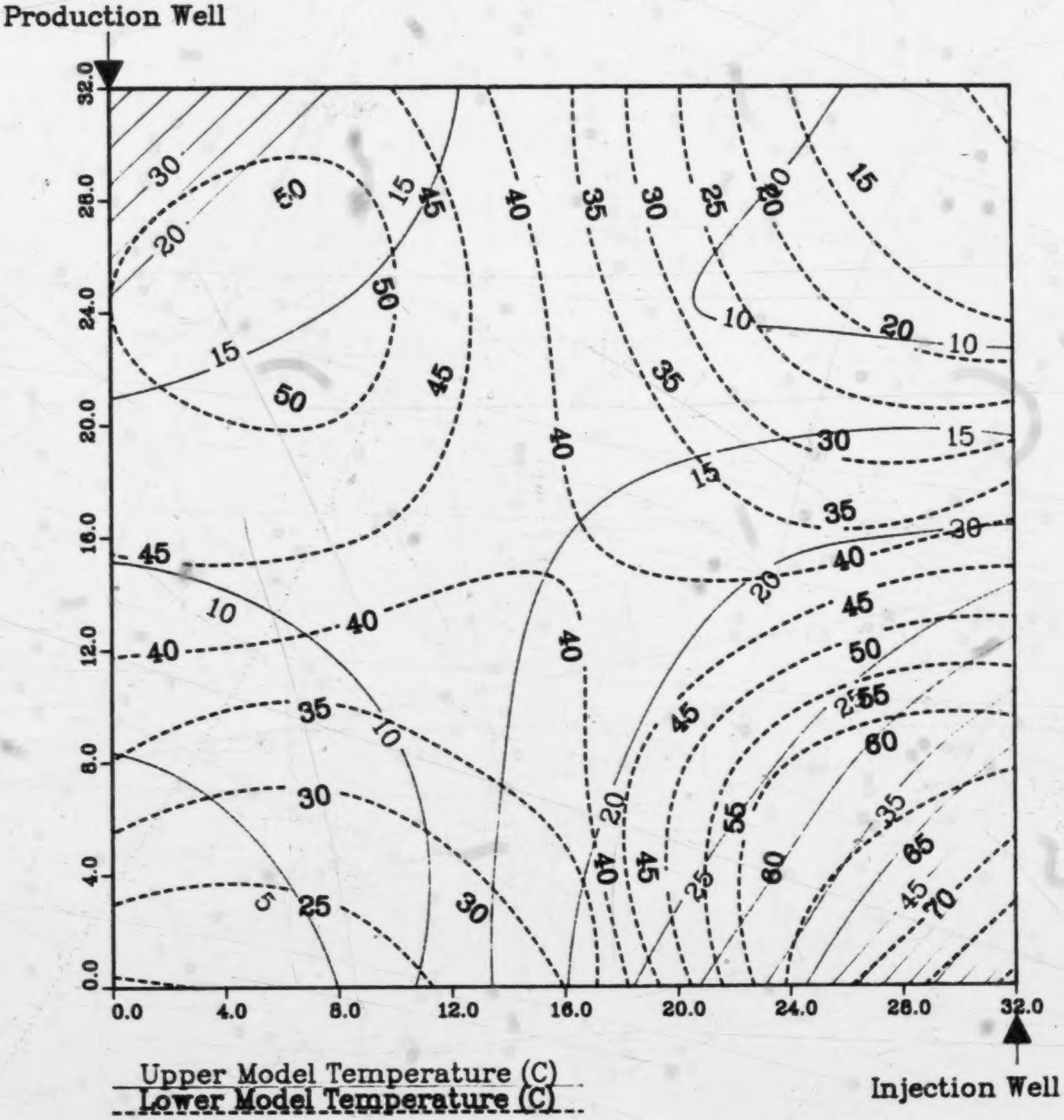
Temperature Profile for
0.75 Pore Volumes Injected

Figure A.4 : Run 39

Steamflood in Bottom Water Model

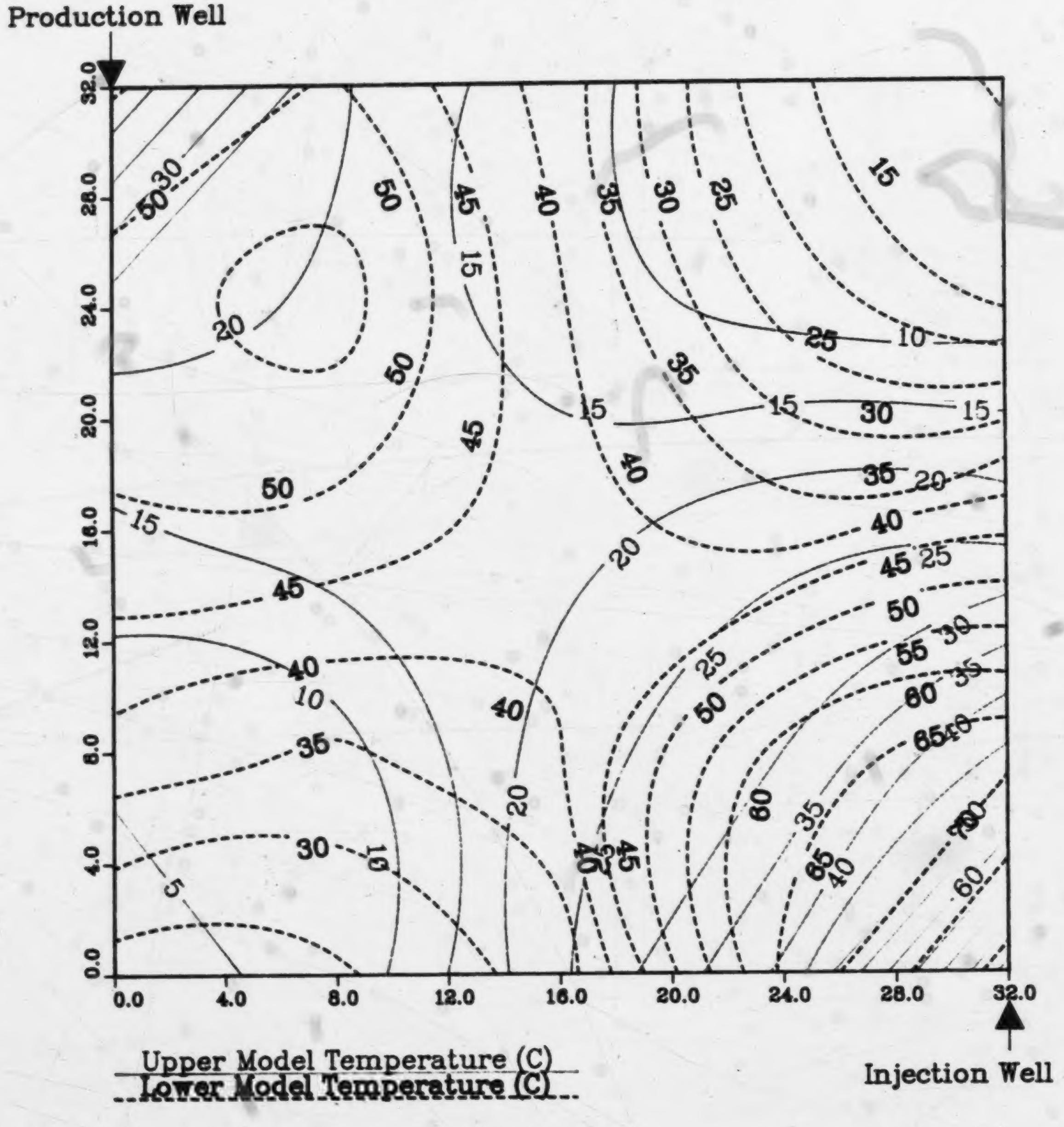

Figure A.5 : Run 39

Steamflood in Bottom Water Model

Temperature Profile for 1.25 Pore Volumes Injected

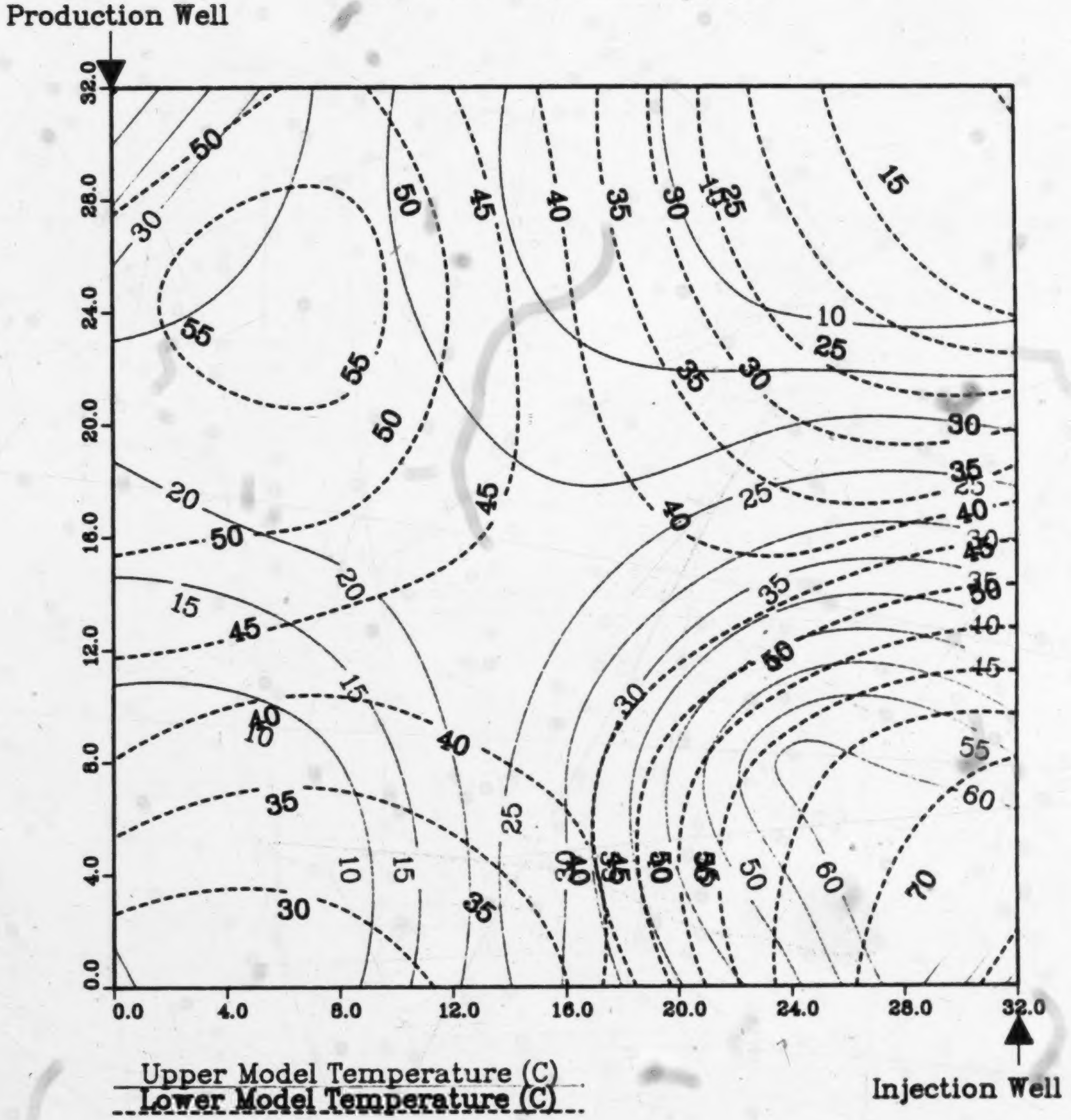

Figure A.6 : Run 39
Steamflood in Bottom Water Model

Temperature Profile for
1.50 Pore Volumes Injected

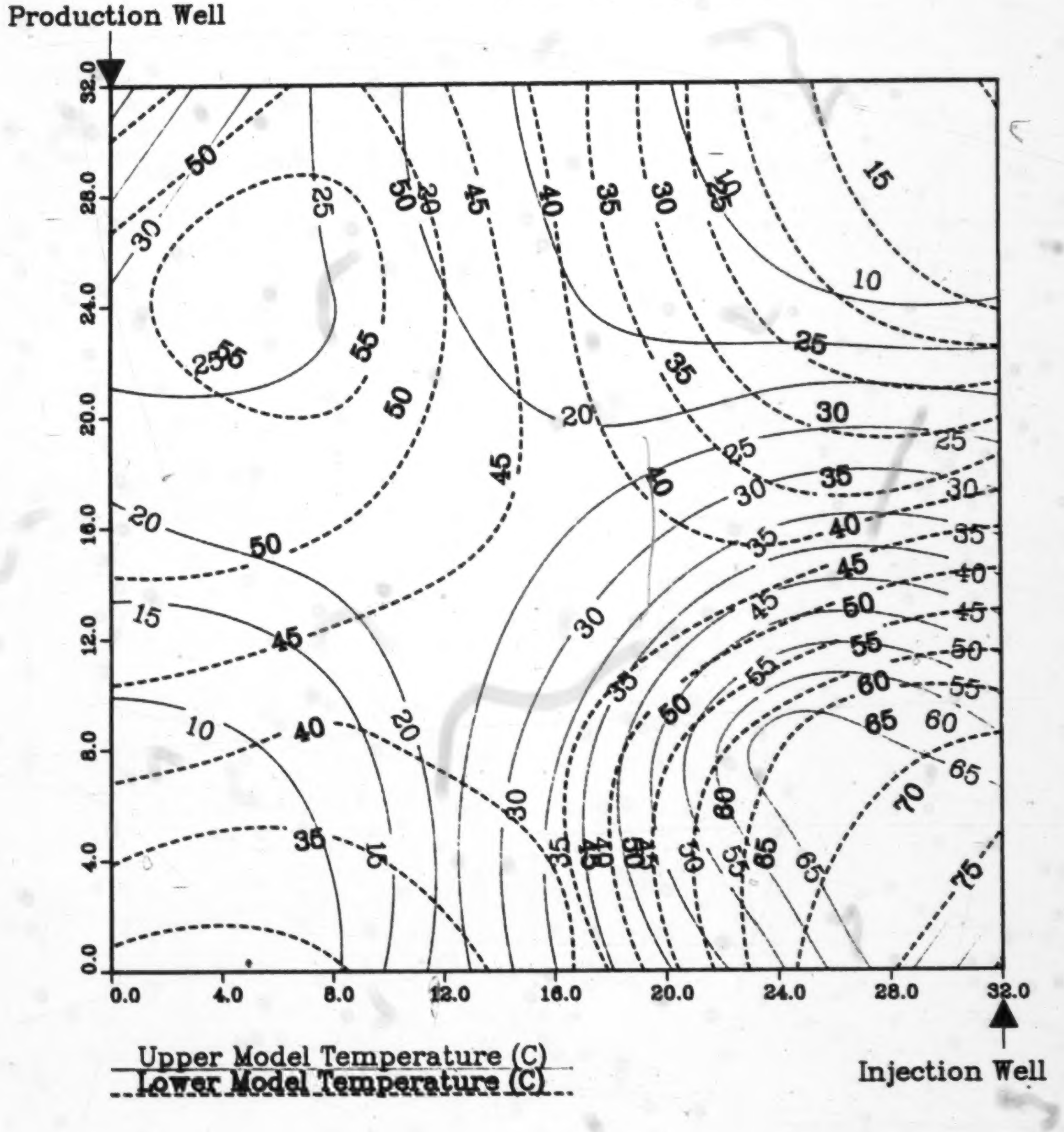

Figure A.7 :Run 39 Temp Profile
Injector to Producer Cross–Section
0.25 Pore Volumes Injected.

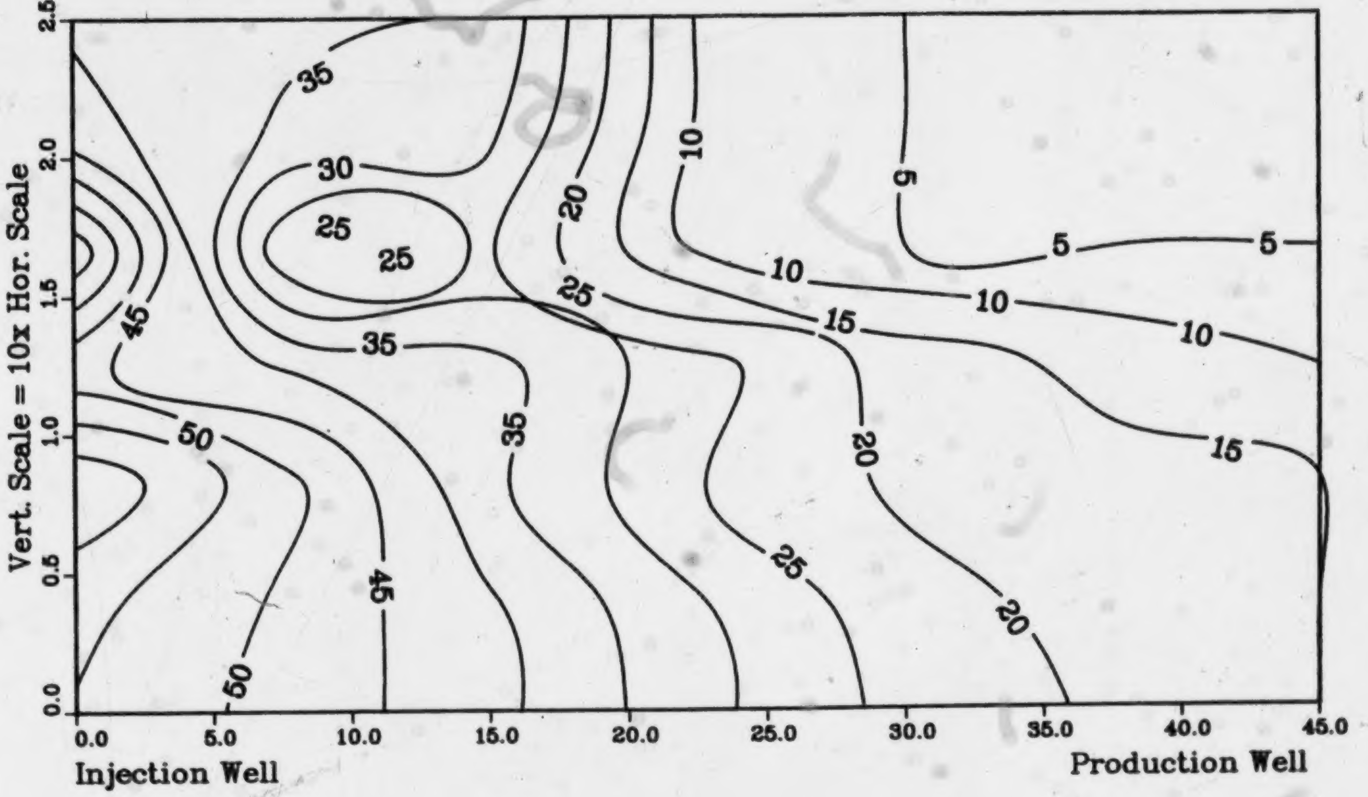

Figure A.8 :Run 39 Temp Profile
Injector to Producer Cross–Section
0.50 Pore Volumes Injected.

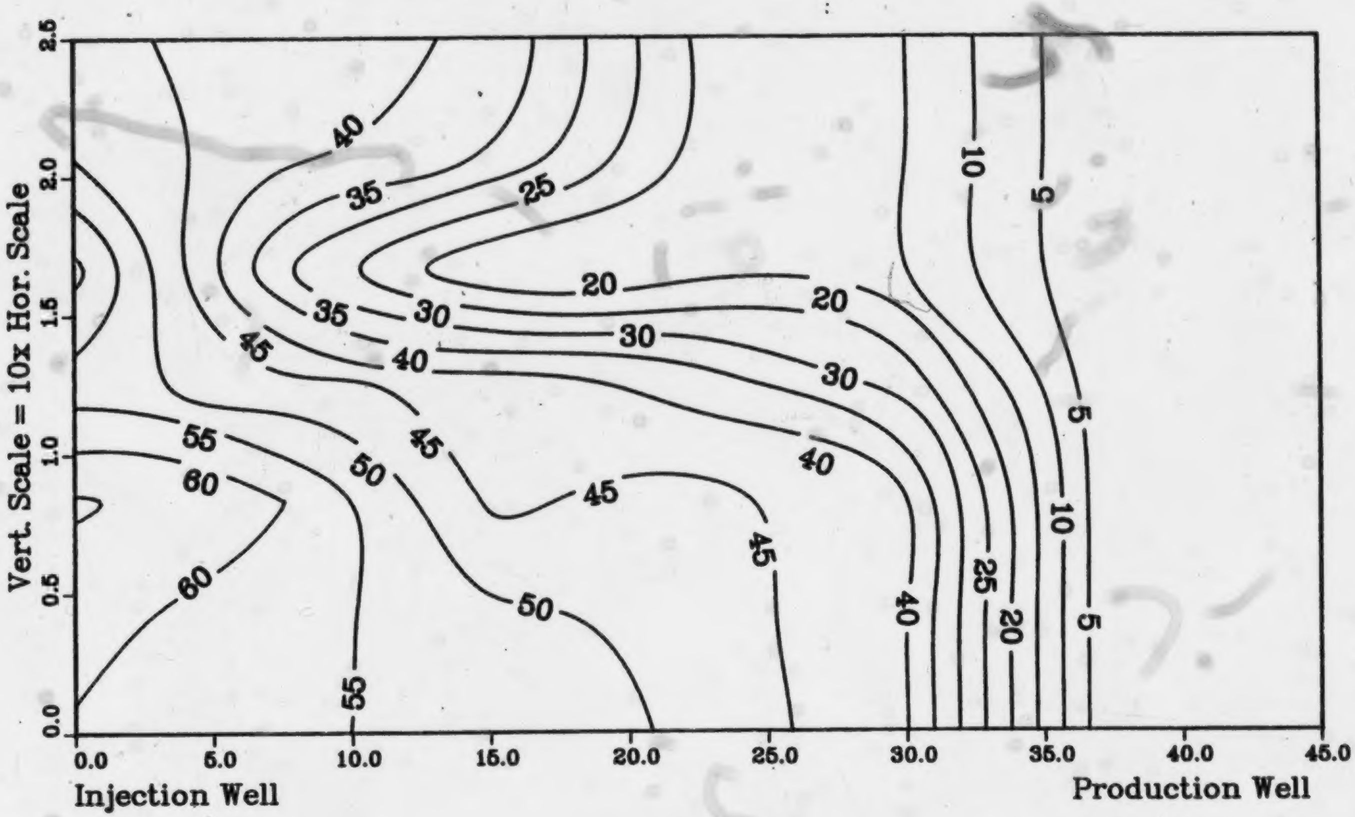

Figure A.9 :Run 39 Temp Profile
Injector to Producer Cross–Section
0.75 Pore Volumes Injected.

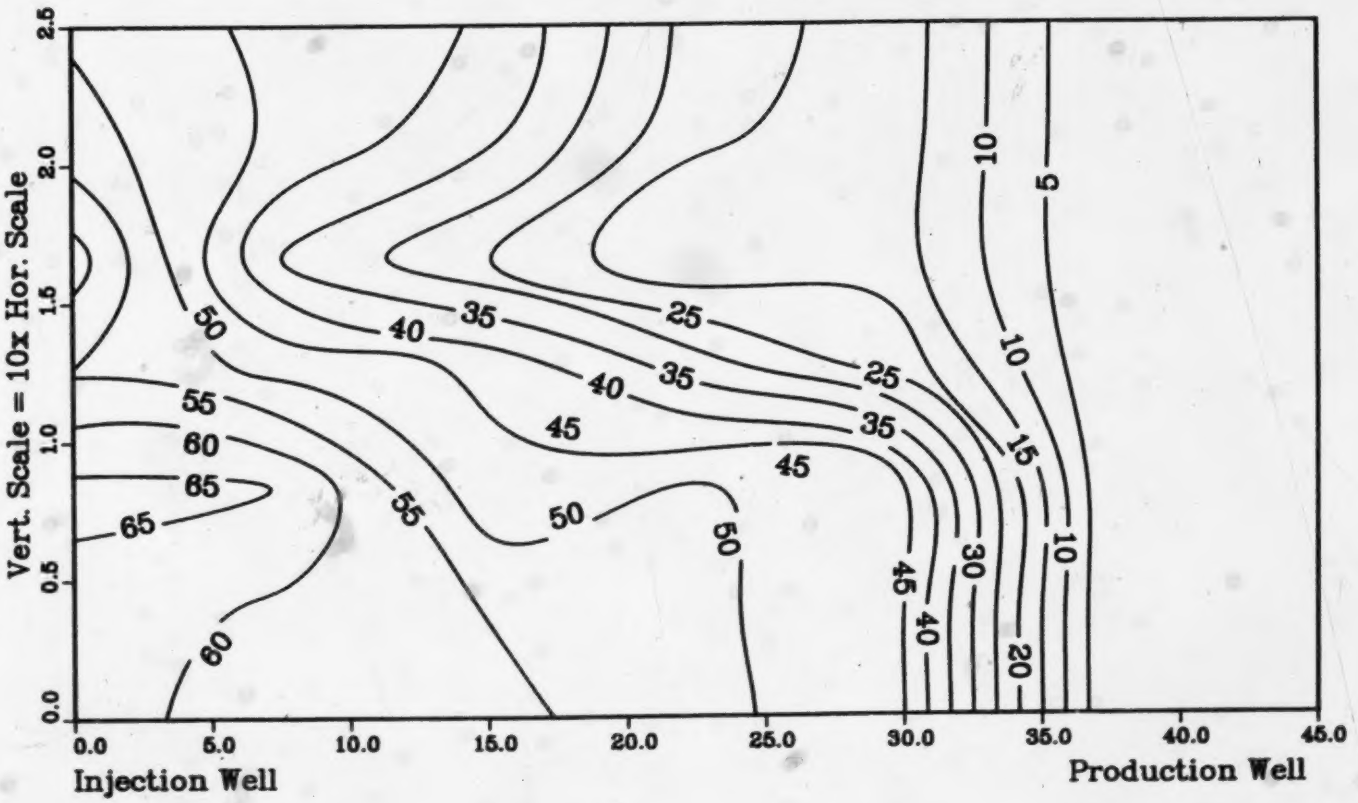

Figure A.10 :Run 39 Temp Profile
Injector to Producer Cross–Section
1.00 Pore Volumes Injected.

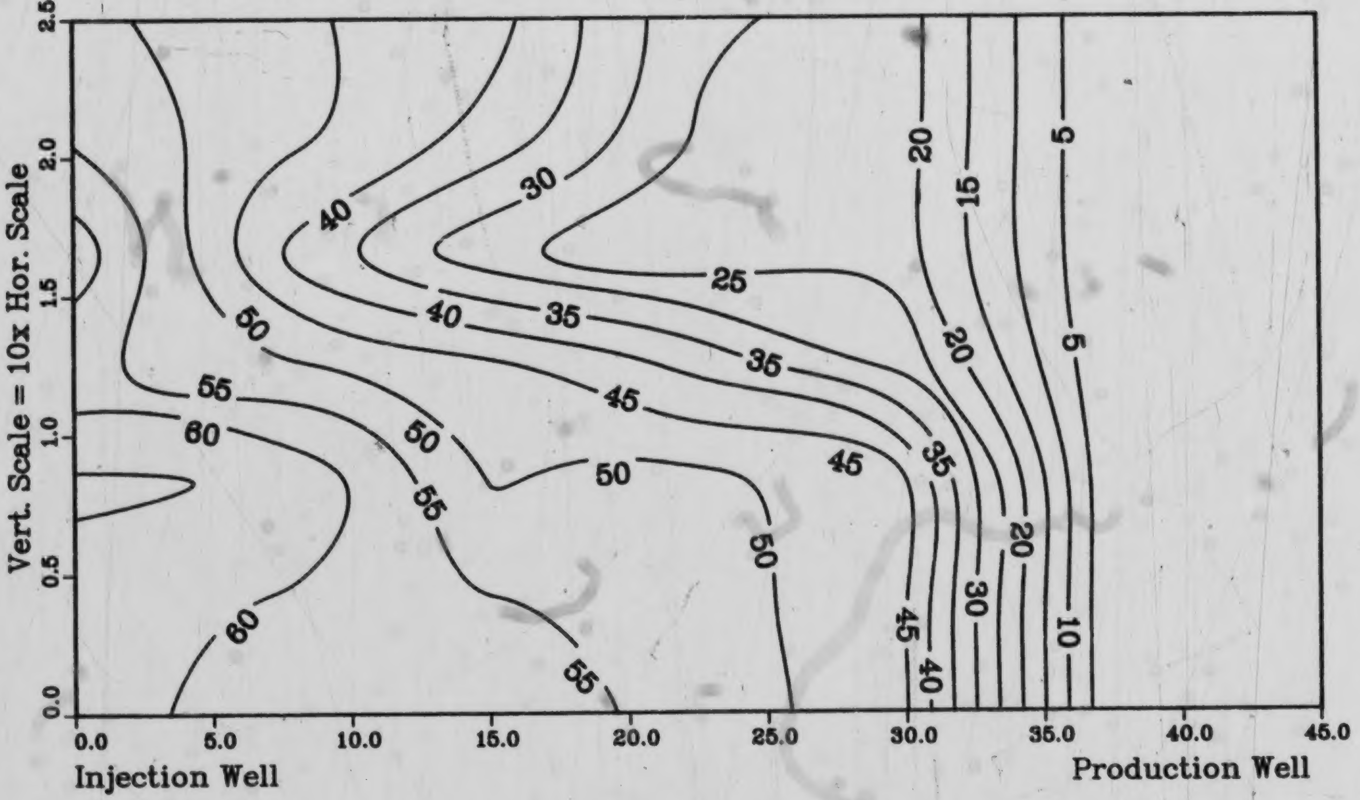

Figure A.11 : Run 40

Solvent Flood in Homogeneous Model

Temperature Profile for
0.25 Pore Volumes Injected

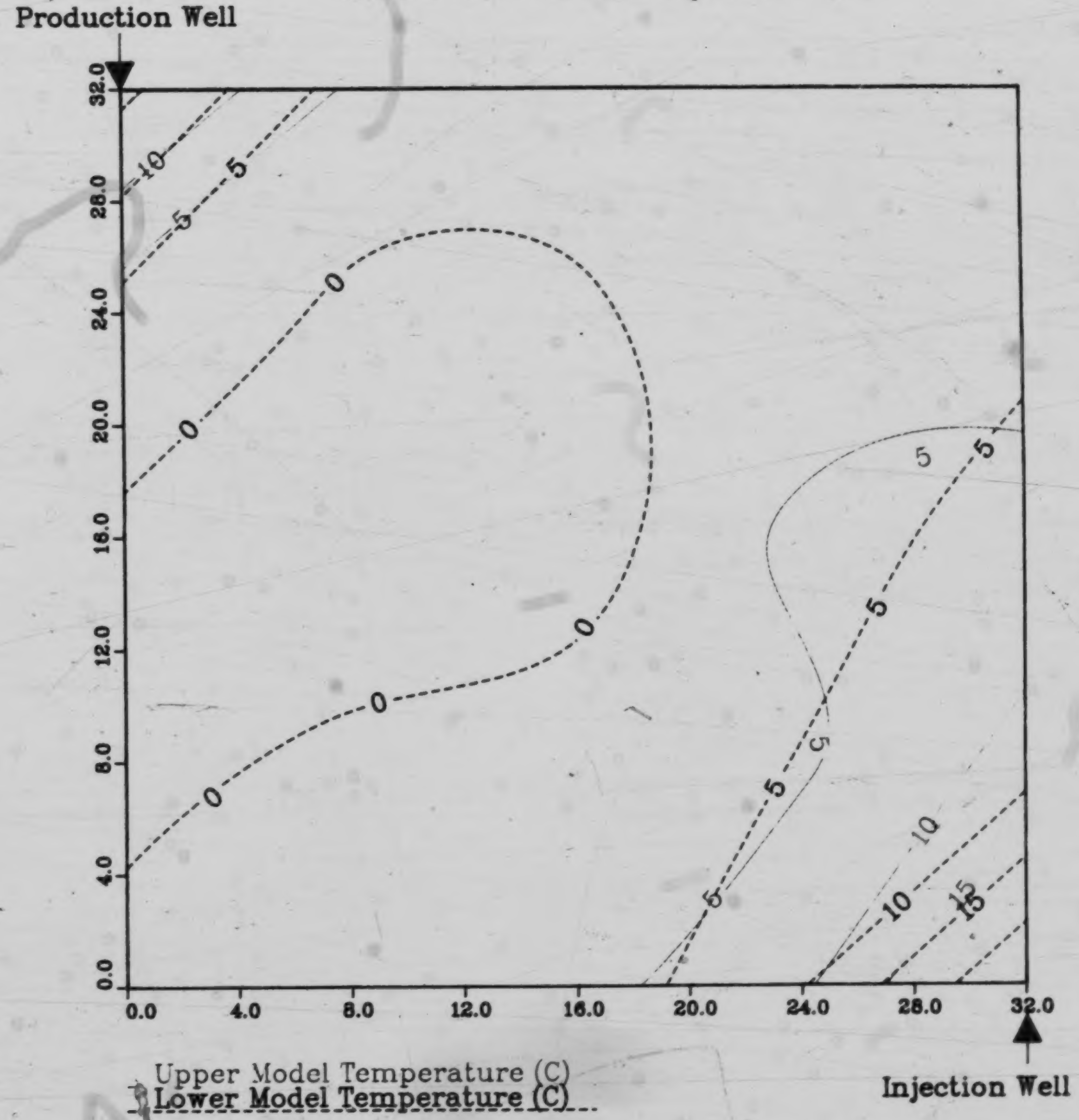

Figure A.12 : Run 40

Solvent Flood in Homogeneous Model

Temperature Profile for
0.50 Pore Volumes Injected

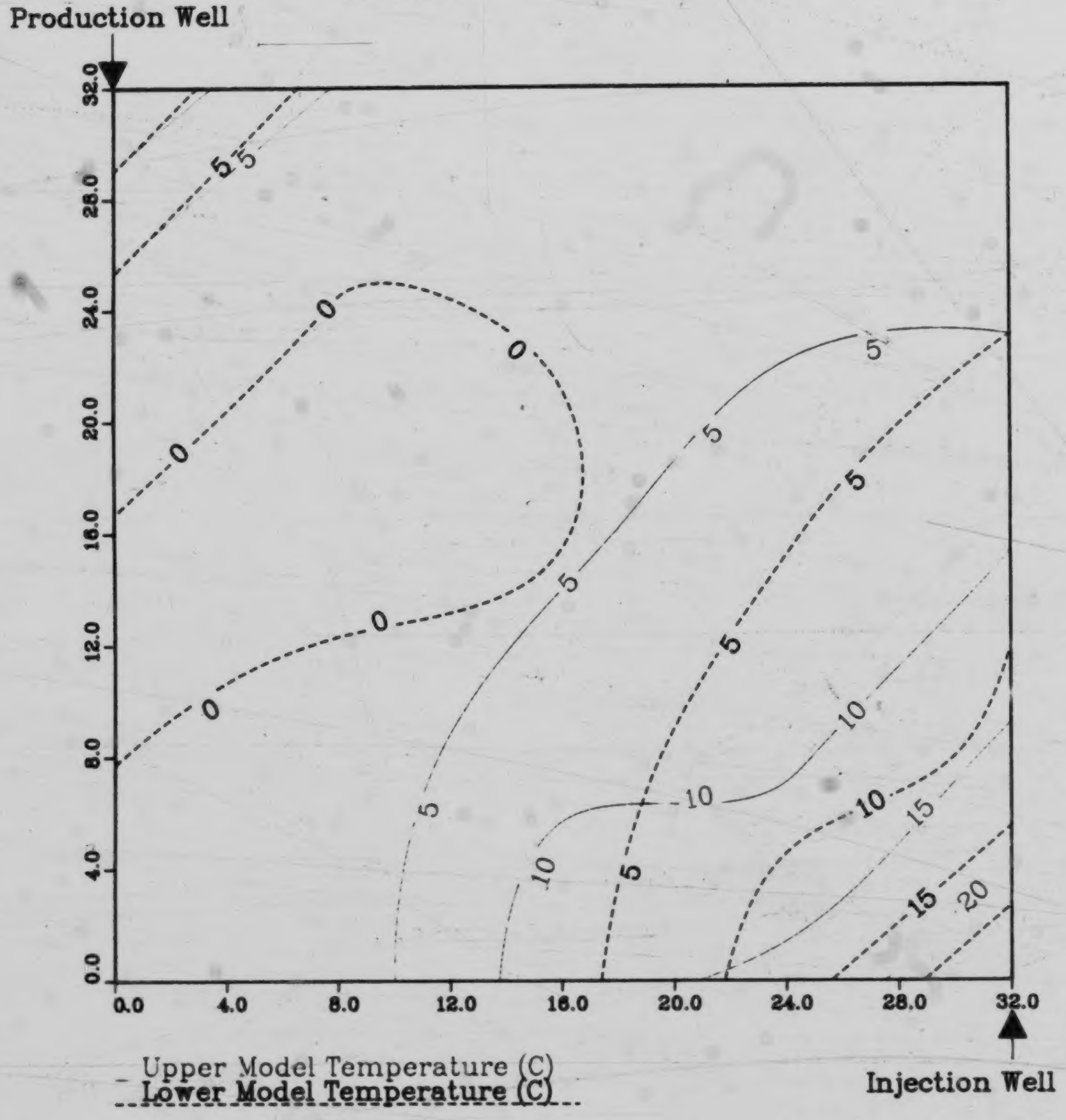

Figure A.13 : Run 40
Solvent Flood in Homogeneous Model

Temperature Profile for
0.75 Pore Volumes Injected

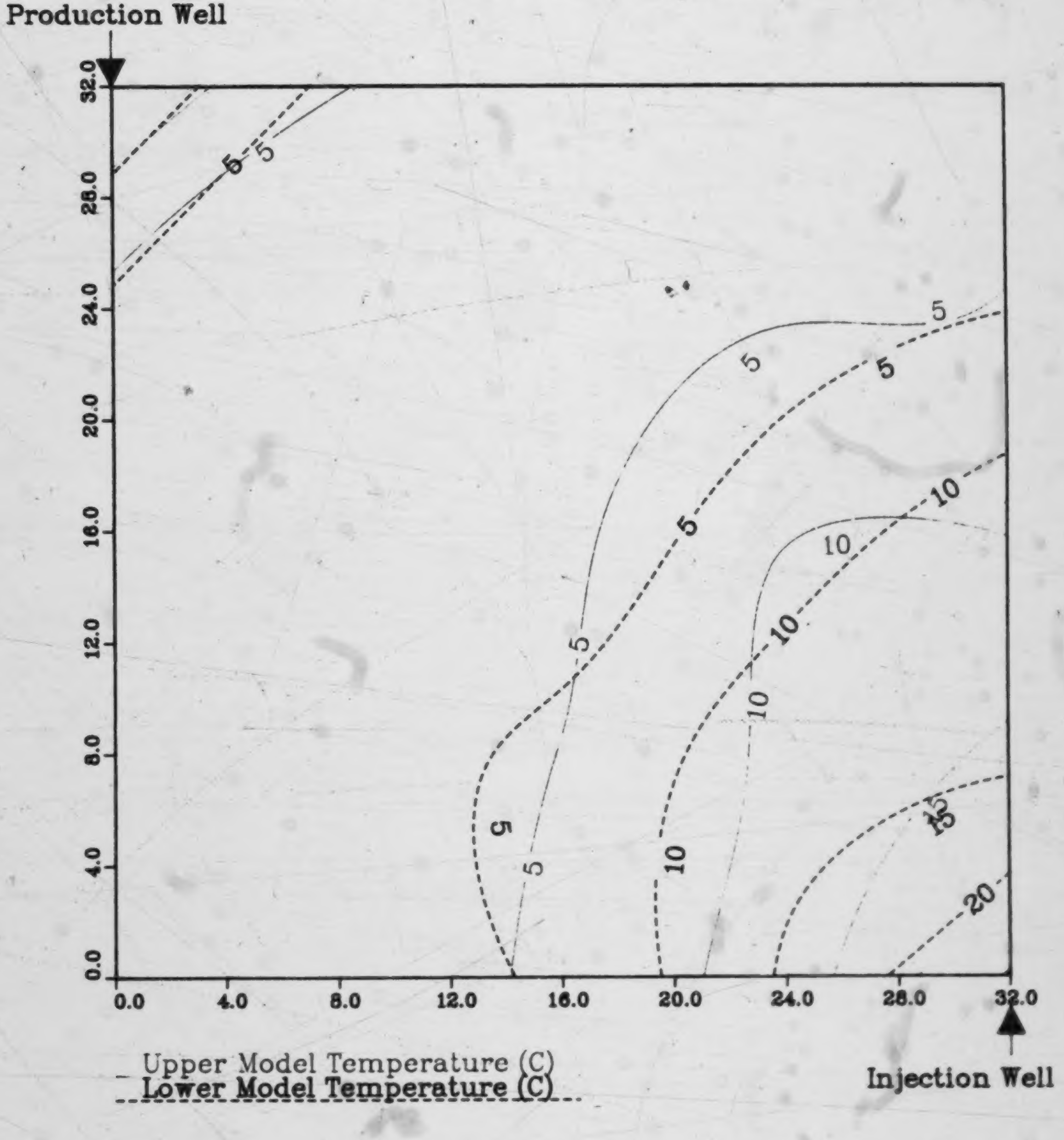

— Upper Model Temperature (C)
- - - Lower Model Temperature (C)

Figure A.14 : Run 40

Solvent Flood in Homogeneous Model

Temperature Profile for
1.00 Pore Volumes Injected

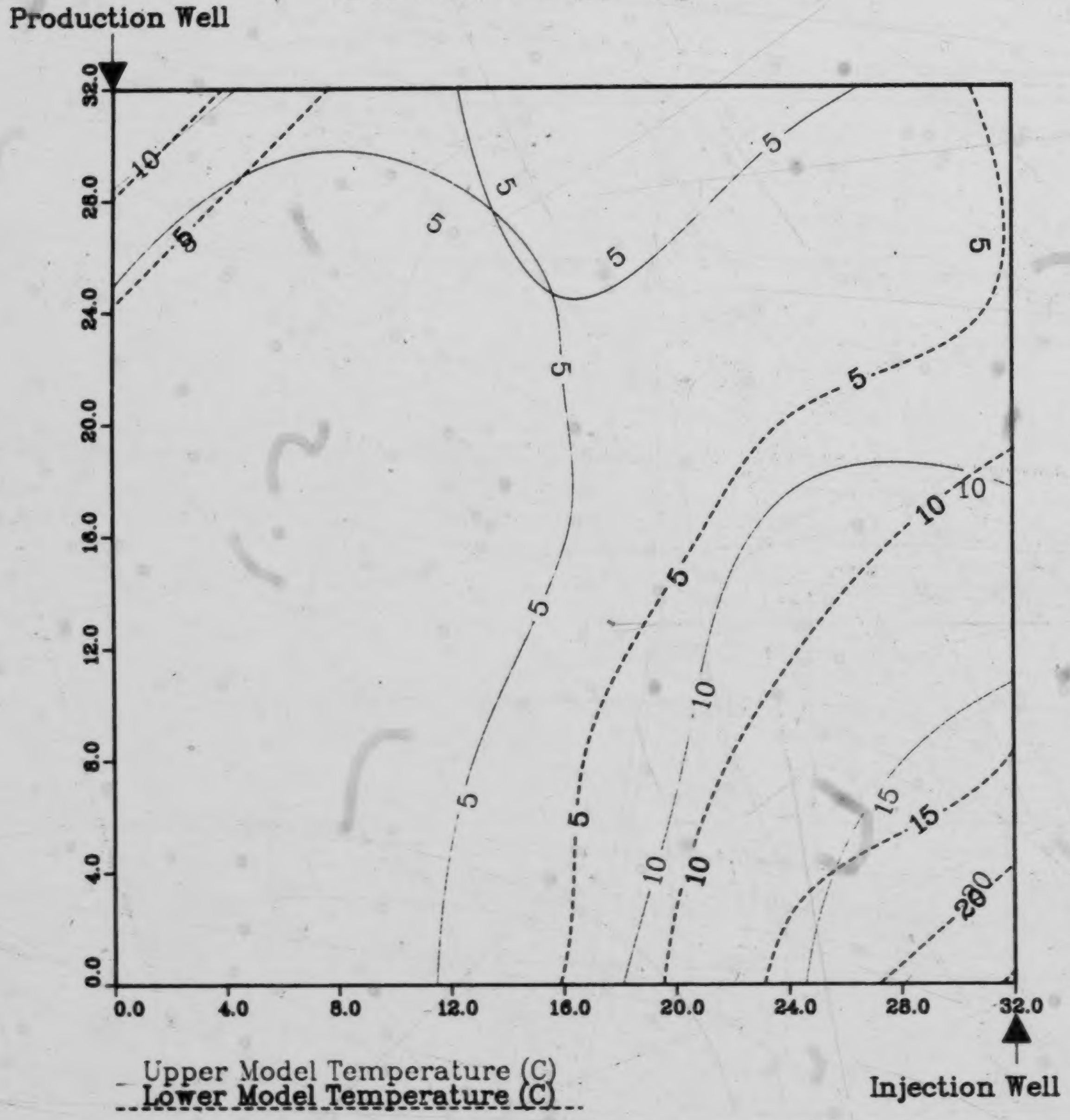

Figure A.15 : Run 40
Solvent Flood in Homogeneous Model

Temperature Profile for 1.25 Pore Volumes Injected

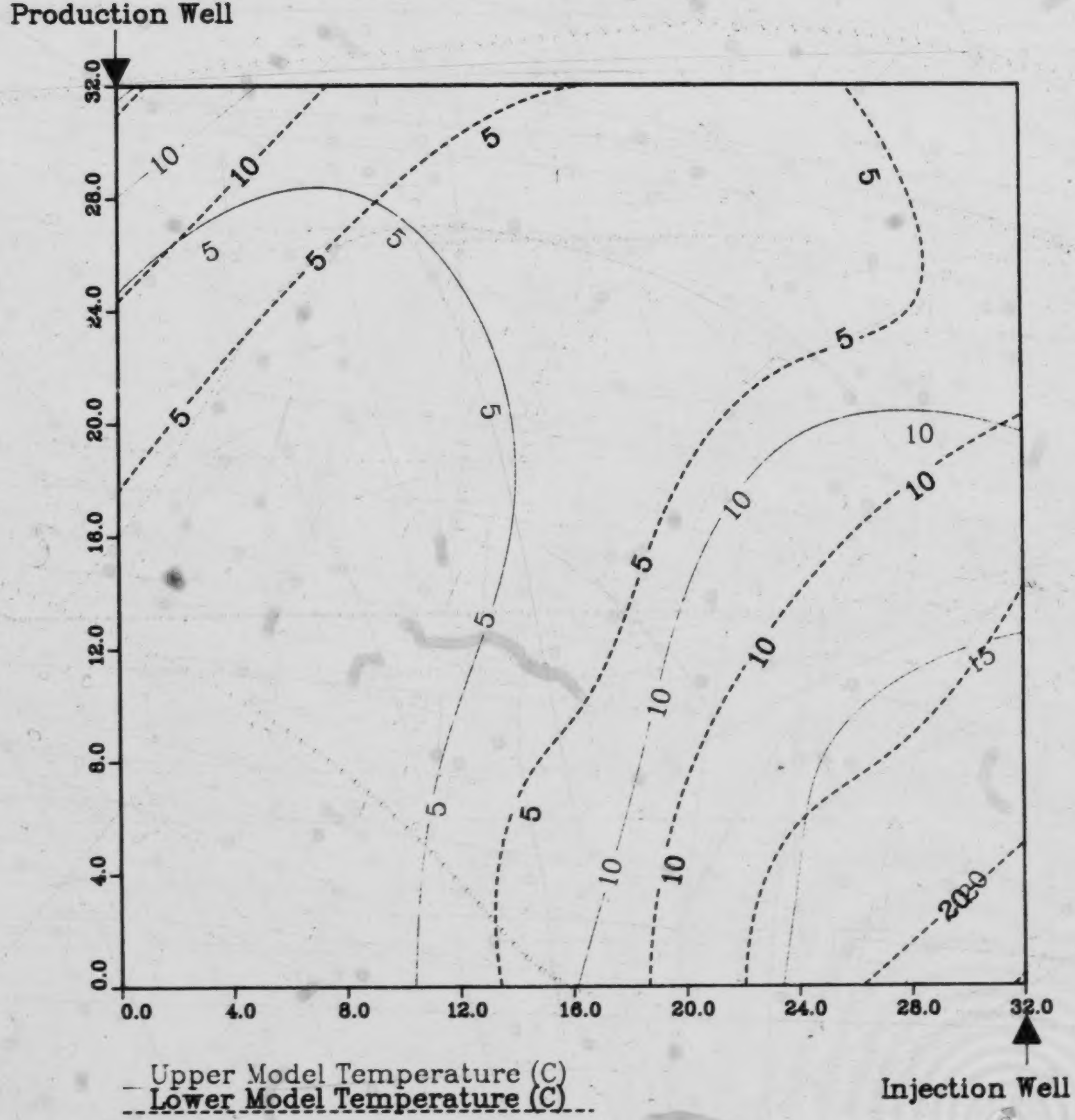

Figure A.16 : Run 40

Solvent Flood in Homogeneous Model

Temperature Profile for
1.50 Pore Volumes Injected

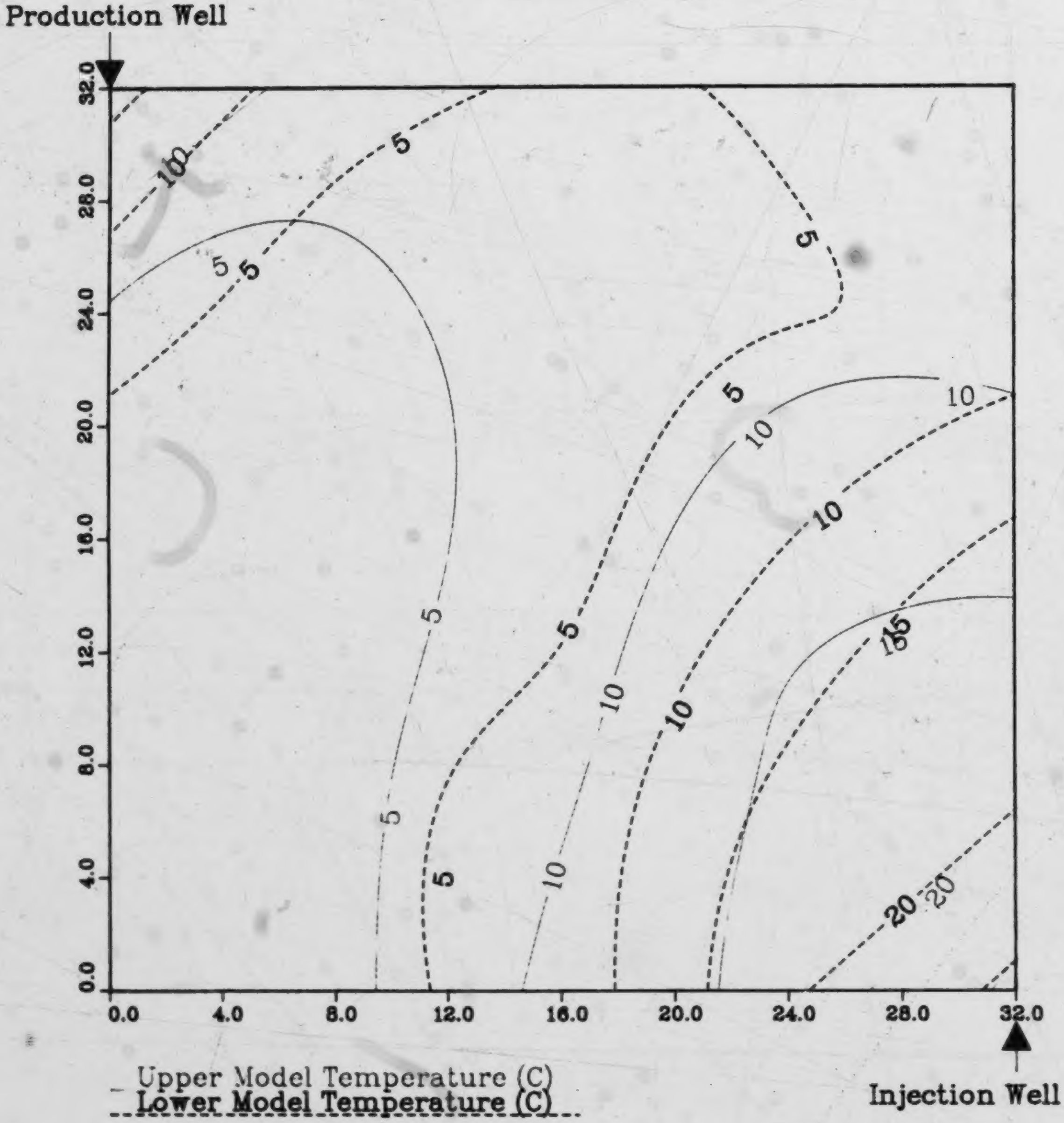

Figure A.17 : Run 40

Solvent Flood in Homogeneous Model

Temperature Profile for 1.75 Pore Volumes Injected

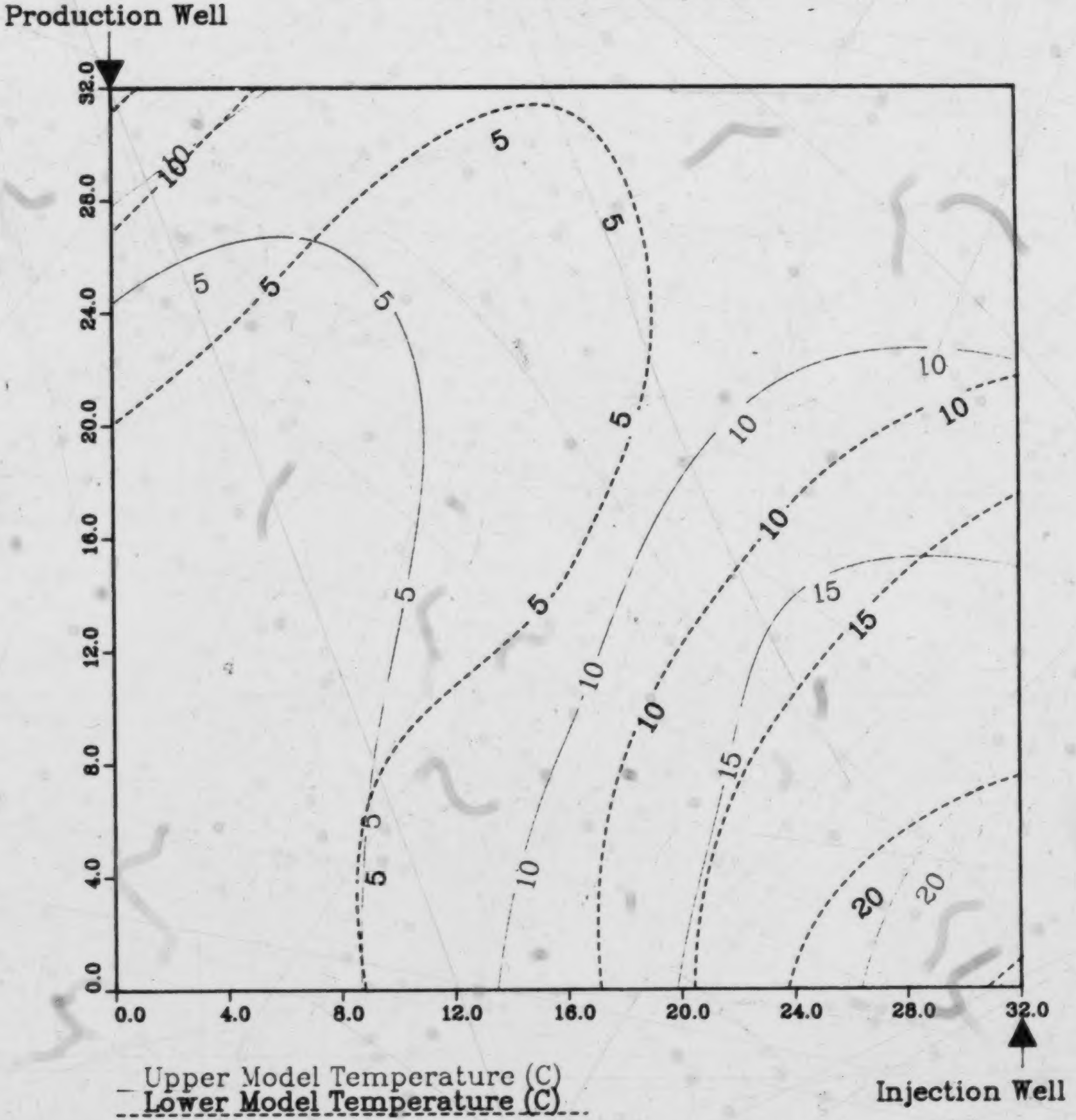

Figure A.18 : Run 40

Solvent Flood in Homogeneous Model

Temperature Profile for 2.00 Pore Volumes Injected

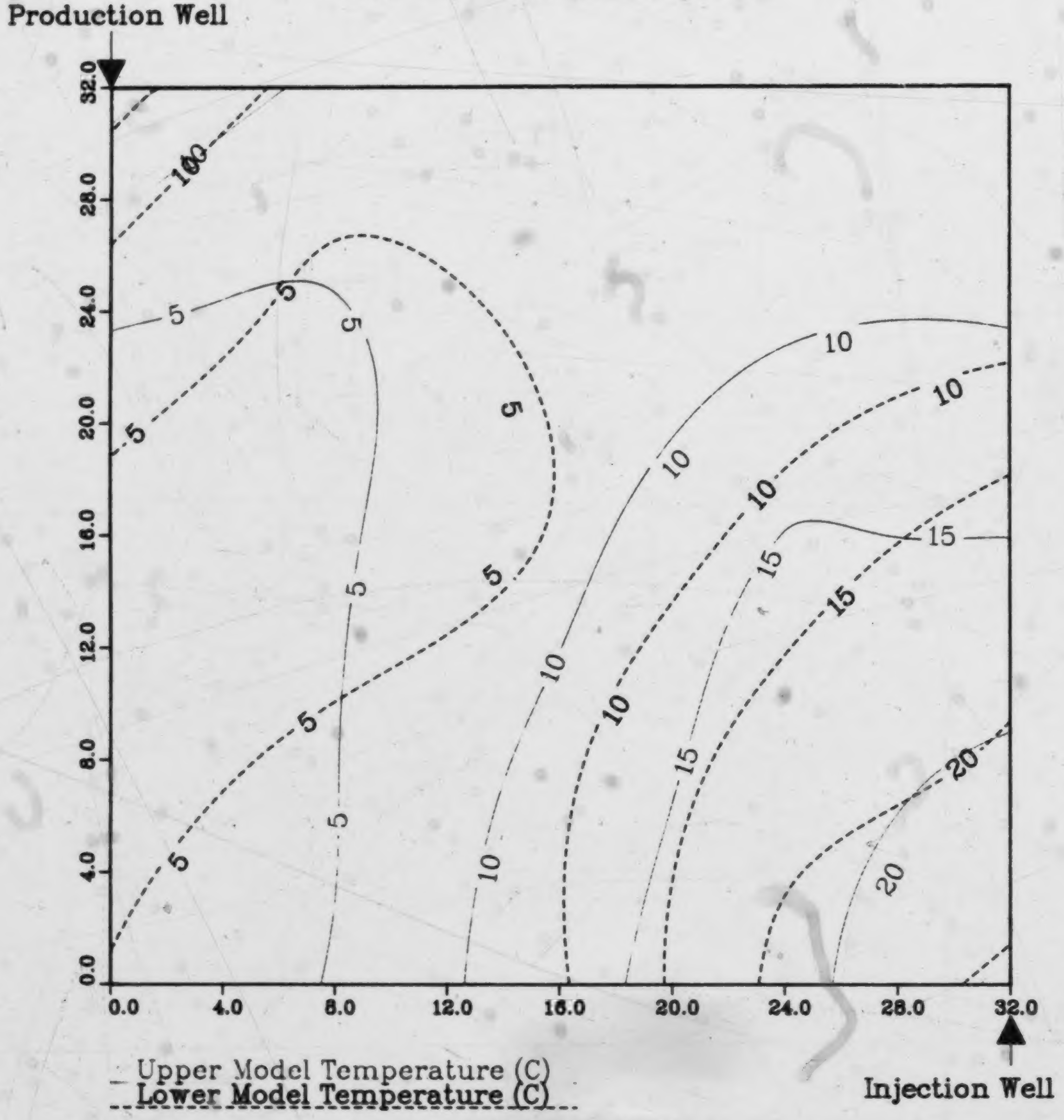

Figure A.19 :Run 40 Temp Profile
Injector to Producer Cross–Section

0.25 Pore Volumes Injected.

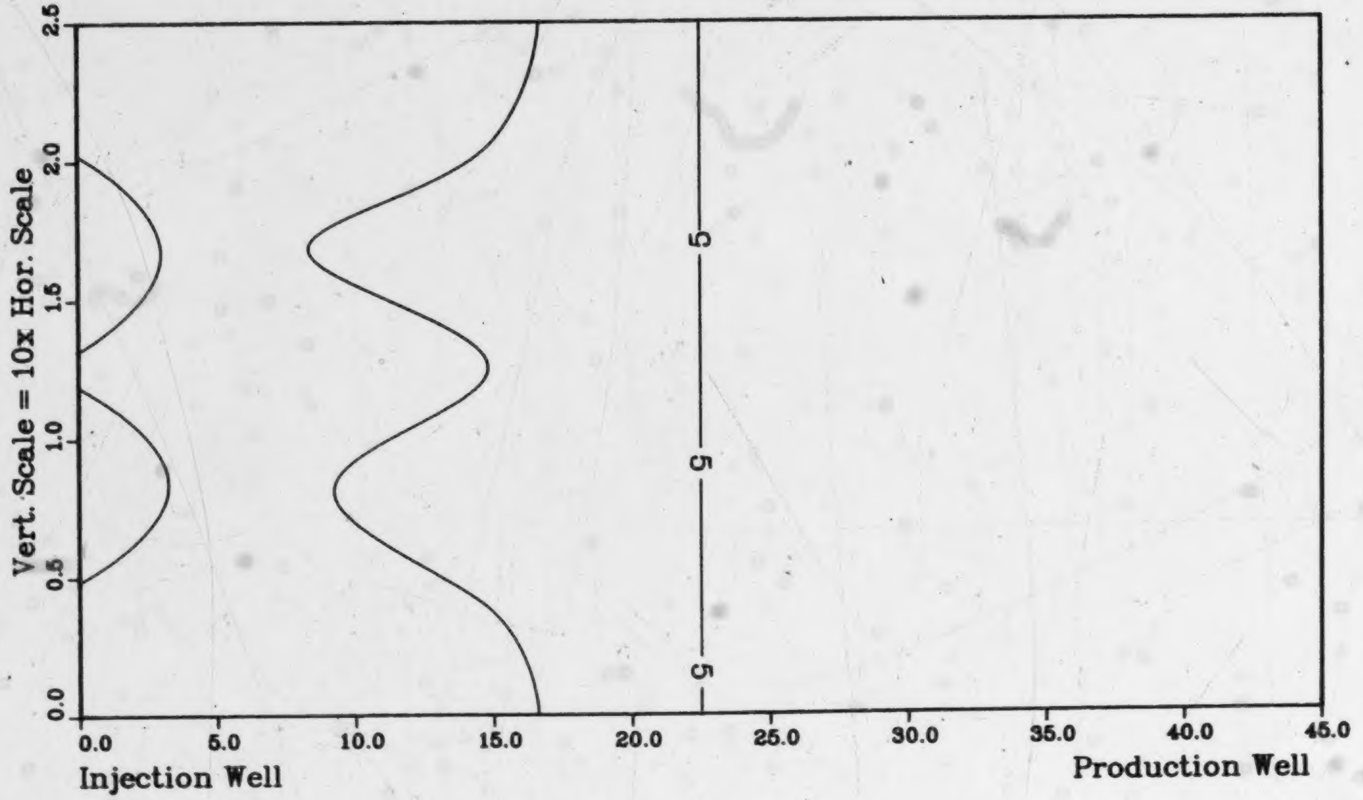

Figure A.20 :Run 40 Temp Profile
Injector to Producer Cross–Section
0.50 Pore Volumes Injected.

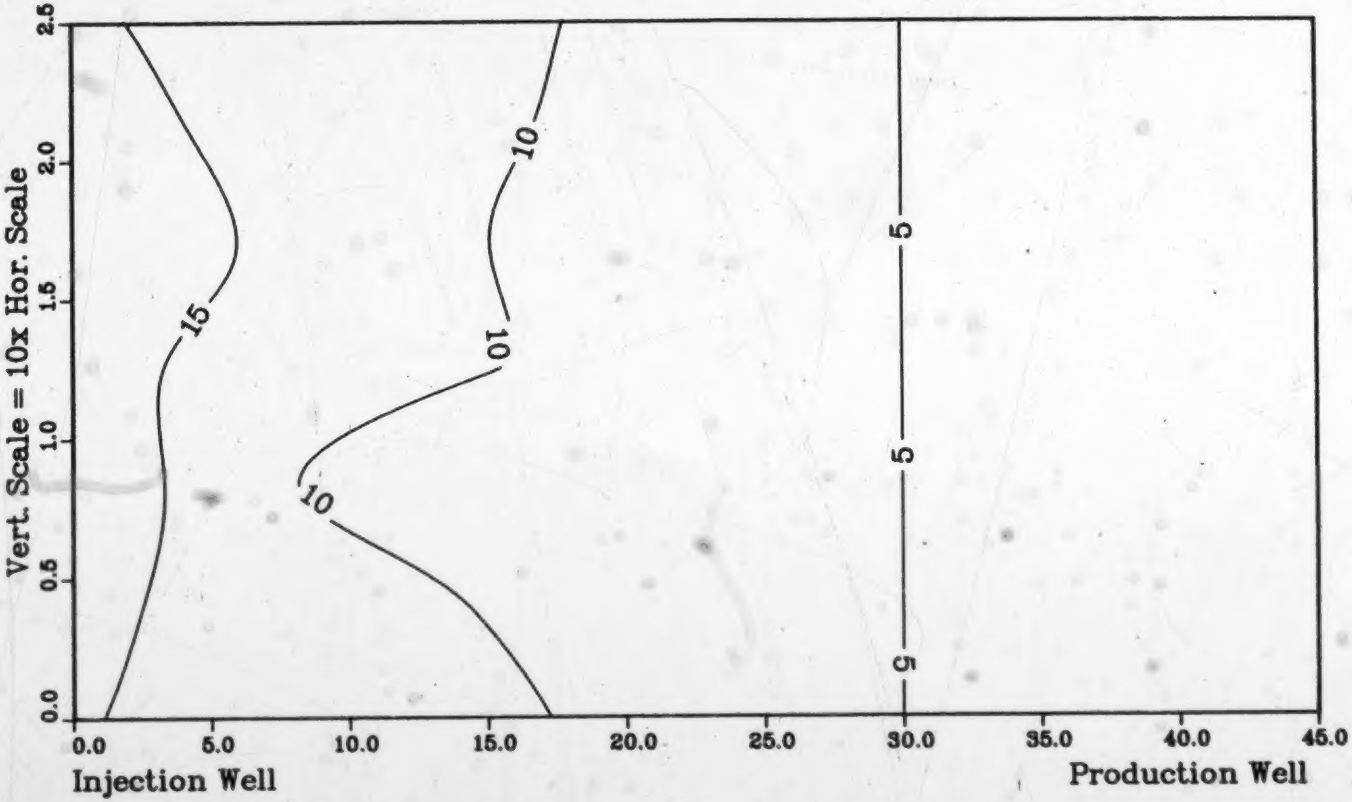

Figure A.21 :Run 40 Temp Profile

Injector to Producer Cross–Section

0.75 Pore Volumes Injected.

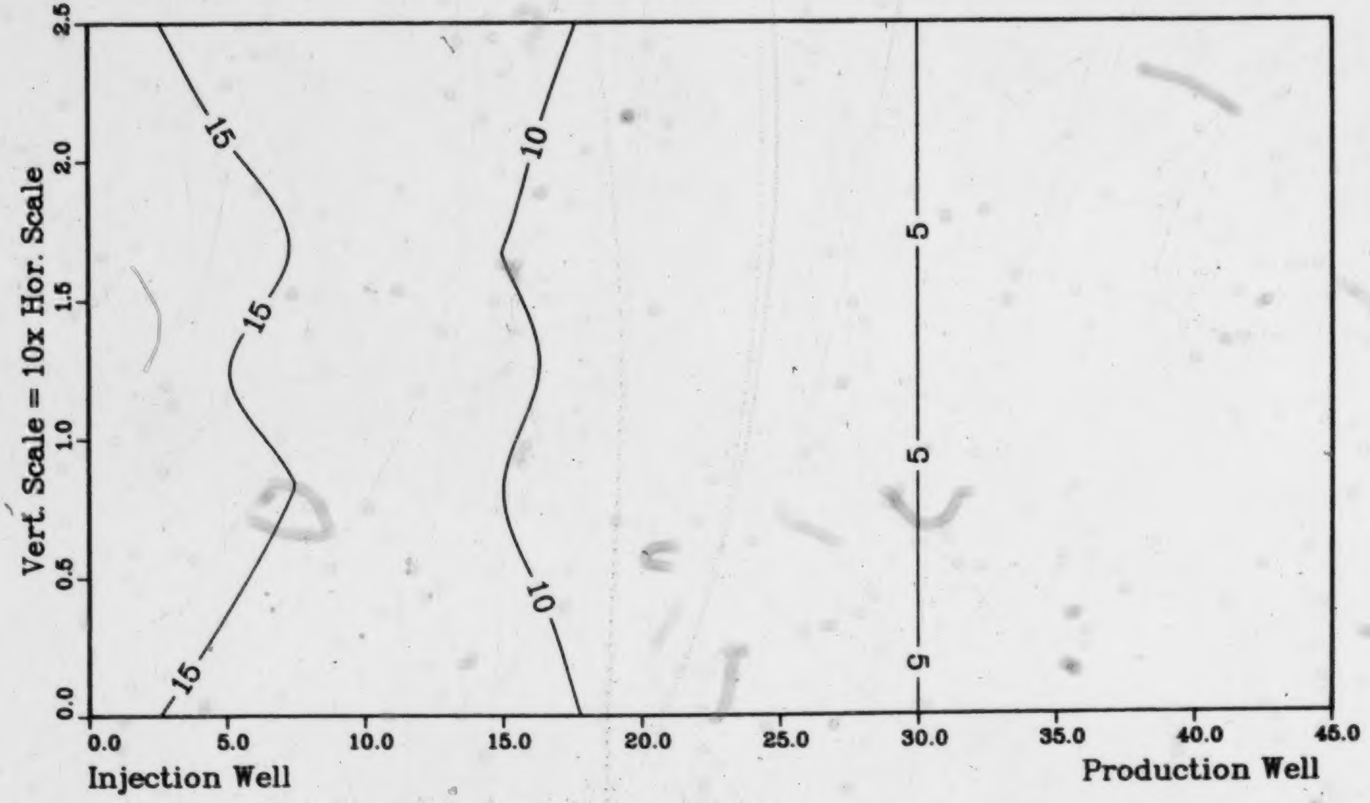

Figure A.22 :Run 40 Temp Profile
Injector to Producer Cross–Section
1.00 Pore Volumes Injected.

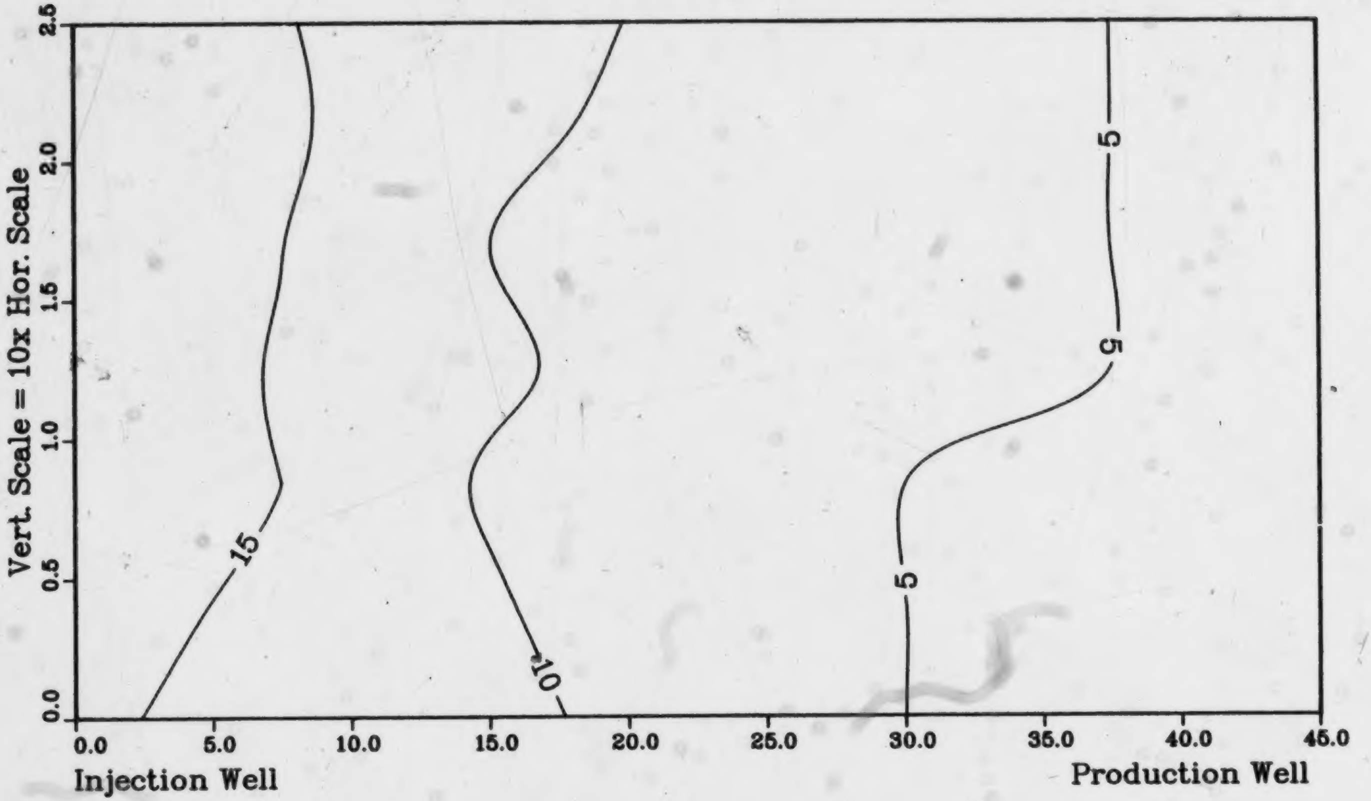

Figure A.23 : Run 44
Solvent–Steamflood in Homogeneous Model

Temperature Profile for 0.25 Pore Volumes Injected

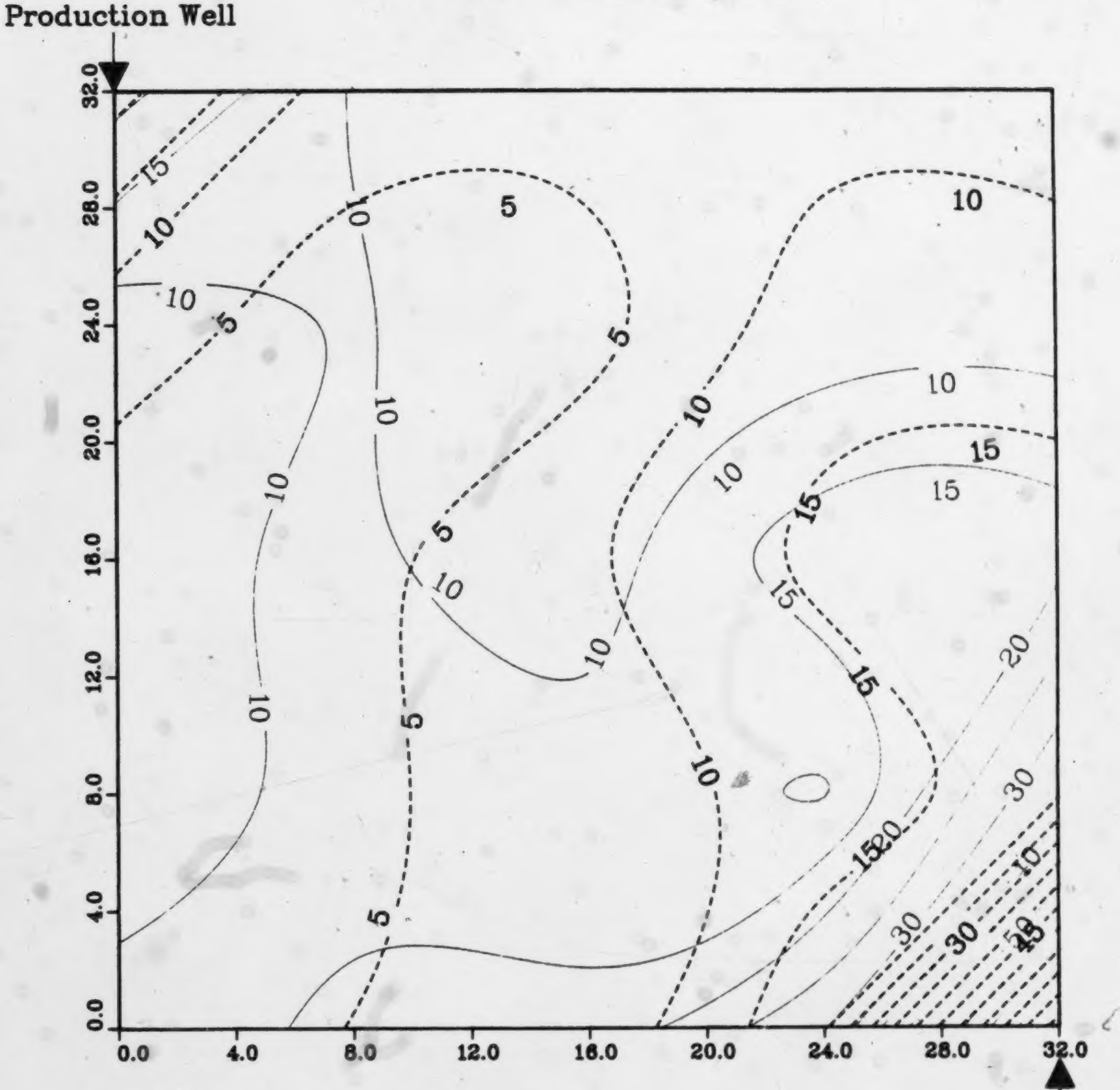

_ Upper Model Temperature (C)
Lower Model Temperature (C)
--------

Figure A.24 : Run 44

Solvent–Steamflood in Homogeneous Model

Temperature Profile for
0.50 Pore Volumes Injected

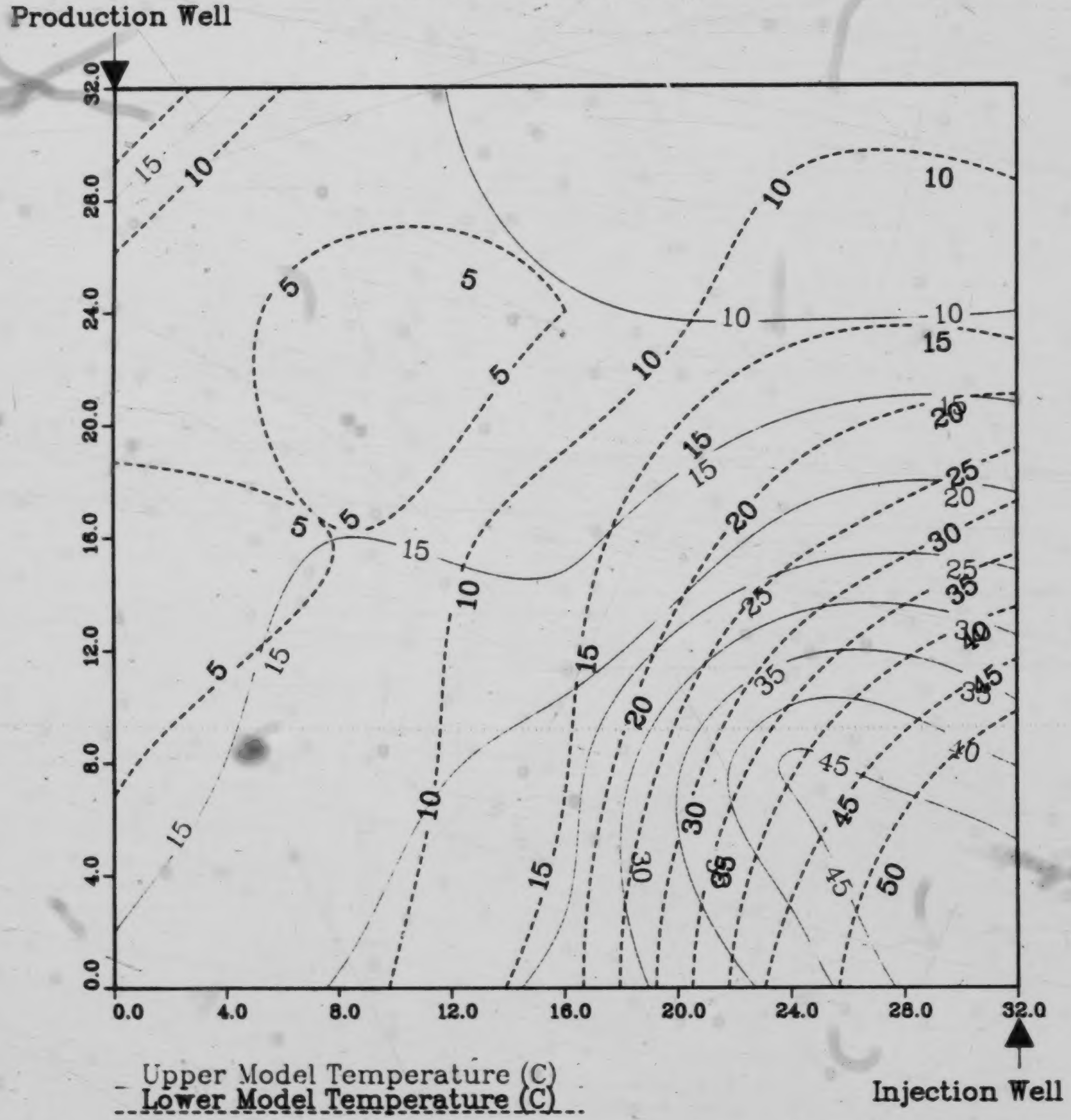

Figure A.25 : Run 44

Solvent–Steamflood in Homogeneous Model

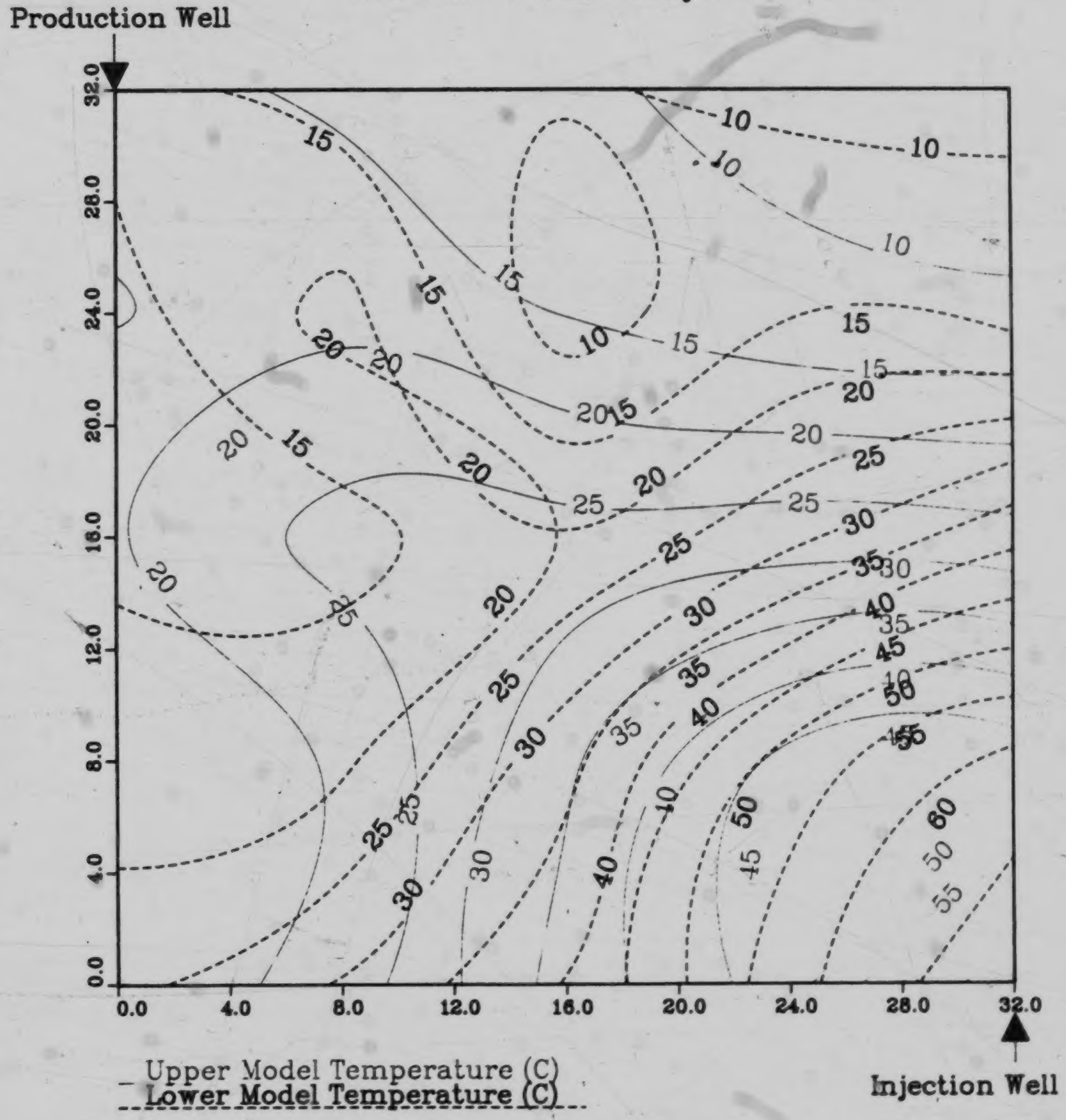

Figure A.26 : Run 44

Solvent–Steamflood in Homogeneous Model

Temperature Profile for 1.00 Pore Volumes Injected

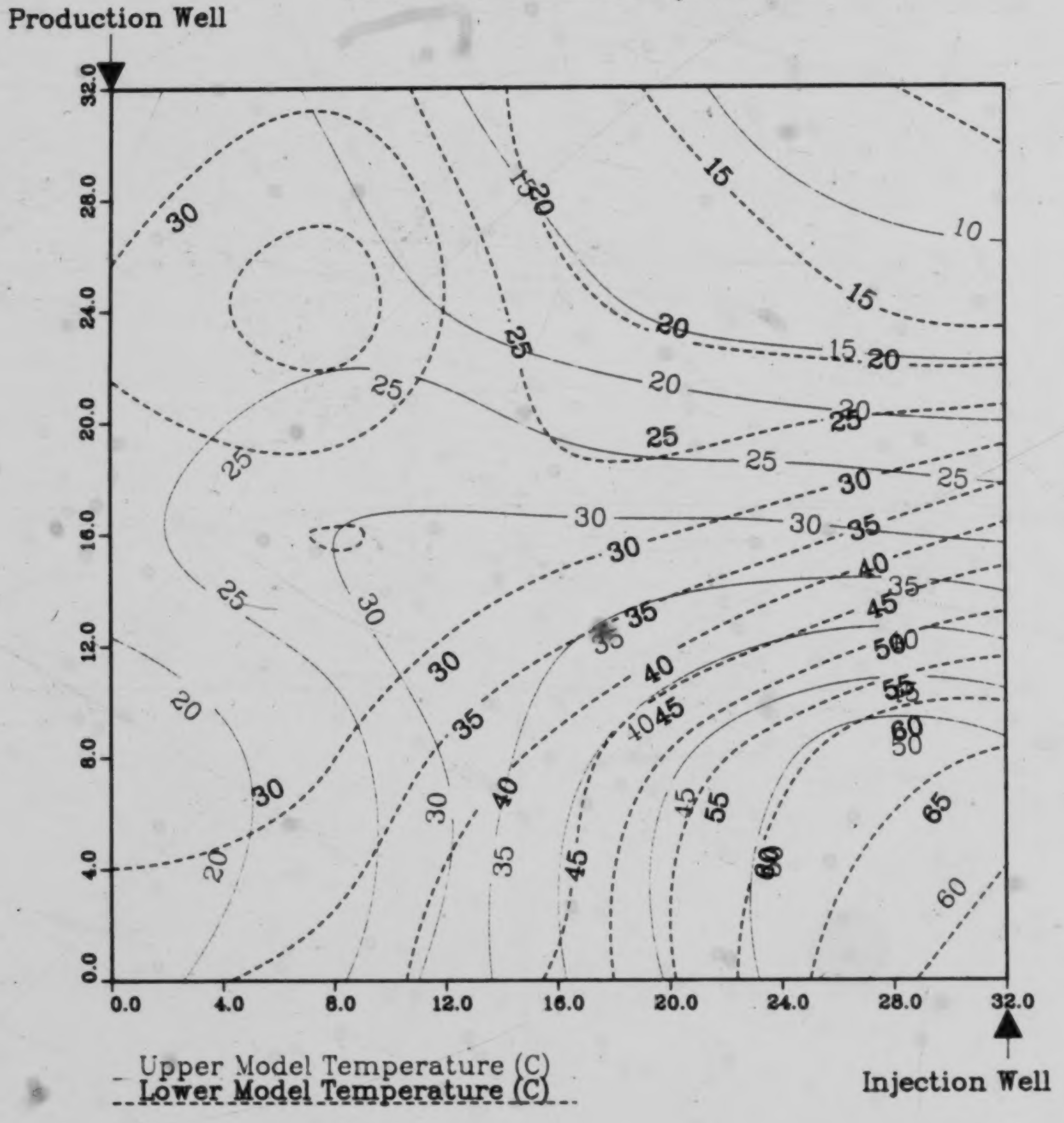

Figure A.27 : Run 44

Solvent–Steamflood in Homogeneous Model

Temperature Profile for 1.25 Pore Volumes Injected

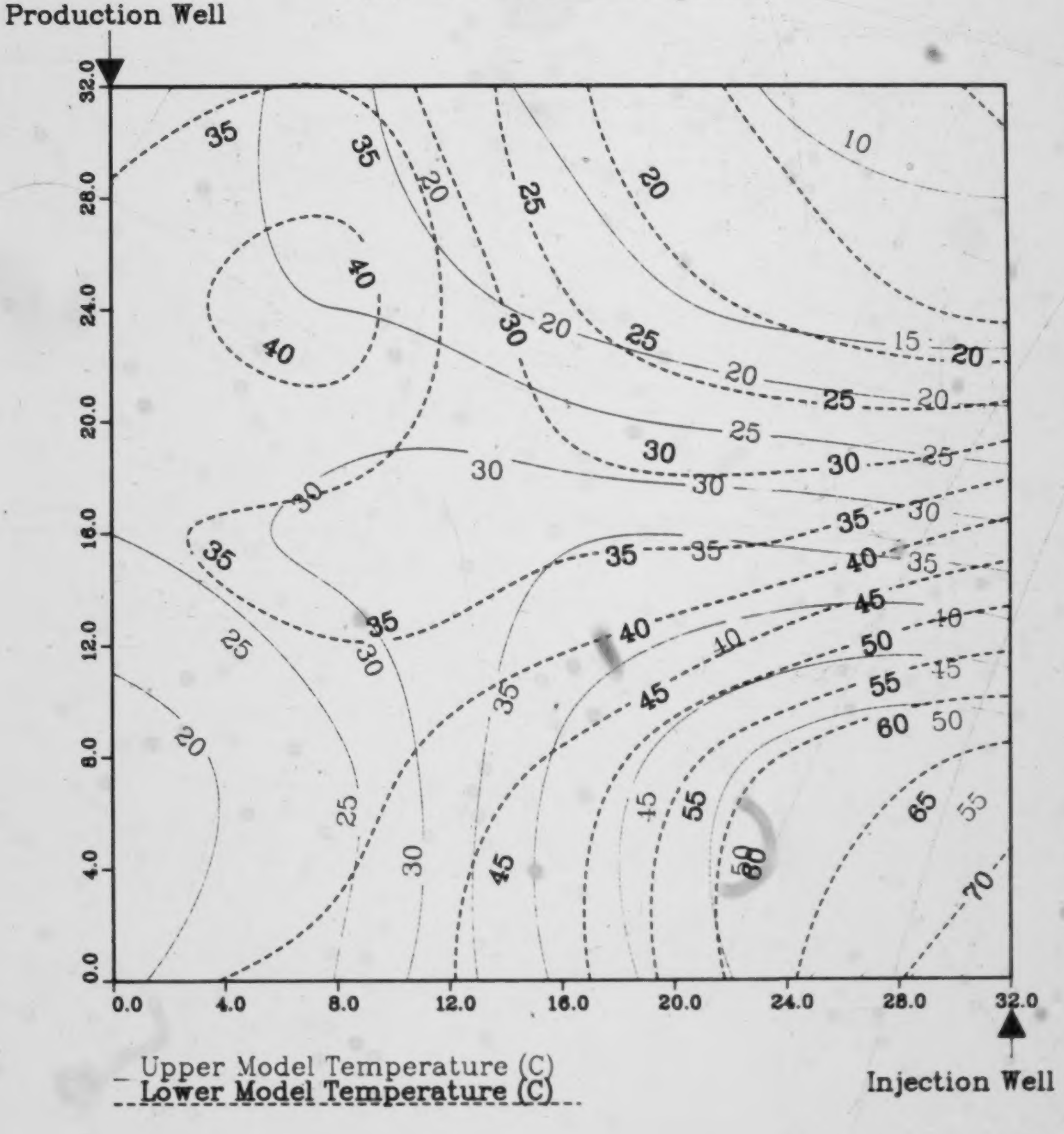

Figure A.28 : Run 44

Solvent–Steamflood in Homogeneous Model

Temperature Profile for 1.50 Pore Volumes Injected

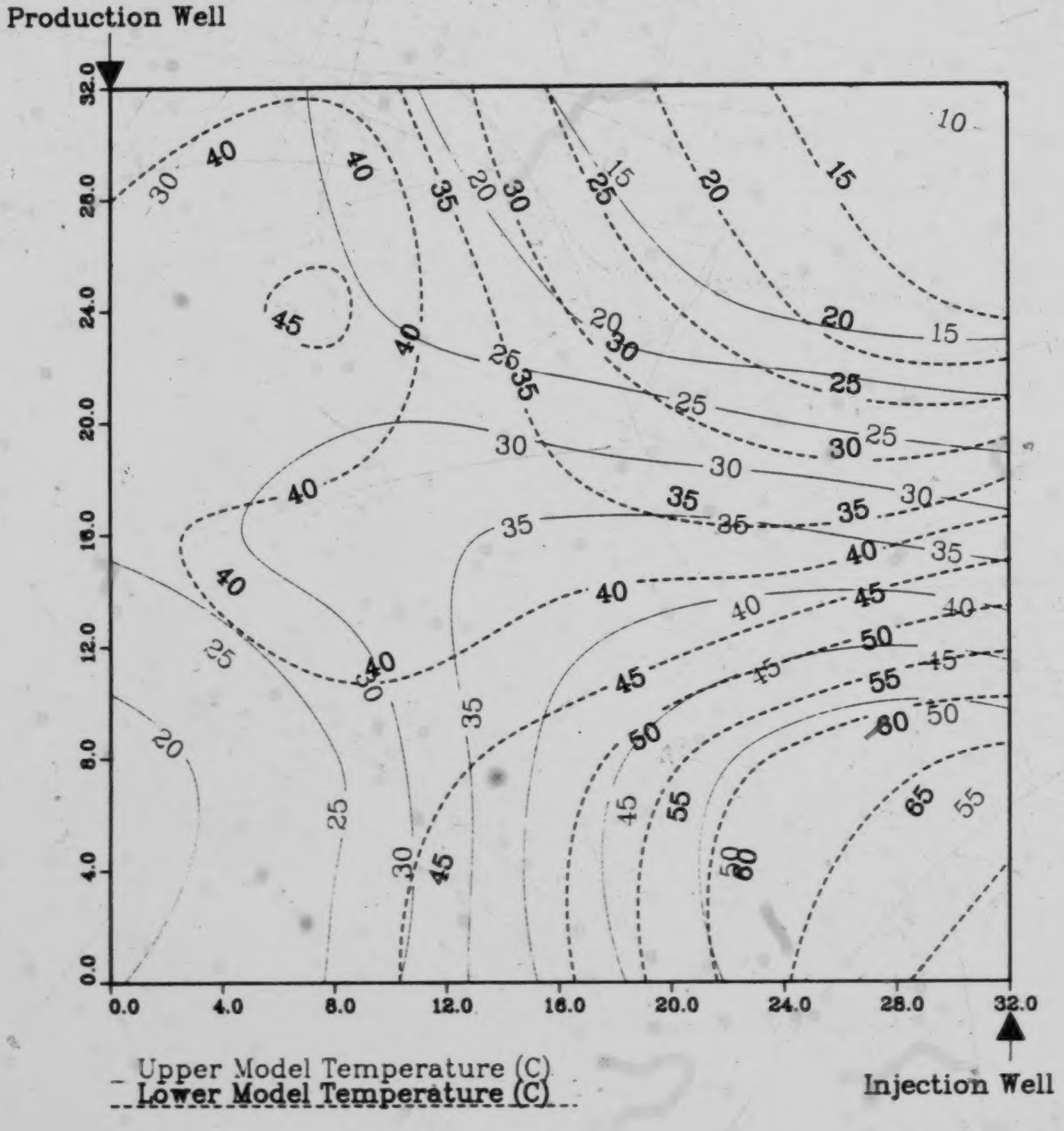

Figure A.29 : Run 44

Solvent–Steamflood in Homogeneous Model

Temperature Profile for 1.75 Pore Volumes Injected

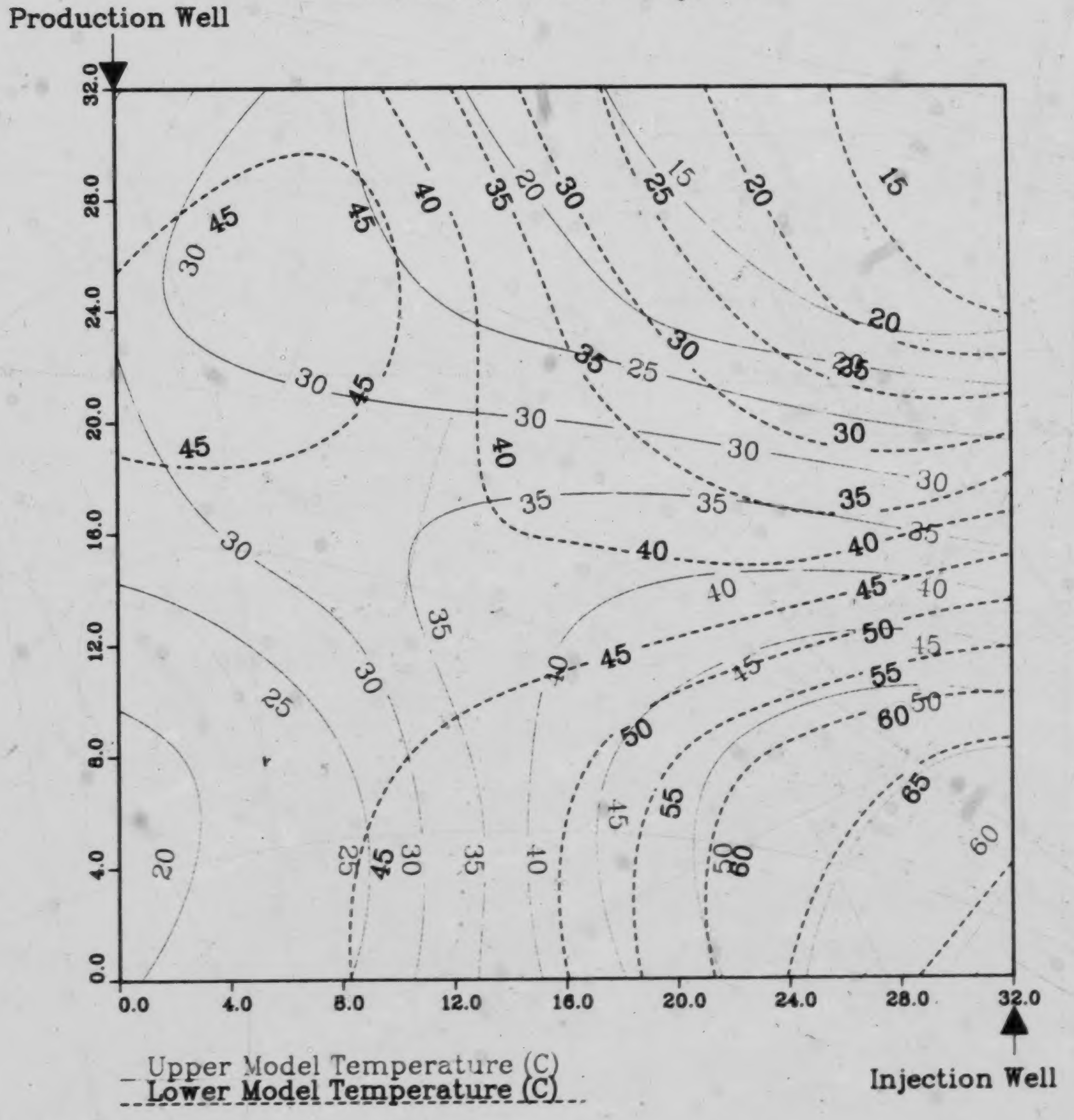

Figure A.30 : Run 44

Solvent–Steamflood in Homogeneous Model

Temperature Profile for 2.00 Pore Volumes Injected

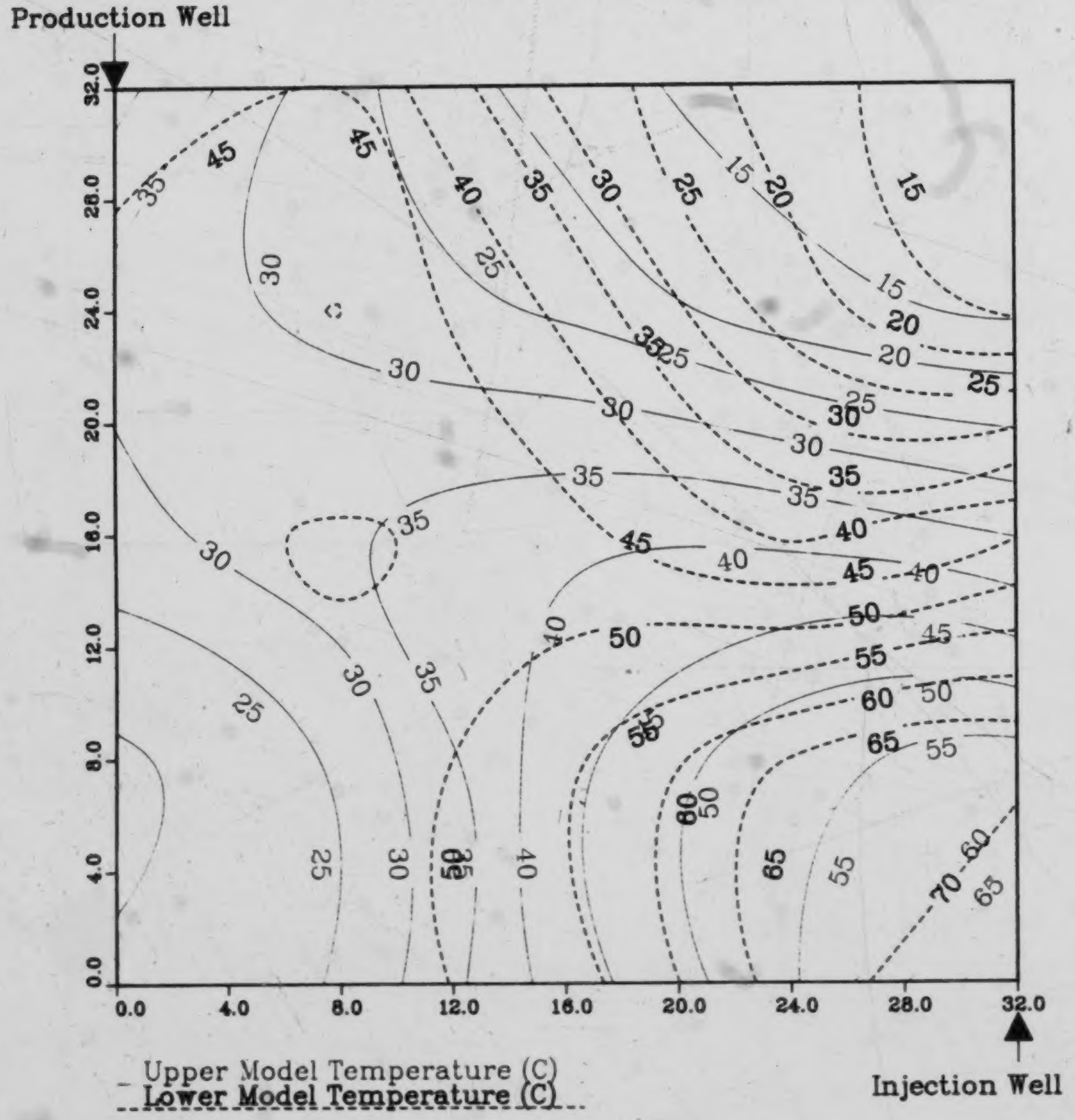

Figure A.31 :Run 44 Temp Profile
Injector to Producer Cross–Section
0.25 Pore Volumes Injected.

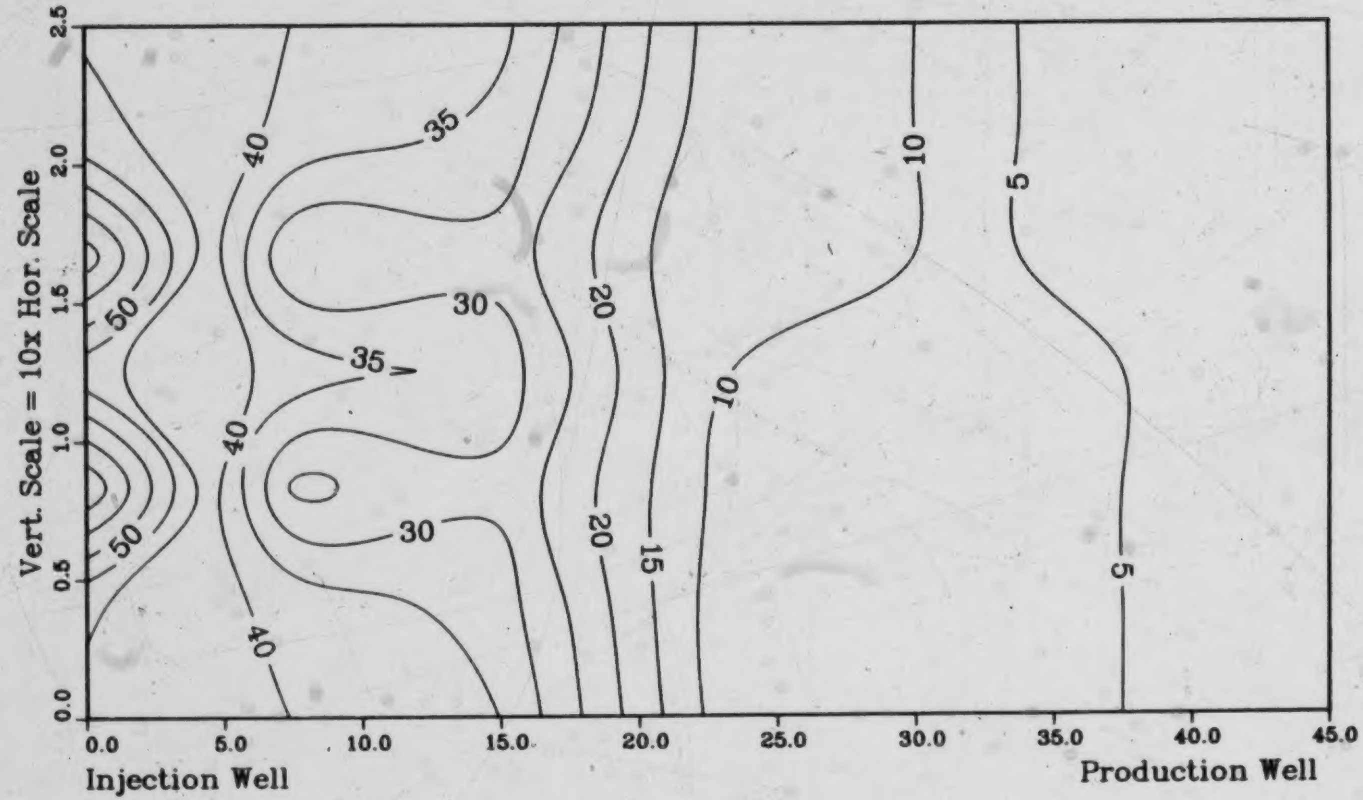

Figure A.32 :Run 44 Temp Profile
Injector to Producer Cross–Section
0.50 Pore Volumes Injected.

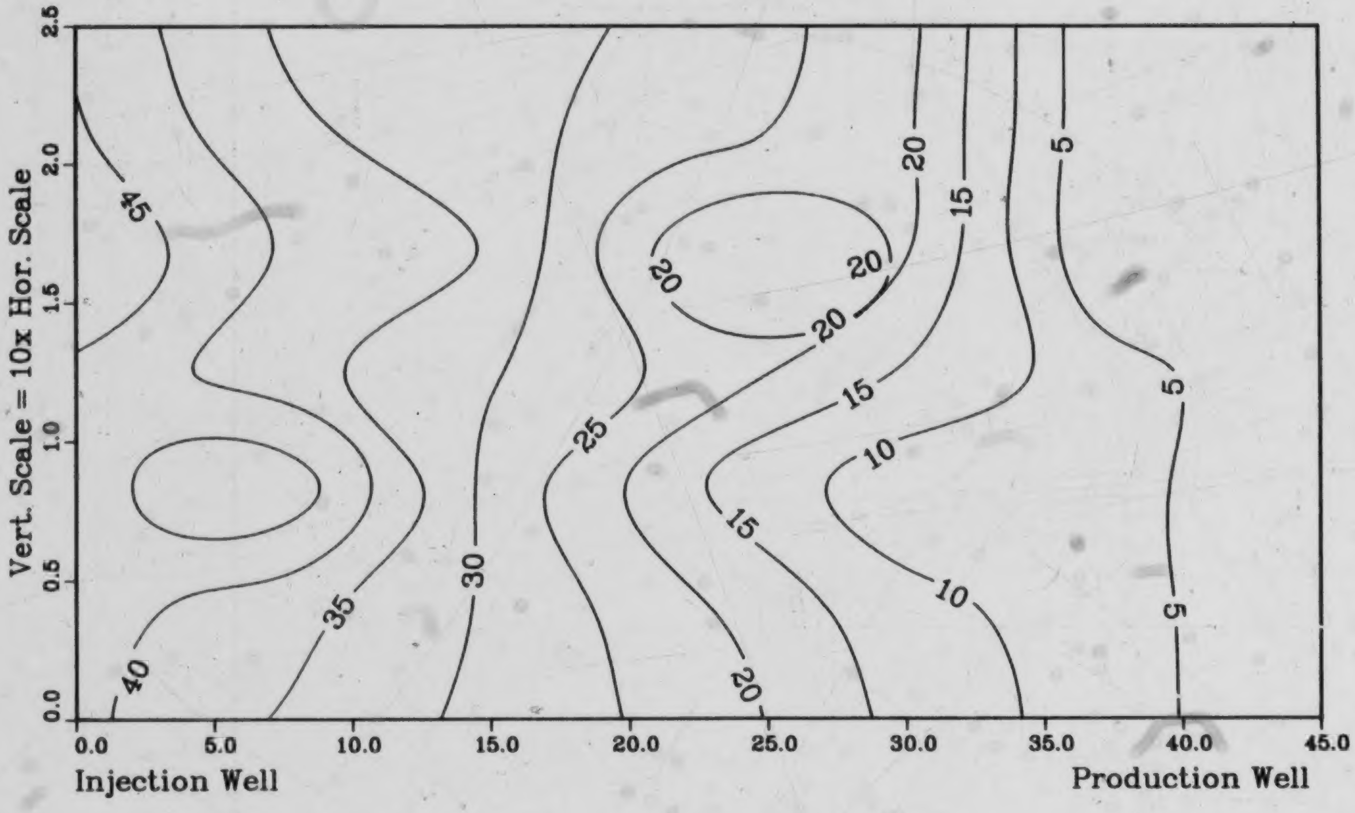

Figure A.33 :Run 44 Temp Profile
Injector to Producer Cross–Section

0.75 Pore Volumes Injected.

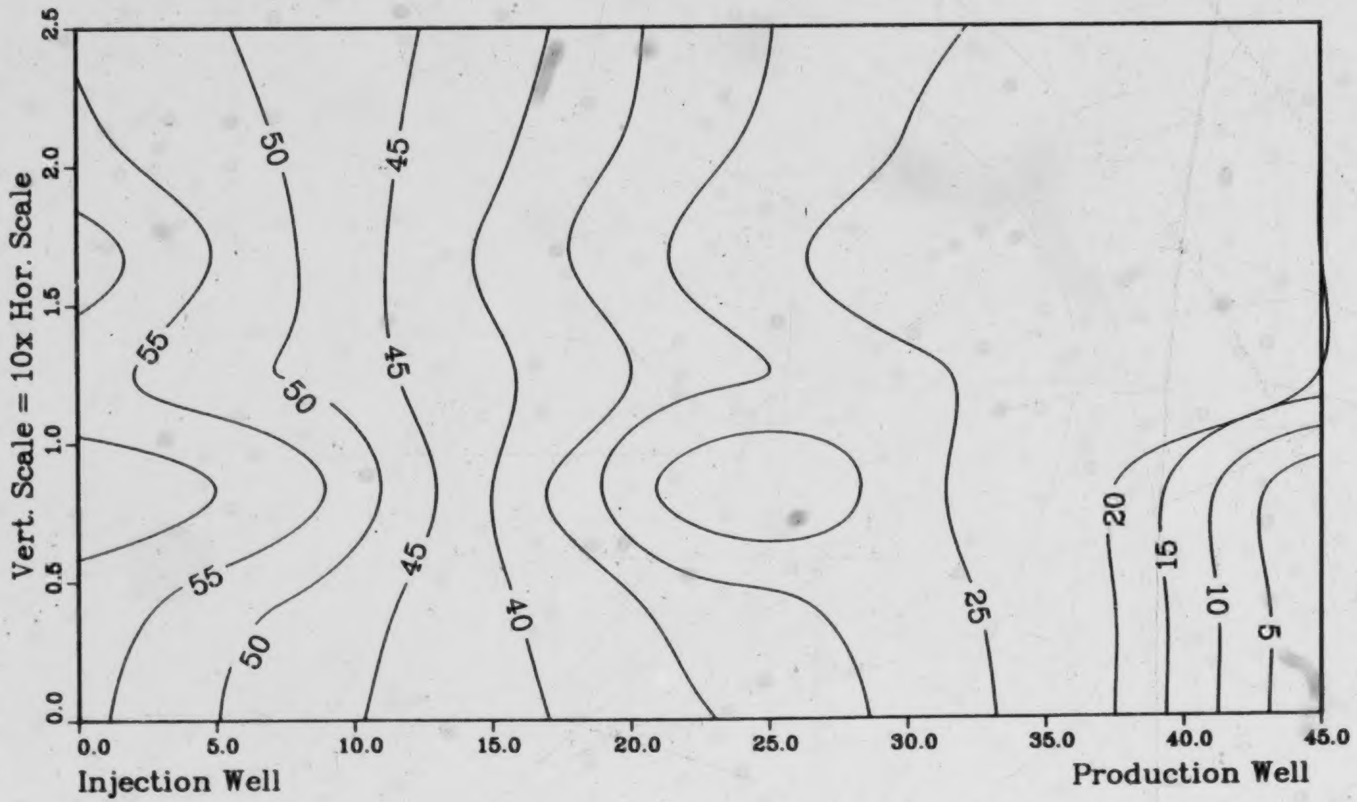

Figure A.34 :Run 44 Temp Profile
Injector to Producer Cross–Section
1.00 Pore Volumes Injected.

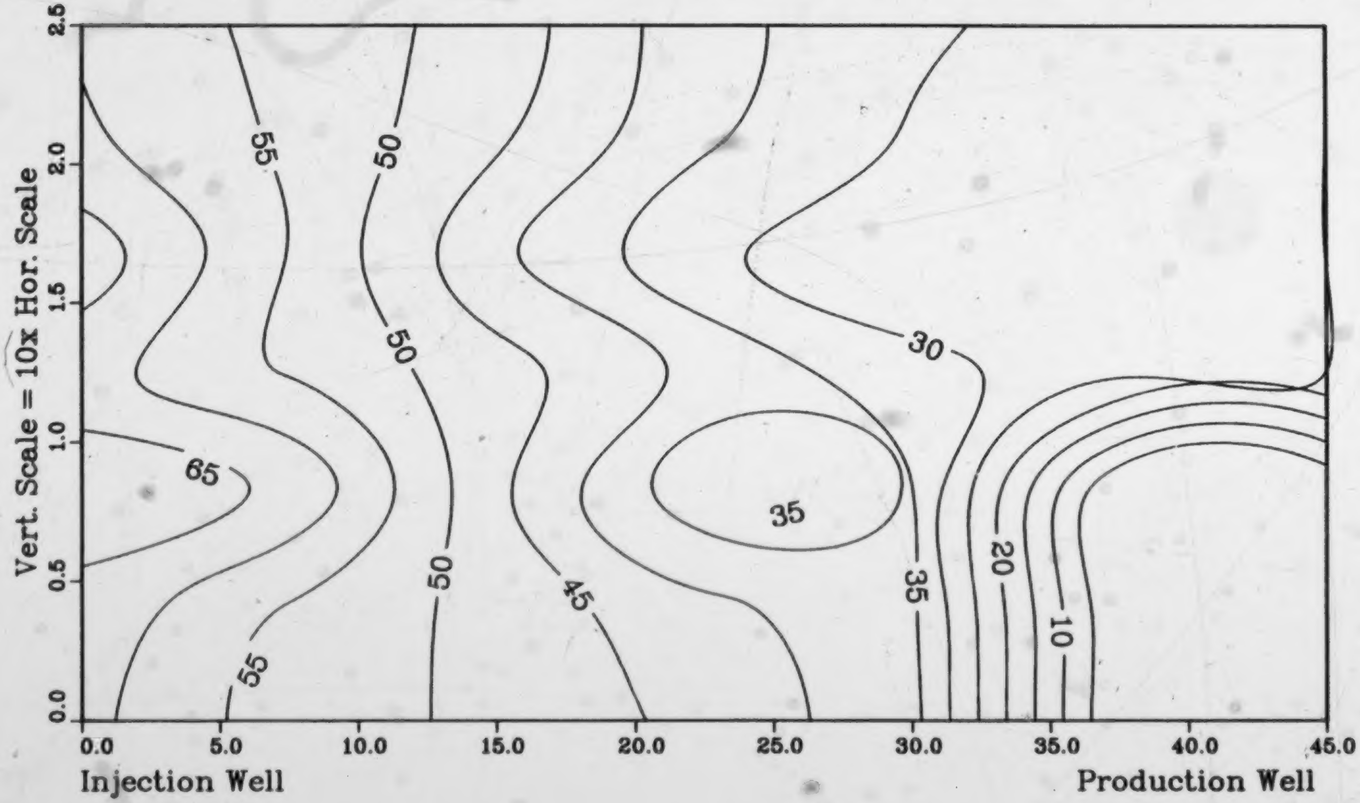

Figure A.35 : Run 45

Solvent–Steamflood in Homogeneous Model

Temperature Profile for 0.25 Pore Volumes Injected

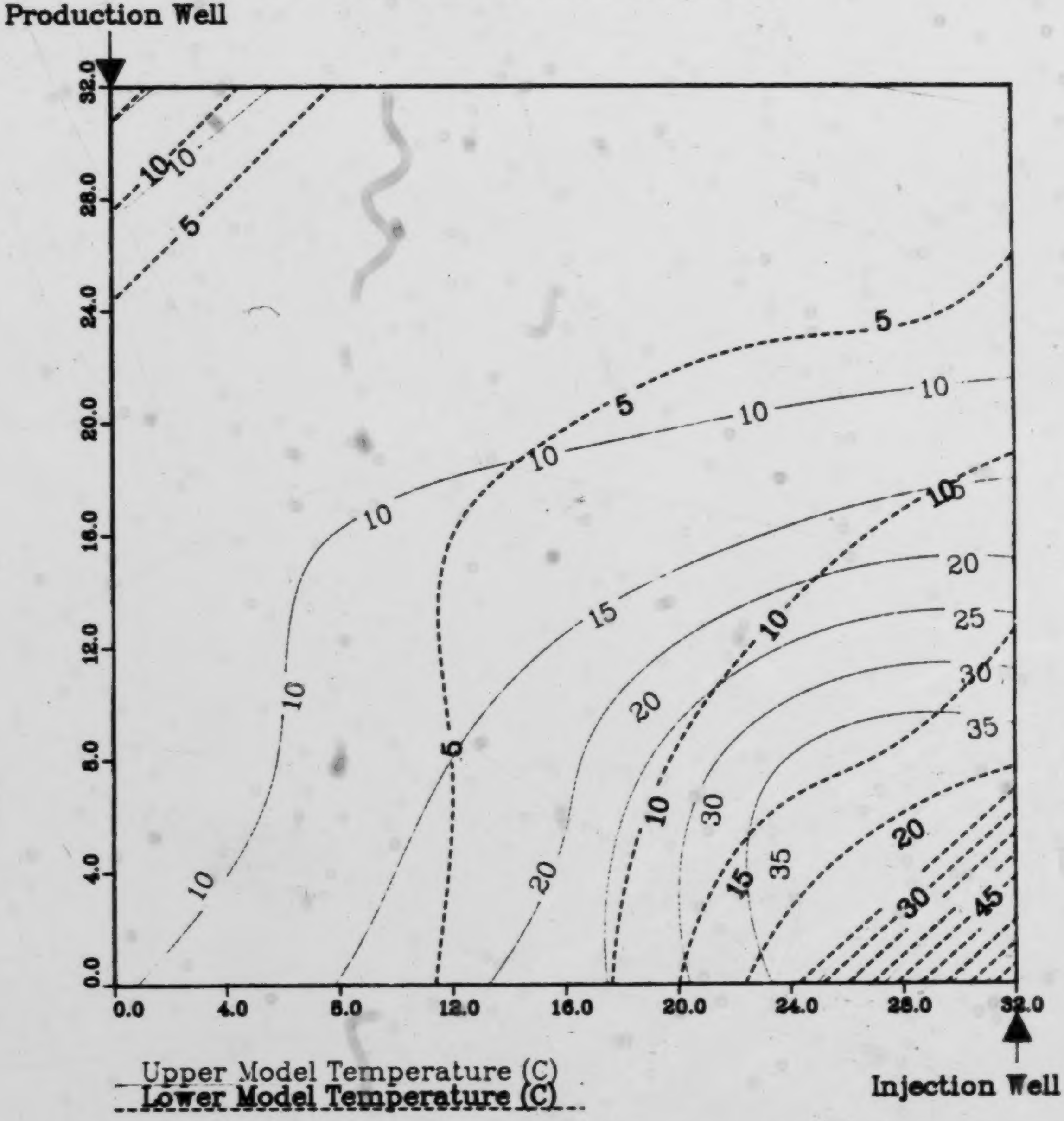

Figure A.36 : Run 45

Solvent–Steamflood in Homogeneous Model

Temperature Profile for 0.50 Pore Volumes Injected

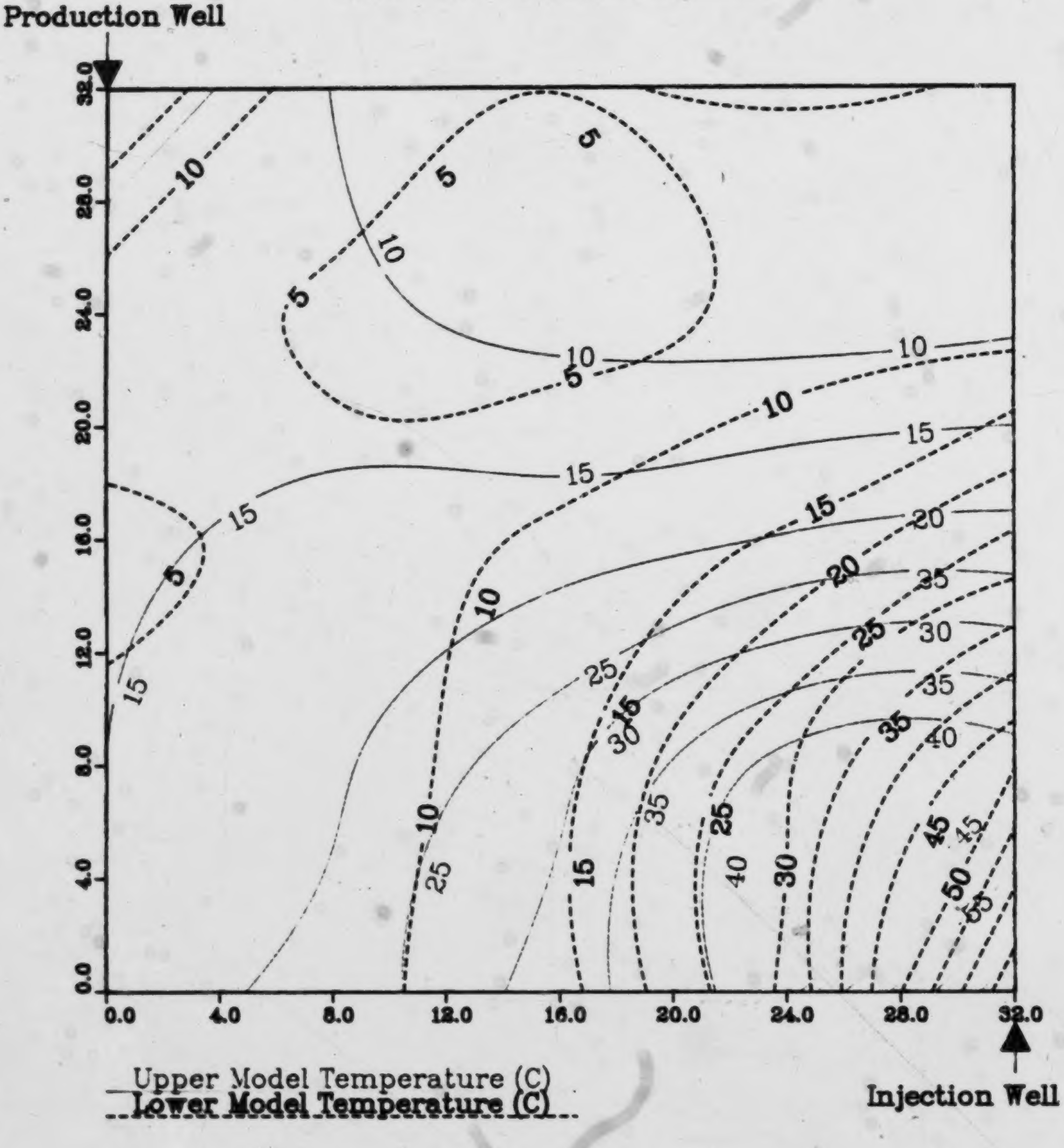

Figure A.37 : Run 45

Solvent–Steamflood in Homogeneous Model

Temperature Profile for 0.75 Pore Volumes Injected

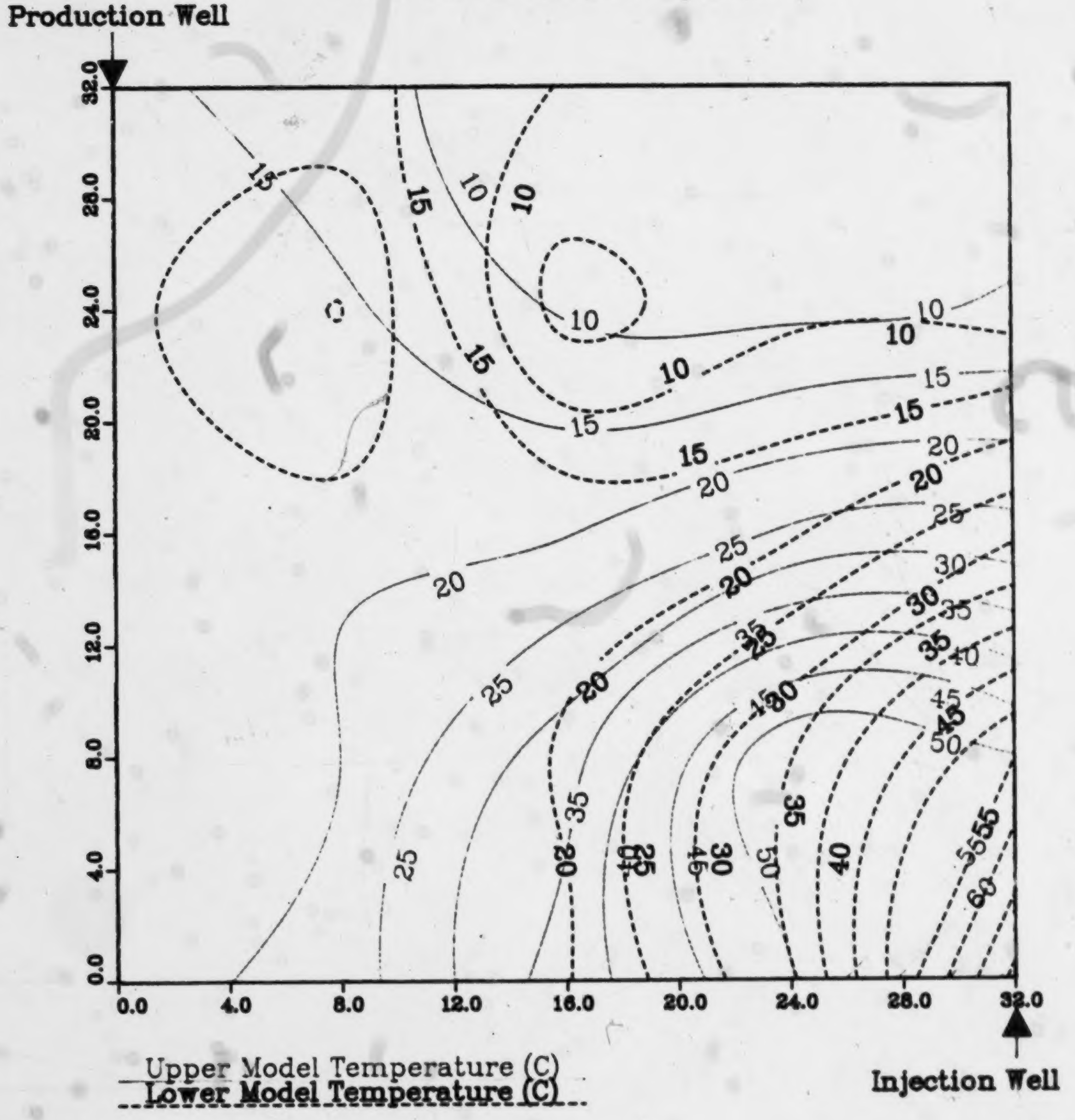

Figure A.38 : Run 45

Solvent–Steamflood in Homogeneous Model

Temperature Profile for 1.00 Pore Volumes Injected

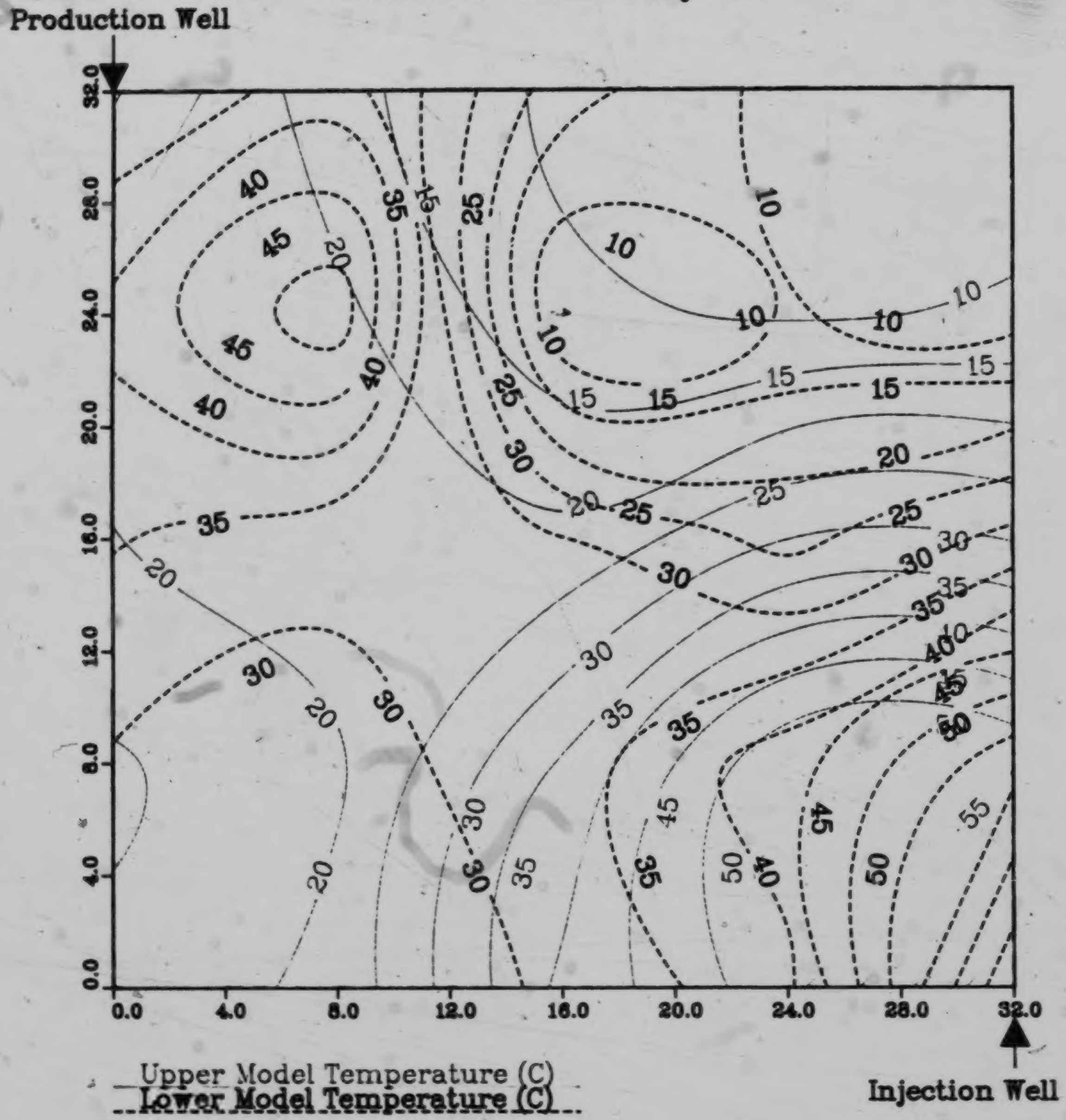

Figure A.39 : Run 45

Solvent–Steamflood in Homogeneous Model

Temperature Profile for 1.25 Pore Volumes Injected

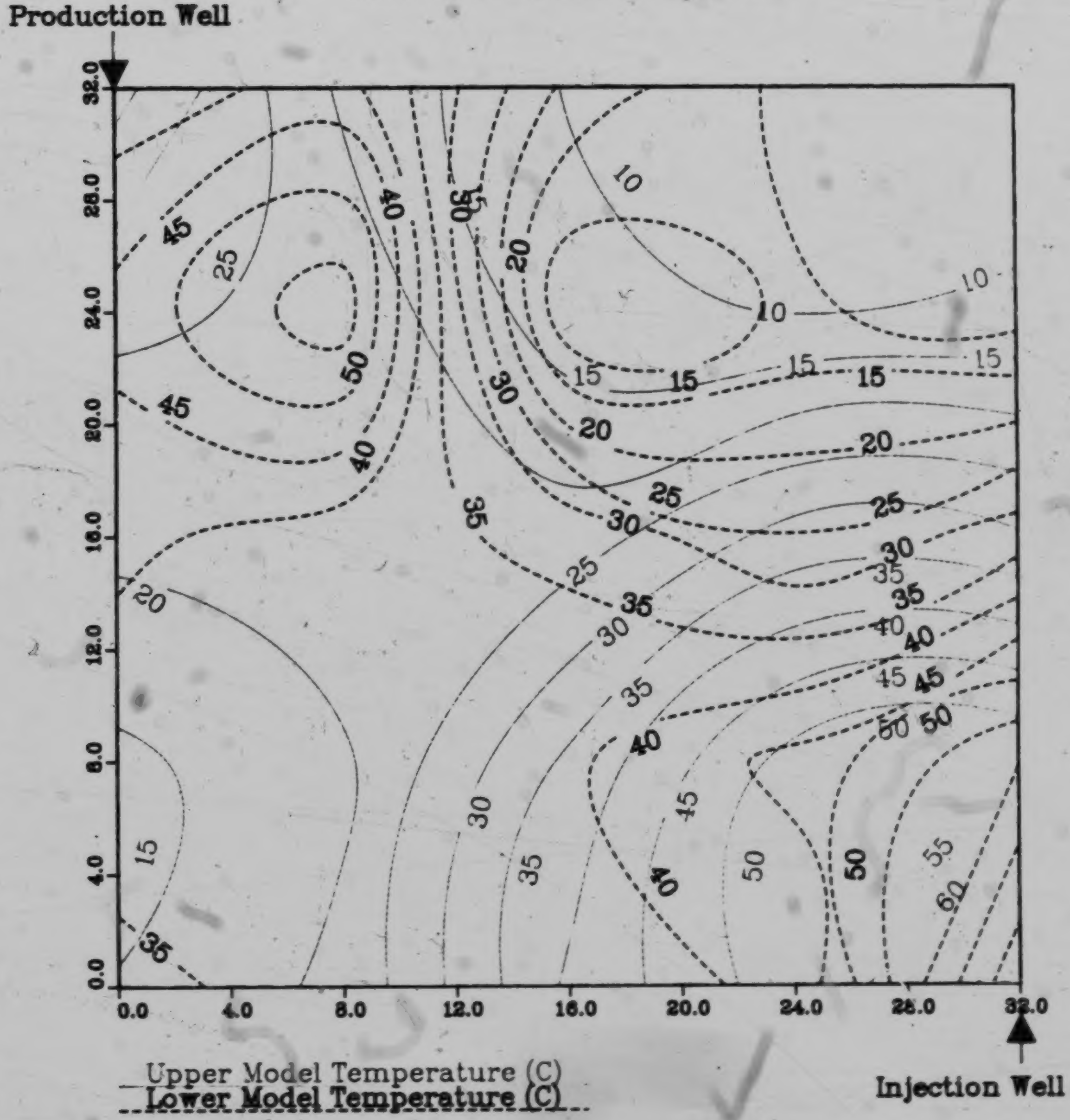

Figure A.40 : Run 45

Solvent–Steamflood in Homogeneous Model

Temperature Profile for 1.50 Pore Volumes Injected

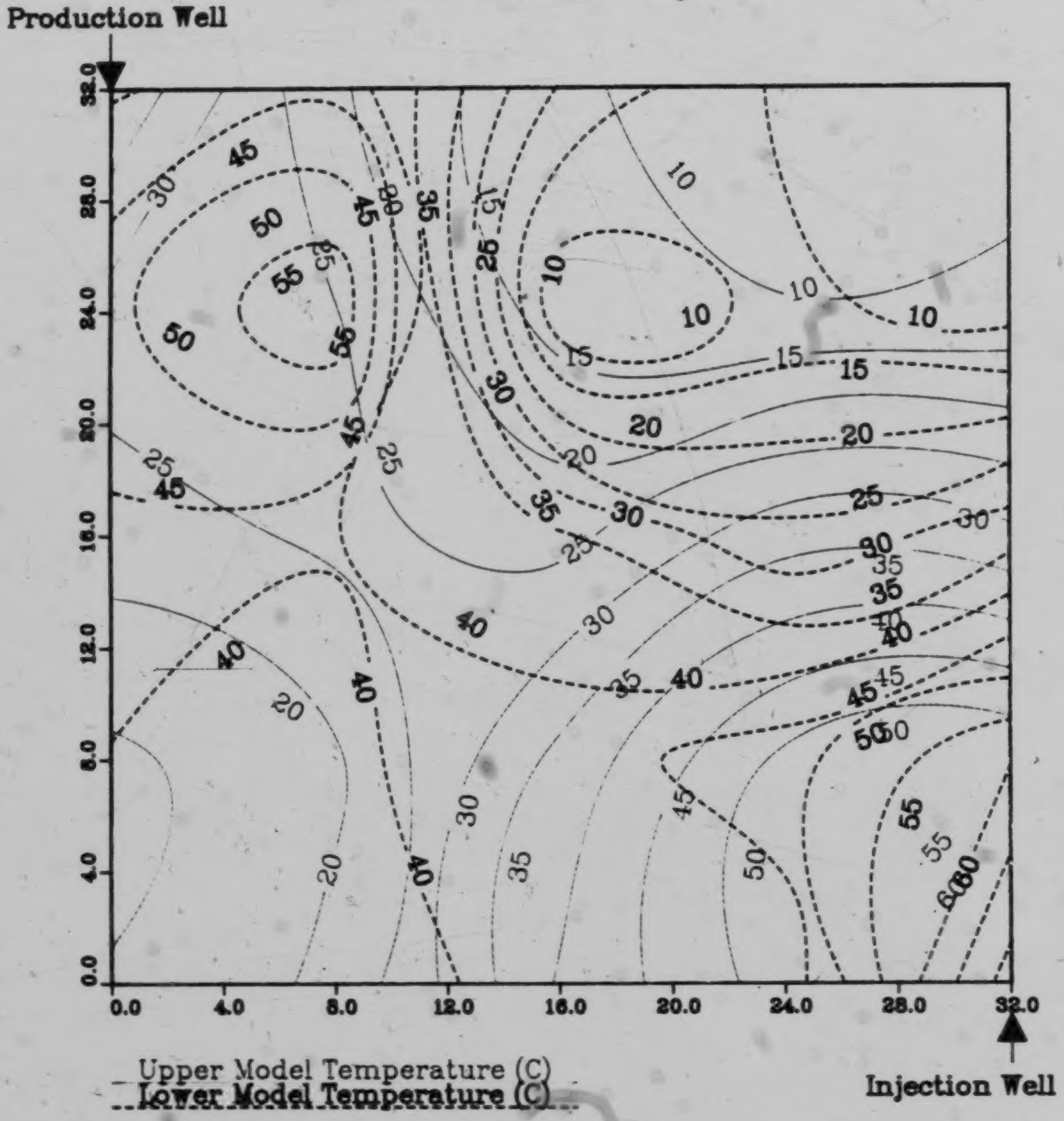

Figure A.41 : Run 45

Solvent–Steamflood in Homogeneous Model

Temperature Profile for
1.75 Pore Volumes Injected

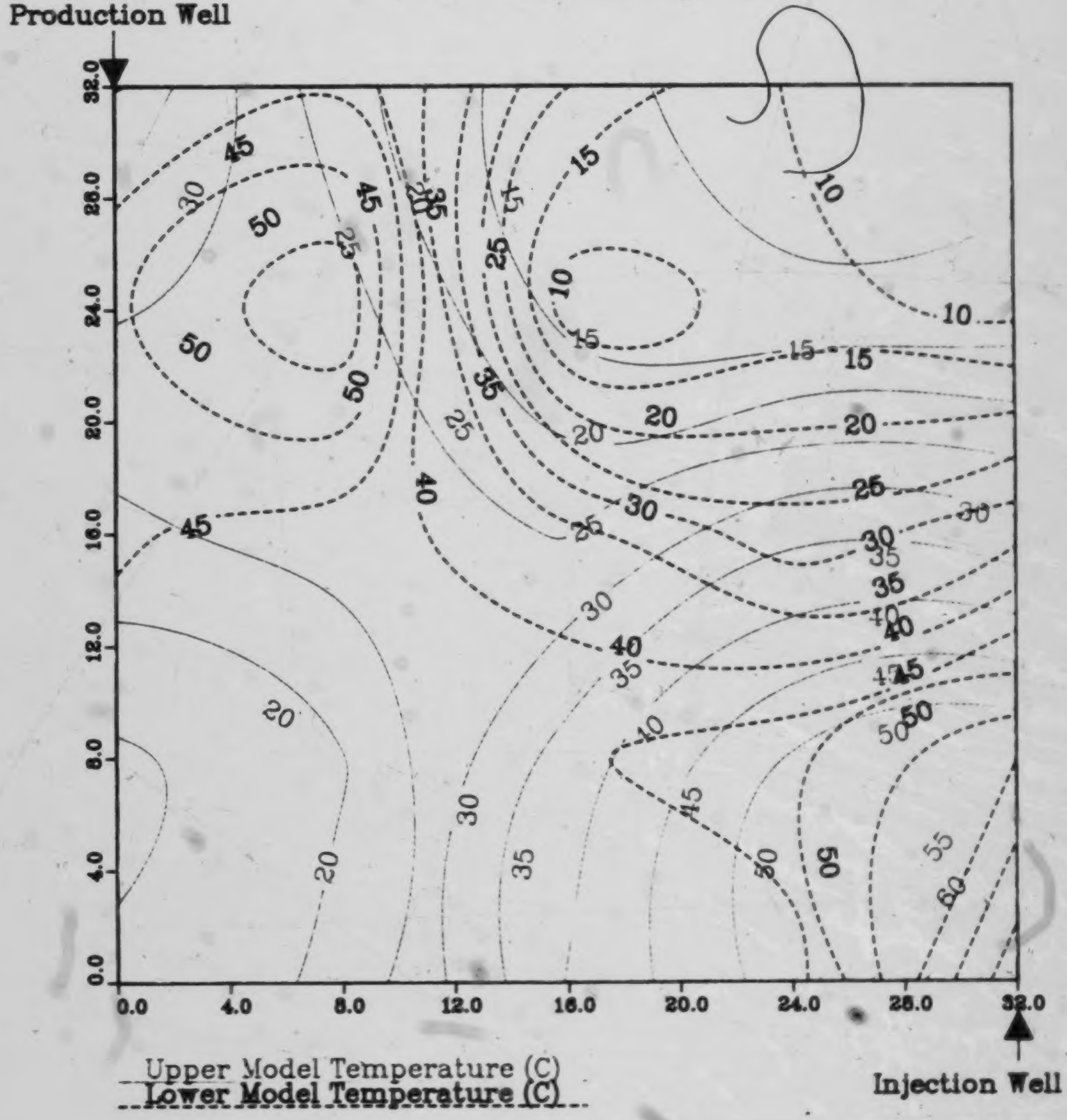

Figure A.42 : Run 45

Solvent–Steamflood in Homogeneous Model

Temperature Profile for 2.00 Pore Volumes Injected

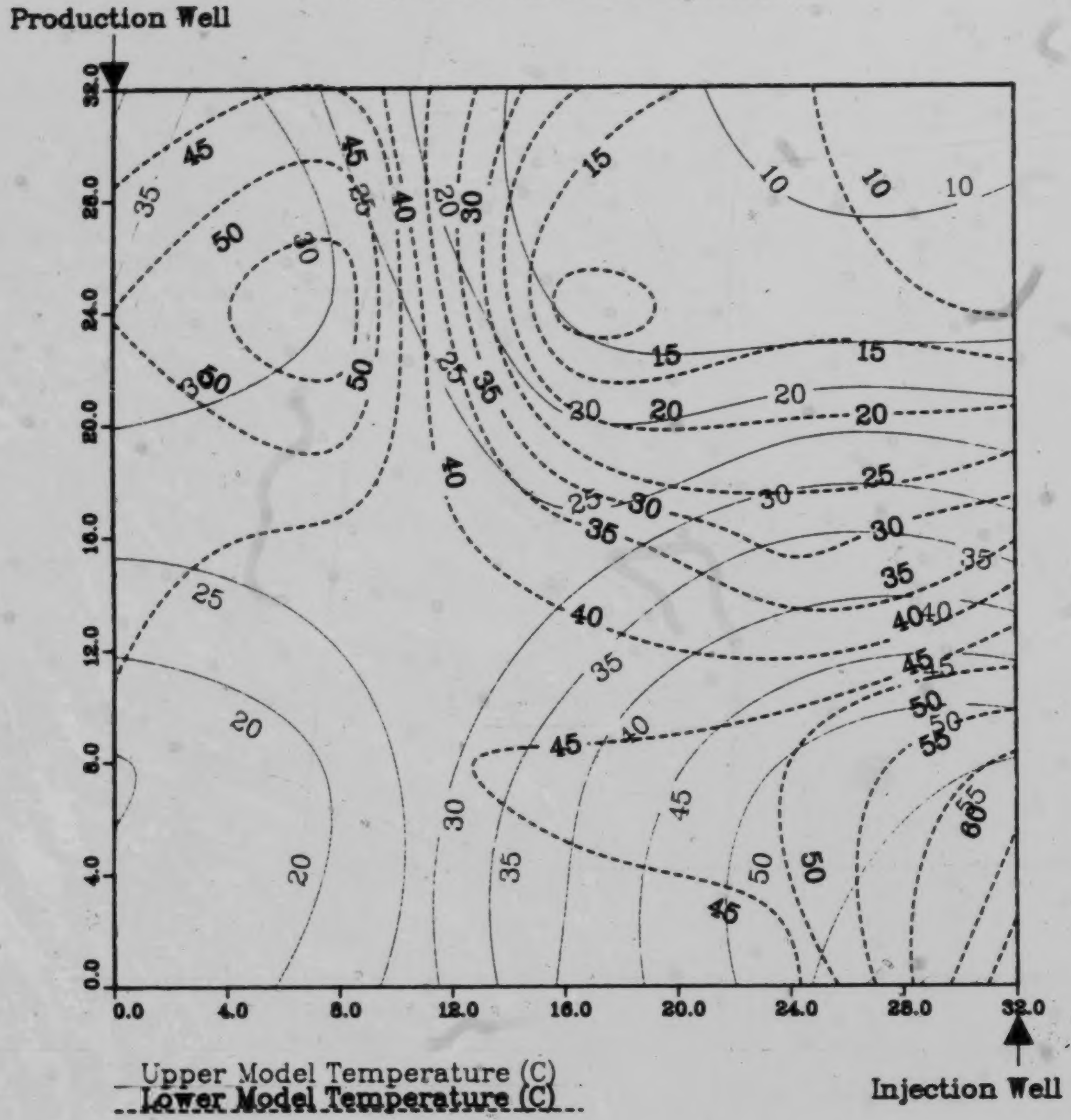

Figure A.43 :Run 45 Temp Profile
Injector to Producer Cross–Section
0.25 Pore Volumes Injected.

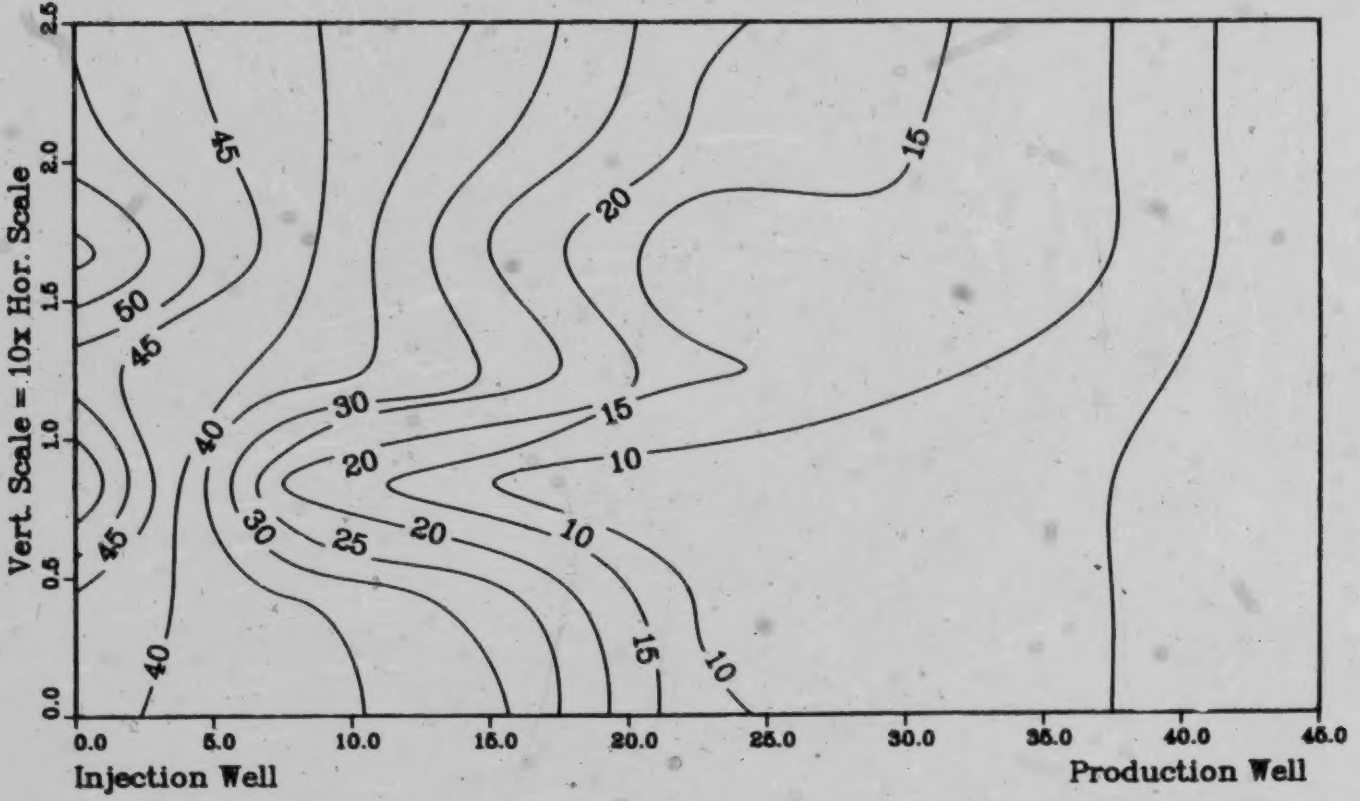

Figure A.44 :Run 45 Temp Profile
Injector to Producer Cross-Section
0.50 Pore Volumes Injected.

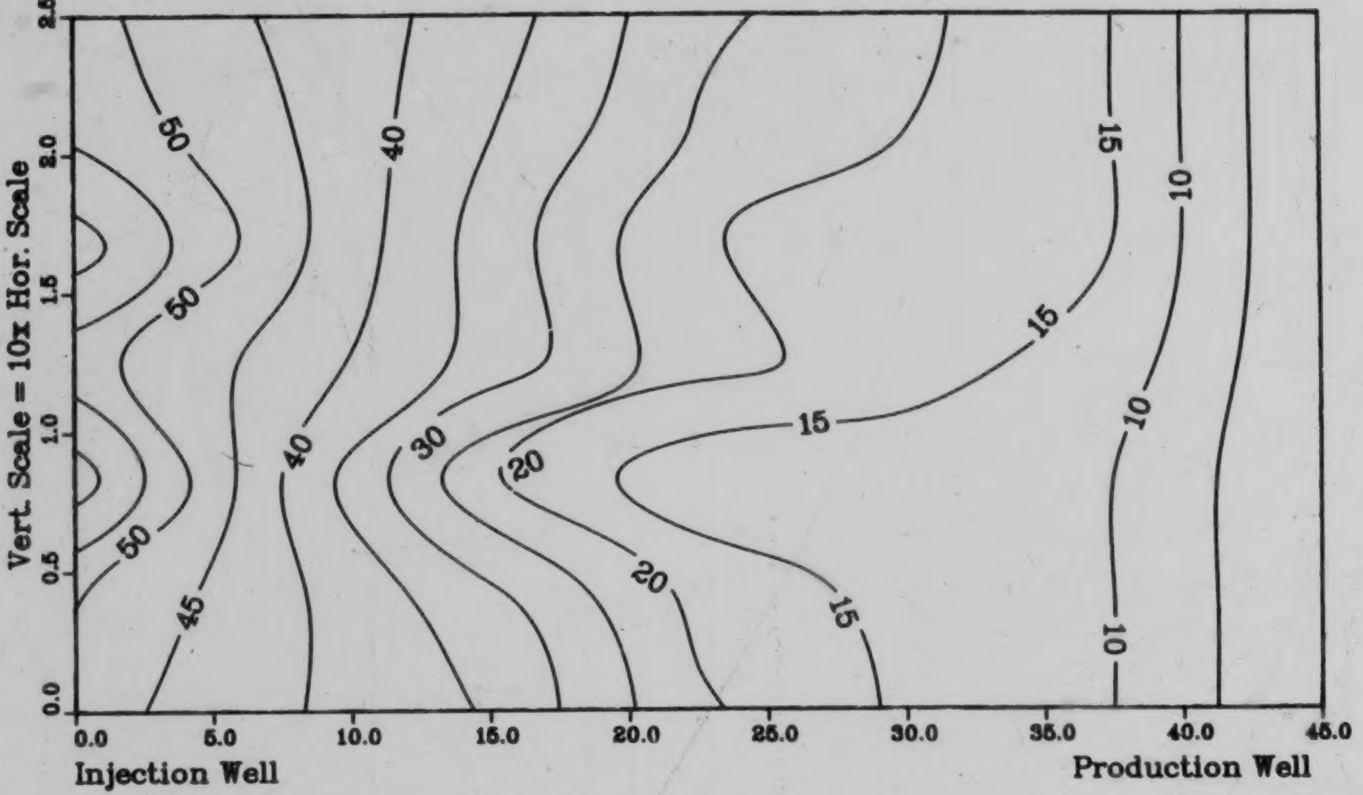

Figure A.45 :Run 45 Temp Profile
Injector to Producer Cross–Section
0.75 Pore Volumes Injected.

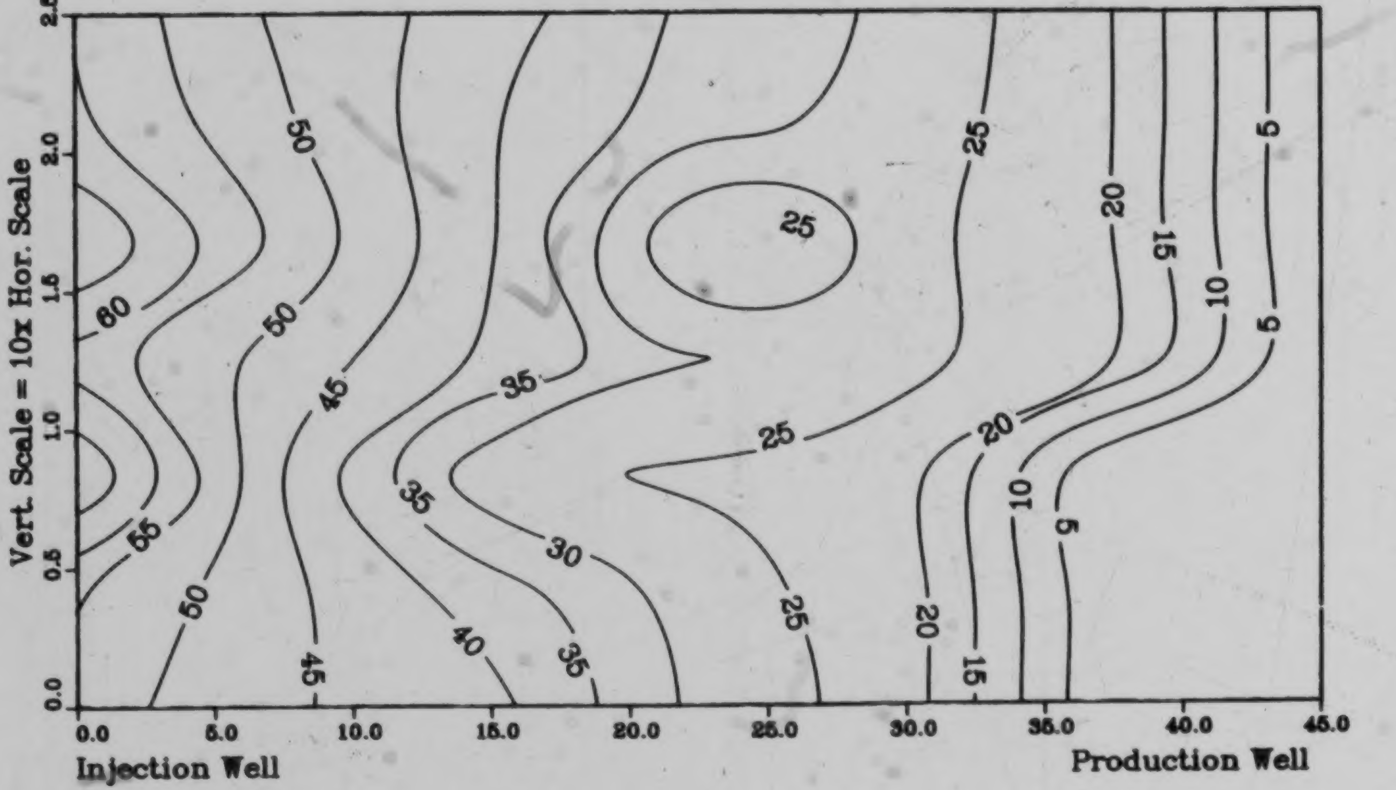

Figure A.46 :Run 45 Temp Profile
Injector to Producer Cross–Section
1.00 Pore Volumes Injected.

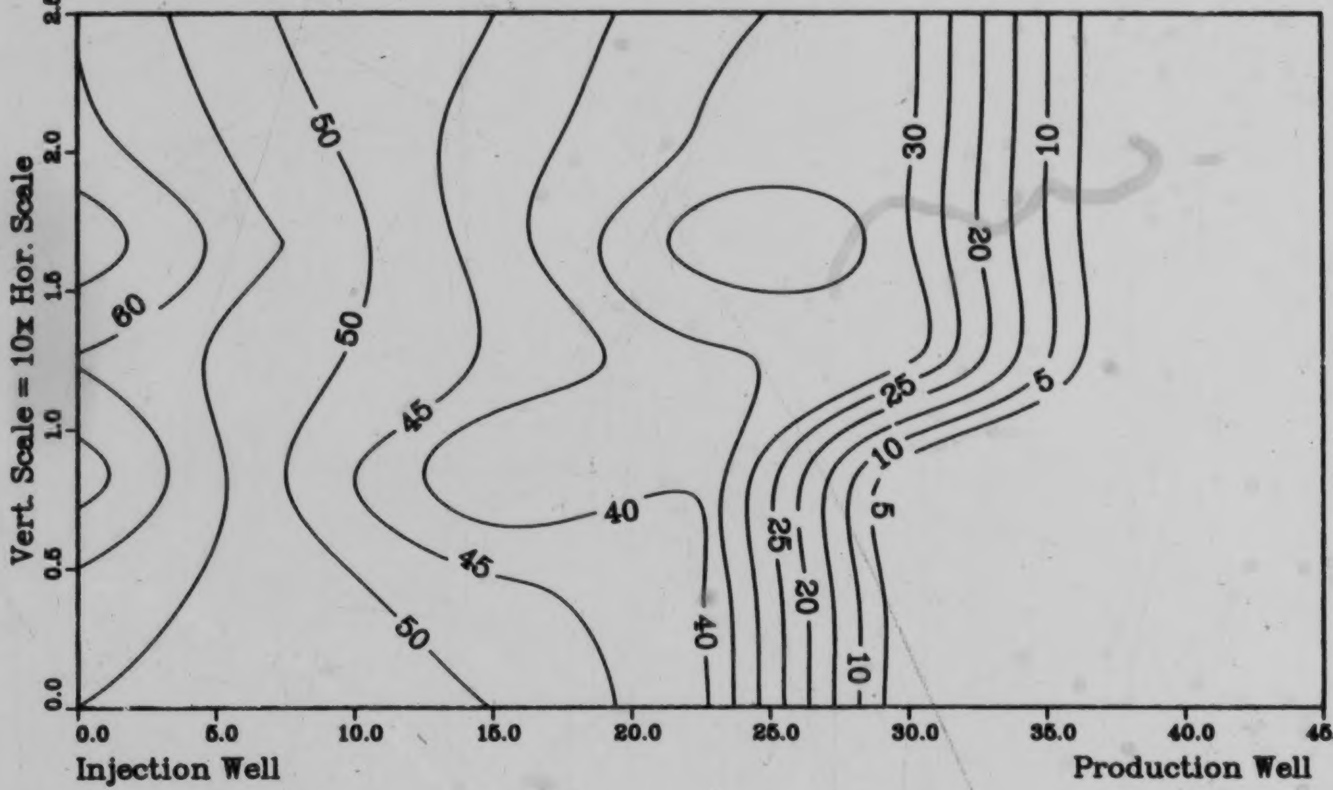

Figure A.47 : Run 46

Solvent–Steamflood in Homogeneous Model

Temperature Profile for 0.25 Pore Volumes Injected

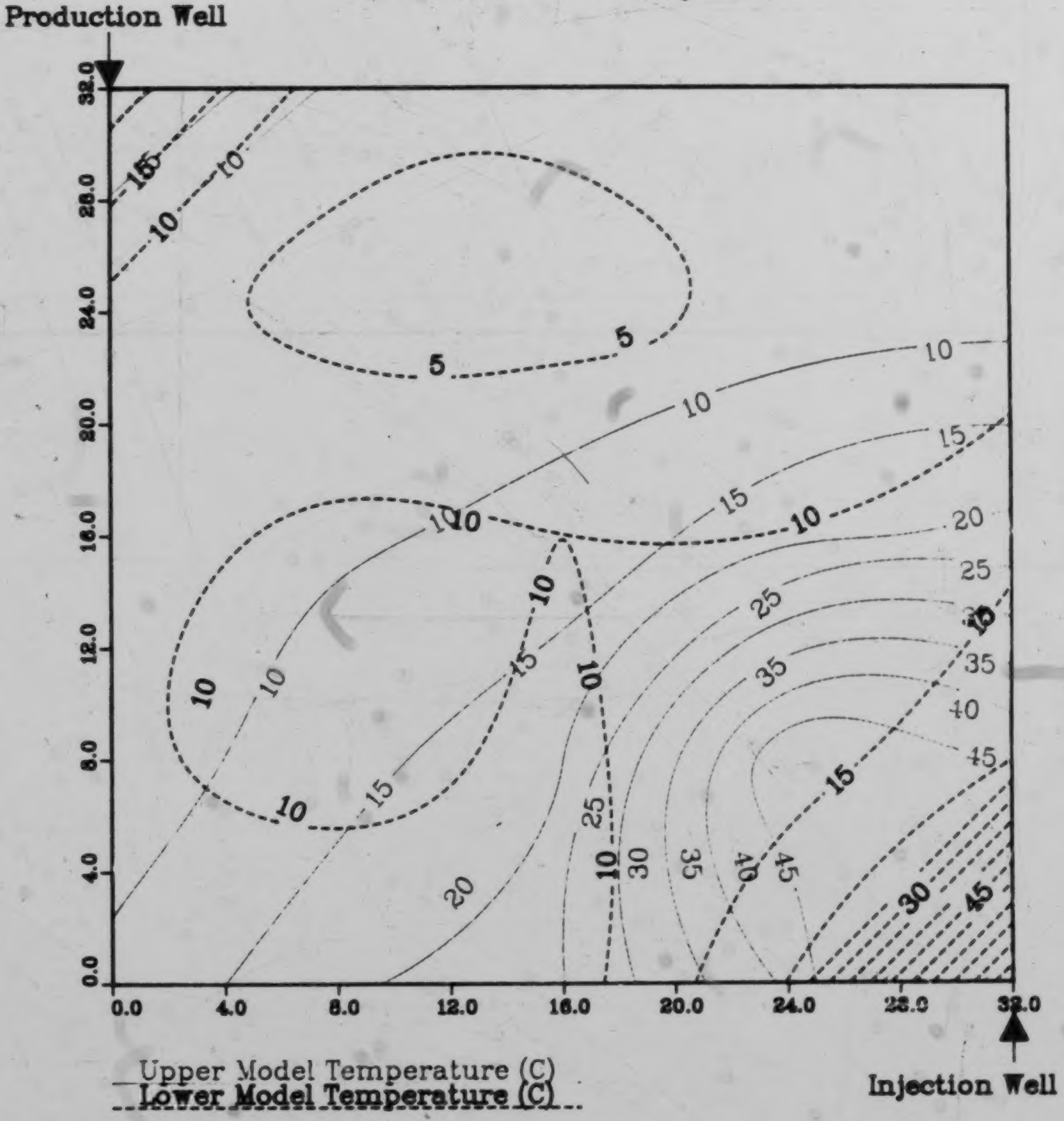

Figure A.48 : Run 46

Solvent–Steamflood in Homogeneous Model

Temperature Profile for
0.50 Pore Volumes Injected

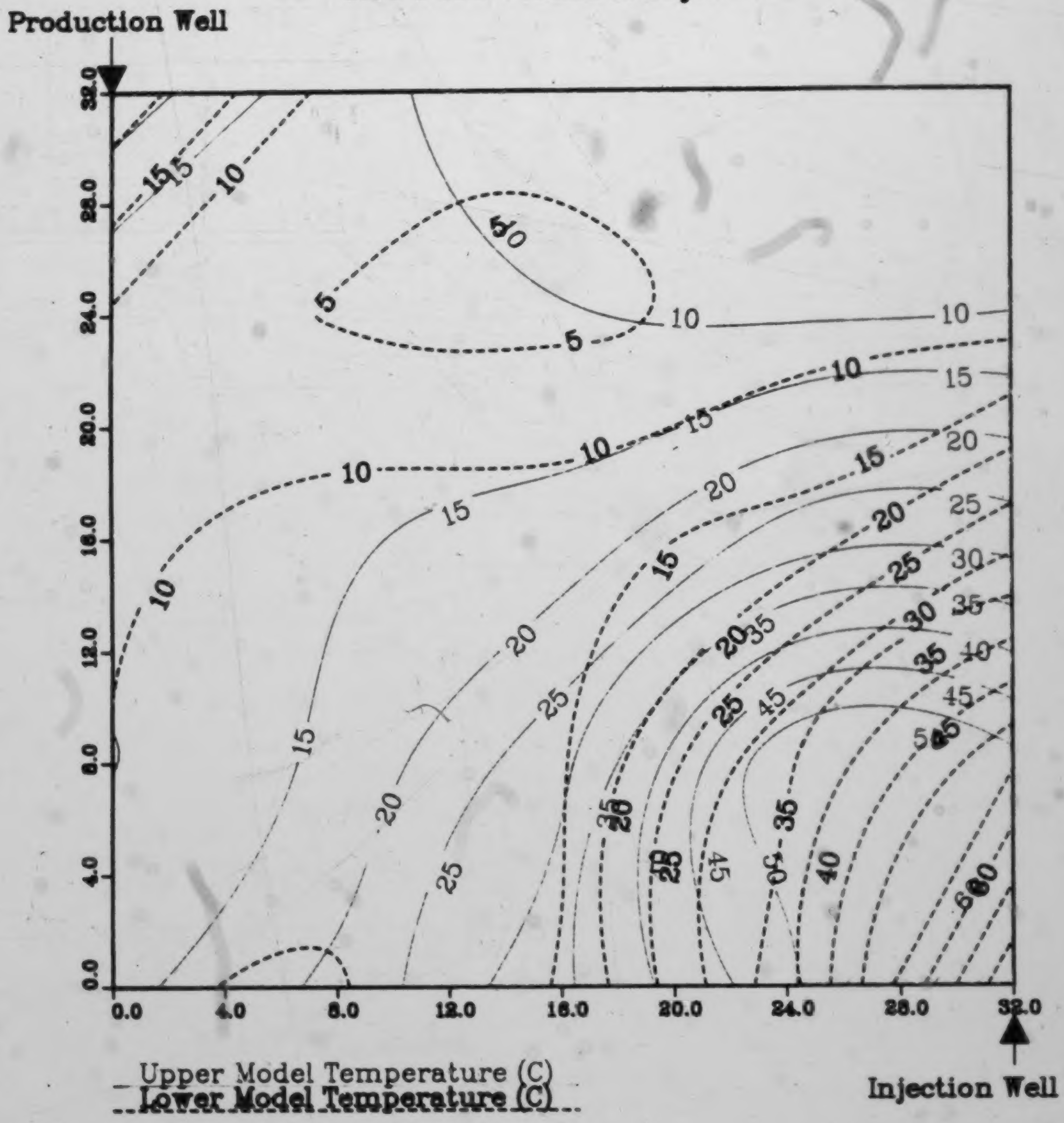

Figure A.49 : Run 46

Solvent–Steamflood in Homogeneous Model

Temperature Profile for 0.75 Pore Volumes Injected

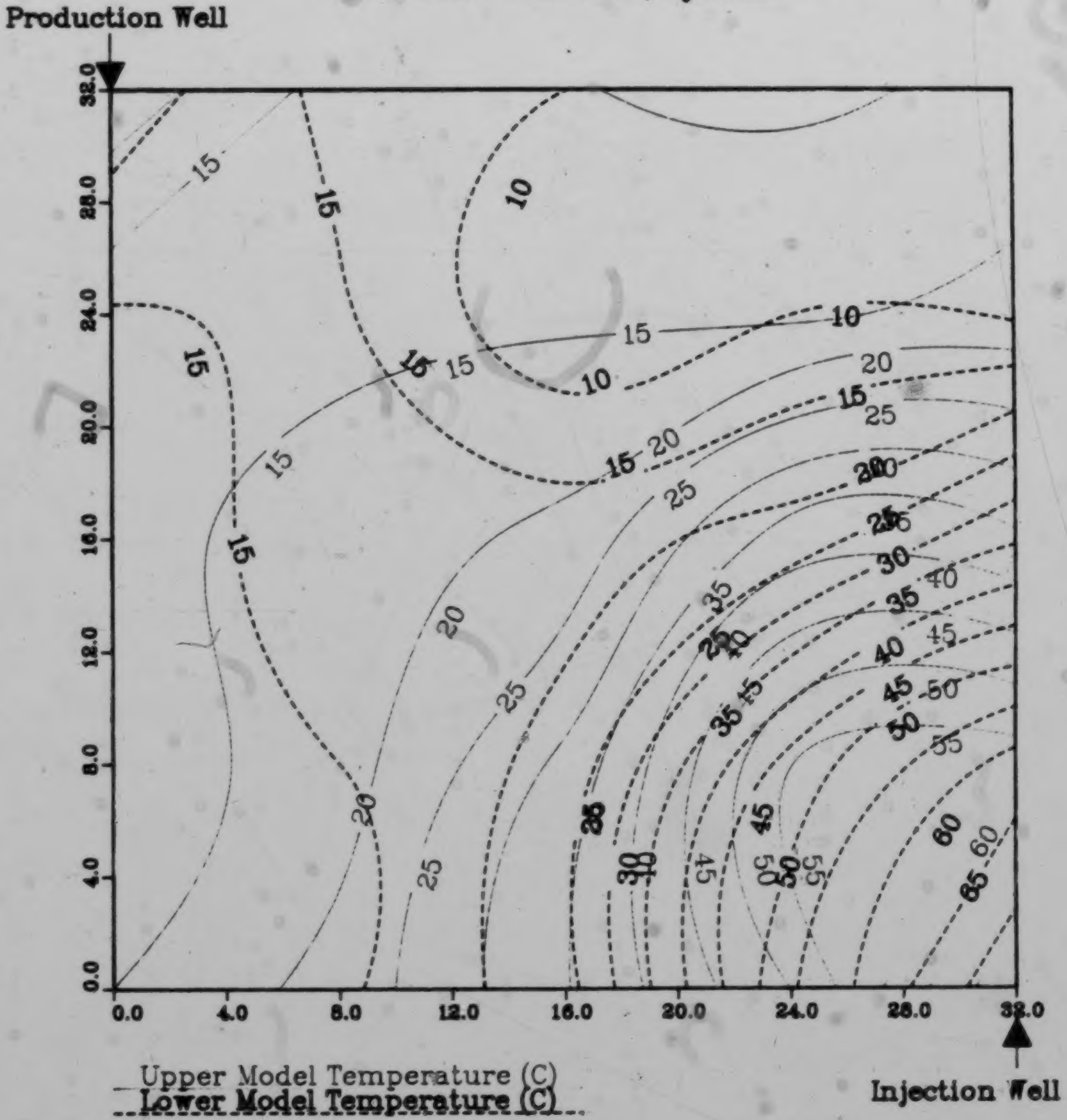

Figure A.50 : Run 46

Solvent–Steamflood in Homogeneous Model

Temperature Profile for 1.00 Pore Volumes Injected

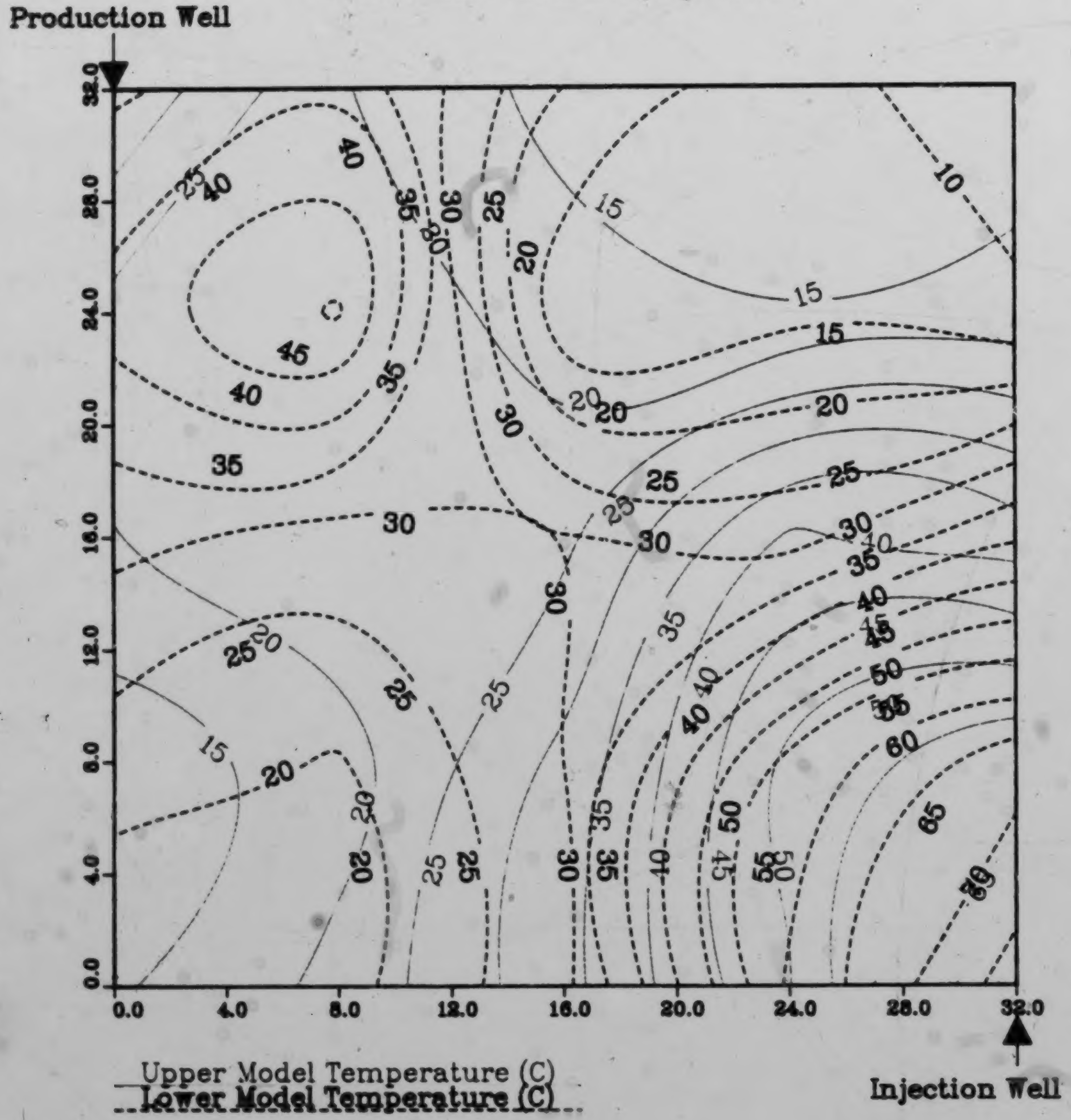

Figure A.51 : Run 46

Solvent–Steamflood in Homogeneous Model

Temperature Profile for 1.25 Pore Volumes Injected

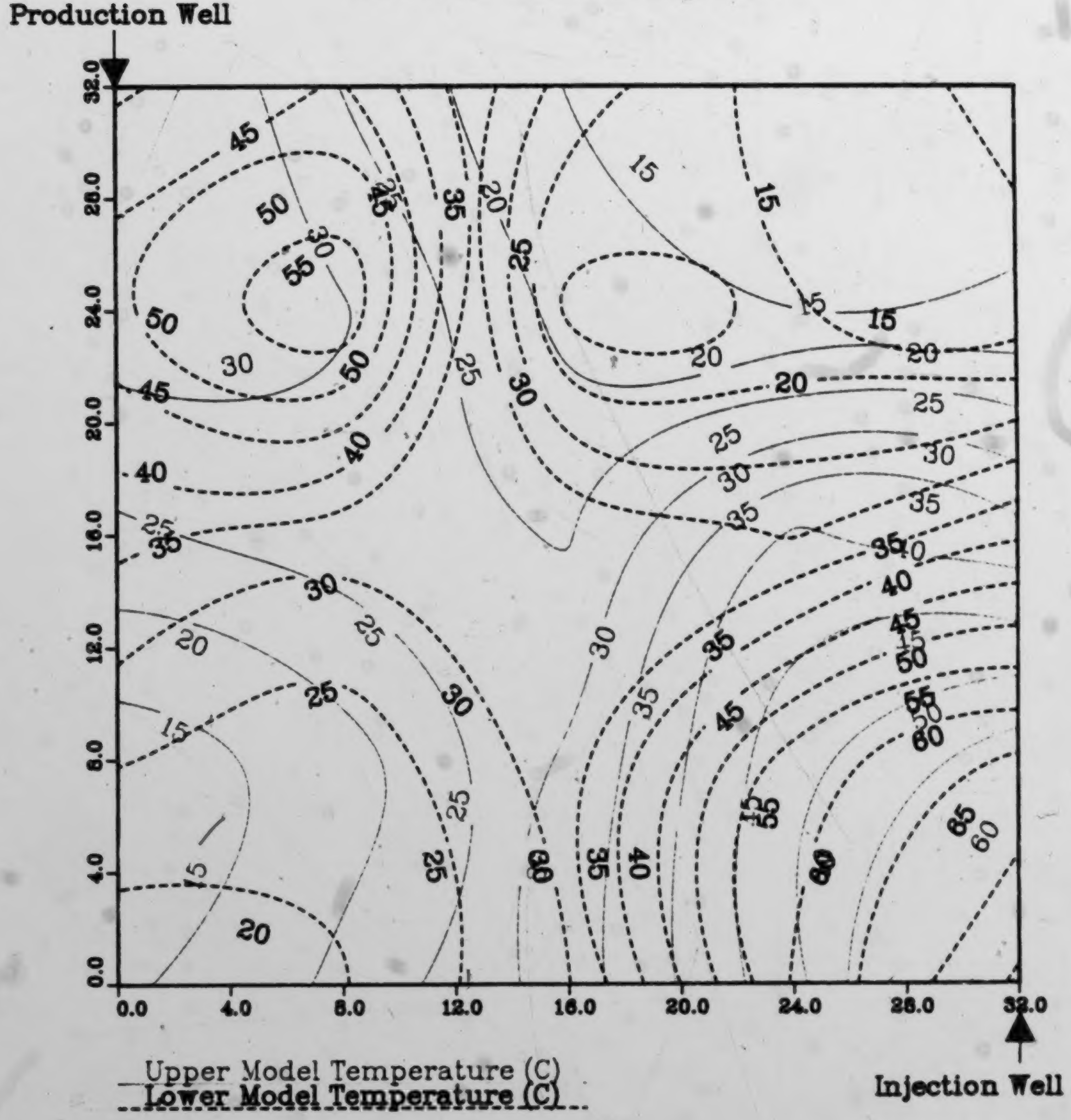

Figure A.52 : Run 46

Solvent–Steamflood in Homogeneous Model

Temperature Profile for 1.50 Pore Volumes Injected

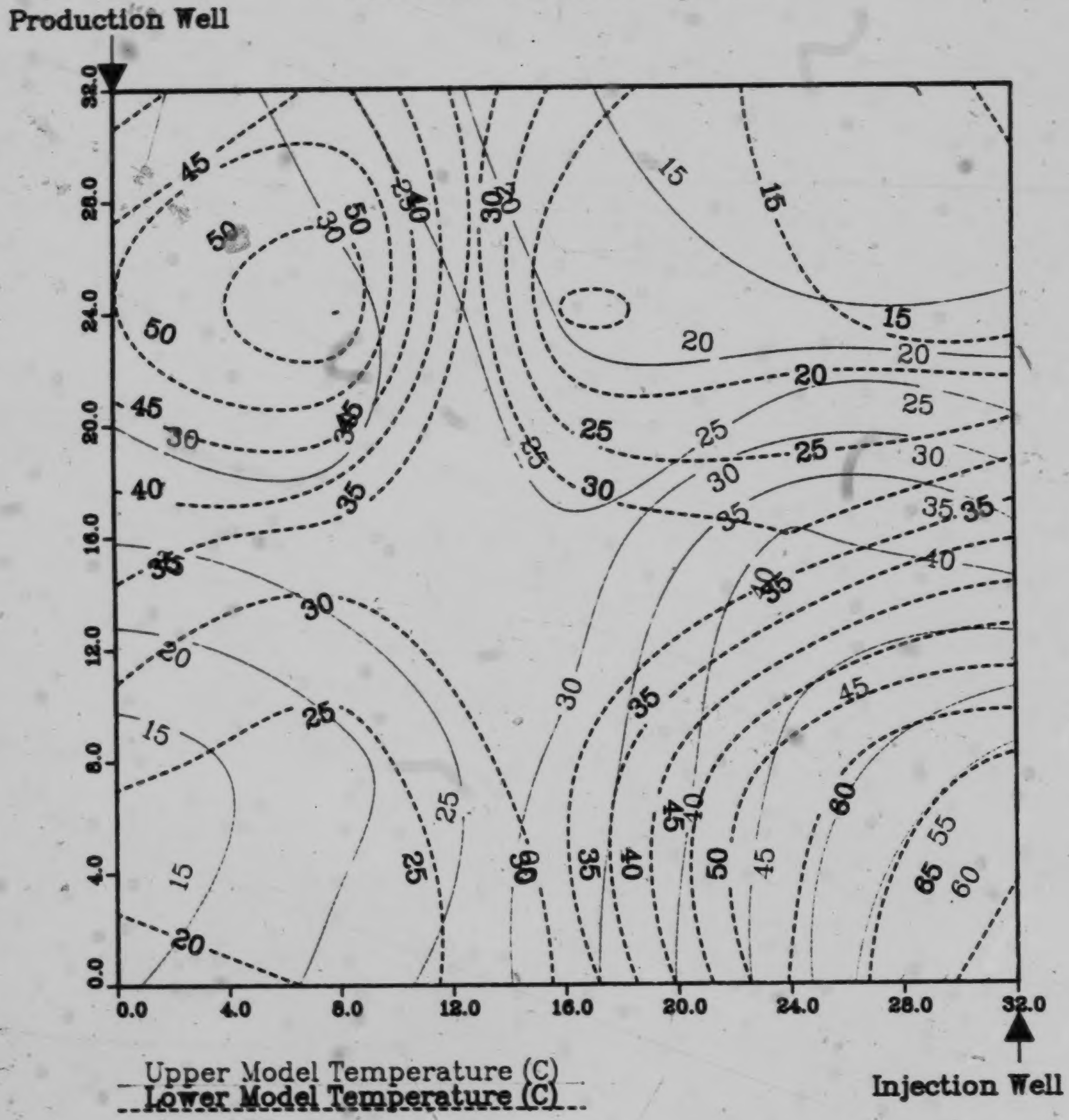

Figure A.53 : Run 46

Solvent–Steamflood in Homogeneous Model

Temperature Profile for
1.75 Pore Volumes Injected

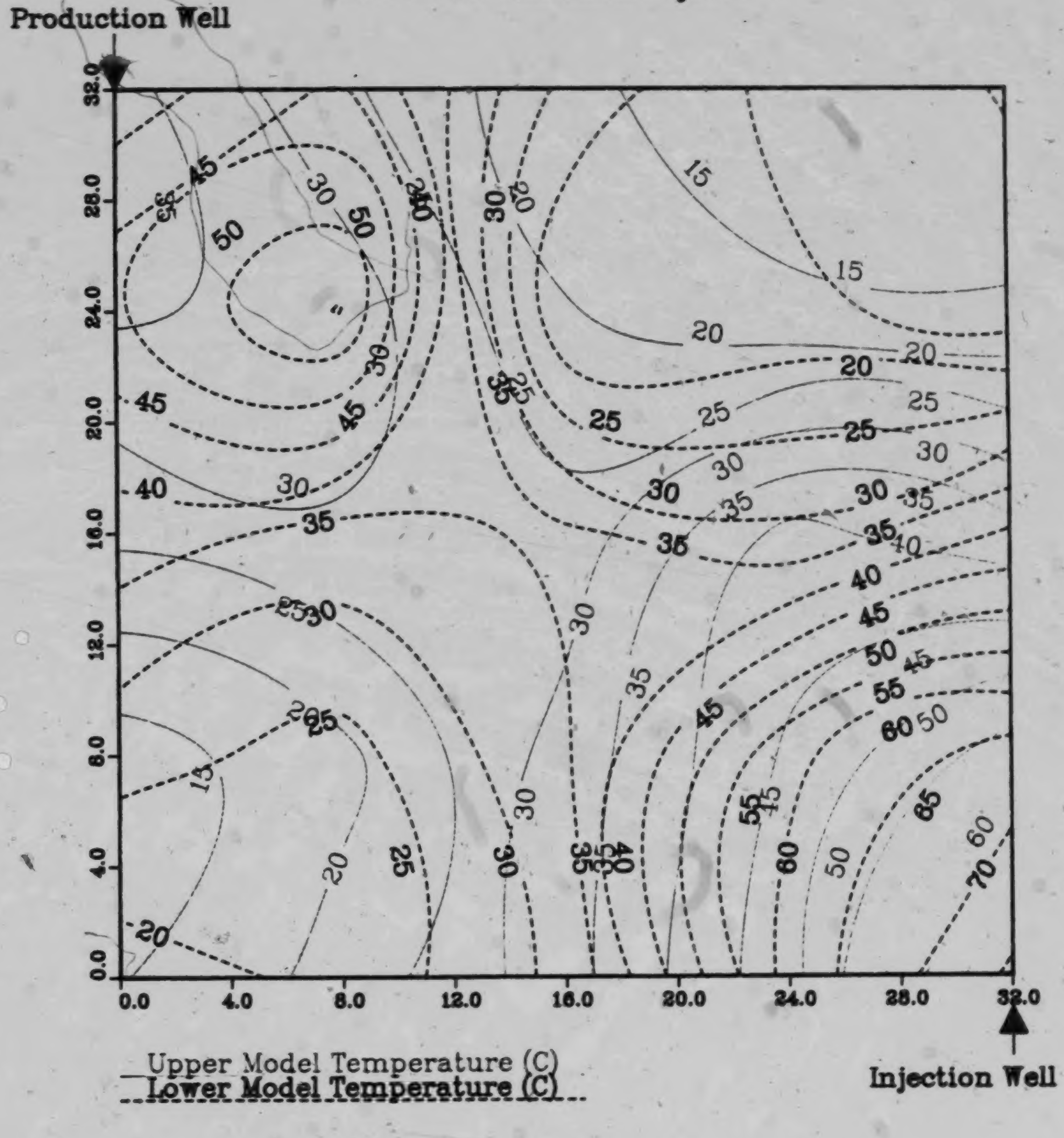

Figure A.54 : Run 46

Solvent–Steamflood in Homogeneous Model

Temperature Profile for
2.00 Pore Volumes Injected

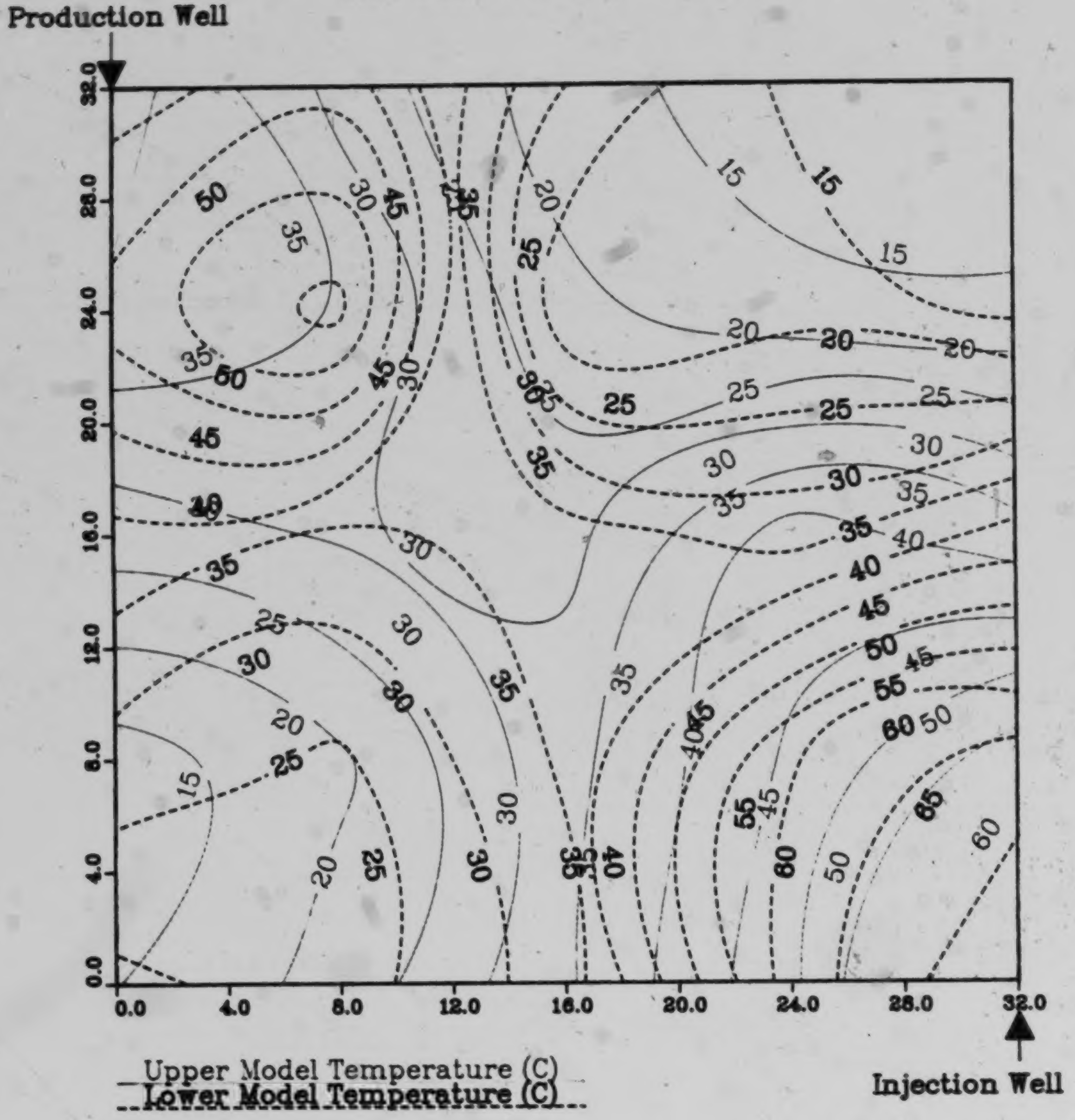

Figure A.55 :Run 46 Temp Profile
Injector to Producer Cross-Section
0.25 Pore Volumes Injected.

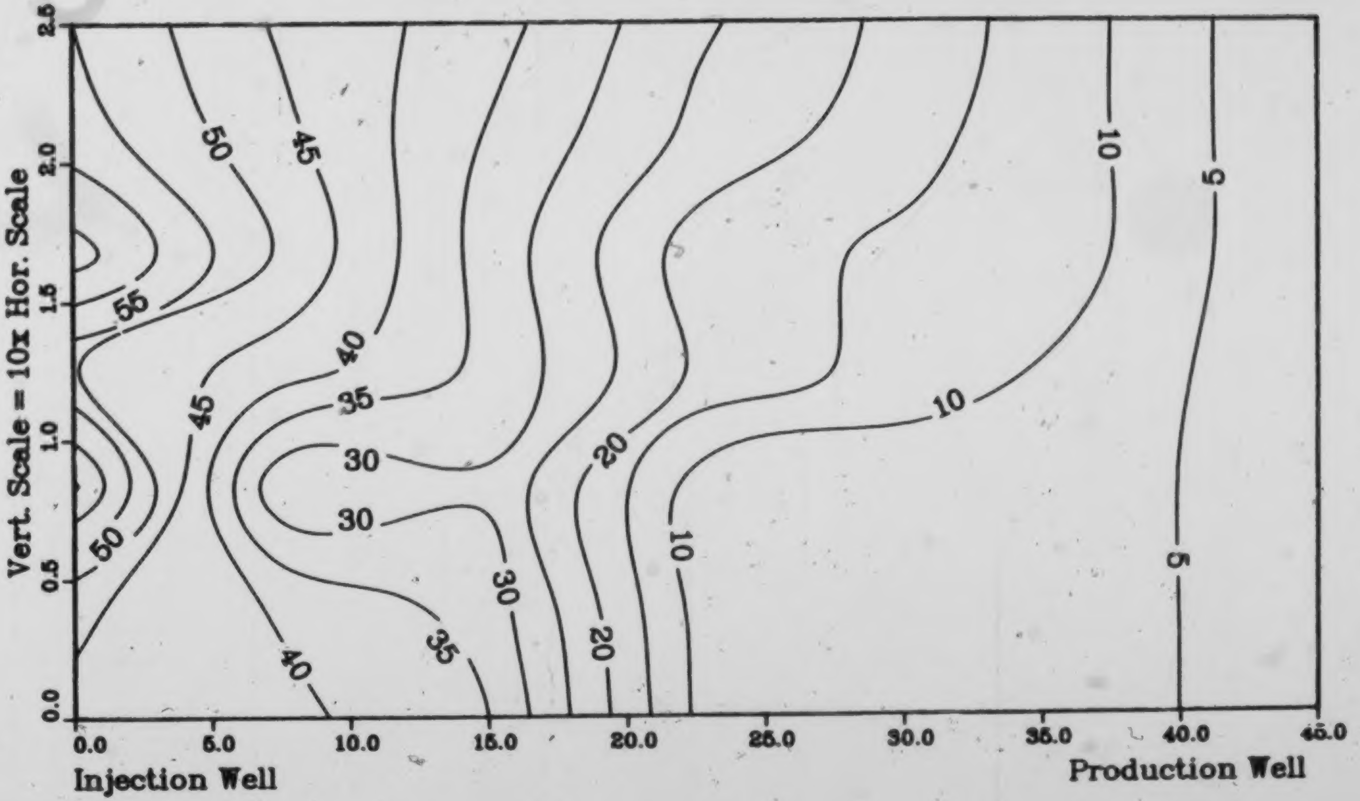

Figure A.56 :Run 46 Temp Profile
Injector to Producer Cross–Section
0.50 Pore Volumes Injected.

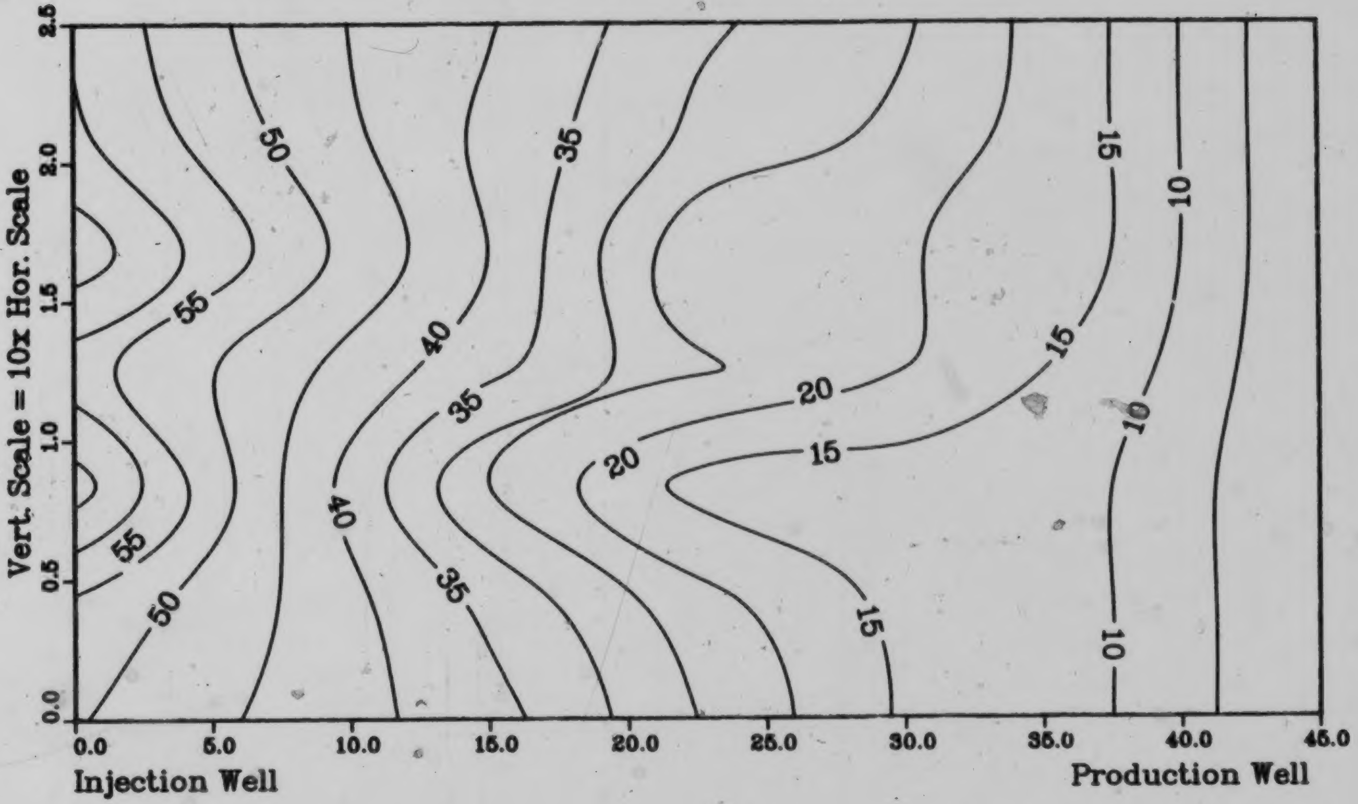

Figure A.57 :Run 46 Temp Profile
Injector to Producer Cross–Section
0.75 Pore Volumes Injected.

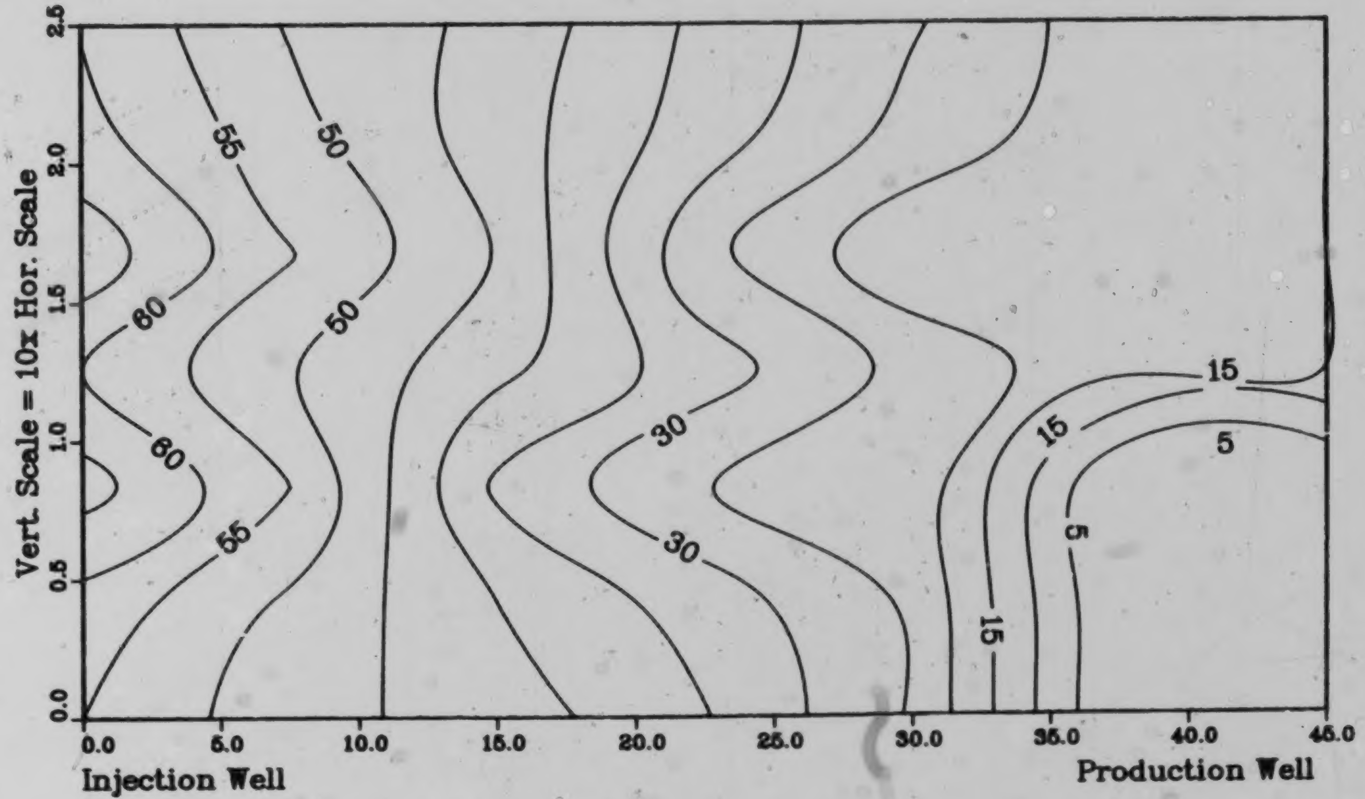

Figure A.58 :Run 46 Temp Profile
Injector to Producer Cross–Section
1.00 Pore Volumes Injected.

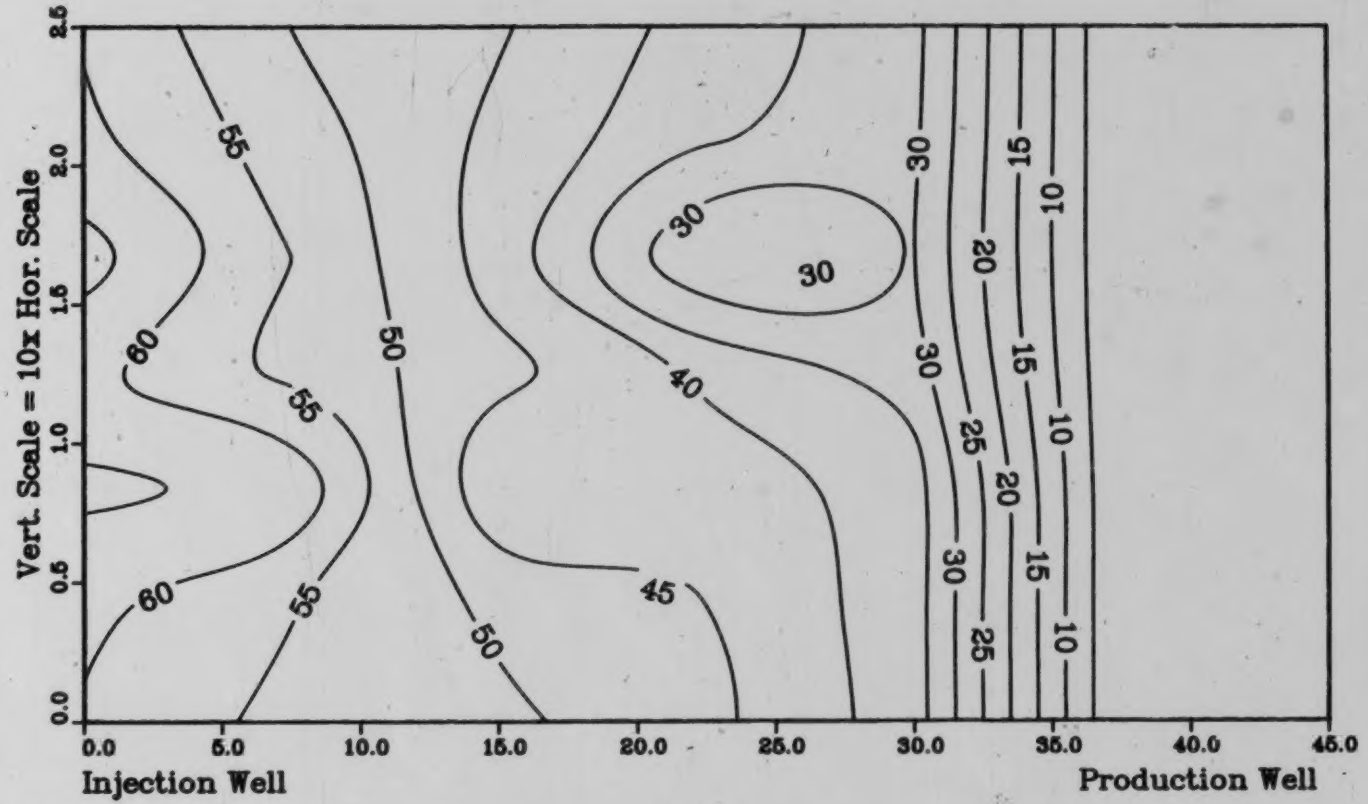

Figure A.59 : Run 60

Gas Inj. & Steamflood in B.W. Model

Temperature Profile for 0.25 Pore Volumes Injected

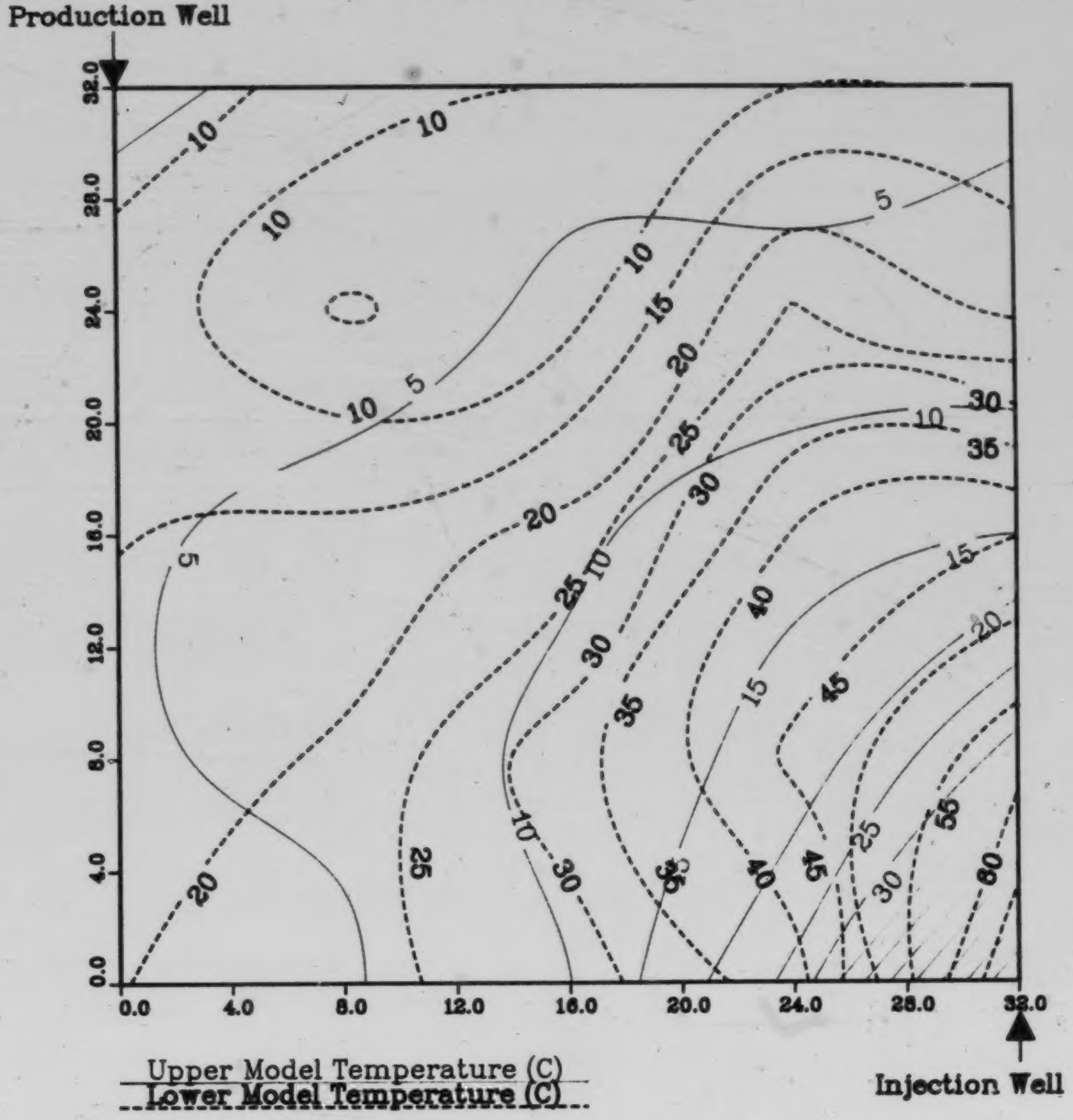

Figure A.60 : Run 60

Gas Inj. & Steamflood in B.W. Model

Temperature Profile for 0.50 Pore Volumes Injected

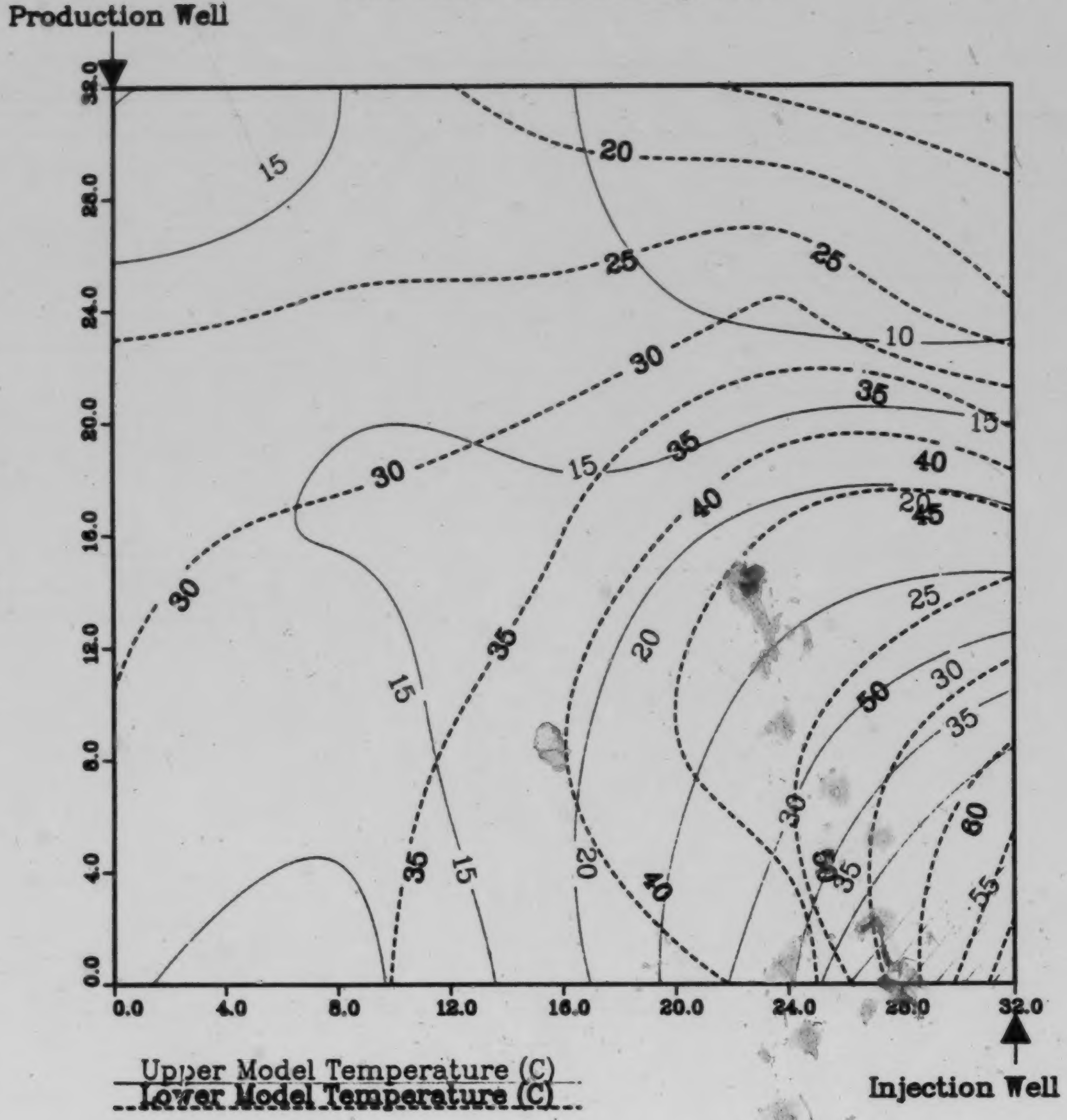

Figure A.61 : Run 60

Gas Inj. & Steamflood in B.W. Model

Temperature Profile for
0.75 Pore Volumes Injected

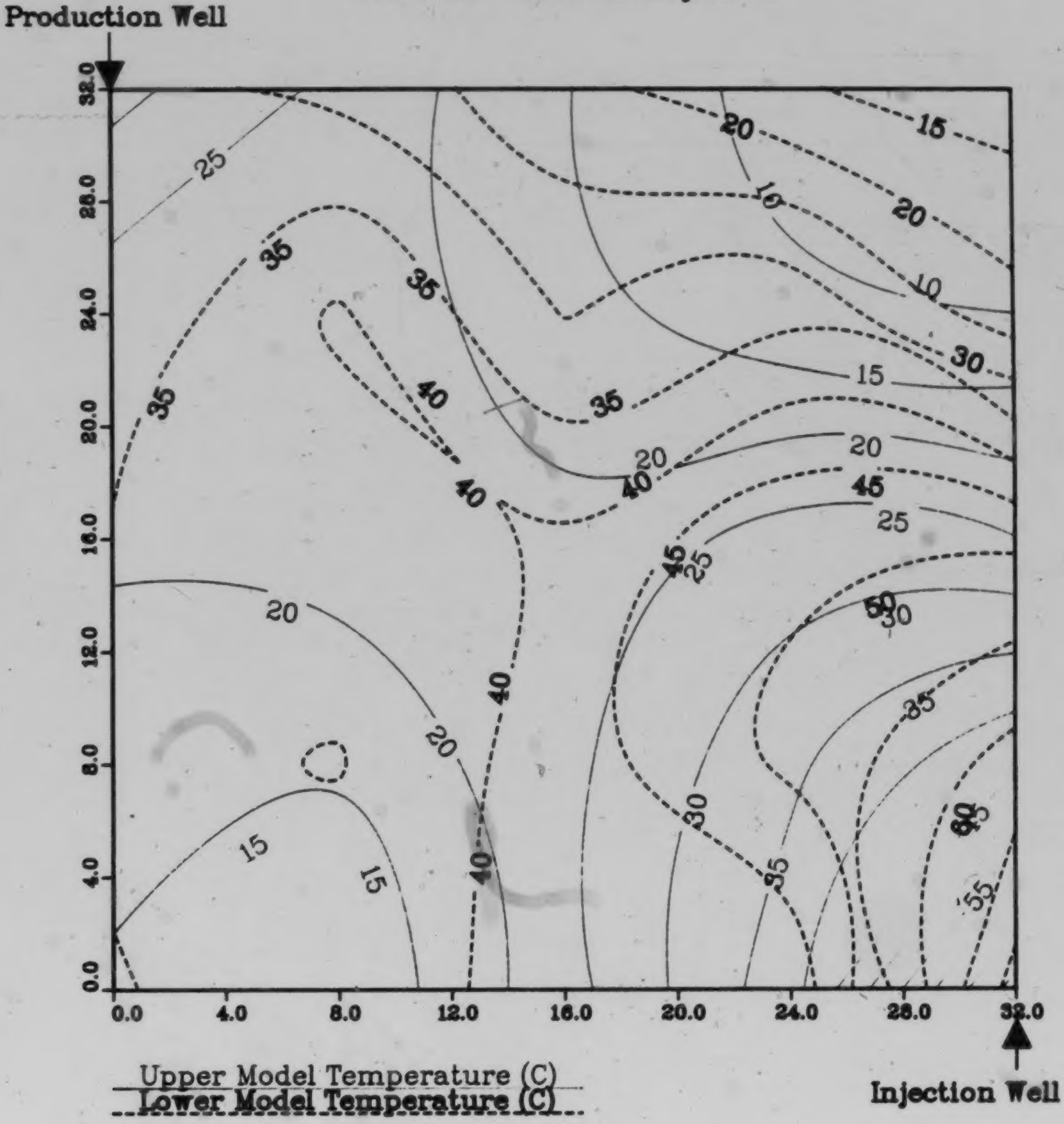

Figure A.62 : Run 60

Gas Inj. & Steamflood in B.W. Model

Temperature Profile for 1.00 Pore Volumes Injected

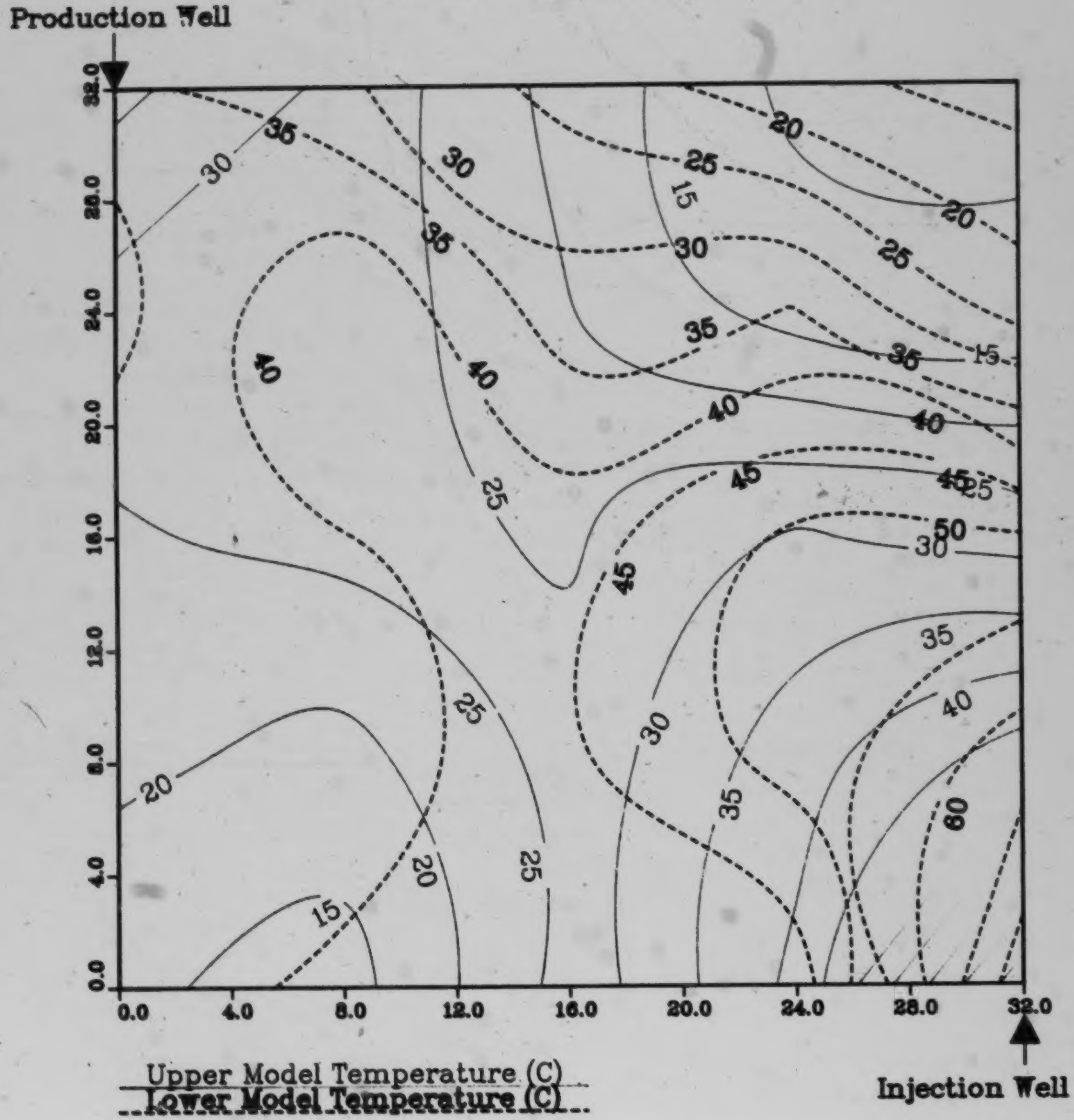

Figure A.63 : Run 60

Gas Inj. & Steamflood in B.W. Model

Temperature Profile for 1.25 Pore Volumes Injected

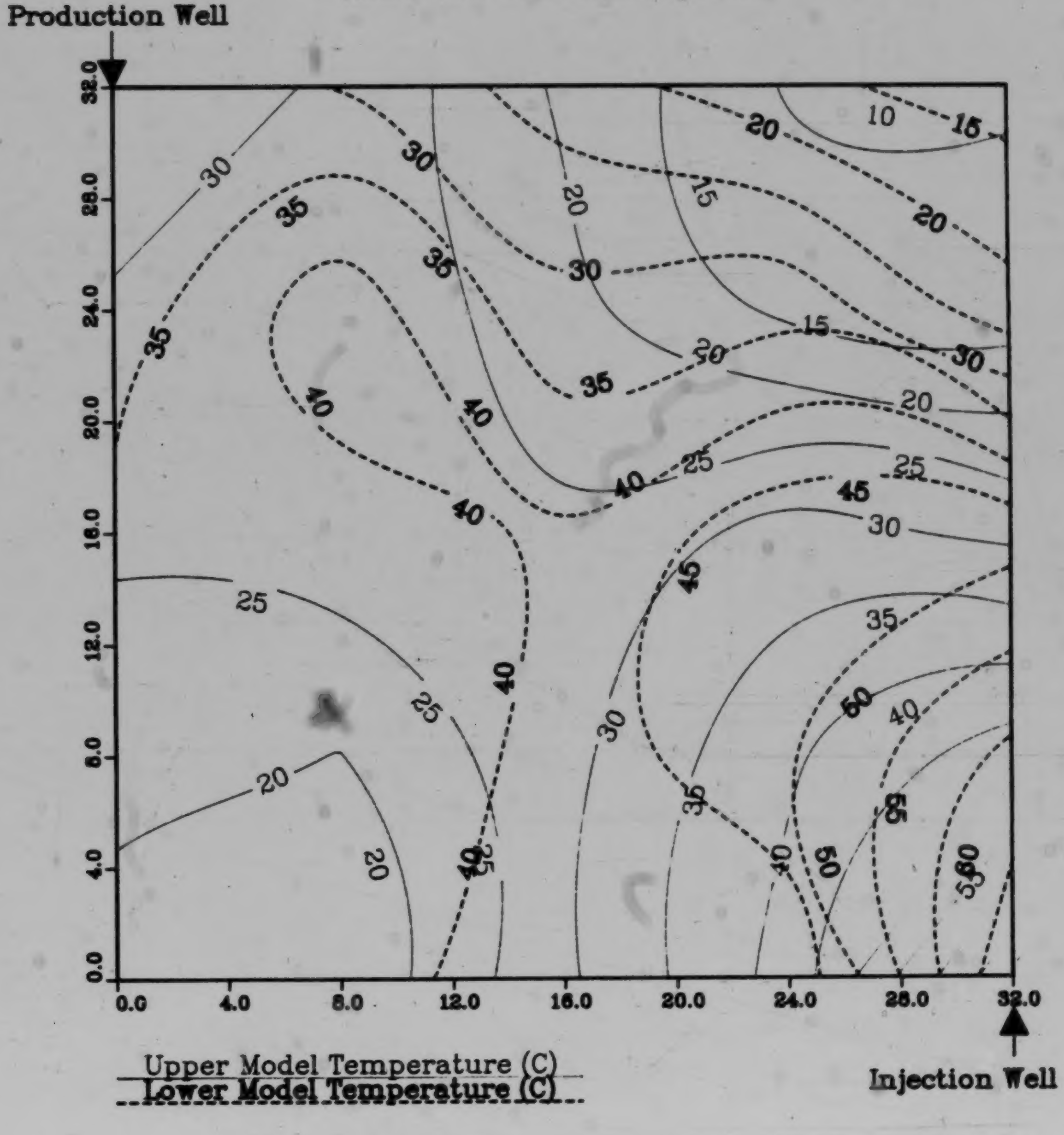

Figure A.64 : Run 60

Gas Inj. & Steamflood in B.W. Model

Temperature Profile for 1.50 Pore Volumes Injected

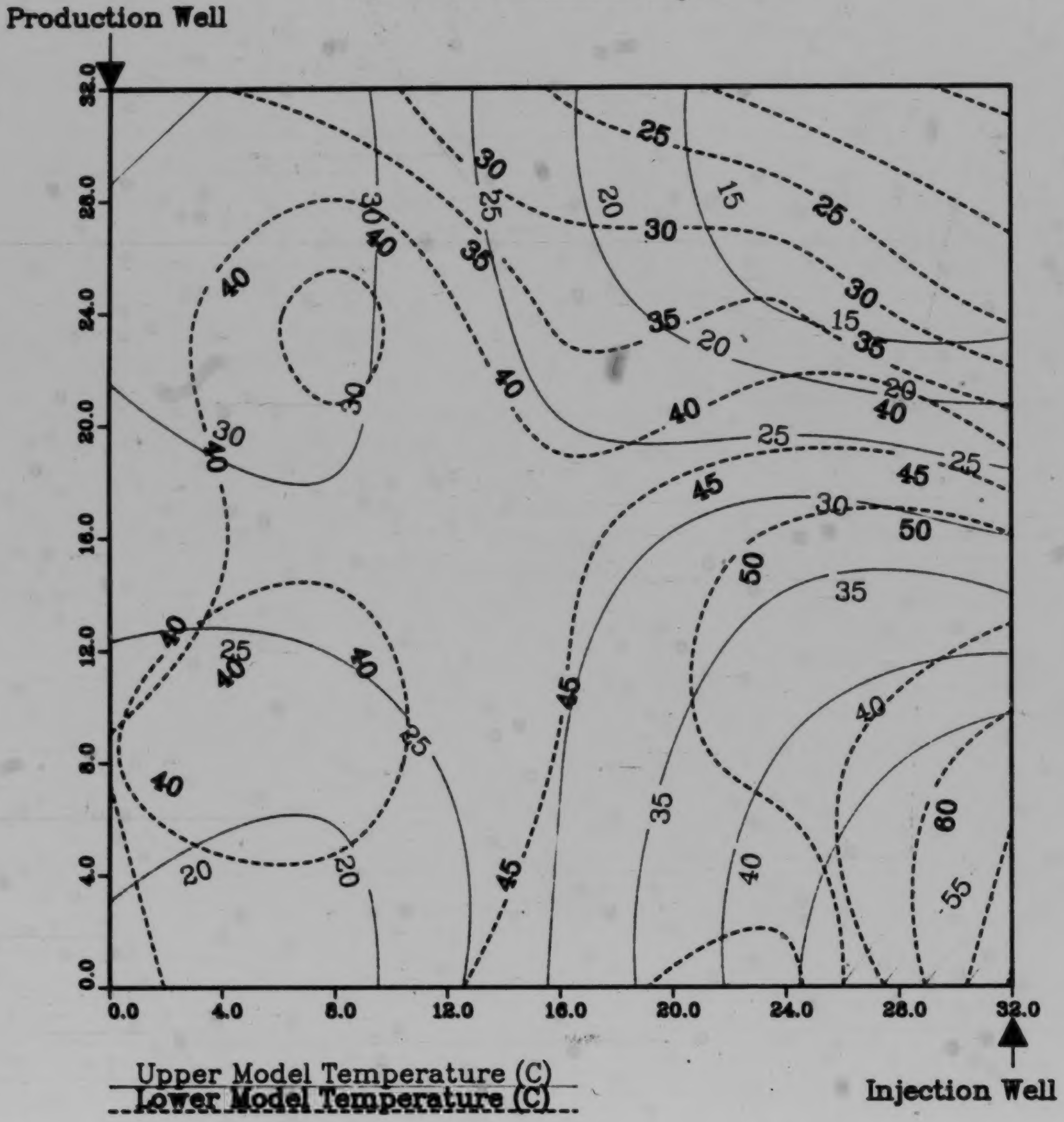

Figure A.65 : Run 60

Gas Inj. & Steamflood in B.W. Model

Temperature Profile for
1.75 Pore Volumes Injected

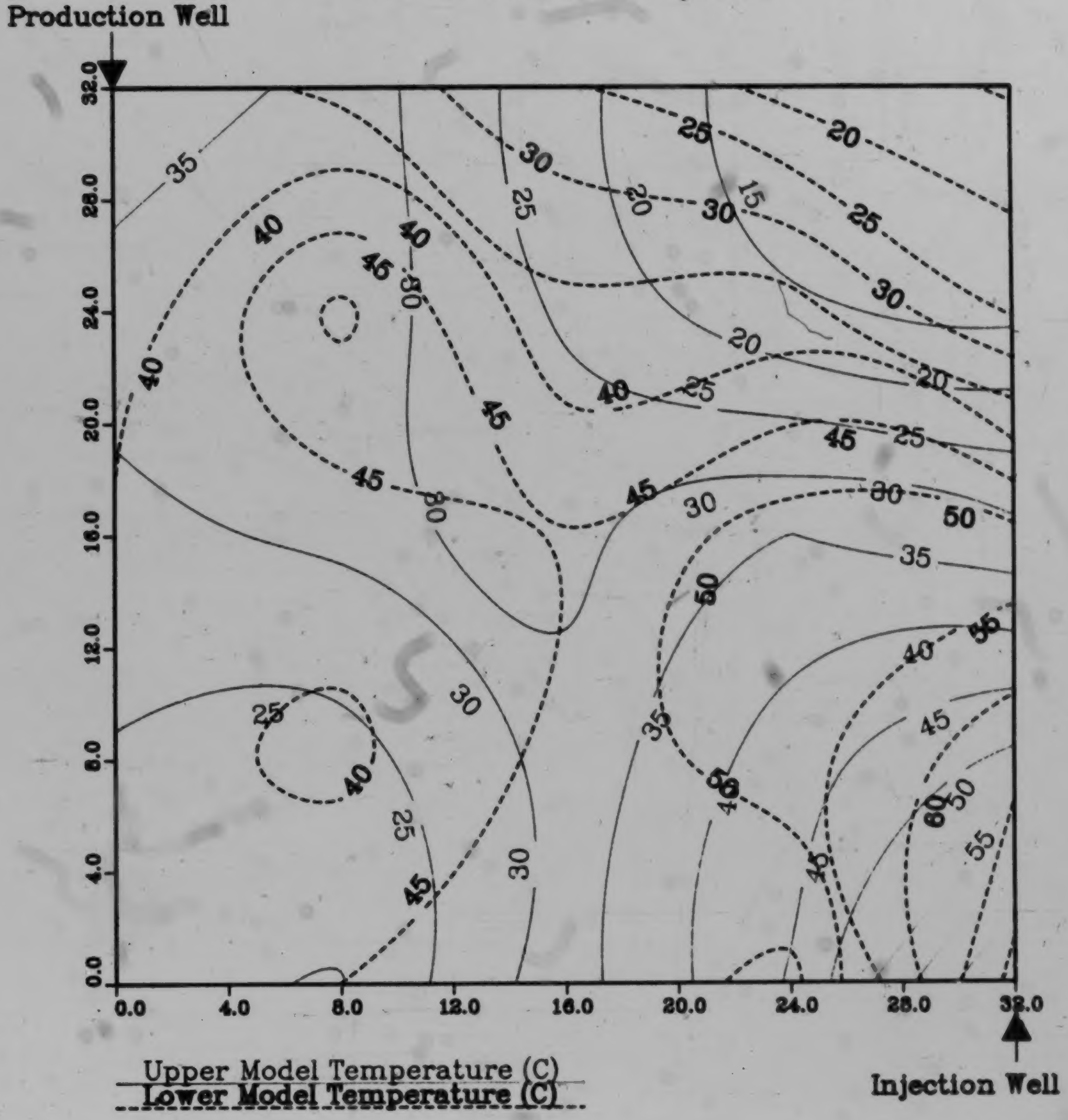

Figure A.66 : Run 60

Gas Inj. & Steamflood in B.W. Model

Temperature Profile for 2.00 Pore Volumes Injected

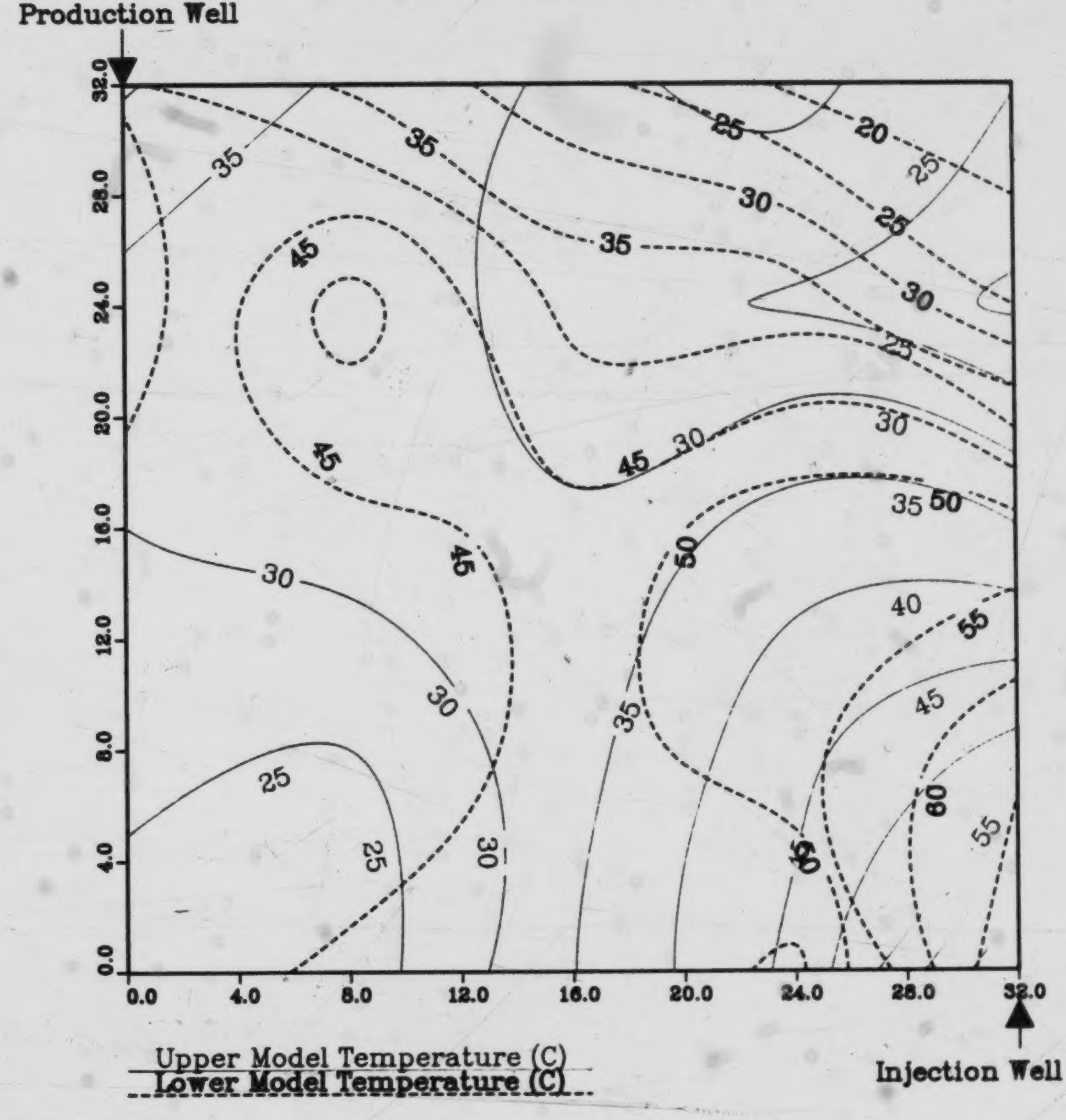

Figure A.67 :Run 60 Temp Profile
Injector to Producer Cross–Section
0.25 Pore Volumes Injected.

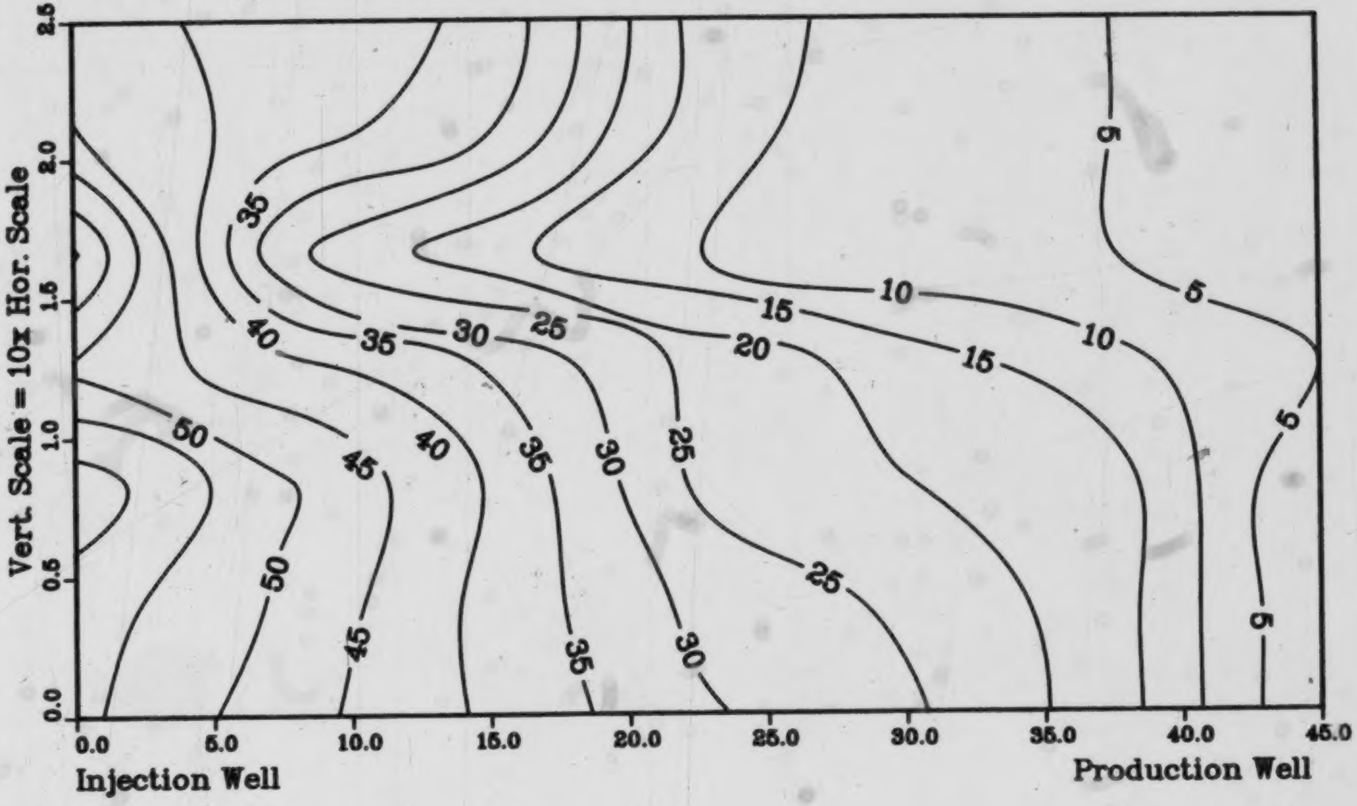

Figure A.68 :Run 60 Temp Profile
Injector to Producer Cross–Section
0.50 Pore Volumes Injected.

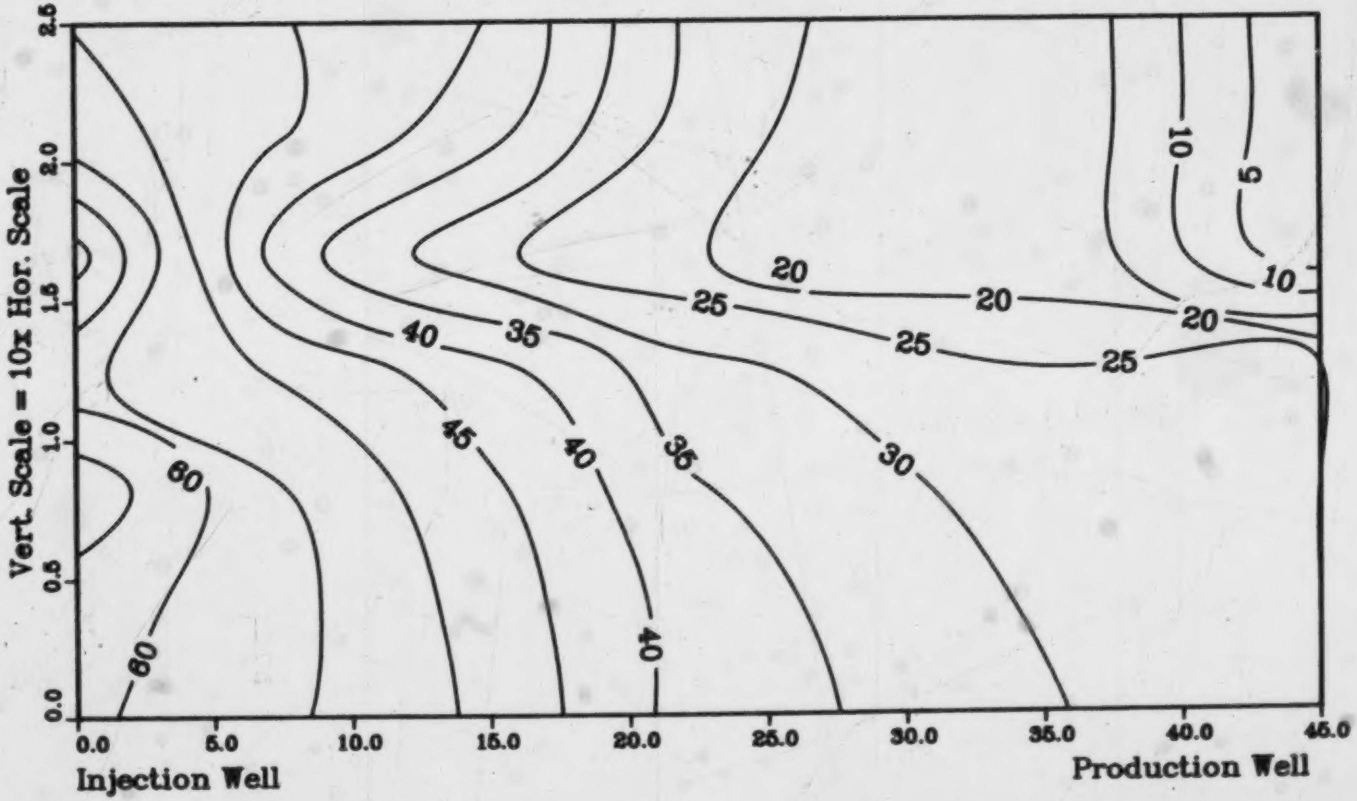

Figure A.69 :Run 60 Temp Profile
Injector to Producer Cross–Section
0.75 Pore Volumes Injected.

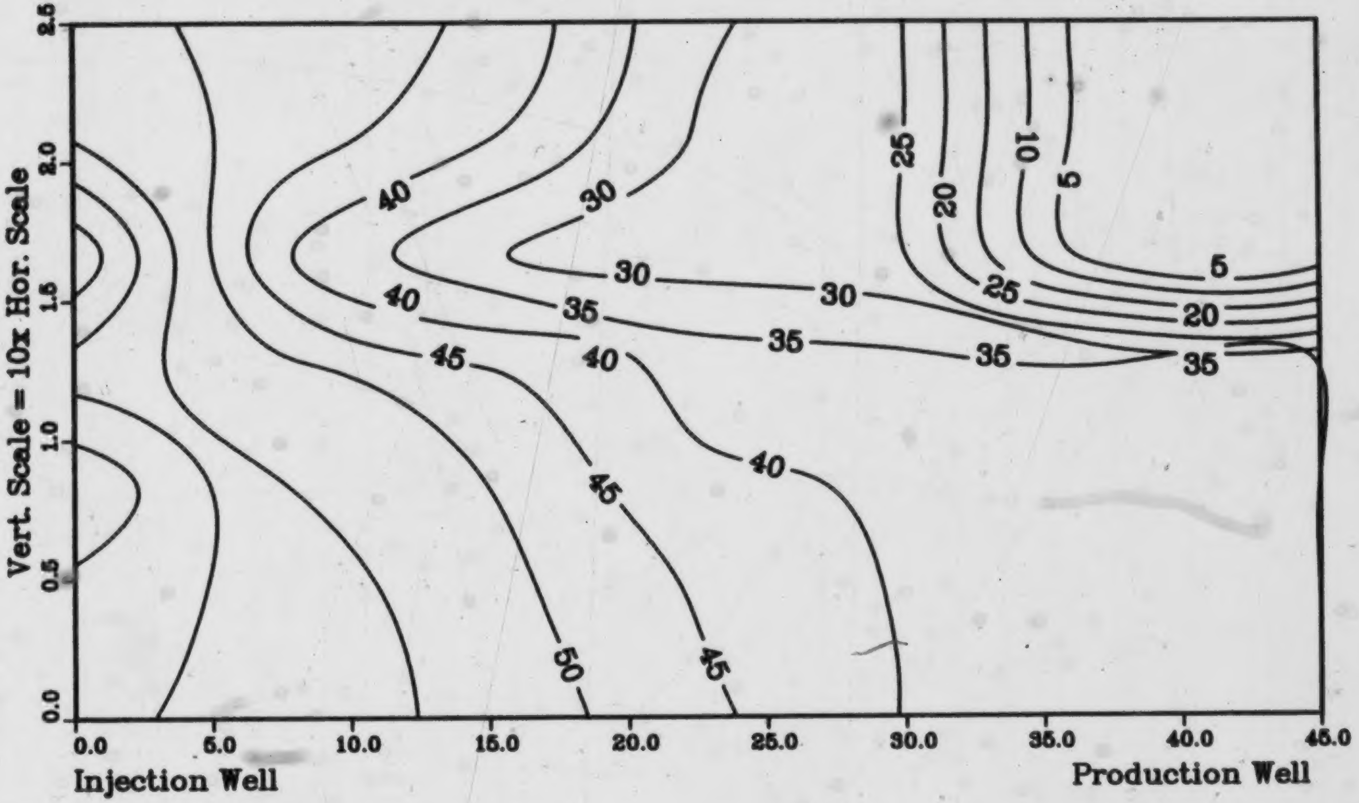

Figure A.70 :Run 60 Temp Profile
Injector to Producer Cross–Section
1.00 Pore Volumes Injected.

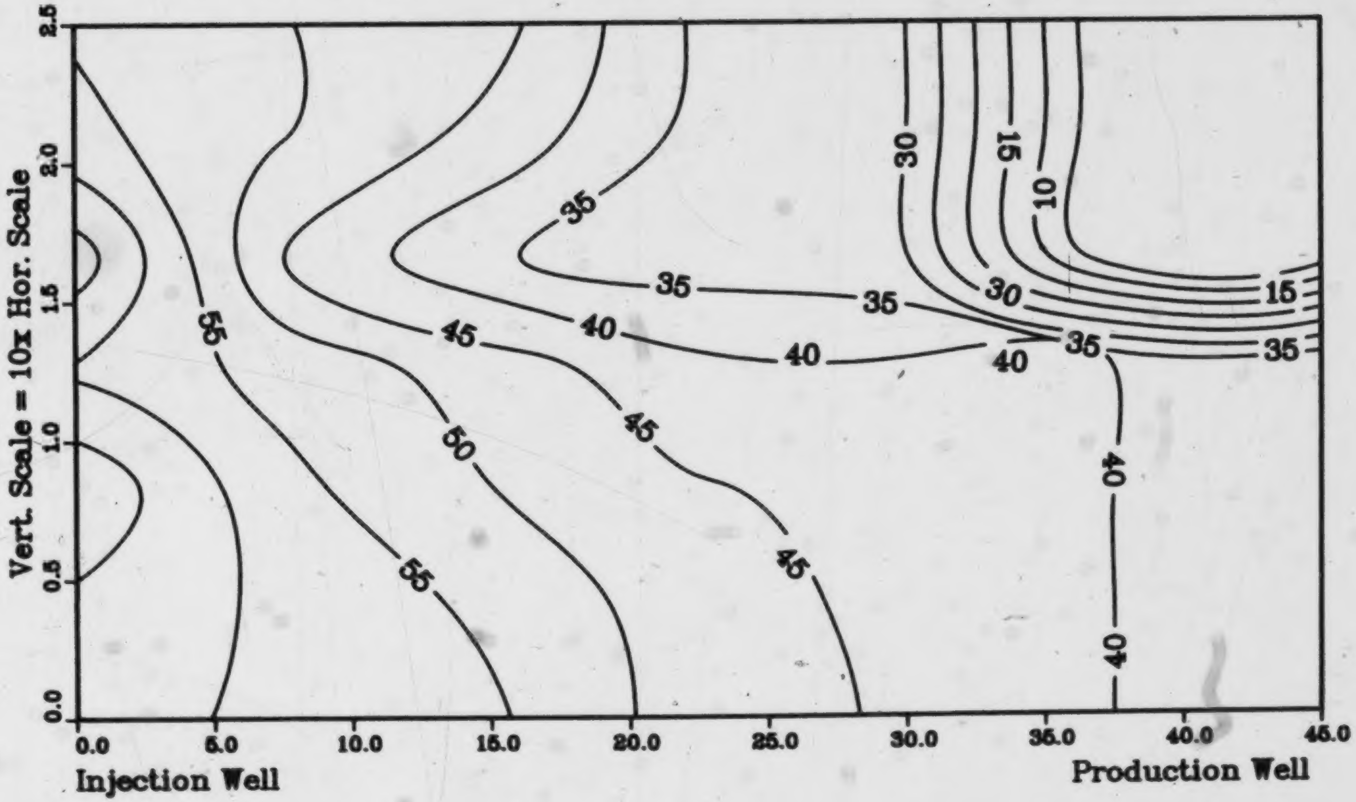

Figure A.71 : Run 61

Gas Inj. & Steamflood in B.W. Model

Temperature Profile for 0.25 Pore Volumes Injected

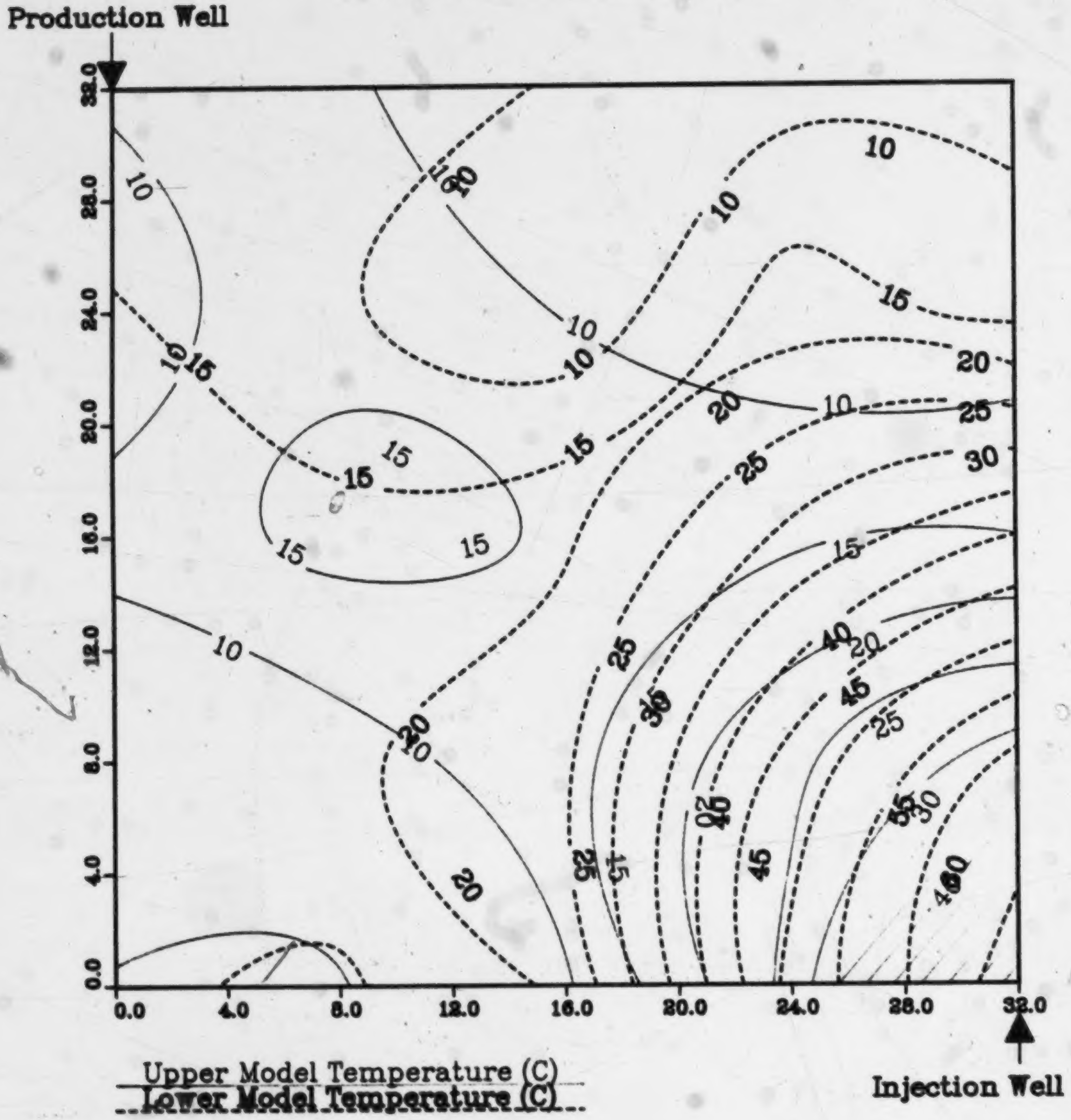

Figure A.72 : Run 61
Gas Inj. & Steamflood in B.W. Model

Temperature Profile for
0.50 Pore Volumes Injected

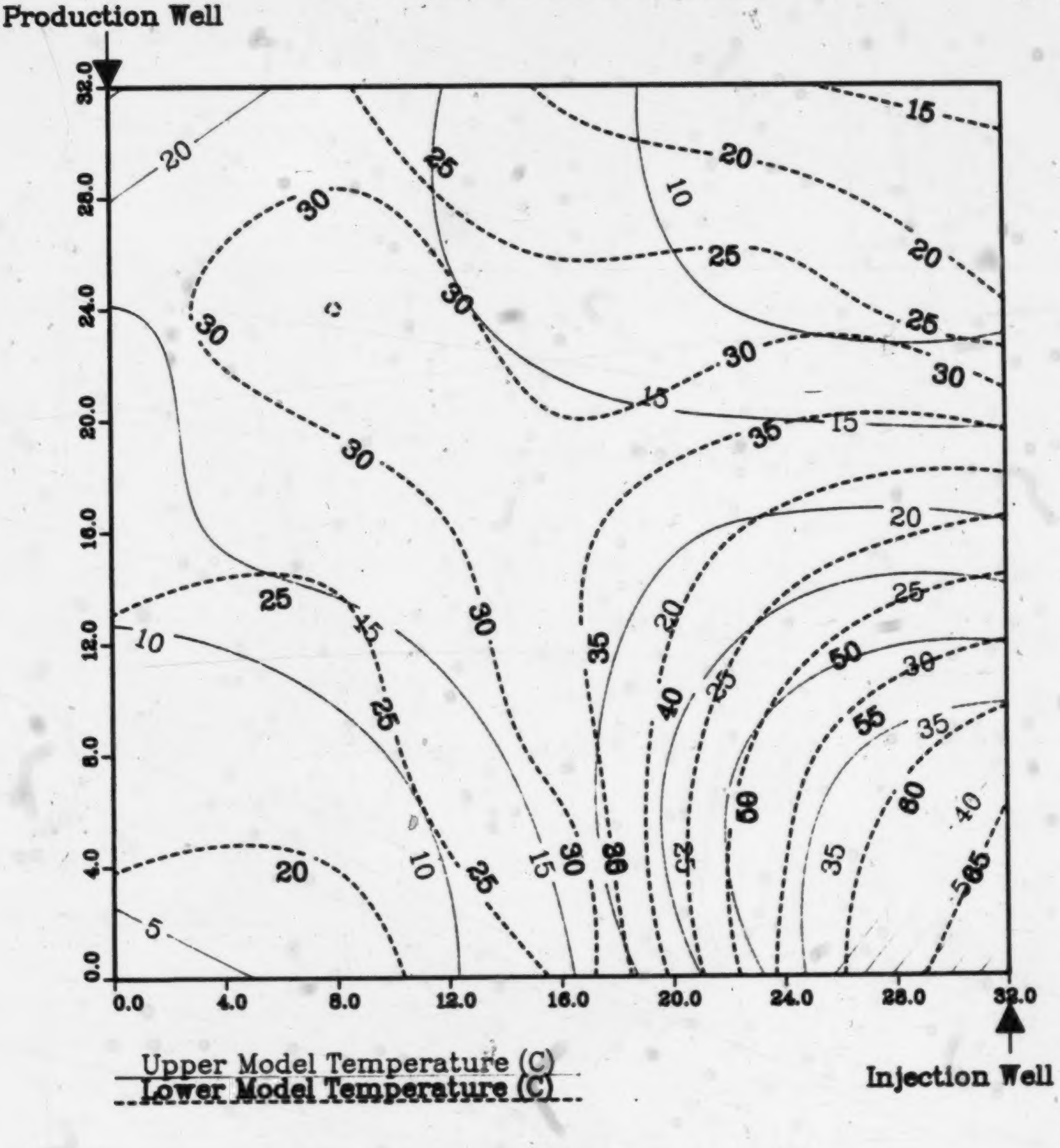

Figure A.73 : Run 61

Gas Inj. & Steamflood in B.W. Model

Temperature Profile for 0.75 Pore Volumes Injected

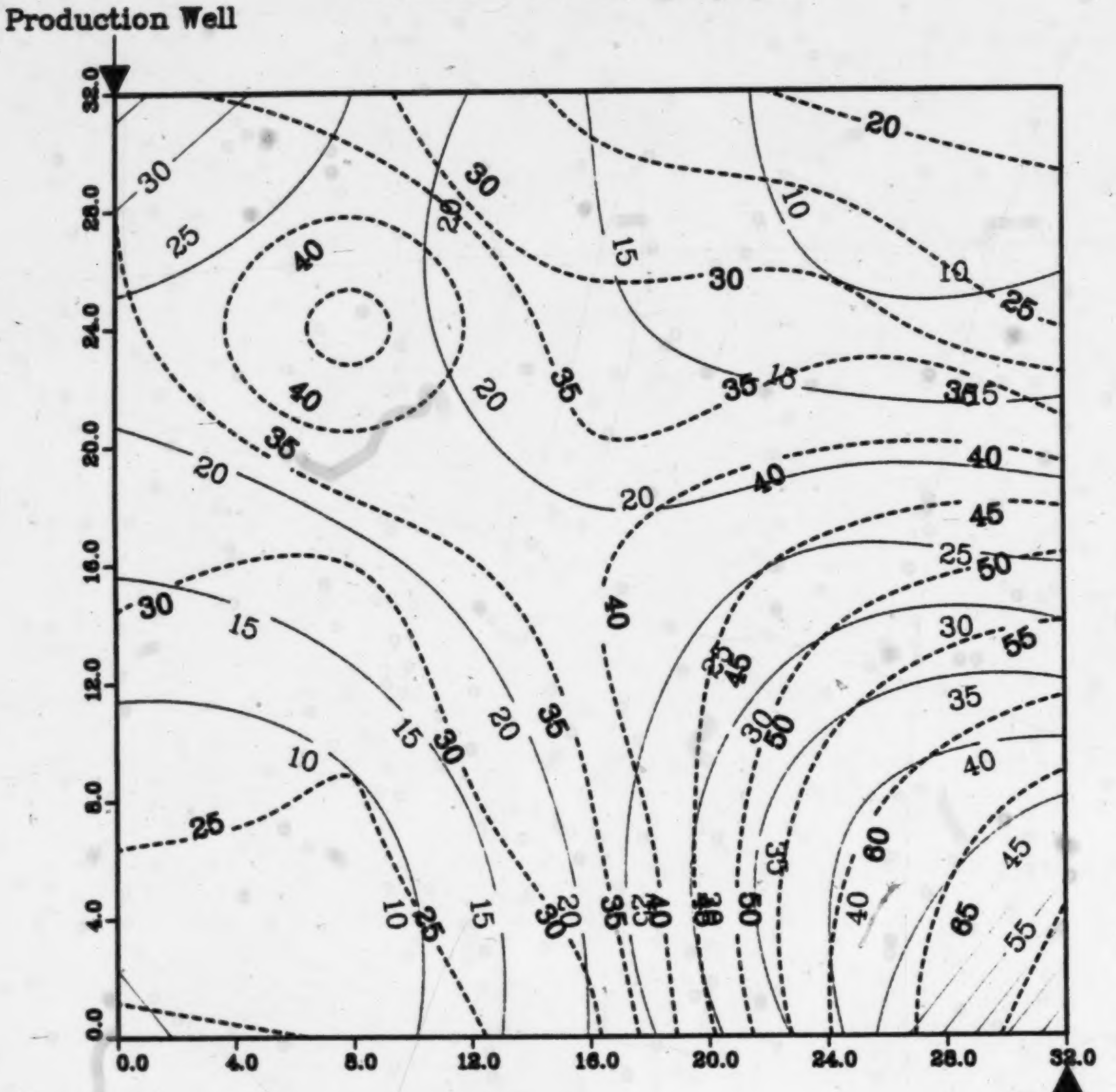

Figure A.74 : Run 61

Gas Inj. & Steamflood in B.W. Model

Temperature Profile for 1.00 Pore Volumes Injected

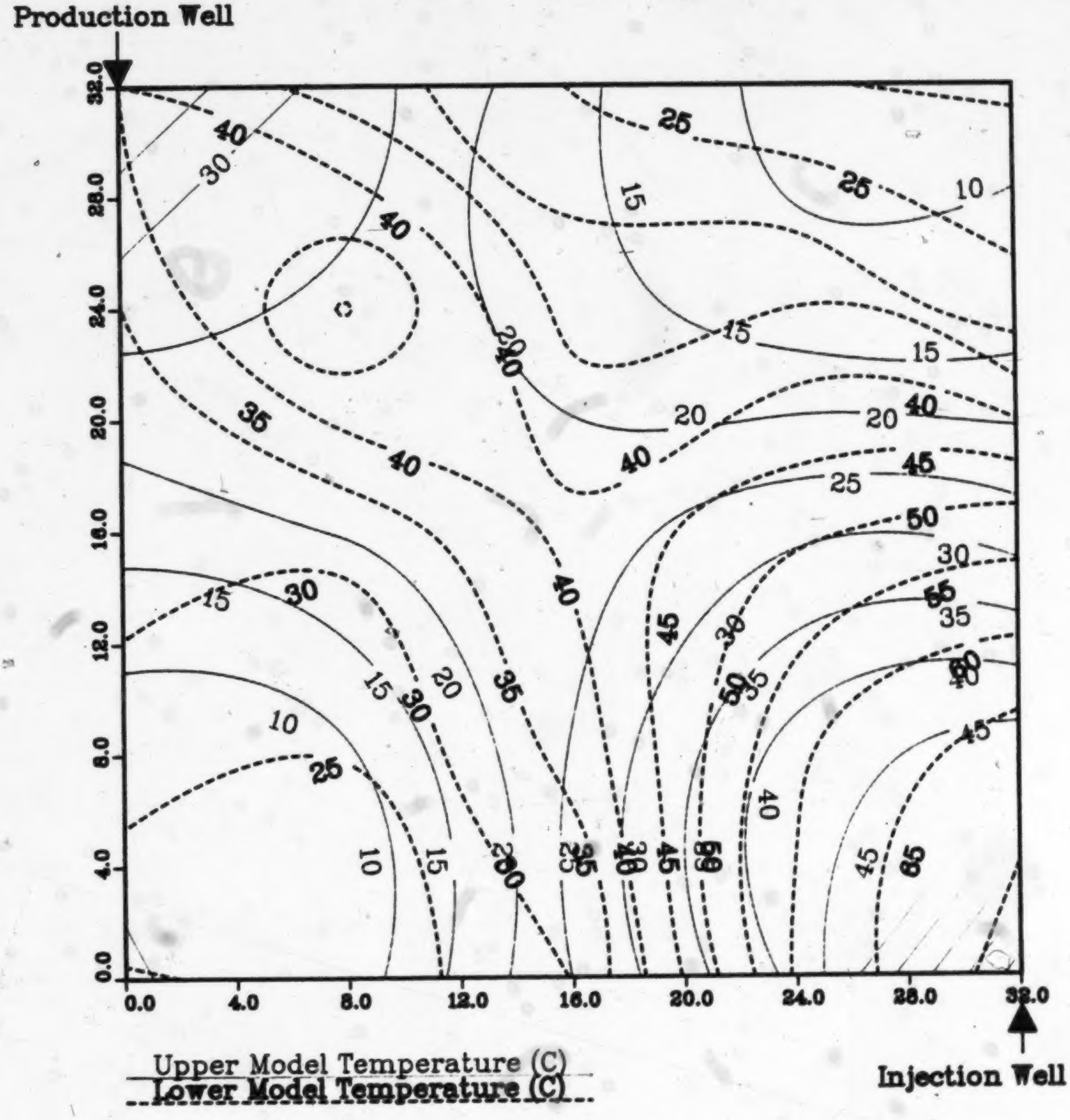

Figure A.75 : Run 61
Gas Inj. & Steamflood in B.W. Model

Temperature Profile for
1.25 Pore Volumes Injected

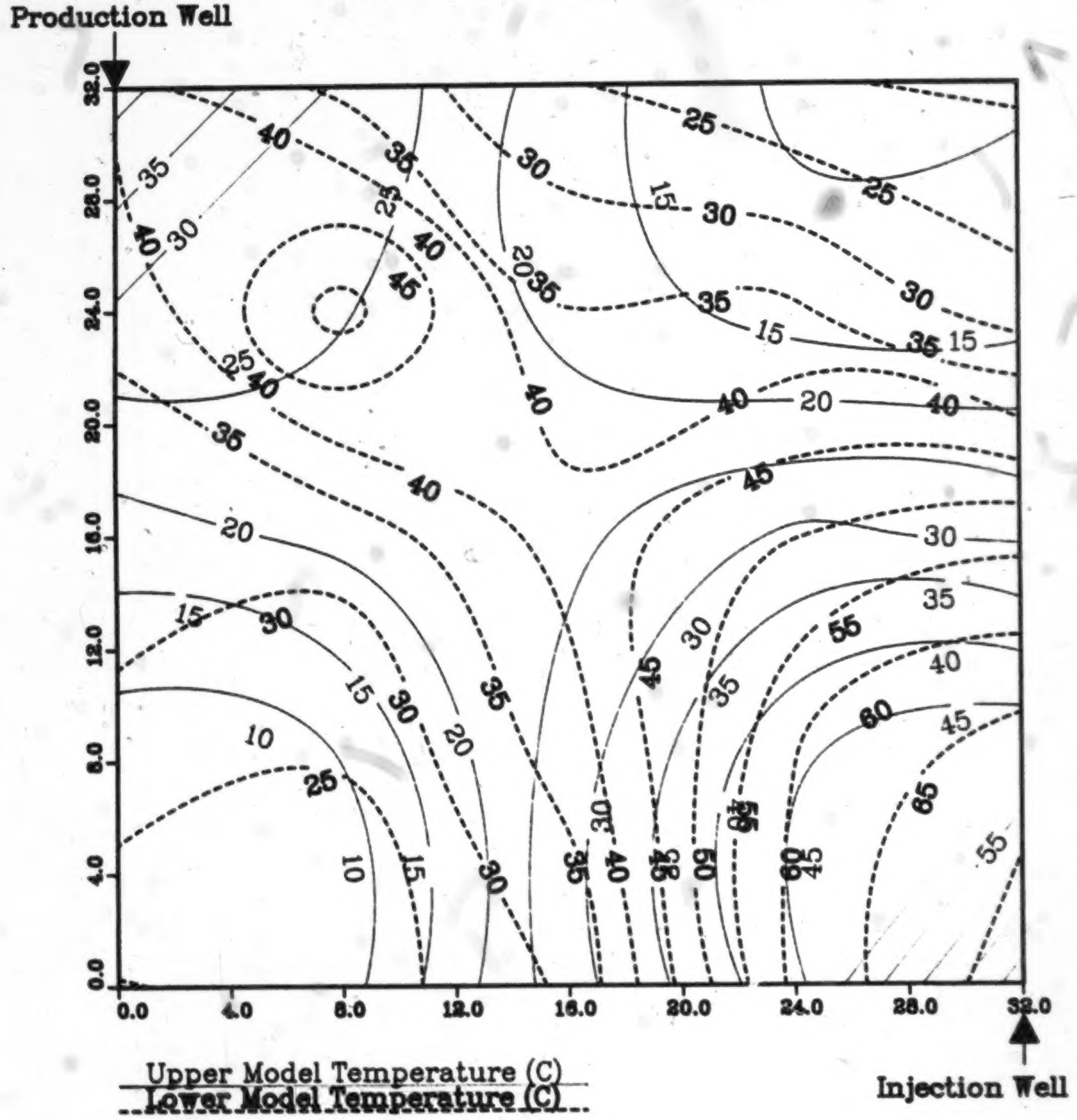

Figure A.76 : Run 61

Gas Inj. & Steamflood in B.W. Model

Temperature Profile for 1.50 Pore Volumes Injected

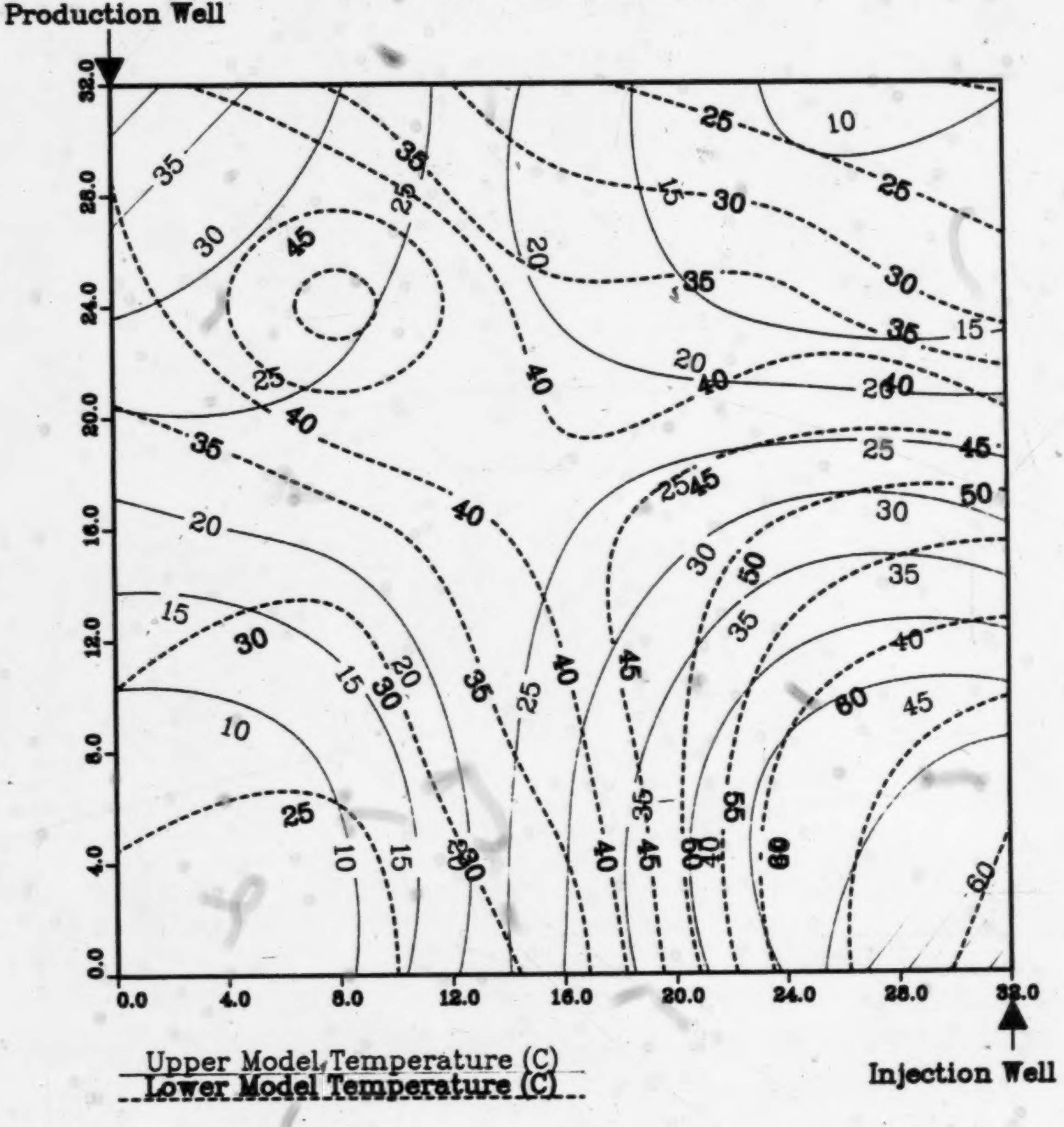

Figure A.77 : Run 61
Gas Inj. & Steamflood in B.W. Model

Temperature Profile for
1.75 Pore Volumes Injected

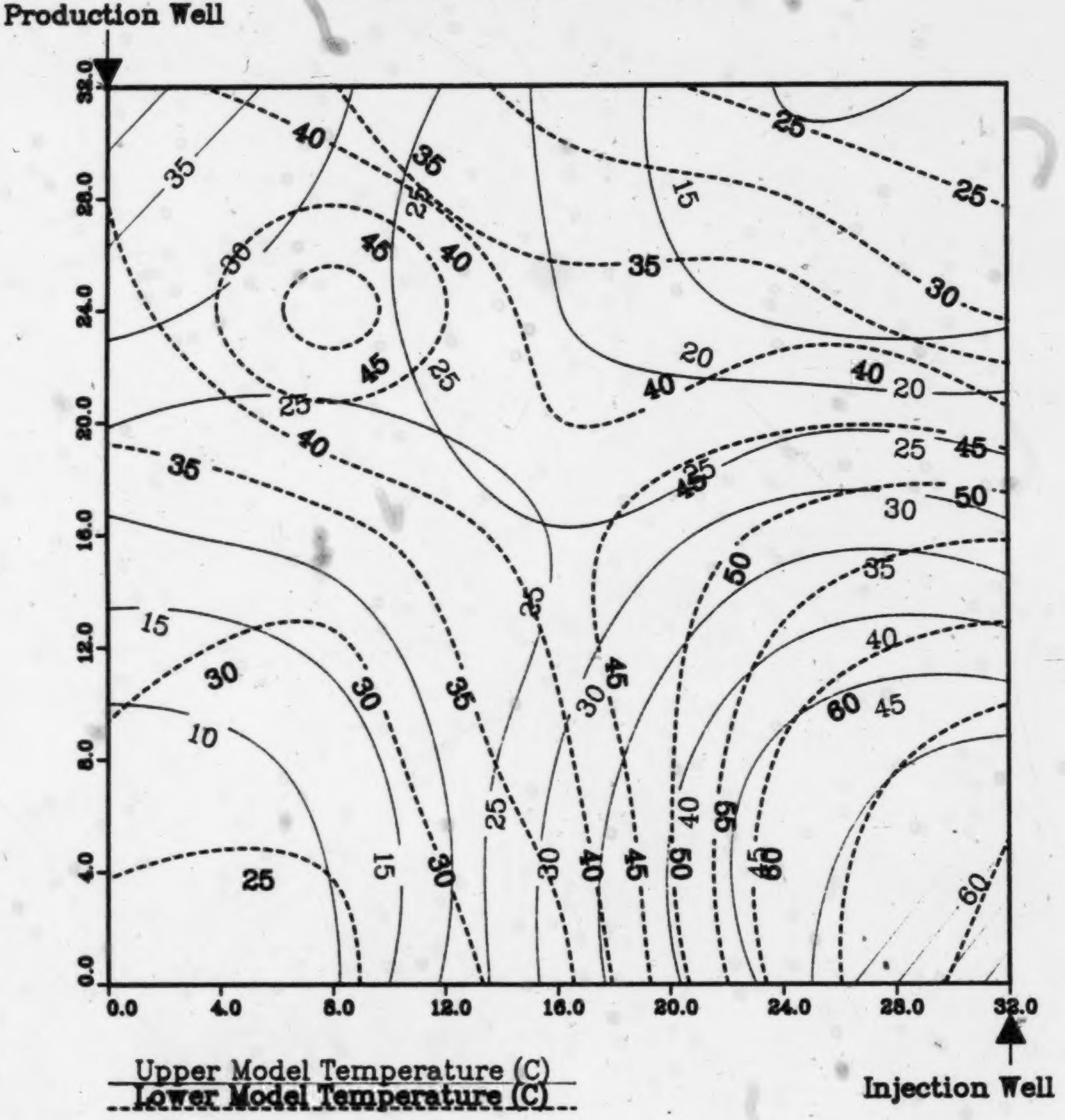

Figure A.78 : Run 61

Gas Inj. & Steamflood in B.W. Model

Temperature Profile for 2.00 Pore Volumes Injected

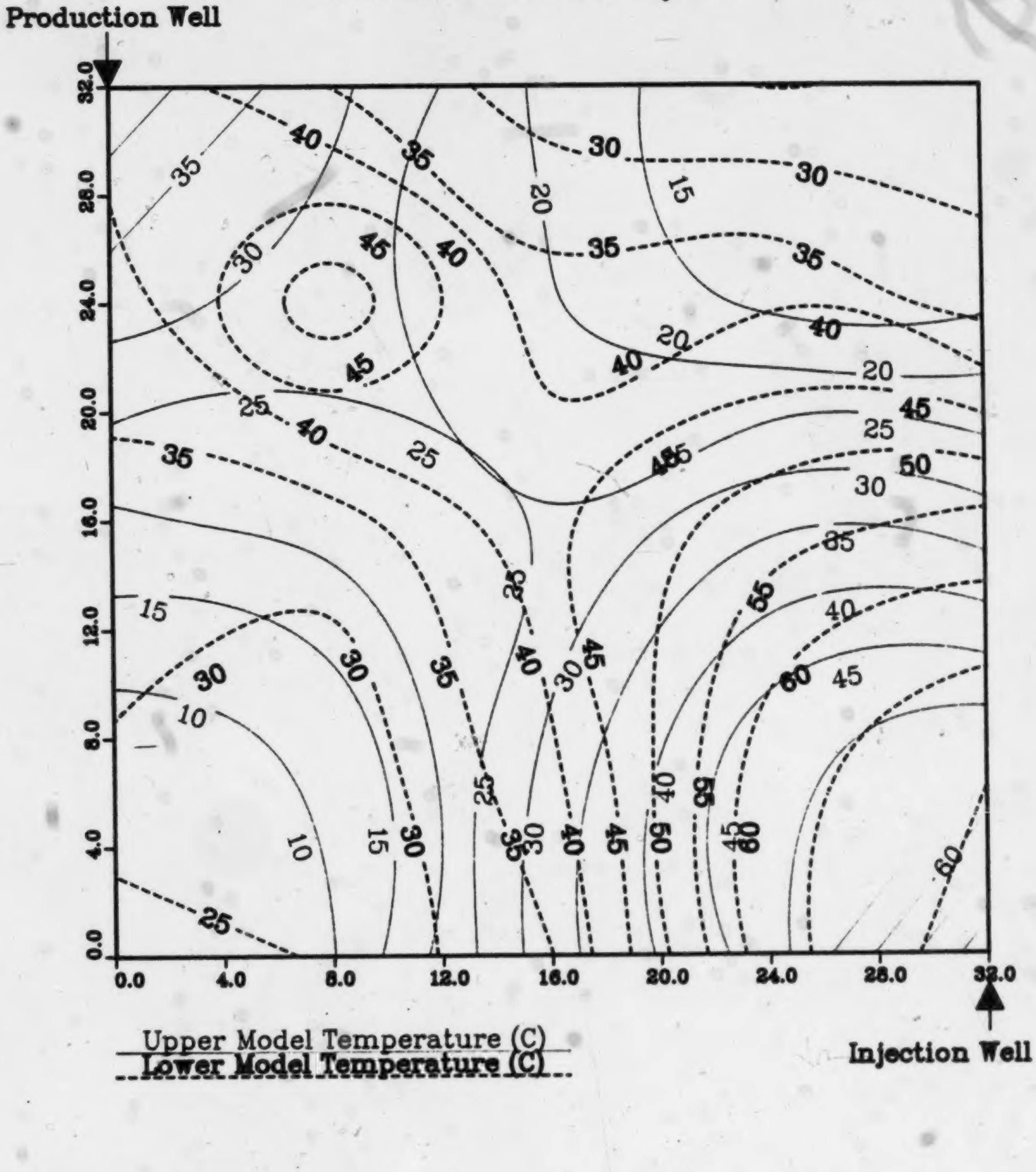

Figure A.79 :Run 61 Temp Profile
Injector to Producer Cross-Section
0.25 Pore Volumes Injected.

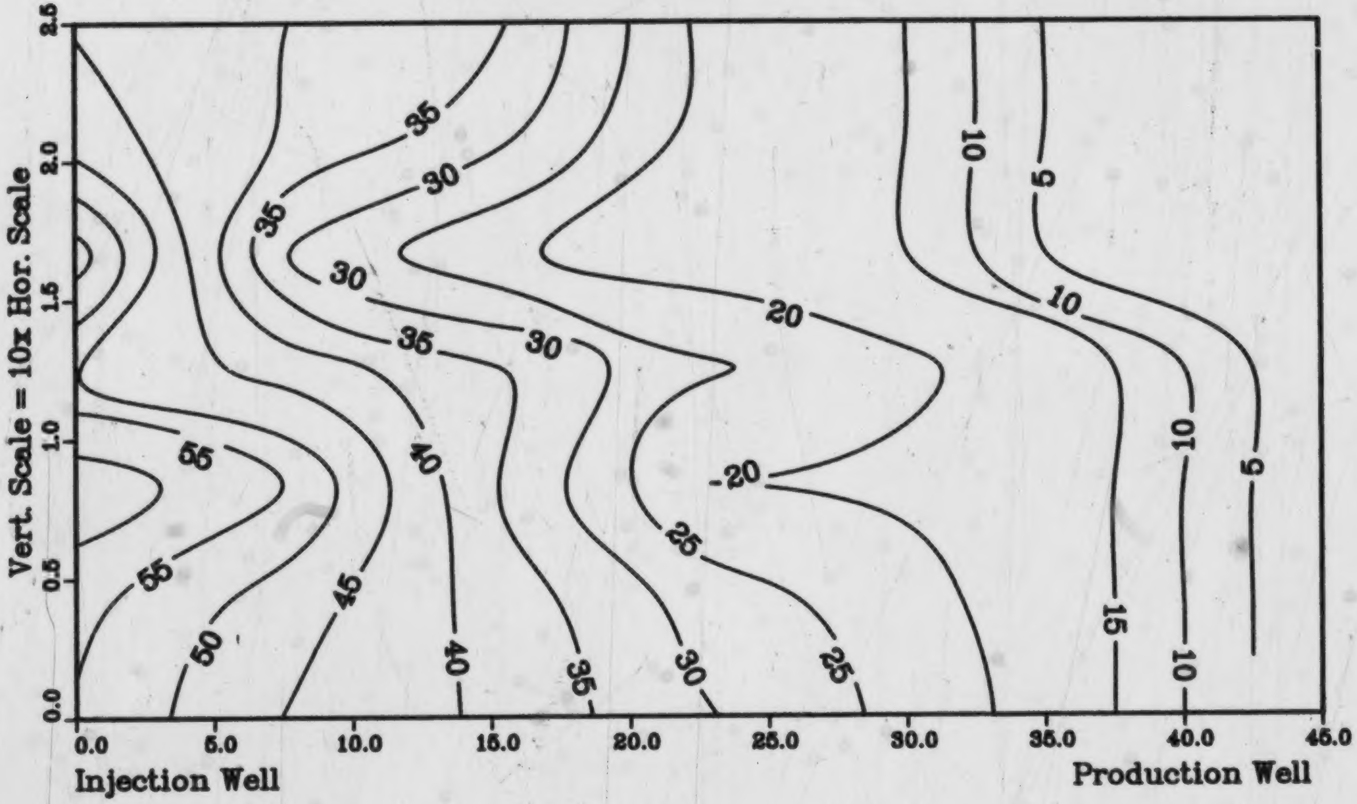

Figure A.80 :Run 61 Temp Profile
Injector to Producer Cross-Section
0.50 Pore Volumes Injected.

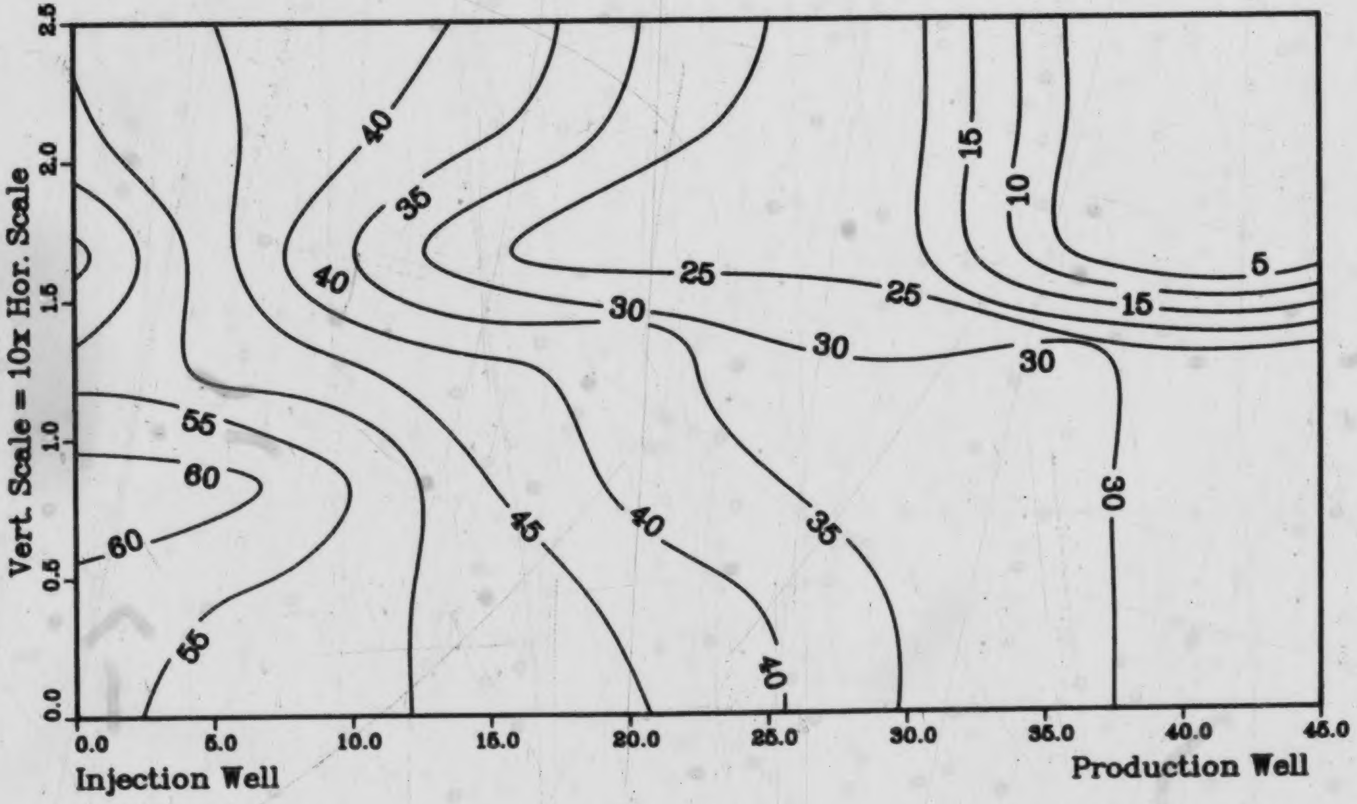

Figure A.81 :Run 61 Temp Profile
Injector to Producer Cross–Section
0.75 Pore Volumes Injected.

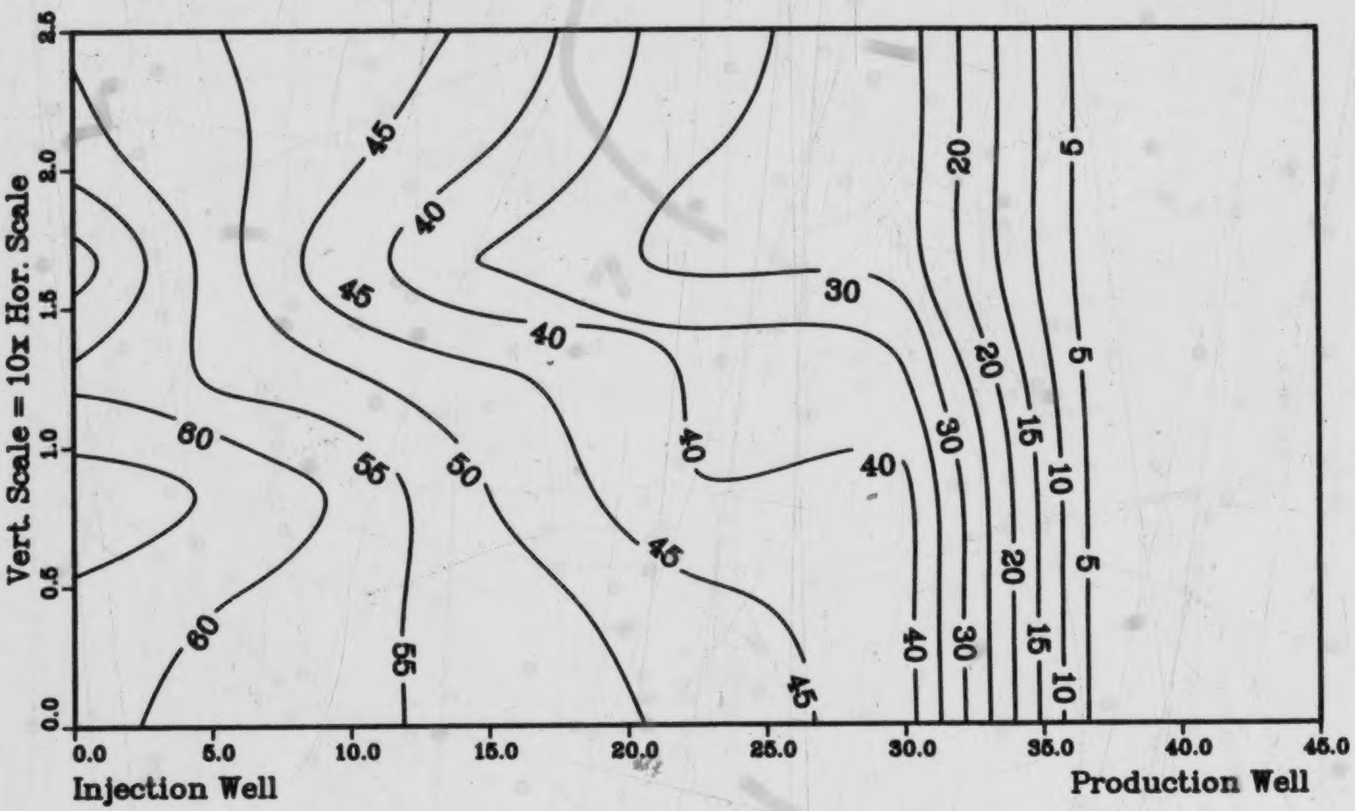

Figure A.82 :Run 61 Temp Profile
Injector to Producer Cross-Section
1.00 Pore Volumes Injected.

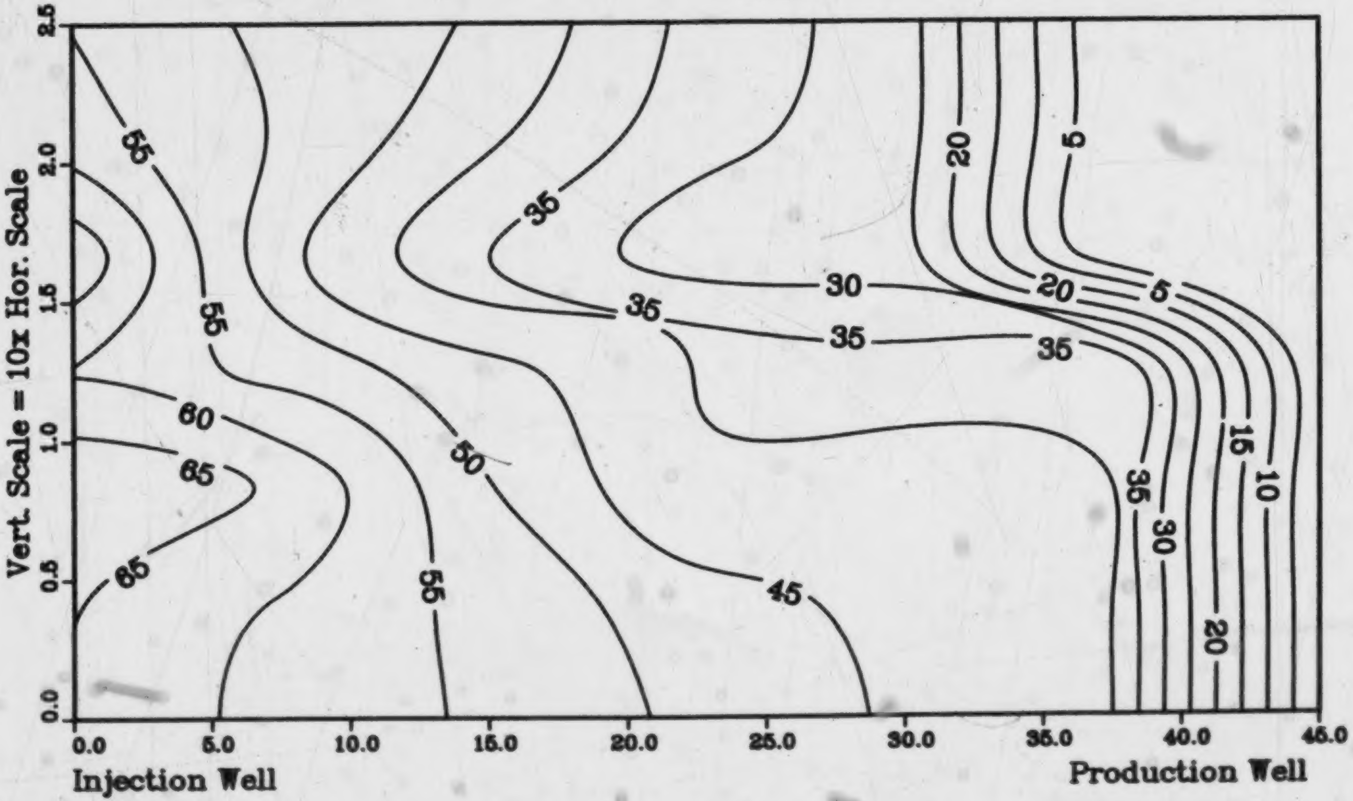

Figure A.83 : Run 65
Solvent–Steamflood in B.W. Model

Temperature Profile for
0.25 Pore Volumes Injected

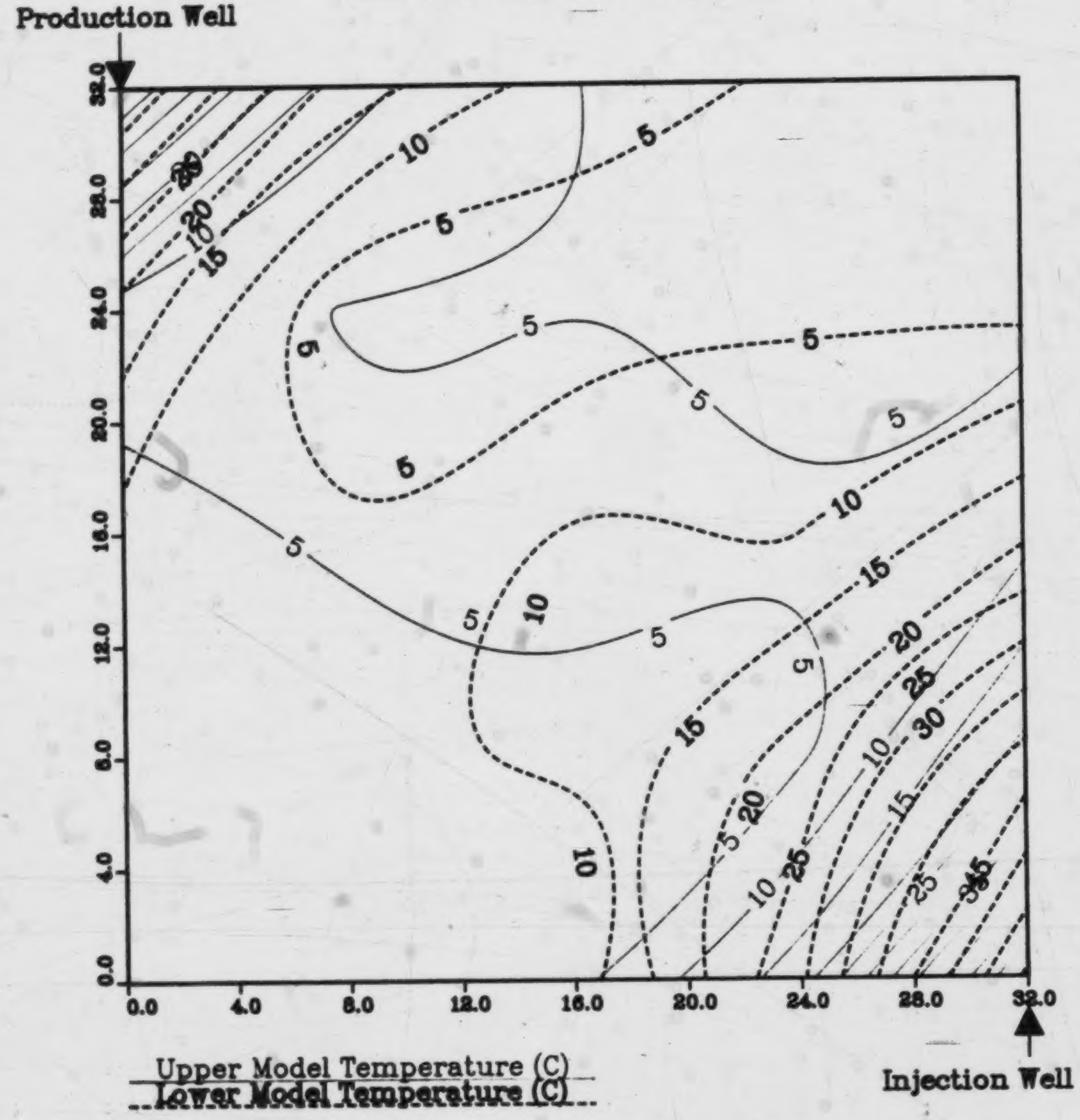

Figure A.84 : Run 65
Solvent–Steamflood in B.W. Model

Temperature Profile for
0.50 Pore Volumes Injected

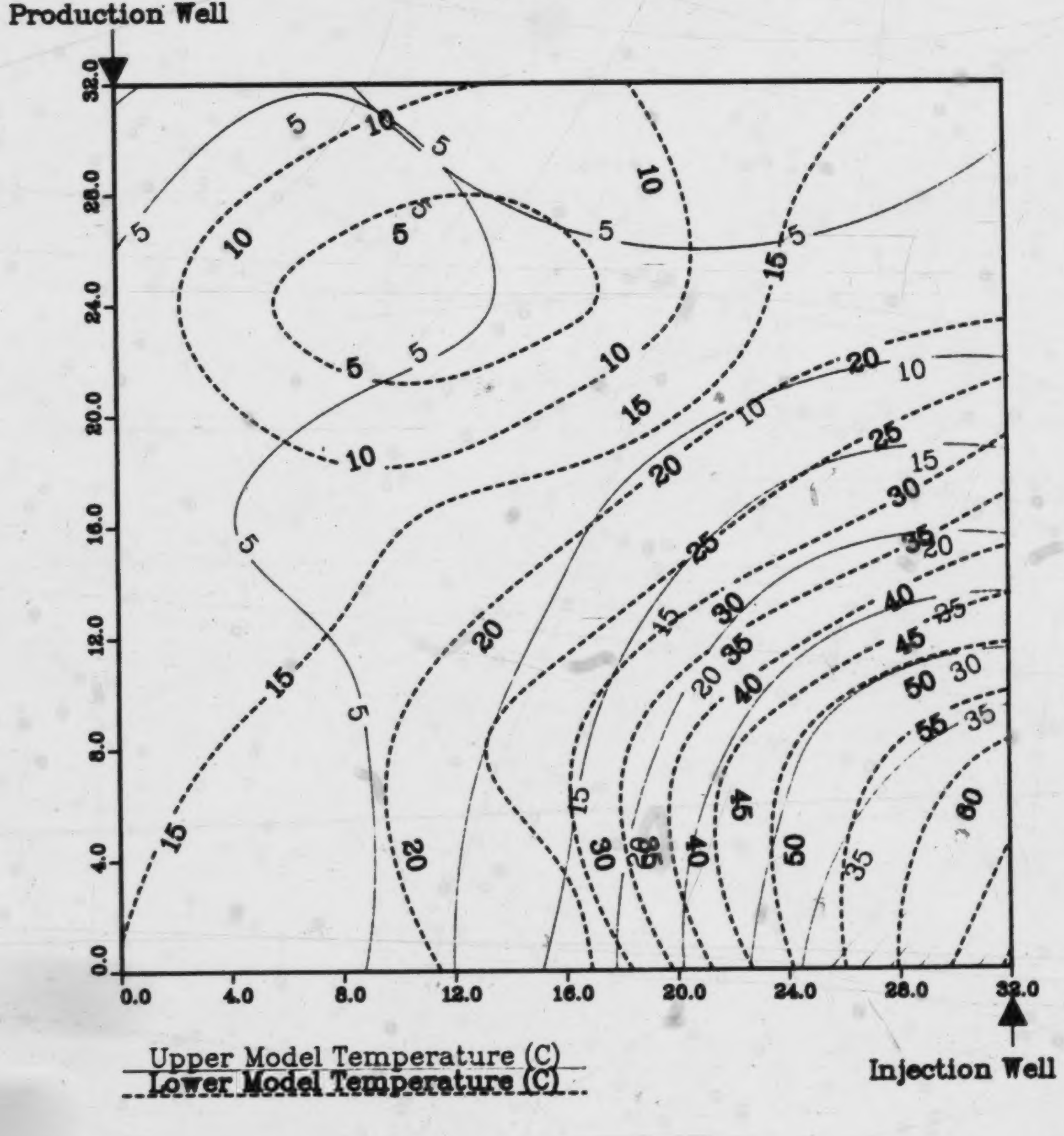

Figure A.85 : Run 65

Solvent–Steamflood in B.W. Model

Temperature Profile for
0.75 Pore Volumes Injected

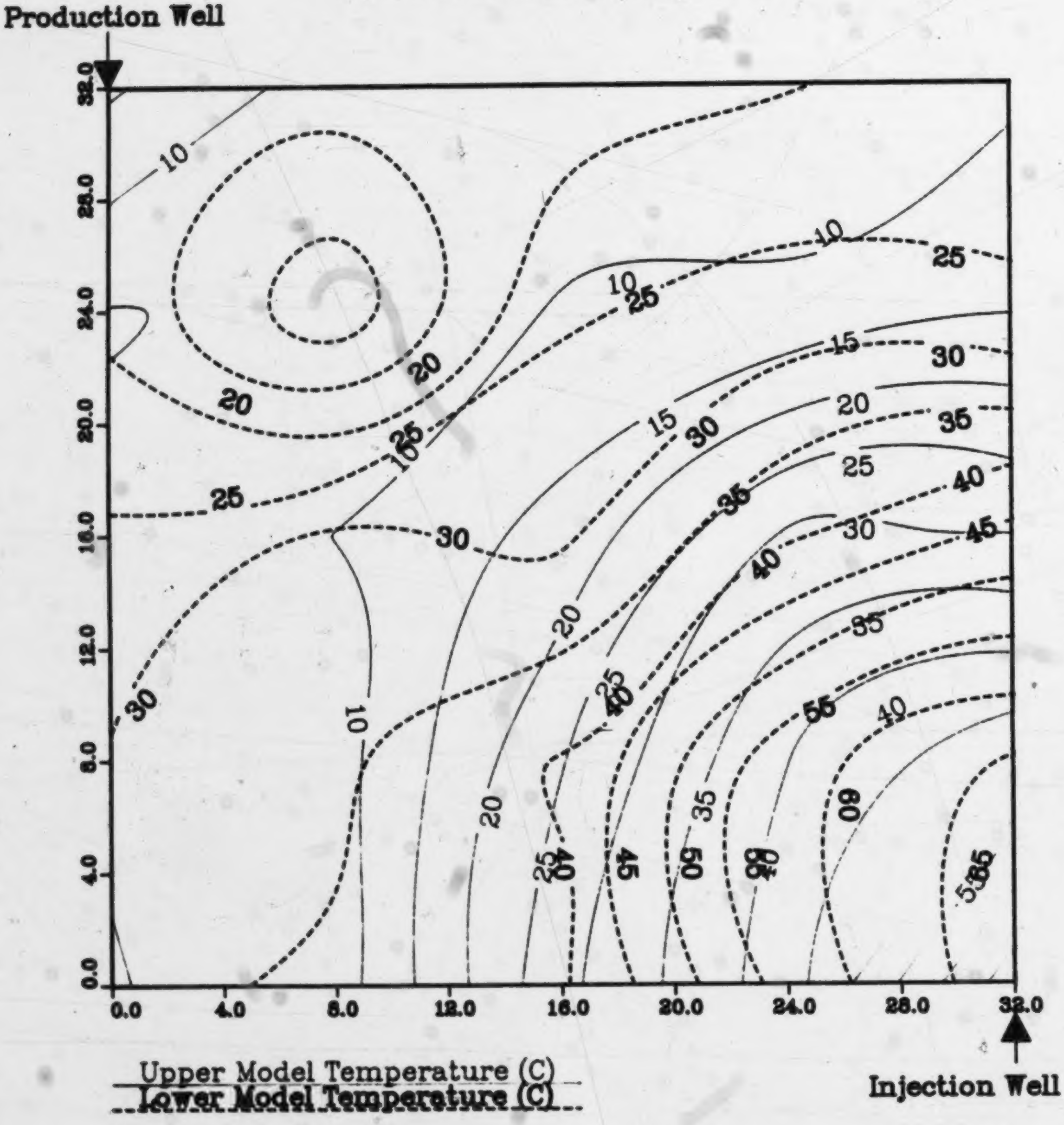

Figure A.86 : Run 65

Solvent–Steamflood in B.W. Model

Temperature Profile for
1.00 Pore Volumes Injected

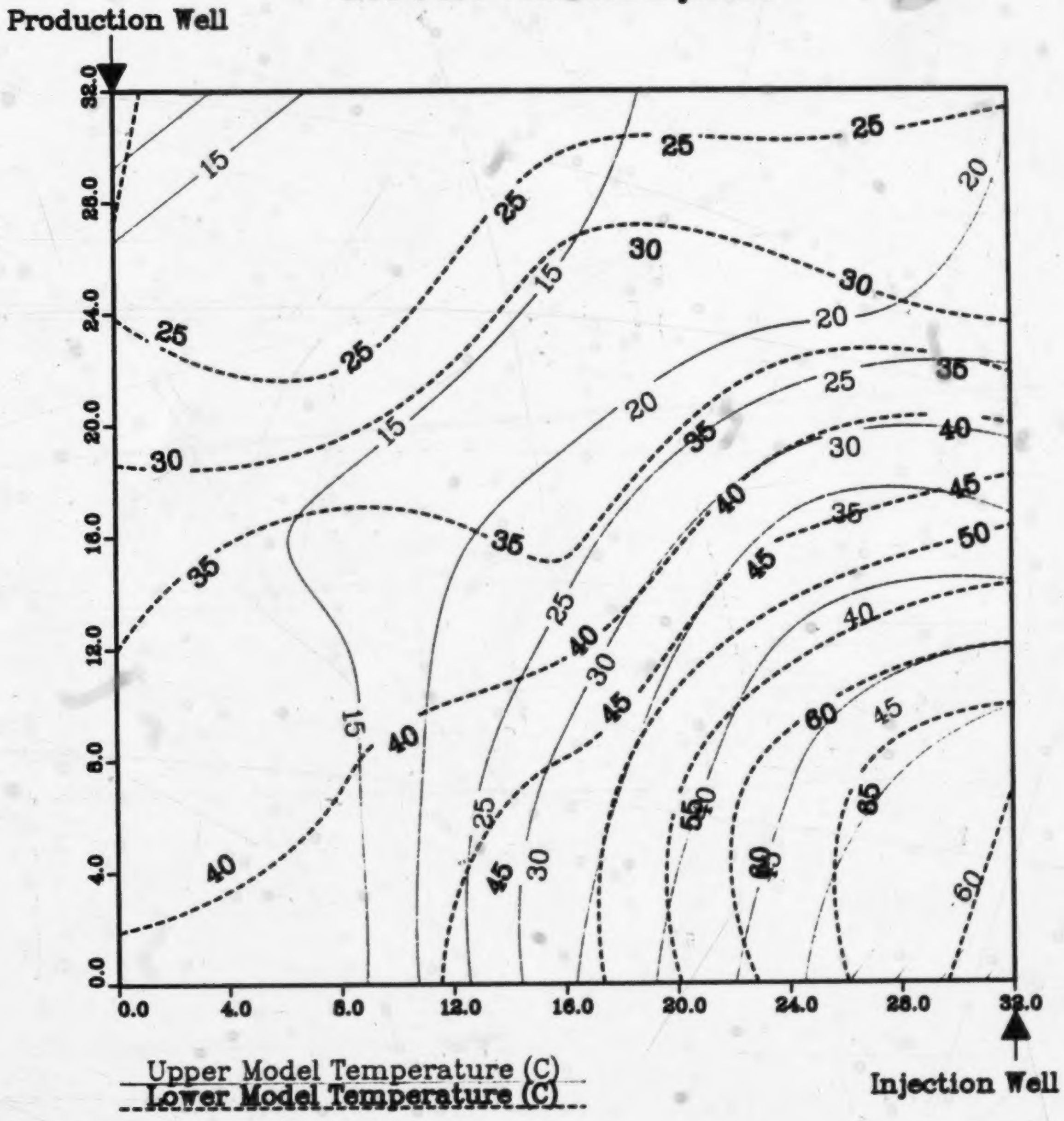

Figure A.87 : Run 65

Solvent–Steamflood in B.W. Model

Temperature Profile for 1.25 Pore Volumes Injected

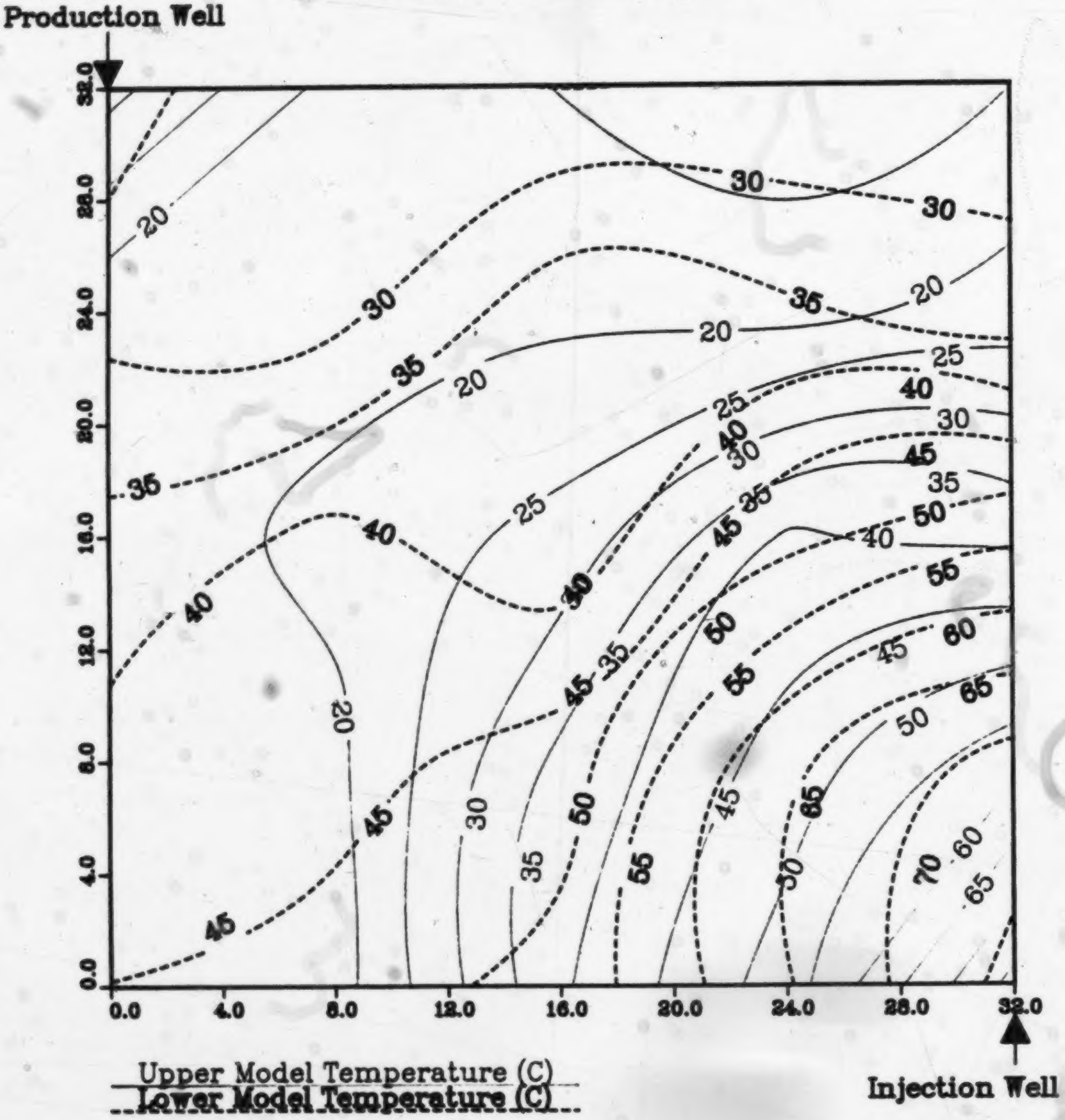

Figure A.88 : Run 65

Solvent--Steamflood in B.W. Model

Temperature Profile for 1.50 Pore Volumes Injected

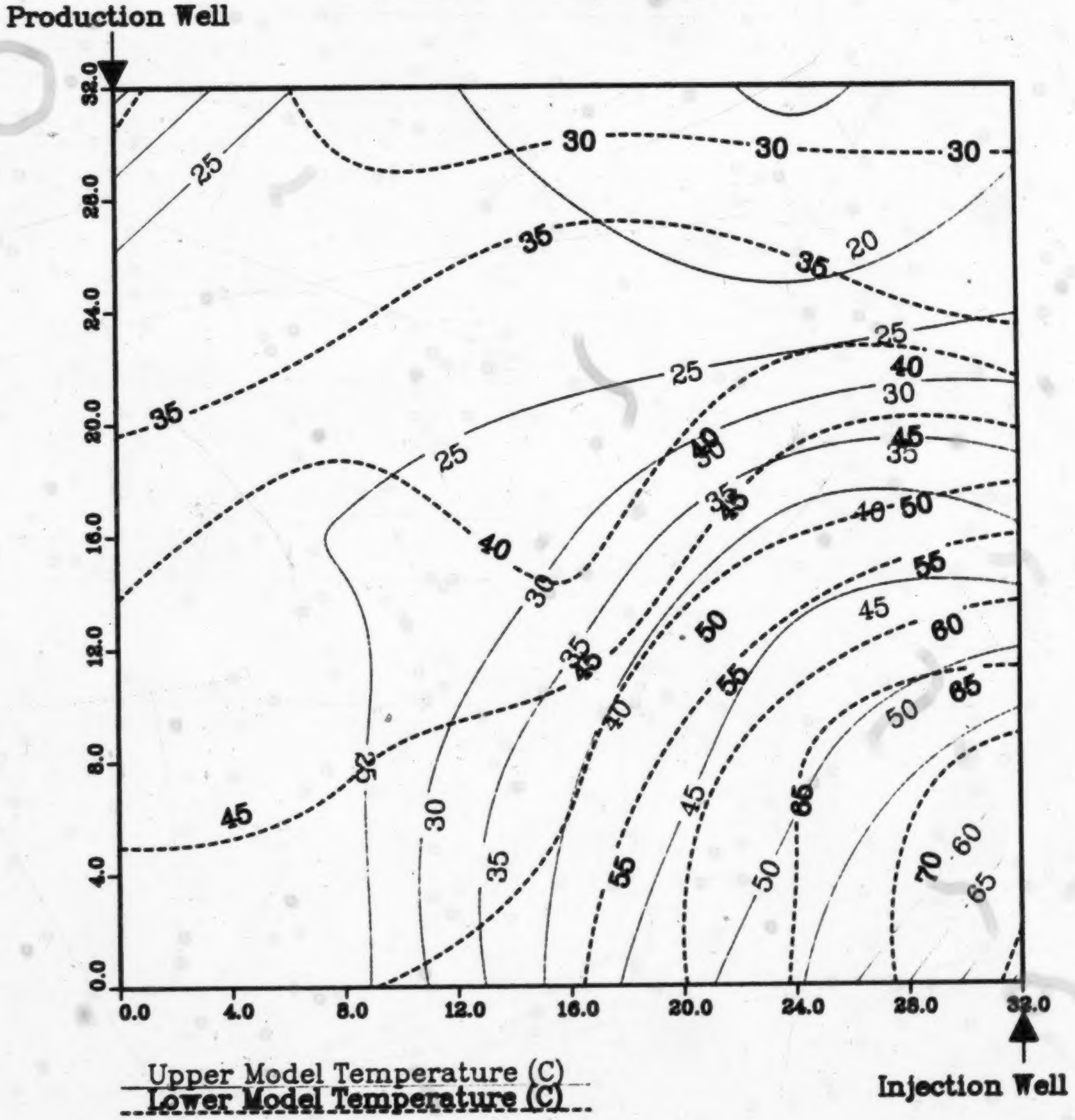

Figure A.89 : Run 65

Solvent–Steamflood in B.W. Model

Temperature Profile for 1.75 Pore Volumes Injected

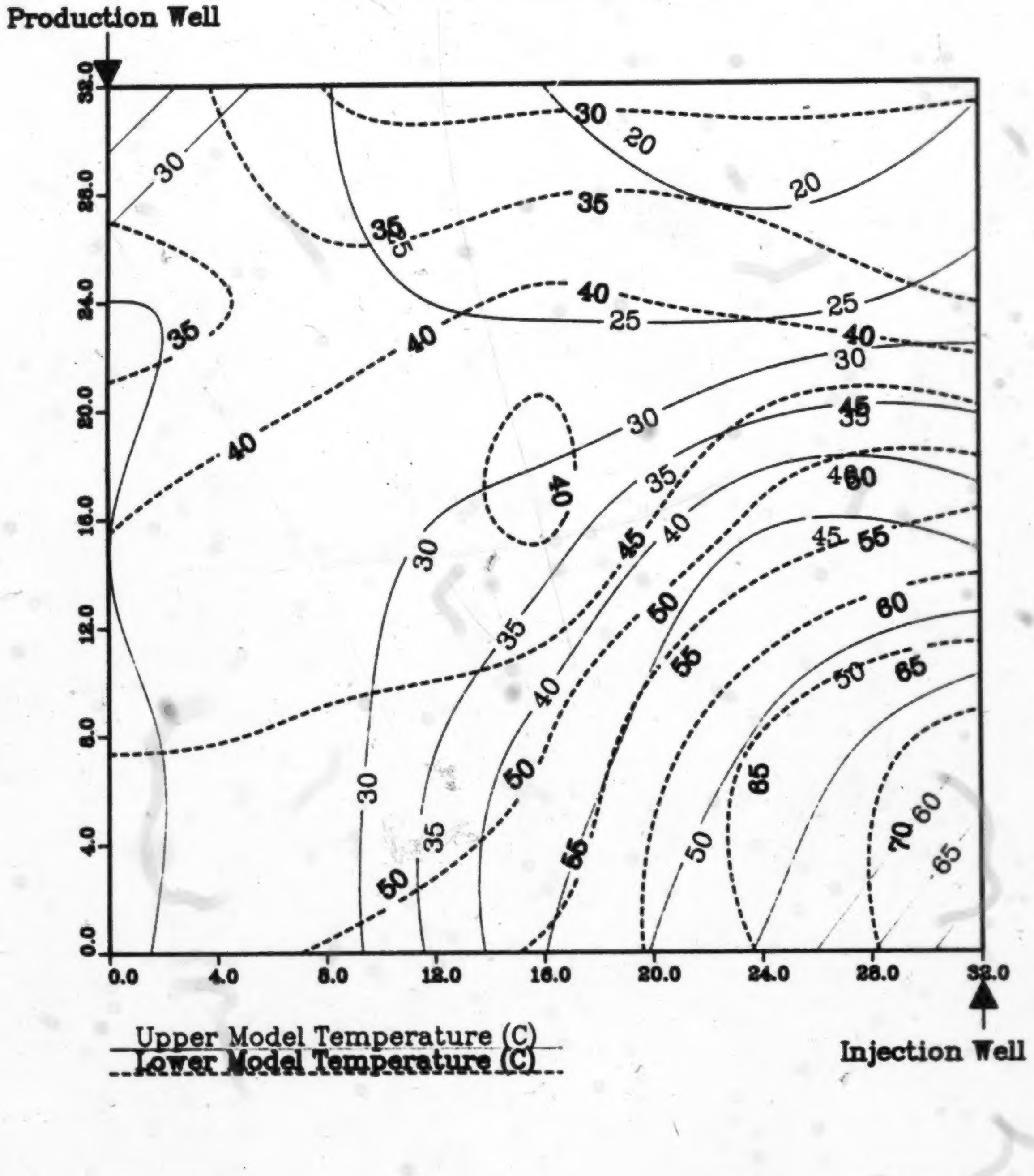

Figure A.90 : Run 65

Solvent–Steamflood in B.W. Model

Temperature Profile for
2.00 Pore Volumes Injected

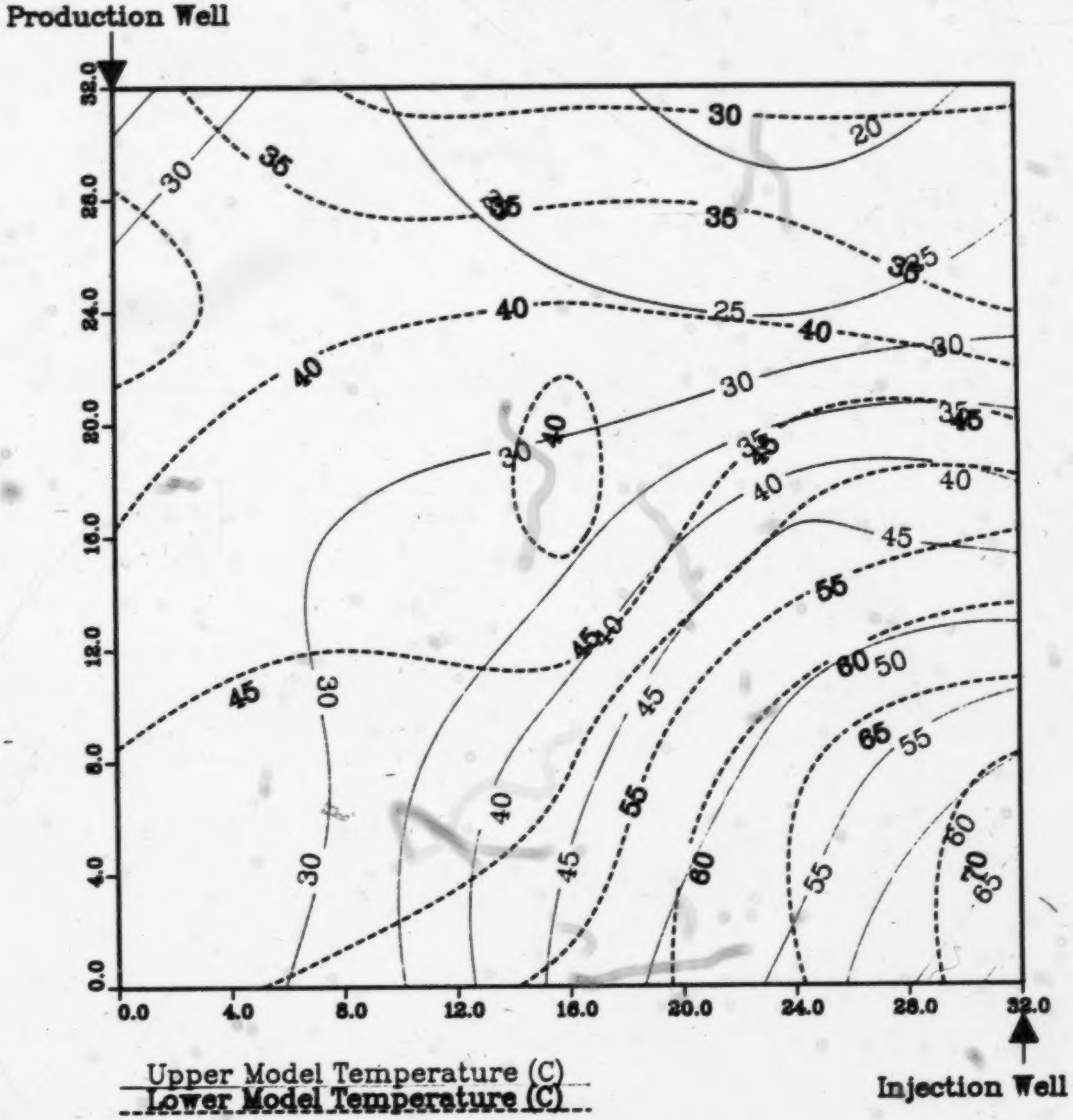

Figure A.91 :Run 65 Temp Profile
Injector to Producer Cross–Section
0.25 Pore Volumes Injected.

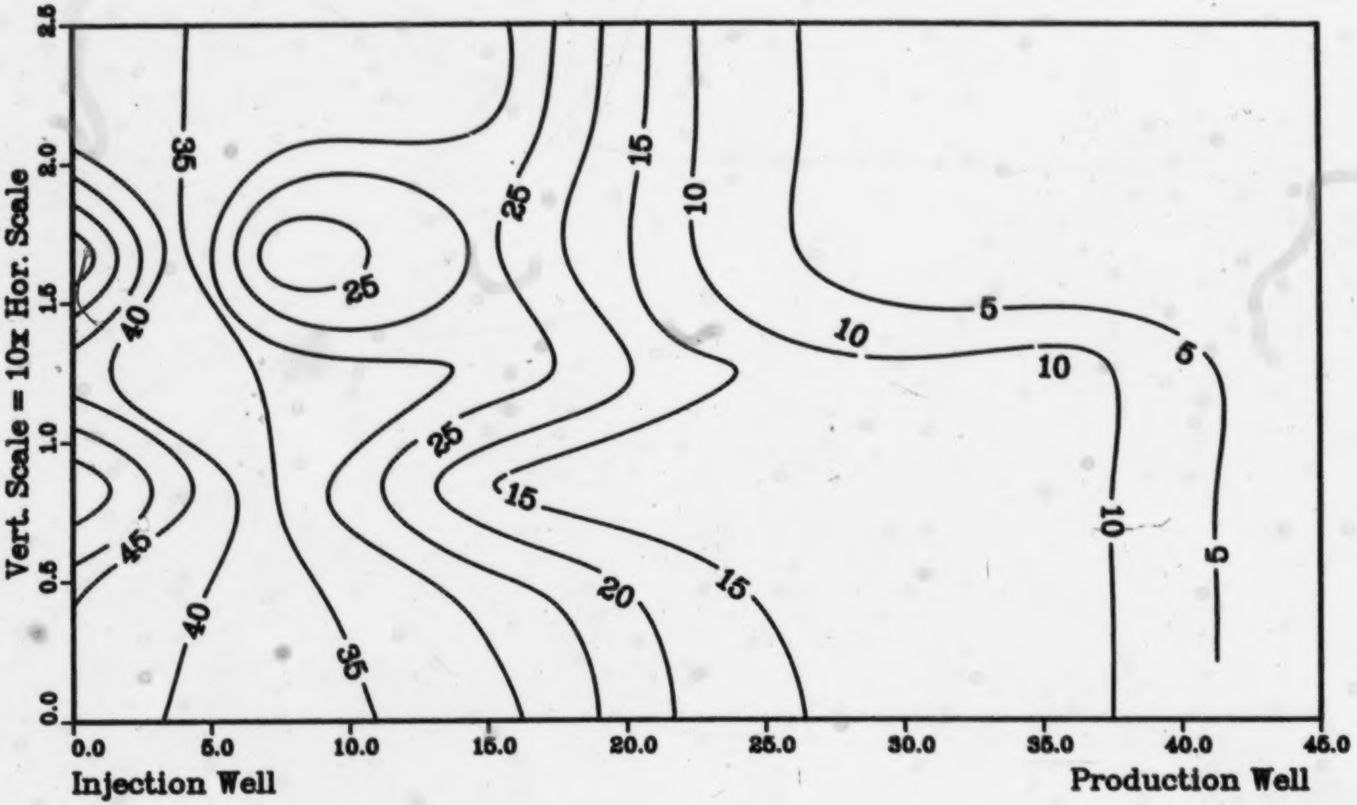

Figure A.92 :Run 65 Temp Profile

Injector to Producer Cross–Section

0.50 Pore Volumes Injected.

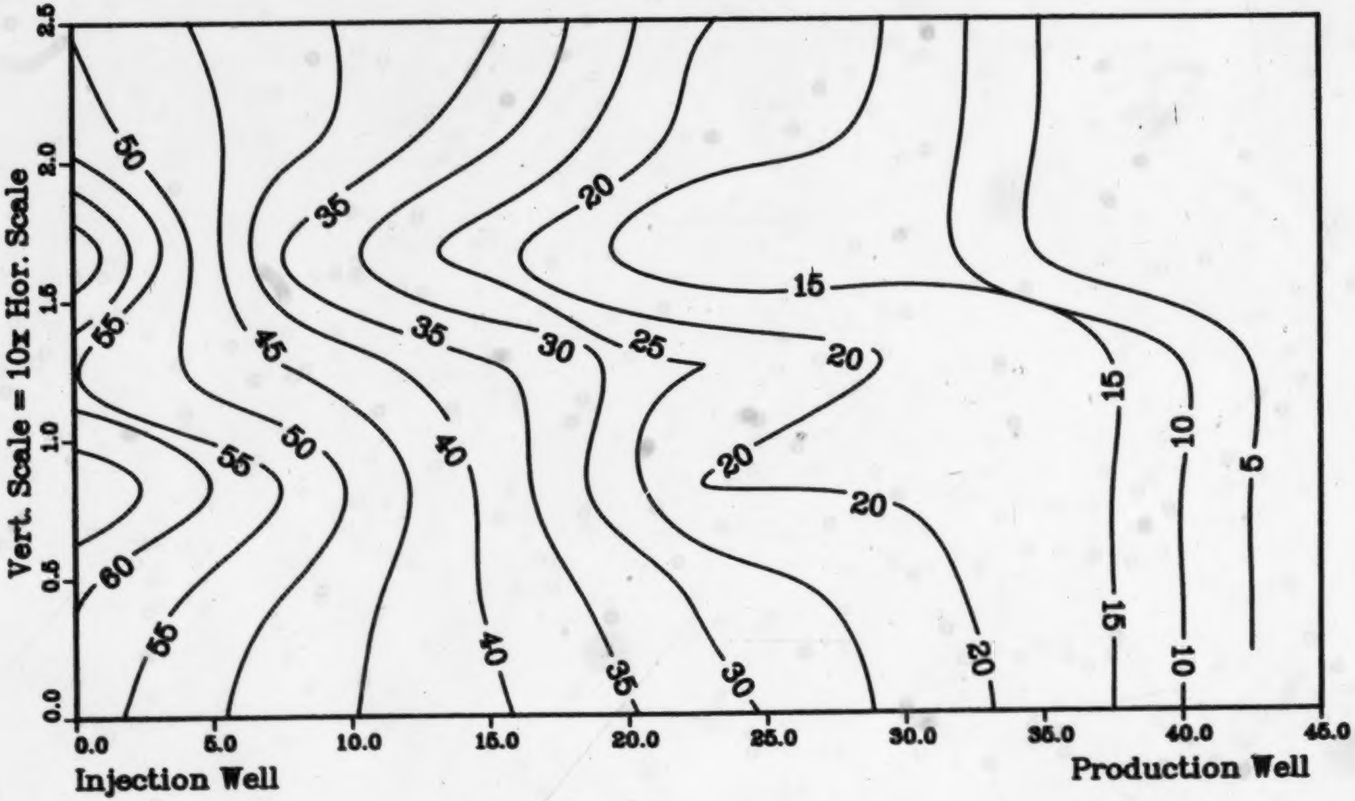

Figure A.93 :Run 65 Temp Profile
Injector to Producer Cross–Section
0.75 Pore Volumes Injected.

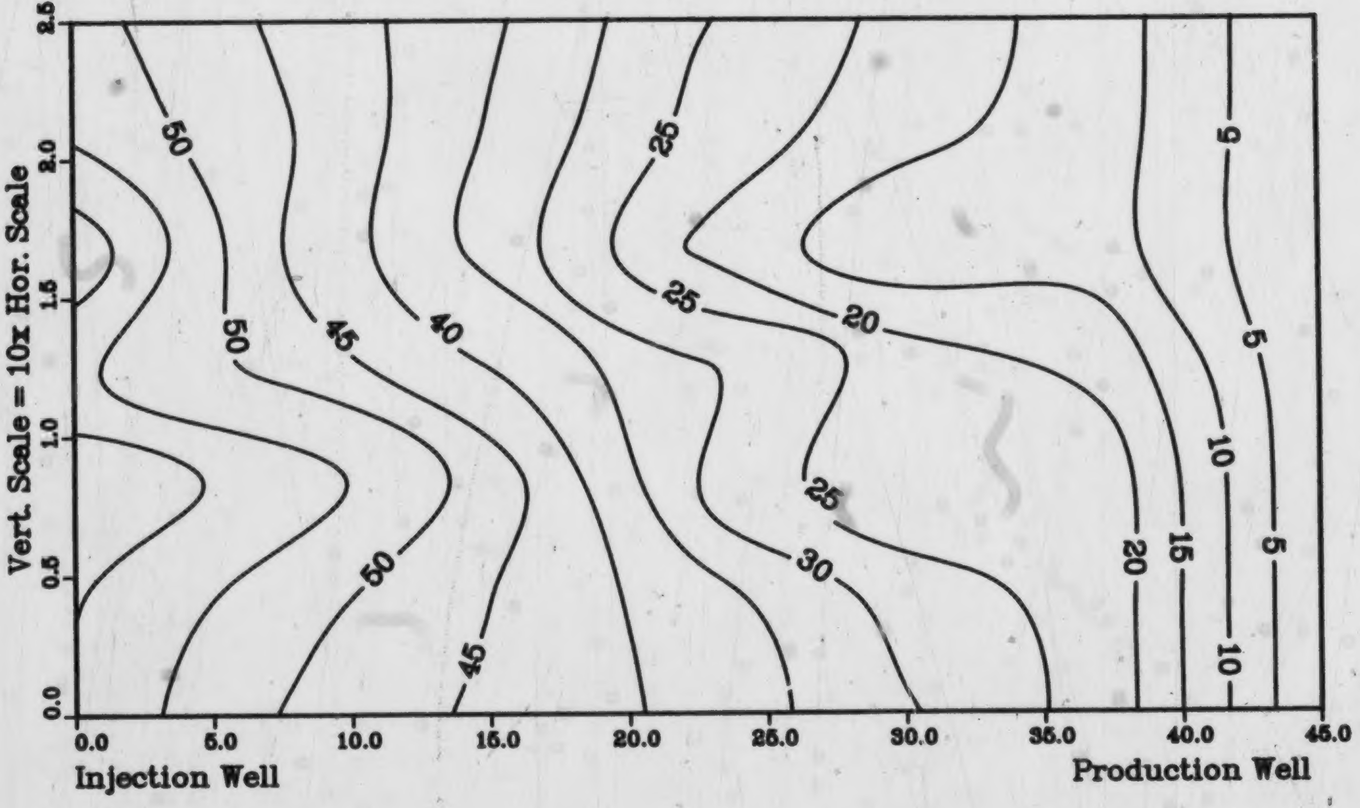

Figure A.94 :Run 65 Temp Profile
Injector to Producer Cross–Section
1.00 Pore Volumes Injected.

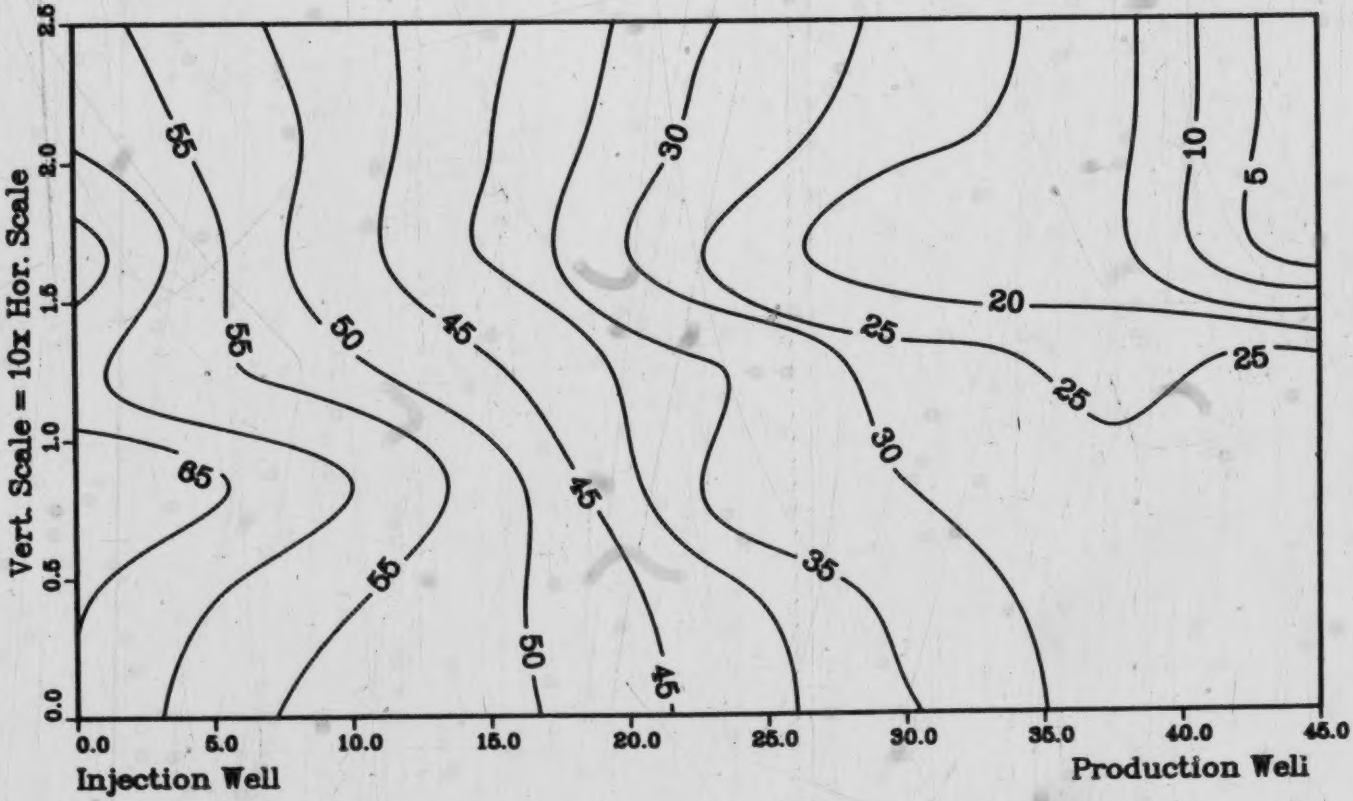

Figure A.95 : Run 66

Solvent–Steamflood in Homo. Model

Temperature Profile for 0.25 Pore Volumes Injected

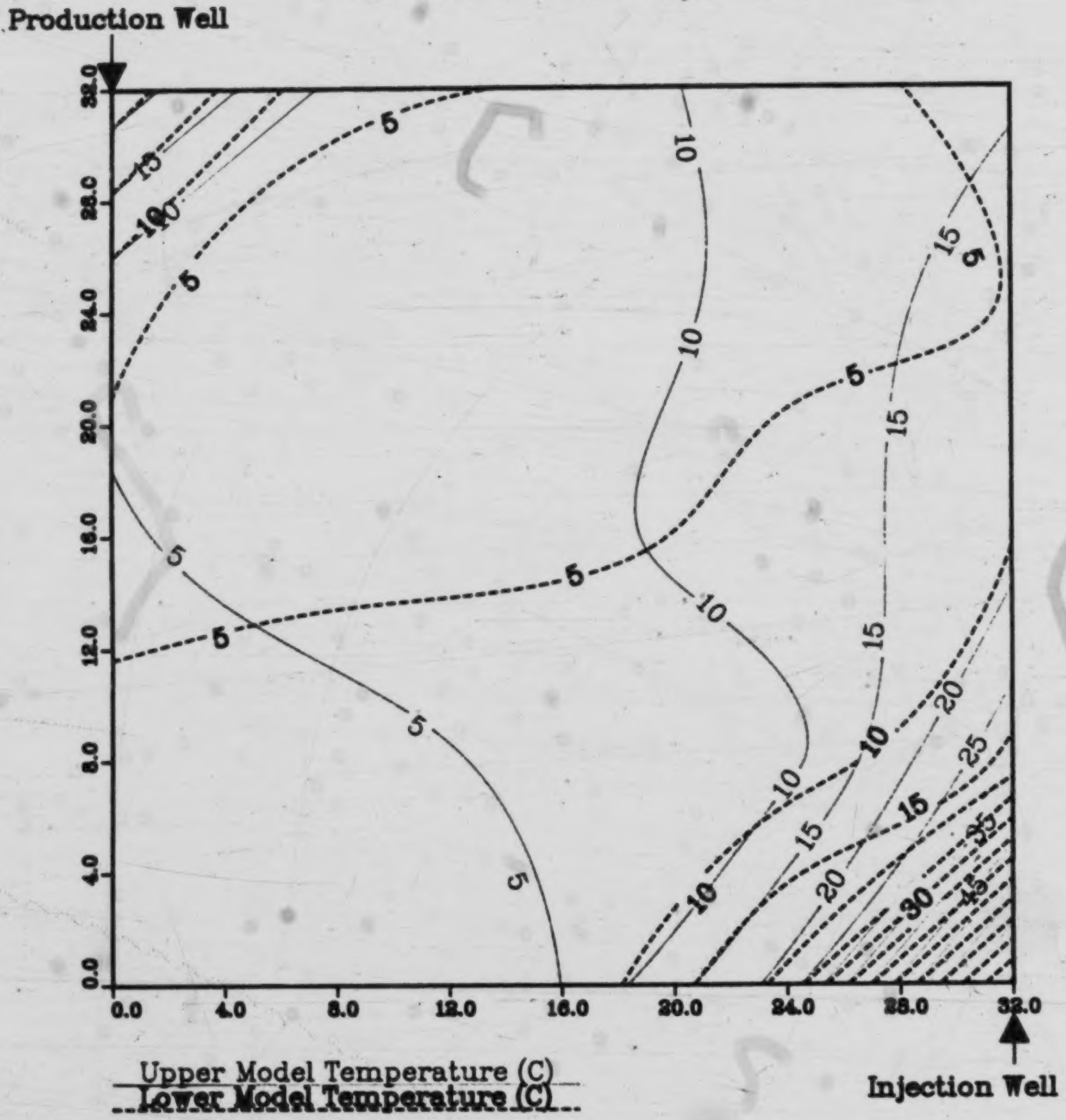

Figure A.96 : Run 66

Solvent–Steamflood in Homo. Model

Temperature Profile for 0.50 Pore Volumes Injected

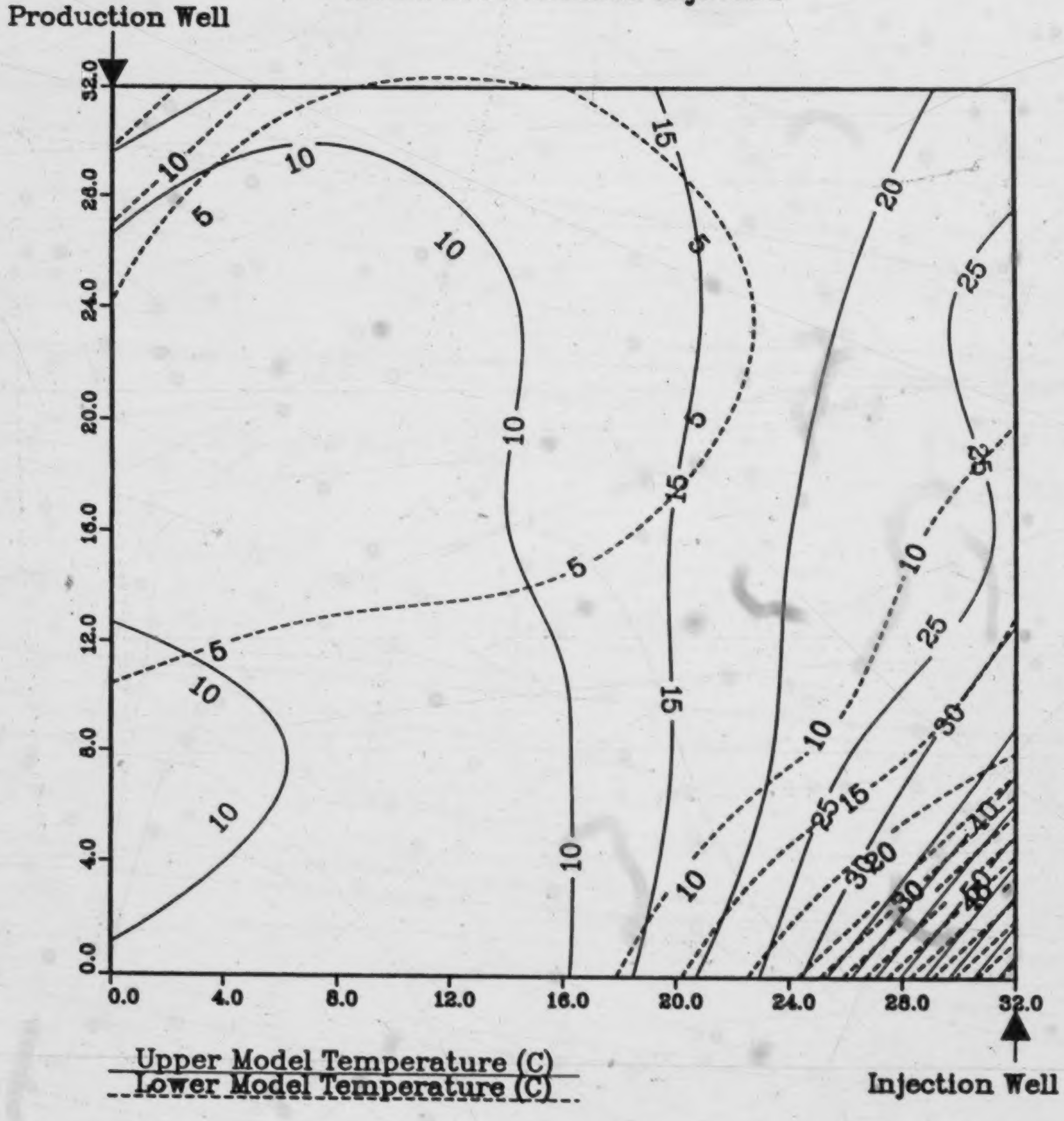

Figure A.97 : Run 66

Solvent–Steamflood in Homo. Model

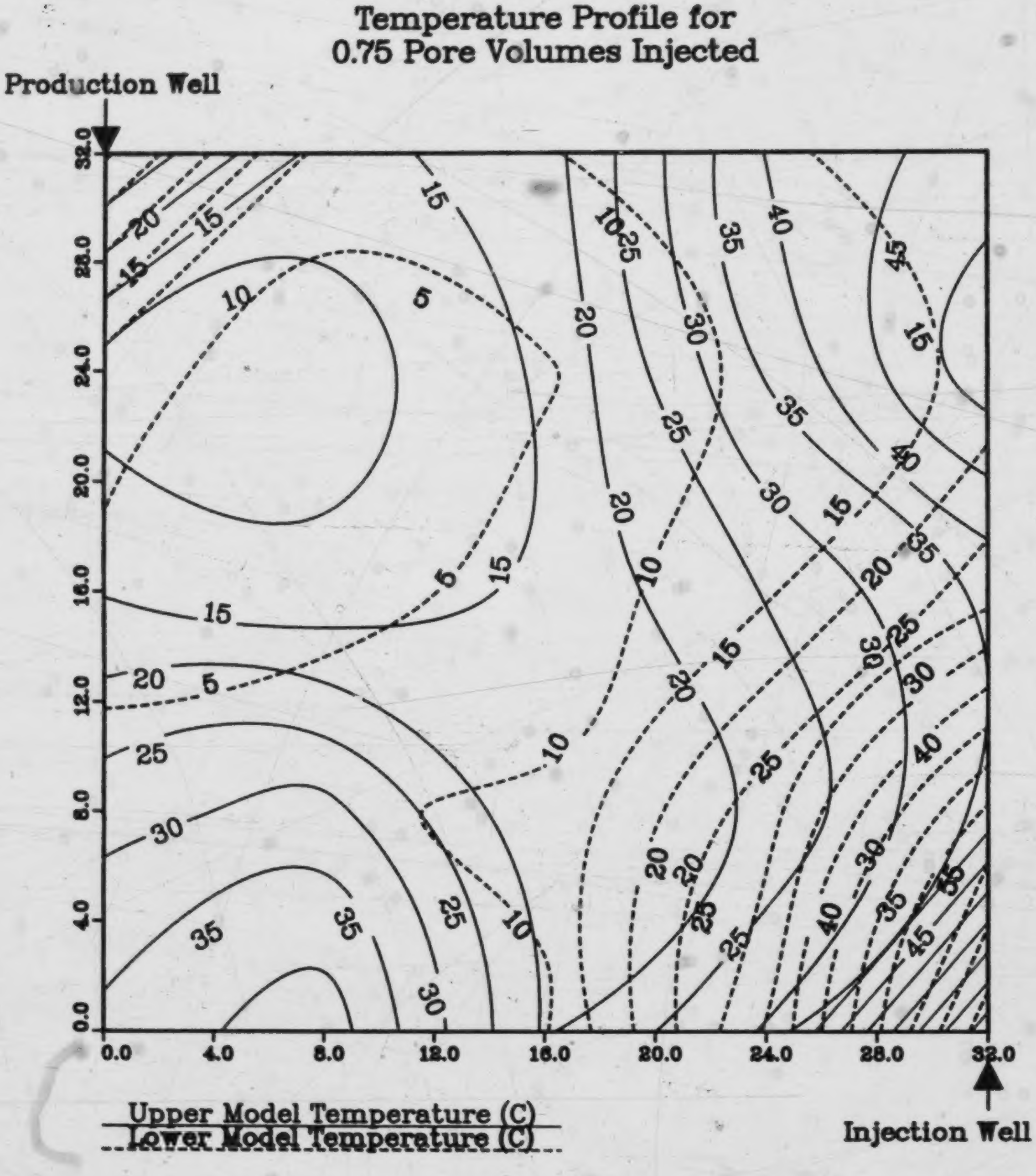

Figure A.98 : Run 66

Solvent–Steamflood in Homo. Model

Temperature Profile for 1.00 Pore Volumes Injected

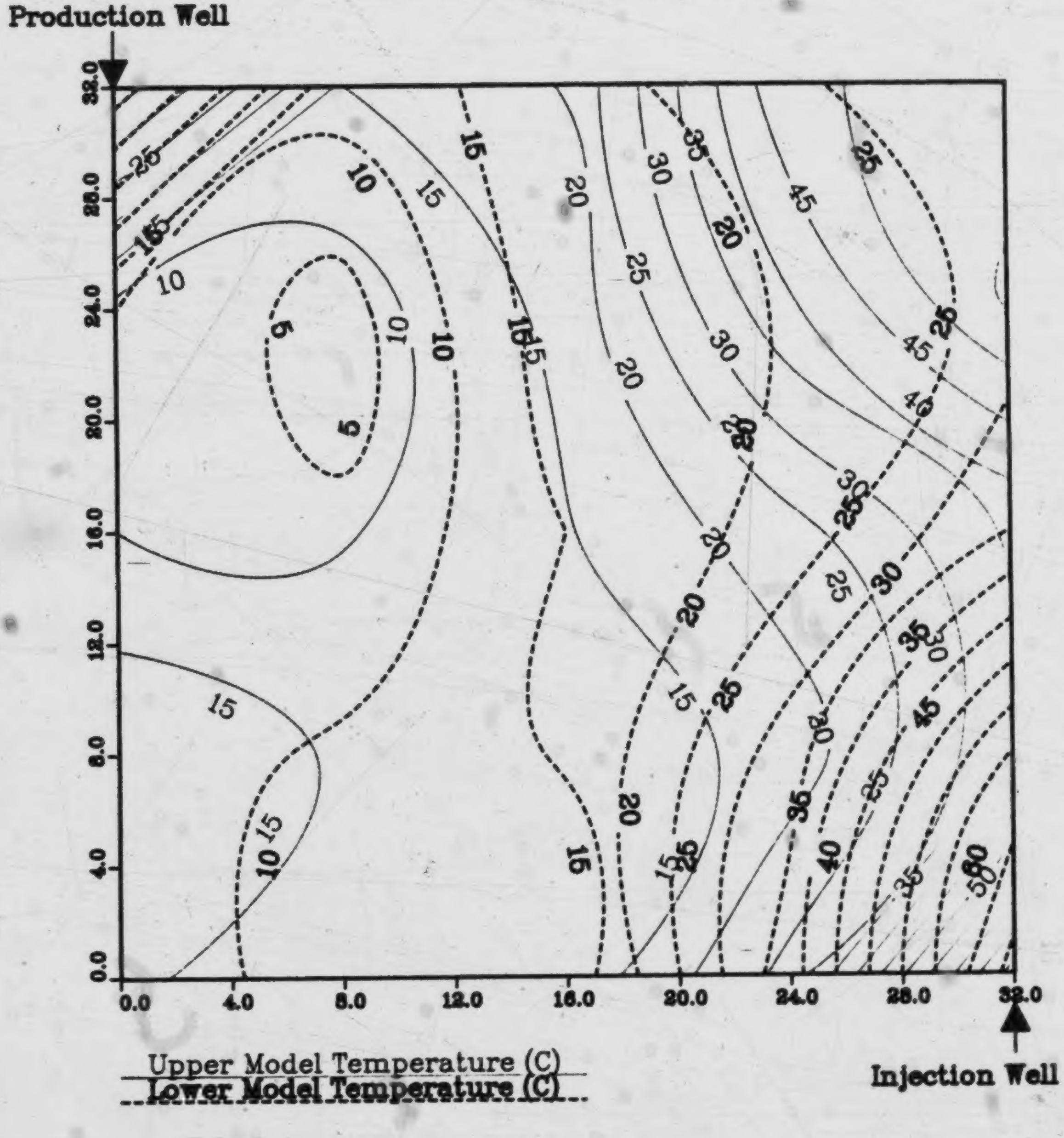

Figure A.99 : Run 66
Solvent–Steamflood in Homo. Model

Temperature Profile for 1.25 Pore Volumes Injected

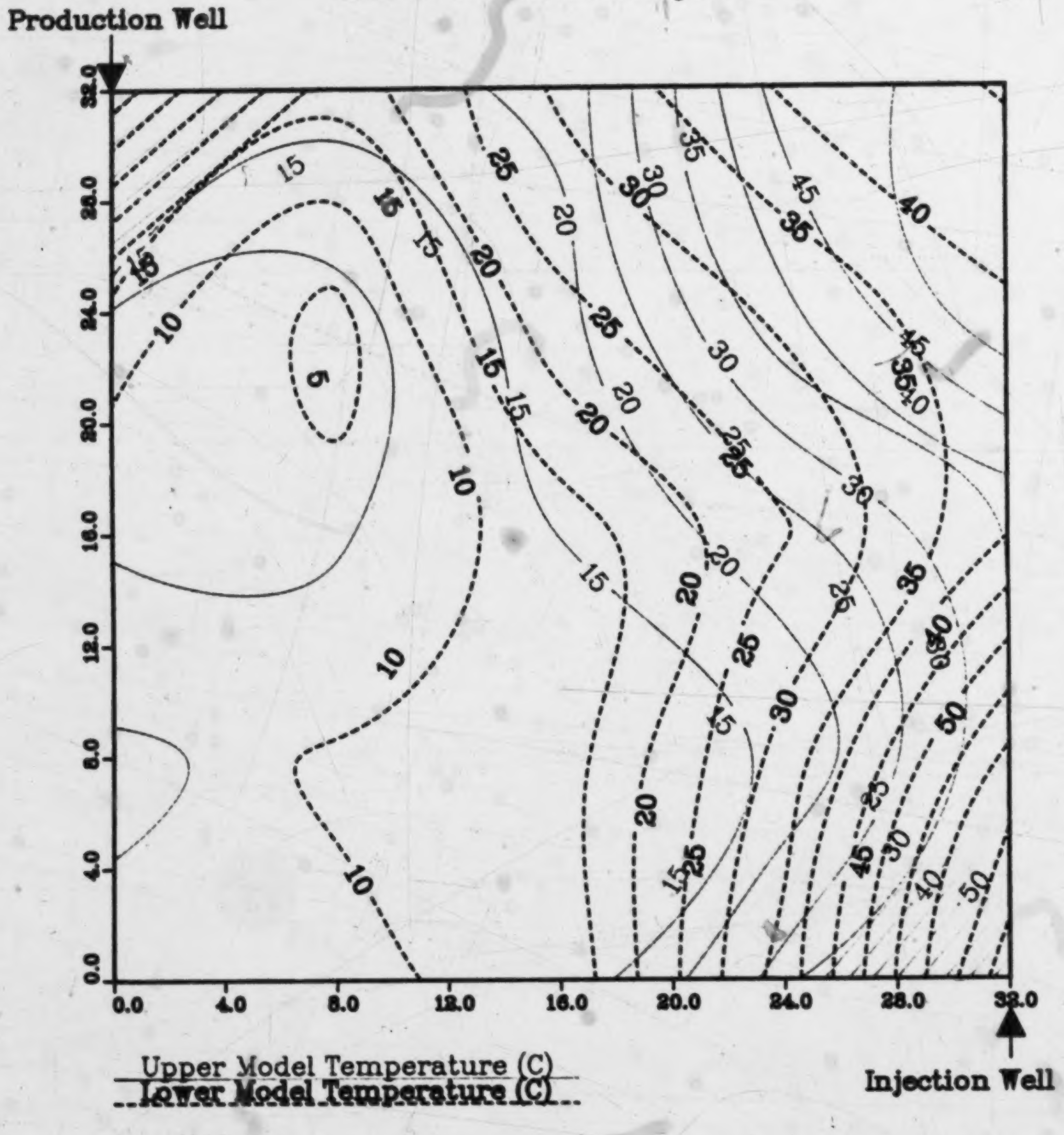

Figure A.100 : Run 66
Solvent–Steamflood in Homo. Model

Temperature Profile for
1.50 Pore Volumes Injected

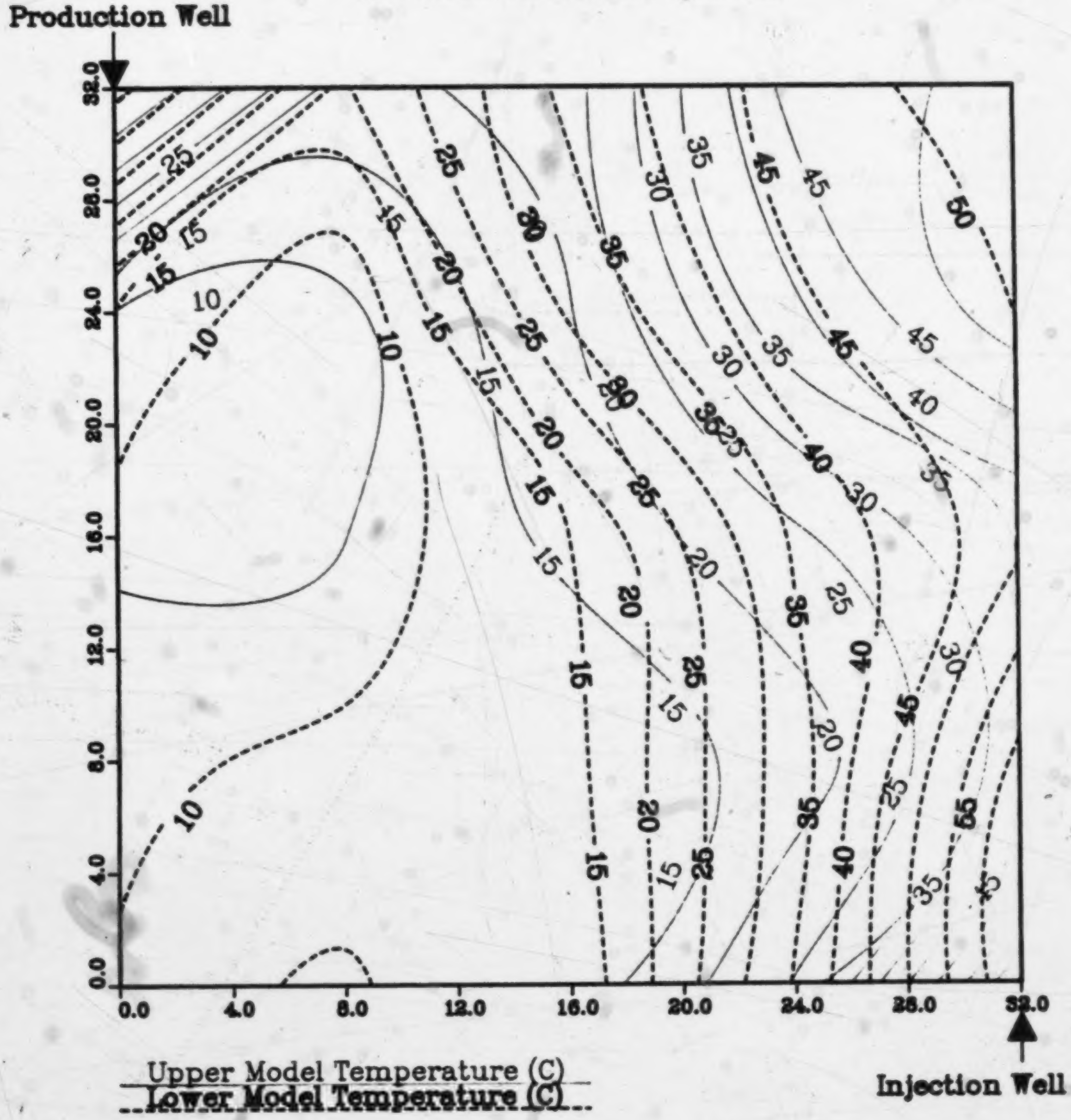

Figure A.101 : Run 66

Solvent–Steamflood in Homo. Model

Temperature Profile for 1.75 Pore Volumes Injected

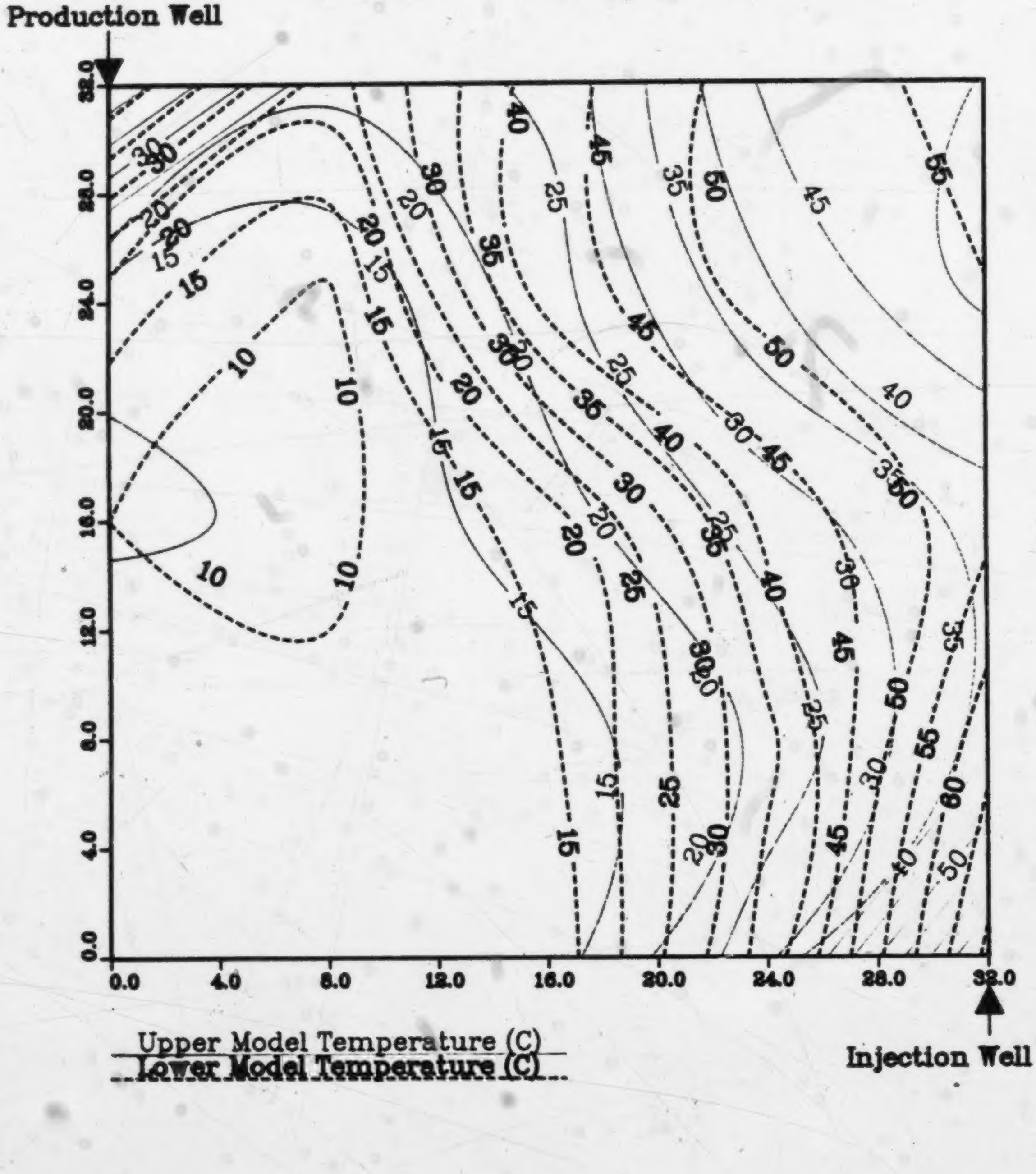

Figure A.102 : Run 66

Solvent–Steamflood in Homo. Model

Temperature Profile for 2.00 Pore Volumes Injected

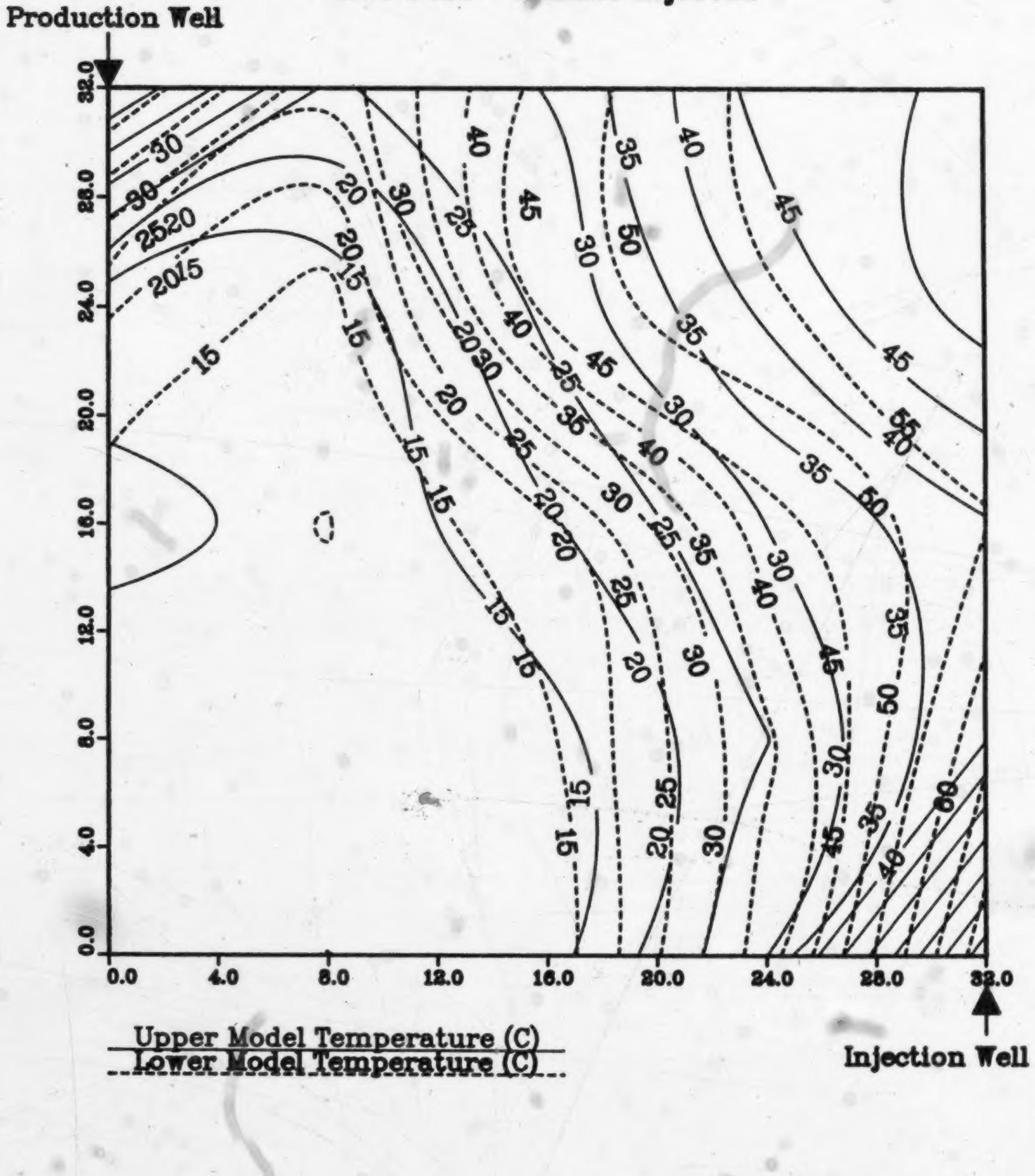

Figure A.103 :Run 66 Temp Profile
Injector to Producer Cross–Section
0.25 Pore Volumes Injected.

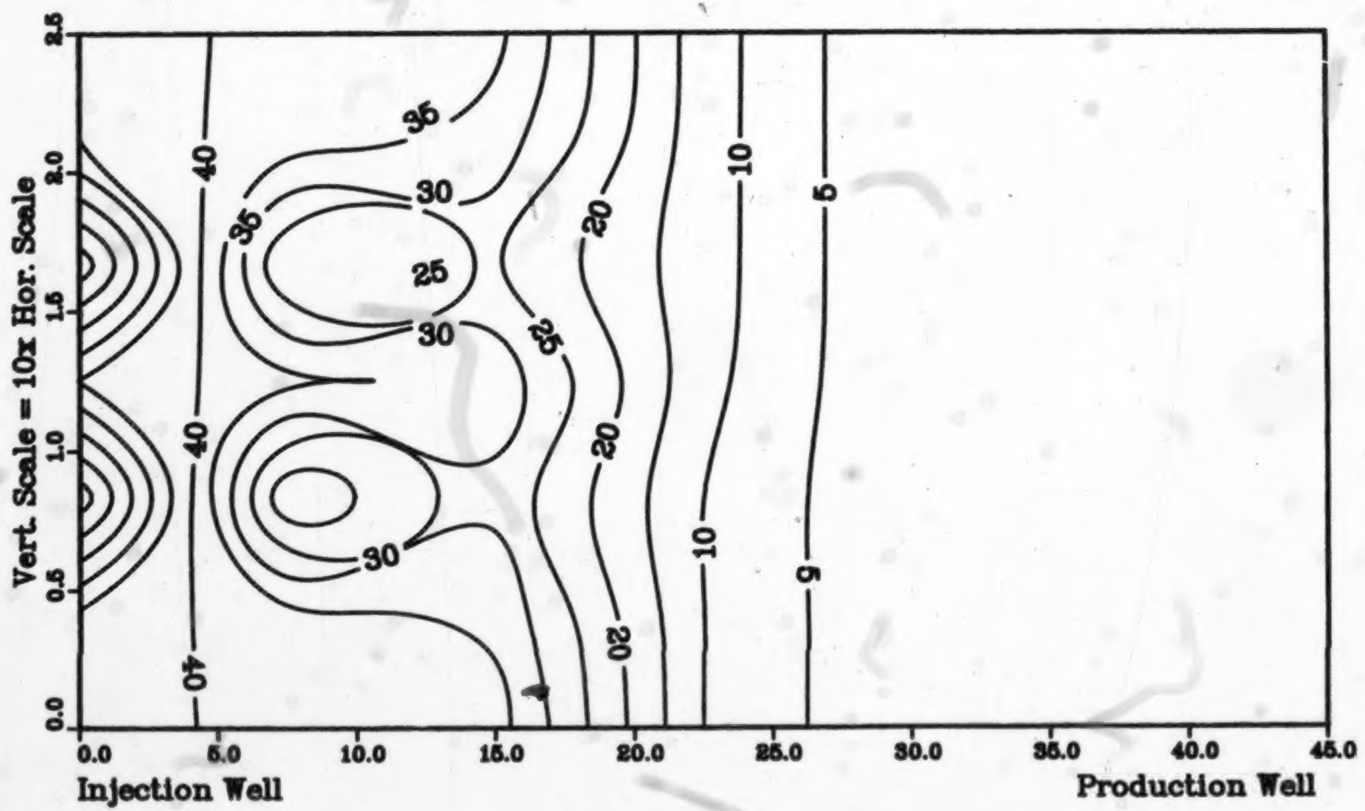

Figure A.104 :Run 66 Temp Profile
Injector to Producer Cross-Section
0.50 Pore Volumes Injected.

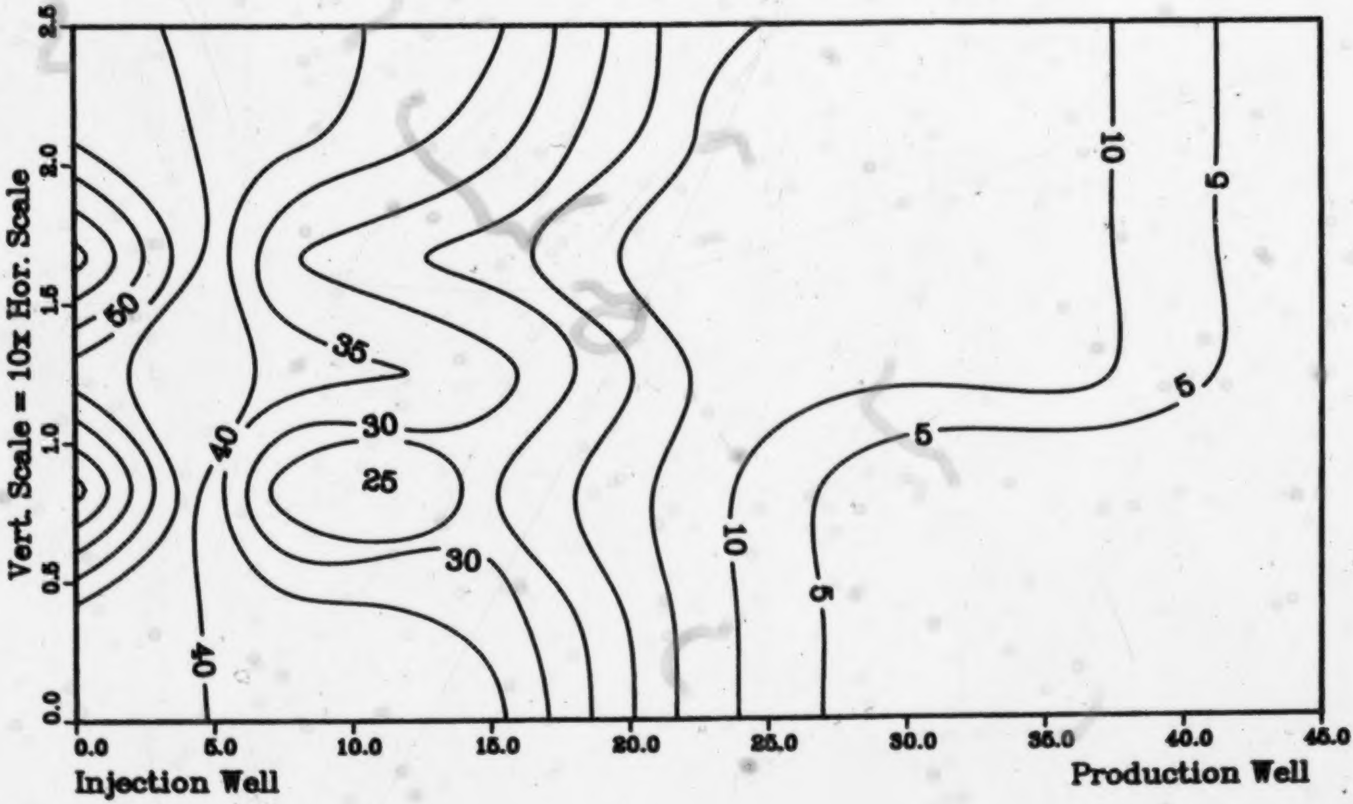

Figure A.105 :Run 66 Temp Profile
Injector to Producer Cross–Section
0.75 Pore Volumes Injected.

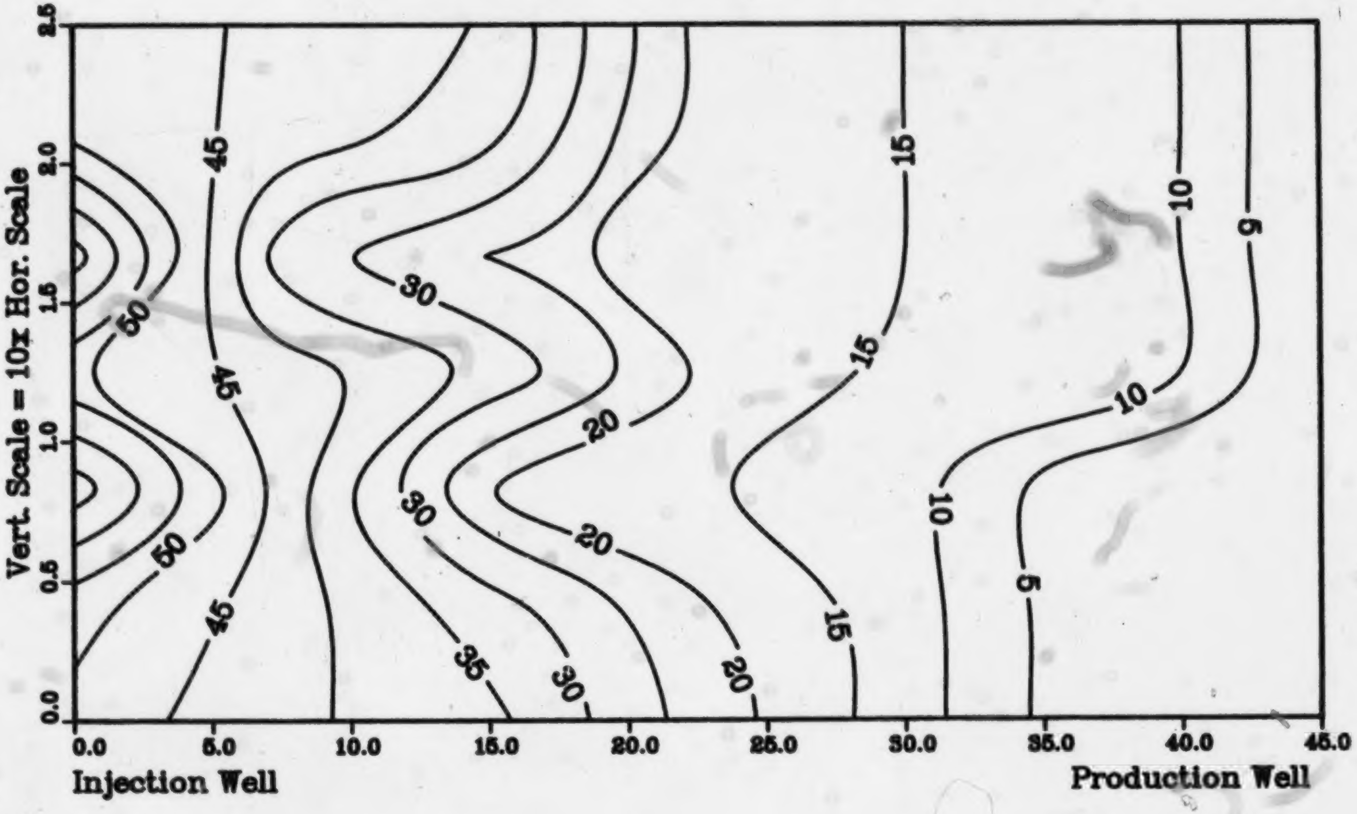

Figure A.106 :Run 66 Temp Profile
Injector to Producer Cross–Section
1.00 Pore Volumes Injected.

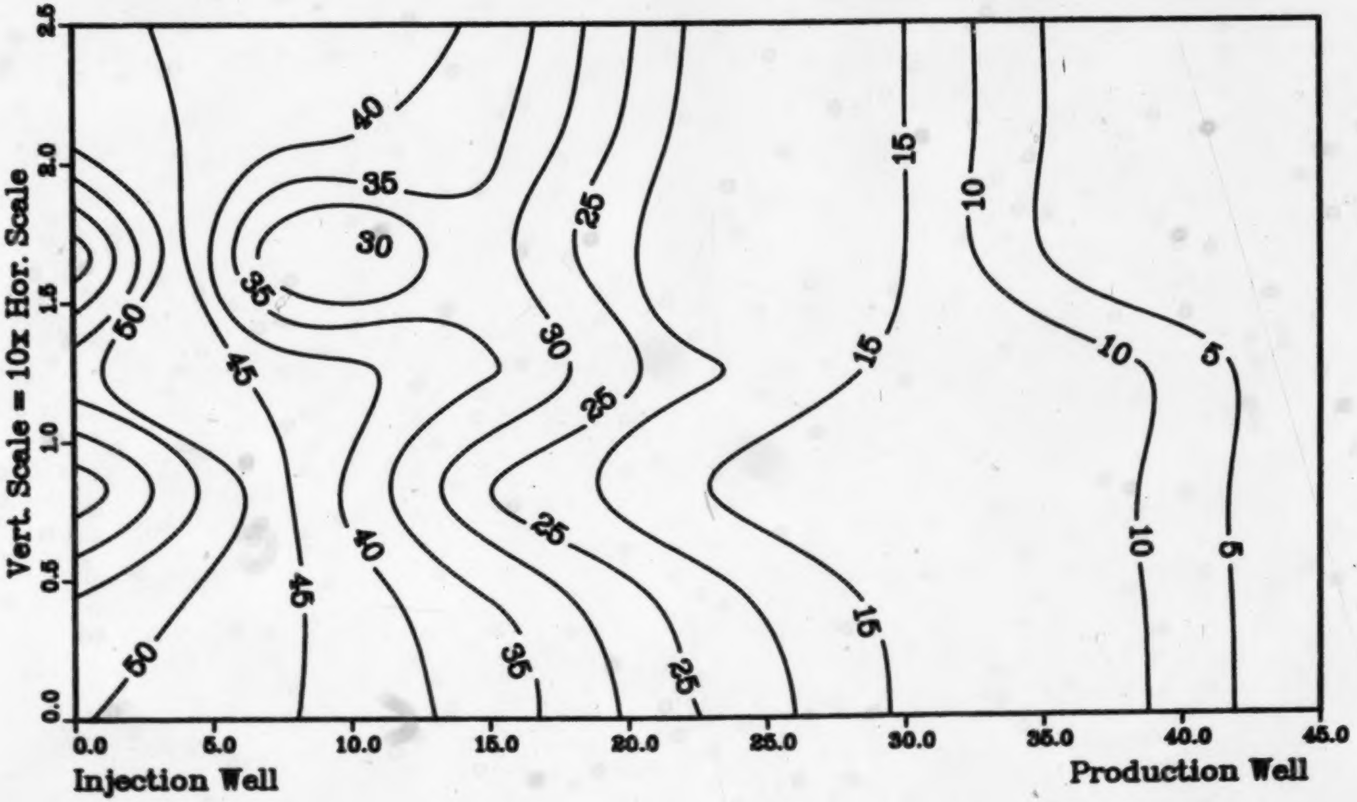

Figure A.107 : Run 67
Solvent–Steamflood in Homo. Model

Temperature Profile for 0.25 Pore Volumes Injected

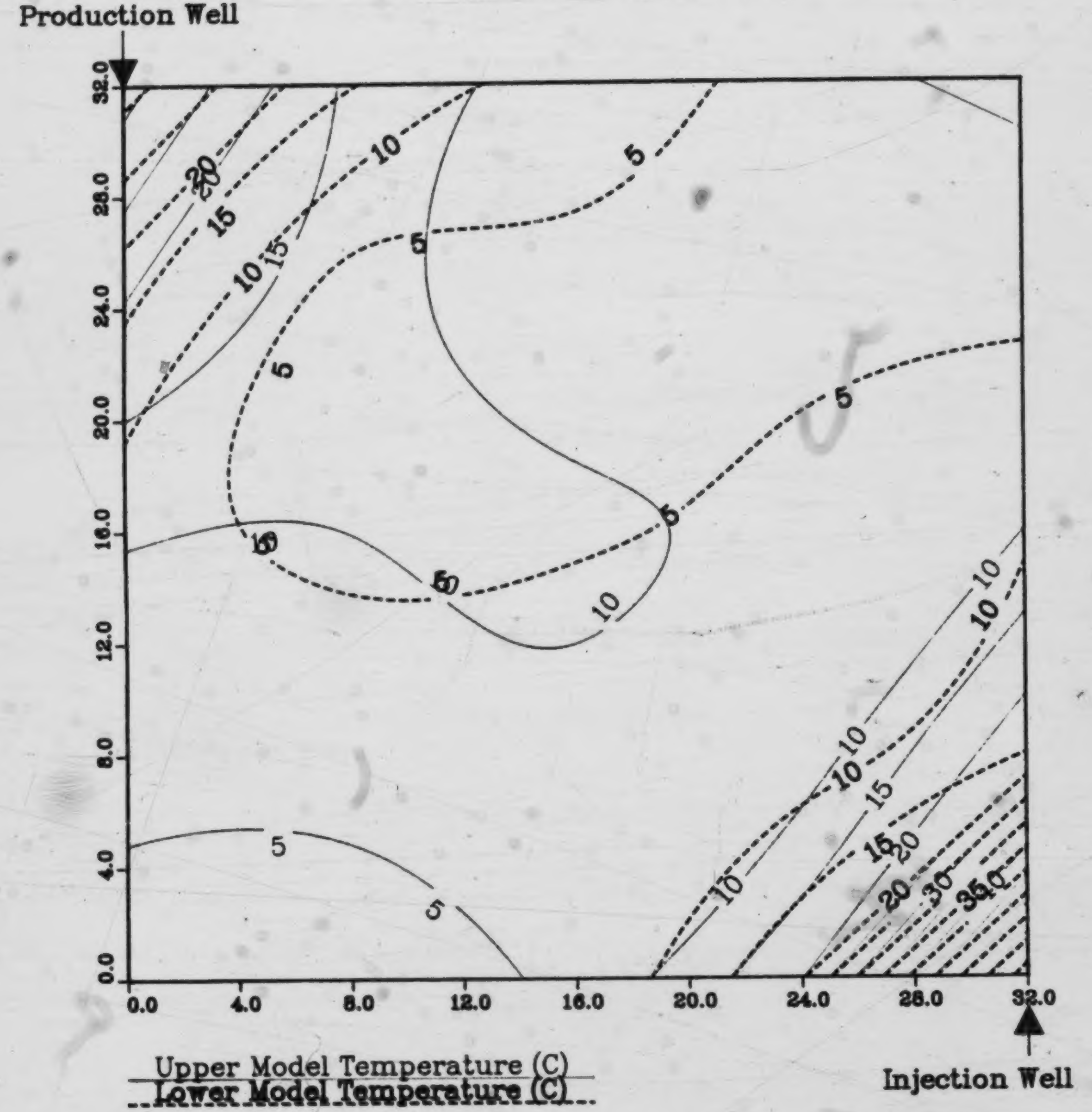

Figure A.108 : Run 67

Solvent–Steamflood in Homo. Model

Temperature Profile for
0.50 Pore Volumes Injected

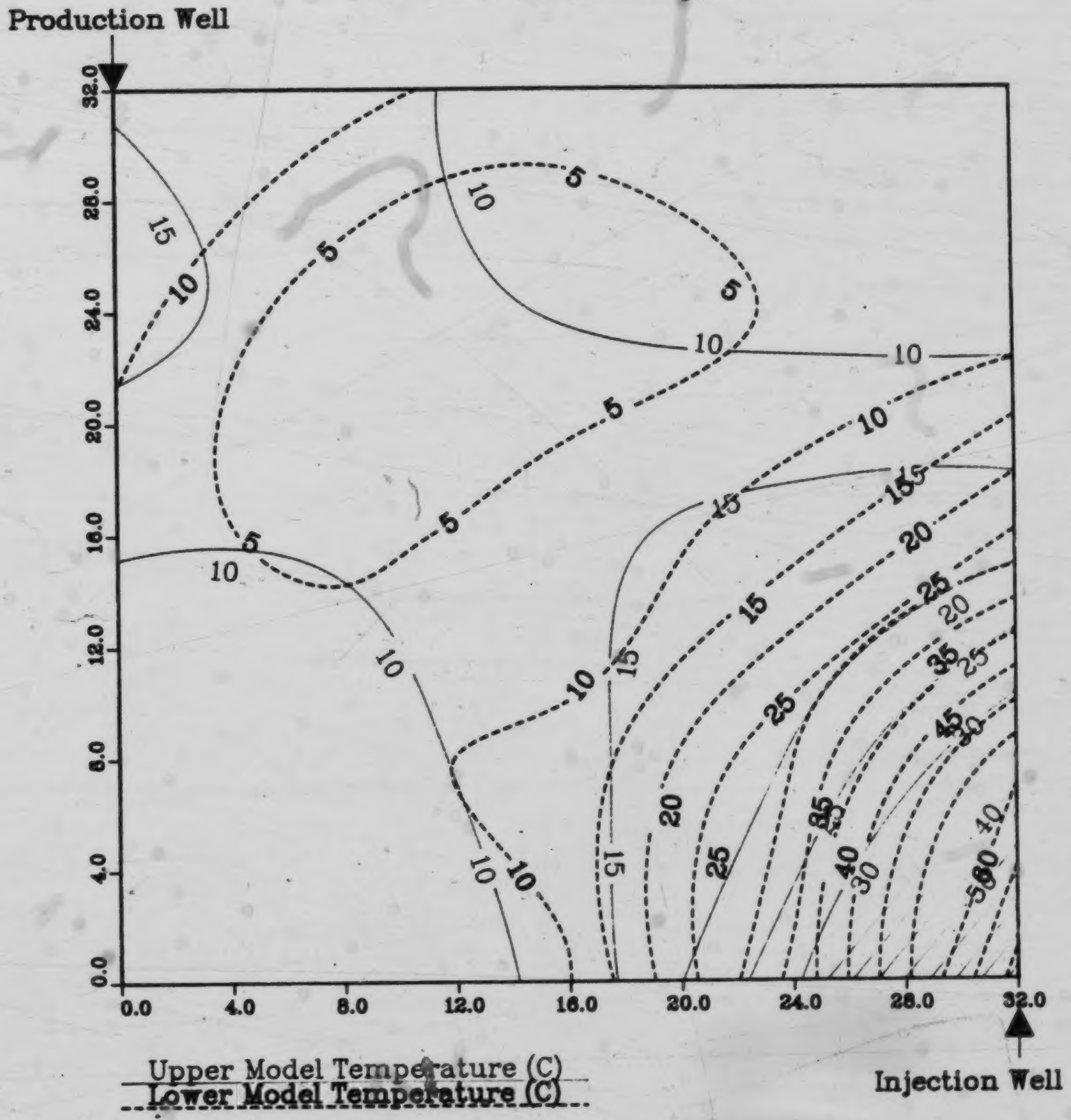

Figure A.109 : Run 67

Solvent–Steamflood in Homo. Model

Temperature Profile for 0.75 Pore Volumes Injected

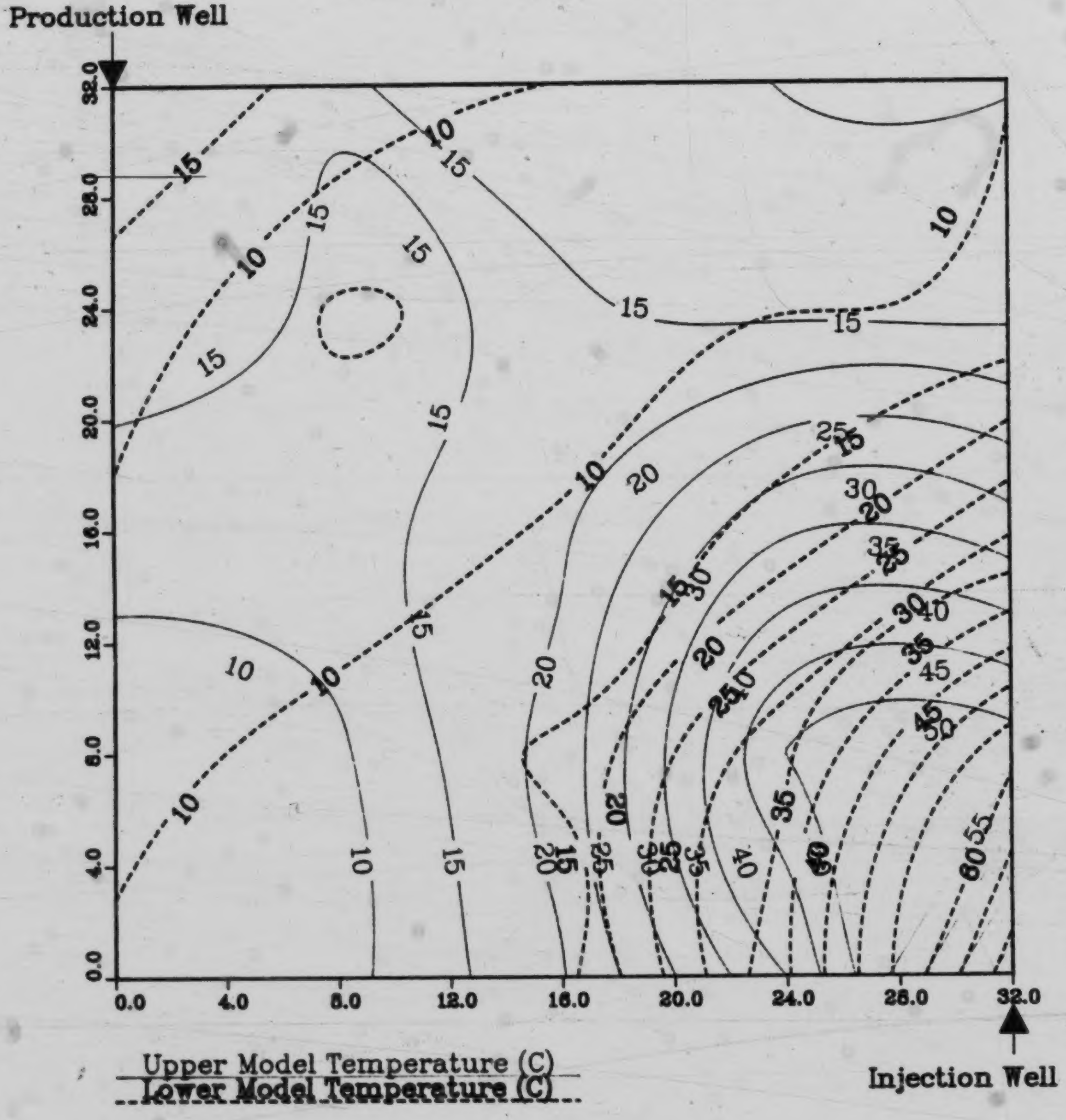

Figure A.110 : Run 67

Solvent–Steamflood in Homo. Model

Temperature Profile for
1.00 Pore Volumes Injected

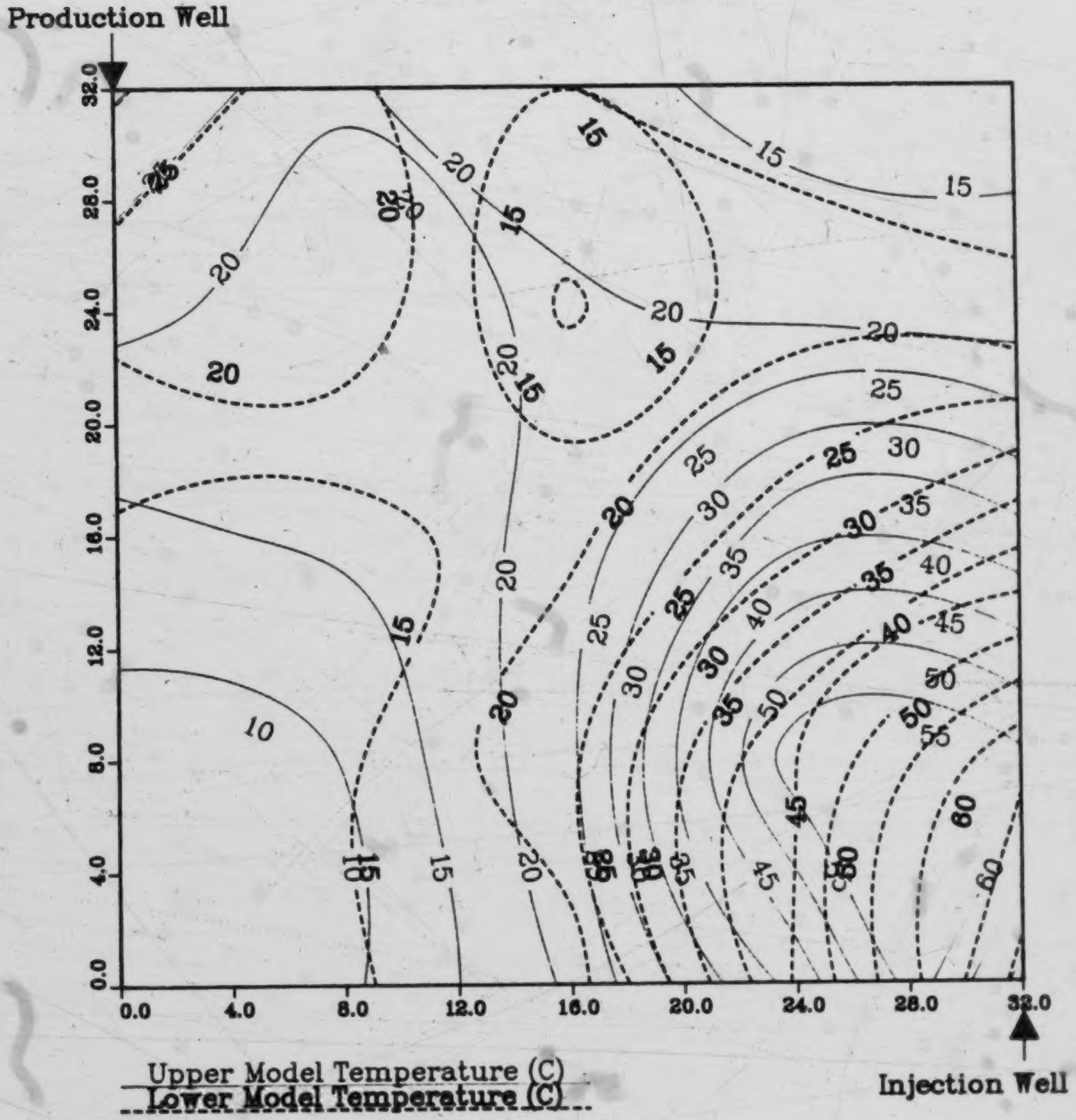

Figure A.111 : Run 67

Solvent–Steamflood in Homo. Model

Temperature Profile for 1.25 Pore Volumes Injected

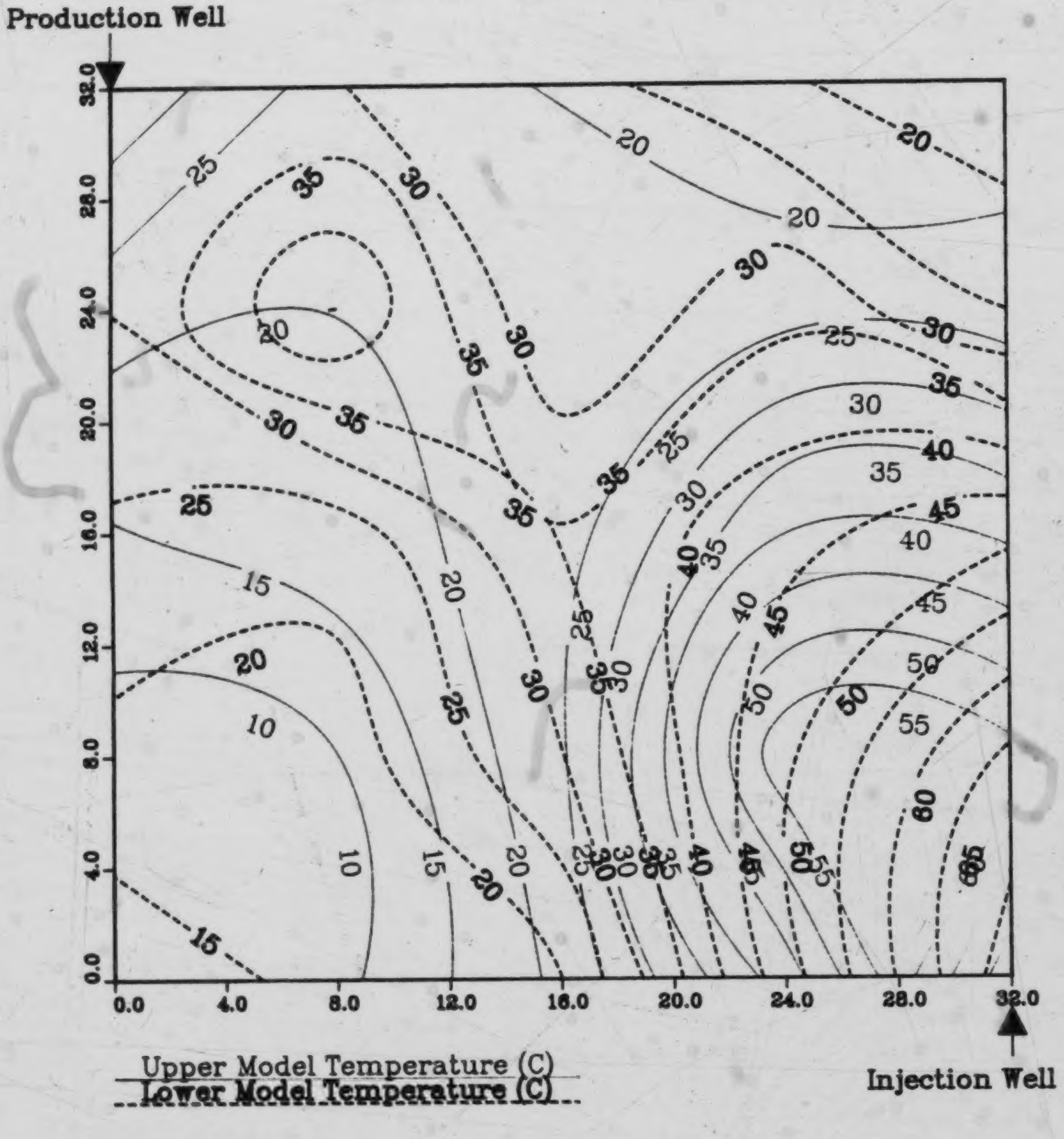

Figure A.112 : Run 67
Solvent–Steamflood in Homo. Model

Temperature Profile for
1.50 Pore Volumes Injected

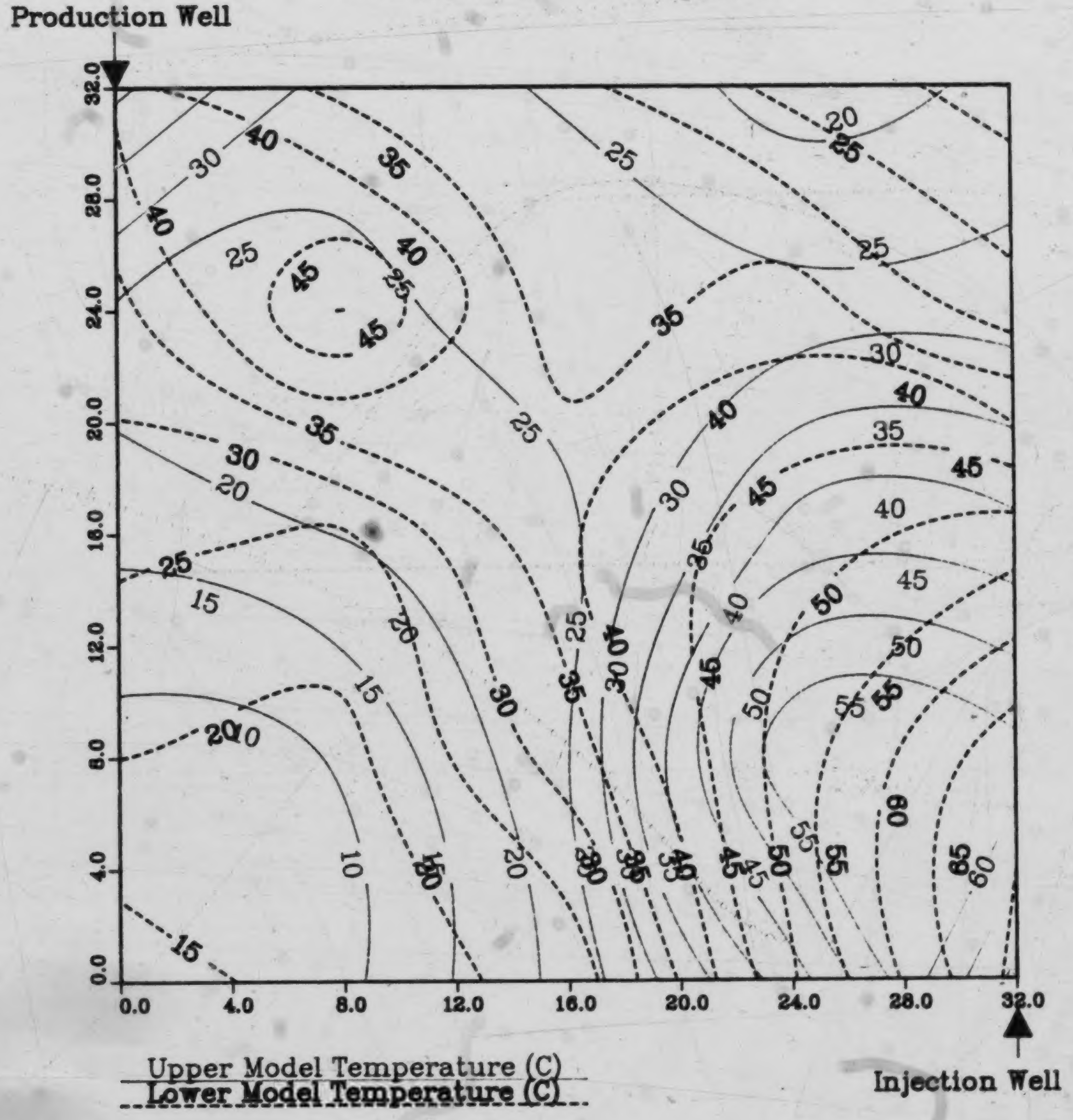

Figure A.113 : Run 67
Solvent–Steamflood in Homo. Model

Temperature Profile for
1.75 Pore Volumes Injected

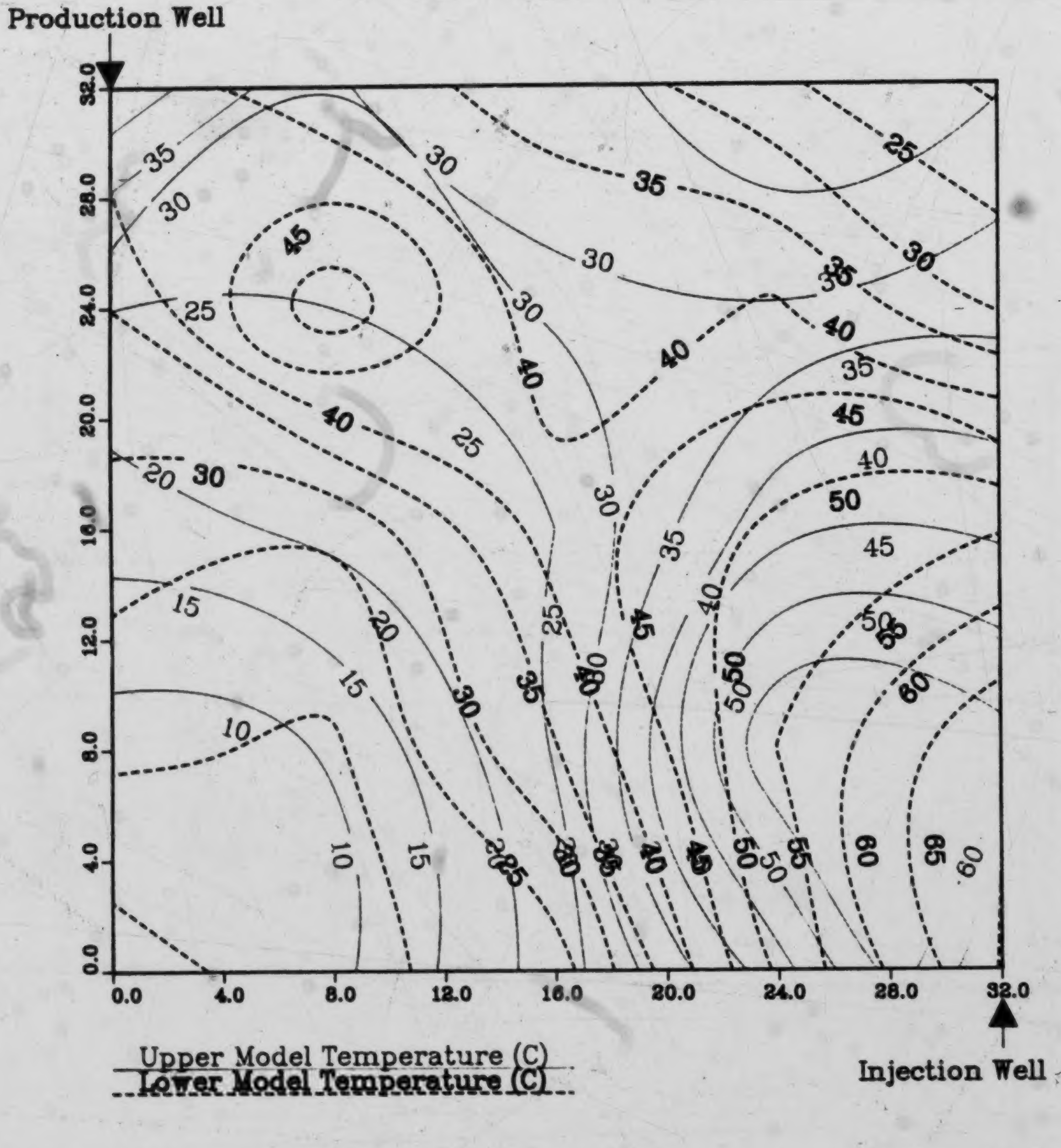

Figure A.114 : Run 67

Solvent--Steamflood in Homo. Model

Temperature Profile for
2.00 Pore Volumes Injected

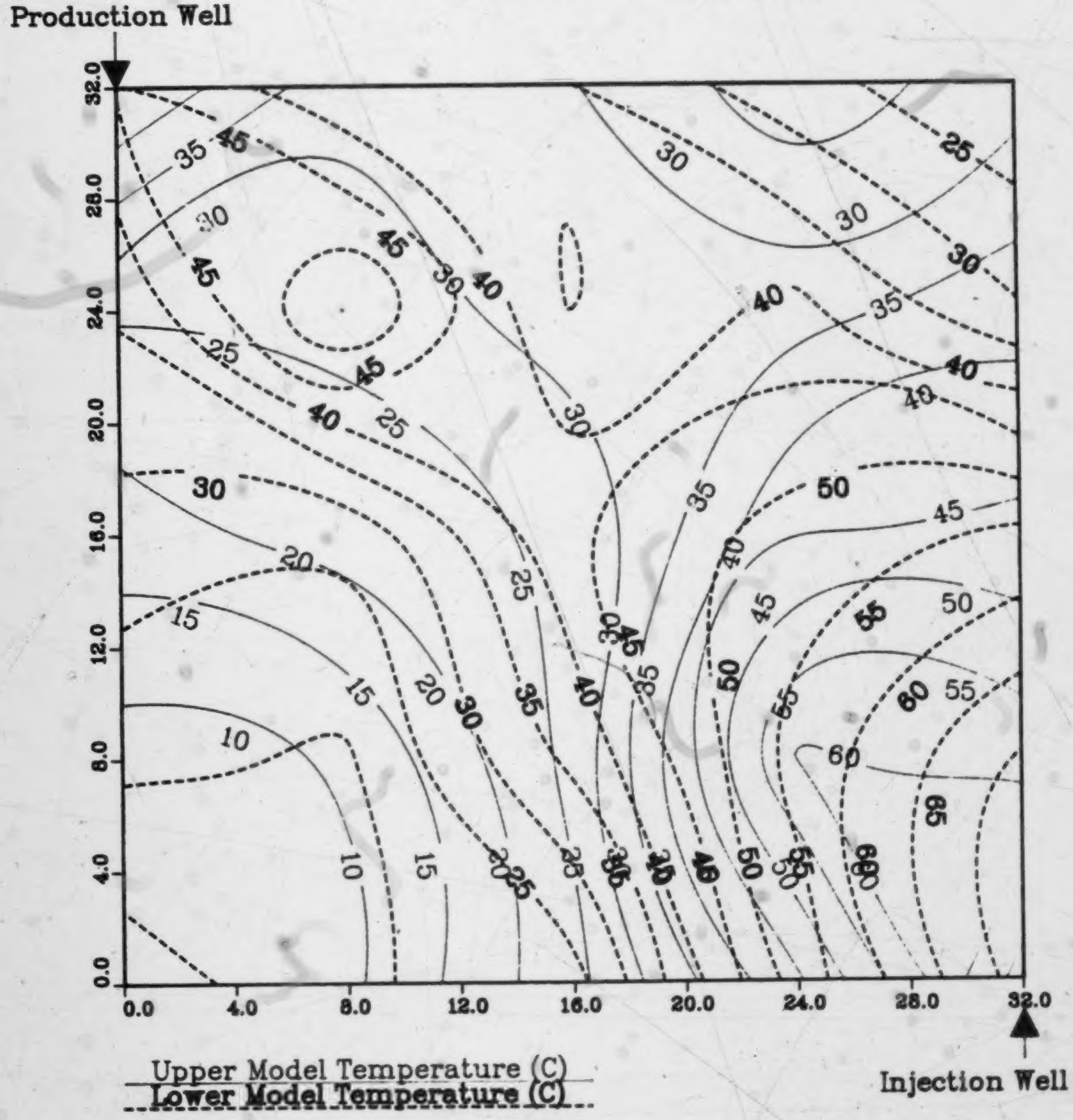

Figure A.115 :Run 67 Temp Profile
Injector to Producer Cross–Section
0.25 Pore Volumes Injected.

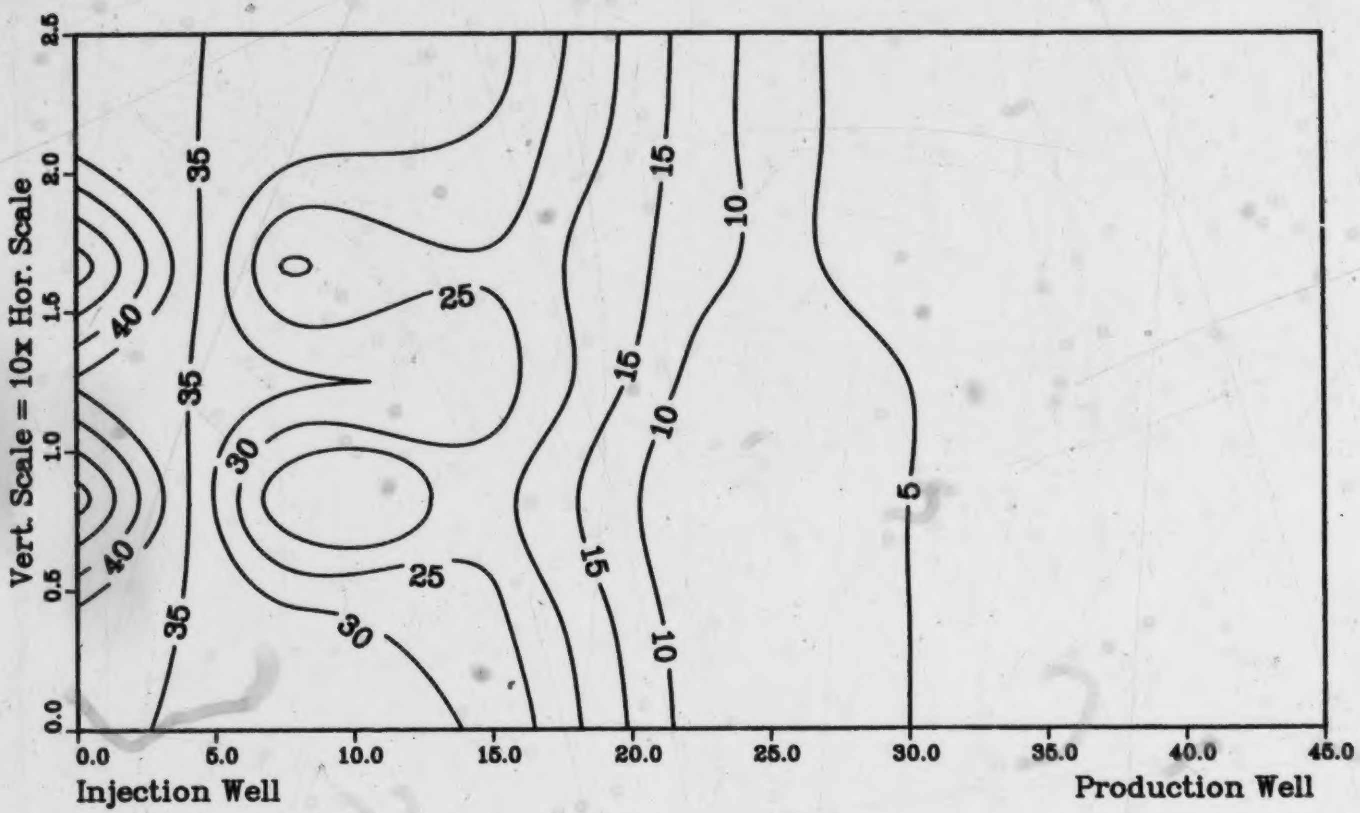

Figure A.116 :Run 67 Temp Profile
Injector to Producer Cross–Section
0.50 Pore Volumes Injected.

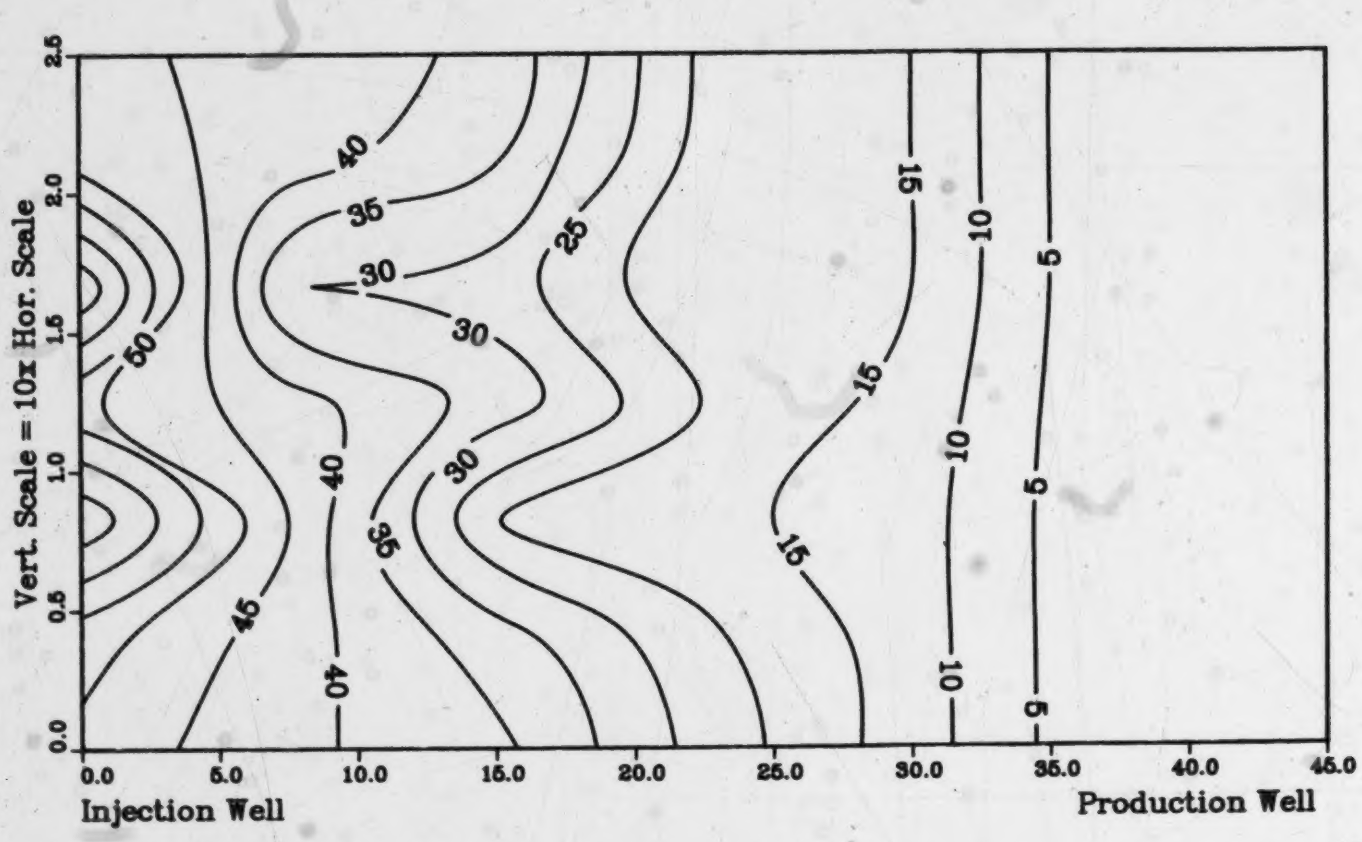

Figure A.117 :Run 67 Temp Profile
Injector to Producer Cross–Section
0.75 Pore Volumes Injected.

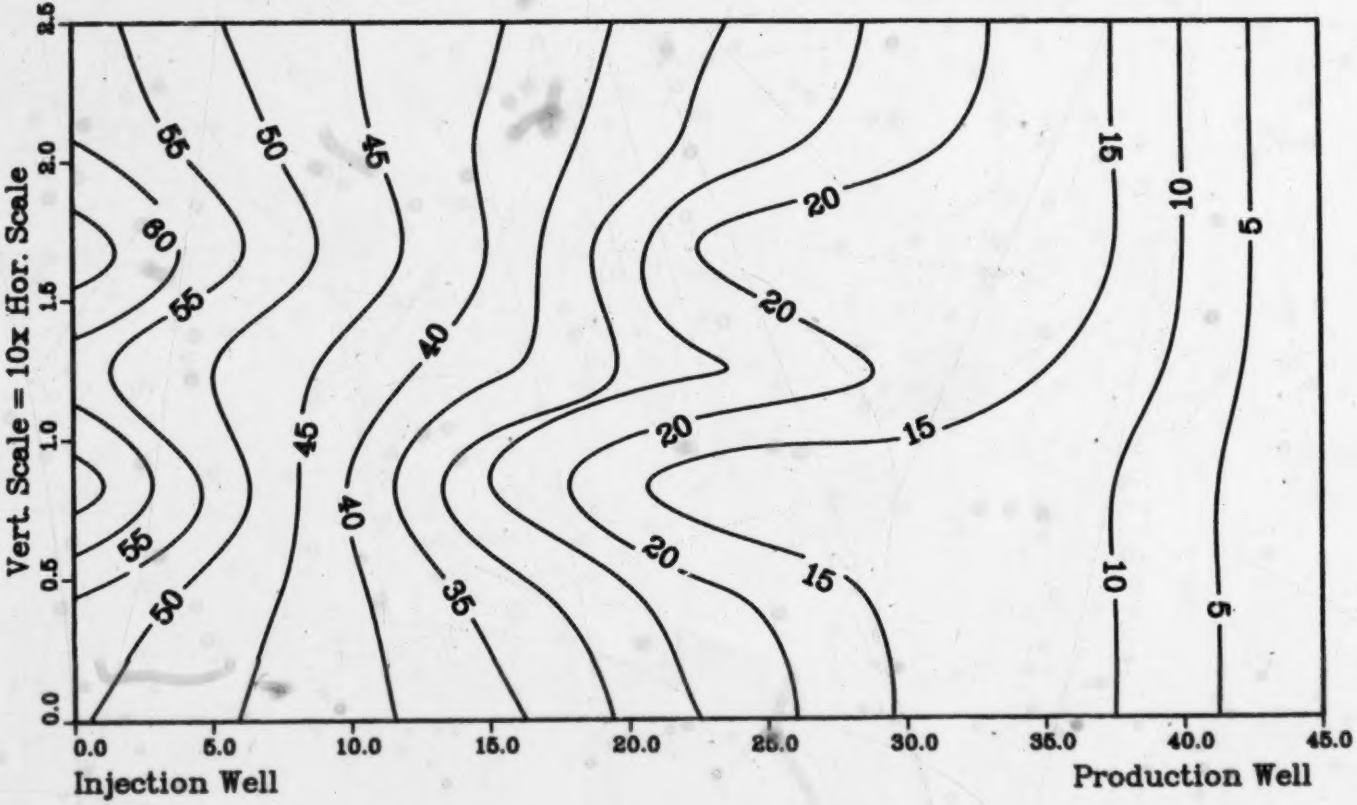

Figure A.118 :Run 67 Temp Profile
Injector to Producer Cross–Section
1.00 Pore Volumes Injected.

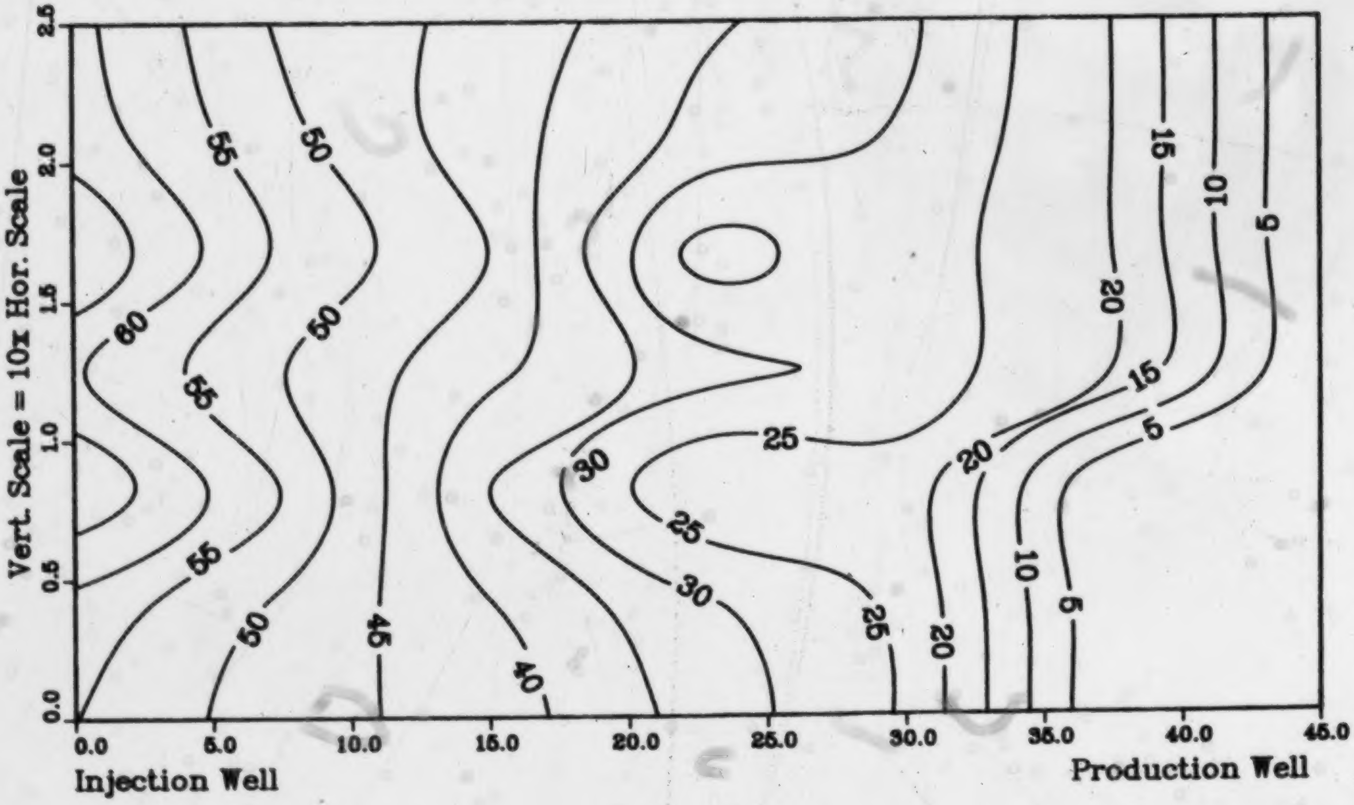

Figure A.119 : Run 49
Solvent–Steamflood in B.W. Model

Temperature Profile for 0.25 Pore Volumes Injected

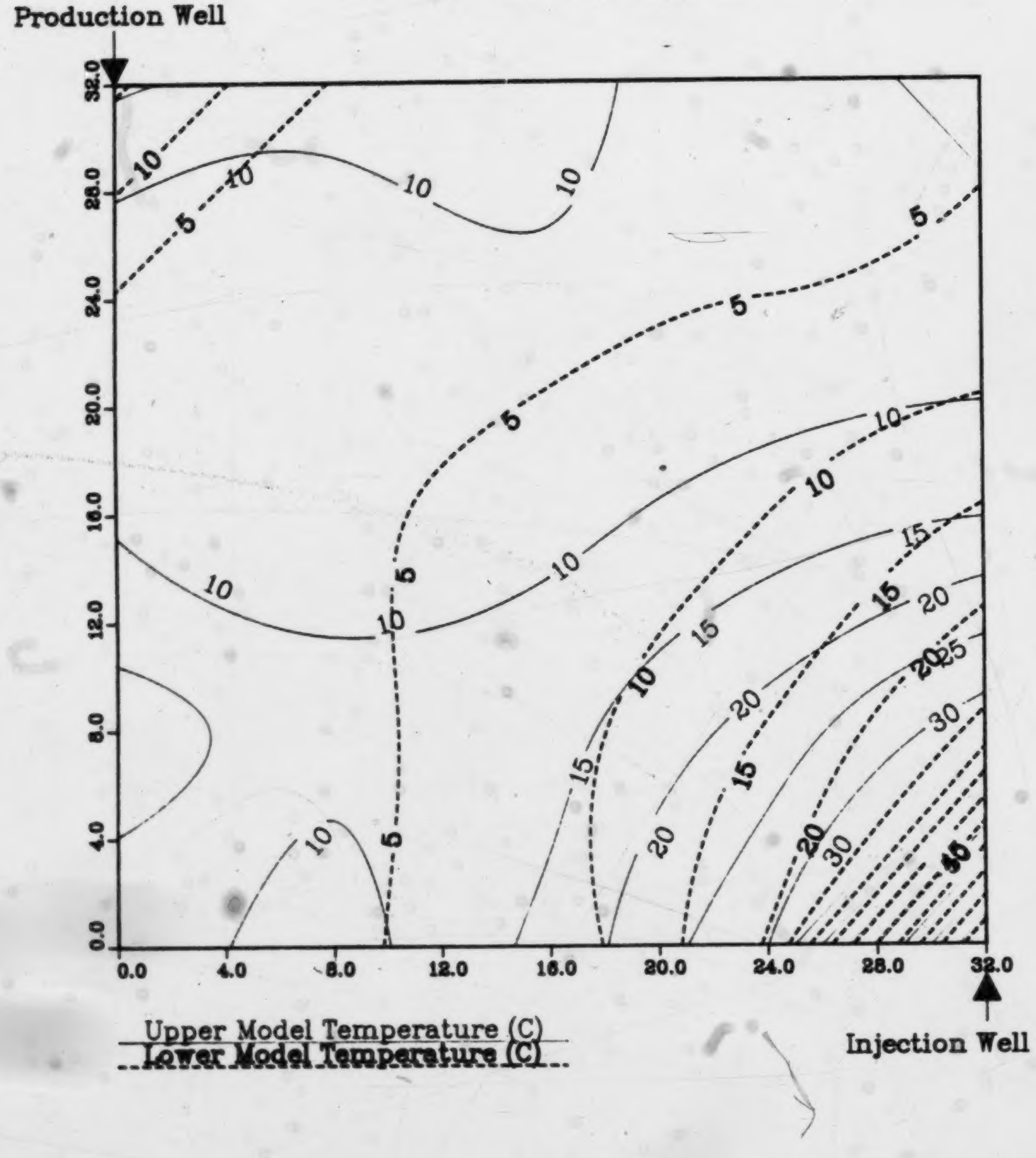

Figure A.120 : Run 49
Solvent–Steamflood in B.W. Model

Temperature Profile for
0.50 Pore Volumes Injected

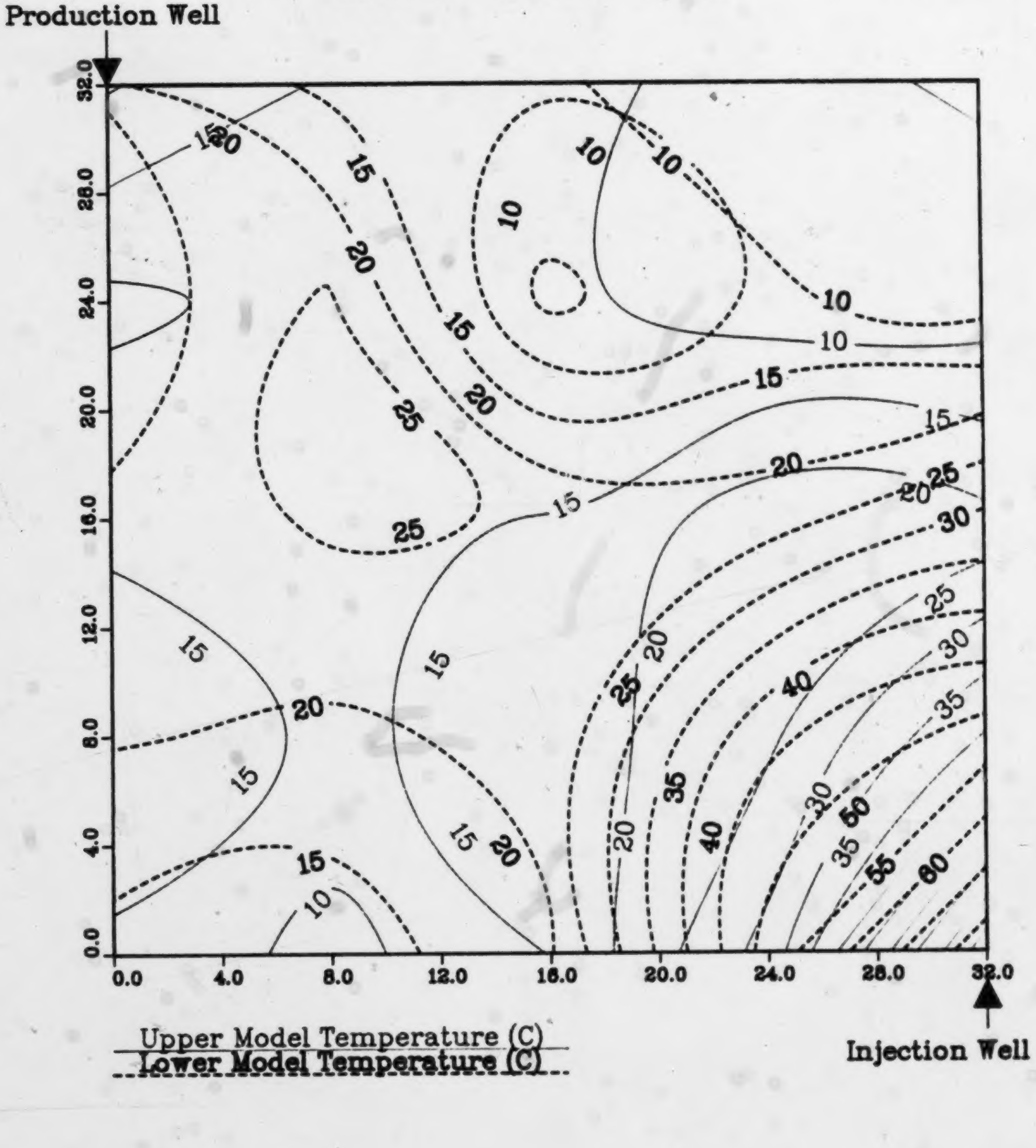

Figure A.121 : Run 49
Solvent–Steamflood in B.W. Model

Temperature Profile for 0.75 Pore Volumes Injected

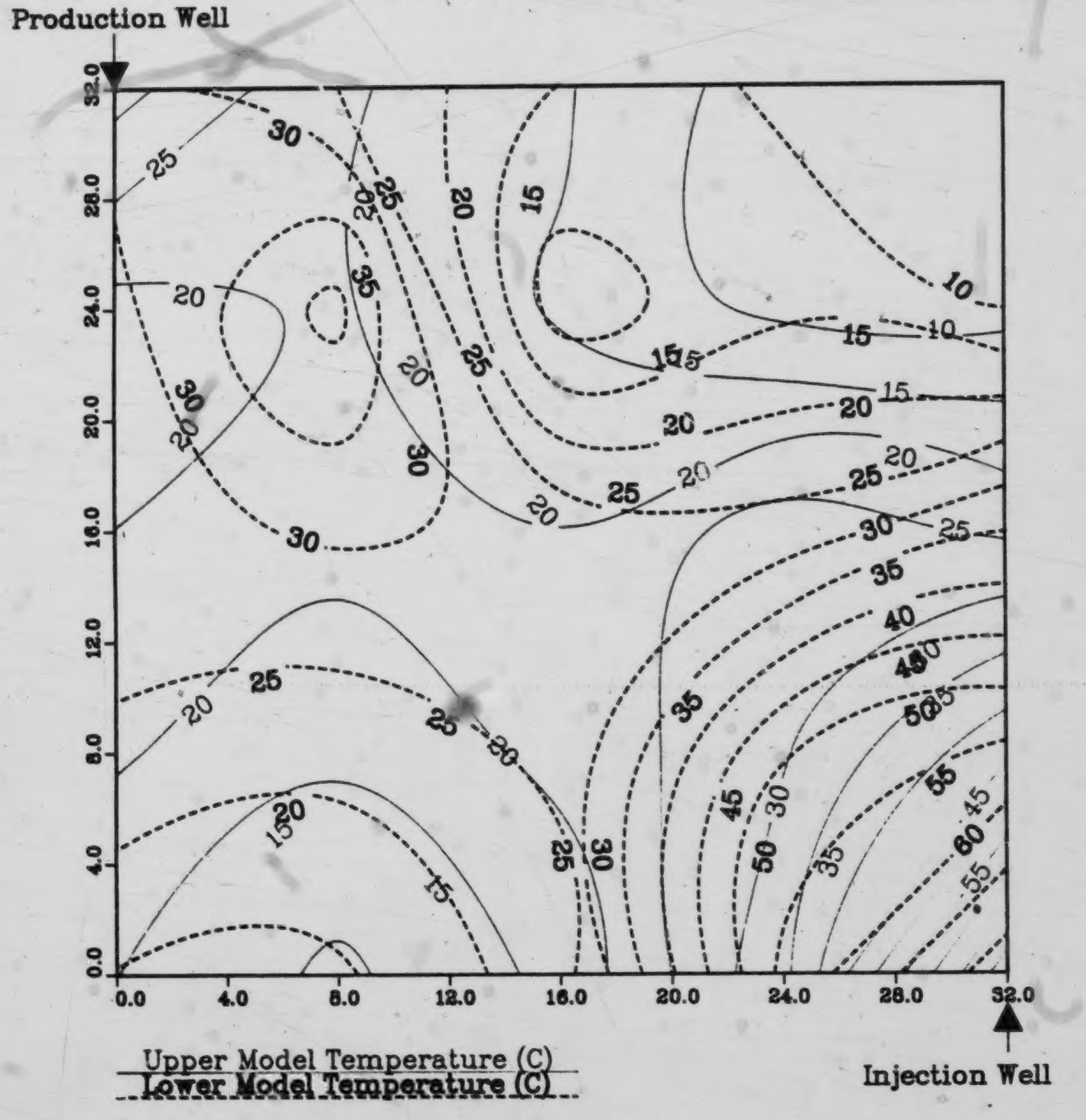

Figure A.122 : Run 49

Solvent–Steamflood in B.W. Model

Temperature Profile for 1.00 Pore Volumes Injected

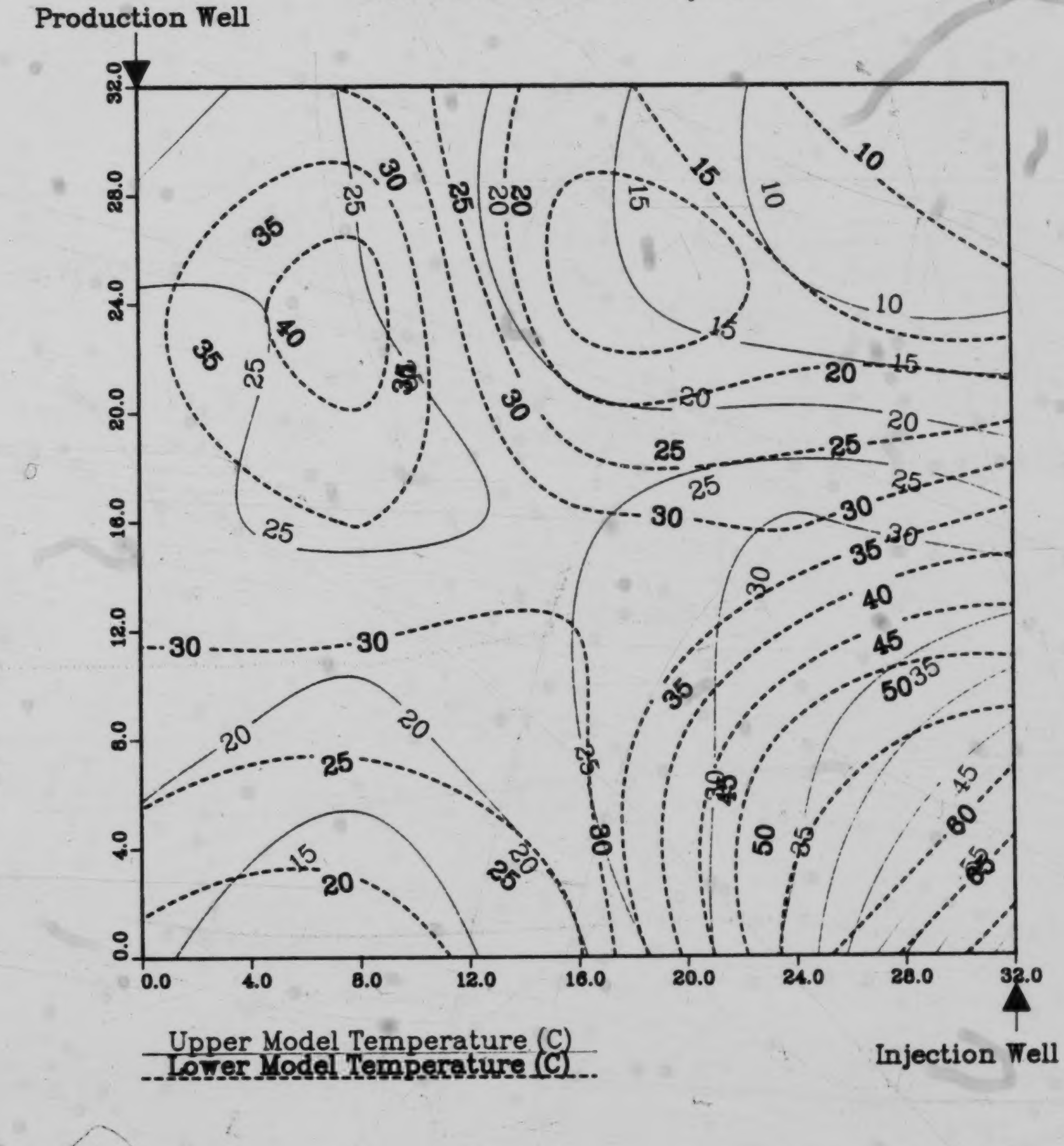

Figure A.123 : Run 49

Solvent–Steamflood in B.W. Model

Temperature Profile for 1.25 Pore Volumes Injected

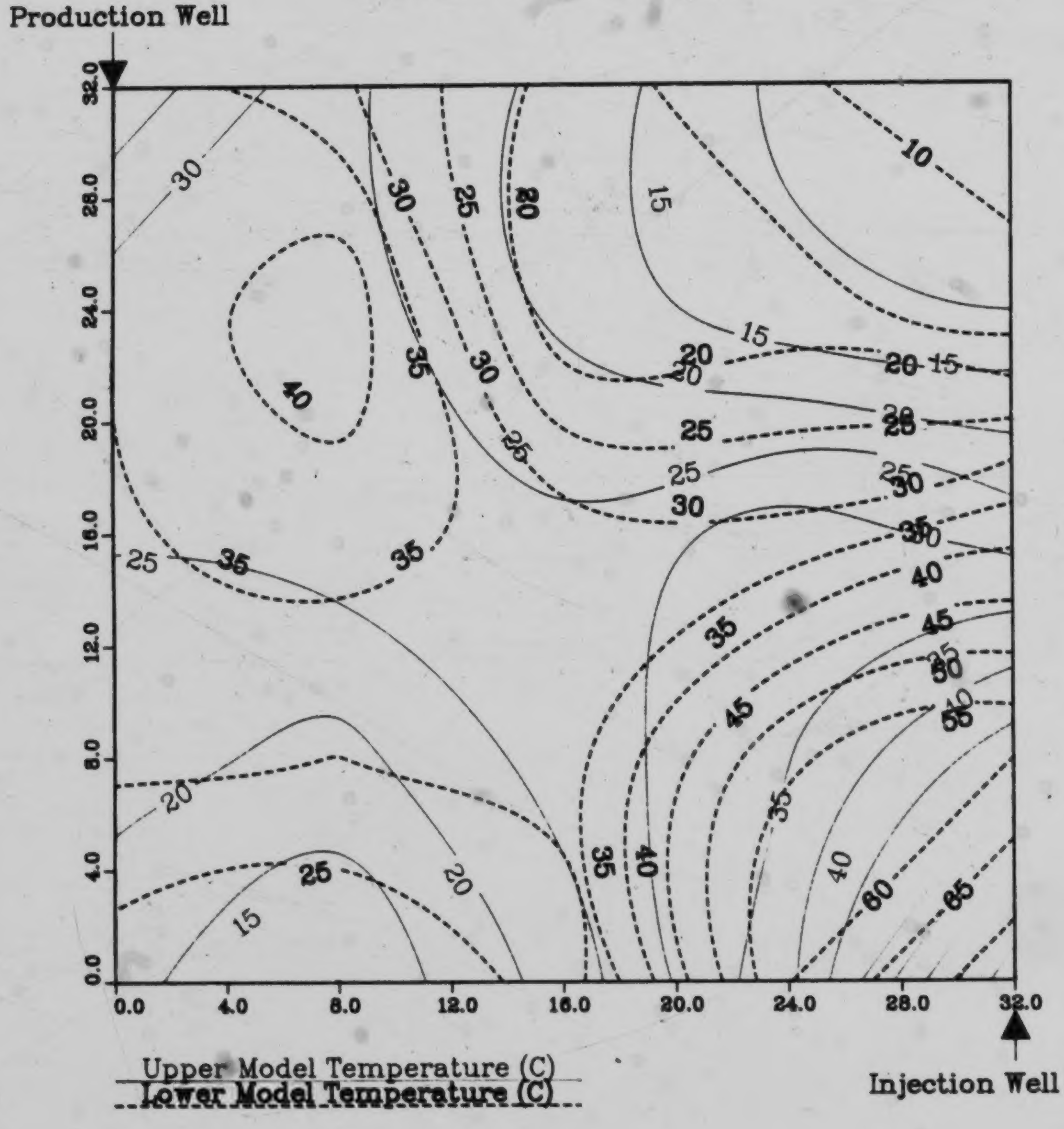

Figure A.124 : Run 49

Solvent–Steamflood in B.W. Model

Temperature Profile for 1.50 Pore Volumes Injected

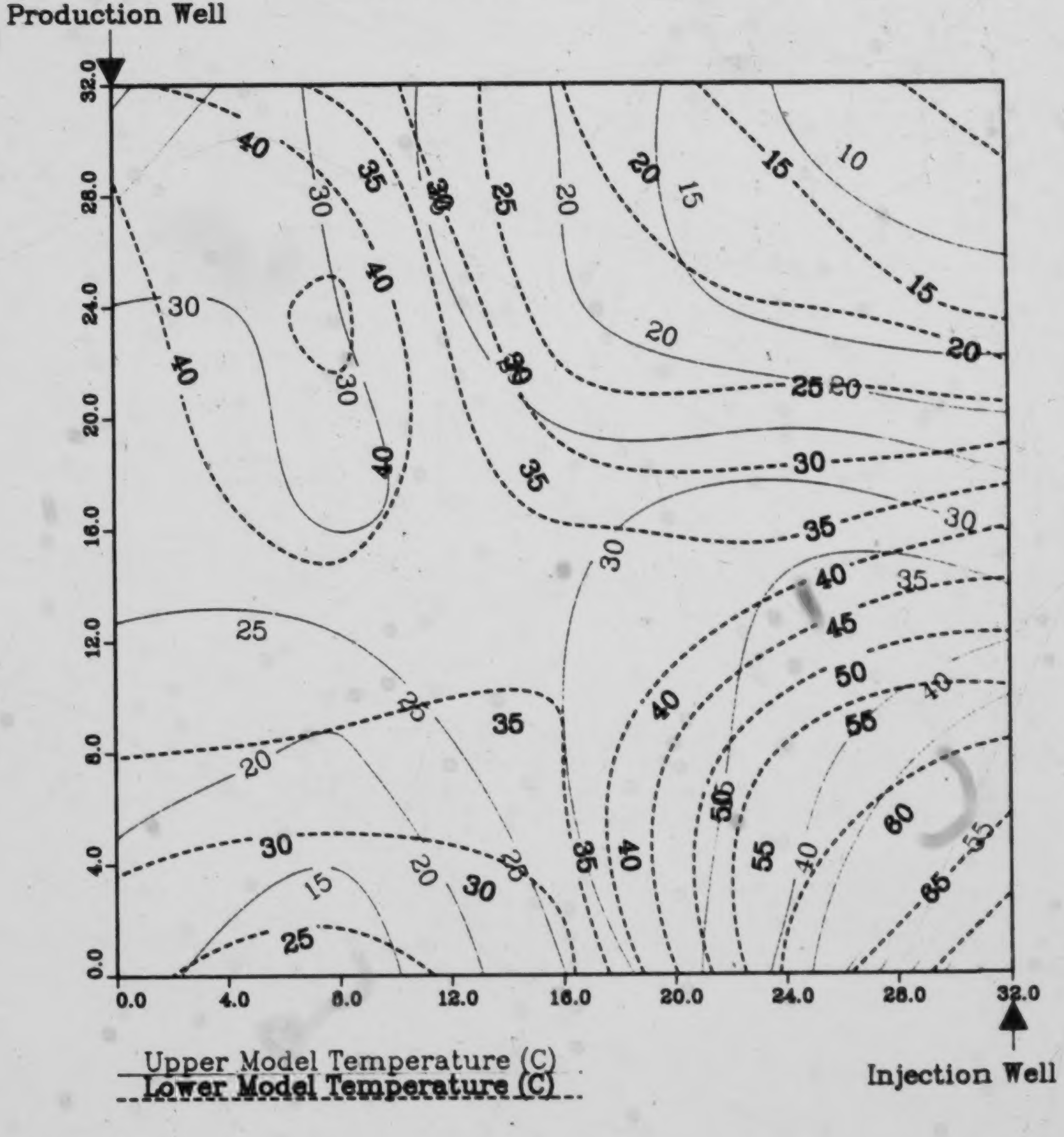

Figure A.125 : Run 49

Solvent–Steamflood in B.W. Model

Temperature Profile for 1.75 Pore Volumes Injected

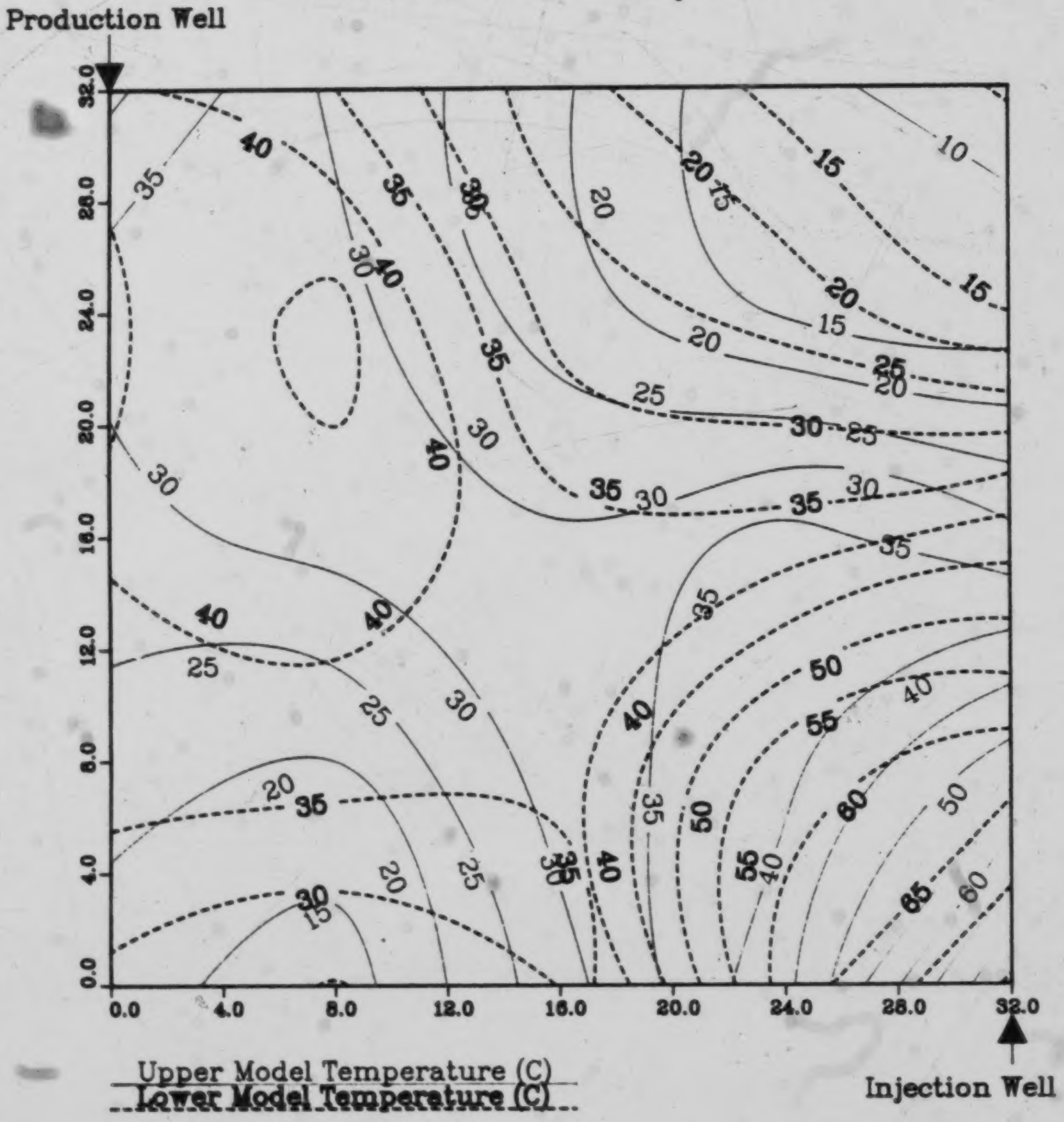

Figure A.126 : Run 49

Solvent–Steamflood in B.W. Model

Temperature Profile for 2.00 Pore Volumes Injected

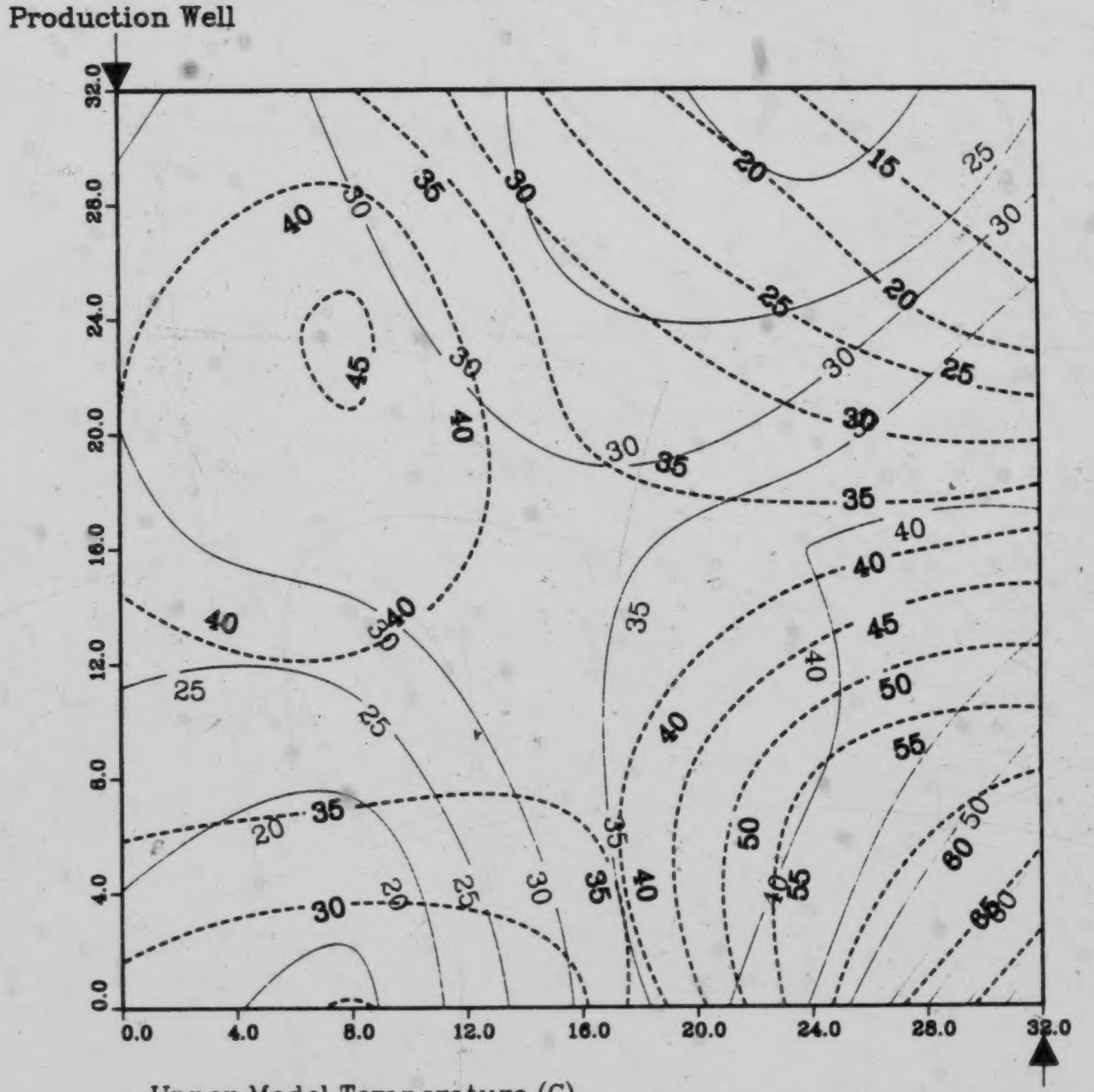

Figure A.127 :Run 49 Temp Profile

Injector to Producer Cross–Section

0.25 Pore Volumes Injected.

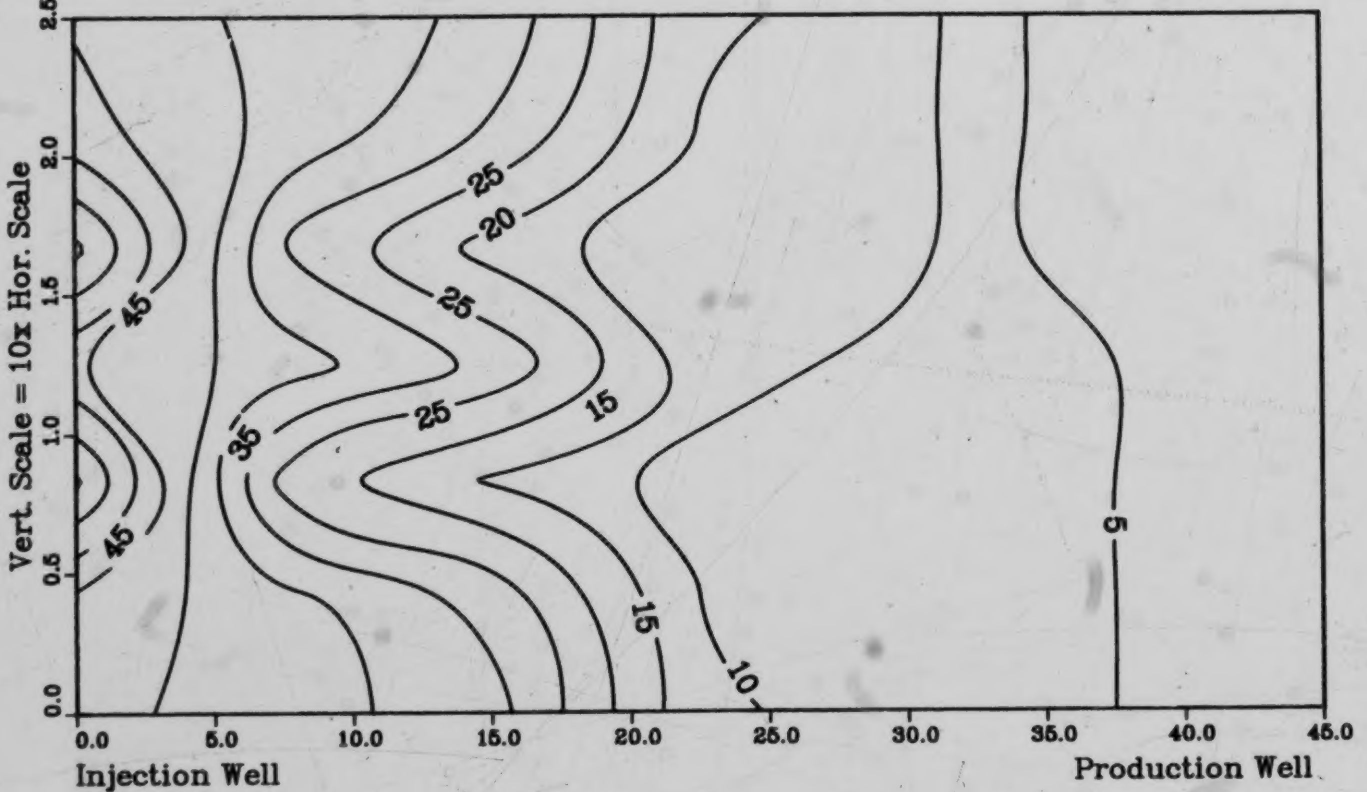

Figure A.128 :Run 49 Temp Profile
Injector to Producer Cross–Section
0.50 Pore Volumes Injected.

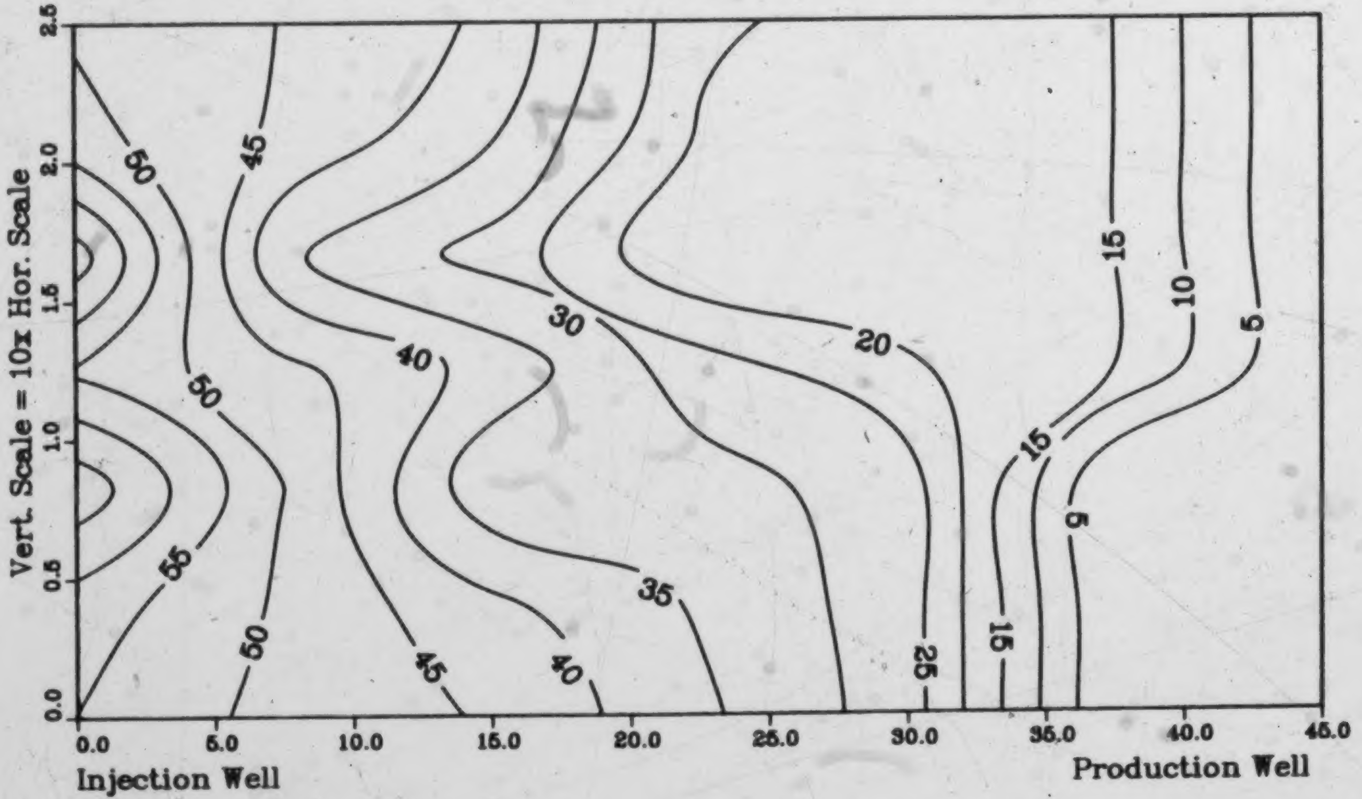

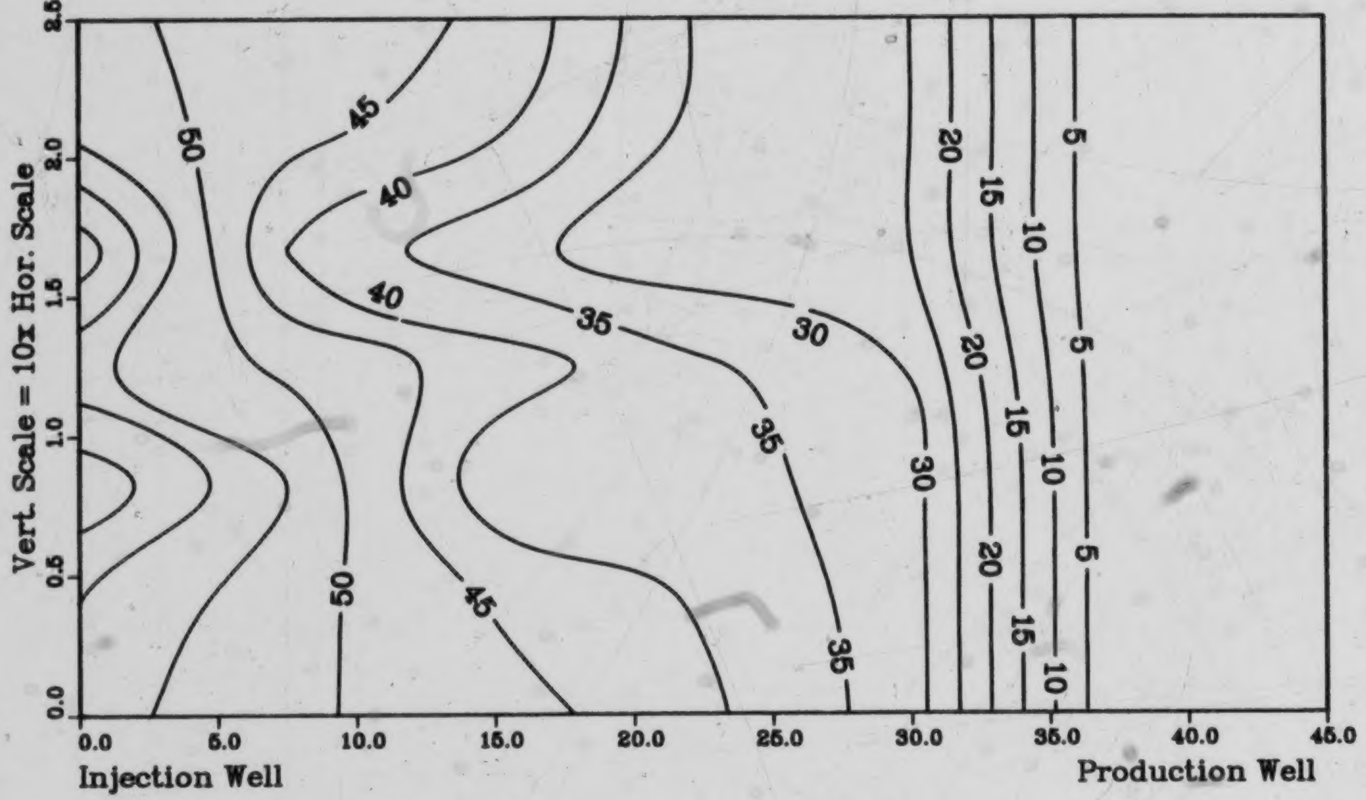

Figure A.129 :Run 49 Temp Profile
Injector to Producer Cross–Section
0.75 Pore Volumes Injected.

Figure A.130 :Run 49 Temp Profile
Injector to Producer Cross–Section
1.00 Pore Volumes Injected.

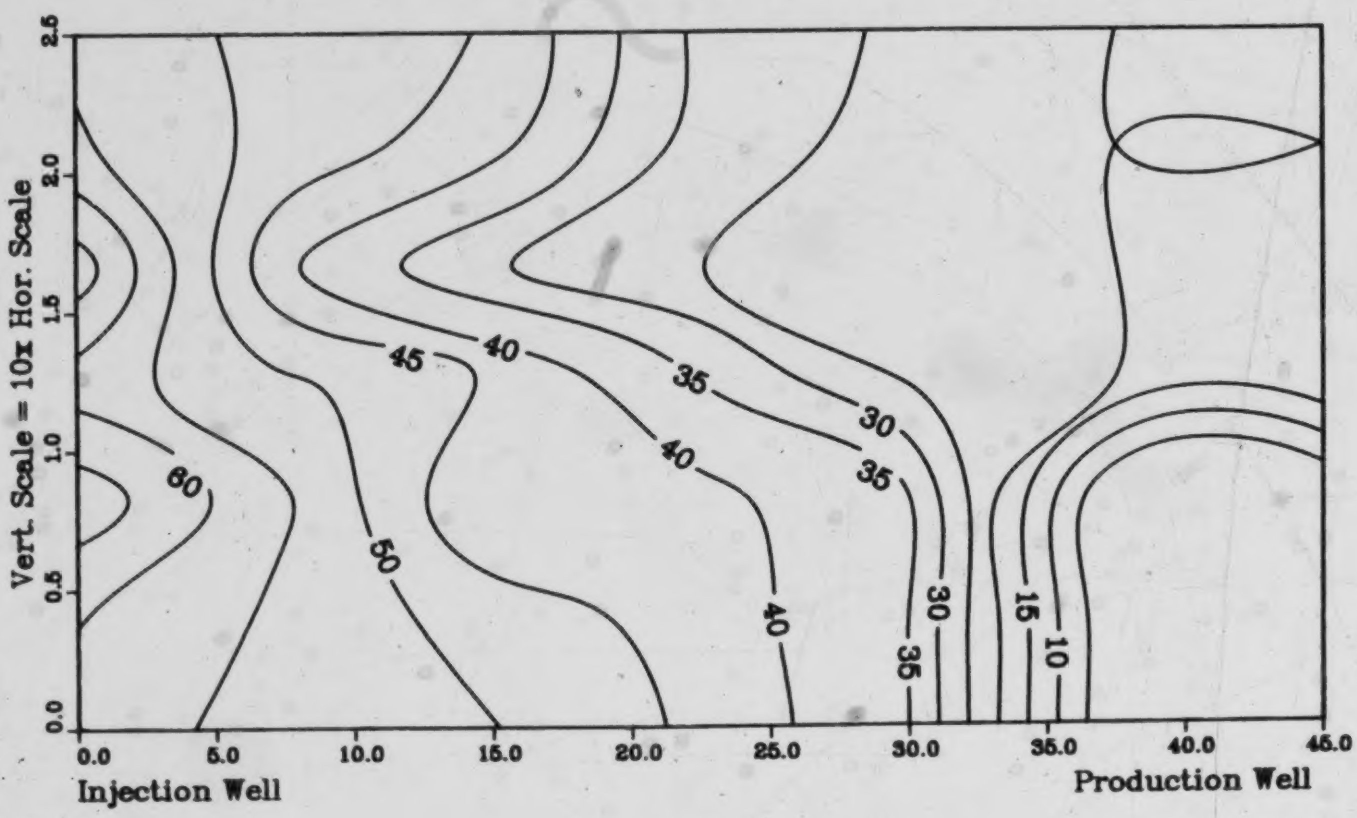

Figure A.131 : Run 50
Solvent–Steamflood in B.W. Model

Temperature Profile for
0.25 Pore Volumes Injected

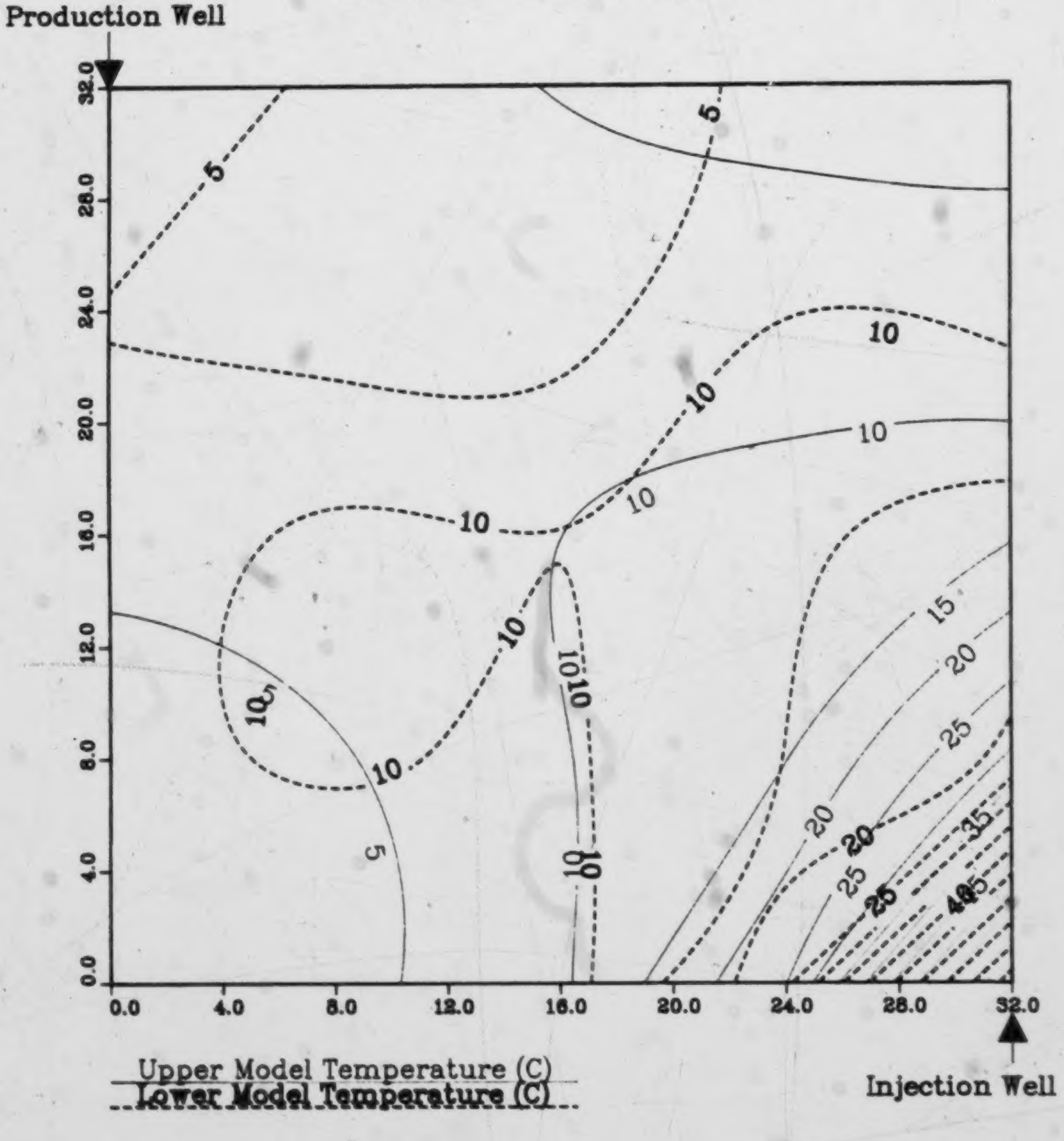

Figure A.132 : Run 50
Solvent–Steamflood in B.W. Model

Temperature Profile for
0.50 Pore Volumes Injected

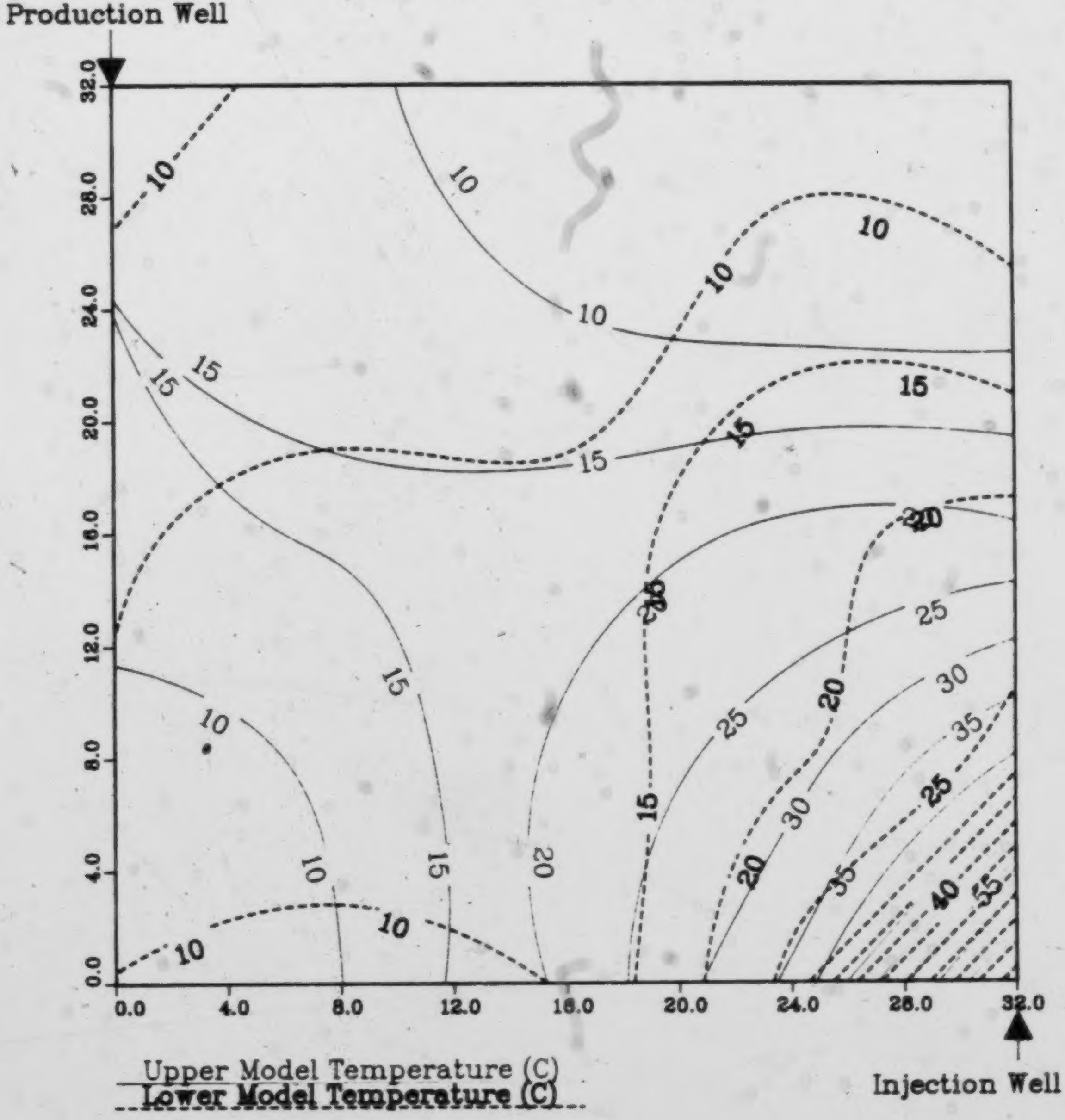

Figure A.133 : Run 50

Solvent–Steamflood in B.W. Model

Temperature Profile for
0.75 Pore Volumes Injected

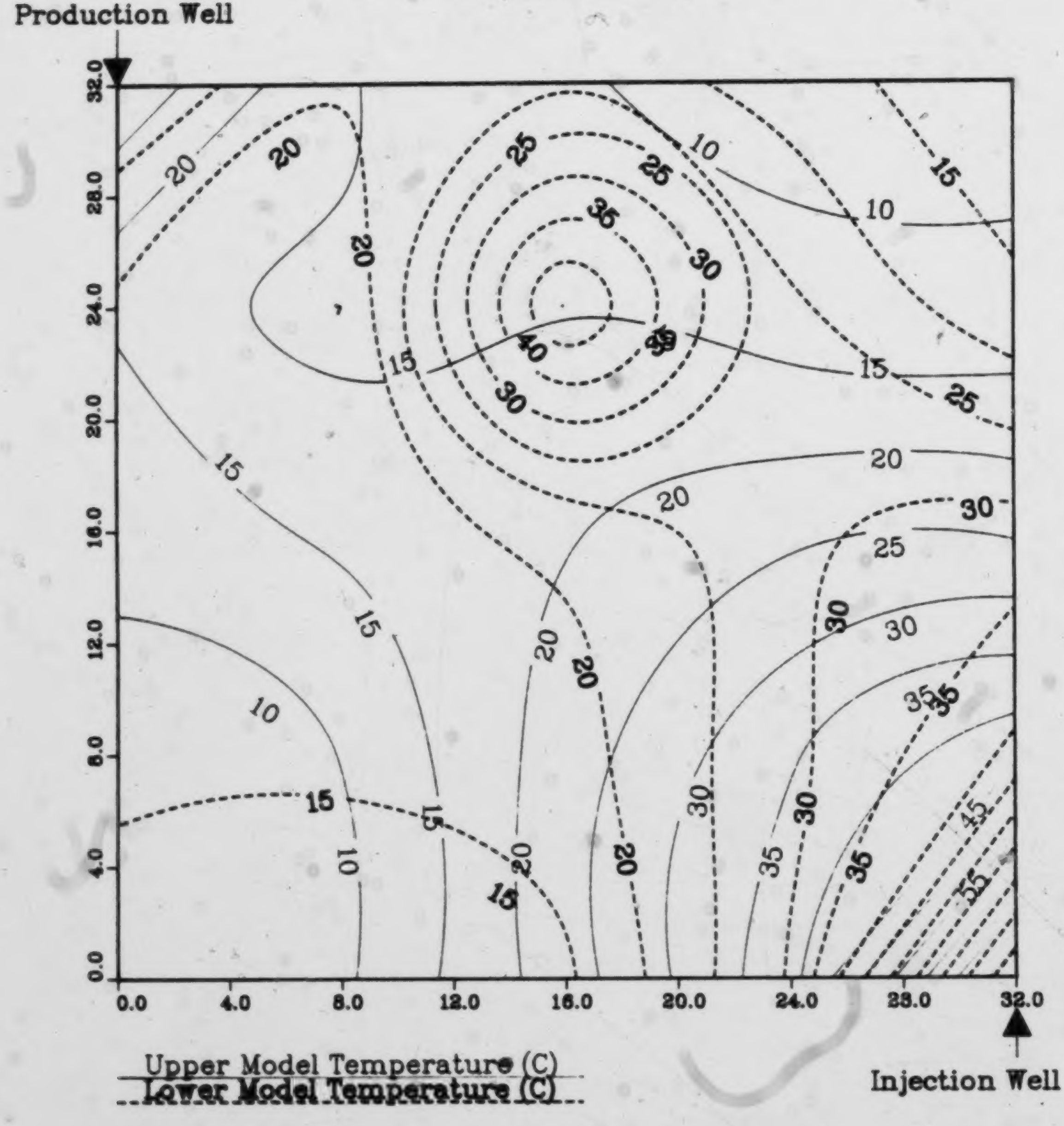

Figure A.134 : Run 50

Solvent–Steamflood in B.W. Model

Temperature Profile for
1.00 Pore Volumes Injected

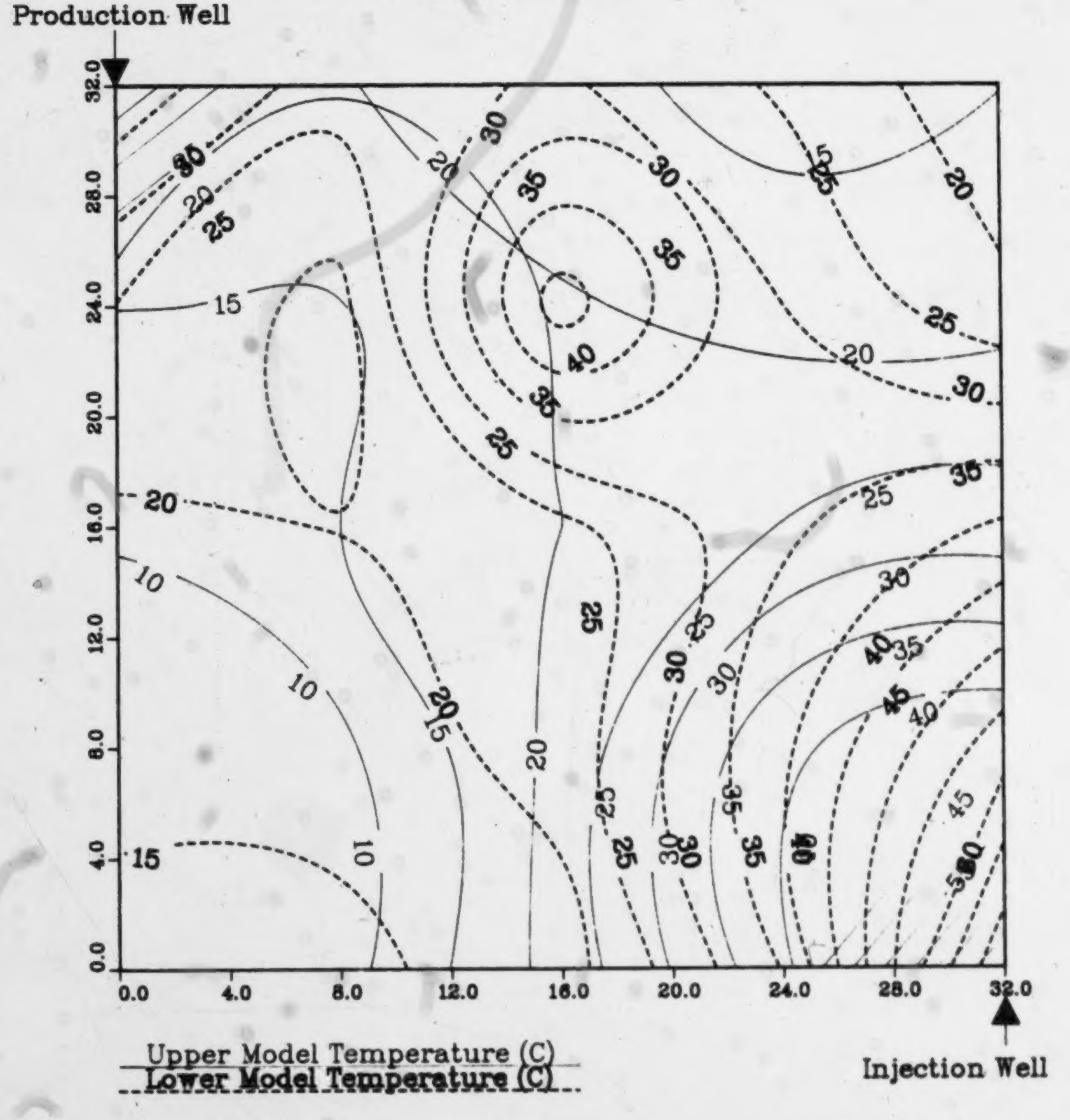

Figure A.135 : Run 50

Solvent–Steamflood in B.W. Model

Temperature Profile for
1.25 Pore Volumes Injected

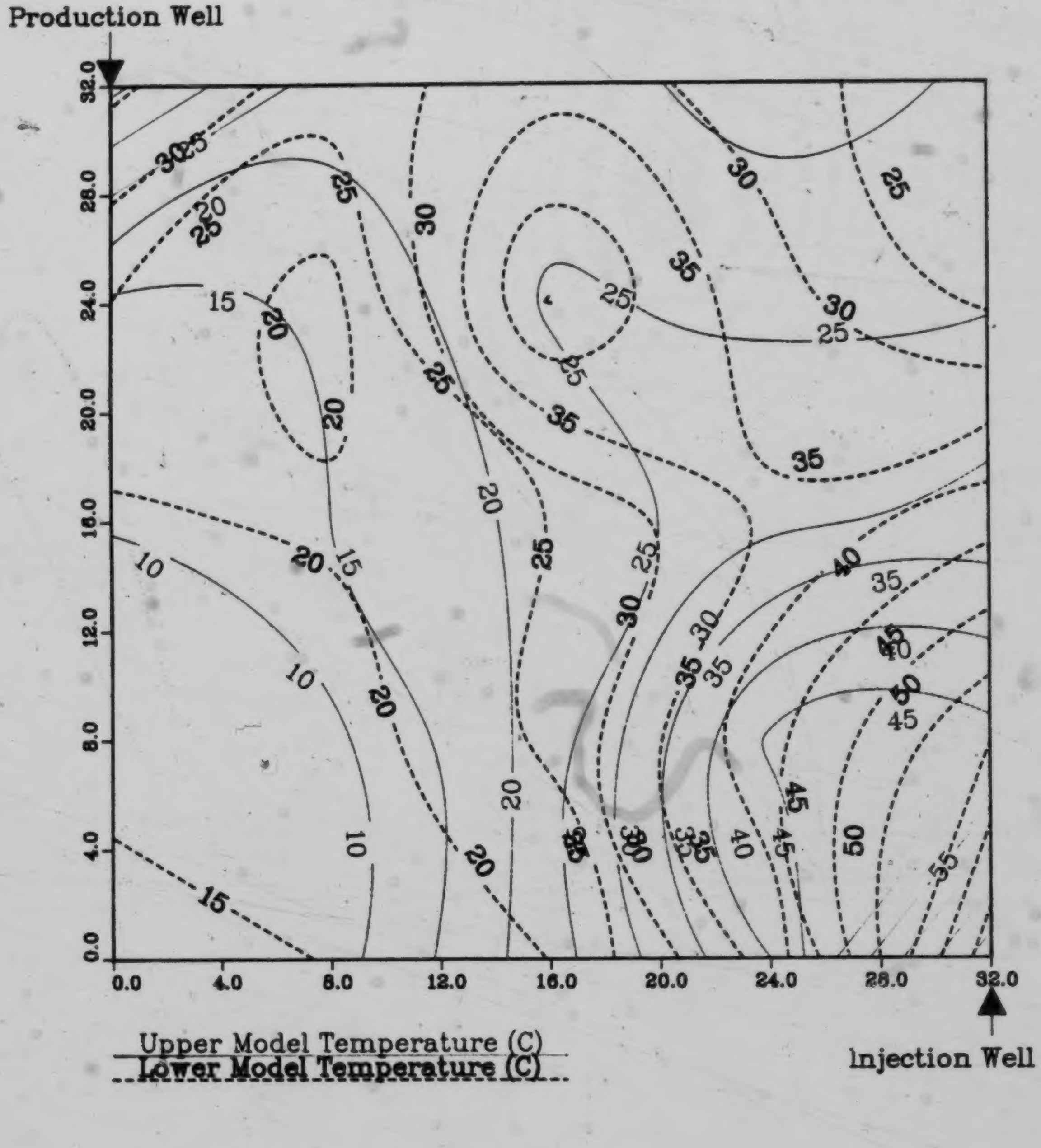

Figure A.136 : Run 50

Sclvent–Steamflood in B.W. Model

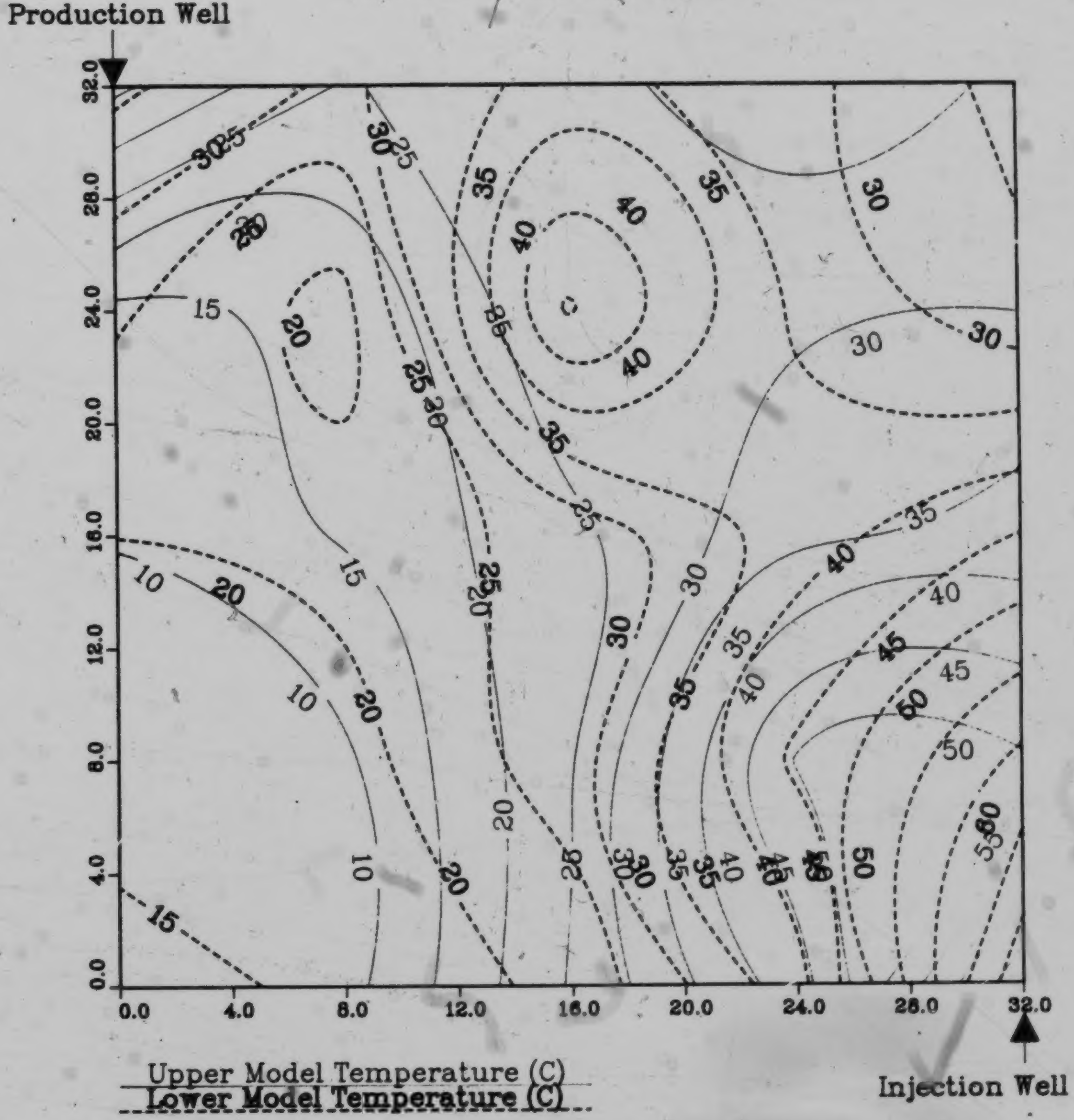

Figure A.137 : Run 50
Solvent–Steamflood in B.W. Model

Temperature Profile for
1.75 Pore Volumes Injected

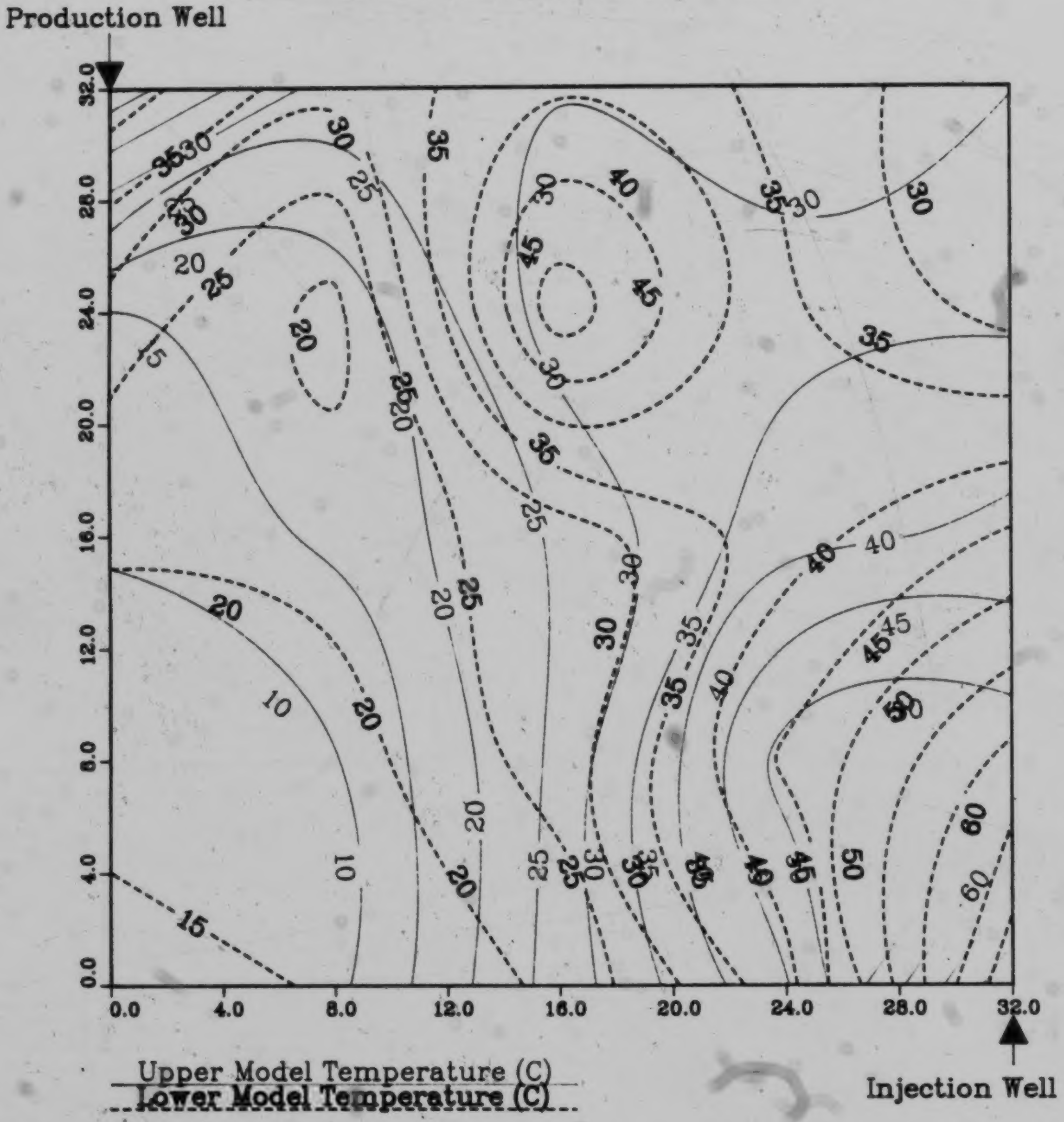

Figure A.138 : Run 50

Solvent–Steamflood in B.W. Model

Temperature Profile for
2.00 Pore Volumes Injected

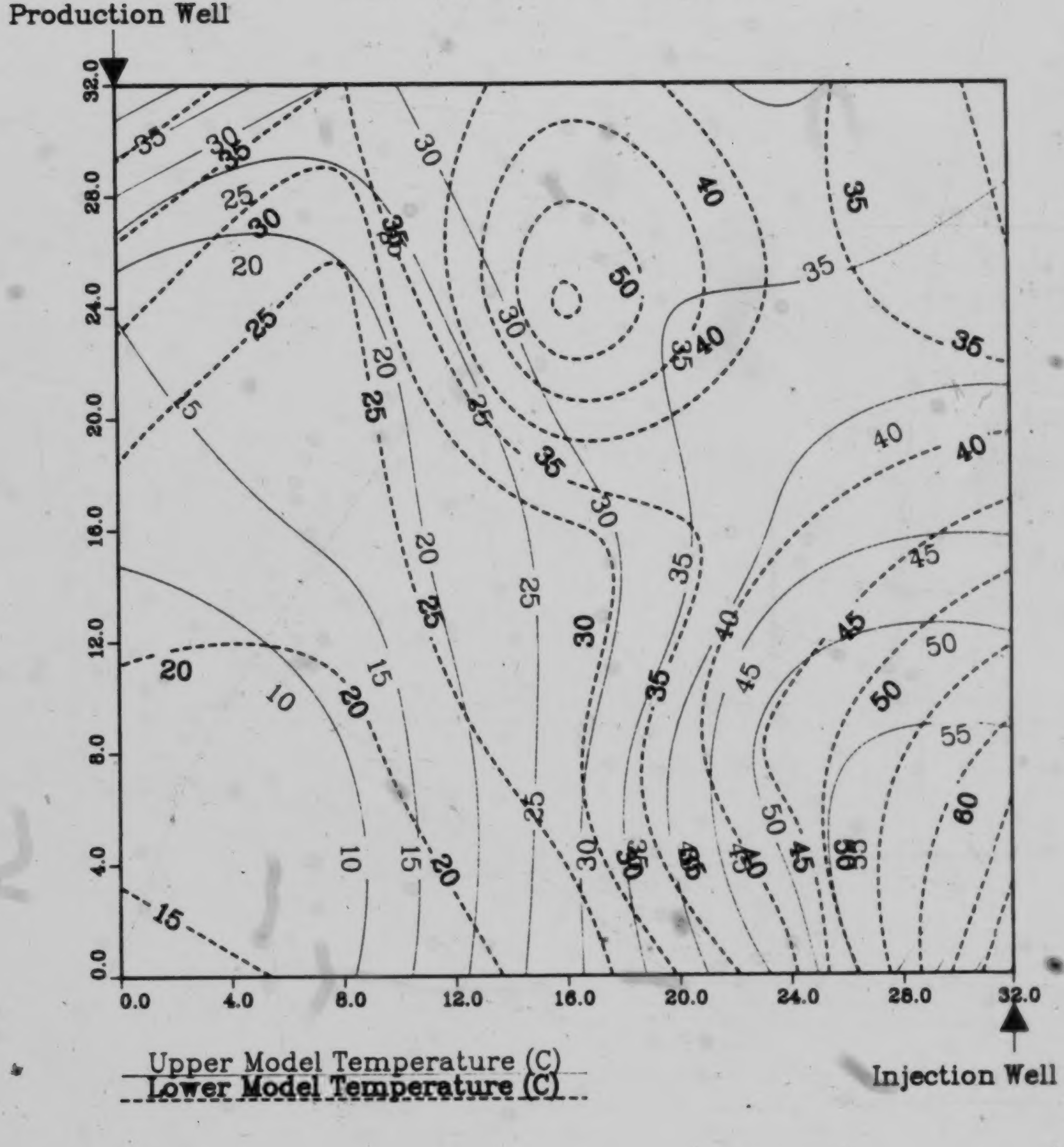

Figure A.139 :Run 50 Temp Profile
Injector to Producer Cross-Section
0.25 Pore Volumes Injected.

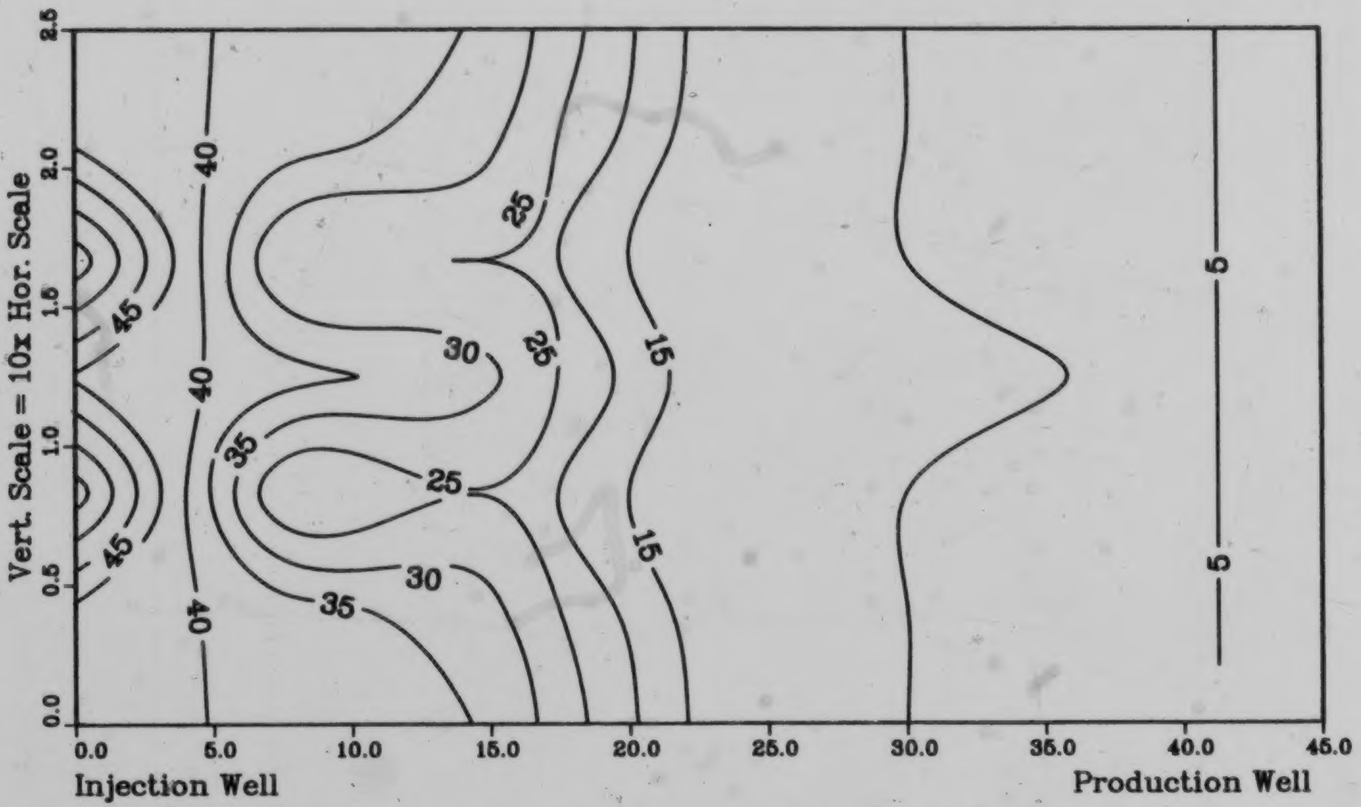

Figure A.140 :Run 50 Temp Profile
Injector to Producer Cross–Section
0.50 Pore Volumes Injected.

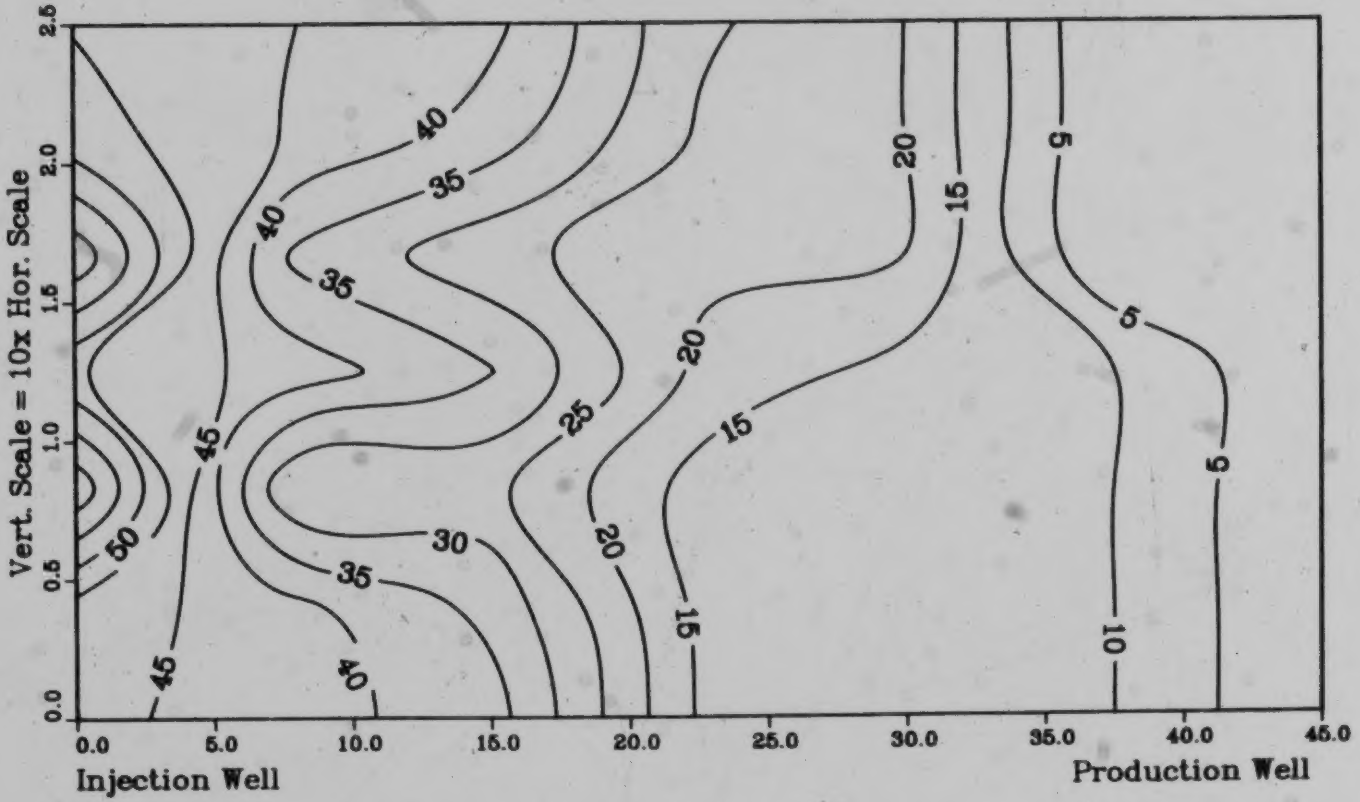

Figure A.141 :Run 50 Temp Profile
Injector to Producer Cross–Section
0.75 Pore Volumes Injected.

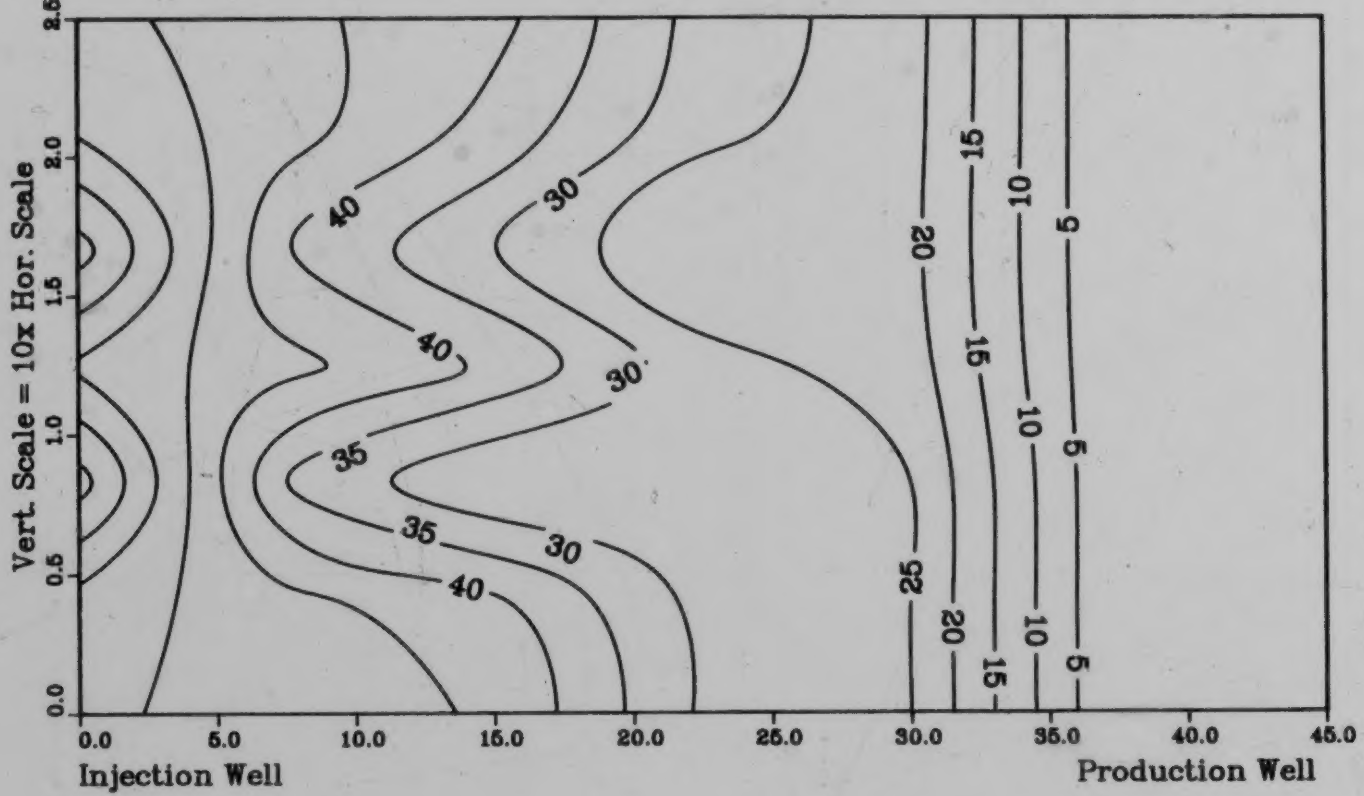

Figure A.142 :Run 50 Temp Profile
Injector to Producer Cross–Section
1.00 Pore Volumes Injected.

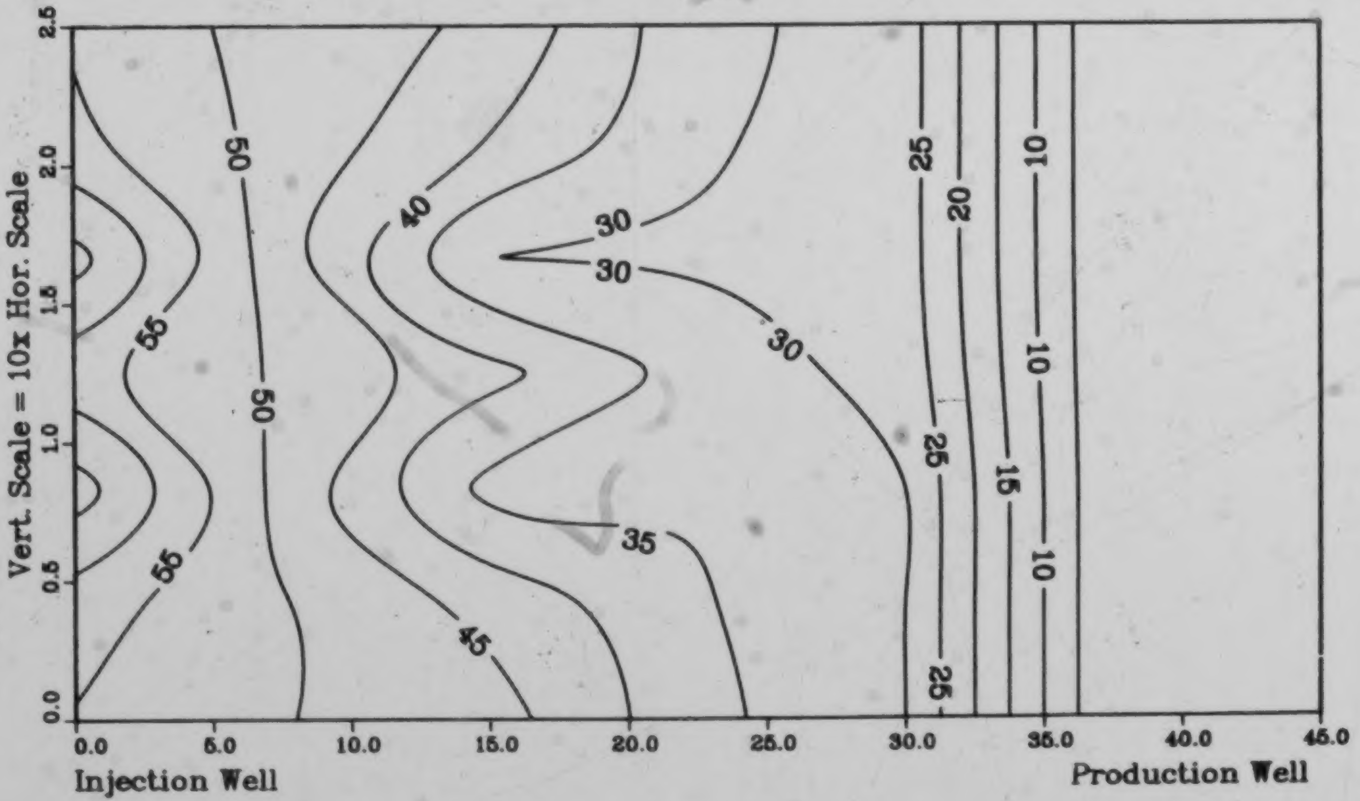

Figure A.143 : Run 51

Solvent–Steamflood in B.W. Model

Temperature Profile for
0.25 Pore Volumes Injected

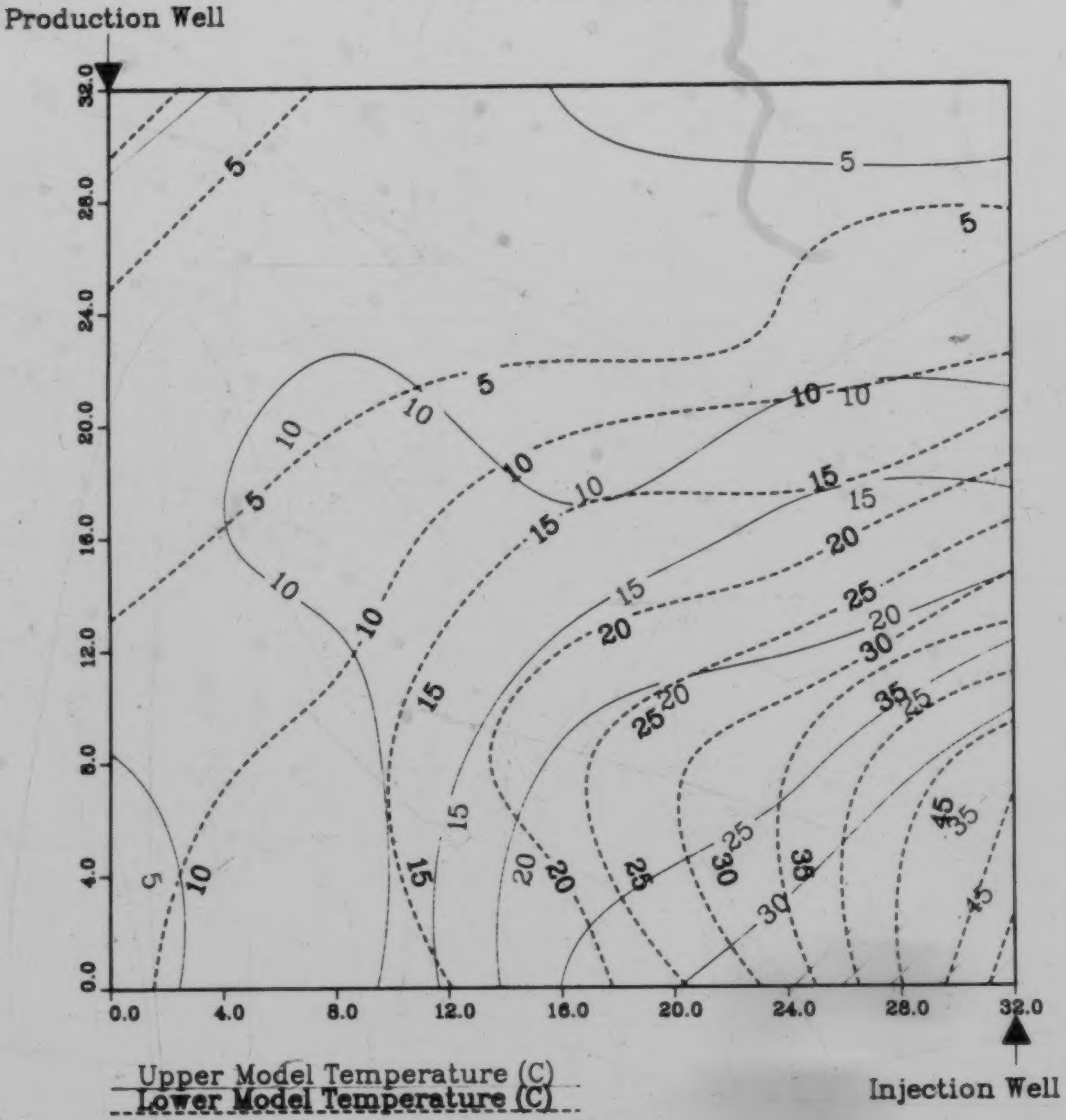

Figure A.144 : Run 51
Solvent–Steamflood in B.W. Model

Temperature Profile for 0.50 Pore Volumes Injected

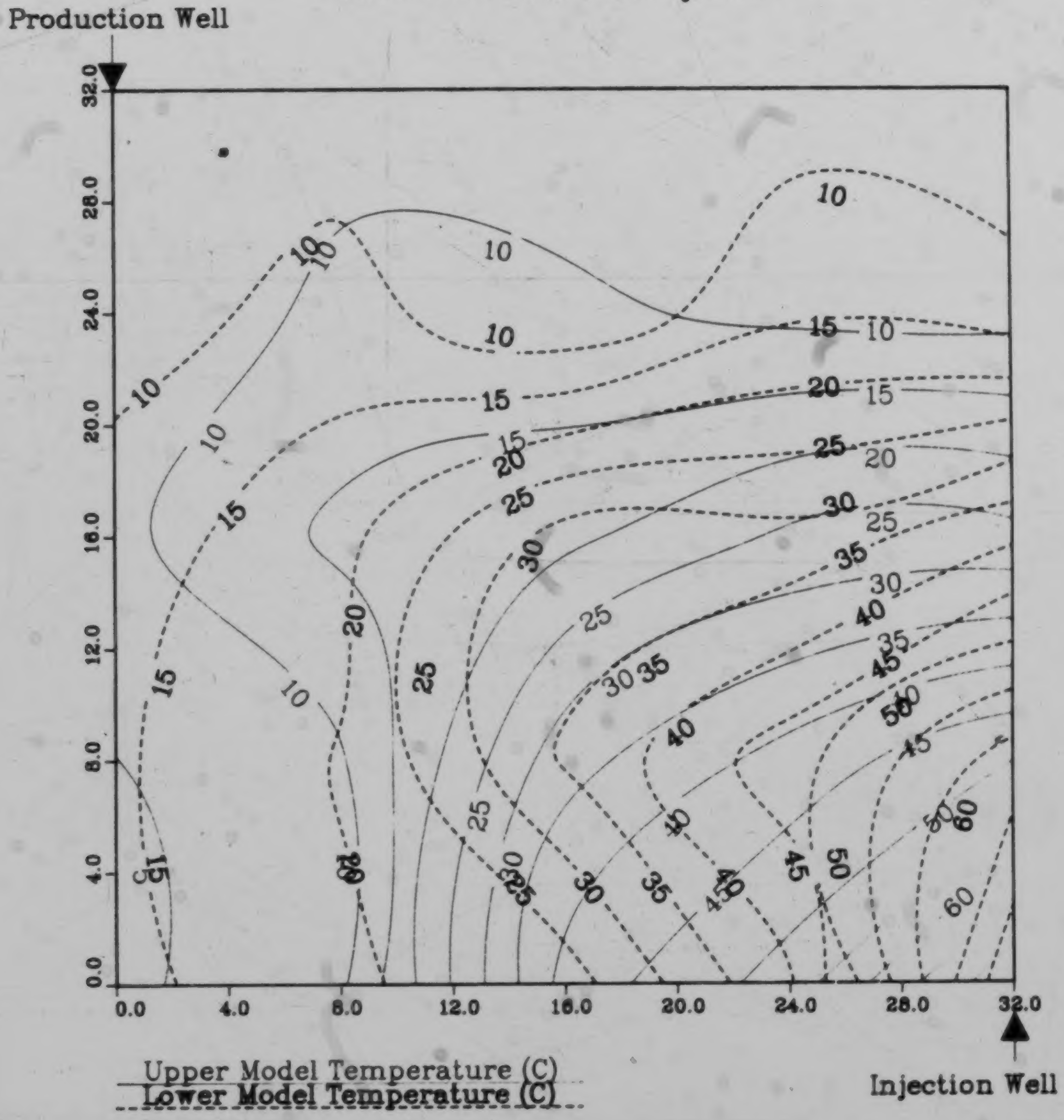

Figure A.145 : Run 51

Solvent–Steamflood in B.W. Model

Temperature Profile for
0.75 Pore Volumes Injected

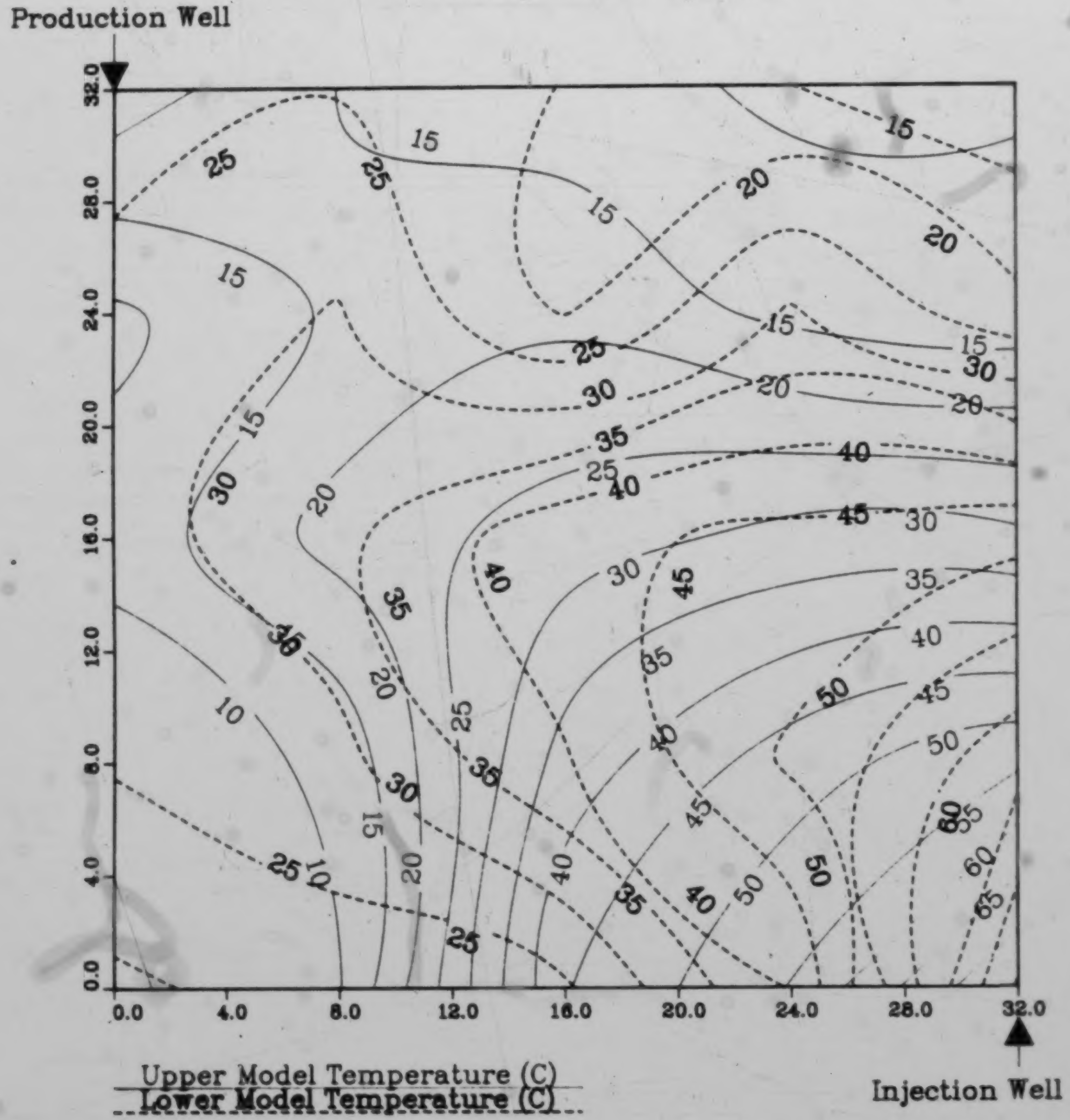

Figure A.146 : Run 51

Solvent- -Steamflood in B.W. Model

Temperature Profile for
1.00 Pore Volumes Injected

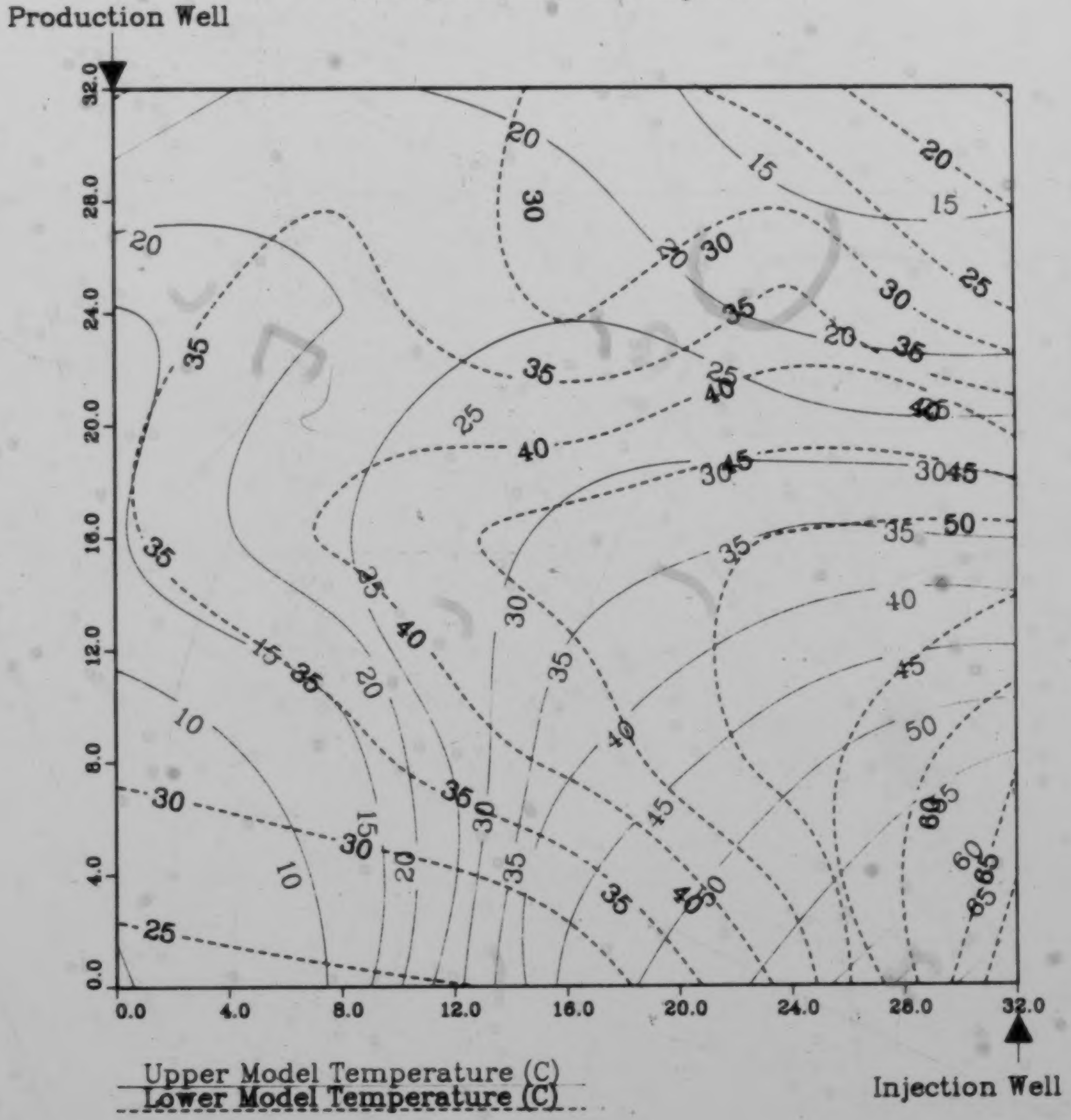

Figure A.147 : Run 51

Solvent–Steamflood in B.W. Model

Temperature Profile for
1.25 Pore Volumes Injected

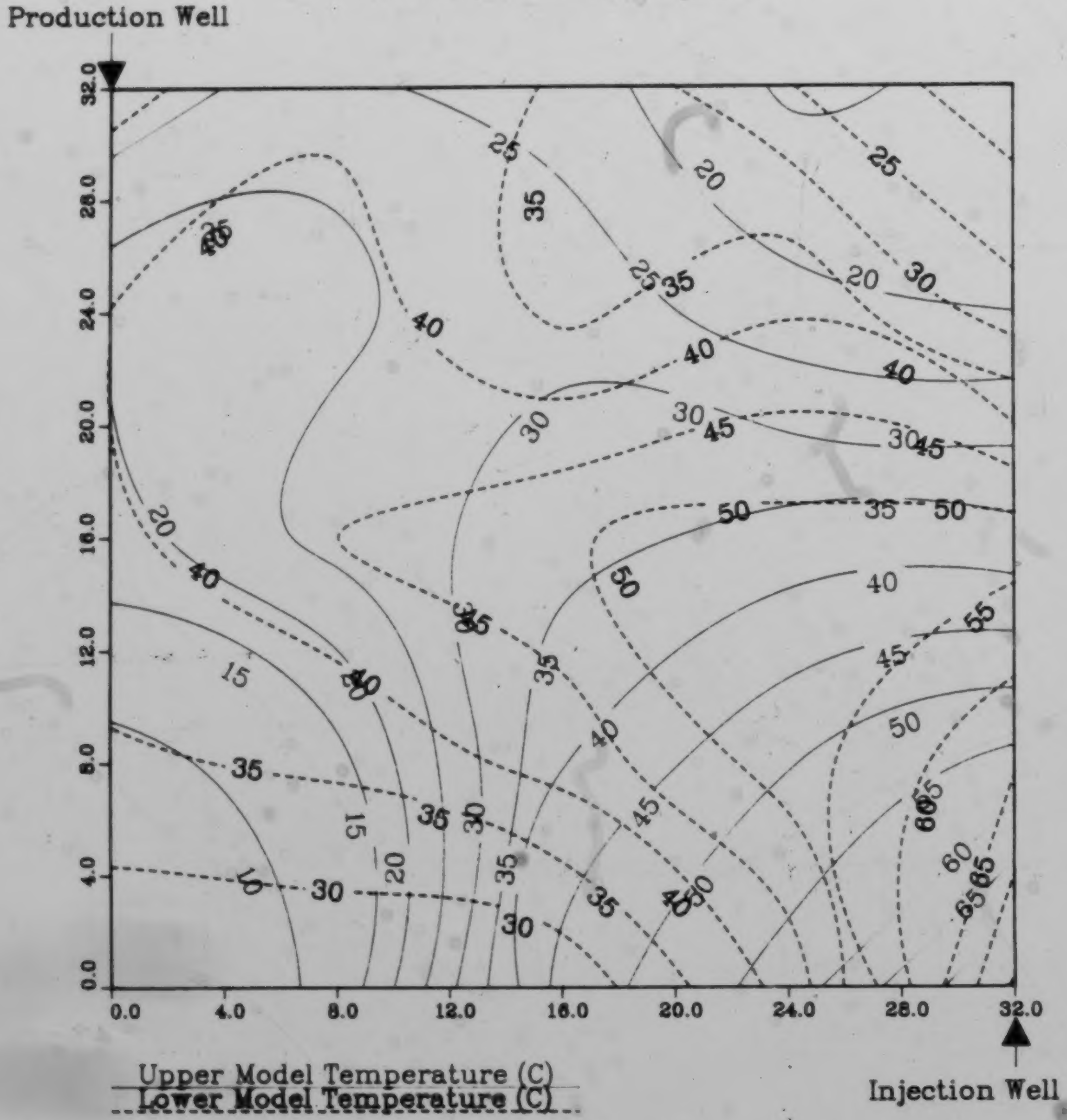

Figure A.148 : Run 51
Solvent–Steamflood in B.W. Model

Temperature Profile for
1.50 Pore Volumes Injected

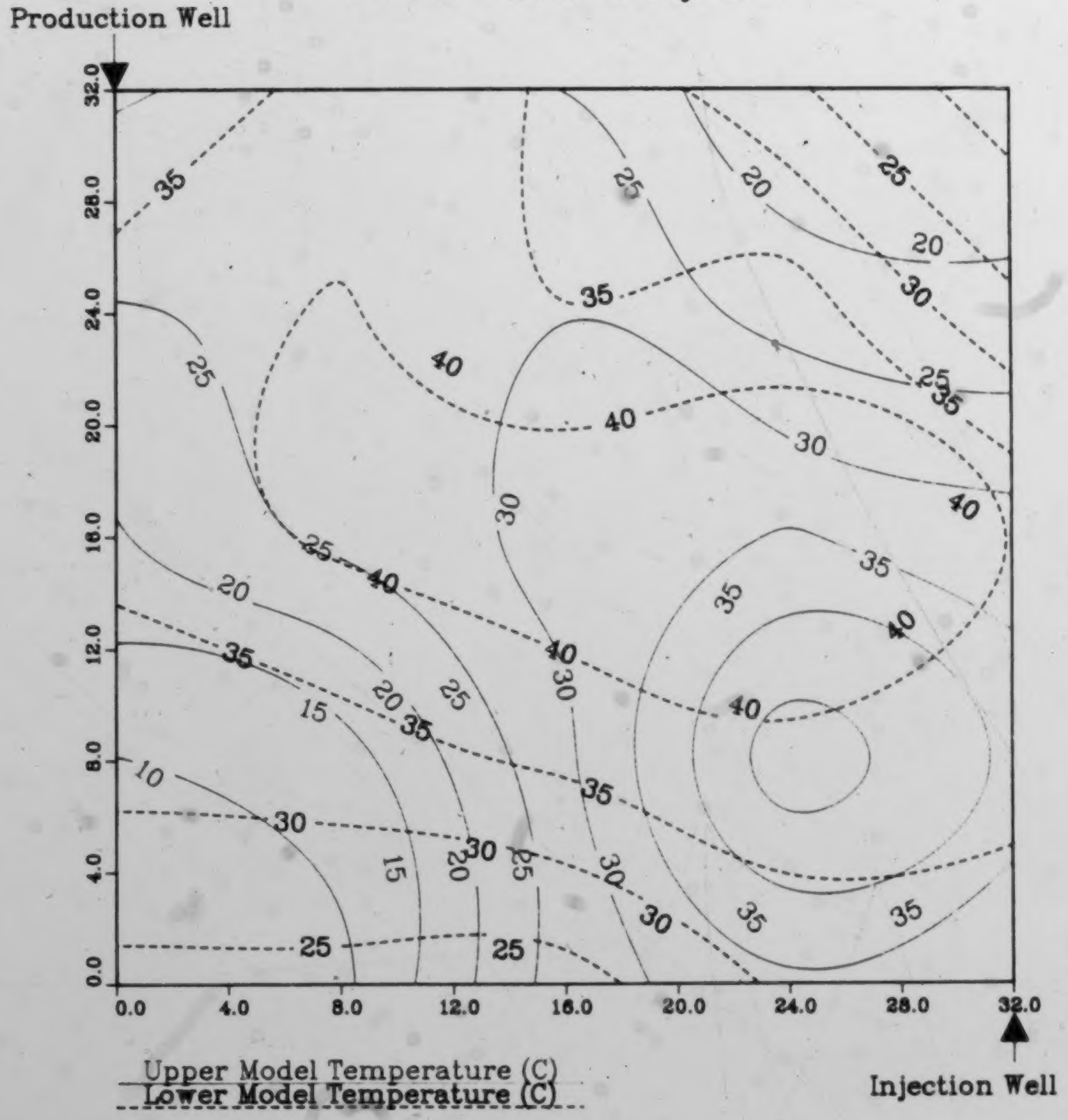

Figure A.149 : Run 51
Solvent–Steamflood in B.W. Model

Temperature Profile for 1.75 Pore Volumes Injected

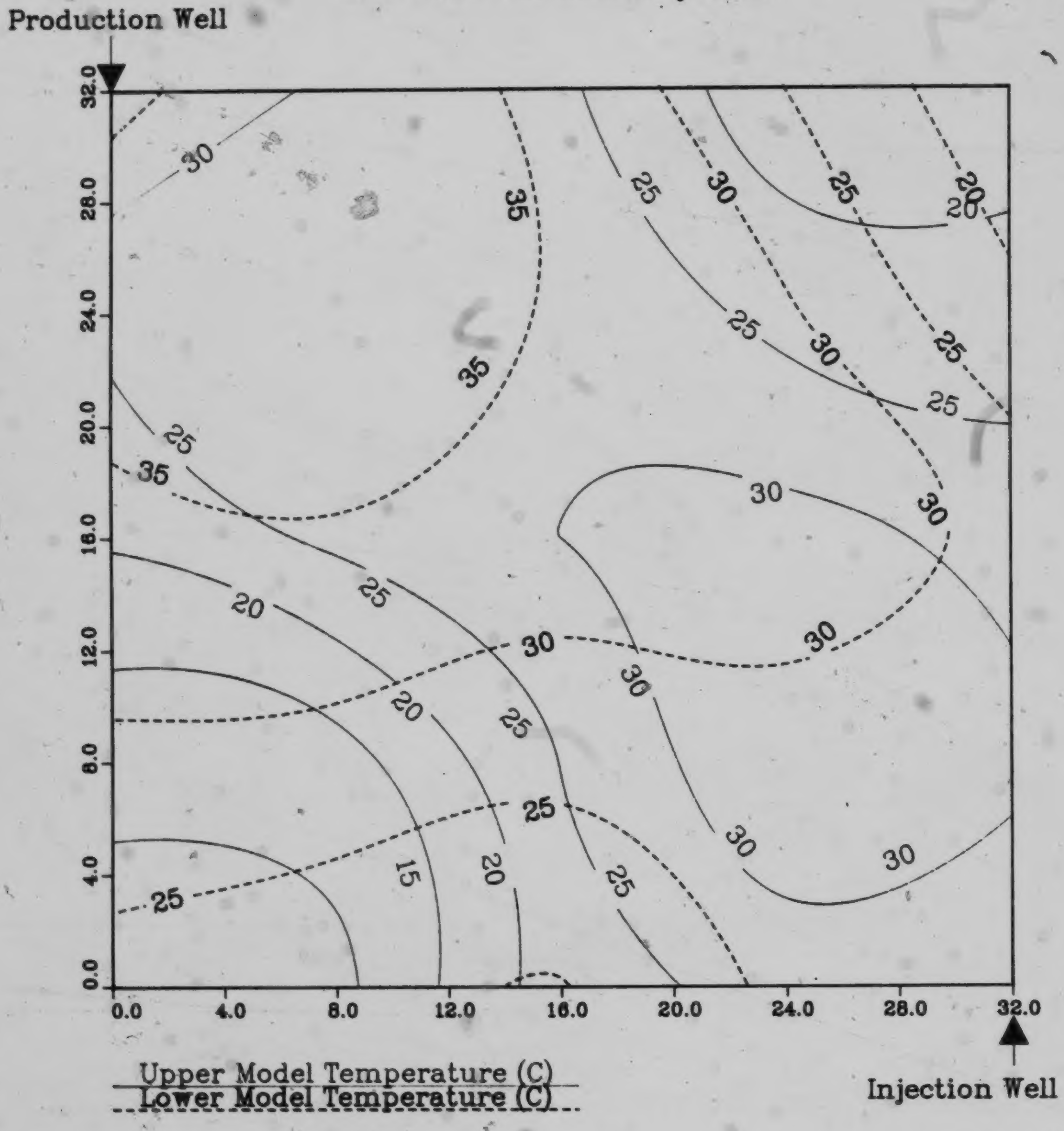

Figure A.150 : Run 51

Solvent–Steamflood in B.W. Model

Temperature Profile for 2.00 Pore Volumes Injected

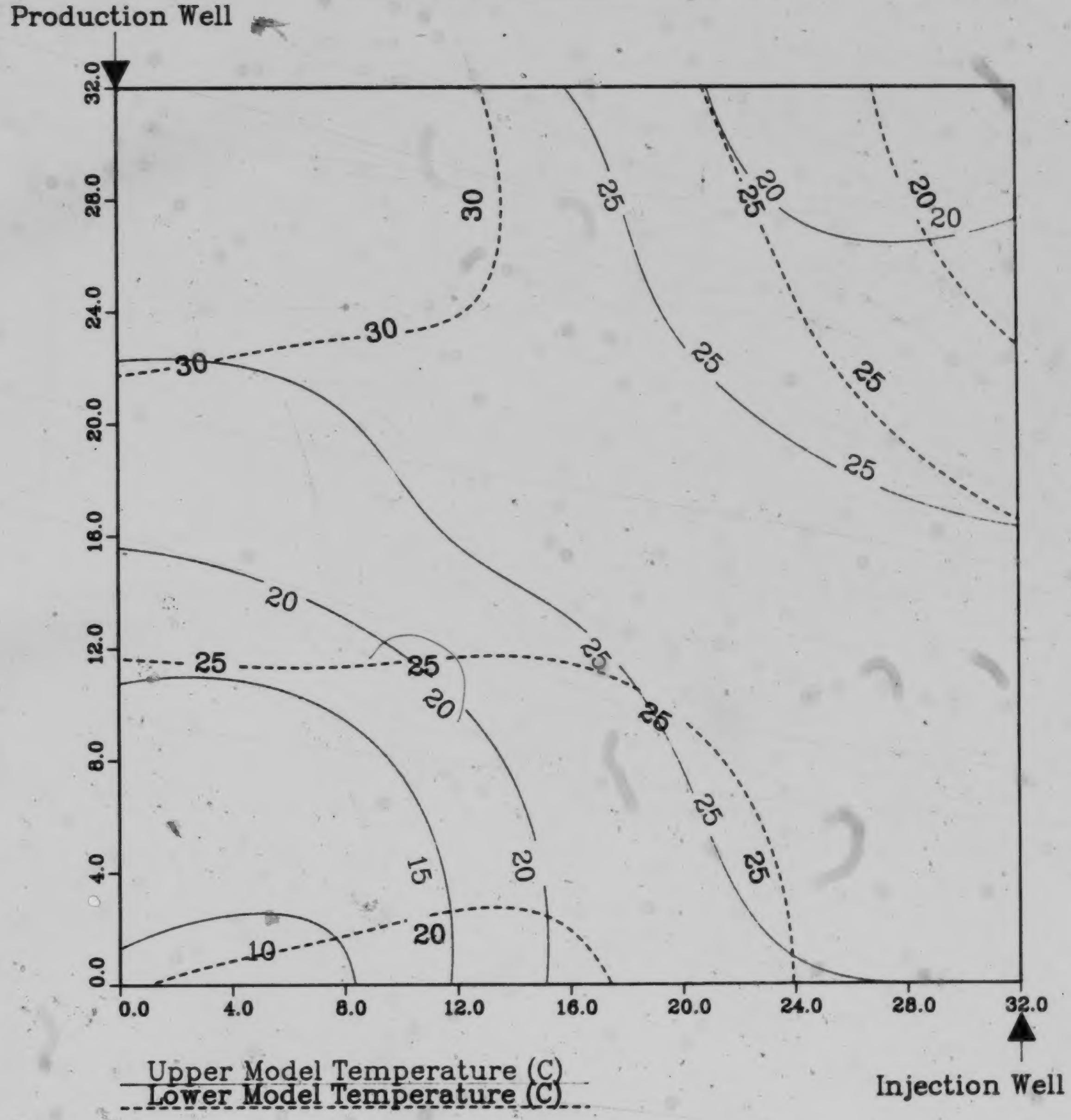

Figure A.151 :Run 51 Temp Profile

Injector to Producer Cross-Section

0.25 Pore Volumes Injected.

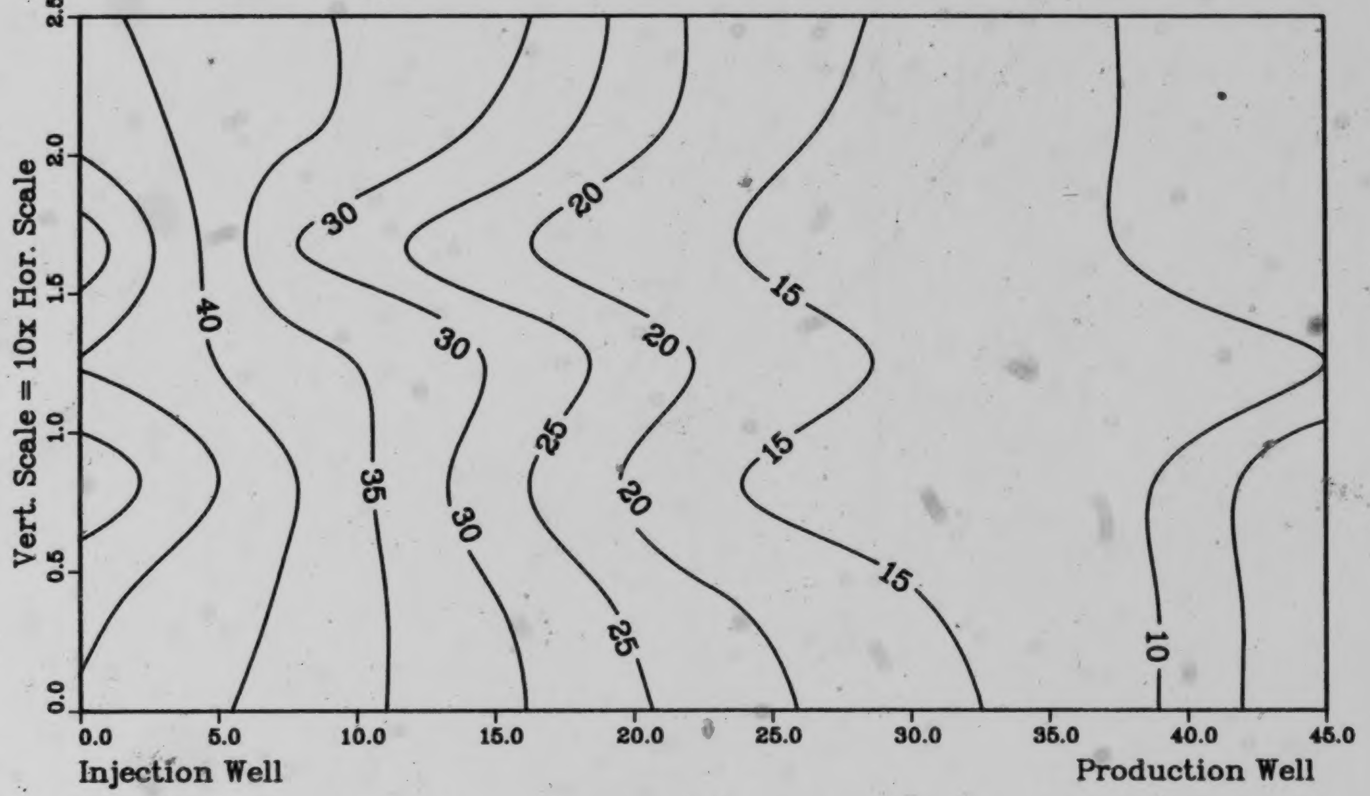

Figure A.152 :Run 51 Temp Profile
Injector to Producer Cross–Section
0.50 Pore Volumes Injected.

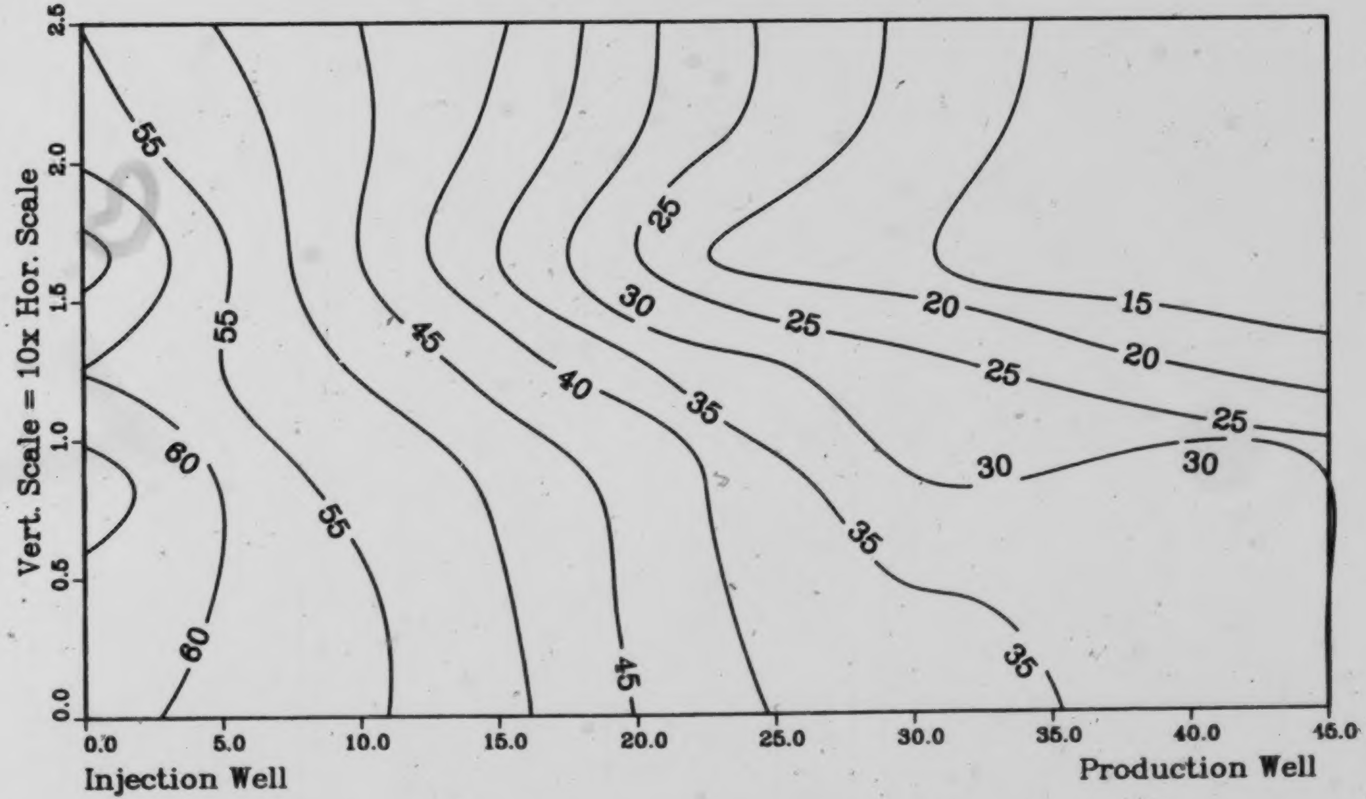

Figure A.153 :Run 51 Temp Profile
Injector to Producer Cross–Section
0.75 Pore Volumes Injected.

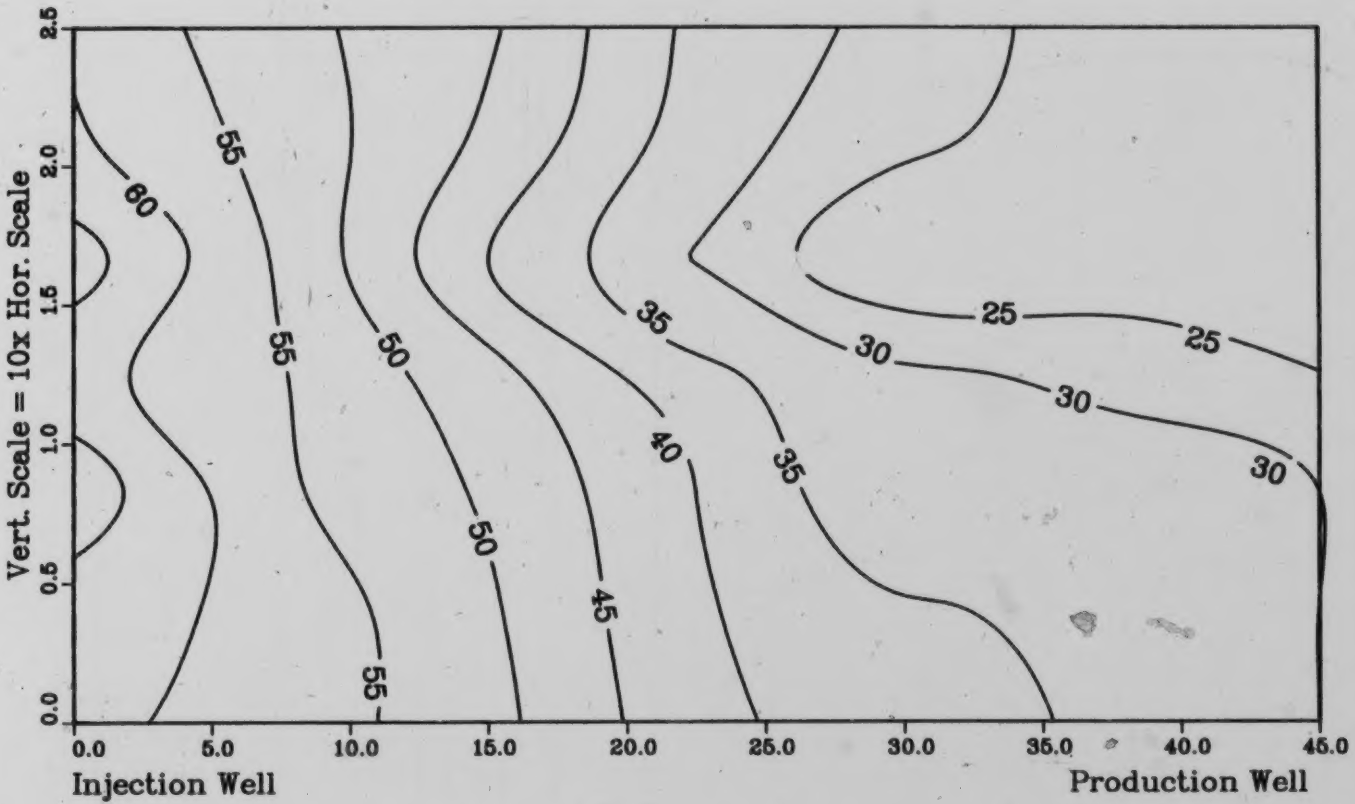

Figure A.154 :Run 51 Temp Profile
Injector to Producer Cross–Section

1.00 Pore Volumes Injected.

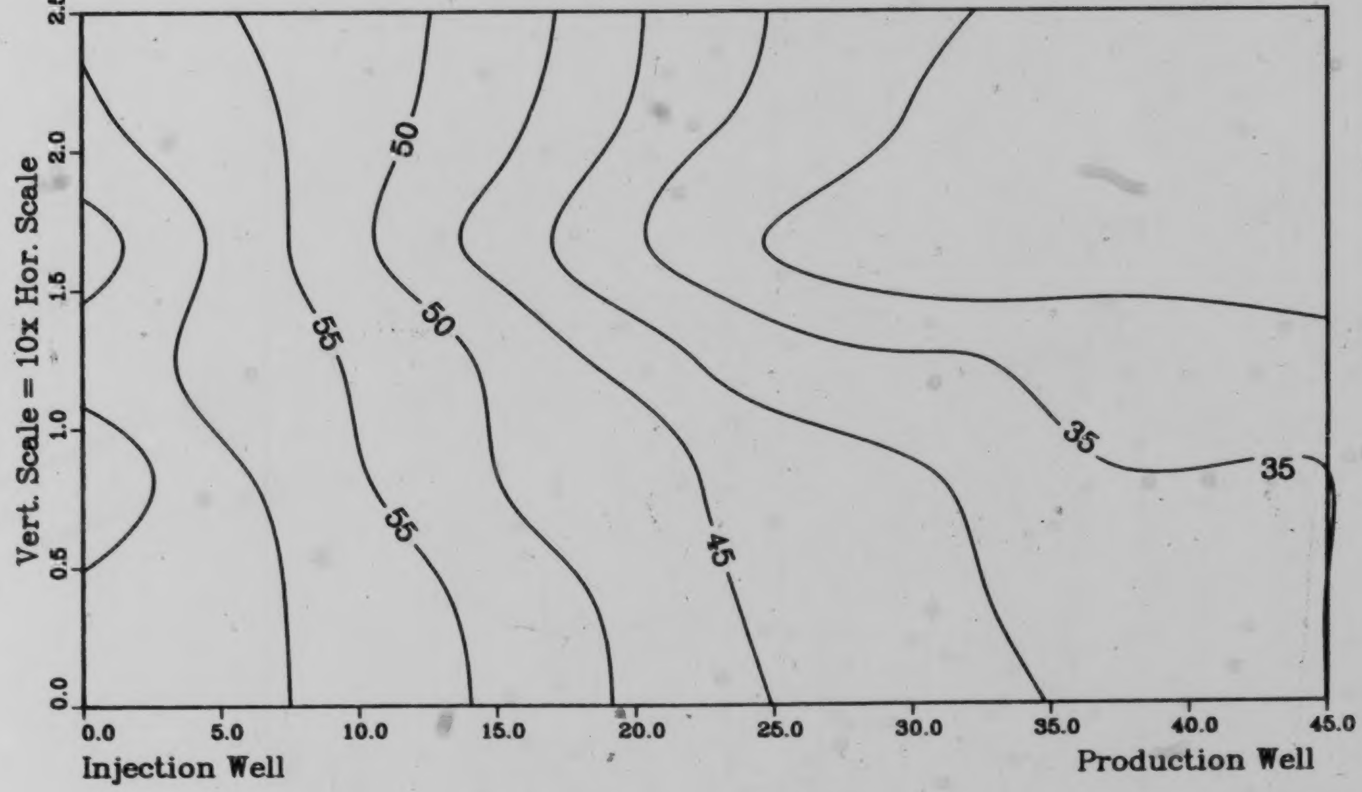

Figure A.155 : Run 53
Solvent–Steamflood in B.W. Model

Temperature Profile for 0.25 Pore Volumes Injected

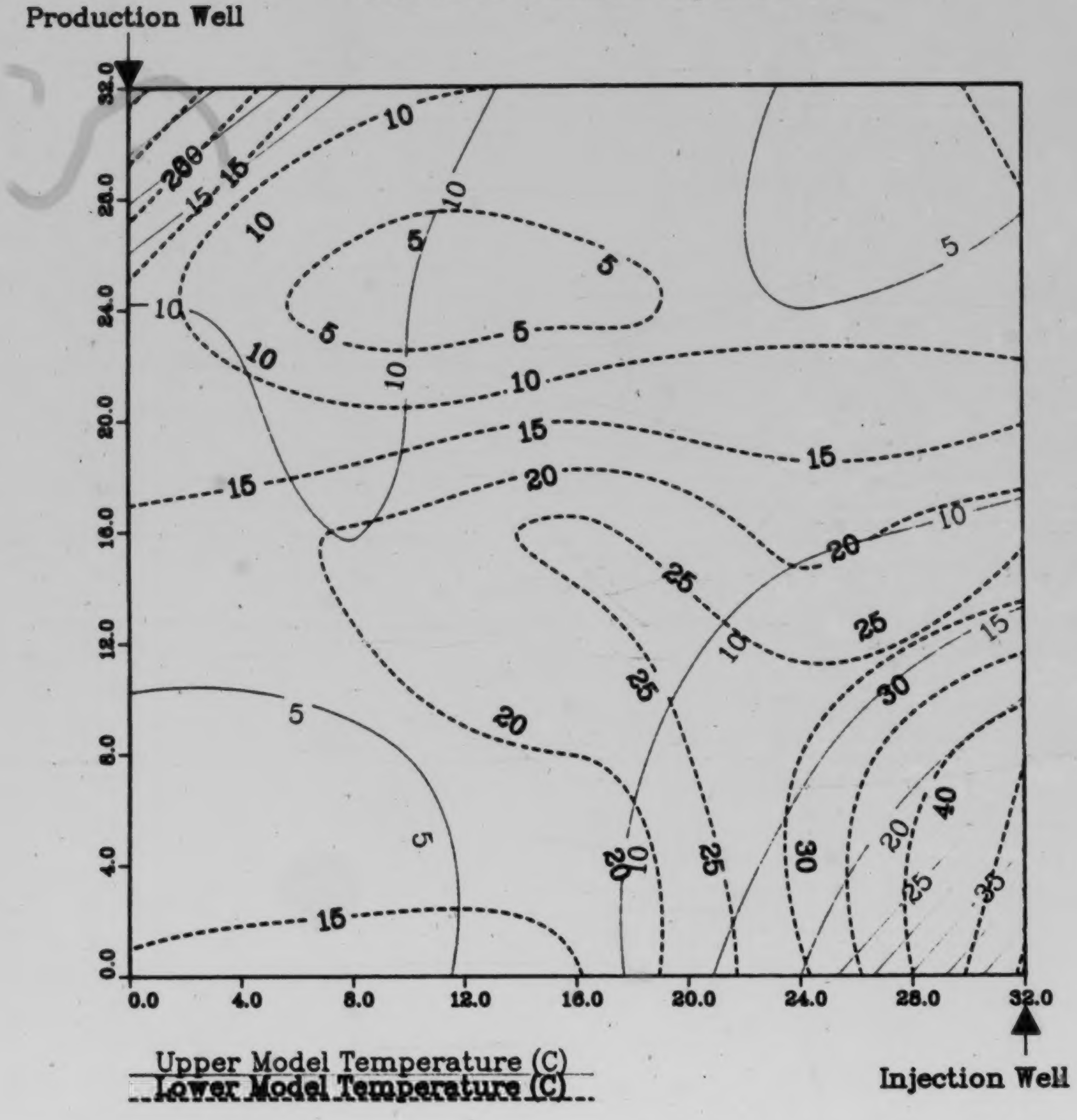

Figure A.156 : Run 53
Solvent–Steamflood in B.W. Model

Temperature Profile for
0.50 Pore Volumes Injected

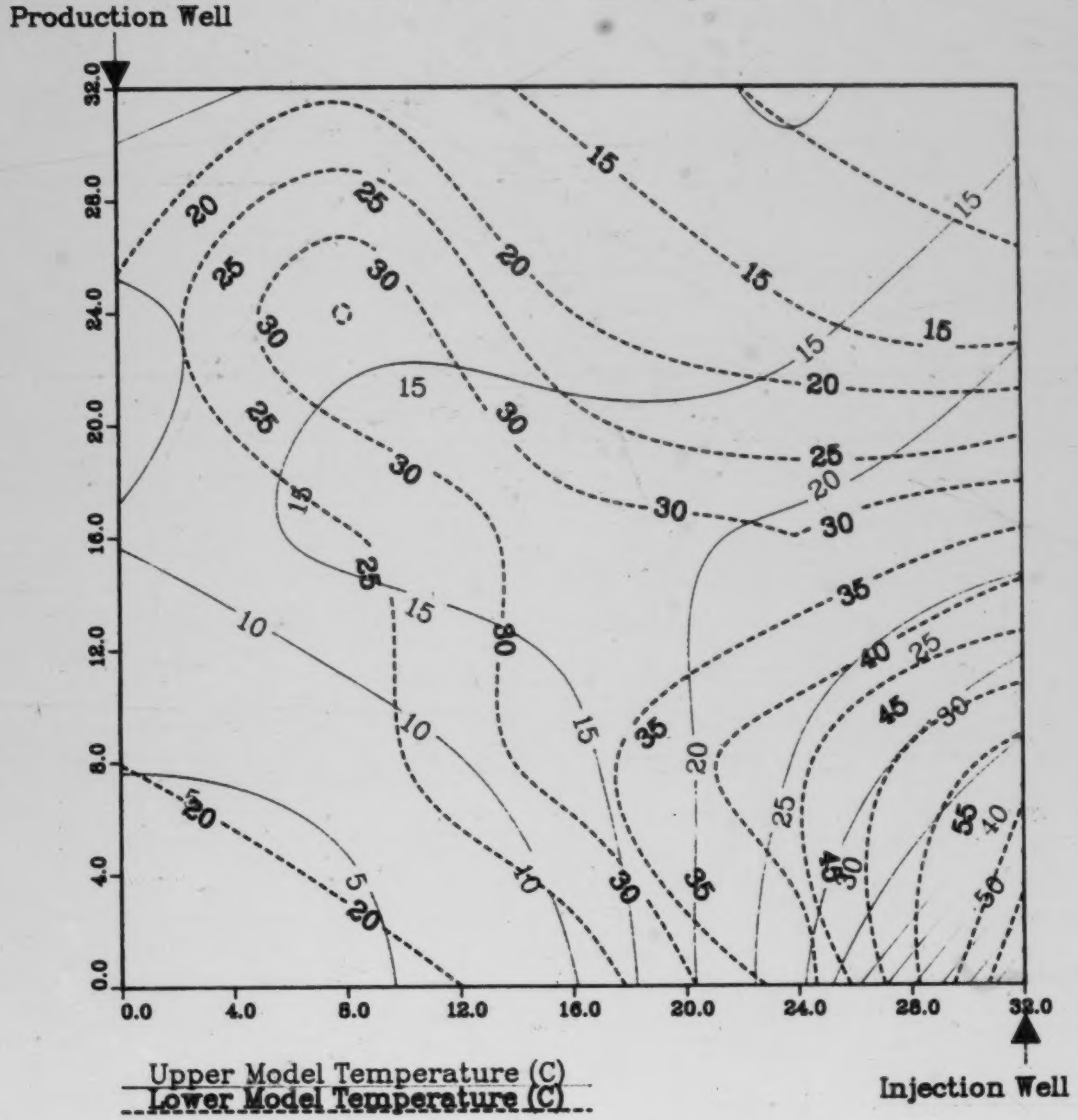

Figure A.157 : Run 53

Solvent–Steamflood in B.W. Model

Temperature Profile for 0.75 Pore Volumes Injected

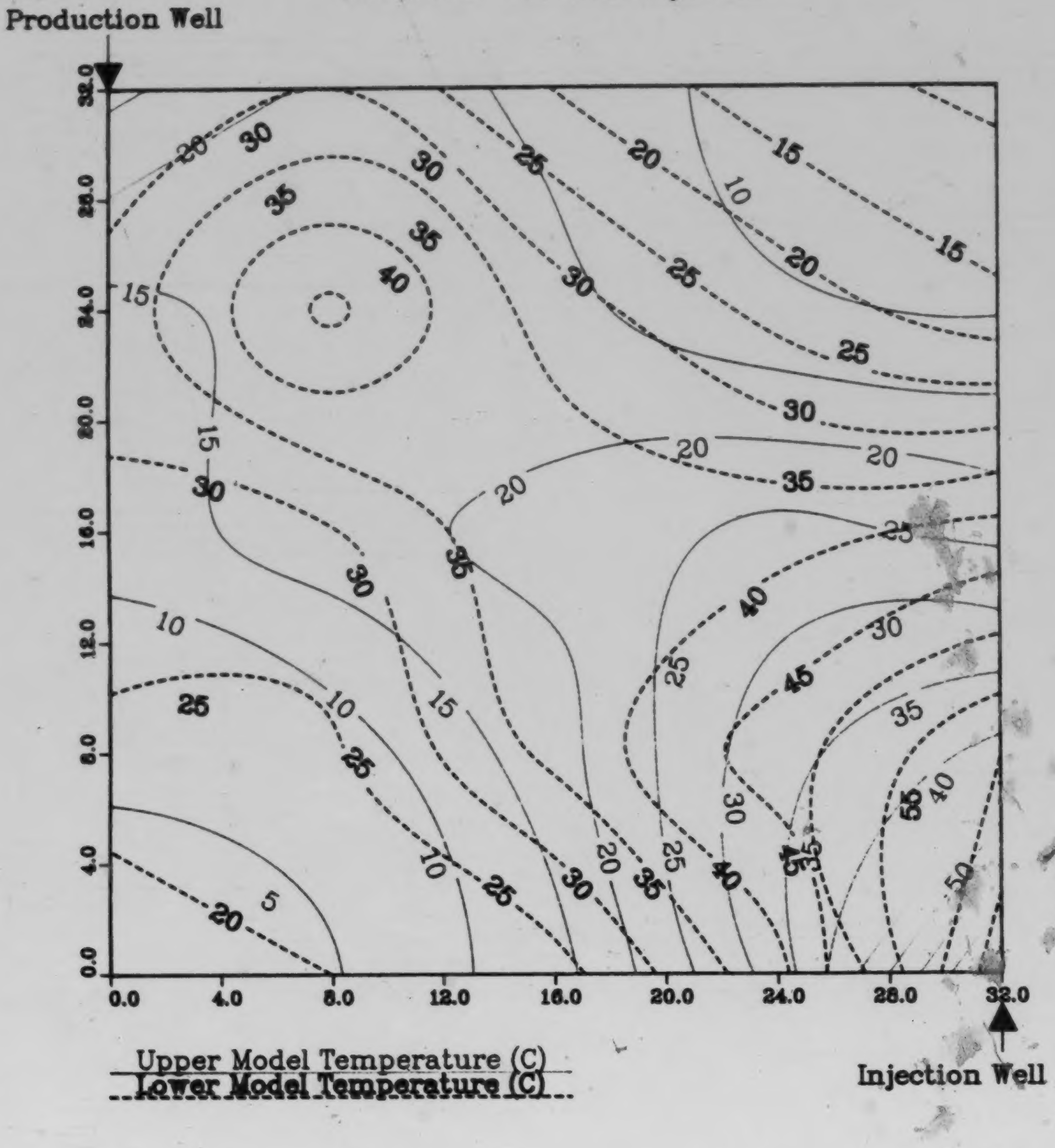

Figure A.158 : Run 53

Solvent–Steamflood in B.W. Model

Temperature Profile for 1.00 Pore Volumes Injected

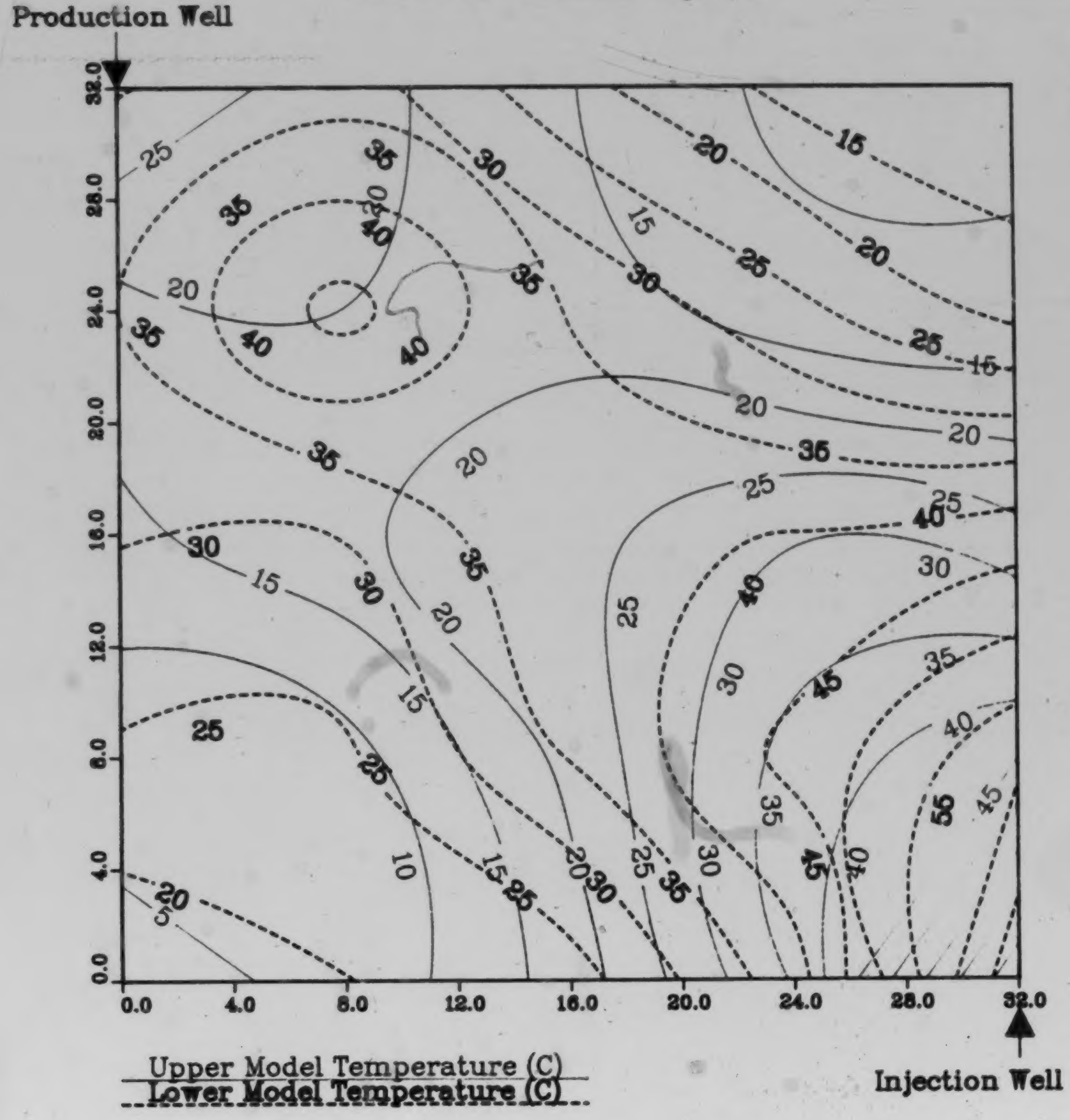

Figure A.159 : Run 53

Solvent--Steamflood in B.W. Model

Temperature Profile for
1.25 Pore Volumes Injected

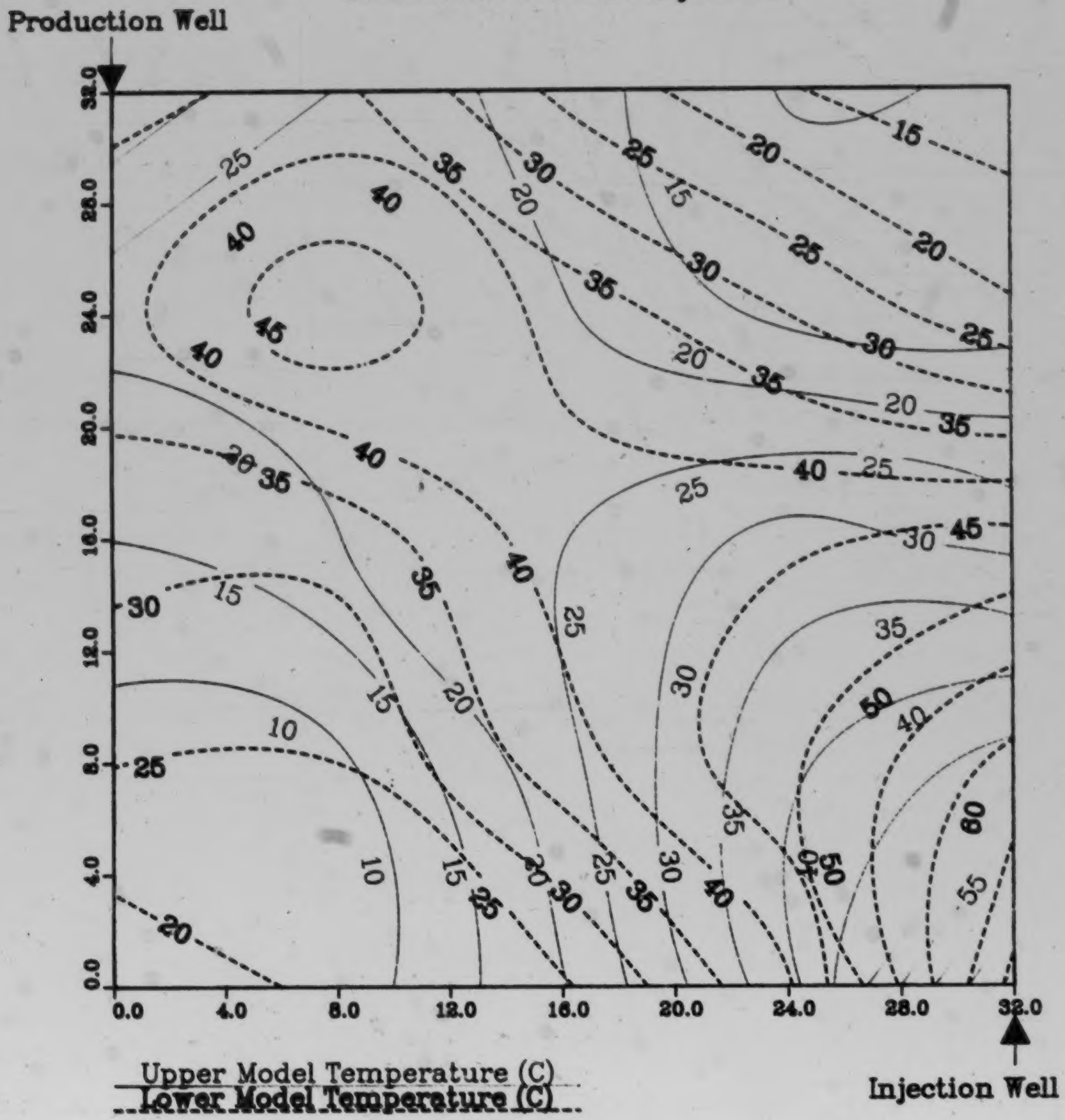

Figure A.160 : Run 53

Solvent–Steamflood in B.W. Model

Temperature Profile for 1.50 Pore Volumes Injected

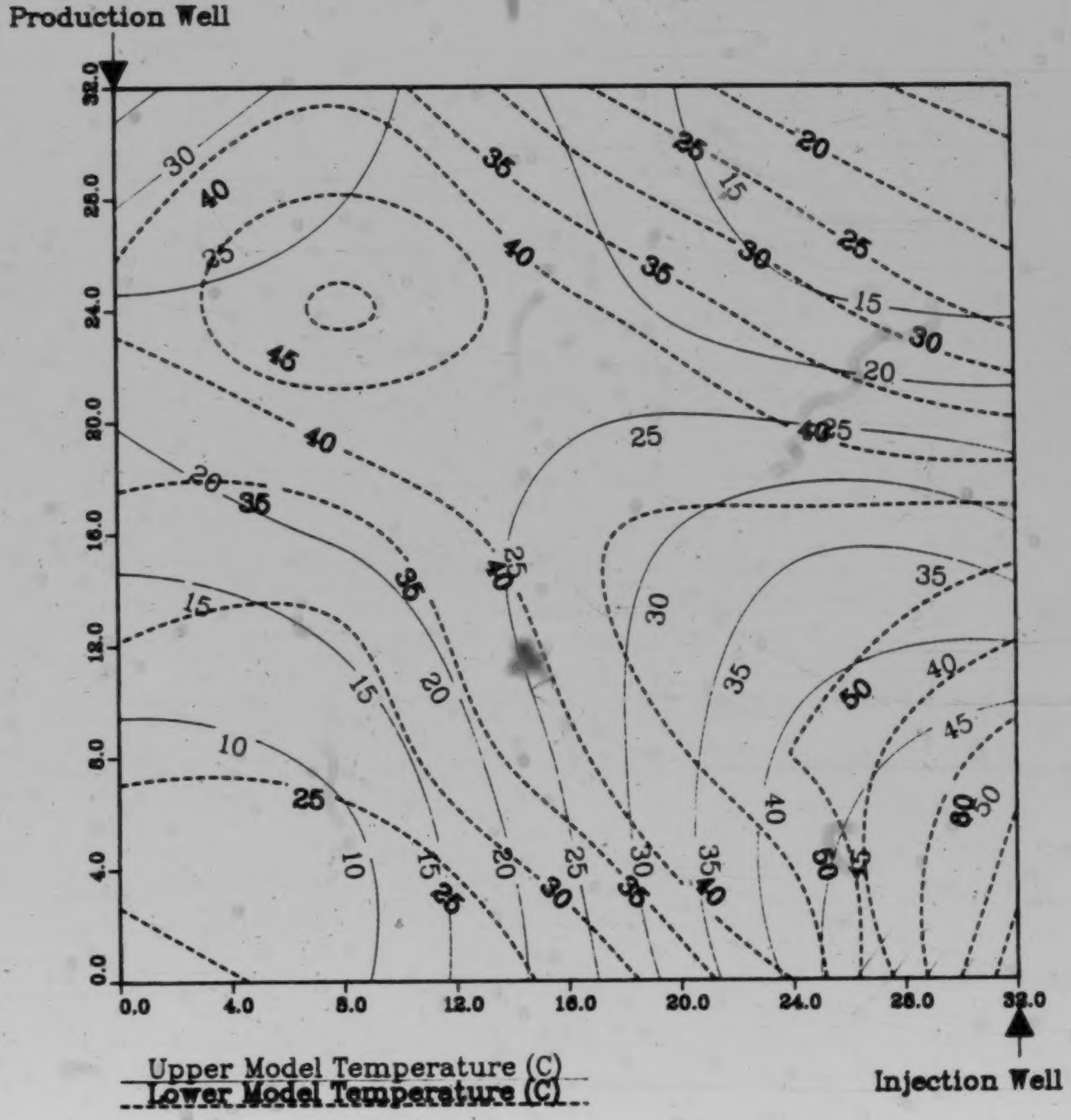

Figure A.161 : Run 53

Solvent–Steamflood in B.W. Model

Temperature Profile for 1.75 Pore Volumes Injected

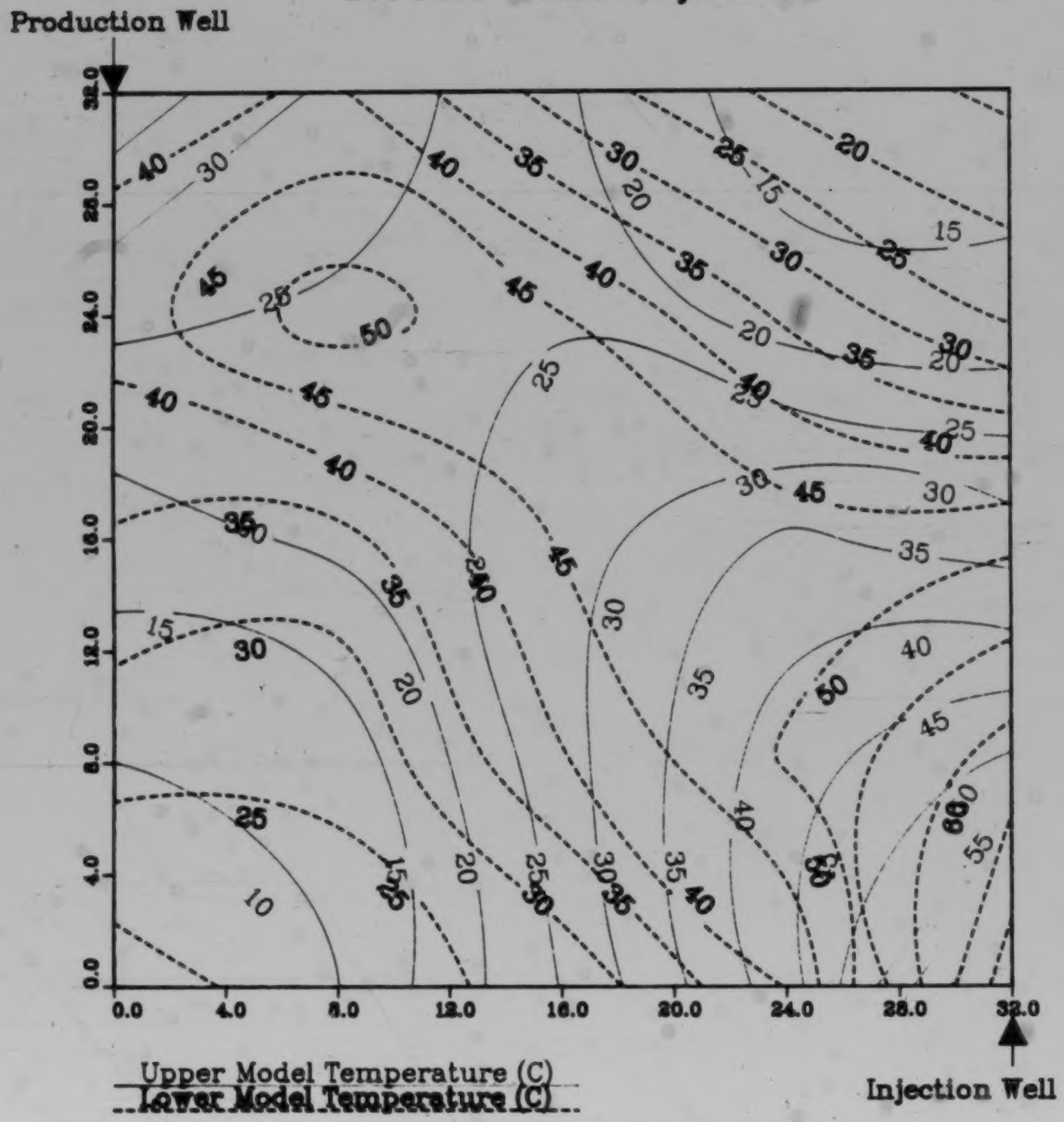

Figure A.162 : Run 53

Solvent–Steamflood in B.W. Model

Temperature Profile for 2.00 Pore Volumes Injected

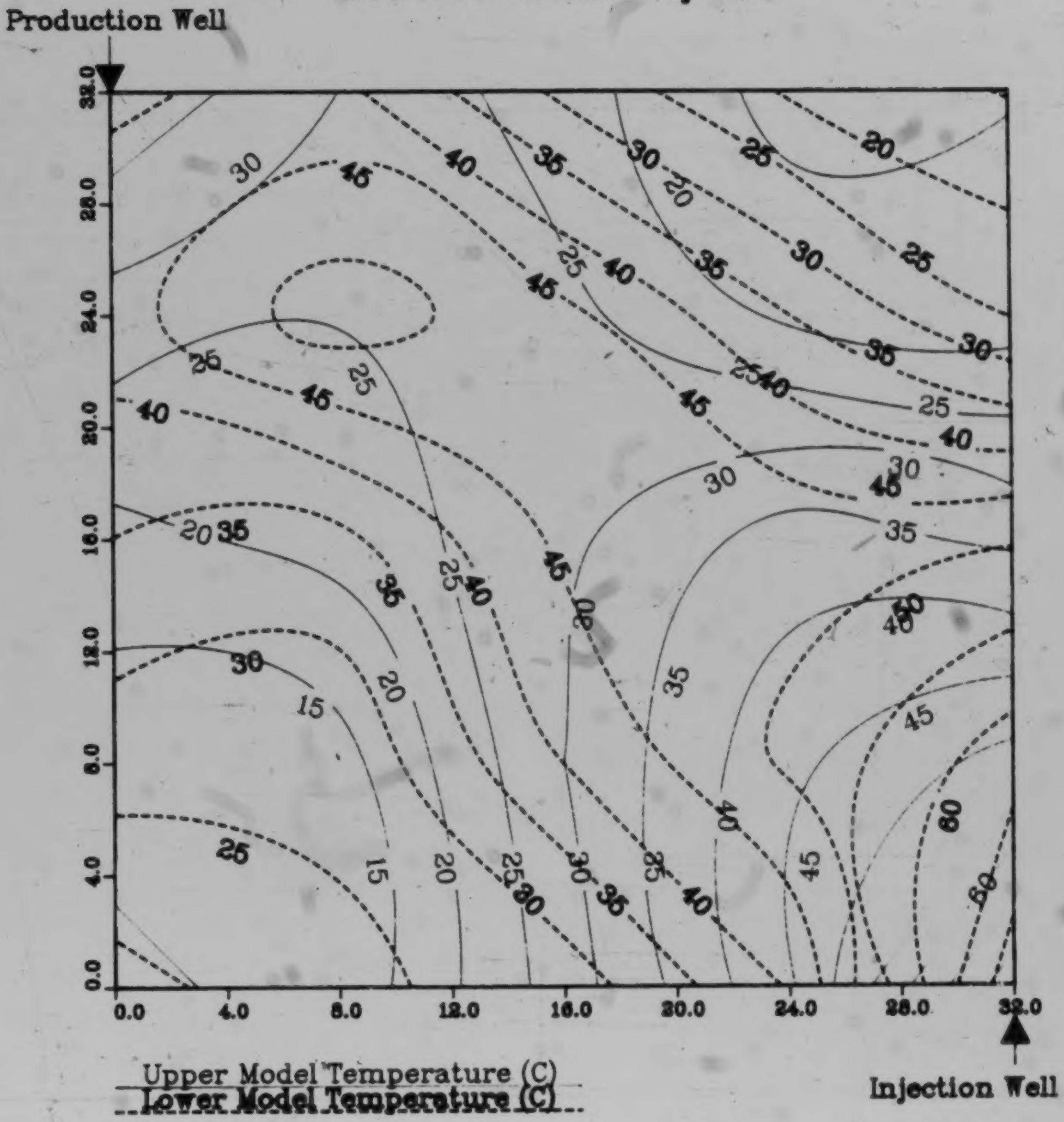

Figure A.163 :Run 53 Temp Profile
Injector to Producer Cross–Section
0.25 Pore Volumes Injected.

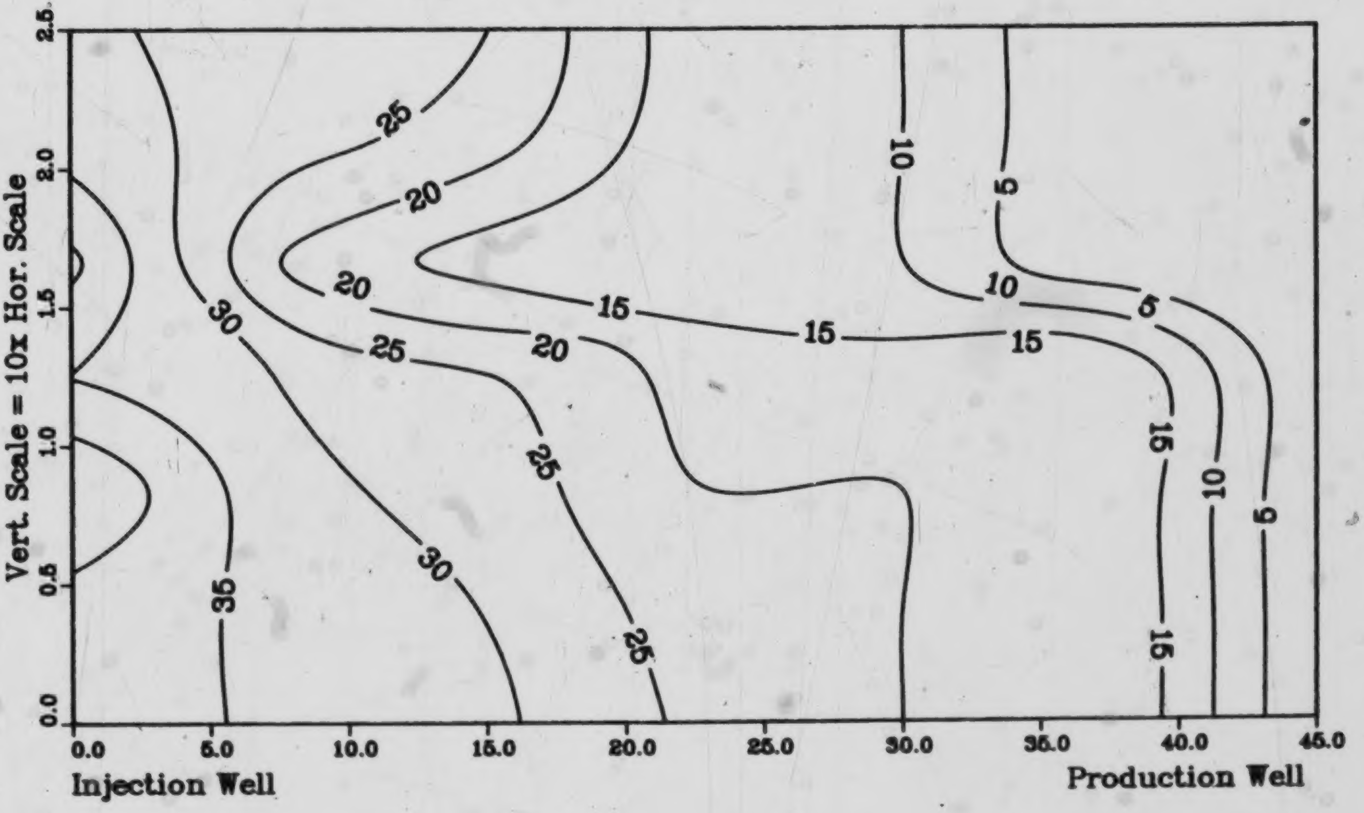

Figure A.164 :Run 53 Temp Profile
Injector to Producer Cross–Section
0.50 Pore Volumes Injected.

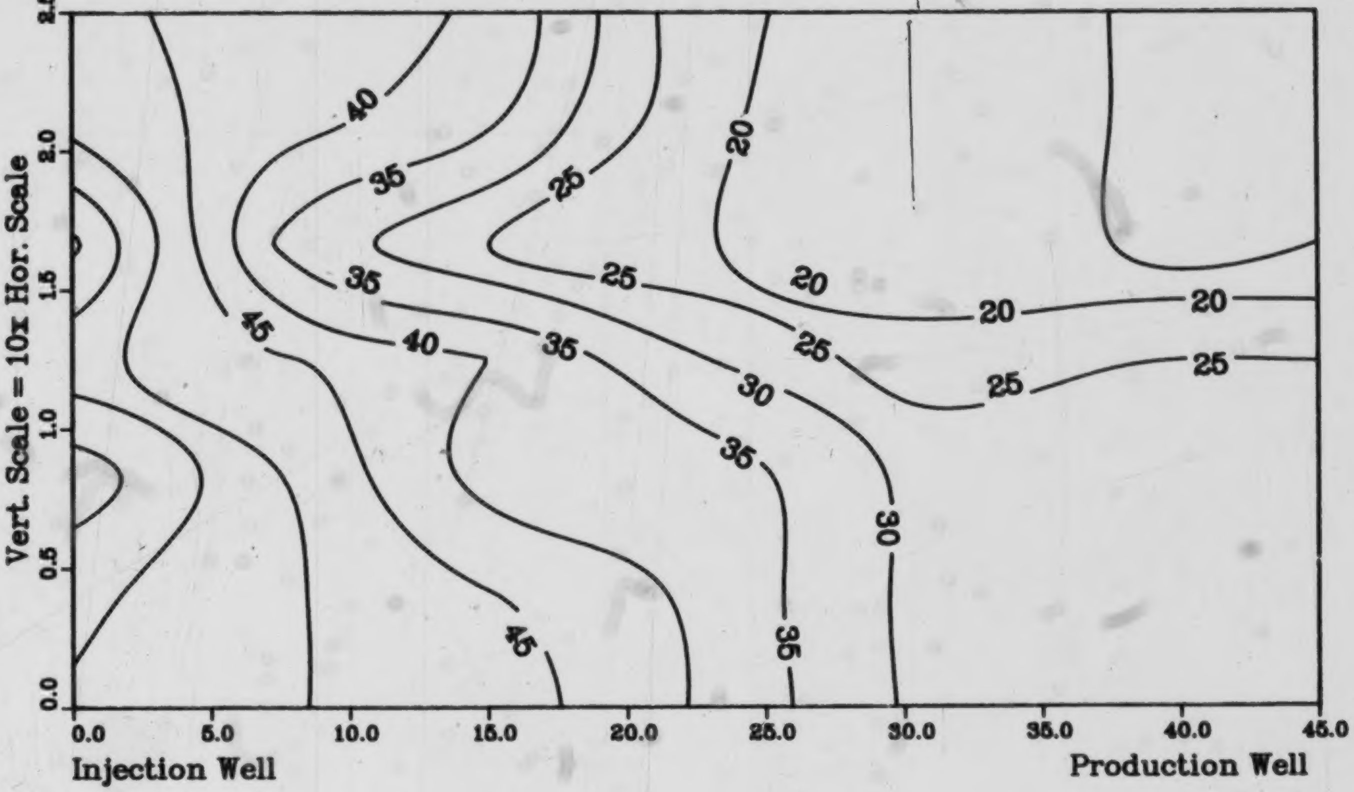

Figure A.165 :Run 53 Temp Profile
Injector to Producer Cross–Section
0.75 Pore Volumes Injected.

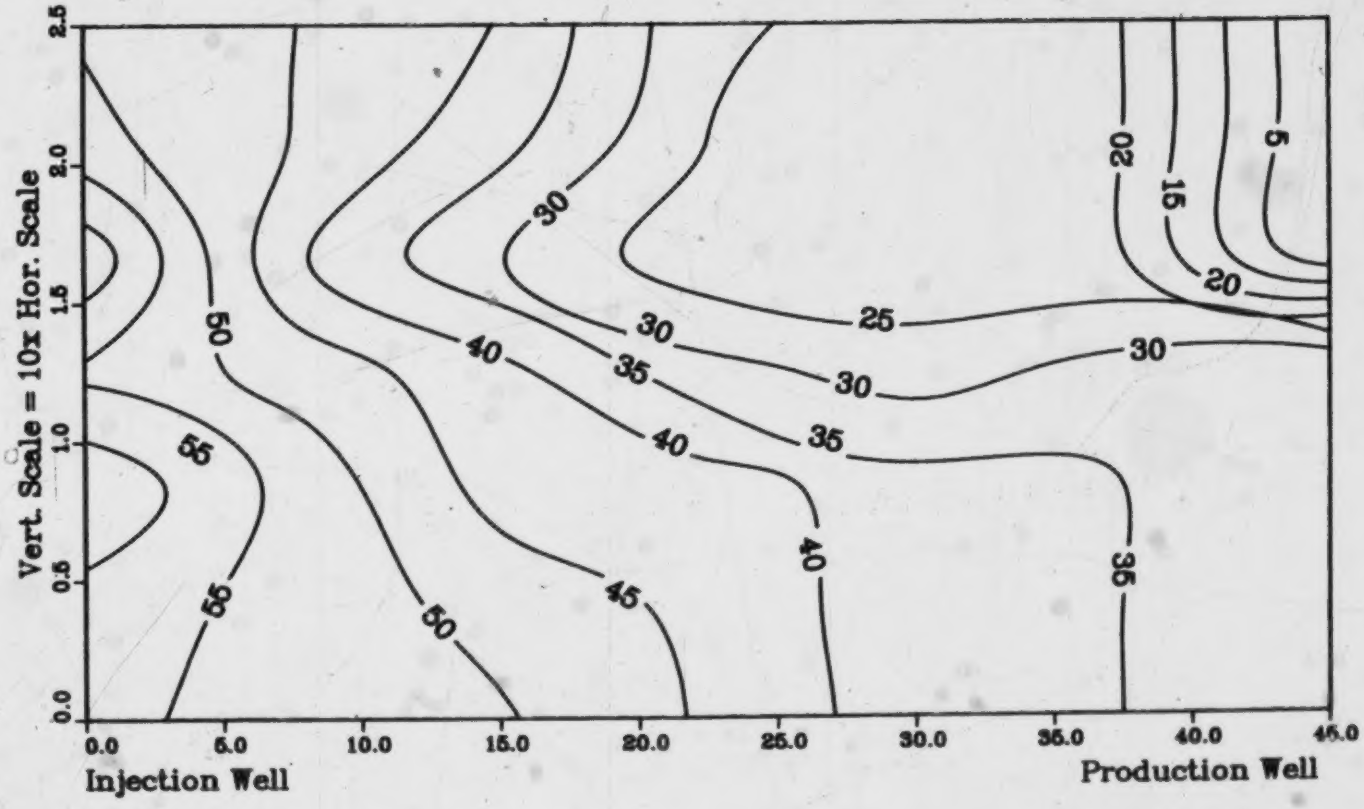

Figure A.166 :Run 53 Temp Profile
Injector to Producer Cross–Section
1.00 Pore Volumes Injected.

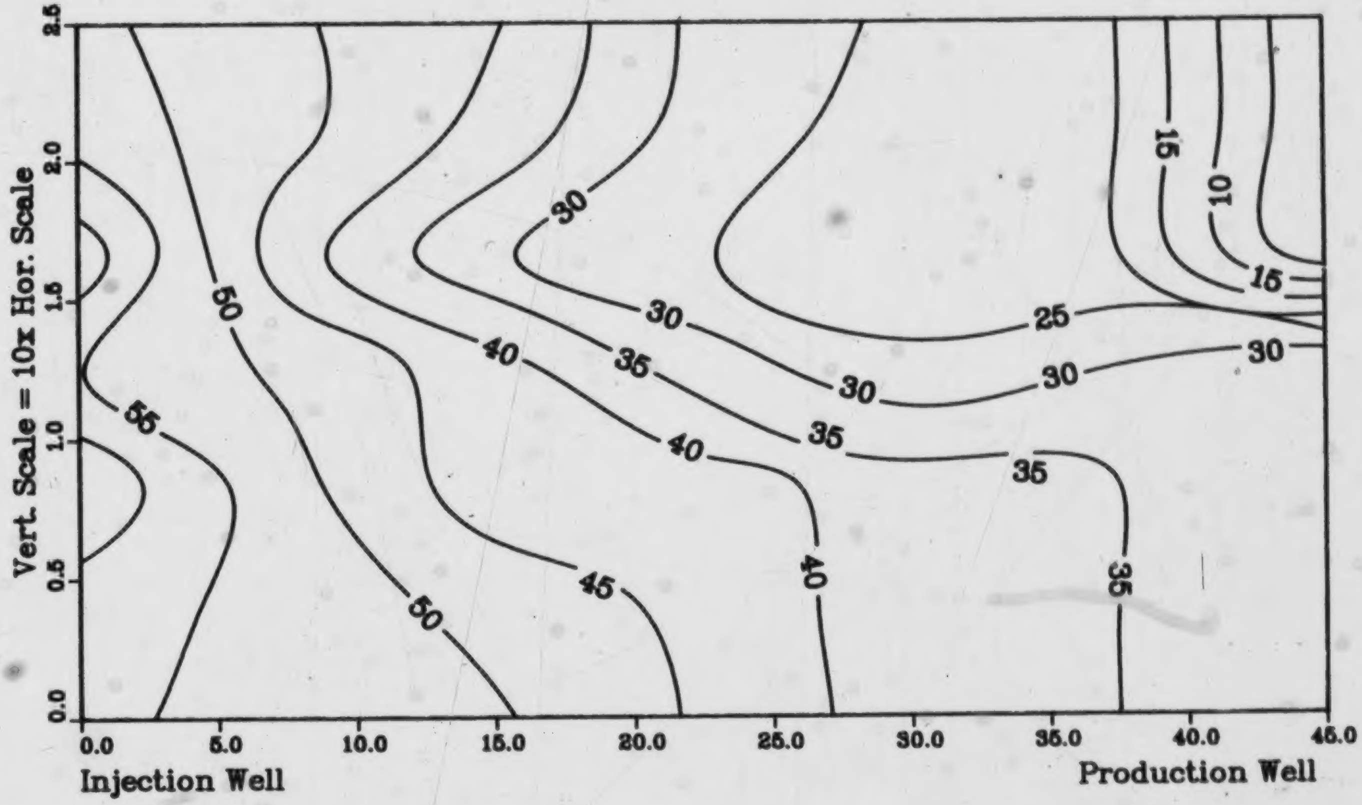

/

Figure A.167 : Run 54
Solvent–Steamflood in B.W. Model

Temperature Profile for
0.25 Pore Volumes Injected

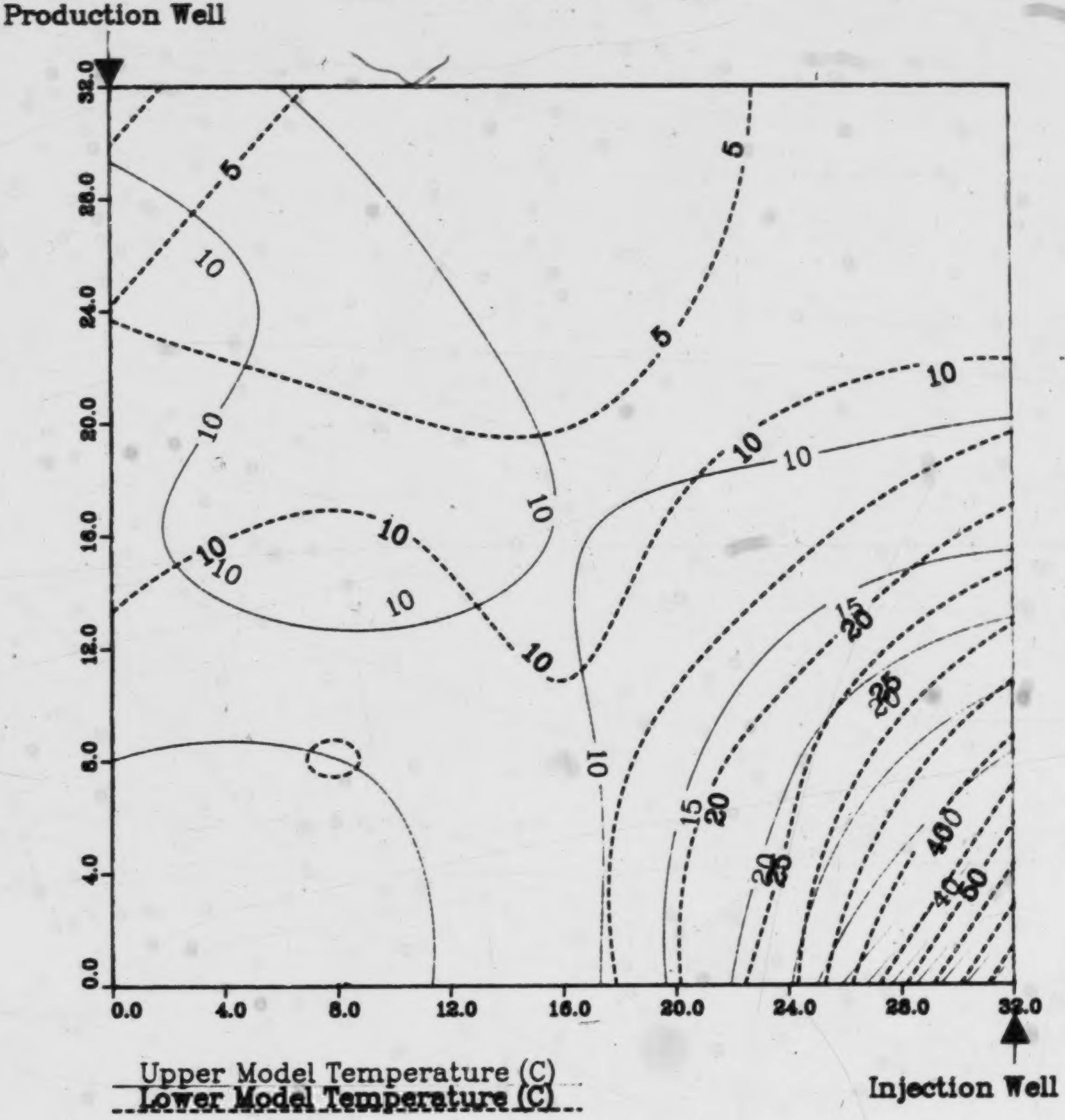

Figure A.168 : Run 54

Solvent–Steamflood in B.W. Model

Temperature Profile for 0.50 Pore Volumes Injected

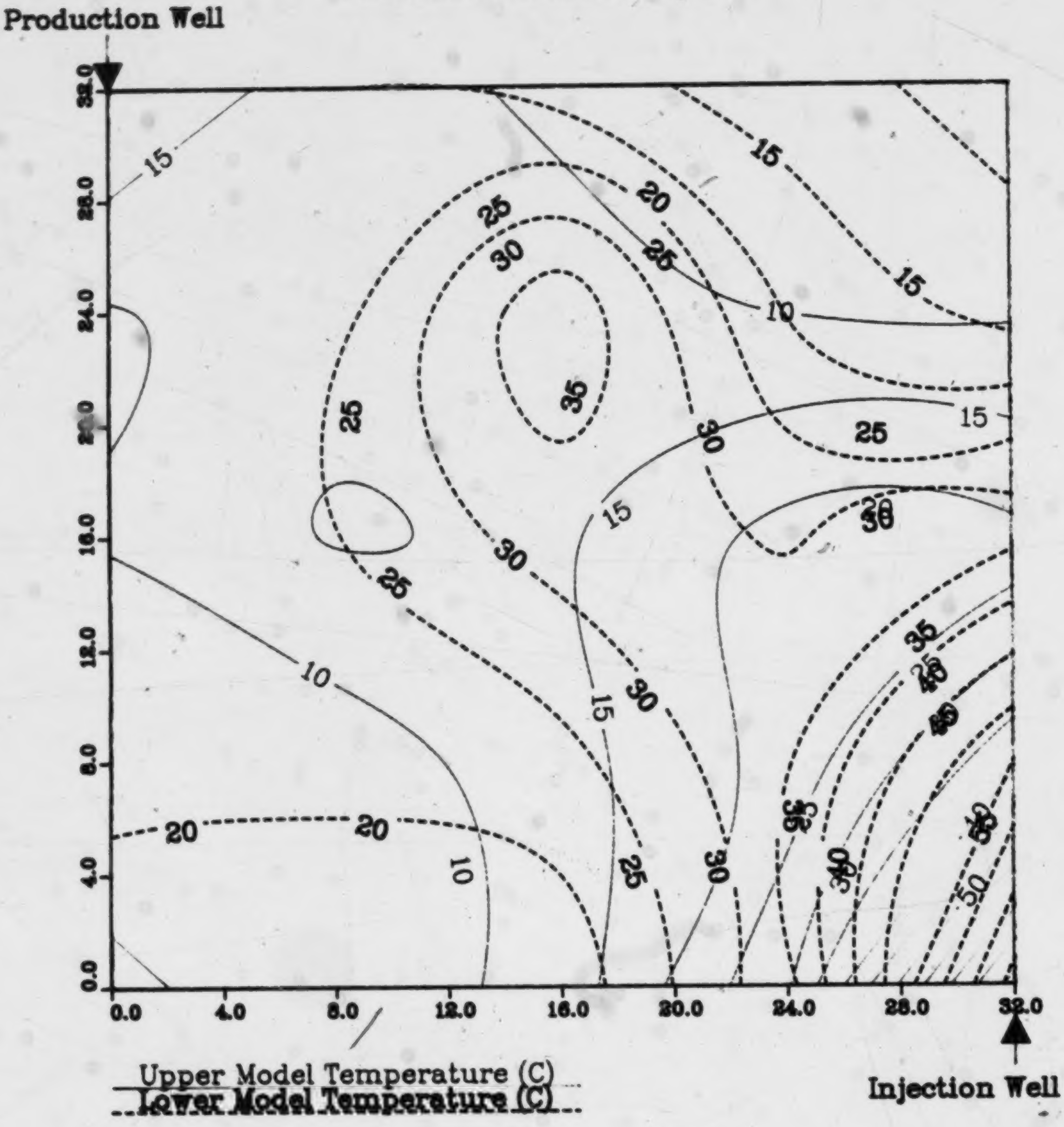

Figure A.169 : Run 54

Solvent–Steamflood in B.W. Model

Temperature Profile for 0.75 Pore Volumes Injected

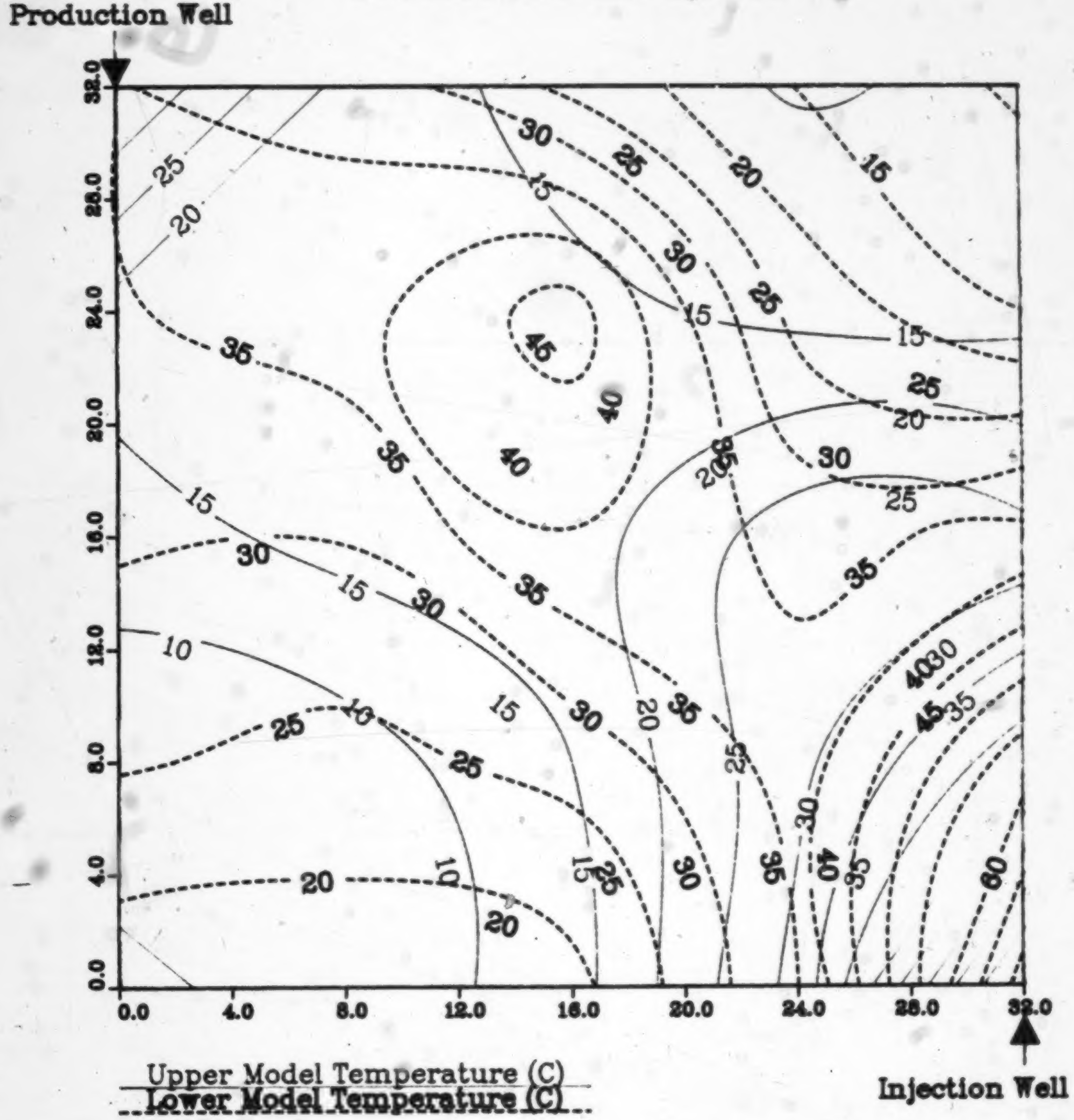

Figure A.170 : Run 54
Solvent–Steamflood in B.W. Model

Temperature Profile for
1.00 Pore Volumes Injected

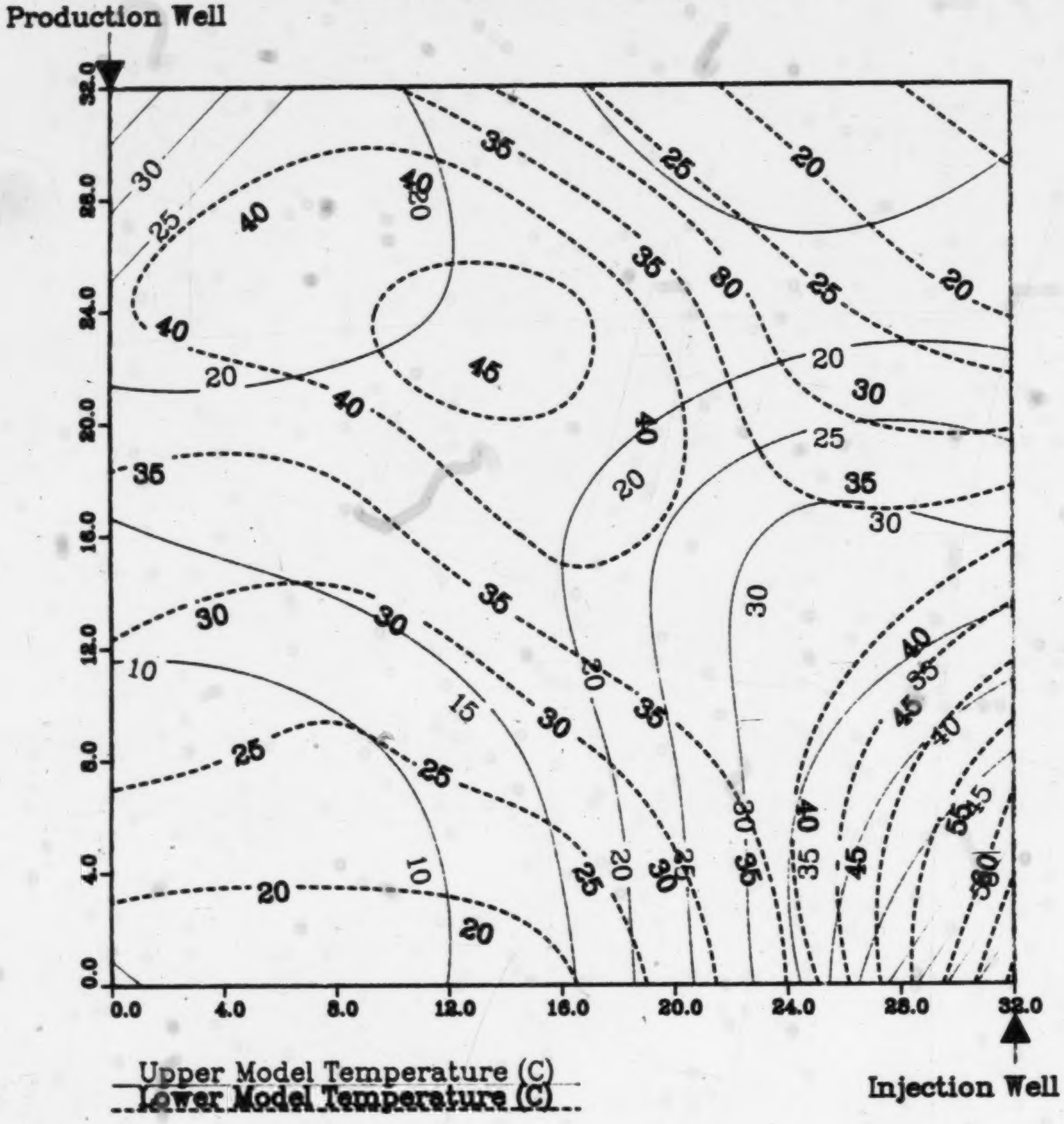

Figure A.171 : Run 54
Solvent–Steamflood in B.W. Model

Temperature Profile for
1.25 Pore Volumes Injected

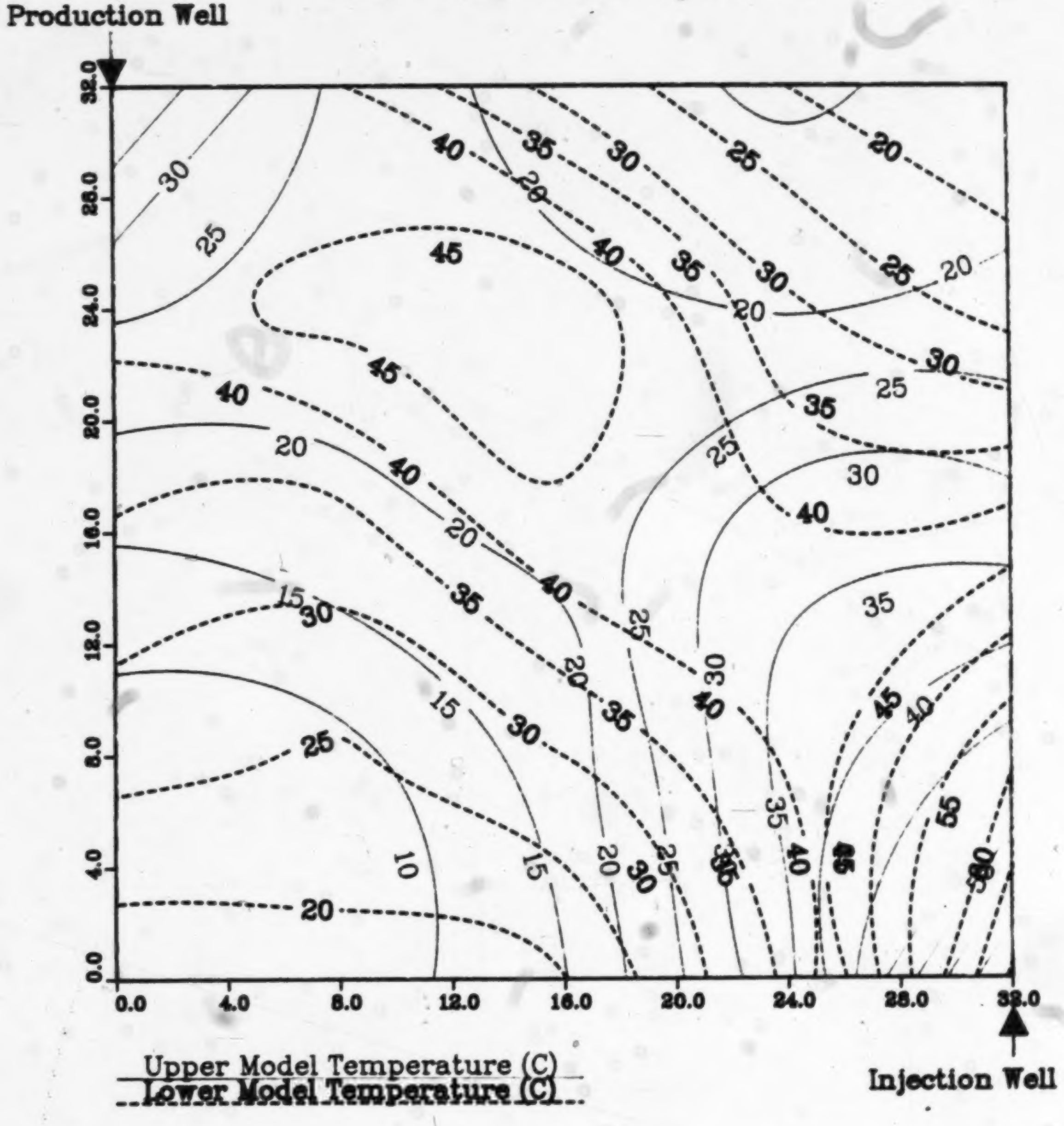

Figure A.172 : Run 54

Solvent–Steamflood in B.W. Model

Temperature Profile for 1.50 Pore Volumes Injected

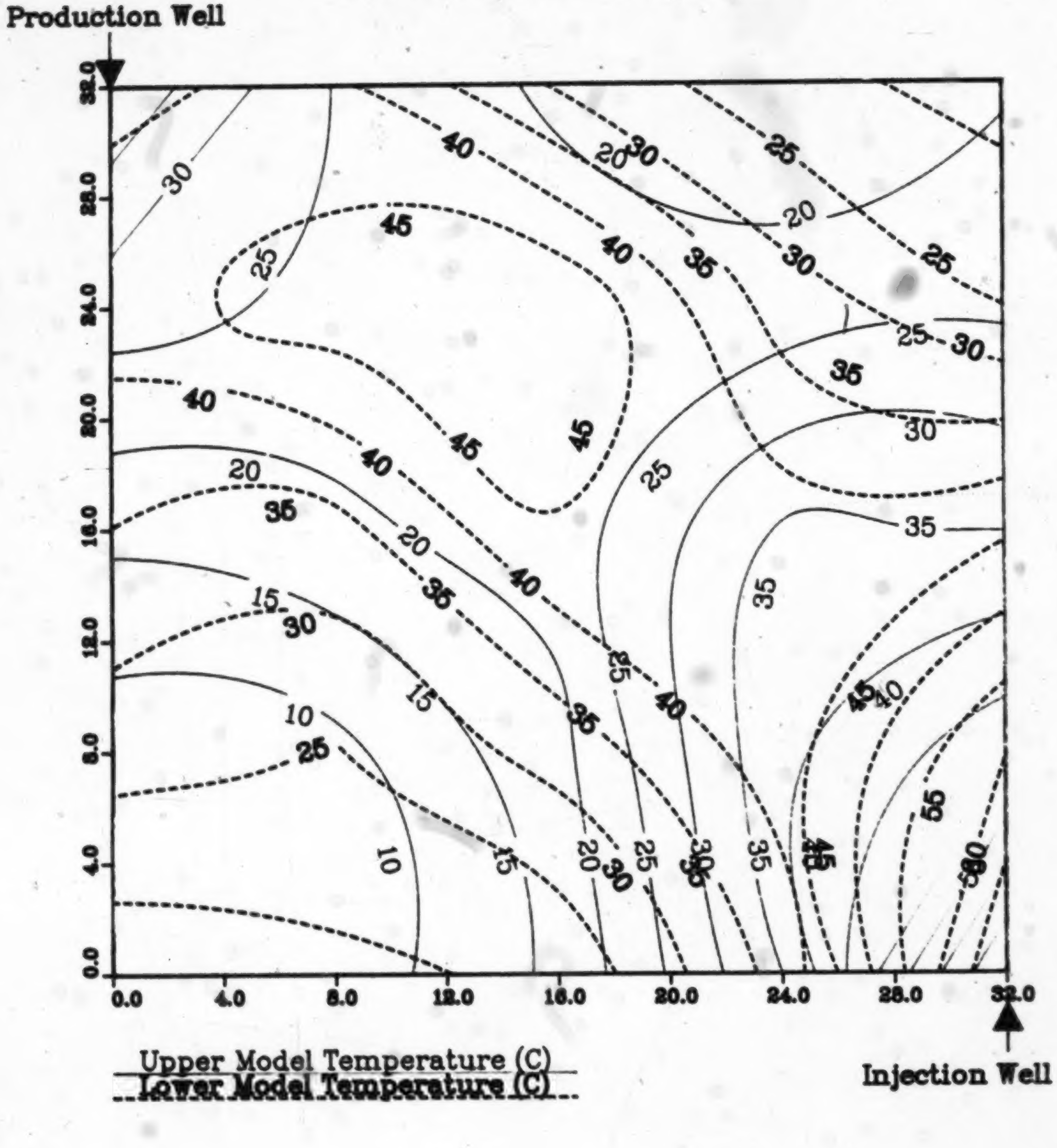

Figure A.173 : Run 54
Solvent–Steamflood in B.W. Model

Temperature Profile for
1.75 Pore Volumes Injected

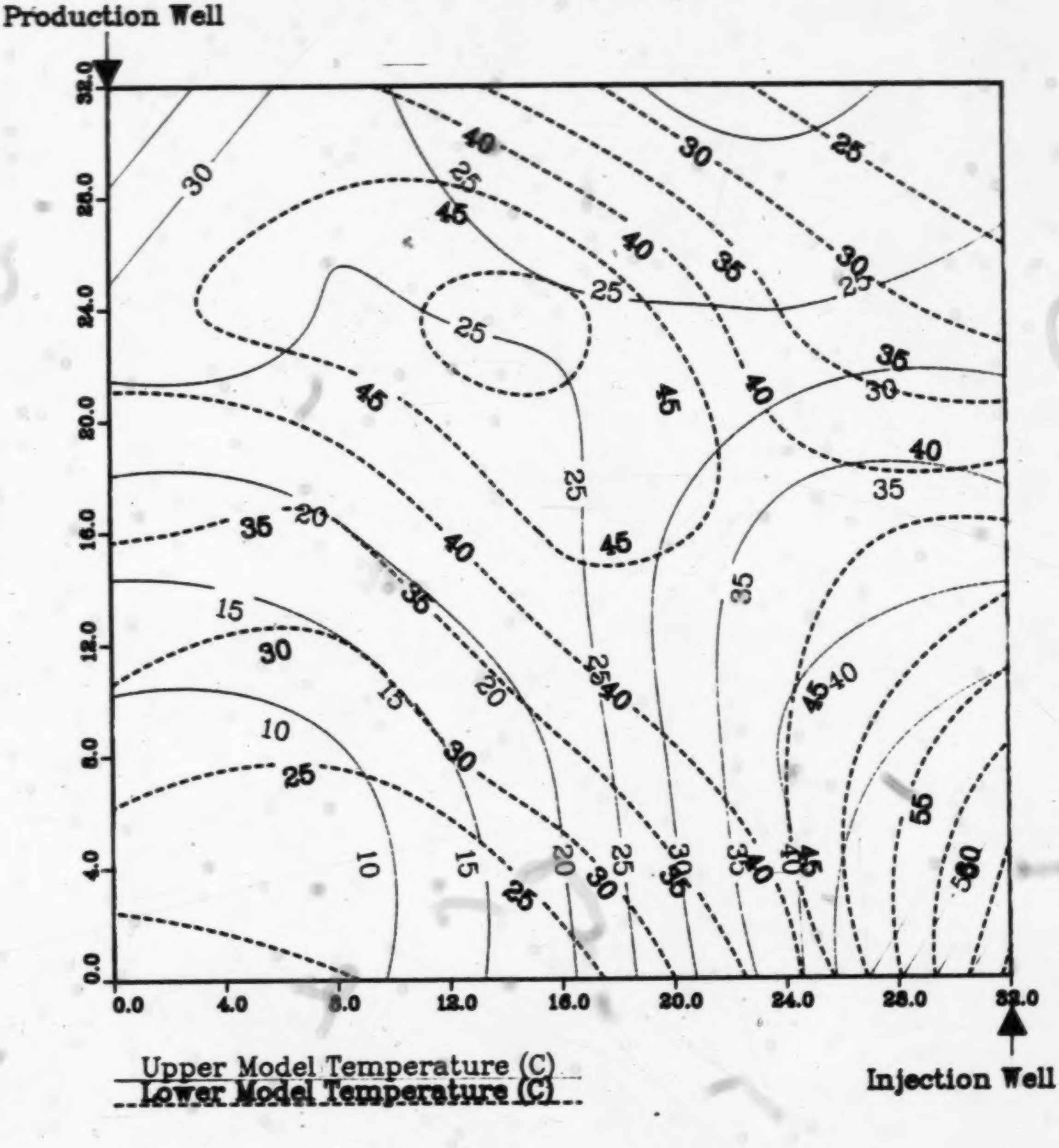

Figure A.174 : Run 54

Solvent–Steamflood in B.W. Model

Temperature Profile for 2.00 Pore Volumes Injected

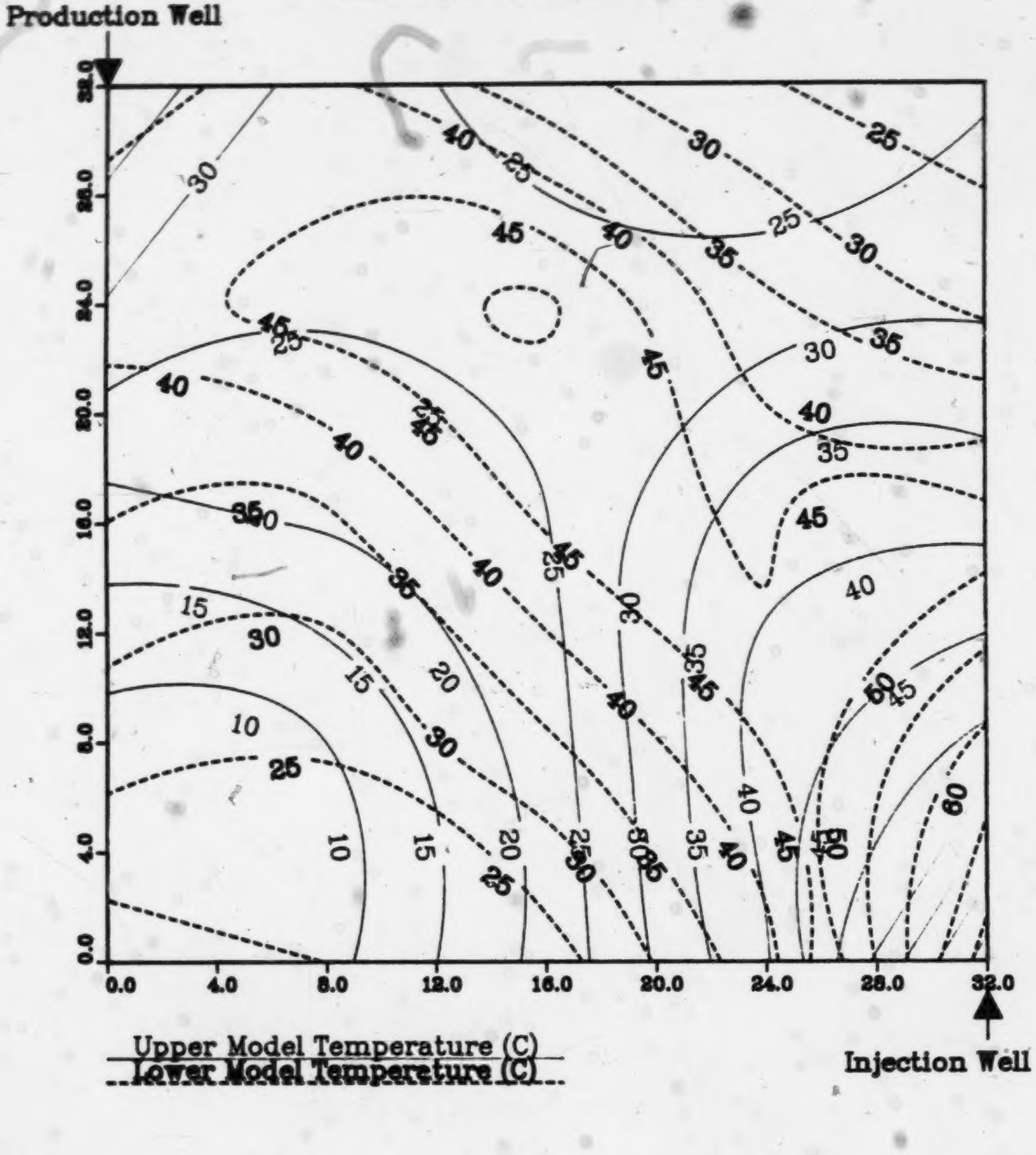

Figure A.175 :Run 54 Temp Profile
Injector to Producer Cross-Section
0.25 Pore Volumes Injected.

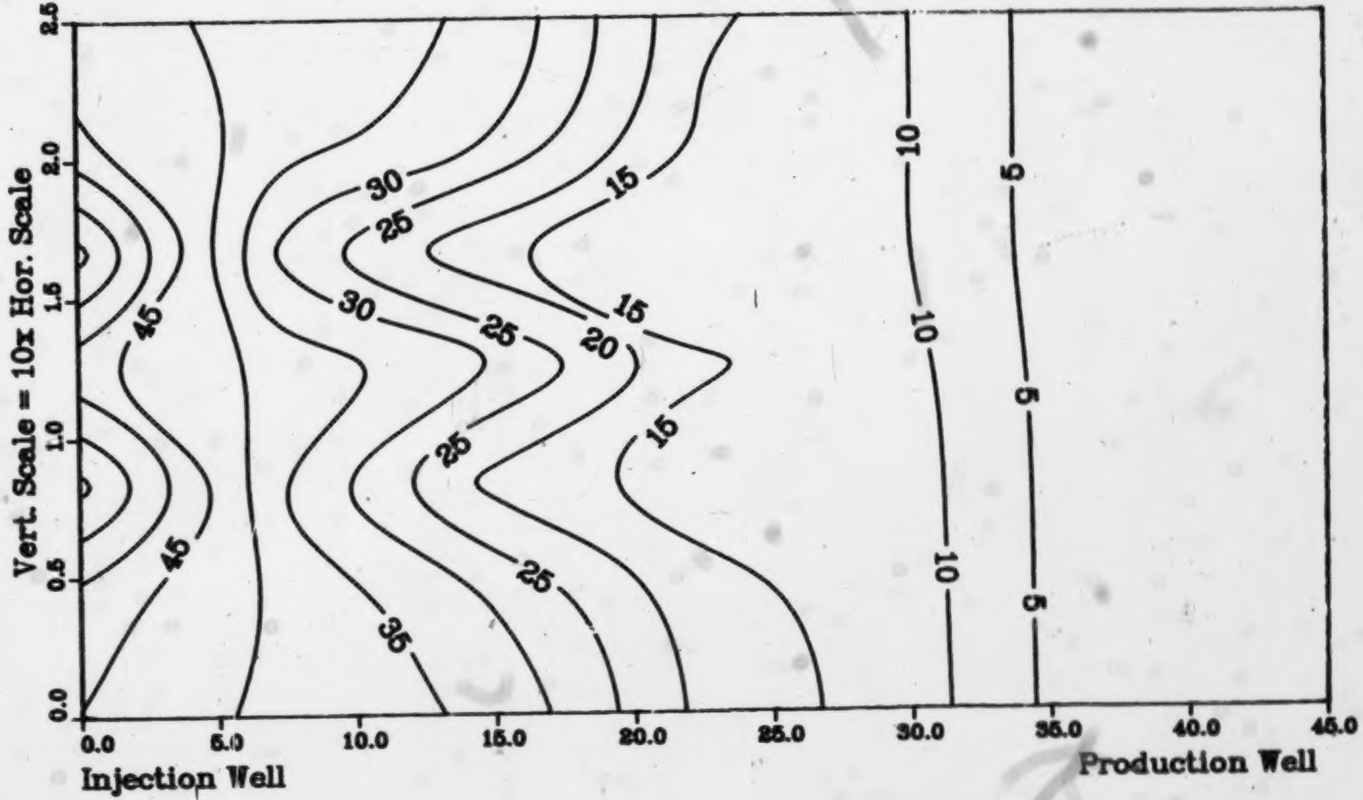

Figure A.176 :Run 54 Temp Profile
Injector to Producer Cross–Section
0.50 Pore Volumes Injected.

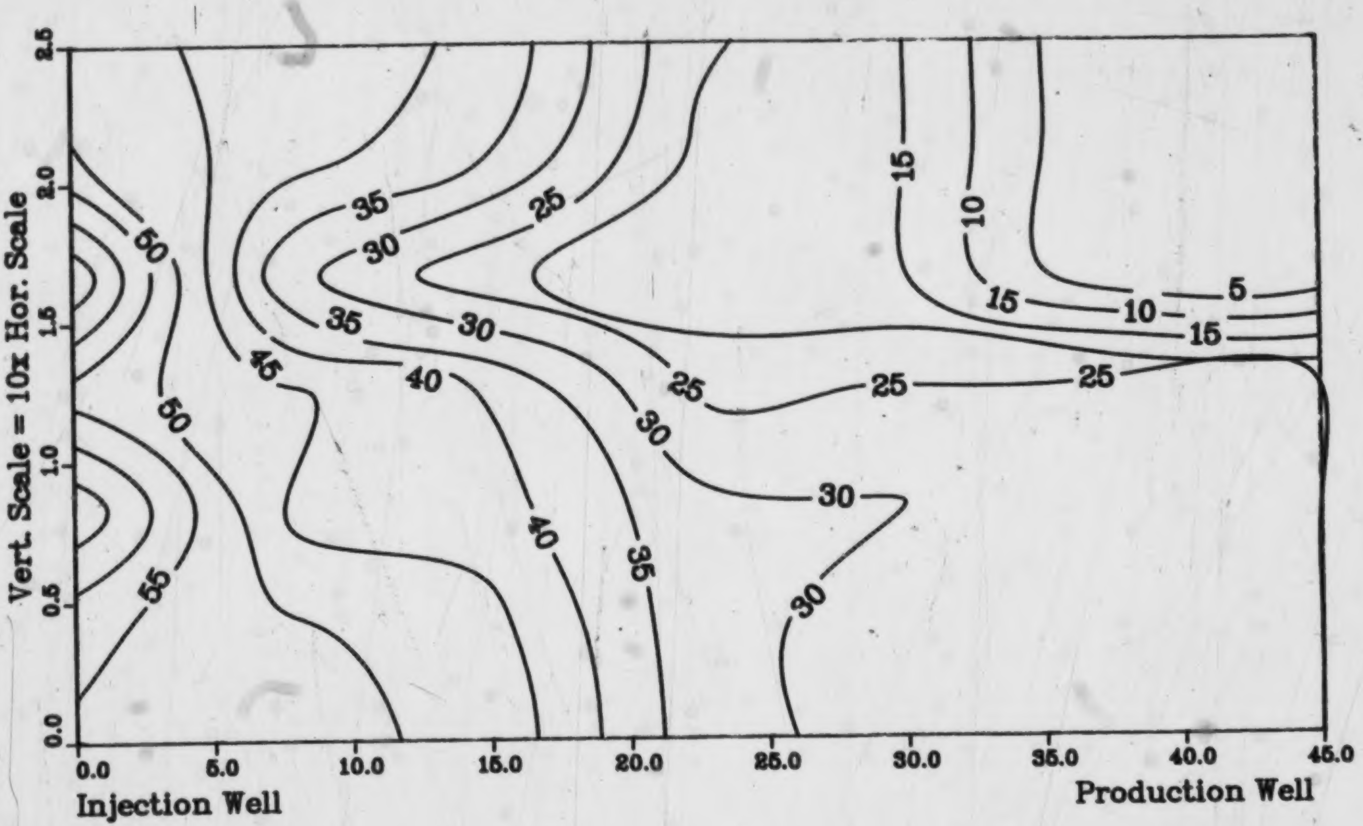

Figure A.177 :Run 54 Temp Profile
Injector to Producer Cross–Section
0.75 Pore Volumes Injected.

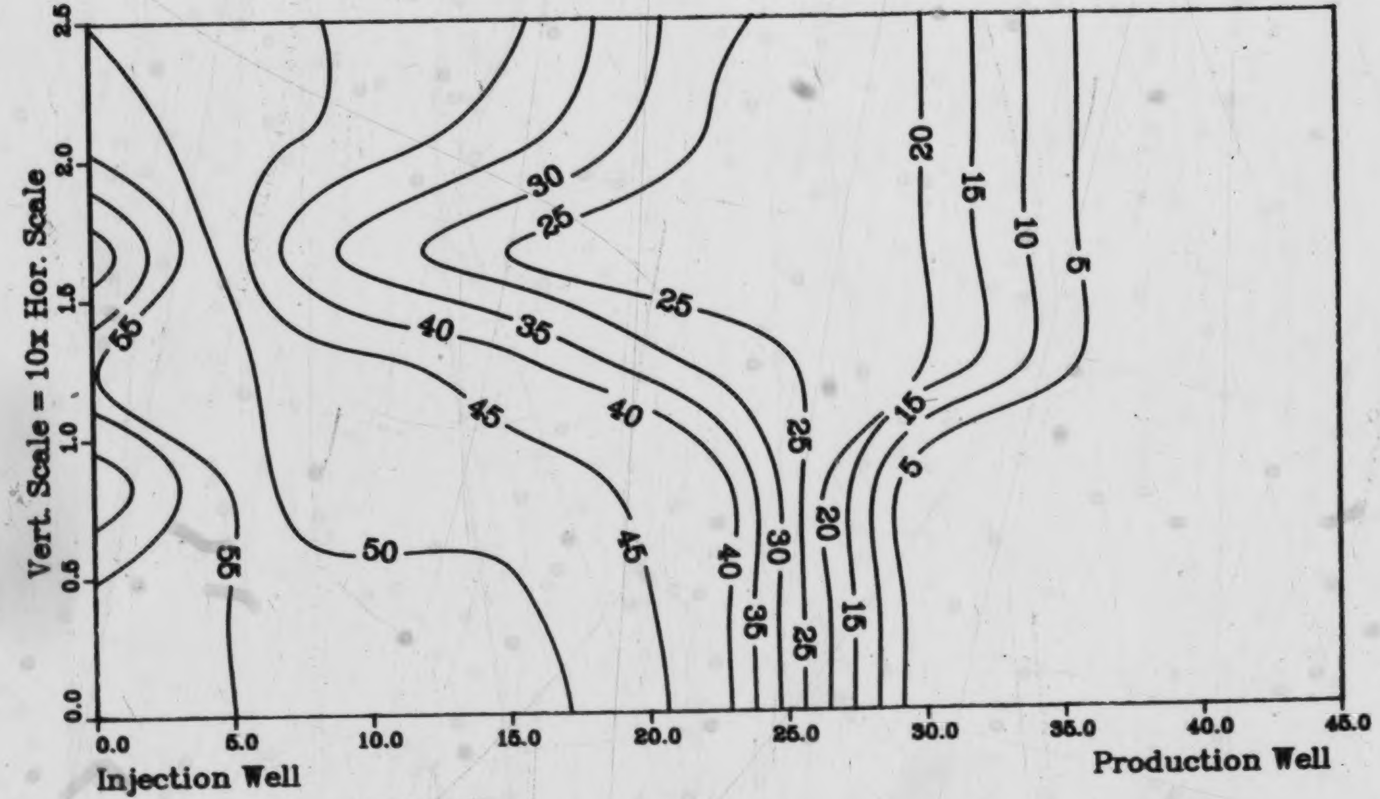

Figure A.178 :Run 54 Temp Profile
Injector to Producer Cross-Section
1.00 Pore Volumes Injected.

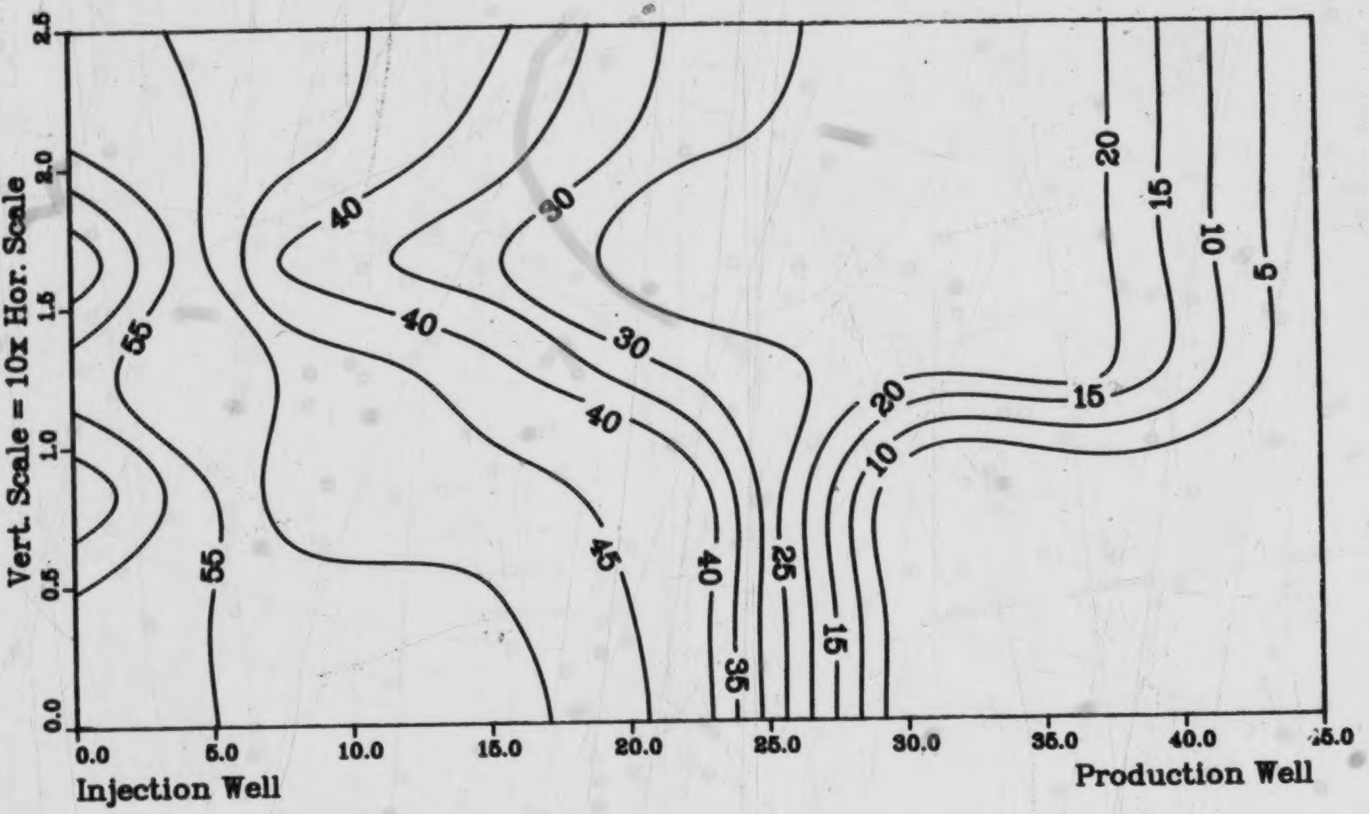

Figure A.179 : Run 55

Gas Inj. Solv.–Stmflood in Homo. Model

Temperature Profile for 0.25 Pore Volumes Injected

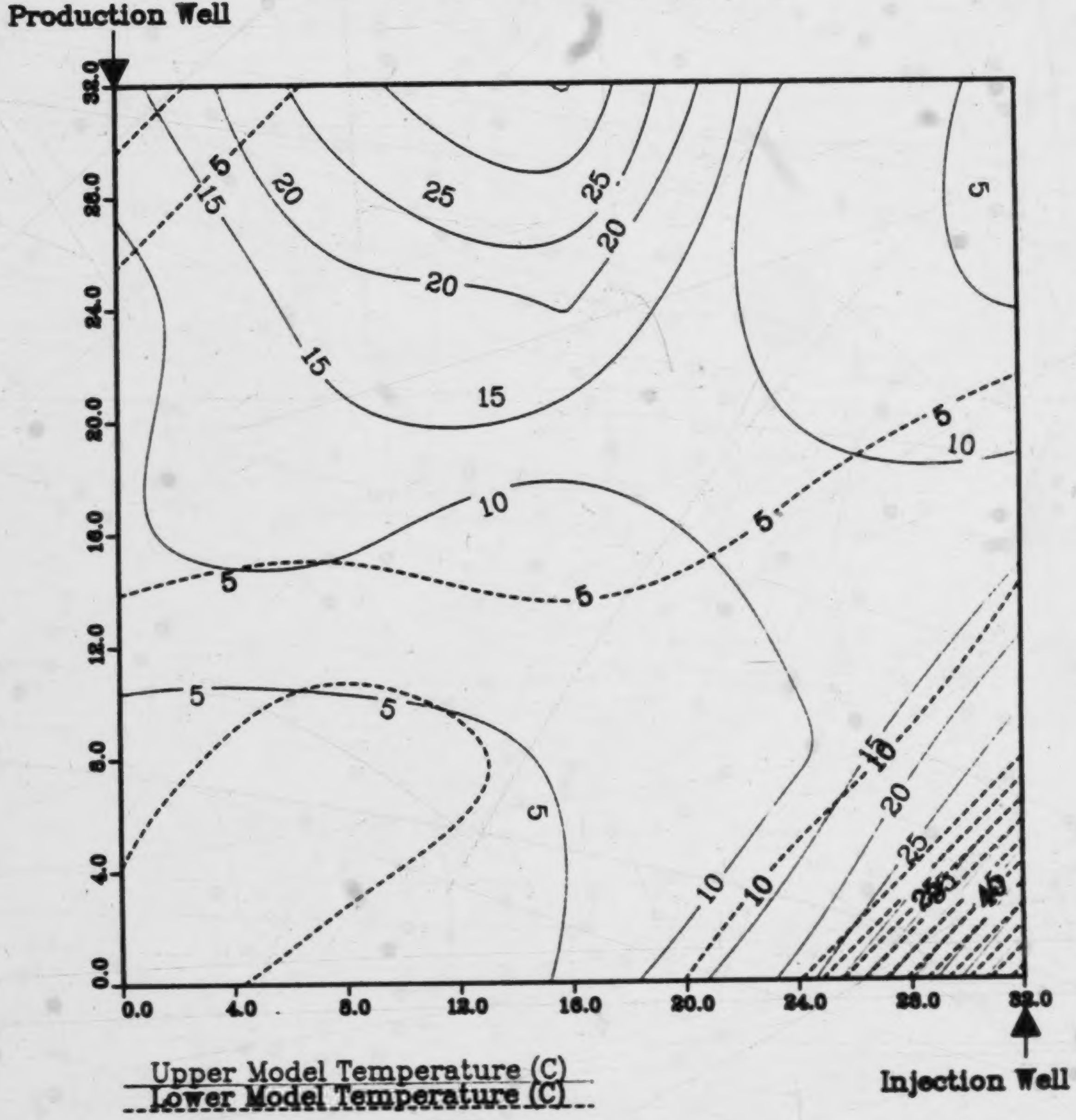

Figure A.180 : Run 55

Gas Inj. Solv.–Stmflood in Homo. Model

Temperature Profile for
0.50 Pore Volumes Injected

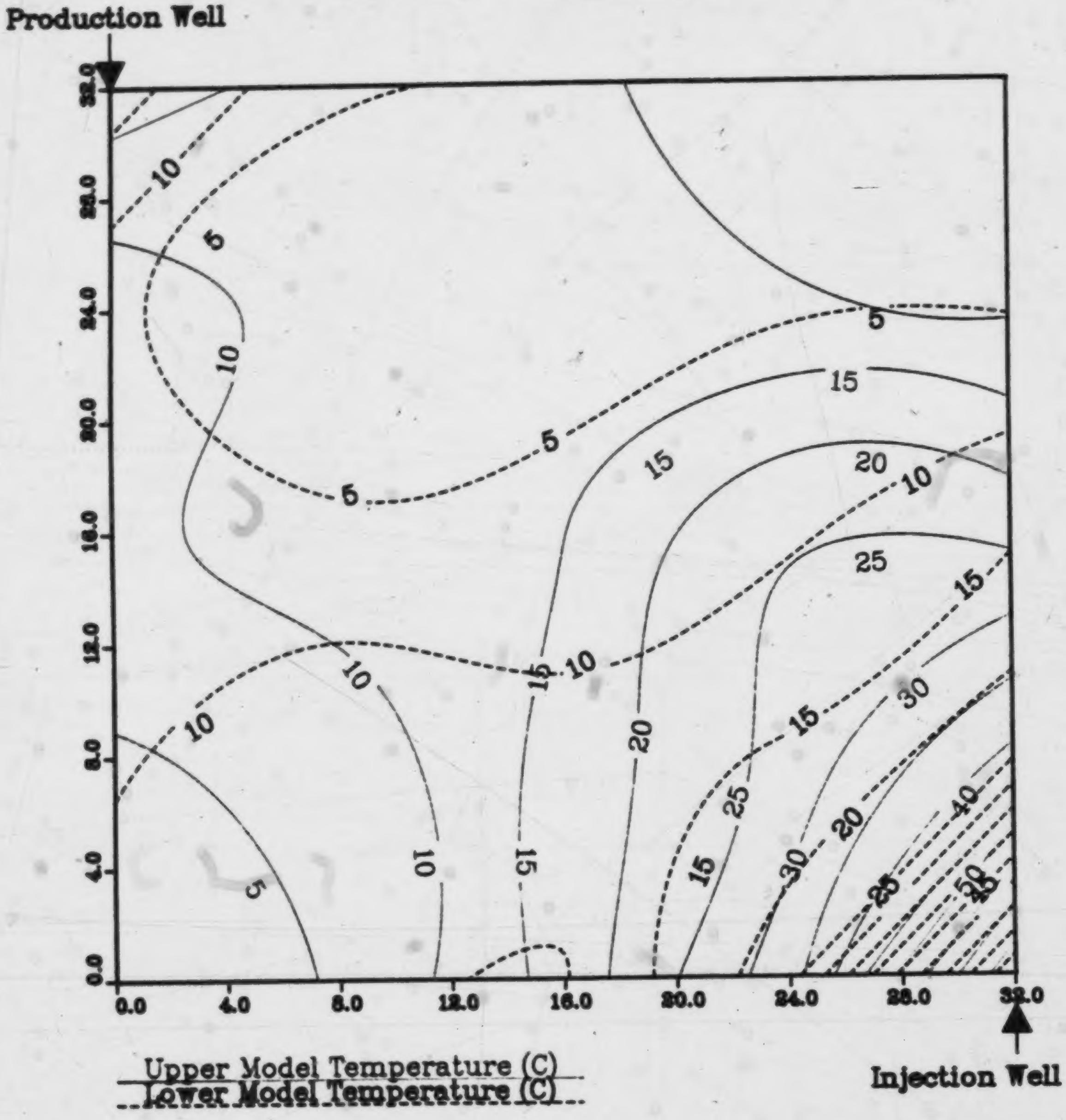

Figure A.181 : Run 55

Gas Inj. Solv.–Stmflood in Homo. Model

Temperature Profile for
0.75 Pore Volumes Injected

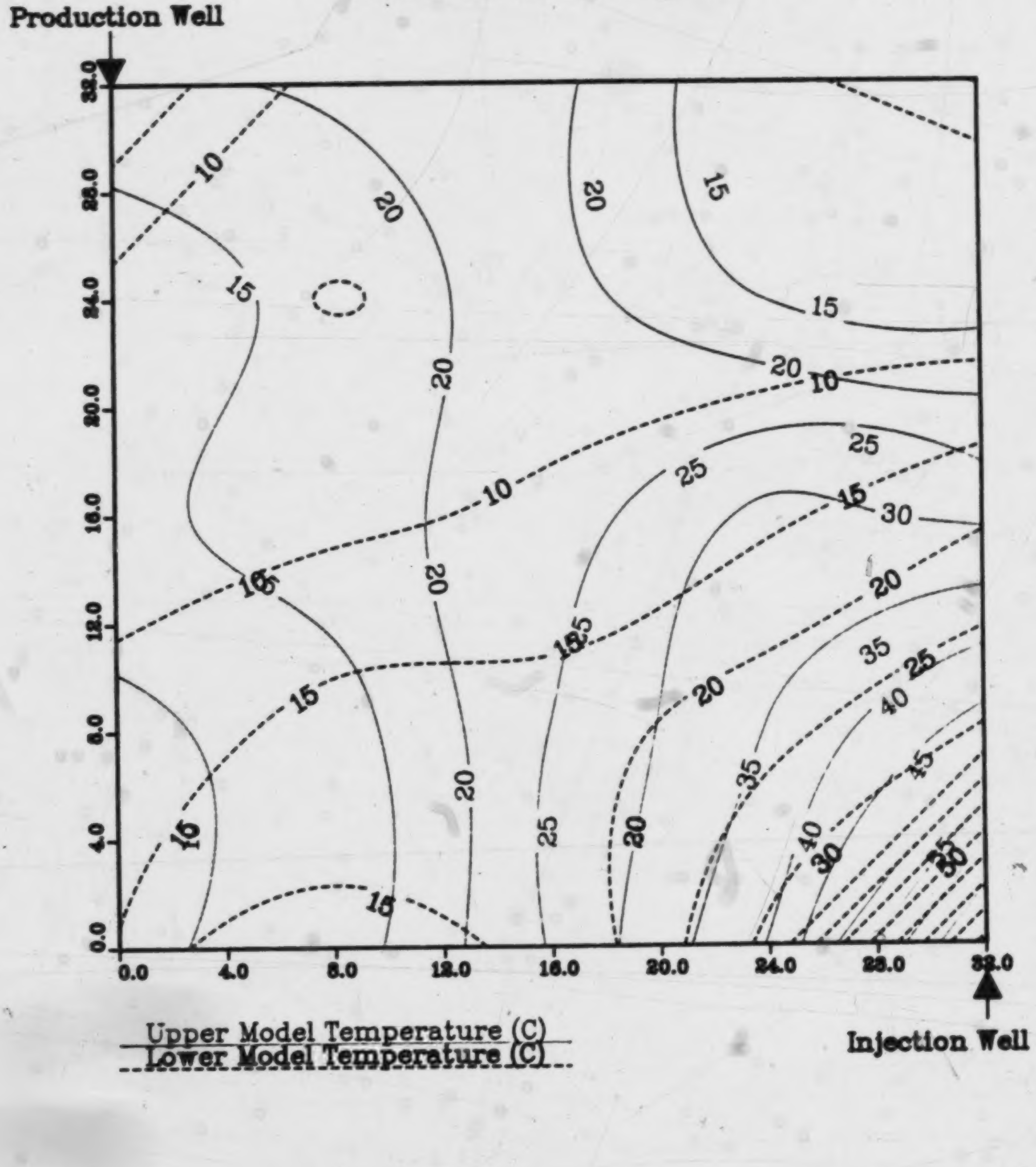

Figure A.182 : Run 55

Gas Inj. Solv.--Stmflood in Homo. Model

Temperature Profile for 1.00 Pore Volumes Injected

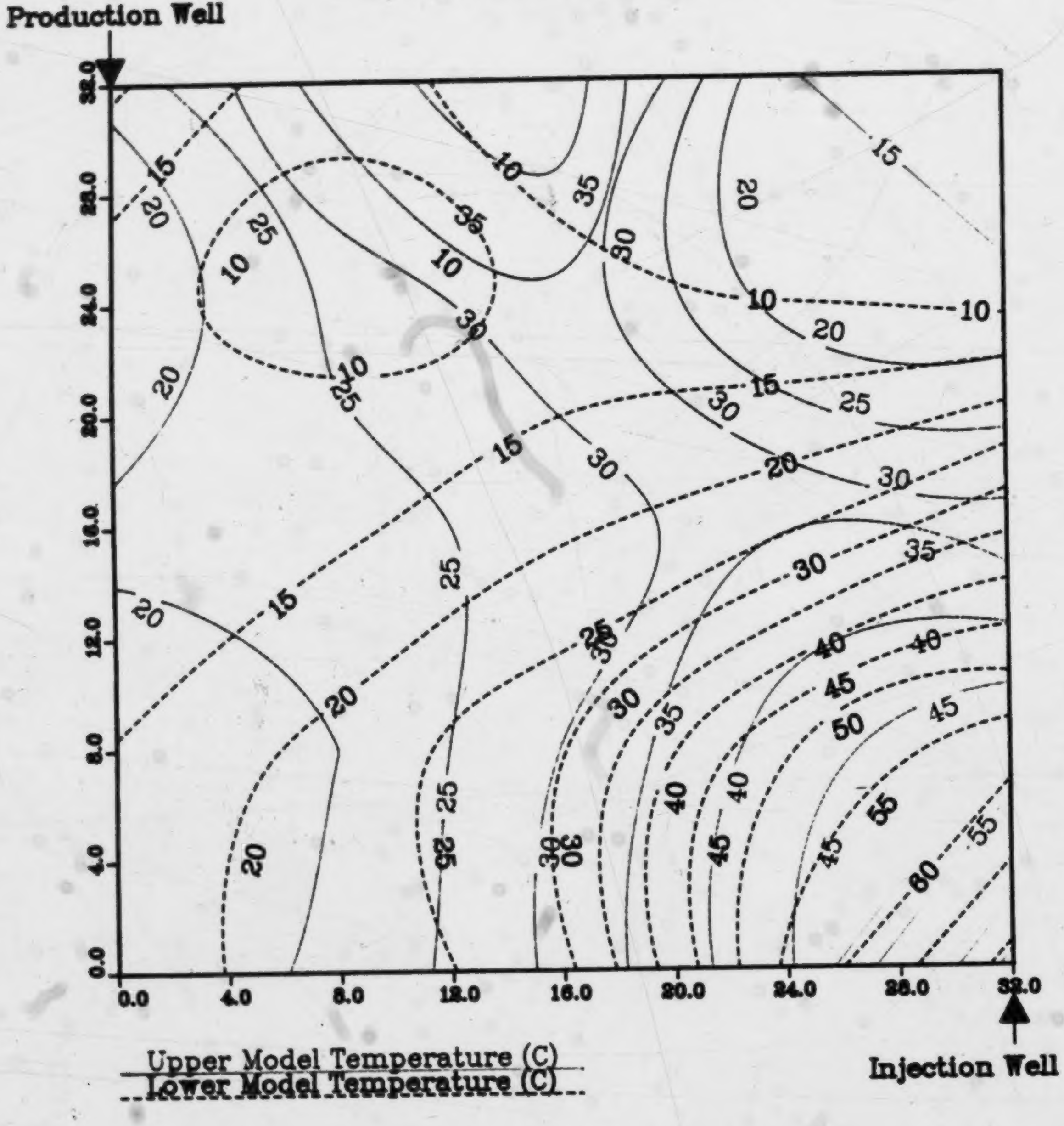

Figure A.183 : Run 55

Gas Inj. Solv.–Stmflood in Homo. Model

Temperature Profile for
1.25 Pore Volumes Injected

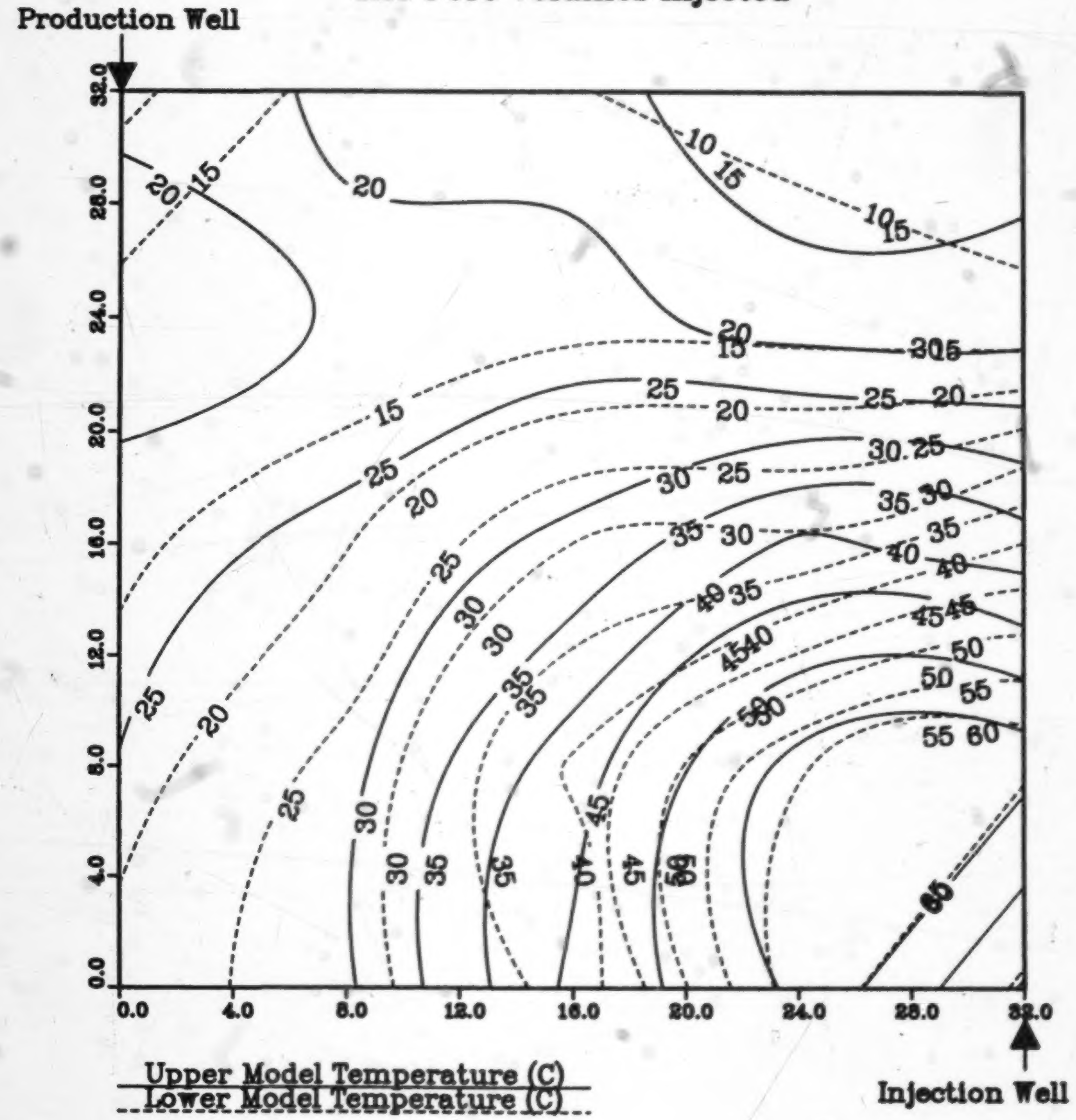

Figure A.184 : Run 55

Gas Inj. Solv.–Stmflood in Homo. Model

Temperature Profile for 1.50 Pore Volumes Injected

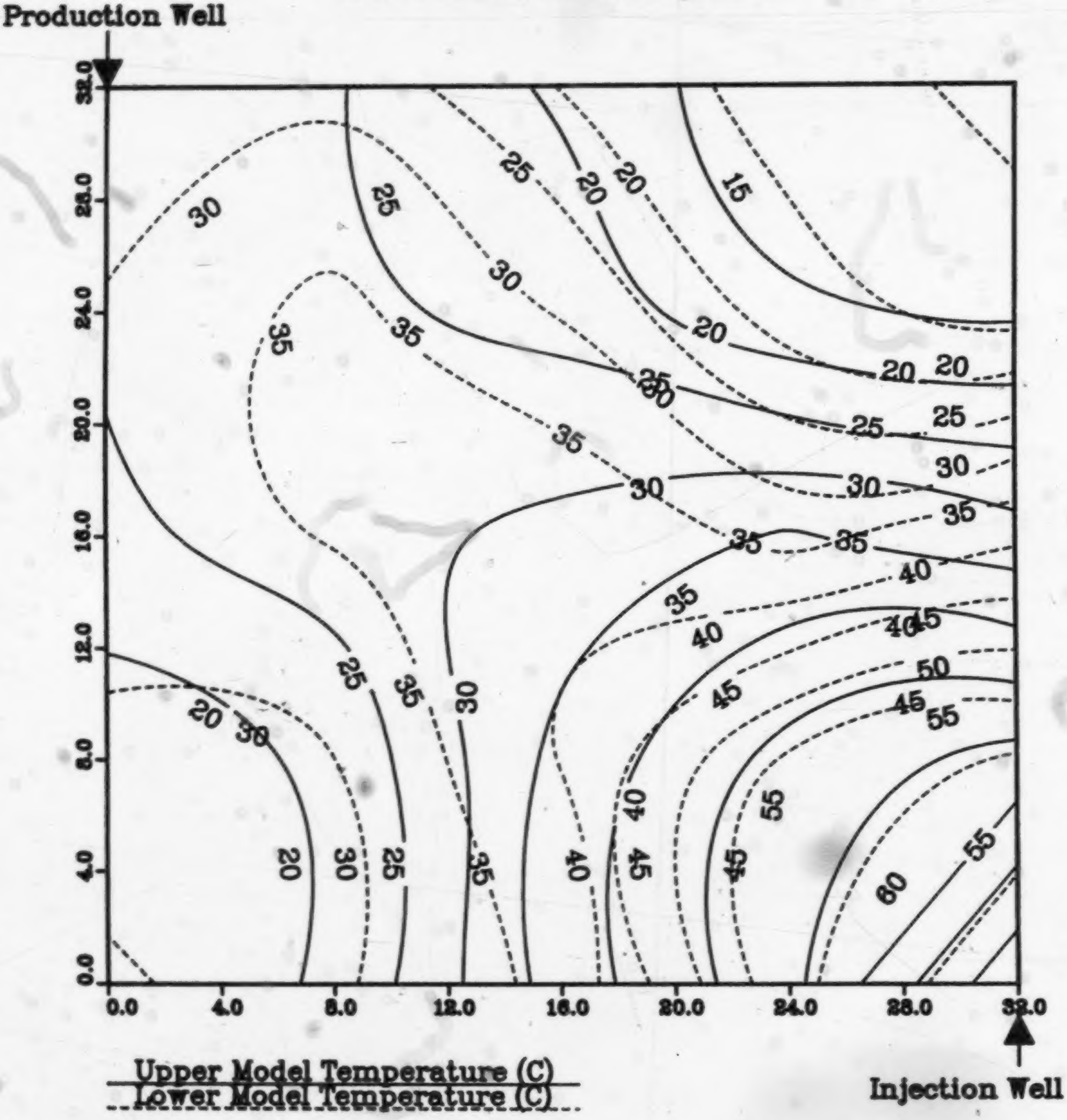

Figure A.185 : Run 55

Gas Inj. Solv.–Stmflood in Homo. Model

Temperature Profile for 1.75 Pore Volumes Injected

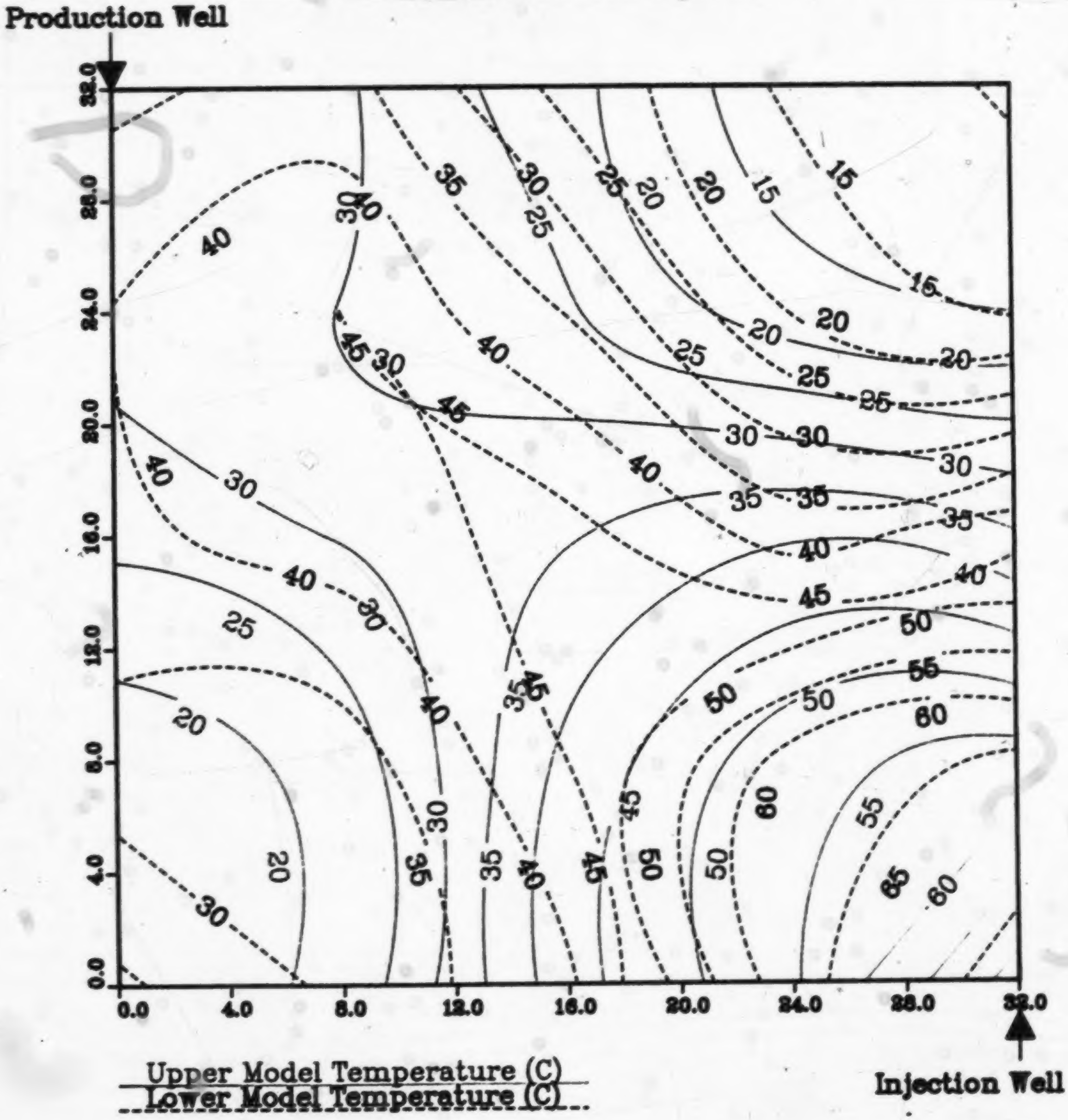

Figure A.186 : Run 55

Gas Inj. Solv.–Stmflood in Homo. Model

Temperature Profile for 2.00 Pore Volumes Injected

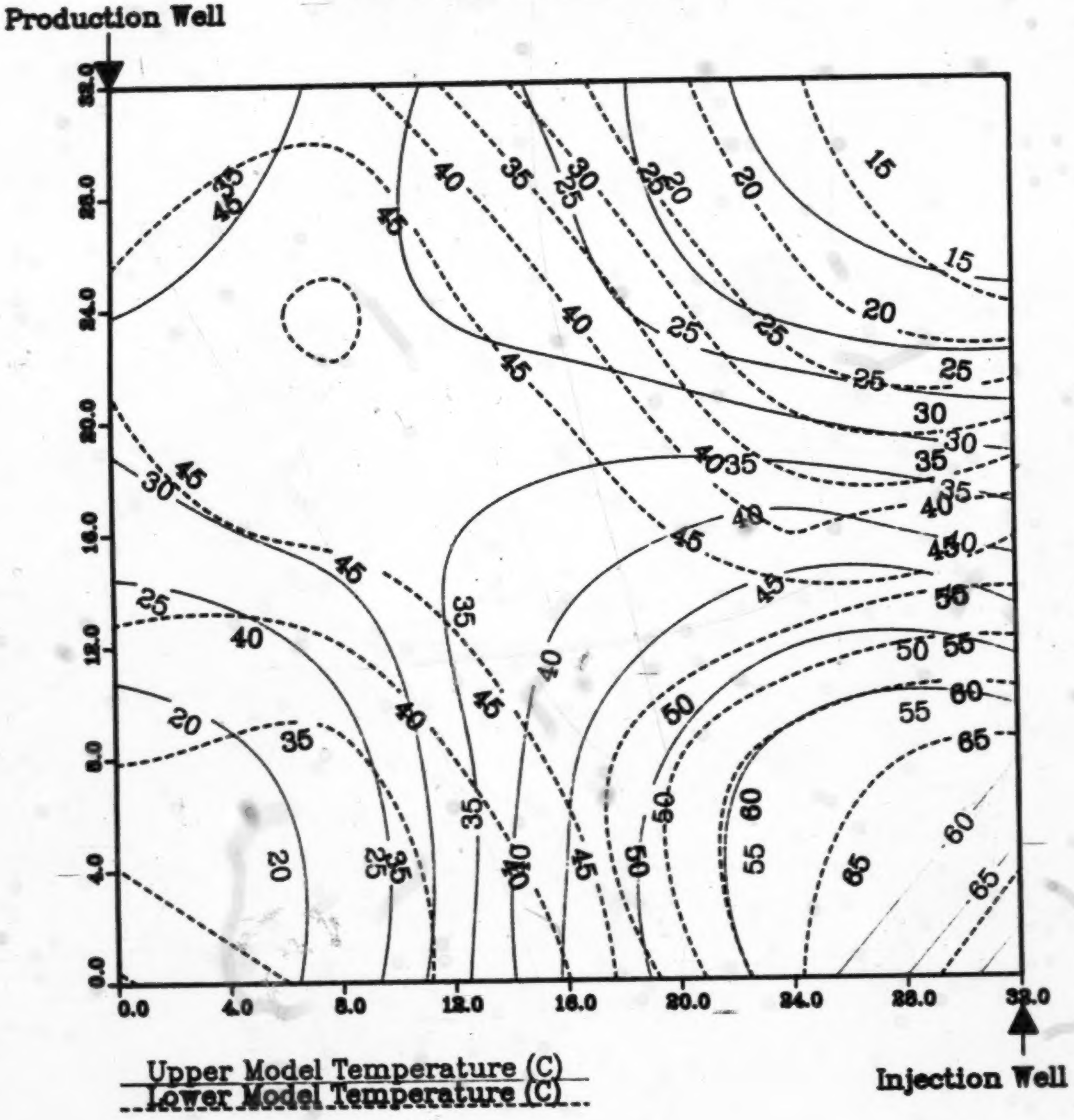

Figure A.187 :Run 55 Temp Profile
Injector to Producer Cross–Section
0.25 Pore Volumes Injected.

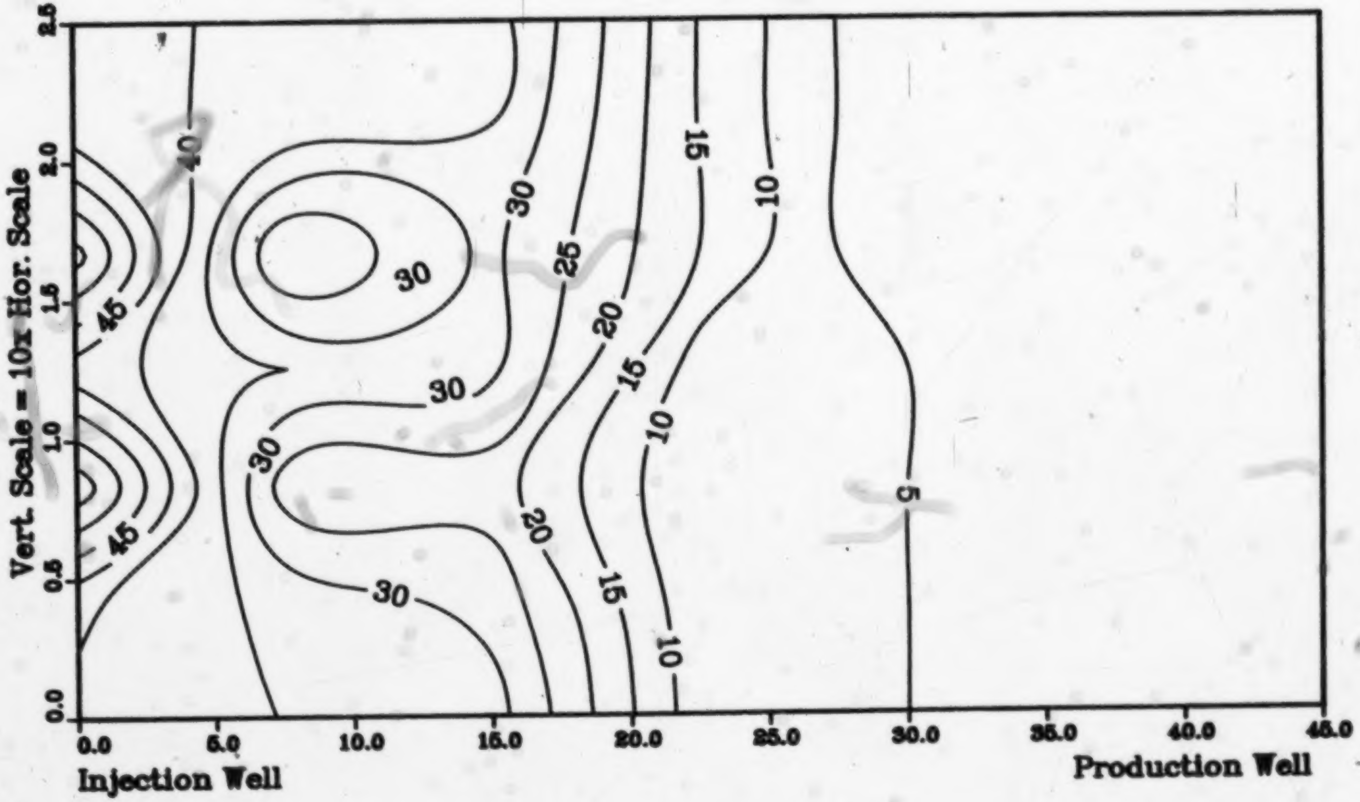

Figure A.188 :Run 55 Temp Profile
Injector to Producer Cross–Section
0.50 Pore Volumes Injected.

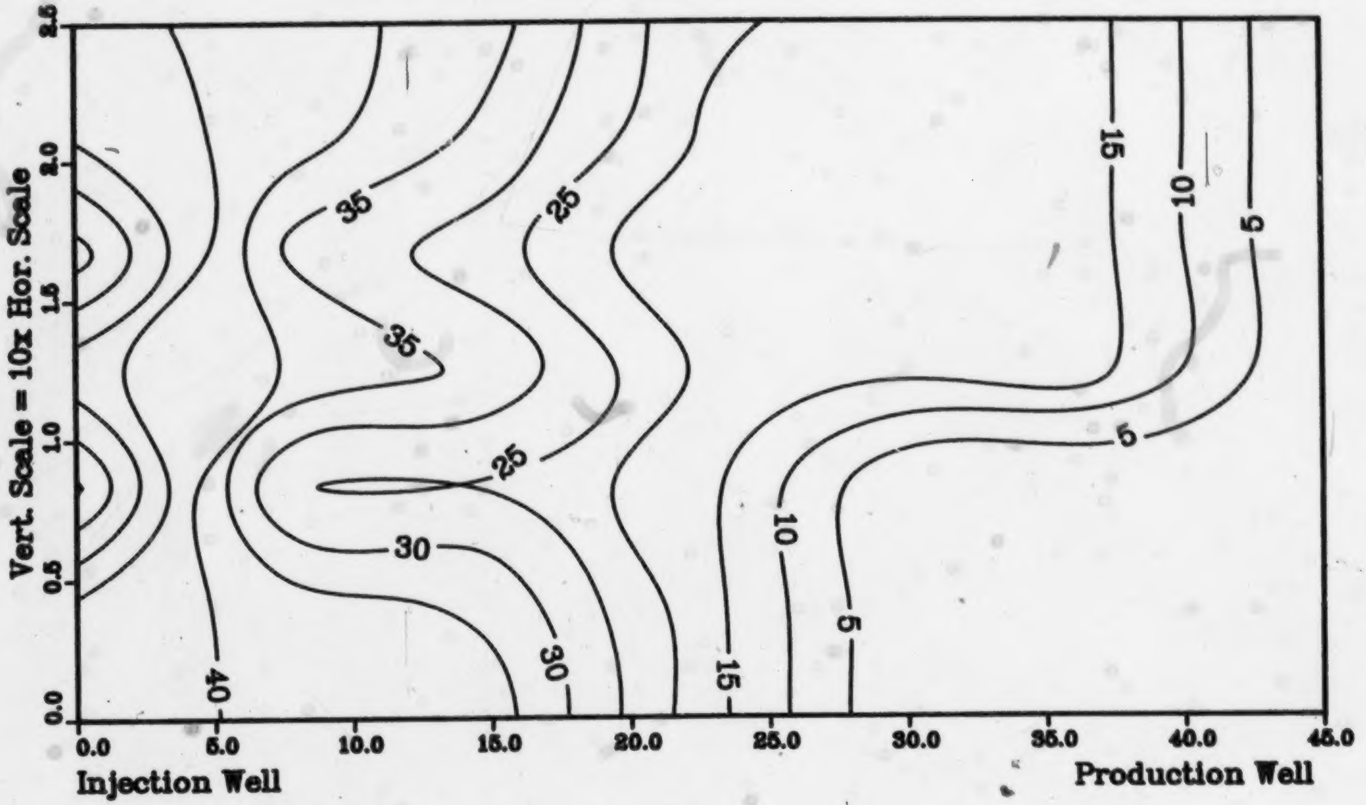

Figure A.189 :Run 55 Temp Profile
Injector to Producer Cross–Section
0.75 Pore Volumes Injected.

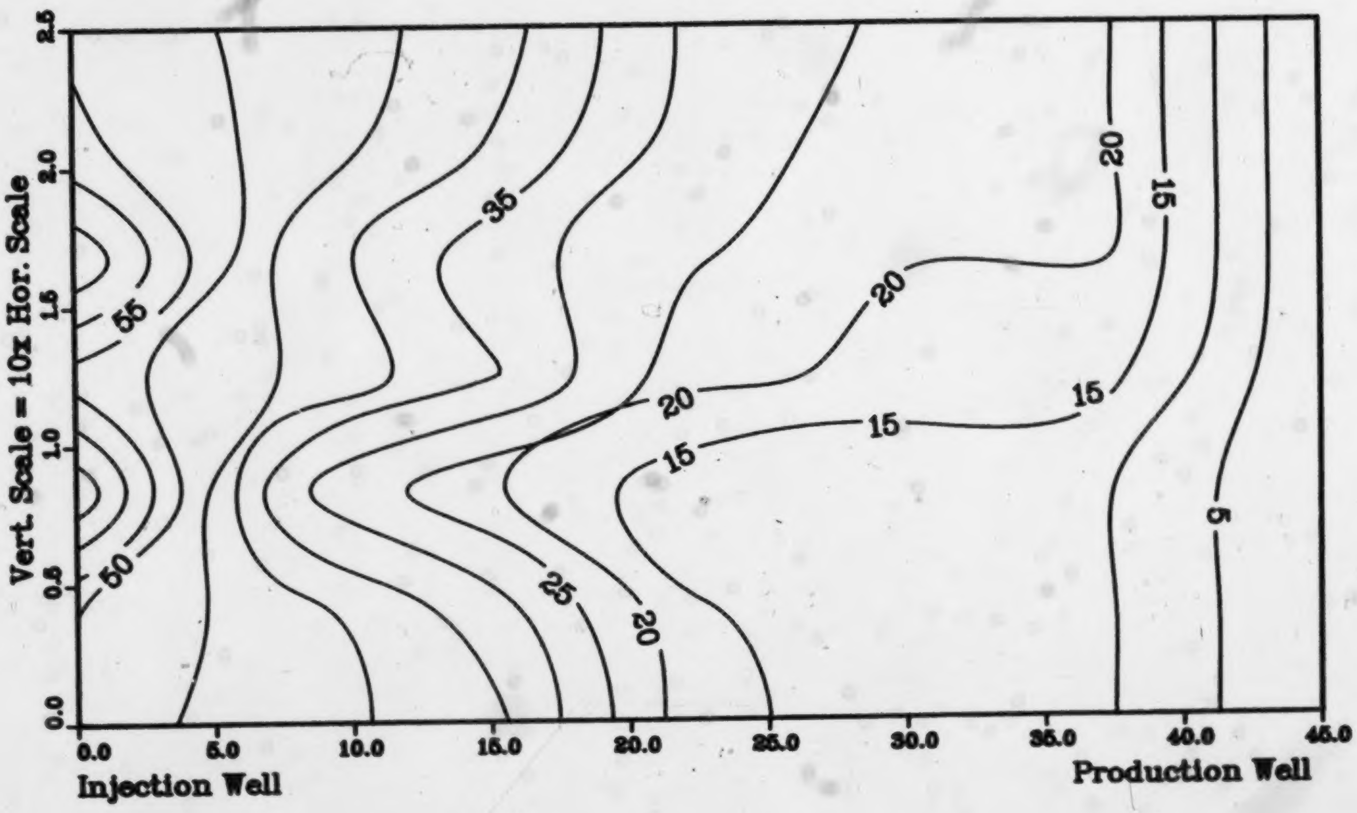

Figure A.190 :Run 55 Temp Profile
Injector to Producer Cross–Section
1.00 Pore Volumes Injected.

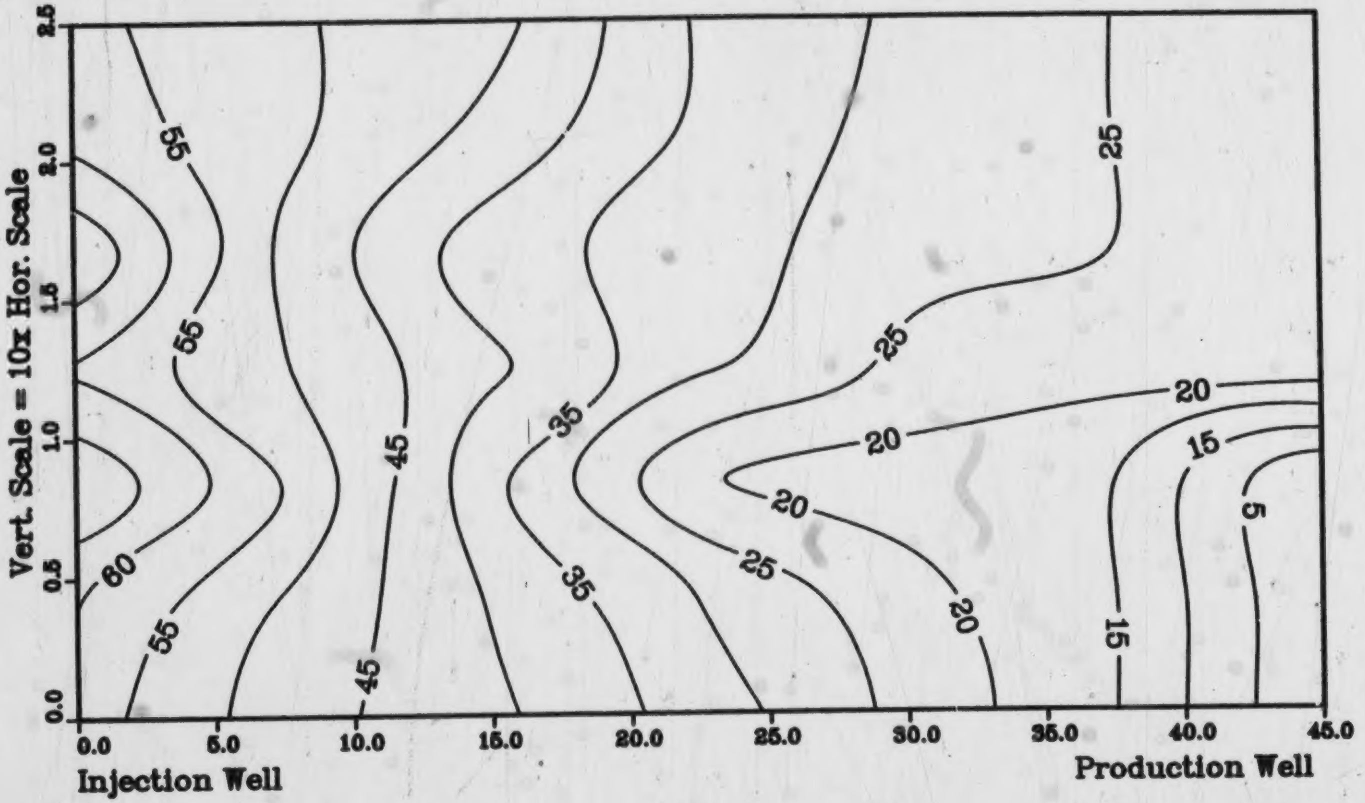

Figure A.191 : Run 56

Gas Inj. Solv.–Stmflood in Homo. Model

Temperature Profile for 0.25 Pore Volumes Injected

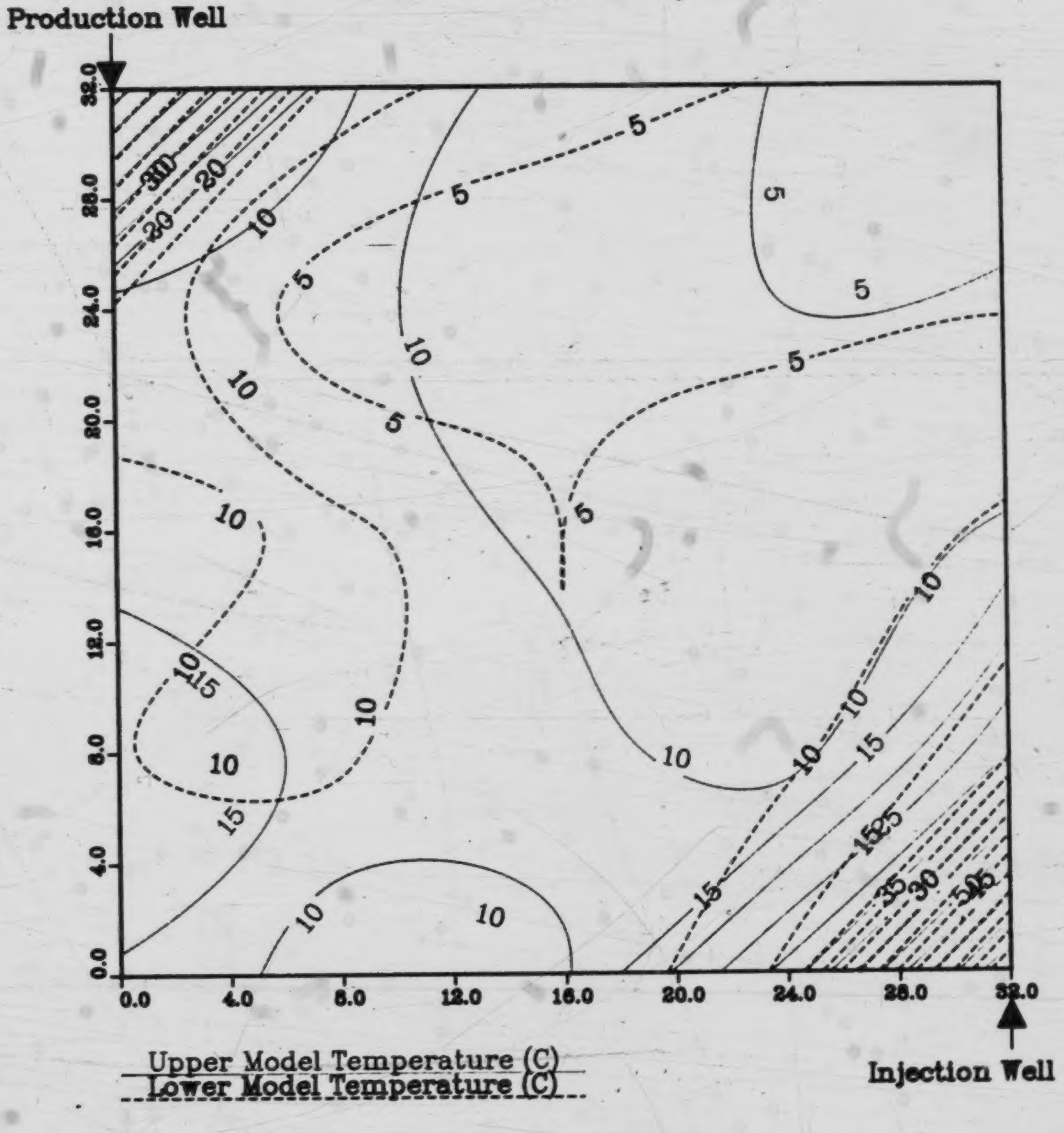

Figure A.192 : Run 56
Gas Inj. Solv.–Stmflood in Homo. Model

Temperature Profile for
0.50 Pore Volumes Injected

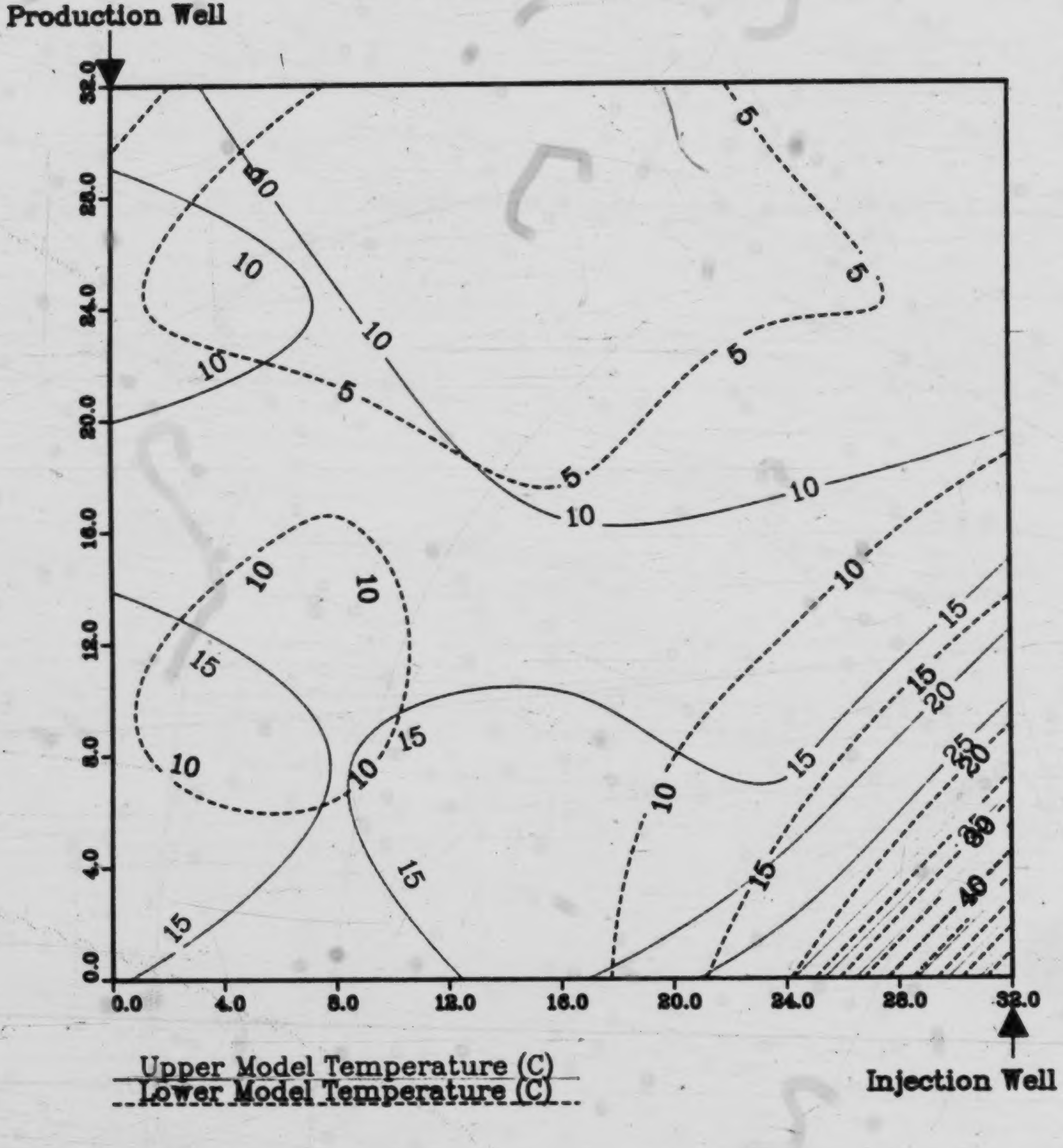

Figure A.193 : Run 56

Gas Inj. Solv.–Stmflood in Homo. Model

Temperature Profile for 0.75 Pore Volumes Injected

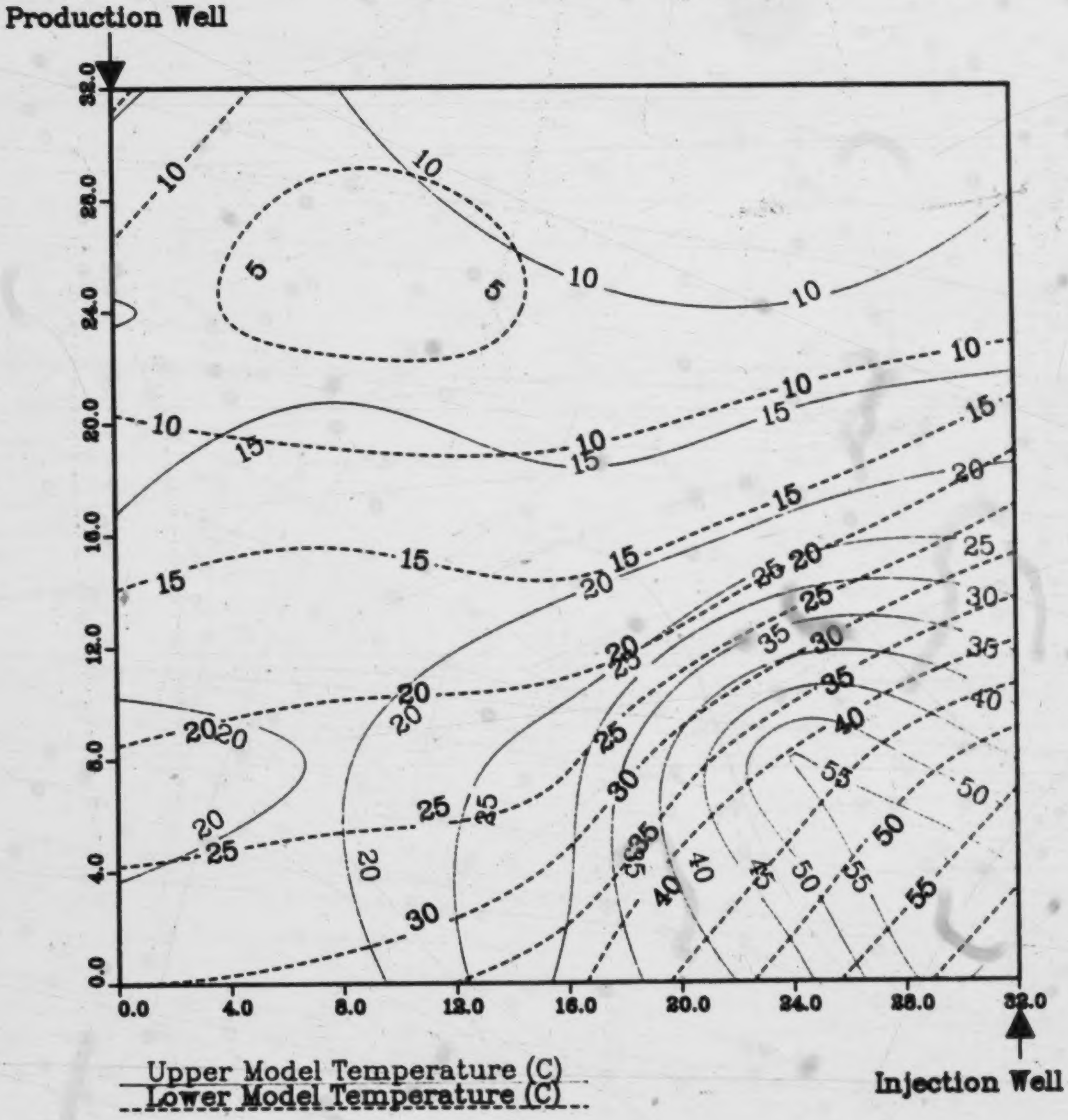

Figure A.194 : Run 56

Gas Inj. Solv.–Stmflood in Homo. Model

Temperature Profile for
1.00 Pore Volumes Injected

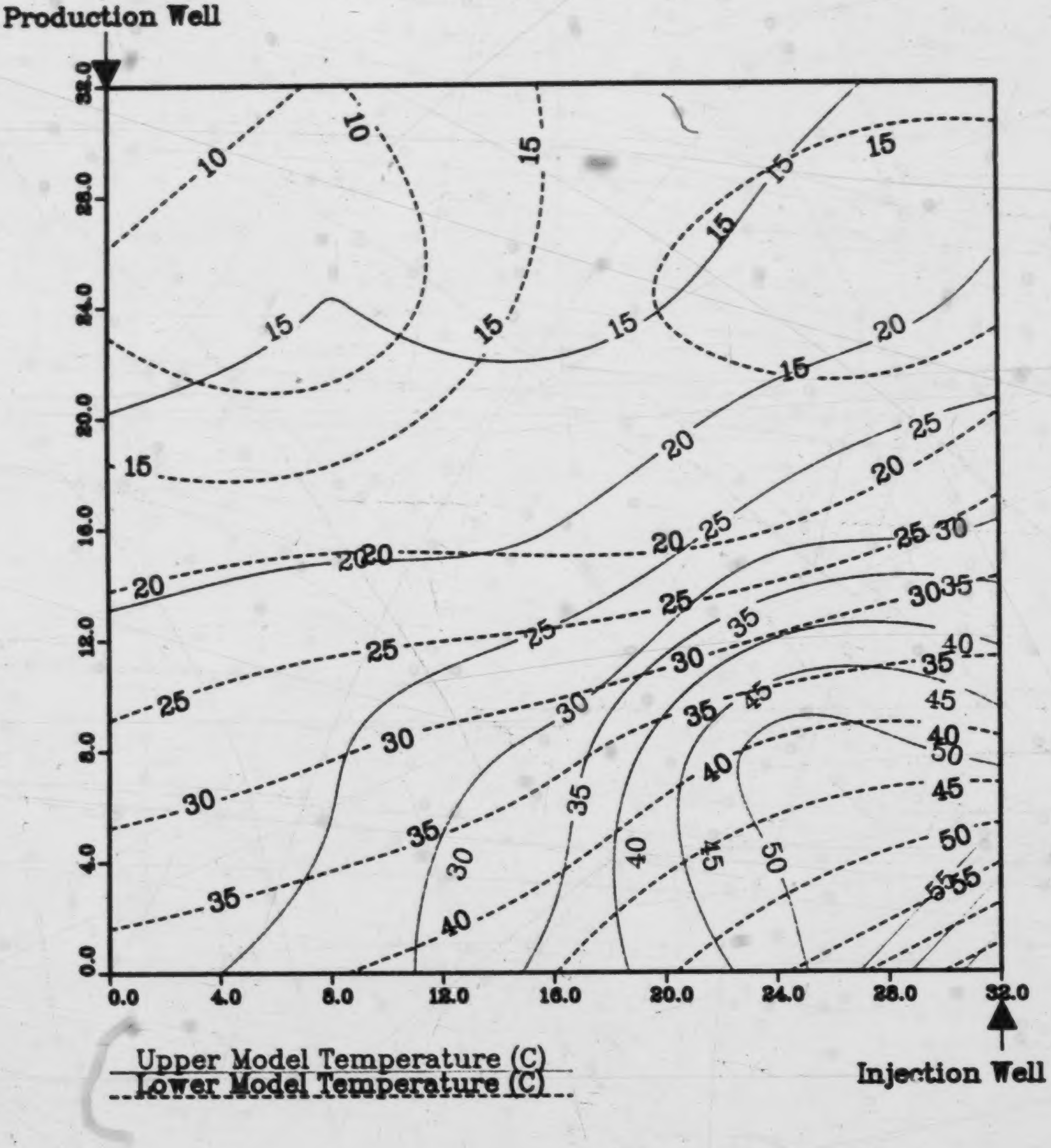

Figure A.195 : Run 56

Gas Inj. Solv.–Stmflood in Homo. Model

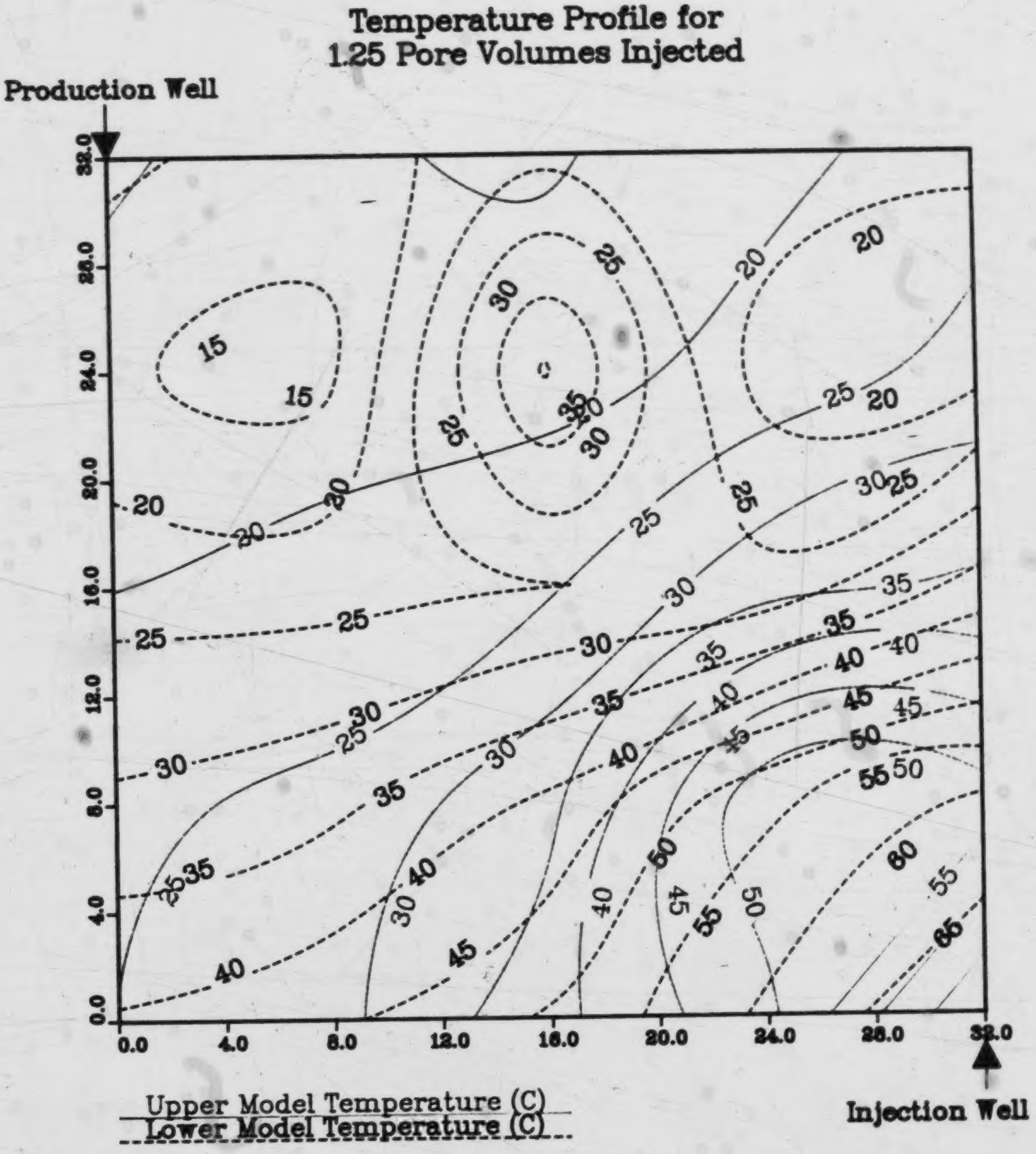

Figure A.196 : Run 56

Gas Inj. Solv.--Stmflood in Homo. Model

Temperature Profile for 1.50 Pore Volumes Injected

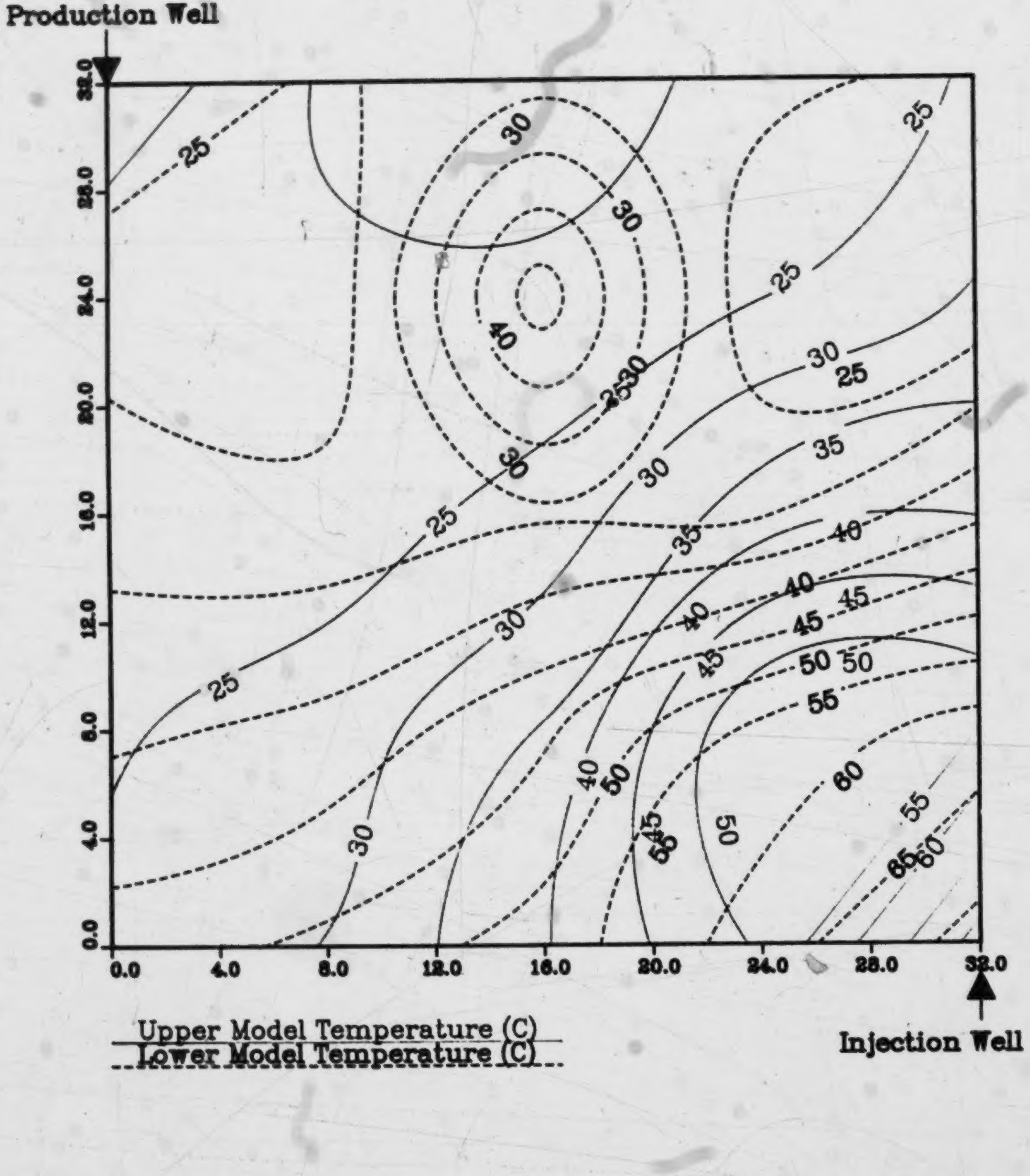

Figure A.197 : Run 56

Gas Inj. Solv.–Stmflood in Homo. Model

Temperature Profile for 1.75 Pore Volumes Injected

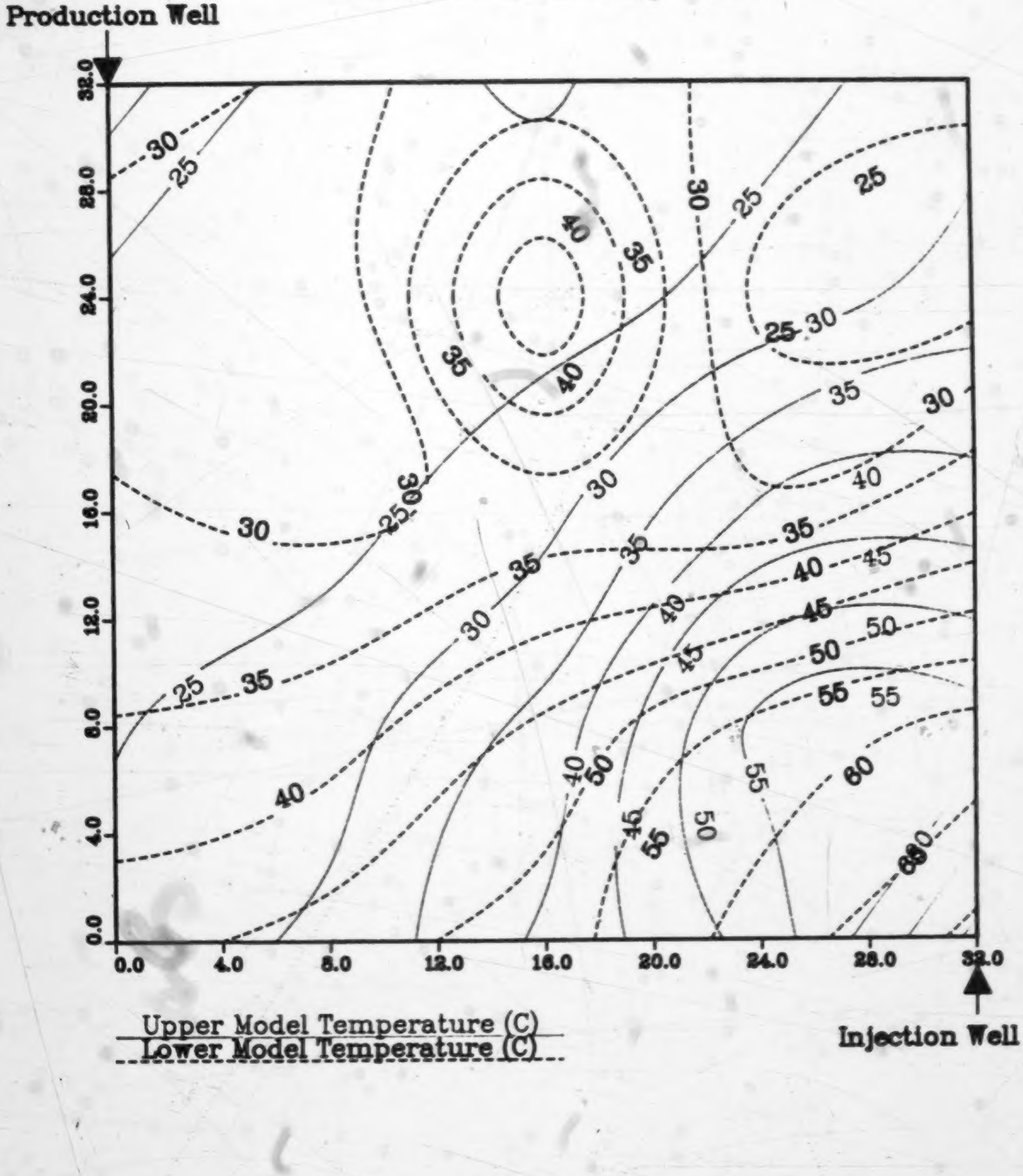

Figure A.198 : Run 56

Gas Inj. Solv.–Stmflood in Homo. Model

Temperature Profile for
2.00 Pore Volumes Injected

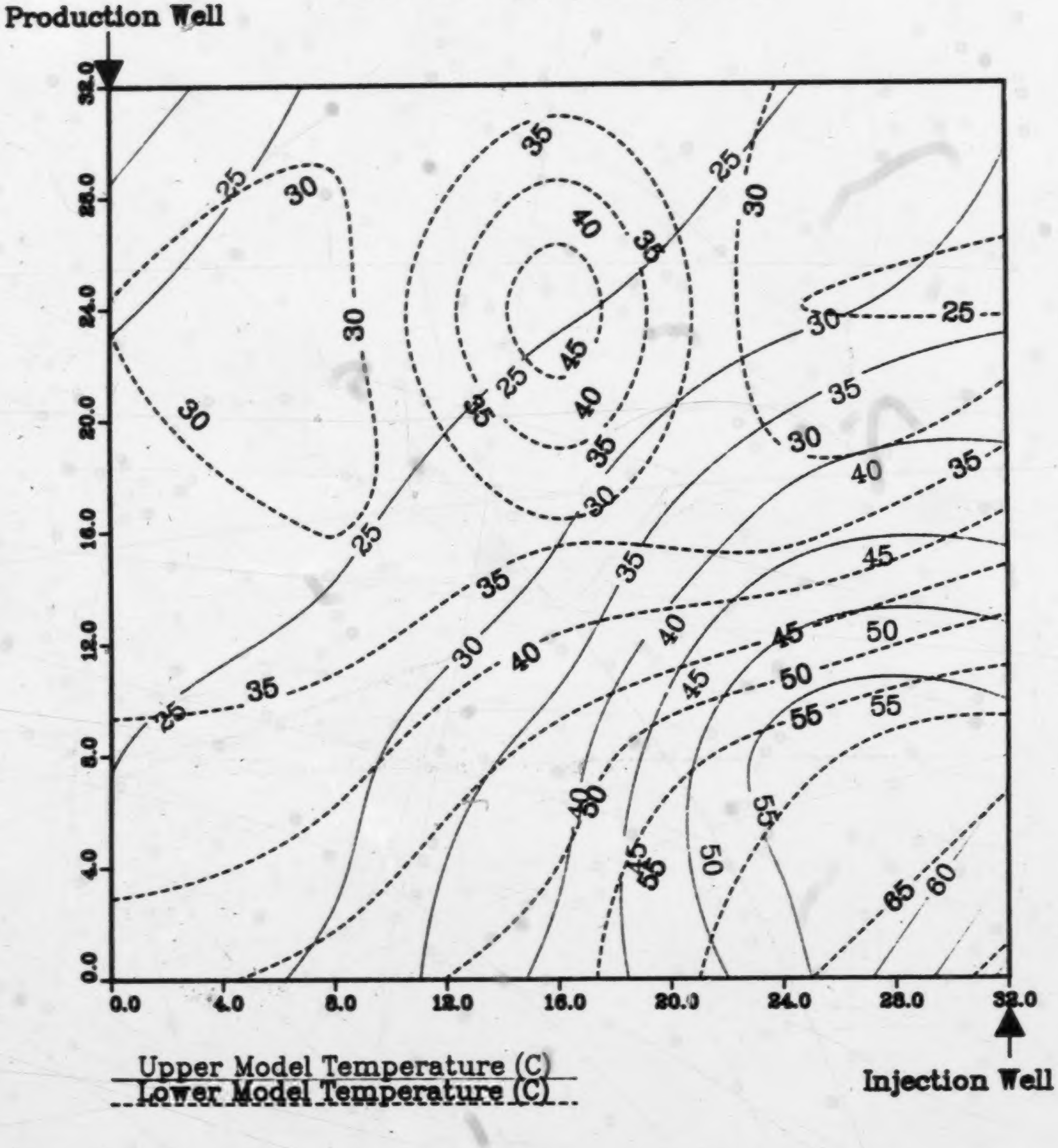

Figure A.199 :Run 56 Temp Profile
Injector to Producer Cross–Section
0.25 Pore Volumes Injected.

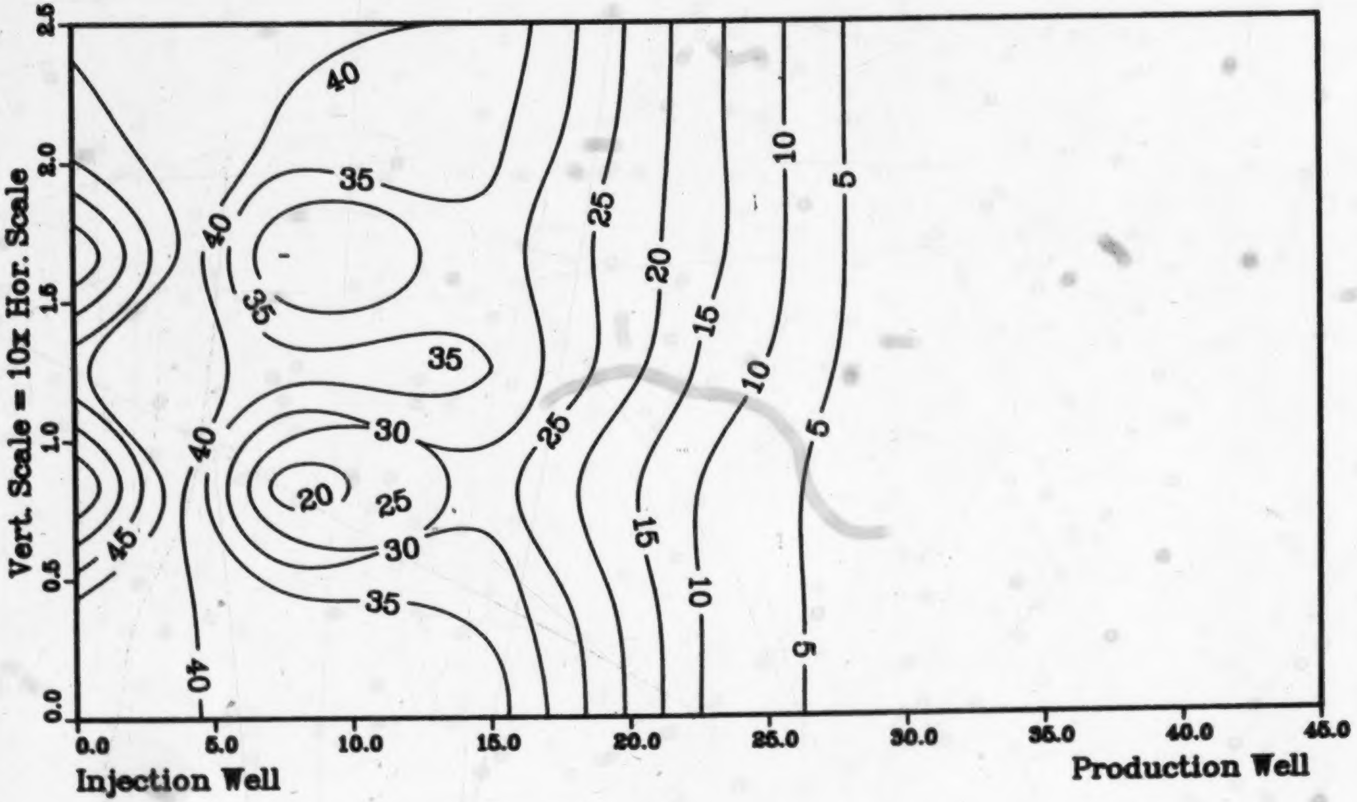

Figure A.200 :Run 56 Temp Profile

Injector to Producer Cross–Section

0.50 Pore Volumes Injected.

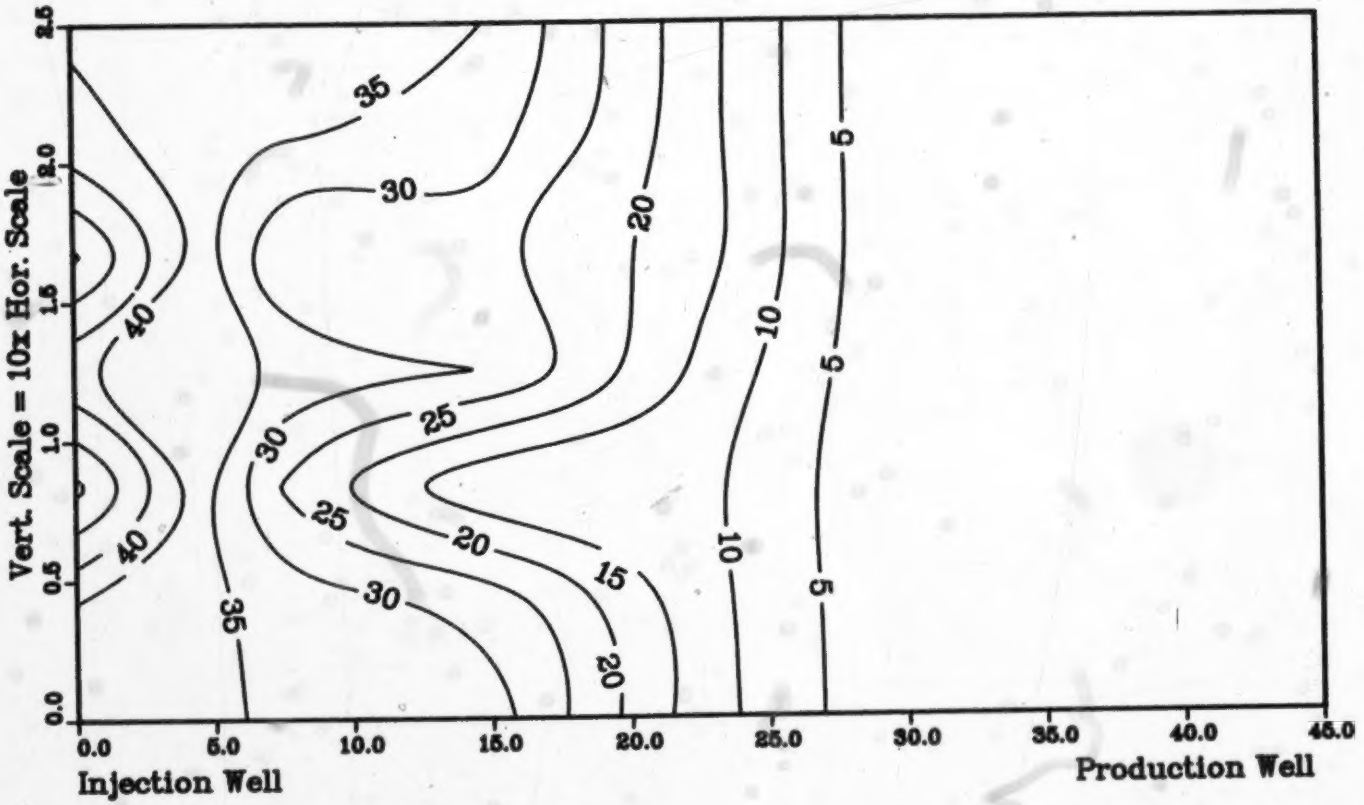

Figure A.201 :Run 56 Temp Profile
Injector to Producer Cross–Section
0.75 Pore Volumes Injected.

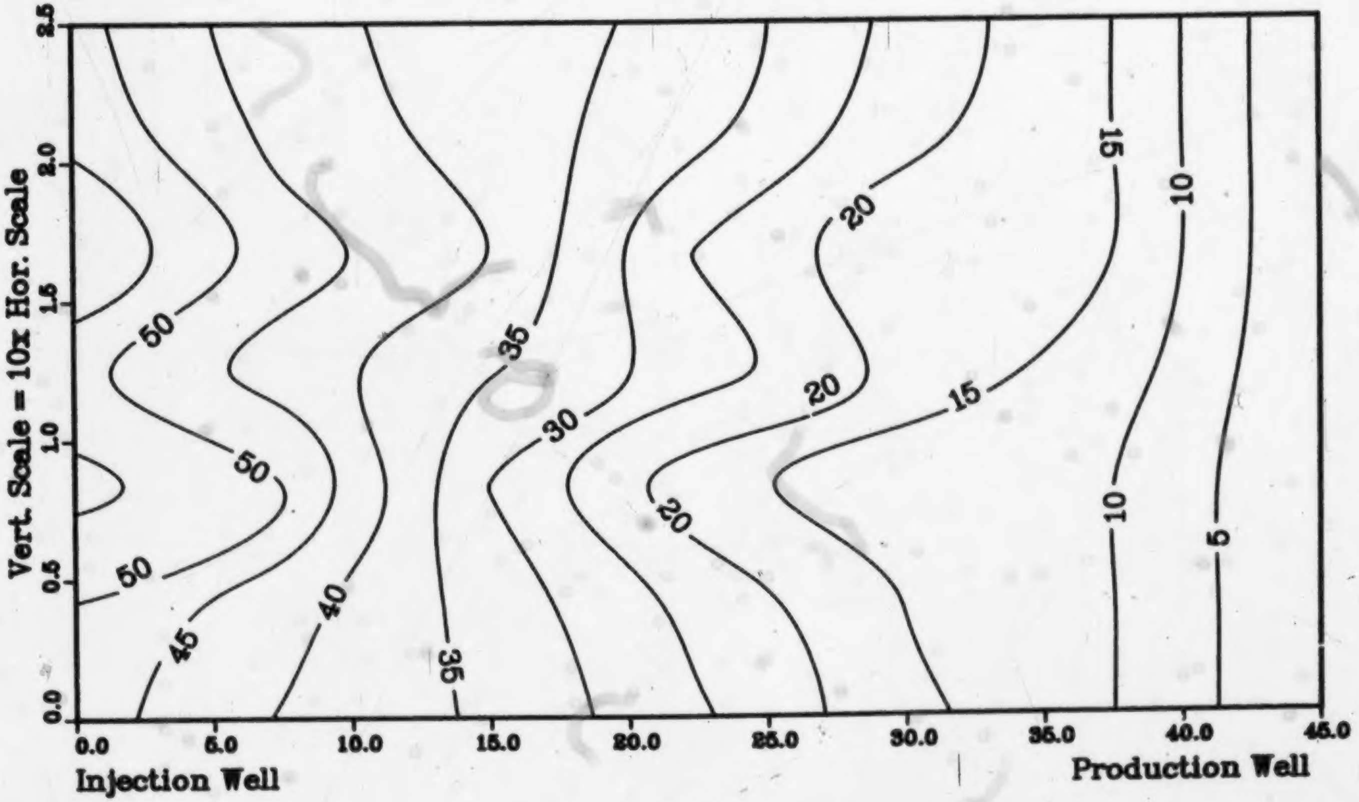

Figure A.202 :Run 56 Temp Profile
Injector to Producer Cross–Section
1.00 Pore Volumes Injected.

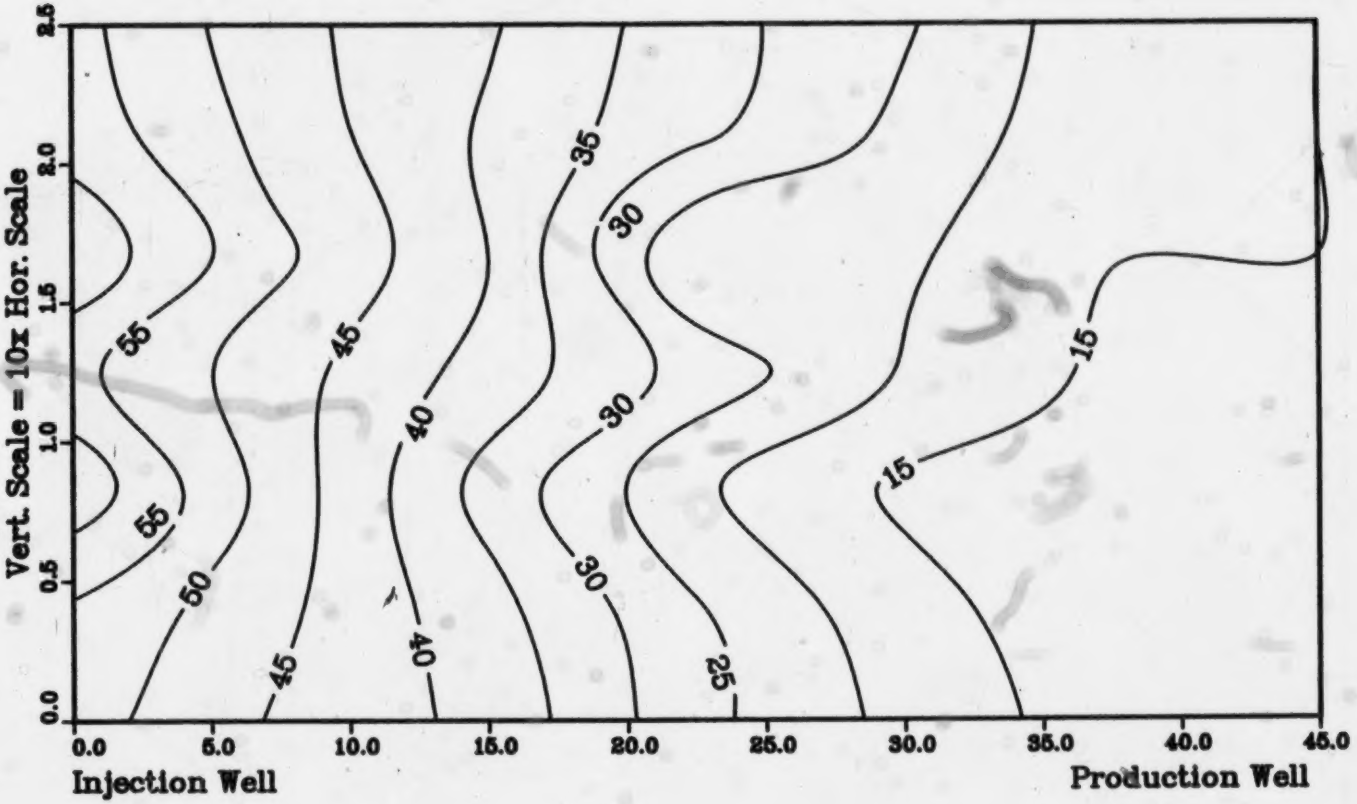

Figure A.203 : Run 58

Gas Inj. Solv.–Steamflood in B.W. Model

Temperature Profile for 0.25 Pore Volumes Injected

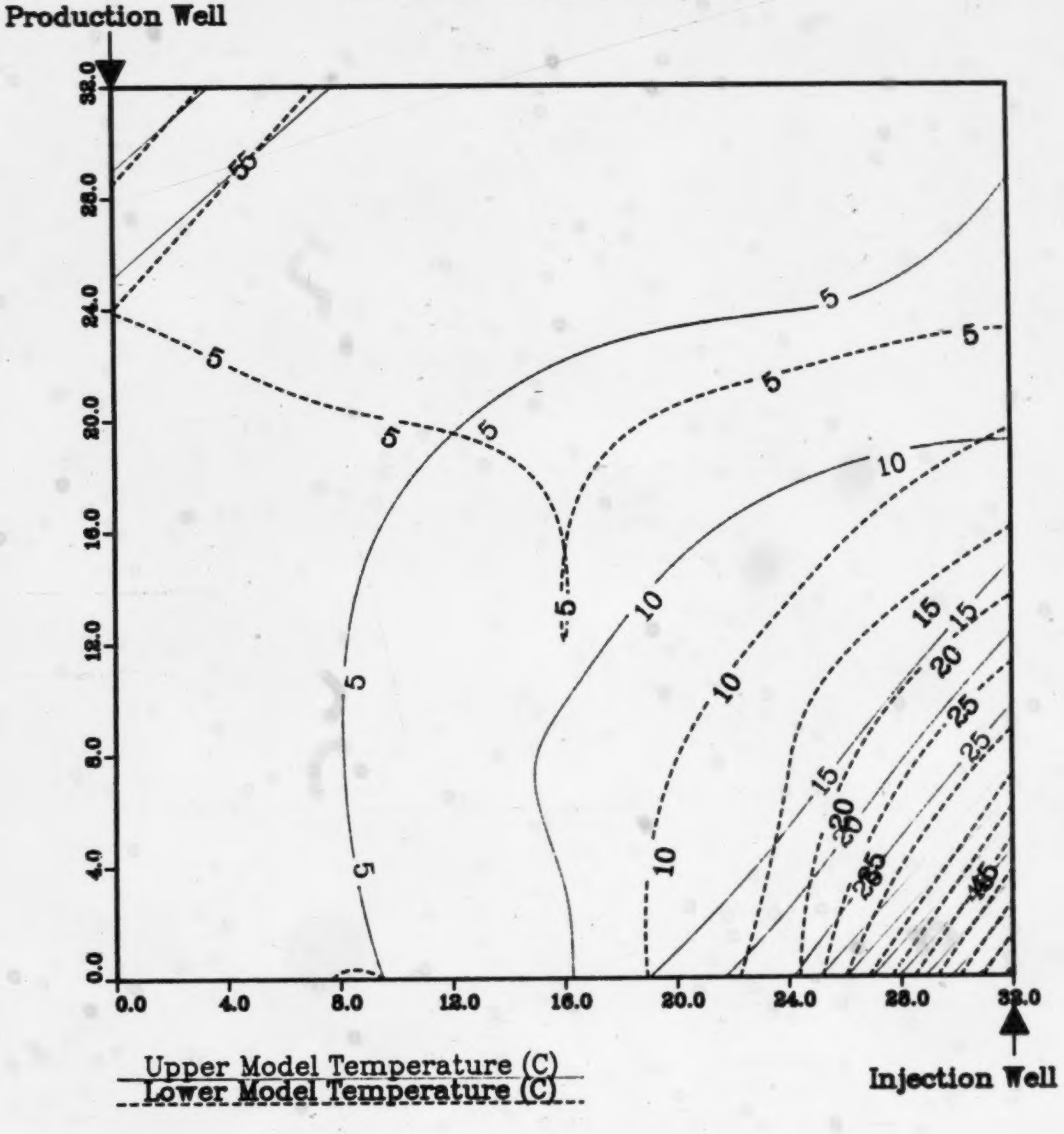

Figure A.204 : Run 58

Gas Inj. Solv.–Steamflood in B.W. Model

Temperature Profile for 0.50 Pore Volumes Injected

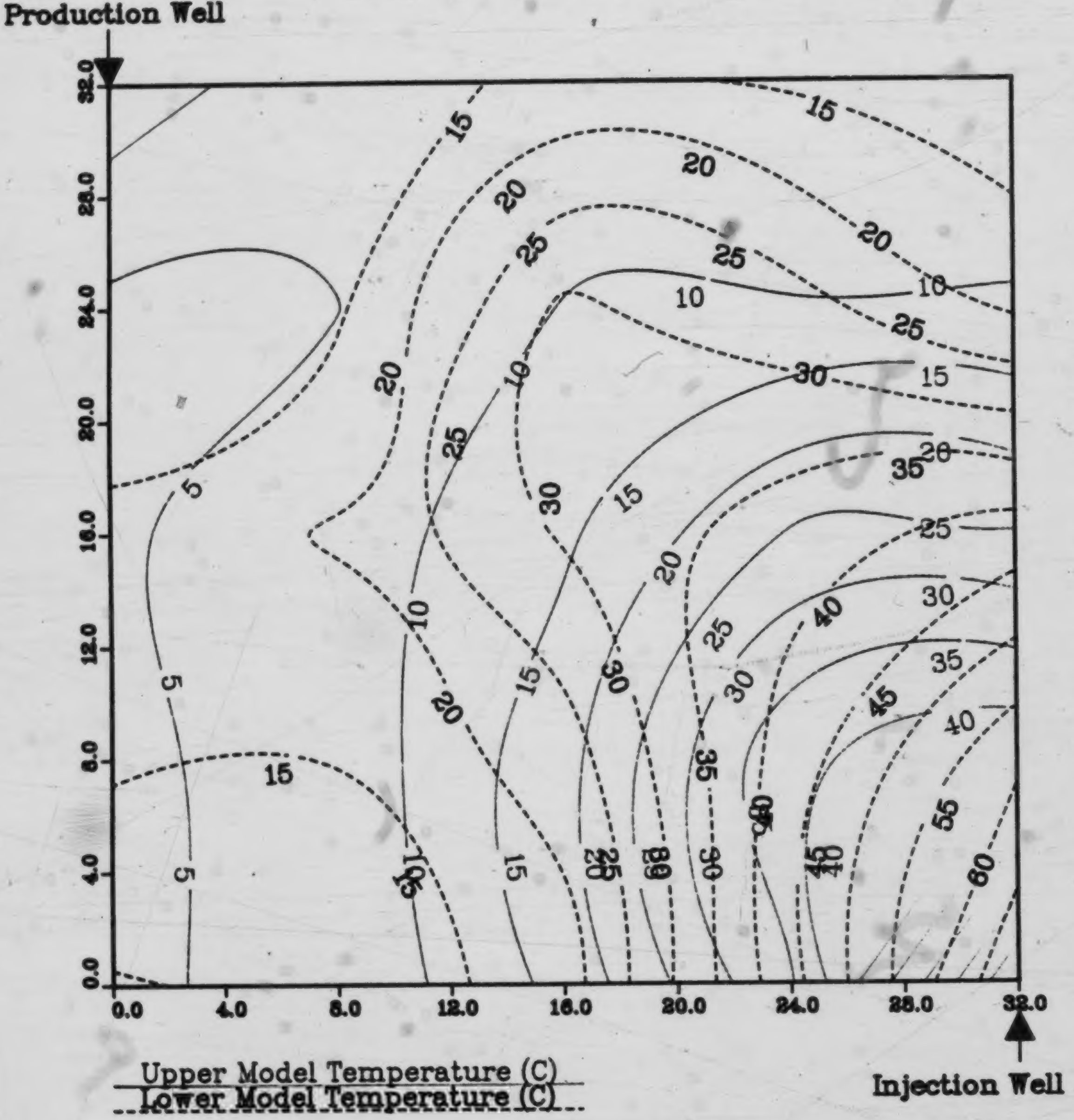

Figure A.205 : Run 58

Gas Inj. Solv.–Steamflood in B.W. Model

Temperature Profile for 0.75 Pore Volumes Injected

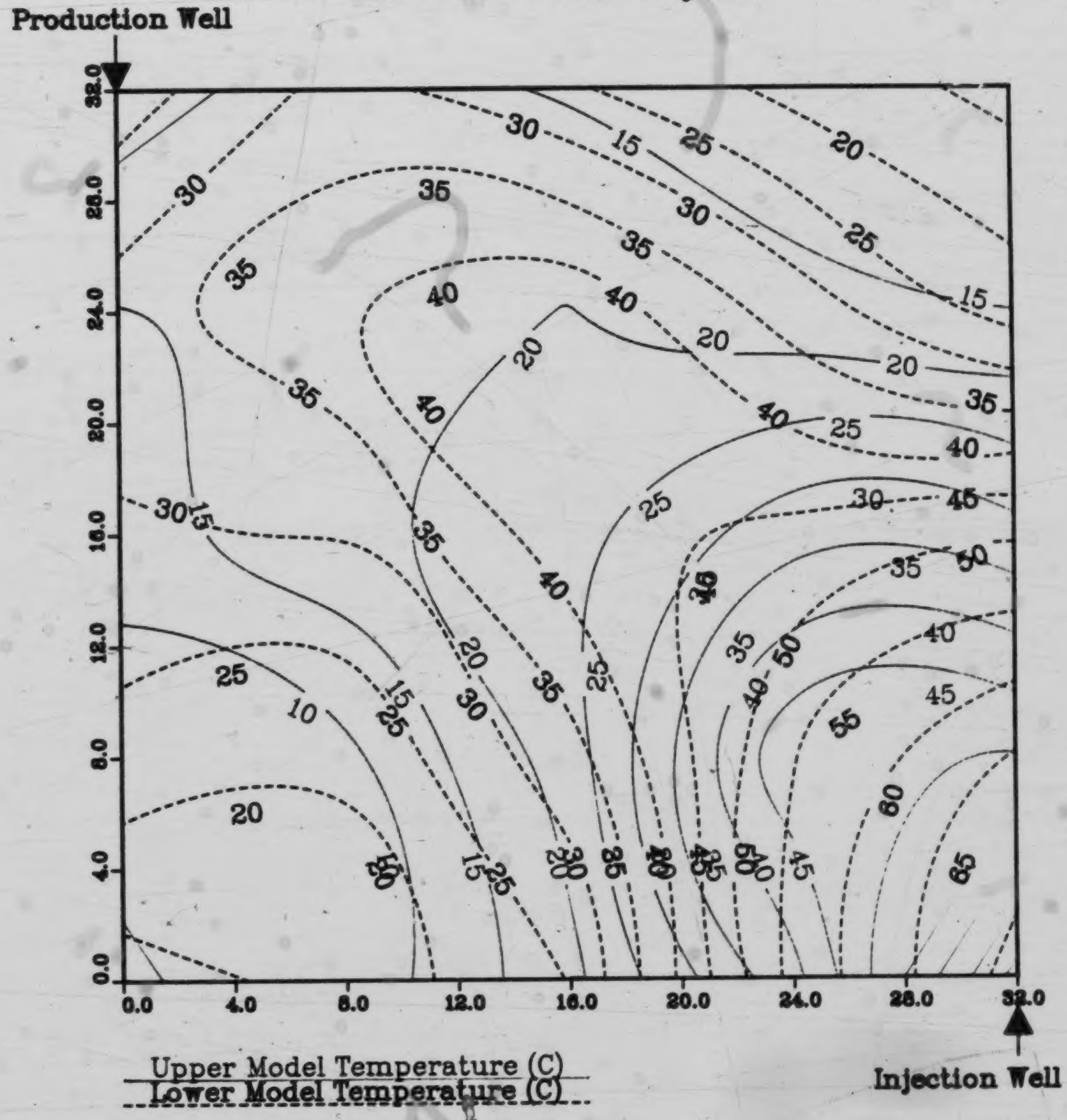

Figure A.206 : Run 58

Gas Inj. Solv.–Steamflood in B.W. Model

Temperature Profile for 1.00 Pore Volumes Injected

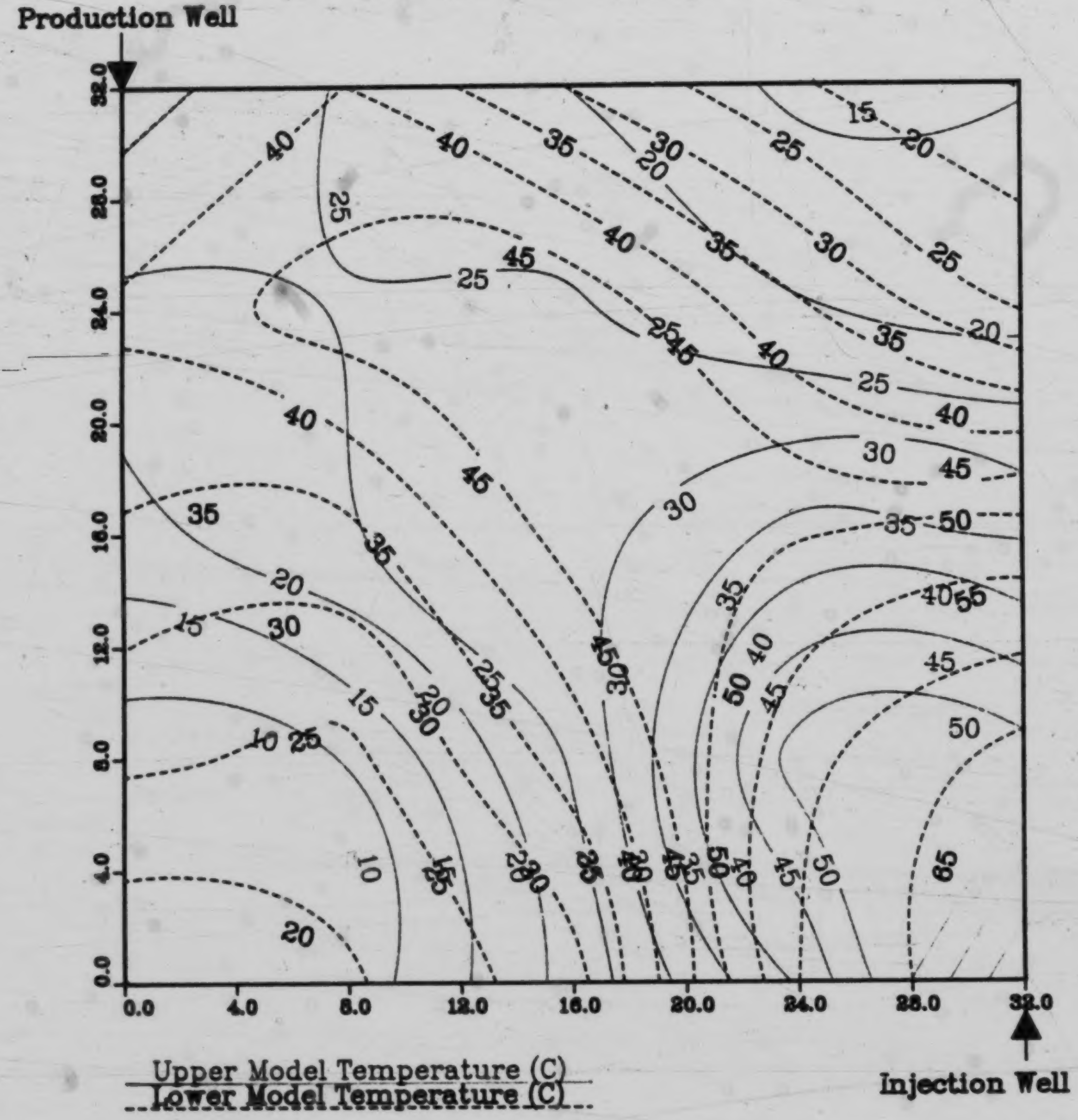

Figure A.207 : Run 58

Gas Inj. Solv.–Steamflood in B.W. Model

Temperature Profile for 1.25 Pore Volumes Injected

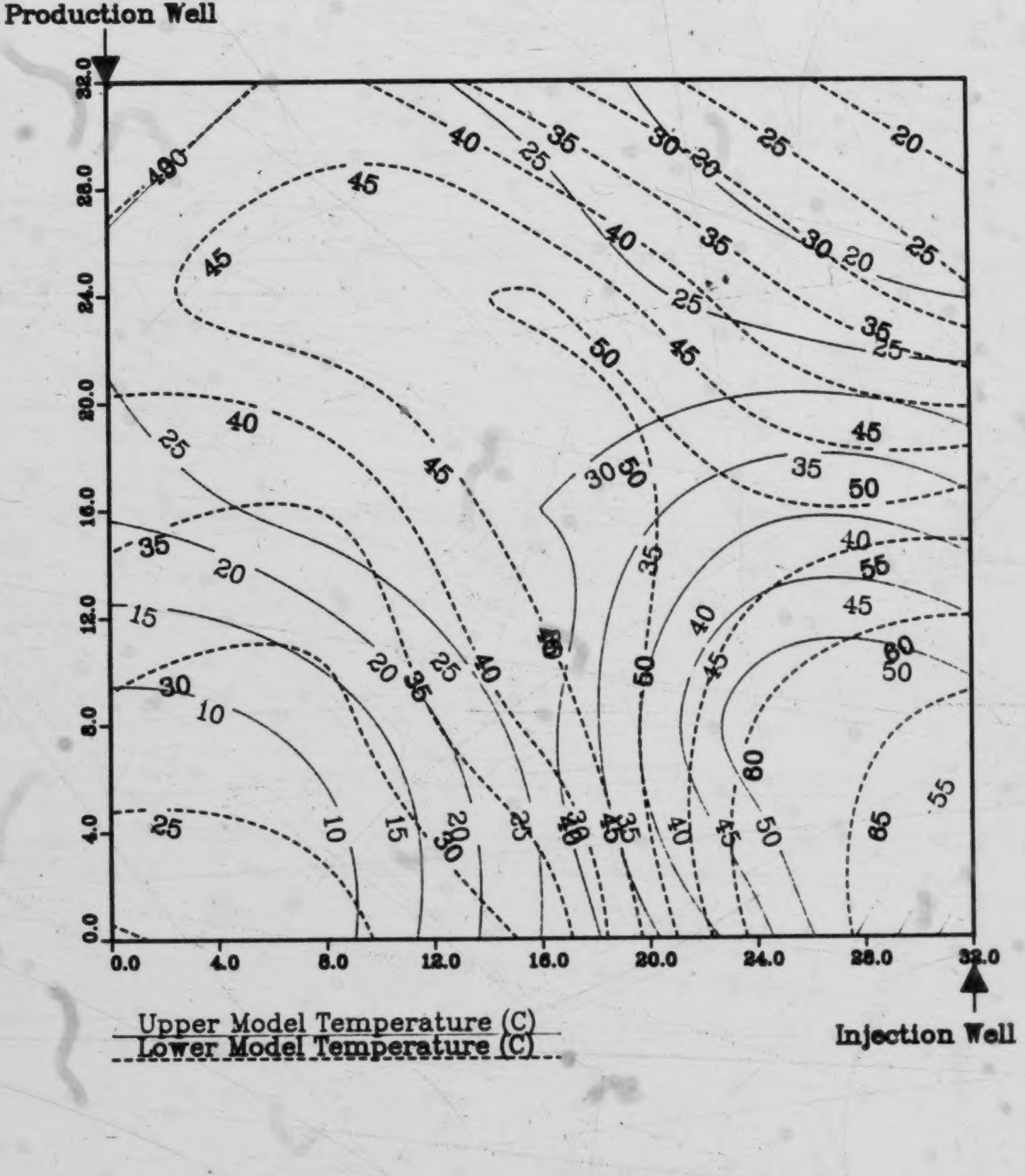

Figure A.208 : Run 58

Gas Inj. Solv.–Steamflood in B.W. Model

Temperature Profile for 1.50 Pore Volumes Injected

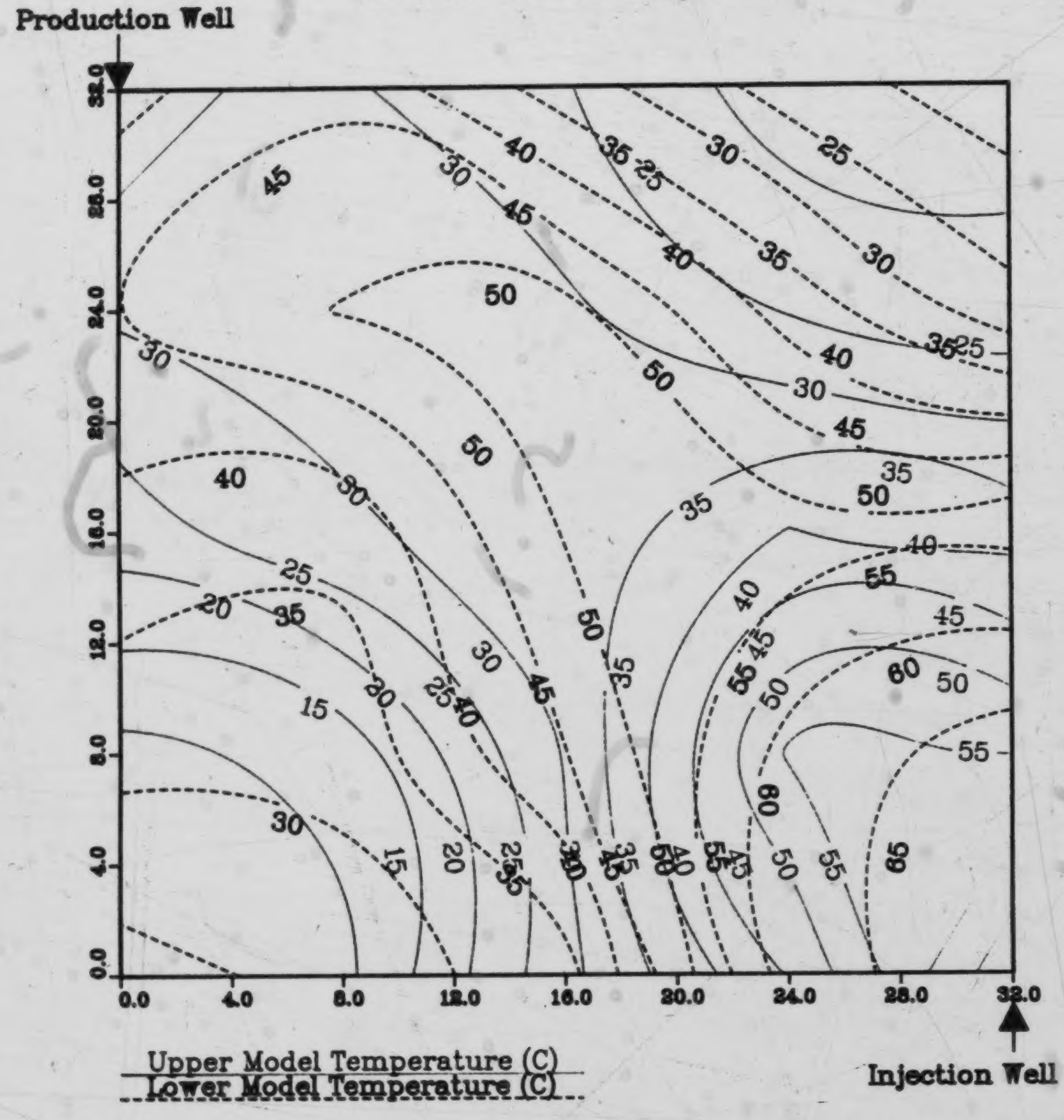

Figure A.209 : Run 58

Gas Inj. Solv.–Steamflood in B.W. Model

Temperature Profile for 1.75 Pore Volumes Injected

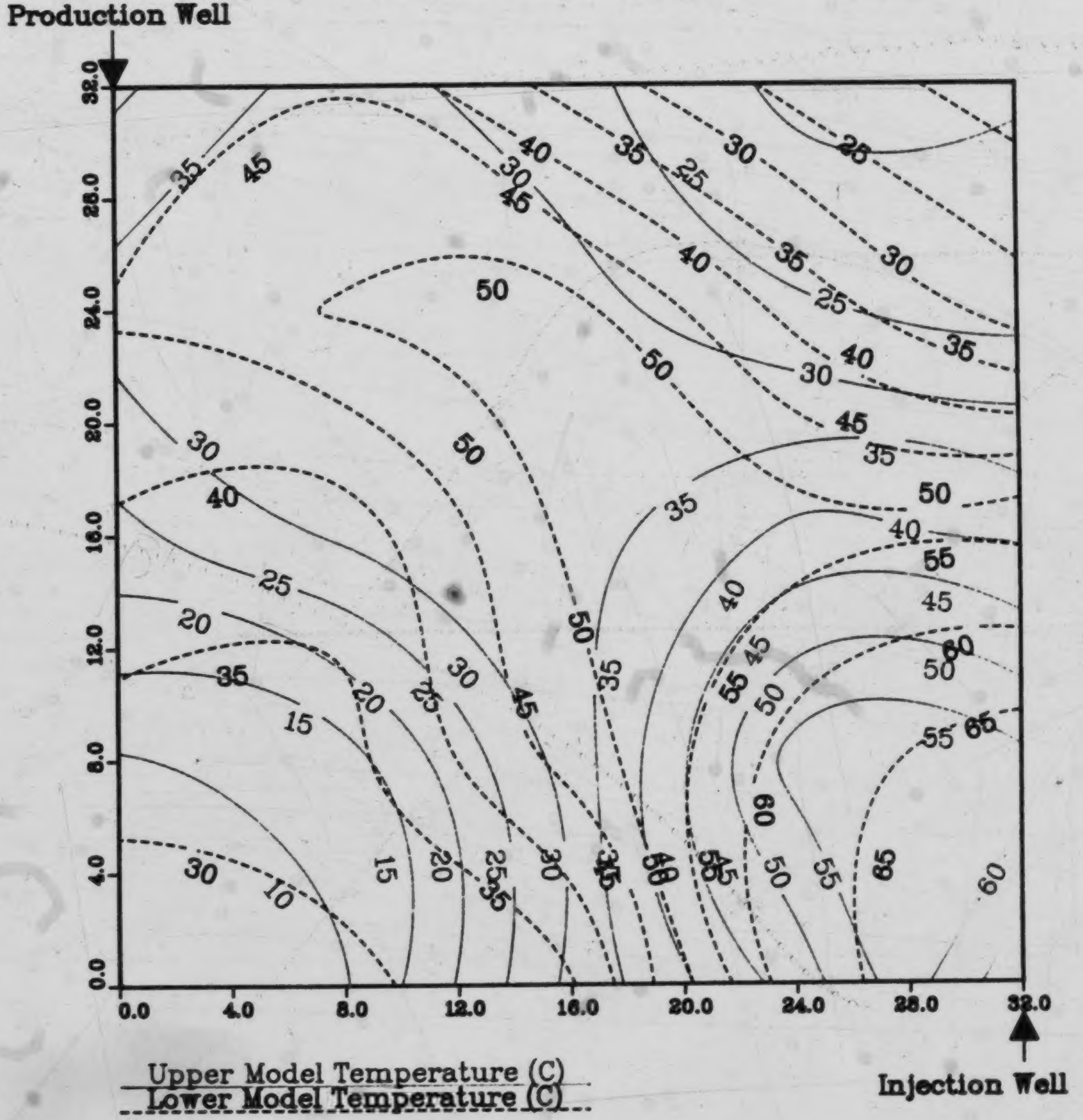

Figure A.210 : Run 58

Gas Inj. Solv.–Steamflood in B.W. Model

Temperature Profile for
2.00 Pore Volumes Injected

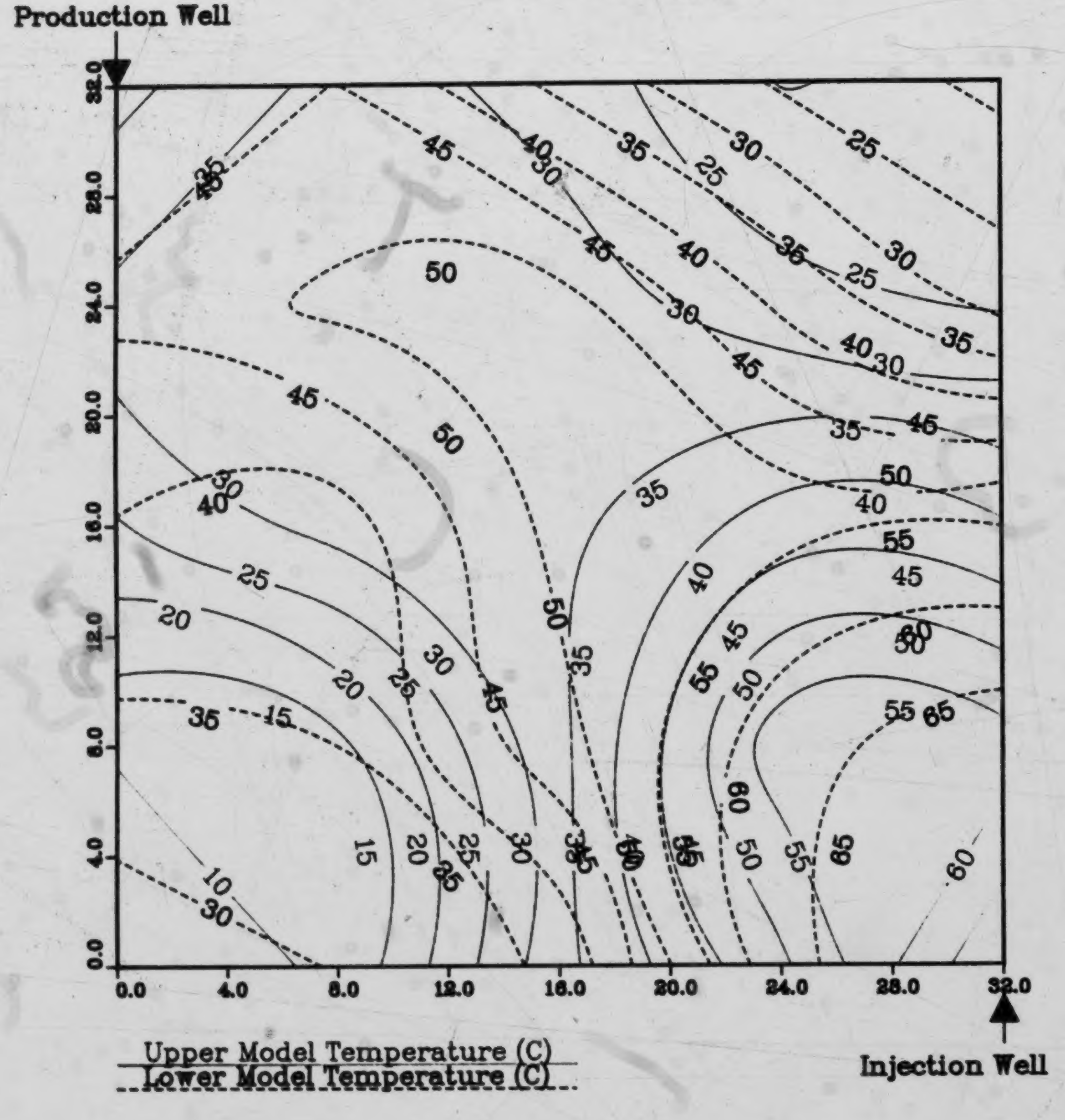

Figure A.211 :Run 58 Temp Profile
Injector to Producer Cross–Section
0.25 Pore Volumes Injected.

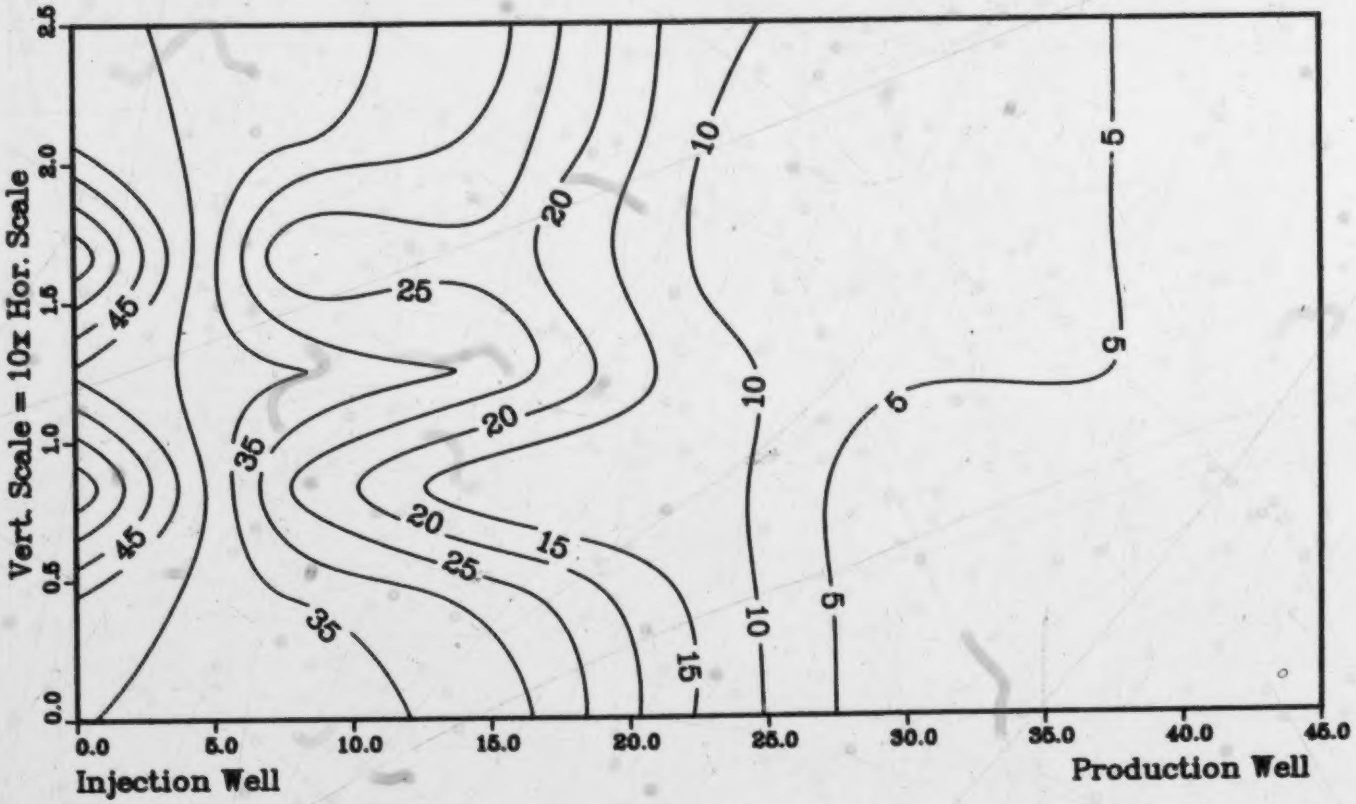

Figure A.212 :Run 58 Temp Profile
Injector to Producer Cross–Section
0.50 Pore Volumes Injected.

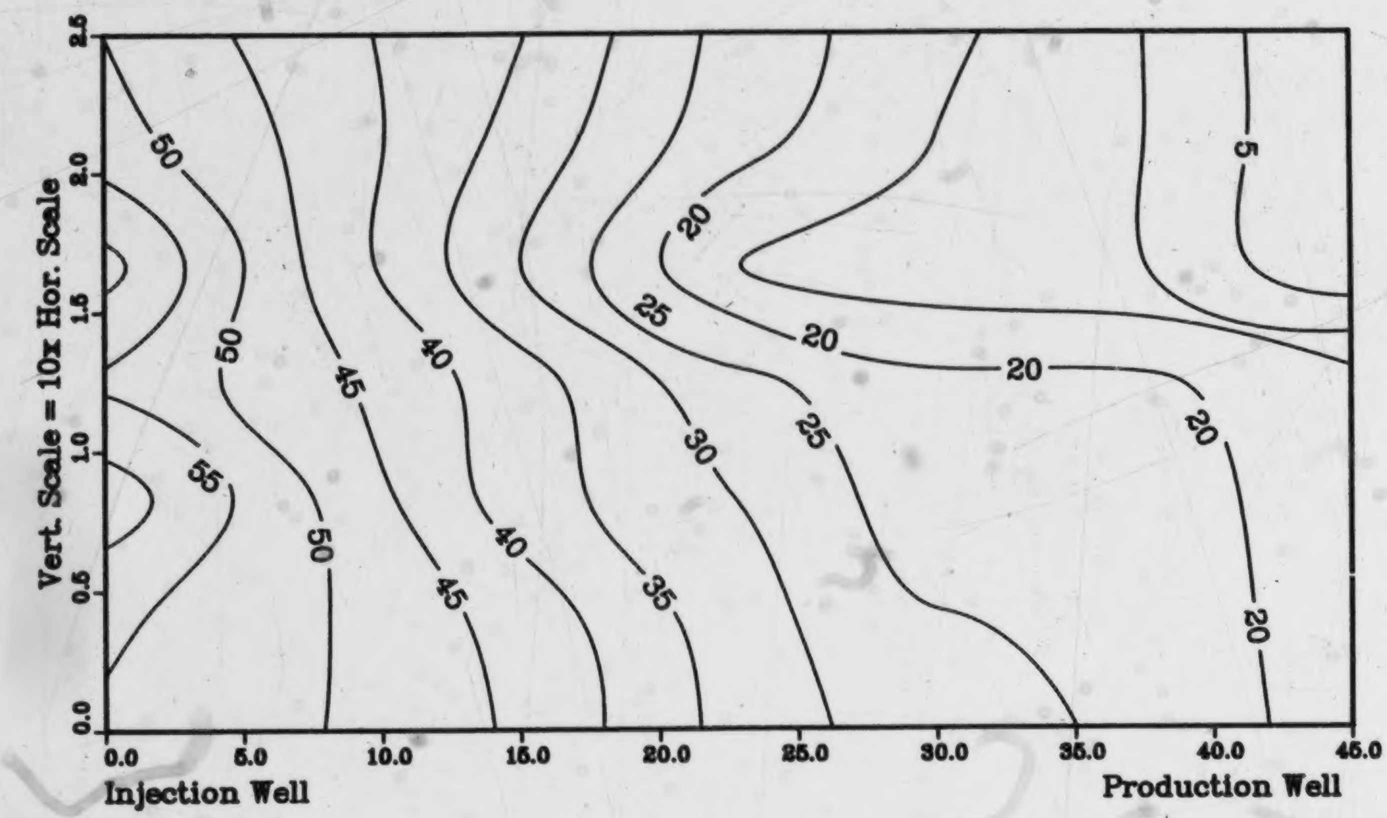

Figure A.213 :Run 58 Temp Profile
Injector to Producer Cross–Section
0.75 Pore Volumes Injected.

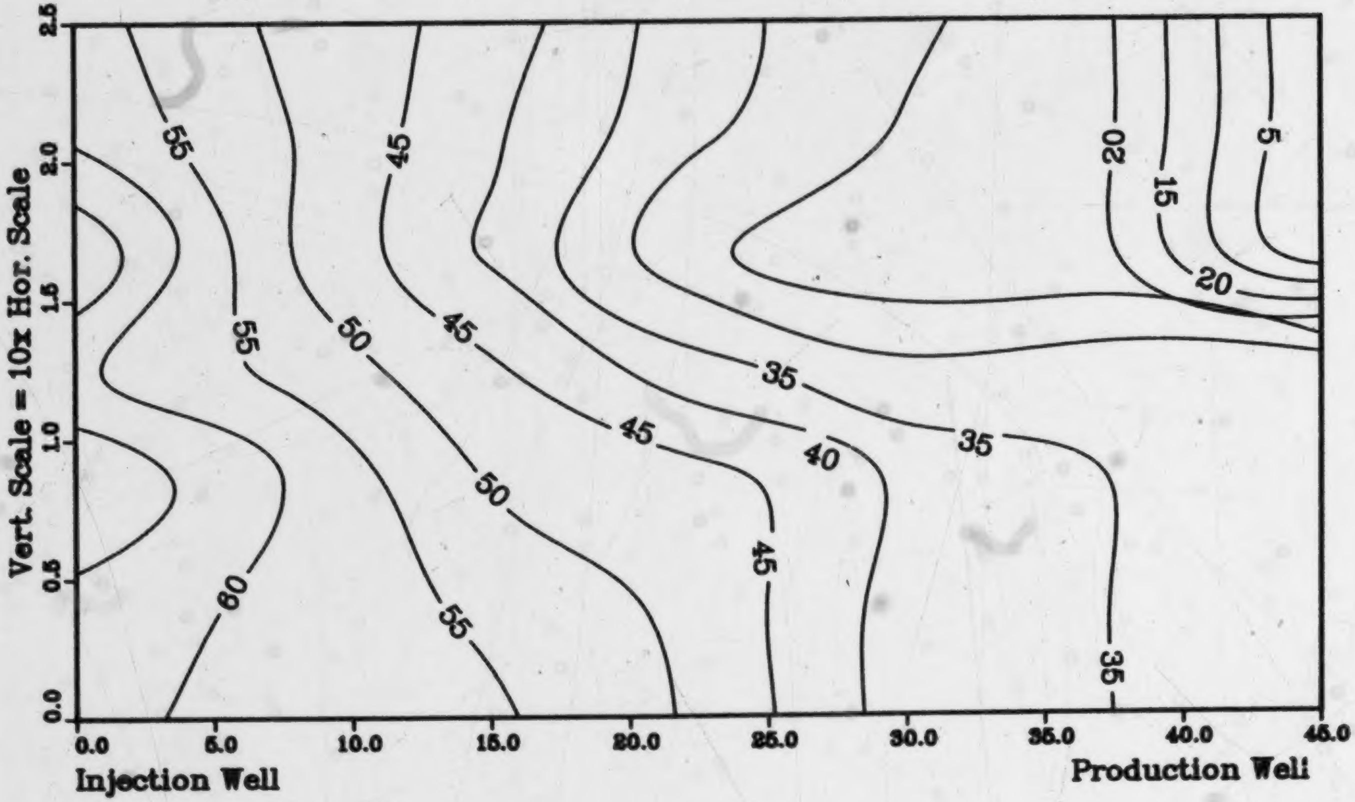

Figure A.214 :Run 58 Temp Profile
Injector to Producer Cross–Section
1.00 Pore Volumes Injected.

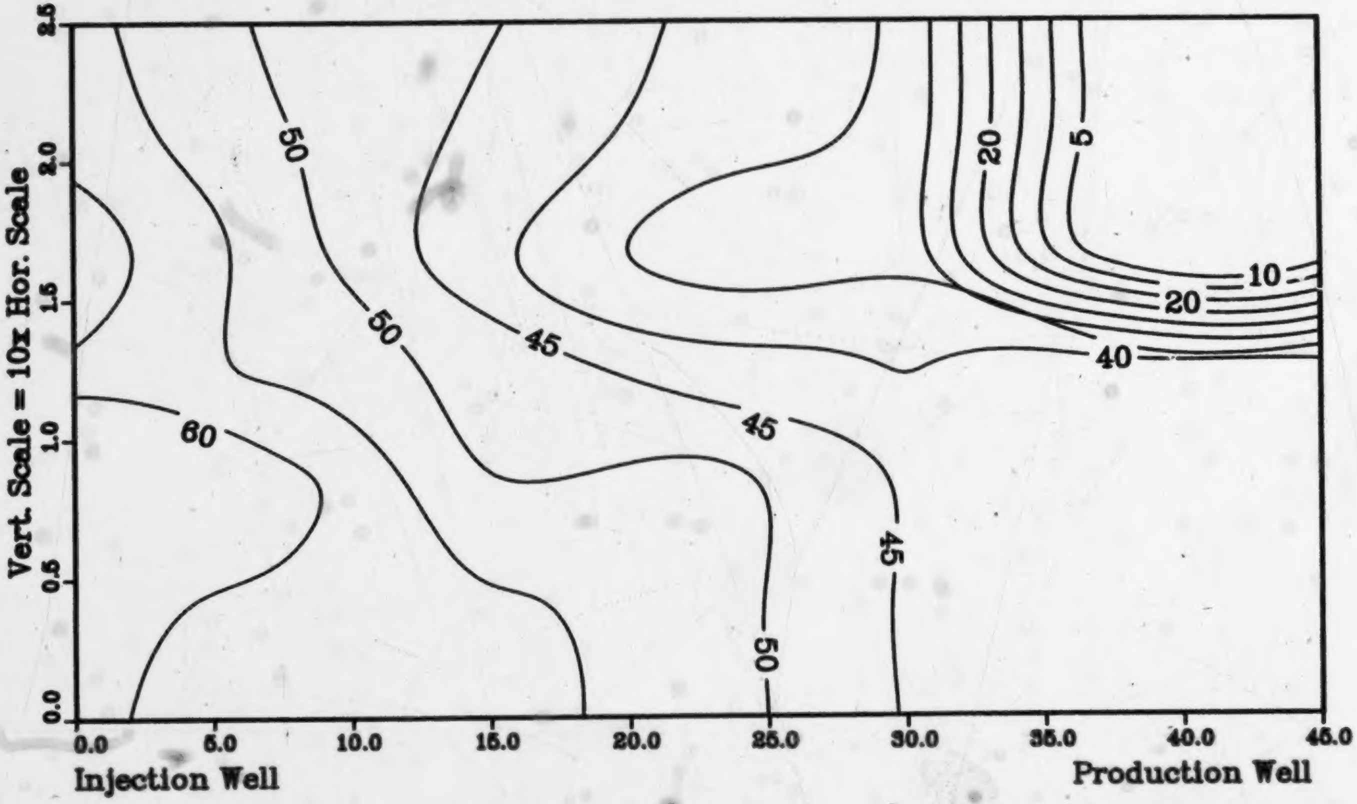

Figure A.215 : Run 59

Gas Inj. Solv.–Steamflood in B.W. Model

Temperature Profile for
0.25 Pore Volumes Injected

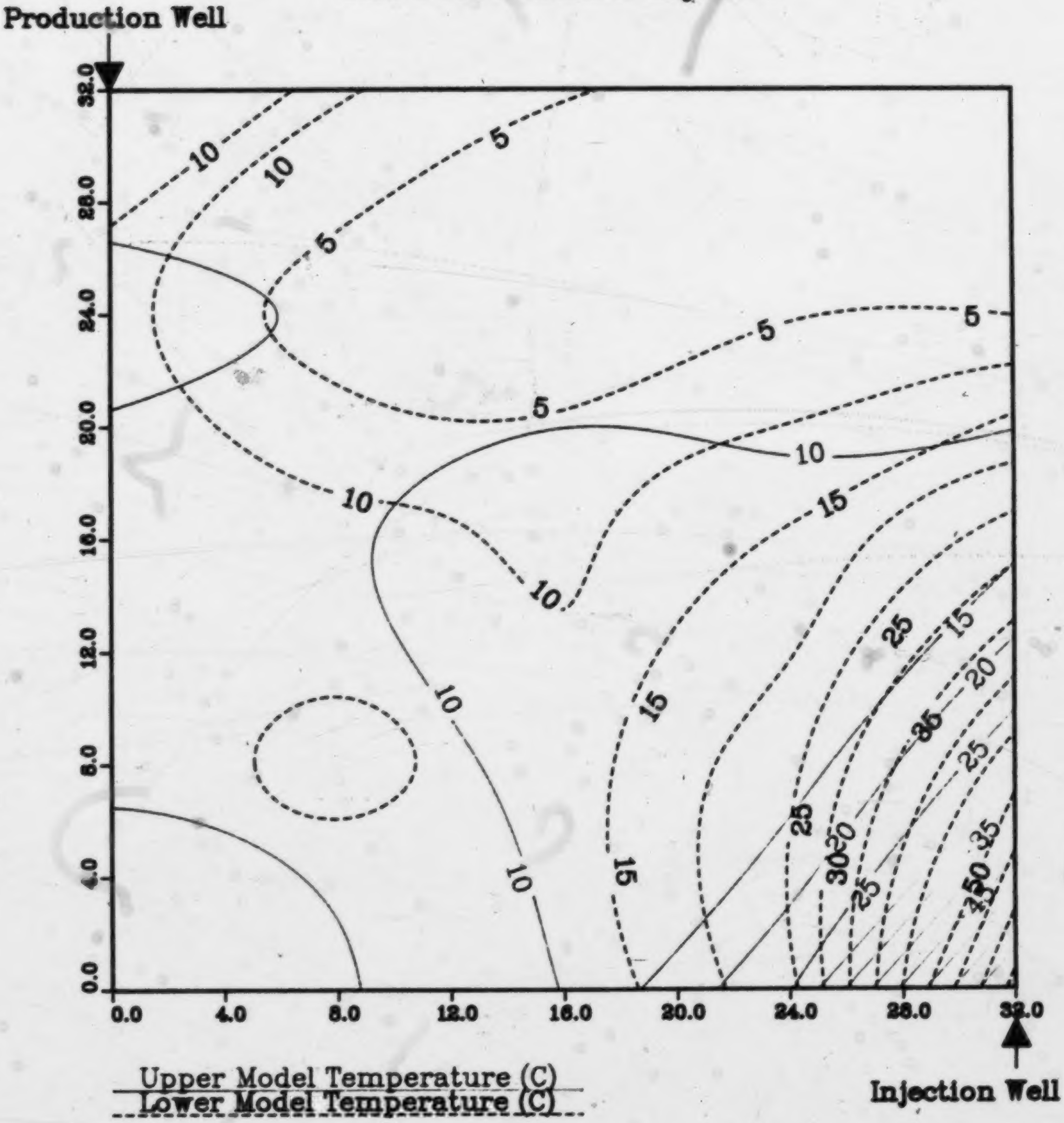

Figure A.216 : Run 59

Gas Inj. Solv.–Steamflood in B.W. Model

Temperature Profile for
0.50 Pore Volumes Injected

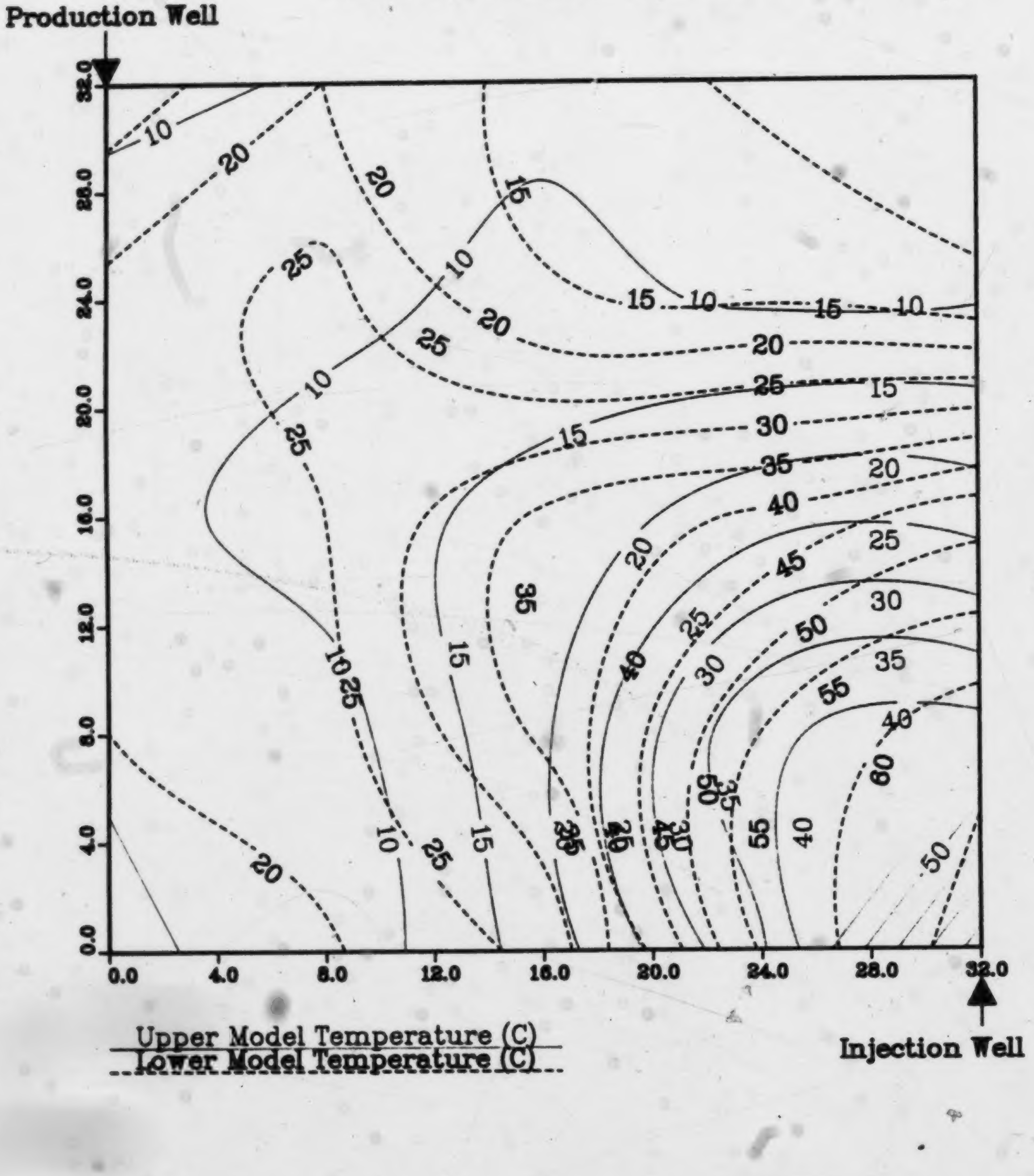

Figure A.217 : Run 59

Gas Inj. Solv.–Steamflood in B.W. Model

Temperature Profile for
0.75 Pore Volumes Injected

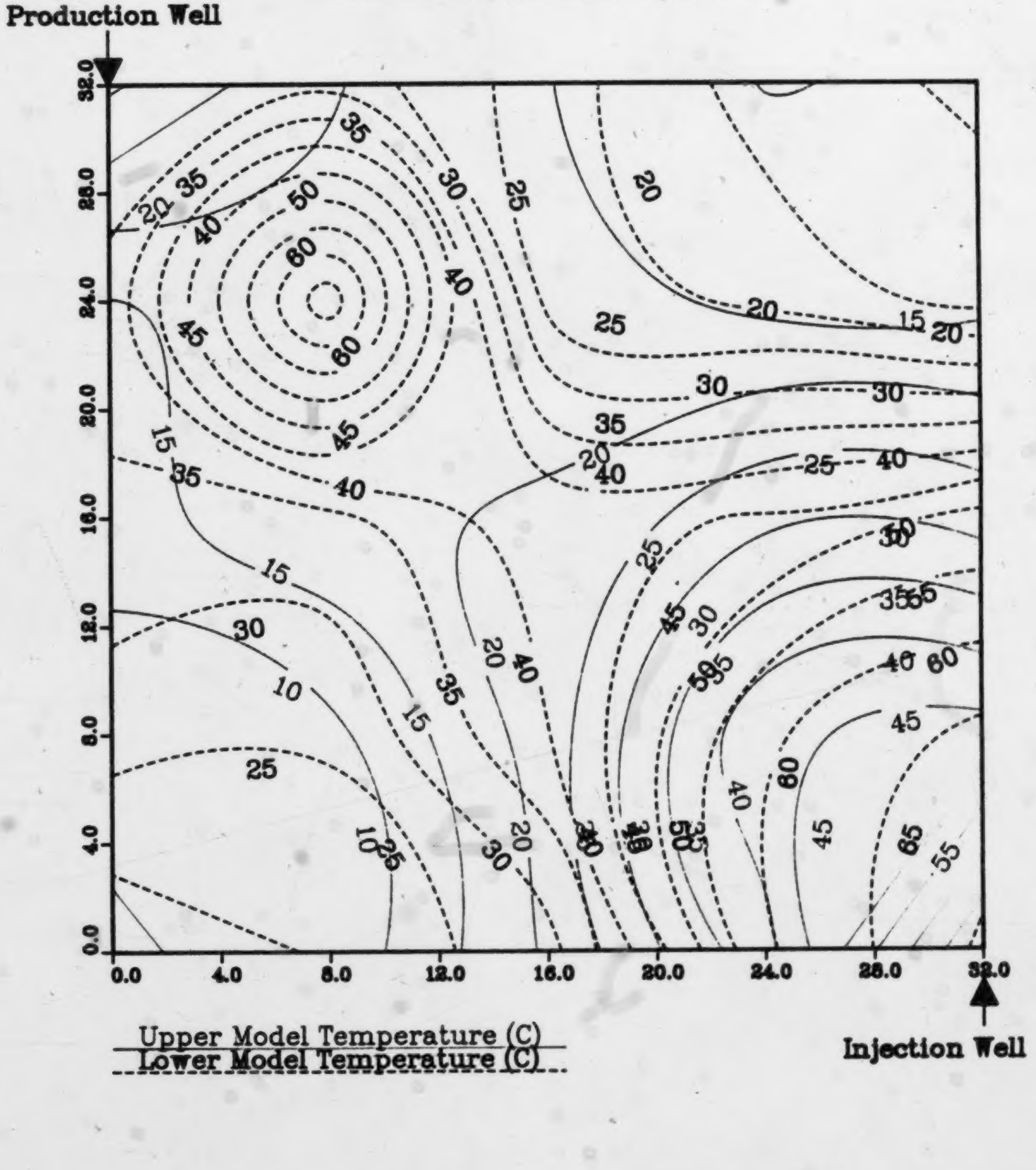

Figure A.218 : Run 59

Gas Inj. Solv.–Steamflood in B.W. Model

Temperature Profile for
1.00 Pore Volumes Injected

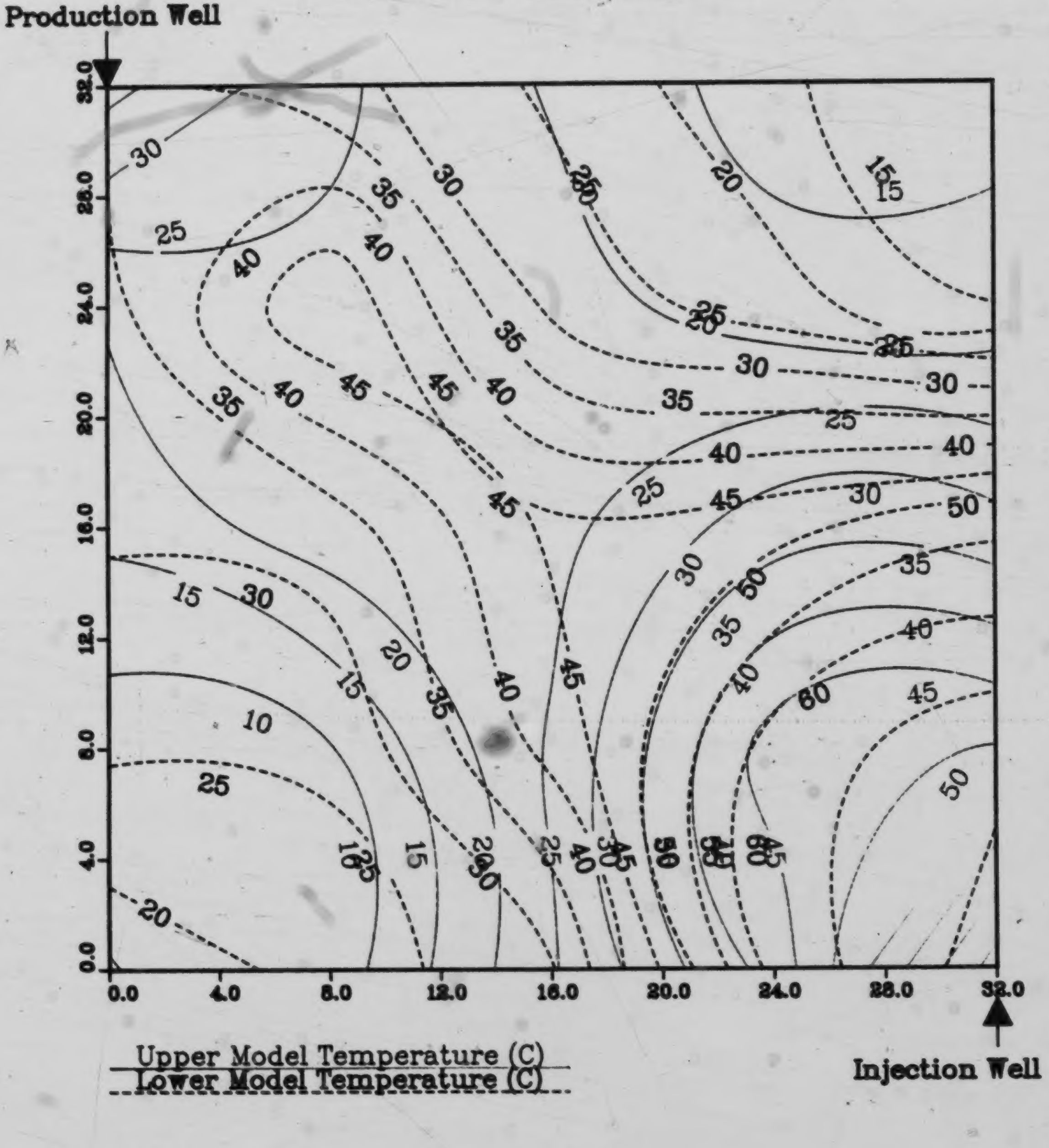

Figure A.219 : Run 59

Gas Inj. Solv.–Steamflood in B.W. Model

Temperature Profile for 1.25 Pore Volumes Injected

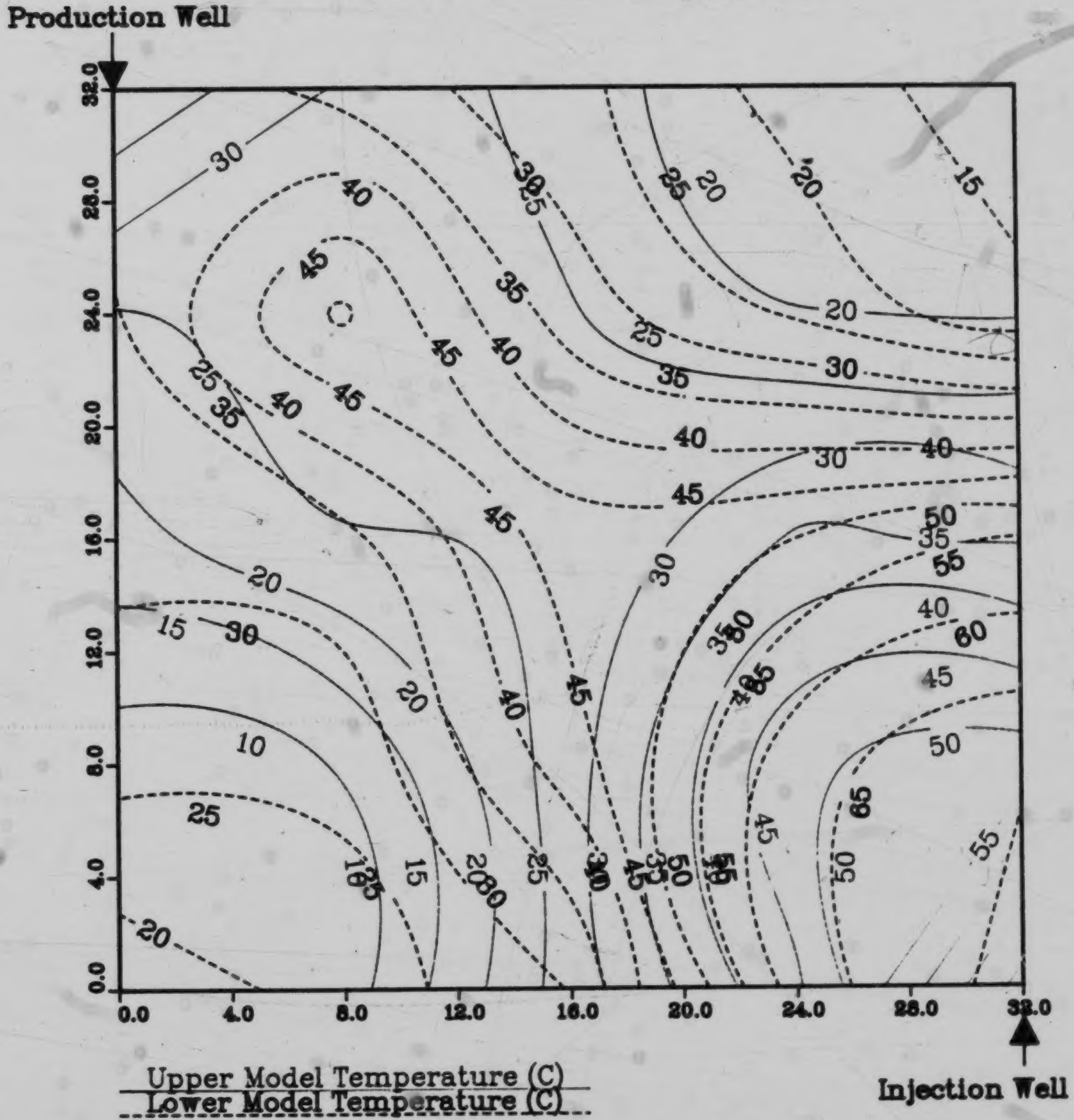

Figure A.220 : Run 59

Gas Inj. Solv.–Steamflood in B.W. Model

Temperature Profile for 1.50 Pore Volumes Injected

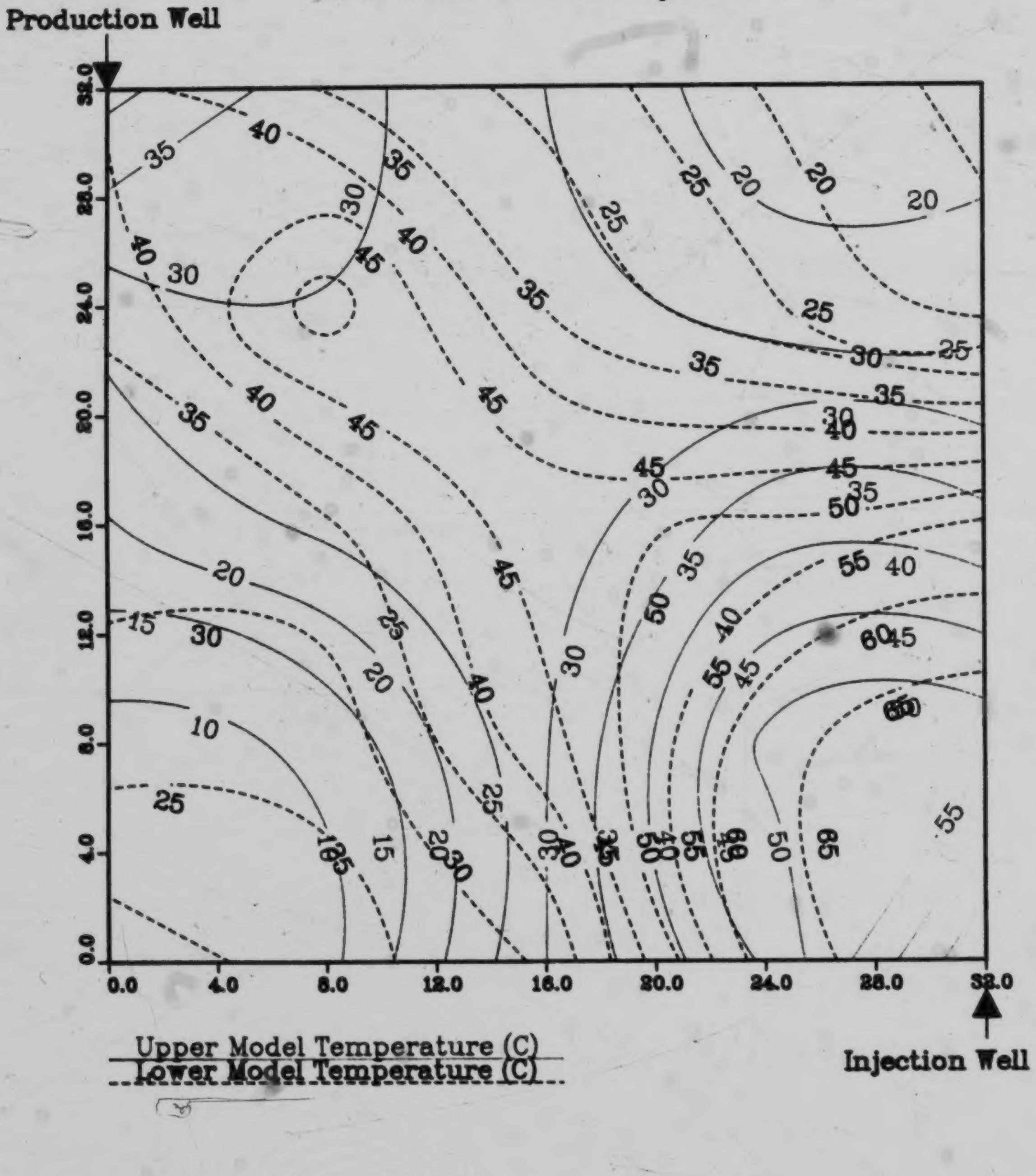

Figure A.221 : Run 59

Gas Inj. Solv.–Steamflood in B.W. Model

Temperature Profile for 1.75 Pore Volumes Injected

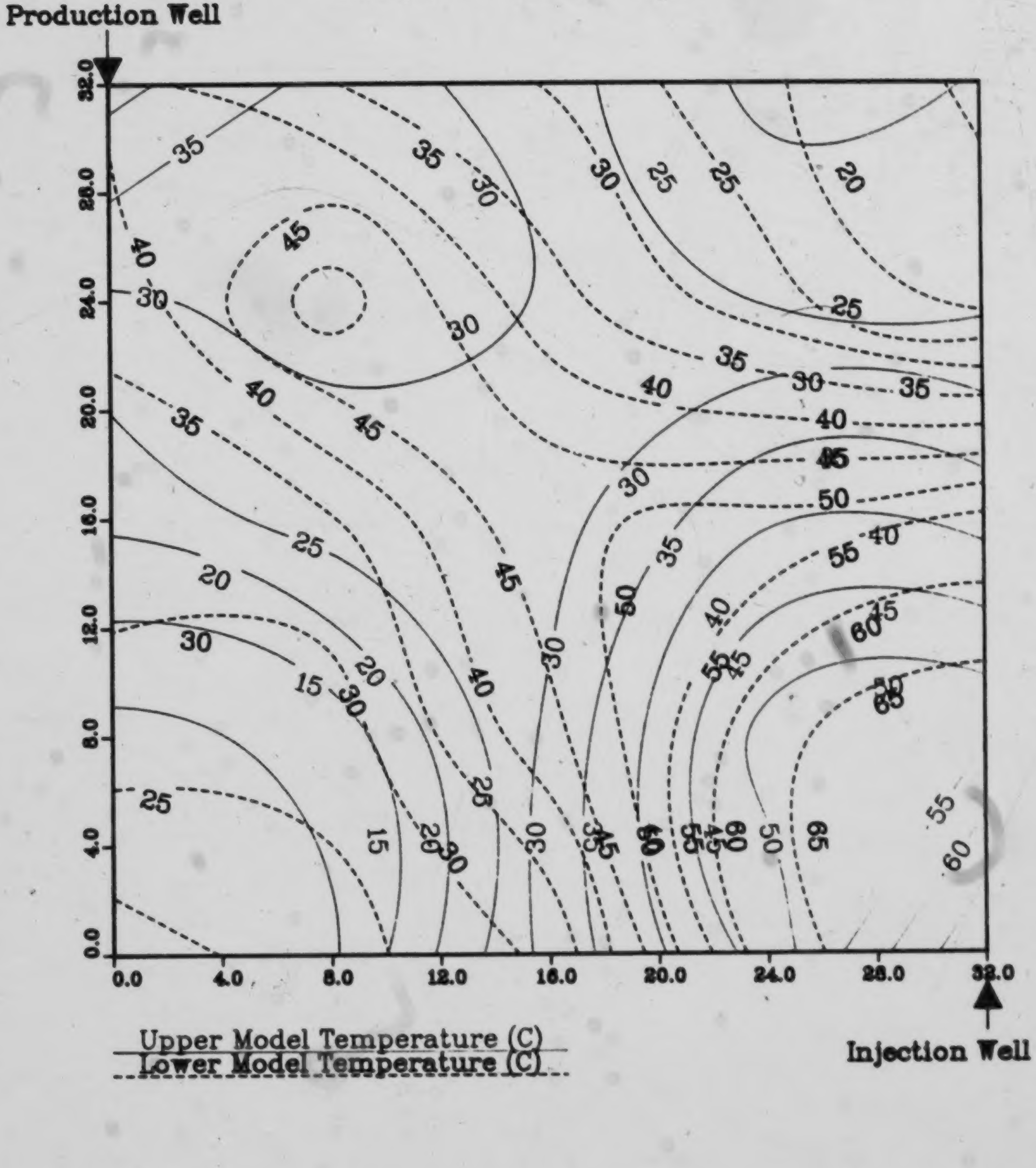

Figure A.222 : Run 59

Gas Inj. Solv.–Steamflood in B.W. Model

Temperature Profile for 2.00 Pore Volumes Injected

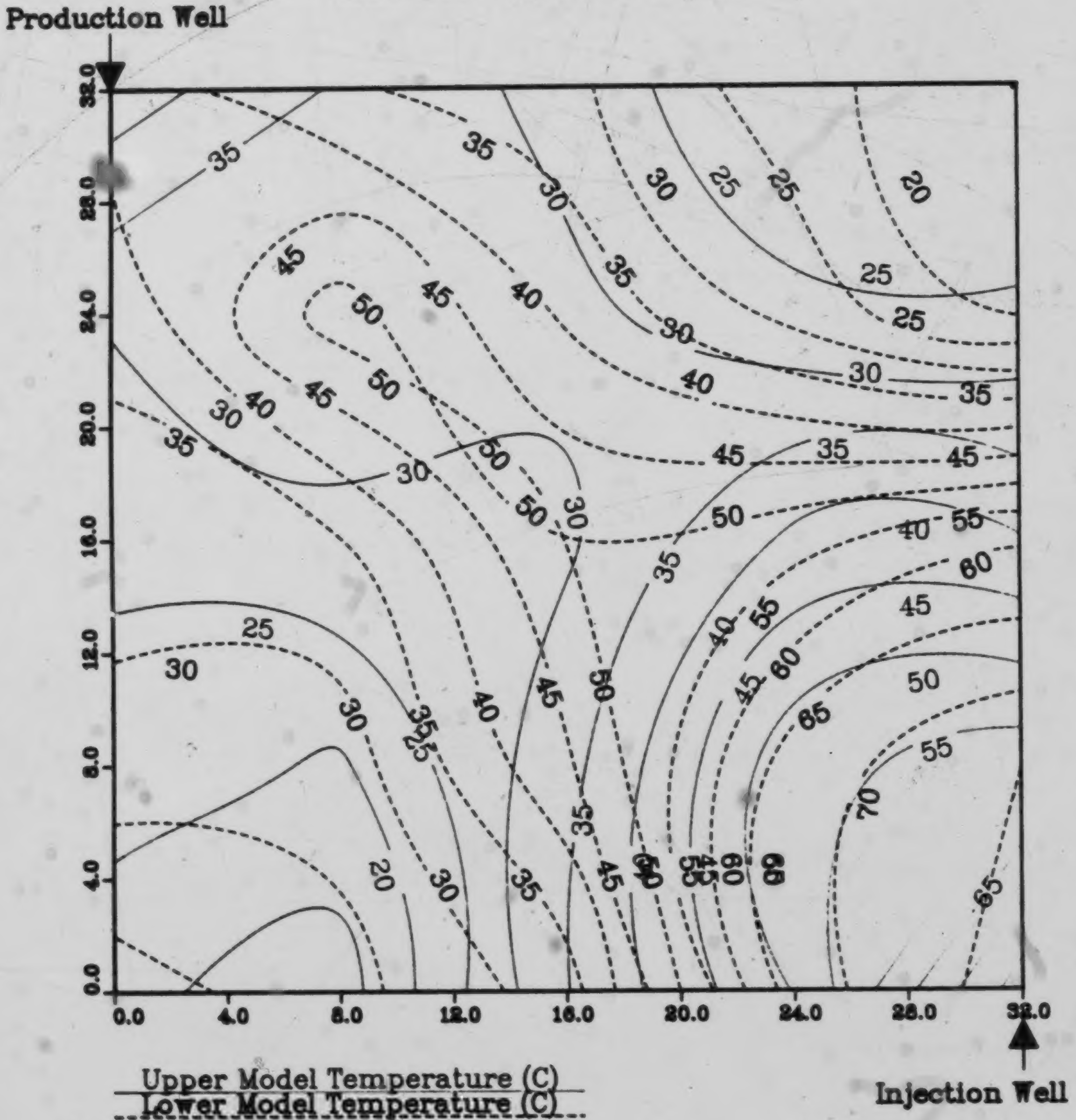

Figure A.223 :Run 59 Temp Profile
Injector to Producer Cross–Section
0.25 Pore Volumes Injected.

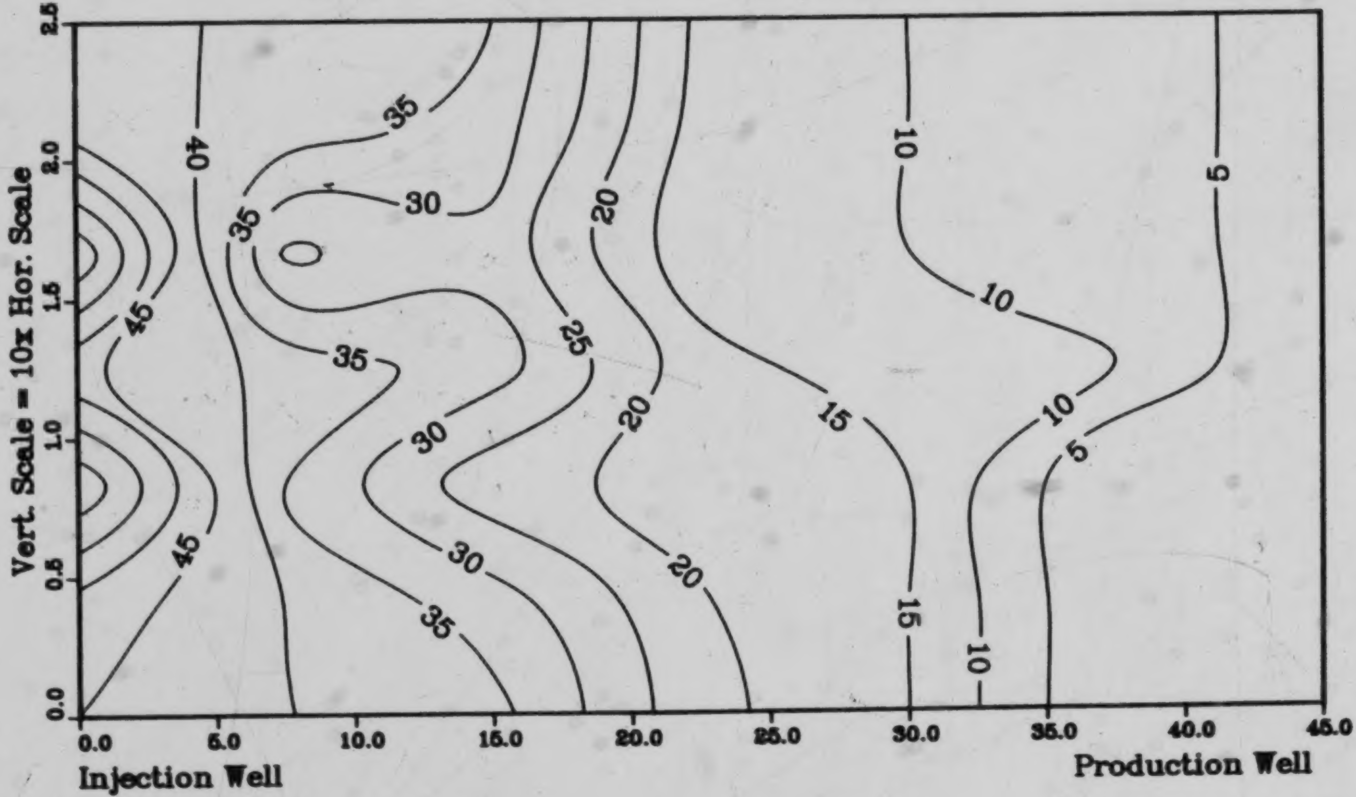

Figure A.224 :Run 59 Temp Profile
Injector to Producer Cross–Section
0.50 Pore Volumes Injected.

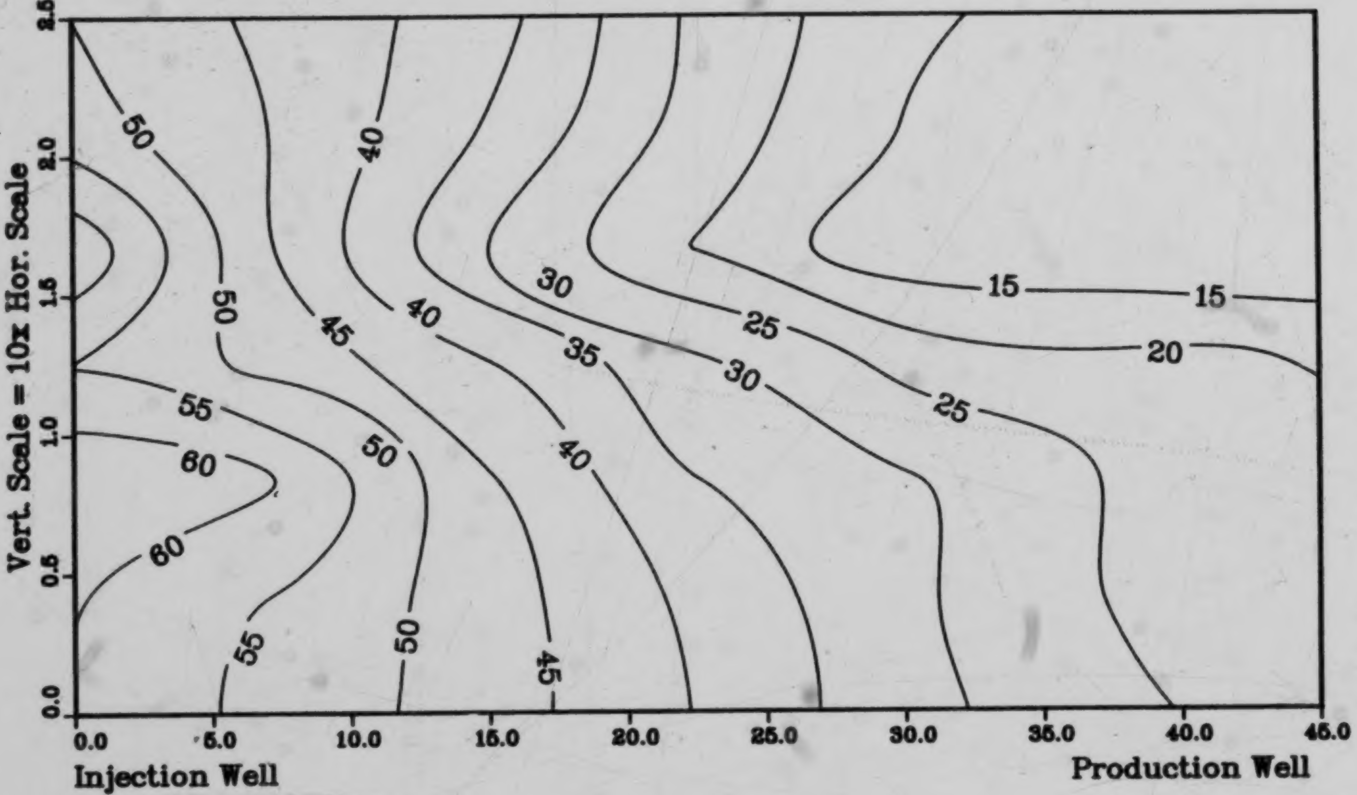

Figure A.225 :Run 59 Temp Profile
Injector to Producer Cross–Section
0.75 Pore Volumes Injected.

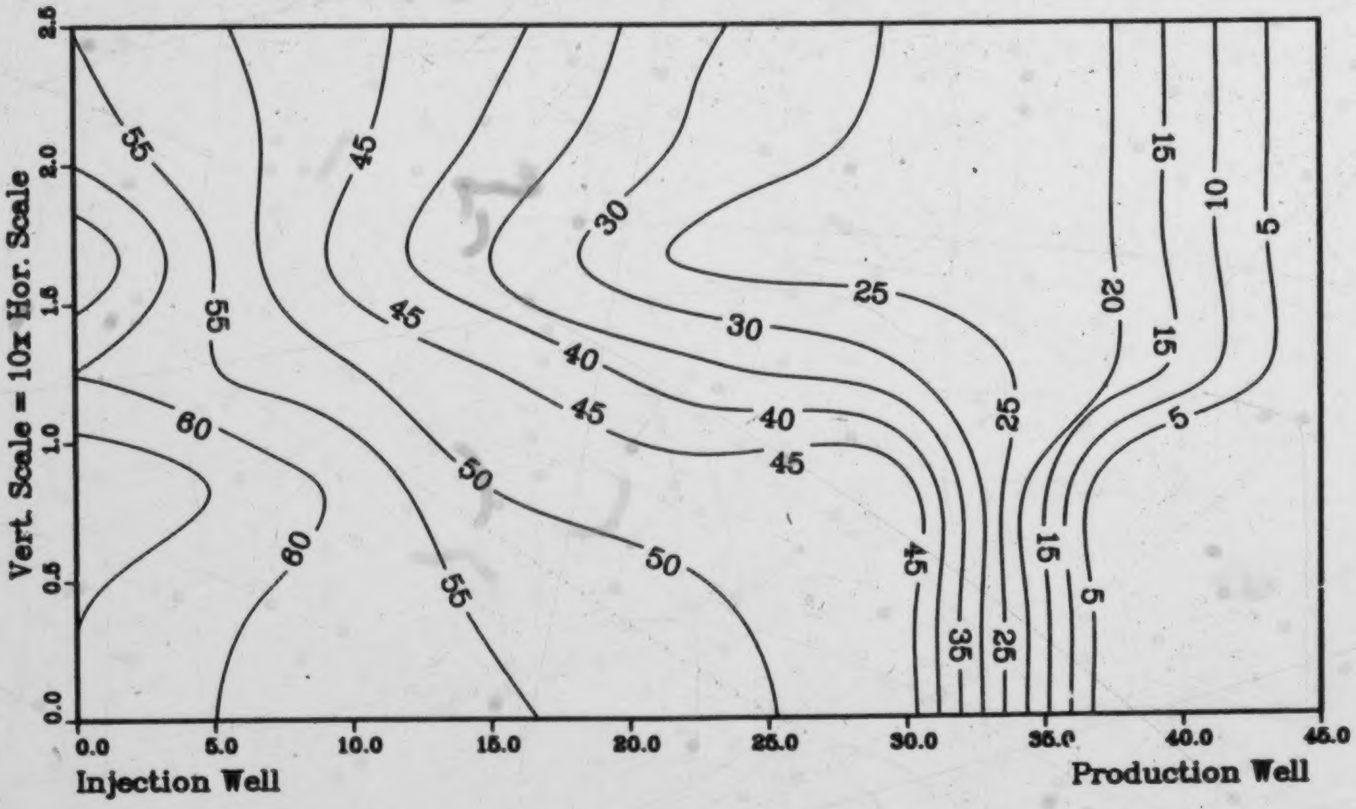

Figure A.226 :Run 59 Temp Profile
Injector to Producer Cross–Section
1.00 Pore Volumes Injected.

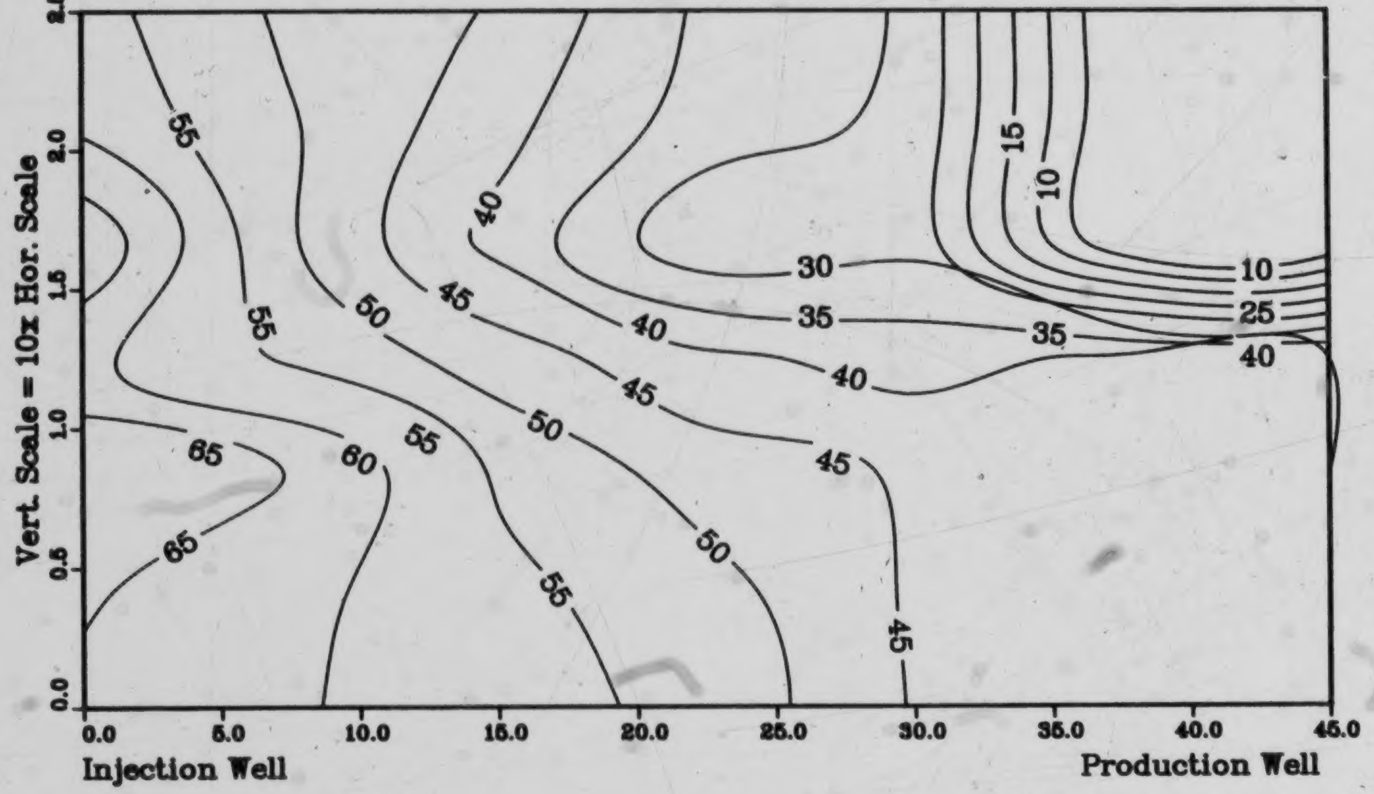

Figure A.227 : Run 62

Gas Inj. Solv.–Steamflood in B.W. Model

Temperature Profile for
0.25 Pore Volumes Injected

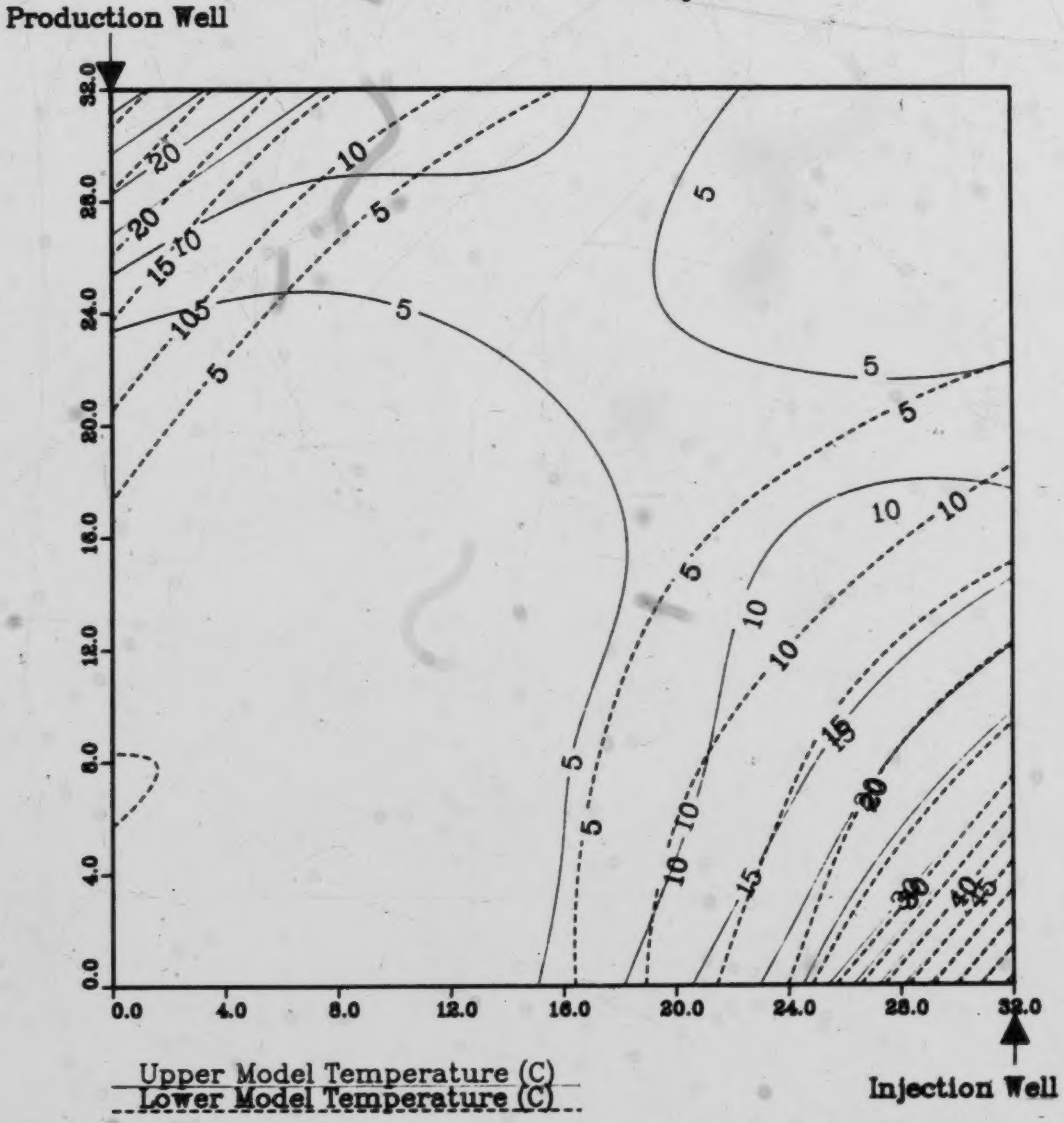

Figure A.228 : Run 62

Gas Inj. Solv.–Steamflood in B.W. Model

Temperature Profile for 0.50 Pore Volumes Injected

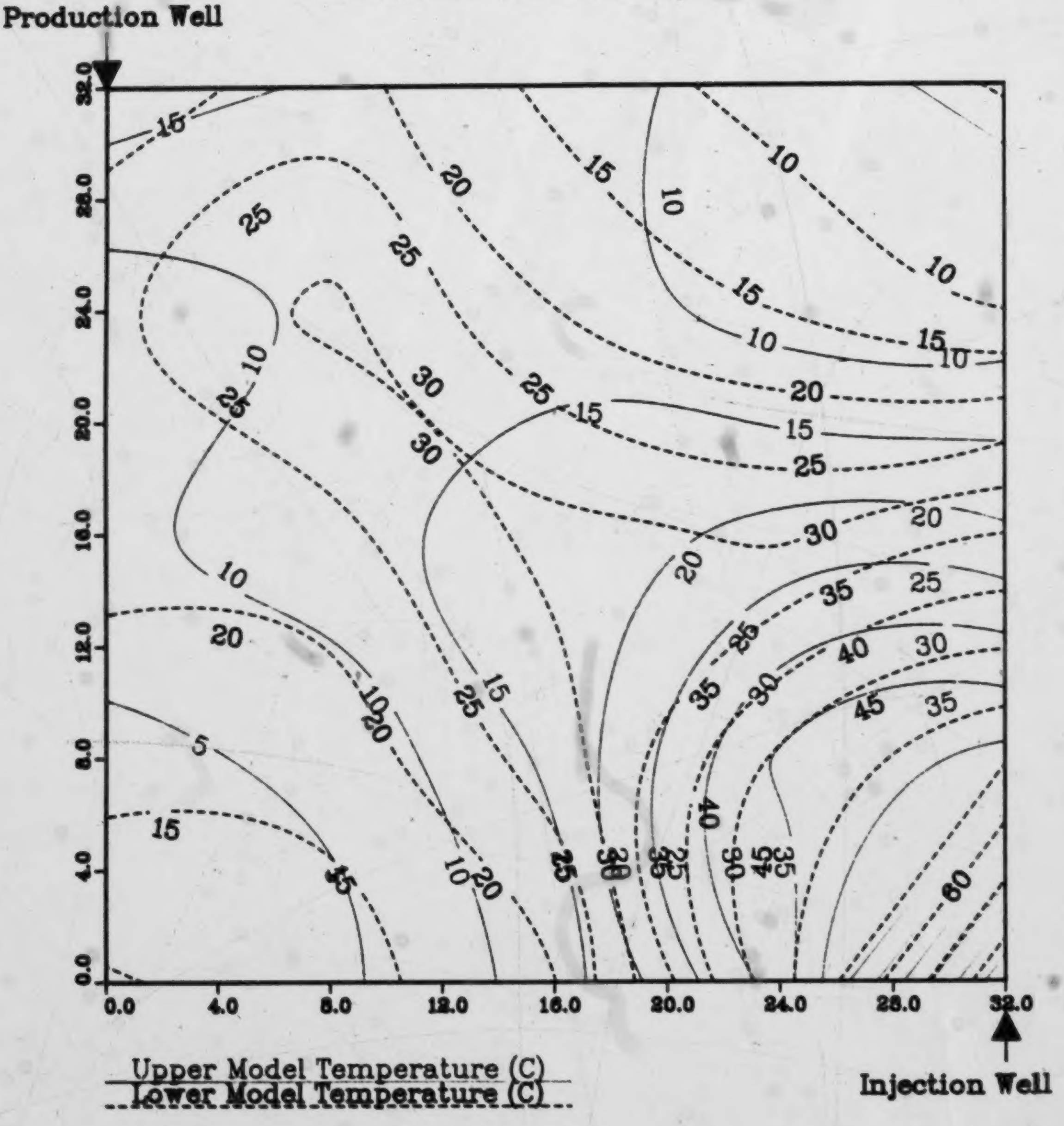

Figure A.229 : Run 62

Gas Inj. Solv.–Steamflood in B.W. Model

Temperature Profile for 0.75 Pore Volumes Injected

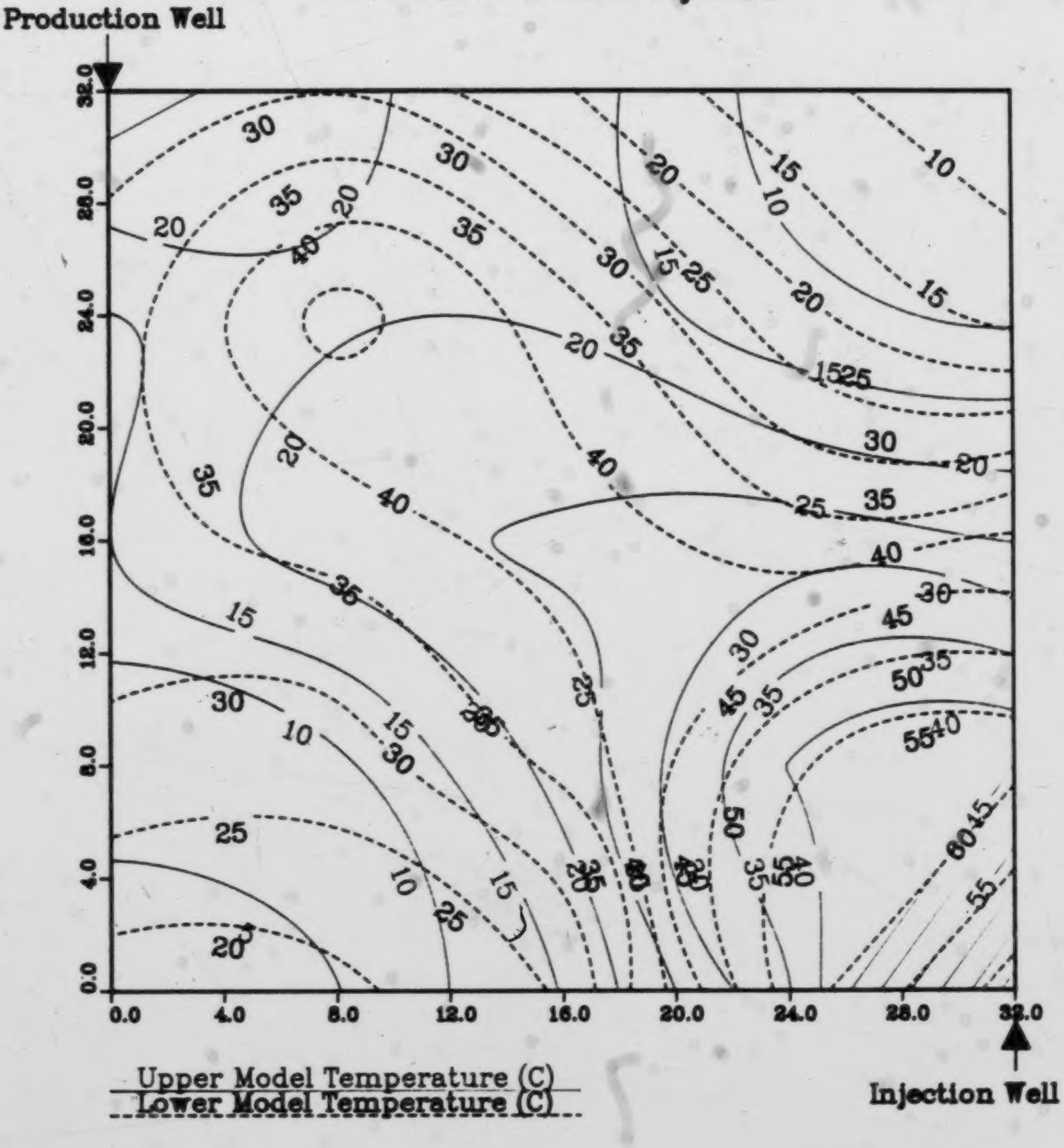

Figure A.230 : Run 62

Gas Inj. Solv.–Steamflood in B.W. Model

Temperature Profile for
1.00 Pore Volumes Injected

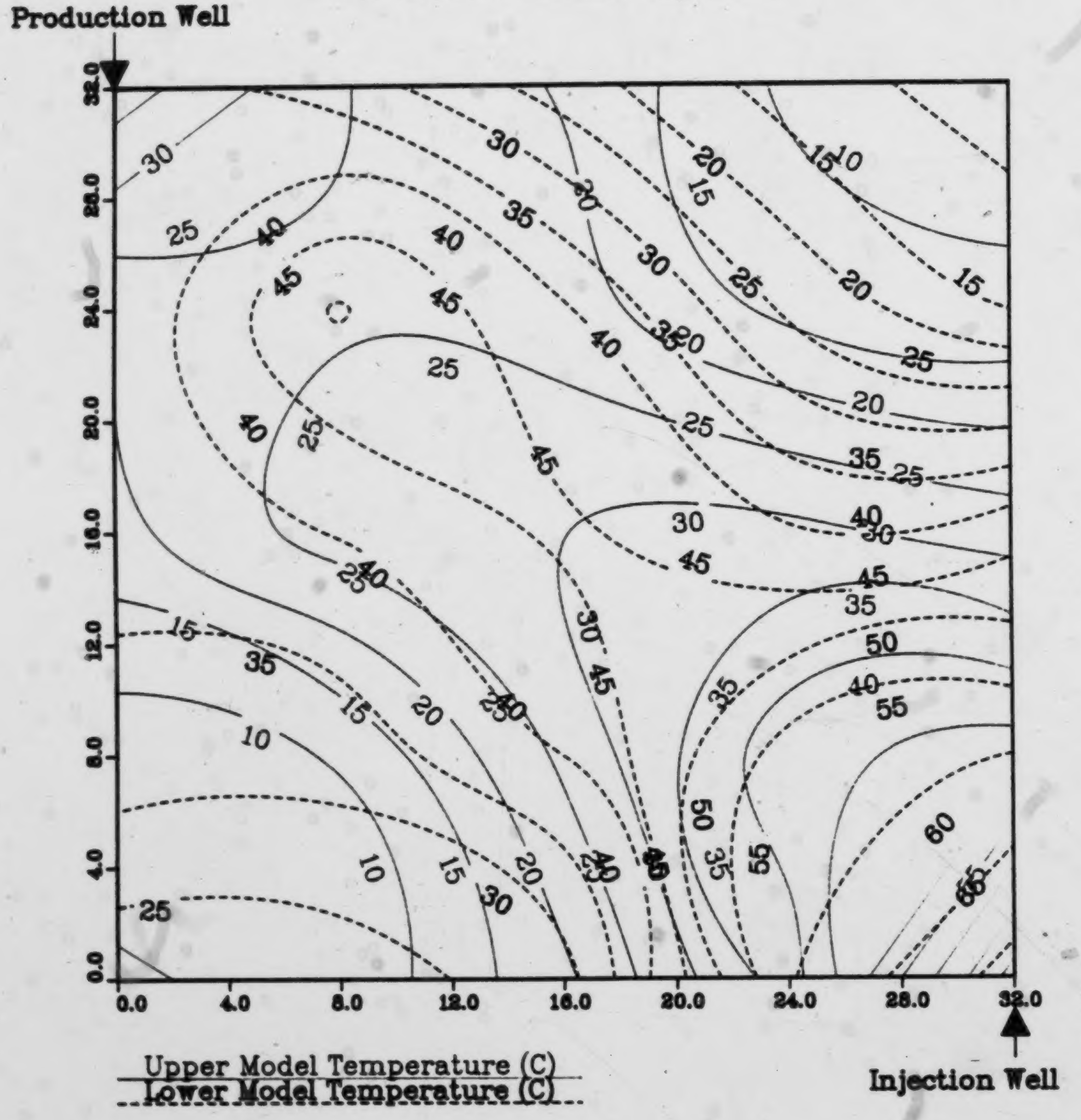

Figure A.231 : Run 62

Gas Inj. Solv.–Steamflood in B.W. Model

Temperature Profile for 1.25 Pore Volumes Injected

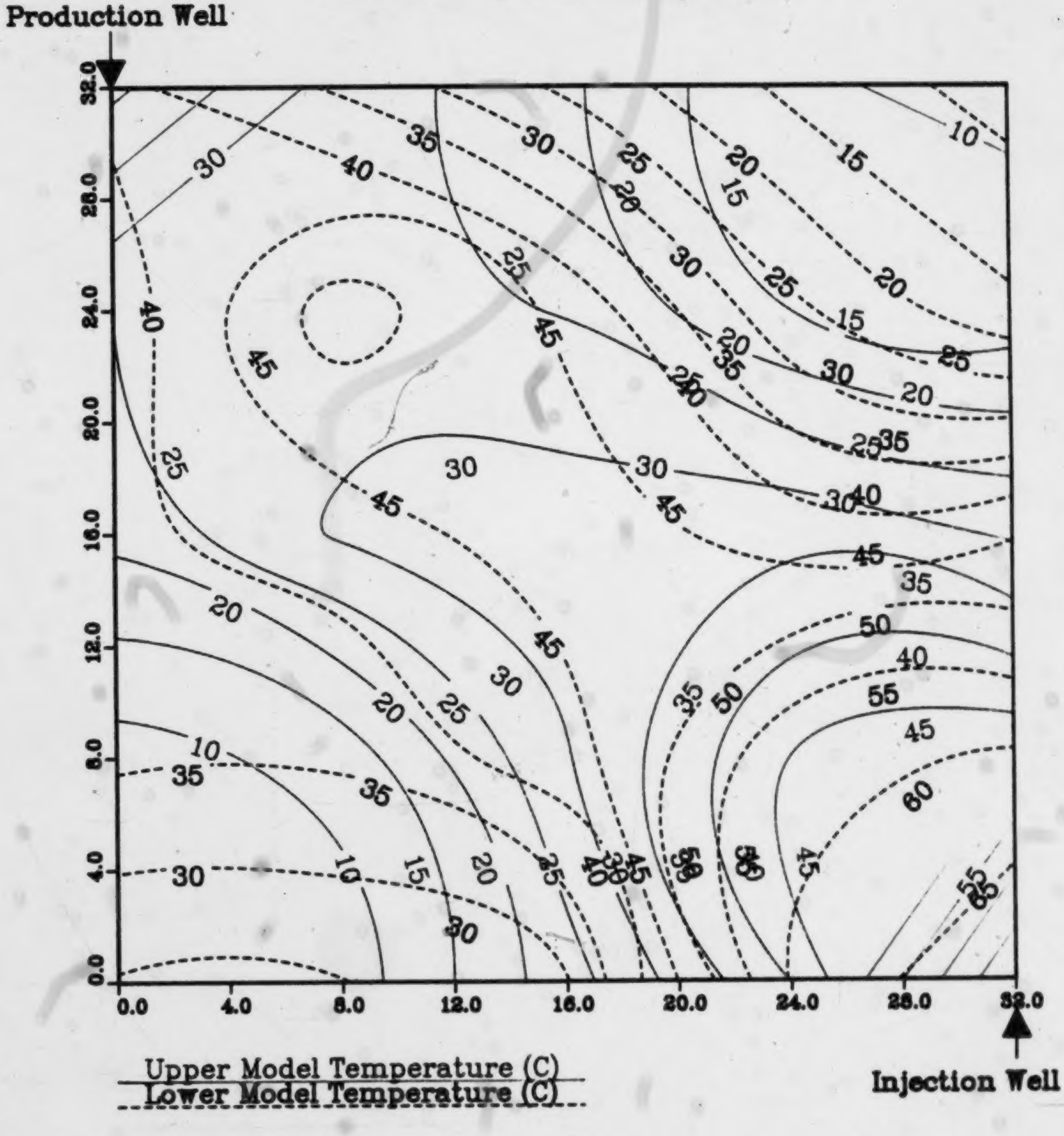

Figure A.232 : Run 62

Gas Inj. Solv.–Steamflood in B.W. Model

Temperature Profile for 1.50 Pore Volumes Injected

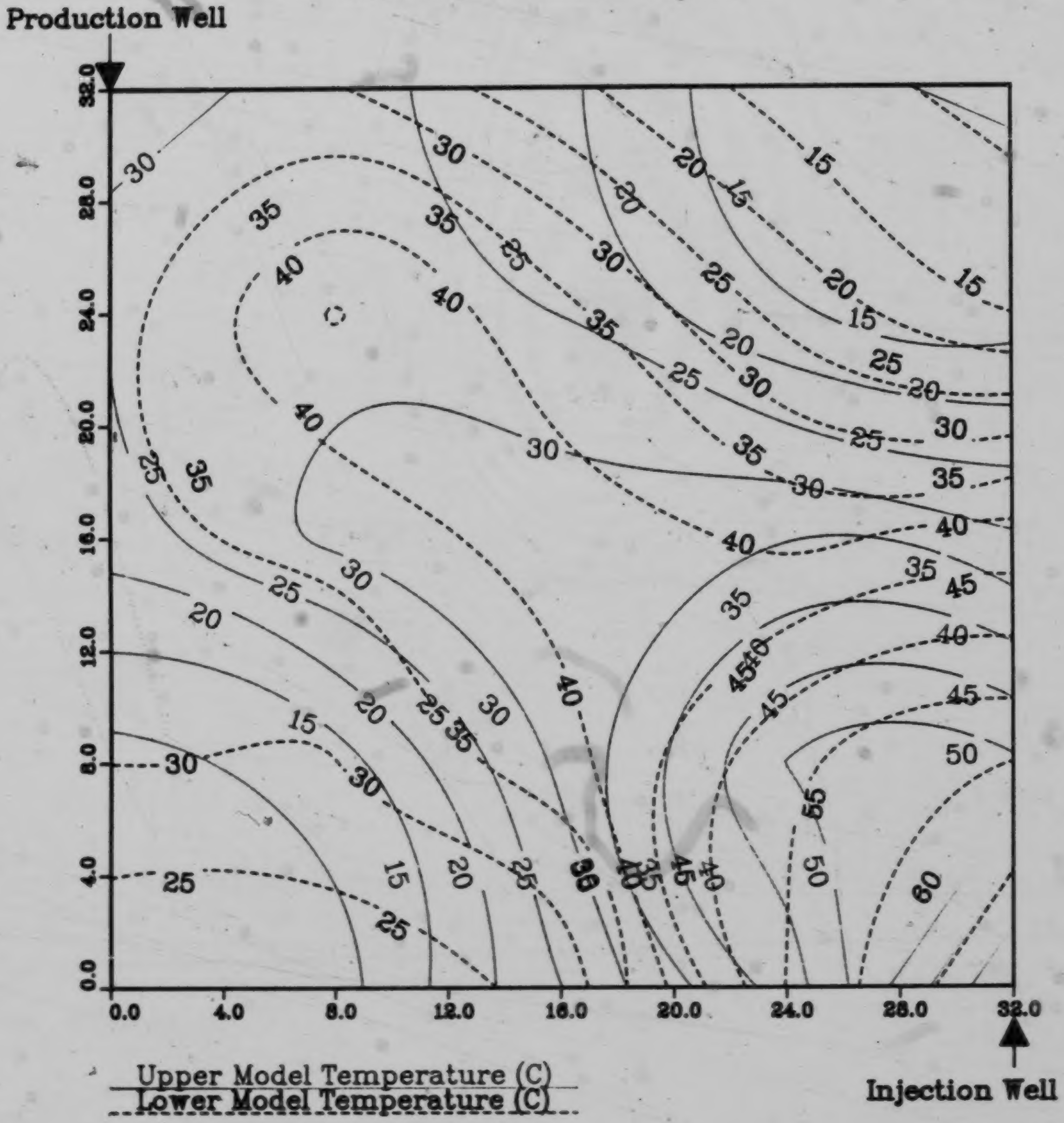

Figure A.233 : Run 62

Gas Inj. Solv.–Steamflood in B.W. Model

Temperature Profile for 1.75 Pore Volumes Injected

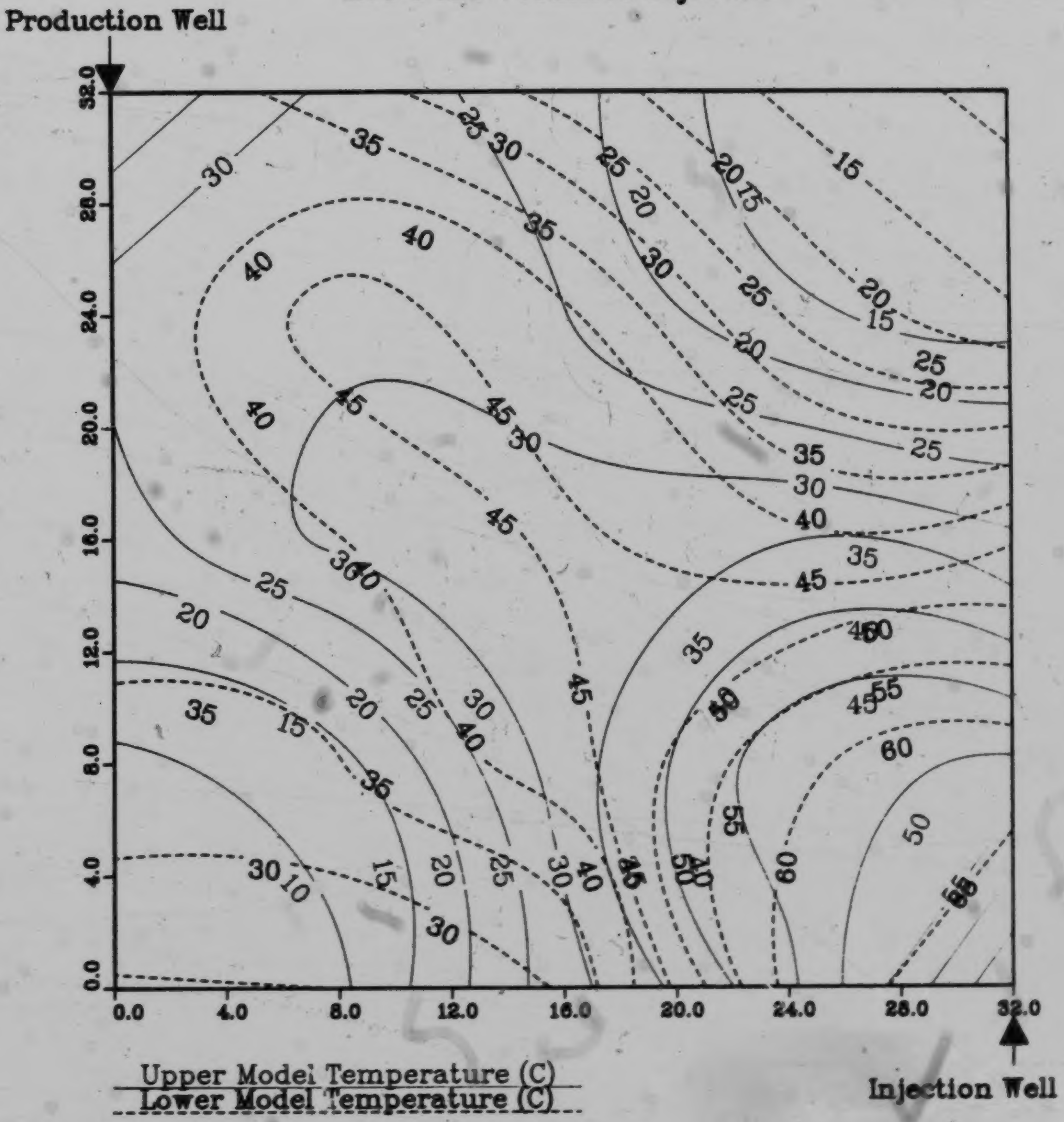

Figure A.234 : Run 62

Gas Inj. Solv.–Steamflood in B.W. Model

Temperature Profile for
2.00 Pore Volumes Injected

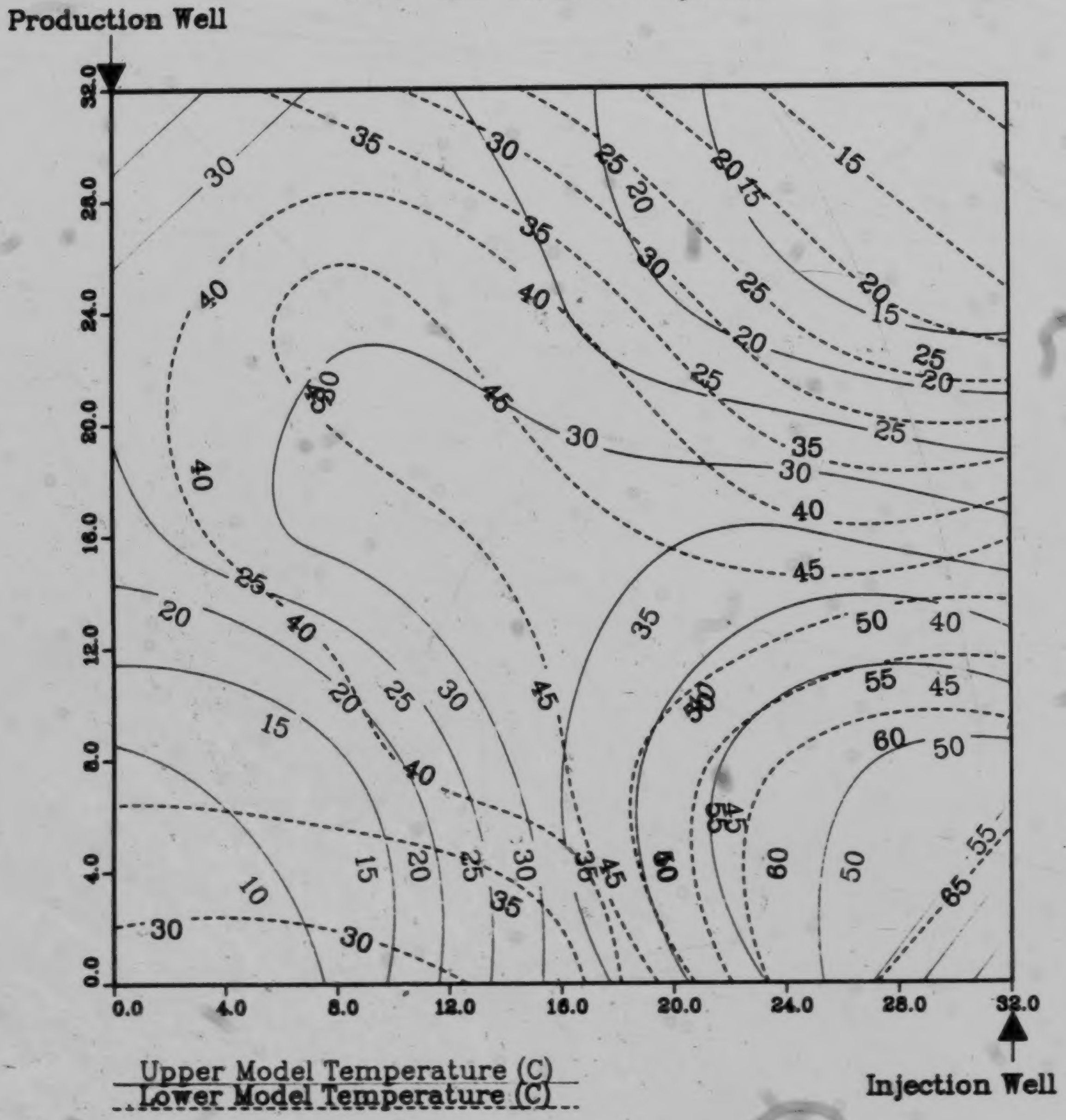

Figure A.235 :Run 62 Temp Profile
Injector to Producer Cross–Section
0.25 Pore Volumes Injected.

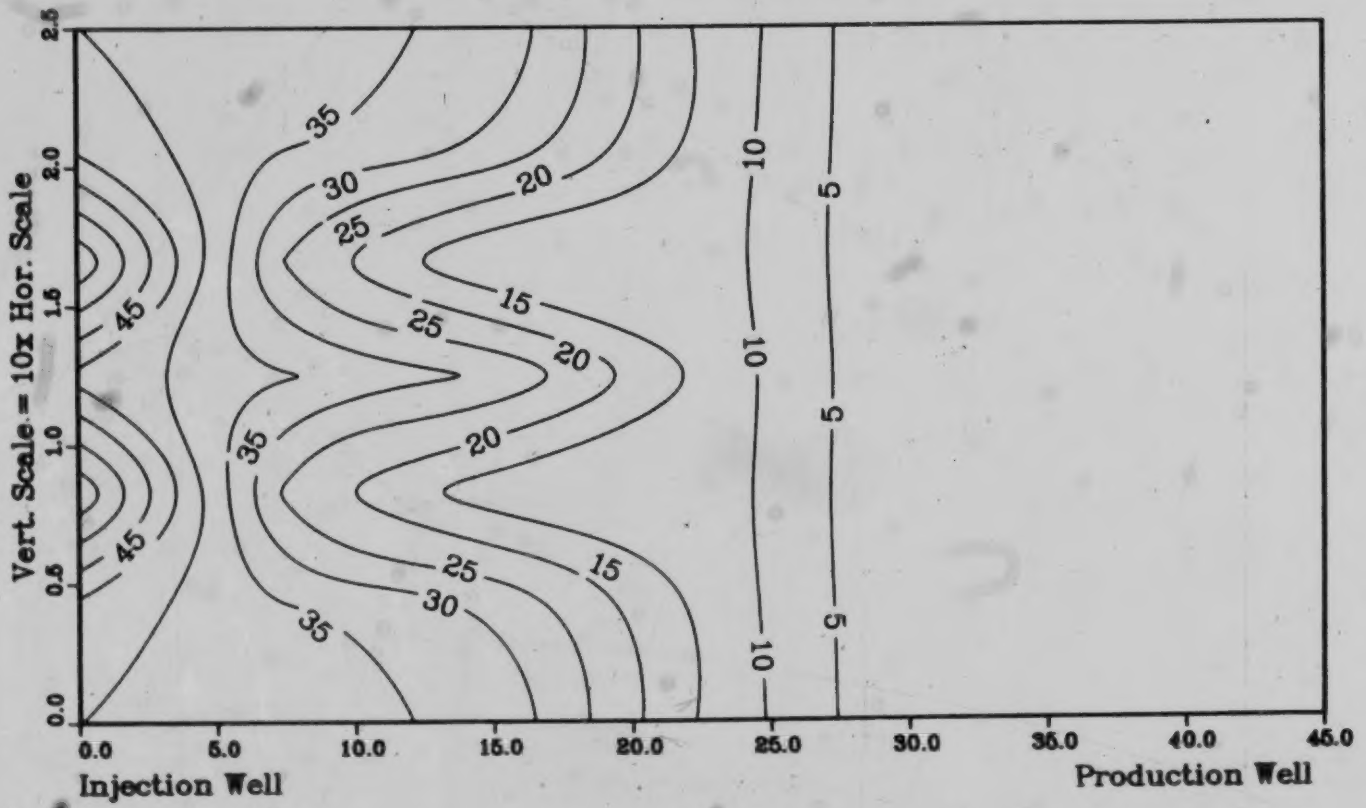

Figure A.236 :Run 62 Temp Profile
Injector to Producer Cross–Section
0.50 Pore Volumes Injected.

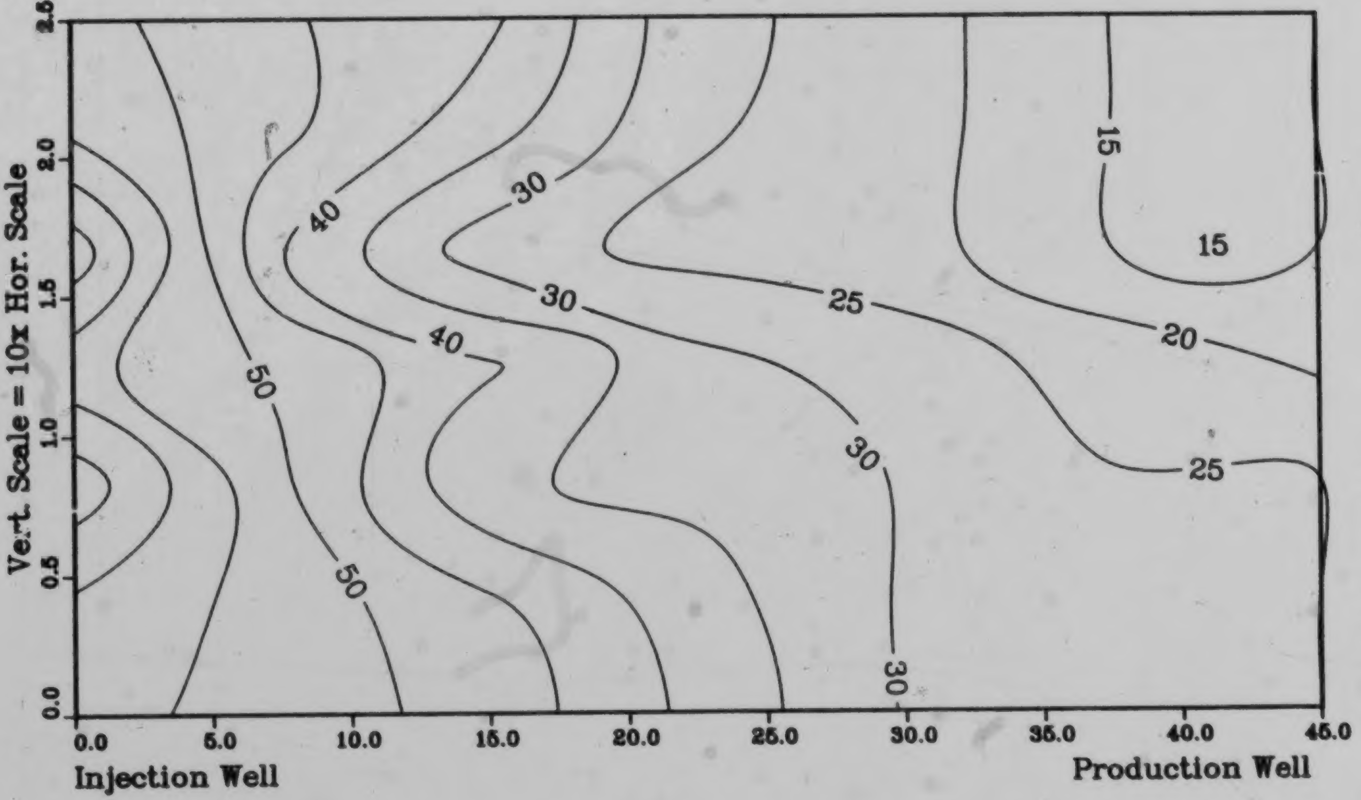

Figure A.237 :Run 62 Temp Profile
Injector to Producer Cross–Section
0.75 Pore Volumes Injected.

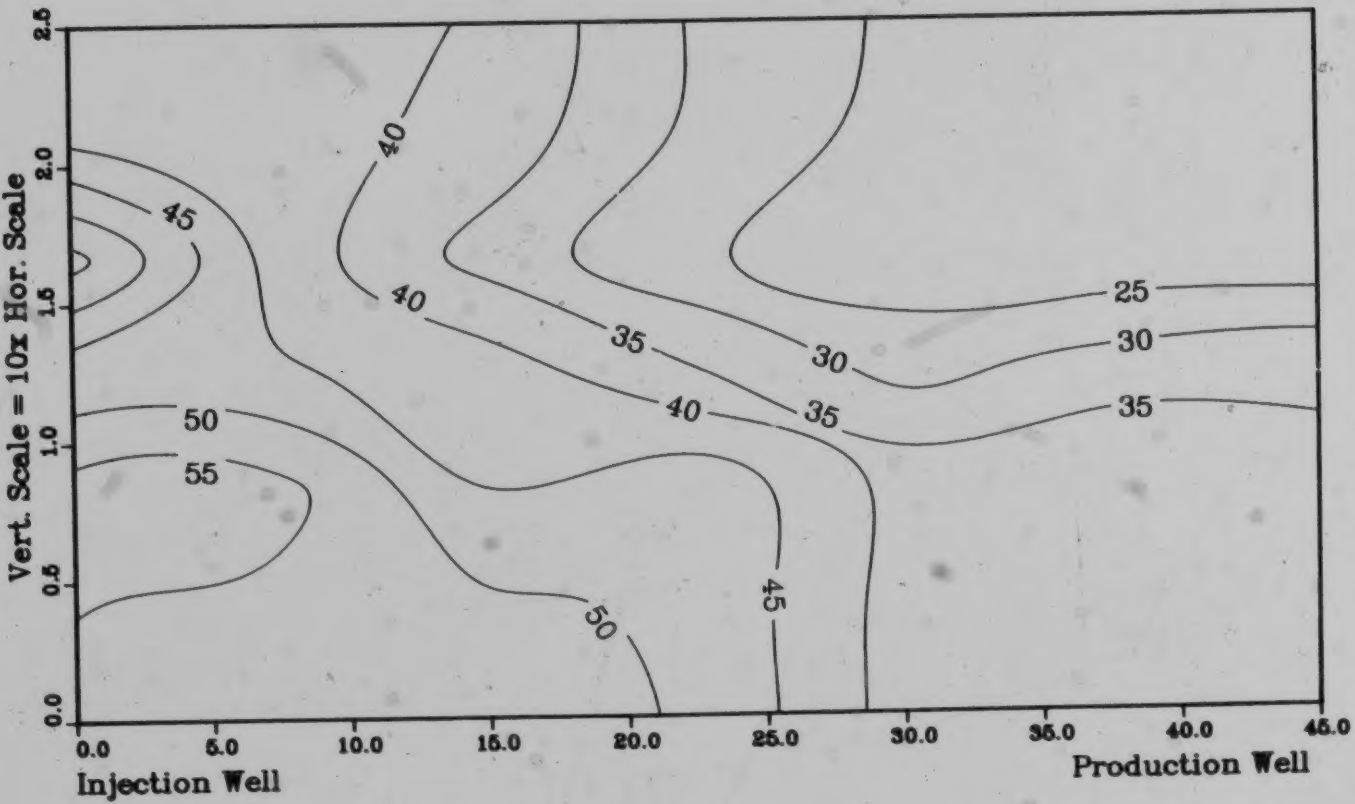

Figure A.238 :Run 62 Temp Profile
Injector to Producer Cross–Section
1.00 Pore Volumes Injected.

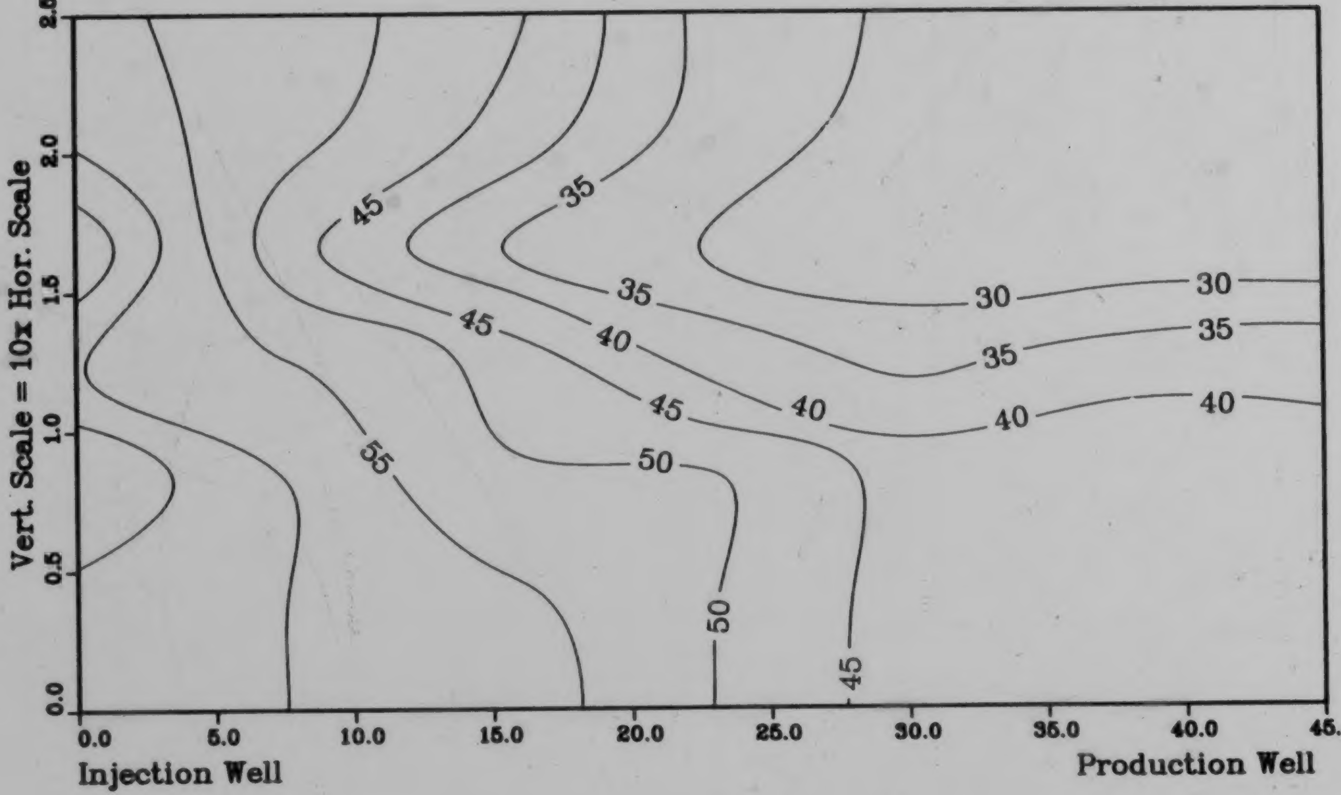

Figure A.239 : Run 63

Steamflood With Partial B.W. Barrier

Temperature Profile for
0.25 Pore Volumes Injected

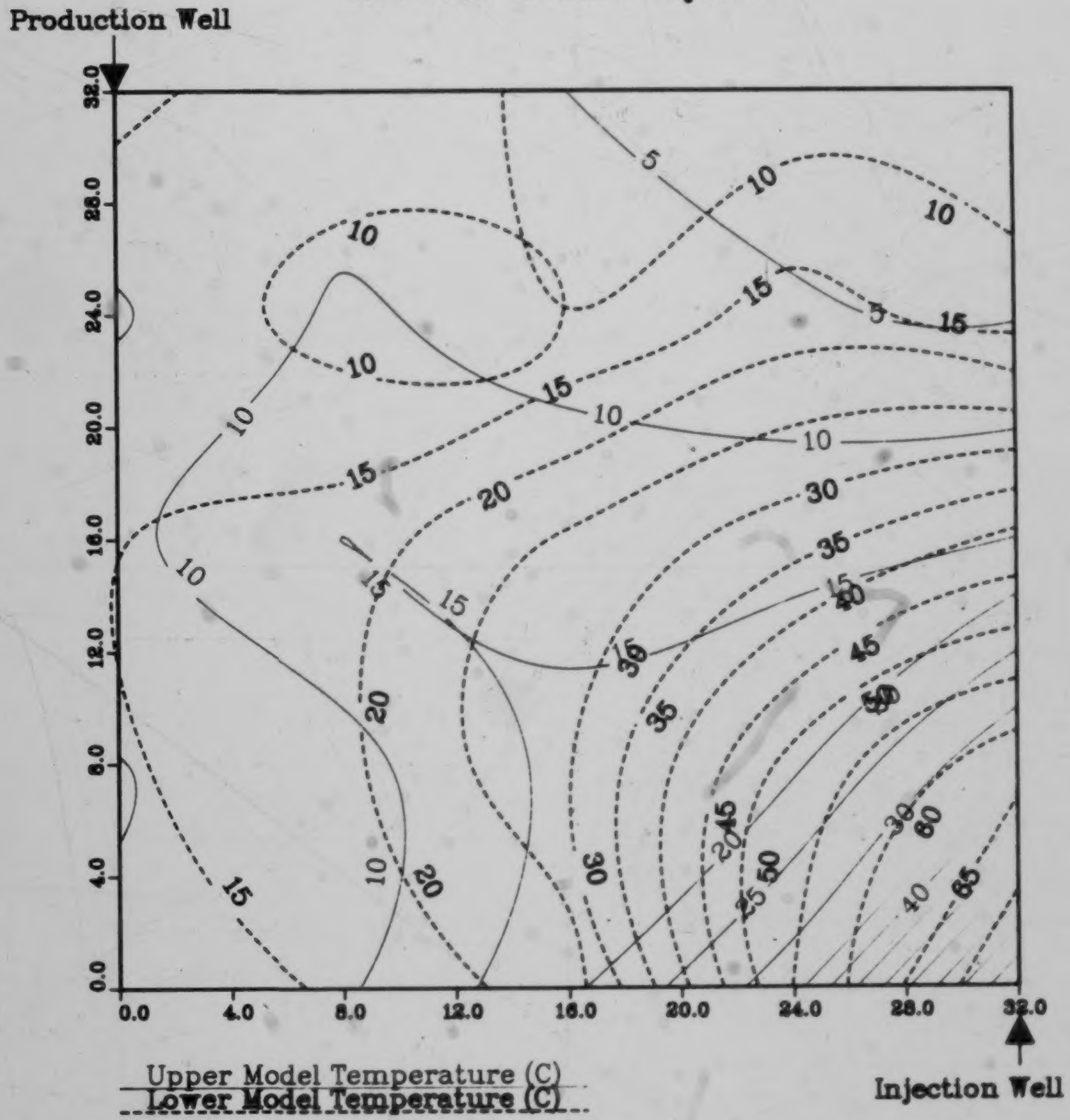

Figure A.240 : Run 63

Steamflood With Partial B.W. Barrier

Temperature Profile for 0.50 Pore Volumes Injected

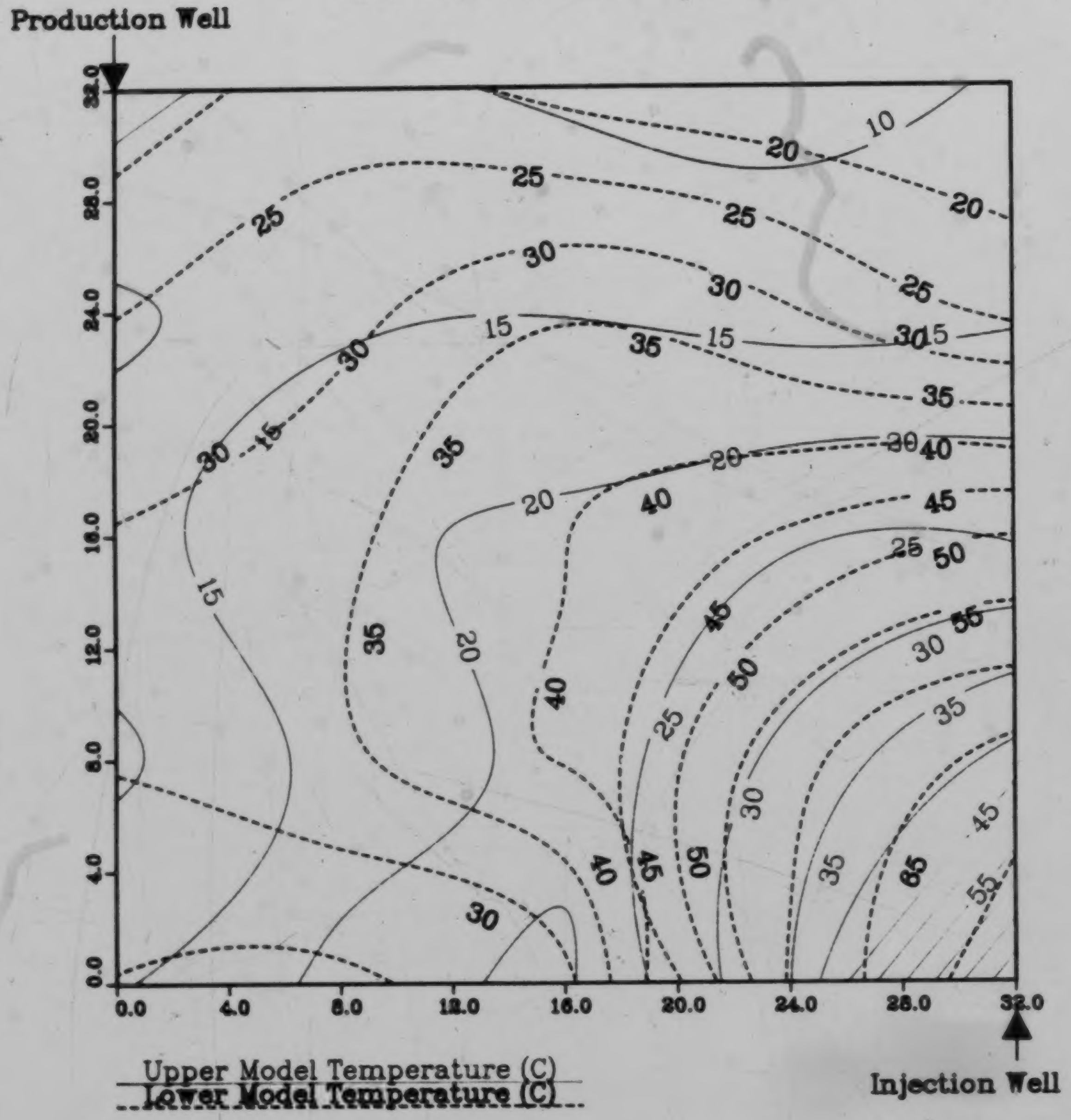

Figure A.241 : Run 63
Steamflood With Partial B.W. Barrier

Temperature Profile for
0.75 Pore Volumes Injected

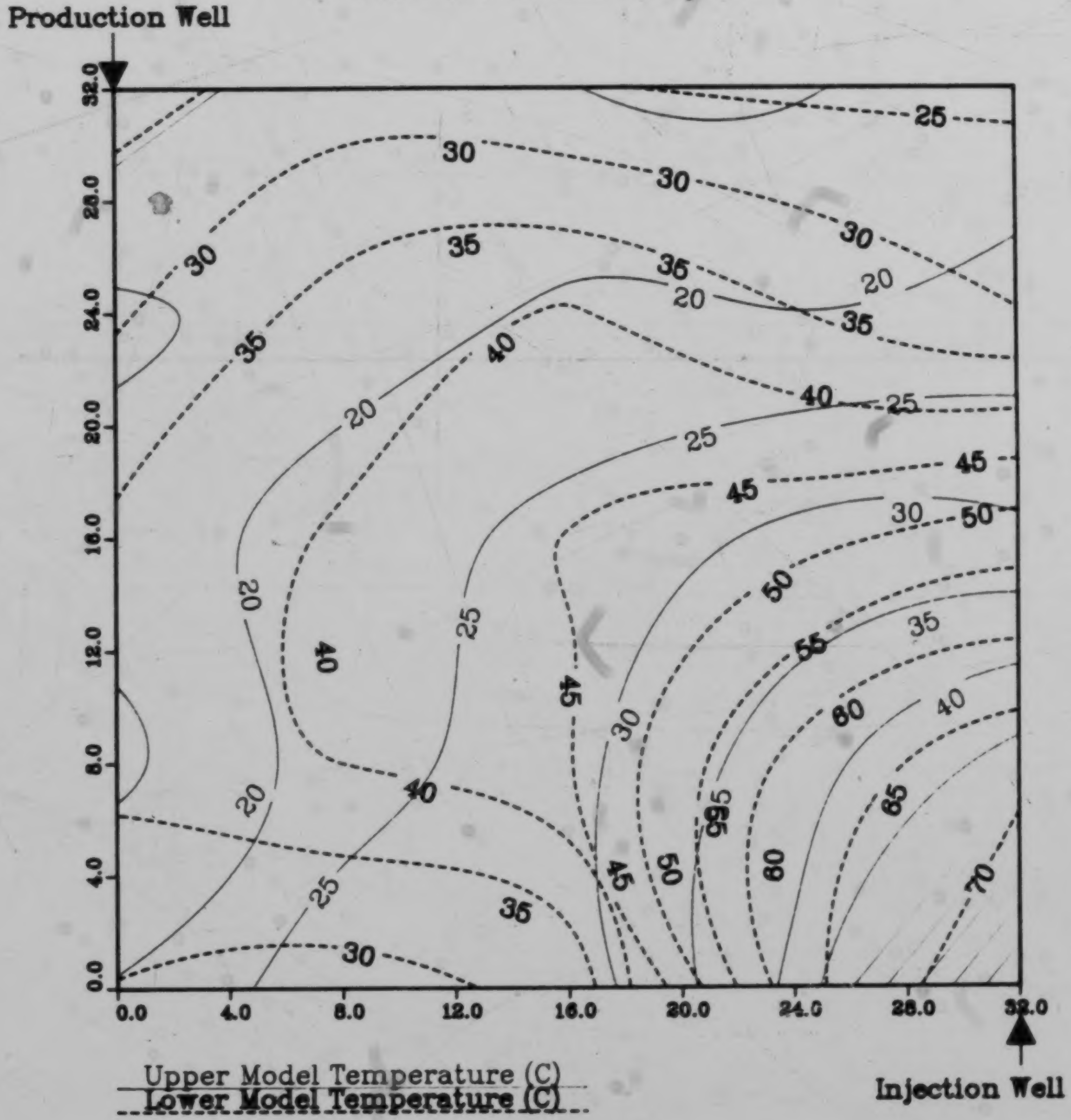

Figure A.242 : Run 63

Steamflood With Partial B.W. Barrier

Temperature Profile for 1.00 Pore Volumes Injected

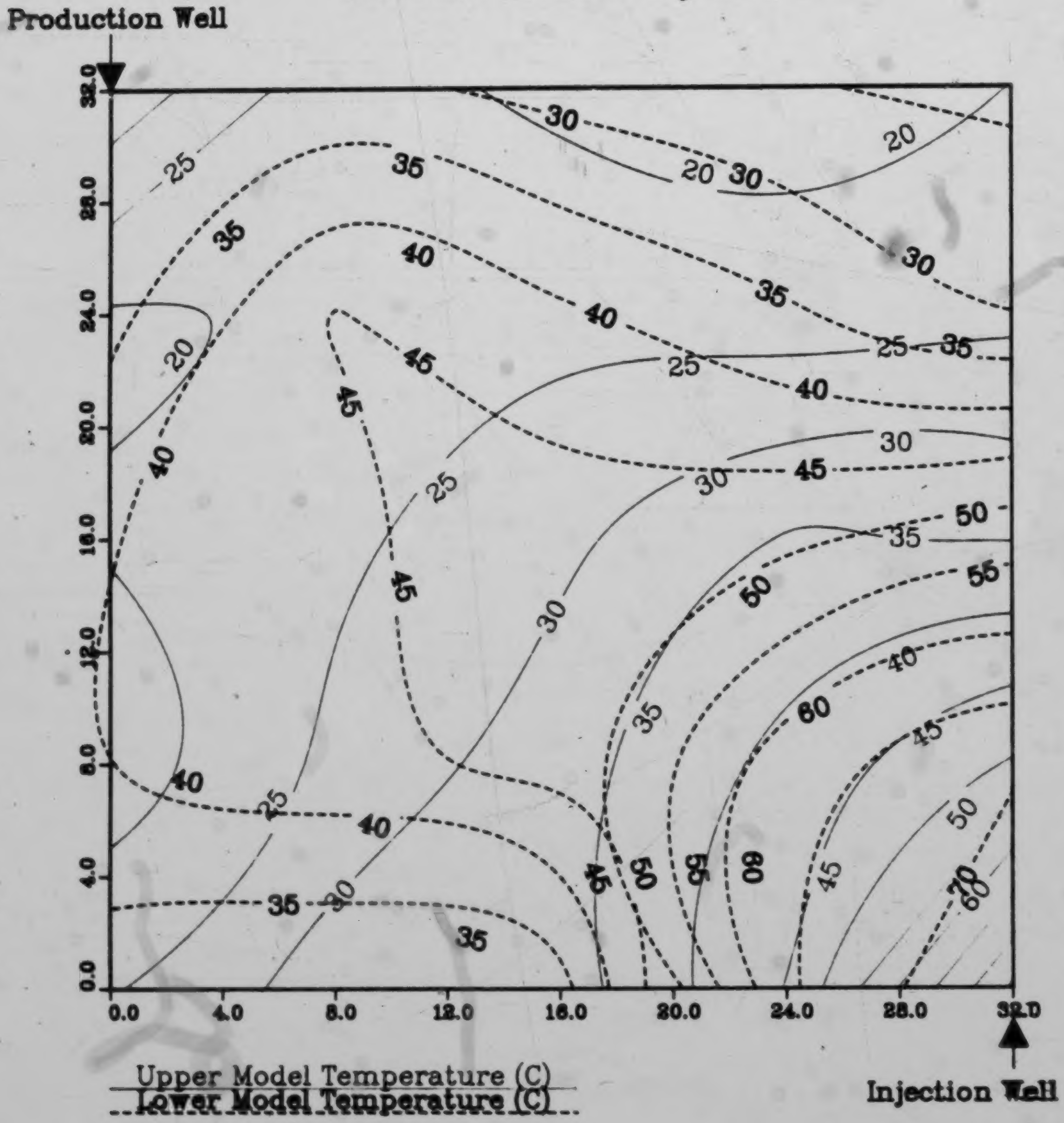

Figure A.243 : Run 63

Steamflood With Partial B.W. Barrier

Temperature Profile for
1.25 Pore Volumes Injected

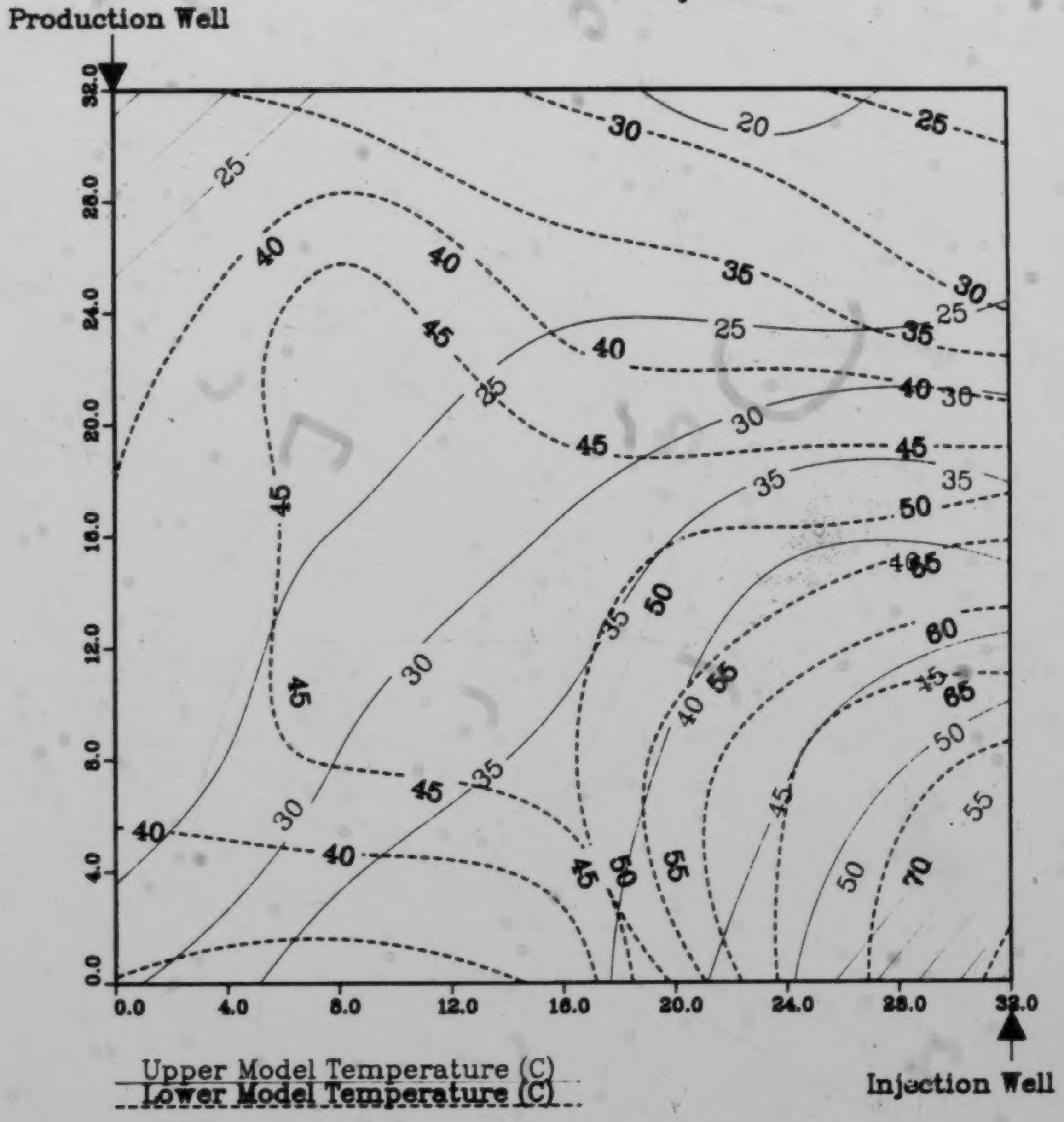

Figure A.244 : Run 63
Steamflood With Partial B.W. Barrier

Temperature Profile for
1.50 Pore Volumes Injected

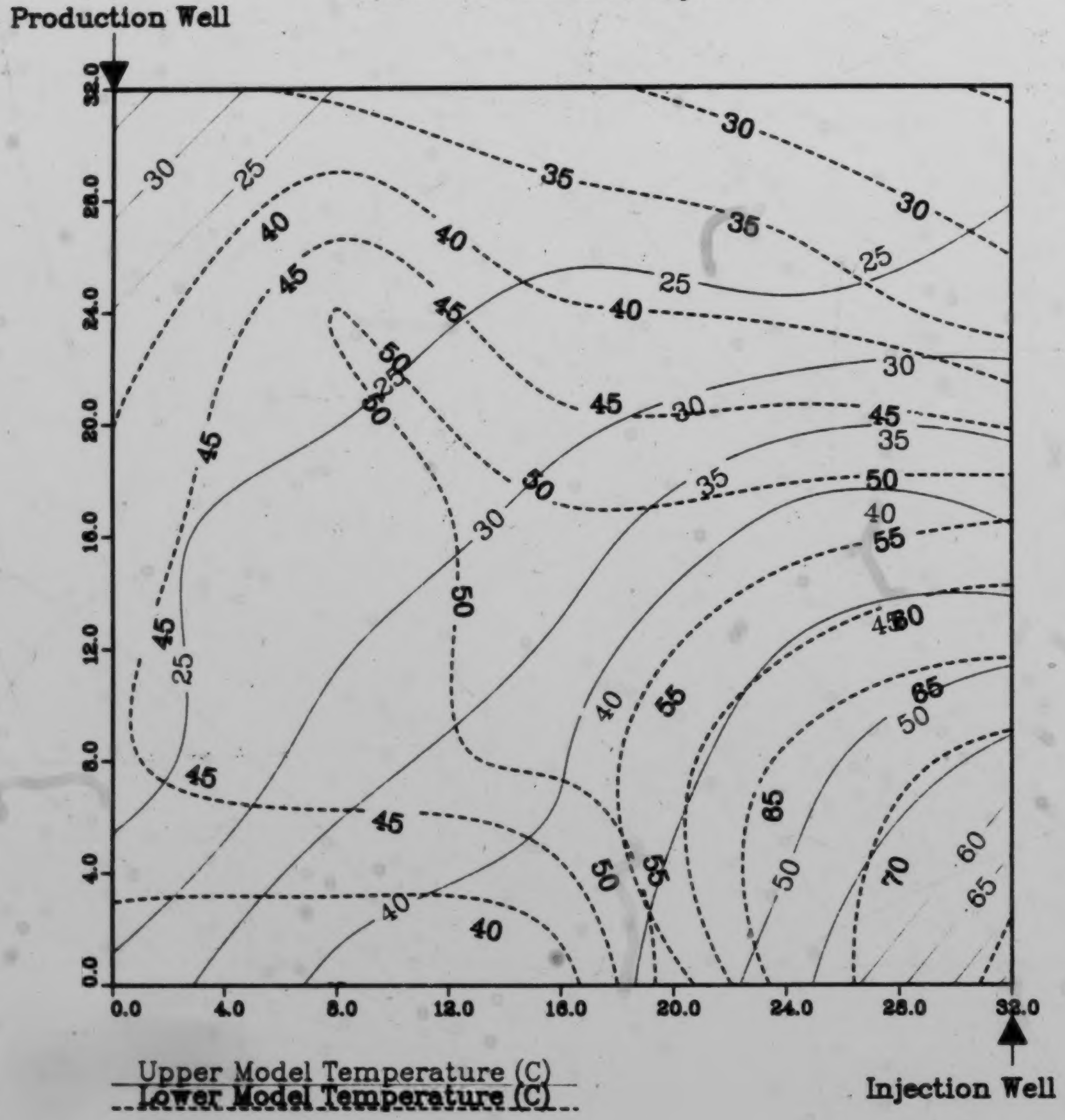

Figure A.245 : Run 63

Steamflood With Partial B.W. Barrier

Temperature Profile for 1.75 Pore Volumes Injected

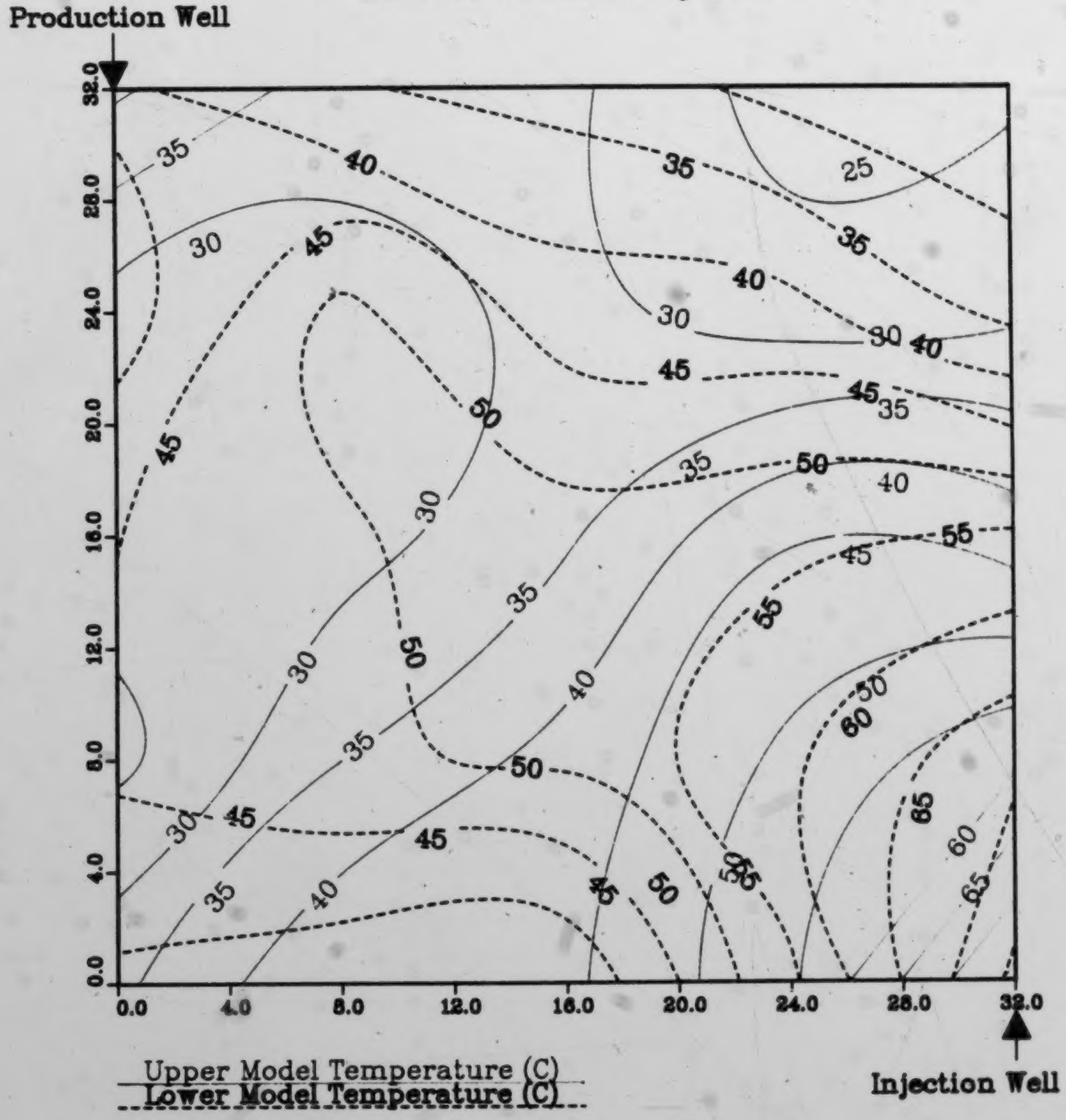

Figure A.246 : Run 63

Steamflood With Partial B.W. Barrier

Temperature Profile for 2.00 Pore Volumes Injected

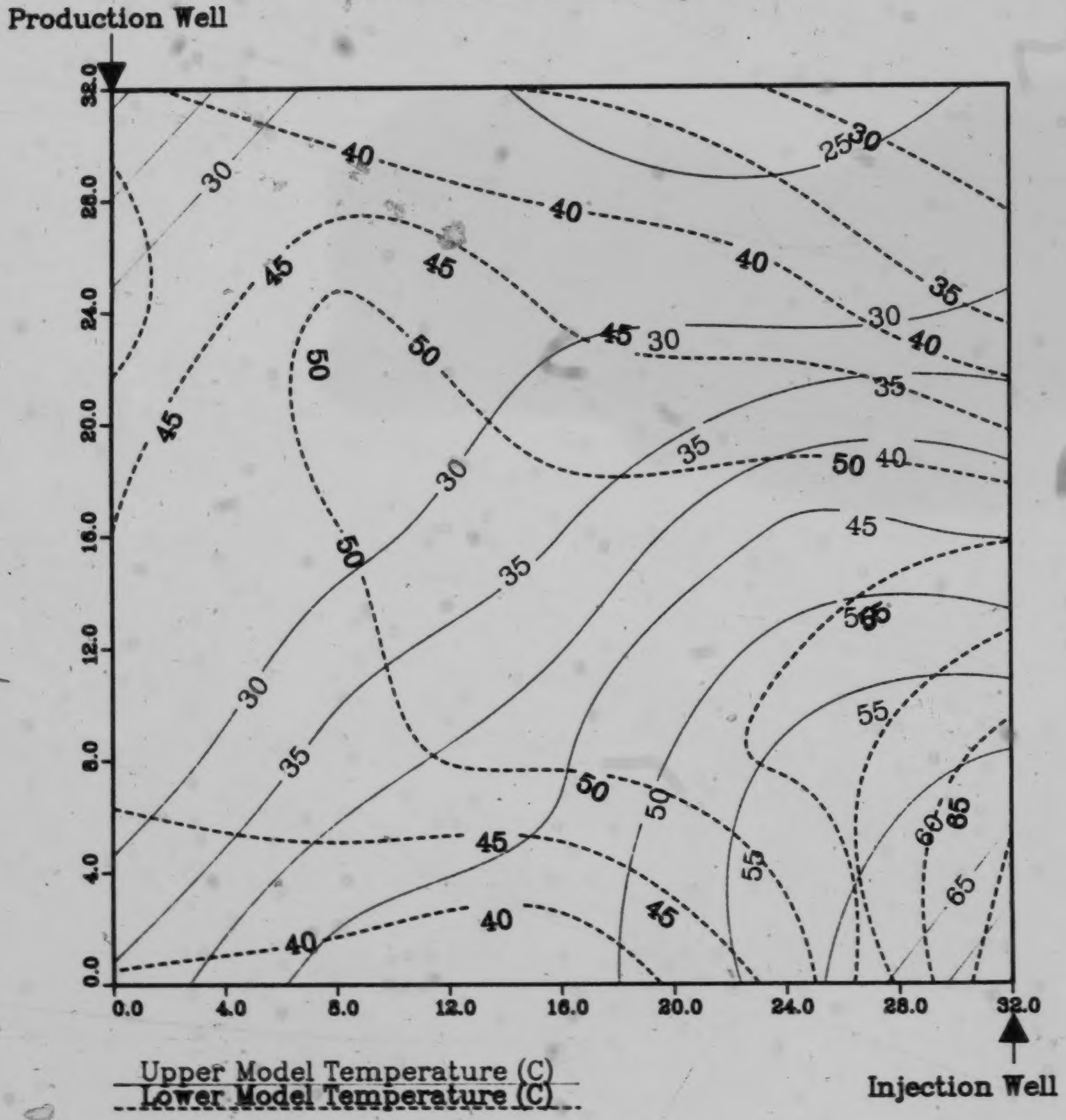

Figure A.247 :Run 63 Temp Profile
Injector to Producer Cross-Section
0.25 Pore Volumes Injected.

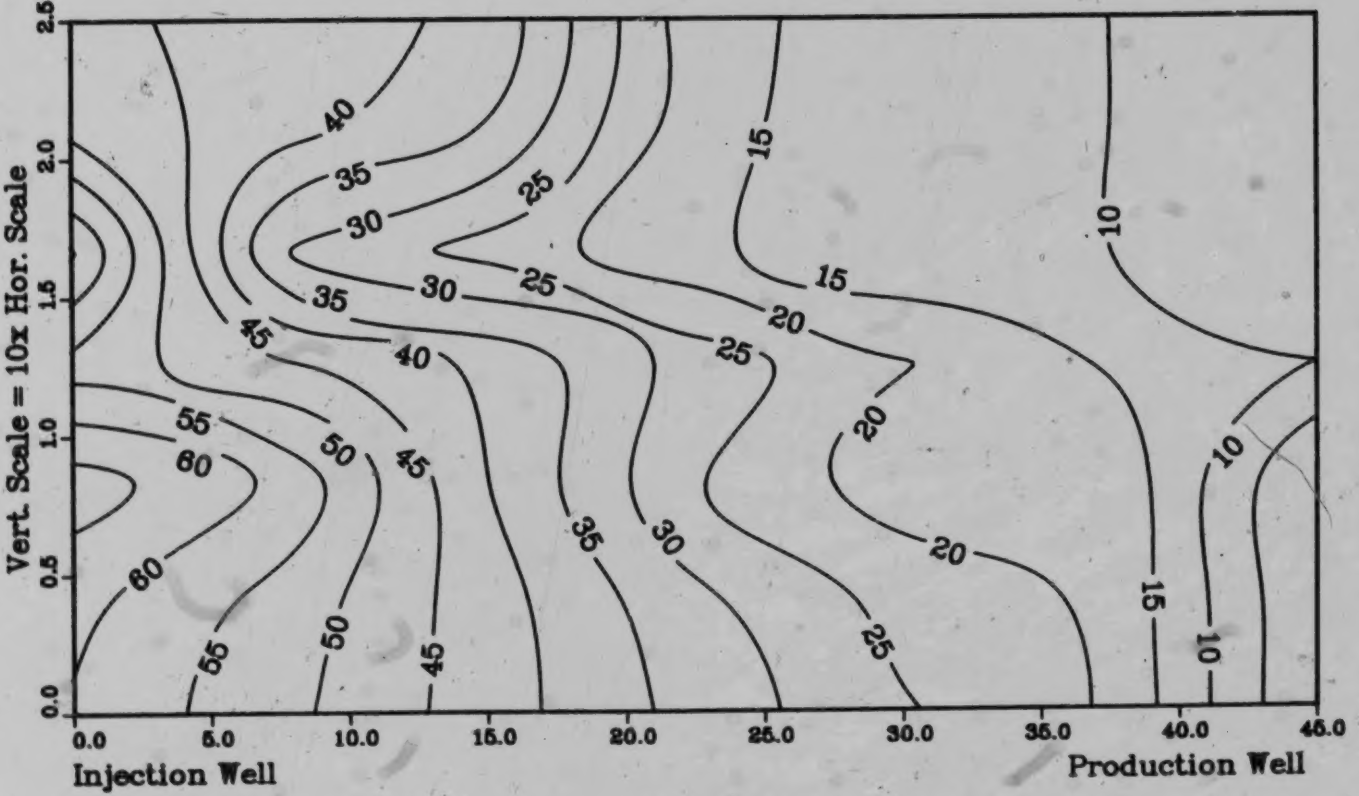

Figure A.248 :Run 63 Temp Profile
Injector to Producer Cross–Section
0.50 Pore Volumes Injected.

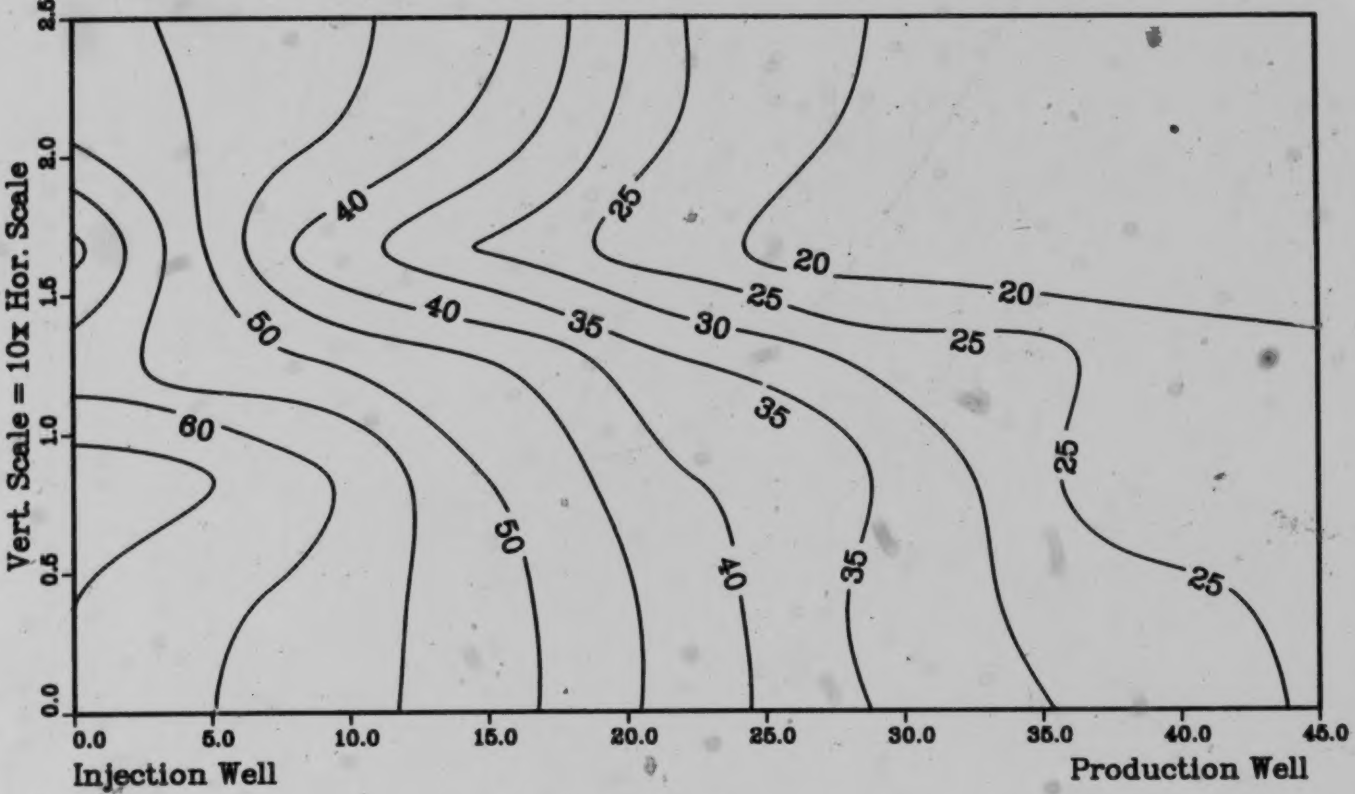

Figure A.249 :Run 63 Temp Profile
Injector to Producer Cross–Section
0.75 Pore Volumes Injected.

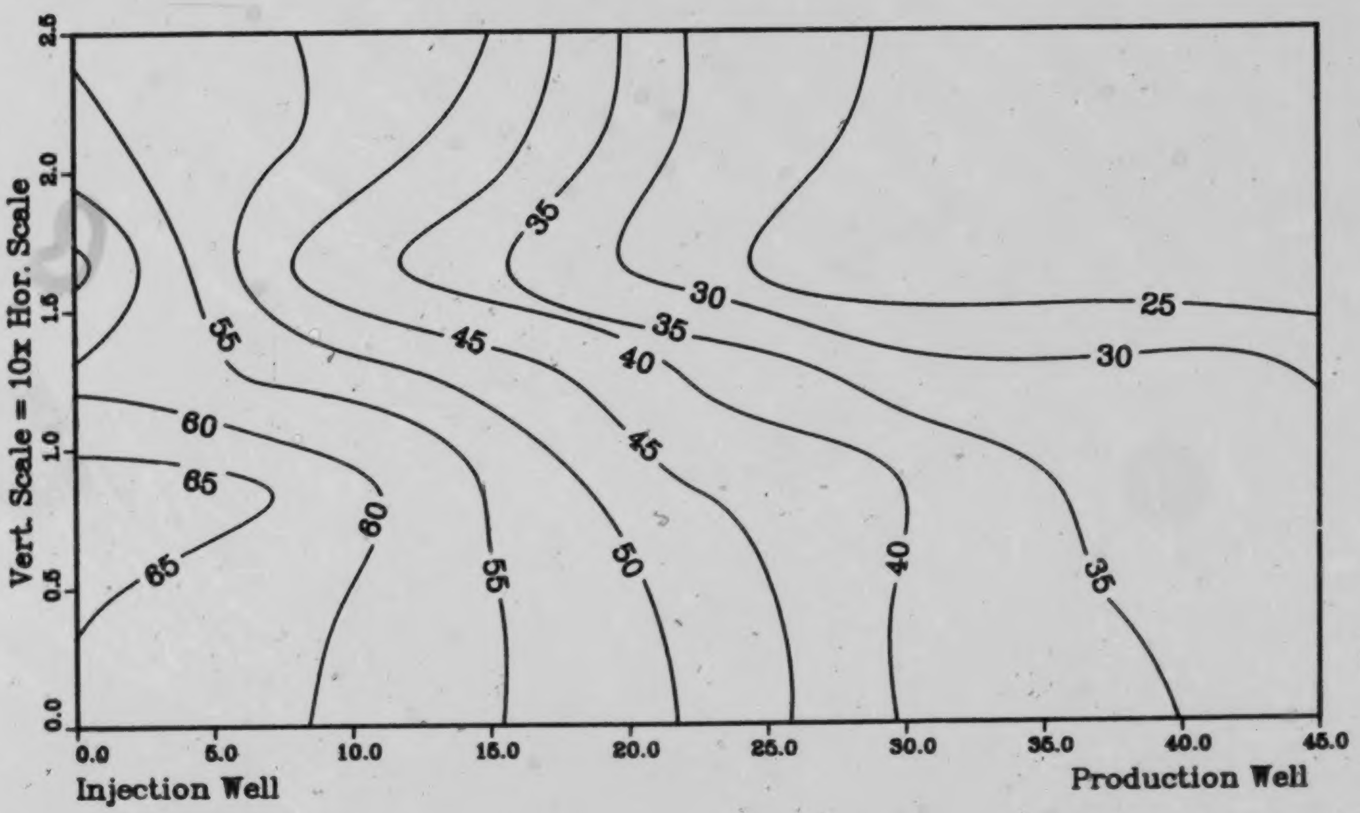

Figure A.250 :Run 63 Temp Profile
Injector to Producer Cross–Section
1.00 Pore Volumes Injected.

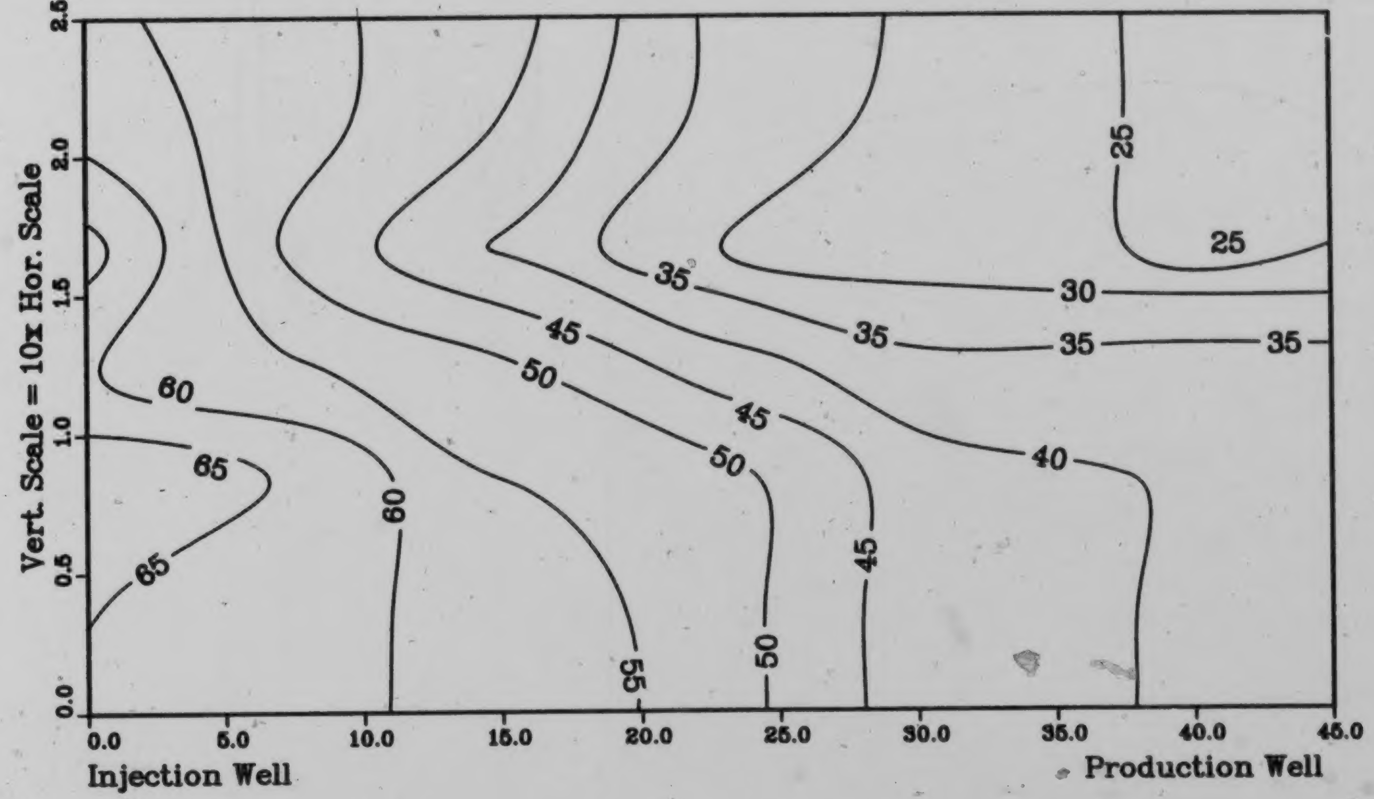

Figure A.251 : Run 64

Steamflood With Partial B.W. Barrier

Temperature Profile for 0.25 Pore Volumes Injected

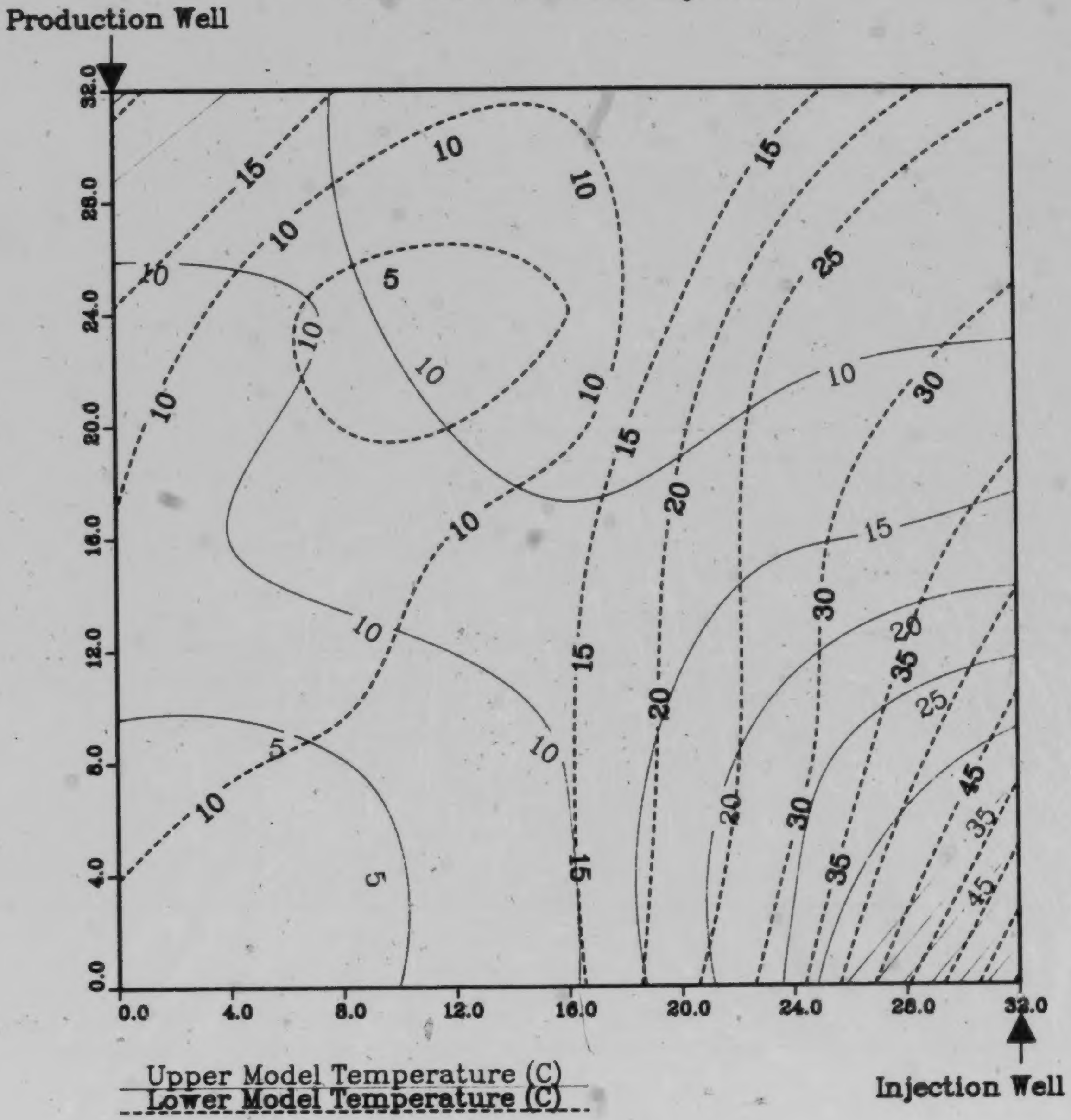

Figure A.252 : Run 64
Steamflood With Partial B.W. Barrier

Temperature Profile for
0.50 Pore Volumes Injected

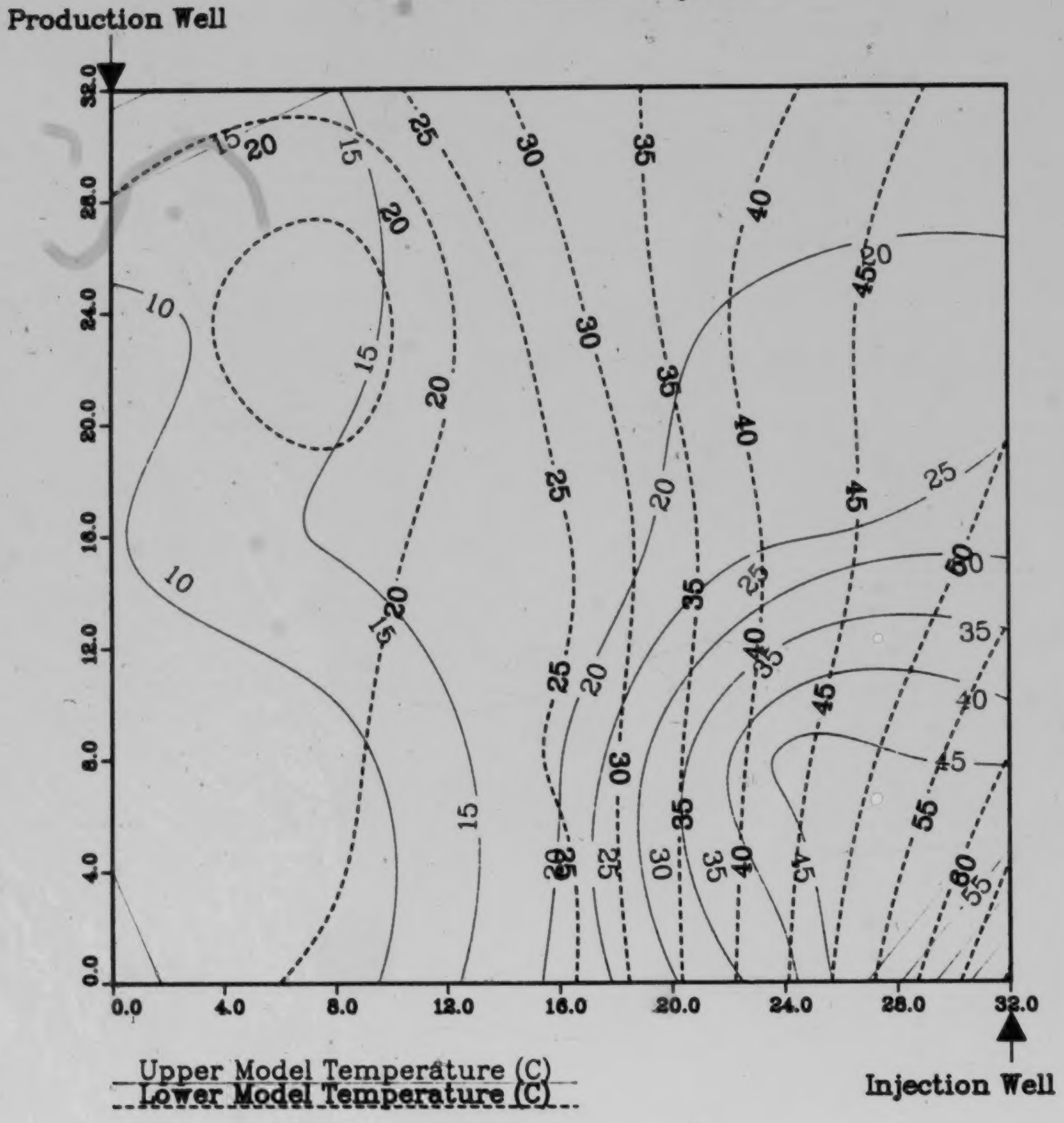

Figure A.253 : Run 64
Steamflood With Partial B.W. Barrier

Temperature Profile for
0.75 Pore Volumes Injected

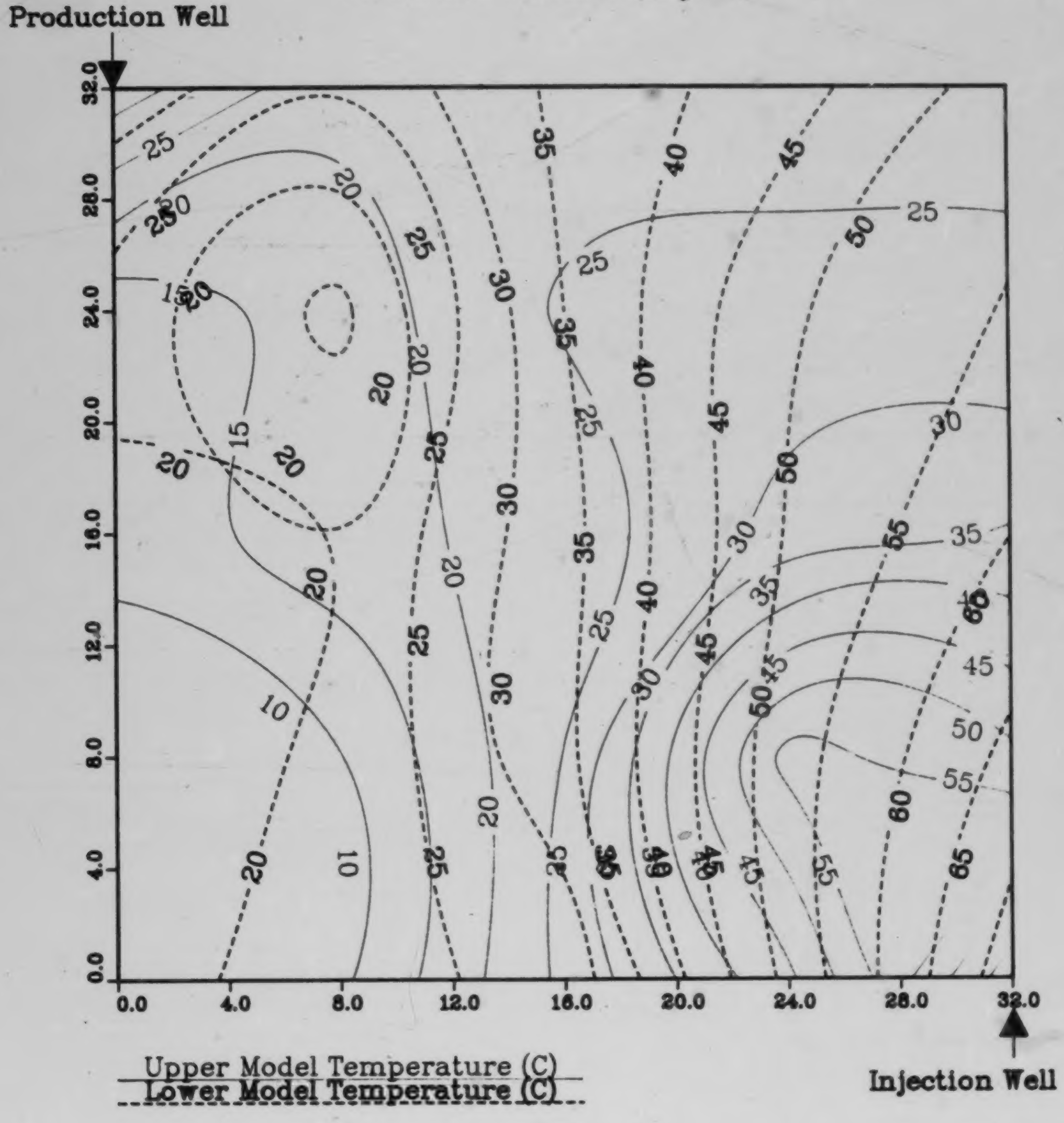

Figure A.254 : Run 64
Steamflood With Partial B.W. Barrier

Temperature Profile for
1.00 Pore Volumes Injected

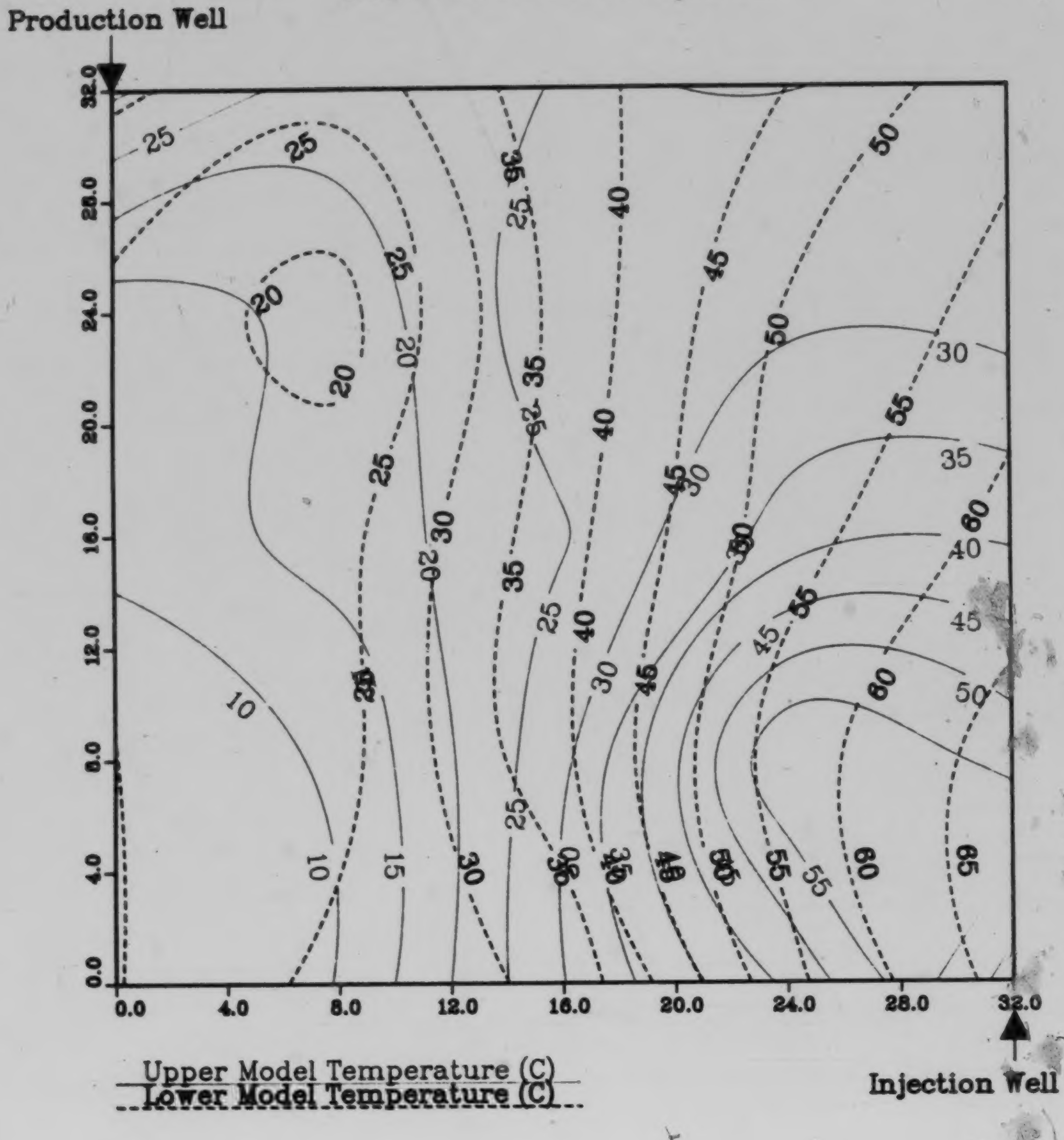

Figure A.255 : Run 64

Steamflood With Partial B.W. Barrier

Temperature Profile for
1.25 Pore Volumes Injected

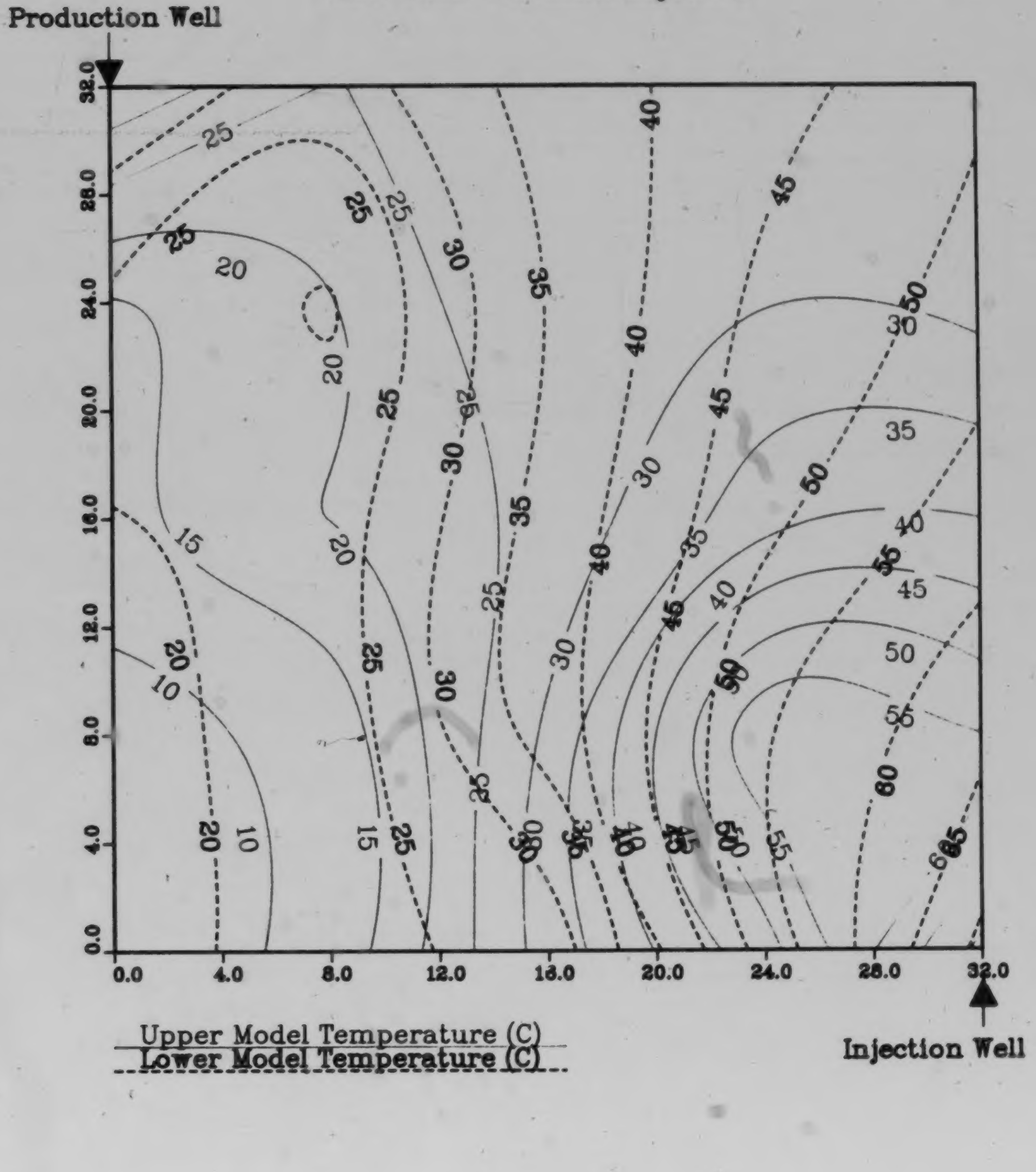

Figure A.256 : Run 64

Steamflood With Partial B.W. Barrier

Temperature Profile for
1.50 Pore Volumes Injected

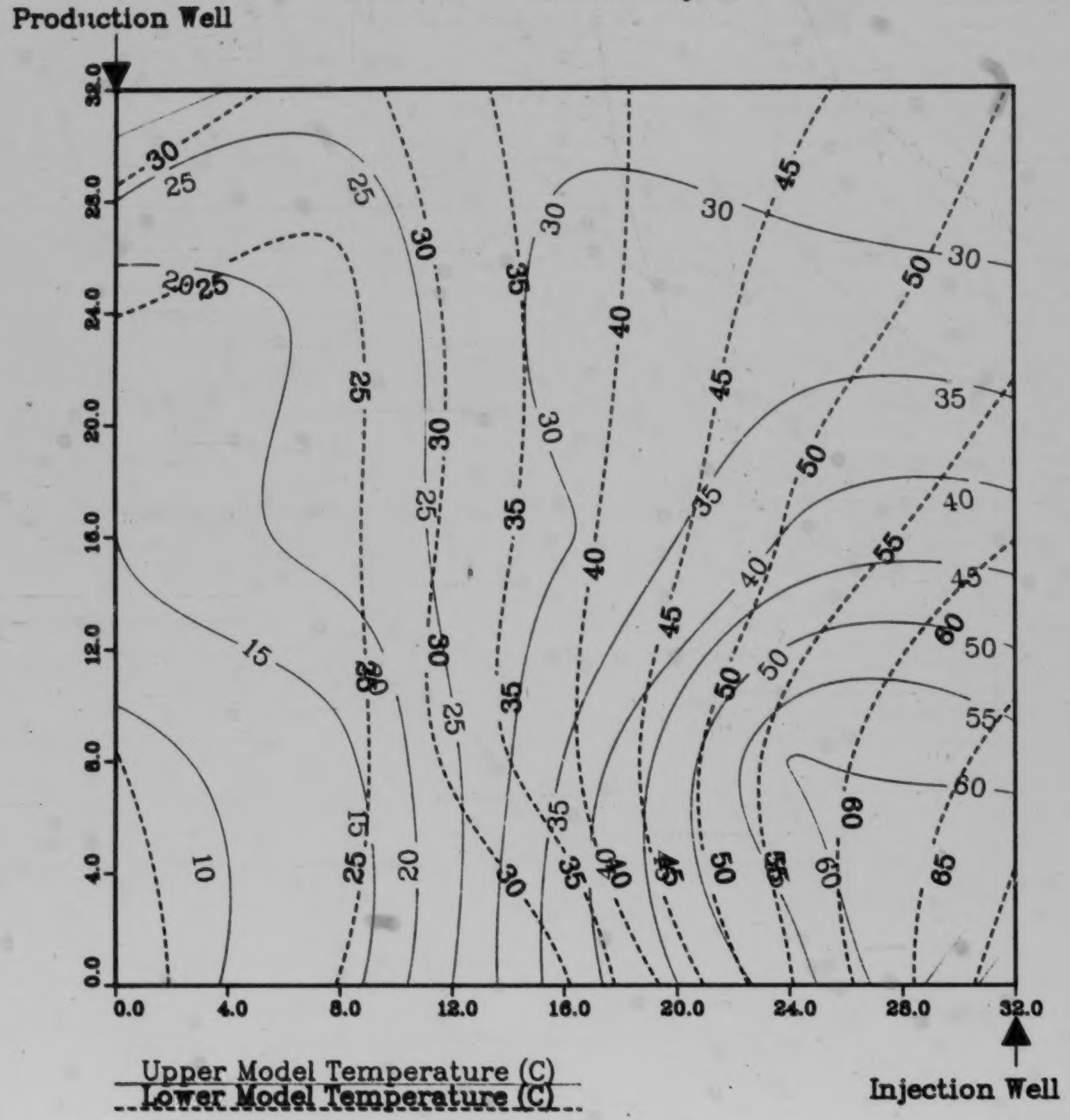

Figure A.257 : Run 64

Steamflood With Partial B.W. Barrier

Temperature Profile for 1.75 Pore Volumes Injected

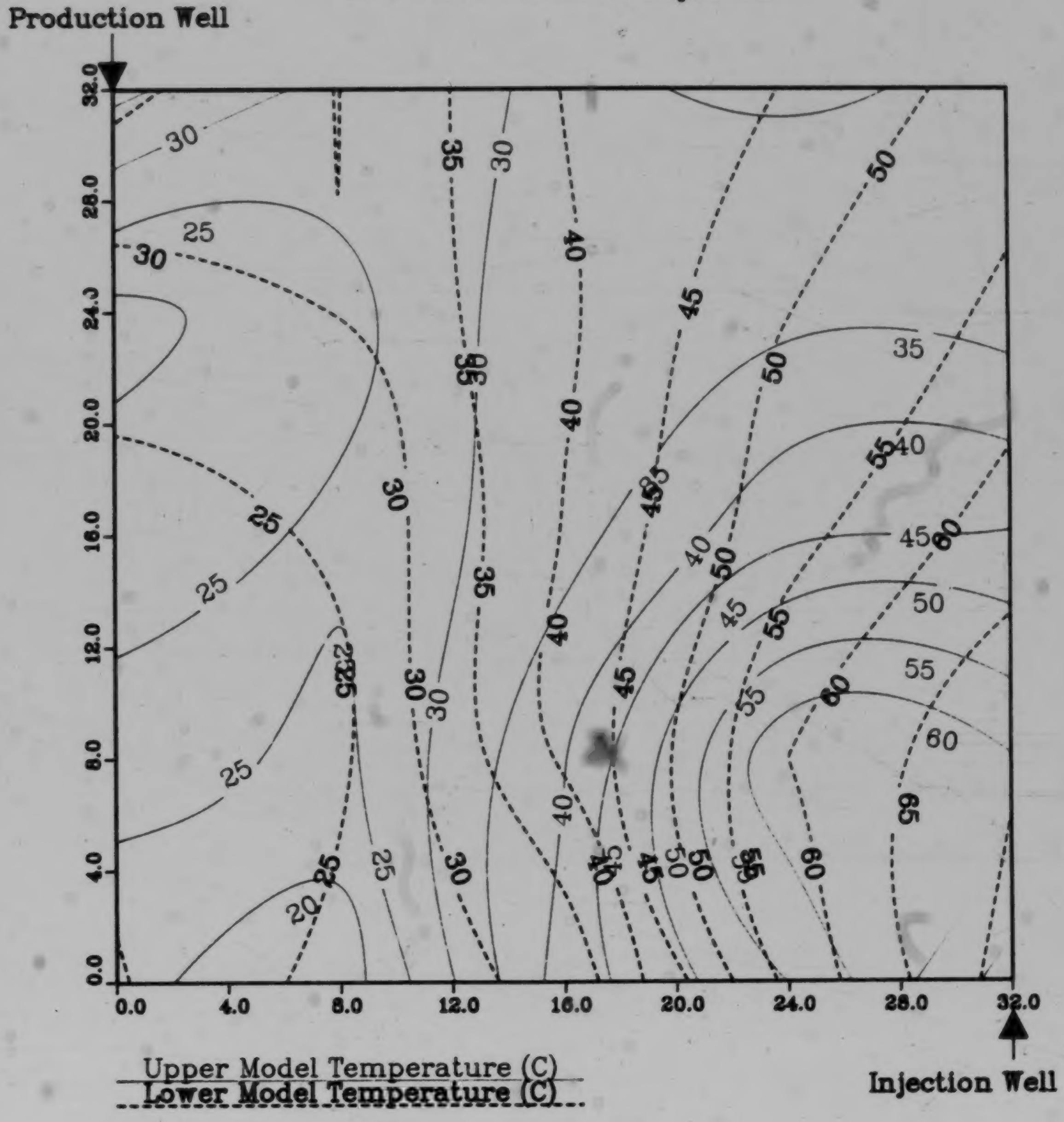

Figure A.258 : Run 64

Steamflood With Partial B.W. Barrier

Temperature Profile for
2.00 Pore Volumes Injected

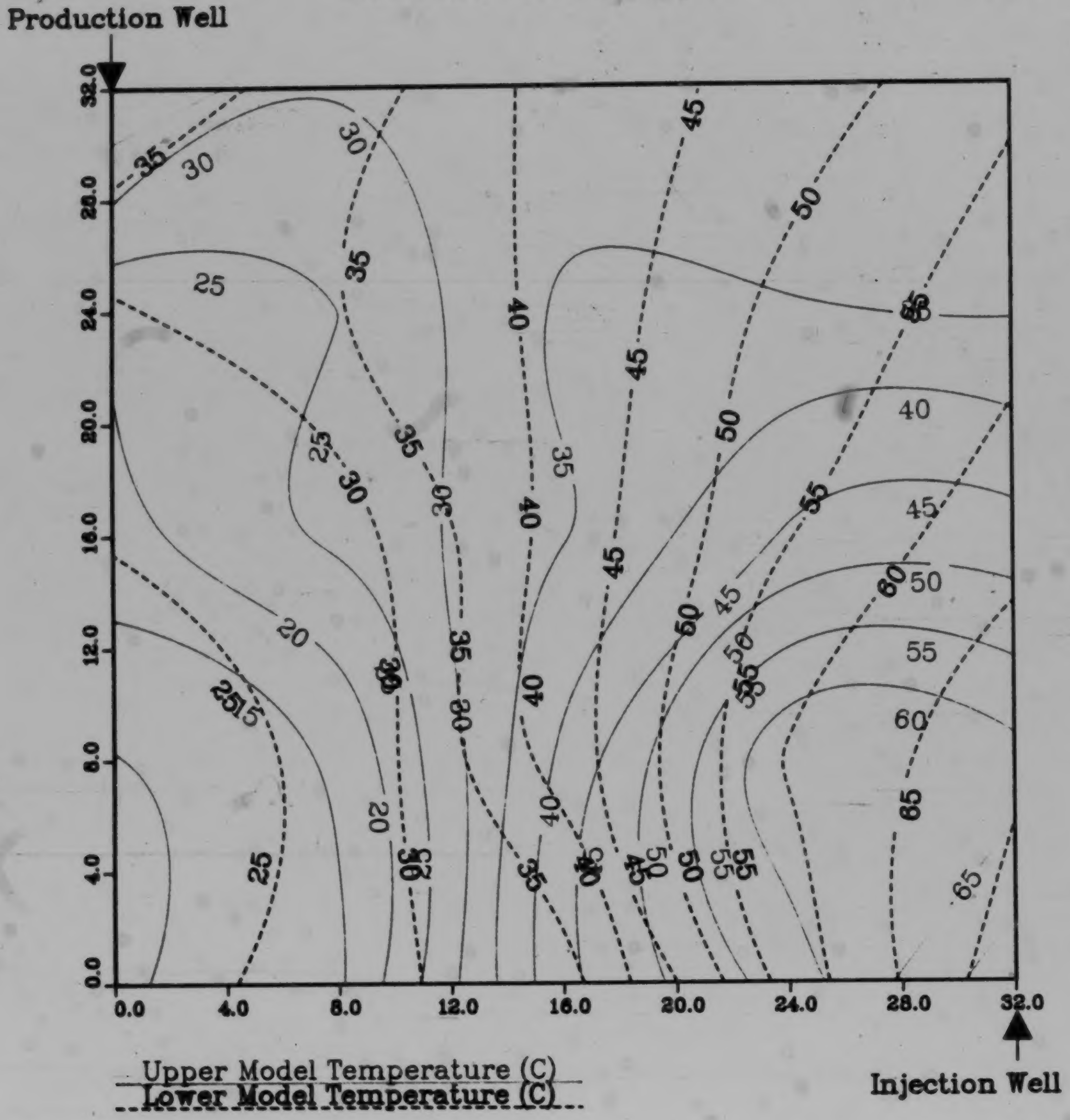

Figure A.259 :Run 64 Temp Profile
Injector to Producer Cross–Section
0.25 Pore Volumes Injected.

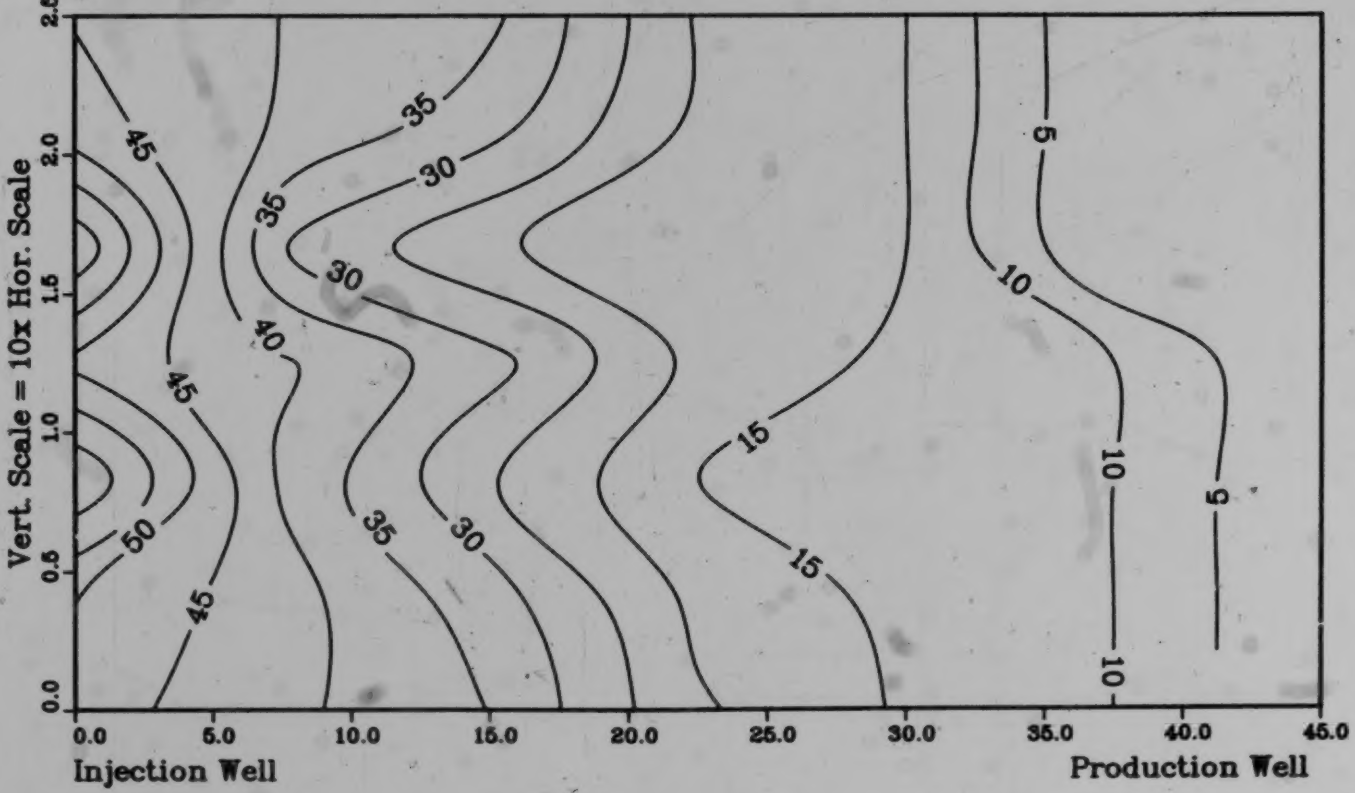

Figure A.260 :Run 64 Temp Profile
Injector to Producer Cross–Section
0.50 Pore Volumes Injected.

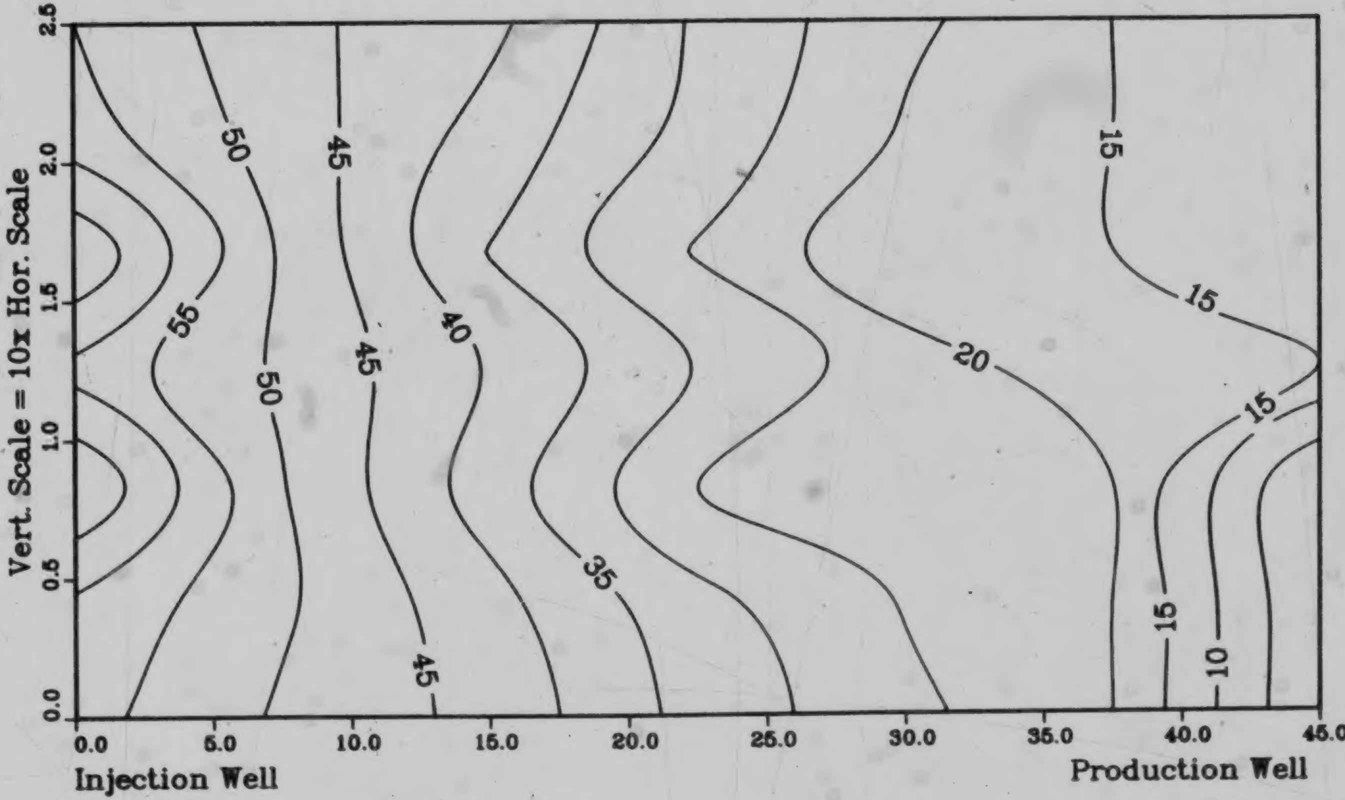

Figure A.261 :Run 64 Temp Profile
Injector to Producer Cross-Section
0.75 Pore Volumes Injected.

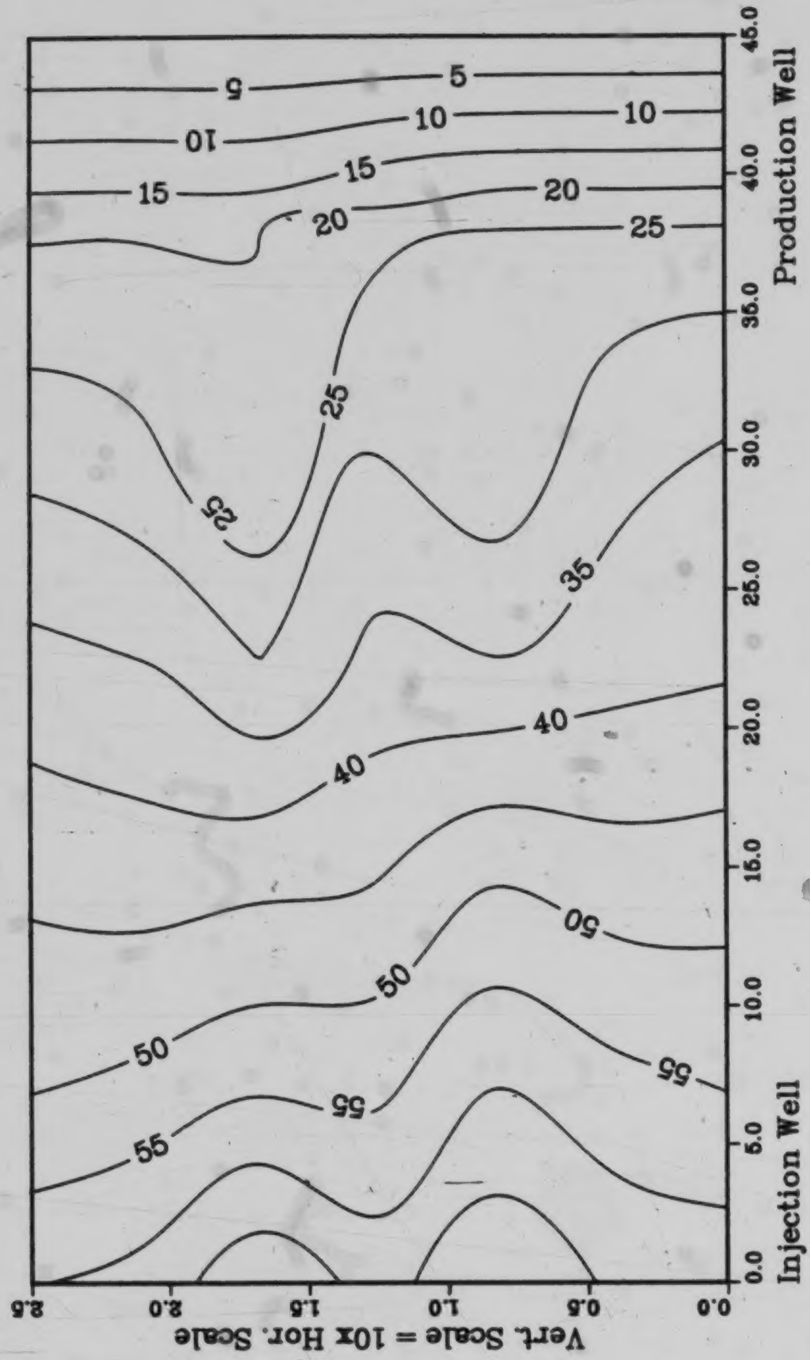

Figure A.262 :Run 64 Temp Profile
Injector to Producer Cross–Section
1.00 Pore Volumes Injected.

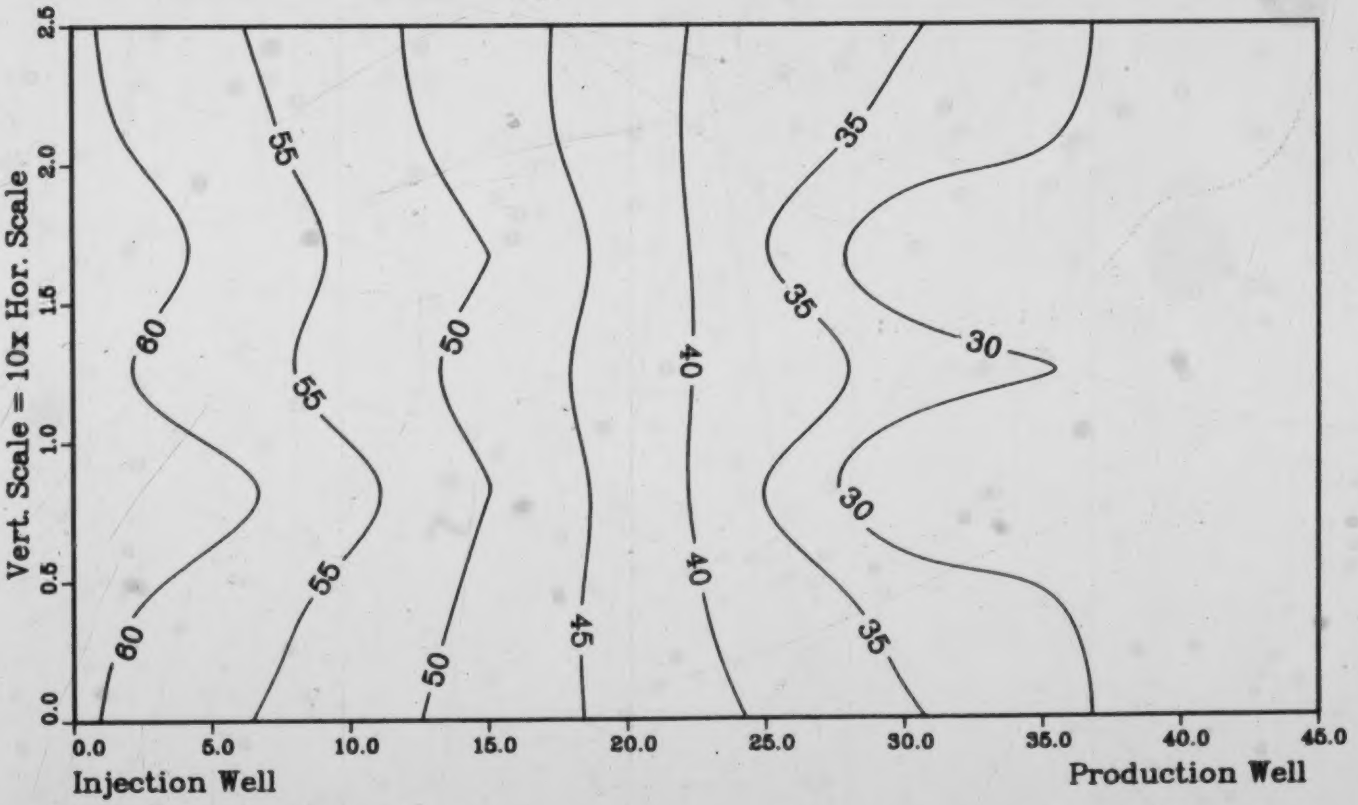

Figure A.263 : Run 47A
Waterflood Prior to Solvent–Steamflood

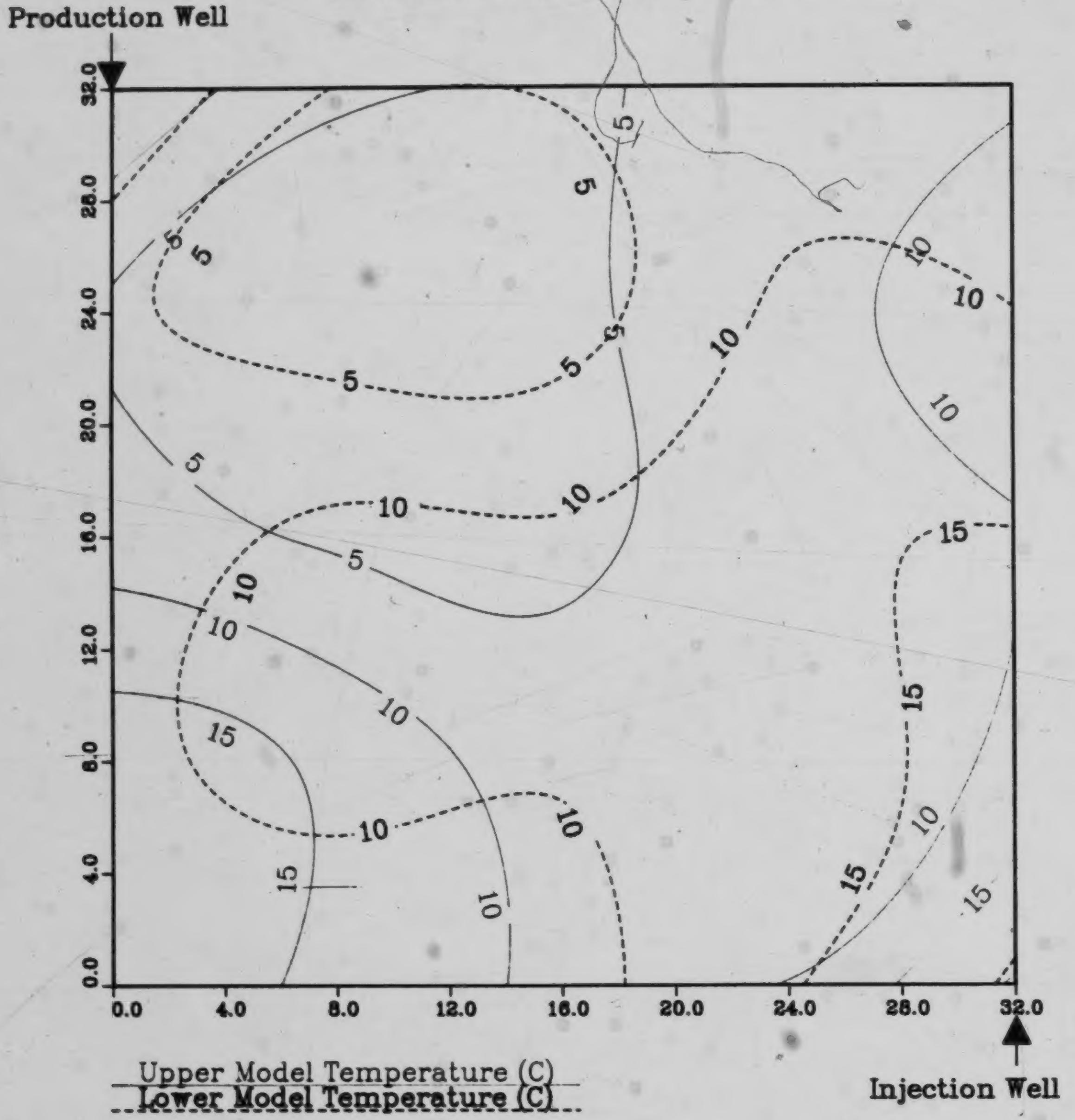

Figure A.264 : Run 47A

Waterflood Prior to Solvent–Steamflood

Temperature Profile for 0.50 Pore Volumes Injected

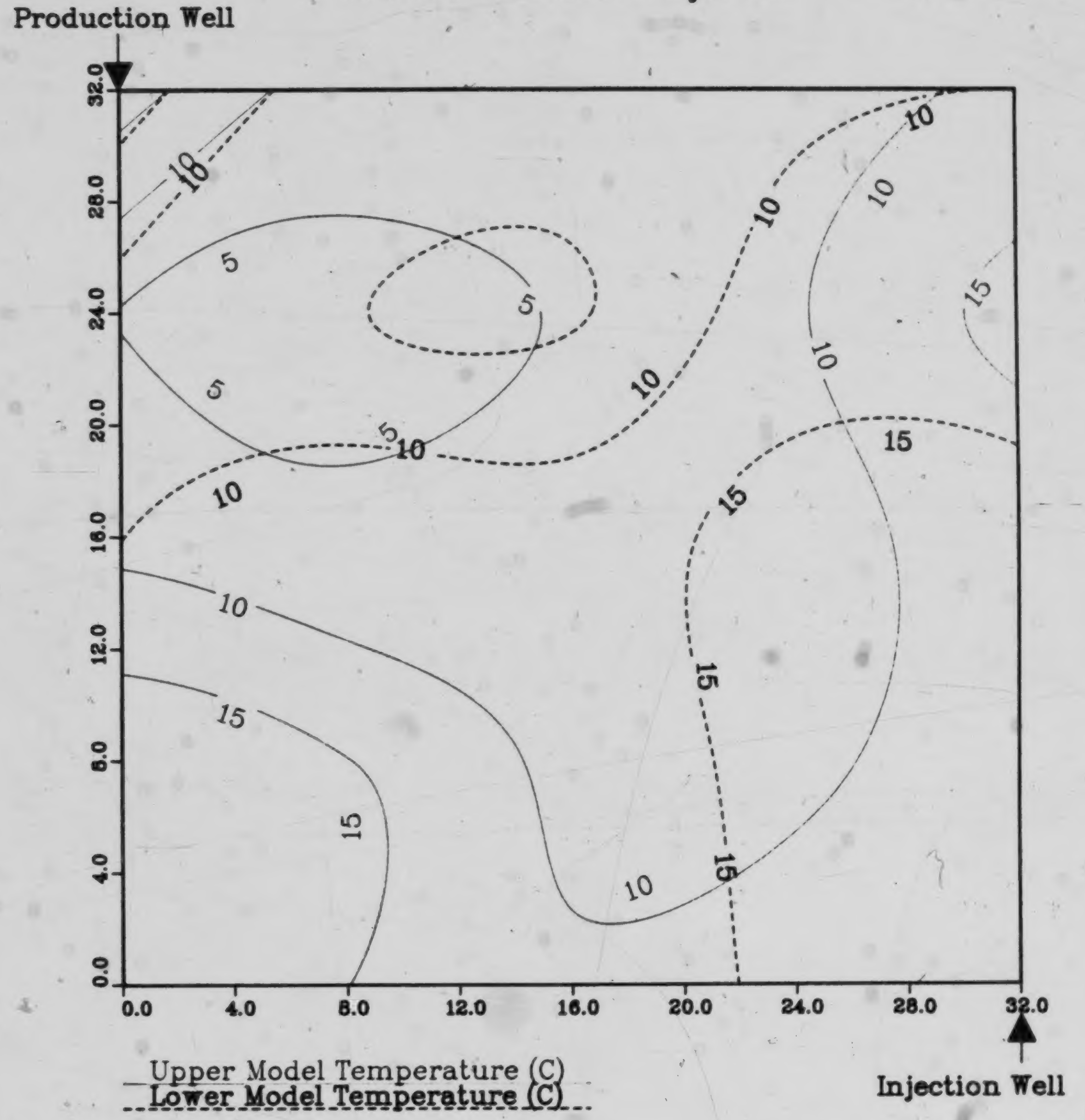

Figure A.265 : Run 47A
Waterflood Prior to Solvent–Steamflood

Temperature Profile for
0.75 Pore Volumes Injected

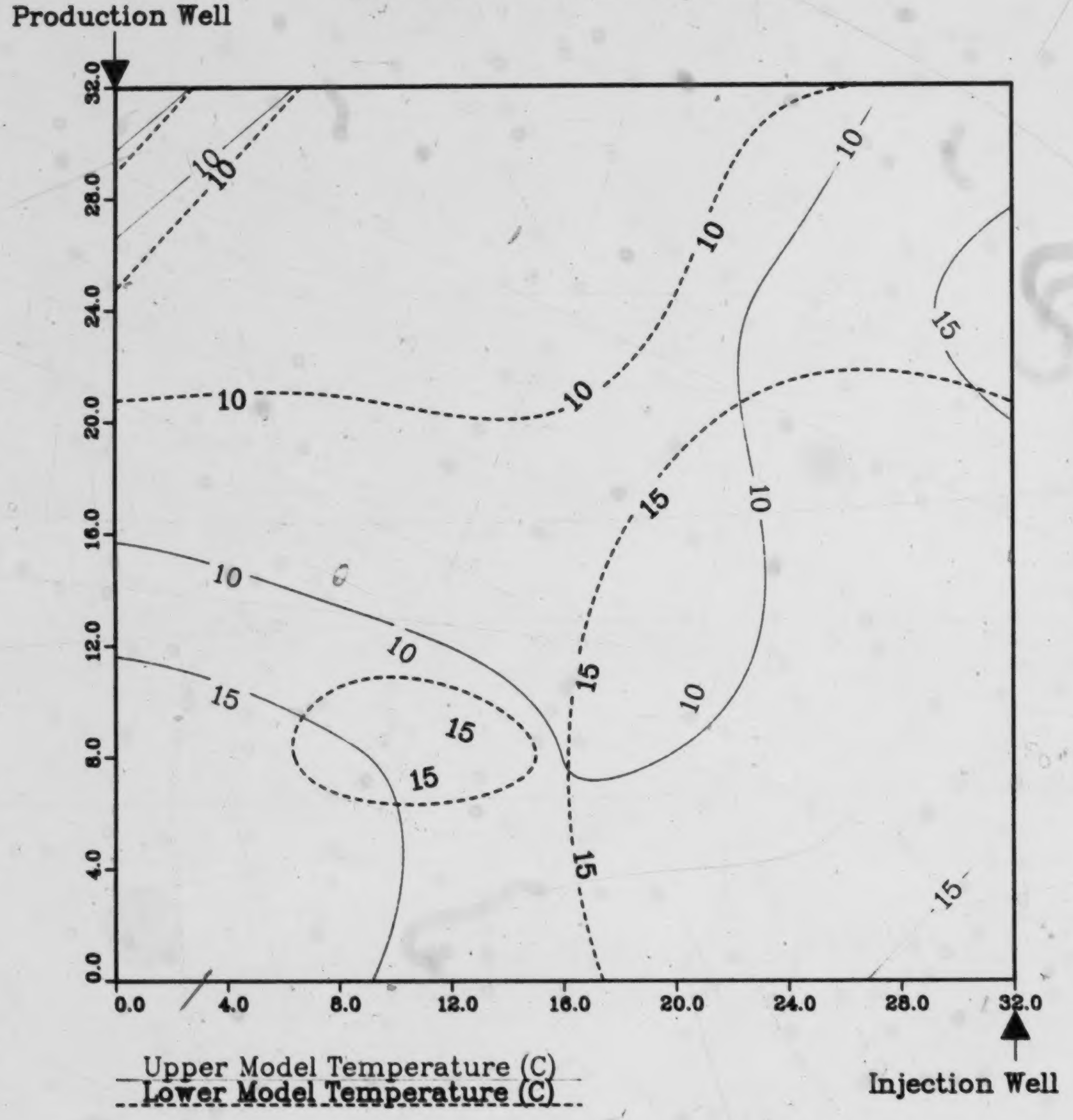

Figure A.266 : Run 47A

Waterflood Prior to Solvent–Steamflood

Temperature Profile for 1.00 Pore Volumes Injected

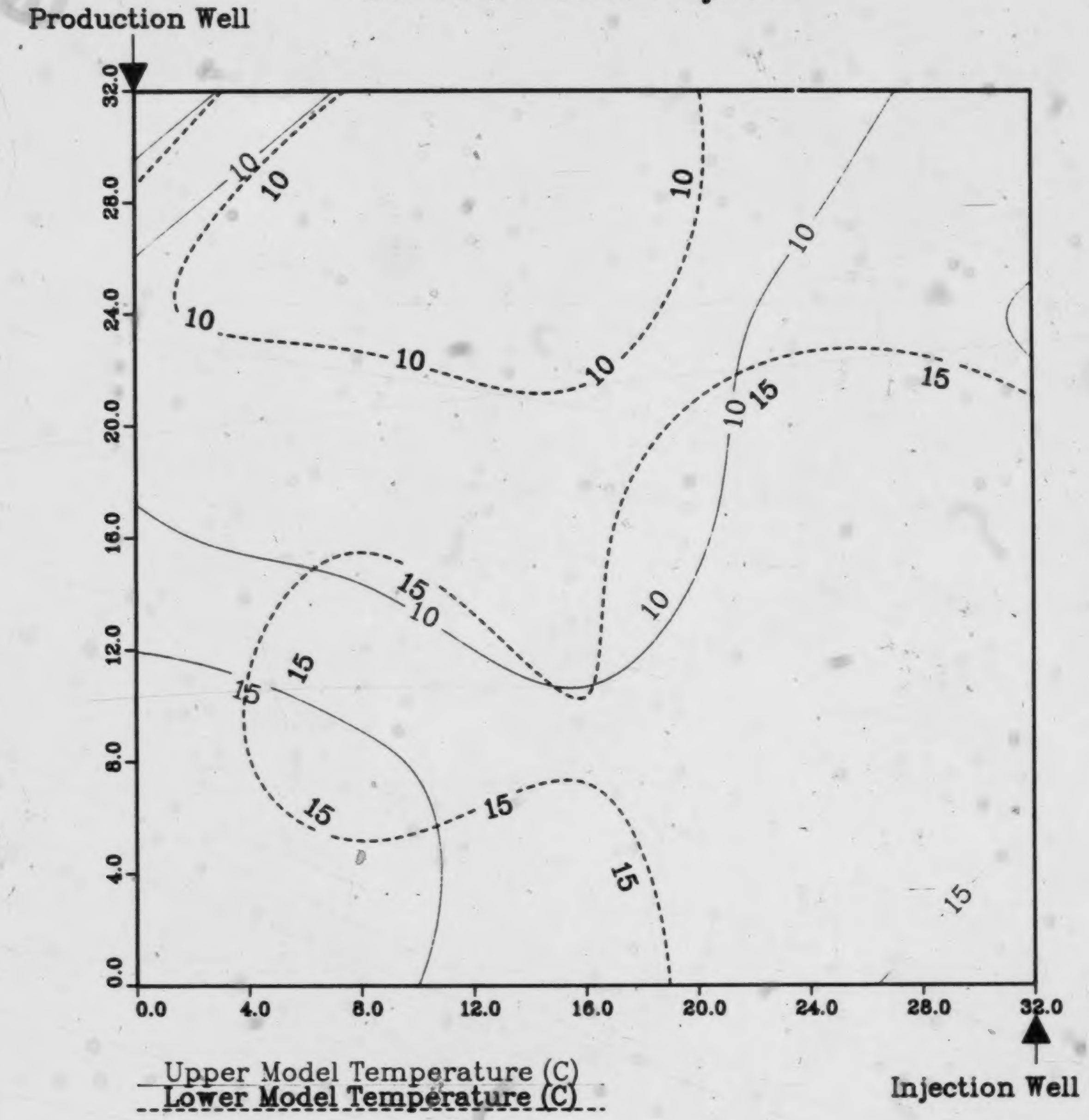

Figure A.267 : Run 47A
Waterflood Prior to Solvent–Steamflood

Temperature Profile for 1.50 Pore Volumes Injected

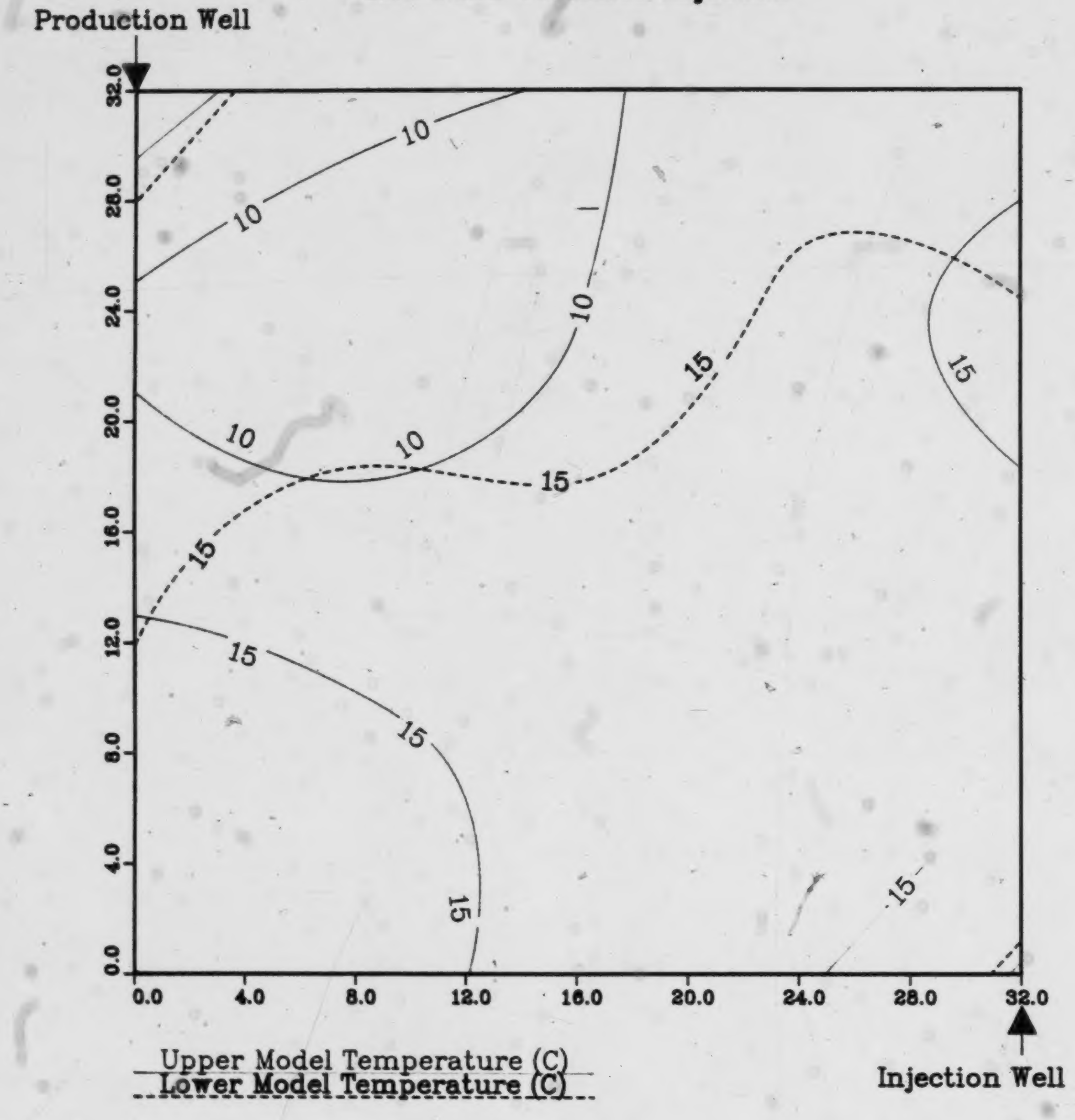

Figure A.268 : Run 47B

Solvent–Steamflood After a Waterflood

Temperature Profile for
2.00 Pore Volumes Injected

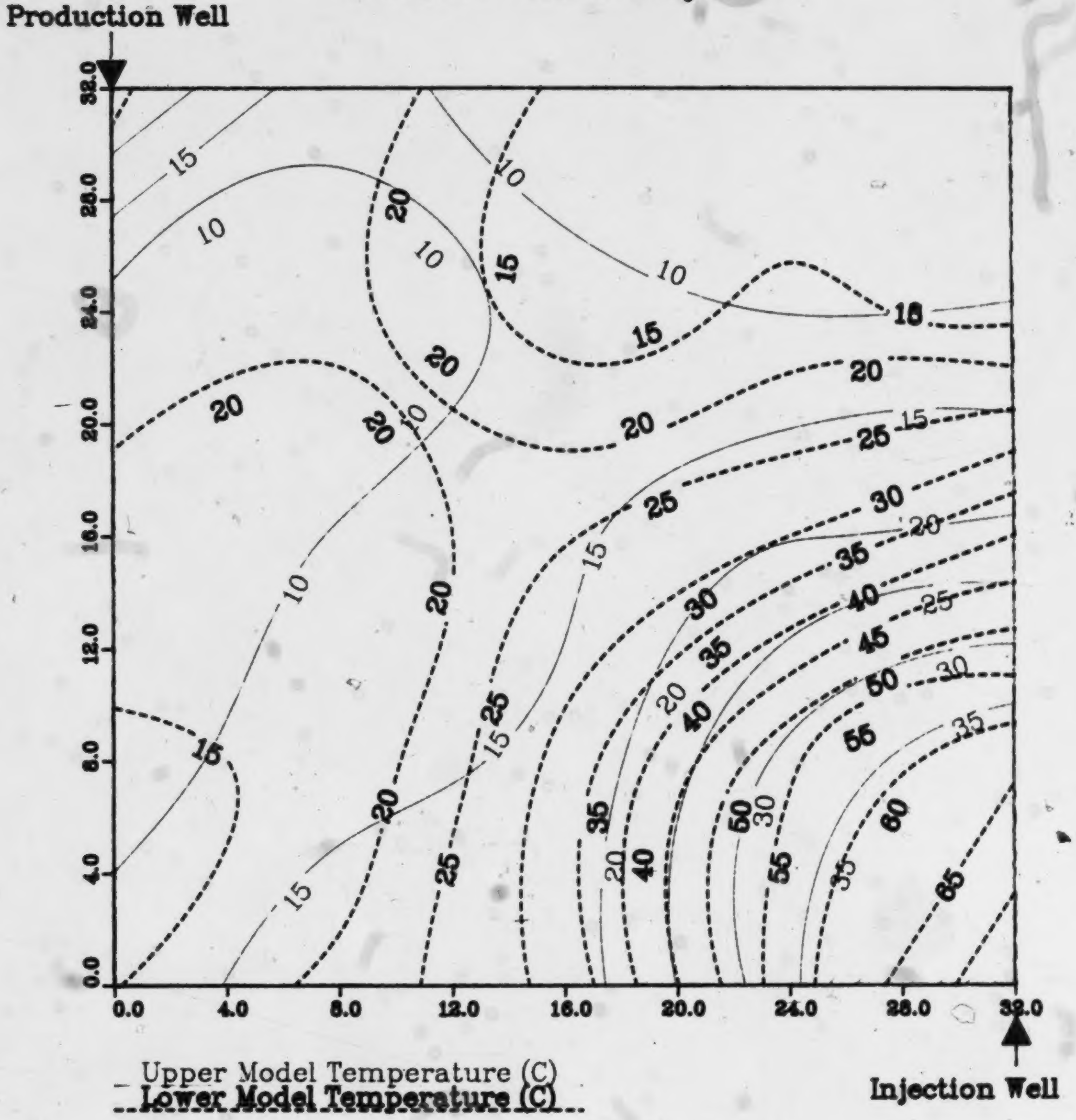

Figure A.269 : Run 47B

Solvent–Steamflood After a Waterflood

Temperature Profile for
2.50 Pore Volumes Injected

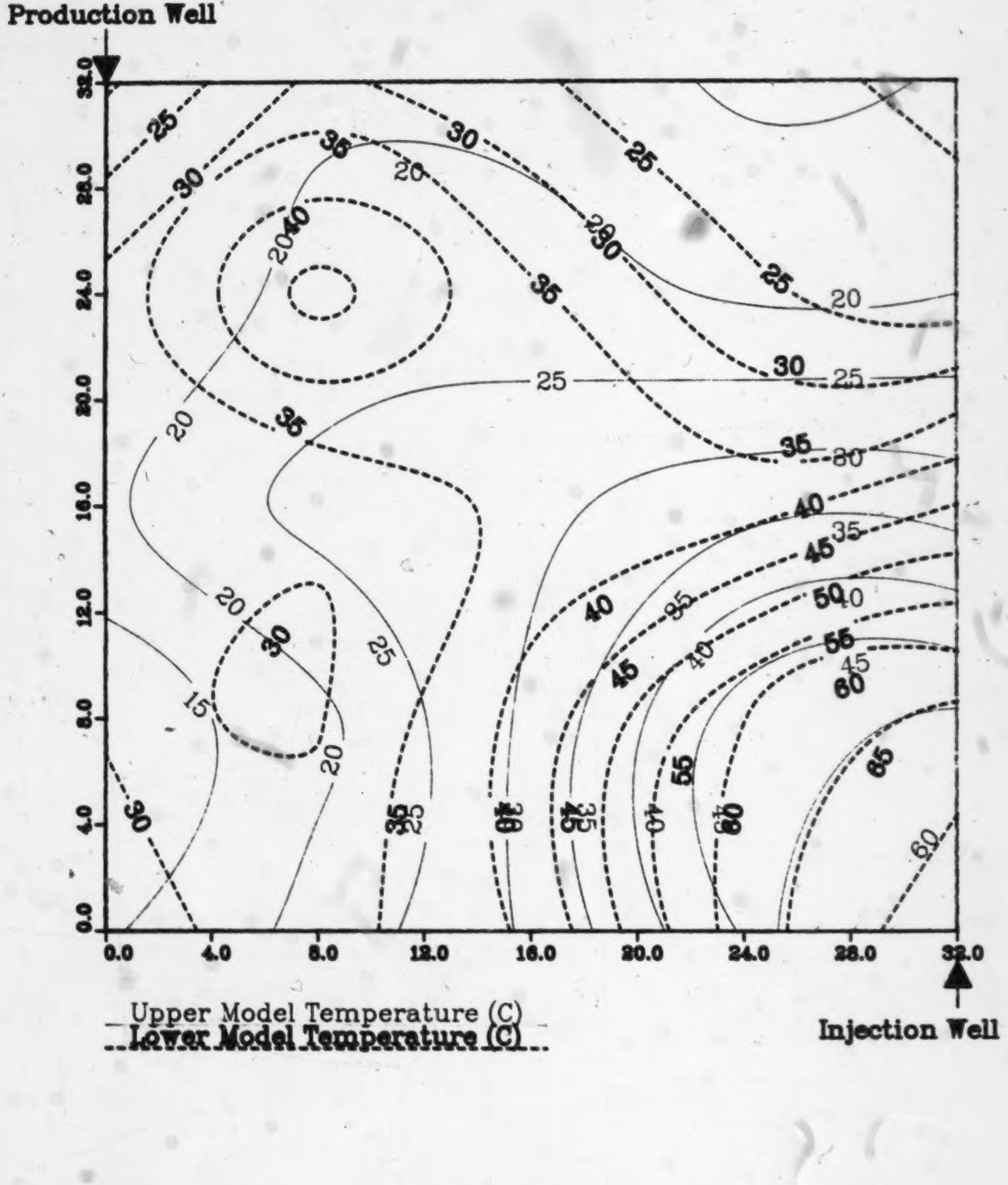

Figure A.270 : Run 47B

Solvent–Steamflood After a Waterflood

Temperature Profile for 3.00 Pore Volumes Injected

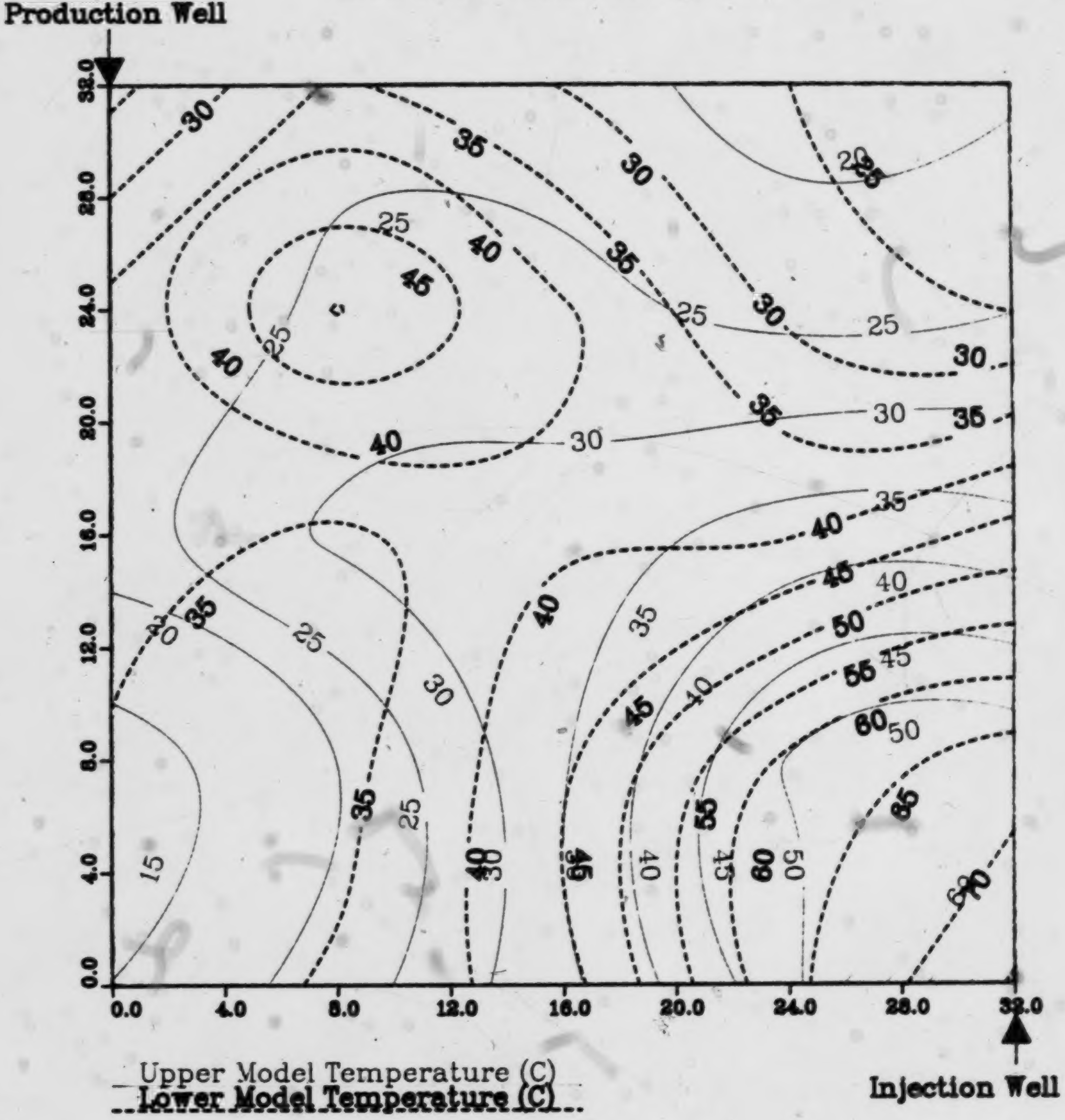

Figure A.271 :Run 47 Temp Profile

Injector to Producer Cross–Section

2.00 Pore Volumes Injected.

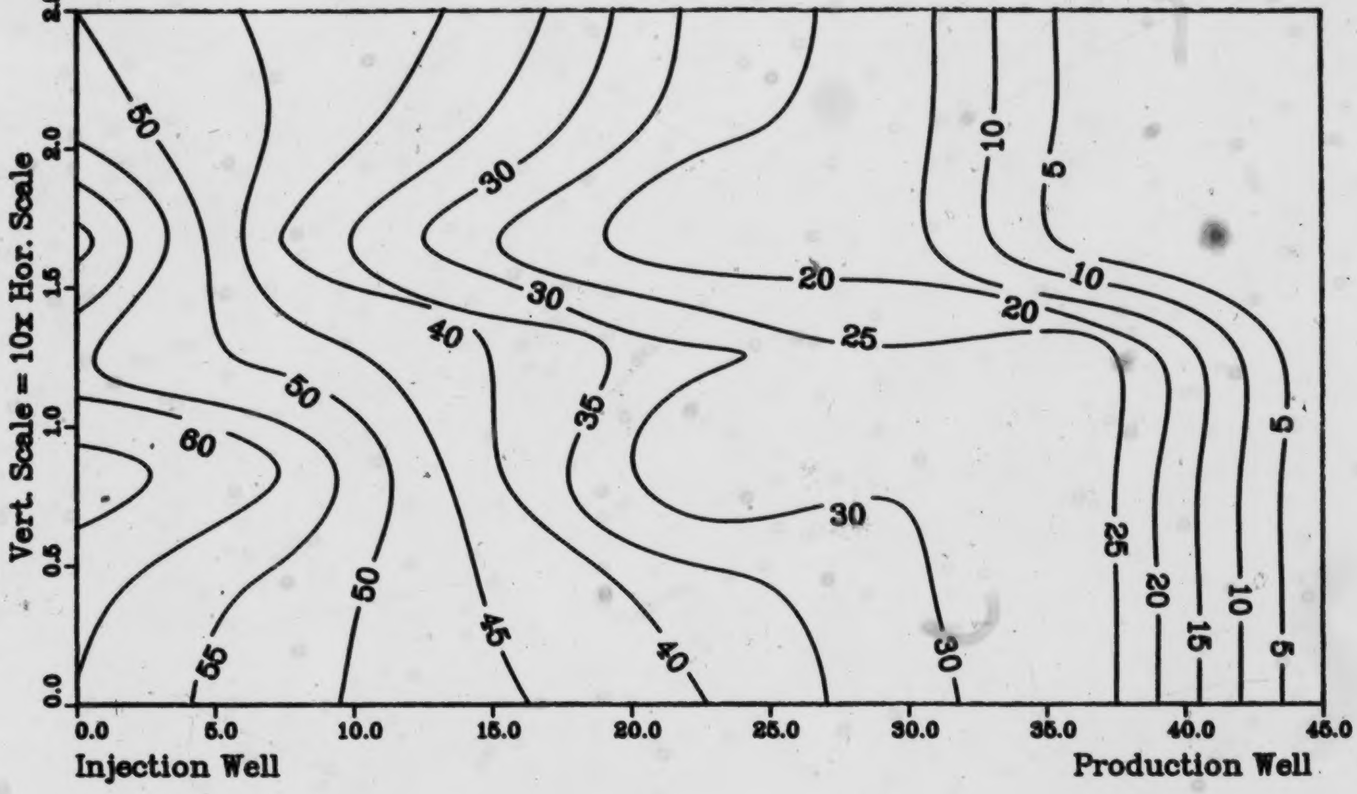

Figure A.272 :Run 47 Temp Profile
Injector to Producer Cross–Section
2.50 Pore Volumes Injected.

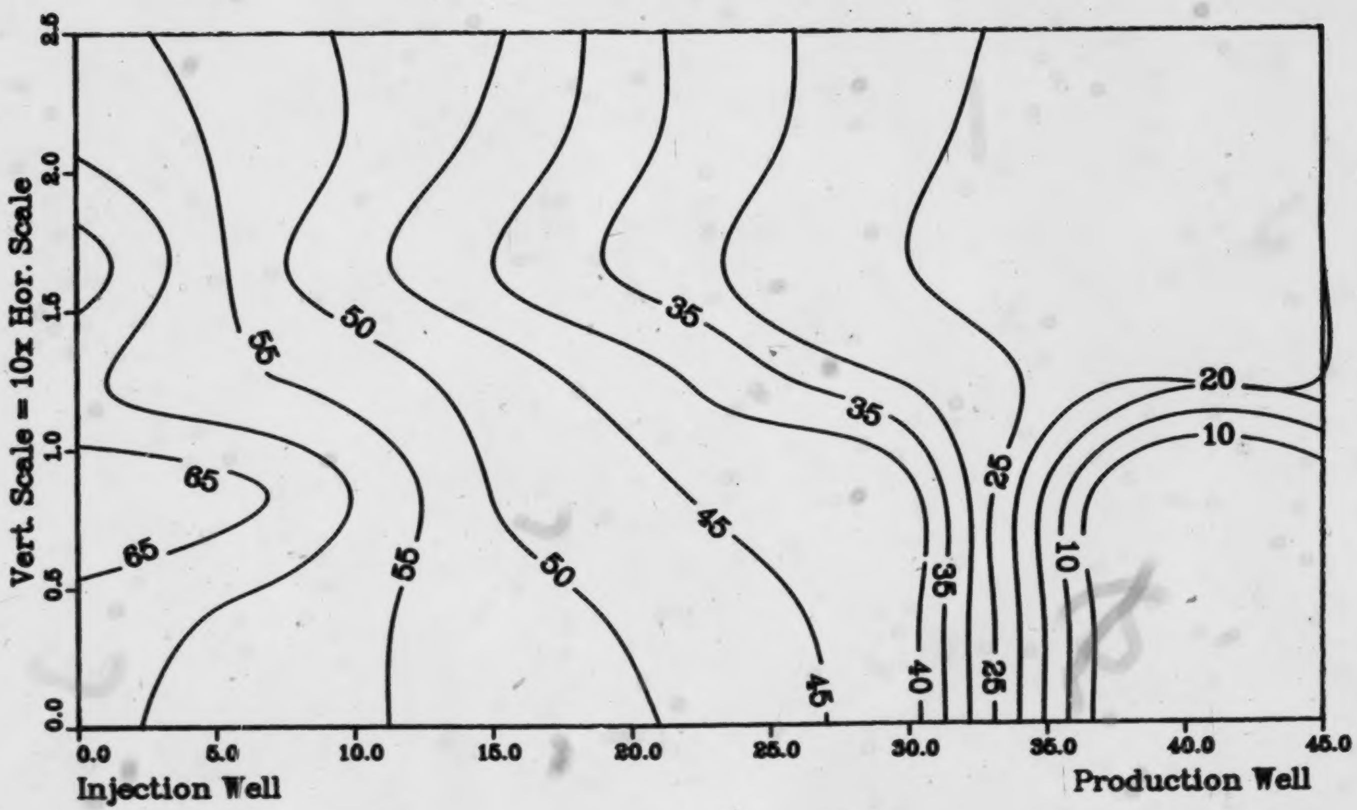

Figure A.273 :Run 47 Temp Profile
Injector to Producer Cross–Section
3.00 Pore Volumes Injected.

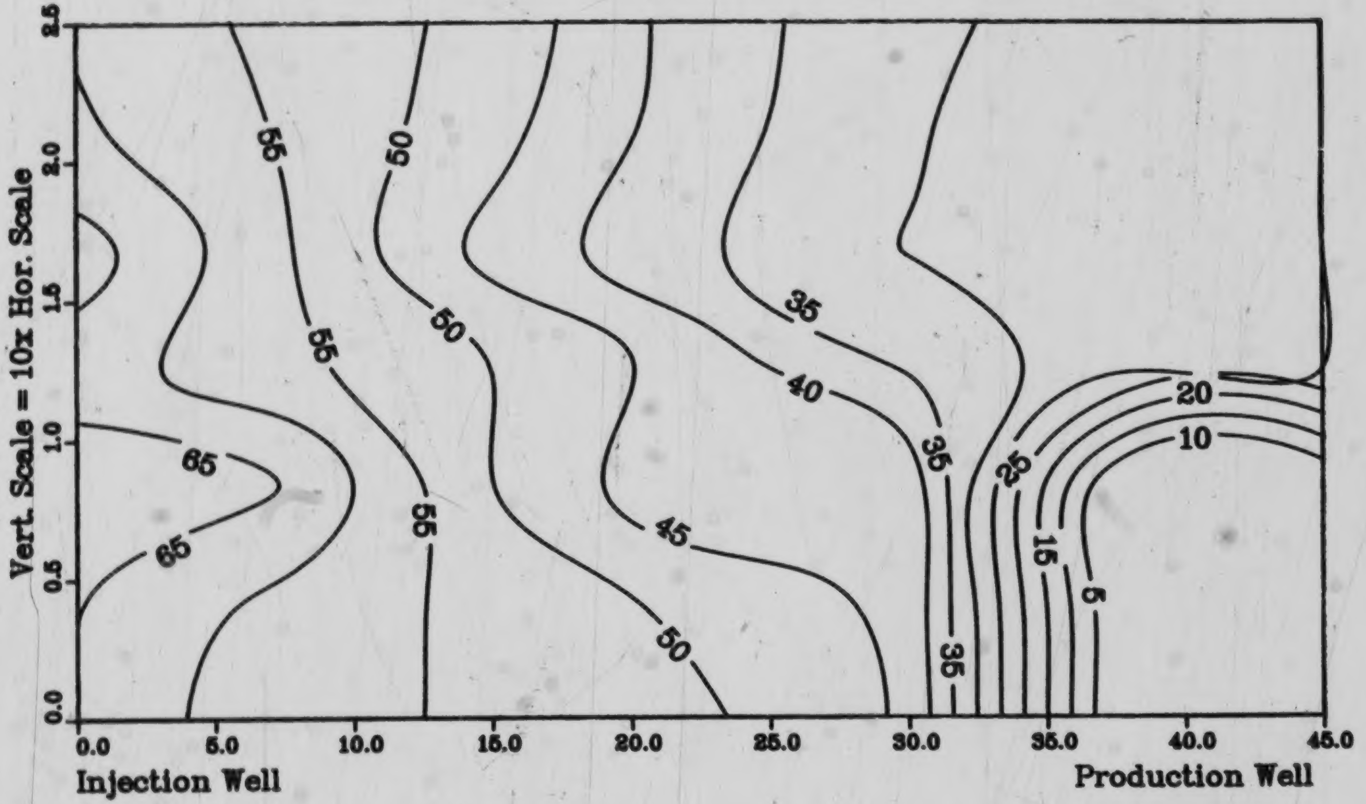

Figure A.274 : Run 48A

Waterflood Prior to Solvent–Steamflood

Temperature Profile for
0.25 Pore Volumes Injected

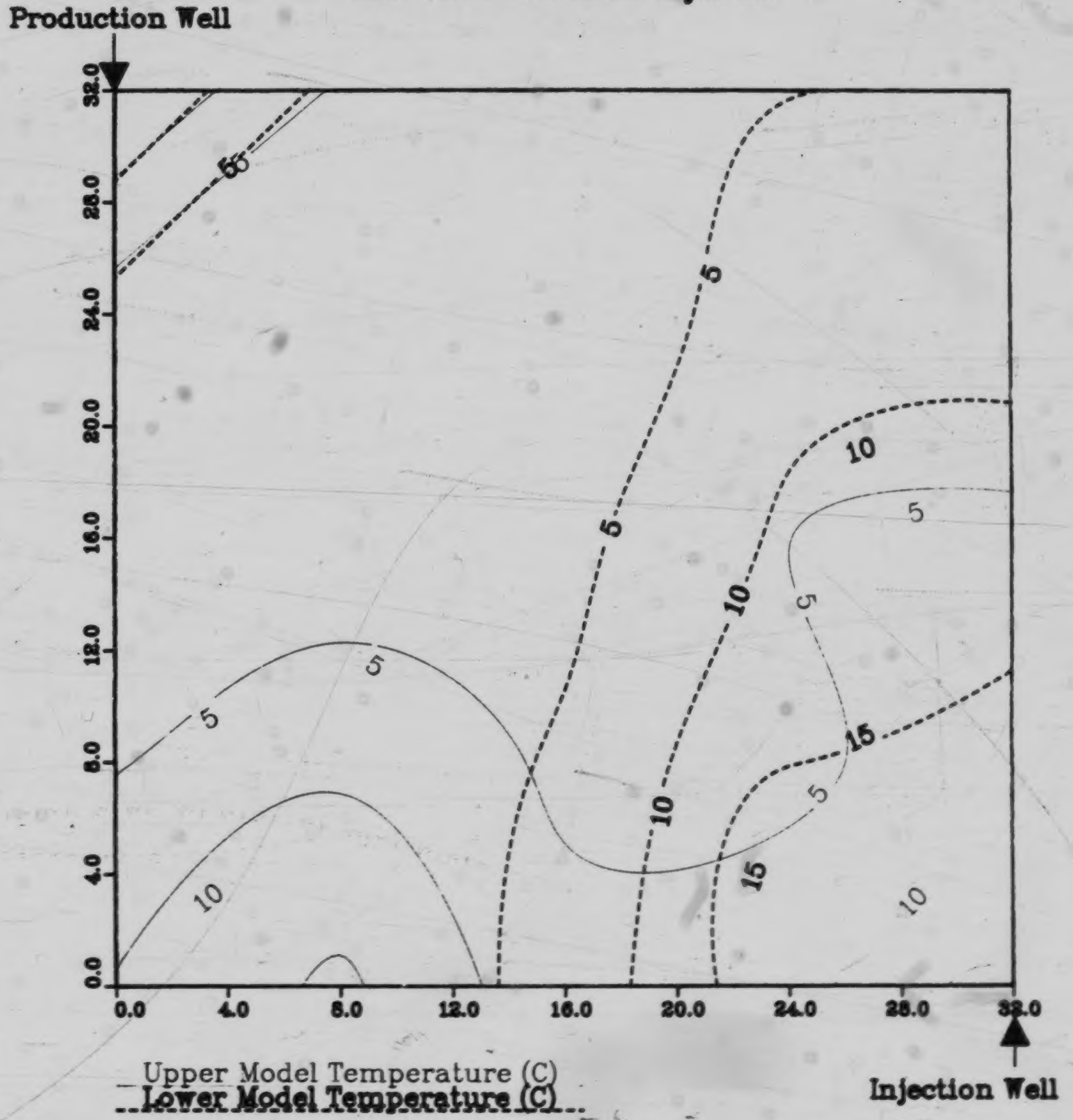

Figure A.275 : Run 48A

Waterflood Prior to Solvent–Steamflood

Temperature Profile for 0.50 Pore Volumes Injected

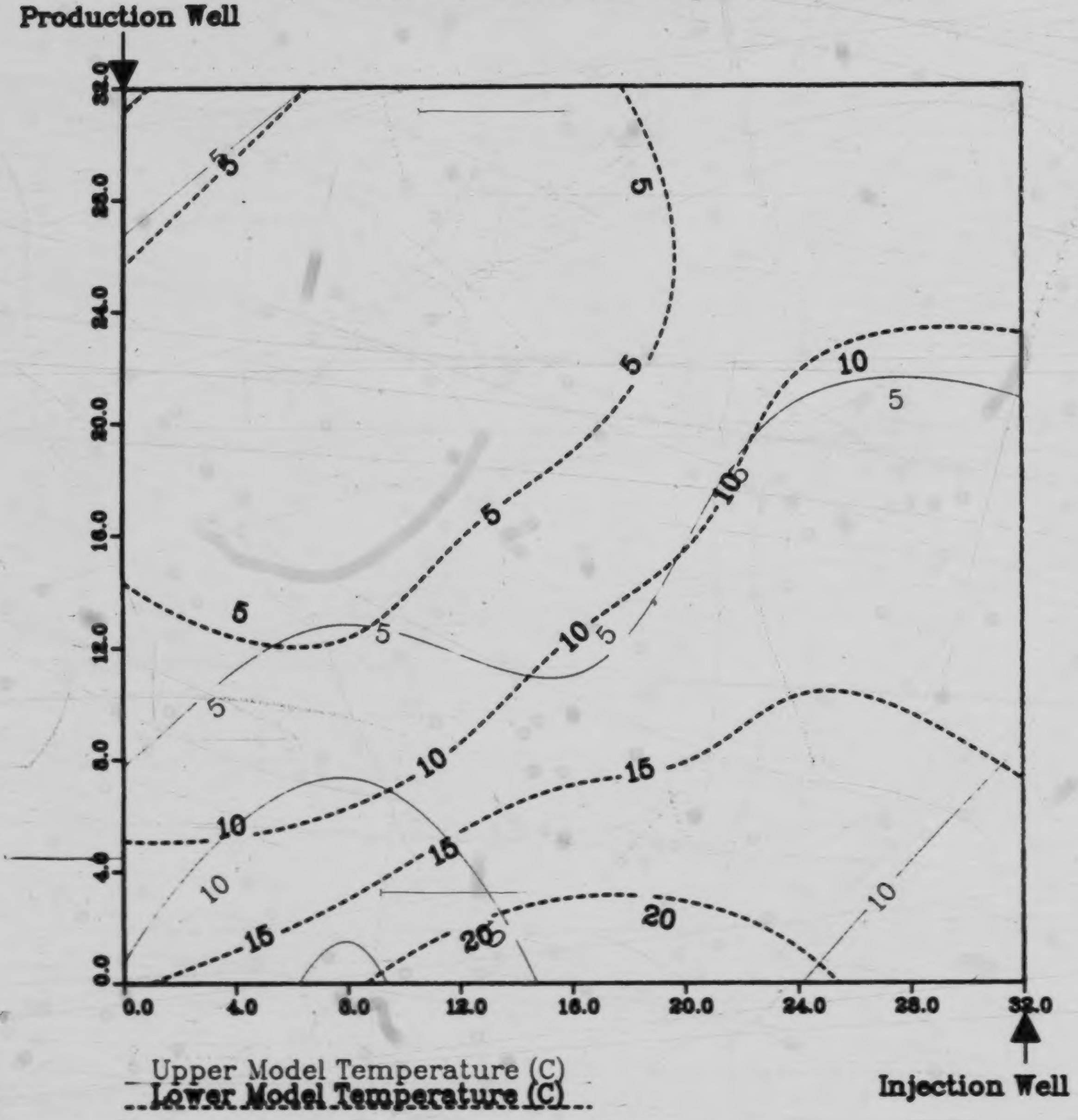

Figure A.276 : Run 48A
Waterflood Prior to Solvent–Steamflood

Temperature Profile for
1.00 Pore Volumes Injected

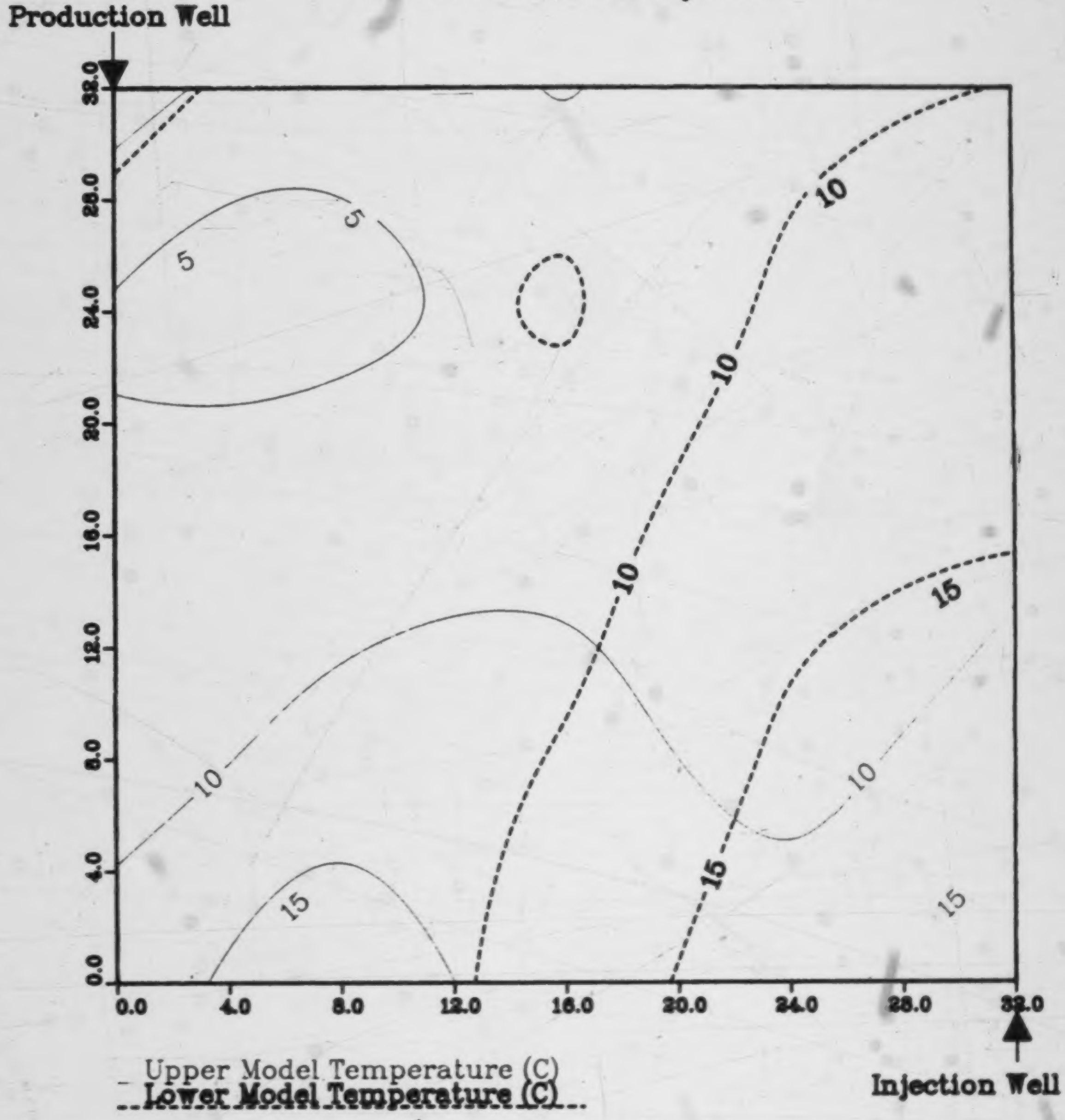

Figure A.277 : Run 48A

Waterflood Prior to Solvent–Steamflood

Temperature Profile for 1.50 Pore Volumes Injected

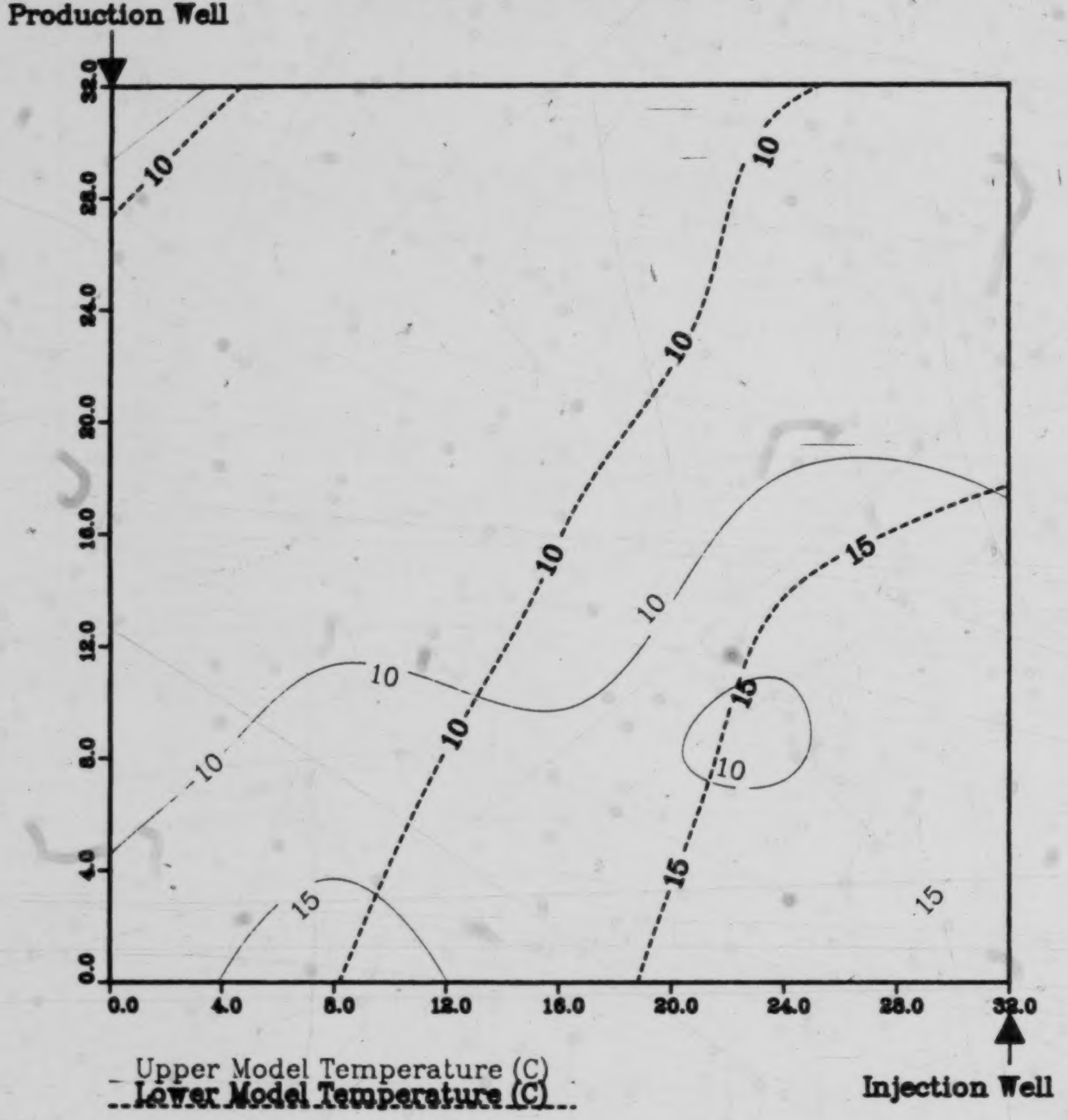

Figure A.278 : Run 48B

Solvent–Steamflood After a Waterflood

Temperature Profile for 2.00 Pore Volumes Injected

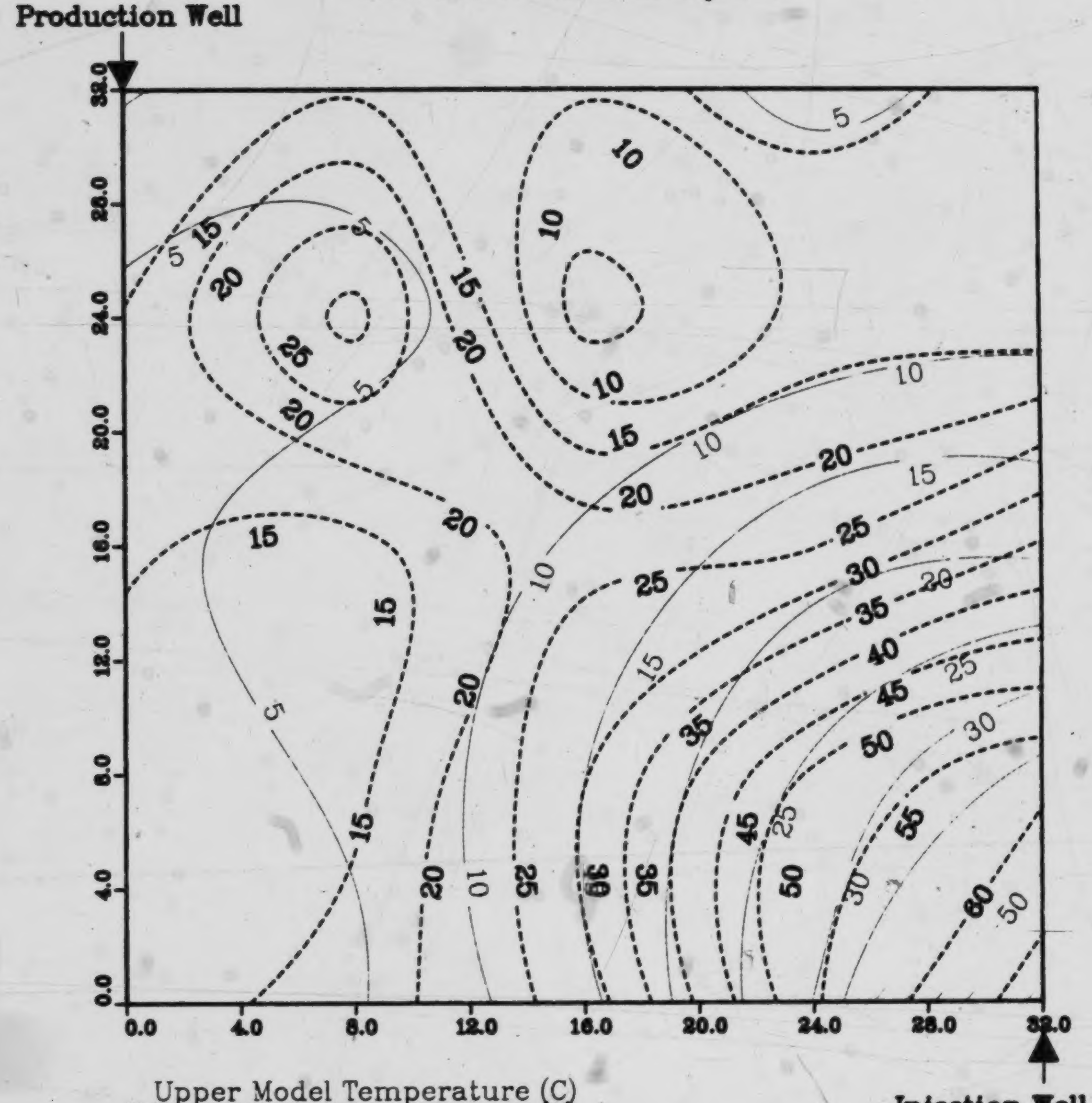

Figure A.279 : Run 48B
Solvent–Steamflood After a Waterflood

Temperature Profile for 2.50 Pore Volumes Injected

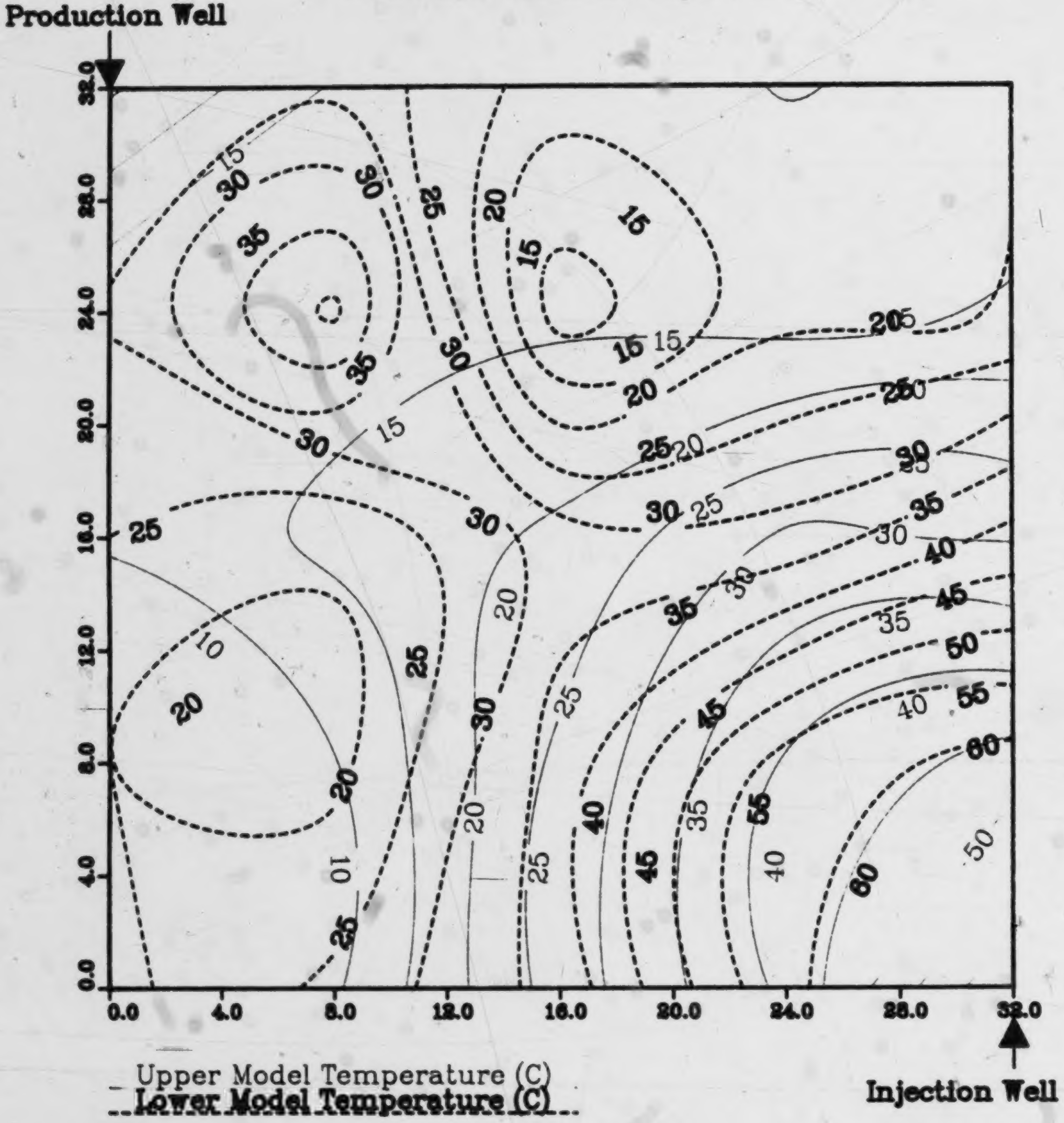

Figure A.280 : Run 48B
Solvent–Steamflood After a Waterflood

Temperature Profile for 3.00 Pore Volumes Injected

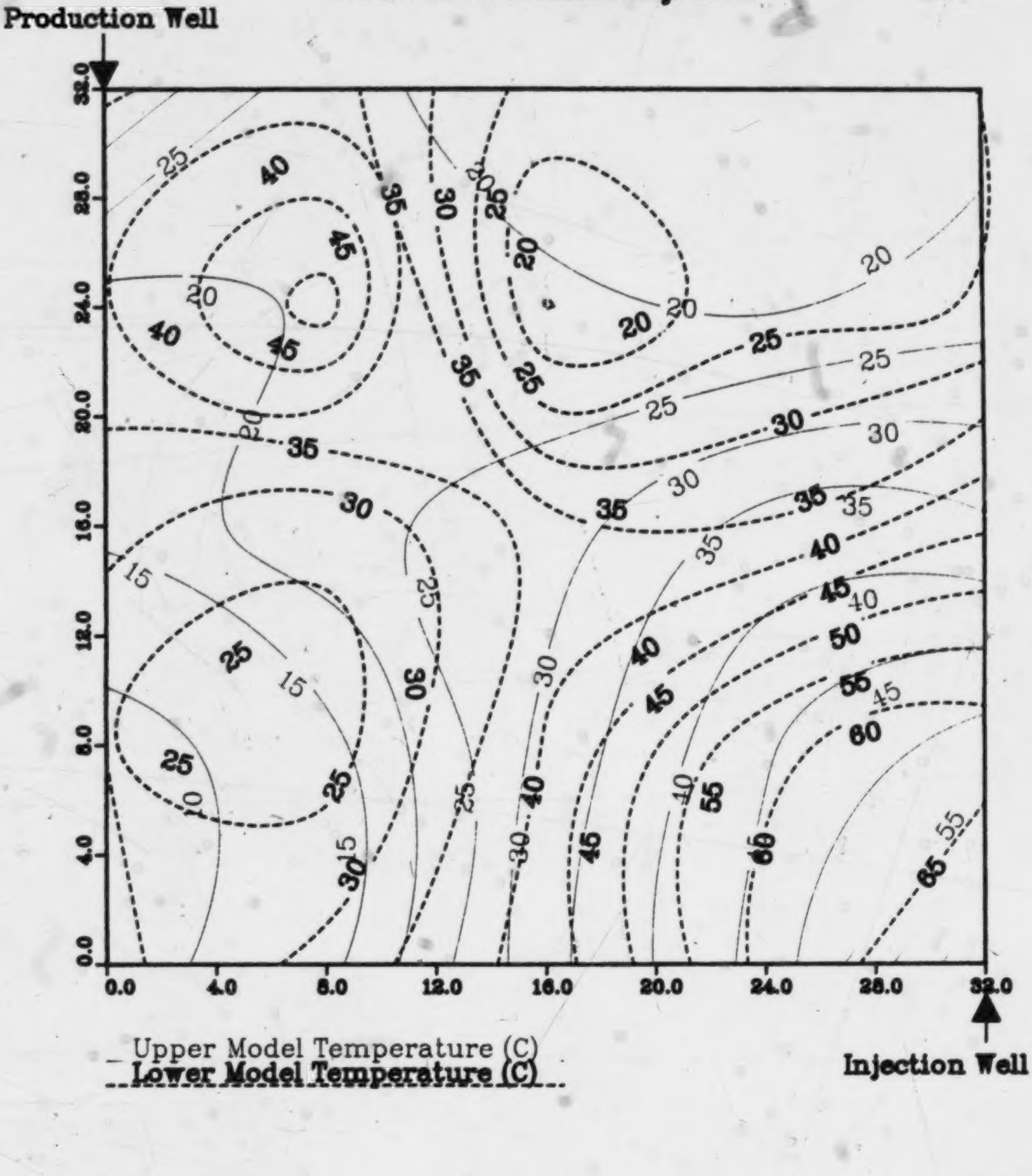

Figure A.281 : Run 48B
Solvent–Steamflood After a Waterflood

Temperature Profile for 3.50 Pore Volumes Injected

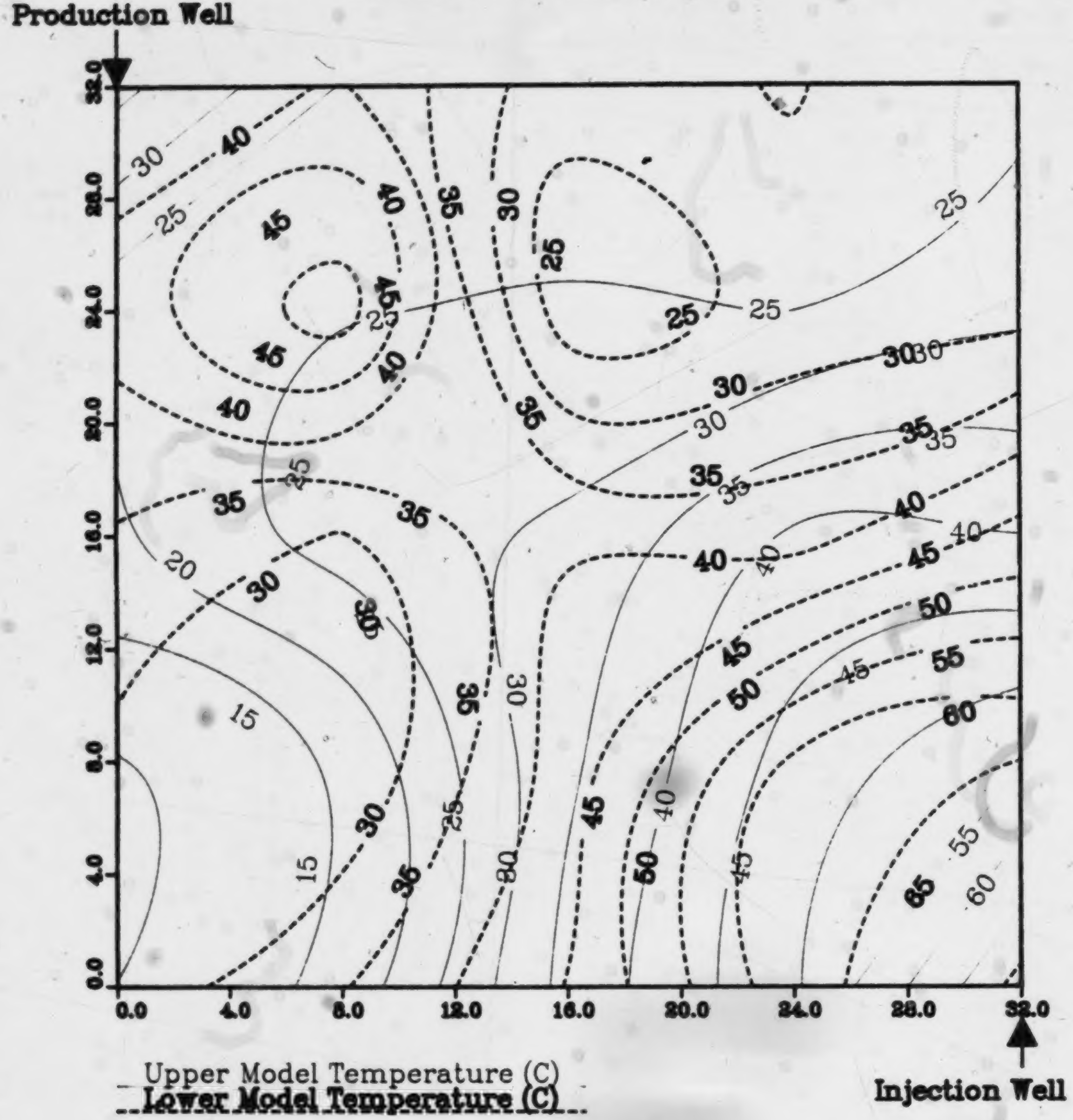

Figure A.282 :Run 48 Temp Profile
Injector to Producer Cross–Section
2.00 Pore Volumes Injected.

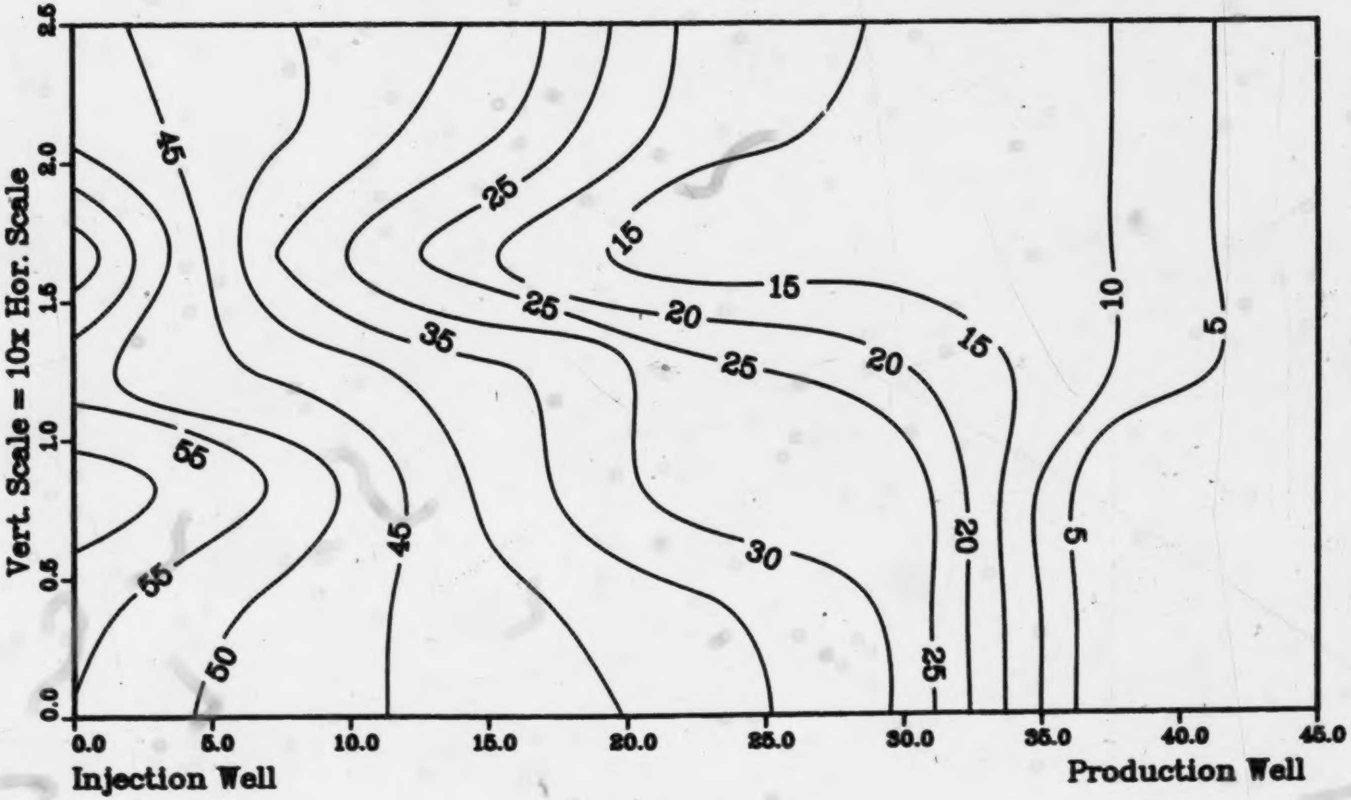

Figure A.283 :Run 48 Temp Profile
Injector to Producer Cross-Section
2.50 Pore Volumes Injected.

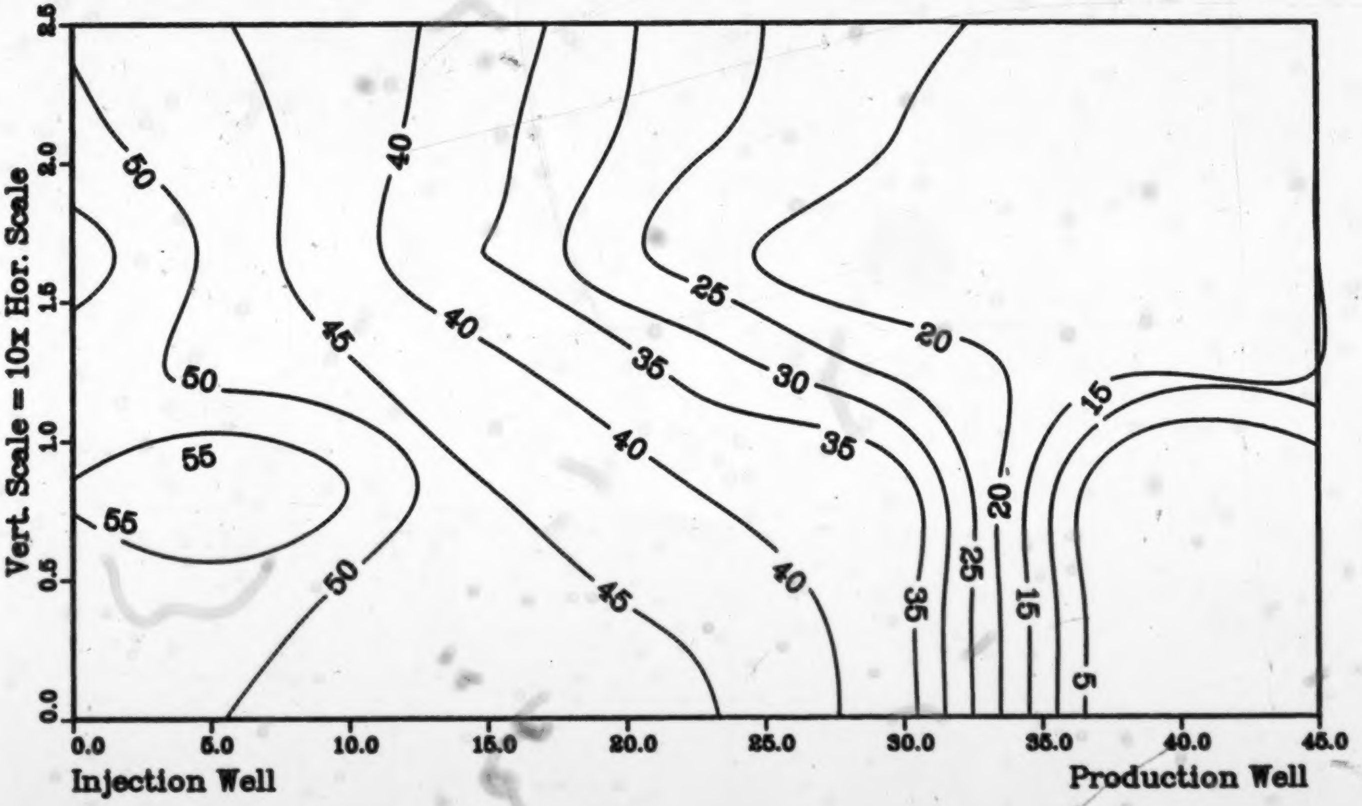

Figure A.284 :Run 48 Temp Profile
Injector to Producer Cross–Section
3.00 Pore Volumes Injected.

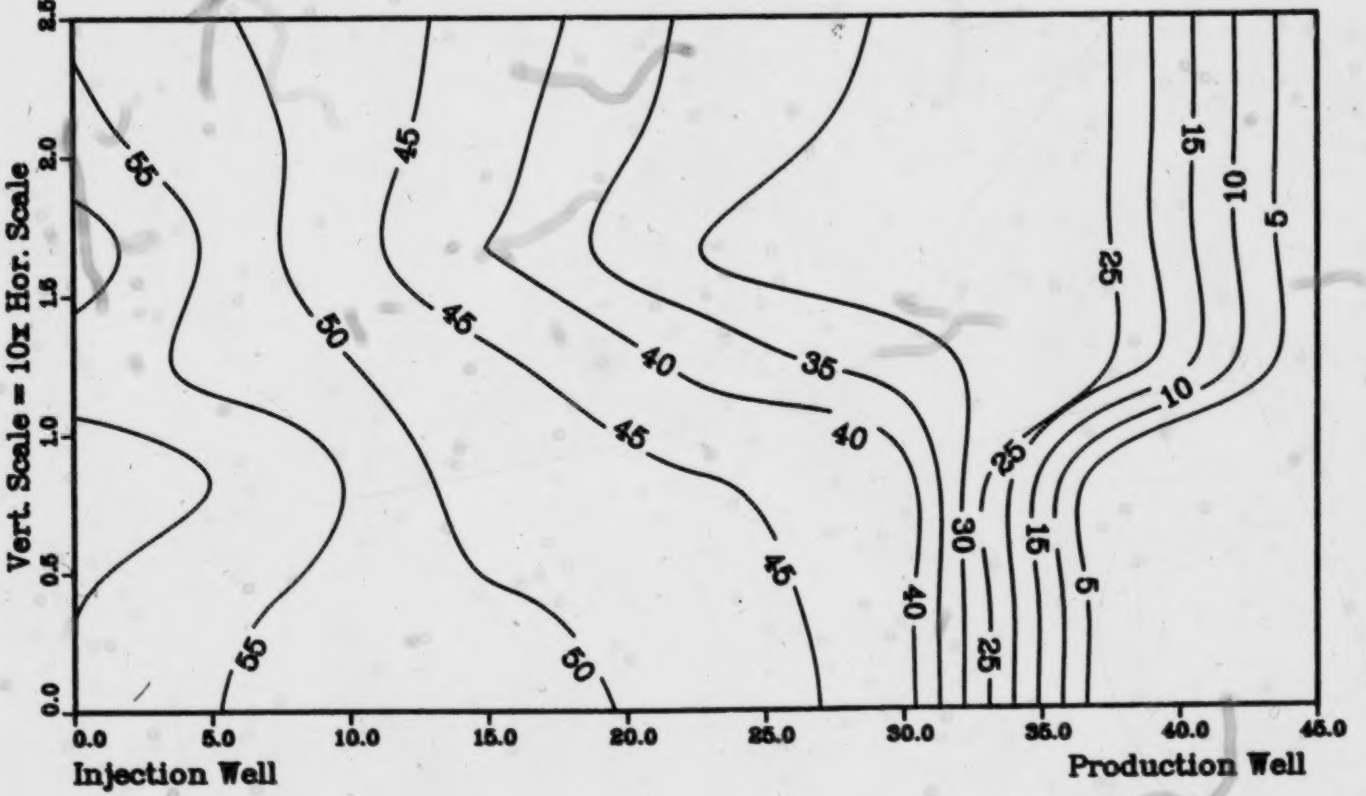

Figure A.285 :Run 48 Temp Profile
Injector to Producer Cross–Section

3.50 Pore Volumes Injected.

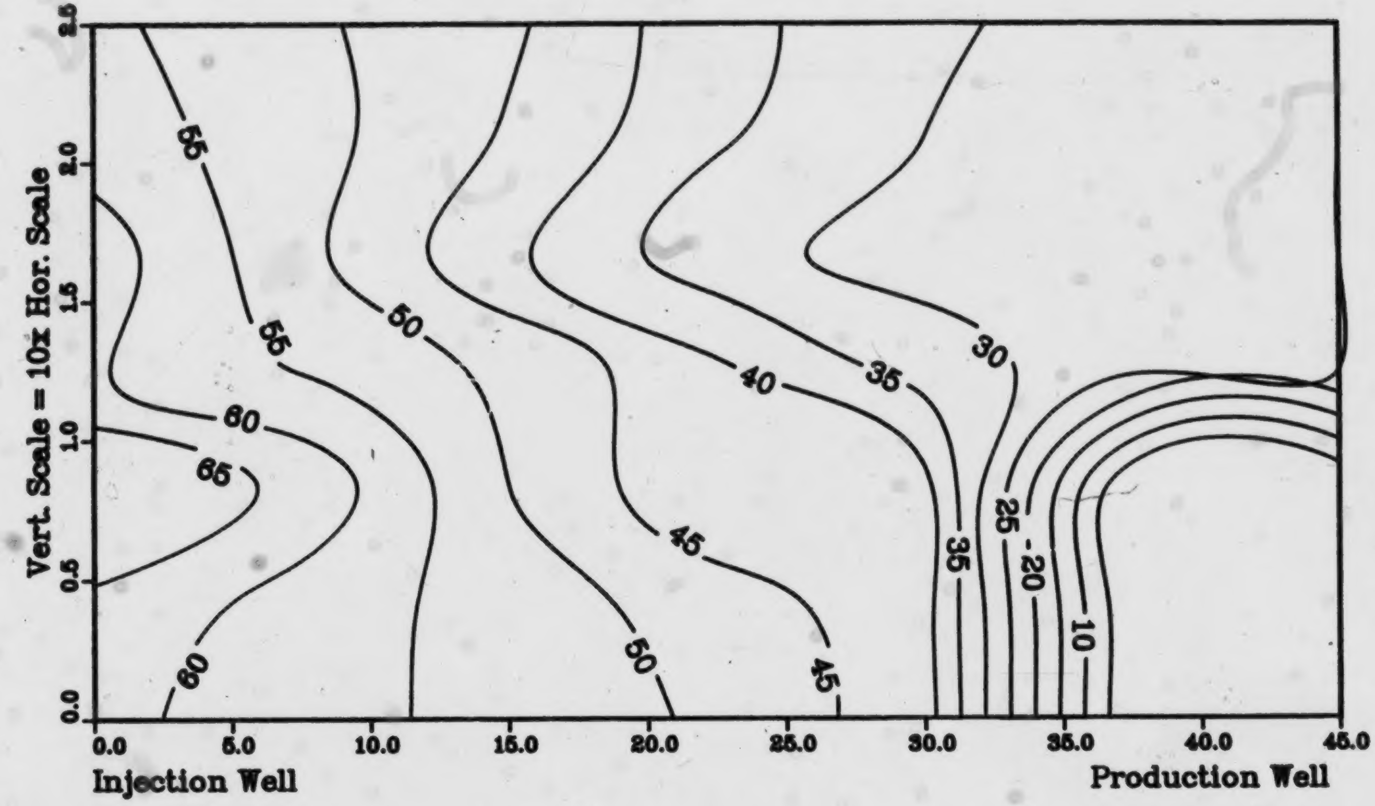

Figure A.286 : Run 26

Steamflood of Homogeneous Model

Temperature Profile for 0.25 Pore Volumes Injected

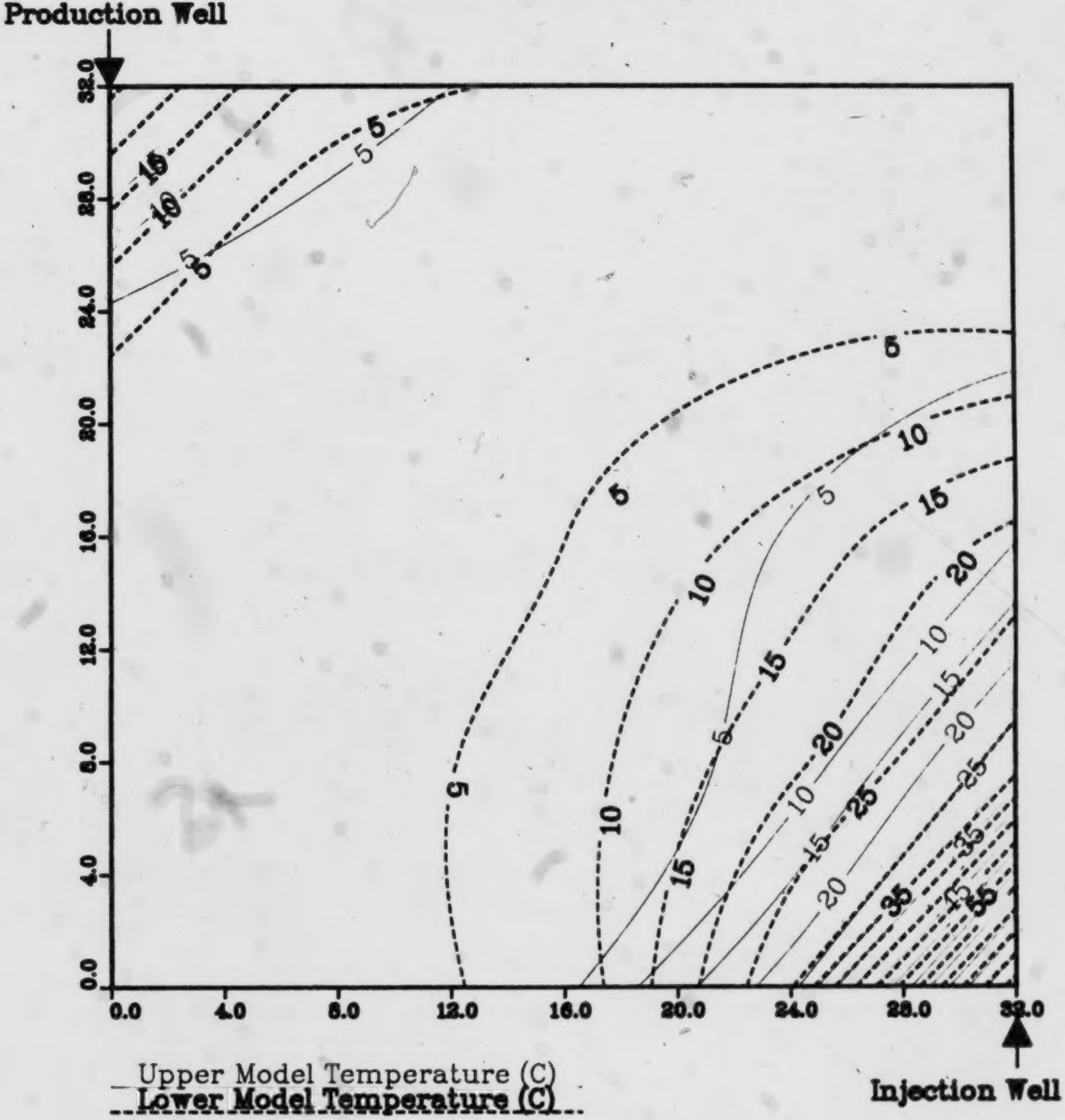

Figure A.287 : Run 26

Steamflood of Homogeneous Model

Temperature Profile for 0.50 Pore Volumes Injected

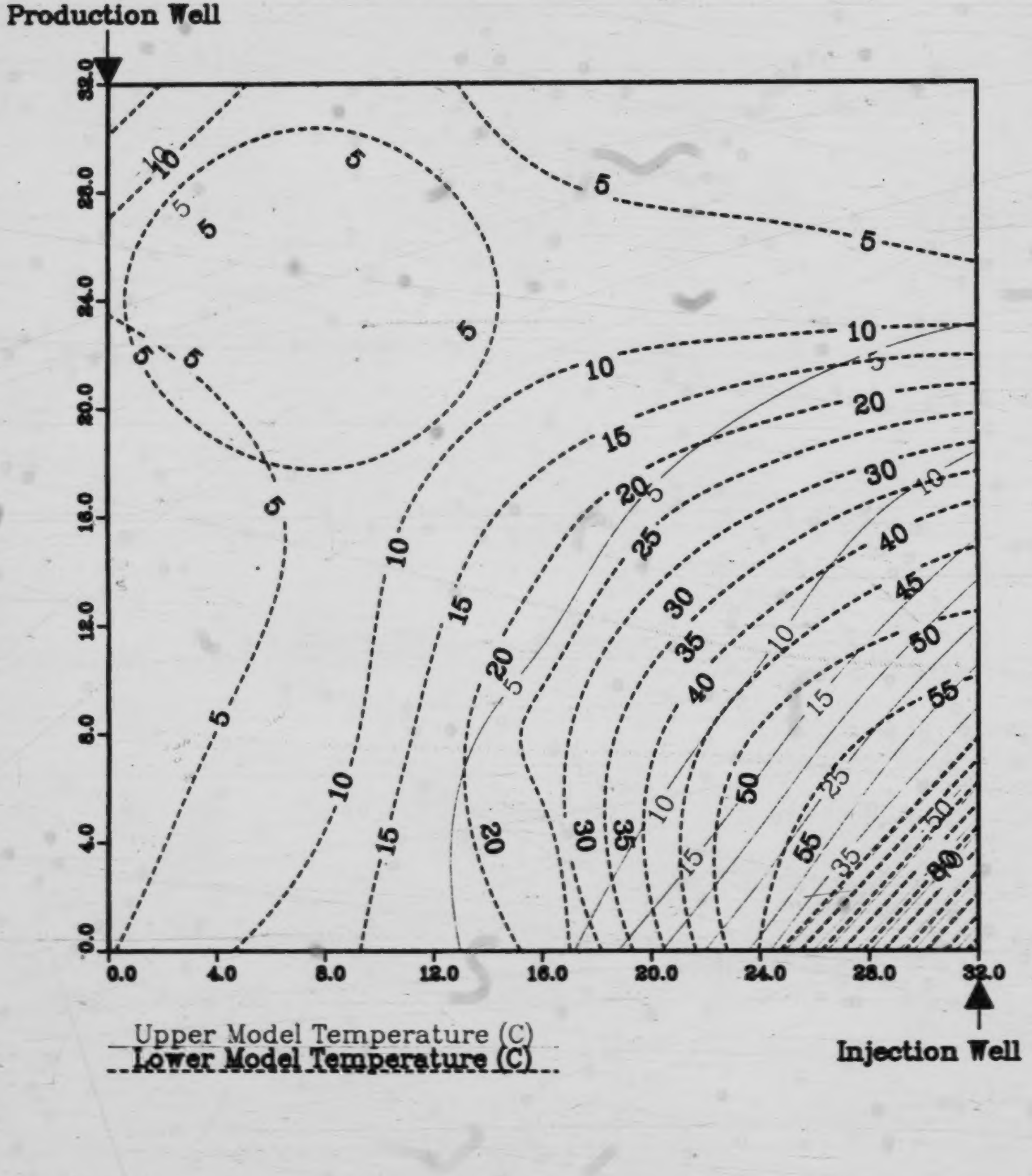

Figure A.288 : Run 26

Steamflood of Homogeneous Model

Temperature Profile for 0.75 Pore Volumes Injected

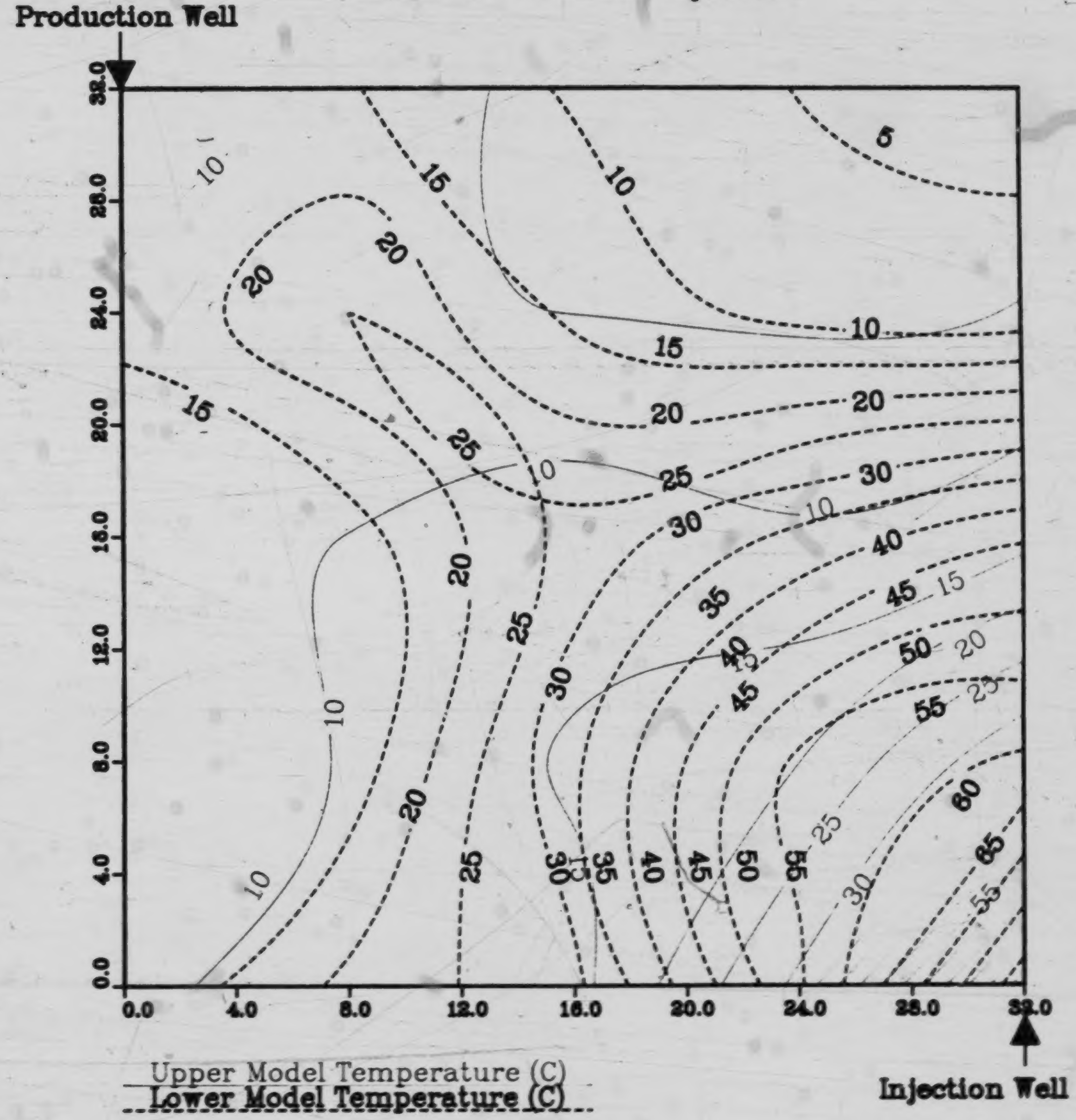

Figure A.289 : Run 26

Steamflood of Homogeneous Model

Temperature Profile for 1.00 Pore Volumes Injected

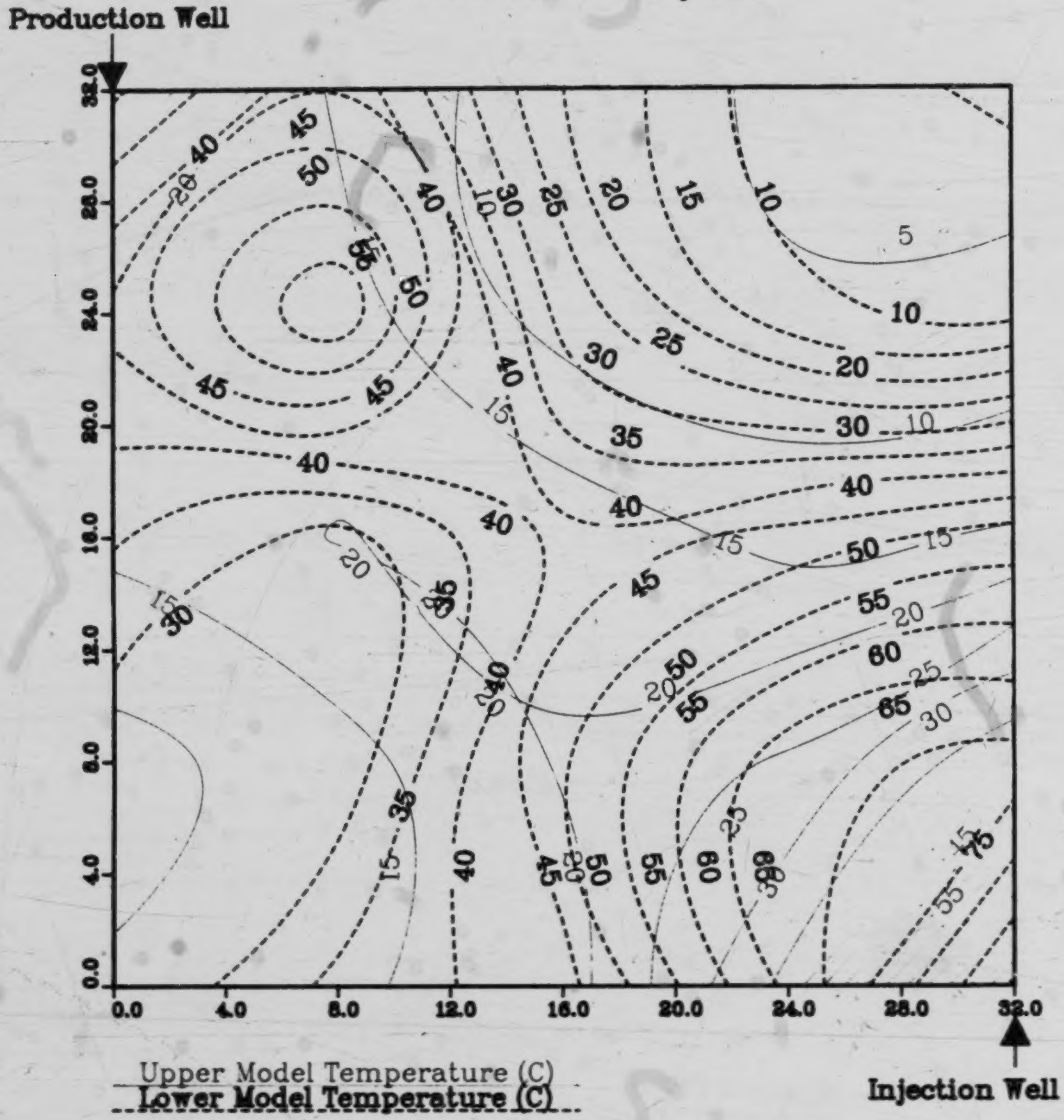

Figure A.290 : Run 26

Steamflood of Homogeneous Model

Temperature Profile for 1.25 Pore Volumes Injected

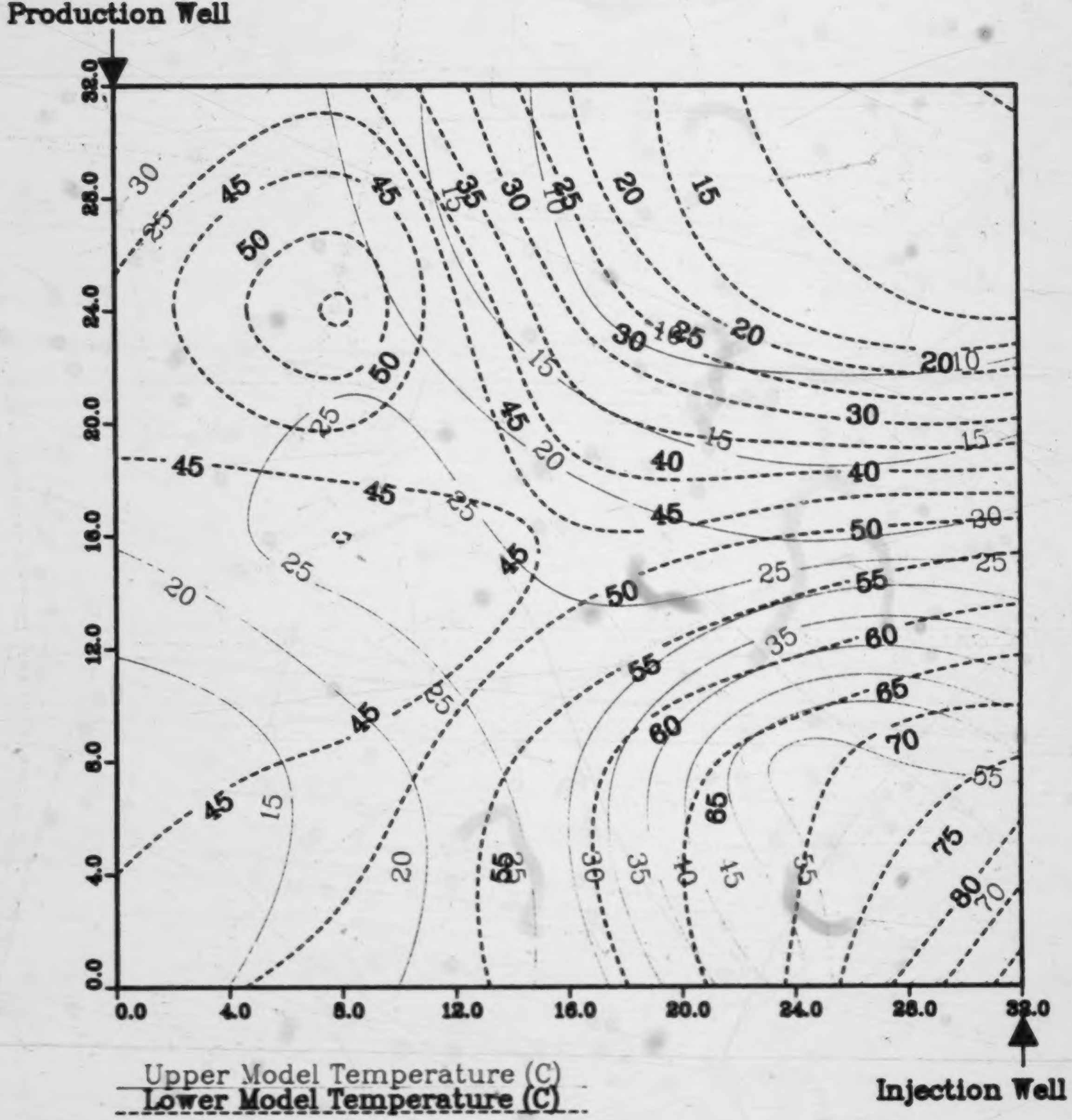

Figure A.291 : Run 26

Steamflood of Homogeneous Model

Temperature Profile for 1.50 Pore Volumes Injected

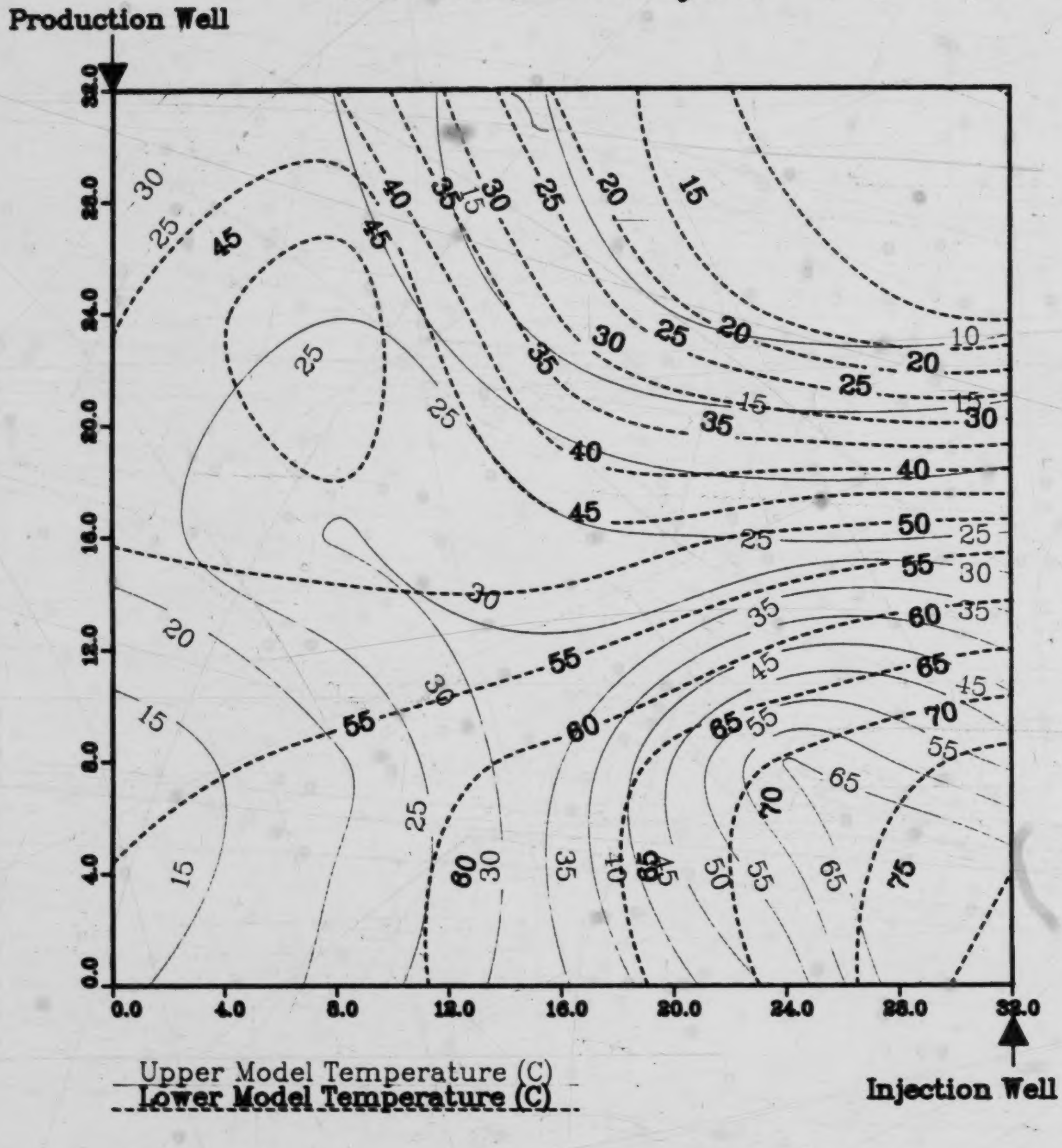

Figure A.292 : Run 26

Steamflood of Homogeneous Model

Temperature Profile for 1.75 Pore Volumes Injected

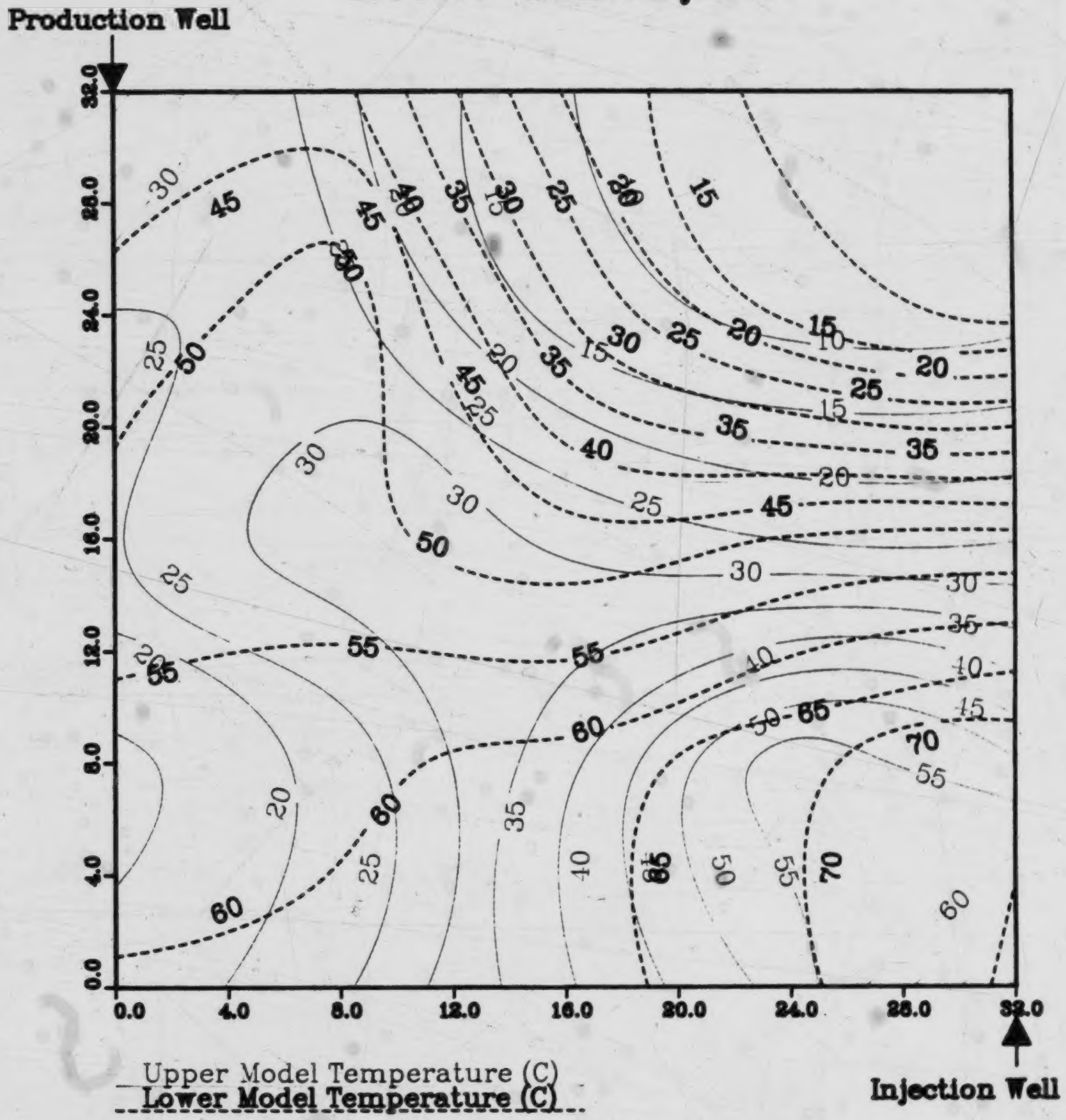

Appendix B

Computer Programs Used in Heat Flow Analysis

University of Alberta

```
C*************************************************************
C
C       The Lauwerier equation was developed to predict
C       formation heating due to Hot Water Injection.
C       (Sensible Heat Only)
C
C       This program utilizes the Lauwerier equation and
C       the temperature contour profiles for Experiment 26
C       (0.25 to 1.00 Pore Volumes).  The area covered by each
C       corresponding temperature on each profile was measured
C       by a planimeter and then substituted into the Lauwerier
C       equation in order to obtain a estimated temperature
C       related to this measured area.
C
C       The contour temperature and the temperature value
C       obtained from the Lauwerier equation are then compared
C       to determine if experiment 26 more closely represents hot
C       water injection instead of the desired continuous
C       steamflood.
C*************************************************************
C
C
      REAL DOIL,COIL,MOIL,DH2O,CH2O,MH2O,KHG,MG,KHOB,MOB,TM,HT,
     @IW,AREA,TR,TF,XD,TD,TEMP,MS,POR,SOIL,SH2O
C
      WRITE(6,33)
33    FORMAT(5X,'ACTUAL TEMP C',5X,'LAUWERIER TEMP C'//)
C
C       Density of Oil (lb/ft3)
      DOIL=38.375
C       Specific Heat of Oil (Btu/lb-F)
      COIL=0.5162
C       Heat Capacity of Oil (Btu/ft3-F)
      MOIL=DOIL*COIL
C       Density of Water (lb/ft3)
      DH2O=61.186
C       Specific Heat of Water (Btu/lb-F)
      CH2O=0.9996
C       Heat Capacity of Water (Btu/ft3-F)
      MH2O=DH2O*CH2O
C       Thermal Condutivity of Glass (Btu/hr-ft-F)
      KHG=0.5
C       Heat Capacity of Glass (Btu/ft3-F)
      MG=25.9
C       Thermal Conductivity of Overburden (Btu/hr-ft-F)
      KHOB=1.46426
C       Heat Capacity of Overburden (Btu/ft3-F)
      MOB=28.8558
C       Thickness (Feet)
      HT=.104167
C       Injection Rate of Fluid (BBl/Day)
      IW=1.5405
C       Temperature of Reservoir (F)
      TR=37.4
C       Temperature of Fluid (F)
      TF=154.71
C       Porosity of Model
      POR=.3346
C       Oil Saturation
      READ(5,*)J,PV,SOIL
```

```
C       Water Saturation
      SH2O=1-SOIL
C       Time(hours)
      TM=PV*14055./(226.8*60.)
C       Heat Capacity of Saturated Porous Medium (Btu/ft3-F)
      MS=POR*SOIL*MOIL+POR*SH2O*MH2O+(1.0-POR)*MG
C
C       Dimensionless Time
      TD=4.0*KHOB*MOB*TM/((MS**2)*(HT**2))
C
C       Read Contour Temperature and Corresponding Area
C       From Data File
      DO 100 I=1,J
      READ(5,*)TEMP,AREA
C
C
C       Dimensionless Distance
      R1=4.*24.*KHOB*MOB*AREA
      R2=5.615*MS*DH2O*CH2O*IW*HT
      XD=R1/R2
C
C       Limits For Lauwerier Equation are Applied
C
      IF(TD-XD) 1,1,2
C
C       If xD is greater than or equal to tD then Lauwerier
C       temperature is equal initial reservoir temperature.
C       (37.4 F)
C
1     WRITE(6,10)
10    FORMAT (10X,'xD is greater than or equal to tD')
      TLAU=3.0
      GO TO 9
C
C       If xd is less than tD then Lauwerier equation can
C       be used
C
2     R3=(TF-TR)*ERFC(XD/(2*SQRT(TD-XD)))
      TLAU=((TR+R3)-32.0)/1.8
C
C       The Contour Temperature and Lauwerier Temperature are
C       written into the output file so these two values can be
C       compared to see how closely experiment 26 represents a
C       hot waterflood.
C
9     WRITE(6,20)TEMP,TLAU
20    FORMAT(12X,F5.2,15X,F5.2)
100   CONTINUE
      STOP
      END
```

University of Alberta

University of Alberta

```
C****************************************************************
C      This program calculates the Steam Zone Volume for every
C      0.25 pore volumes of steam injected for Experiment 26 using
C      the Marx-Langenheim Model for Formation Heating by Steam
C      Injection.
C
C      Marx-Langenheim assumes that the latent heat injection
C      rate is greater than the rate of its comsumption.
C
C
C****************************************************************
      REAL DOIL,COIL,MOIL,DH2O,CH2OT,MH2O,KHG,MG,KHOB,MOB,TM,HT,
     @IW,TR,TF,XD,TD,MS,POR,SOIL,SH2O,FST,QI,LV,F1,VS,SST,PV,CH2O
C
C
C      Quality of Steam
      FST=0.08324
C      Latent Heat of Vaporization (Btu/lb)
      LV=1017.755
C      Density of Oil (lb/ft3)
      DOIL=38.375
C      Specific Heat of Oil (Btu/lb-F)
      COIL=0.5162
C      Heat Capacity of Oil (Btu/ft3-F)
      MOIL=DOIL*COIL
C      Density of Water (lb/ft3)
      DH2O=61.186
C      Specific Heat of Water (Btu/lb-F)
      CH2O=1.01495
C      hw-hr (Btu/lb)
      CH2OT=101.23
C      Heat Capacity of Water (Btu/ft3-F)
      MH2O=DH2O*CH2O
C      Thermal Condutivity of Glass (Btu/hr-ft-F)
      KHG=0.5
C      Heat Capacity of Glass (Btu/ft3-F)
      MG=25.9
C      Thermal Conductivity of Overburden (Btu/hr-ft-F)
      KHOB=1.46426
C      Heat Capacity of Overburden (Btu/ft3-F)
      MOB=28.8558
C      Thickness (Feet)
      HT=.104167*2.0
C      Injection Rate of Fluid (BBl/Day)
      IW=2.054
C      Temperature of Reservoir (F)
      TR=37.4
C      Temperature of Fluid (F)
      TF=154.71
C      POROSITY OF MODEL
      POR=.3346
C
      DO 100 I=1,8
C      Fraction of Pore Volume Injected into the Model
      PV=0.25*I
C      Calculate Time Using the Pore Volume Injected (hrs)
      TM=PV*14055./(226.8*60)
C      Oil Saturation
      SOIL=0.15
```

```
C       Steam Saturation
      SST=0.50
C       Water Saturation
      SH20=1-SOIL-SST
      MS=POR*SOIL*MOIL+POR*SH20*MH20+(1.0-POR)*MG
C
C       Dimensionless Time
      TD=4.0*KHOB*MOB*TM/((MS**2)*(HT**2))
      WRITE(6,22)PV
22    FORMAT(/10X,F4.2,' Pore Volumes Injected')
C
C
C       Calculate Heat Injection Rate (Btu/hr)
      QI=350.*IW*(CH20T+FST*LV)/24.
C
      F1=EXP(TD)*ERFC(SQRT(TD))+2.*SQRT(TD/3.141592)-1.
      R1=QI*MS*(HT**2.0)*F1
      R2=4.*KHOB*MOB*(TF-TR)
C
C       Steam Zone Volume as a Percentage of
C       Total Model Bulk Volume
C
      VS=(R1/R2)/1.481481*100
      WRITE(6,20)VS
20    FORMAT(10X,'Vs is  ',F5.2,2X,'% of Models Bulk Volume')
100   CONTINUE
      STOP
      END
```

University of Alberta

University of Alberta

```
C*****************************************************************
C       This program calculates the Steam Zone Volume for every
C       0.25 pore volumes of steam injected in Experiment 26
C       using the Mandl-Volek Model of Formation Heating by
C       Steam Injection.
C
C       The Mandl-Volek Model allows for the convective heat
C       transport by hot water ahead of the condensation front.
C
C
C*****************************************************************
      REAL DOIL,COIL,MOIL,DH2O,CH2OT,MH2O,KHG,MG,KHOB,MOB,TM,HT,
     *IW,TR,TF,XD,TD,MS,POR,SOIL,SH2O,FST,QI,LV,F1,VS,SST,PV,CH2O
     *TC,TDC
      INTEGER A
C
C      Quality of Steam
      FST=0.08324
C      Latent Heat of Vaporization (Btu/lb)
      LV=1017.755
C      Density of Oil (lb/ft3)
      DOIL=38.375
C      Specific Heat of Oil (Btu/lb-F)
      COIL=0.5162
C      Heat Capacity of Oil (Btu/ft3-F)
      MOIL=DOIL*COIL
C      Density of Water (lb/ft3)
      DH2O=61.186
C      Specific Heat of Water (Btu/lb-F)
      CH2O=1.01495
C      hw-hr  (Btu/lb)
      CH2OT=101.297
C      Heat Capacity of Water (Btu/ft3-F)
      MH2O=DH2O*CH2O
C      Thermal Condutivity of Glass (Btu/hr-ft-F)
      KHG=0.5
C      Heat Capacity of Glass (Btu/ft3-F)
      MG=25.9
C      Thermal Conductivity of Overburden (Btu/hr-ft-F)
      KHOB=1.46426
C      Heat Capacity of Overburden (Btu/ft3-F)
      MOB=28.8558
C      Thickness (Feet)
      HT=.104167*2.0
C      Injection Rate of Fluid (BBl/Day)
      IW=2.054
C      Temperature of Reservoir (F)
      TR=37.4
C      Temperature of Fluid (F)
      TF=154.71
C      POROSITY OF MODEL
      POR=.3346
C      Oil Saturation
      SOIL=0.15
C      Steam Saturation
      SST=0.50
C      Water Saturation
      SH2O=1-SOIL-SST
C      Heat Capacity of Saturated Reservoir
```

```
      MS=POR*SOIL*MOIL+POR*SH2O*MH2O+(1.0-POR)*MG
C
C      Dimensionless Critical Time (From Table 5.1 of SMFA Text)
      TDC=0.4726
C      Critical Time (Hours)
      TC=MS**2.*HT**2.*TDC/(4.*KHOB*MOB)
C
C
C
      DO 100 I=1,8
C      Fraction of Pore Volume Injected into the Model
      PV=0.25*I
C      Calculate Time Using the Pore Volume Injected (hrs)
      TM=PV*14055./(226.8*60)
C
C
C      Dimensionless Time
      TD=4.0*KHOB*MOB*TM/((MS**2)*(HT**2))
C
C      Check if time is past critical time and then
C      Mandl-Volek equation applies otherwise Marx-Langenheim
C      is used.
C
      IF(TM-TC)1,1,2
C      Marx-Langenheim
1     F1=EXP(TD)*ERFC(SQRT(TD))+2.*SQRT(TD/3.141592)-1.
      A=1
      GO TO 3
C      Mandl-Volek
2     X1=EXP(TD)*ERFC(SQRT(TD))+2*SQRT(TD/3.141592)-1.
      X2=(1/(1+(FST*LV/CH2OT)))-(TD-TDC)/(3.*SQRT(3.141592*TD))
      X3=((TD-TDC-3.)/3.)*EXP(TD)*ERFC(SQRT(TD))
      X4=SQRT((TD-TDC)/3.141592)
      F1=X1-X4*(X2+X3)
      A=2
3     WRITE(6,22)PV
22    FORMAT(/10X,F4.2,' Pore Volumes Injected')
C
C
C      Heat Injection Rate(Btu/hr)
      QI=350.*IW*(CH2OT+FST*LV)/24.
C
      R1=QI*MS*(HT**2.0)*F1
      R2=4.*KHOB*MOB*(TF-TR)
C
C      Steam Zone Volume as a Percentage of
C      the Model's Bulk Volume (1.481481 ft3)
      VS=(R1/R2)/1.481481*100.
C
C
      WRITE(6,20)VS
20    FORMAT(10X,'Vs is ',F5.2,2X,'% of Models Bulk Volume')
100   CONTINUE
      STOP
      END
```

University of Alberta

```
C*****************************************************************
C      This program calculates the total heat injected into the
C      model, the amount of heat contained in the model and the
C      amount of heat lost from the model in Experiment 26 which
C      was a base steamflood.
C
C      After planimetering all of the Run 26 temperature profiles
C      one could then use this program to calculate the above
C      mentioned values for Experiment 26.
C
C      In general this program does a simple heat balance on the
C      model during Experiment 26.  Where the heat in the model
C      is determined by summing heat contained in each
C      temperature's incremental volume which is calculated by:
C
C      Heat=Ms*Vol. for partial temp.*Change in temp.
C
C      The total heat in the model is obtained by the summation
C      of these Volumes.
C
C*****************************************************************
      REAL DOIL,COIL,MOIL,DH2O,CH2OT,MH2O,KHG,MG,KHOB,MOB,TM,HT,
     @IW,TR,MS,POR,SOIL,SH2O,FST,QI,LV,SST,PV,CH2O,
     @AREA1,AREA2,VTEMP1,VTEMP2,QM,QM1,QM2,TOTALQ,LOSTQ
      INTEGER A
C
C      Quality of Steam
      FST=0.08324
C      Latent Heat of Vaporization (Btu/lb)
      LV=1017.755
C      Density of Oil (lb/ft3)
      DOIL=38.375
C      Specific Heat of Oil (Btu/lb-F)
      COIL=0.5162
C      Heat Capacity of Oil (Btu/ft3-F)
      MOIL=DOIL*COIL
C      Density of Water (lb/ft3)
      DH2O=61.186
C      Specific Heat of Water (Btu/lb-F)
      CH2O=1.01495
C      hw-hr  (Btu/lb)
      CH2OT=101.297
C      Heat Capacity of Water (Btu/ft3-F)
      MH2O=DH2O*CH2O
C      Thermal Condutivity of Glass (Btu/hr-ft-F)
      KHG=0.5
C      Heat Capacity of Glass (Btu/lb-F)
      MG=25.9
C      Thermal Conductivity of Overburden (Btu/hr-ft-F)
      KHOB=1.46426
C      Heat Capacity of Overburden (Btu/ft3-F)
      MOB=28.8558
C      Thickness (Feet)
      HT=.104167
C      Injection Rate of Fluid (BBl/Day)
      IW=2.054
C
C      Since the lowest temperature on the contours is
C      5.0 C (41.0 F) then this is assumed as the initial
```

University of Alberta

University of Alberta

```
C       reservoir temperature.
C
C       Temperature of Reservoir (F)
      TR=41.0
C       POROSITY OF MODEL
      POR=.3346
C       Calculate Heat Injection Rate (Btu/hr)
      QI=350.*IW*(CH2OT+FST*LV)/24.
C
C
      DO 10 I=1,7
          READ (5,*)PV,SOIL
          QM=0.0
          QM1=0.0
          QM2=0.0
          LOSTQ=0.0
          TOTALQ=0.0
C          Time (hours)
          TM=PV*14055./(226.8*60.)
C          Water Saturation (fraction)
          SH2O=1.-SOIL
          MS=POR*SOIL*MOIL+POR*SH2O*MH2O+(1.0-POR)*MG
C
C       Calculate Total Amount of Heat Injected (Btu)
      TOTALQ=QI*TM
C
         DO 20 J=1,13
C
C       Reads Temperature and its corresponding areal extent
C       in the upper and lower portion of the model, respectively.
C
             READ(5,*)TEMP,AREA1,AREA2
C          Convert Temperature to Fahrenheit
             TEMP=TEMP*1.8+32.
C       Upper Portion
C       Volume in Upper Portion of Model Corresponding to
C       the Temperature is Calculated
C
             VTEMP1=AREA1*2.9941052*HT
C
C       Heat contained in this volume is calculated and summed
C       up.for the entire upper portion of the model.
C
             QM1=QM1+(MS*VTEMP1*(TEMP-TR))
C       Lower Portion
C       Same procedure as was performed for the upper portion
C       of the model is carried out for the lower portion.
C
             VTEMP2=AREA2*2.9941052*HT
             QM2=QM2+(MS*VTEMP2*(TEMP-TR))
20       CONTINUE
C
C
C
C
C       Heat Remaining in the Model
      QM=QM1+QM2
C       Heat Lost to Surroundings is Calculated
      LOSTQ=TOTALQ-QM
```

```
C
C       Percentage of Heat Remaining in the Model
      QM=QM/TOTALQ*100.
C       Percentage of Heat Lost from the Model
      LOSTQ=LOSTQ/TOTALQ*100.
C
      WRITE(6,2)PV,TOTALQ,QM,LOSTQ
2     FORMAT(/10X,'After ',F4.2,' P.V.s'/10X,'Tot. Heat ',
     @'Inj. into Model is ',F8.2,' BTUs'/10X,'% of Tot. Heat ',
     @'Inj. that is Remaining in Model is ',F5.2,' %'/10X,'% ',
     @'of Tot. Heat Inj. Lost from the Model was ',F5.2,' %')
C
C
10    CONTINUE
      STOP
      END
```

University of Alberta